AD-A259 235

(2)

Proceedings of the
Forty-First

IWCS



DTIC
ELECTE
DEC 2 9 1992
S A D

INTERNATIONAL WIRE AND CABLE SYMPOSIUM

November 16 thru 19, 1992

This document has been approved for public release and sale; its distribution is unlimited.

Sponsored by
International Wire and Cable Symposium, Inc. (IWCS)
Eatontown, New Jersey

With Participation by
US Army Communications-Electronics Command (CECOM)
Fort Monmouth, New Jersey

PROCEEDINGS OF 41ST INTERNATIONAL WIRE AND CABLE SYMPOSIUM

Sponsored by
International Wire and Cable Symposium, Inc. (IWCS)
Eatontown, New Jersey

With Participation by
US Army Communications-Electronics Command (CECOM)
Fort Monmouth, New Jersey

RENO HILTON RESORT HOTEL
RENO, NEVADA
NOVEMBER 16, 17, 18 and 19, 1992

APPROVED FOR PUBLIC RELEASE: DISTRIBUTION UNLIMITED

92-33061
8555

92 12 29 021

MISSION

The International Wire and Cable Symposium provides a forum for the exchange of technical information amongst suppliers, manufacturers, and users on technological advancements in materials, processes, and products used for voice, data and video signal transmission systems.

TECHNICAL PAPERS

Tuesday, November 17, 1992

9:00 am	SESSION I	The Future of Cable Communications
1:00 pm	SESSION II	Fiber Optic Cable Design I
1:00 pm	SESSION III	Application & Field Evaluation I
1:00 pm	SESSION IV	Splicing/Enclosures

Wednesday, November 18, 1992

8:00 am	SESSION V	Fiber Optic Cable Design II
8:00 am	SESSION VI	Application & Field Evaluation II
8:00 am	SESSION VII	Fiber Optic Coatings
2:15 pm	SESSION VIII	Materials Processes & Manufacturing
2:15 pm	SESSION IX	Fire Resistance
2:15 pm	SESSION X	Submarine Cables
4:00 pm	SESSION XI	Poster Papers

Thursday, November 19, 1992

8:30 am	SESSION XII	Medium and High Voltage Power Cables and Accessories
8:30 am	SESSION XIII	Fiber Optic Reliability I
8:30 am	SESSION XIV	Technology in Military Applications
1:00 pm	SESSION XV	Fiber Optic Reliability II
1:00 pm	SESSION XVI	Copper Cable/Wire
1:00 pm	SESSION XVII	Fiber Optic Interconnects

PAPERS

The papers in this volume were printed directly from unedited reproducible copies prepared by the authors. Responsibility for contents rests upon the authors and not the symposium committee or its members. All rights reserved by the International Wire and Cable Symposium, Inc., 174 Main Street, Eatontown, New Jersey 07724.

PROCEEDINGS/PUBLICATIONS
INTERNATIONAL WIRE AND CABLE SYMPOSIUM (IWCS)

Proceedings – Bound – Available from IWCS

31st IWCS Proceedings – 1982 – $8.00
32nd IWCS Proceedings – 1983 – $8.00
33rd IWCS Proceedings – 1984 – $10.00
34th IWCS Proceedings – 1985 – $10.00
35th IWCS Proceedings – 1986 – $15.00
39th IWCS Proceedings – 1990 – $25.00
40th IWCS Proceedings – 1991 – $35.00
41st IWCS Proceedings – 1992 – $50.00

Publications – Bound – Available from IWCS

Index of IWCS Papers (1983–1990); PUB #1001RP-1991 – $15.00
PIC Insulation Testing & Field Experience; PUB #1003RP-1992 – $25.00
Fiber Optic Cables; PUB #1004RP-1992 – $25.00

Extra Copies of the 1992 Proceedings: 1–3, $50.00 per copy; 4–10, $40.00 per copy; 11 and above $30.00 per copy

Shipping/Handling:

Proceedings

$ 5.00 per copy USA only
$13.00 per copy Surface Mail (overseas – 4 to 6 weeks)
$35.00 per copy Airmail (Europe)
$40.00 per copy for (Asia)

Publications

$ 3.00 per copy USA Only
$ 5.00 per copy Surface Mail (overseas – 4 to 6 weeks)
$10.00 per copy Airmail (Europe and Asia)

Payment: Make a check or bank draft payable in U.S. Dollars drawn on U.S. Bank only to the INTERNATIONAL WIRE & CABLE SYMPOSIUM, INC. or use your VISA/MasterCard by providing number and expiration date and forward request to: International Wire and Cable Symposium, Inc., 174 Main Street, Eatontown, NJ 07724. Telephone inquiries may be directed to Pat Hudak (908) 389-0990.

Photocopies are available for complete sets of papers for 1964 thru 1991. Information on prices and shipping charges should be requested from the:

US Department of Commerce
National Technical Information Service (NTIS)
Springfield, Virginia 22151
Telephone: (703) 487-4650

Include Title, Year and "AD" Number

13th Annual Wire & Cable Symposium (1964) — AD 787164
15th Annual Wire & Cable Symposium (1966) — AD A006601
16th International Wire & Cable Symposium (1967) — AD 787165
17th International Wire & Cable Symposium (1968) — AD 787166
18th International Wire & Cable Symposium (1969) — AD 787167
19th International Wire & Cable Symposium Proceedings 1970 — AD 714985
20th International Wire & Cable Symposium Proceedings 1971 — AD 733399
21st International Wire & Cable Symposium Proceedings 1972 — AD 752908
22nd International Wire & Cable Symposium Proceedings 1973 — AD 772914
23rd International Wire & Cable Symposium Proceedings 1974 — AD A003251
24th International Wire & Cable Symposium Proceedings 1975 — AD A017787
25th International Wire & Cable Symposium Proceedings 1976 — AD A032801
26th International Wire & Cable Symposium Proceedings 1977 — AD A047609
27th International Wire & Cable Symposium Proceedings 1978 — AD A062322
28th International Wire & Cable Symposium Proceedings 1979 — AD A081428
29th International Wire & Cable Symposium Proceedings 1980 — AD A096308
30th International Wire & Cable Symposium Proceedings 1981 — AD A110859
31st International Wire & Cable Symposium Proceedings 1982 — AD A125662
32nd International Wire & Cable Symposium Proceedings 1983 — AD A136749
33rd International Wire & Cable Symposium Proceedings 1984 — AD A152119
34th International Wire & Cable Symposium Proceedings 1985 — AD A164384
35th International Wire & Cable Symposium Proceedings 1986 — AD A180828
36th International Wire & Cable Symposium Proceedings 1987 — AD A189610
37th International Wire & Cable Symposium Proceedings 1988 — AD A200903
38th International Wire & Cable Symposium Proceedings 1989 — AD A216023
39th International Wire & Cable Symposium Proceedings 1990 — AD A233634
40th International Wire & Cable Symposium Proceedings 1991 — AD A244038
Kwic Index of Technical Papers, International Wire & Cable Symposium (1952–1982) — AD A027588

DTIC QUALITY INSPECTED 5

Codes
1/or
Dist | Special
A-1



MESSAGE FROM THE PRESIDENT/DIRECTOR

As the director of the symposium, it is always my pleasure on behalf of the International Wire and Cable Symposium (IWCS) Committee and CECOM, Fort Monmouth, New Jersey to welcome all attendees to the conference. This symposium represents the 41st year of continued service to the wire and cable industry. I constantly ask myself, where have the years gone. It seems as if it was only a few years ago that we were in Atlantic City or Cherry Hill, New Jersey. Many changes have taken place during this period, the most notables are the introduction of poster papers and a suppliers forum. Also the addition of educational short courses have been quite successful. It is hoped that these activities plus the technical presentations will provide the interest and stimulation to maintain the support and participation of the entire cable industry. I can assure you, the committee will continue to provide the latest information on copper and fiber optic technology during each symposium.

This should be another exciting year for symposium attendees. The response to the "Call-for-Papers" was outstanding, especially from our international representatives. The program includes over seventy speakers from nineteen different countries. The program's opening session, entitled "The Future of Cable Communications" should be of interest to all attendees, especially since the panel of invited speakers will be discussing the future of cable communication as it relates to their country or worldwide.

The "Call-for-Papers" for the 1993 Symposium is being circulated during this symposium. Each one is encouraged to obtain a copy and to submit an abstract for the committee's review. *Papers are specifically requested on materials and copper* cable/wire designs and usage.

Committee Member Dave Fallowfield, the committee's present chairman's term on the committee expires this year. Dave and his company, AGT Limited, are strong supporters of the symposium and its program. I extend to Dave on behalf of the IWCS Committee, a very special thanks for his dedication, cooperation and most of all his individual contributions as a committee member. I wish to express my sincere appreciation and thanks to all Committee Members for their dedication, cooperation and technical assistance.

The committee solicits the support and suggestions of all symposium attendees, cable manufacturers, material suppliers and cable users. We are constantly seeking and exploring new and innovative ideas for technical growth, and also provide a convivial and pleasant environment for the interchange of information.

The symposium schedule for the next three years is as follows:

Adam's Mark Hotel, St. Louis, MO – November 15th thru 18th, 1993
Hilton Hotel, Atlanta, GA – November 14th thru 17th, 1994
Marriott Hotel, Philadelphia, PA – November 13th thru 16th, 1995

Elmer F. Godwin

ELMER F. GODWIN
President/Director, IWCS









IWCS REGISTRATION













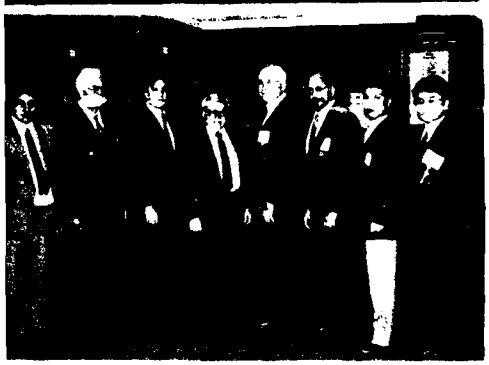




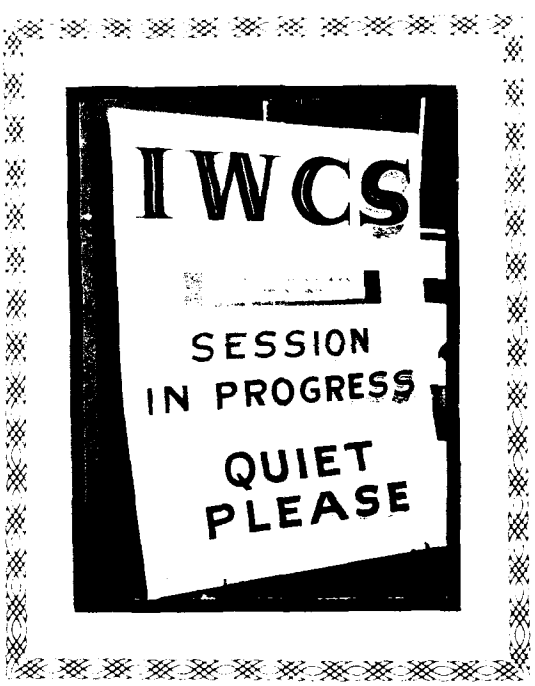









IWCS
SESSION
IN PROGRESS
QUIET
PLEASE



















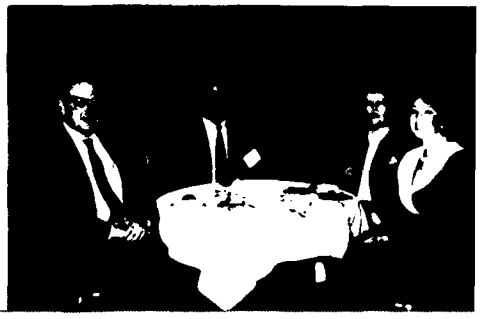

HOSPITALITY HOUR





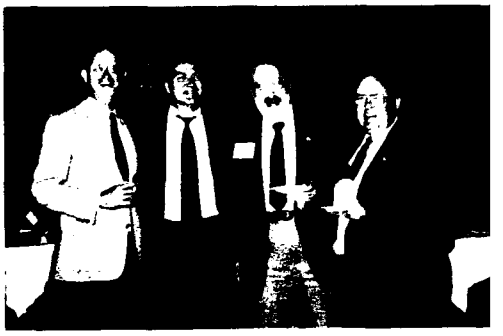






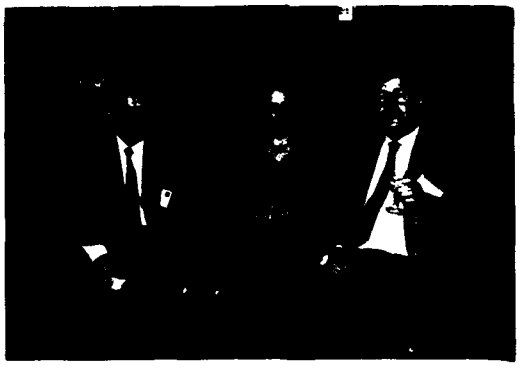


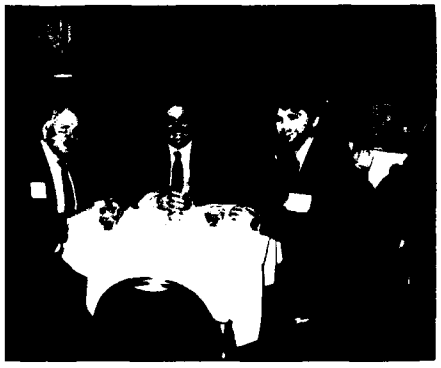


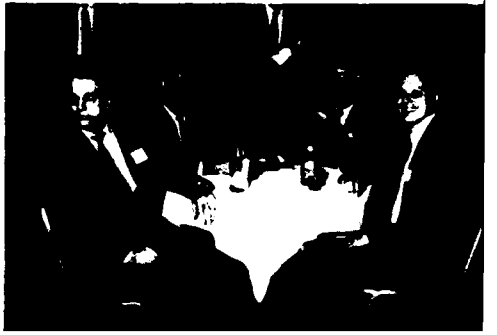

HOSPITALITY HOUR











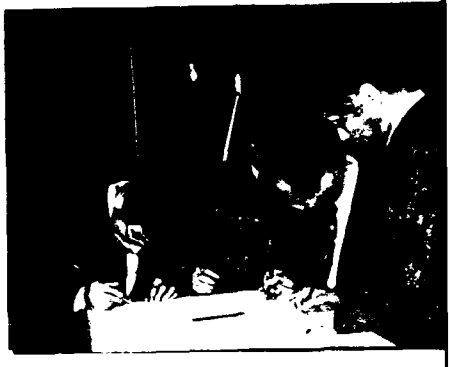
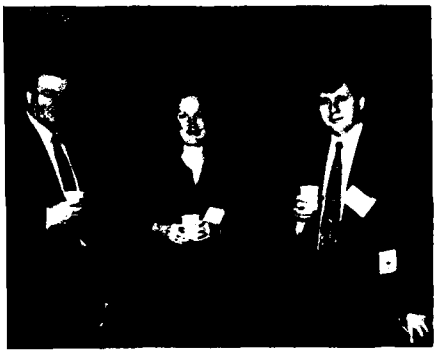






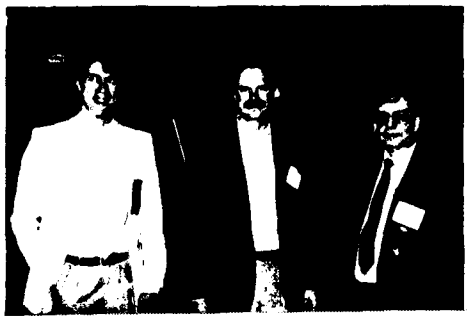




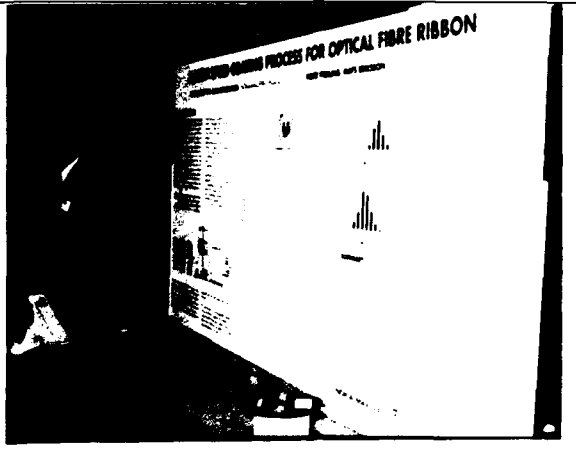







1991...**IWCS**...1991







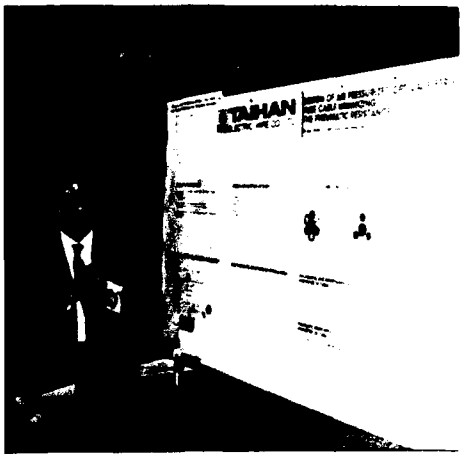


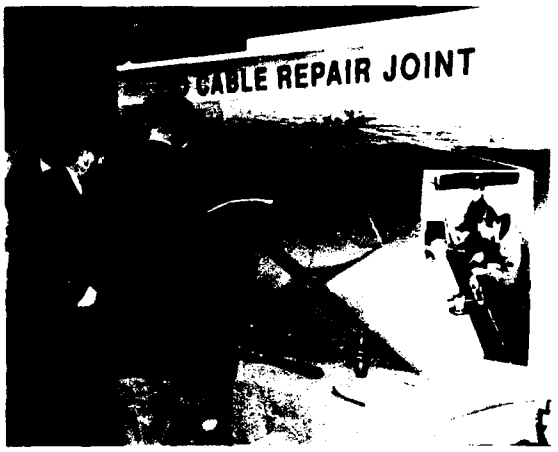
IWCS

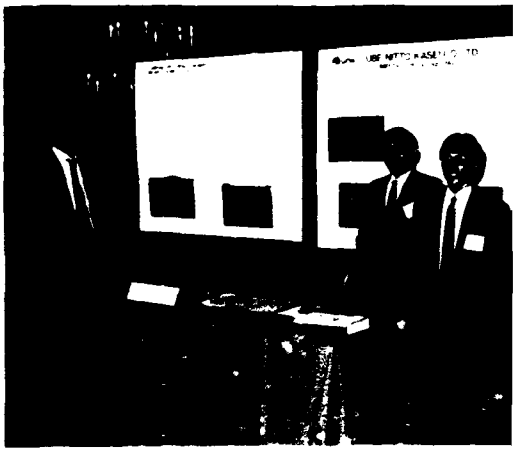
DISPLAYS

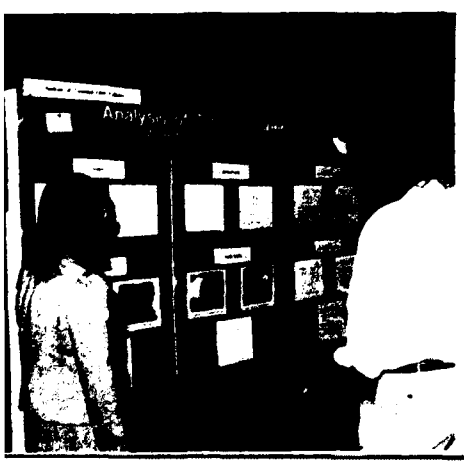




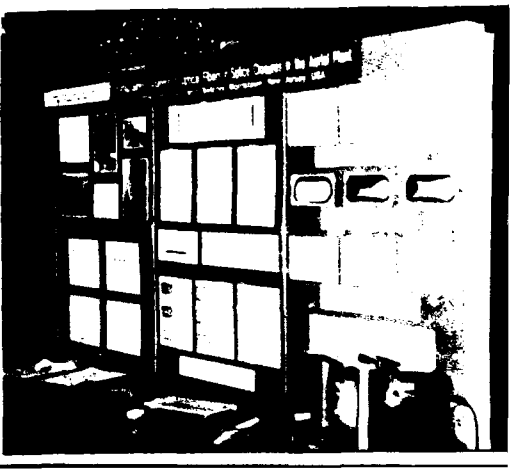












AWARDS

Outstanding Technical Paper

H. Lubars and J. A. Olszewski, General Cable Corp – "Analysis of Structural Return loss in CATV Coaxial Cable"

J. P. McCann, R. Sabia and B. Wargotz, Bell Laboratories—"Characterization of Filler and Insulation in Waterproof Cable"

D. E. Setzer and A. S. Windeler, Bell Laboratories—"A Low Capacitance Cable for the T2 Digital Transmission line"

R. Lyenger, R. McClean and T. McManus, Bell Northern Research—"An Advanced Multi-Unit Coaxial Cable for Toll PCM Systems"

J. B. Howard, Bell Laboratories—"Stabilization Problems with Low Density Polyethylene Insulations"

Dr.H. Margin, Kabelmetal—"High Power Radio Frequency Coaxial Cables, Their Design and Rating"

D. Doty, AMP Inc. – "Mass Wire Insulation Displacing Termination of Flat Cable"

T. S. Choo, Dow Chemical U.S.A. – "Corrosion Studies on Shielding Materials for Underground Telephone Cables"

N. J. Cogelia, Bell Telephone Laboratories and G. K. Lavoie and J. F. Glahn, US Department of Interior – "Rodent Biting Pressure and Chemical Action and Their Effects on Wire and Cable Sheath"

T. K. McManus, Northern Telecom Canada Ltd. and R. Beveridge, Saskatchewan Telecommunications, Canada—"A New Generation of Filled Core Cable"

F. Suzuki, S. Sato, A. Mori and Y. Suzuki; Sumitomo Electric Industries, Ltd. Japan—"Microcoaxial Cables Insulated with Highly Expanded Polyethylene By Chemical Blowing Method"

S. Masaki, Y. Yamazaki and T. Ideguchi, Nippon Telegraph and Telephone Public Corporation, Japan—"New Aluminum Sheath Cable Used for Electromagnetic Shielding"

P. Kish and Y. BeBorgne, Northern Telecom Canada Limited,Motreal, Canada—"General Crosstalk Model For Paired Communication Cables"

C. J. Arroyo, N. J.Cogelia, Bell Laboratories, and B. J. Darsey, Western Electric—"Thermal Behavior of Experimental Plenum Cable Sheaths Determined in a Radiant Heat Chamber"

R. H. Whiteley. Raychem Ltd.—"A Comprehensive Small Scale Smoke Test"

V. A. Fentress, Raychem Corp. and D. V. Nelson, Stanford University—"Fracture Mechanics Evaluation of the Static Fatigue Life of Optical Fibers in Bending"

M. Fujise and Y. Iwamoto, KDD Research & Development Laboratories, Tokyo, Japan—"Self-Core-Alignment Arc-Fusion Splicer Based on a Simple Local Monitoring Method"

James A. Krabec and John W. Kincaid, Jr., Belden Technical Research Center—"Advances in the Optimization of Multi-Layer Shield Design"

Simon D Dadakarides and Bruce B. Lusignam, Stanford University—"Magnetically Loaded Cables"

Best Presentation

1968 N. Dean, B.I.C.C. – "The Development of Fully Filled Cables for Distribution Network"

1969 J. D. Kirk, Alberta Government Telephones—"Progress and pitfalls of Rural Buried Cable"

1970 Dr. O. Leuchs, Kable and Metalwerke—"A New Self-Extinguishing Hydrogen Chloride Binding PVC Jacketing Compound for Cables"

1971 S. Nordblad, Telefonaktiebolaget L. M. Ericsson—"Multi-Paired Cable of Nonlayer Design for Low Capacitance Unbalance Telecommunications Network

N. Kojima Nippon Telegraph and Telephone – "New Type Paired Cable for High Speed PCM Transmission"

1972 S. Kaufman, Bell Laboratories—"Reclamation of Water-Logged Buried PIC Telephone Cable"

1973 R. J. Oakley, Northern Electric Co., Ltd.—"A Study Into Paired Cable Crosstalk"

1974 G. H. Webster, Bell Laboratories—"Material Savings by Design in Exchange and Trunk Telephone Cable"

1975 J. E. Wimsey, United States Air Force—"The Bare Base Electrical Systems"

1976 Michael DeLucia, Naval Ship Research and Development – "Highly Fire-Retardant Navy Shipboard Cable"

1977 William L. Schmacher, AMP Inc.—"Design Considerations for Single Fiber Connector"

1978 Richard C. Mondello, Bell Labs.—"Design and Manufacture of an Experimental Lightguide Cable For Undersea Transmission Systems"

1979 I. Wadehra, IBM Corporation—"Performance of Polyvinyl Chloride Communication Cables in Modified Steiner Tunnel Test"

1980 J. J. Refi, Bell Laboratories—"Mean Power Sum Far-End Crosstalk of PIC Cables as a Function of Average Twist Helix Angle"

1981 G. S. Anderson, Belden Corporation—"Installation of Fiber Optic Cable on 457 Meter Tower"

1982 A. Yoshizawa, The Furukawa Electric Co., Ltd.—"Structure and Characteristics of Cables for Robots"

1983 J. R. Bury, Standard Telecommunication Laboratories, Ltd., Hailow, England—"Development of Flame Retardant, Low Aggressivity Cables"

1984 William E. Dennis, Dow Corning Corporation, Midland, Michigan—"Hydrogen Evolving Tendencies of Cable Fillers and Optical Fiber Coatings"

1985 Stephen Hornung, British Telecom Research Laboratories—"Manufacture and Performance of Fibre Units for Installation by The Viscous Drag of Air"

1986 Dave Fischer, Superior Cable Corp.—"Progress Towards the Development of Lighting Test for Telecommunication Cables"

John C. Chamberlain, Siecor Corp.—"Zero Halogen Fire Retardant Fiber Optic Shipboard Cable"

Outstanding Technical Paper	*Outstanding Poster Paper*	*Best Presentation*
1987 Stephen B. Pierce—Conel Laboratories—"Digital Transmission on Customer Premises Wiring"	William Wood—Bell Communication Research "Performance Analysis of Optic Fiber Cleavers"	Richard Rossi—General Cable Company "Cable Sheathing Design and Performance Criteria"
1988 Martin C. Light Jr., James A. Moses, Mark A. Sigmon and Christopher A. Story – Siecor Corp. – "Design and Performance of Telecommunication Cable Optimized for low Fiber Count"	Dr. R. Raman - Contel Laboratories —"Loss at Dissimilar Fiber Splices"	Janice B. Haber - AT&T Laboratories "Single-Mode Media and Apparatus for Fiber to the Home"
1989 Michel Plasse, Lise Desroches and Paul-Andre Guilbert - Northern Telecom Canada Limited - "High Performance Twisted-Pair Cable for LAN Systems"	Werner Bernard and Susan C. Grant - Siecor Corporation - "Fiber Optic Drop Cables in the Subscriber Loop"	Michel de Vecchis - Les Cables de Lyon - "Results on a Large Scale Installation of a Fibre Optic Distribution Network"
1990 Trevor N. Bowmer, Russell J. Miner, Irene M. Plitz, Joseph N. D'Amico and Lal M. Hore - Bellcore - "Thermal Stability Tests for Polyolefin Insulations"	Steve Lischynsky, Helmut Lukas, Robin McIntyre and Grant Pacey - Bell-Northern Research Ltd. - "New Technology for a Single Mode Mechanical Splice"	Harold W. Friesen - AT&T Bell Laboratories - "An Improved Characteristic Impedance Measurement Technique"
1991 Shigeru Tomita, Michito Matsumoto, Tetsuro Yabuta and Takuya Uenoya – NTT – "Preliminary Research into Ultra High Density and High Count Optical Fiber Cables"	G. Scott Glaesemann – Corning Inc. – "The Effect of Proof Testing on the Minimum Strength of Optical Fiber"	Sue V. Wolfe – STC Submarine Systems – "Structure and High Voltage DC Behaviour of Submarine Cable Mouldings"

GOLD and SILVER CONTRIBUTORS

GOLD SUSTAINING CONTRIBUTORS

AFA Industries
20 Jewell Street
Garfield, NJ 07026

Akzo Fibers Inc.
801-F Blacklawn Road
Conyers, GA 30207

Alcatel Kabelmetal Electro GmbH
Hannover, Germany

Alcoa Fujikura Ltd.
P.O. Box 5631
Spartanburg, SC 29304

Amoco Chemical Company
150 West Warrenville
Naperville, IL 60566

Anixter Bros., Inc.
4711 Golf Road
Skokie, IL 60076

AT&T Bell Laboratories
2000 Northeast Expressway
Norcross, GA 30071

Bell Canada
700 La Gauchetiere W., Rm 18E2
Montreal, Quebec, Canada H3B 4L1

Camden Wire, Co., Inc.
12 Masonic Ave.
Camden, NY 13316

Chase & Sons
19 Highland Ave.
Randolph, MA 02368

Comm/Scope, Inc.
3642 US 70 East
Claremont, NC 28610

Communication Line Products Association of Japan
Toranomon Bldg, 1-1-12 Toranomon
Minatoku, Tokyo 105
Japan

Corning Inc.
35 W. Market St.
Corning, NY 14831

DCM International Corp.
2930 Faber Street
Union City, CA 94587

The Dow Chemical Company
2020 Willard H. Dow Center
Midland, MI 48674

DSM Desotech Inc.
1122 St. Charles Street
Elgin, IL 60120

Du Pont Company
Chestnut Run Plaza
Wilmington, DE 19880-0711

Elf Atochem North American, Inc.
Three Parkway
Philadelphia, PA 19102

Facile Holdings, Inc.
185 Sixth Avenue
Paterson, NJ 07509

The Furakawa Electric Co., Ltd.
6, Yawata-Kaigardori
Ichihara, Chiba 290, Japan

Fusion UV Curing Systems
7600 Standish Place
Rockville, MD 20855-2798

Gary Corp.
Pioneer Industrial Park
P.O. Box 808
Leominster, MA 01453

GE Plastics
One Plastics Avenue
Pittsfield, MA 01201

GTE TestMark Labs
3050 Harrodsburg Road
Lexington, KY 40503

Hargro Industrial Packaging
Church Street Extension
Flemington, NJ

KT Industries Ltd.
1130 Wall Street
Winnipeg, MB
Canada R3E 2R9

Lantor BV, FIRET Cable Wrappings
P.O. Box 45
3900 AA Veenendaal
The Netherlands

GOLD SUSTAINING CONTRIBUTORS

LITESPEC, Inc.
76 Alexander Drive
Research Triangle Park, NC 27709

Master Adhesives, Inc.
996 A Norcross Industrial Court
Norcross, GA 30071

MM Cables Communication Products
71 Whiteside Road
Clayton, Victoria 3168
Australia

Mohawk Wire & Cable Corp.
9 Mohawk Drive
Leominster, MA 01453

NEPTCO, Inc.
30 Hamlet Street
Pawtucket, RI 02861-0323

Nippon Telegraph and Telephone Corp.
Tokai, Ibaraki, 319-11
Japan

Nokia-Maillefer, Inc.
749 New Ludlow Road
South Hadley, MA 01075

Norscan Instruments Ltd.
7 Terracon Place
Winnipeg, Manitoba
Canada R2J 4B3

Northern Telecom
6201 Oakton Street
Morton Grove, IL 60053

Olex Cables A Division of Pacific Dunlop Ltd.
207 Sunshine Road
Tottenham, VIC 3012
Melbourne, Australia

Optical Fibres
Second Avenue
Deeside Industrial Park
Deeside, Clwyd CH5 2NX
United Kingdom

Owens-Corning
Fiberglas Tower - T/8
Toledo, OH 43659

PENRECO
138 Petrolia Street
Karns City, PA 16041

Photon Kinetics, Inc.
9405 S.W. Gemini Drive
Beaverton, OR 97005-7160

Quantum Chemical Corp.
11500 Northlake Drive
Cincinnati, OH 45249

Rimtec Corporation
Beverly Road
Burlington, NJ 08016

Siecor Corp.
P.O. Box 489
Hickory, NC 28603-0489

SpecTran Corporation
50 Hall Road
Sturbridge, MA 01566

The Stewart Group Ltd.
259 Steelcase Rd., W.
Markham, Ontario
Canada L3R 2P6

Sumitomo Electric U.S.A., Inc.
21221 S. Western Ave., Suite 200
Torrance, CA 90501

Teknor Apex Company
505 Central Avenue
Pawtucket, RI 02861

UBE Industries (America), Inc.
666 Fifth Avenue, 14th Floor
New York, NY 10103

Union Carbide Chemicals and Plastics Company, Inc.
2970 Clairmont Road, Suite 500
Atlanta, GA 30329

WaterGuard Cable Products, Inc.
P.O. Box 1079
Houston, TX 77530

Weber & Scher Mfg. Co., Inc.
263 Sussex Avenue
Newark, NJ 07107

Witco Corporation
520 Madison Avenue
New York, NY 10022-4236

SILVER SUSTAINING CONTRIBUTORS

ANT-Nachrichtentechnik GmbH
Offenburg, Germany

AT Plastics Inc.
Brampton, Ontario, Canada

AT&T Fitel
Carrollton, GA 30117

Barcel Wire and Cable Corp.
Irvine, CA 92714-5885

Breen Color Concentrates, Inc.
Lambertville, NJ 08530-3411

Cooper Industries/Belden Division
Richmond, IN 47375

Du Pont Canada, Inc.
Mississauga, Ontario, Canada

Dussek Campbell Ltd.
Belleville, Ontario, Canada

Dussek Campbell Pty. Ltd.
Auburn, New South Wales, Australia

Ericsson Cables AB
Hudiksvall, Sweden

Essex Group, Inc.
Decatur, IL 62525

General Cable Corporation
Highland Heights, KY 41076-9753

Glastic Corp.
Cleveland, OH 44121

H.B. Fuller GmbH
Lùneburg, Germany

Kabel Rheydt Aktiengesellschaft
Mönchengladbach, Germany

Kroschu-Kabelwerke
Kromberg & Schubert GmbH u. Co.
Wuppertal, Germany

Philips Kommunikations Industrie AG
Köln, Germany

RXS Schrumpftechnik-Garnituren GmbH
Hagen, Germany

Siemens AG
München, Germany

Superior Teletec
Atlanta, GA 30339

Telia Research
Haninge, Sweden

Texas Instruments Inc.
Attleboro, MA 02703

41ST INTERNATIONAL WIRE AND CABLE SYMPOSIUM (IWCS)

SYMPOSIUM COMMITTEE

ELMER F. GODWIN
(President/Director)
GEF Associates
3A Buttonwood Drive
Shrewsbury, NJ 07702
Office: (908) 389-0990
Fax: (908) 389-0991
Home: (908) 741-8864

IRVING KOLODNY
(Director's Assistant)
80-56 230th Street
Bellerose Manor, NY 11427
Tel & Fax: (718) 464-9197

DAVE FALLOWFIELD
(Chairman)
AGT Limited
15015 123 Ave.
Edmonton, Alberta
Canada T5V 1J7
Tel: (403) 453-7467
Fax: (403) 451-0763

Dr. Robert Baboian
(Treasurer)
Texas Instruments, Inc.
34 Forest Street
MS 10-13
Attleboro, MA 02703
Tel: (508) 699-1350
Fax: (508) 699-3476

Dr. Koichi Inada
Fujikura Ltd.
Opto-Electronics Laboratory
1440 Mutsuzaki, Sakura-shi
Chiba-ken, 285 Japan
Tel: 011-81-434-84-3940
Fax: 011-81-434-84-3988

Richard Rossi
General Cable
One Cragwood Road
P.O. Box 1012
South Plainfield, NJ 07080
Tel: (908) 412-3800
Fax: (908) 769-6909

Dave Fischer
Superior Cable Corp.
150 Interstate North Parkway
Suite 300
Atlanta, GA 30339
Tel: (404) 953-8338
Fax: (404) 980-2808/2812

Dr. Joyce P. Kilmer
Bellcore
445 South Street, Rm 2K-134
Morristown, NJ 07962-1910
Tel: (201) 829-5035
Fax: (201) 829-5965

Manuel R. Santana
AT&T Bell Laboratories
2000 NE Expressway
Norcross, GA 30071
Tel: (404) 447-2754
Fax: (404) 441-7154

Rene G. Freeman
Union Carbide Chemicals and Plastic Company, Inc.
2970 Clairmont Road
Suite 500
Atlanta, GA 30329
Tel: (404) 320-3527
Fax: (404) 320-3520

Xavier Mann
(Secretary)
AT&T Fitel
P.O. Box 486
Carrollton, GA 30117
Tel: (404) 830-6616
Fax: (404) 836-8820

Homer Vela
(Vice-Chairman)
AT&T Network Cable Systems
505 North 51st Avenue
P.O. Box 13369
Phoenix, AZ 85002
Tel: (602) 233-5552
Fax: (602) 233-5798

Brian D. Garrett
Comm/Scope, Inc.
P.O. Box 879
Claremont, NC 28610
Tel: (704) 459-5003
Fax: (704) 459-5097

Dieter S. Nordmann
Kabelmetal Electro
P.O. Box 260
Kebelkamp 20
D-3000 Hannover 1
Germany
Tel: 011-49-511-676-2020
Fax: 011-49-511-676-2664

ADVISORY

Dr. Peter R. Bark
Siecor Corporation
P.O. Box 489
489 Siecor Park
Hickory, NC 28603
Tel: (704) 323-6205
Fax: (704) 323-6264

Leo Chattler
DCM Industries, Inc.
2930 Faber Street
Union City, CA 94587
Tel: (510) 429-9500
Fax: (510) 429-1250

Michael A. DeLucia
Naval Surface Warfare Center
Carderock Div., Annapolis Detach.
Energy R&D Office, Code 2759
Annapolis, MD 21402-5067
Tel: (410) 267-3825
Fax: (410) 267-2875

CONSULTANTS

Dr. Reiner J. Gerdes
Gerdes Consulting
812 Oakdale Rd., N.E.
Atlanta, GA 30307
Tel: (404) 377-8608
Fax: (404) 378-5658

Dr. Raymond E. Jaeger
SpecTran Corporation
50 Hall Road
Sturbridge, MA 01566
Tel: (508) 347-2261
Fax: (508) 347-2747

Hans A. Mayer
Olex Cables A Division of Pacific Dunlop Ltd.
207 Sunshine Road
Tottenham, VIC 3012
Melbourne, Australia
Tel: 011-61-3-316-2222
Fax: 011-61-3-314-0383

TABLE OF CONTENTS

TUESDAY MORNING—9:00 AM–12:00 PM (NOON)
Broadway Room

Announcements/Greetings
Elmer F. Godwin, President/Director, IWCS, Inc., Eatontown, NJ
Dave Fallowfield, AGT Limited, Alberta, Canada, Chairman, IWCS
Joseph J. Pucilowski, Jr., Director, Command, Control and Communications Systems, U.S. Army CECOM, Fort Monmouth, NJ

SESSION I: THE FUTURE OF CABLE COMMUNICATIONS

Chairperson: Mr. Manuel R. Santana, AT&T Bell Laboratories, Norcross, GA

Panelists (Invited Presentations):
Mr. J.P. (Jack) Bucter, President, AT&T Network Cable Systems, Morristown, NJ
Mr. Michel de Vecchis, Chairman of Technical Affairs of EUROPACABLE, Bruxelles, Belgium
Mr. Shunji Kaibuchi, Executive V.P., Nippon Telegraph and Telephone Corporation (NTT), Osaka, Japan
Mr. Phil W. Black, Technical Director, STC Submarine Systems, London, United Kingdom

TUESDAY AFTERNOON—1:00 PM–5:00 PM
Capital Rooms

SESSION II: FIBER OPTIC CABLE DESIGN I

Chairperson: Dr. Peter R. Bark, Siecor Corporation, Hickory, NC

Preliminary Research into High-Count Pre-Connectorized Optical Fiber Cable—*S. Tomita, M. Matsumoto, S. Nagasawa, T. Tanifuji,* NTT Telecommunication Field Systems R&D Center, Ibaraki-ken, Japan; and *T. Uenoya,* NTT Network Systems Development Center, Tokyo, Japan 5

Microbending Loss of Thin Coating Single Mode Fiber for Ultra-High-Count Cable—*W. Katsurashima, Y. Kitayama, K. Oishi, T. Kakuta, N. Akasaka,* Sumitomo Electric Industries, Ltd., Yokohama, Japan 13

Design of Downsized Coated Optical Fibers to Minimize Microbending Loss—*M. Hara, S. Okagawa, A. Otake,* The Furukawa Electric Co., Ltd., Chiba, Japan 20

An International Development on Ribbon Technology and Evaluation of Applicability to National Specification—*JP. Bonicel,* Alcatl Cable, Lyon, France; *D. Keller,* Alcatel NA, Claremont, NC; *G. Kylen,* Alcatel IKO Kabel AB, Grimsas, Sweden; *J. Schulte,* Alcatel Kabelmetal Electro, Stadthagen, Germany; *G. Patternostro,* Alcatel Cavi, Latina, Italy; *G. Berthelsen,* Alcatel Kable Norge AS, Oslo, Norway; *C.G. Cortines,* Alcatel Cable Iberica, Cantabria, Spain; and *C. Lasne,* Alcatel Alsthom Research, Marcoussis, France 25

High Count Trunk Optical Fiber Cable and Related Technology Development—*K. Yoshioka, N. Ohno, K. Sato, O. Yamauchi,* NTT Network Systems Development Center, Tokyo, Japan 32

Analysis on Shift Phenomena Between Cable Constructing Elements Under External Force—*S.-I. Yonechi,* Sumitomo Electric Industries, Ltd., Yokohama, Japan 38

Characteristics and Applications of a Non-Metallic, Waterproof, Non-Halogen Flame-Retardant Optical Wire With an Elliptical Construction—*T. Amano, H. Horima,* Sumitomo Electric Industries, Ltd., Yokohama, Japan; and *K. Fukuoka, T. Yamazaki,* Tsushin Kogyo Electric Wire & Cable Co. Ltd., Tokyo, Japan 46

TUESDAY AFTERNOON—1:00 PM–5:00 PM
Bijou Complex

SESSION III: APPLICATION & FIELD EVALUATION I

Chairperson: Mr. David Fischer, Superior Cable Corporation, Atlanta, GA

Flexible Architecture and Plant for Optical Access Networks—*S. Hornung, P. Frost, J. Kerry, J. Warren,* BT Laboratories, Martlesham Heath, Ipswich, IP5 7RE 53

Monitoring Trials on All-Dielectric, Self-Supporting, Optical Cable for Power Line Use—*G. Carlton,* Scottish Power, Glasgow, Scotland, UK; *C. N. Carter,* National Grid Company, Leatherhead, England, UK; *A. J. Peacock,* Telephone Cables Ltd., Dagenham, England, UK; and *R. Sutehall,* Pirelli Cables Ltd., Newport, Wales, UK 59

Cable Hauling Tension and Optical Fibre Reliability—*R.-C. Hsieh, P. Boes, A. Kruijshoop,* Australian and Overseas Telecommunications Corporation, Melbourne, Australia 64

Fiber Optic Guided Underwater Vehicles—*V. Kölschbach, H. Tröndle,* Philips Kommunikations Industrie AG, Köln, Germany 75

Optical Fiber Line Surveillance System for Preventive Maintenance Based on Fiber Strain and Loss Monitoring—*I. Sankawa, Y. Koyamada, S.-I. Furukawa, T. Horiguchi,* NTT Telecommunication Field Systems R&D Center, Ibaraki, Japan 81

Wide Dynamic Range Optical Talk System Using External Loss Modulation—*Y. Unami, K. Sakurai, T. Yamada,* Fujikura Ltd., Chiba, Japan; *N. Kuwaki,* NTT Technical Assistance & Support Center, Tokyo, Japan; and *M. Yumoto,* Suzuki Technical Engineering, Chiba, Japan 88

Non-Destructive Optical Fiber Amplitude Modulator for Optical Talk System over 80 km—*Y. Azuma, Y. Shibata, S. Tamura, N. Kuwaki,* NTT Technical Assistance & Support Center, Tokyo, Japan 97

TUESDAY AFTERNOON—1:00 PM–5:00 PM
Goldwyn Ballroom

SESSION IV: SPLICING ENCLOSURES

Chairperson: Mr. Dieter S. Nordmann, Kabelmetal Electro., Hannover, Germany

Splice Verification and Active Fiber Identification - A Strategy for Optimal Network Restoration—*G. F. De Veau, W. S. Konik, J. L. Mock, M. J. Presnell,* AT&T Bell Laboratories, Norcross, GA; and *W. B. Westfall,* AT&T Network Services Division, Raleigh, NC 104

High-Strength Spliced Optical Fiber Manufactured Using A Localized Carbon Coating Technique with a CO2 Laser—*K. Oohashi, T. Shimomichi, S. Araki, N. Sato,* Fujikura Ltd., Chiba-ken, Japan 111

The Hermetic Carbon Layer Restoration of the Fusion Spliced Portion of Carbon Coated Fiber—*I. Fijita, M. Hamada, H. Aikawa, K. Nagayama, Y. Asano,* Sumitomo Electric Industries, Ltd., Yokohama, Japan 119

Intelligent Lid Systems in the Multi-Fiber Technology—*M. Loch, R. Kossat, G. Ruegenberg*, Siemens AG, Munich, Germany; and *G. Boscher*, RXS Schrumpftechnik-Gerniturен GmbH, Hagen, Germany 126

Development of Full Automatic Fusion Splicer—*Y. Sugiyama, S. Mishima, Y. Sanshige*, The Furukawa Electric Co., Ltd., Chiba-ken, Japan 132

Development of Compact Fusion Splicer for 4-Fiber Ribbon and Single Fiber—*K. Ohzawa, S. Toyoshige, H. Taya, I. Suzuki, M. Yoshinuma*, Fujikura Ltd., Chiba-ken, Japan 140

TUESDAY EVENING—6:30 PM–8:00 PM
Hospitality Hour & Suppliers Forum
Broadway Room

Admission by tickets issued to all registrants

WEDNESDAY MORNING—8:00 AM–11:45 AM
Capital Rooms

SESSION V: FIBER OPTIC CABLE DESIGN II

Chairperson: Mr. Manuel R. Santana, AT&T Bell Laboratories, Norcross, GA

Situation and Influence of Standardization for Fibres and Cables—*M. de Vecchis*, Alcatel Cable, Clichy, France 145

Development of Ribbon Loose Tube Cable for Optical Subscriber Loop—*Y. Kurosawa, H. Sawano, M. Miyamoto, N. Sato*, Fujikura Ltd., Chiba-ken, Japan ... 151

A Fiber-Optic Cable for Hostile Environments—*K. Kathiresan, A. J. Panuska, J. W. Shea, W. H. Ficke, M. R. Santana, C. R. Taylor, L. T. Carlton*, AT&T Bell Laboratories and AT&T Network Cable Systems, Norcross, GA 158

Polarization Mode Dispersion of Single Mode and Dispersion Shifted Fibers—*Y. Terasawa, Y. Kubo, Y. Suetsugu, S. Tanaka*, Sumitomo Electric Industries, Ltd., Yokohama, Japan 171

Fiber Strain Measurement in Optical Cables Employing Brillouin Gain Analysis—*M. Kamikatano, H. Sawano, M. Miyamoto, N. Sato*, Fujikura Ltd., Chiba-ken, Japan 176

WEDNESDAY MORNING—8:00 AM–11:45 AM
Bijou Complex

SESSION VI: APPLICATION AND FIELD EVALUATION II

Chairperson: Mr. Brian D. Garrett, Comm/Scope, Incorporated, Claremont, NC

The Development of Optical Fiber Cable Network and Optical Fiber Cable Industry in China—*Z. Y. Kun, T. H. Chen, X. N. Ying*, Chengdu Cable Plant of P&T Ministry, Chengdu, China 183

Investigations on a Radiation Hardened Multimode Fibre—*M. Emmerich*, Kabelwerk Oberspree GmbH, Berlin, Germany 197

Optical Cable Identifier Utilizing the External Photoelastic Polarization Modulation—*H. Nimura, A. Fujisaki*, The Furukawa Electric Co., Ltd., Chiba, Japan; and *K. Kinoshita*, Tokyo Electric Power Company, Tokyo, Japan 208

Optical Cable with Lateral Pressure Sensor—*S. Shimizu, K. Suzuki, A. Takase, A. Otake*, The Furukawa Electric Co., Ltd., Tokyo, Japan 213

A Real-Time Configuration Management System Using Two-Pin Optical Fiber Identification Devices for Optical Fiber Cable Networks—*K. Yamashita, F. Ohtsuki, Y. Yamamoto*, NTT Telecommunication Field Systems R&D Center, Ibaraki-ken, Japan 220

Intelligent Building: Design Considerations—*C. Di Minico*, Digital Equipment Corporation, Maynard, MA 228

An 8-Fiber 3-State 2x2 High Speed Switch—*H. Furukawa, S. C. Yow, Y. Nomura, H. Yokosuka*, Fujikura Ltd., Chiba, Japan 234

WEDNESDAY MORNING—8:00 AM–11:45 AM
Adelphi Room

SESSION VII: FIBER OPTIC COATINGS

Chairperson: Dr. Koichi Inada, Fujikura Limited, Chiba-ken, Japan

Fiber Protective Coating Design for Evolving Telecommunication Applications—*H. C. Chandan, J. R. Petisce, J. W. Shea, C. R. Taylor*, AT&T Bell Laboratories, Norcross, GA; and *L. L. Blyler, D. Inniss, and L. Shepherd*, AT&T Bell Laboratories, Murray Hill, NJ 239

Application of FT-IR to the Cure Degree Measurement of UV Curable Optical Fiber Coating—*A. Mizutani, D. Saitho, S. Endo, N. Yoshioka*, Sumito Electric Industries, Ltd., Yokohama, Japan 249

Vinyl Ethers, A New Material Technology For Ultra-Violet Curable Optical Fiber Coatings—*G. D. Green, J. R. Snyder*, Allied-Signal Inc., Morristown, NJ; *A. C. Levy, R. J. Kovac*, Alvin C. Levy & Associates, Inc., Norcross, GA; and *P. R. Foy*, Fiber Optic Materials Research Program, Piscataway, NJ 253

The Effect of Drawing Rate on Mechanical Properties of UV Curable Polyurethane Acrylate Coatings for Optical Fiber—*T. Ukachi, A. Aoyama, Y. Naito, K. Igarashi*, Japan Synthetic Rubber Co., Ltd., Kawasaki, Japan 261

Differential Quantitative Determination of the Extent of the Radiation Cure of Both the Primary and the Secondary Component for Double Coated Fibres—*J. L. Jostan*, Daimler Benz AG, Ulm, Germany; and *R. G. Sommer, M. Hoffart*, AEG Kable AG, Mönchengladbach, Germany 267

A Study of Hermetically Coated Optical Fiber—*T. Zushi, S. Nakahara, T. Takeda, T. Kaide, H. Tanaka*, Mitsubishi Cable Industries, Ltd., Hyogo, Japan 273

The Effects of Aging on Optical Fibers with Incompletely Cured Coatings—*R. A. Frantz, H. H. Yuce*, Bellcore, Morristown, NJ; and *I. M. Plitz, O. S. Gebizlioglu*, Bellcore, Red Bank, NJ 279

WEDNESDAY AFTERNOON—11:45 AM–2:15 PM
Awards Luncheon
Goldwyn Ballroom

Admission by tickets issued to all registrants

WEDNESDAY AFTERNOON—2:15 PM–5:00 PM
Capital Rooms

SESSION VIII: MATERIALS PROCESSES & MANUFACTURING

Chairperson: Mr. Rene G. Freeman, Union Carbide Chemicals and Plastic Company, Inc., Atlanta, GA

Development of Co-Extruded Polyethylene/Polyamide 12 Insect Resistant Telecommunications Cable—*P. Boes, P. Latoszynski*, Telecom Australia, Melbourne, Australia; *J. Rachcoff*, MM Cables Communication Products, Melbourne, Australia; and *M. Styzinski*, ICI Australia, Melbourne, Australia 285

On the Development of an Aramid Yarn With Water-Blocking Properties—*O. Grabandt, S. Willemsen, J. H. v. Leeuwen*, AKZO Fibers, Arnhem, The Netherlands 293

Evaluation of Antioxidant Uniformity in Polyethylene Insulations—*Y. Gau*, Union Carbide Corporation, Somerset, NJ; *E. D. Nelson*, AT&T Bell Laboratories, Norcross, GA; and *K. D. Dye*, AT&T Network Systems, Phoenix, AZ 298

Investigation of Factors Affecting Long Term Heat Stability of Polyolefin Insulation Resins—*K. Tonyali*, Quantum Chemical Corporation, Cincinnati, OH 304

Remedial Strategies for Polyolefin Insulations in Outside Plant—*T. N. Bowmer, J. N. D'Amico*, Bellcore, Red Bank, NJ 310

WEDNESDAY AFTERNOON—2:15 PM–5:00 PM
Bijou Complex

SESSION IX: FIRE RESISTANCE

Chairperson: Mr. Richard Rossi, General Cable, South Plainfield, NJ

Short and Long Term Behaviour of Halogen Free Fire Retardant Cable Materials in Different Environments—*L. Grüner-Nielsen, P. Hasløv, N. H. Skovgaard*, NKT Elektronik A/S, Broendby, Denmark 321

Shipboard Hardened Fiber Optic Cables Utilizing Thermoset Jackets—*H. J. Russell III, E. J. Joseph*, GE Aerospace, Moorestown, NJ; *M. Connaughton*, Brand-Rex Company, Willimantic, CT; and *L. Rogers*, Naval Sea Systems Command, Washington, DC 332

Recent and Future Developments in Cable Technology in the UK Royal Navy—*T. Dawson*, UK Ministry of Defence, Bath, England 338

Implementing the Canada–United States Free-Trade Agreement: Harmonizing Fire Requirements for Cables—*S. Kaufman*, AT&T Bell Laboratories, Norcross, GA 345

WEDNESDAY AFTERNOON—2:15 PM–5:00 PM
Adelphi Room

SESSION X: SUBMARINE CABLES

Chairperson: Mr. Dave Fallowfield, AGT Limited, Alberta, Canada

New Unrepeatered Cable Design Testing Methodology and Results—*S. C. Beech, I. R. Doble, J. R. Ford, C. J. Rochester*, STC Submarine Systems, Southampton, UK 349

The Application of Electric Stress Analysis and Breakdown Statistics to Inspection Criteria for Submarine Cable Systems—*J. Bishop*, STC Submarine Systems, Southampton, UK; and *A. E. Davies*, University of Southampton, Southampton, UK 356

Development of An Alternate Undersea Armored Cable Protective Coating Compound—*W. B. Wargotz*, AT&T Bell Laboratories, Holmdel, NJ 362

The Flexible Tubular Splice. – A Technique for Manufacturing Very Long Continuous Submarine Fibre Optic Cable, Without Diameter Increase at the Splice—*J. Wardeberg, K. Nyaas*, Alcatel Kabel Norge AS, Oslo, Norway 369

WEDNESDAY AFTERNOON—4:00 PM–6:30 PM
Broadway Room

SESSION XI: POSTER PAPERS

Chairpersons: Dr. Reiner J. Gerdes, Gerdes Consulting, Atlanta, GA and Mr. Dieter S. Nordmann, Kabelmetal Electro, Hannover, Germany

A New Cable Family for the Optical Fiber Subscriber Network—*P. Delage, R. Girbig, G. Hög, M. Hoffart, H. Moers, P. E. Zamzow*, Kabel Rheydt AG, Mönchengladbach, Germany 373

Fabrication and Evaluation of 40-Fiber Array—*R. Matsuoka, Y. Shindo, N. Okada, N. Kume*, The Furukawa Electric Co., Ltd., Chiba, Japan 384

A Study on Self-Supporting Optical Fiber Cable With Four Fiber Ribbons—*H. Sawano, S. Saito, M. Miyamoto*, Fujikura Ltd., Chiba-ken, Japan 389

Optical Fiber Ribbon Containing High Strength Splices for Long Span Submarine Cable—*H. Ishikawa, I. Fujita, Y. Kitayama, K. Osaka, S. Tanaka*, Sumitomo Electric Industries, Ltd., Yokohama, Japan 395

Newly Developed, Small Diameter Optical Link Cord Using Compound Glass Fiber—*T. Machida, M. Saegusa, N. Sugiyama*, Showa Electric Wire & Cable Co., Ltd., Kanagawa, Japan 401

Extendable Optical Fibre Curled-Cord—*H. W. Brückner, G. Franken, D. S. Parmar*, Kromberg & Schubert GmbH u. Co., Rhede, Germany 406

Failure Rate as the True Parameter of Optical Fibre Reliability—*J. G. Titchmarsh*, BNR Europe, Harlow, UK 411

Development of a Dual Layer Core Loose Tube Fiber Optic Cable and Its Tensile Window Analysis—*O. Daneshvar, J. Hill, Y. Miayazaki*, AT&T Fitel Company , Carrollton, GA 417

Degradation Study for Stressed Optical Fibres in Water. New Worst Case Life Time Estimation Model—*P. Hasløv, K. B. Jensen, N. H. Skovgaard*, NKT Elektronik A/S, Broendby, Denmark 423

Design and Qualification of Optical Fiber Coating for Ribbon Fiber—*N. Akasaka, W. Katsurashima, T. Nonaka, T. Hattori, Y. Matsuda*, Sumitomo Electric Industries, Ltd., Yokohama, Japan 428

Effects of Waterproofing Compounds on the Long Term Reliability of Polymeric Coated Optical Fibers—*J. M. Hsiao, S. I. Wang, K. Y. Chen, T. C. Chang, D. M. Fann, Y.-C. Lin*, Telecommunication Laboratories, M.O.C., Taiwan, Republic of China 435

Aspects of Thermo-Oxidative and Hydrolytic Degradation in Optical Fiber Cable Matrix Materials—*T. Bishop, C. Chawla, D. Szum, E. Poklacki*, DSM Desotech Inc., Elgin, IL 442

The L^4 Splice—A New Mechanical OWG Splice—*L. Finzel*, Siemens AG, München, Germany; *L. Mendat*, RXS, Kernersville, NC; and *G. Boscher*, RXS Schrumpftechnik-Garnituren GmbH, Hagen, Germany 447

Universal Jointing for Optical Fibre Undersea Cables—*C. A. Gould, D. J. Tibbetts*, BT Labs, Ipswich, UK 451

Optical Fiber Stresses Produced During Storage in Splice Organizers—*P. B. Grimado, L. A. Reith, A. Pellegrino*, Bellcore, Morristown, NJ 457

Mechanical Reliability of Multi-Fiber Fusion Splices—*H. H. Yuce, J. P. Varachi, Jr., A. Pellegrino*, Bellcore, Morristown, NJ; *P. L. Key*, Bellcore, Red Bank, NJ; and *T. Wei*, GTE Laboratories Inc., Waltham, MA 462

Fiber Coating and Tight Buffer Degradation Induced by Index-Matching Gels and Adhesives—*R. A. Frantz, L. A. Reith*, Bellcore, Morristown, NJ; and *I. M. Plitz*, Bellcore, Red Bank, NJ 467

Testing of 4- and 8-Fiber Ribbon Strippability—*G. A. Mills*, Siecor Corporation, Hickory, NC 472

Miniature Optical Filter—*S. Yodo, I. Ohta, H. Hayakawa, A. Hasemi, M. Shimizu*, The Furukawa Electric Co., Ltd., Chiba-ken, Japan 476

Novel Spiral-Air System for Optical Fiber and Cable Installation—*K. Horii, Y. Matsumae*, Shirayuri Women's College, Tokyo, Japan; *K. Ohsumi*, Toa Kikai Kogyo Co., Ltd., Yamaguchi, Japan; *Y. Tomita*, Kyushu Institute of Technology, Fukuoka, Japan; *T. Hamade, Y. Shimo*, NTT, Ishikawa, Japan 481

An All Dielectric Fiber Optic Cable Monitoring System—*D. Vokey, K. Sontag*, Norscan Instruments Ltd., Winnipeg, Canada; and *J, Ritchie*, Manitoba Telephone System, Winnipeg, Canada 486

Installation of Submarine Fiberoptic Cables in Rugged Coastal Terrain—*S. Hopland, A. Klykken*, Norwegian Telecom, Oslo, Norway 492

Characterization and Development of Foam-Skin Polyethylene Insulation Resins—*K. Tonyali, P. L. Fernando*, Quantum Chemical Corporation, Cincinnati, OH 497

Highly Expandable Compound and Processing Techniques for Coaxial Cable—*S. Hashimoto, T. Sakamoto, Y. Moritani, J. Hakozaki*, Nippon Unicar Co., Ltd., Kawasaki, Japan 506

Interactive Manufacturing & Costing System (I_MACS) for Multi-Pair Telecommunication Cables—*M. J. Khan*, Saudi Cable Company, Jeddah, Saudi Arabia 511

The Development of a Cost Effective, Environmentally Friendly Method for Lagging Wire and Cable Shipping Reels—*J. A. Hill*, AT&T Fitel, Carrollton, GA; *C. E. Hall*, Sonoco Products Company, Hartselle, AL; and *K. B. Shields*, C&S Associates, Pittsburgh, PA 521

Moisture Permeability of Steam Resistant Telephone Cables—*J. N. D'Amico, O. S. Gebizlioglu*, Bellcore, Red Bank, NJ 526

The Removal of Copper Pairs of Distribution Cables to Create Paths for Placing Fiber Cables—*P. R. Briggs, Jr., L. M. Slavin, E. E. Hershkowitz, J. P. Varachi, Jr.*, Bellcore, Morristown, NJ; and *S. A. Khan*, Bellcore, Red Bank, NJ 533

A High Productivity, Low Smoke, Zero Halogen Compound for Sheathing Power and Telecommunication Cables—*J. Taylor, J. Preston, D. Sawyer, L. P. Cheng*, Lindsay & Williams Limited, Manchester, England 539

Techniques to Characterize the Corrosivity of Cable Fire-Products—*F. L. Chu*, Factory Mutual Research Corporation, Norwood, MA 545

Quantitative Determination of a Thioester Antioxidant in Cable Filling Compounds Based on Fourier Transform-Infrared Spectroscopy and Correlation to Oxidation Induction Time—*W. J. Thalman, A. Eckard, A. Debska*, Witco Corporation, Oakland, NJ 548

On-Line Temperature Measurement of Optical Fiber and Telephone Wire—*D. Willett*, Luxtron Corporation, Santa Clara, CA 552

THURSDAY MORNING—8:30 AM–12:00 (NOON)
Capital Rooms

SESSION XII: MEDIUM AND HIGH VOLTAGE POWER CABLES AND ACCESSORIES

Chairperson: Mr. Hans A. Mayer, Olex Cables, A Division of Pacific Dunlop Limited, Melbourne, Australia

Invited Presentations

Long Term Service Experience of XLPE and EPR Cables in MV and HV Networks—*F. Kraehenbuehl, J. J. Wavre*, Câbles Cortaillod SA, Cortaillod, Switzerland 556

Development of a 220/230kV XLPE High Voltage Cable and Accessories—*H. A. Mayer, E. Buczma, J. A. Adcock*, Olex Cables (A Division of Pacific Dunlop Ltd.), Melbourne, Australia; and *V. J. Boliver, M. Uzelac*, G&W Electric Company, Blue Island, IL 561

The Application of 154kV Transition Joint in Korea—*S. C. Hwang, C. S. Lee, W. K. Park*, Gold Star Cable Co., Ltd., Seoul, Korea; and *J. Y. Koo*, Hanyang Univ., Seoul, Korea 573

Estimation of Temperatures During Dry Crosslinking of High Voltage XLPE Insulated Cable—*R. C. Kemp*, CSIRO Division of Applied Physics, Sydney, Australia; and *A. Stringer, Y. Zlatsin*, Olex Cables (Division of Pacific Dunlop Ltd.), Melbourne, Australia 578

New Developments in Medium and High Voltage Cable with Laminate Sheaths as Moisture Barriers—*K. E. Bow*, The Dow Chemical Company, Granville, OH 583

An Experimental Investigations on the Degradation Characteristics of 22.9kV XLPE Insulated Power Cables Installed in Korea—*Y.-O. Cho, H.-S. Ryoo, C.-H. Sun*, Korea Electrotechnology Research Institute, Changwon, Korea; *J.-Y. Koo*, Hangyang University, Seoul, Korea; and *D.-W. Chung, S.-J. Kim*, Korea Electric Power Cooperation, Daejeon, Korea 594

THURSDAY MORNING—8:30 AM–12:00 (NOON)
Bijou Complex

SESSION XIII: FIBER OPTIC RELIABILITY I

Chairperson: Mr. Xavier Mann, AT&T Fitel, Carrollton, GA

Invited Presentations

Current Issues in Mechanical Reliability of Optical Fibers—*C. R. Kurkjian, D. Inniss*, AT&T Bell Laboratories, Murray Hill, NJ; and *H. Chandan*, AT&T Bell Laboratories, Norcross, GA 599

Aging Behavior of Optical Fibers—*H. H. Yuce*, Bellcore, Morristown, NJ 605

Reliability Considerations for Long Optical Fibers—*S. T. Gulati*, Corning Incorporated, Corning, NY 612

Ageing of Optical Fibres in Water—*W. Griffioen*, PTT Research, Leidschendam, The Netherlands 622

Maximum Values of Strength and Fatigue Parameter *n* for Hermetically Coated Optical Fibers—*M. M. Bubnov, E. M. Dianov, S. L. Semjonov*, General Physics Institute, Moscow, Russia 629

Reliability of Waterproof Optical Fiber Cables—*M. Kawase*, NTT Telecommunication Field Systems R&D Center, Ibaraki, Japan 637

THURSDAY MORNING—8:30 AM–12:00 (NOON)
Adelphi Room

SESSION XIV: TECHNOLOGY IN MILITARY APPLICATIONS

Chairperson: Mr. Michael A. DeLucia, Naval Surface Warfare Center, Annapolis, MD

Moderators: Dr. Howard Wichansky and Mr. Vasilios E. Kalomiris, US Army CECOM, Fort Monmouth, NJ

Invited Presentations

Overview of the Tri-Service Fiber Optic Technology Program—*B. M. Hendrickson*, Rome Laboratory, Griffiss AFB, NY 645

GaAs Integrated Optoelectronic Transceiver for Fiber-Optic Link Applications—*R. W. Ade, D. E. Bossi, J. M. Berak, R. N. Sacks, L. A. Newman*, United Technologies Research Center, East Hartford, CT 650

Test Patterns of Optically Controlled Two-Band Phased Array Antenna—*S. Thai, N. Bernstein, J. Hunter*, Rome Laboratory, Griffiss AFB, New York ... 654

Single Mode Fiber Optic Cable for Space Applications—*P. A. Michaels*, AT&T Bell Laboratories, Whippany, NJ; *A. E. Miller, M. F. Yan*, AT&T Bell Laboratories, Murray Hill, NJ; and *V. E. Kalomiris*, U.S. Army CECOM, Fort Monmouth, NJ... 659

Fiber Optic Cable Systems for Navy Ships—*D. R. Knudsen, J. P. Ingold, G. D. Brown*, Naval Surface Warfare Center, Dahlgren, VA 667

THURSDAY AFTERNOON—1:00 PM–5:00 PM
Capital Rooms

SESSION XV: FIBER OPTIC RELIABILITY II

Chairperson: Dr. Robert Baboian, Texas Instruments, Inc., Attleboro, MA

Hydrogen-Caused Signal Attenuation in Buried Optical Fiber Cables—*G. Schick, K. A. Tellefsen, C. J. Wieczorek, R. M. Kanen, A. J. Johnson*, Bell Communications Research, Morristown, NJ..... 673

Analysis of Fiber Optic Cable Design Conditions in Vicinity of Steam Lines - Ruptured and Pristine—*N. E. Hardwick, III and K. Kathiresan*, AT&T Bell Laboratories, Norcross, GA; and *J. G. Hartley*, Georgia Institute of Technology, Atlanta, GA 679

Static Fatigue Testing of Optical Fibers in Water Immersion—*E. Cuellar, M. T. Kennedy, D. R. Roberts*, Raynet Corporation, Menlo Park, CA..... 689

The Mechanical Behavior of Large Flaws in Optical Fiber and Their Role in Reliability Predictions—*G. S. Glaesemann*, Corning Incorporated, Corning, NY 698

Fiber Reliability Study of Field Aged Optical Cables—*H. H. Yuce, R. Estes, C. J. Wieczorek, J. P. Kilmer, J. P. Varachi, Jr.*, Bellcore, Morristown, NJ; and *T. Wei, B. T. Devlin*, GTE Laboratories Inc., Waltham, MA 705

Predicting the Lifetime of Optical Fibre Cables Using Applied Stress Histories and Reliability Models—*K. G. Hodge, C. S. Pegge*, BICC Cables Ltd., Cheshire, UK; and *G. S. Glaesemann, M. Hopiavuori*, Corning Incorporated, Corning NY 713

Distributed Strain—A Rational Test of Fiber Fatigue—*T. Svensson, E. Sundberg*, Telia Research AB, Haninge, Sweden 725

THURSDAY AFTERNOON—1:00 PM–5:00 PM
Bijou Complex

SESSION XVI: COPPER CABLE/WIRE

Chairperson: Mr. Homer Vela, AT&T Network Cable Systems, Phoenix, AZ

Moderator: Mr. Larry G. Romig, Building Industry Consulting Service International (BICSI), Tampa, FL

Ultra-High-Bandwidth Heat Resistant Leaky Coaxial Cable—*K. Aihara, Y. Sakata, N. Tago*, Sumitomo Electric Industries, Ltd., Yokohama, Japan 732

Leaky or Radiating? Radiation Mechanisms of Radiating Cables and Leaky Feeders—Channel Tunnel Applications—*A. Levisse*, Alcatel Cable, Bezons, Cedex, France 739

Leaky Coaxial Cable with Length Independent Antenna Receiving Level—*H. G. Haag, K. Schulze-Buxloh, G. Thönneßen*, AEG Kabel AG, Mönchengladbach, Germany; and *A. Coraiola*, SIRTI S.p.A., Milano, Italy..... 748

Return Loss of Metallic Telecommunications Cables Due to Periodic and Random Structural Variation and Temperature—*L. M. Hore*, Bellcore, Morristown, NJ 757

Radio-Frequency Cables in Russia—*A. A. Pavlov, I. B. Peshkov, M. F. Popov*, Institute of the Russian Cable Industry, Moscow, Russia 765

Automated Equipment to Assemble Connectors for Telecommunication Cables—*T. Harakawa, N. Nakao, S. Matsuhashi*, NTT Telecommunication Field System R&D Center, Ibaraki-ken, Japan 777

THURSDAY AFTERNOON—1:00 PM–5:00 PM
Adelphi Room

SESSION XVII: FIBER OPTIC INTERCONNECTS

Chairperson: Dr. Joyce P. Kilmer, Bellcore, Morristown, NJ

Evaluation Method and Performance of Advanced Low-Reflection Optical Connectors—*K. Kanayama, Y. Ando, S. Iwano*, NTT Opto-Electronics Laboratories, Ibaraki, Japan; and *R. Nagase*, NTT Communication Switching Laboratories, Tokyo, Japan 785

Performance of Ceramic-Ferrule Optical Connectors—*L. A. Reith, G. D. Kiss, W. W. Wood, H. H. Yuce*, Bellcore, Morristown, NJ; and *R. M. Fagerstrom, E. M. Vogel*, Bellcore, Red Bank, NJ..... 792

Push-On Pull-Off Multi-Fiber Connector—*Y. Nomura, Y. Kikuchi, H. Hirao*, Fujikura Ltd., Chiba, Japan 801

Development of High-Density Extensible Mechanical Switching System—*T. Komiya, S. Mizuno, T. Sano, K. Ozawa, K. Osaka, Y. Asano*, Sumitomo Electric Industries Ltd., Yokohama, Japan 806

Mechanical-Type Optical Switch for DSF—*K. Yoshida, T. Ohta, H. Sueki, H. Yamada, T. Shigematsu, T. Kimura*, The Furukawa Electric Co., Ltd., Chiba-ken, Japan..... 813

MT-Type Fiber Selector for Optical Fiber Monitoring Systems—*Y. Tamaki, Y. Isono, S. Goto*, Fujikura Ltd., Chiba, Japan..... 820

A Large-Scaled 1xN Optomechanical Matrix Switch—*S. Mizuno, H. Maki, N. Hakamata, Y. Asano*, Sumitomo Electric Industries, Ltd., Yokohama, Japan..... 826

OPENING SPEAKERS



Dave Fallowfield
AGT Limited
Edmondton, Canada

Dave Fallowfield was born in 1957 in British Columbia, Canada. He received a Bachelor of Science in Electrical Engineering from the University of Manitoba in 1979 and began working for AGT (formerly Alberta Government Telephones) in that same year. After a series of assignments in the Maintenance Engineering and Cable Systems Design sections, he became Manager Outside Plant Standards in 1986. In 1990 he joined his company's international subsidiary ATI and worked as Network Design and Integration Manager constructing a 3000 km fibre optic network in Thailand. He returned to Canada in June 1992 and assumed the position of Network Design Manger with AGT.



Joseph J. Pucilowski, Jr.
Director, CECOM Center for C3 Systems
U.S. Army Communications-Electronics
Command and Fort Monmouth
Fort Monmouth, New Jersey

Mr. Joseph J. Pucilowski, Jr. was appointed as Director of the Center for Command, Control and Communications (C3) Systems, U.S. Army CECOM, in August 1990. He has command responsibility for formulating, coordinating, managing and implementing internal and external research, development and engineering programs to fill the Army's tactical C3 needs, while also providing full technical support to U.S. Army Program Executive Officers and Project Managers in C3. Recipient of the Presidential Meritorious Rank Award in 1991.

He was awarded a Bachelor of Arts in Physics, with a minor in mathematics from Rutgers University, and a Master of Science in electrical engineering from Fairleigh Dickinson University. He was appointed by the Secretary of the Army to the Senior Executive Service in November 1986.

Mr. Pucilowski was appointed Acting Deputy Chief of Staff for Concurrent Engineering at the U.S. Army Materiel Command Headquarters from February 1991 to September 1991. In that capacity he had command responsibility for Concurrent Engineering planning and implementation as well as test and evaluation, production base planning and product assurance for AMC.

Mr. Pucilowski began his government career in 1963 as a physicist for the U.S. Atomic Energy Commission. He transferred to Fort Monmouth in 1967 and has held various technical and managerial assignments at Fort Monmouth to include: Director of the CECOM Product Assurance and Test Directorate; Associate Director for Research & Technology, CECOM RD&E Center; Associate Director for Information Processing Technology, Center for COMM/ADP and Deputy Director and Acting Director of the Center for Tactical Computer Systems.

He has served as the NATO U.S. Dept. of Defense (DOD) Representative to SubGroup IX, Defense Equipment Reliability and Maintainability (R&M) Assurance and as a member of the American British Canadian Australian (ABCA) Committee on R&M.

Mr. Pucilowski served as President of the Armed Forces Communications-Electronics Association (AFCEA) Fort Monmouth Chapter and as the Chairman of the 14th and 17th Annual AFCEA Symposia. He also serves as an Honorary Advisor Member of the Board of AUSA. He has been a member of the NJ Dept of Higher Education's Panel on Faculty Development in Telecommunications and Army Member of the Joint Directors of Laboratories Subcommittee on C3. He has published or presented over thirty-five technical papers.

A native of New Jersey, Mr. Pucilowski currently resides in Howell with his wife Maryann. They have six children--Adam, Joseph, Linda Ann, Mary, Kristin and Francine.



Manuel R. Santana
AT&T Bell Laboratories
Norcross, Georgia

Manuel R. Santana is Supervisor of the Outside Plant Cable Group with research and development responsibility for fiber-optic cables used in the outside plant. He has been involved in research and product development in fiber-optic cable and he has been awarded nine patents and has twenty-five publications to his credit.

Mr. Santana joined AT&T Bell Laboratories in 1970, having received his B.S.E.E. from the University of Hartford, and M.S.E.E. from Georgia Institute of Technology. He is a senior member of the IEEE.



J.P. (Jack) Bucter
President
AT&T Network Cable Systems
Morristown, New Jersey

Jack Bucter assumed his present position as President, AT&T Network Cable Systems (NCS) effective September 15, 1991. NCS designs, manufactures and markets fiber, fiber optic and copper cable, and associated apparatus for systems solutions that meet peoples' needs in the information society. Prior to his current assignment, Mr. Bucter served as President of AT&T Business Communications Systems (BCS), starting in April, 1989. BCS developed, manufactured, serviced and sold communications systems for AT&T's large business and government customers.

During his AT&T career, Mr. Bucter has held management positions in marketing, product management, engineering, manufacturing and finance. Previously, Mr. Bucter held the position of Vice President, Product Management and Marketing in AT&T's Communications Systems Division.

Mr. Bucter has a bachelor's degree in mathematics from Hobart College and a master's degree in management from MIT, where he was a Sloan Program participant. His office is located at AT&T Network Systems, 475 South Street, Morristown, New Jersey.



Michel de Vecchis
Chairman of Technical Affairs
of EUROPACABLE
Bruxelles, Belgium

Michel de Vecchis was born in 1946. He is graduated from Ecole Nationale Supérieure des Télécommunications (1969). He joined LTT in 1970 where he worked on microwave components. He started to work on fiber optics in 1974 and has been Technical Director of the Cable Division until the merging in 1986 of LTT cable activities with Les Cables de Lyon now Alcatel Cable. He is now Director of Technical International Marketing at Alcatel Cable Telecommunication Branch. Since 1991 he is the Chairman of the Technical Committee of Eurotelcab, the Telcom Business Group of Europacable.

He is involved in International Standardization of optical fibers and cables (Chairman of CECC WG 28 and Secretary of IEC SC 86 A)



Shunji Kaibuchi
Executive Vice President of NTT
General Manager of NTT Kansai
Telecommunications Service Region
Osaka, Japan

Shunji Kaibuchi was born in Tokyo, Japan in 1937. He received his Bachelor's degree in Electrical Engineering in 1959 from the University of Tokyo.

In 1959 he joined Engineering Bureau of Nippon Telegraph and Telephone Public Corporation, and was engaged in metallic cable development and outside plant planning. He has held the positions of Executive Manager of Engineering Bureau in 1974, General Manager of Shikoku Regional Headquarters in 1985, and Senior Executive Manager of Procurement and Supply Department in 1988.

His work has greatly contributed to the development of optical fiber cable and related technologies. He is now an Executive Vice President of NTT (Nippon Telegraph and Telephone Corporation) and General Manager of the NTT Kansai Telecommunications Service Region.

He is a member of Institute of Electronic, Information and Communication Engineers of Japan (IEICE).



Phil W. Black
Technical Director
STC Submarine Systems
Greenwich, London
United Kingdom

Phil Black is the Technical Director of STC Submarine Systems, a division of Northern Telecom Europe and one of the world's leading suppliers of undersea telecommunication cable systems.

Phil studied Electrical Engineering at London University and gained a B.Sc (Eng) honours degree in 1966. He joined Standard Telecommunication Laboratories Ltd (STL) from university. STL was then the Central Research facility for ITT and source of the original paper on fibre optic communications in 1966 and is now BNR Europe.

After four years on materials and component developments Phil joined the optical communications group and took charge of the silica fibre research team. This work advanced very rapidly in the early seventies and the technology developed was used to set up fibre manufacturing facilities in the USA, Germany and the UK.

Phil has published a number of papers, been granted more than twenty patents and served on CCITT, IEC and BSI committees on fibre and cable standards.

As his career developed he became involved in management of a wider range of components, and system activities including developments for the earliest undersea cable systems.

From this research base he transferred to STC Submarine Systems in London first as Assistant Technical Director concentrating on advanced technology and components, before being appointed to his present position. As Technical Director he has responsibility for advanced research work, product development and the performance of installed turnkey systems. This includes cable activities in the UK (Southampton) and USA (Portland), and repeaters, terminals and power feed in the UK (Greenwich).



McAvoy Layne
as Mark Twain
Incline Village, Nevada

When asked how he got started portraying Mark Twain, McAvoy Layne responds, "Well I had all these white suits hanging in my closet..."

But actually it was a fortunate freak of nature that left McAvoy snowbound on the shores of Lake Tahoe in the winter of '75...1975, with nothing but a dart board and some books. He threw darts for three days, then reached down and picked up the works of Mark Twain. When rescued two days later, delirious with cabin fever, he was reciting passages of Twain.

For five years now, McAvoy Layne has been delivering the wit & wisdom of The Wild Humorist of the Pacific Slope, retracing his steps from Virginia City to Russia. "It's like being a Monday through Friday preacher, whose sermon, though not reverently pious, is fervently American."

Preliminary Research into High-Count Pre-Connectorized Optical Fiber Cable

Shigeru TOMITA, Michito MATSUMOTO, Shinji NAGASAWA
Tadatoshi TANIFUJI and Takuya UENOYA*

NTT Telecommunication Field Systems R & D Center
*NTT Network Systems Development Center

Abstract

We present a cable with a new structure called U-groove unit cable. With this structure, the cable cross sectional area is about 30% less than that of the well-known slotted-core cable under the same conditions such as holding the same number of fiber ribbons with the same clearances. In this paper, we describe the characteristics of a 1500-fiber cable which contains 12-fiber ribbons. This cable shows good performance in conventional cable tests.

Next, we present a 16-fiber connector and describe its performance. This connector was designed for use with a 16-fiber ribbon which contains small diameter coated fibers. The connection loss is the same as that of conventional MT-connectors.

In addition, we describe our concepts toward a 4000-fiber cable and a pre-connectorized cable end.

1. Introduction

NTT is currently discussing an FTTH (Fiber To The Home) construction program called OFL21[1]. In order to construct FTTH networks, very high count optical fiber cables and connectors are needed. We presented a new cable concept and new connector structures which are useful for this purpose in the 40th IWCS.[2],[3]

This paper is the second report on these developments. First, we describe the design and performance of 1500- and 360- fiber U-groove unit cables both of which contain 12-fiber ribbons. Next, we describe the structure and performance of a 16-fiber connector. In addition, we present 4000-fiber cable and pre-connectorized cable end design.

2. U-groove unit cable

In order to replace all existing copper cables, optical fiber cables are required which have the same core count as the copper cable pair count. The highest count cable in copper networks, has 3600 pairs. Therefore, we began to study high density and high count cable which can hold 4000 fibers, taking into account to the potential future increase in subscribers. The U-groove unit is a useful basis from which to develop a high density and high count cable. Figure 1 shows a cross section of U-groove unit cable.

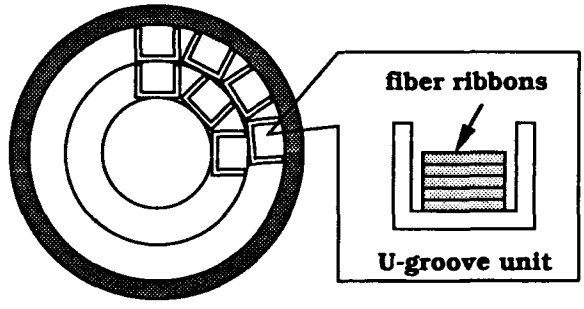


Figure 1 U-groove unit cable structure

2.1 Benefits of U-groove unit cable

The biggest benefit of this structure is that the fiber density is much higher than conventional cable. Figure 2 shows the well-known slotted-rod cable. This 1000-fiber cable contains 8-fiber ribbons, and its diameter is 40 mm. [4] If we use the U-groove unit cable design, the diameter will be reduce to 33 mm, with no change in the other conditions such the number of fiber

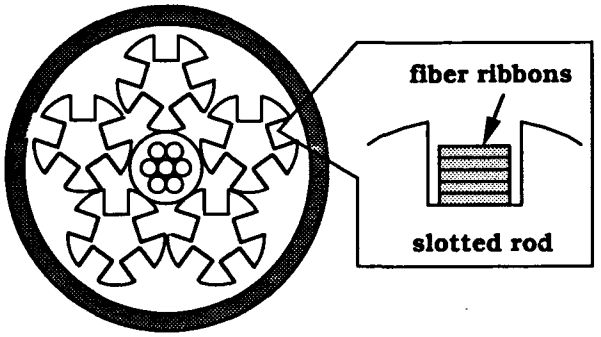


Figure 2 Slotted rod cable structure

ribbons and the clearances. This means that the cable cross sectional area is about 30% less than that of slotted-core cable.

Another benefit is that we can handle the U-groove units separately. All cables can be divided into units at the cable splicing points. With conventional copper cables, we branch several units which contain 100 or 200 pairs at splicing points. U-groove unit cable can meet this requirement because its units are stranded around the central member, but not fixed to it.

2.2 Experimental cable structure

Next, we describe our experimental cable structures.

2.2.1 Coated fiber

The coated fiber we use is conventional 0.25 mm diameter 2-layer (soft and hard) coated fiber as shown in figure 3. The fiber is matched cladding single-mode fiber standardized by CCITT.

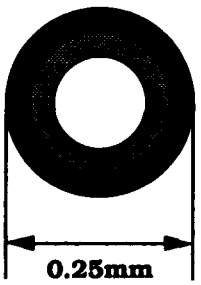


Figure 3 Coated optical fiber

2.2.2 12-fiber ribbon

We use 12-fiber ribbons in this experiments as the use of higher count fiber ribbon is an effective way of increasing fiber density. Ribbon coating thickness of a 12-fiber ribbon is the same as that of conventional 4- and 8-fiber ribbons. A cross section of a 12-fiber ribbon is shown in figure 4.

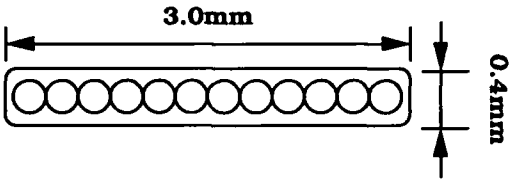


Figure 4 12-fiber ribbon

2.2.3 U-groove unit

For our experiments, we designed a U-groove which contains five 12-fiber ribbons as shown in figure 5. The U-groove units are stranded, as shown in figure 1. The inscribed circle radius R_i of the stranded U-groove units is shown in figure 6 and is expressed below as equation 1.

$$R_i = b/2(1/\tan(\pi/n)) \qquad (1)$$

where a is unit height, b is unit width and n is the number of stranded units.

The circumscribed circle radius R_o is expressed as equation 2.

$$R_o = ((b/2)^2 + (a+R_i)^2)^{1/2} \qquad (2)$$

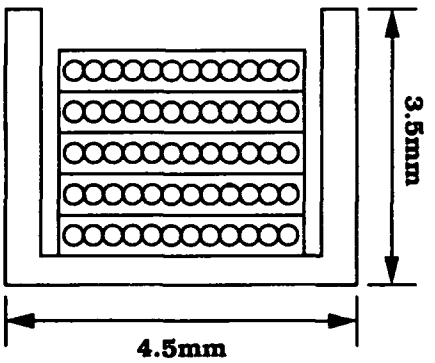


Figure 5 U-groove unit

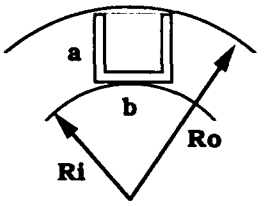


Figure 6 U-groove cable size calculation model

2.2.4 Cables

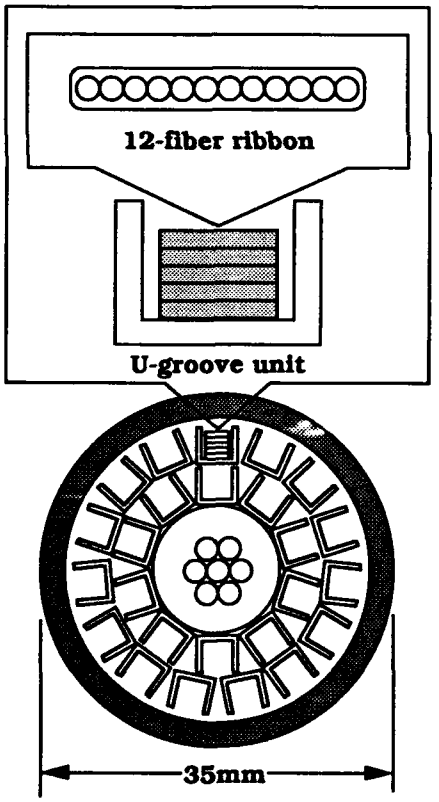
We manufactured two cables as shown in figure 7. Cable A is a 1500-fiber cable 100 m in length. Cable B is a 360-fiber cable 500 m in length. The cable lengths are different because of the limitation of the manufacturing equipment. Cable A is composed of 25 U-groove units which are stranded in two layers. 10 U-groove units are stranded in an inner layer and 15 U-groove units are stranded in an outer layer.

Cable B is composed of 6 stranded U-groove units in one layer.

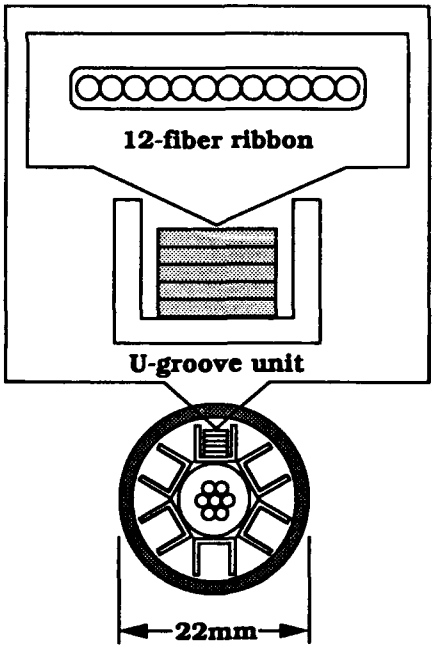
Both cables have a 2.5 mm thick sheath and a strength member composed of seven stranded steel wires 2.0 mm in diameter.

2.3 Performance of U-groove unit cable

We believe that the two cables shown in figure 7 would exhibit similar results with regard to loss variation during manufacture, because loss variation depends on both fiber ribbon and U-groove size. They exhibit similar results in heat cycling test, because loss variation and fiber elongation both depend on the temperature characteristics of the cable materials. However, in other cable tests such as bending, squeezing and crushing, the two cables may exhibit different characteristics, because these test results depend on cable size.



(a) cable A; 1500-fiber cable



(b) cable B; 360-fiber cable

Figure 7 Experiment Cable Structure

2.3.1 Loss variation during manufacture

A long length of cable is required for a detailed study of loss variation during manufacture in order to ensure measurement accuracy. Cable A is too short and so we use cable B for this measurement. Figure 8 shows the measurement results. It appears that the maximum loss of cabled fiber is a little higher than that of original fiber. However, the average loss is almost the same and the maximum loss increase is very small, so we think that this apparent difference is not a big problem.

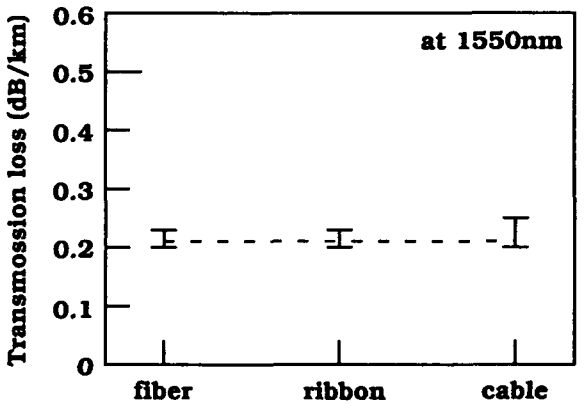


Figure 8 Transmission loss during manufacture

2.3.2 Temperature characteristics

Figure 9 shows the loss variation of cable B due to temperature change. The loss variation is less than 0.05 dB/km in the -30°C to +60°C temperature range. This value is almost same as that of conventional optical fiber cables. Therefore, we think that this test results is satisfactory.

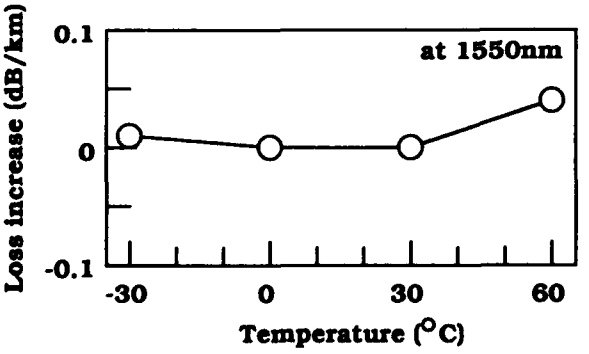


Figure 9 Temperature characteristics

2.3.3 Bending characteristics

Cable A was bent with a radius ranging from 200 to 600 mm and the loss increase and maximum elongation were measured. The results are shown figure 10 and 11 respectively. With a radius of 200 mm, we detected a small loss increase and the maximum elongation is about 0.17%. The loss increase values are the same as those of 1000-fiber slotted rod core cable. In this bending radius range, the maximum elongation is less than that of 1000-fiber slotted core cable. Therefore, we found that cable A is reliable when the cable bending radius is higher than or equal to 300 mm.

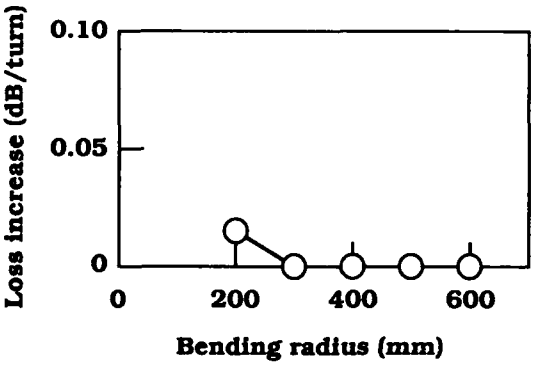


Figure 10 Loss increase due to bending

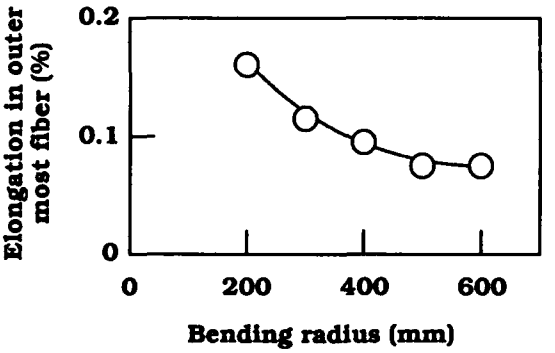


Figure 11 Elongation due to bending

2.4.4 Other test results

We measured the cable characteristics under the following conditions.

(1) Crushing

There was no loss increase in either cable A or B with a crushing force of up to 2000 N applied to 100 mm of cable.

(2) Tension

There was no loss increase in either cable, when a 100 m length was subjected to a pulling force of up to 8000 N.

(3) Squeezing

There was no loss increase when the cables were squeezed across a mandrel radius of 600 mm with a pulling force of up to 8000 N.

These test conditions are the same as those used for conventional 1000-fiber slotted rod core cable, so we consider cables A and B to be suitable for application under conventional installation condition.

2.4 Toward a 4000-fiber cable

It is confirmed above that U-groove unit cable is reliable in conventional test. Next, we describe how to increase the fiber count in the cable. In the last IWCS, we reported to decrease the coated fiber diameter and to increase the fiber count in a ribbon.[2] In that paper, we described 0.16 mm diameter coated fiber and 16-fiber ribbon. If these components can be used in practice, we will be able to fabricate a 4000-fiber cable 35 mm in diameter by replacing the five 12-fiber ribbon stack with a ten 16-fiber ribbon stack as shown in figure 12. Recently, we manufactured a 16-fiber ribbon with coated fibers less than 0.2 mm in diameter. Its transmission attenuation is almost the same as that of conventional fiber ribbons, and its other characteristics are now being measured.

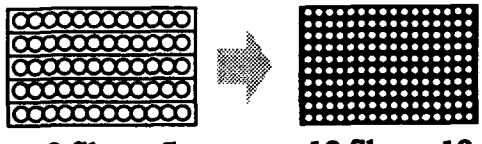


Figure 12 Next step to develop 4000-fiber cable

3. 16-fiber connector

Using the 16-fiber ribbon mentioned above, we evaluate a newly developed 16-fiber connector.

3.1 Structure

Figure 13 shows a 16-fiber connector with a structure similar to that of conventional MT-connectors.[4] It consists of a pair of plastic ferrules, two guide pins and a clamp spring. At the ferrule end, sixteen fibers are positioned between two guide pin holes. The ferrules are aligned by inserting the two guide pins fitted into the guide pin holes and are held by the clamp spring.

The distance between the fiber holes is less than that in conventional connectors. This is because, 16-fiber ribbons contain coated fiber which is less than 0.2 mm in diameter. The 16-fiber connector is slightly larger than conventional connectors.

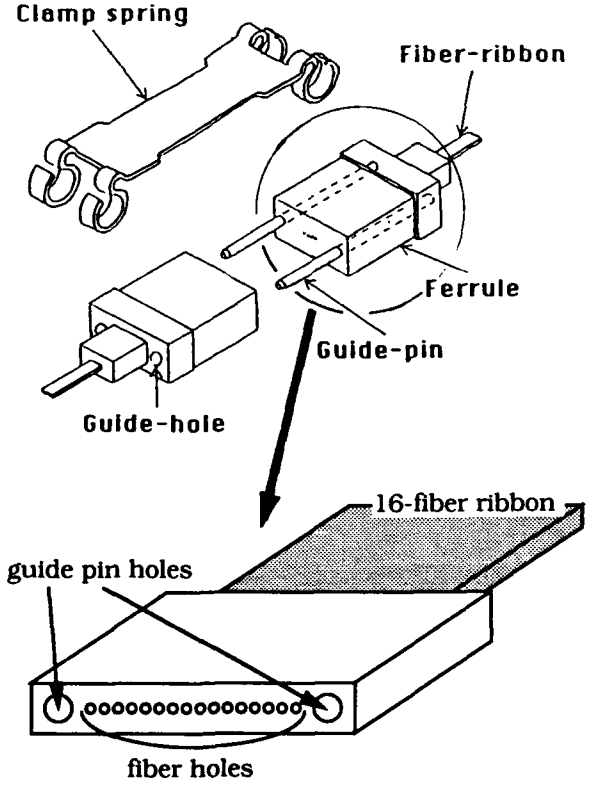


Figure 13 16-fiber connector

3.2 Performance

We measured the connection loss of 16-fiber connectors as shown in figure 14. The mean value was 0.31 dB and the standard deviation was 0.16 dB. These are almost the same as the values for MT-connectors. This means that MT-connector manufacturing technologies are also useful for 16-fiber connectors.

However, in the age of FTTH, a connection loss is less than 0.2 dB will be required. Therefore, we should refine these technologies.

Other characteristics such as temperature and humidity, are currently being studied.

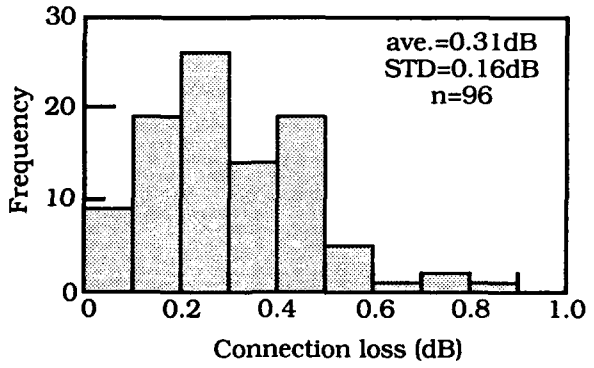


Figure 14 Connection loss in 16-fiber connector

3.3 Toward pre-connectorized cable

The 16-fiber connector mentioned above, is the key component of a connectorized cable end. At the last IWCS, we presented the unit connectors and cable end design for high count fiber connection shown in figures 15 and 16. The aim was to reduce connection time. When we use 40-fiber unit connectors which are composed of 8-fiber connectors, it is possible to connect 200-fiber pre-connectorized cable in 20 minutes.[3] It takes 10 minutes to remove the pulling eyes and to install the lower and upper covers. Therefore, the connection time is 2 minutes for each connector.

If we use an 80-fiber connector composed of five 16-fiber connectors as shown in figure 17, we can connect a 4000-fiber cable in 110 minutes. This is based on a connection time of about 2 minutes for each connector, and a closure assembly time of about 10 minutes.

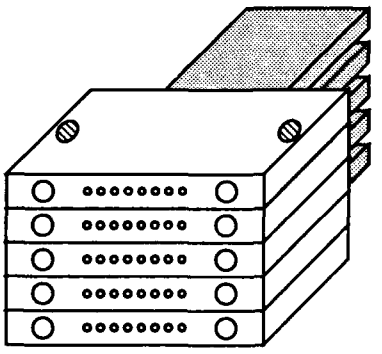


Figure 15 40-fiber unit connector (8-fiber connector x 5)

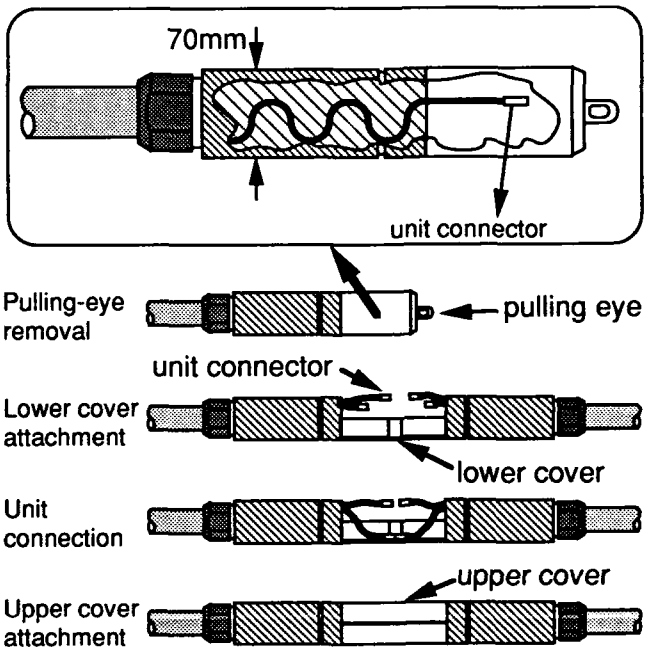


Figure 16 Cable-end structure for unit connector and procedures

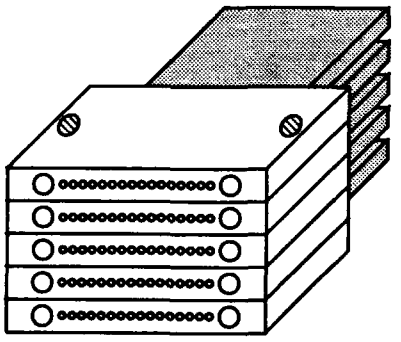


Figure 17 80-fiber unit connector (16-fiber connector x 5)

4. Conclusions

In the past year we have begun to study on high-count and high-density cables and connectors in order to construct optical subscriber cable networks for FTTH. Thus for we have clarified the following items.
(1) U-groove units are useful for the development of high count cable.
(2) 1500-fiber cable, 35 mm in diameter is reliable under conventional installation conditions.
(3) 16-fiber connector performance is the same as that of a conventional MT-connector.

We are continuing to study this cable and connector with the aim of developing 4000-fiber pre-connectorized cable, towards the ultimate goal of an all optical fiber subscriber network.

5. References

[1] T. Uenoya "The optical fiber loop 21 plan", OEC, 1990.

[2] S. Tomita, M. Matsumoto, T. Yabuta and T. Uenoya "Preliminary research into ultra high density and high count optical fiber cables", 40th IECS, pp.8-15, 1991

[3] T. Haibara, S. Tomita, M. Matsumoto and T. Yabuta "High-speed low-loss connection techniques for high count pre-connectorized cables", 40th IWCS, pp.296-302, 1991

[4] M. Kawase, T. Fuchigami, M. Matsumoto, S. Nagasawa, S. Tomita, and S. Takashima "Subscriber Single-Mode optical fiber ribbon cable technologies suitable for midspan access", J. of Lightwave Technology, Vol.7, No.11, November, 1989.

Shigeru TOMITA



NTT
Telecommunication
Field Systems Research
& Development Center
Tokai, Ibaraki,
319-11, JAPAN

Shigeru Tomita is a Senior Research Engineer. He was born in 1960 and received a B.E. degree in electrical engineering from Nihon University in 1983.

He joined NTT in 1983. Since 1990 he has been engaged in research on High-density and Pre-connectorized optical fiber cable.

Mr. Tomita is a member of IEEE.

Michito MATSUMOTO



NTT
Telecommunication
Field Systems Research
& Development Center
Tokai, Ibaraki,
319-11, JAPAN

Michito Matsumoto is an Executive Research Engineer. He was born in 1952 and received B.E. degree in electrical engineering from Kyushu Institute of Technology. He received M.E. and Ph.D. degrees in electronics engineering from Kyushu University in 1977 and 1987, respectively.

He joined NTT in 1977. Since 1990 he has been engaged in research on High-density and Pre-connectorized optical fiber cable.

Dr. Matsumoto is a member of IEEE.

Shinji NAGASAWA



NTT
Telecommunication
Field Systems Research
& Development Center
Tokai, Ibaraki,
319-11, JAPAN

Shinji Nagasawa is an Executive Research Engineer. He was born in 1950 and received B.E. degree in electrical engineering from Chiba University in 1974 and 1976, respectively.

He joined NTT in 1976. Since 1990 he has been engaged in research on multi fiber connectors.

Mr. Nagasawa is a member of IEEE.

Tadatoshi TANIFUJI



NTT
Telecommunication
Field Systems Research
& Development Center
Tokai, Ibaraki,
319-11, JAPAN

Tadatishi Tanifuji is the leader of high count optical fiber cable reseach group. He was born in 1949. He received B.E. and M.E. degrees in electronics engineering from Hokkaido University in 1972 and 1974, respectively.

He joined NTT in 1974. Since 1991 he has been engaged in research on High-density and Pre-connectorized optical fiber cable.

Dr. Tanifuji is a member of IEEE.

Takuya UENOYA



NTT
Yamaguchi branch office
Kumano, Yamaguchi
753, JAPAN

Takuya Uenoya is a Director of NTT Yamaguchi branch office. He received B.E. and M.E. degrees in electronics engineering from Waseda University in 1971 and 1973, respectively.

He joined NTT in 1973. Since 1988 he had been engaged in Development on Transmission cable systems including both Metallic and optical. Mr. Uenoya is a member of IEICE of Japan.

Microbending Loss of Thin Coating Single Mode Fiber for Ultra - High - Count Cable

W. Katsurashima, Y. Kitayama, K, Oishi, T. Kakuta, N. Akasaka

Sumitomo Electric Industries, Ltd.

Abstract

For the higher count and higher density optical cable, we manufaicured downsized coated optical fibers and evaluated their microbending behavior. Theoretical and experimental evaluation revealed that a 160 μm fiber was seven times more sensitive to lateral forces than conventional 250 μm diameter fiber.

We also investigated the improvement of microbending resistivity and confirmed that fibers with the secondary coatings of higher modulus of elasticity showed less microbending loss increase than these with conventional coating materials.

1. Introduction

In 1990, NTT revealed the idea of telecommunications services on the 21st century, named VI&P. (1) To realize this concept, it is necessary to extend optical fiber cables to all users. We must replace conventional copper pair cable consists of several thousands of copper pairs by almost the same fiber core count optical cable.

Now, up to 1000 fiber core count cable is introduced as subscriber optical cable and installed only in metropolitan area where we have feeder points within 700 m. However to realize FTTH conception, we must extend optical fiber loops into rural areas and lengthen the installation length up to the 1500 m. To achieve this target, optical fiber cables with diameter of about 35 mm are required. (2)

Downsizing single mode optical fiber is one of the most promising method to realize several thousands fiber count cable with small cable diameter. However coatings has two essential functions, namely protection of the fiber from abrasion and microbending losses caused by lateral forces. Hence, in reducing the coating diameter, we should pay careful attention to these effects.

In this paper, we studied the microbending characteristics of thin coated optical fibers. Diameter of the fiber glass is remained to be 125 μm considering the connection with existing lines through this paper. We manufactured optical fibers of several sizes in coating diameter and evaluated microbending characteristics. Presumed Microbending Loss (PML) method is also introduced to compare microbending loss of fibers with different parameters.

2. Coated Optical Fiber

Coatings are duly attached around fiber glass for protection of glass from breakage. These coatings have another fundamental functions of increasing resistivity against microbending caused by lateral forces.

2 - layer coating structure (Fig. 1) is simple and effective design to reduce external force that reaches the surface of glass. Secondary layer lessens the deformations caused by outer force and primary layer functions as cushion. We deal with this 2 - layer coating structure throughout this paper.

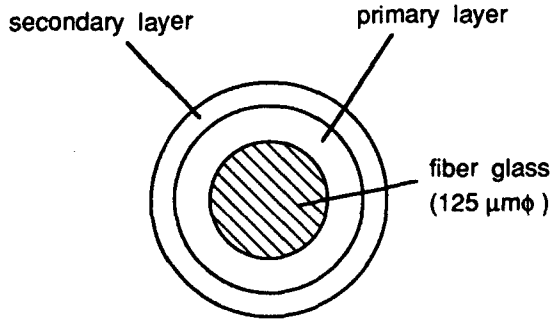


Fig. 1 2 - layer coating structure

For the given optical fiber diameter, optimum primary diameter is also determined in terms that minimum stress on glass surface is achieved against lateral forces. (3) However this optimum structure in terms of minimum stress does not coincide with that in terms of microbending loss increase due to cabling. We discuss it later.

3. Measuring Method

To estimate microbending characteristics, plates method is well known. (Fig. 2) In this method, optical fiber is set between two plates (probably metal plates with or without sandpapers) , and plates pushes fibers. We measure microbending loss increase due to deformations.

However applied loads are extremely larger compared to that given in actual cabling process. Plates can damage the coatings of diameter diminished optical fibers at worst and it is likely that it ends up only a abrasion test not for microbending test.

To give adequate lateral forces uniformly, long span winding test (Fig. 3) was adopted. Sand papers of #1000 (according to JIS) was wound around a reel and fibers on it.

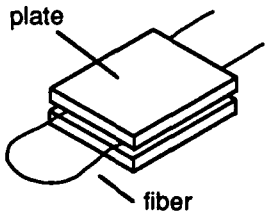


Fig. 2 plates test

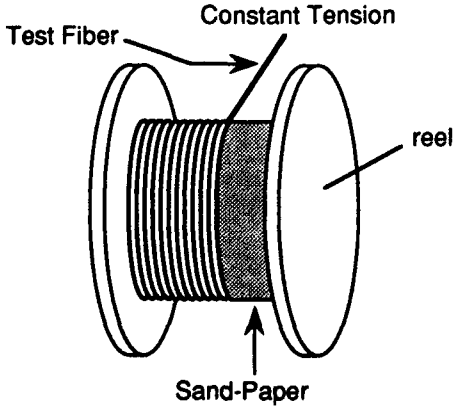


Fig. 3 Long Span Winding Test

In this way, we can measure the optical loss caused by adequate loads because the sample length reaches several hundreds of meters. Chromatic loss spectrum is measured before and after winding test (Fig. 4) and we get a loss increase by subtraction.

4. Presumed Microbending Loss (PML)

It is well known that microbending loss depends on fiber parameters. Hence, in the actual experiment, it is rather difficult to compare the detected loss increase of individual fiber with different parameters. In order to overcome this problem, we introduced presumed microbending loss (PML) method.

By fitting the measured data to microbending formula of Petermann (4), given by follows,

$$\Delta\alpha = \frac{1}{4}\left(\overline{\frac{1}{R^2}}\right)(k_0\, n_1\, w_0)^2\, f(\Delta\beta)$$

where

$$\Delta\beta = \frac{1}{w_0^2 k_0^2 n_1}, \quad \phi(\Omega) = \sqrt{\pi}\, L_c \exp\left[-\left(\frac{\Omega L_c}{2}\right)^2\right]$$

we get the correlation length Lc and average bending radius R. These parameters are assumed to be inherent to the bending condition and not to be influenced by fiber parameters. Hence the effect of fiber parameter difference on the induced loss increase is compensated. Substituting Lc and R again into the equation presuming standard fiber, whose mode - field - diameter is 9.5 μm and effective cut - off wavelength is 1.25 μm, and we get presumed microbending loss (PML) that is fairly converted microbending loss increase.

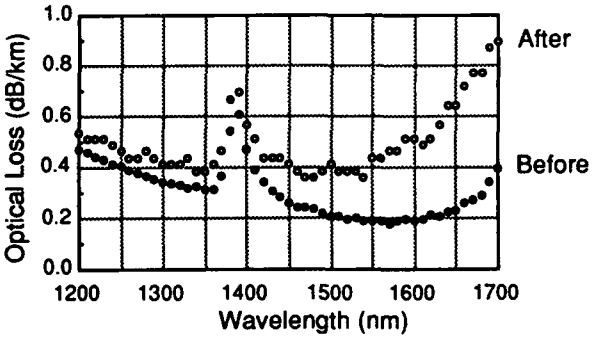


Fig.4 chromatic loss spectrum before and after winding test

5. Preliminary Experiment

5-1 Spool Tension and Correlation Length

Correlation length reflects the periods of bending of fiber. This physical assumption naturally leads us that fibers wound on a reel with different tension should have the same correlation length Lc provided we use same fiber and same reel.

To examine this assumption, we manufactured coated optical fibers with diameter of 160 μm. It has 2 - layer coating structure with 145 μm primary layer and 160 μm secondary layer. Diameter of glass fiber is 125 μm. We wound this fiber around sand - paper reel with tension of 27 g, 37 g and 47 g respectively.

Fig. 5 shows the measured loss increase by long - span winding test. We get the microbending parameters Lc by fitting this measured data. Calculated parameter Lc is plotted in Fig. 6. Lc remains constant regardless of winding tension. This result indicates that correlation length is determined by only fiber structure and the surface conditions of reel and we confirmed that our experiment is efective by this preliminary experiment.

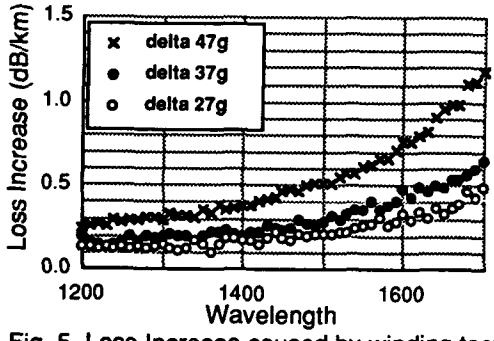


Fig. 5 Loss Increase caused by winding test (fiber diameter is 160 μm)

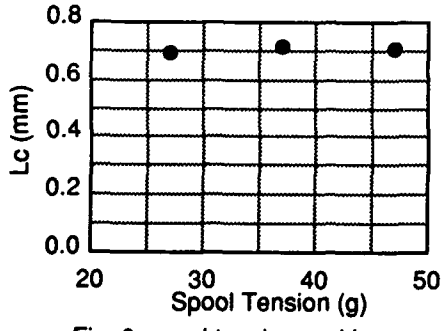


Fig. 6 spool tension and Lc

5-2 Temperature Dependence on Loss Increase

A reel has its thermal coefficient of liner expansion in itself. Environmental condition variation can do harm in our experiment. And also the stiffness of reel might affect the data. To examine this problem, we had another preliminary experiment.

Sand - papers were attached on the surfaces of the two reels made of plastic and aluminum respectively. Test fibers were wound around the reel with the tension of 50 g and put into a heat chamber. Temperature around the winding machine was 25.5 °C. We changed the tempereture in the chamber by 5 degrees centigrade around 25.5°C, so temperature range was 25.5 ± 5 °C. Optical loss at the wavelength of 1.55 μm was measuted using OTDR.

Fig. 7 shows the measured optical loss. Open circle indicates the plastic reel and closed one the aluminum reel. Optical Losses indicate clear linear dependence on temperature and we can read the gradient of loss increase in terms of temperature. We got 0.048 dB / km / °C by alminum reel and if we assume that loss increase is proportional to the tension, we have $2.5 * 10^{-5}$ [1/ °C] for the coefficient of linear expansion of aluminum reel. The coefficient of linear expansion of aluminum is $2.3 * 10^{-5}$ [1/ °C], that is described in ref. (5) for example. And we get $7.9 * 10^{-5}$ [1/ °C] for plastic reel by the same way and this fugure is also very close to the data we can find in many books that treat various coefficients including linear expansion of plastics.

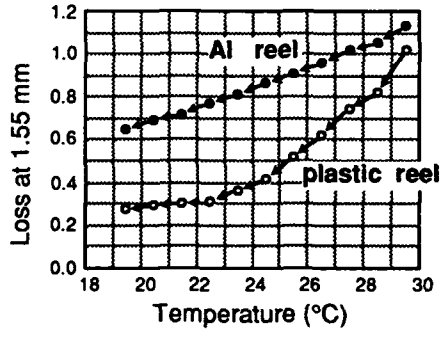


Fig. 7 optical loss by winding test in terms of temperature

And also from Fig. 7, we must notice that if we use different reels for this experiment, we can not expect same loss increase any more. Plastic reel lessen the effect of lateral force and the mesured induced loss tends to be smaller than when we use aluminum reel. And we also can not expect the surface and the base of sand - papers commercially available to be uniform. We should use same reel during concerned experiences.

From this preliminary experiment, we know clarify important points,

(1) We should keep emvironmental temperarute to be constant as possible.

(2) Microbending loss increase is proportional to the tension. This result is consistent with the result of previous preliminary experiment.

(3) We must not change test reel during concerned experiments.

6. Experiment

6.1 Microbending Loss of Downsized Fibers

To construct ultra - high - density and high - fiber - count optical cable, downsizing optical fibers is one of the most promising technologies. Diameter of the glass fiber should be 125 μm considering the connection with existing lines. So downsizing the coated optical fiber means to thin the coatings. At first we must know the sensitivity against microbending in terms of the coating thickness.

We manufactured four downsized fibers and a conventional 250 μm diameter fiber to refer. In table 1, fiber dimensions and parameters are indicated for our test samples.

Fig. 8 shows the measured microbending loss and PML at 1.55 μm. Close circle indicates the measured data. It can not be clarified which fiber is superior in terms of microbending from the measured data as our test fibers have different fiber paremeters respectively. The open circles indicate PML. These circles show a clear dependence on coating diameter and we confirmed these measurement done well. We now know the sensitivity against microbending compared with 250 μm fiber. Loss increase at the wavelength of 1.55 μm is about 6.5 times more sensitive by 160 μm fiber, 4 times by 180 μm fiber, and 3 times by 200 μm fiber.

Fig. 9 shows the ratio of PML at 1.55 μm to that of 1.3 μm. Experimental result shows that if we downsize the coated fiber, these fibers have smaller wavelength dependence and the loss increase at 1.3 μm may be compatable to that at 1.55 μm. It means that correlation length Lc become shorter as fiber coatings is diminished(Fig. 10 indicates the measured Lc). It can be explained by the physical effect of the coatings to cut off the minute fluctuation on the reel surface. Thick coatings translate only relatively long span sluctuations to fiber glass and thin coatings can translate shorter ones to the glass. So the wavelength dependence become smaller.

Table 1 Test Sample

Sample	Secondary Diam.	Primary Diam.	MFD	λc
A	160 μm	145 μm	9.6 μm	1.26 μm
B	170	150	9.7	1.25
C	180	155	10 0	1.25
D	200	165	9.9	1.25
E	250	180	9.7	1.25

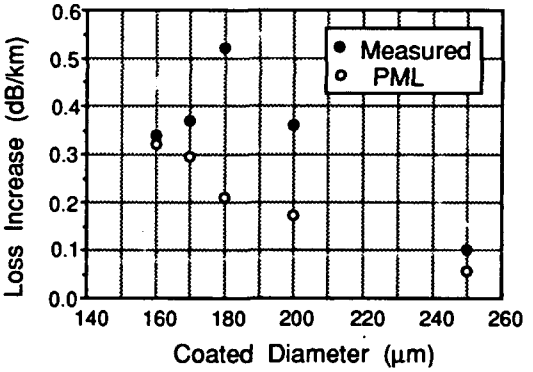


Fig. 8 Measured and PML at 1.55 μm

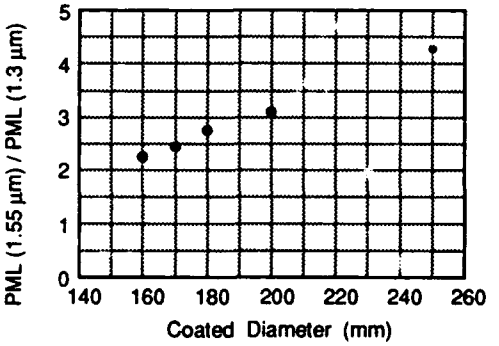


Fig. 9 ratio of PML at 1.55 μm to 1.3 μm

6-2 Lc and Primary Diameter

It is very interesting that correlation length Lc in Fig. 10 increases in order as the fiber diameter increases in spite that we choosed primary diameter without an intention. We had another experiment to confirm the effect of primary diameter on microbending.

We intended to manufacture the smallest diameter fiber of 160 μm at first. However it is very difficult to make 160 μm fiber with different primary diameters. So we used 180 μm diameter fiber for instead. Three samples were manufactured with thier primary diameter of 150 μm, 160 μm and 170 μm respectively. They were wound around sand - paper reel (different reel from the reel that was utilized in the chap. 6-1) with the tension of 50 g.

Fig. 11 indicates the PML of these fibers. Microbending loss indicates clear dependence on primary diameter and 170 / 180 μm fiber has the best resistivity against microbending. It is very interesting result compared to the analysis result of the stress on fiber calculated by FEM (Fig. 12) . According to this FEM analysis, stress on fiber glass is the least when primary diameter is about 150 μm. This experiment indicates that we can not know the microbending characteristics by the stress on glass fiber only.

Fig.13 shows the correlation length Lc and average bending radius R. Lc has little dependence on primary diameter, however R shows the relationship

$$R \propto 1 / \sqrt{k_s}$$

from the experiment. k_s is the spring constant determined by FEM.

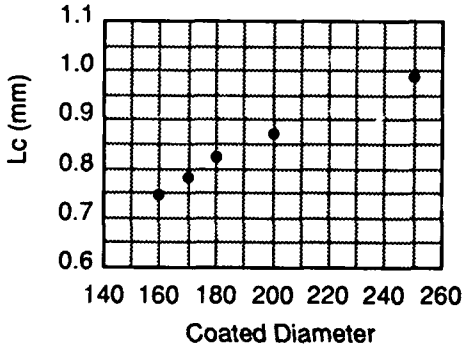


Fig. 10 coated diameter and correlation length

Now we know two important things from the experiments,

(1) Once fiber coating material, deameter and bending condition (reel for spool) is given, Lc is generally determined and affected little by primary diameter.

(2) Average bending radius R is proportional to $R \propto 1 / \sqrt{T k_s}$ where T is the spool tension.

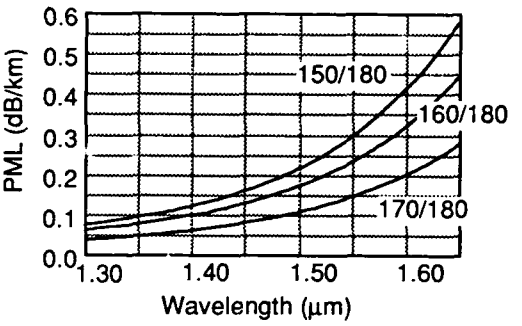


Fig. 11 PML of downsized optical fiber with different primary diameter

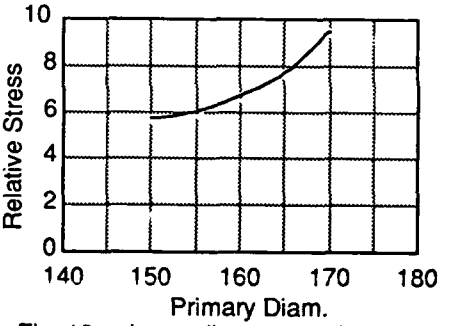


Fig. 12 primary diameter and relative stress on fiber glass (Coated diameter is 180 μmϕ)

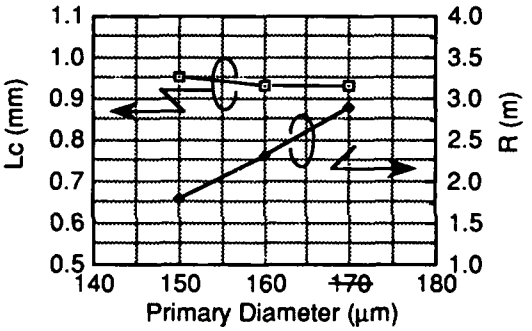


Fig. 13 Lc and R of downsized fiber with different primary diameter

7. Improvement of Resistivity against Microbending

So far we manufactured test samples using the same coating materials. To improve the resistivity against microbending, technologies of ultra high modulus of elasticity for secondary layer and low modulus of elasticity for primary layer are promising for long correlation length Lc and large bending radius R respectively.

In this paper, we studied the effect of high Young's modulus for secondary coating. We prepared 2 test samples with their diameter of 160 μm. Modulus of elasticity of these fibers are 50 kgf / mm^2 and 150 kgf / mm^2 respectively.

Fig. 14 shows the PML of these test samples. Samples with higher coating material indicates stronger wavelength dependence compared to another sample and shows less microbending loss increase during the communication wavelength window of 1.3 to 1.55 μm. From this experiment, we confirmed that coating material of higher modulus of elasticity is effective for the resistivity against microbending.

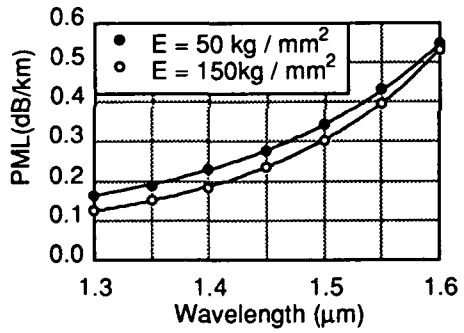


Fig. 14 PML of fibers with different secondary coating material

8. Conclusions

To realize FTTH, ultra high fiber count cable with small diameter is indispensable. Diminishing fiber diameter is one of the promising technique to complete this cable and we clarified the fundamental characteristics of microbending loss for these downsized coated optical fibers.

We introduced presumed microbending Loss method and by compensating fiber parameters we can compare the fibers with different paremeters. And we clarified that

(1) Downsized optical fiber is from 3 to 7 times more sensitive against microbendig than conventional 250 μm fiber if compared at 1.55 μm.

(2) Once fiber diameter, coating material and the bending condition (reel) are given, correlation length is determined and primary diameter affects little.

(3) By using material with higher modulus of elasticity for secondary layer, we can achieve longer Lc and lower loss increase during the communication window.

We have still many promlems left to realize downsized optical fibers for practical use. Primary coating material with lower modulus of elasticity, microbending characteristics after ribbon coating and cable design suitable for these fibers are the problems that should be conquered for example.

References

(1) M.Kuwabara,"21st Century Telecommunication and Optielectronics" , (Plenary Talk), OEC 90
(2) S.Tomita et. al. "Preliminary research into ultra high density and high count optical fiber cables." IWCS '91
(3) K.Ishihara et al , "Determination of Optimum Structure in Coated Optical Fiber and Unit ", Trans. IEICE '84/4 Vol.J.64-B, No.4, pp71-76 (in Japanese)
(4) K. Petermann, AEU , 1986, 30, pp.337-342
(5) Rika Nenpyo (chronological Scientific Tables) Maruzen '91 (in Japanese)
(6) W.Katsurashima et al, "Downsizing Optical Fiber Coatings and Microbending Chararacteristics", OEC '92 pp. 48-49



Wataru Kasturashima

Sumitomo Electric Industries, Ltd.

1, Taya-cho, Sakae-ku
Yokohama , Japan

Wataru Katsurashima graduated from Tokyo University in 1987. He joined Sumitomo Electric Industries, Ltd in 1987 and has been engaged in optical fiber and cables. Mr. Katsurashima is a member of Institute of Electronics and Communication Engineers of Japan.



Yoshinobu Kitayama

Sumitomo Electric Industries, Ltd.

1, Taya-cho, Sakae-ku
Yokohama , Japan

Yoshinobu Kitayama received his M.S. degree in Electrical Engineering from Kyoto Univ. in 1982. He then joined Sumitomo Electric Industries and has been engaged in research and development of optical fiber and cables. Mr. Kitayama is a senior engineer of Communication R&D Department in Yokohama Research Laboratories, and a member of the Institute of Electronics & Communication Engineers of Japan.



Kazumasa Oishi

Sumitomo Electric Industries, Ltd.

1, Taya-cho, Sakae-ku
Yokohama , Japan

Kazumasa Oishi received his M.S. degree in Geochemistry fromTsukuba University and joined Sumitomo ElectricIndustries, Ltd in 1991. Mr. Oishi is a member of Transmission Media R & D Department in Yokohama Laboratories and is engaged in opticalfibers and cables.



Tatsuya Kakuta

Sumitomo Electric Industries, Ltd.

1, Taya-cho, Sakae-ku
Yokohama , Japan

Tatsuya Kakuta was born in Osaka, Japan, on February 17 1960. He received the B.S. and M.S. degrees in Applied Chemistry from Osaka University in 1983 and 1985, respectively. He joined Sumitomo Electric Industries, Ltd. in 1985, and has been engaged in research and development of optical fibers and cables. Mr. Kakuta is a member of Institute of Electronics and Communication Engineers of Japan.



Nobuhiro Akasaka

Sumitomo Electric Industries, Ltd.

1, Taya-cho, Sakae-ku
Yokohama , Japan

Nobuhiro Akasaka received a M.S. degree in Chemical Engineering from Tokyo University in 1983. He joined Sumitomo Electric Industries, Ltd. in 1983, and has been engaged in research and development of optical fiber and cables. Mr. Akasaka is a member of Transmission Media R & D Department in Yokohama Research Laboratories.

DESIGN OF DOWNSIZED COATED OPTICAL FIBERS TO MINIMIZE MICROBENDING LOSS

M.HARA, S.OKAGAWA and A.OTAKE

THE FURUKAWA ELECTRIC CO., LTD.

6, YAWATA KAIGAN-DORI, ICHIHARA, CHIBA, 290, JAPAN

Abstract

Several studies on the lateral pressure characteristics of coated optical fibers were made so far. In this paper, we have introduced a regression formula of microbending loss by multi-regression analysis to study the effects of coating structure on the lateral pressure characteristics of downsized coated optical fibers. From this regression formula, it was considered that a larger Young's modulus of secondary coating and a larger diameter of the primary coating are advantageous in improving the lateral pressure characteristics of downsized coated optical fibers. Based on these results, we have manufactured downsized coated optical fibers with a high Young's modulus secondary coating and obtained good results both in lateral pressure and temperature characteristics.

I Introduction

NTT is promoting a plan to apply optical fibers to the whole subscriber network and ultra-high-density and high-count optical cable is required to implement such plan.[1] In this optical cable, coatings of optical fibers must be downsized. However, the coating structure of optical fibers is closely related to the lateral pressure characteristics, and reduction of coating diameter leads to deterioration of lateral pressure characteristics. In order to downsize the coating, therefore, it is necessary to clarify the optimum coating structure that does not induce deterioration of the lateral pressure characteristics. However the relationship between microbending loss and coating structure in single mode optical fiber has not been clarified completely.

Therefore, we have made examinations to clarify the relationships between microbending loss and coating structure by introducing an experimental formula on microbending loss through multi-regression analysis using parameters related to coating structure.

II Multi-regression Analysis

1. Experiments

We prepared two-layer UV curable urethane acrylates coated single mode optical fibers with 9.2 ± 0.1 μ m of MFD and 1.25 ± 0.01 μ m of cutoff wavelength. And the diameters of the secondary coating and the primary coating, Young's moduli of the secondary coating and the primary coating were varied.

The microbending losses of these fibers were measured as the loss increase at the wavelength of 1.55 μ m by winding a length of 1 km into multi-layer at a tension of 40 gf/fib. on a bobbin with a diameter of 160 mm (Multi-layer Drum-winding Microbending Testing).

2. Parameters

As the parameters for expressing the coating structure, we used D, H which were the parameters employed by Gloge in a paper determining the loss increase in a multi mode optical fiber.[2] The parameters D and H are shown in equations (1) and (2), respectively.

$$D = Ep + Es \cdot (b/Rs)^3 \quad (1)$$

$$H = Ef \cdot If + Ep \cdot Ip + Es \cdot Is \quad (2)$$

Where, Ep, Es, and Ef represent the Young's moduli of the primary coating, secondary coating, and glass, respectively ; b and Rs are the thickness and the radius of the secondary coating ; and Ip, Is, and If are the moments of inertia of the primary coating, secondary coating, and glass, respectively.

3. Results

Using D, H, D^2, H^2, also higher-order terms and logD and logH as parameters, the loss increase of Multi-layer Drum-winding Microbending Testing was analyzed by multi-regression analysis. As a result, the optimum formula for expressing the loss increase was found to be expressed in up to the second-order terms of D, H. The multi-regression formula is shown in equation (3).

$$\alpha = 9.03 \times 10^{-2} D^2 - 2.51 \times 10^{3} H^2 + 4.42 \times 10^{2} H - 19.4 \quad (3)$$

Where α denotes the loss increase of Multi-layer Drum-winding Microbending Testing (dB/km) (expressed in the loss increase after this). The relation between the loss increase calculated by using equation (3) and the loss increase obtained in experiment is shown in Figure 1. The correlation coefficient of the calculated loss increase and the experimental loss increases is 0.63, which is significant at the level of significance of 5%. This result shows that equation (3) expresses the loss increase in a considerably high accuracy.

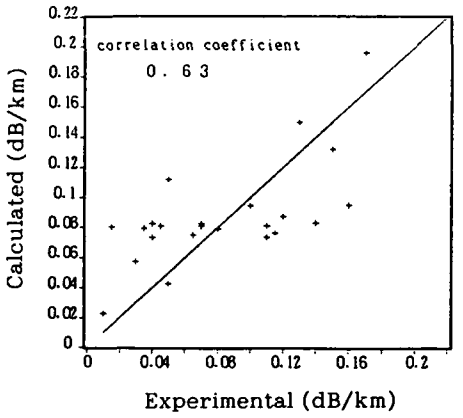


Fig. 1 Relation between experimental loss increase and calculated loss increase

III Discussion

1. Parameters D and H

Using equation (3), the relation between the microbending loss and coating structure was investigated. Figure 2 shows the range of D and H that are required to suppress loss increase to below a certain level. From this figure, it can be found that a smaller value of D and a larger value of H are advantageous in reducing microbending loss. Gloge called D rigidity and H stiffness, and D seems to represent the buffer effect of coating, and H is a parameter expressing the degree of difficulty in bending of optical fiber. A smaller D means a greater buffer effect, and a larger H means more difficulty in bending.

2. The Effect of Parameters

Figure 3 shows the relationships between the diameter of the secondary coating and calculated loss increase. From this figure, it can be found that a smaller diameter of the secondary coating results in a larger loss increase and smaller Young's modulus of primary coating results in a smaller loss increase. Also, the ratio of the thickness of the secondary coating to the radius of the secondary coating, that is, b/Rs gives influences on loss increase and such influences are larger than those of the Young's modulus of the primary coating. So, it can be understood that b/Rs is a considerably important parameter.

When looking into b/Rs, a smaller b/Rs results in a smaller loss increase when the diameter of the secondary coating is 230 μ m or less and, on the contrary, a larger b/Rs results in a smaller loss increase when diameter is more than 230 μ m. It is considered that, in a region of more than 230 μ m, H is larger and the stiffness H becomes more effective than the buffer effect D, and the loss increase seems to be smaller when H is somewhat larger.

From the above result, even in the region of small outer diameter, the loss increase is expected to be smaller by further increasing H by raising the secondary Young's modulus.

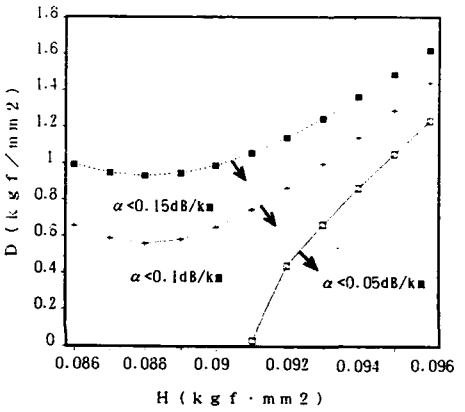


Fig. 2 Ranges of D and H

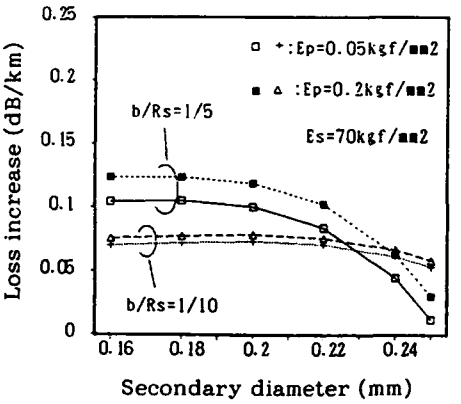


Fig. 3 Relation between secondary diameter and loss increase

Ⅳ Characteristics of Downsized Coated Optical Fibers with a High Young's Modulus Secondary Coating

1. Lateral Pressure Characteristics

Taking the above discussions into consideration, we have made trial manufacture of downsized coated fibers and evaluated these fibers. And also actual loss increases of the fibers were compared with calculated loss increases. The coating structures of the fibers are shown in Table 1.

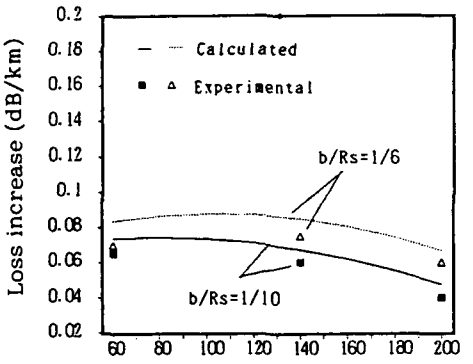
Table 1 Coating structures of downsized coated fibers

outer diameter (μ m)	secondary Young's modulus (kgf/mm²)	b/Rs
200	60, 140, 200	1/6, 1/10
180	60, 140, 200	1/6, 1/10
160	60, 140, 200	1/10

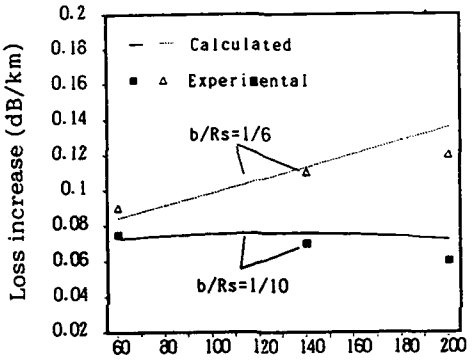
The fiber with b/Rs=1/6 and outer diameter of 160 μ m could not be manufactured because the prima y coating diameter was too small.

The actual loss increase of the fibers and calculated value are shown in Figure 4. Although the absolute value of the loss increase was somewhat different from the calculated value, the tendency to the secondary Young's modulus nearly coincided. The figures indicate that the tendency of loss increase varies with the values of outer diameter and b/Rs. At the outer diameter of 200 μ m, by raising the Young's modulus, the loss increase becomes smaller, but at the outer diameter of 160 μ m, to the contrary, the loss increase becomes larger. Also, at the outer diameter of 180 μ m, when b/Rs is 1/10, the loss increase becomes smaller by raising the Young's modulus, but when b/Rs is 1/6, it becomes larger. It is considered that, in fibers with small outer diameter and large b/Rs, H dose not become larger compared with increase of D when the secondary Young's modulus is raised, therefore the loss increase becomes larger .

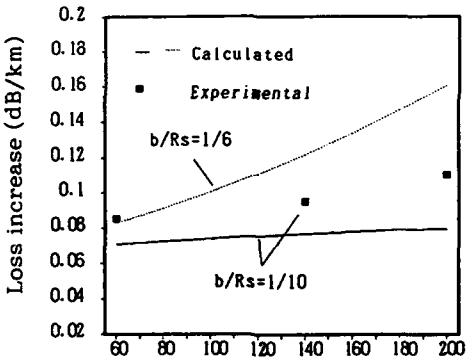
This result suggests that there are two cases depending on the outer diameter of coating and the value of b/Rs : in one case, a larger Young's modulus is advantageous in reducing loss increase and in another case, a smaller Young's modulus is advantageous. Moreover, in order to suppress the loss increase by raising the secondary Young's modulus, it is necessary to reduce b/Rs as the outer diameter of coating decreases.



(a) Outer diameter 200 μ m, Ep=0.1kgf/mm²



(b) Outer diameter 180 μ m, Ep=0.1kgf/mm²



(c) Outer diameter 160 μ m, Ep=0.1kgf/mm²

Fig. 4 Relation between secondary Young's modulus and loss increase

From the above examinations, it is considered that the application of a large diameter for primary coating and a high Young's modulus for the secondary coating is effective for reducing microbending loss in downsized coated optical fiber. However, there is a problem that a too small thickness of the secondary coating results in a reduced strength, so the dimensions must be designed also taking this aspect in consideration.

2. Other Characteristics

Then, other characteristics of fibers with a high Young's modulus secondary coating were investigated.

The losses in a loose coil was the same as that of conventional fiber with a diameter of 250 μ m in all fibers. For example, the spectral attenuation of the fiber with outer diameter 200 μ m, Es=200kgf/mm^2, and b/Rs=1/6 is shown in Figure 5, in which the loss increase at the long wavelength side was not found, in spite of applying the high Young's modulus in secondary coating.

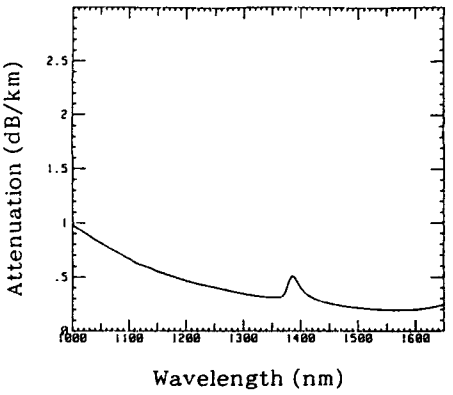


Fig. 5 Spectral attenuation

Also, no problem was found on temperature characteristics in any size of fiber. For example, figure 6 shows the temperature characteristics at a wavelength of 1.55 μ m in fiber with outer diameter 200 μ m, Es=200kgf/mm^2, and b/Rs=1/6. The loss changes of all fibers were less than 0.01 dB/km from -60 ℃ to 80 ℃. When a material with a high Young's modulus is used in the secondary coating, the shrinking force at low temperature becomes larger. But, since the cross-section of coating was smaller by reduction of coating diameter, good temperature characteristics seemed to be obtained.

Thus, by the applying of a large diameter for the primary coating and a high Young's modulus for the secondary coating, we have succeeded in obtaining downsized coated optical fibers that are superior in lateral pressure and temperature performance.

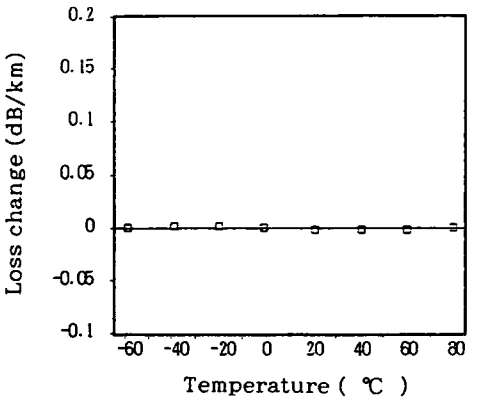


Fig. 6 Temperature characteristics

V Conclusions

An experimental formula of microbending loss was deduced by multi-regression analysis. Using this formula, it has been found that b/Rs gives a large influence on microbending loss. Further, it has also been known effective to raise the secondary Young's modulus for reducing microbending loss of downsized coated optical fibers.

On the basis of these results, downsized coated optical fibers with a high Young's modulus secondary coating were fabricated, and the fibers having excellent lateral pressure and temperature characteristics were obtained.

VI Future Plans

Ribbons and cables are being manufactured by using downsized coated optical fibers with a high Young's modulus secondary coating, and their characteristics will be evaluated.

References

1) S. Tomita et al., IWCS(1991) pp. 8-15.
2) D. Gloge, B.S.T.J., Vol. 54, No. 2, Feb. 1975, pp. 245-262.



Masami HARA

The Furukawa Electric Co., Ltd.

6, Yawatakaigandori, Ichihara, Chiba, 290, Japan

Mr. Hara graduated from Osaka University in 1987 with a M.E. in physics. Then he joined The Furukawa Electric Co., Ltd., Chiba, Japan, and has been engaged in research and development of optical fiber cables.

He is now a research engineer of Optical Fiber Transmission Section, Opto-Technology Laboratory, The Furukawa Electric Co., Ltd.



Akihiro OTAKE

The Furukawa Electric Co., Ltd.

6, Yawatakaigandori, Ichihara, Chiba, 290, Japan

Mr. Otake graduated from Tohoku University and joined The Furukawa Electric Co., Ltd. in 1974. He has been engaged in research and development of optical fiber cables and those accessories.

He is now a manager of optical fiber transmission research section.



Shuji OKAGAWA

The Furukawa Electric Co., Ltd.

6, Yawatakaigandori, Ichihara, Chiba, 290, Japan

Mr. Okagawa graduated from Osaka University in 1981 with a M.Sc. in chemistry . Then he joined The Furukawa Electric Co., Ltd., Chiba, Japan, and has been engaged in research and development of plastic materials and manufacturing methods for optical fiber cable.

He is now a senior research engineer of Optical Fiber Transmission Section, Opto-Technology Laboratory, The Furukawa Electric Co., Ltd.

AN INTERNATIONAL DEVELOPMENT ON RIBBON TECHNOLOGY AND EVALUATION OF APPLICABILITY TO NATIONAL SPECIFICATIONS

JP BONICEL, D. KELLER, G. KYLEN, J. SCHULTE , G. PATERNOSTRO, G. BERTHELSEN, CG. CORTINES, C. LASNE

ALCATEL CABLE, ALCATEL NA, ALCATEL IKO KABEL, ALCATEL KABELMETAL, ALCATEL CAVI, ALCATEL KABEL NORGE, ALCATEL CABLE IBERICA, ALCATEL ALSTHOM RECHERCHE

ABSTRACT

This paper reports the development of optical fiber ribbon technology on an international basis considering the specific requirements of the different countries involved.

The basic premise has been to define a common technology foundation for optical fiber ribbons which can be used by the different international cable manufacturing units. Work on detailed development specific to individual countries or specifications will be the responsability of the each individual manufacturing unit.

1. INTRODUCTION

Optical fiber ribbon technology is already widely used in the international market due to advantages in small cable size and mass splicing. Due to differences in specifications from country to country, there are many resulting ribbon and cable structures which have a common technical foundation. The international ribbon development program has been established based on the common technical foundation.

The parameters which have been analyzed include the following :

- ribbons : fibers
 primary coatings
 colouring
 ribbonning : encapsulated
 edge bonded
 4 to 12 fibers
- cables . cable structure : unitube
 multitube
 slotted core
 tight structure.

It has been shown that it was possible to establish a common technical foundation for ribbons because fundamental problems concerning materials and processing must be solved in order to achieve good results.
Development of different families of ribbon cables have resulted from the common technical foundation, and some of those cables are now in standard production in different Alcatel Cable manufacturing units. Ribbon splicing, particularly using mass fusion splicing techniques has been thoroughly analyzed using different kinds of fibers.

With the introduction of fiber in the loop (FITL) looming on the horizon, there is currently a great deal of investigation into the best technical/ economic solution for next generation telecommunication systems. The use of ribbon technology has been analyzed as a possible solution for these evolving systems.

2. MULTIFIBER RIBBON TECHNOLOGY

2.1. Main characteristics on multifiber ribbons : National specifications

Basically we can consider two kinds of ribbons : thin and encapsulated ribbon as presented on figure 1.

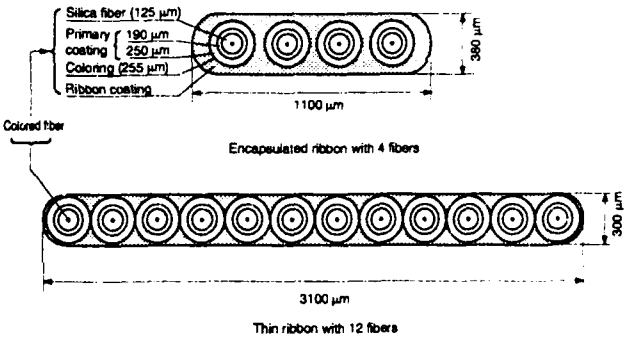


Figure 1 : Thin and encapsulated ribbons.

The figure 2 gives the typical geometrical characteristics that we can meet.

N° of fibers	Type of ribbon	Width (µm)	Height (µm)
2	Encapsulated	610	380
	Thin	510	300
4	Encapsulated	1120	380
	Thin	1020	300
6	Encapsulated	1630	380
	Thin	1530	300
8	Encapsulated	2140	380
	Thin	2040	300
10	Encapsulated	2650	380
	Thin	2550	300
12	Encapsulated	3160	380
	Thin	3060	300

Figure 2 : Main geometrical characteristics

Some of these ribbons are already specified or used in some countries by telecommunication operators and are under considerations in other countries as synthetized in figure 3.

COUNTRIES	INTRODUCED	UNDER CONSIDERATION
BELGIUM	-	4 - 6 fibers
FRANCE	-	6 fibers, encapsulated (1) (2)
GERMANY	-	10 - 4 fibers (3) (4)
ITALY	4 fibers, encapsulated	- (5)
JAPAN	4 fibers, encapsulated	- (6)
	8 fibers, encapsulated	- (6)
		16 fibers (7)
NORWAY	-	4 fibers
SPAIN	-	4 fibers
SWEDEN	4 fibers, encapsulated	- (8)
USA	12 fibers, thin	- (9)

Figure 3 : Use of ribbon cables in the world
((1) (2) .. are bibliography references)

From the different specifications or specification projects, the main characteristics that we have to consider on the ribbons or on the ribbon cables are summarized on figures 4 and 5.

CHARACTERISTICS	REQUIREMENTS
Geometry Width and height Flatness Distance between the fibers	According to particular specification
Color coding	U.C
Transmission $\Delta\alpha$ ribbon/fibers Sensitivity to microbending Sensitivity to bending	$\Delta\alpha \leq 0.01$ dB/km at 1300 and 1550 nm U.C. U.C.
Temperature cycling	$\Delta\alpha \leq 0.05$ dB/km at 1300 and 1550 nm - 40°C + 70°C
Mechanical characteristics Strippability Break out Torsion Crush Tear resistance	U.C.
Environmental tests Compatibility ribbon/filling compound Dry air Humidity Water	U.C.

Figure 4 : Main requirements on ribbons.

This figure 4 gives only an overview of the main requirements and it should be too difficult to present in a such simplified figure all the particular specifications required by different customers. However, in addition to these requirements there are some specific requirements that have a strong influence on ribbon development, such as «water sink test» from SIP (Italy).

CHARACTERISTICS	REQUIREMENTS
Geometry Maximum compactness	According to national specifications
Mechanical tests Tensile Crush Impact Bending Torsion Kink Watertightness	According to national specifications
Temperature cycling	- 40°C + 70°C No significant increase in attenuation at both windows

Figure 5 : Main requirements on ribbon cables

2.2. Multifiber ribbon developments

Considering the different characteristics on ribbon and ribbon cables, different Alcatel units have been involved in a general R & D program for the development of ribbons and ribbon cables. To make a precise presentation of all these R & D activities should be too long. So we will present hereafter only some aspects of these works and final results that we achieved on some ribbon cables.

2.2.1. Ribbon development

R and D activities have been oriented on ribbons with 4 to 12 fibers per ribbon.The main activities are up to now on ribbons with 4, 6, 8 and 12 fibers.

From extensive works that we have made on the 2 kinds of ribbons, the encapsulated ribbons are less sensitive to microbending and the ribbon layer material gives a better mechanical protection of the fiber than in the case of thin ribbons. *This point must be carefully analyzed* for applications such as fiber in the loop (FITL). However, in the example of a 4 fiber ribbon, an encapsulated ribbon will require 2 to 3 times more U.V. curable material than the same thin ribbon and it is well known that this kind of material is expensive. So, a cable with thin ribbon will be more cost effective for two reasons :

- it uses less expensive material in the ribbon.
- *because the ribbons are smaller (- 25 % on the* thickness) it is possible to reduce the cable size.

We have shown during this research that it was very important to keep the ribbon geometry as symmetrical as possible to avoid differential strain due to the differencies in the thermomechanical material characteristics (Young modulus, time/temperature behaviours....)

For the ribbon manufacturing process we have used a machine as presented on figure 7 with U.V. curable systems and the possibility to produce ribbons up to 12 fibers.

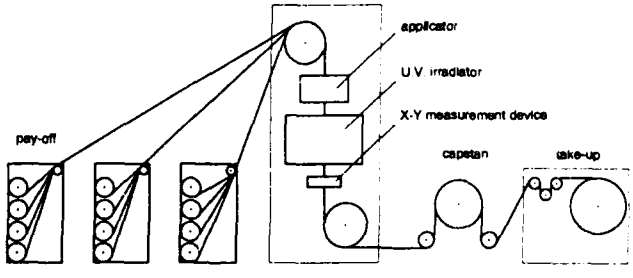


Figure 6 : Ribbon machine system.

In standard production tandem lines with coloring systems are also used.

A large part of this research has been focused on materials to know the impact of each parameter on the ribbon quality. The figure 7 gives an overview of the ribbon characteristics as a function of materials characteristics.

MATERIAL	MAIN PARAMETER	IMPACT ON RIBBON CHARACTERISTICS
Fiber	- mode field diameter - λ_c - index profile	micro and macrobending
primary coating	- Young modulus = f (T) - glass transition temperature - fiber adhesion -sensitivity to water and filling compound - processability	- microbending sensitivity - thermal stability - ageing stability - spliceability (strippability) - fiber stress corrosion factor
Secondary coating	- Young modulus = f (T) - glass transition temperature - compatibility with primary coating - compatibility with coloring systems - sensitivity to water and filling compounds - processability - adhesion to secondary coating	- microbending sensitivity - thermal stability - ageing stability - break out - spliceability
Coloring	- viscosity = f (T) - curing speed - color quality - Young modulus = f (T) - compatibility with secondary coating and ribbon matrix - sensitivity to water and filling compound - smooth surface - processability	- microbending sensitivity - thermal stability - ageing stability - break out - fiber identification - spliceability
Ribbon matrix	- viscosity = f (T) - Young modulus = f (T) - compatibility with coloring - sensitivity to water and filling compound	- ribbon geometry - break out - strippability - ageing stability

Figure 7 : Overview of the relations ribbon characteristics/material characteristics

A great deal of analyses has been made on these different parameters and as an example we present 2 points to show the relation material / characteristics :

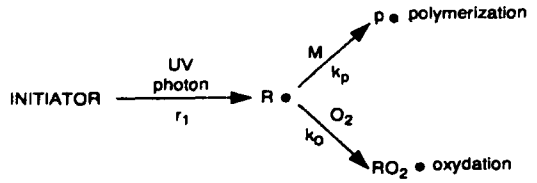
- Break out : to have a good break out the colored fibers must be «clean» (without ribbon matrix adhesion) when the fibers are separated. To meet this requirement we have demonstrated the strong relation between :

 - the secondary coating
 - the coloring layer
 - the ribbon matrix

The coloring layer must be well cured and bonded to the secondary coating, and the ribbon matrix must have a low adhesion to the coloring layer. So it is important to carefully control the ink quality and its processability.

In the case of U.V. curable inks it is fundamental to control the evolution of double carbon links (C = C) but we must note that the curing rate is a function of inks (matrix, opacity of pigments to the UV rays, use of T_iO_2 or not, photocuring kinetics and inhibition by oxygen....)

The mechanism of photocuring inhibition by oxygen is shown in figure 8.



if $k_o > k_p$ photocuring is inhibited

Symbols have the following meaning :

r_1 : formation rate of free radicals R
M : monomer
k_p : rate constant of polymerization
k_o : rate constant of peroxydation

Figure 8 : Mechanism of photocuring inhibition by oxygen.

All the photocurable materials (fiber coatings, UV coloring, ribbon matrix) have been intensively analyzed by infrared absorption and some analyses have been made in situ by microscopic analysis associated to an infrared system.

- water sink test : to meet the water sink test requirement ($\Delta\alpha_{1550} \leq$ 0.1 dB/km during 22 days in water at 20°C and 60°C) it is also necessary to develop special materials for fiber coatings, inks and ribbon matrix. All these materials and their processability have been intensively analyzed. The figure 9 shows two results. In one case (figure 9 - 1) the result is very bad and the change in attenuation can reach more than 1 dB/km at 1550 nm. In the other case the result is good with a change in attenuation lower than 0,1 dB/km at 1550 nm (figure 9 - 2).

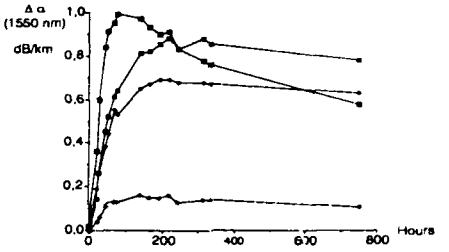


Figure 9 - 1 : Bad ribbon in water sink test.

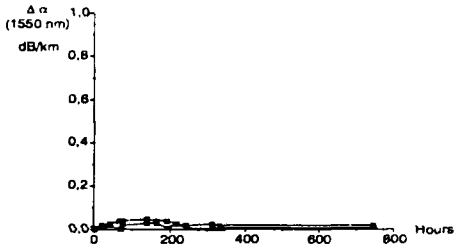


Figure 9 - 2 : Good ribbon in water sink test.

The ribbons have been also submitted to more standard tests as :

- pulling test
- torsion test
- twist test
- ageing test
- strippability
- spliceability.

As an example we give hereafter some OTDR results that we have obtained on mass fusion splice test with 4 fiber encapsulated ribbons made with different kinds of fibers (matched cladding and depressed cladding). Figures 10 present two histograms that we have obtained in laboratory environment using an automatic ribbon fusion splicing machine.

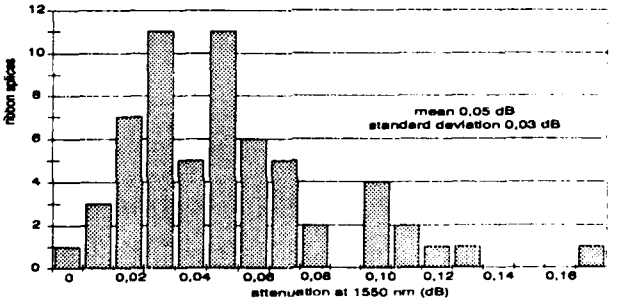


Figure 10 - 1 : Mixed ribbons with matched cladding fibers.

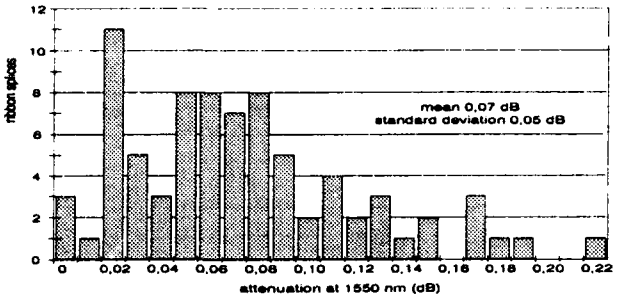


Figure 10 - 2 : Mixed ribbons with matched and depressed cladding fibers.

2.2.2. Ribbon cable development

Considering the customers requirements we have developed different families of ribbon cables. Here also it would be too long to present in details all these specifications. So we will give only some examples as presented on next figures. Some of these cables are in production; some other are still under development.

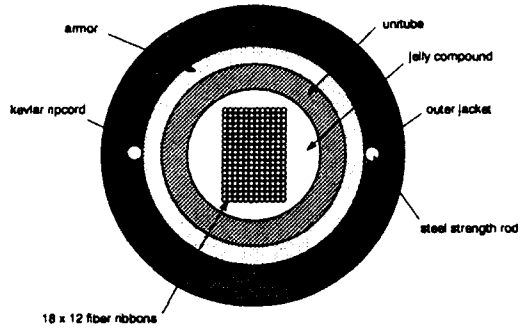


Figure 11 : Unitube cable (up to 216 fibers) (nominal diameter = 16 mm)

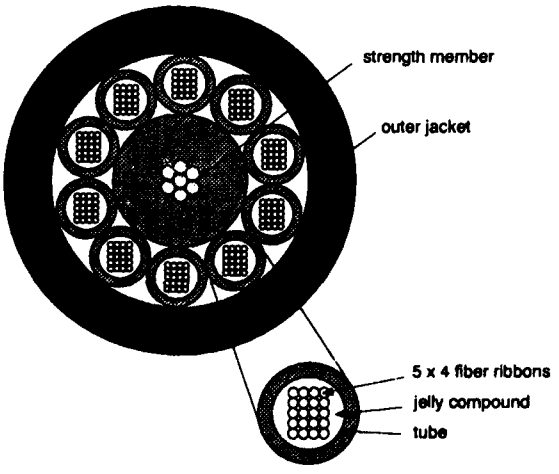


Figure 12 : Multitube ribbon cable (up to 200 fibers) (nominal diameter = 20 mm)

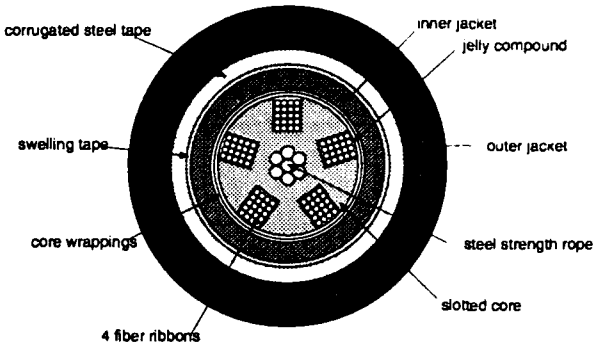


Figure 13.1 : slotted core ribbon cable (up to 100 fibers) (nominal diameter = 19,5 mm)

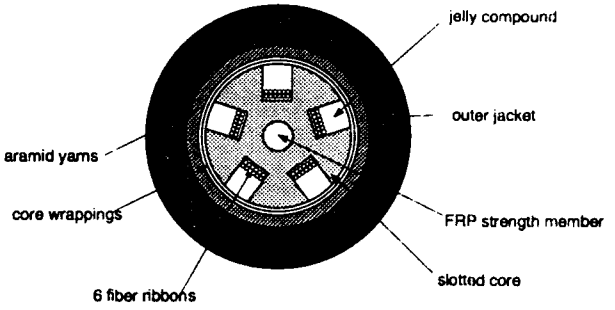


Figure 13 - 2 : slotted core ribbon cable (up to 60 fibers) and 150 *in the future (nominal diameter = 12 to 16 mm)*

Similar cable is now in production with 6 slots and with 2 ribbons/slot (48 fiber dielectric cable).

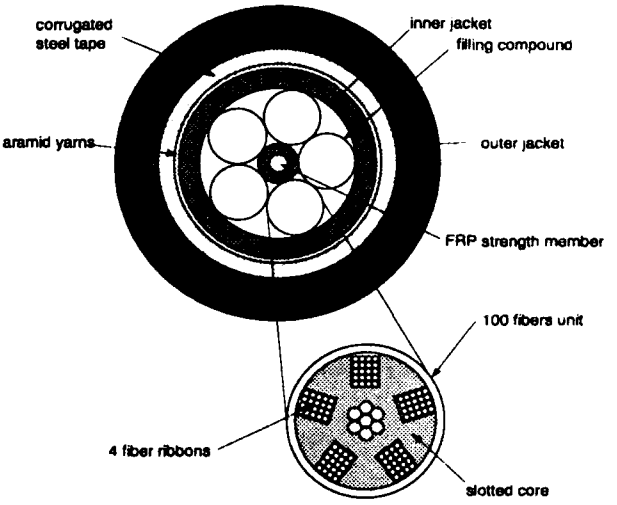


Figure 14 : slotted core ribbon cable (up to 500 fibers) (nominal diameter = 40 mm)

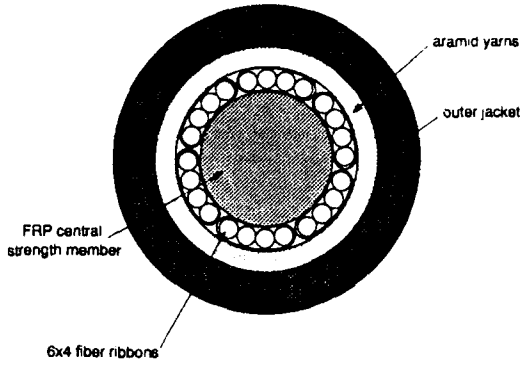


Figure 15 : tight ribbon structure (nominal diameter = 6 mm)

Different ribbons that we have developed have been tested in these different structures. The figure 16 presents results that we have obtained in a 100 fiber ribbon cable as presented on figure 14 - 1. The parameters tested on the ribbon in this experience are :

- glass fiber design,
- primary coating,
- inks,
- ribbon matrix.

FIBERS	RIBBON	$\Delta\alpha_{1550}$ in cable 10 cycles - 40 + 70°C dB/km	
		Average	Max
A	1	0.23	0.70
B	2	0.30	0,76
C	3	0.05	0,07
D	4	0.04	0.05
E	5	0.035	0.06

Figure 16 : Thermal test on ribbon cables using different fibres and different ribbons.

Fibers A and B give bad results because their primary coatings are not suitable for ribbon applications.

We can see that one of the good results has been got with fibers E and ribbon 5. Our fibers have been used to produce this ribbon n° 5 and their main characteristics are presented in figure 17.

CHARACTERISTICS	VALUE	UNIT
Geometrical properties		
Core non-circularity	6 max.	%
Clad diameter	125 ± 2	µm
Clad non-circularity	2 max	%
Core/clad concentricity error	1 max	µm
Coating diameter	245 ± 10	µm
Coating/clad concentricity error	15 max	µm
Optical properties		
Mode field diameter	9.1 ± 0.5	µm
Cut off wavelength	1150 - 1280	nm
Zero dispersion wavelength	1310 ± 10	nm
Slope at zero dispersion wavelength	0.093 max	ps/nm^2.km
Chromatic dispersion at 1285 - 1330 nm	3. 5 max	ps/nm.km
Chromatic dispersion at 1550 nm	19 max	ps/nm.km

Figure 17 : Fibre characteristics
(Attenuation is within CCITT recommandation)

These fibers use a special «coating» developed for ribbon applications.

With fibers C, D, and E and ribbons 3, 4, 5 we have produced 100 fiber ribbon cables and the figure 18 presents the results on thermal test with a maximum change in attenuation at 1550 nm of 0.07 dB/km in the range of - 40 to 70°C.

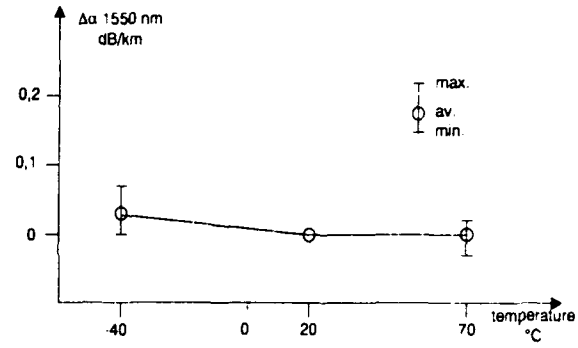
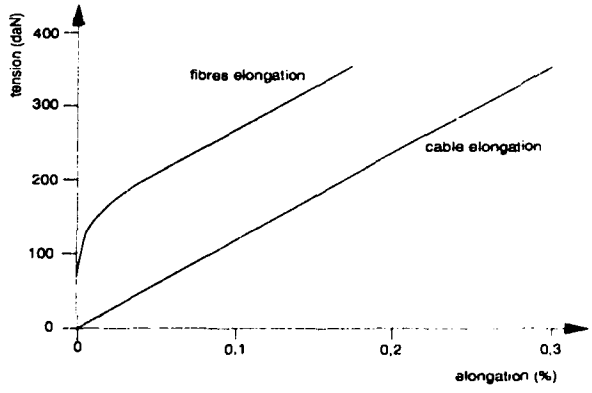


Figure 18 : thermal test on 100 fiber ribbon cables.

This cable has been submitted to a pulling test with a pulled length of 200 m. Figure 19 presents stress/strain relation on the cable, the change in attenuation on fibers at 1550 nm and the stress/strain on fibers measured by the phase shift method.



The change in attenuation is less than 0.05 dB/km at 1550 nm

Figure 19 : Stress/strain on cable and fibers and $\Delta\alpha$ at 1550 nm

As it is well known the stress/strain on the cable is a function of strength members included in the cable. So the parameter is easily ajustable. The most important point is the low change in attenuation on the different fibers when cable strain and fiber strain increase.

A great deal of mechanical or ageing tests have been performed on different ribbon cables and are not presented here (mainly according to IEC 794 - 1 or Bellcore TR TSY 000020 specification).

Today some of these cables are intensively used by some operators in standard networks applications.

3. MULTIFIBER TECHNOLOGY AND FIBER IN THE LOOP APPLICATION

For Telecommunications Operators the most important challenge for the end of the 20th century and the beginning of the 21st century is the FITL for narrowband and broadband applications. All large telecommunication equipment suppliers are also working on this challenge. Many field trials have been done worldwide and in France 600,000 subscriber lines for cable TV fiber to the home application have been already installed (10).

Today the main targets are :

- to increase the transmission capacity of the copper distribution network,
- to maintain the same reliability for fiber narrowband transmission than on the present copper network,
- to try not to have specific civil works for the FITL,
- to have a competitive cost with standard copper system,
- to have a «flexible» FITL system where it is easy to connect new subscribers during the system life time.

The analysis of these different targets can give different «cable plant» solutions based on :

- star network (point to point),
- star network with splitters (point to multipoint),
- ring network.

Depending of the different systems the number of fibers per cable may be radically different. Some systems require cable plant with high fiber count cables (200 or more); for some other with high share ratio it could be necessary to use only low fiber count cable (100 or less). So we can understand that the FITL system will influence the cable structures.

With ribbon cables it is possible to have a large fiber count in a small size cable. For example it is possible to have 200 fibers in less than 17 mm diameter cable. And if mass splices are usable ribbon cables are very good candidates, particularly for point to point transmissions. On the other side if shared fibers are used with different splitting ratio and different splitting points it is necessary to analyze if ribbon cable is the best choice.

The figure 20 summarizes the different advantages of ribbon cables.

- HIGH FIBRE COUNT)) HIGH DENSITY
- SMALL DIAMETER)
- MASS SPLICING)) REDUCTION ON SPLICING
- POSSIBILITY OF AT LEAST ONE FACTORY PRETERMINATED END) COSTS
- EASY AND CORRECT IDENTIFICATION (EVEN FOR LOW FIBRECOUNTS)
- HANDLABILITY OF RIBBON BETTER THAN THAT OF INDIVIDUAL FIBRES (EXCEPT TORSION)

Figure 20 : Advantages of ribbon cables.

The best cases for the applicability of ribbon structure are :

- very high fiber count cables
- fixed structure cable plant

In these cases mass splicing and/or preconnectorization are convenient and it is a way to reduce the connexion cost on the field. However the different experiences on preconnectorized copper cable and preconnectorized optical cable have shown that a lot of problems must be solved to prove the efficiency of the preconnectorization (cable length, cable plant planning....). So the optical cable preconnectorization for FITL application must be carefully analyzed.

4. CONCLUSION

We have presented the development of an international basis of an optical ribbon technology considering the specific requirements of the different countries involved. We have developed a family of ribbons and a family of cables and the main parameters that influence the product quality have been presented.

The ribbon technology is now an integral part of fibre optics world. It is used on several countries and seems to be especially convenient for high fibre count cables. Whether it is fitted or not to FTTH applications is still under consideration but this is a very important point for the future development of optical fibre networks. For that purpose, future new developments can be anticipated such as ribbon improvements or new possible candidates as presented in figure 15 (tight ribbon structure).

REFERENCES

(1) F. Legros, J-L Rochefort, Y. Roussel, D. Brault «Câbles à rubans de fibres optiques», OPTO 92.

(2) JP. Bonicel, PJ. Giraud, M. de Vecchis «Overview of optical fibre ribbon technology», OPTO 92.

(3) HG. Haag, GF. Hög, PE. Zamzow, «Optical fiber cable for subscriber loop», J. of Lightwave Technology, vol. 7, n° 11, November 1989.

(4) G.D. Maltz, «Stranding of strength members in F.O. cables». Proceedings, Nr 12 of FOCA 90. Symposium for the Telecom cable trade, 27 and 28 th september 1990, Geneva.

(5) F. Esposito, F. Montalfi, F. Nanni «OF ribbon cable system technology : the Italian experience» 40th IWCS, 1991.

(6) T. Matsuo, Y. Sataka «Development of single mode optical fiber cable for NTT», Sumitomo Electric technical review, n° 29, January 1990.

(7) S. Tomita, M. Matsumoto, T. Yabuta, T. Uchiya «Preliminary research into ultra high density and high count optical fiber cable» 40th IWCS, 1991.

(8) L. Sundeman «First trial of optical fibre in local network», Swedish Telecom publication «TELE», Issue 2, 1991.

(9) KW. Jackson, PD. Patel, ML. Pearsall, JR. Petisce, GA. Lochkovic «An enhanced ribbon structure for high fiber count cables in the loop» 38 th IWCS, 1989.

(10) JP. Boinet, M. de Vecchis, J. de Vitry «Fibre to the Home : No more a trial, an operational reality» ISSLS April 1991, Amsterdam.

AUTHORS

JP. BONICEL - ALCATEL CABLE
170 Av.Jean Jaurès - 69344 LYON
FRANCE



Jean-Pierre BONICEL was born in 1952. He received his engineer degree from the Institut des Sciences de l'Ingénieur de MONTPELLIER (ISIM) in 1976. He joined Les Câbles de Lyon now Alcatel Cable in 1977 where he was in charge of material and mechanical problems for telecommunication cables. Now he is the head of telecommunication cables laboratory and the manager for the Alcatel Optical Cable Competence Center.

DA. KELLER - ALCATEL NA
PO Box 39 - Penny road
CLAREMONT, NC 28610
USA



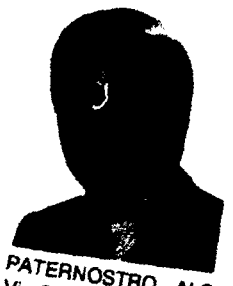
David A. KELLER was born in Harrodsburg, Kentucky in 1960. He received his bachelor of Science degree in Mechanical Engineering from the University of Kentucky in 1983. He held several positions in the Wire and Cable Industry in both Product Development and Process Engineering prior to joining Alcatel in 1987 as a Process Engineer. He is currently employed as a Senior Product Development Engineer in Alcatel's Product Development Department. Since September 1991 he has held the position of Team Leader of Alcatel NA's Ribbon Cable Development Team.

G. KYLEN - ALCATEL IKO Kabel
S-510 94 GRIMSÅS
SWEDEN



Goran KYLEN was born in 1954. He received his degree in electrical engineering from Chalmers University of Technology, Gothenburg, in 1979. In 1986 he joinded Alcatel IKO Kabel, where he is in charge of fiber optic cable development.

J. SCHULTE - ALCATEL KABELMETAL
Gubener Str. 1 - 3060 STADTHAGEN
GERMANY



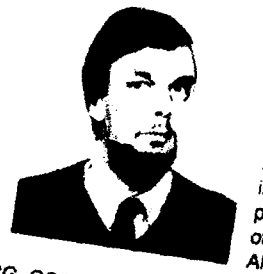
J. SCHULTE received his physics degree in quantum optics in 1981 and his Ph.D. in engineering in 1986 from the Technical University Hannover. After a research fellowship at IBM, Yorktown Heights, he joined Kabelmetal in 1987, where he has been engaged in the development of fiber optic cables.

G. PATERNOSTRO - ALCATEL CAVI
18 Via Crocifisso - 04100 LATINA
ITALY



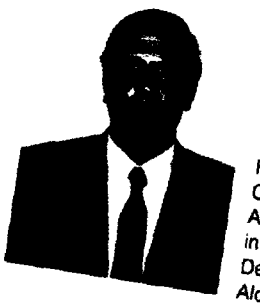
Giovanni PATERNOSTRO was born in 1946 and received his Dott. Ing. degrees in electronics engineering from Roma university. He is manager of Telecom Cables design and development of Alcatel Cavi.
He is author of technical papers and patents on cable process and measures.

G. BERTHELSEN - ALCATEL KABEL NORGE AS
Østre Aker vei 33 Postboks 130 Økern
509 OSLO 5
NORWAY



G. BERTHELSEN is 44 years old and received a B.SC in Electrical Engineering from Heriot-Watt University in Edinburgh in 1971. He joined STK (now Alcatel Kabel Norge) the same year as a cable design engineer. He started work with fibre optics in 1977 and has been involved in cable and systems development. His present position is Technical Manager of the Communications cable division at Alcatel Kabel Norge.

CG. CORTINES - ALCATEL CABLE IBERICA
Ruiz de Alda s/n
39600 MALIANO - CANTABRIA
SPAIN



Carlos G. CORTINES has received his Master Degree in Physic from Valiadolid University in 1968. He joined Standard Electrica, ITT, today Alcatel, and worked in the Engineering Department of the Telecommunication Cable Division. From 1982 he was the head of the Optical Fiber Development Group in Alcatel Standard Electrica, Cable Factory in Maliano-Cantabria. At present is the Development Engineering Manager of Alcatel Cable Iberica.

C. LASNE - ALCATEL ALSTHOM RECHERCHE
Route de NOZAY
91460 MARCOUSSIS
FRANCE



Claude LASNE is a member of the Materials and Characterization Group at Alcatel Alsthom Recherche, the main research center of Alcatel Alsthom, located at Marcoussis. After many years devoted to the analytical applications of mass spectometry techniques, he now coordinates the use of the means of Analytical Physics available in the Group, to investigate technological materials used under development inside the company.

HIGH COUNT TRUNK OPTICAL FIBER CABLE AND RELATED TECHNOLOGY DEVELOPMENT

Kenji Yoshioka, Naohito Ohno, Kiminori Sato, and Osamu Yamauchi

NTT Network Systems Development Center
Uchisaiwaicho, Chiyoda, Tokyo, 100 JAPAN

1. Abstract

We have developed a 300-Fiber Single Slotted Rod Cable. In order to deploy this new cable for trunk networks, a new trunk optical fiber cable closure has been developed, and a cable transfer and supervisory system called the Fiber Transfer and Test System (FITAS) has extended the number of measurable fibers. This cable and equipment have been in commercial service since August 1991. This paper describes the new cable and related technologies.

2. Introduction

In order to construct a digital network, NTT has been deploying trunk optical fiber cable networks. The maximum number of fibers in one trunk optical fiber cable has been 100, but a higher-count trunk optical fiber cable is needed to minimize the financial outlay for construction. Especially, to reduce new installation of underground facilities. However, existing cables with more than 100 fibers have been designed for use in subscriber loops, and they have a multi-slotted rod structure. Such a multi-slotted rod cable can not be applied to trunk networks because the length which can be wound in one drum is too short. Consequently, the cable diameter had to be reduced to extend the cable length in one drum, and this led to the development of a high count single-slotted rod optical fiber cable with water blocking (WB) technology (1).

In particular, the new trunk optical fiber closure had to accomodate 300-fiber WB cables. While the number of fibers here is three times that of previous optical fiber cable closures, the volume of the new closure had to be as small as possible. In addition, bending loss, which arises from maintenance of the closure, had to be low so as not to cause short breaks in signals.(2)

NTT has deployed the Fiber Transfer and Test System I (FITAS I) since 1990. It was developed for the operation, administration and maintenance of trunk optical fiber cable. FITAS I however, could only maintain up to 100-fiber trunk optical fiber cables, and as the maximum number of fibers in one trunk optical fiber cable became three times larger, the cable transfer and supervisory system had to be modified accordingly. The new system is named FITAS II.(3)

3. High Count Trunk Optical Fiber Cable

Since 1989, NTT has been deploying water blocking optical fiber cable for trunk and subscriber networks. Water blocking optical fiber cable is constructed with polyethylene sheath, water blocking tape and slotted rod in which 4 or 8-fiber ribbons are inserted.

There are three types of water blocking cable. The first one has the structure of a single-slotted rod and can hold 25 4-fiber ribbons at maximum. The second is the multi-slotted rod cable with six slotted rods, and each slotted rod can contain 25 4-fiber ribbons. The third one is also a multi-slotted rod cable, but it is constructed with only five slotted rods, where each slotted rod contains 25 8-fiber ribbons. For the trunk optical network, single-slotted rod cable has been used as mentioned above, and the maximum number of fibers in one trunk optical fiber cable here is 100. All three types of cables have been installed for the subscriber optical network. The new cable was developed based on the technologies of these water blocking cables.

3.1 Cable Structure

Based on the demand forecasted for the trunk optical network, we determined that the new trunk optical fiber cable should contain 300 fibers. To satisfy this requirment, we initially proposed both single-slotted rod and multi-slotted rod cables.

The multi-slotted rod cable's diameter is 30 mm, and that of the single-slotted rod is 23 mm. As shown in Fig. 1, the length of the single-slotted rod cable which canl be wound in one drum is 133% that of the multi-slotted rod cable, and we chose the single-slotted rod structure that allows a longer span length during installation. We designed the new single-slotted rod cable as two types: one is a water blocking cable with a metallic strength member, and the other is a non-metallic cable (see Fig. 2).

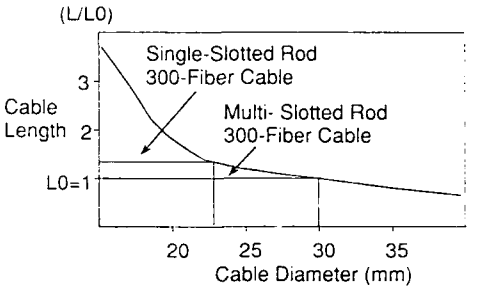


Fig. 1 Relation Between Cable Diameter and Cable Length
(LO : Length of Multi-Slotted Rod 300-Fiber Cable)

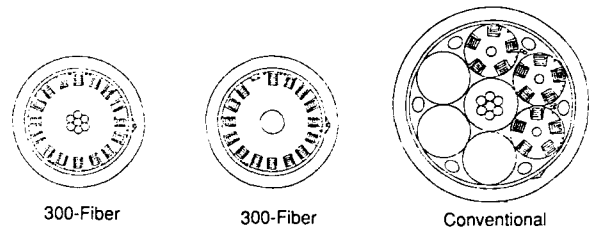


Fig.2 Cross Sectional Structures of Single-Slotted Rod Cable and Multi-Slotted Rod Cable

3.2 Cable Flexibility

The slotted rod diameter of the new cable becomes 120% that of the conventional slotted rod. This may cause an increase in cable rigidity which can create problems during installation or housing accomodation work. To evaluate and compare the new cable rigidity with that of the previous cable, we measured the side force that produces the same cable bending. Fig. 3 shows the set-up for measuring cable rigidity, and Table 1 the results of measurements. The new cable rigidity is lower than the multi-slotted rod subscriber cable, and we therefore regard the new cable as having enough flexibility for commercial use.

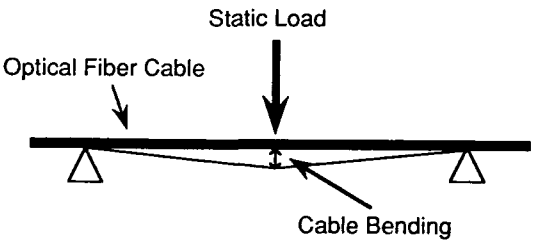


Fig. 3 Cable Rigidity Measurement

3.3 Characteristics of The New Trunk Cable

Optical losses at each stage of the manufacturing process were measured. The losses did not change during the cabling process at both 1.3-μm and 1.55-μm wavelengths for both cable types (see Fig. 4 and 5).

Table 2 shows the characteristics of the new trunk cable in comparison with the conventional 100-fiber water blocking cable. Each item indicates that the new 300-fiber water blocking cable has almost the same properties of the 100-fiber water blocking cable, which again indicates that we can deploy this new cable in trunk optical network.

Table 3 compares the previous 300-fiber water blocking subscriber cable with the new 300-fiber water blocking trunk cables. The new cable has 67% the diameter, 47% the weight and 250% the maximum cable

Table 1 Cable Rigidity

Cables	Cable Sturucture	Ratio of Load
100-Fiber WB Cable	Single Slotted-Rod	1
600-Fiber WB Cable	Multi Slotted-Rod	20
1000-Fiber WB Cable	Multi Slotted-Rod	20
300-Fiber WB Cable	Single Slotted-Rod	6

length of the 300-fiber multi-slotted rod cable. This new 300-fiber single-slotted rod cable can be applied not only for trunk networks but for subscriber loops as well; due to its superior flexibility and light weight.

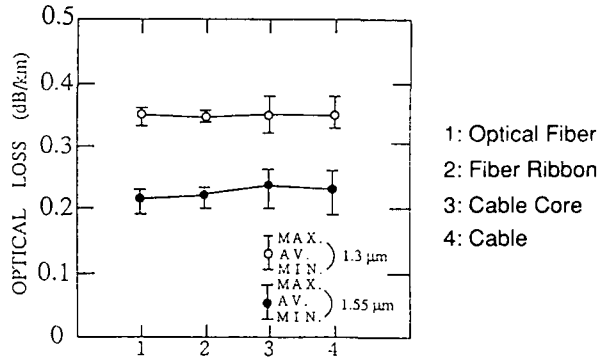


Fig. 4 Optical Loss in Cabling Process (300-Fiber Water Blocking Cable)

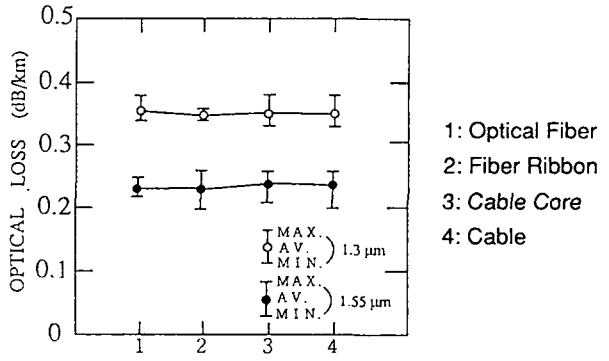


Fig. 5 Optical Loss in Cabling Process (300-Fiber Non Metallic Cable)

Table 2 Test Results of Manufactured Cable

Items		Results of 300-Fiber Cable	Results of 100-Fiber Cable
Optical Loss		<0.36 dB/km	<0.36 dB/km
Change In Loss	Heat Cycle:-30℃ - +60℃	<0.1 dB/km	<0.1 dB/km
	Repeated Bend : IEC 794-1	<0.1 dB/km	<0.1 dB/km
	Crush : IEC 794-1	<0.1 dB/km	<0.1 dB/km
	Torsion : IEC 794-1	<0.1 dB/km	<0.1 dB/km
	Impact : IEC 794-1	<0.1 dB/km	<0.1 dB/km

Table 3 Main Features of Single-Slotterd Rod Cable and Multi-Slotted Rod Cable

Item	300-Fiber Single Slotted-Rod Cable		Conventional 300-Fiber Multi-Slotted Rod Cable
	Water Blocking	Non-Metallic	
Outer Diameter (mm)	24	23	36
Weight (km/kg)	0.52	0.39	1.1
Length in One Drum (km)	4.0	4.0	1.6

4. Trunk Optical Fiber Cable Closure

Along with the 300-fiber single-slotted rod cable, the trunk optical fiber cable closure has also been altered. The main functions of an optical fiber cable closure are to store and protect reinforced fiber splicing points and spare optical fibers. Moreover, a trunk optical fiber closure is required to enable access to individual fiber ribbons with no increase in loss to other fibers. an in-service trunk optical fiber closure must be maintainable without stopping service.

4.1 Closure Structure

Fig. 6 shows the structure of the new trunk optical fiber closure, which consists of three main parts. The first part is a cylinder-shaped waterproof case that also has the function of cable clamping. The second part is the frame in the waterproof case, and the last is protective trays and other fiber protection materials.

4.2 Frame

The frame holds the protective trays and other materials for fiber protection. It also clamps the strength member of cables to protect the fibers from pistoning of the cable core. It can hold a maximum of 44 protective trays. Tray holder have a drawer structure, which makes for easy access to each protective tray.

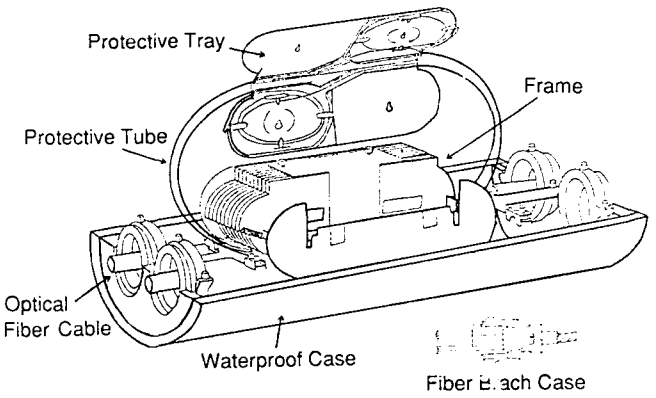


Fig.6 New Trunk Optical Fiber Cable Closure

4.3 Protective Tray

This new protective tray accomodates two 4-fiber ribbons. Excess ribbon and its joint are inserted in two oval spaces provided for each ribbon.

4.4 Fiber Distribution

The unit of fiber distribution is five 4-fiber ribbons inserted in one slot of the cable. Individual fibers branch at the bottom of tray holder. Each fiber is covered with a protective tube or a fiber branch case throughout distribution.

4.5 Characteristics of New Closure

Table 4 compares the old 100-fiber closure and the new 300-fiber closure. The new closure can accomodate over 300 fibers in almost the same space as the old closure. The increase in loss during closure maintenance and cable transfer work was measured; the results are shown in table 5. Maximum increase in loss is small enough to maintain a new closure while in service. Under FITAS, we can transfer a cable at this closure without stopping service.

5. Cable Transfer And Supervisory System

As mentioned above, NTT introduced FITAS I into trunk networks in 1990. Due to the multiplication of trunk optical fiber cables, we developed a new system named FITAS II which can accomodate the new 300-fiber cable.

Table 4 Comparison Between Old and New Closure

Items		Old Closure	New Closure
Protective Tray	Height	90 mm	100 mm
	Length	150 mm	290 mm
	Width	11 mm	5 mm
	Max. Number of 4-Fiber Ribbons	1 (4 Fibers)	2 (8 Fibers)
Closure Frame	Height	140 mm	140 mm
	Length	550 mm	550 mm
	Width	160 mm	220 mm
	Max. Number of Protective Trays	25	44
	Max. Number of Fibers	100	352

Table 5 Increase in Loss Due To Maintenance Work

Maintenance Work	Max. Increase in Loss(dB)
Closure Assembly	0.2
Assembly and Removal of Protective Tray	0.1
Assembly and Removal of Fiber Branch Case	0.2

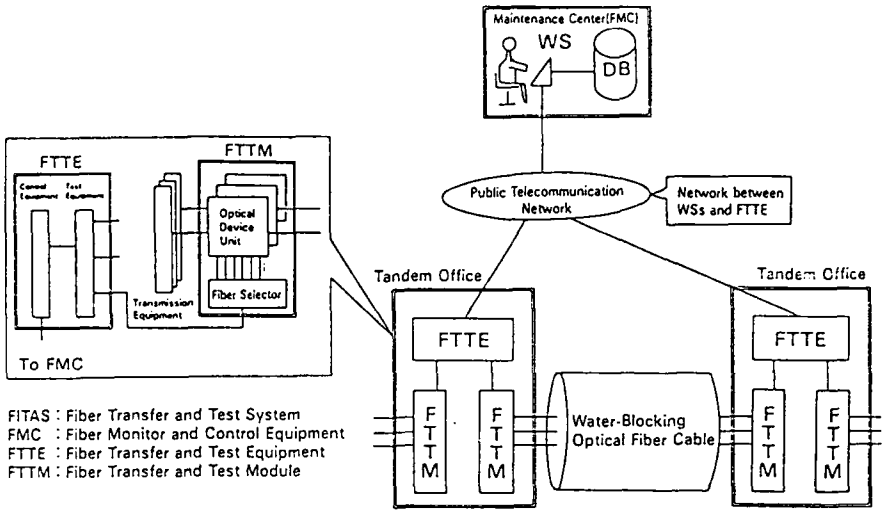


Fig.7 System Configuration of FITAS

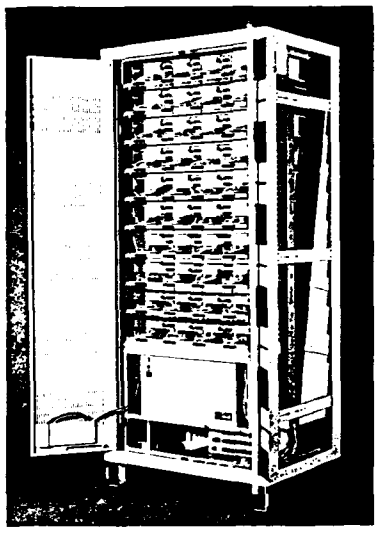


Fig.8 New FTTM

5.1 System Configuration

The system configuration of FITAS is shown in Fig. 7. It consists of three main elements: a Fiber Transfer and Test Module (FTTM), Fiber Transfer and Test Equipment (FTTE), and Fiber Monitor and Control Equipment (FMC). Table 6 compares FITAS I and FITAS II. FTTE has become 10 FTTM controllable by changing operating software. We have newly developed FTTM, which can now accomodate a maximum of 320 fibers.

5.2 New FTTM

A FTTM consists of fiber selectors and optical device units. A fiber selector connects the test equipment in the FTTE with the optical device unit. The optical fiber unit accomodates WDM couplers, filters, and multifiber mechanical switches. It enables the tests and operations with no interruption in services.

To splice fibers in a conventional FTTM, we applied fusion splicing and connectors; in the new FTTM, single and multi-fiber push-on connectors[4] replaces previous splicing equipment. These connectors don't need spare fibers and protective trays for storage; this allows to teminate fibers with higher density. Fig. 8 shows a photograph of the new FTTM.

Table 6 Main system specifications of FITAS

Items	FITAS II	FITAS I
Optical Device Unit	8 Fibers/Unit Maximum	4 Fibers/Unit Maximum
FTTM	320 Fibers	100 Fibers
FTTE	Maximum 10 FTTM Contorollable	Maximum 5 FTTM Contorollable
FMC	Maximum 20 FTTE Contorollable	Maximum 20 FTTE Contorollable

6. Conclusions

(1) A 300-fiber single-slotted rod optical fiber cable has been developed. In comparison with conventional multi-slotted rod cables, the new cable is 67% the diameter, 47% the weight, allowing 2.5 times as much cable length to be wound in one drum.

(2) A trunk optical fiber cable closure which can accommodate more than 300 fibers has developed.

(3) A new version of FITAS (Fiber Transfer and Test System) has been developed. The total amount of fiber in one system is now six times that of conventional systems.

Acknowledgments

The authors are would like to express their sincere appreciation to Mr. T. Uenoya and Mr. Y. Yuuki for their helpful discussion and suggestions.

References

(1) S. Tomita, et al. ,"1000-Fiber Water Blocking Cable" The Transactions of The IEICE, Vol. E73, NO.9, 1990.
(2) Y. Banda, et al. ,"Optical Receiver Adjustment Method Considering Fiber Loss Fluctuation" 1989 Autumn National Convection Record, The Institute of Electronics, Information and Communication Engineers, B-483, 1989.
(3) H. Matumoto et al. ,"Cable Transfer and Supervisory System for Trunk Optical Fiber Cables" 40th IWCS, 1991.
(4) S. Nagasawa et al. ,"A High-Performance Single-Mode Multifiber Connector Using Oblique and Direct Endface Contact Between Multiple Fibers Arranged in a Plastic Ferrule" IEEE Photonics Technology Letters, Vol. 3, No. 10, 1991.



Kenji Yoshioka

NTT Network Systems
Development Center
Tokyo, Japan

Kenji Yoshioka received his B.S. degree from Hokkaido University in 1990. He joined NTT in 1990. He is a engineer in the Telecommunications Cable Systems & Outside Plant Group in NTT Network Systems Development Center.



Naohito Ohno

NTT Network Systems
Development Center
Tokyo, Japan

Naohito Ohno received his B.E. degree in electrical communication from Tohoku University in 1986. He joined NTT in 1986. He is a engineer in the Telecommunications Cable Systems & Outside Plant Group in NTT Network Systems Development Center.



Kiminori Sato

NTT Network Systems
Development Center
Tokyo, Japan

Kiminori Sato received his B.E. degree in electorical engineering from Kyoto University in 1979. He joined NTT in 1979. He is a senior engineer in the Telecommunications Cable Systems & Outside Plant Group in NTT Network Systems Development Center.

He is a member of the Institute of Eectrical and Electronics Engineers, and the Institute of Electronics, Information and Communication Engineers of Japan.



Osamu Yamauchi

NTT Network Systems
Development Center
Tokyo, Japan

Osamu Yamauchi received his B.E. and M.E. degree in electrical communication from Tohoku University in 1978 and 1980, respectively. He joined NTT in 1980. He is senior engineer, superviser in the Telecommunications Cable Systems & Outside Plant Group in NTT Network Systems Development Center.

He is a member of the Institute of Electronics, Information and Communication Engineers of Japan.

ANALYSIS ON SHIFT PHENOMENA BETWEEN CABLE CONSTRUCTING ELEMENTS UNDER EXTERNAL FORCE

Shin-ichi Yonechi

Sumitomo Electric Industries, Ltd.
1, Taya-cho, Sakae-ku, Yokohama, 244, Japan

ABSTRACT

Most of cables from optical fiber to composite cable consist of several longitudinal elements linking each other with friction. The element on which external tension act directly transfers some part of the tension to the neighbor element through the medium of the friction. In this scheme, if the elongation rates are different for two elements, mutual longitudinal shift must be produced. This paper shows the analysis on this shift phenomena with some actual applications and the experimental result which shows good correspondence with this theory. The general design concept useful to control shift phenomena in a cable is also obtained.

1. INTRODUCTION

The theory describing relation between elongation and tension for a solid material had been already established perfectly, and threr is no experimental exception which does not obey the theory. On the other hand, the shift phenomena induced by external tension between two longitudinal elements combining together by friction have not been sufficiently investigated theoretically nor experimentally.
This paper describes trial analysis on this subject. Generally, a cable from optical fiber cable to power cable contains plural longitudinal elements which are supposed to suffer tension. Hence, all cables have a potnetial to generate shift phenomena. Since some cable accidents which seem to be caused by shift between cable elements are actually reported, this theory will be widely applied including the cases of those accidents.

2. BASIC THEORY

In the simple case shown in Fig.1, two elements are linked together by friction. External tension F is acting on the elements "A" at the two points separating with interval of 2Lo. All values for elemtns "A" are denoted with capital letters and for elements "B" with small letters. Longitudinal tension distrbution T(x) and t(x) may take a form shown as Fig.2, where x denotes longitudinal co-ordinate. In the section $[l_1,l_2]$, tension varies in accordance with the equations

$$\frac{dT}{dx}=\sigma \qquad \frac{dt}{dx}=-\sigma$$

where σ denotes frictional force per unit length (kg/m). These relations and the boundary conditions provide concrete expression for T(x) and t(x).
Since the tension is symmetry around the origin, it is sufficient to consider only the portion of x>o. Elongation of "A" and "B" are determined by E(x)=T(x)/K, e(x)=t(x)/k respectively where K or k is tensile elasticity defined by the product of Young's modulus and cross section of the element.

The shift amount between "A" and "B" at point x is given by the following equation.

$$S(x)=\int_0^x \{E(x)-e(x)\}dx$$

This is the basic theory in this paper. If S>O, "A" shifts to the direction of x>0 from "B". The beginning point of shift: l_1 and the ending points of shift: l_2 are also determined from T(x), t(x) and the boundary conditions. If "A" and "B" are cylindrical, σ is the force per unit length needed to pull out each other.

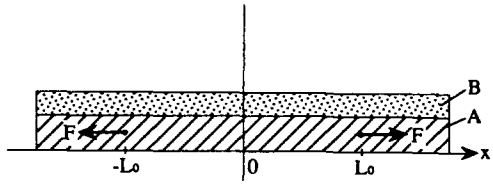


Fig.1 Simplified model

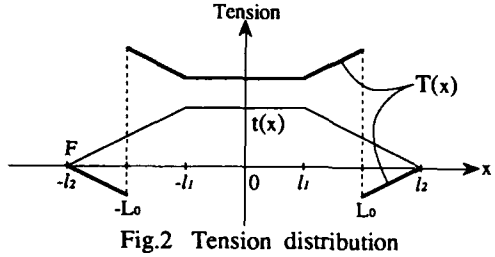


Fig.2 Tension distribution

3. DERIVATION OF FORMULA

Table 1 shows the concrete expressions concerning the model shown in Fig. 1.

Table 1 Concrete expression

	$0 \le x \le l_1$	$l_1 \le x \le Lo$	$Lo \le x \le l_2$
T(x)	$F-\sigma(l_2-l_1)$	$F-\sigma(l_2-x)$	$-\sigma(l_2-x)$
t(x)	$\sigma(l_2-l_1)$	$\sigma(l_2-x)$	$\sigma(l_2-x)$
E(x) - e(x)	$(F/K)-G(l_2-l_1)$	$G(x-l_1)$	$G(x-l_2)$
S(x)	0	$G(x-l_1)^2/2$	$G(l_2-x)^2/2$

In this table, $G=\sigma(K+k)/Kk$.
The conditons: $E=e(0\le x\le l_1)$ and $S(l_2)=0$ determine l_1 and l_2 as follows

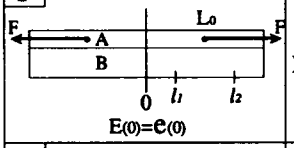
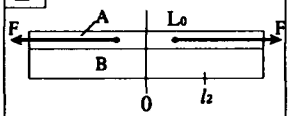
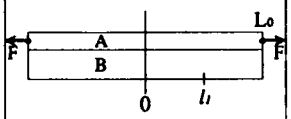
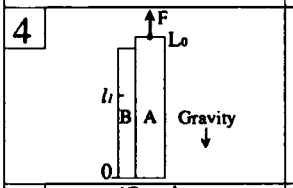
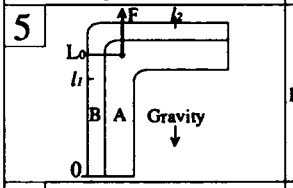
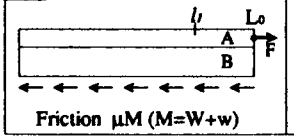
$$L_0-l_1=l_2-L_0=\frac{Fk}{2\sigma(K+k)}$$

Total elongation in the section $[-l_2,l_2]$ is then,

$$\varepsilon=\int_{-l_2}^{l_2}edx=\int_{-l_2}^{l_2}Edx=\frac{2L_0F}{K+k}$$

Table 2 shows the formulas derived by the similar method for various cases including the case of Fig. 1. Besides of $l_1,l_2,S(L_0)$ and ε shown in Table 2, concrete expression of $S(x)$ is also derived for every cases.

Table 2 Formulas for various cases

Case	l_1 (Beginning point of shift)	l_2 (Ending point of shift)	$S(L_0)$	Elongation	Comment
1  $E(0)=e(0)$	$L_0-\frac{Fk}{2\sigma(K+k)}$	$L_0+\frac{Fk}{2\sigma(K+k)}$	$\frac{kF^2}{8K(K+k)\sigma}$	In$[-l_2,l_2]$ $\int Edx=\int edx$ $=\frac{2L_0F}{K+k}$	
2  $E(0)\neq e(0)$	0	$\sqrt{\frac{2kFL_0}{\sigma(K+k)}}$	$\frac{\sigma(K+k)(l_2-L_0)^2}{2Kk}$	In$[-l_2,l_2]$ $\int Edx=\int edx$ $=\frac{2L_0F}{K+k}$	This case appears when $2L_0<\frac{kF}{\sigma(K+k)}$ then $l_2>L_0$
3 	$L_0-\frac{Fk}{\sigma(K+k)}$	Nonexistent	$\frac{kF^2}{2K(K+k)\sigma}$	$\int_{-L_0}^{L_0}(E+\frac{k}{K}e)dx$ $=\frac{2L_0F}{K}$	
4 	$\frac{(\sigma-w)L_0}{\sigma-\nu}$	Nonexistent	$\frac{(K+k)(w-\nu)^2L_0^2}{2Kk(\sigma-\nu)}$ $=\frac{kF^2}{2K(K+k)(\sigma-\nu)}$	$\int_0^{L_0}Edx=\frac{L_0^2}{2K}(W+\delta)$ $\int_0^{L_0}edx=\frac{L_0^2}{2k}(w-\delta)$ where $\delta=\nu+\frac{(w-\nu)^2}{\sigma-\nu}$	$\nu=\frac{Kw-kW}{K+k}$ W: weight per unit length for A (kg/m) w: weight per unit length for B(kg/m)
5 	$L_0-\frac{(w-\nu)L_0}{\sigma-\nu+\sqrt{\sigma(\sigma-\nu)}}$	$L_0+\frac{(w-\nu)L_0}{\sigma+\sqrt{\sigma(\sigma-\nu)}}$	$\frac{(K+k)(w-\nu)^2L_0^2}{2Kk(\sqrt{\sigma}+\sqrt{\sigma-\nu})^2}$ $=\frac{kF^2}{2K(K+k)(\sqrt{\sigma}+\sqrt{\sigma-\nu})^2}$	$\int_0^{l_2}Edx\cong\frac{(W+\nu)L_0^2}{2K}$ $\int_0^{l_2}edx\cong\frac{(w-\nu)L_0^2}{2k}$	The left approximation can be used when $2L_0\cong l_1+l_2$ $L_0^2\cong l_1\,l_2$
6  Friction μM $(M=W+w)$	$\frac{(\sigma-\mu M)L_0}{\sigma-\nu}$	Nonexistent	$\frac{(K+k)(\mu M-\nu)^2L_0^2}{2Kk(\sigma-\nu)}$ $=\frac{kF^2}{2K(K+k)(\sigma-\nu)}$ $F=\mu ML_0$	$\int_0^{L_0}Edx=\frac{L_0^2\delta}{2K}$ $\int_0^{L_0}edx=\frac{L_0^2}{2k}(\mu M-\delta)$ where $\delta=\nu+\frac{(w-\nu)^2}{\sigma-\nu}$	The substitution $W\to0$, $w\to\mu M$ in the case 4 yield these formulas Hence, $\nu=\frac{K\mu M}{K+k}$

4. APPLICATIONS

Several applications of the formulas in Table 2 were examined.

4-1 Cramping of Aerial Cable

Aerial cable are often cramped between 2 poles as shown in Fig. 3. If the curvature in the slack portion is ignored, the case 1 will be applicable. The calculated results for four examples are listed in Table 3.

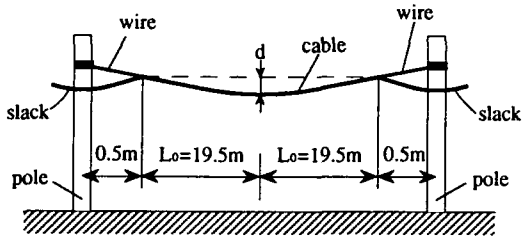


Fig.3 Cramping of aerial cable

(2) If the external messenger wire is cramped, the smaller k of the core the better.

(3) If large k of the core is required for another reason, σ should be large enough correspondingly.

As the pulling end also has possibility of generating shift, it is desirable to connect both core and sheath firmly at the pulling end.

4-2 Optical Fiber

When the coating of optical fiber shown in Fig. 4 is tentioned, shift between silica glass and coating may be induced. Employing formulas of case 1 in Table 2, shift amount is calculated as shown in Table 4.

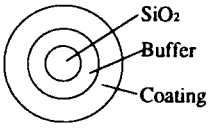
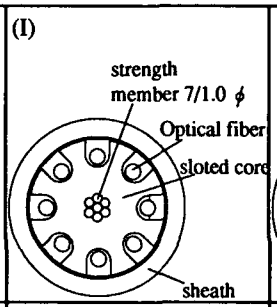
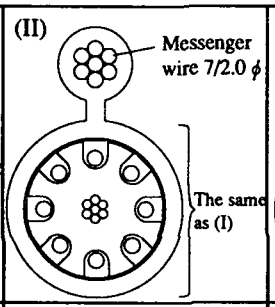
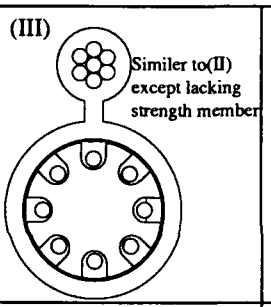


Fig.4 Optial fiber

Table 3 Calculated results for the shift in aerial cable

Cable	(I) 	(II) 	(III) 	(IV) The same as (II) σ is increased
Cramping Portion	Sheath	Messenger wire	←	←
K (kg)	5×10^4	45×10^4	←	←
k (kg)	10×10^4	←	0.2×10^4	10×10^4
Span (m)	40	←	←	←
d (m)	0.5	←	←	←
Cable Weight (kg/m)	0.15	0.35	0.31	0.35
F (kg)	60	140	124	140
σ (kg/m)	5	←	←	50
l_1 (m)	15.5	17	19.45	19.25
l_2 (m)	23.5	22	19.55	19.75
S (Lo) (mm)	1.2	2.0	0.04	0.2

Followings are remarkable points come from the results.

(1) If k of the cable core is large, cramping only the sheath is not preferable.

Those results show that the maximum shift of several hundread μm might occur in the section of several mm around the tensioned point. In the case of optical fiber, k of the silica glass is inherently large, so the σ should have large value.

Table 4 Shift in optical fiber

Item \ Example	I	II
Coating	Nylon	UV resin
Coating dia.	600 μmϕ	400 μmϕ
K (kg)	14.9	3.52
k (kg)	89.8	89.8
σ (kg/m)	60.0	40.0
F (0.5% elongation)	0.52 kg	0.47 kg
$l_2 - l_1$ (mm)	3.7	5.7
S (L0) (mm)	0.03	0.19

4-3 General Concept for Cable Design

A cable generally have plural slidable interfaces between elements. In the case 1 of Table 2, length of shifting section and shift amount are $\lambda = \varepsilon/G$, $S(L_0)=\varepsilon^2/8G$ respectively where $G=\sigma(K+k)/Kk$ and $\varepsilon=F/K$.

Since F, K and k are given, λ and S(L0) are determined by G which depends only on σ. On the base of this consideration, generalized design method for Fig. 5 can be discussed. When G_{ij} and σ_{ij} denote the G and σ between elements i and j, condition $G_{01}=G_{02}$ which will be the consistent design yields

$$\frac{\sigma_{01}}{\sigma_{02}} = \frac{k_1}{k_2} \cdot \frac{K_0+k_2}{K_0+k_1}$$

if $K_0 >> k_1$, $K_0 >> k_2$

$$\frac{\sigma_{01}}{\sigma_{02}} \cong \frac{k_1}{k_2}$$

This implies that the element with larger k should combine tighter with common neighbour element.

In the case of Fig. 6, assuming $G_{12}=G_{23}$ yields

$$\frac{\sigma_{12}}{\sigma_{23}} \cong \frac{k_1}{k_3} \cdot \frac{k_2+k_3}{k_2+k_1}$$

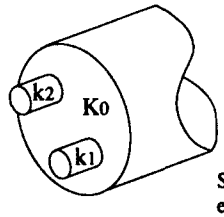
which dictates to followings:

i) if k1 is extra large, σ_{12} should be large

ii) if k2 is extra large, $\sigma_{12}/\sigma_{23} \cong k_1/k_3$

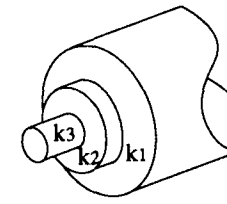
iii) if k3 is extra large, σ_{23} should be large

Taking optical fiber cord as a actural example of Fig. 6, the round values k_1=200kg, k_2=5000kg, k_3=150kg correspond to ii), and result in $\sigma_{12} \cong 1.3\sigma_{23}$. If we use larger k2, we should increase σ_{12} correspondingly.



Suffix denote element's number

Fig.5 Parallel model



Suffix denote element's number

Fig.6 Series model

All results for those consideration commonly guide to the fundamental concept that the element with larger tensile elasticity should be connected more tightly with neighbour element. This concept can be extended to more complicated constructions.

4-4 Vertical Installation

Installing a submarine cable before reaching sea bed is a typical example of vertical installation. An example of submarine cable is shown in Fig. 7 and Table 5. Four states corresponding to case 4 and case 5 in Table 2 are assumed for the calculation of shift in this cable. The calculated results are summerized in Table 6.

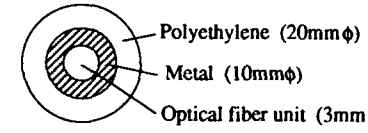


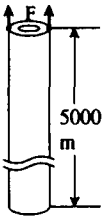
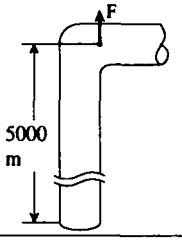
Fig.7 Submarine cable model

Table 5 Characteristic values

Portion	Weight in water	K or k
Polyethylene	- 0.012 kg/m	18900 kg
Metal	0.426 kg/m	994000 kg
Fiber unit	0.0035 kg/m	6500 kg

If $v \ll \sigma$, formulas for S(L0), l_1, l_2 is expressed by very simple form. For example, in the case 5 of table 2, these formulas are approximately expressed by those of case 1.

Table 6 Calculated results for submarine cable

Example	(I)	(II)	(III)	(IV)
State		←		←
Case in Table 2	Case 4	←	Case 5	←
Slidable interface (Assumption)	Fiber Unit / Metal	Metal / Polyethylene	Fiber Unit / Metal	←
W (kg/m)	0.414	- 0.012	0.414	←
w (kg/m)	0.0035	0.4295	0.0035	←
K (kg)	1012900	18900	1012900	←
k (kg)	6500	1000500	6500	←
F (kg)	2088	←	←	←
ν (kg/m)	0.0084	0.0197	0.00084	←
σ (kg/m)	50	500	50	25
S(L0) (m)	0.274×10^{-3}	0.226	0.0677×10^{-3}	0.137×10^{-3}
l_1 (m)	5000 - 0.2665	5000 - 4.1	5000 - 0.133	5000 - 0.266
l_2 (m)	Nonexistent	←	5000 + 0.133	5000 + 0.266

4-5 Installation into a Duct

Formulas for case 6 in Table 2 are obtained by the substitution W→0, w→μM(M=W+w) in the formulas for case 4 in the same Table. Using the formulas for case 6, shift phenomena in a cable which is pulled into a duct can be caluculated. For the cable shown in example (I) of Table 3, the shift at the pulling top end is calculated as follows:

(1) Pulling sheath only
S(L0)=0.0048 (m) l_1=991.97 (m)

(2) Pulling cable core only
S(L0)=0.0012 (m) l_1=995.97 (m)

where the total length is L0=1000m
It is apparent that the element with large tensile elasiticity should be pulled. Of course connecting all elements firmly at the pulling top end is the best way to avoid the shift.

4-6 Shift in Winding Portion

Shift phenomena in the winding portion is much more difficult to analize. In the model shown in Fig. 8, T0 is the initial tension acting on "A" at the origin point. If the shift occurs in the section of [o,l_1], tension distribution will take a pattern shown in Fig. 9. At the point of x=L0, the elements take off the sheave.

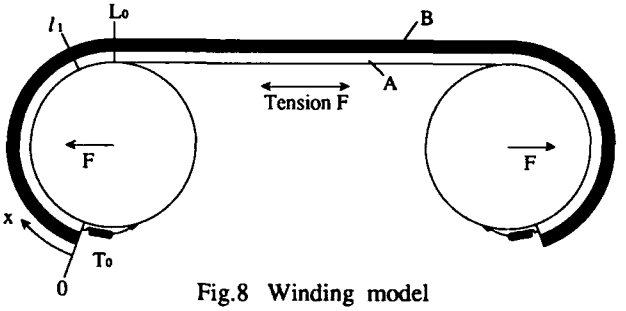


Fig.8 Winding model

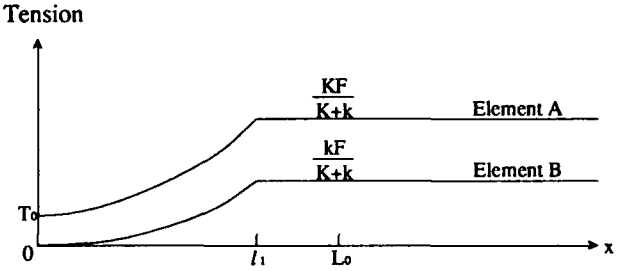


Fig.9 Tension distribution

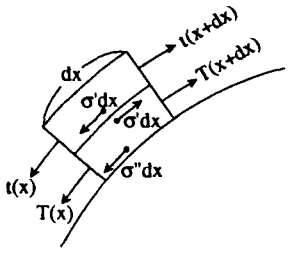


Fig.10 Analysis model

Refering to Fig. 10, frictional forces are expressed as follows:

$$\sigma' = \mu_2(P_0+\frac{t}{R})$$
$$\sigma'' = \mu_1(\frac{T}{R}+\frac{t}{R})$$

where μ_1 and μ_2 are frictional co-efficients and P_0 is the contact pressure in straight state. So $\mu_2 P_0 = \sigma$ implies the pulling out force per unit length if "A" and "B" are concentric. Static balance conditions are expressed by following simultaneous differential equations.

$$\frac{dt}{dx} = \frac{\mu_2}{R}t + \mu_2 P_0$$
$$\frac{dT}{dx} = \frac{\mu_1}{R}T + \frac{\mu_1-\mu_2}{R}t - \mu_2 P_0$$

The solutions are

$$t(x) = \frac{R\sigma}{\mu_2}\left\{\exp(\frac{\mu_2}{R}x) - 1\right\}$$
$$T(x) = T_0 \exp(\frac{\mu_1}{R}x) - \frac{R\sigma}{\mu_2}\left\{\exp(\frac{\mu_2}{R}x) - 1\right\}$$

Since $t(l_1)$,$T(l_1)$ should take the values shown in Fig. 9,

$$l_1 = \frac{R}{\mu_2} ln\left\{1 + \frac{\mu_2 kF}{(K+k)R\sigma}\right\} = \frac{R}{\mu_1} ln\frac{F}{T_0} \quad (1)$$

so that

$$T_0 = \frac{F}{\left\{1+\frac{\mu_2 kF}{(K+k)R\sigma}\right\}^{\frac{\mu_1}{\mu_2}}} \quad (2)$$

are derived.
S(x) is written as

$$S(x) = S(0) + \int_0^x (\frac{T}{K} - \frac{t}{k})dx$$
$$= S(0) + \frac{T_0}{K}\frac{1}{\zeta}\left\{\exp(\zeta x) - 1\right\}$$
$$- \frac{(K+k)\sigma R}{Kk\mu_2}\frac{1}{\eta}\left\{\exp(\eta x) - 1\right\} + \frac{(K+k)\sigma R}{Kk\mu_2}x \quad (3)$$

where $\zeta = \mu_1/R$, $\eta = \mu_2/R$
The boundary condition $S(l_1)=0$ yields

$$S(0) = \frac{FR}{K}(\frac{1}{\mu_2} - \frac{1}{\mu_1}) + \frac{FR}{K\mu_1\left\{1 + \frac{\mu_2 kF}{(K+k)R\sigma}\right\}^{\frac{\mu_1}{\mu_2}}}$$
$$- \frac{(K+k)R^2\sigma}{Kk\mu_2^2} ln\left\{1 + \frac{\mu_2 kF}{(K+k)R\sigma}\right\}$$
$$= \frac{FR}{K}(\frac{1}{\mu_2} - \frac{1}{\mu_1}) + \frac{T_0 R}{K\mu_1} - \frac{(K+k)R\sigma l_1}{Kk\mu_2} \quad (4)$$

Using eq. (1) (2) (3) and (4),l_1,To,S(0) and S(x) can be calculated. If t(Lo)<kF/(K+k), the ending point of shift will extend to l_2(>Lo), therefore the tension distribution will be shown as Fig. 11. As the two values of T(Lo) or t(Lo) calculated by two different equations defined in two different section[0,Lo] and [Lo,l_2] should be the same, l_2 and To are expressed by eq.(5) and eq.(6) respectively.

$$l_2 - L_0 = \frac{kF}{(K+k)\sigma} - \frac{R}{\mu_2}\left\{\exp(\frac{\mu_2 L_0}{R}) - 1\right\} \quad (5)$$

$$T_0 = \frac{F}{\exp(\frac{\mu_1 L_0}{R})} \quad (6)$$

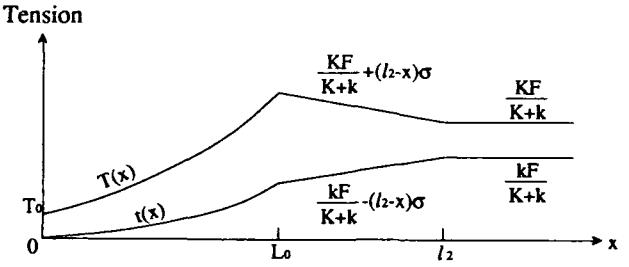


Fig.11 Tension distribution

In the section[0,Lo], S(x) takes the same form as eq.(3). In the section [Lo,l_2], the shift is

$$S(x) = S(L_0) + \frac{(K+k)\sigma}{2Kk}\left[(l_2-L_0)^2 - (l_2-x)^2\right]$$

The boundary condition $S(l_2)=0$ leads to

$$S(L_0) = -\frac{(K+k)\sigma}{2Kk}(l_2-L_0)^2 \quad (7)$$

so that

$$S(x) = -\frac{(K+k)\sigma}{2Kk}(l_2-x)^2 \quad (8)$$

Since S(Lo) calculated by eq.(3) and (7) should be the same value,

$$S(0) = \frac{FR}{K}\left[\frac{1}{\mu_2}\left\{\exp(\frac{\mu_2 L_0}{R}) - 1\right\} + \frac{1}{\mu_1}\left\{\exp(-\frac{\mu_1 L_0}{R}) - 1\right\}\right]$$
$$- \frac{kF^2}{2K(K+k)\sigma} - \frac{(K+k)R^2\sigma}{2Kk\mu_2^2}$$
$$\times\left\{\exp(\frac{2\mu_2 L_0}{R}) - 4\exp(\frac{\mu_2 L_0}{R}) + \frac{2\mu_2 L_0}{R} + 3\right\} \quad (9)$$

S(x) in [o,Lo] is calculated from eq.(9) and eq.(3), on the other hand in [Lo,l_2], eq.(8) gives S(x). If l_2=Lo, both equations give the same value of S(Lo)=0. This particulaer situation apears when F=Fc: where

$$F_c = \frac{(K+k)\sigma R}{k\mu_2}\left\{\exp(\frac{\mu_2 L_0}{R}) - 1\right\} \quad (10)$$

As a practical example, the calculated results for nylon coated optical fiber are shown in from Fig. 12 to Fig. 17.
Fig. 12,13,14 and 15 show l_1,l_2,To,S(0),S(Lo) when F varies. Fig. 16 and Fig. 17 show T(x), t(x) and S(x) when F is fixed at 3 kg(>Fc). This fiber has 600μmφ diameter of nylon coating, and 125μmφ diameter of silica glass and values nesessary for calculation are as follows:

K=15kg , k=90kg , μ_1=0.5 , μ_2=0.2 , R=0.05m
σ=10kg/m , Lo=0.157m(half circle).

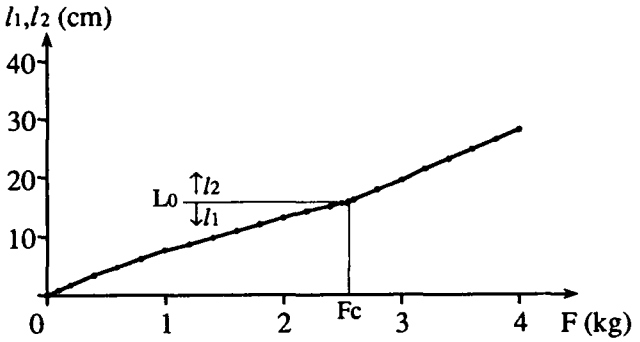


Fig.12 F vs. l_1 or l_2

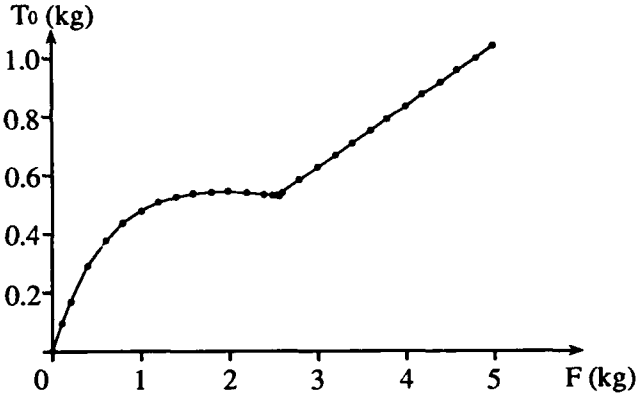


Fig.13 F vs. To

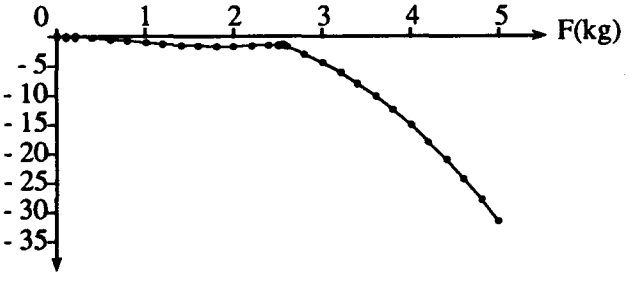


Fig.14 F vs. S(0)

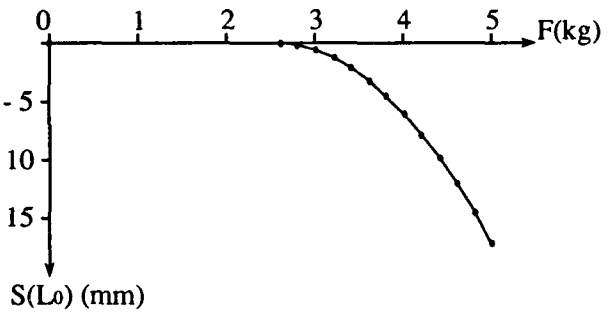


Fig.15 F vs. S(Lo)

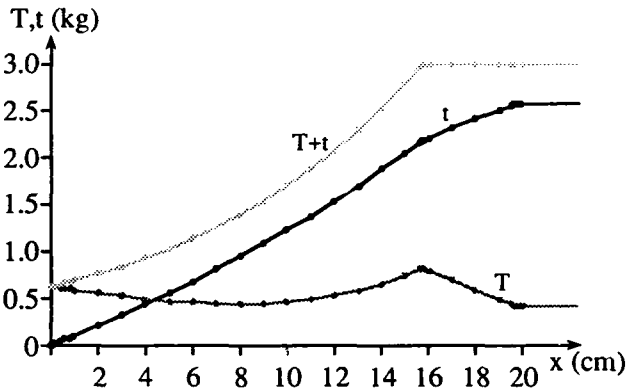


Fig.16 Longitudinal tension distribution when F=3kg

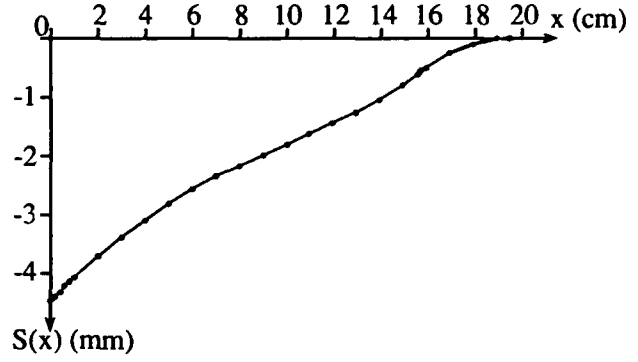


Fig.17 S(x) when F=3kg

Here, σ and μ_2 are assumed so as to exist l_2(>Lo) when F>Fc which is 2.55kg in this case.

5. EXPERIMENT

In the experiment, 0.9mmφ nylon coated optical fiber was wound on the sheave with 15cmφ dia. by half turn. The shift occurs at the interface between nylon and silicone resin buffer layer of which diameter is 0.4mmφ.

S(0) was measured varying the tension F in the range from 0 to 3kg which dose not go beyond Fc=5,37kg. The schematic view of the experiment is illustlated in Fig. 18. The values needed for theoretical calculation are as follows:

K=50kg , k=90kg , μ_1=0.16 , μ_2=0.32 , R=0.075m
σ =8.5kg/m , L_0=0.2356 m (half circle)
The measured values and calculated values are shown in Fig. 19. Both values are approximately coinside with each other showing varidity of this theory.

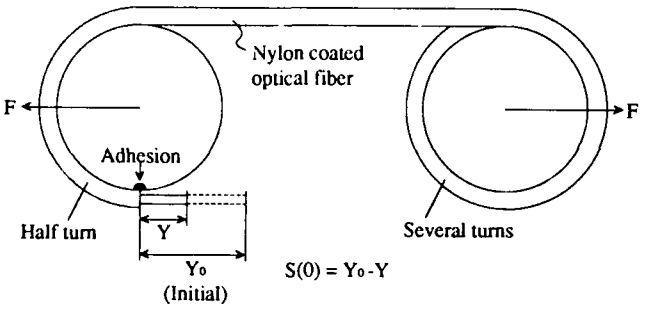


Fig.18 Outline of the experiment

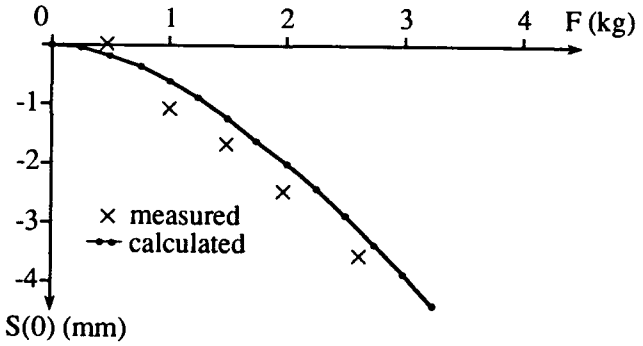


Fig.19 Experimental result

6. CONCLUSION

This paper describes analysis on shift phenomena between to elements contained in a cable and derives several formulas useful for practical calculation. Generally, followings are effective to decrease shift amount.

(1) External tension should act first on the element which has large tensile elasticity.

(2) The neighbour element is preferable to have small tensile elasticity.

(3) If the neighbour element is required to have large tensile elasticity for another reaseon, frictional link between both elements should be large enougth.

On the contrary, weak linkage between two elements which have both large tensile elasticity is most likely to occur shift phenomena. Although these concept is understandable to some extent from experiences in manufacturing and handling cables, exact understanding of this phenomena could be clarified by this analysis. This theory will be widely applied to varieties of problems which relate to shift phenomena in cables.



Shin-ichi Yonechi
Sumitomo Electric
Industries, Ltd.
1, Taya-cho,
Sakae-ku
Yokohama 244, Japan

Shin-ichi Yonechi received a B.S. in 1966 from Tohoku University. He joined Sumitomo Electric Industries, Ltd. in 1971, and had been engaged in research and development of communication cables. He is now chief engineer in the Fiber Optics Division. He is a member of the Institute of Electronics, Information and Communication Engineers of Japan.

CHARACTERISTICS AND APPLICATIONS OF A NON-METALLIC, WATERPROOF, NON-HALOGEN FLAME-RETARDANT OPTICAL WIRE WITH AN ELLIPTICAL CONSTRUCTION

T. Amano*, H.Horima*, K. Fukuoka**, T. Yamazaki**

*Sumitomo Electric Industries,Ltd.,
**Tsushin Kogyo Electric Wire & Cable Co. Ltd.

1. Abstract

In FTTH (fiber to the home), the most significant target of public communications, an ultra high density multi fiber cable has been developed which accommodates more than 1,000 cores of optical fiber.① The small core fiber cable for dropping and wiring to each household, on the other hand, has been making remarkable progress, too. In addition, the application range of optical fiber has been extending over the field of various sensors. A fiber-optic distributed temperature sensor has been developed by utilizing the dependency of the optical fiber's Raman back-scattered light. And the optical fiber cable for this sensor has been studied continuously. In particular, an ultra-high voltage power cable is being applied more and more to temperature monitoring, fault monitoring and position detection systems. Recently, We have developed and evaluated, a small-sized, optical cable, which is oval in shape and can be applied to such a wide range of uses.

2. Introduction

Optical fiber has been achieving remarkable development in the field of communications making effective use of its low attenuation and large capacity. In recent years, research has been actively pursued to apply the optical fiber itself as a sensor, resulting in a remarkable expansion of its application range.

In the public communications field, progress has been made in 1.55 μm band transmission long-distance large-capacity communications with dispersion-shifted fiber and a fiber amplifier applied. On the other hand, a subscriber system optical linkage technology has been researched continuously and an ultra-high density multi-fiber cable mainly aimed at FTTH with more than 1,000 cores has also been developed. And studies are being vigorously made on small-core optical cable for dropping and wiring to each subscriber as a important technology for FTTH.

important technology for FTTH.

On the other hand, as an example of the application of optical fiber to sensors, a fiber-optic distributed temperature sensor has been progressively applied in many fields, which permits us to determine a temperature range of -150°C through +300°C, utilizing the dependency of the Raman back-scattered light intensity of optical fiber's upon temperature.

Figure 1 shows a fiber-optic distributed temperature sensor system configuration. Storks light and Anti-Storks light, two components of the Raman back-scattered light in optical fiber, have their respective intensities varied, depending upon temperature. With the laser incident to the optical fiber at one end, the Raman back-scattered light returned over the optical fiber width is determined by application of OTDR (optical time domain refractometry), thereby determining the temperature.

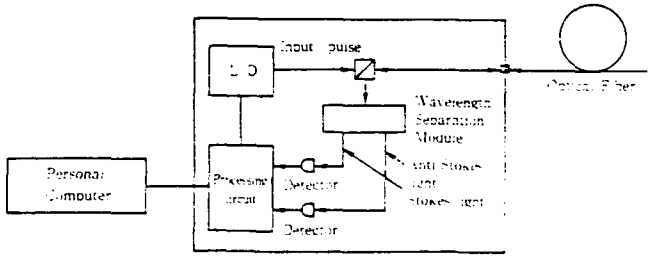


Fig.1 Fiber-Optic Distributed Temperature Sensor System

This sensor is to determine the scattered light of optical fiber itself. It is capable of determining temperatures longitudinally in succession. In the electric power field, in particular, attention has been paid to two points: one is that the optical fiber applied distribution type temperature sensor be non-metallic and the other that it be capable of determining a longitudinal succession of temperatures. As a result, studies have been made concerning the feasibility of applying this system to the establishment of a maintenance system, which permits us to monitor an ultra-high tension power cable temperature regularly, to detect a failure point in the event of fault, and to assess the magnitude of such a fault promptly.

The author et al. have developed an oval-shaped, small-sized, non-metallic, non-halogenized and flame-retardant optical cable, which has a wide enough range of applications to cope with such an expansion of the application optical fiber as referred to above.

3. Required Characteristics

In an optical subscriber cable network, the optical drop wire, optical indoor cable and optical cable for LAN are installed through a variety of wiring roots, such as an aerial root from power transmission cable posts, underground root leading into households by use of a existing duct, etc. and in-door piping and undercarpet, etc. Such optical cable is required to be small-sized of flexible construction and low cost. With an underground root assumed as an environment resistance requirement, moreover, the optical cable is called upon to be waterproof, and flame-retardant with consideration given to household-oriented wiring disaster prevention. Besides, a non-metallic construction is also required in the sense of both insulation and safety.

The distributed temperature sensor, on the other hand, has been having its applicability studied as a sensor for monitoring power cable temperature regularly and to detect a failure point in the power cabling. Regularly monitoring of power cable temperature would not raise any special problem since a power cable changes temperature gradually. If however, a fault such as grounding accident or the like, is detected, the optical cable's temperature follow ability relative to a temperature change of a determined object will turn out to be a key point since such a fault is accompanied by a slight degree of temperature change and is local as well. As a result, the optical cable is required to have an excellent level of radiated heat absorption efficiency and a low thermal capacity, that is , a delicate construction of high mountability onto any determined object.

A tunnel or the like could turn out to be the installation environment of the optical cable. Nevertheless, the tunnel may be internally flooded with water. The optical cable, therefore, is required to have a water-proof and flame-retardant construction for disaster prevention as well.
Moreover, with consideration given to the effects of electromagnetic induction, etc., the optical cable is desired to have a non-metallic construction from a safety point of view.

4. Cable Construction

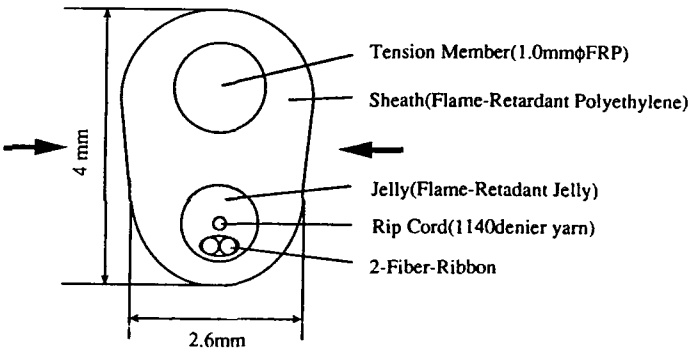


Fig.2 Cable Construction

As far as the cable construction is concerned, a study was made, with consideration given to the conformability to a change in temperature and to ease of handling in wiring work.

To improve the radiated heat absorption efficiency, a ideal optical cable should have a section shaped into a rectangle from a contact area point of view. From an adherence point of view, however, a round shaped is more advantageous in terms of flexibility. As shown in Figure 2, therefore, the cable was designed into an elliptic shape constructed to be highly workable in wiring and efficient in absorbing radiated heat, with the characteristics of both the rectangular and round shaped. Moreover, this design shows excellent crush characteristics, for loading on the tension member in relation to a lateral load (indicated with arrows in Figure 2).

Considering that not only the outer jacket material but also the fitting compound should be flame retardant, a flame retardant jelly[2] has been applied. On the supposition that it is mounted onto a high-tension power cable, the optical cable has adopted a non-metallic construction from a safety point of view, with an FRP tension member applied. And this optical cable is also designed the two ϕ250 μm UV-cured fibers or a 2-fiber-ribbon[3] can be built in together with a rip cord made of aramid yarn. Photo 1 shows sectional view of a 2-fiber-ribbon built-in optical cable actually manufactured. This cable is of a low-cost-oriented design, produced by a single process.

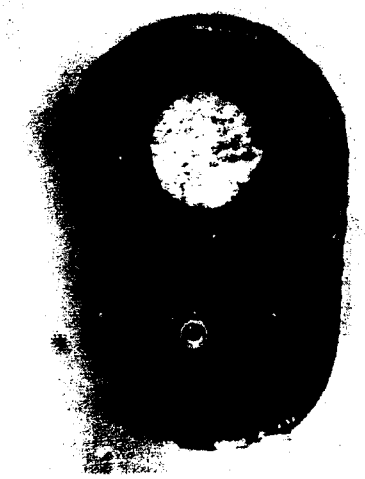


Photo 1 Cross Sectional View of Optical Cable

5. Compact Jelly Filling Facility

To fill a sufficient amount of jelly into the small-sized cable core designed as reported herein, the author et al. developed a compact jelly filling facility, too. figure 3 shows the configuration of the facility developed. This compact jelly filling facility is composed of a cylindrically shaped jelly feeder vessel, a rotary disc with controllable speed, a squeezing die and a recipient.

The jelly feeder vessel and the rotary disc are provided with a clearance of 1 or 2 mm. The optical fiber, and the rip cord are led into the cross head of the extruder, the main device for cabling passing through the squeezing die by way of that clearance.

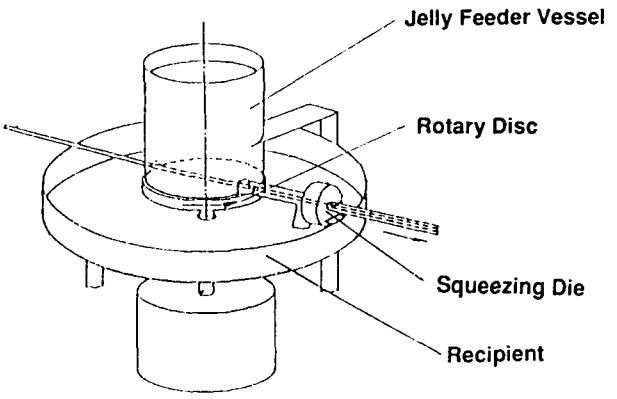


Fig.3 Compact Jelly Filling Facility

The jelly in the jelly feeder vessel is fed into the lower clearance by a weight placed thereon in addition to the gravity of the jelly itself. As a result, the disc rotates so that the jelly will stick to the fiber. The quantity of jelly sticking to the fiber varies with its viscosity, feedrate (drop speed), disc turning rate, and fiber-passing speed. A desired quantity of jelly may be continuously obtained by selecting the disc turning speed, weight load, clearance breadth and so on. In addition, the jelly which has stuck to the fiber is squeezed into an appropriate quantity while passing through the squeezing die. After the jelly is simultaneously formed into an appropriate shape, it is extruded together with the tension member and made into a cable.

The compact jelly filling facility permits the jelly to be filled longitudinally and uniformly into a small-sized optical cable. Photo 2 shows the jelly filling facility actually developed.

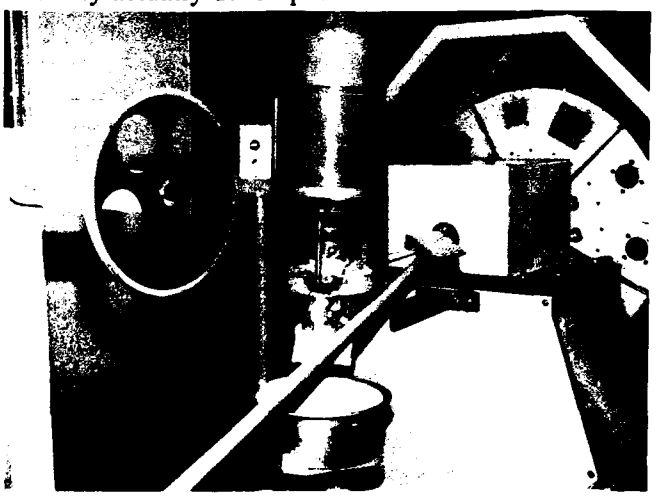


Photo2 View of Compact Jelly Filling Facility

6. Characteristics of Optical Cable

The extremely flexible, elliptically shaped, small-sized, non-metallic , non-halogenized and flame-retardant optical cable recently designed as shown in figure 2 was actually manufactured and evaluated for its characteristics. Results involved are described below.

6.1 Transmission Characteristics

Both GI SM ϕ250 μm UV cured fiber and 2-fiber ribbon were manufactured. For GI and SM fibers were evaluated at 1.3 μm and 1.5 μm, respectively.

From the evaluation of loss variation during the process, GI and SM showed loss variations stabilizing at 0.04 dB/km or less and 0.02 dB/km or less, respectively. From this, it may be gathered that the loss variation during the process is scarcely affected by a difference in the fiber coating structure of the optical fibers.

6.2 Mechanical Characteristics

With application as a temperature sensor for the power cable taken into consideration, the optical cable was required to have an especially small-sized, highly flexible construction. For flexibility, the optical cable was studied concerning the directionally of bend and bendability with a load applied, as shown in Figures 4. From this, it may be gathered that the optical cable has no directionally of bend and good bendablity. With wiring workability taken particularly into account, the optical cable was designed with special attention paid to crush characteristics, which showed an excellent value as shown in Figure 5. Other mechanical characteristics obtained are summarized in Table 1, showing satisfactory values for the construction proposed herein.

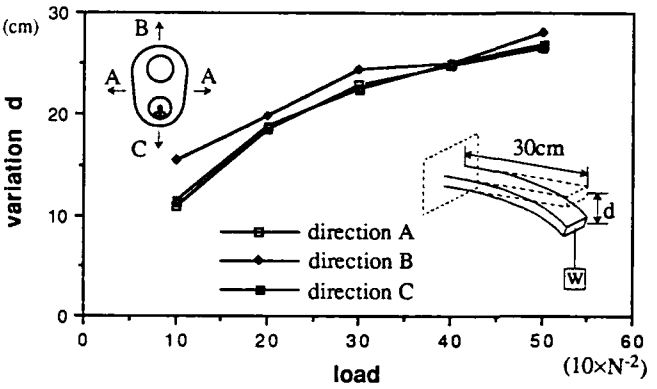


Fig.4 Result of Flexibility Test

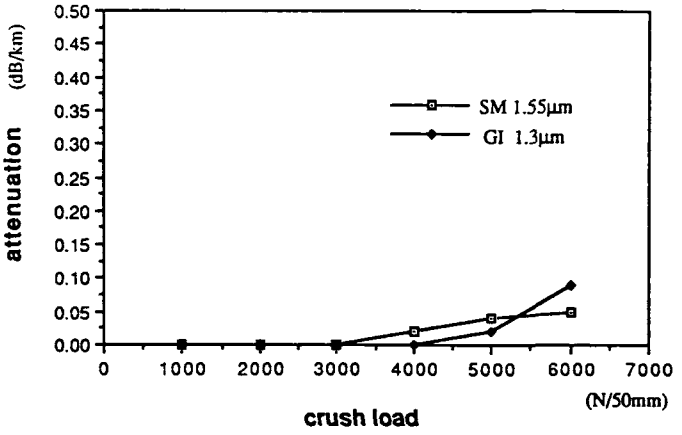


Fig.5 Crush Characteristics

Table 1 Mechanical Characteristics of the Optical Cable

Item	Test conditions	Test results	
Tensile performance	T ◄——► T	SM 1.55μm GI 1.3μm	at T<300N No loss increase
Crush	W Flat plate 50 mm wide	SM 1.55μm GI 1.3μm	at W<3000N/50mm No loss increase
Mandrel winding	d	SM 1.55μm GI 1.3μm	at d>60mm No loss increase
Impact	W, 1m A cylinder (25mmφ) is dropped onto 10 different spots	SM 1.55μm GI 1.3μm	at W=500g No loss increase

6.3 Temperature Characteristics

For temperature characteristics, GI and SM were studied concerning 1.3 and 1.55 μm, respectively. Results involved are as shown in Figure 6. Any of these values pose no problem in the practical use of the optical cable.

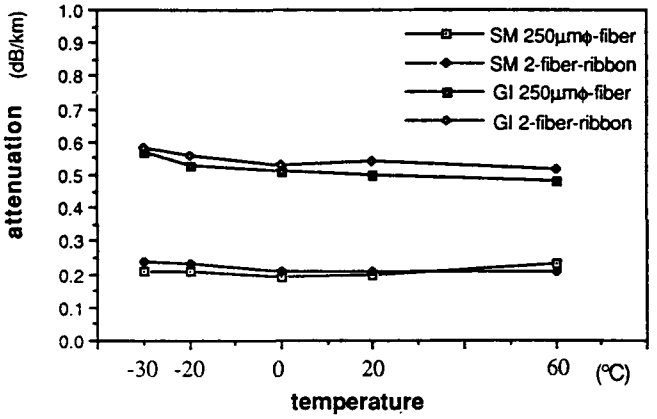
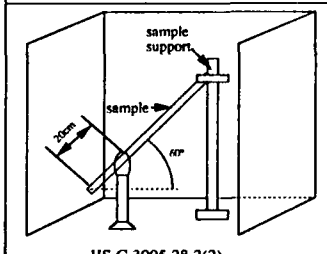


Fig.6 Temperature Characteristics

6.4 Flame Retardancy

A flame retardant test was conducted in accordance with JIS C 3005 28.2 (2). Table 2 shows the related test method and results, demonstrating sufficiently satisfactory characteristics. Moreover, even if it is mounted on the power cable applicable to the vertical tray method subject to the IEEE383 2.5, the optical cable was also verified not to adversely affect the flame retardancy of the power cable.

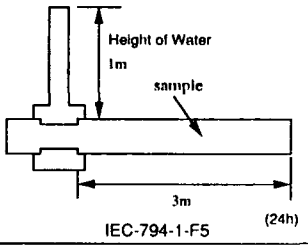
Table 2 Result of Flame RetardancyTest

Test Condition	Result
	No spread of flame

6.5 Water Proofness

A water-proof test was conducted in accordance with the IEC-794-1-F5. Table 3 shows the related test method and results. From these results, it could be verified that the optical cable could be installed in a tunnel, underground duct, etc.

Table 3 Result of Water Penetration Test

Test Condition	Result
	No Penetration

7. Characteristics as a Temperature Sensor

As referred to above, the optical cable proposed showed satisfactory characteristics while being capable of accommodating two fibers or a 2-fiber ribbon. Thus, it could be confirmed that the optical cable was applicable to the FTTH as a dropping cable.

Subsequently, therefore, the optical cable was checked to verify its characteristics as a temperature sensor. In this case, an evaluation was made on GI fiber whose Raman back-scattered light was stable and easy to determine. Figure 7 shows the results of determining temperatures in environments with locally given temperature difference of 50 °C distribution on a spectrum analyzer. From the results, it may be gathered that the optical cable proposed herein is applicable as an ordinary thermometric sensor. In addition, testing was conducted to detect a grounding fault in a power cable. Figure 8 shows the results of determining a change in temperature with regards to the proposed optical cable when the power cable suffered from a grounding fault. The optical cable detected a temperature rise of 4 or 5 °C relative to the grounding fault which had taken place. Thus, it could be verified that the optical cable proposed herein is applicable as a grounding fault sensor, as well.

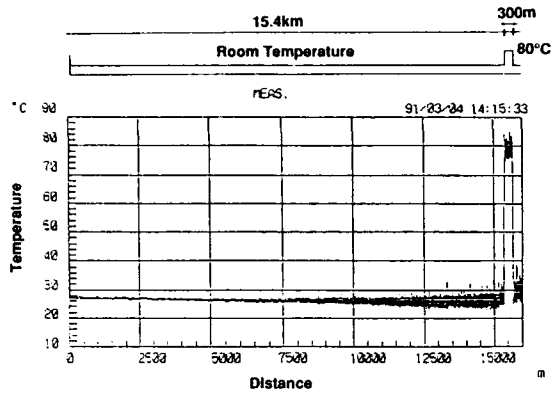


Fig.7 Measurement of Temperature

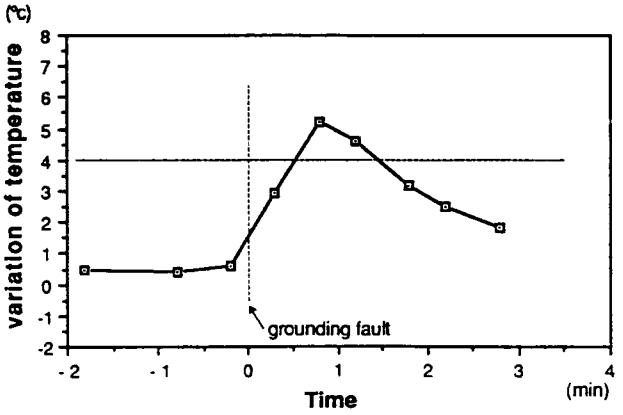


Fig.8 Determination of Temperature Variation

8. Conclusion

We designed, fabricated, and evaluated an oval, small-diameter, non-metallic, waterproof and non-halogenized flame-retardant optical cable that can be easily used for dropping to the home, or for wiring in a duct, or for wiring under carpets in the home and can be easily mounted to the object to be measurement as a part of a distributed temperature sensor.

As a result, it has been revealed that the oval optical cable we have developed has adequate temperature characteristics, transmission characteristics, mechanical characteristics, waterproofness, and flame retardancy together with temperature following characteristics when applied to distributed temperature sensors.

The results of this evaluation prove that this cable can be applied to the fields mentioned above without any practical problem.

References

① S. Tomita, M. Matsumoto, T. Yabuta and T. Uenoya, "Preliminary Research into Ultra High Density and High Count Optical Fiber Cables", 40th I.W.C.S., pp8-15, (1991).

② H. Horima, K. Niikura, N. Akasaka, T. Yamanishi:"Development of Flame Reterdant Halogen-Free Jelly-Filled Non-Metallic Optical Cable", 38th I.W.C.S.pp295-300, (1989).

③ N. Okada, A. Mogi, N. Misono, T. Hayakawa, M. Miyazaki, M. Kurokawa and K. Niikura, "A SZ slot Ribbon IBER Cable for Subscriber Network", 38th I.W.C.S., pp155-161, (1989).



Tsuguo Amano
Sumitomo Electric
Industries, Ltd.
1, Taya-cho,
Sakae-ku,
Yokohama 244, Japan

Tsuguo Amano received the B.E. degree in engineering from Keio University in 1987 and jointed Sumitomo Electric Industries, Ltd. He has been engaged in design and development of optical fiber cables. He is now an engineer of Fiber Optics Division. He is a member of the Institute of electronics, Information and Communication Engineers of Japan.



Koichiro Fukuoka
Tsushin Kogyo Electric
Wire & Cable Co., Ltd.
2-14-2, Tsukiji, Chuo-
ku, Tokyo 104, Japan

Koichiro Fukuoka graduated from Kawagoe Agricultural High School in 1951. He jointed Tsushin Kogyo Electric Wire and Cable Co. Ltd. in 1954. He has been engaged in design , and development of product engineering of communication cables. Thereafter, concentrated on the development of product engineering of optical cables. He is now Manager of Fiber Optics Development Office.



Hiroaki Horima
Sumitomo Electric
Industries, Ltd.
1, Taya-cho,
Sakae-ku,
Yokohama 244, Japan

Hiroaki Horima received the M.S. degree in engineering from Osaka University in 1972. He then joined Sumitomo Electric Industries, Ltd. and worked on the development of CATV coaxial cables, multipair PEF-insulated junction cables and low loss unbalanced type cables. Thereafter, concentrated on the development of optical fiber cables. He is now Manager of the Fiber Optics Engineering Department of Fiber Optics Division at Sumitomo Electric Industries, Ltd. He is a member of the Institute of Electronics, Information and Communication Engineers of Japan.



Tsuneo Yamazaki
Tsushin Kogyo Electric
Wire and Cable Co., Ltd.
2-14-2, Tsukiji,
Chuo-ku, Tokyo
104, Japan

Tsuneo Yamazaki received the B.E. degree in engineering from Toyo University in 1977 and jointed Tsushin Kogyo Electric Wire and Cable Co. Ltd. He has been engaged in development of product engineering of optical cables and connectors. He is now Sub Manager of Fiber Optics Development Office.

FLEXIBLE ARCHITECTURE AND PLANT FOR OPTICAL ACCESS NETWORKS

S Hornung P Frost J Kerry J Warren

BT Laboratories, Martlesham Heath, IPSWICH, IP5 7RE

Abstract

In the UK, BT's copper access network is predominantly underground cable housed in preinstalled ducts. Flexibility is provided at two points on route to the customer; firstly, at street side cabinets serving up to 600 lines; and secondly, at distribution points serving around 10-15 lines. In total BT has about 250,000km of underground duct, 83,000 cabinets, 3.1 million distribution points and 3.7 million manholes and joint boxes.

In progressing towards a fully fibred network exploitation of this valuable infrastructure is essential and this paper examines a process for economic role out of a thin fibre overlay with high resilience and a future proof capacity.

1. Fibre Access Philosophy

The ultimate goal is a fixed, resilient, transparent optical access network, with capacity for all foreseeable service requirements. The aim must be to create a fully managed fibre network in the form of a thin widespread overlay for the whole access topography. Such a network can be equipped as the need arises and thereby results in capital expenditure savings, since the major part of the investment will be the provision of terminal equipment on a 'just in time' basis. The design and management concepts should enable the rapid provision of extra lines to new or existing customers, and flexible provision or reconfiguration of telephony services. Continuous monitoring of the health of the whole system will be essential, to make service, fault free and transparent to the customer.

In order to be completely future proof the network should be single mode optical fibre, with no bandwidth limiting active electronics within the infrastructure. Consequently, only passive optical networks which can offer this total transparency and complete freedom for upgrade, should be considered.

The most common passive optical network (PON) is the simplex single star, with point to point fibre for each transmit and receive path, from the exchange head end (HE), and the customer network terminating equipment (NTE). This network design has been used throughout the world and by BT [1] and meets all the access criteria. It involves high fibre count cables and unique electro-optic provision at HE and NTE for each customer. The resulting inherent cost can only be justified for large business users, who generally also require the security of diverse routing, which increases the cost still further.

The advent of optical splitters, based on fused fibre [2] and the ability to make wavelength flattened devices, demonstrated by BT in 1985, [3] has enabled the concept of the PON to be taken one step further. These passive components allow the power transmitted from a single transmitter device to be distributed amongst several customers, thereby reducing and sharing the capital investment. In 1987 BT has demonstrated splitter technology in a system for telephony on a passive optical network (TPON) with a 128 way split and using time division multiplex (TDM) running at 20Mb/s [4]. This combination enabled basic rate integrated service digital network (ISDN) to be provided to all customers. In practice, the competitive cost constraint of the existing copper network, precludes domestic customers from having just telephony over fibre, due to the high capital cost of equipment. However, telephony for small business users, with >5 lines can probably break this barrier.

The wider range of service and higher capacity required by business customers makes a 32 way split more attractive for a 20 Mb/s system and this has been demonstrated by BT's local loop optical field trial (LLOFT) at Bishop's Stortford, [5] [6].

The additional digital capacity available at each NTE with this lower split level, enables the customer to be offered a wide range of service options. These would typically be single channel telephony (POTS); ISDN 2; ISDN 30; Megastream; Kilostream and Analogue private circuits (PC's). Each NTE would have capacity for 1 Megastream (2Mb/s) plus 30 POTS channels or equivalent.

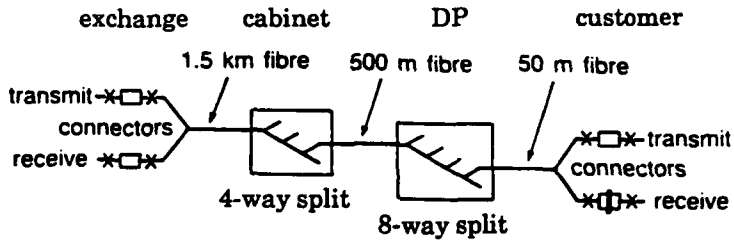


Figure 1. The 32 way PON used by BT for LLOFT

Achieving this level of flexibility implies a complex time management process and the TPON bit transport system (BTS) [7] enables any number of the 240 available 64 Kbit/s time slots, from any of the 8 connected 2 Mb/s exchange ports at the HE, to be allocated to any customer terminal, to suit demand; and this choice can be reconfigured in seconds from customer service desks. This ensures that all 2Mb/s ports are efficiently utilised. Additionally, time delay in the network return paths and the amplitude of each NTE laser power level is monitored and controlled by the HE equipment, to ensure perfect matching and multiplexing of the return signals. This monitoring feature also offers a powerful diagnostic tool for supporting maintenance, equipment health and fault location; giving advanced warning of problems and thus enabling quality of service standards for above those currently available.

In summary, the use of splitter based PON architecture will reduce the cost of fibre deployment in the access network. When compared with point-to-point fibre, savings will result form:-

- reducing the number of fibres at the exchange and in the network.
- reducing the amount of terminal equipment at the exchange
- sharing the cost of equipment amongst a number of customers
- providing a thin, widespread, low cost, fibre infrastructure
- providing a high degree of flexibility and allowing 'just in time' equipment and service provision.

Additionally, PON architecture can be tailored to suit the existing infrastructure resources (duct and other civil works).

2. Achieving the Goal

Total network transparency retains the option for future services to be provided on different wavelengths to the telephony band, which for TPON is in the 1300nm window. By transmitting at other wavelengths, other services, such as broadband access for cable television and high definition TV, or business services, such as high bit rate data, video telephony or video conferencing, can be provided. The huge bandwidth potential of fibre promises virtually unlimited capacity for the transparent network. Eventually it will be possible to transmit hundreds of wavelengths simultaneously, as the development of technology in optical components such as, narrow band lasers, wavelength division multiplexers (WDM'S), optical filters, fibre amplifiers and tunable devices, moves forward.

For this potential to remain available and for the access network to be used to provide many and varied services, the network must be designed and engineered to provide very high levels of security and resilience. Even for simple POTS, advance warning and live maintenance are essential to limit disruption; these have been demonstrated with TPON [8].

Resilience implies diverse routing, and exploiting the existing infrastructure of underground ducts and other civil works is a prime requirement of the design philosophy. Analysis of this resource has indicated that diversity, from creating primary ring topographies, could be achieved by linking the spine cables which currently feed many primary connection points (PCP's) in the existing star type network. This would allow the generic PON architecture shown in Figure 2. The route lengths shown are typical of the majority of BT's local networks.

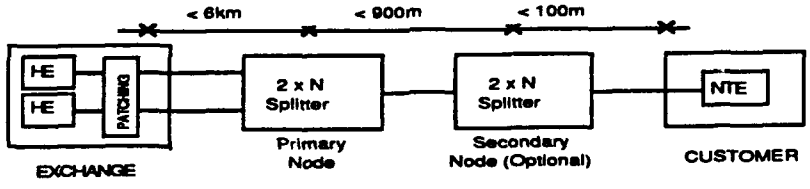


Figure 2. PON with distributed split and primary route diversity.

Figure 2 also shows duplication of the HE opto-electronic equipment. This simple solution is preferred to alternatives which add complexity, for instance the use of optical fibre switches, as it reduces the component count and gives increased reliability from duplication of essential high risk components.

In order to create rings from the existing star configurations some localities will have existing ducts that will allow the link cables to be installed. In BT's suburban networks analysis has shown that on average 60% of PCP's can be served on rings using existing duct, and by adding new duct links of 200m or less, a further 30% can be covered.

A typical existing topography is shown in Figure 3 with proposed new duct links shown dotted.

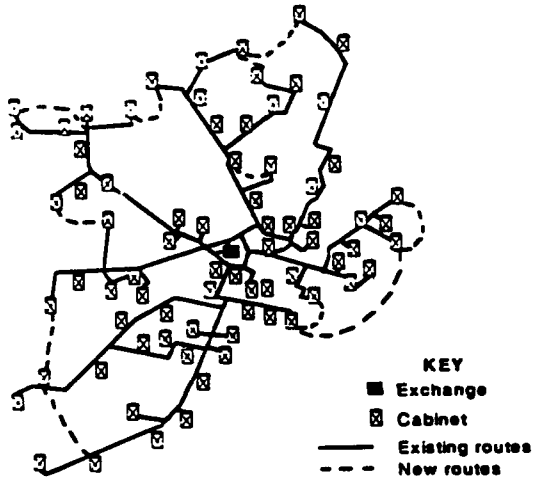


Figure 3.

Primary local duct and cabinet topography.

In some cases there will be natural or man made boundaries where physical rings cannot be provided and in these cases duplicate fibres in the same duct route i.e. across rivers or over railway bridges, may be the only choice.

For the majority of customers the primary ring will give adequate resilience, and this will be the preferred option in most cases, but if further protection is considered necessary or is requested, then duplication of fibre in the secondary cables would be the second option, with the third option being alternative routing to a different PCP, giving a totally diverse solution.

Figure 4 shows a generic ring architecture with these various options. Each primary node on the ring will be at an existing PCP position in the network and is fed from fibres in both directions round the ring. Both primary and secondary nodes contain splitters for several PONs and also straight through fibres for point to point links to large business customers.

3. PON Topology and Component Options

The architecture adopted for the PON topography will be influenced by transmission technique and the availability of suitable splitter components. Transmission options are simplex (two fibre paths) and duplex, half duplex or diplex (single fibre path).

Simplex working increases the complexity of the infrastructure due to the two fibre circuits required, however it benefits from the lowest optical insertion loss, due to the absence of duplexing couplers, and the lowest return loss since reflections are virtually not a problem with separate transmit and receive paths.

Duplex and half duplex working have an insertion loss penalty of 7dB from the duplexing couplers and diplex working replaces these with WDM's, with a reduced penalty of 2dB.

Figure 5 shows schematically the effect of the PON transmission technique on the insertion loss specification for the devices. This assumes a fixed overall power budget and shows that because simplex working has the lowest loss, the splitter specificaion could be relaxed.

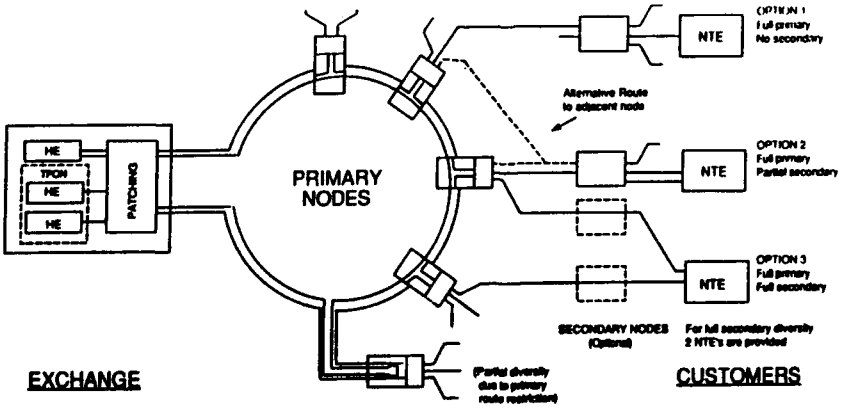


Figure 4. Primary Ring with secondary route diversity options.

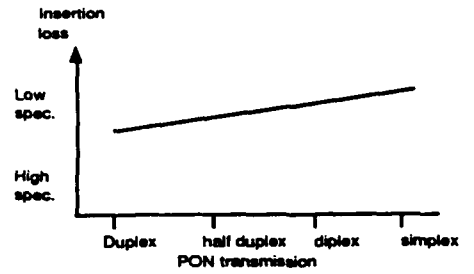


Figure 5. The effect of PON topography on the insertion loss specification.

The return loss of components used in duplex systems must be tightly controlled since reflections from these can cause deterioration in the signal to noise ratio of the sytem, [9]. A discussion on reflections is presented elsewhere, [10, 11]. Simplex, half duplex and diplex working imposes less of a constraint on the return loss. Typically, reflections in these scenarios do not introduce errors unless they are high enough to introduce transmitter problems at the head end. Figure 6 shows schematically the effect of PON transmission systems on the return loss specification for the devices.

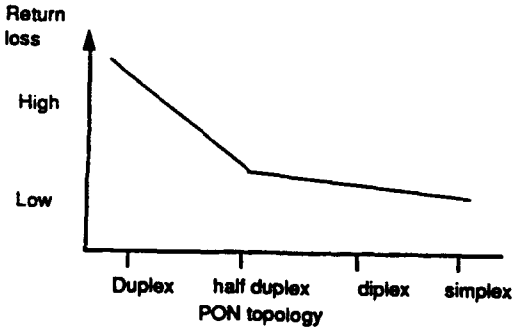


Figure 6. The effect of PON topography on the return loss specification.

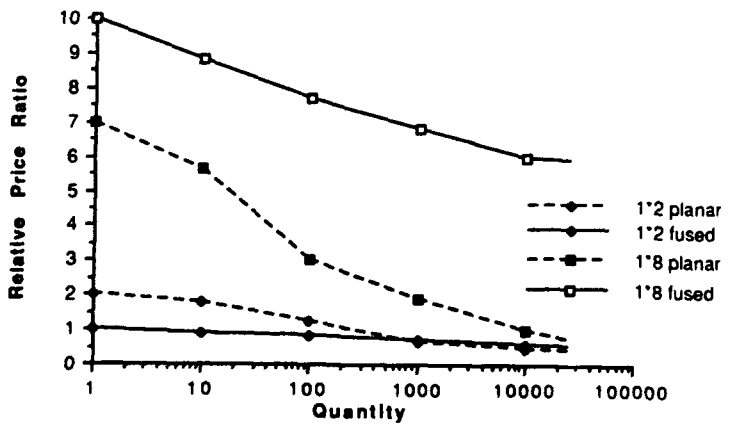


Figure 7. Relative price / Volume purchase, for fused and planar splitters.

The chosen level of split will be dependent on the available power budget and the degree of flexibility required in the network. As already discussed there is little advantage in providing a high level of split if the channel capacity of the transmission equipment cannot adequately service a large number of customers.

In view of the long term aim to provide a total fibre infrastructure and the present early state of passive technology components, it is considered beneficial to opt for simplex working and a relatively low level of split (<32) for initial role out of PON networks. High quality components should be used, as this will enable future conversion to single fibre working by the simple addition of 2x2 duplexing couplers at the network terminations.

The choice and position of splitters in the network must be a balance between the requirements of geographical customer base and the aim of providing maximum flexibility with a low fibre penetration. There is no single right answer and the field planner requires a range of kit and simple rules to allow each case to be addressed on its merits. There would seem to be little benefit in positioning the splitters at the exchange as they will not contribute to reduced fibre in the network. We are therefore left with a choice of distributed split at the primary and secondary nodes, or single location in either of these positions. These choices can be met with a limited range of splitter sizes and this should be the aim, in order to gain cost benefit from volume purchase.

Splitter technology has advanced in recent years and mass production techniques are beginning to reduce the price of fused fibre devices, however, the complex and intricate handling required to assemble these products will always tend to be costly. New techniques are being developed worldwide to produce planar light-wave circuits, by depositing silica glass waveguides on or in silicon substrates. This technology promises to provide integrated planar splitter arrays at an economic price for large quantities. They have a major advantage in reduced physical size over the fused fibre devices. Figure 7 shows the likely price trend for fused and planar devices.

The solid lines indicate the range of price variation in fused splitters from 1x2 to 1x8 devices, and the dotted lines show the same range in planar. It is clear that for quantities of 1000+ the 1x2 planar devices start to be cheaper. This effect is far more marked as the splitting ratio increases, because the fused device becomes much more difficult to make, whereas the planar price is only volume related. It can be concluded that planar devices will soon be the technology of choice.

The requirement to provide route diversity dictates that all splitters should have at least two input fibres and therefore complete flexibility can be achieved by procuring 2x2; 2x4; 2x8 and 2x16 modules which will allow the 32 way split to be achieved using combinations of only two modules in single or distributed positions.

4. Node Design

The physical design of nodes received considerable attention in preparation for the BT, LLOFT installation [12]. Of particular concern was the need to provide designs with ease of use in mind. Ability to re-enter housings to connect new customers and to allow maintenance testing of live fibres, without introducing transient losses and transmission failure, was of paramount importance. These requirements are still valid.

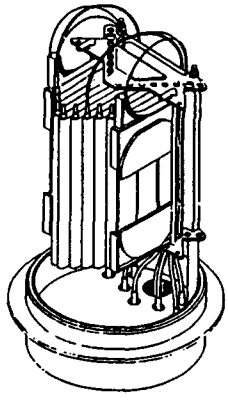


Figure 8. The PON secondary node used at Bishop's Stortford.

For LLOFT a simple modular concept was adopted using single circuit splice trays to limit transient effects caused by the handling of live fibre. This facility was very successful and the design of new nodes, to meet the wider requirements of the new fibre access networks, will expand the modular concept to its logical conclusion. By providing all components and splice trays in a similar modular format, and by providing a range of re-enterable housings of various suitable sizes, any combination of PON designs and point to point fibre paths can be accommodated up to the physical, modular, capacity of each housing. This will give the flexibility required by the field planners and benefit from uniform products and procedures throughout the network.

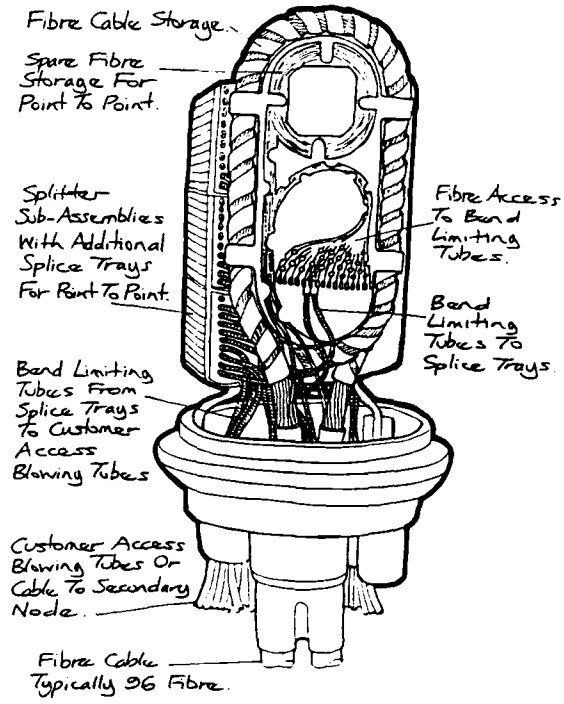


Figure 9. Schematic proposal for an expandable modular node.

The modular provision required in a given node for each PON, will depend on the split ratio at that point in the network. An expandable concept with add-on modules and a range of dome closures could cope with the individual needs and expansion requirements for both primary and secondary nodes. For instance, consider a simplex PON with a distributed split of 2x4 at the primary node and 2x8 at each of the resulting four secondary nodes. For that PON, the primary node will require a main and standby circuit on the primary ring (four fibres), and two 2x4 splitter modules. Hence, two single circuit splice trays for the 'input' legs of the splitter and four single circuit trays for the 'output' legs are needed. Assuming planar splitters, then the splitter modules will be no thicker than the splice trays and the total requirement in the node will be equivalent to eight trays. Similarly, in the secondary node a i2 tray capacity would be required to provision this PON.

It will be normal for primary nodes to have several PONS radiating from their geographical position in the network and also some point-to-point fibre circuits spliced out of the ring. Secondary nodes will generally be smaller than primary nodes, as the fibre density reduces at the outskirts of the network.

If we consider a 'five PON' simplex primary node with a 2x4 split on each PON, and additionally, with five main and five standby point-to-point simplex circuits; then the total modular capacity requirement for that node will be equivalent to 50 single circuit splice trays. If a higher level of split was used at this point in each PON, say 2x8, then assuming the same point-to-point provision, the modular capacity requirement would increase to 70 trays. It is feasible to consider coping with such a range of primary and secondary node sizes in an underground dome ended closure.

In the access network the primary cable ring will contain many fibres and therefore primary nodes will also be required to allow fibres on the ring to pass through, without the need to cut and splice. BT uses primary cable of a 96 fibre loose tube design and in the above example, 20 fibres from the ring (giving 20 main + 20 standby) will be cut and spliced into the node and 76 will pass through. A 96 fibre ring has capacity for five such nodes, approximately, but in some instances a larger node may be needed. Therefore both cabinet and underground versions will be provisioned, and as it is considered unwise to mix fibre and copper technologies in the same enclosure, new cabinets will be provided at PCP positions. However in many instances, it is likely that the high capacity benefit of optical plant, will enable underground primary nodes to replace, or compliment, the existing copper network cabinets. The 'five PON' node considered above will have >1000 line capacity, which is greater than the average copper PCP. The aesthetic and security benefits of putting plant underground are obvious and this should be the preferred solution where ever possible.

5. Conclusions

Optical cables have been installed in BT trunk networks for about 15 years and more recently have been used in single star passive access networks to provide telephony service to large business customers. This paper has described methods and topographies that would enable these star networks to be converted to primary ring architectures. It has been shown how these architectures could support universal nodes with optical splitter technology and diverse routing, and alternatives for diverse routing in the secondary network have been suggested. It is argued that these changes, would provide highly resilient shared access infrastructures, would allow live fibre operations and maintenance to occur and would enable cost effective telephony to be provided to small/medium business customers.

The effect of different transmission techniques on the specification of passive optical splitters has been discussed and the cost implications of recent developments in the technology for manufacturing optical splitter arrays has been presented. It is concluded that planar arrays will become the components of choice when large scale purchase occurs.

The LLOFT exercise at Bishop's Stortford demonstrated that it was possible to deploy optical plant to meet the requirements of a fibre based infrastructure in the Access Network. Building upon that success and with the improvements in technology that have taken place in the intervening time, BT is to roll out passive optical networks to provide service to the business sector for customes of 5 line capacity or greater.

Finally the concept of a universal, expandable, modular access node has been proposed and issues related to its design, operation and use, have been discussed. It is concluded that underground nodes are to be preferred.

Acknowledgements

The author would like to thank his many colleagues who contributed to the work described in this paper and particularly Tim Finegan and Nick Achurch for their work on splitter analysis.

References

1. Dufaun I G: 'Flexible Access Systems', BT Technology Journal, 7, No.4, pp 233 January 1989.
2. Georgian, G, and Boucouvaias, A.C, 'Low-loss Single-mode Optical Couplers' IEE Proceedings, vol. 132, Pt. J No. 5, October 1985.
3. Mortimore, D.B, 'Wavelength-flattened Fused Couplers; Electronics Letters, Vol. 21, No. 17, pp 742-743 15 August 1985.
4. Stern, J.R, Faulkner, D.W, Hornung, S, Ballance, J, & Payne, D.B, Electronics Letters Vol. 23, pp 1255 to 1257, 1987.
5. Rowbotham, T.R, "Plans for a British Trial of Fibre to the Home', BT Engineering Journal 8 Pt. 2 pp 78-82 July 1989.
6. Newman, D., Stern, J.R, 'Last Link In the Loop' Physics World pp 45-48 September 1991.
7. Hoppitt, C.E, Clarke, D.E.A, 'The Provision of Telephony over Passive Optical Networks' BT Technology Journal 7 No. 2 April 1989.
8. Hoppit, C.E, Rawlson, J.W.D. "The UK Trial of Fibre in the Loop' BT Engineering Journal 10 Pt. 1 1991.
9. Rosher, P, "Receiver penalty calculations in duplex systems," IEE International Conference on Communications, June 1989.
10. Finegan, T, and Hunwicks, A, "A statistical approach to modelling the network performance of fibre in-the-loop systems' Globecom 91, pp1828-1833.
11. Clift, D, Finnegan, T and Hunwicks, A, 'The return loss performanc of opto-electronic components for PON systems; to be published at EFOC/LAN 92, June 1992.
12. Reeve, M.H, Hornung, S, Bickers, L, Jenkins, P, and Mallinson, S. 'Design of Passive Optical Networks' BT Technology Journal 7 No. 2 April 1989.

Monitoring trials on all-dielectric, self-supporting, optical cable for power line use

G Carlton,[1] C N Carter,[2] A J Peacock[3] and R Sutehall[4]

1 Scottish Power, Glasgow, Scotland UK
2 National Grid Company, Leatherhead, England, UK
3 Telephone Cables Ltd., Dagenham, England, UK
4 Pirelli Cables Ltd., Newport, Wales, UK

Summary

All-dielectric, self-supporting, optical cables installed on power transmission lines can suffer from sheath damage, caused by dry-band arcing induced by electrical coupling with the power circuits. There is a lack of data from actual installations on the duration, frequency and magnitudes of these low-current arcs. This information is necessary for the evaluation of accelerated testing regimes. This paper reports results of a trial mounted in Scotland to monitor such events.

Introduction

All-dielectric, self-supporting (ADSS), optical cables offer the dual advantages that they can be mounted on existing overhead line supports and that their flexible non-metallic construction and light weight allows installation on spans of up to 500 m without the requirement for a power system outage. Self-supporting cable is totally separate from the power system and this allows work on either system without affecting the other.

Ranges of fittings to attach cables to the supports are well developed and consist of preformed liners and dead-end grips, suspension clamps, sag-adjusters and vibration dampers. Tensile tests on ADSS cables have shown that ultimate tensile strengths in the region of 80 kN are achievable. Cable installations are arranged so that under worst case conditions the load will not exceed 25 kN, to prevent overload of the support structures.

ADSS optical cables have to date performed well on lines operating up to 150 kV. The ease of installation and operation has allowed electrical utilities to set up high capacity optical transmission networks for private operational use, and more recently in the UK to begin to provide utility based public telecommunications services.

In the UK, the performance of ADSS cable sheath materials on lines where the system voltage is above 150 kV is still the subject of development. The aim is to prove materials which are resistant to electrical degradation at these higher voltages.

It is possible to mount a cable on a UK, double-circuit, 400 kV line at a point of minimum electrical induction, where we can be sure that during double-circuit working no electrical degradation will occur. However, should the line then be operated with one of these circuits switched out, the threat of degradation will return. This is the remaining area where further information is required. The present paper discusses progress in this investigation.

Background

ADSS optical cables began to be installed on overhead power lines in around 1979. These early cables were mostly used on 110 kV lines in Europe, and have performed satisfactorily ever since. A few years later, reports began to be received of sheath degradation, apparently caused by electrical phenomena, on ADSS cables which had been installed on higher voltage power transmission lines. Various laboratory experiments and field trials subsequently indicated that this sheath degradation was being caused by dry-band arcing, a well known phenomenon in the field of high-voltage, outdoor insulation.[1 2 3]

It has been shown recently that there exists a threshold product of induced voltage and earth-leakage current below which stable dry-band arcing does not occur.[4] This may explain why degradation has rarely, if ever, been encountered on lines whose system voltage is below 150 kV, and why lines which are subject to marine pollution have been more prone to sheath degradation than those which are not.

In 1987, STC (now Pirelli) and the CEGB (now NGC) mounted a trial of ADSS cable on a double-circuit, 400 kV line at Fawley on

the south coast of England. The cable was lowered for examination every few months. It performed well for two and a half years with no sign of damage, but before the end of the third year had suffered severe sheath degradation.

Independently, a year or so later TCL and the SSEB (now Scottish Power) mounted a similar trial, also on a double-circuit, 400 kV line, at Hunterston on the west coast of Scotland. This cable suffered sheath degradation within a matter of months. Subsequent calculation showed that whereas the cable at Fawley had experienced a maximum induced voltage of around 25 kV, that on the failed sections at Hunterston had been more than double this.

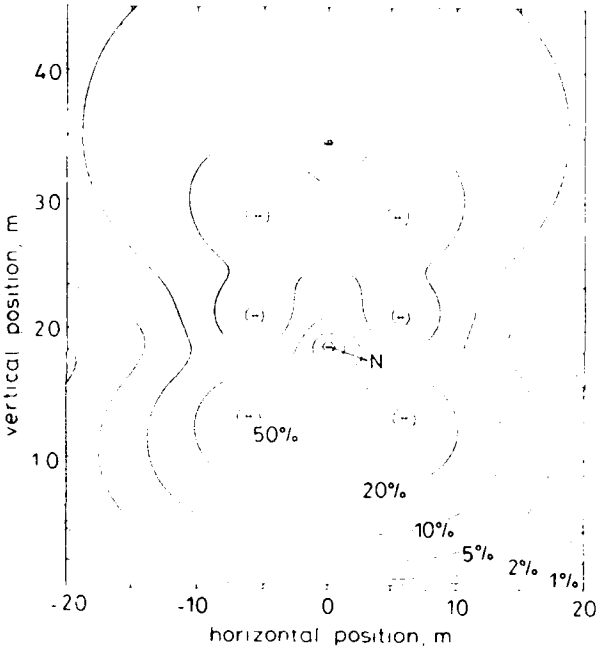


Figure 1 Both circuits live

As knowledge of the degradation mechanism increased, so various testing regimes were developed for evaluating the degradation resistance of candidate sheath materials.[5] [6] [7] Modern sheath materials are very much better able to withstand arcing than those used in the early trials. However, there has been a lack of data on the actual conditions that a typical cable installation might experience in the field, making it difficult to know how representative the various testing regimes are.

It was decided that all four parties participating in the earlier trials would pool their resources to mount new trials at Hunterston with the aim of gathering the necessary information. Hunterston was chosen for its harsh electrical conditions, its wet and windy, marine climate and position exposed to prevailing winds from the sea.

The cables

Both cables are designed to meet the stringent requirements of the Electricity Supply Industry as efficient telecommunications media for the transmission of data for supervisory, maintenance, control and telephony purposes. Both cables employ glass reinforced plastic strength members. The Pirelli design carries fibre ribbons in a single slotted cylindrical strength member, while the TCL design carries fibres in loose tubes placed in the interstices between four cylindrical strength members.[8] [9]

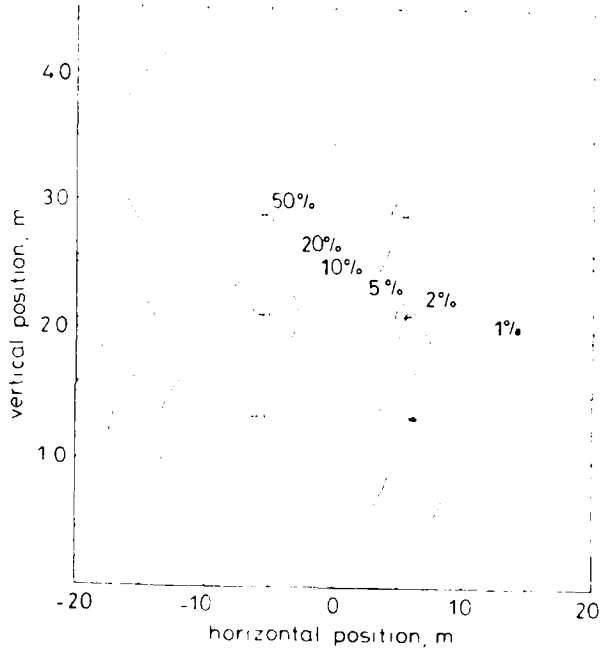


Figure 2 One circuit live

The cables are installed by conventional tension-stringing techniques with lightweight equipment developed from existing installation plant. This minimises damage to land beneath the power line and inconvenience to the general public. There is no need to de-energise the power circuits.

Tension and suspension fittings, based on conventional preformed fittings, have been developed which are designed to provide a safety factor of at least two. Vibration control devices such as spiral vibration dampers and modified stockbridge dampers effectively control aeolian vibration.

Installation and monitoring

Four, three-phase, 400 kV circuits are

lead away from Hunterston Power Station on two, double-circuit, overhead lines, each with the same relative phasing pattern (RYB, RBY). Two spans of Pirelli and three spans of TCL ADSS cable were strung, one on each of the two lines in the spring of 1990. Figures 1 and 2 show induced-voltage, contour plots for the lines at Hunterston, with both circuits live and with one circuit live and the other earthed.[4] Voltage levels are expressed as a percentage of the phase to ground voltage, so that for instance 10 % on a 400 kV line would represent 23.1 kV (0.1 x 400/√3).

When both circuits are live there is, because of the relative phasing of the two circuits, a position of minimum induced voltage, marked N. When the cables were first installed, the end of each cable was attached to the terminal tower at or near this calculated position.

Monitoring equipment was set up which recorded the output from a weather station on the roof of the nearby indoor sub-station, and the earth-leakage current flowing from each of the two cables at the terminal towers. Data logging equipment, located in the telecommunications room within the sub-station, was connected to the towers, several hundred metres distant, with buried coaxial cables and to the weather station by a multiple-pair cable. Data collected throughout the day is stored for later transmission to the National Grid Laboratories via a modem and the public telephone network.

The monitoring of the weather parameters is by conventional instruments, but the earth-leakage current monitoring deserves a few words of explanation. On each cable a dummy of the mouth of the dead-end fitting has been constructed, and placed about 20 cm beyond the actual dead-end mouth. This 20 cm of cable has been heavily greased to maximise the resistance of the alternative path to earth. The inner of the coaxial cable is then connected to the dummy dead-end on the cable and its other end earthed through a 10 Ω measuring resistor at the data logger. In the interests of safety the measurement resistor, protected by gas discharge tubes, is housed in a sealed box to which access can only be gained when the signal lead is earthed.

The monitored parameters are: Wind speed, wind direction, temperature, relative humidity, rainfall rate, specific resistance of cable samples and of a similarly sized glass rod and finally filtered and unfiltered earth-leakage current from each of the cables. The filtered earth-leakage currents have been conditioned by a 50 Hz notch filter. They give a measure of the quantity of the higher frequency components of the current, only present during arcing activity, and thus provide a measure of the periods during which arcing had been taking place.

Results

When new, both cables were very hydrophobic, so that when wetted, water formed discrete droplets rather than a film. As they aged this hydrophobicity was gradually lost, until after they had been in service for about a year they were fully wettable. As has been mentioned, the cables were originally installed in positions of minimum induced voltage, and remained in that position for about eighteen months. During this period earth-leakage currents never exceeded 10 μA, the discrimination level of the monitoring system. This result tends to validate the calculation which pinpointed the position of minimum induced voltage.

Hunterston is a nuclear power station and so the circuits carrying its output are rarely switched out. In order to simulate the conditions which would be experienced during single-circuit working, the monitored end of the terminal span of each of the two cables was lowered into a position of higher induced voltage. All the results discussed below relate to this new positioning.

It can be shown theoretically that the earth leakage-current is given by:

$$I = (2V_oJ_o/R)^{0.5} \qquad \ldots(1)$$

where V_o is the induced voltage on an insulating cable, J_o is the charging current per unit length to an earthed conducting cable and R is the resistance per unit length of the wet polluted cable.[4] The first two of these parameters will vary little for a given cable installation. Calculated values for this installation are around 25 kV and 6.25 x 10^5 A/m, depending a little on weather conditions which will cause small variations in the relative positions of cable and phase conductors. Only R will change dramatically with time.

When the cable is dry, R will be very high and virtually no current will flow. The results confirm this, currents are only seen either after rainfall or when the relative humidity approaches 100 %, when we might expect condensation on the cable from fog or dew.

When the cable is wet, R will be determined by the concentration of pollutants dissolved in the moisture. Again the results confirm this, significant earth-leakage currents are only seen after very

gentle rain or when condensation might have been expected. Heavier rain presumably washes off the salt, the main conducting pollutant at the site of this trial.

Significant earth-leakage currents do not always flow when the moisture levels are favourably low, but only when there is also enough salt pollution present. We might have expected that this would have occurred after winds had been blowing from the sea, but the data is inconclusive on this point.

The best correlation, although by no means perfect, is between the earth-leakage currents from the two cables. There is also good correlation, although less good than that between the currents from the two cables, between earth-leakage current and the specific resistance of the cable samples on the roof of the sub-station.

The inference is that salt deposition can vary locally. To put these results in perspective numerically, leakage currents have rarely exceeded 1 mA and the resistance per unit length of the cable samples has rarely been less than 1 MΩ/m, values which match very well with calculations based on equation (1).

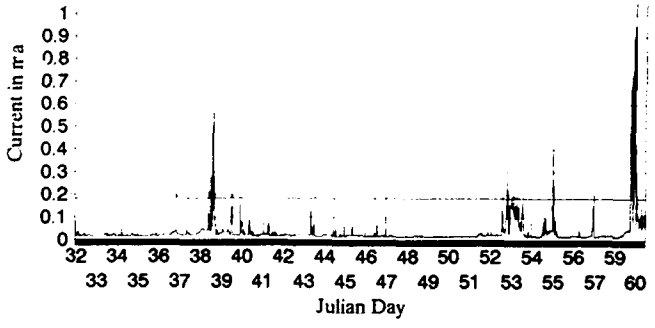


Figure 3 Earth-leakage currents for February 1992

Arcing activity occurs, as might be expected, towards the end of the periods when leakage currents have been flowing. It is observed that arcing is generally limited to occasions when the leakage current has exceeded 300 μΩ, which is in line with the theoretical understanding.[4] Before this monitoring exercise, it had been thought that arcing activity might occur towards the end of every rain event. We can now see that, for reasons which had not previously been appreciated, arcing occurs much less often than had been expected. Figure 3 shows the leakage current pattern for one of the cables for February 1992; the filtered trace is displaced upwards for clarity. Although it is not easy to see on this black and white trace, there were just three bursts of arcing activity in this period, on days 38, 55 and 60. This is typical of the measurements being made.

Discussion

World experience to date appears to indicate that damage only occurs when induced voltages are in excess of 10 to 20 kV. Theoretical studies have yielded a plausible explanation for this.[4]

The same studies have also added the knowledge that, not only must the induced voltage be above a certain level, but the resistance per unit length must also below a threshold value before stable dry-band arcing is possible. The fact that in this monitoring exercise, dry-band arcing did not occur when currents were less than 300 μA tends to confirm this view. We have also seen that by judicious positioning of the optical cable on the structure it is possible to minimise the induced voltage.

Taken together, these facts indicate that with proper care most installations away from areas of conducting pollution will never experience stable dry-band arcing or the risk of sheath damage. For that minority of installations where the possibility of arcing is high, then the cable must be shown to be proof against it. The magnitude of earth-leakage currents and the frequency of arcing incidents will obviously be dependant on location. However, the findings of this study should be of use in devising realistic test regimes.

Conclusions

A trial has been set up to monitor weather and earth-leakage current parameters on an ADSS cable strung on a 400 kV, double-circuit, power-line. The site of the trial and the type of line used presents a particularly severe threat of electrical damage. To date, both cables have remained undamaged.

The experimental results have supported the techniques used to calculate electrical threat parameters. The existence of positions of minimum induced voltage on certain lines has been verified. The frequency of dry-band arcing activity has been shown to be considerably less than had previously been assumed.

Acknowledgements

The authors would like to thank all their colleagues who have contributed much thought and effort into the establishment and monitoring of this trial. The trial is mounted jointly by Scottish Power, The National Grid Company, Telephone Cables Ltd. and Pirelli Cables Ltd. This paper is published by their permission.

References

1. Berkers, A.G.M., and Wetser, J.M., 1988, Proc. 5th DMMA, Canterbury, June 1988. IEE Conf. Pub. No. 289, pp 69-72.

2. Carter, C.N. 1988, Proc. 37th IWCS, Reno, November 1988, pp 117-121.

3. Rizk, F.A.M., 1981, Electra 78, October 1981.

4. Carter, C.N. and Waldron, M.A., 1992, Proc. IEE Part C. 139, No 3, May 1992, pp 185-196.

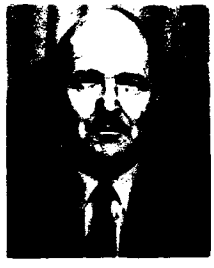
5. Roland, S.M. and Carter, C.N., 1988, Proc. 5th DMMA, Canterbury, June 1988. IEE Conf. Pub. No. 289, pp. 77-80.

6. Wheeler, J.C.G., Lissenburg, M.L., Hinchcliffe, J.D S. and Slevin, M.E., 1988 Proc 5th DMMA, Canterbury, June 1988, IEE Pub. No. 289 pp 73-76.

7. Dissado, L.A., Parry, M.J., Wolfe, S.V., Summers, A.T. and Carter, C.N. 1990, Proc. 39th IWCS, Reno, November 1990, pp 743-751.

8. Roland, S.M., Craddock, K., Carter, C.N., Houghton, I. and Delme-Jones, D. 1987 36th IWCS, Arlington, Va 1987, pp 449-456.

9. Bartlett, A.D., Carlton, G., Carter, C.N. and Peacock, A.J. 1989, CIRED Brighton, May 1989, IEE Conf. Pub. No. 305, pp 252-258.



Gerry Carlton
Scottish Power
Roman Road
Kirkintilloch
GLASGOW
G66 1DZ
UK

Gerry Carlton was born and educated in Glasgow and trained initially with the then UK Government Telecommunications Service. He has been the Telecommunications Manager of ScottishPower plc since 1981, where his responsibilities have included modernising their telecommunications assets by setting up an integrated digital data network embracing all the utility services. Married with two grown chidren, he is a Fellow of the Institution of Electrical Engineers.



Alan J Peacock
Telephone Cables Ltd.
Chequers Lane
DAGENHAM
Essex
RM9 6QA
UK

Alan James Peacock is a qualified telecommunications engineer and has worked for Telephone cables Ltd. for 35 years. During this period he has worked in cable design and development of balanced pair, coaxial and optical fibre cables. This work has involved serving on many National and International committees. He has had a particular responsibility for developing the TCL ADSS featured in the Hunterston trial.



Chris N Carter
National Grid
Technology and
Science
Laboratories
Kelvin Avenue
LEATHERHEAD
Surrey
KT22 7ST
UK

Chris Carter graduated from the University of London with a B Sc Honours degree in Mathematics and Physics in 1963. He has since carried out research work on magnetohydrodynamic power generation, superconducting magnet design, ac loss measurements in superconductors, failure mechanisms in the joints of power cables and, since 1979, on the development of optical communications on power lines.



Ralph Sutehall
Pirelli Cables Ltd.
Wednesbury Street
NEWPORT
Gwent
NP9 0WS
UK

Ralph Sutehall is employed by the Technical Department of Pirelli Cables Ltd. as a Senior Project Engineer. Having worked on all aspects of optical cables for the past twenty years, he is currently involved in the application and installation of aerial cables, including investigating the vibrational performance of ADSS cables.

CABLE HAULING TENSION AND OPTICAL FIBRE RELIABILITY

Rong-Chang Hsieh, Paul Boes, Alfred Kruijshoop

Australian and Overseas Telecommunications Corporation
Melbourne, Australia

ABSTRACT

Cable tension models representing cable tension during and after hauling are first established, followed by mathematical expression of optical fibre strain functions for practical installations of various cable designs. The optical fibre strain as a function of time and installed length is converted to the equivalent strain, from which the reliability of installed optical fibres can be determined. Based upon this method the maximum allowable cable hauling tension can be defined precisely and maximised to facilitate cost-effective cable design, efficient installation and high reliability. Optical fibre strains and cable hauling tensions were measured in the field.

1. INTRODUCTION

The link between the reliability of fibre installed in underground ducts and the hauling tension during installation has been far from being well-defined. The lack of a physical model or mathematical analysis on the effect of time and length dependent tension on the fibre reliability has led to two extreme views. One view allows the cable to be hauled at a tension that does not break the optical fibres during installation. This approach neglects the long-term effects caused by residual strain, and consequently premature fibre breaks may occur in the future. The other more conservative view takes the worst case optical fibre strain during installation as a long-term constant strain, which limits the maximum allowable hauling tension of the cable. The latter approach under-utilises the optical fibre strength and results in the less efficient use of cable materials and lower productivity hauling than the optimised design approach can achieve. This paper establishes a quantitative method to link the hauling tension to the overall reliability of the optical fibres installed in underground duct.

2. METHODOLOGY

The major issues in relating the practical hauling conditions to the lifetime of optical fibres installed in ducts are:

- How to model the time and length dependent cable tensions during and after hauling, in practical duct routes including straight ducts and bends;
- How to find the mathematical expressions for fibre strains in cables with or without a strain free window during and after installation;
- How to convert the time and length dependent fibre strains to equivalent constant strains in order to apply fibre lifetime equations;
- How to determine the combined effect of fibre strains during and after hauling on the overall reliability.

The solutions found can be applied to maximise the cable tensile strength for practical hauling conditions at a required reliability. The cable tensile strengths of cable designs with and without a strain free window are compared. Field measurements of hauling tensions and fibre strains have been carried out.

3. CABLE HAULING TENSION MODELS

Cable hauling tension models for duct routes with a straight duct, one bend and two bends are illustrated in this section. Only level duct will be discussed in this paper. In all cases the cables are installed at the

maximum allowable hauling tension. It will be shown that the maximum residual cable tension of a cable installed in a straight duct is greater than or equal to that of cables intalled in ducts with one bend and two bends.

3.1 Straight duct

The maximum hauling tension F in a straight duct is given by:

$$F = \mu mgL \qquad (3.1)$$

where μ is coefficient of friction of hauling,
m is cable mass per unit length,
g is gravitational acceleration and
L is the maximum cable length that can be installed in a straight duct at the maximum hauling tension.

The hauling tension is proportional to installed length. Also the tension is time dependent at a given position of the cable as the hauling operation progresses. After hauling, the cable at the hauling winch end retracts into the duct as if the cable were being hauled from the opposite direction until an equilibrium tension distribution is reached. The maximum residual cable tension is half the maximum hauling tension at the mid-point of the duct route.

Fig.1a shows the cable hauling tension in a straight duct as a function of cable length x. The maximum installed cable length is L.

Fig.1b-e show the strains at various locations during and after the hauling duration T. The strain is both time-variant and length-dependent during installation and becomes time-invariant and length-dependent after installation.

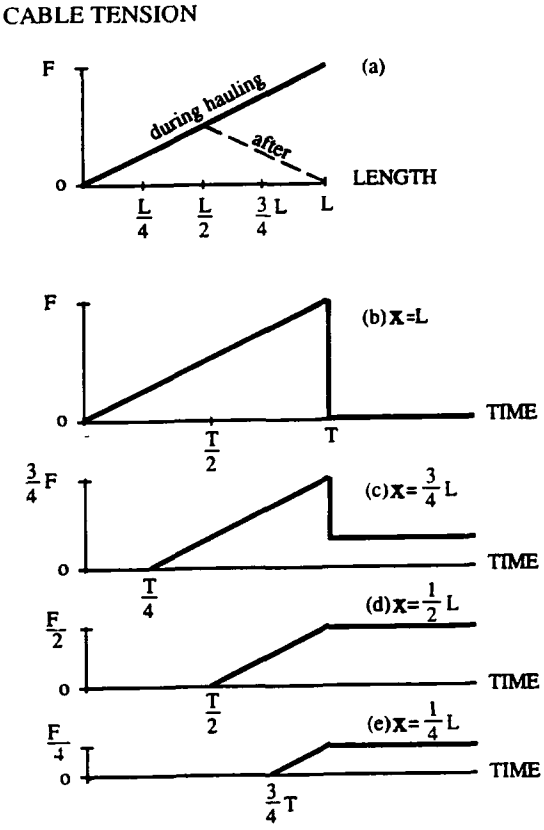


Fig.1 Cable tension in a straight duct

3.2 Duct with one bend

Figs.2 & 3 depict the cable tension of a duct route containing a bend. A bend is defined by the angle of bend determined by the ratio of the arc length and the bend radius. (Ref. Fig.2). The maximum installed length in a duct with a bend is shorter than L as the bend requires extra hauling tension. The maximum hauling tension F in a duct with a bend is given by[1]:

$$F = \mu mg(L1e^{\mu\theta} + L2) \qquad (3.2)$$

where L_1 and L_2 is the straight length of the first and second straight duct forming an angle θ, and
θ is the angle of bend of a duct route ($s=r\theta$ where s is the arc length and r is the radius of the bend).

The example in Fig.2 shows that the maximum residual tension in this case is half the maximum hauling tension, being exactly the same as in the case of a straight duct.

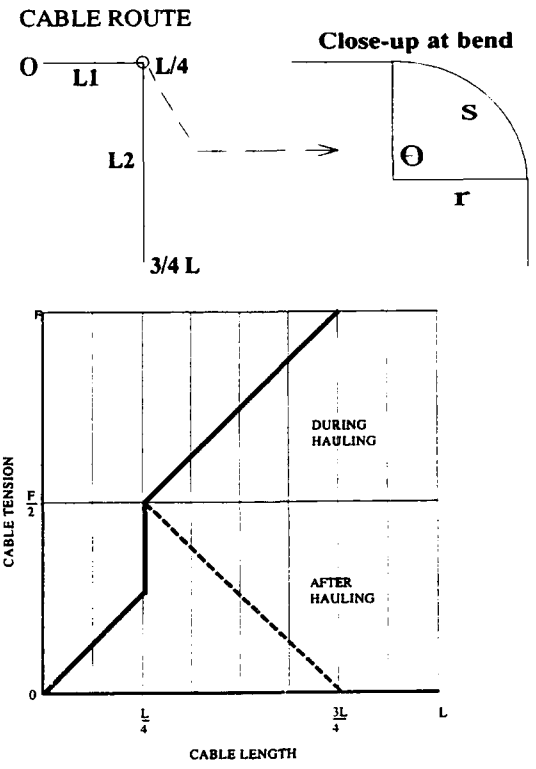


Fig.2 Cable tension in a duct with one bend

It is not apparent from the example in Fig.3 what the maximum residual tension would be at the bend. Therefore, a significant outcome of this analysis is that it can be proved that the maximum residual cable tension is always no greater than half the maximum hauling tension:-

$$\theta_1+\theta_2=\theta \tag{3.3}$$

where θ is the angle of bend and θ_1 is the angle between the start of the bend from the L_1 side to the point of the maximum residual tension at the bend and θ_2 is the angle from that point to the end of the bend on the L_2 side.

At the equilibrium of the tension distibution, the maximum residual tension at the bend is given by:

$$F_1=\mu mg\, L_1 e^{\mu\theta_1}=F_2=\mu mg\, L_2 e^{\mu\theta_2} \tag{3.4}$$

Solving Eqs.3.3 & 3.4,

$$\theta_1=\frac{1}{2}(\theta-\frac{1}{\mu}\ln\frac{L_1}{L_2}) \tag{3.5}$$

Insert Eq.3.5 into Eq.3.4, the maximum residual cable tension at the bend is given by:

$$F_1=\mu mg\, L_1 e^{\mu\theta/2}(\frac{L_2}{L_1})^{1/2} \tag{3.6}$$

From Eq.3.2, half the maximum hauling tension in the case of a cable installed in a straight duct is given by:

$$\frac{F}{2}=\mu mg\, L_1(\frac{1}{2}e^{\mu\theta}+\frac{1}{2}\frac{L_2}{L_1}) \tag{3.7}$$

Let $e^{\mu\theta}=a$, $L_2/L_1=b$, $\mu mgL_1=c$, then

$$(\frac{F}{2})^2-F_1^2=c^2[\frac{1}{4}(a+b)^2-ab]=c^2[\frac{1}{4}(a-b)^2]\geq 0$$

Therefore, $\frac{F}{2}\geq F_1$.

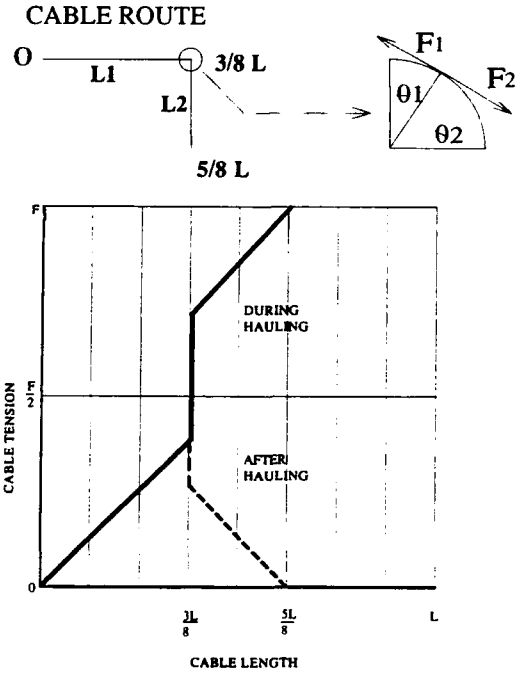


Fig.3 Cable tension in a duct with one bend

For the example in Fig.3, $L_2/L_1=2/3$ and $e^{\mu\theta}=2$, so $F/2=1.333\ \mu mgL_1$. $F_1=1.155\ \mu mgL_1$, so $F_1=0.43F$.

This result confirms the finding that $F/2\geq F_1$. Therefore a simple and conservative approach would be to analyse the maximum residual cable tension in the duct with a bend by using the straight model.

3.3 Duct with two bends

Figs.4 & 5 depict the cable tension installed in a duct containing two bends. The method described in Section 3.2 can be applied to calculate the maximum residual tension at the bend. It was calculated that the maximum residual hauling tension at the bend is 34% and 43% of the maximum hauling tension for the example in Fig.4 and Fig.5 respectively. In both cases the maximum residual tension is less than half the maximum hauling tension.

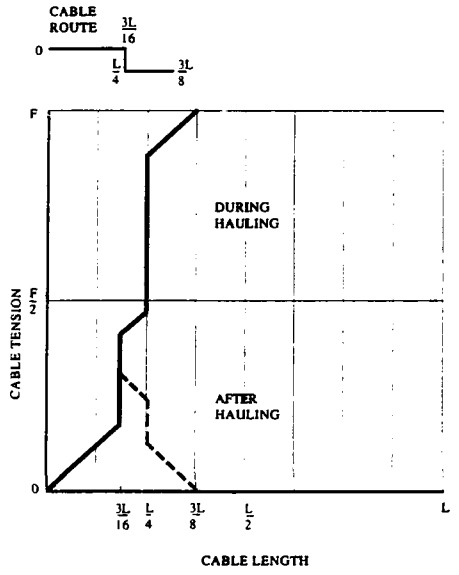


Fig.4 Cable tension in a duct with two bends

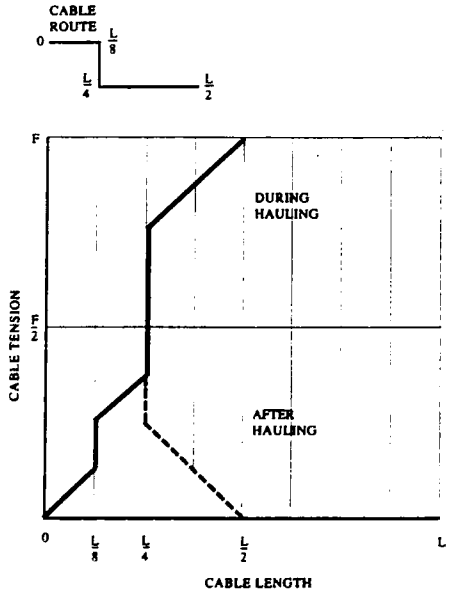


Fig.5 Cable tension in a duct with two bends

4. FIBRE STRAIN FUNCTION AND EQUIVALENT FIBRE STRAIN

Since cable strain is proportional to cable tension for cables with a linear cable tension to cable strain relationship, the findings with regard to cable tension for such cables is also applicable to cable strain. The vertical axis of Figs 1,2,3,4&5 can be either cable tension or cable strain with a linear cable tension-cable strain relationship. The maximum cable strain E_c corresponds to the maximum cable tension F.

The fibre strain as a function of time and distance can be converted to an effective constant strain by Eq.4.1 for the purpose of optical fibre lifetime calculation[2]:

$$E_{eq} = \{ \frac{1}{L} \int_0^L [\frac{1}{T} \int_0^T E^n(t,x)\, dt]^b\, dx \}^{1/bn} \qquad (4.1)$$

where E_{eq} is the equivalent strain for the duration T of installation,

L is the installed length at the maximum hauling tension,

E(x,t) is the strain as a function of time and length,

n_p is stress corrosion factor in the environment of proof test (room condition),

$b=(n_p-2)/(n-2)$ and

n is stress corrosion factor of the installation environment.

Cable designs can be classified into tight construction and loose construction. There is little or no fibre strain free window in the case of tight construction. Fibre strain increases with the cable strain for fibres in the tight cable construction. The loose construction provides some degree of decoupling between cable strain and fibre strain. Both types of cable design will discussed in the following sections.

4.1 Straight duct

4.1.1 Optical fibre strain during installation

i). The optical fibre strain for a tight construction cable during installation is the same as the cable strain depicted in Fig.1 and is given by:

$$E(x,t) = \frac{E_o}{T} [t-(1-\frac{x}{L})T]\, \mathbf{u}[t-(1-\frac{x}{L})T] \qquad (4.2)$$

where E_O is the maximum fibre strain at x=L and t=T, **u**[t - (1 - x/L)T] is the step function.[3]

Inserting Eq.4.2 into Eq.4.1, the equivalent fibre strain for a tight construction cable during hauling is:

$$E_{eq} = \frac{E_o}{[(n+1)(n+2)]^{1/n}} \qquad (4.3)$$

The equivalent strain of a tight construction cable during hauling is 76% of the maximum fibre strain if $n=n_p=23$.

ii) The optical fibre strain of a loose construction cable during hauling shown in Fig.6 is given by:

$$E(x,t) = \frac{E_o}{T}\,[t-(1-\frac{x-a}{L})\,T]\;\mathbf{u}[t-(1-\frac{x-a}{L})T \qquad (4.4)$$

where $a = \frac{E_f}{E_o + E_f} L$ and

E_f is the strain free window.

Insert Eq.4.4 into Eq.4.1, the equivalent fibre strain of a loose construction cable during hauling becomes:

$$E_{eq} = \frac{E_o}{[(n+1)(n+2)]^{1/n}} (\frac{E_o}{E_o+E_f})^{\frac{n+2}{n}} \qquad (4.5)$$

The equivalent fibre strain during hauling a loose construction cable with Ef=0.3% is 52% of the maximum fibre strain if n=23 and E_o=0.73%.

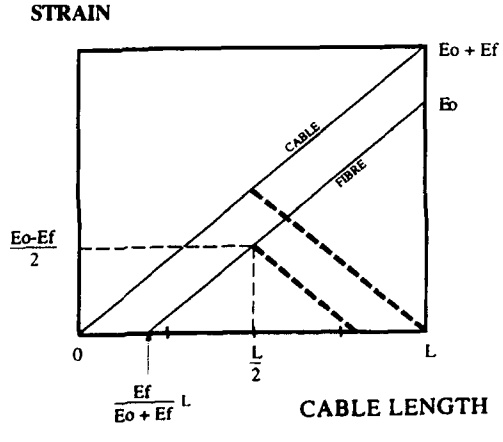


Fig.6 Optical fibre strain (loose construction cable)

4.1.2 Optical fibre strain after installation

The cable strain function is depicted in Fig.1a and is given by:

$$E(x,t) = E(x) = E_o\, x/L \quad \text{when } x \le L/2 \qquad (4.6)$$

The strain curve for $x \ge L/2$ is symmetrical to the strain curve for $x \le L/2$.

i)The optical fibre strain of a tight construction cable after hauling is the same as the cable strain given by Eq.4.6 and is depicted in Fig.1.

Insert Eq.4.6 into Eq.4.1, the equivalent optical fibre strain of a tight construction cable after installation is given by:

$$E_{eq} = \frac{E_o}{2} (\frac{1}{bn+1})^{1/bn} \quad \text{when } t \ge T \qquad (4.7)$$

The equivalent strain is 44% of the maximum strain if n_p=23, n=17.

ii) The optical fibre strain of a loose construction cable after installation is depicted in Fig.6 and is given by:

$$E(x,t) = E(x) = (E_o + E_f)\frac{x}{L} - E_f, \quad x \le L/2 \qquad (4.8)$$

The strain curve for $x \ge L/2$ is symmetrical to the strain curve for $x \le L/2$.

The equivalent strain for a loose construction cable is given by:

$$Eeq = \frac{E_o - E_f}{2}\,[(\frac{E_o - E_f}{E_o + E_f})\,(\frac{1}{bn+1})]^{1/bn}, t \ge T \qquad (4.9)$$

The equivalent fibre strain after hauling a loose construction cable with a strain free window of 0.3% is 25% of the maximum fibre strain if E_o=0.73%, E_f=0.3%, n=17, n_p=23.

4.1.3 Max. fibre strain and equivalent strain

Using Eqs.4.3, 4.5, 4.7, & 4.9, equivalent strains can now be determined by the maximum fibre strain

during hauling, stress corrosion factors and fibre strain free window. Fig.7 shows equivalent strain as a function of maximum fibre strain during and after hauling (T1=duration of hauling), given a proof strain of 1% and a strain free window of 0 or 0.3%. The constant equivalent strains will be used to determine fibre reliability in Section 5.

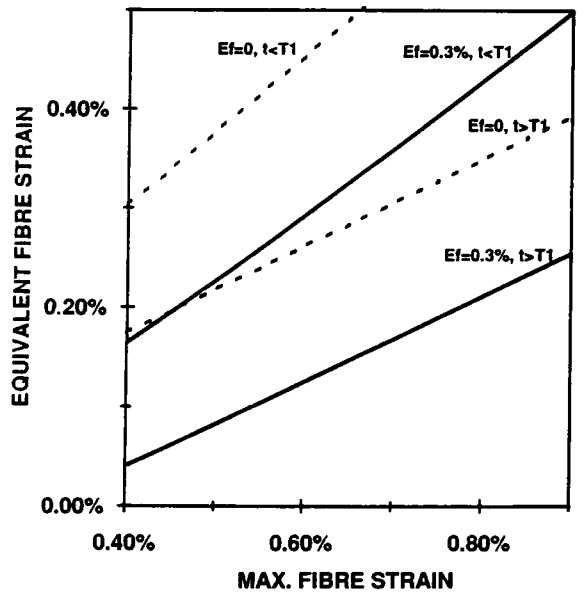


Fig.7 Max. fibre strain and equivalent fibre strain

4.2 Duct with one and two bends

It has been proven in Section 3 that the maximum residual cable tension/strain of a cable installed in a duct with one or two bends is no greater than that of a cable installed in a straight duct, and in Section 4 that for a given strain free window and stress corrosion factor, the equivalent fibre strain of a cable installed in a straight duct is determined by the maximum fibre strain during installation. It follows that the equivalent strain of a cable installed in a duct with one or two bends after hauling is no greater than that of a cable installed in a straight duct.

For example, in Fig.2 the lower residual cable strain in the length L_1, compared with the case of a straight duct results in a lower effective fibre strain over the length L_1, while the remaining length of the cable has an effective fibre strain equal to that of a cable installed in a straight duct of length L. Consequently the effective fibre strain of the whole length is smaller than that of a cable in a straight duct. (Refer Fig.1). This means that the fibre strain and reliability analysis for the case of a straight duct can be conservatively applied to the cases of more complex ducts with bends.

5. FIBRE RELIABILITY AND CABLE DESIGN APPLICATIONS

This section will study the effect of maximum fibre strain on reliability, followed by examples of cable design applications at a required reliability.

5.1 Optical fibre reliability

Eqs. 5.1 and 5.2 are examples of optical fibre reliability estimation. Eq.5.1 is a minimum time-to-failure lifetime model[4]:

$$t_{s(min.)} = B\sigma_p^{n-2}\sigma_s^{-n} \qquad (5.1)$$

where $t_{s(min)}$ is service life, n is stress corrosion factor, σ_p is proof stress, σ_s is service stress,and B is a constant for a given environment and material composition and geometry.

Eq.5.2 is a system length failure probability lifetime model[5]:

$$ts = tp\left(\frac{Ep}{Es}\right)^n\left\{\left[1 - \frac{\ln(1-f)}{NpL}\right]^{\frac{n-2}{m}} - 1\right\} \qquad (5.2)$$

where t_p is the duration of proof test, f is the failure probability of the system length L, N_p is the number of breaks per unit length during proof test and m is the Weibull modulus.

Fig.8 is an example of the system failure probability approach if E_p=1%, m=10, N_p=0.05/km, n=23 (50% Relative Humidity) or n=17 (97% R.H.) and a failure probability of 0.01 per 1000 fibre.km.

The method presented in this paper is equally applicable to Eqs.5.1 and 5.2. and indeed also applicable to any lifetime calculation which requires the knowledge of a constant service strain. Eq.5.2 will be used in this paper as Eq.5.2 uses the statistics of fibre strength over a very long length thus more closely represents a practical system length.[6,7]

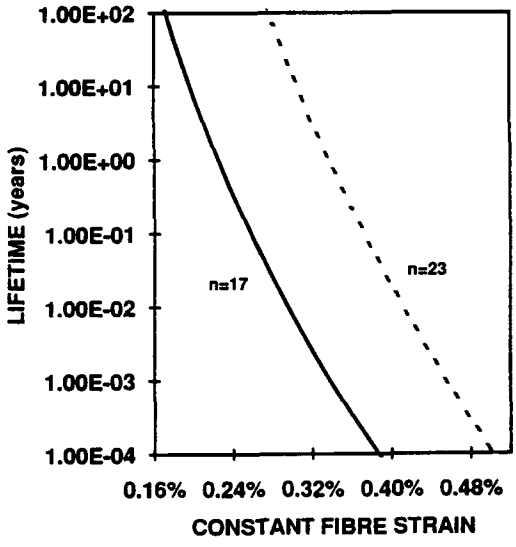


Fig.8 Optical fibre lifetime at constant fibre strain

Optical fibres are subject to strain during and after hauling. The design criterion for reliability is that degradation of fibre strength (flaw growth) in the duration of hauling must not compromise the required overall lifetime, as given by[8]:

$$T_2 - T_1 \left(\frac{E_{eq1}}{E_s}\right)^n \geq T_{min} \qquad (5.3)$$

where T_1 is the duration of hauling,
E_{eq1} is the equivalent fibre strain during hauling,
T_2 is the fibre lifetime determined by E_{eq2}, which is the equivalent strain after hauling,
Es is the constant strain which would meet the required fibre lifetime of T_{min} in the environment during hauling,
n is the stress corrosion factor in the environment of hauling and usually $n=n_p$ during hauling,
T_1, T_2 and T_{min} must be in the same units.

If a minimum lifetime of 40 years is required, and $n=n_p=23$ at 50% Relative Humidity (R.H.) in air during hauling, $E_p=1\%$, $N_p=0.05$/km, L=1000 km and f=0.01 then $E_s=0.28\%$ from Eq.5.2. The duration of actual hauling is generally no greater than 2 hours. After hauling, n=17 at 97% R.H. is used for calculating T_2 for optical fibre cables under wet condition. Table 5.1 shows the maximum fibre strains during installation, their equivalent strains and effect on fibre reliability for cables with strain free windows of 0 and 0.3%.

TABLE 5.1
MAX. FIBRE STRAIN AND RELIABILITY
(1% fibre proof strain)

Strain free window	Max. fibre strain during hauling	Equivalent strain during hauling	Reduction in lifetime due to hauling (year)	Equivalent fibre strain after hauling	Lifetime at the equivalent fibre strain after hauling (year)	Overall lifetime (year)
Ef	Eo	Eeq1		Eeq2	T2	Tmin
0	0.41%	0.31%	0.00	0.18%	40.11	40.11
0	0.53%	0.40%	0.25	0.23%	0.60	0.35
0.30%	0.73%	0.38%	0.07	0.18%	40.10	40.03
0.30%	0.81%	0.44%	1.67	0.22%	2.03	0.36

The first two examples in Table 5.1 show that for a tight construction cable, a maximum fibre strain during hauling of 0.41% and 0.53% would have a lifetime of 40 and 0.35 years respectively. The next two examples show that a cable with a strain free window of 0.3%, a maximum fibre strain of 0.73% and 0.81% would result in 40 and 0.36 years lifetime respectively. The equivalent strain after hauling dominates the long-term lifetime requirement. The criterion of no fibre breaks during hauling does not guarantee the long-term reliability.

It is interesting to note that given the same reliability requirement of 40 years, a cable with a strain free window of 0.3% allows a fibre strain during hauling of 0.73%, compared with 0.41% in the case of no strain free window. This means a cable with a larger strain free window utilises the fibre strength more effectively during hauling and would permit a much higher maximum hauling tension.

It is also interesting to note that the equivalent strain during hauling is 76% and 52% of the maximum fibre strain during hauling for cables with $E_f=0$ and $E_f=0.3\%$ respectively. This is not suprising as only a small portion of the fibre is subject to the maximum strain and only when the hauling is close to finish. The equivalent strain after hauling is also much smaller than the maximum strain during hauling: 44%

and 25% of the maximum strain for E_f=0 and E_f=0.3% respectively. This means that "worst-case" approach assuming that after hauling the fibre would stay at the maximum strain is very conservative.

5.2 Cable design applications

Cable tensile strength can now be defined on a scientific basis. In practice, the maximum fibre strain has two components: a tensile strain component due to hauling and a non-tensile strain component due to fibre stranding, torsion and bending of the cable construction. In addition, there is a need for an error margin to "buffer" the sensitive strain- lifetime curve. The cable strain is given by:

$$Ec = Et + Ef = Eo - Em + Ef \quad (5.4)$$

where E_c is the cable strain,
E_t is the maximum fibre tensile strain due to hauling,
E_f is the strain free window.
E_o is the maximum fibre strain (all inclusive) and
E_m is the fibre non-tensile strain and margin.

Table 5.2 shows cable design examples which maximise the cable tensile strength at a required reliability of 40 years under wet condition. 0.1% is used for the non-tensile strain component and margin. All the conditions are the same as in Table 5.1. A Glass Reinforced Plastic (GRP) rod strength member with a diameter of 2.8 mm and Young's modulus of 52GPa is used in the examples. It shows that a cable with a strain free window of 0.3% can achieve a cable tensile strength of 3 kN compared with 1 kN in the case of no strain free window. The tripled cable tensile strength is due to better utilisation of fibre strength during hauling and a greater cable strain made possible by the strain free window.

TABLE 5.2
CABLE TENSILE STRENGTH DESIGN
(1% fibre proof strain, E_m=0.1%, 2.8mm OD FRP)

Strain free windows	Max. fibre strain during hauling	Max. fibre strain due to tensile force	Cable tensile strain	Cable tensile strength
Ef	Eo	Et	Ec	*F*
0	0.41%	0.31%	0.31%	1.0 kN
0.30%	0.73%	0.63%	0.93%	3.0 kN

Fibre lifetime is only one of the many considerations for the design of the cable tensile strength. The cable tensile strength is also subject to additional requirements such as cable crush resistance for bending under maximum hauling tension, optical attenuation limit, yield strength and breaking strength of strength member and hauling eyes, error sensitivity etc..

6. FIELD TEST METHOD

6.1 Test objectives

The objectives of the field test were:
(i) to measure the cable tension at the cable head to ensure that the maximum hauling tension had been reached;
(ii) to investigate whether or not the residual fibre strain in a duct with multiple bends is less than the strain calculated from the straight duct model, as the residual strain dominates the long-term fibre lifetime calculation;
(iii) to ascertain that the fibre strain reaches a stable level in a very short period after the hauling is stopped.
(iv) to evaluate the improvement of the cable tensile strength using the new design method.

The field test aimed to use a maximum fibre tensile strain of 0.63% and a strain free window of 0.3% as per Table 5.2.

6.2 Cable tension measurement

The pulling force on the head of the optical fibre cable was measured with a commercially available device. The measuring system utilises a measuring transducer attached to the hauling eye of the cable, which detects the pulling force by the winch rope. The detected pulling force is translated into a frequency varying signal which is transmitted, via the copper pairs contained in a Kevlar winch rope, to the receiving analyser located at the winch truck. With the assistance of a length counter the instrument is then able to provide a plot of the pulling force on the cable as a function of the length of cable hauled in by the winch truck.

6.3 Optical fibre strain measurement

The fibre strain is measured using commercially available equipment which provides a real time, readout of both the change in power throughput and optical propagation delay. From these, attenuation and fibre optical length with millimetre resolution are computed. Generally one reading per second is taken and displayed as a function of time in graphical format, providing an overview of fibre strain and attenuation. This can be observed by field staff during the cable hauling operation and stored in memory for further analysis.

It is recognised that methods such as this are capable of highly accurate measurement of total optical link length, and changes thereof, but cannot determine the distribution of strain along the length of the fibre being monitored.

The strain measuring equipment uses the principle of the phase shift of a high frequency modulated optical signal, first at five optical wavelengths for unambiguous absolute length determination, followed by monitoring at one wavelength (selectable as 1310 or 1550 nm) for continuous strain recording.

The fibre reflective end is housed in a standard cable hauling eye (inside diameter 11 mm), thereby avoiding the need for an unusually large hauling eye, as would be required to house a fibre loop for the return signal. The signal can be transmitted along one particular fibre in the cable, used bi-directionally with a reflective layer of silver applied directly to the cleaved fibre end.[9] Since the launch/detect end of the cable needs to be permanently connected to the optical equipment during the haul, it is necessary to remove the cable from the drum and lay it out on ground.

7. FIELD TEST RESULT

7.1 Field test route

The field test route is shown in Fig.9. The duct length is 1.5 km. The cable went through many bends, including a change-of-direction wheel with a radius of 0.2 m at the manhole between Sections E and F.

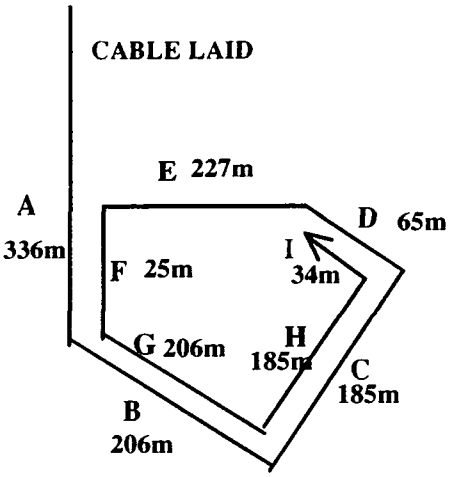


Fig.9 Field test route

7.2 Cable hauling tension

The solid line in Fig.10 represents the measured cable hauling tension during the field test. The maximum hauling tension was 3.2 kN. The dotted line in Fig.10 is the residual tension estimated from the measured tension. The maximum residual cable tension installed in a duct with multiple bends is no greater than half the maximum hauling tension, as predicted.

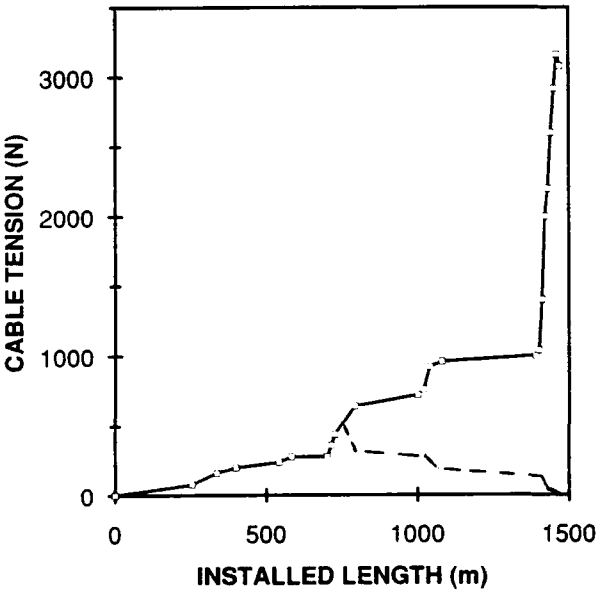


Fig.10 Cable hauling tension during field test

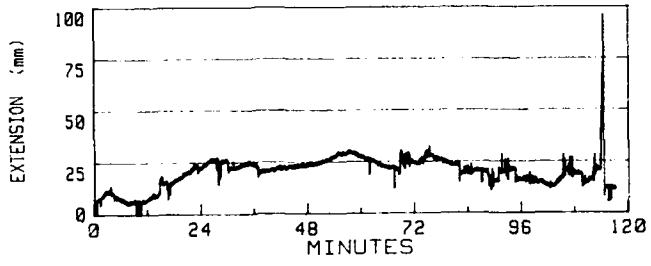
7.3 Optical fibre strain

Fig.11 shows the optical fibre elongation recorded in the field test. The measured average strain after hauling is 0%, which is less than the average strain of 0.015% calculated from the straight duct model in Fig.6, thus confirming the finding that the straight duct model can be safely applied to complex duct routes with multiple bends.

Fig.11(a) indicates that the optical fibre had not been under significant strain for most of the time during installation until the cable tension reached a level which had depleted the excess fibre length.

Fig.11(b), which expands the time scale of the strain curve at the end of the hauling, shows that the optical fibre elongation returned to the base level immediately upon removal of the hauling tension. This confirms the elastic property of the cable and fibres.

(a) Full trace



(b) Expanded time scale at the end of trace

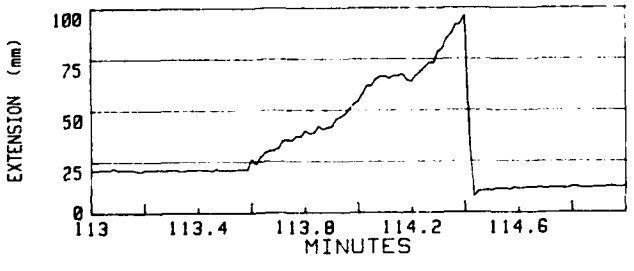


Fig.11 Optical fibre strains during and after hauling

7.4 Cable tensile strength improvement

The maximum hauling tension applied to the cable in the field test was 3.2 kN, which is significantly greater than the 2 kN that would normally be applied to the same cable. The tensile strength improvement shows the potential of facilitating more efficient hauling with cost-effective cable design.

8. CONCLUSION

A method to determine the reliability of optical fibre installed in underground ducts has been developed on a scientific basis. It has been found that the risk of optical fibre breakage during hauling is low, but the effect of post-installation residual strain on fibre reliability limits the maximum allowable fibre strain during installation.

The method can be applied to achieve cost-effective cable design, efficient cable hauling and high reliability of installed fibres in the underground duct.

ACKNOWLEDGMENTS

The permission of the Group Managing Director, Telecom Australia Commercial and Consumer Business Units, and the Director of Research, Telecom Research Laboratories to publish the above paper is hereby acknowledged. We thank the staff at Maidstone Technical Development and Evaluation Site for their involvement in the field tests.

REFERENCES

[1] M.Reeve, R.Kashyap, S.Hornung, S.Cassidy, "Continuous Optical Fibre Strain Measurement During Optical Cable Installation", Proc. International Wire & Cable Symposium, 1981.

[2] Y.Mitsunaga, Y.Katsuyama, H.Kobayashi, Y.Ishida, "Strength Assurance of Optical Fiber Based on Screening Test", Electr. & Comm. in Japan, Vol.66B, No.7, July 1983.

[3] R.Hsieh, P.Boes, A.Kruijshoop, "Lifetime of Optical Fibres Installed in Underground Plant", 16th Australian Conference on Optical fibre Technology, 1991.

[4]. A.Evans and S.Wiedrhorn, "Proof Testing of

Ceramic Materials-An Analytical basis for Failure Predictions", Int. J. Frac. 10, 1974
[5] Y.Mitsunaga et al., Electronic Letter, Vol.17, No.16, p567, 1981.
[6] G.Glaesemann, S.Gulati, "Design Methodology for the mechanical Reliability of Optical Fibre", Optical Engineering, Vol.30 No.6, June 1991.
[7] D.Roberts, E.Cuellar, M.Kennedy, "Calculation of Static Fatigue Lifetime of Optical Fibre", Optical Engineering, Vol. 30 No.6, June 1991.
[8] D.Kalish, "Effect of Moisture on the Strength of Optical Fibres", Proc. 27th International Wire & Cable Symposium, 1978.
[9].Swiss PTT, "Single End System for Strain/Length Measurements in Optical Fibres", CCITT COM VI-39-E, September 1990.



Paul Boes joined AOTC in 1986 after graduating with a B.E. degree in communication engineering from the Royal Melbourne Institute of Technology in the same year. After a brief period with a regional administration he joined the National Office, Melbourne, in 1988 where he has mainly been involved with cable technology. He is currently Principal Engineer with Customer Access Fibre Network Section of Technology & Engineering Practices Branch, Commercial & Consumer Business responsible for the development, implementation and technical management of copper and optical fibre cable mainly in the Customer Access Network.



Rong-Chang Hsieh received the BSEE degree from Taipei Tatung Institute of Technology in 1973 and the MSEE degree from the University of Colorado, USA, in 1979. He has extensive experience in TV design, optical fibre cable design, testing, fault location techniques, training, development of national cable standards, international project consultancy and management of AOTC Customer Access Network cable design. He is currently Principal Engineer with Customer Access Planning Branch of Commercial & Consumer Business responsible for the Fibre-to-the-Curb and Fibre-To-The-Customer-Premises field trials.



Alfred W. Kruijshoop graduated with an M.Sc. in applied physics from Delft University of Technology and worked in the Netherlands with Shell Research on metal-fluid interfaces. He then lectured in Physics at the University of Papua New Guinea, with research and consulting in atmospheric and soil physics and energy and environmental monitoring projects. He joined the AOTC Telecom Research Laboratories in 1986 as Principal Physicist to work on the environmental reliability of telecommunication plant and materials with an emphasis on optical fibre cable, interconnection technology and passive devices.

FIBER OPTIC GUIDED UNDERWATER VEHICLES

Veit Kölschbach, Hubert Tröndle

Philips Kommunikations Industrie AG
Nachrichtenkabel und -anlagen
Piccolominstr. 2
5000 Köln 80
Federal Republic of Germany

Abstract

This paper reviews the development of an optical fiber link for bi-directional data communication between an underwater vehicle and a control station. The development is intended for applications, where high speed deployment and long lengths of cable are required. It focuses on the choice of an appropriate winding technique and a suitable design of minicable.

The solution aims to minimize tensile forces during payout. This is achieved with a lattice wound coil that shows negligible loss increase due to winding. A well suited secondary coating was developed taking into account the winding behavior. Properties of secondary coated fibers under severe environmental conditions are discussed.

Laboratory tests allowed the measurement of tensile forces and attenuation behavior in water at pay-off velocities up to 25 m/sec. Consequently launching tests were performed under realistic conditions.

Introduction

Today guided underwater vehicles are used in research and military applications. Although guidance by copperwire is well established, this technique is subject to severe limitations. Obviously, guidance applications benefit from the properties of optical fiber transmission known from telecommunication:

- low signal attenuation
- high speed data transmission due to fiber bandwidth in GHz-range
- low weight and small cable diameter
- simple, reliable transmission techniques compared to complex conventional techniques

The development is intended for applications, where high speed deployment and long length transmission are required, and where only limited space for the cable is available. The minicable is wound to a self-supporting coil which is positioned in a container inside the underwater vehicle. The fiber is deployed while the vehicle moves through the water.

Design Considerations

One aim of the project was to develop a solution based on standard singlemode fibers according to CCITT G. 652 at the operation wavelength 1300 nm. Optical fiber characteristics are given in Table 1. On this premise, the concept has to avoid small bending radii, which would cause additional attenuation. Additional attenuation caused by a single sharp bend with a radius in the range 5 ... 10 mm is hard to control with standard singlemode fibers[1]. Such sharp bends may occur at the peel-off point. There are mainly two parameters influencing this behavior: the flexural strength of the cable and the tensile force acting on the cable which, for its part, depends on the presence of an adhesive.

Unlike high speed deployment in air, where usually multiple layer windings wound within a canister are preferred, a self-supporting coil with payout from the inside is considered to be most appropriate in water. The coil is fixed in a container at the faces and the outer side.

Mode field diameter	9 ± 0.9	µm
Cutoff-wavelength λ_c	1200 ... 1280	nm
1550 nm loss performance diameter 75 mm	< 0.1	dB / 100 turns
chromatic dispersion coefficient 1285 ... 1330 nm	< 2.7	ps/nm/km

Table 1 Fiber characteristics

At first sight, the multiple layer winding technique seems to be most suitable to the fiber properties with respect to bending radii. But on closer examination, the universal winding technique, often referred to as basket weave or lattice wound coil, clearly offers some advantages, because a self-supporting and stable coil can be achieved without continuous use of an adhesive.

The concept of minimal tensile forces during payout allows small cable diameters because there is no necessity for additional strength members. Preliminary minicable designs consist of one or two singlemode fibers with a thermoplastic coating. Composite buffered designs with a thin layer of gel between primary and secondary coating and tight secondary coated fibers were tested (compare Fig. 1). Both designs were studied as singlefiber cable (type A and C) and as well as dual fiber cable (type B and D). Preselected coating materials are thermoplastic polyurethane (TPU), polyvinylchloride (PVC non-rigid) and polybutyleneterephthalate (PBT).

The development steps are shown in Figure 2. Special attention was given to attenuation increase due to winding and also to minimum tensile forces during payout.

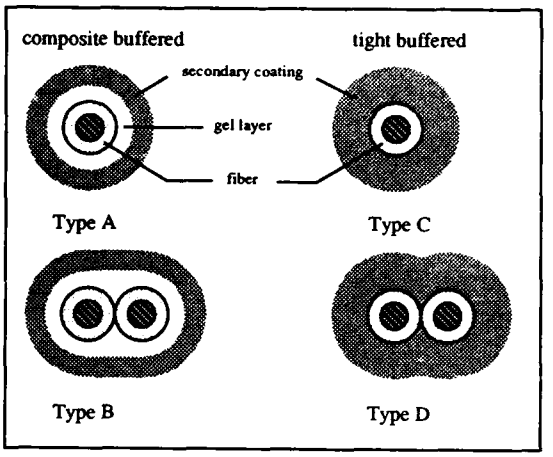


Fig. 1 Minicable designs

Winding Technique

The performance of coils was evaluated by visual inspection and measuring of optical attenuation. A series of winding tests was carried out with universal winding and layer winding equipment. Lengths of 2000 m cable were used for the comparative tests.

Precision multiple layer winding was done in two ways: The first one involved radial winding on a mandrel starting with the innermost layer. The second one was axial winding starting with the face side on a disk. Axial winding turned out to be more difficult, because winding a layer from larger to smaller radii generates a radial force which pulls the cable towards the axis of the winding disk. Therefore it is necessary to fix the cable in the right position immediately with an adhesive. To form a self-supporting coil, layer windings have to be fixed with an adhesive in a similar manner. Deployment was only moderately reliable for both types of windings due to the adhesive. The absence of a core in the self-supporting coil poses a risk of two or more turns being pulled off the spool at one time.

A lattice wound coil demonstrates sufficient stability even without adhesive. Its payout reliability is excellent, and well proven in many other applications in the textile industry.

One disadvantage of universal winding is that more space per unit length may be required. Looking at the space factor, which is defined as the ratio of cable-volume and coil-volume including interstices, universal winding shows a factor of 60 % whereas layer winding reaches values of up to 85 %. The universal coil thus requires more volume than layer winding.

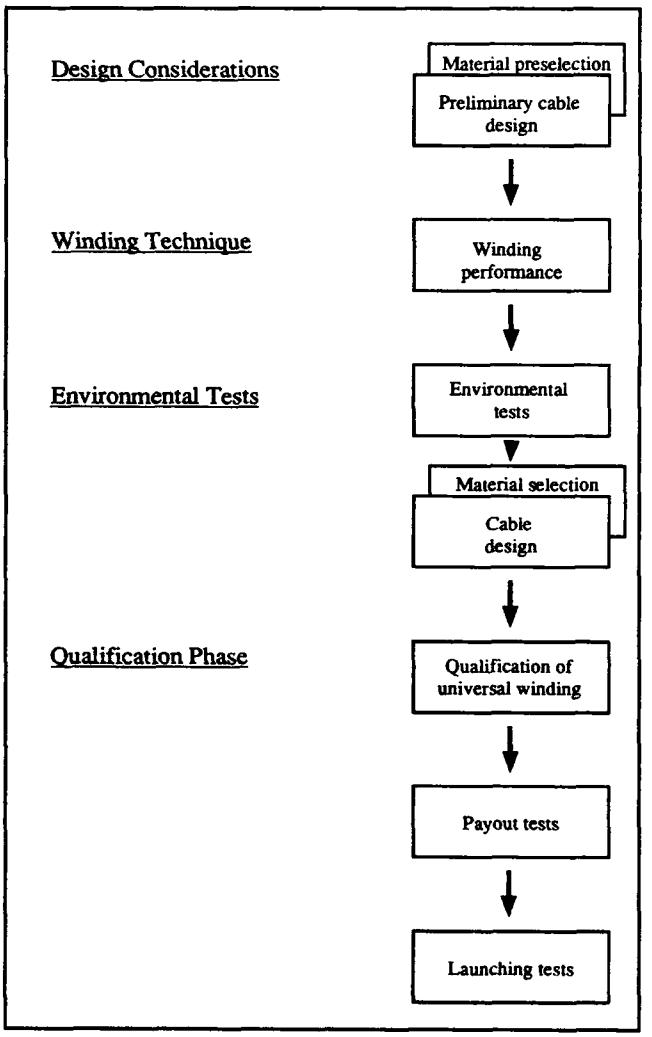


Fig. 2 Development steps for fiber optic guidance of underwater vehicles

Normally long lengths of fiber need to be accommodated within the vehicle. This requires a high layer count for the coil. This is quite easily achieved with universal winding. With layer windings it is much more complicated and the layer count is strongly limited by the geometrical tolerances of the cable.

With standard G. 652 fibers, the universal coils show attenuation increases at 1550 nm that do not permit reliable transmission at this wavelength. Thus transmission is limited to the wavelength 1300 nm, unless the fiber is upgraded to special bend-insensitive fiber type.

A qualitative summary of the test results is given in Table 2 . The findings clearly favor the universal winding technique for the planned application.

A stable and self-supporting coil is obtained with universal winding when the angle between the cable and coil axis lies within 75 deg. to 86 deg[2]. Besides the winding angle the relevant parameters determining geometry and optical attenuation are: winding force, guide pressure and spacing between two adjacent turns. The parameters have to be chosen carefully so as not to distort the geometry of the coil or to lead to an unacceptable increase of attenuation.

One effect, for example, is that the coil does not obtain a plain surface, but becomes raised near the crossing points. Crossing points here are understood as points where a turn passes over the preceding turn. Figure 3 compares two surface patterns, the first one with a "good spool geometry", the second one with distortions in geometry near the crossing points.

characteristics	layer winding	universal winding
stability without adhesive	not applicable	very good
payout reliability	moderate	excellent
space factor	85 %	60 %
high layer count	poor	very good
transmission window	1300 nm and 1550 nm	1300 nm for G. 652 fibers

Table 2 Comparison of winding techniques

Attenuation behavior depends on cable design and on the material used. For tight buffered minicables (types C and D) and especially type C, a higher added loss was detected in comparison with types A and B. This resulted from the need for higher winding forces and guide pressures. The loss arising from the type of material used was examined by comparing coils with equal winding parameters. This effect is attributed to Young's modulus of the secondary coating. For our winding diameters and the geometrical conditions, an upper limit for Young's modulus can tentatively be given. For type C and D cables, the limit is in the range of 0.7 to 1 GPa. With type A and B designs, uniform winding patterns with tolerable attenuation changes are achieved even with Young's modulus of 2 GPa.

Cable designs with an attenuation increase less than 0.1dB/km due to winding were found to be worth testing in environmental tests for further evaluation.

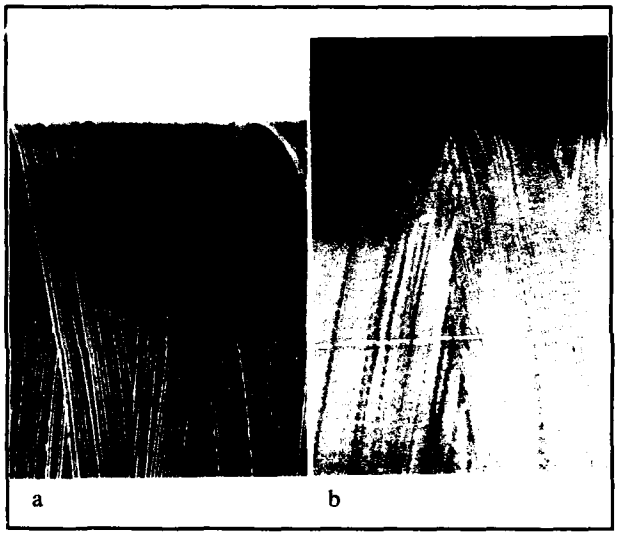


Fig. 3 Surface patterns of universal windings
a) uniform pattern, b) distorted geometry

Environmental Tests

Coils containing 2 km of fiber were studied in environmental conditions given in Table 3. Critical tests for the tight buffered types turned out to be the water immersion test and the hydrostatic pressure test, whereas type A and B cables produced excellent results. Examples of test results on types A and C are given in Figure 4. Type A shows smaller attenuation increases in thermal cycling, water immersion and hydrostatic pressure tests. The test findings indicated that only A and B type cables are suitable for this application.

To obtain a smaller volume per cable length than that of existing copper-wire systems, a diameter of 0.6 mm was chosen for the single fiber cable. All subsequently discussed test results refer to this cable diameter.

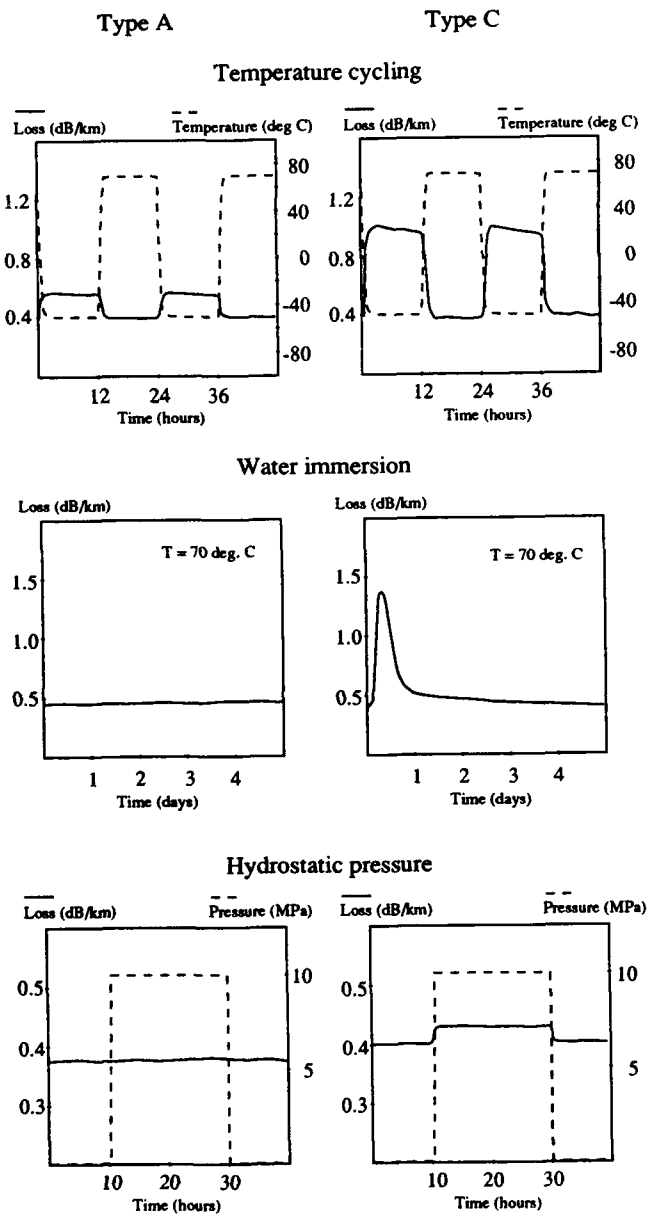


Fig. 4 Test results for Type A and C cables under environmental conditions

Characteristics	Parameter	Time	Standard
attenuation	1310 nm	-	IEC 793-1-C1C
temperature cycling	-50 ... +70 deg C period t_1 21 cycles	12 h	IEC-794-1-F1
water-humidity cycling	- water 20 deg C - drying 25 deg C and rel. humidity 30 % - humidity 40 deg C and rel. humidity 95 % 21 cycles	7 h 5 h 12 h	internal
water immersion	70 deg C	21 d	internal
hydrostatic pressure	10 MPa (100 bar) - rise time: - dwell time: - fall time: 2 cycles	 10 min. 20 h 1 min.	internal
low pressure cycling	50 hPa - rise time: - dwell time: - fall time: 1000 hPa 2 cycles	 5 min. 30 min. 5 min. 6 h	internal
vibration	frequency range from 10 to 150 Hz acceleration 40 m/s^2 3 cycles	30 min.	IEC 874-1-18.2

Table 3 Environmental test procedures

Qualification of Universal Winding

The expected high layer count for universal winding was verified during a test series. Starting on coil forms with diameters varying from 100 to 350 mm, outer diameters in the range of 150 to 400 mm were realized. Universal winding proofed to be a stable process even with lengths 25 km, but longer lengths are also possible.

As a result, it can be stated that universal winding allows geometries with a small coil width and large outside diameters. For a coil form with a diameter of 100 mm and a coil width of 150 mm, a diameter/width ratio of 2.5 can be achieved.

The winding tests show that universal winding is insensitive to deviations of the cable cross-section. This attribute could be useful when splicing and carrying out secondary coating repair.

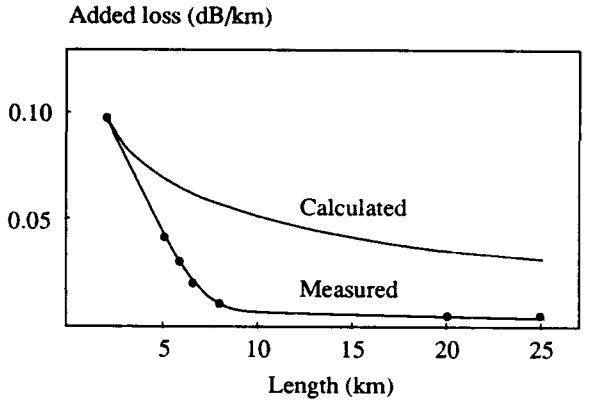


Fig. 5 Attenuation increase due to universal winding

Characteristics	Parameter	attenuation change / resp. other criteria
temperature cycling	-50 ... +70 deg C 21 cycles	0 ...70 deg C: 0.04 dB/km -50 ...70 deg C: 0.30 dB/km
water-humidity cycling	- water 20 deg C - drying 25 deg C and rel. humidity 30 % - humidity 40 deg C and rel. humidity 95 % 21 cycles	0.02 dB/km
water immersion	70 deg C	0.03 dB/km
hydrostatic pressure	10 MPa 2 cycles	0.02 dB/km
low pressure cycling	50 hPa ... 1000 hPa 2 cycles	0.02 dB/km
vibration	10 ... 150 Hz , 40 m/s^2 3 cycles	no distortion of layers

Table 4 Qualification test results

Winding slightly increases attenuation at 1300 nm but its effect is negligible in actual practice. Most of this additional attenuation can be attributed to the bends near the crossing points, that occur twice per turn. The attenuation coefficient becomes less for larger winding radii, because the number of bends per length is smaller the larger the winding diameter.

Figure 5 shows measured values and a calculated curve, that is adjusted to the measuring length of 2 km. The calculated curve predicts higher attenuation coefficients for longer lengths, because this simplified model takes into account only the number of bends, and neglects the fact that the bending radii at the crossing points become larger as the winding diameter increases. Nevertheless transmission at 1300 nm is not seriously affected by the attenuation increase reported here.

The results of the environmental tests for the chosen cable design and parameters evaluated for universal winding are given in Table 4.

Payout Tests

Payout performance was simulated with a reel-off model (Fig. 6). The model is designed for payout velocities of up to 25 m/sec.

The coil was submerged in water. A steady flow of water in the tube behind the coil simulated a moving vehicle. The desired test velocities were obtained by using an additional pulley. Tensile forces acting on the minicable during payout were measured. At velocities up to 25 m/sec., the continuous forces were well below 5 N. They are independent of the winding diameter, but approximately increase linearly with increasing payout-velocity.

In addition to the tensile force, a sinusoidal signal was recorded to observe possible loss increase. There was no attenuation increase due to payout. That means the bending radius at the peel-off point is uncritical as regards attenuation (Fig. 7).

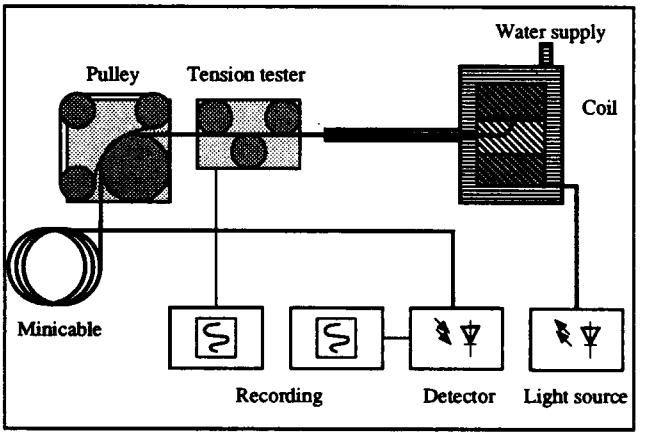


Fig. 6 Reel-off model

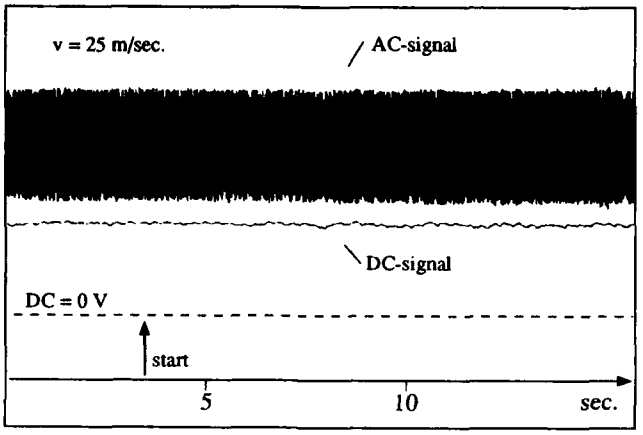


Fig. 7 Signal pattern during payout test

Launching Tests

For launching tests under realistic conditions, a trial torpedo was modified to take up the coil consisting of a single fiber A-type cable.

The optical source in the transmission system was a high radiance 1300 nm LED. The LED was attached to the fiber by means of a fusion coupler. Guidance commands from the control station and sensor signals from the vehicle were transmitted as FSK coded binary signals. The modulation frequencies indicated the transmission direction.

During the test series, a cable length of 12 km was successfully deployed several times. Like the payout tests, the launching tests confirmed that payout does not increase attenuation. The total tested length of fibers was more than 100 km. During the launching tests, no transmission error was caused by the optical part of the transmission system.

Summary

To evaluate the advantages of optical fiber transmission for underwater vehicle guidance, a development project with standard singlemode fibers was successfully performed.

More than 40 km of the developed minicable can be packaged to a universal winding.

Operation at 1550 nm wavelength is possible with bend-insensitive fibers.

Acknowledgment

The authors would like to thank Mr. G. Pies, Mr. U. Meissner and all members of the PKI development laboratories for their extensive support.

References

1. D. Biswas, K. Karbassiyoon, L. Hodgers, Singlemode Bend-Insensitive Fiber, International Wire and Cable Symposium Proceedings 1988 , pp. 603-606, 1988

2. WM. Querfurth, Coil Winding, Geo. Stevens MFG. Co., Chicago - Illinois, 1968



Veit Kölschbach was born in 1959. He obtained a degree in experimental physics from the Rheinische Friedrich-Wilhelms-Universität Bonn.

He joined Philips Kommunikations Industrie AG in 1986. In 1990, he was appointed head of the product development section for optical fiber cables.



Hubert Tröndle was born in 1952. He obtained a degree in electrical engineering from the Rheinisch-Westfälische Technische Hochschule Aachen in 1981. In the same year he joined Philips Kommunikations Industrie AG. He was employed initially on the development of cable measurement equipment and later on optical fiber cables. He is now Product Manager Advanced Cable Systems.

Optical Fiber Line Surveillance System for Preventive Maintenance Based on Fiber Strain and Loss Monitoring

Izumi Sankawa, Yahei Koyamada, Shin-ichi Furukawa
and Tsuneo Horiguchi

NTT Telecommunication Field Systems R&D Center
Tokai, Ibaraki, 319-11, Japan

Abstract

A surveillance system is demonstrated for use with an optical fiber line network. It provides a warning, based on fiber strain and loss monitoring, when there is a need to initiate preventive maintenance. This system monitors for two types of fiber fault. One is caused by tensile strain in a fiber which induces fiber failure and the other is caused by fiber bending and the absorption of hydrogen molecules which induces loss increase. The system automatically calculates the fiber fault probability.

1. Introduction

During the last decade, optical fiber transmission systems have played a vital part in trunk line and subscriber line networks. As these networks expand and optical transmission systems with high fiber count cables come into use, fiber operations such as testing, fault location and the supervision of transmission characteristics will become more complicated. Recently, a number of reports have appeared that propose automatic operation, administration, and maintenance systems for optical fiber line networks.[1]-[5] In these systems, the optical characteristics of fiber lines at communication band wavelengths have been automatically and remotely monitored by using conventional equipment such as light sources, optical power meters and optical time domain reflectometers. However, fiber failure and loss increase in a cable or a cable joining closure can not be predicted with this equipment. Since system failure due to fiber or cable faults may seriously affect many customers, there is an urgent need to develop an optical fiber line surveillance system which can diagnose fiber and cable degradation and warn of the need for preventive maintenance. This paper presents key technologies and the system configuration of such an optical fiber line surveillance system.

Two new techniques have been developed which can be used to predict fiber failure and loss increase. One is Brillouin Optical Time Domain Analysis (BOTDA) which measures the tensile strain distribution in fibers.[6] [8] The other is Optical Time Domain Reflectometry (OTDR) in the 1.6 - 1.7 μm wavelength range, which is suitable for the detection of loss increases due to bending and/or hydrogen absorption before the service is affected at communication wavelengths (1.3 to 1.6 μm). A prototype surveillance system is constructed, which automatically and remotely accesses fibers, diagnoses fiber degradation and anticipates fiber failure probability.

2. Basic concepts for Preventive Maintenance of Fiber Line Networks

Table 1 outlines the sites and causes of fiber faults. Fiber faults are classified into two types; fiber failure and fiber loss increase. The former is caused by tensile strain inside a fiber in a cable and by fiber bending in a cable joining closure. In addition to this strain, the strength of optical fibers is generally reduced by water penetration. The latter is caused by fiber bending and by the absorption of hydrogen molecules.

Table 1 Sites and causes of fiber faults.

Site	Fiber fault	Cause
At cable joining point	Fiber failure	Water penetration and fiber bending
	Loss increase	Fiber bending and fiber joint
In fiber cable	Fiber failure	Tensile strain and water penetration
	Loss increase	Fiber bending and/or water penetration

Table 2 Items of fiber measurement.

Site	Cause	Items of measurement
At cable joining point	Water penetration	Time and date of penetration
	Variation in fiber bending radius	Fiber bending loss
In fiber cable	Water penetration	Time and date of penetration
	Tensile strain in fiber cable	Tensile strain

Items for fiber line measurement are shown in Table 2. Recently, a water sensor module has been proposed[10], in which absorbent material expands and bends the fiber causing additional optical loss in the monitor fiber. It is clear that a technique is needed for measuring the tensile strain and bending loss increase of fibers with high sensitivity.

The fiber fault probability in the new surveillance system is estimated based on BOTDA and OTDR for tensile strain and bending loss increase, respectively. First, the fiber failure probability, F, is calculated from the measured tensile strain, δa, as follows;

$$F = 1 - \exp\left[Np\ L \left\{ 1 - \left(1 + \left(\frac{\delta a}{\delta p}\right)^{n} \left(\frac{ta}{tp}\right)\right)^{m/(n-2)} \right\} \right] ,$$

where Np is the failure number per unit length during proof testing, L is the fiber length under tensile strain, δp is the tensile strain during proof testing, n is the crack growth parameter, ta is the loading time under δa, tp is the loading time during proof testing and m is the slope of a distribution in a Weibull probability chart.[11] The system warns operators based on this equation. For fiber bending, the loss distribution is periodically measured by high sensitivity OTDR at longer wavelengths and recorded as past data. The time dependence of loss increase at longer wavelengths is calculated automatically, based on the measured loss values, and loss values in the near future are estimated. If these estimated loss values are larger than the prescribed ones, the system gives a warning. It is noted that the loss increase due to water penetration is also detected and estimated.

Therefore, operators can diagnose fiber degradation on the basis of these results and deal with it before the service is affected.

3. Key Technologies for preventive maintenance

This section introduces newly developed techniques for measuring fiber strain distribution.

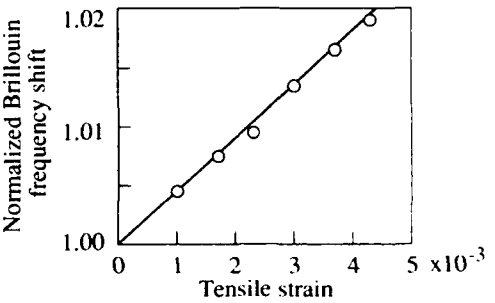


Fig.1 Normalized Brillouin frequency shift versus tensile strain.

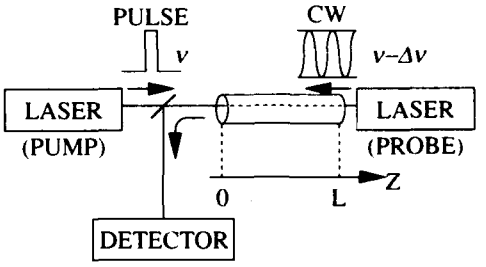


Fig.2 Basic configuration of BOTDA.

3.1 Tensile Strain Measurement

If tensile stress is applied to a fiber over a long time, it causes degradation in fiber strength, leading finally to fiber failure, even if the tensile stress is considerably lower than that which causes immediate failure. The time to failure depends on the magnitude of the applied tensile stress and environmental conditions as described above. In order to predict fiber reliability, it is necessary to measure the tensile strain or stress in fibers. Recently, Brillouin Optical Time Domain Analysis (BOTDA) has been developed for this purpose. This technique is briefly explained below.[6]-[8]

The tensile strain induces a change in the Brillouin frequency shift in fibers as shown in Fig.1. From this figure, it can be seen that the magnitude of Brillouin frequency shift varies linearly with the tensile strain. It is possible, therefore, to estimate the tensile strain in the fiber by measuring the Brillouin frequency shift. Figure 2 shows the basic configuration for BOTDA. A pulsed lightwave and a continuous lightwave with a frequency difference $\Delta\nu$ are launched into the test fiber from opposite endfaces so that they counterpropagate. When their optical frequency difference $\Delta\nu$ coincides with the Brillouin frequency shift, the CW lightwave is amplified by the pulsed lightwave through Brillouin scattering. Thus, by repeated measurement of time-dependent CW light power for various $\Delta\nu$ values, the Brillouin frequency shift in any part of the test fiber can be measured as the optical frequency difference $\Delta\nu_{max}$ at which the CW light power is maximized.

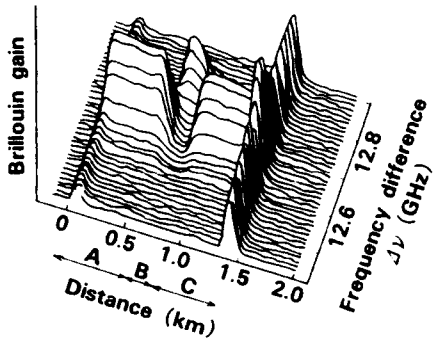


Fig.3 Brillouin amplification gain distribution.

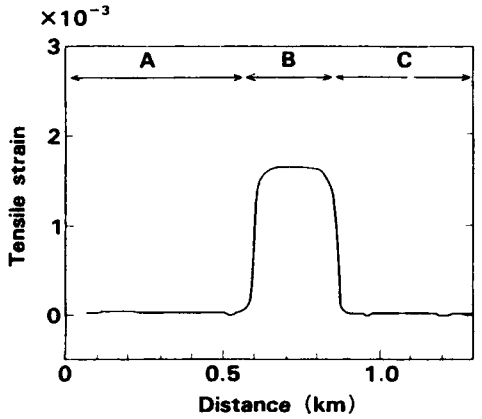


Fig.4 Fiber strain distribution.

Tensile strain distribution in a fiber in the test cable was measured using BOTDA. Figure 3 shows the experimental results for a fiber, which consists of three sections A, B and C. Tensile stress is applied uniformly throughout section B. The CW light power increase (Brillouin amplification gain) is three-dimensionally displayed on a plane which is determined by the distance z and the optical frequency difference Δν. In this figure, the Brillouin gain datum at any point represents the average Brillouin gain value within half a pump pulse around that point. The ridges at either end are Fresnel reflection lights at the measurement ends. The Brillouin frequency shift Δvmax, at which the CW light amplification is maximized, is shifted for section B from those for the other sections. This shift indicates the strain induced by the applied stress in section B. Figure 4 shows the tensile strain distribution, which is calculated from the distribution of Δvmax. From this figure, it is clear that a uniform tensile strain of 0.16% appears in section B. This result coincides with the mechanically measured value with an error of less than 10%. This result shows that the variation in tensile strain can be obtained by using the Brillouin scattering phenomenon.

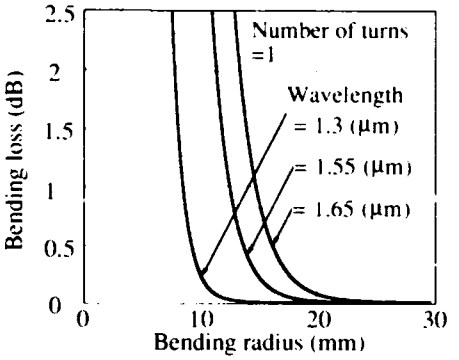
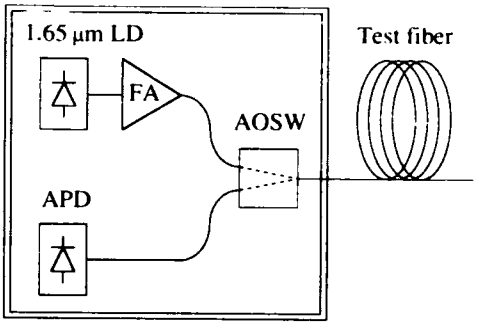


Fig.5 Bending loss versus bending radius.



FA : Fiber amplifiers, AOSW : Acousto-optic switch

Fig.6 Basic configuration of OTDR at 1.65μm.

3.2 Bending Loss Measurement

Fiber bending induces fiber loss increase as described in section 2. The loss value depends on the bending radius and is generally larger at longer wavelengths as shown in Fig.5 for single mode fibers. From this figure, it is clear that the bending loss increase can be sensitively detected by monitoring the loss distribution periodically at longer wavelengths. Therefore, Optical Time Domain Reflectometry (OTDR) at longer wavelengths is suitable for the detection of loss increases due to bending before the service at communication wavelengths (1.3 to 1.6 μm) is affected.

Figure 6 shows the basic configuration for OTDR at longer wavelengths. Two kinds of optical amplification technique in the 1.6 - 1.7 μm wavelength range are used to improve the OTDR performance. One is the erbium-doped aluminosilicate fiber amplifier [12] and the other is the stimulated Raman fiber amplifier.[9]

(1) Erbium-doped aluminosilicate fiber amplifier

In erbium-doped fiber amplifiers (EDFAs), the spectral bandwidth of optical gain is expanded by doping the silica glass with aluminum. Recently, a 15 dB gain has been obtained for a signal wavelength of 1.6 μm using an erbium-doped

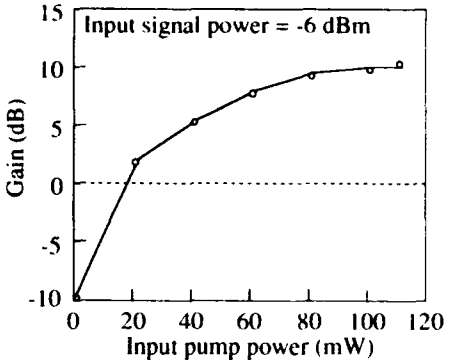


Fig.7 Gain characteristics of EDFA.

aluminosilicate fiber amplifier pumped by a color center laser.[13] The color center laser is so bulky that this configuration can not be combined with optical measurement equipment. We have investigated a practical EDFA pumped by semiconductor laser diodes. The pump light sources were two 1.48 μm laser diodes (LDs) whose outputs were combined with a polarizing beam splitter, providing a total optical power of 110 mW. The signal light source was a 1.617 μm DFB-LD. Figure 7 shows the gain characteristics of an erbium-doped aluminosilicate fiber amplifier at a wavelength of 1.617 μm. A gain of 10 dB has been obtained.

(2) Stimulated Raman fiber amplifier

We have investigated a stimulated Raman fiber amplifier (RFA) operating at around 1.65 μm. The RFA setup is shown in Fig.8. The pump pulses were output optical pulses from a 1.555 μm laser diode, amplified by the EDFA. Signal pulses from a tunable color center laser modulated by an acoustooptic modulator were combined with the pump pulses by a WDM coupler and synchronized at the input to a Raman fiber. The Raman fiber was a 20 km long dispersion-shifted fiber with a fiber loss of 0.21 and 0.26 dB/km at 1.55 and 1.66 μm, respectively. Figure 9 shows the measured spectral characteristics of the RFA. This figure reveals that the RFA gain is 23 dB at a center wavelength of 1.665 μm and the 3 dB bandwidth is 33 nm.

The fiber bending loss was measured by using OTDR. Figure 10 shows the measured bending loss dependence on the bending radius for a dispersion-shifted fiber ribbon. From this figure, we found that a larger bending loss value is obtained at longer wavelengths. This result coincides with the loss value measured using a light source and an optical power meter. Therefore, it is possible to detect fiber bending by OTDR at

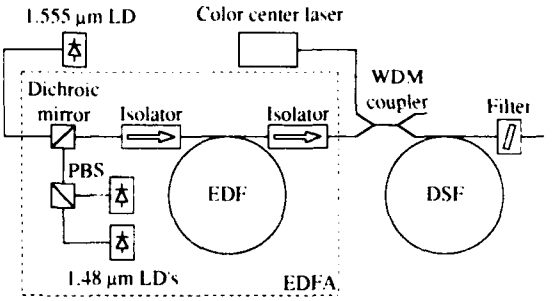


Fig.8 Setup of Raman fiber amplifier.

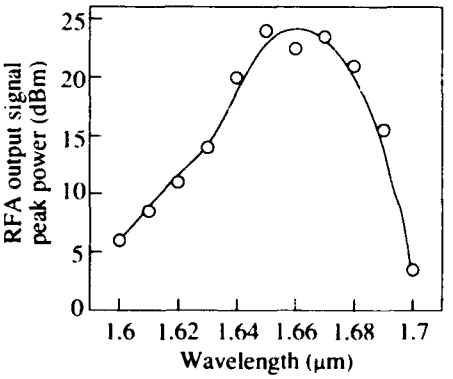


Fig.9 Spectral characteristics of RFA.

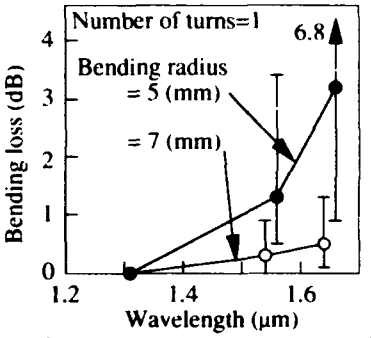


Fig.10 Bending loss versus wavelength.

longer wavelengths before the service is affected.

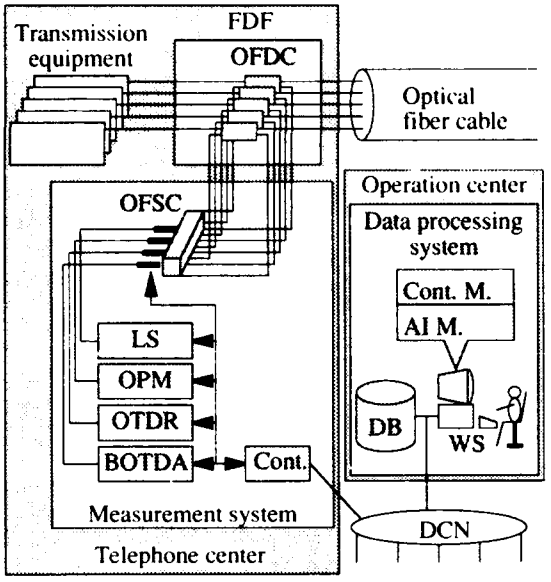
4. System Configuration and Performance

We constructed a prototype system which can remotely and non-intrusively access fibers and automatically diagnose fiber line degradation. This system is now being examined for use in preventive maintenance. Figure 11 shows the system configuration. The system consists of a measurement system installed in a telephone office and a data processing system installed at an operation center. Key structural elements of the measurement system are as follows:

(1) Optical fiber directional coupler for measurement access,

(2) Optical fiber selecting connector,

(3) Measuring equipment such as LS, OPM, OTDR operating at long wavelengths and BOTDA,



FDF : Fiber distribution frame
OFDC : Optical fiber directional coupler
OFSC : Optical fiber selecting connector
LS : Light source
OPM : Optical power meter
OTDR : Optical time domain reflectometer
BOTDA : Brillouin optical time domain analizer
DCN : Data communication network
DB : Data base
WS : Workstation
Cont.M. : Controlling software module
AI M. : AI software module

Fig.11 Configuration of Fiber line surveillance system.

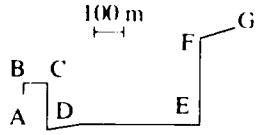


Fig.12 Conduit route for cable installation.

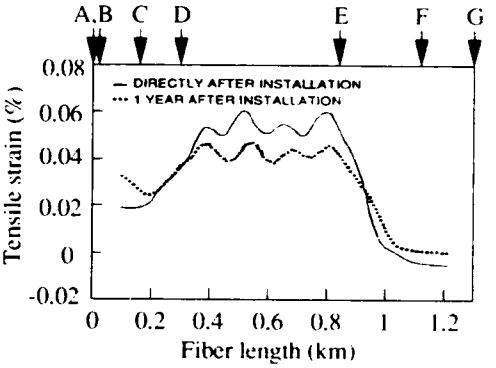


Fig.13 Tensile strain distribution.

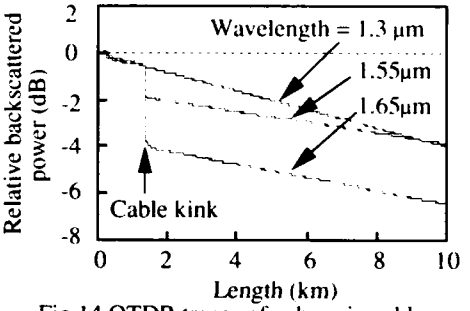


Fig.14 OTDR traces of submarin cable after laying trials.

(4) Multi-job measurement controller.

In the data processing system, a database, which stores the periodically measured data on fiber strain and loss, and an AI module are installed in order to anticipate fiber fault probability. Based on this estimation of tensile strain and bending loss of fibers, the prototype system diagnoses fiber degradation and warns operators. This is described below.

4.1 Tensile strain

The prototype system was used to measure the distributed tensile strain in single mode fibers in a field-installed cable and estimate its fiber failure probability. This cable was installed into the conduit route as shown in Fig. 12. Letters A-G in the figure denote the cable ends and corners in the conduit route. Figure13 shows the measured tensile strain distributions in the fiber in this cable. The solid line shows the tensile strain distribution measured immediately after installation and the broken line shows that measured one year after installation. The letters with arrows in the figure correspond to the cable ends and corners in the conduit route. From Fig.13, it is found that a maximum residual tensile strain in the DE section is decreased. This strain decrease is evaluated as 0.01%. Based on this data, the data processing system calculated a fiber failure probability. As a result, the tensile strain value was found to be sufficiently small compared to the tolerable maximum tensile strain of about 0.17% for a 20 year lifetime against 10 FIT / 100 km.[14]

4.2 Bending loss

The system measured the bending loss of fibers in a submarine optical cable during laying trials by using the 1.65 μm OTDR. This cable contained 48 dispersion-shifted fibers. A kink was intentionally made in the cable at a distance of about 1.3 km from the fiber end during the cable laying process. Figure 14 shows measured OTDR traces of the 38th fiber line at 1.3, 1.55 and 1.65 μm, respectively. From this figure, it is clear that a bending loss appears at a fiber length of about 1.3 km, which corresponds to the length of the cable kink, and is

larger at longer wavelengths. A loss increase also appeared at longer wavelengths in OTDR traces of the 39th and 40th fibers. The prototype system gives a warning, based on these results, which indicates the occurrence of abnormal loss increase in fiber lines.

5. Conclusions

This paper described an optical fiber surveillance system for preventive maintenance based on fiber strain and loss monitoring. Key measuring technologies and elements for in-service strain and loss monitoring were explained. A prototype system which will lead to the development of centralized and automated fiber line measurement system was also presented.

Several areas need further study before optical fiber lines can be measured in practice. Lengthy and careful consideration should be given to these problems.

Acknowledgment

The authors thank T.Kurashima for useful discussions. The authors gratefully thank K.Ishihara and Y.Wakui for their encouragement.

References

(1) F.A.Huszarik, et al.,"Installation and testing of multiservice fiber links in the subscriber loop: a case study", Proceedings of 37th I.W.C.S., pp.158-162, (1988).

(2) Y.Koyamada, et al.,"Basic concepts of optic subscriber loop operation systems", Proceedings of IEEE I.C.C., pp.1540-1544, (1990).

(3) T.Uenoya, et al.,"Operation, administration and maintenance systems of the optical fiber loop", Proceedings of GLOBECOM, pp.1493-1497, (1990).

(4) H.Takasugi, et al.,"Design and evaluation of automatic optical fiber operation support system", Proceedings of 39th I.W.C.S., pp.623-629, (1990).

(5) H.Matsumoto, et al.,"Cable transfer and supervisory system for trunk optical fiber cables", Proceedings of 40th I.W.C.S., pp.787-792, (1991).

(6) T.Horiguchi, et al.,"Tensile strain dependence of Brillouin frequency shift in silica optical fibers",IEEE Photon. Technol. Lett., vol.1, pp.107-108, (1989).

(7) T.Horiguchi, et al.,"BOTDA-Nondestructive measurement of single-mode optical fiber attenuation characteristics using Brillouin interaction:Theory", J. Lightwave Technol., vol.7, pp. 1170-1176, (1989).

(8) M.Tateda et al.,"First measurement of strain distribution along field-installed optical fibers using Brillouin spectroscopy", J. Lightwave Technol., vol.8, pp.1269-1272, (1990).

(9) T.Horiguchi et al., "Stimulated Raman amplification of 1.6 μm band pulsed light in optical fibers", IEEE Photon. Technol. Lett., vol.4, pp.64-66, (1992).

(10) S.Tomita et al.,"Water sensor with optical fiber", IEEE J. Lightwave Technol., vol.8, pp.1829-1832, (1990).

(11) Y.Mitsunaga et al.,"Failure prediction for long length optical fiber based on prooftesting", J. Appl. Phys., vol.53, pp.4846-4853, (1982).

(12) I.Sankawa et al.,"Fiber measurement techniques for passive double star networks", Proceedings of 3rd IEEE Workshop on Local Optical Networks, pp.4.2.1-4.2.10, (1991).

(13) J.F.Massicott et al.,"High gain, broadband, 1.6μm Er^{3+} doped silica fiber amplifier", Electron. Lett., vol.26, pp.1645-1646, (1990).

(14) Y.Mitsunaga et al.,"Strength assurance of optical fiber based on screening test"(in Japanese), Trans.IECE Japan, vol.J66-B, pp.829-836, (1983).



Izumi Sankawa
NTT Telecommunication
Field Systems R&D Center
Tokai, Ibaraki Japan

Izumi Sankawa is a senior research engineer with the Optical Subscriber Cable Systems Laboratory in the Telecommunication Field Systems R&D Center in NTT. He was born in 1956 and received B.E. and D.E. degrees in electrical engineering from Waseda University in 1979 and 1991, respectively.

He joined NTT in 1979. Since 1987, he has been engaged in the development of optical fiber measuring technologies and optical fiber surveillance systems. He is a member of IEICE of Japan who presented him with the 1985 Young Engineer Award.



Yahei Koyamada
NTT Telecommunication
Field Systems R&D Center
Tokai, Ibaraki Japan

Yahei Koyamada is a group leader with the Optical Subscriber Cable Systems Laboratory in the Telecommunication Field Systems R&D Center in NTT. He was born in 1947 and received B.E., M.E. and D.E. degrees in electrical engineering from Osaka University in 1970, 1972, and 1978, respectively.

He joined NTT in 1972. Since 1988, he has been engaged in the development of optical fiber measuring technologies and surveillance systems. He is a member of IEEE and IEICE of Japan.



Tsuneo Horiguchi
NTT Telecommunication
Field Systems R&D Center
Tokai, Ibaraki Japan

Tsuneo Horiguchi is a supervisor with the Optical Subscriber Cable Systems Laboratory in the Telecommunication Field Systems R&D Center in NTT. He was born in 1953 and received B.E. and D.E. degrees in electronic engineering from the University of Tokyo in 1974 and 1988, respectively.

Since he joined NTT in 1974, he has been engaged in the development of optical fiber measuring technologies and surveillance systems. He is a member of IEEE, the Optical Society of America, and IEICE of Japan.



Shin-ichi Furukawa
NTT Telecommunication
Field Systems R&D Center
Tokai, Ibaraki Japan

Shin-ichi Furukawa is a supervisor with the Optical Subscriber Cable Systems Laboratory in the Telecommunication Field Systems R&D Center in NTT. He was born in 1952 and received B.E. and D.E. degrees in electrical engineering from Kyushu University in 1974 and 1988, respectively.

He joined NTT in 1976. Since 1989, he has been engaged in the development of optical fiber measuring technologies and surveillance systems. He is a member of IEEE and IEICE of Japan.

Wide Dynamic Range Optical Talk System Using External Loss Modulation

Y.Unami K.Sakurai T.Yamada N.Kuwaki(*) M.Yumoto(**)

Fujikura Ltd. Chiba, Japan
* NTT Technical Assistance & Support Center Tokyo, Japan
** Suzuki Technical Engineering Chiba, Japan

Abstract

The external loss modulation has been applied to a new optical talk system that requires no fiber end in any intermediate point of an optical fiber. The system has a wide dynamic range and is capable of simultaneous communication between multi-points on an optical fiber. To realize such performances, the local light detection and the pulse amplitude modulation (PAM) techniques are adopted with the external loss modulation.

This paper focuses on the prototype system for 1550nm and describes the methods to realize some key functions of the system in both technical and operational aspects. The excellent properties and easy operations of the prototype system are also reported.

1. Introduction

Recently optical talk sets are becoming indispensable instruments during installation and maintenance of optical cables. Conventional talk sets require the access of the ends of a fiber for optical signal launching and detection, therefore, fiber cutting and splicing operations are unavoidable. An optical talk set free from such complicated and loss inflicting operations is strongly desired as an ideal instrument.

External modulation to an optical fiber and local light injection[1] are known to be useful methods to realize such kind of talk sets that operate without fiber ends. Furthermore, two external modulation methods for talk sets are already reported, one is the external loss modulation[2] and another is the polarized wave external modulation[3].

The external loss modulation method is adopted into the talk system in this paper, because the method provides the widest dynamic range and simultaneous communication between all talk sets on a fiber.

The principle of the talk system is based on the external loss modulation method, local light detection[1] technique, and PAM applied to a laser diode (LD). The local light detection is the fundamental technique used in fiber identifiers[4].

The prototype system for 1550nm on a single mode fiber (SMF) has demonstrated communication performance to be viable in many applications.

2. General Description

2.1 System Configuration

The talk system consists of master units and local units operated on a fiber. Fig.1 shows an example of system configuration comprising two master units and two local units. The two master units at both fiber ends are indispensable as light sources for external loss modulation utilized by local units in any configuration.

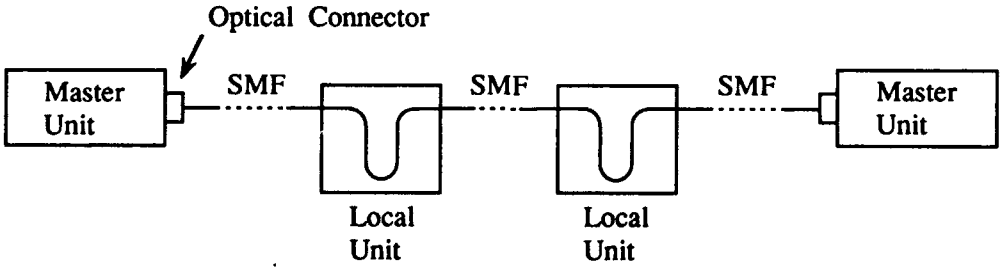


Fig.1 An Example of System Configuration

2.2 Master Unit

The master unit includes a LD, a photo diode (PD) and a 3dB optical fiber coupler for full duplex communication on a fiber as shown in Fig.2. The light signal access is achieved through the fiber end that is terminated with an optical connector normally. The LD drive current is directly modulated by voice signals as transmitted from the master unit, so called direct modulation.

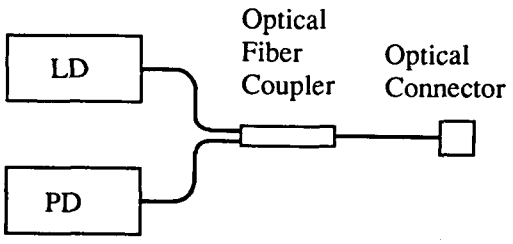


Fig.2 Basic Configuration of Master Unit

2.3 Local Unit

An external loss modulator and a PD for local light detection are the main components of the local unit shown in Fig.3. The loss modulator is a kind of electromagnetic vibrator. The variation of fiber bending width caused by the vibrator corresponds to the variation of the fiber loss. In this way, optical intensity modulation is achieved and the modulation index is basically in proportion with the vibration amplitude.

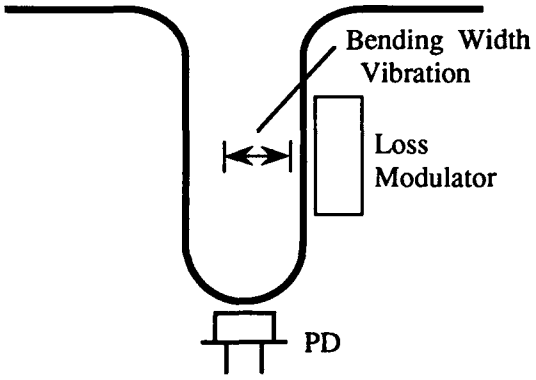


Fig.3 Basic Configuration of Local Unit

The vibration amplitude of such an electromagnetic vibrator is inversely proportional to the signal frequency. The maximum frequency capable to be transmitted is approximately 3kHz.[5]

In addition, the PD for local light detection has a large diameter in order to detect the leaked light power from the bending point of the fiber efficiently, but has a slow response. Furthermore, the bandwidth limitation of the internal electronic circuit improves the signal to noise ratio (S/N).

In the local unit, the voice signal is modulated in baseband because of those reasons above.

2.4 System Operation

The system operations of the light modulation and detection between master and local units are described as follows;

(1) Master to Master

The way between two master units is basic full duplex communication on a fiber using fiber ends similar to ordinary talk sets.

(2) Master to Local

The light modulated by the direct modulation within the master unit is detected by the local unit using local light detection method.

(3) Local to Master

The light from the master unit is externally modulated in the local unit and detected in the other master unit.

(4) Local to Local

The light from the master unit is externally modulated in one local unit and detected by the local light detection method in the other local unit.

3. System Design

3.1 Optical Isolator

It is well known that light injected into a LD not only damages the LD but also degrades the transmitted signal quality. The master unit in the system is also susceptible to such harmful light injected into a LD, such as the reflections from optical connectors included in an optical line and the light from the other master unit at the opposite fiber end. When the system is used in short fiber length applications, the light power from the other master unit is especially of high intensity.

An optical isolator is an effective solution to prevent these lights injected into the LD. A polarization independent optical isolator is adopted in the system shown in Fig.4, as the lights of two LDs from each of the master units have no correlation in polarization.

3.2 PAM

As mentioned before, an optical line normally includes some optical connectors or other optical components that cause reflections indicated in Fig.4. Furthermore, an optical fiber itself has an intrinsic property known as Rayleigh

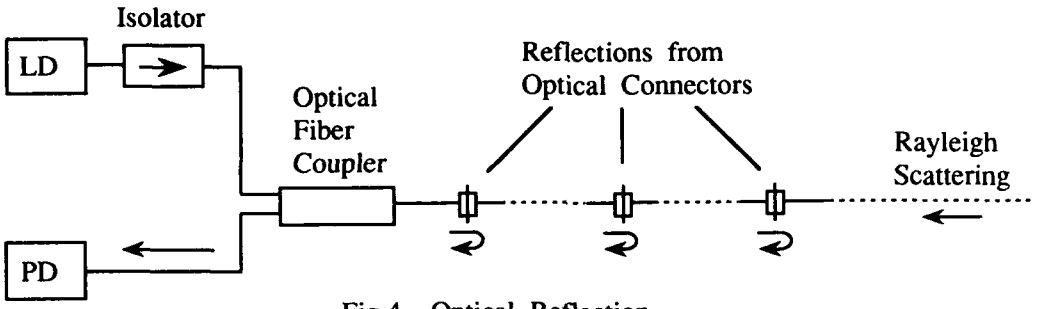


Fig.4 Optical Reflection

scattering that causes reflection of the transmitted light along the fiber. The source of these reflected lights from multi-points is the same LD in the master unit. If the length between reflected points is shorter than the coherent length of the LD, their interference results optical power fluctuations. This optical power fluctuation directly affects to the optical intensity modulation in baseband. The fluctuation is observed as the noise mixed with the demodulated voice signal in the master unit. The more the number of reflected points and the nearer they are to the master unit, the higher the noise level.

Generally, to prevent the degrading effect of reflected lights, wavelength multiplexing in optical region or multiple frequency carriers in electrical region are useful. The properties of the external loss modulation and local light detection is strongly dependent on the wavelength of the light used. Thus, two different frequency carriers are assigned to each master unit in the system. The master unit includes an electrical filter to exclude its own carrier frequency and a demodulator for amplitude modulation (AM) signals.

The modulated light signal from the master unit should be demodulated as a baseband signal in the local unit. The PAM method is adopted because the PAM signal can be demodulated as either a baseband signal or an AM signal.

The PAM signal from the master unit is demodulated as an AM signal in the other master unit and as a baseband signal in the local unit as shown in Fig.5. The external loss modulation to the light pulses from the master unit is an equivalent effect to the direct modulation of PAM to a LD.

The carrier of pulses has harmonics in frequency region shown in Fig.6. The two carrier frequencies satisfies the following relationship to simplify the electrical filters in master units.

$$f_1 : f_2 = 2 : 3$$

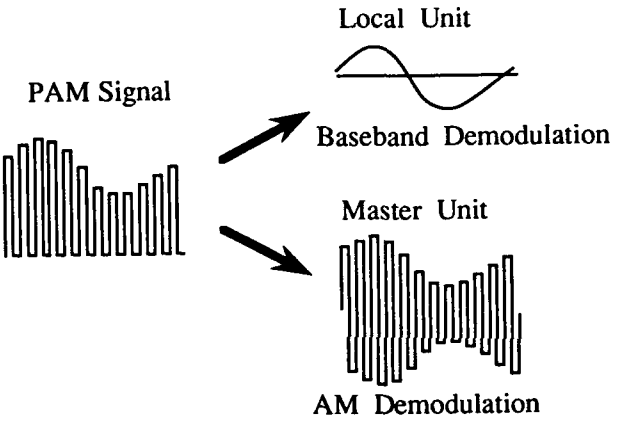


Fig.5 Demodulation of PAM Signal

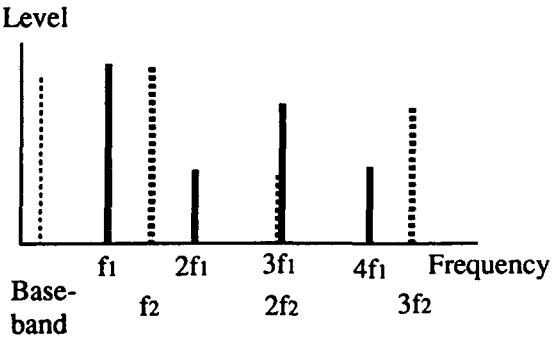


Fig.6 Carriers and Harmonics

3.3 Bending Width Adjustment

Fig.7 shows an example of the loss curve of a single mode optical fiber to the bending width. Generally it is known that the curve dose not show a simple relationship.[6] The best modulation width for the external loss modulation is the steepest and most linear portion of the curve. The curve is dependent on the fiber parameters, the fiber coating materials or the condition of the boundary between the glass and the coating. Each fiber has a different characteristic, and so adjustment of bending width is necessary to obtain the optimum point for the modulation index and linearity of the external loss modulation in the local unit.

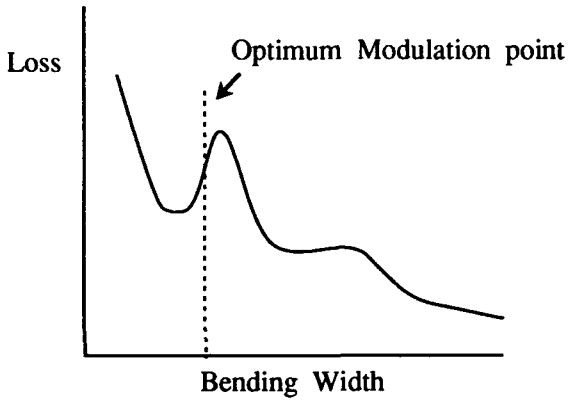


Fig .7 Example of Fiber Loss vs. Bending Width

4. Prototype System

The prototype system is designed to be applicable to FITAS (Fiber Transfer and Test System)[7] of NTT. The target fiber is specified to be a single mode 4-fiber ribbon divided into 2-fiber ribbons at 1550 nm wavelength.

4.1 Master Unit

Fig.8 shows the block diagram of the master unit. The frequencies of two carriers for PAM are f_1=33kHz and f_2=50kHz in the prototype system. When the master unit sends carrier f_1, the center frequency of the electrical band pass filter (B.P.F.) is automatically switched to f_2 to allow the detection of signals from the other master unit which sends carrier f_2.

The light emitting device is an InGaAsP/InP 1550nm LD with APC (Automatic power control) and temperature control. The light detecting device is a small diameter InGaAs PIN-PD used together with a preamplifier to detect the carriers. The optical input/output is a SC type optical connector.

The internal electronic circuit includes an automatic range control function and an automatic gain control function for optimal signal detection.

The outside view of the master unit is shown in Fig.9.

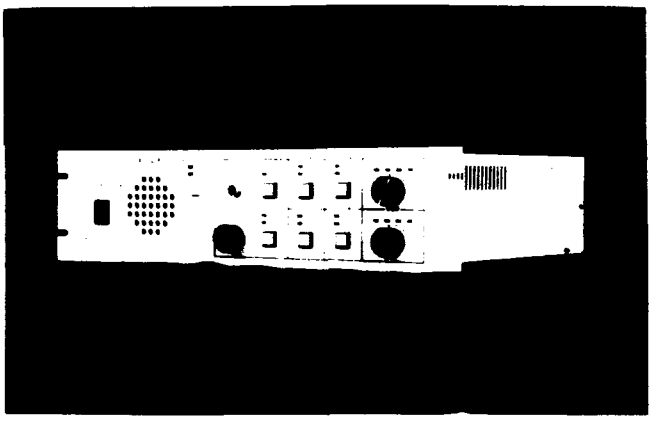


Fig.9 Outside View of Master Unit

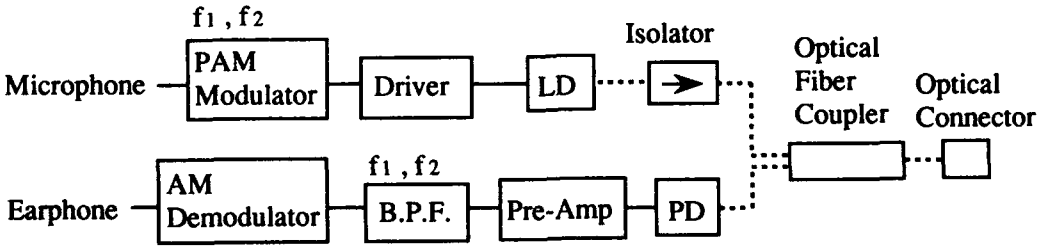


Fig.8 Block Diagram of Master Unit

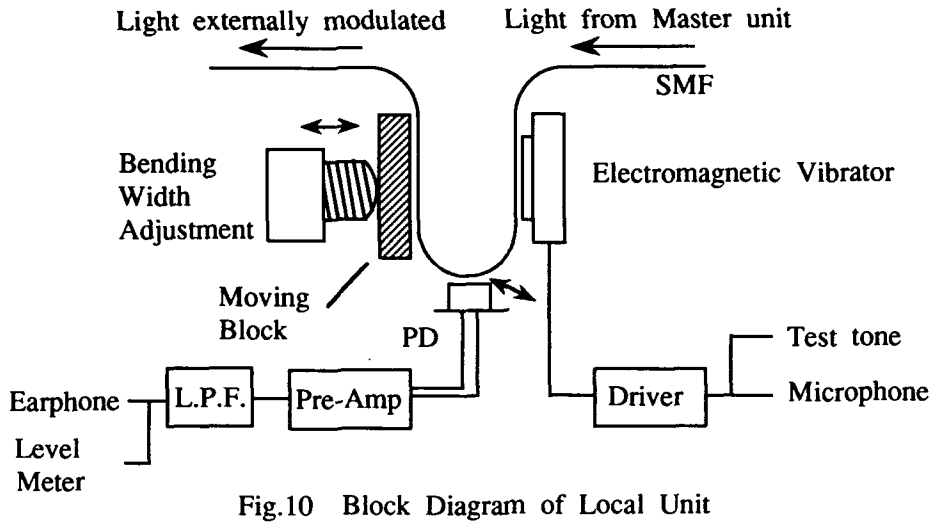


Fig.10 Block Diagram of Local Unit

4.2 Local Unit

Fig.10 shows the block diagram of the local unit and Fig.11 shows the outside view. The local unit includes a detachable attachment for setting the fiber ribbon to the electromagnetic vibrator. The local unit requires only two simple operations of setting a fiber ribbon onto the attachment and the bending width adjustment.

The PD for the local light detection is a large diameter InGaAs PIN-PD.

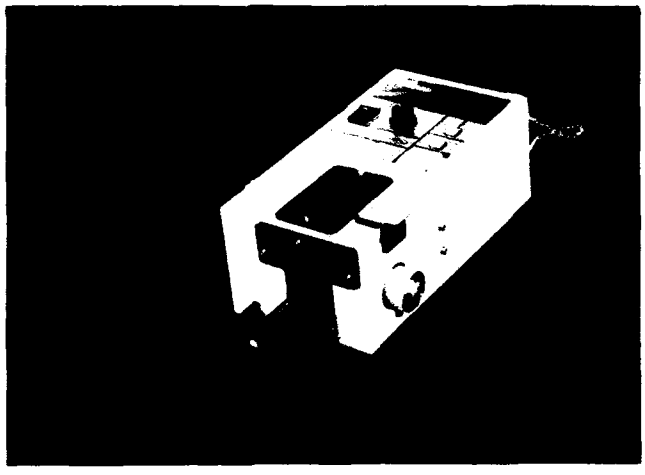


Fig.11 Outside View of Local Unit

Fiber Setting Attachment

The attachment holds the fiber ribbon and provides a secured U-shape bend to the fiber ribbon easily. Fig.12 shows the operation of the attachment. The attachment consists of two stages, two fiber holders and a pivot. The stages are designed to rotate about the pivot. Fig.12-a shows the initial state, the stages are open and the pivot is out of the line between the holders. The fiber is stretched and slid in the holder until the state shown in Fig.12-b. Fig.12-c shows the final state of the operations. In this way, the initial sag of the fiber in the state of Fig.12-a is absorbed by this mechanism. The fiber setting operation is completed by inserting the attachment back into the local unit.

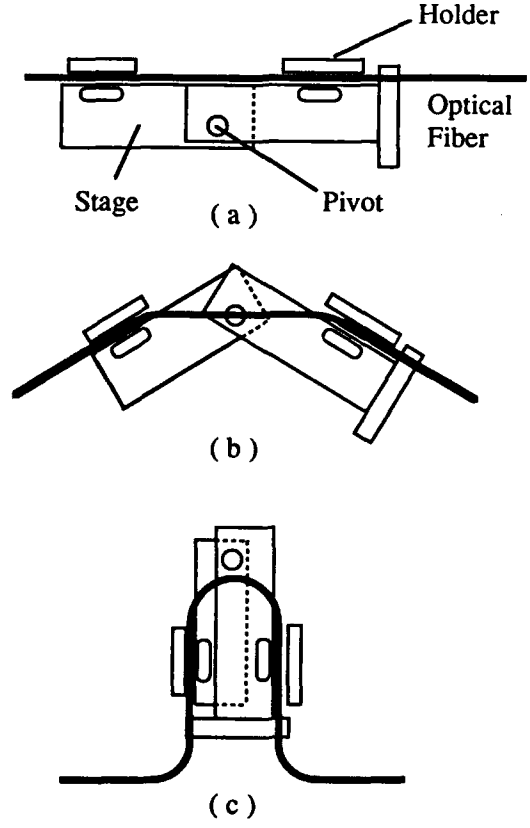


Fig.12 Operation of Attachment

Bending Width Adjustment

The local unit includes a test tone, a level meter and a moving block to adjust the fiber bending width as shown in Fig.10. After fiber setting, a 1kHz test tone is applied to the vibrator. The light from the master unit is externally modulated by the test tone and detected by the PD in the same local unit. The level meter indicates the detected test tone level. The fiber bending width adjustment is performed such that a maximum level of received signal is indicated in the level meter. While the moving block is under adjustment, the PD is slid to keep the same relative location to the top of the U-shape bend fiber.

Electromagnetic Vibrator

The electromagnetic vibrator shown in Fig.10 is based on normal audio speakers. Fig.13 shows the structure of the vibrator used in the local unit. The vibrator consists of a magnet, a moving coil and two dampers. The two dampers realize the efficient vibration of Z-axis, the vibrations of X and Y-axis do not contribute to the loss modulation.

The vibration amplitude of more than 30um to the fiber ribbon is obtained at 1kHz with this violator.

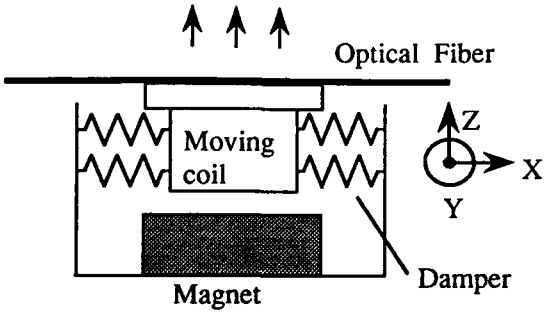


Fig.13 External Loss Modulator

4.3 Repeater Function

The repeater function of the master unit enables communication between a master unit and local units.

Fig.14 shows the operation of the repeater function. Light signal from the master unit A is attenuated at the location of the local unit and the master unit B because of the transmission loss of the long distance. The local light detection method has an intrinsic loss called coupling loss defined in the next section. This coupling loss weakens the already attenuated signal received at the local unit, resulting the S/N received beyond satisfactory level for communication. On the other hand, the master unit B can detect enough power through the fiber end and demodulate the signal with sufficient S/N. The repeater function in the master unit B can then be used to re-modulate the demodulated signal from the master unit A, and transmit to the nearby local unit at a stronger signal level. The S/N of the local unit is improved in this way.

This function is also effective in improving communication performance of the overall system, between the master unit to local units and local units to local units.

5. Properties of Prototype System

5.1 Properties of Local Unit

The modulation index is defined as shown in Fig.15. The local unit provides about 5% modulation index when the fiber bending width is more than 20mm. This bending exerted does no damage to the fiber.

Fig.16 shows the definitions of the insertion loss and the coupling loss due to the local light detection. P_2 is a portion of leaked power detected by the PD. Insertion loss that is less than 2dB

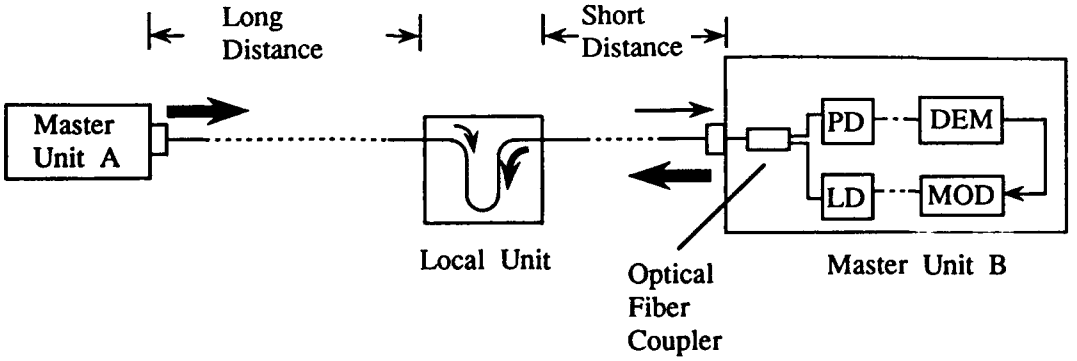


Fig.14 Repeater Function

and coupling loss averaging 20dB are obtained respectively when the prototype local unit is installed onto the fiber. The minimum detectable power of the PD is -48dBm at 1kHz with 20dB S/N for a transmitted signal of 5% modulation index. So the local unit requires incoming optical power P_0 to be more than -48+20+1=-27dBm for sufficient communication quality.

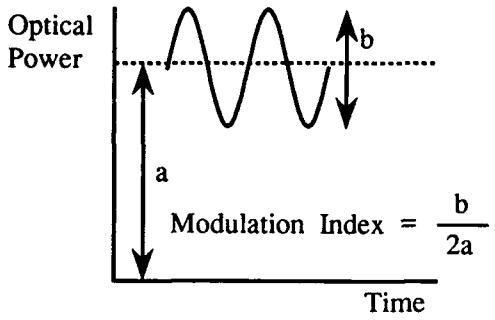


Fig.15 Modulation Index

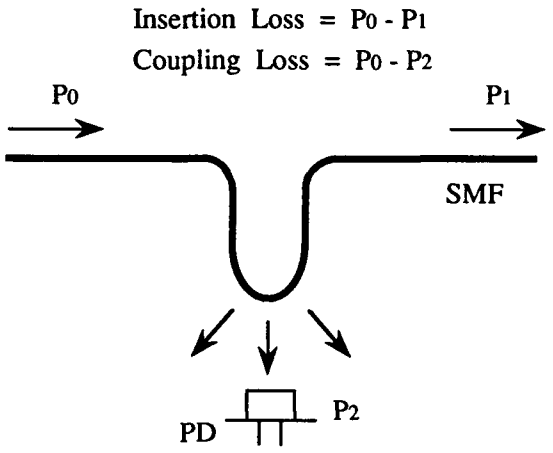


Fig.16 Loss of Local Unit

5.2 Dynamic Range

The launching optical power of the master unit into a single mode fiber is more than -7dBm, and the minimum detectable power is at least -45dBm at 1kHz with 20dB S/N for a light signal of 5% modulation index. The modulation index of the direct modulation in the master unit is set to 5%, same as that of the local unit.

The dynamic range between two master units is -7-(-45)=38dB, and the dynamic range from a master unit to a local unit is -7-(-27)=20dB according to the above discussion. However, the overall system dynamic range is still 38dB as the repeater function can be used to compensate for the smaller dynamic range of the local unit. The dynamic range is independent to the number of operating local units.

5.3 S/N and Distortion

Fig.17 and Fig.18 shows the typical frequency characteristics of the S/N and distortion of a 40km single mode fiber respectively for all combinations of the master and the local units. The degradation of the characteristics from 2kHz onwards is due to the electrical B.P.F. used in each unit. Compared with the direct modulation, the linearity and modulation index of the external loss modulation are inferior, which influences the characteristics of the local to master and of the local to local units.

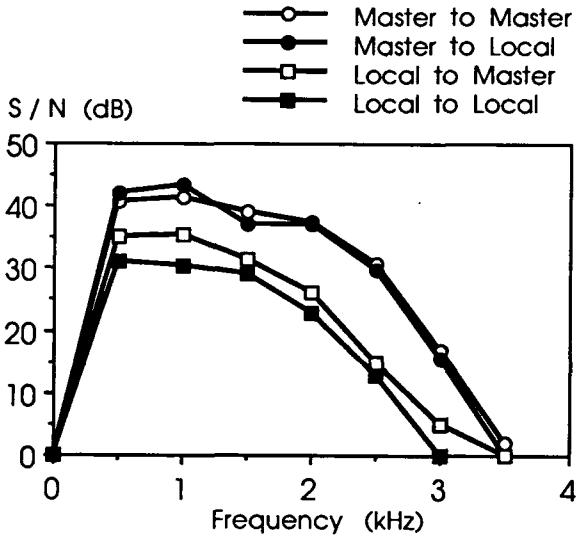


Fig.17 S/N vs. Frequency

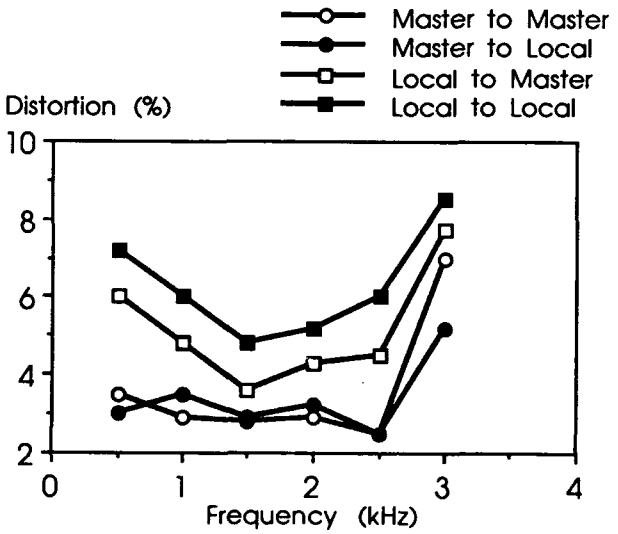


Fig.18 Distortion vs. Frequency

6. Conclusion

The availability of the external loss modulation applied to the talk system is proven by the prototype system designed in this paper.

For the present, the system is suitable for optical cable maintenance systems that can equip two master units in telephone stations permanently.

By modifying the system for better performance and increasing the number of applicable fibers, the system described is expected to be an essential instrument in optical fiber systems.

References

(1) M.Shimizu et al.: Identification Method for Optical Fiber Transmission Operation Lines with Local-Light Injection and Detection Coupling System, 39th IWCS, 1990

(2) N.Kuwaki et al.: Characteristics of Optical Modulator using Single-Mode Fiber, IEICE of Japan, B-693, Fall 1990

(3) A.Fujisaki et al.: Optical Talk Set and Optical Cable Identifier using Polarised-Wave-External-Modulation Method, 39th IWCS, 1990

(4) K.Arakawa et al.: A Method for Identifying Single-mode Fibers in an Operating Fiber Cable System, 38th IWCS, 1989

(5) Y.Azuma et al.: Characteristics of Optical Fiber Amplitude Modulator, IEICE of Japan, B-897, Spring 1991

(6) A.J.Harris et al.: Bend Loss Measurements on High Numerical Aperture Single-Mode Fibers as a Function of Wavelength and Bend Radius, J. Lightwave Tech. Vol. LT-4, No.1, January 1986

(7) H.Matsumoto et al.: Cable Transfer and Supervisory System for Trunk Optical Fiber Cables, 40th IWCS, 1991



Yoshiharu Unami

Fujikura Ltd.

1440, Mutsuzaki, Sakura, Chiba, 285, Japan

Yoshiharu Unami was born in 1961. He joined Fujikura Ltd. after his graduation from Chiba University with the B.E. degree in 1982 and has been engaged in research and development of optical systems. He is now an engineer of optical communication system section and a member of IEICE of Japan.



Kouichi Sakurai

Fujikura Ltd.

1440, Mutsuzaki, Sakura, Chiba, 285, Japan

Kouichi Sakurai was born in 1962. He joined Fujikura Ltd. after his graduation from Chiba University with the B.E. degree in 1988 and has been engaged in research and development of optical systems. He is now an engineer of optical communication system section and a member of IEICE of Japan.



Takeshi Yamada

Fujikura Ltd.

1440, Mutsuzaki, Sakura, Chiba, 285, Japan

Takeshi Yamada was born in 1950. He joined Fujikura Ltd. after his graduation from Waseda University with the B.E. degree in 1973 and has been engaged in research and development of optical systems. He is now a manager of optical communication system section and a member of IEICE of Japan.



Nobuo Kuwaki

NTT Technical Assistance & Support Center

3-9-11, Midori,
Musashino, Tokyo, 180,
Japan

Nobuo Kuwaki was born in Tochigi Prefecture on March 25, 1958. He received the B.S. degree in electronic engineering and Ph.D. degree from Chiba University, Chiba, Japan in 1980 and 1991, respectively.

He joined Musashino Electrical Communications Laboratories, Nippon Telegraph and Telephone Public Corporation, Musashino in 1980. He was engaged in research on the balanced pair cable design and the dispersion-modified optical fiber design for high bit-rate transmission system. Since 1989, he was engaged in the research of evaluation for optical fiber and device transmission characteristics at Technical Assistance & Support Center, Nippon Telegraph and Telephone Corporation.

He is a member of the IEICE of Japan.



Motoaki Yumoto

Suzuki Technical Engineering

3-24-7, Botan,
Koto, Tokyo, 135,
Japan

Motoaki Yumoto was born in 1933. He joined Fujikura Ltd. after his graduation from Tokyo Denki University with B.E. degree in 1957, and joined Suzuki Technical Engineering Co.Ltd. in 1989. He is now a chief engineer (M.D.) and a member of IEICE and SICE of Japan.

Non-destructive Optical Fiber Amplitude Modulator for Optical Talk System over 80 km

Yuji Azuma, Yoshihiro Shibata*, Shinji Tamura**, and Nobuo Kuwaki

NTT Technical Assistance & Support Center
Midori-cho, Musashino-shi, Tokyo, 180 Japan

* NTT Hokuriku System Development Center
** NTT Hyogo Network Center

Abstract We have developed a new method of local amplitude modulation using the bending loss property of optical fiber without cutting the fiber. It is shown that a high modulation index is obtained by choosing the optimum bending radius with low insertion loss. Using this technology, we have fabricated a talk system among six intermediate points and the ends of an 80-km-long optical transmission line.

1. Introduction

Non-metallic optical fiber cables that have the advantage of being induction-free and lightweight are used for subscriber loops and trunk communication lines[1][2]. During cable installation and maintenance, it is often necessary to be able to talk via the optical fiber. This is usually performed by cutting the optical fiber to send and detect a signal light. This method, however, requires fusing the optical pigtail cords with optical connectors, which takes a long time and reduces operational efficiency. Therefore, there is a need to be able to talk from any point without cutting the fiber. We have theoretically shown that bending loss is proportional to small changes in the bending radius for a U-bend optical fiber. Using this property, we propose the local amplitude modulator to enable non-destructive operation of an optical fiber which is transmitting light signal. This paper discusses amplitude modulation characteristics using the radius changes of a U-bend fiber.

2. Modulation Principle

It is well known that the fiber bending loss is larger when the bending radius is smaller. Figure 1 shows the general dependence of the transmitted optical power through the fiber on bending radius. The transmitted optical power can be changed by variations of the bending radius, and modulated by input vibration signals. This property enables local amplitude modulation without cutting the fiber. However, the bending loss characteristics needs to be linear for high modulation. The fiber bending loss characteristics is therefore an important factor for the amplitude modulation.

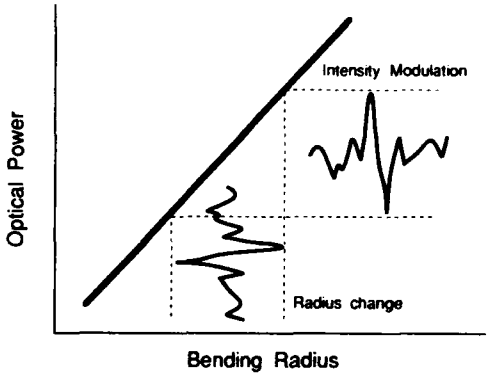


Fig. 1. Amplitude modulation principle.

3. Fiber Bending Loss Characteristics

In order to modulate the transmitted light using the bending loss changes, we have to investigate the fiber bending loss characteristics in detail. In this section, we indicate the experimental results for the dependence of fiber bending loss on bending radius.

3-1 Experimental Results

Figure 2 shows the theoretical bending loss characteristics[3]. The fiber used is a step-index single-mode (SM) optical fiber for 1.3-μm wavelength, where the mode-field diameter $2W$ is 9.5 μm (at λ =1.3 μm), the effective cut-off wavelength λ_{ce} is 1.29 μm , and the refractive index difference Δ is 0.28%. The incident light wavelength is 1.55 μm, because 1.55-μm- wavelength light transmitted in a 1.3-μm SM fiber radiates in a simple way from the bending region. The insertion losses are calculated on the assumption that the fiber is bent into a U-shape to make it easy to change the radius. The calculated bending loss characteristics decrease exponentially when the bending radius is large. Amplitude modulation by changing the bending radius needs linearity of the bending loss characteristics. The calculated curve is ideal for modu-

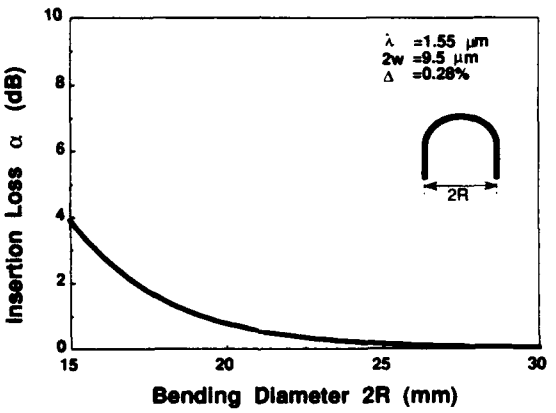


Fig. 2. Theoretical bending loss characteristics.

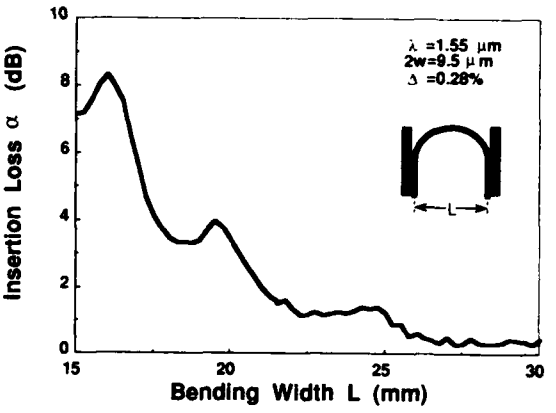


Fig. 3. Measured results for dependence of insertion loss on bending width.

lating easily without the need for careful adjustment of the bending radius.

However, the measured results of the bending loss characteristics have a few dips and peaks as shown in Fig. 3, for a used fiber with the same parameters as used for the calculated results in Fig. 2, and the incident light wavelength is 1.55 μm. These dips and peaks may cause distorted modulation waveforms. We discuss the generation mechanism of these dips and peaks in section 3-2.

3-2 Mechanism of Dip/Peak Generation

The mechanism of dip/peak generation in the fiber bending loss characteristics is discussed in Ref.[4][5]. Here, we discuss the mechanism applied to a U-bend fiber. In general, the fiber bending losses are divided into radiation loss and a mode-transfer loss. Figure 4 shows the behavior of the mode-transferred light. The transmitted light through the straight region of the core is radiated to the cladding, and transferred to non-transmitted light at the changing point of curvature. When the mode-transferred light arrives at the inner wall of the cladding, a part of it is radiated out of the cladding, and the other part is reflected in the cladding. The reflected light is transmitted in the cladding until the next arrival at the inner wall of the cladding. This multi-reflection continues transmission in the cladding of the bent region. The multi-reflected light arriving at the next change in bending curvature is again coupled to the transmitted mode under the condition of a specific bending width L_2 as shown in Fig. 4(b). The angle between the start-point of U-bend and the point on the inner wall where mode-transferred light initially arrived is θ. Therefore the angle of the multi-reflection cycle is 2θ, if the bending shape is a true semicircle. The requirement for coupling the transmitted mode at the end-point of the bending region is

$$\begin{aligned} \pi &= 2M\theta \\ &= 2M\cos^{-1}\{R/(R+r)\} \\ &= 2M\cos^{-1}\{L/(L+2r)\}, \end{aligned} \qquad (1)$$

where R is the bending radius, r is the fiber cladding radius, L is the bending width, and M is the number of reflections in

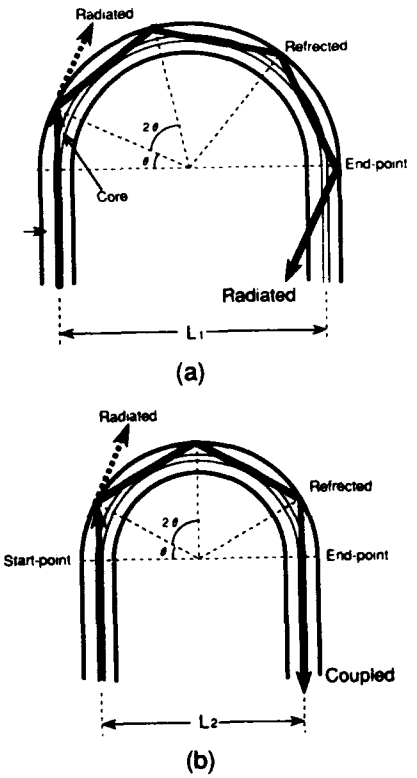


Fig. 4. Multi-reflected light behavior in the bending region. (a) Radiation condition. (b) Coupling condition.

the bending region. When the bending radius R satisfies with Eq. 1, the multi-reflected light is coupled with the transmitted mode. This causes the dips to be generated on the curve in Fig. 3. Figure 5 shows the coupling condition calculated from the relationship between the bending width L and the multi-reflection number M. The reflection numbers M are from 13 to 17 times between the bending widths

L=15 and 30 mm. We estimate that the coupling conditions are satisfied 4 or 5 times between these bending widths. These values correspond with the number of dips measured in Fig. 3. These dip/peak characteristics depend on the fiber cladding radius and fiber coating materials. The fiber structure parameters such as mode-field diameter and relative refractive index difference are unrelated to these dip/peak characteristics. The generated positions of these dips/peaks are irregular, but the generated interval between a dip and a peak is identical with the characteristics of any other fiber. Therefore, we can avoid using bending widths that are difficult to modulate, by changing the longer bending width rather than the dip/peak interval.

4. Structure of Local Modulator and Detector

4-1 Local Modulator

The structure of an optical fiber local amplitude modulator is shown in Fig. 6. An optical fiber is bent into a U-shape, between the diaphragm and the stationary plate, with fiber bending width L. The stationary plate possesses a fine adjustment knob used to adjust the bending width L to the best position. The diaphragm is vibrated by the electromagnetic transducer which uses an audio speaker. When the voice band signals are put into the electromagnetic transducer, the diaphragm vibrates and L is changed microscopically by the input voice band signal frequency f. Therefore, the transmitted light through the fiber is modulated as shown in the previous chapter.

4-2 Local Detector

We also need a technique which can locally detect the transmitted light signals from other points without cutting the fiber. The local detection technique is achieved by an optical identification system[6][7]. However, the bending shape using the optical fiber identification system is different from a U-bend. Therefore, we investigated suitable positions for detecting radiated light from a U-bend fiber. Figure 7 shows the measured results of the coupling loss η, which is the ratio of transmitted to radiated optical power. The photodetector was an InGaAs-photodiode with a diameter of 3 mm. The results showed that positioning the photodetector at the center of the top of the U-bend fiber provides the smallest coupling loss, and enables efficient detection. The coupling loss η is then approximately 20 dB.

5. Modulation Characteristics

5-1 Theory

The non-destructive fiber amplitude modulator is based on the principle that the U-bend width vibration changes the transmitted optical power. When the amplitude of the diaphragm is A mm, and the bending loss slope for the bending width L is $d\alpha/dL$ dB/mm, the bending loss difference $\Delta\alpha$ is given by

$$\Delta\alpha=(d\alpha/dL)A. \qquad (2)$$

When the maximum optical power of the modulated light

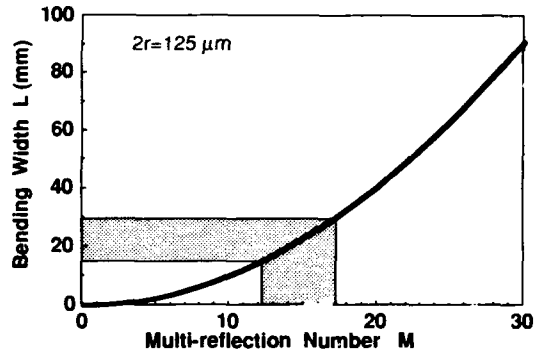


Fig. 5. Calculated condition for the transmission mode.

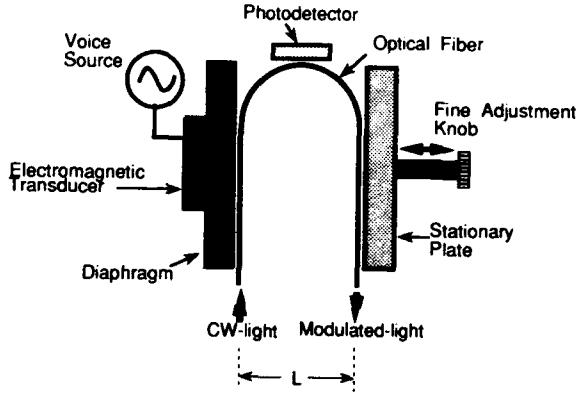


Fig. 6. Structure of non-destructive optical fiber modulator and detector.

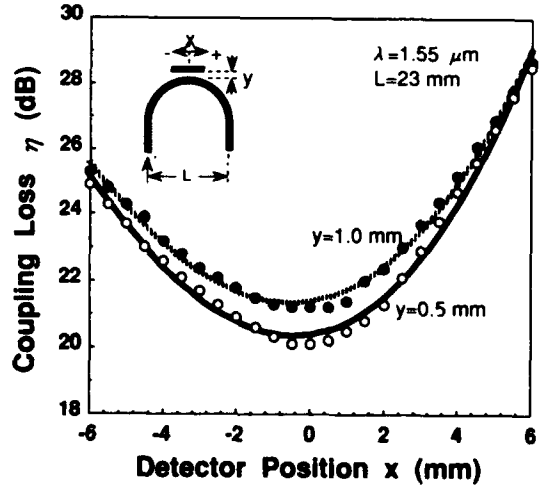


Fig. 7. Measured coupling loss for the light radiated from the bending region.

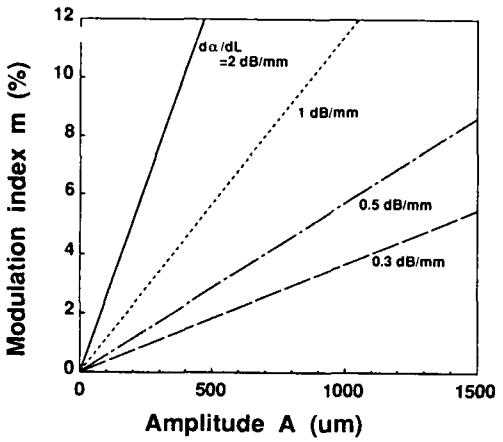


Fig. 8. Dependence of modulation index on amplitude.

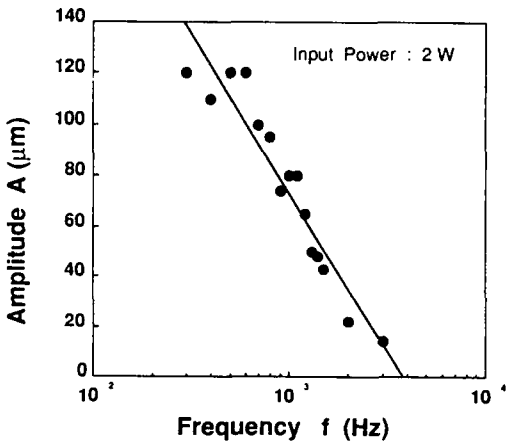


Fig. 9. Dependence of diaphragm amplitude on vibration frequency.

signal is P_1, minimum optical power is P_2, and the average power is P_0, the modulation index m is given by

$$m=(P_1-P_2)/2P_0$$
$$=(1-10^{-\Delta\alpha/10})/(1+10^{-\Delta\alpha/10}). \quad (3)$$

Figure 8 shows the dependence of the modulation index m on amplitude calculated using Eq. 3. In order to get a modulation index m=3% when $d\alpha/dL$=1 dB/mm, the amplitude A has to be larger than 250 μ m.

The measured amplitude A of the diaphragm is shown in Fig. 9. When the vibration frequency f increases, the amplitude A decreases. A is 100 μ m at f=1 kHz. Comparing with the results of Fig. 8, it is found that m is approximately 1% at $d\alpha/dL$=1 dB/mm.

5-2 Experimental Results

Figure 10 shows the measured and calculated characteristics of bending loss α and modulation index m, where the modulation index is measured at f=1 kHz. The measured bending loss characteristic has a few dips and peaks. It is clear that m increases when $d\alpha/dL$ increases. The measured results are identical with this trend. In the case of A of the diaphragm is 100 μm at f=1 kHz obtained in Fig. 9, the modulation index m calculated from the measured results in Fig. 10(a) are shown by the dotted line in Fig. 10(b). This is not identical with the measured characteristics. The amplitude A which fits the measured result is 900 μm as shown by the dash dotted line. Therefore the U-bend fiber is found to vibrate with an amplitude of 900 μm for 100 μm ampli ude of diaphragm vibration. This result expects the U-bend fiber to jump without following the vibration of the diaphragm. Consequently a higher modulation index can be obtained by jumping of the U-bend fiber vibration.

On the other hand, Fig. 10(c) shows the modulation index m calculated using A=900 μm by the theoretical loss characteristics in Fig. 10(a). The measured maximum modulation index m (=5.5%) is larger than the calculated values. Therefore, it is clear that a higher modulation index than the theoretical modulation index is achieved effectively by utilizing the dip/peak characteristics.

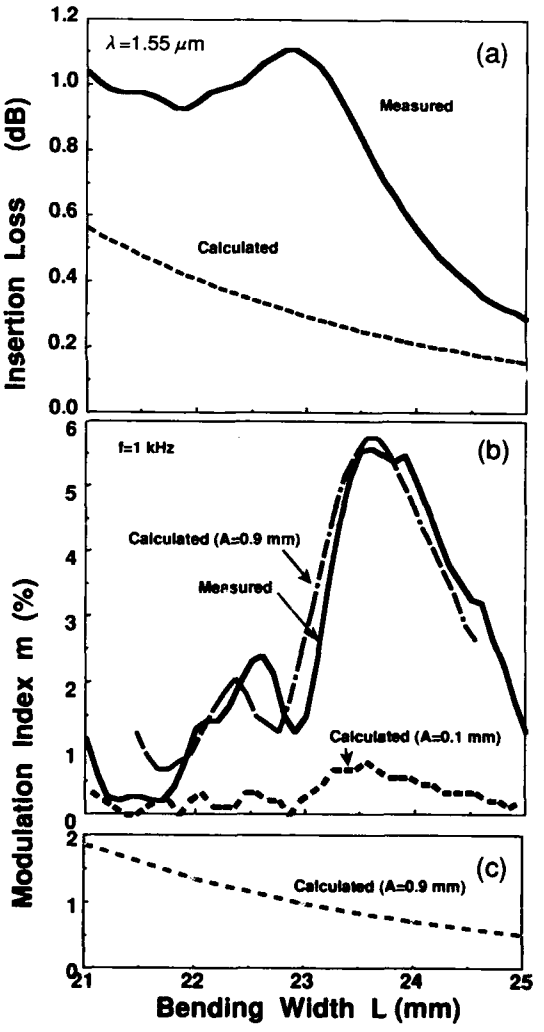


Fig. 10. Relationship between the bending loss and the modulation index. (a) Dependence of the bending loss on bending width. (b) Measured and calculated modulation index. (c) Modulation index calculated from theoretical bending loss.

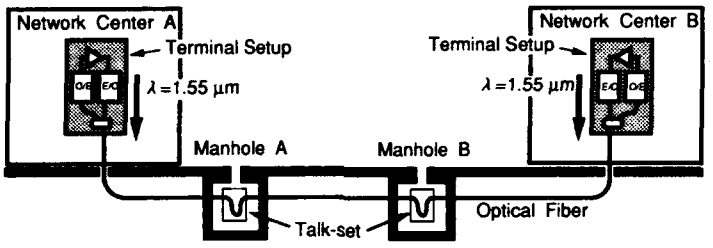


Fig. 11. Construction of optical talk system.

6. Optical Talk System

6-1 Construction

In this section, the optical talk system of a non-destructive optical fiber talk-set using the optical fiber amplitude modulator is explained.

The construction of the talk system is shown in Fig. 11. This system uses an optical fiber for 1.3 μm-wavelength. 1.55 μm-wavelength light is transmitted from both terminal network centers which are at the ends of the fiber. At an intermediate point such as a manhole, the intermediate talk-set is mounted by bending the fiber into a U-shape without cutting. The terminal setup has a repeater function which sends the restored and amplified light signals into the same fiber. This function is effective in obtaining a good signal/noise (S/N) ratio. This system has been used to talk between network centers and manholes.

6-2 Talk Characteristics

The S/N ratio characteristics using the optical talk system are evaluated. The measured characteristics show the dependence of S/N ratio on optical line loss. In order to avoid S/N decrease caused by the reflected light at fiber end faces, optical line losses vary by changing the bending radius at an intermediate point of the fiber.

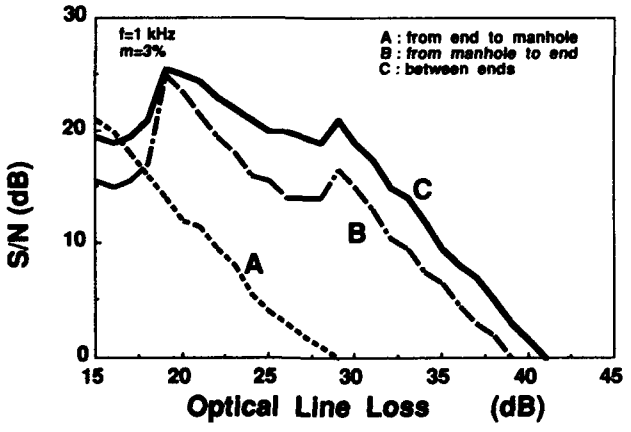


Fig. 12. Dependence of S/N ratio on optical transmission line loss.

Figure 12 shows the experimental results for S/N ratio measured using this optical talk system. Lines A, B, and C indicate the S/N ratios from a network center to a manhole, from a manhole to a network center, and between network centers, respectively. However, the repeater of both terminal setups is not used. The humps of these characteristics are caused by changing the detection sensitivity at the terminal.

The minimum S/N ratio for a satisfactory signal during cable installation and maintenance work is experimentally obtained 5 dB. At 5 dB, the optical transmission line losses of A, B, and C are 24.2, 35.8, and 38 dB, respectively. Assuming that the fiber line loss including splice losses is estimated to be 0.35 dB/km at 1.55 μm-wavelength, the optical transmission line loss (24.2 dB) of the characteristics A *is equivalent to 70-km line length.* Assuming that the maximum insertion U-bend loss of an intermediate point is 1.5 dB, the line loss increases by 9.0 dB for six intermediate points. Therefore, the applied optical transmission line loss is 15.2 dB. This value is equivalent to 43 km of optical line length. A longer optical line can be used, if a terminal-type repeater is used. Using the repeaters, it is possible to talk at any points within the 43 km area from a terminal network center, because the light signals sent from a terminal network center or intermediate points are detected at other terminal network center, and again sent to the same fiber. Therefore, six intermediate points can be set up an optical transmission line of over 80 km.

Table 1 shows the performance characteristics of the system.

7. Conclusion

We have developed a new amplitude modulator that can be used at any point along on optical fiber without cutting the fiber. The required modulation index of this modulator is obtained by choosing the optimum bending width with low insertion loss. Talk systems using the proposed modulator enables conversation among the workers at six intermediate points and at both ends of an 80-km optical transmission line. This non-destructive optical fiber talk-set will be used on local area network system after further investigations of the bending characteristics and system construction.

Table 1 Performance of the talk system.

Fiber :	Single-mode fiber for 1.3-μ m-wavelength use	
	Line length	< 80 km
Terminal setup :	Output wavelength	1.55 μ m
	Output optical power	-4 dBm
Intermediate setup :	Insertion loss	< 1.5 dB
	Coupling loss	20 dB
	Maximum number used	< 6

Acknowledgements

The authors wish to thank M. Hirai, A. Sakamoto, N. Ikawa, K. Arita, Y. Yamazaki, and K. Yoshida for their helpful suggestions and encouragement.

References

[1] K. Hogari, K. Takagi, and F. Ashiya, "Nonmetallic 1000-fiber cable," J.Lightwave Technol., vol.10, no.2, pp.130-134, 1992.

[2] S. Tomita, F. Ashiya, and M. Kawase, "1000-fiber water-blocking cable," Trans.IEICE Japan, vol.E73, no.8, pp.1511-1516, 1990.

[3] D. Marcuse, "Bending losses of the asymmetric slab waveguide," Bell Syst. Tech. J., vol.50, no.8, pp.2551-2563, 1971.

[4] H. Renner, "Bending losses of coated single-mode fibers," J.Lightwave Technol., vol.10, no.5, 1992.

[5] W. A. Gambling and H. Matsushita, "Propagation characteristics of curved optical fiber," Trans.IEICE Japan, vol.E61, no.3, pp.196-201, 1978.

[6] K. Arakawa, K. Yoshida, and H. Ikeya, "A method for identifying single-mode fibers in an operating fiber cable system," IWCS, pp.88-93, 1989.

[7] M. Shimizu, S. Takashima, and H. Kobayashi, "Identification system for optical fiber transmission operation lines with local-light injection and detection coupling system," J.Lightwave Technol., vol.10, no.5, pp.686-692, 1992.



Yuji Azuma

NTT Technical Assistance & Support Center
Midori-cho, Musashino-shi, Tokyo, 180 Japan

Yuji Azuma reseived the B.S. degree in electrical engineering from Doshisha University, Kyoto, Japan, in 1984, and then joined NTT Laboratories. He was engaged in reserch on characteristics of high-density optical fiber cable, and fiber nonlinearity. Since 1989, he was engaged in reserch of evaluation for optical device reliability, and optical fiber transmission characteristics, at Technical Assistance & Support Center. He is now an engineer of the Fiber Optics Group.

He is a member of the Institute of Electronics, Information and Communication Engineers of Japan.



Shinji Tamura

NTT Hyogo Network Center
Hyogo-ku, Kobe-shi, Hyogo, 652 Japan

Shinji Tamura graduated from Sumoto Vocational Senior High School, Hyogo, Japan, in 1975, and then joined NTT. Since 1989, he was engaged in reserch on evaluation of thunderstruck cable, and development of non-destructive optical fiber talk-set at Technical Assistance & Support Center. Since 1992, he was engaged in developement of transmission line infomation system at Hyogo Network Center.



Yoshihiro Shibata

NTT Hokuriku System Development Center
Dewa-cho, Kanazawa-shi, Ishikawa, 920 Japan

Yoshihiro Shibata received B.S. and M.E. degree in chemical engineering from Toyama University, Toyama, Japan, in 1986 and 1988, respectively. He joined NTT in 1988. Since 1989, he was engaged in development of non-destructive optical fiber talk-set at Technical Assistance & Support Center. Since 1992, he was engaged in development of transmission line tools at Hokuriku System Developement Center.

He is a member of the Institute of Electronics, Information and Communication Engineers of Japan.



Nobuo Kuwaki

NTT Technical Assistance & Support Center
Midori-cho, Musashino-shi, Tokyo, 180 Japan

Nobuo Kuwaki received the B.S degree in electric engineering and Ph.D. degree from Chiba University, Chiba, Japan in 1980 and 1991, respectively. He joined NTT Laboratories in 1980. He was engaged in reserch on the balanced pair cable design and the dispersion-modified optical fiber design for high bit-rate transmission system. Since 1989, he was engaged in the reserch of evaluation for optical fiber and device transmission characteristics at Technical Assistance & Support Center. He is now a senior engineer of the Fiber Optics Group.

He is a member of the Institute of Electronics, Information and Communication Engineers of Japan.

SPLICE VERIFICATION AND ACTIVE FIBER IDENTIFICATION - A STRATEGY FOR OPTIMAL NETWORK RESTORATION

George F. DeVeau, Walter S. Konik, Joel L. Mock, Mary J. Presnell

AT&T Bell Laboratories
Norcross, GA 30071

William B. Westfall
AT&T Network Services Division
Raleigh, NC 27601

Abstract

As the traffic density and numbers of fiber-optic long-haul communications networks increase, so does the need to promptly identify and repair total or partial fiber-optic cable cuts. In response to increasing demands to minimize network downtime, an optimal restoration strategy has been implemented for AT&T's fiber network. Key to this restoration strategy is a restoration kit which includes a 36-fiber lightweight bridging cable with two closures attached, splices, and all necessary sheath access and splicing hand tools.

Unique additions to this 500LG RESTORATION KIT are a second-generation Fiber Identifier and a Go/No-Go splice verifier. The 956A Fiber Identifier provides positive directional identification of fibers operating at 1310 nm and/or 1550 nm with an insertion loss well below 1 dB. The splice verifier, integrated into a splice workstation, utilizes the 1310 nm or 1550 nm regenerator signal to verify that splice loss is below a preset maximum value. Unlike fiber macro-bending devices, the 955A Verifier takes advantage of the relationship between scattered infrared light and actual splice loss in an optically clear mechanical splice.

Introduction

Since the first telephone "network" formally opened on January 28, 1878 in New Haven, Connecticut serving 21 customers[1], service interruption from natural or manmade causes has been of concern to the telecommunications industry. As the outside-plant transmission media evolved from iron and steel open wire to paired copper cable and coaxial cable with analog and digital carrier systems, higher traffic densities increased concerns of catastrophic cable damage. These concerns have intensified because present-day fiber-optic long-haul networks with extreme traffic densities make service interruption a very serious event causing enormous revenue losses and dissatisfied customers.

Reducing the impact of cable damage has been accomplished by providing clearly marked routes, regular close surveillance, electrical/mechanical protection, redundant routes, and faster more-efficient fiber/cable restoration. AT&T Network Services Division (NSD), the "long-lines" of AT&T, has formal guidelines for cable restoration that are detailed in a comprehensive restoration handbook. This document covers all aspects of cable restoration: training, responsibilities, safety, communications, test sets and the most efficient procedures to for repair. Complementing this restoration handbook is the "500LG LIGHTGUIDE CABLE RESTORATION KIT" which provides a 36-fiber lightweight bridging cable on a rapid deployment spool with closures, mechanical splices and all necessary tools for achieving a restoration.

In a restoration, the first activities performed (after establishing communications and preparing the site) are to identify any remaining active fibers and then to splice in the bridging cable across the break. After all disrupted fibers have been re-joined, successfully restored fibers and non-successfully restored fibers are identified, and troubleshooting begins on those, which for as yet undetermined reasons, have not returned to service. **It is this activity, identifying the causes of failure to return to service, that may cause additional serious delays in restoring full service.** Of course, the most likely possibilities for trouble are the two bridging splices - new additions to the path. Or, the splices may be good and the end terminations, which have been disturbed during the repair sequence, are now defective.

NSD has commissioned the design and development of test sets to complement the 500LG for:

- Identifying active fibers and direction of traffic without causing damage to the fiber or loss of traffic.
- Verifying that the splice losses of the bridging cable splices are less than 1 dB each.
- Having sufficient compactness to fit into the 500LG restoration kit.

This paper presents an overview of the 500LG Restoration Kit and the two new test sets that satisfy and exceed NSD's network requirements.

500LG Lightguide Restoration Kit

The 500LG is designed for temporary restoration and protection of a damaged fiber-optic cable. This kit, shown below in Figure

1, as presently used by NSD, has all tools and consumables needed to perform up to a 72-fiber repair except for fiber identifier and splice verifier test sets.

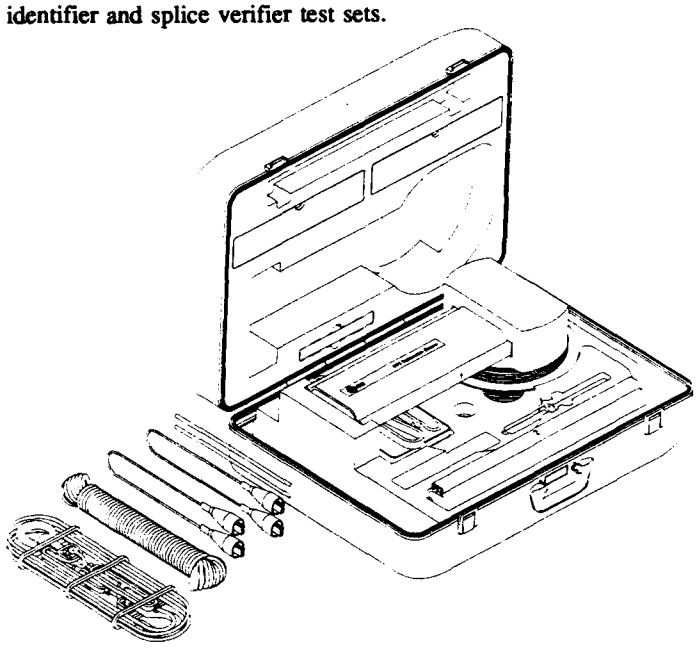


Figure 1 - 500LG Lightguide Restoration Kit

Outside-plant technicians are equipped with a 500LG containing a 500-feet 36-fiber cable stored on a rapid-deployment-reel fixed on both ends with temporary closures. Figure 2 shows the fiber reel positioned on the spindle ready for deployment.

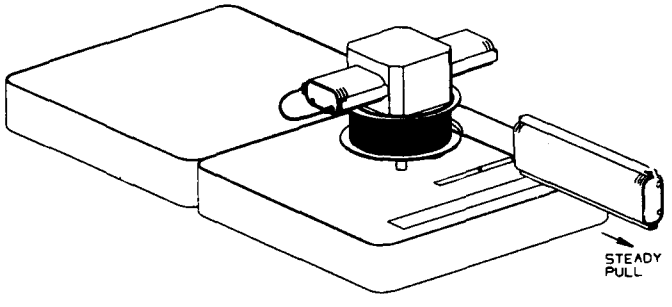


Figure 2 - Bridging Cable Deployment

Included in the 500LG are assorted tools, ropes, turn-buckles, and other miscellaneous accessories selected to perform the restoration operation. Also included are a VHS video tape and instruction manual showing restoration methods for a total cable failure with no slack, total cable failure with slack, and partial cable failure (taut-sheath).

The temporary closures organize, store and protect up to seventy-two fiber splices while strain relieving the 36-fiber cable. Figure 3 is a diagram of organized splices in a typical restoration of a total cable failure with slack. When two kits are available, the two 36-fiber cables can be combined into one set of closures to make a total 72-fiber repair. For NSD's network, however, thirty-six fibers will suffice in the majority of the restoration occurrences.



Figure 3 - Typical Closure Arrangement

Customer Requirements - Splice Verifier/Fiber Identifier

Prior to the development of splice verifier and fiber identifier, *AT&T Bell Labs and AT&T Network Cable Systems (NCS)* met with NSD to determine the requirements for these new test sets. They are listed in Tables 1 and 2.

Table 1	
Verifier Functional Requirements	
Operation	Use Regenerator traffic or idle signal as source
	Acceptable or unacceptable indication only (Go/No-Go)
	Self-test function
	Low-battery indication
	Unit must retrofit into the 500LG Restoration Kit
Dynamic Range	0 dBm to -30 dBm
Operating Wavelength	1300 nm and 1550 nm
Operating Temperature	-20°C to 50°C (95% R.H.)
Storage Temperature	-40°C to 60°C (80% R.H.)
Power	Standard Alkaline batteries (minimum 8 hour operation)
Weight	≤ 5 pounds

Table 2	
Identifier Functional Requirements	
Operation	No traffic indication at ≤ -35 dBm
	Traffic and direction at ≥ -25 dBm
	2 KHz tone indication
	low-battery indication
	self-test indication
	Easy fiber access into taut-sheath entry
	Unit must retrofit into the 500LG Restoration Kit
Insertion loss	≤ 1.0 dB at 1310/1550 nm
Operating temperature	-20°C to 50°C (95% R.H.)
Storage temperature	-40°C to 60°C (80% R.H.)
Power	Standard Alkaline batteries (minimum 8-hour operation)
Weight	≤ 2 pounds

955A Splice Verifier

Preliminary Design Considerations

AT&T Bell Laboratories has investigated macro-bend and scattered-light methods to locally measure and verify splice loss. Following, in Table 3, are some of the more significant advantages and disadvantages of each of these two methods.

Table 3

Method →	Macro-bend Technology	Scattered-light Technology
Description	Controlled fiber bends on either side of splice. Difference between signal levels should be representative of splice loss.	Fiber core misalignment results in light lost or scattered from the junction. Amount of scattered light is proportional to splice loss.
Advantages	May be used for any splice, mechanical or fusion.	Insensitive to fiber color or fiber parameters. This is a proven technology used with the AT&T Rotary splice.
Disadvantages	Detected core power is subjected to fiber parameters and coating colorants. Expensive electronics and hardware is required. Costly.	All splice components must be clear in order to pass scattered-light signal.

To keep costs as low as possible and to utilize the transparency of some available mechanical splices, it is technologically prudent to choose scattered-light technology and the CSL LightSplice™ [2] for the verifier for NSD.

Preliminary Development

Previously, scattered-light measurements for Rotary Mechanical Splices were readily accomplished. As is shown in Figure 4, light scattered from this splice follows a repeatable, slightly diverging, uniform pattern from the transparent splice housing.

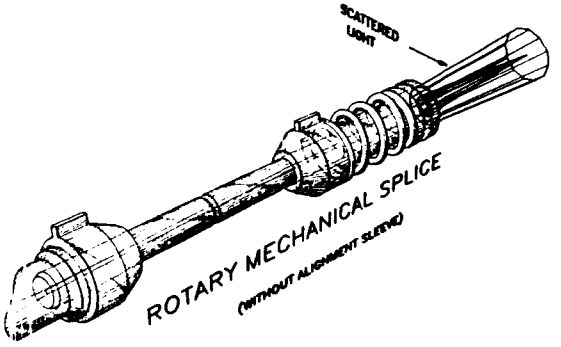


Figure 4 - Scattered Light From The Rotary Splice

In fact, observation with infrared devices show a uniform annulus of constant shape at the rear of the splice housing. The intensity of this ring is directly proportional to splice loss and the detector, placed on axis with the splice, collects a calibrated portion of the scattered light. The ratio of the collected scattered light to the reference measurement taken before the splice ferrules are assembled is the Rotary-Splice local splice-loss measurement.

An infrared vision system, set up in the laboratory, showed, however, that the scattered light from a CSL splice is not uniform. Instead, scattered light exits at various positions and angles at the end of the clear housing.

Figure 5 shows infrared photographs of two CSL splices with similar splice losses and identical input power levels at 1310 nm wavelength. Note the differences in the patterns and light concentrations.



Figure 5 - Scattered 1310 nm Light From CSL Splices

Further investigations showed that the radiation-pattern differences from splice-to-splice were caused by slight variations in the position of the glass capillary within the splice housing, index-matching-grease placement, the complex geometry of the clear CSL housing (compared to the cylindrical/symmetrical Rotary Mechanical Splice) and the longitudinal location of the cleaved-fiber joint within the splice. These patterns, do not measurably shift due to changes in wavelength or power levels.

It was clear that sufficient scattered power was available, but some focus or guidance was needed to collect the light in a repeatable calibrated way.

The most efficient and mechanically simple method for this proved to be a plastic lightpipe closely abutting the CSL splice.

Figure 6 shows the lightpipe aligned with the splice and a graphical representation of the scattered light "pinballing" through the housing and guided by the plastic lightpipe.

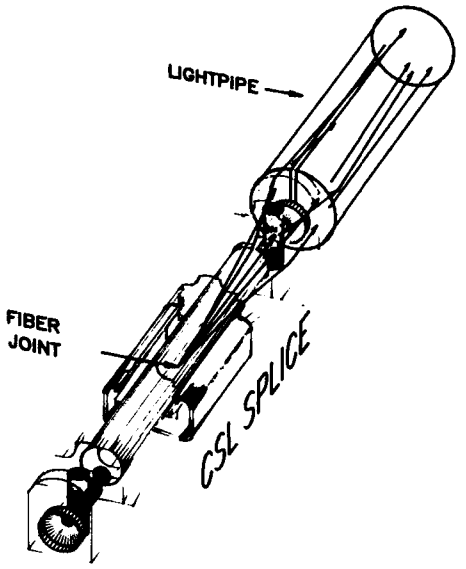


Figure 6 - CSL Lightpipe Collector

Verifier Mechanical Design

The lightpipe technique is used in the 955A CSL Splice Verifier which is shown without its case-cover in place in Figure 7. The 955A consists of a basic CSL workstation with splice holder (1), fiber grips (2) and spring closing lever (3). The 955A differs mechanically from a standard workstation by its ambient light cover and baffle arrangement. The lightpipe (4) is housed in a protective fiber-guiding pivoted sleeve. Pivoting allows a slot in the lightpipe to align with the entrance to the splice for fiber insertion. When the lever is closed to engage the splice's fiber-retention spring, the lightpipe pivots to align axially with the end face of the splice to complete the scattered-light measurement.

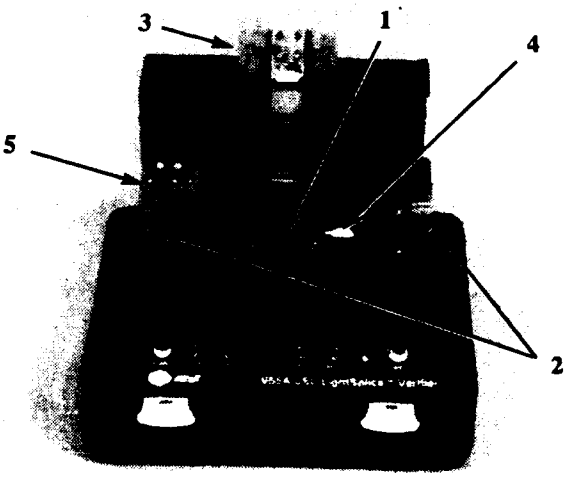


Figure 6 - 955A CSL Splice Verifier

The hinged covered Reference Module, (5), is fitted with a fiber V-groove with fiber-coating stop to correctly position the active fiber to take a signal (source) reference level. This reference signal is used to determine the appropriate threshold for subsequent pass/fail determination.

Verifier Electronics

The control panel, Figure 7, has two switches: POWER off/on, and REF START (Reference Start). The bank of LED indicators show power on, low-battery condition, self-test operation, reference pass (sufficient fiber signal) and splice pass/fail indication.



Figure 7 - Control Panel

Reinforcing the LED indications are tone sequences for self-test pass/fail, proper reference signal between 0 and -30 dBm, and, ultimately, splice-loss pass or fail.

A microprocessor controls the operations of the 955A. This 8-bit microcontroller allows the designers to change the operational sequence, measurement and go/no-go calculations for optimum performance and to suit customer needs.

Verifier Operation

The primary design intent for the CSL-splice-verifier operation was to enable the restoration splicer to quickly and simply determine that the subject splice was of sufficiently low loss to permit system operation without needing time consuming meter or display interpretations. Additionally, if a splice-fail condition exists, the verifier allows the splicer to reposition the fibers in the splice and re-test quickly using the existing splice without recleaving, re-referencing or performing any other time-consuming procedures.

Briefly, the operation of the 955A is as follows:

1. Lower the lever closing the cover and turn the power on - This blocks ambient light and starts and completes the self-test sequence.

2. Cleave and strip the active fiber and insert into the reference module - To correctly align with the reference photodiode.

3. Press the REF START button - If the signal level is between 0 dBm and -30 dBm, the REF PASS LED will illuminate and this level will be retained by the processor.

4. Insert both the fibers into the CSL Splice - Using standard fiber preparation, insertion and fiber bowing procedures,

NOTE: Since the CSL LightSplice is transparent, fiber insertion and contact is visible and magnified by the lensed housing.

5. Close the lever/cover to engage the fiber retention spring - This will complete the splice and signal the processor to begin the scattered-light measurement sequence. A calculation comparing the average of thirty-two scattered light measurements to the stored reference measurement will determine splice pass/fail.

» **SPLICE PASS LED Illuminates** - In conjunction with a single, short tone indicates that a satisfactory splice has been made. The REF PASS LED will extinguish and the 955A is set to make the next splice.

» **SPLICE PASS LED Unlit** - In conjunction with three, short, rapid tones indicates that the splice is unsatisfactory. The processor will retain the reference level as indicated by the REF PASS LED remaining on. When this condition occurs, without removing the fibers from the splice, the fiber-retention spring on the splice is disengaged, the fibers are repositioned, the spring is closed and the scattered-light measurement sequence is repeated. This operation may be repeated as often as necessary however, the first remake is usually successful.

956A Fiber Identifier

Preliminary Design Considerations

Early during AT&T's development of a new-generation fiber identifier, two candidate methods of signal extraction, Macro-bends and periodic micro-bends, were explored. Macro-bend technology is commonly used in the fiber identifiers available today. AT&T chose a combination of micro-bend and macro-bend technology because it creates nearly the same insertion loss at both 1310 and 1550 nm. Unlike pure macro-bends, this approach prevents excess insertion loss at one wavelength while attaining sufficient signal strength at both wavelengths.

Important to NSD was the design of the identifier detection head. Existing fiber identifiers make fiber access into a taut-sheath entry, where the partial damage gives no slack, very difficult. For this reason, a tapered head design to allow easy individual-fiber access was essential. The final design makes accessing a fiber simple during a taut-sheath entry as shown in Figure 8.

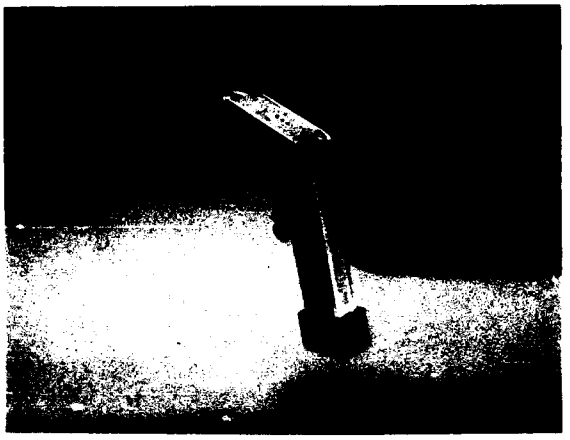


Figure 8 - 956A Fiber Identifier

Identifier Mechanical Design

The 956A Identifier's extruded aluminum handle houses the electronics and a molded-plastic head contains the periodic micro-bend and micro-bend components. The fiber-clamp/release actuator is placed where the operator's thumb can operate the fiber-access function without disturbing the balance of the unit and thereby causing possible fiber breakage.

Identifier Electronics

Picked up by the periodic micro-bends, the optical signal is amplified and filtered. This processing of the signal enables the provision of directional indicators and indication of 2 KHz modulation, if present. The power LED shows that the power is on and that sufficient time has elapsed for the circuit to complete signal processing. Simultaneously, the absence of indicator LED's after the power LED has come on is an indication of no signal on the fiber.

In addition to the circuit-power switch, activated by the load/measure mechanism, an LED-test switch has been incorporated to illuminate all LED's and place the voltage regulator in the low-battery mode which causes the power LED to flash.

Identifier Operation

Fiber access, during a taut-sheath entry, is accomplished by slipping the tapered blade beneath the fiber in question. The guide slots deliver the fiber to the optical assembly where a gentle thumb movement captures the fiber.

The identifier control panel, Figure 9, indicates the unit is functioning with the illuminated POWER LED. This LED illuminates when the thumb slide switch is pulled toward the operator to capture the fiber.

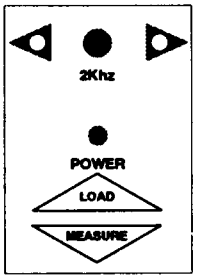


Figure 9 - Fiber Identifier Control Panel

After approximately 4-seconds a signal direction LED will show the direction of propagation and, if the signal is modulated at 2 KHz, the 2 Khz LED will illuminate. No directional LED's indicate an absence of signal on the fiber under test.

Conclusion

Over the past several years, restoration tools and procedures have impressively reduced the time required to reestablish communication links. The objective of AT&T's concept of "Optimal Restoration" is to restore service as quickly as possible once an intrusion has occurred. This restoration plan may range from a 1-person repair at the damage site to a full restoration *deployment.*

The addition of two new tools, 955A Splice Verifier and 956A Fiber Identifier, will have a pronounced effect on the time required to restore service. The splice verifier will permit the restoration crew to bridge a severed cable and instantly verify the quality of the bridging splices. Additionally, non-serviceable splices can be remade and immediately verified locally by one person without far-end test equipment.

The 956A Fiber Identifier is a second-generation identifier designed with direct customer input. The identifier is designed to make fiber access during taut-sheath restorations far easier than with previous tools. The identifier utilizes the inherent advantages of periodic micro-bend technology to provide low-stress, low insertion loss at both 1310 and 1550 nm while simultaneously providing high sensitivity to low-level signals.

Acknowledgements

The authors would like to acknowledge the contributions to the design and development of the 956A Fiber Identifier from B.B. Boehlke, B.V. Darden, C.H. Duvall, J.J. Hayes, S.C. Mettler and G.E. Mock.

References

1. Fagen, M.D., ed. 1975. "A History of Engineering and Science in the Bell System: The Early Years (1875-1925)," Bell Telephone Laboratories, Inc. 20.

2. G.F. DeVeau, J.A. Aberson, and J.K. Lo, "A New Generation of Fiber Splices and Installation Results," 39th International Wire and Cable Symposium Proceedings, Reno, 1990.



George F. DeVeau is a Member of Technical Staff at AT&T Bell Laboratories, Norcross, Georgia. After joining Bell Laboratories in 1967, he was involved in multipair cable design and development. Since 1980 Mr. DeVeau has been engaged in the design and development of fiber optic splicing systems. He has been granted five patents with two more pending.



Walter S. Konik is a Member of Technical Staff at AT&T Bell Laboratories, Norcross, Georgia. After joining Western Electric in 1969, he was involved with design and development in the area of manufacturing automation. Since 1986, his involvement has been with the design and development of fiber optic apparatus. He has a B.S. degree from Polytechnic of Krakow, Poland.



Joel L. Mock is a Member of Technical Staff at AT&T Bell Laboratories, Norcross, Georgia. Since joining Bell Laboratories in 1981, he has been involved in the design of fiber optic test equipment.



Mary J. Presnell joined AT&T Bell Laboratories, Norcross, Georgia in 1986 as a Member of Technical Staff. She has been involved in the design and development of fiber optic building cable and apparatus. Ms. Presnell received her B.S. and M.S. in Electrical Engineering, both from the University of Kentucky, Lexington, Kentucky.

(photograph unavailable)

William B. Westfall joined AT&T Network Services Division in 1956 and since then has been involved in network operations and engineering. He is currently technical-support and subject-matter expert for fiber and coaxial outside-plant cable systems for the eastern United States.

HIGH-STRENGTH SPLICED OPTICAL FIBER MANUFACTURED USING A LOCALIZED CARBON COATING TECHNIQUE WITH A CO2 LASER

K. Oohashi, T. Shimomichi, S. Araki, and N. Sato

Opto-Electronics Laboratory, Fujikura Ltd.
1440 Mutuzaki, Sakura-shi, Chiba-ken 285 Japan

Abstract

In order to improve the reliability of the fusion spliced portions of the carbon-coated optical fibers, we have studied the carbon recoating of spliced bare fiber surfaces with a local carbon coating technique that uses a CO2 laser as a heat source. As a result, we have achieved a maximum splice strength of 4 GPa and an "n" value of 85. These are clearly high levels of strength and fatigue resistance compared with the levels resulting from normal splices without carbon recoating. We have also used the local carbon coating technique to recoat mass fusion splices of carbon-coated optical 4-fiber ribbons. In the case of the 4-fiber ribbon, we have succeeded in forming a smooth carbon film. We have also verified that there are no adverse effects in terms of splice loss.

1. Introduction

In recent years, as the use of long-distance, high-count optical submarine cables for large capacity transmission increases, splices of optical fibers are required to be highly reliable. In the meantime, since a carbon film deposited on a silica-based optical fiber surface increases the fiber's long-term reliability by preventing the permeation of moisture and hydrogen molecules, studies have been conducted on the application of carbon-coated fibers in lines such as submarine cables[1]. However, there is concern about the reliability of spliced portions formed from carbon-coated fibers, because carbon film can be removed from spliced portions by an arc discharge generated during the fusion splicing process. We think that it is necessary to recoat the spliced portions with carbon film in order to maintain the fiber reliability[2,3]. To further increase the reliability of the spliced portions of the fiber, stronger splices are necessary. In the case of the arc fusion splicing process, the splice strength is at most 3 GPa. It seems that this decrease in strength is the result of the permanent elongation in the fibers that develops during the fusion splicing process by arc discharge. We think that such permanent elongation can be eliminated by applying a local heat treatment, and that strong spliced portions can thereby be formed.

First, this paper describes the carbon-coated fiber splice method and discusses its relation to splice strength. Then, this paper illustrates a method of carbon coating on the spliced portions of a carbon-coated fiber. It goes on to describe the characteristics of the carbon-coated fibers, including the strong spliced portions coated with the carbon film. This coating method employs a local carbon coating technique that uses a CO2 laser as a heat source. Finally, this describes the characteristics of the carbon recoating trial produced in the spliced portions of a 4-fiber ribbon by the specified technique.

2. Test Samples

A germanium-doped, silica-core SM fiber was used for this study. In the drawing process, this fiber was coated with pyrolytic carbon film with a thickness of about 500 Å. Subsequently, the dual coatings of the UV curable resins were applied with in-line applicators. The diameters of the fiber and dual coatings were 125 μm and 250 μm, respectively. Table 1 shows the parameters of this fiber. Fig. 1 illustrates the sectional figure of a 4-fiber ribbon, which uses the specified fiber.

3. Carbon-Coated Fiber Splice Method

The following section describes the splicing process of carbon-coated fibers through arc fusion.

Table. 1 The parameters of the fiber

Parameters	Value
Cladding diameter	125 μm
M.F.D	10 μm
λc	1.18 μm
Core eccentricity	< 1.0 μm

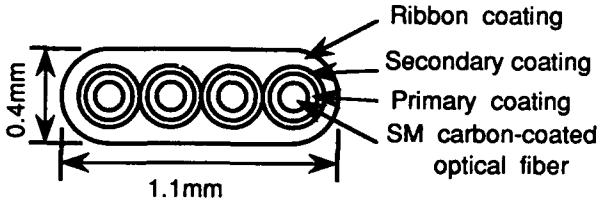


Fig. 1 Structure of the manufactured carbon-coated 4-fiber ribbon

(1) Remove the UV resin coatings from the fibers and fix the fibers in V-grooves. At this time, be careful not to allow the bare fiber parts to come into contact with the grooves.

(2) Perform a prior discharge with a core-direct-monitoring arc fusion splicer. This operation will burn away the carbon film on the tips of the fibers.

(3) Align the core axes of the fibers to prepare for the fusion splice.

(4) Splice the fibers after the core axes aligning.

(5) Recoat the bare parts of the fibers with UV curable resin.

The purpose of a prior discharge is essentially to clean the fiber surface. However, this prior discharge also serves to burn the carbon film on the carbon-coated fibers to allow for direct core monitoring. If the splicing process is initiated without a prior discharge, carbon film will be burned away when the fibers are fusion spliced, and these burned carbon particles may damage the spliced portion. Fig. 2 shows the Weibull plots of splice strength achieved both with a prior discharge and without it. The splice strength achieved without a prior discharge varied widely and was generally low compared to that achieved with a prior discharge. Fig. 3 shows the Weibull plots of the splice strength of carbon-coated fibers and normal(non-carbon-coated) fibers achieved with a prior discharge. The figure shows almost the same failure strength distribution between both sets of spliced fibers, but no signs are observed that the burned carbon particles damaged the fiber surface during a prior discharge. These results indicate that a prior discharge process to burn carbon film is necessary for splicing carbon-coated fibers.

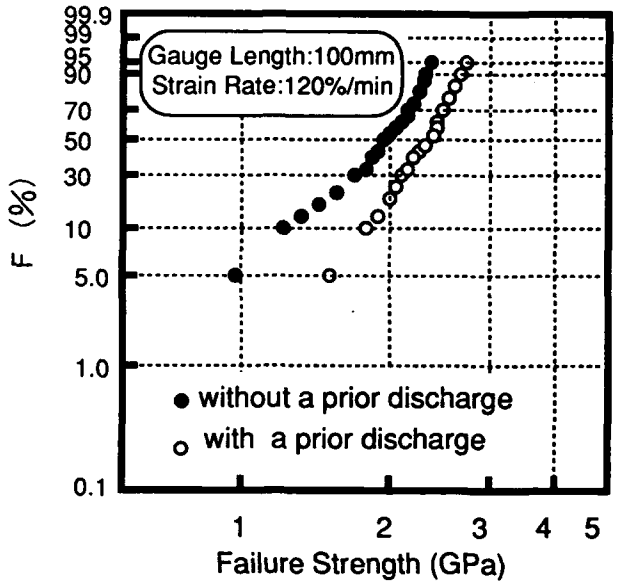


Fig . 2 Weibull plots of the splice strength of the carbon-coated fibers

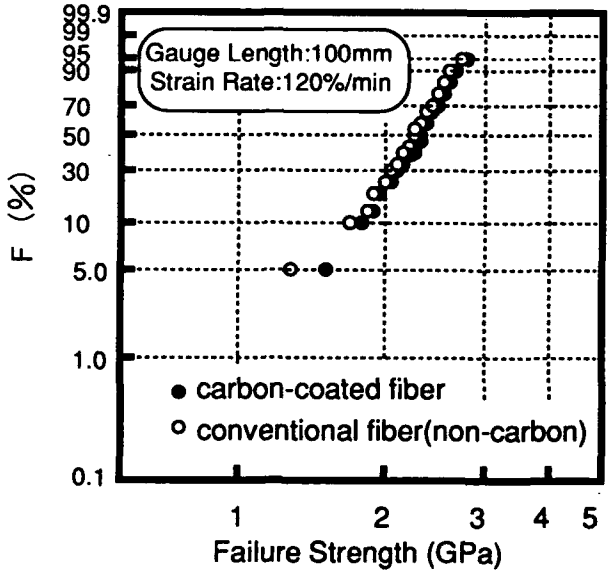


Fig . 3 Weibull plots of the splice strength achieved with a prior discharge

4. Local Carbon Recoating of Fusion Spliced Portions

Fig. 4 shows the local carbon coating process of the spliced portions of the carbon-coated fibers. The fibers have been fusion spliced, and the area where the carbon film has been burned away has been coated with carbon film, using local carbon coating equipment. This procedure has created the need for a lapping allowance of about 2 mm between the carbon film on the carbon-coated fiber and the newly recoated carbon film. Finally, the bare parts of the fibers have been recoated with a UV curable resin. Fig. 5 shows the schematic figure of the local carbon coating equipment that uses CO2 laser as a heat source. During this process, a high-strength spliced fiber is set in a reaction chamber. Then the chamber is charged with a hydrocarbon gas, and a CO2 laser beam is introduced into the chamber through a zinc selenide window. This laser converges on the bare fiber surface and heats up the region of the spliced bare fiber surface without carbon film. Because of this heat treatment, carbon film becomes deposited on the region through thermal chemical vapor deposition. The reaction chamber then moves at the appropriate speed to coat carbon film of about 7 mm in length along the spliced portion.

5. Results and Discussion

5.1 Local Carbon Recoated Surface

Fig. 6 shows a photograph of the carbon recoating on the spliced portion. This photo shows that the newly recoated carbon film becomes a little darker than the carbon film on the carbon-coated fiber. Fig. 7 shows the STM (scanning tunnel microscope) images of the local carbon film on the spliced portion. Using the analysis method for STM images, the surface roughness is determined to be 4 nm. The surface roughness value describes the difference in height between the highest point and the lowest point on the carbon film's surface. This is nearly equal to the surface roughness of a carbon-coated fiber whose fiber surface is coated with a carbon film during the drawing process. This surface roughness indicates no difference in the carbon recoating film quality.

5.2 Splice Strength

Fig. 8 shows the tensile failure strength distribution of the carbon-coated fiber whose spliced portions have been recoated with carbon film through the local carbon coating technique. The maximum failure strength is 3.0 GPa, while the median failure strength is 2.7 GPa.

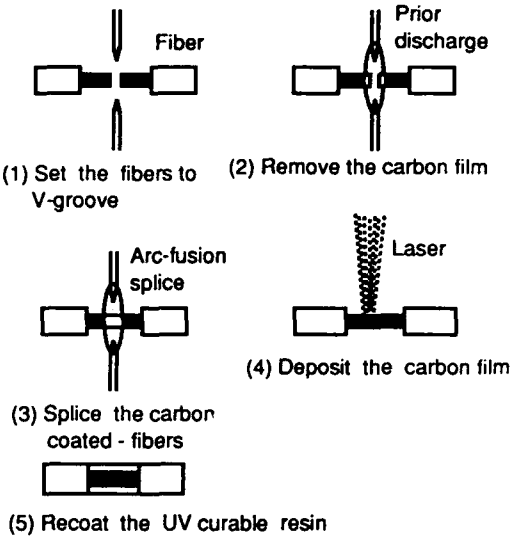


Fig . 4 Splicing process of the carbon-coated fiber

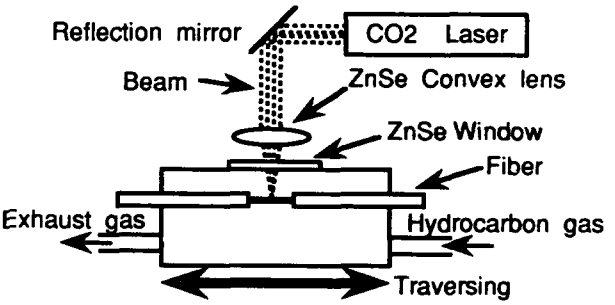


Fig . 5 Schematic diagram of the local carbon coating equipment

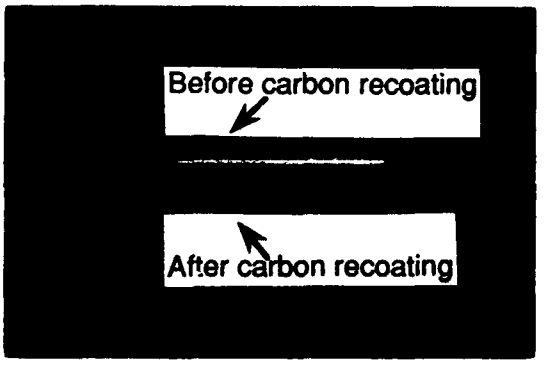
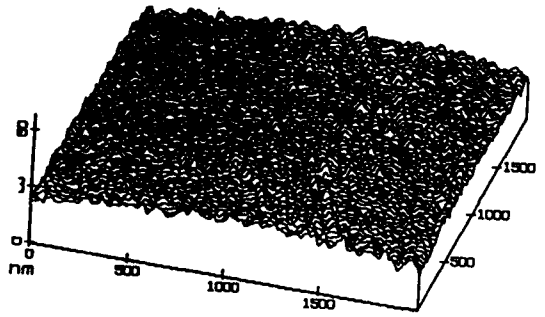
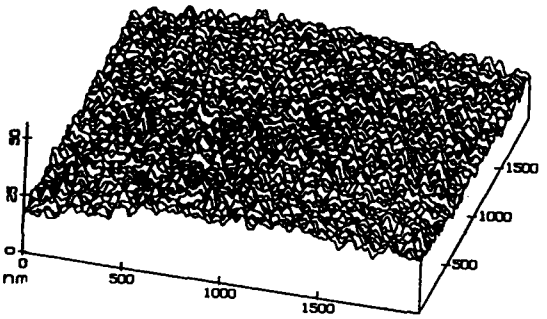


Fig. 6 Photograph of the carbon recoating



Carbon film(carbon-coated fiber's surface)



Local carbon film(carbon recoating)

Fig. 7 STM images of the carbon film

On the other hand, the spliced portion without carbon recoating has a maximum strength of 2.8 GPa and a median strength of 2.3 GPa. This indicates that the carbon recoating has only a slight annealing effect. To reduce elongation of the fibers, we studied the relationship between the annealing time during the carbon recoating and the splice strength. Fig. 9 shows the relationship between the splice strength and the annealing time needed to carry out the carbon recoating. The splice strength increases as the annealing time increase; however, the splice strength peaks after a certain annealing time. Fig. 10 shows the Weibull plot indicating the strength of the spliced portions recoated with carbon film whose annealing time has allowed the greatest splice strength. The maximum strength is 4 GPa, while the median strength is 3.2 GPa. These strength values are substantially higher than those of normal fiber splices. To confirm that carbon recoating is an effective annealing method for eliminating the elongation of the fiber caused by fusion splicing, we have investigated the splice strength of a fiber whose spliced portion is only irradiated by a CO2 laser without carbon recoating. These results are shown in Fig.11. The irradiated spliced portion shows less strength than normal fibers(non-irradiated), indicating that there is no annealing effect on the spliced portion without carbon recoating. This may be because moisture absorbed on the fiber surface reacts with heat, and forms silanol groups(Si-OH).

Consequently, we think that the carbon film coating of the spliced portions using the local carbon coating technique is an effective means of

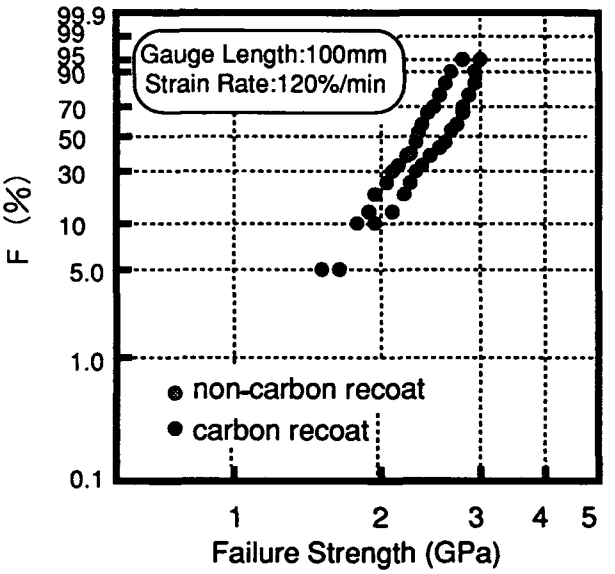


Fig . 8 Weibull plots of the splice strength of the carbon-coated fibers

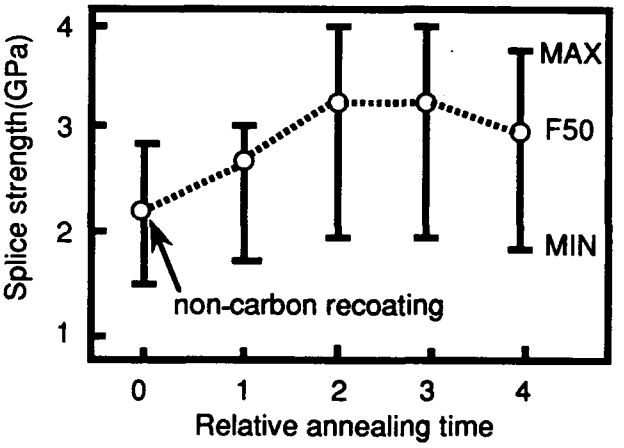


Fig. 9 Relationship between the splice strength and the annealing time needed to carry out the carbon recoating

eliminating the elongation in the fibers. Therefore, we believe that it will contribute to improvements in the strength of fiber splices.

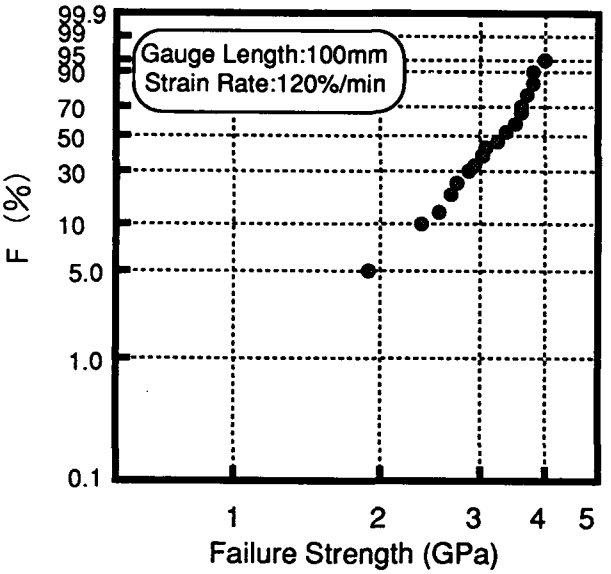


Fig. 10 Weibull plot of the strength of spliced portion recoated carbon film whose annealing time allowed the greatest splice strength

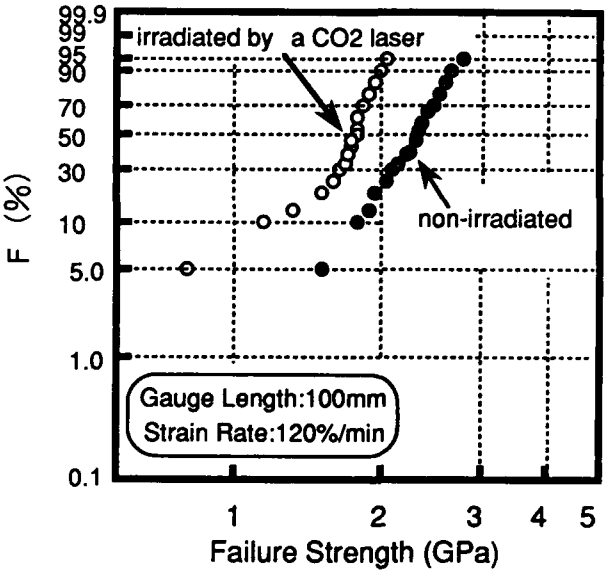


Fig. 11 Weibulle plots of the strength of splice portions irradiated by a CO2 laser without carbon recoating

5.3 Fatigue Characteristics of the Splices

We conducted a tensile dynamic fatigue test to evaluate the reliability of the spliced portions. Fig. 12 shows the dynamic fatigue parameter "n" value determined by the median failure strength. The "n" value of the carbon-coated fibers whose spliced portions have not been coated with carbon film is 23. On the other hand, the spliced portion that has been recoated with carbon film has an "n" value of 85. However, this "n" value is slightly lower than that of the original carbon-coated fibers without the spliced portions. This degradation in the "n" value is presumably due to the presence of moisture on the spliced bare fiber surface before the carbon recoating process begins. It is expected that eliminating this moisture before carbon recoating will improve the "n" value.

5.4 Temperature Loss Characteristics at the Splice

We manufactured 1000 m of a carbon-coated fiber including 10 spliced portions that had been recoated with carbon film. The splice loss is 0.5 dB or 0.05 dB for each splice. This value is almost equal to a normal splice loss. This sample was subject to a heat cycle test of -40 °C to 60 °C to monitor loss variations. The results of this test are shown in Fig. 13. The increase in the loss on the low-temperature side is about 0.01 dB. Therefore, the amount of loss per splice is negligible, indicating that the carbon recoating process has no adverse effects.

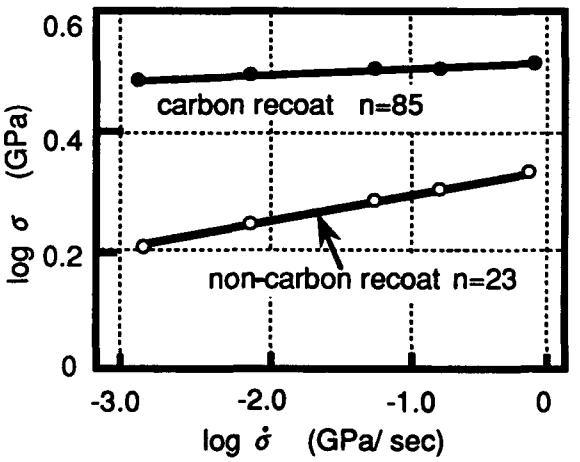


Fig . 12 Dynamic fatigue test of the spliced portions of the carbon-coated fibers

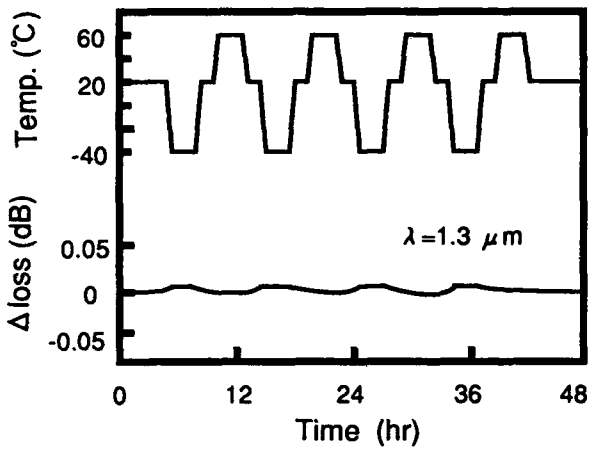


Fig. 13 Loss change of the carbon-coated fiber including 10 spliced portions that have been recoated with carbon film

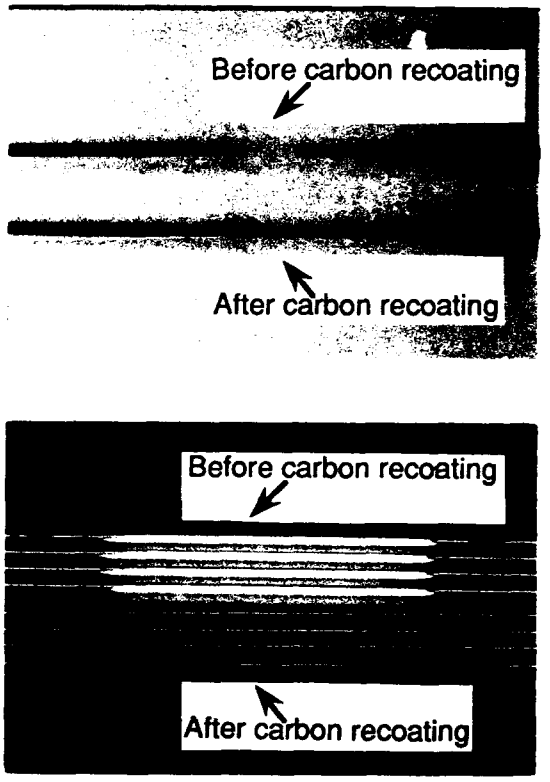


Fig. 14 Photographs of the mass fusion splice

5.5 Trial Manufacture of 4- Fiber Ribbon with Carbon Coater, Splices and Splice Characteristics

We coated the mass fusion splice of a carbon-coated 4-fiber ribbon with a carbon film, core by core, using the local carbon recoating method. Fig. 14 shows two photographs of the mass fusion splice before and after carbon recoating. Fig. 15 shows the Weibull plots of the splice strength. The median tensile strength is 1.7 GPa, which is equal to the splice strength of a 4-fiber ribbon without carbon film on the spliced portions. Presumably, carbon recoating does not improve the splice strength because the fiber surface is damaged by fixing the fiber in the V-groove during the mass fusion splicing process, thereby nullifying the annealing effects of the carbon coating. Fig. 16 shows the STM image of the carbon film recoated on a 4-fiber ribbon splice. The surface roughness is about 4 nm, which is the same as it is in the spliced portion of a single core, carbon-coated fiber recoated with carbon film formed by applying the same process. Fig. 17 provides a histogram of the splice losses. The mean splice loss is 0.048 dB. The standard deviation is 0.037 dB, which is equal to the splice loss of 4-fiber ribbons whose spliced portions have not been carbon coated. This indicates that the local carbon coating does not adversely effect the spliced portions of fiber ribbons.

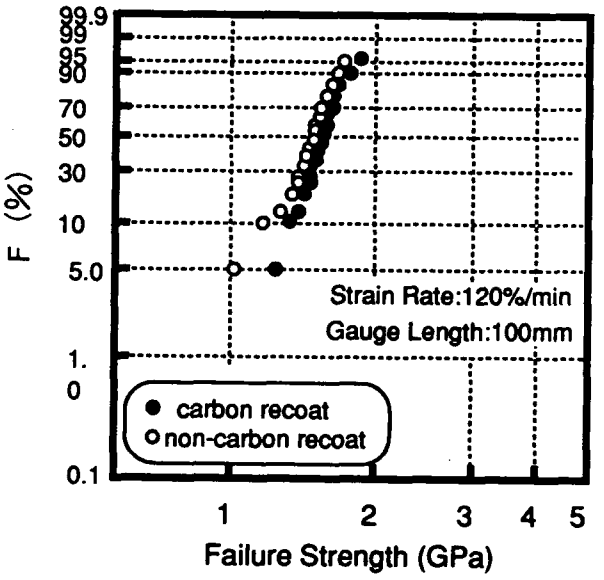


Fig. 15 Weibull plots of the splice strength of the carbon-coated 4-fiber ribbon

6. Conclusion

On the basis of the experimental results presented above, we have drawn the following conclusions.

(1) It was confirmed that a local carbon recoating technique that uses a CO2 laser could produce a smooth carbon film on spliced bare fiber surfaces

(2) By optimizing the carbon recoating conditions of the spliced portions, carbon-coated fiber splice-strength could be improved to a maximum of 4 GPa.

(3) The fatigue characteristics of the spliced portion show that an "n" value of dynamic fatigue is 85. We therefore think that the carbon film coating on the spliced portion can improve the fatigue.

(4) The splice loss of the carbon-coated fiber whose spliced portions have been coated with carbon film is 0.05 dB per splice, which is a normal splice loss. This indicates that carbon recoating has no adverse effects. The temperature loss of these splices is the same as that of normal fiber splices.

(5) The splice strength, splice loss, and temperature loss characteristics of the 4-fiber ribbon whose mass fusion splice is carbon-coated are the same as those of normal mass fusion splices of 4-fiber ribbons. Therefore, no particular adverse effects on these characteristics caused by carbon recoating could be observed.

We expect that the carbon recoating of the spliced bare fiber surface will increase reliability in large capacity transmission lines that are composed of carbon-coated fibers.

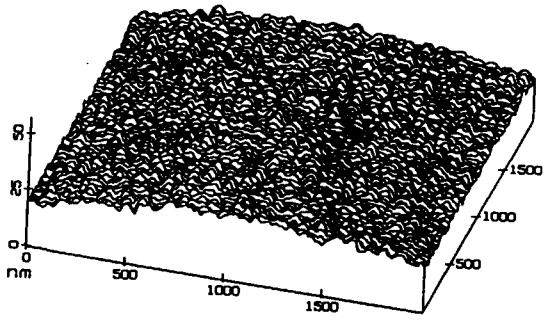


Fig. 16 STM image of the carbon film recoated on the 4-fiber ribbon

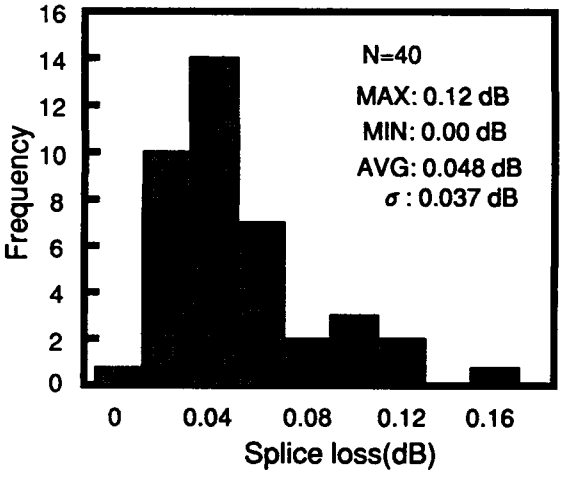


Fig. 17 Distribution of splice loss of the carbon-coated 4-fiber ribbon

7. References

[1] N.Yoshizawa, Y.Miyajima, and Y.Katuyama, "A one-hundred-fiber submarine cable composed of hermetically coated fiber ribbons inserted into slots", IWCS, p603-610, 1989.

[2] D.Inniss and J.Krause, "Hermetic splice overcoating", OFC, 1991, Paper ThG4.

[3] T.Shimomichi, S.Ishimaru, K.Oohashi, and S.Araki, "Carbon recoating on the splicing portion of carbon coated optical



Keiji Oohashi

Fujikura Ltd.

1440 Mutuzaki,
Sakura, Chiba,
285, Japan

Mr. Oohashi was born in 1956. He graduated from Tokyo Institute of Technology with a B.E. degree in 1980. After eight years'work as an engineer in materials for motor viecles he joined Fujikura Ltd. and has been engaged in research and development of optical cables. He is now an engineer of Telecommunication Cable Material Section and a member of IEICE of Japan.



Shinji Araki

Fujikura Ltd.

1440 Mutuzaki,
Sakura, Chiba,
285 Japan

Mr. Araki was born in 1950. He joined Fujikura Ltd. after his graduation from Tokyo Metropolitan University with a B.E. degree in 1974. He has been engaged in research and development of optical fibers and optical fiber coatings. He is now the chief of the Telecommunication Cable Material Section and a member of IEICE of Japan.



Tsuyoshi Shimomichi

Fujikura Ltd.

1440 Mutuzaki,
Sakura, Chiba,
285 Japan

Mr. Shimomichi was born in 1960. He joined Fujikura Ltd. after his graduation from Nagasaki University with a M.E. degree in 1986. He has been engaged in research and development of optical fibers and optical fiber coatings. He is now an engineer of Telecommunication Cable Material Section and a member of IEICE of Japan.



Nobuyasu Sato

Fujikura Ltd.

1440 Mutuzaki,
Sakura, Chiba,
285 Japan

Mr. Sato was born in 1943. He joined Fujikura Ltd. after graduation from Tohoku University with a B.E. degree in 1966 and has been engaged in research and development of transmission cables. He is now the manager of Transmission Line Department and a member of IEICE of Japan.

THE HERMETIC CARBON LAYER RESTORATION ON THE FUSION SPLICED PORTION OF CARBON COATED FIBER

Isamu FIJITA, Masahiro HAMADA, Haruhiko AIKAWA,
Katsuya NAGAYAMA, Yasuo ASANO

YOKOHAMA RESEARCH LABORATORIES
SUMITOMO ELECTRIC INDUSTRIES, LTD.

Abstract

Conventional fusion splicing methods remove the carbon layer of a hermetically carbon coated optical fiber locally. The vanishment of the carbon layer degrades its fatigue characteristics drastically. In this study, hermetic carbon layer restoration technology on the fusion spliced portion of a carbon coated fiber filament has been developed with a thermal decomposition process using a CO_2 laser as a local heat source. The tensile strength of 3kgf, and the fatigue parameter n of 94, have been attained on the spliced portion by this restoration process.

1.Introduction

Mechanical reliability of silica-based optical fibers is described by two natures. One is its initial fracture strength and the other is its fatigue characteristics. The latter is expressed by a fatigue parameter(n-value), and is ruled by the water molecules corroding the silica surface. Conventional optical fibers have a n-value of around 20. A carbon coated optical fiber(CCF) has a much larger n-value of around 150, which extends its life remarkably. This is caused by the carbon layer on the silica surface intercepting moisture penetration. However, when CCFs are spliced with conventional arc fusion, the carbon layer exposed to the discharge is locally burned off. The vanishment of the carbon layer degrades the spliced portion to around 20 in n-value. As for a CCF cable elongated by factory splicing, spliced portions become the weakest points through the total length of an optical fiber cable against fatigue. This fact becomes a very important issue in circumstances requiring very long-term reliability such as in submarine cables. This paper describes a method for restoring the carbon film on the fusion spliced portion of a CCF with a thermal chemical vapor deposition using a CO_2 laser, and gives experimental results of the tensile strength and the fatigue parameter n.

2.Experimental Apparatus

Figure 1 shows the experimental apparatus for the carbon restoration process, which consists of: a CO_2 laser with 10.6 um wave length, which heats the optical fiber through a ZnSe window; a reaction chamber equipped with a horizontal traverse table which moves the fiber horizontally; a reactant gas supplier which controls the fraction and flow rate of a mixture of organic gas and inert gas, and feeds it into the chamber; and an infra-red thermometer for temperature measurement of the fiber surface in the wave length from 1 to 2 micrometers through a CaF window.

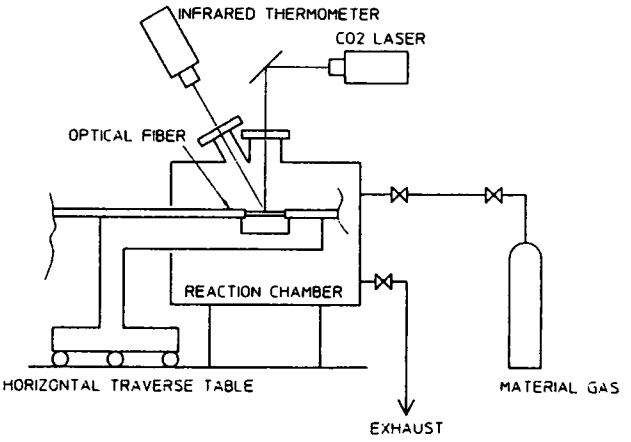


Fig.1 Experimental Apparatus

3.Experimental Procedures

Figure 2 shows the flowchart of the experimental procedures. The processes from 1 to 5 are conventional high strength splicing methods. In the 1st step, the resin jacket around the fiber is removed in hot sulfuric acid and cleaned in an organic solvent using ultrasonic vibration. In the 2nd step, the original carbon layer is removed for several millimeters from the end face using a discharge in inert gas. This step is indispensable for a commercial splicer to align the fiber cores with image processing. In step 3, the fiber is cut with a cleaver designed not to damage the fiber. In step 4, a resin thin film is fabricated again around the bare silica with a thickness of several micrometers, in order to prevent the silica surface from direct contact to the V-shaped grooves of the splicer. In step 5, arc fusion is performed using a commercially standard splicer. In step 6, a 1.5% screening test is applied onto the spliced portion in order to eliminate the weak samples due to the handling error in the previous steps. This process gives samples whose strengths fit well to a single mode Weibull distribution. In the 7th step, the carbon layer is restored on the region where the carbon was removed previously and about 1 mm on the original carbon layer on either side of the removed section as shown in figure 3. Fracture strength of the fiber was measured with a tensile test, and an n-value is calculated from the set of 50% failure strengths at different strain rates.

1:Chemical removal of resin jacket
↓
2:Removal of carbon later with discharg
↓
3:Cleaving fibers
↓
4:Fabrication of a resin film layer onto the bare section
↓
5:Arc fusion splicing
↓
6:Screening test with a strain of 1.5%
↓
7:Carbon film restoration

Fig.2 Flowchart of the experimental proc

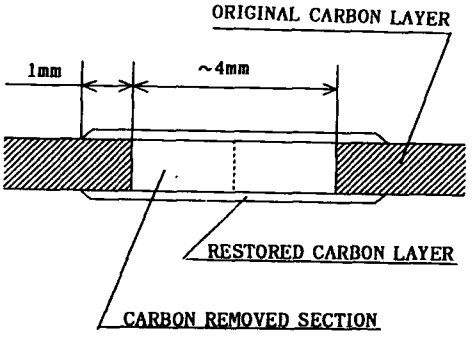


Fig.3 Geometry of restored portion

4.Experimental results and Discussion

4-1.Strength distribution

Figure 4 and 5 show the distribution of fracture strength of non-restored and restored spliced portion, respectively. 'Non-restored' means the samples without only step 7 in this study. The data shown in the figures were collected at the strain rate of 85%/min. The figures show that restored spliced portion has higher strength than the non-restored ones. The 50% failure strength of the restored is nearly 0.26kgf higher than that of the non-restored. Especially, improvement of the strength is remarkable in the high strength region. This is suspected to be caused by the annealing effect of the CO_2 laser such as closing cavities on the silica surface, which is probably more effective on smaller Griffith flaws. This effect might result in the transition of the Weibull mode around 20% failure probability. Such a transition was observed at other strain rates. Table 1 shows the results of a tensile test at different strain rates. The 50% failure strength and its precision index, which is almost same to the standard deviation when there is much data, are calculated from each Weibull plot using a statistical method including a regression with the least square method, whose details are explained in section 5.

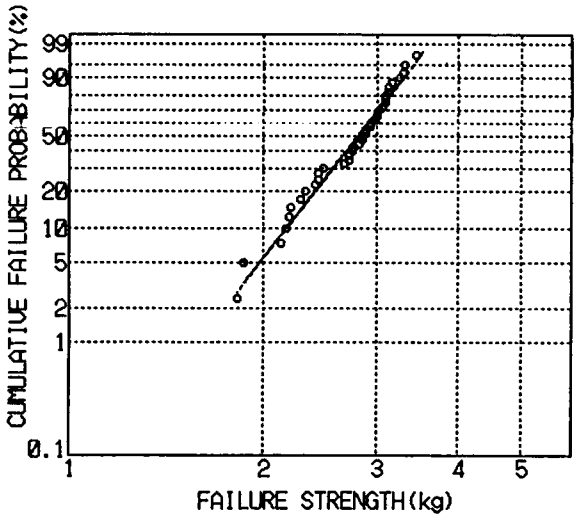


Fig.4 Fracture strength distribution of non-restored spliced portion

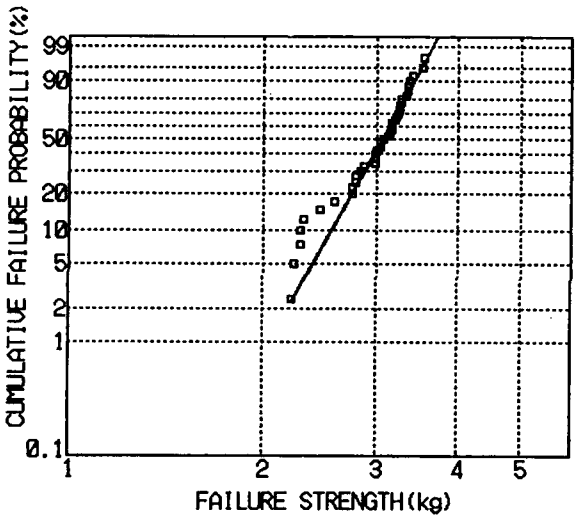


Fig.5 Fracture strength distribution of restored spliced portion

Table1.Fracture strength of restored and non-restored spliced portion

Fracture strength(kg)	Precision index(kg)	Strain Rate(mm/min)	Remarks
2.927	0.007	3.31	restored
2.937	0.005	22.93	restored
3.048	0.006	171.00	restored
2.453	0.003	3.31	non-restored
2.526	0.011	22.93	non-restored
2.799	0.012	171.00	non-restored

Gauge length is 200mm

Number of samples is 40 at each strain rate.

4-2.Fatigue parameter n

Figure 6 and 7 show the relation between fracture strength and strain rate for the non-restored and the restored,respectively. The lines, whose slope is the inverse of 'n-1', are drawn from the values in table 1 using the least square method. The figures show that the fatigue parameter n is improved from 28 for the non-restored spliced portion to 94 for the restored portion by the restoration process . Errors of the n-value are ± 2 for the non-restored and ± 15 for the restored in 95% confidence level.

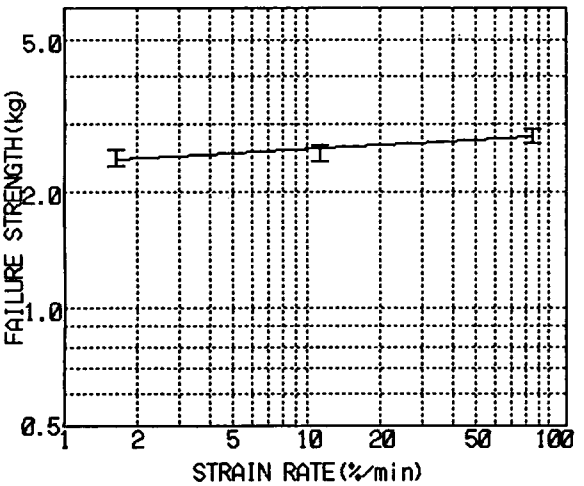


Fig.6 Relation between fracture strength and strain rate for non-restored spliced portion (n-value is 28)

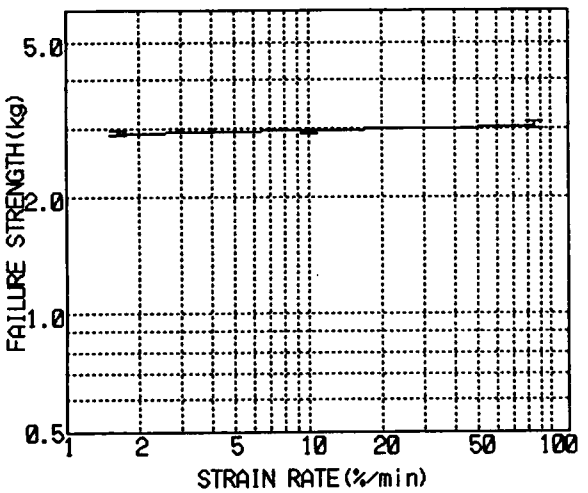


Fig.7 Relation between fracture strength and strain rate for restored spliced portion (n-value is 94)

4-3.Microscopic observation

An SEM image of the cross section of the restored region (photo.1) indicates that the thickness of the carbon layer is around 35 nm, which is slightly thinner than 50 nm for the original carbon layer. Photos 2 and 3 give the atomic force microscope (AFM) images of the restored and original carbon surface, respectively. Comparing these photos, there is no significant difference of surface roughness between the two. The common parameter Ra indicating roughness is 0.57nm for the original and 0.66nm for the restored. Original carbon layer usually has an n-value of more than 150. The difference of the n-value between the restored carbon layer and the original carbon layer is supposed to be depending on the thickness of the layer.

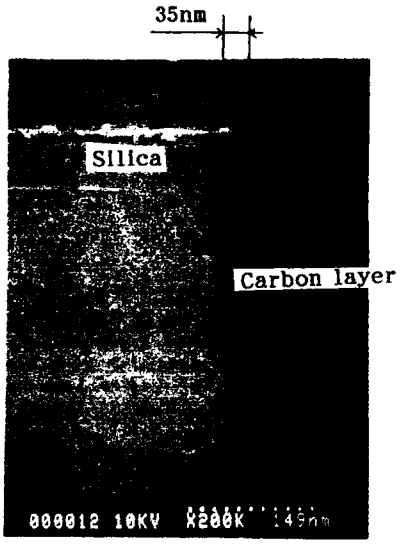


Photo.1 SEM image of the cross section of the restored region

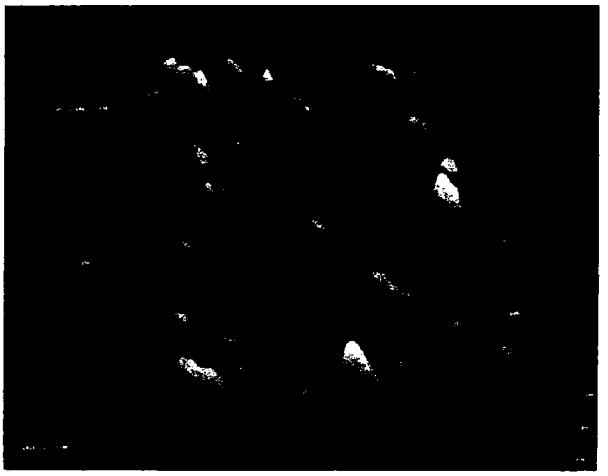


Photo.2 Surface of an original carbon layer (AFM image)



Photo.3 Surface of a restored carbon layer (AFM image)

5.Error estimation of n value

Fatigue characteristics of optical fibers are usually represented by the fatigue parameter n which is obtained by the well-known dynamic fatigue test, in which fibers are loaded to fracture at several strain rates. Results of the dynamic fatigue test give good estimation of the n-value when it is executed on intrinsic fibers, owing to its steep line on the Weibull chart. Usually the m parameter of original fibers is around 100. However, spliced portions have lower m values and more scattered strengths from the ideal Weibull distribution than the original fibers, and in some cases they don't have unique mode but multiple Weibull mode instead. In the dynamic fatigue test, 50% fracture strength are usually taken as the representative values. However, in case of spliced portions, the 50% fracture strength is supposed to have more error compared with that of the original fiber, which might result in low reliability of n value. Therefore discussion of error is indispensable to determine the n-value, especially for spliced portions. In this study, a simple statistical method is proposed, which gives an estimated error of the n-value. In this method, the following assumptions and procedures are adopted.

(1)Fracture strength distribution is essentially the Weibull distribution.

(2)Each fracture data has the same uncertainty around the ideal Weibull distribution, and its distribution is Gaussian.

(3)Ideal Weibull distribution can be estimated by the least square method.

(4)Each fracture strength having the same failure probability at different strain rates corresponds to the same initial flaw size.

Experimental fracture data are plotted on the Weibull chart and regressed with the well-known Weibull distribution as follows;

$$P=1-\exp\{-(\sigma/\xi)^m\} \qquad \cdots\cdots[1]$$

where P is the cumulative failure probability
σ is the failure strength
m and ξ are the weibull parameters

The two Weibull parameters m and ξ, and their errors are solved by using the least square method and partial derivative as below;

$$m=(C_{22}d_1-C_{12}d_2)/(C_{11}C_{22}-C_{12}C_{21})$$
$$\xi=\exp(-b/m)$$
$$dm=\Sigma\frac{\partial m}{\partial X_1}dX_1$$
$$d\xi=\exp(-\frac{b}{m})\Sigma(-\frac{1}{m}\frac{\partial b}{\partial X_1}+\frac{b}{m^2}\frac{\partial m}{\partial X_1})dX_1 \qquad \cdots\cdots[2]$$

where $C_{11}=\Sigma X_1^2$ $\quad X_1=\ln\sigma_1$
$C_{12}=\Sigma X_1$ $\quad Y_1=\ln(-\ln(1-P_1))$
$C_{21}=\Sigma X_1$
$C_{22}=\Sigma 1$
$d_1=\Sigma X_1Y_1$
$d_2=\Sigma Y_1$
$b=(-C_{21}d_1+C_{11}d_2)/(C_{11}C_{22}-C_{12}C_{21})$

On the assumption (2), a precision index of each strength data with 95% confidence level is estimated with the equation [3].

$$\Delta\sigma=\sqrt{\frac{\Sigma(\bar{\sigma}(P_1)-\sigma_1)^2}{n-1}} \qquad \cdots\cdots[3]$$

Fracture strength of any failure probability and its error are given by eq.[4] and [5]

$$\bar{\sigma}(P)=\exp(\frac{1}{m}\ln(-\ln(1-P))) \qquad \cdots\cdots[4]$$

$$d\bar{\sigma}=\frac{\partial\bar{\sigma}}{\partial m}dm+\frac{\partial\bar{\sigma}}{\partial\xi}d\xi$$
$$=\Sigma(\frac{\partial\bar{\sigma}}{\partial m}\frac{\partial m}{\partial X_1}+\frac{\partial\bar{\sigma}}{\partial\xi}\exp(-\frac{b}{m})(-\frac{1}{m}\frac{\partial b}{\partial X_1}+\frac{b}{m^2}\frac{\partial m}{\partial X_1}))dX_1 \qquad \cdots\cdots[5]$$

Using the equation [3] and [5], The error propagation from the data to the 50% failure strength can be expressed in eq.[6].

$$\Delta\bar{\sigma}=\sqrt{\Sigma\{(\frac{\partial\bar{\sigma}}{\partial m}\frac{\partial m}{\partial X_1}+\frac{\partial\bar{\sigma}}{\partial\xi}\exp(-\frac{b}{m})(-\frac{1}{m}\frac{\partial b}{\partial X_1}+\frac{b}{m^2}\frac{\partial m}{\partial X_1})\}^2\frac{\Delta\sigma^2}{\sigma_1^2}} \qquad \cdots\cdots[6]$$

Also using the least square method, Both of the n-value and the error propagation from the 50% fracture strength to the n-value can be expressed in the following two equations.

$$\frac{1}{n-1}=\frac{S_{22}t_1-S_{12}t_2}{S_{11}S_{22}-S_{12}S_{21}} \qquad \cdots\cdots[7]$$

$$\Delta n=2\sqrt{\Sigma(\frac{\partial n}{\partial\sigma_1}\Delta\bar{\sigma}_1)^2} \qquad \cdots\cdots[8]$$

where $S_{11}=\Sigma(\ln\dot{\sigma}_1)^2$
$S_{12}=\Sigma\ln\dot{\sigma}_1$
$S_{21}=\Sigma\ln\dot{\sigma}_1$
$S_{22}=\Sigma 1$
$t_1=\Sigma\ln\dot{\sigma}_1\ln\bar{\sigma}_1$
$t_2=\Sigma\ln\bar{\sigma}_1$

Equation [8] gives the error in 95% confidence level. Applying this method to the experimental data, the error of $\pm$ 2 for the non-restore and the error of $\pm$ 14 for the restored are assured. That fact proves that the carbon layer restoration technology improves the n parameter for certain.

6.Conclusion

Hermetically carbon layer restoration technology has been developed using a thermal chemical vapor deposition with a CO_2 laser as a local heat source. Using this technology, the fracture strength of 3kgf, and the fatigue parameter n of 94 with the estimated error of 15 in 95% confidence level have been realized.

The failure strength is comparably high, but the n-value is lower than the original CCF. Perhaps higher n-values can be obtained by thickening the restored carbon layer to the thickness of the original.

References

[1]N.YOSHIZAWA, H.TADA, Y.KATSUYAMA, J. Lightwave tech., vol 9 pp417-412, 1991

[2]K.OSAKA et al., "Fusion splicing characteristics of hermetically carbon coated fiber.", WeP6, ECOC, 1990.

[3] J.T.KRAUSE, C.R.KURKJIAN, Electronics letters, vol.21, pp533-535, 1985.

[4]ANSI/ASME PTC19.1-1985.



Isamu Fujita

Sumitomo Electric Industries, Ltd.

1, Taya-cho, Sakae-ku Yokohama, Japan

Isamu Fujita was born in 1965 and received his M.S. degree in mechanical engineering from Tokyo University in 1990. He joined Sumitomo Electric Industries the same year and has been engaged in research and development of fusion splicing technologies for optical fibers. He is a member of Japan Society of Mechanical Engineers.



Masahiro Hamada

Sumitomo Electric Industries, Ltd.

1,Taya-cho, Sakae-kuYokohama, Japan

Masahiro Hamada was born in 1962 and received his M.S. degree in electronic engineering from Shizuoka University in 1987. He joined Sumitomo Electric Industries the same year and has been engaged in research and development of fusion splicing technologies for optical fibers. He is a member of the Institute of Electronics, Information and Communication Engineering of Japan.



Haruhiko Aikawa

Sumitomo Electric Industries, Ltd.

1,Taya-cho, Sakae-kuYokohama, Japan

Haruhiko Aikawa was born in 1964 and received his M.S. degree in metallurgical engineering from Tofoku University in 1989. He joined Sumitomo Electric Industries the same year and has been engaged in research and development of optical fiber fabrication. He is a member of the Japan Institute of metals.

Katsuya Nagayama



Sumitomo Electric
Industries, Ltd.

1,Taya-cho,
Sakae-kuYokohama,
Japan

Katsuya Nagayama was born in 1963 and received his M.S. degree in mechanical engineering from Tokyo University in 1988. He joined Sumitomo Electric Industries the same year and has been engaged in research and development of drawing and coloring technologies for optical fibers.

Yasuo Asano



Sumitomo Electric
Industries, Ltd.

1,Taya-cho,
Sakae-kuYokohama,
Japan

Yasuo Asano received his B.S. degree in mechanical engineering from Waseda University in 1968. He joined Sumitomo Electric Industries in 1971, and has been engaged in development of jointing technologies for coaxial cables and optical fiber cables. He is now a manager of Optomechatronics System R&D Dept. Yokohama Research Labs. and a member of Japan Society of Mechanical Engineers and the Institute of Electronics, Information and Communication Engineering of Japan.

INTELLIGENT LID SYSTEMS IN THE MULTI-FIBER TECHNOLOGY

M. Loch, R. Kossat, G. Ruegenberg

Siemens AG
Munich, Germany

G. Boscher

RXS Schrumpftechnik-Garnituren GmbH
Hagen, Germany

ABSTRACT

The essential advantages of Light Injection and Detection (LID) Systems, which are prerequisite to reliable low loss splicing technique and highly accurate loss measurement of single-mode fibers, are transferred to multi-fiber/ribbon technology. In this paper we discuss in detail the main advantages of intelligent LID Systems and compare different techniques for the realization of fiber selective multi-fiber/ribbon LID Systems. The structure and technique of different systems are presented and discussed. Novel systems based on bend couplers have been developed and tested in the laboratory. Results of measurements are shown to illustrate the benefits of this technique. The optimum concept has been implemented in a new microprocessor controlled multi-fiber fusion splicer for single-mode fibers. Consequently, all established measuring and controlling procedures using intelligent single-fiber LID Systems are now applicable to the multi-fiber/ribbon structure in the same way.

INTRODUCTION

The increasing demand for information necessitates the extension of existing communication systems, re-arrangement of local distribution networks and subsequent requirement for many fiber optic cables. Cost and time expenditures can be minimized by utilizing a reliable and easy to operate splicing technique for single-fiber and multi-fiber/ribbon structures. Past and present single-mode fiber (SMF) splicing techniques have shown that splice loss is mainly predetermined by accurate core-to-core positioning of the fibers, preparation of the fiber end face, and the optimum selection of fiber-specific fusion parameters. The accurate determination of splice loss is also a very important element for reliable and prompt optical fiber splicing. Two different methods are commonly used to detect local splice loss when using fusion splicers. The "core monitoring" method uses the digitized video signal of the splice area to calculate the splice loss from the detected core offset and the tilt of the core axes[1,2]. However, differences between the assumptions necessary for the calculation, e.g. spot size, and the actual given conditions can lead to significant estimation errors. A more reliable concept to determine the splice loss and to control all above mentioned critical parameters is to use a LID System combined with the so-called "air gap method"[3]. Initially, LID Systems allow an automatic control of the fusion time: the power through the splice during fusion is monitored, and at the time of maximum transmission a microprocessor shuts off the fusion arc guaranteeing a minimum splice loss. This provides for optimum fusion time resulting in the lowest splice loss under prevailing conditions. Hence, this system automatically compensates for non-optimal fiber-specific splice parameters. Extensive examinations in the field show a significant reduction of the splice loss using this automatic control of the fusion process. Secondly, using the measured power levels P_b and P_a before and after the fusion process[4] the splice loss a_s can be determined as follows

$$a_s = 10 \log \frac{P_b}{P_a} + a_b \qquad (1)$$

Here a_b denotes the loss of the optimally aligned splice before fusing (air splice). Analysing the mutual end face tilt in a single-mode fiber air splice based on the physics of the Fabry-Perot resonator[5,6] the preparation of the fiber end faces is controlled, guaranteeing a highly accurate splice loss measurement. In[2] the transmission properties of a single-mode fiber air splice caused by Fresnel reflections and fiber alignment errors are investigated comprehensively. Particularly analyzed is the influence of end face angles on splice loss and measurement error of the "air gap method". The oscillation amplitude of the loss of a single-mode fiber air splice, which is observed while moving the fiber ends in an axial direction, is directly related to an effective tilt angle of the fiber end faces. Using this method for automatically evaluating the end face quality of the fibers to be spliced, which is implemented in modern fusion splicers provided with LID Systems, a maximum error of splice loss measurement of +/- 0.05 dB is guaranteed, rejecting unsatisfactorily prepared fiber end faces. Additionally, because of the measuring possibilities, the LID System also allows the determination of optimum parameters without any additional measuring device.

Consequently, when using the LID System, the automatic end face check and the controlled fusion process make fusion splicing easy and less operator intensive resulting in low splice losses and highly accurate splice loss measurement. This system is available and has been successfully applied in the long distance communication system to reduce splice loss in the single-fiber technology. However, until now, no equivalent system has been developed for the simultaneous joining of several fibers or ribbons.

This paper investigates the fundamental advantages of single-fiber LID Systems to multi-fiber/ribbon technology. Different concepts utilizing different transmitters and different operating wavelengths are explored. A new method is described for optimum implementation of the multi-fiber LID System into a microprocessor controlled multi-fiber/ribbon fusion splicer.

FUNDAMENTALS

An effective intelligent multi-fiber LID System allows a local fiber-selective measurement of transmission in a multi-fiber structure; that is, the transmitted light of each fiber can be detected independently of the transmission properties of the other fibers. In principle, there are two different fundamental procedures to solve this problem: fiber-selective coupling of light and fiber-selective detecting of transmitted light. For both concepts different techniques are conceivable.

There are three different techniques for fiber-selective, quasi simultaneous coupling of light in one or more fibers within a multi-fiber structure:
First, to launch light into the fibers of a multi-fiber structure, separate sources which emit different modulated signals can be used. Practically, the number of separate light sources should correspond to the number of fibers.
Secondly, the light spot of a single source is moved in the plane of the multi-fiber structure orthogonally to the fiber axes to launch light in each fiber successively. This can be done by a relative movement of the light spot in relation to the multi-fiber structure. To realize this, a movable mirror to deflect the focused beam, e.g. a rotating multifaced polygon of a galvanometer scanner, is applicable.
Finally, the light source is designed to launch light into all fibers simultaneously, however a moving slit, which allows only a small light beam to pass through, acts as the fiber-selective element.
For the application of all these different coupling techniques within a multi-fiber LID System one large area photodiode is sufficient for the detection of the transmitted light of all fibers. Using a suitable evaluation method the separation of the detected light for each fiber within the multi-fiber structure is possible. This is especially true with time-division multiplexing, as the system automatically identifies each fiber by analyzing the detected signal. This allows recognition of the actual position of each fiber within the multi-fiber struture.

For the fiber-selective detecting of transmitted light, which is coupled simultaneously in a multi-fiber structure using only one light source, a high number of photosensitive elements is necessary. To get a high local resolution the number of photosensitive elements should be much higher than the number of separate fibers. The transmitter identifies the number of fibers automatically and is insensitive to the actual fiber position within the multi-fiber structure. Practically, this requirement can be realized by using a photodiode array or a line scan sensor.

PRACTICAL REALIZATION

Two different techniques based on LID Systems for local transmission measurement on fiber ribbons were realized and tested in the laboratory. The setup is designed for 1 to 12 fibers or 2- to 12-fiber ribbons. The first system works with a fiber-selective receiver. The experimental setup shown schematically in Fig. 1 was used. The light of a laser diode (output power: 30 mW) operating at the wavelength of 780 nm is launched on the left side of the ribbon under test. To launch light into all individual fibers within the multi-fiber structure simultaneously, the light passes through a special optical system obtaining cylindrical elements to form a suitable light spot. The signals propagate through the object to be measured - an air gap splice - and are detected on the opposite side. A second optical system adapted to the ribbon structure images the transmitted signals of all fibers to a self-scanning photodiode array (line scanner) consisting of 256 separate photosensitive elements. Each photosensitive element is associated with a storage capacitor on which the photocurrent is integrated. With a built-in multiplex switch for periodic readout via an integrated shift register scanning circuit and an external A/D converter, the voltage values for each capacitor are transmitted to the microprocessor for calculating the detected relative power level of each fiber.

A 4-fiber ribbon with differently colored fibers was used as a test ribbon. The measured intensity distribution (Fig. 2) shows a very good separation of the fibers. The distance of adjoining distribution peaks is about 1.35 mm corresponding to a distance of fiber axes of 260 µm at the given optical magnification of 5.2.

The second system is designed for a fiber-selective transmitter with an operating-wavelength of 1310 nm. The correspondent setup is shown in Fig. 3. As selective light source a laser scanner is used. A pre-objective scanning system, which is characterized by a flat image plane, is used. The parallel beam of the laser diode (output power 25 mW) is deflected by a movable mirror performing as a galvanometer scanner. The following scan lense

is designed for sufficient light for up to 12 single-mode fibers. However, pre-objective scanning results in high requirements for the scan lens. The dimension of the scanning spot and the intensity distribution within the spot is shown in Fig. 4 for one fiber in the middle and one fiber at the edge of the multi-fiber structure, and in each case for two positions of the image plane (scan line) to demonstrate the depth of the focus. Scanning the multi-fiber structure orthogonally to the fiber axes, light is launched into each fiber separately. The signals pass through the air gap splice under test and are detected by the bend coupler based receiver using a simple optical system and a large area InGaAs photodiode. The output of the photodiode triggered with the position of the scanning unit is shown in Fig. 5. As ribbon for testing we used a generally available 10-fiber ribbon. The separate signals of 10 single-mode fibers are visible. The different heights of the peaks are caused by different color coatings of the fibers within the ribbon.

APPLICATION

Fig. 6 compares the two presented multi-fiber LID Systems with regard to the application in a multi-fiber fusion splicer. Both systems allow automatic control of the fusion time to optimize the fusion process. In addition, the multi-fiber LID System at 1310 nm enables splice loss measurement at the operation wavelength of the fibers to be spliced according to equation (1). As known, the matched wavelength is prerequisite for high-precision loss measurement since there is no strict relationship between the losses at different wavelengths. Therefore a multi-fiber LID System based on a fiber-selective transmitter corresponding to Fig. 3 has been integrated into a microprocessor controlled multi-fiber fusion splicer, which allows the transversal alignment of the fiber ribbon.

Since there is no need to monitor the power through all single-fiber splices within a multi-fiber splice simultaneously during the fusion process, it is necessary to make an efficient selection. For this we have chosen the digitized video signal of the optimal x, y, z-aligned air splice of the multi-fiber structure to control the parameters decisive to low splice loss, e.g. transversal disalignment, preparation of fiber end face and air gap. To optimize the alignment of the multi-fiber structure before fusion there are different algorithm, e.g. minimizing the maximal loss within the multi-fiber structure. Analyzing the information of the video signal, we select the fibers with the highest loss before fusing. Conscious that the fusion parameters are not as critical for well aligned single-fibers as they are for badly aligned fibers, we restrict the monitoring of the fusion process to these disaligned fibers. This leads to the lowest splice loss of these fibers under prevailing conditions without significant changes in the loss of the well aligned fibers of the multi-fiber/ribbon structure. In Fig. 7, the relative transmitted power through one single-fiber splice within a 10-fiber ribbon is shown. The optimal fusion time t_s is marked. At this time the microprocessor shuts off the fusion arc as indicated by a slight decrease of the transmitted signal which is caused by the cooling of the glass.

CONCLUSION

Different solutions for local fiber-selective coupling and detecting of transmitted light in the multi-fiber/ribbon structure are available. A multi-fiber LID System consisting of a bend coupler based transmitter and receiver operating at 1310 nm has been developed. The system is designed for up to 16 individual fibers or 2 to 16 fiber ribbons controlling the transmitted light of each fiber separately. It works independent of the actual fiber numbers. This novel system has been incorporated in a new microprocessor controlled and piezo driven multi-fiber fusion splicer for single-mode fibers, and the mode of operation and the benefits of the intelligent systems have been verified experimentally. Thus, the fundamental advantages of single-fiber LID Systems could be transferred to the multi-fiber/ribbon technology. Optimization of fusion process by automatic control of fusion time guarantees the optimum multi-fiber/ribbon splice under the prevailing conditions. Consequently, a more accurate splice loss measurement is possible. By this, the reliability and the handling of multi-fiber splicing technique are improved by reducing the repetition rate and the average splice loss.

ACKNOWLEDGMENT

We would like to express our sincere gratitude and appreciation to Prof. Dr. Lieber for the valuable advice, input, and guidance provided.

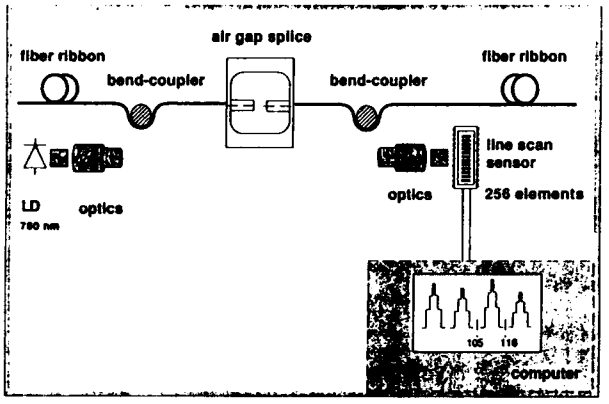


Fig. 1: Multi-fiber LID System for 1 to 12 fibers/ 2- to 12-fiber ribbons; fiber-selective receiver; operating wavelength 780 nm

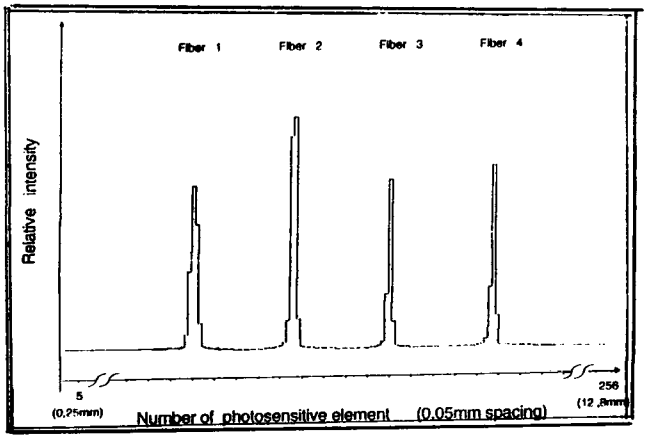


Fig. 2: Measured intensity distribution using fiber-selective receiver; integration time: 45 msec; ribbon under test: four fiber ribbon with different colored single-mode fibers

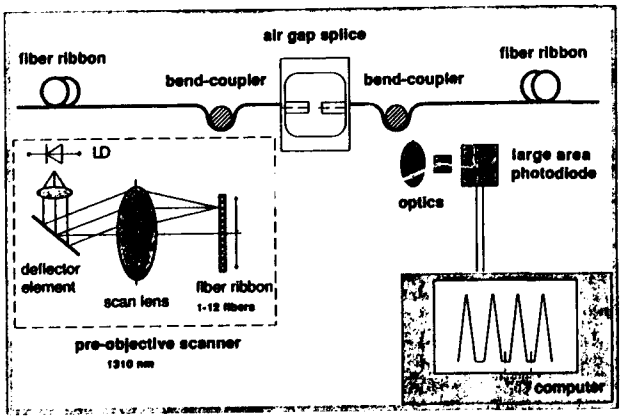


Fig. 3: Multi-fiber LID System for 1 to 12 fibers/2- to 12-fiber ribbons; fiber-selective transmitter using pre-objective scanning; operating wavelength: 1310 nm

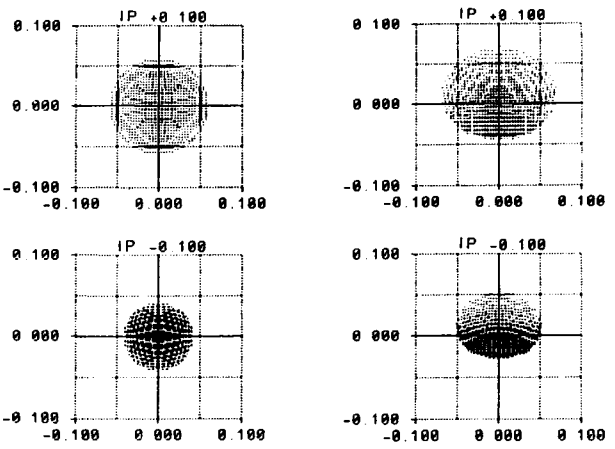


Fig. 4: Intensity distribution within the focused beam before (IP = + 0,100 mm) and behind (IP = - 0.100 mm) the image plane (IP); all dimensions in mm; a) in the middle of the scanning range; b) at the edge of the scanning range

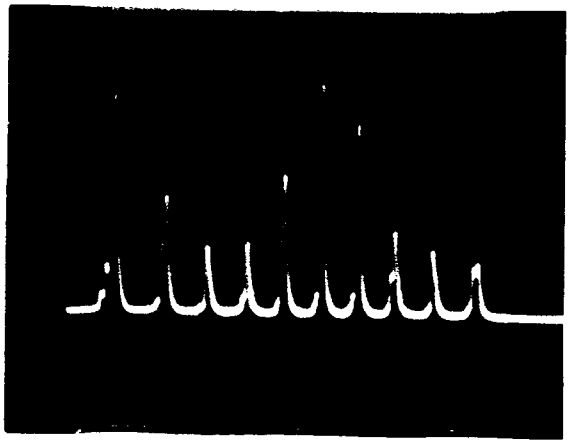


Fig. 5: Detected signals using fiber-selective transmitter; ribbon under test: 10 fiber ribbon

	Fiber-selective receiver	Fiber-selective transmitter
Fiber selection technique:	photodiode array for selective detection of light	scanning system for selective coupling of light
Operation wavelength:	780 nm	1310 nm
Light spot:	simultaneous illumination of all fibers	separate illumination of all individual fibers
Coupling efficiency of transmitter:	↓ bad	↓ good
Automatic control of fusion time:	yes	yes
Loss measurement:	probably not	yes

Fig. 6: Comparison of different techniques of multi-fiber LID Systems

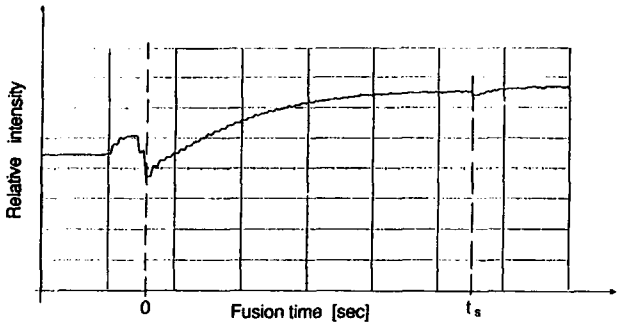


Fig. 7: Automatic control of fusion time: transmitted power versus time for a single-fiber within the 10-fiber ribbon; the fusion splicer automatically shuts off the fusion arc at the time t_s



Manfred Loch received his diploma degree and Ph.D. degree in electrical engineering from the University of Kaiserslautern, Germany in 1983 and 1989 respectively. He was concerned with refractive-index profile measurements and characteristics of birefringent fibers. Since 1989 he has been employed at Siemens AG, Munich, Germany. He is responsible for the development of fusion splicing equipment and optical measurement systems.

REFERENCES

/1/ T. Halbara, M. Matsumoto, T. Tanifuji, M. Tokuda: Monitoring method for axis alignment of single-mode optical fiber and splice-loss estimation. Optics Letters, Vol. 8, No. 4, April 1983, pp. 235-237

/2/ C. M. De Blok and P. Matthijsse: Core alignment procedure for single-mode-fibre jointing. Electron Lett., Vol. 20, Feb. 1984, pp. 109-110

/3/ T. Eder, W. Lieber, M. Heier: Evaluation of fiber end face tilts during automatic fusion splicing of single-mode fibers. Proceedings of 37th IWCS, Nov. 1988, pp. 407-411

/4/ T. Eder, R. Engel: Einmodenspleiße automatisch messen und herstellen. Nachrichtentechnische Zeitschrift, Vol. 41, No. 4, April 1988, pp. 230-233

/5/ T. Eder: Messung und Analyse der Resonatoreigenschaften von Einmodenfaserverbindungen zur Abschätzung und Reduzierung der Dämpfung thermischer Spleiße. Fortschrittsberichte VDI Verlag, Reihe 21, No. 54, 1989

/6/ R. Wagner, C. Sandahl: Interference effects in optical fiber connections. Applied Optics, Vol. 21, No. 8, April 1982 pp. 1381-1385



Rainer Kossat received his diploma in electrical engineering from the Fachhochschule in Munich in 1984. For a period of two years he was employed at the Department of Telecommunications at the Fachhochschule in Munich. Starting in 1986, he worked at Siemens AG on the design of fiber optic test equipment and optical CATV systems. Since 1991 he has been concerned with the development of fusion splicing equipment.



Gervin Ruegenberg studied electrical engineering at the University of Kaiserslautern, Germany. In 1984 he joined Siemens AG and worked on the development of optical transmitters and receivers. Since 1988 he has been working on the development of fusion splicers. He is responsible for electronics and software of fusion splicers and optical measurement systems.



Georg Boscher received his diploma degree in physics from the University of Munich, Germany in 1967. He joined Siemens AG and worked for several departments. In 1970 he became responsible for the development and testing of accessories in the Telecommunications Cable Division. Since 1985 he has been working as a deputy director and head of Marketing and Management of RXS Schrumpftechnik-Garnituren GmbH, a fully-owned subsidiary of Siemens AG. RXS manufactures and markets accessories for the telecommunications and power industries.

DEVELOPMENT OF FULL AUTOMATIC FUSION SPLICER

THE FURUKAWA ELECTRIC CO., LTD

Yuji Sugiyama Seiryo Mishima Yutaka Sanshige

< Summary >

We have completed a full automatic fusion splicer for splicing and reinforcing both SM 8 and 4-fiber ribbons. The performance measures up to a splice loss of 0.05 dB or less, tact time 3 min. or less, and yield of 90% or more.

1. Introduction

With optical fiber ribbons multiplied in a single cable for subscriber networks, a staggering length of time has been required of the splicing work.

Even though there has been existent a fiber fusion splicer[1] for a 4-fiber ribbon or 8 fiber ribbon, which was commercialized, no full automated fusion splicer is yet available for sequential processes starting with stripping of coating from the surface of fiber ribbon, and cleaving fibers, and reinforcing fused fibers. More specifically, stripping of coated material and cleaving of fiber ribbon, are still made manually, depend on of the operators who are required to have considerable proficiency. In order o lay down the solution for the incovenience as explained, we have completed full automatic fusion splicer in collaboration with Nippon Telegraph & Telephone Corporation.

Hereafter, we are reporting on the machine developed as being in the vanguard of the world, which can greatly facilitate fusion sp' ,g work, producing remarkable efficiency and unloading most troublesome work on the operators.

2. Abstract of Equipment

2.1 Appearance, Outline

This equipment is comprised of two components: a main body and a controller which are connected to each other with a control cable. All the splicing works are done on the main body with primary functions. The controller merely maintains a TV monitor and switches to output conditions of a splicing process.

The manual opeations include setting an optical fiber ribbon in a fiber supply cassette, setting a reinforcing material in a reinforcing material casset, and switching work and cleaning work according to instructions shown in the TV monitor. All the other operations are performed automatically. Shown in Figure 1 is the outlook of this equipment, while the dimensions and weight are given in Table 1.



Fig.1 Outlook of machine

Table 1 Physical specifications

Size (mm)	Main body	260W × 230D × 350H
	Controller	198W × 294D × 156H
Weight (kg)	Main body	18.0
	Controller	4.2

2.2 System and component

As shown in Figure 2, the equipment is comprised of the following.

1) Fiber supply cassette
2) Fiber feed assembly
3) Fiber holder
4) Stripping assembly
5) Cleaving assembly
6) Fusion assmbly
7) Handling assembly
8) Reinforcing assembly

The above compoents are assembled into equipment as shown in Figure 3.

Functions and applications of each assembly are shown in Table 2.

Table 2 Functions and applications of each assembly

Assembly	Functions and applications
Fiber supply cassette	To raise a following fiber To lead a fiber to fiber feed assembly
Fiber feed assembly	To lead a fiber to holder To detect an existent or nonexistent of fiber
Fiber holder	To hold a fiber ribbon Tensing aid in stripping coated material Tensile test after splice Positioning for stripping, cleaving, insertion into V-groove To set ends, stuffing aid at discharging
Stripping assembly	To unfold and fold stripping blade Removal of fiber
Cleaving assembly	To hold a bare fiber To move a blade, to apply tending tension to a fiber
Fusion assembly	Switching positions for stripping and fusion Forcusing a fiber To set and release fiber holder in V-groove Discharging arc for fusion splicing Discharging arc for cleaning
Handling assembly	Transferring aid from fusion assembly to reinforcing assembly, releasing after splicing
Reinforcing assembly	To supply reinforcing material from cassette To hold the upper reinforcing material (alloy plate side) To hold the lower reinforcing material (glass plate side) To detect existence or nonexistence of reinforcing material

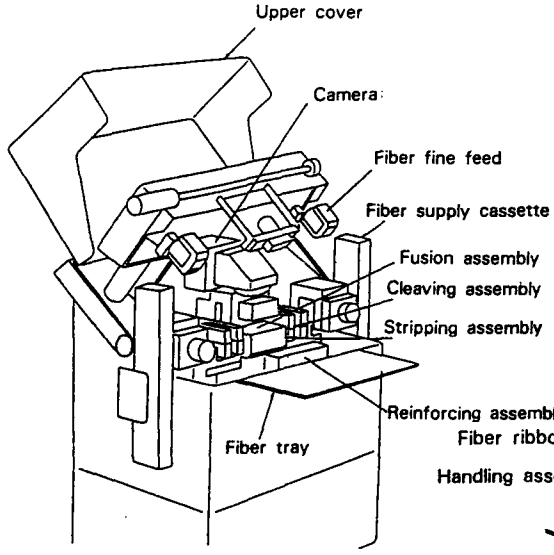


Fig. 2 Discription of main body

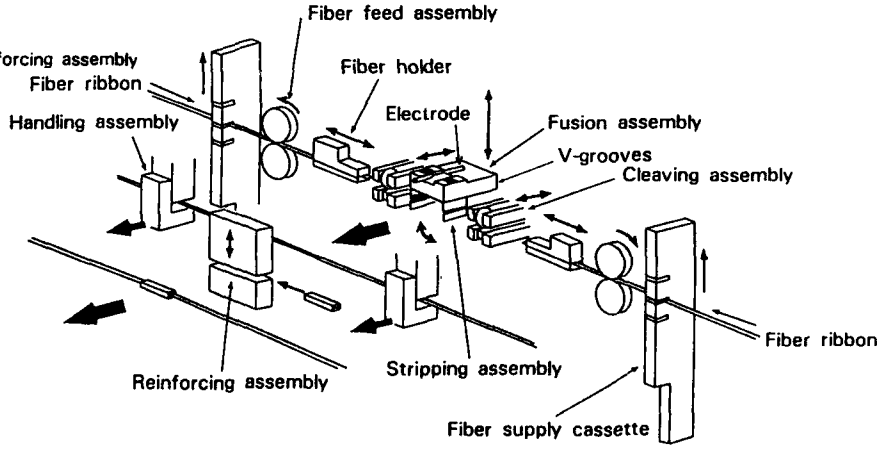


Fig. 3
Configuration of functional assemblies of S101 fusion splicer

2.3 Splicing Process

We are explaining about the operation process of this equipment, while showing the operation flowchart in Figure 6.

First and foremost, a fiber ribbon is set in a fiber cassette. At this moment, if the fiber cassette is set on a fiber setting stand, and the fiber ribbon is fixed, an optimum fiber length is prepared the insertion into a main body. And 12 fiber ribbons can be installed at the maximum.

Second, reinforcing material for a fused fiber is set in a reinforcing material cassette, which can house 12 sets in full.

With a fiber cassette and a reinforcing material cassette set in a main boby, when pressing a start button, automatically spliced and reinforced fibers begin to come out in sequence. In addition, the discharge arc test mode as an examination of strength is selectable for measuring an amount of fused lengh. Figure 4 shows fiber setting stands, and appearing in Figure 5 is reinforcing material set for the processing.

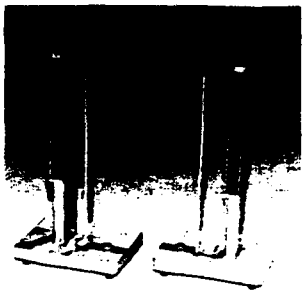


Fig. 4 Setting stand



Fig. 5 Setting reinf. material

Hereafter, explained stage-by-stage are the automatic processes available on the splicing machine.

1) Fiber supply process

A fiber ribbon housed in a fiber supply cassette is led onto fiber holder by fiber supply rollers. Then, fiber holder cramp a fiber ribbon, which, thereafter, is supplied to stripping assembly where a coating length to be stripped is fixed.

2) Fiber stripping process

After a fiber ribbon inserted into stripping assembly is heated by a heater and cramped by stripping blades, the coated material is peeled off with fiber holder drawn back.

3) Fiber cleaving process

When bare fiber holder on cleaving assmbly between fiber holder and stripping assembly, fold to cramp a fiber, and cleaving blades advance to notch the surface, the fiber is instantly cleaved in to mirror surface by bending stress on opposite side of the notch.

4) Coating dust removing process

Coating dust remaining inside stripping assembly is swept out by a cleaning brush and gathered in a dust box.

5) Cleaning discharge process

After finishing fiber ends, remaining dust of coating is cleaned from a fiber ribbon by arc discharging with cleaning electrodes of both sides of a V-groove at the same time of procsss of advancing to the position into V-groove.

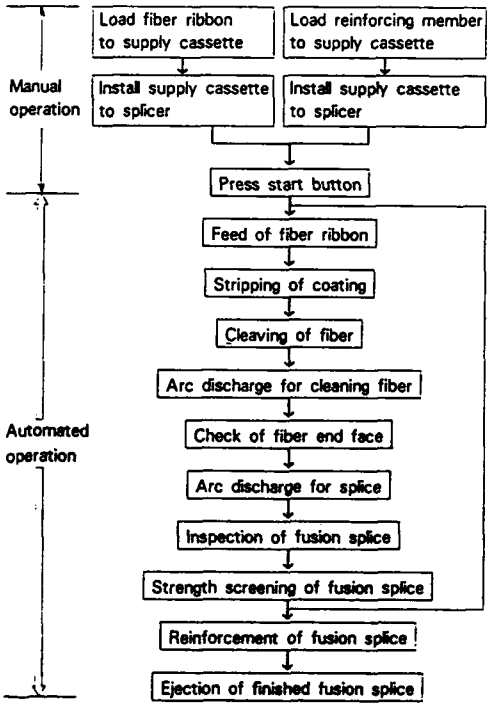


Fig. 6 Flowchart showing operation

6) Fiber-axis aligning process

A fiber placed in a camera sight is axialy adjusted and V-groove is raised. Then, the fiber is inserted into the V-groove and fixed.

7) Setting gap between fiber ends process

Both fibers are moved to the middle area in a camera sight and adequate gap is set.

8) Inspection and fusion process

Axial misalighnment between counterpart fibers is delermined, and gap between fi ber ends and cleaved condition of an end surface are examined. Accordingly, passable fibers are spliced under arc fusion discharging. Faulty fiber are returned to supply process for a retrial.

9) Testing process of fused part

A spliced fiber is tested for the fused condition. Unpassable fibers are returned to supply process, after cutting away with discharge.

10) Screening process

After testing spliced part, to which 200g of tension is applied, unpassable fibersr-are returned to supply process for a retial.

11) Handling process, Heat-rein forcement process.

After splicing, handling assembly hold and carry the fiber ribbon to reinforing assembly. Then, heat-reinforcement is ready to start. On the instant that handling assembly hold the fiber ribbon, the paired reinforcing materials are separated into the upper material (alloy side) and the lower material (glass ceramics side).

12) Fiber ejecting process

After heating, spliced and reinforced fiprocesses. Also, as often as a handling process ends, the following fiber ribbon is sequentially set for splicing. In this case, the fiber supply cassette is raised by one slot, and splicing work is started.

2.4 Monitor Display

2.4.1 Indication Pattern

Even though this splicing machine is fairly complicated when an fault occurs somplace, exact and adequate information must be timely prepared for searching out trouble and a recovery. Otherwise, the automated device could be unable to work at length. Against this background, and from the stand point of operators, instructions for switching operation, cleaning points, and precise breakdown of process are arranged on a TV monitor as shown in Figure 7, providing for easy handling about operation, maintenance, etc..

On the uppermost stage, appearing are a type of error (ex, axial misalignment), an identification number of cleaning point, which is shown on the main boby.

On the middle stage, appearing are items of operation, selector buttons (ex, splicing/arc discharge test mode, applicable fiber mode), a cleaning method/point, and brief description.

The lower three stages indicate a type of processing on fusion section, and a type of processing on reinforcement area, and a fiber mode and time of arc discharge in literal order.

Figure 8 shows some tangibility. This indicationtion refers to a fault that the

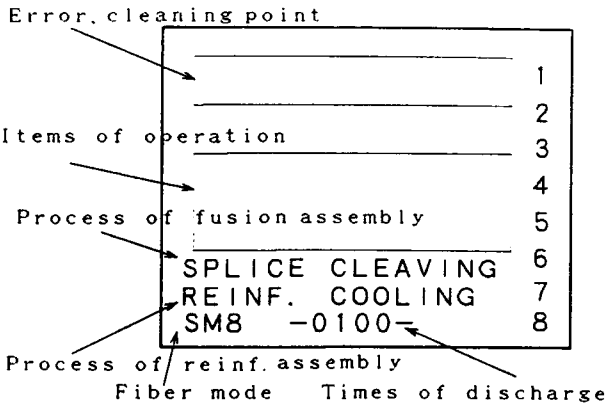


Fig. 7 TV monitor

◆CLEANING ③④⑤⑥◆
Cleaning up
Stripping, cleaving
Retry
Fusion-reset-button
SPLICE RIGHT
REINF. RETURN

Fig.8 Example for T.V indication

fiber ends of right-side fibers have been processed unfavorably. By showing identification numbers of cleaning points on the uppermost stage, an operator is required to clean the right-side cleaving and stripping assembly. After cleaning, fustion reset-button is pressed to restart a shown in the monitor.

2.4.2 Indication System

The configuration of indication as previously described was realized by the application of event-dribble type multi-task operating system to the CPU. This system enables independent operations of controling each assembly, indication, key board, etc.. That being, fusion area and reinforcement area become inde pendent in control. And, a faulty assembly can only be shut down unless any effect extends from the defect, and the other assemblies continue operation. Accordingly, an operator learns about faults from the indication and cope with them according to recovery procedures shown. Then, even if faults would be coincidental, the events are shown one by one, including recovery procedures.

This arises from the ingenious application of cue-entry type FIFO baffer and Cemalfor control, which has often been taken up in the discussion of multi-task O.S.. In reality, a controller has only five switches, which, in turn, would functionaly vary with a type of task working then. So we have several contrivances at the softw-are.

2.5 Reinforcing Procedures

On this splicing machine, sandwiching reinforcement method is applied, by which a fiber ribbon is sandwiched between reinforcing plates, unlike sleeves of thermal shrink. As shown start as shown in the monitor.

in Figurre 9, reinforcing material is comprised of the upper and lower plates. The upper plate is an alloy of Invar, and the lower plate is glass ceramics. A hot-melt

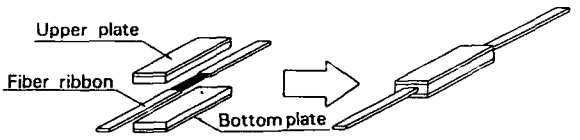


Fig. 9 Reinforcing member

adhesive is coated on one side of both plates.

When a fiber ribbon is sandwiched between reinforcing plates, the Invar alloy is high-frequency heated to melt coated adhesive inside the sandwich.

The applied procedures can greatly facilitate automatic feeding of a reinforcing material by contrast with a feeding system of sleeves. Moreover, high-frequenc heating shortens a length of proccessing duration.

3. Performance

3.1 Characteristics of Splice

Figure 10-1 and 10-2 show splice loss of fiber ribbon with 8 fibers and 4 fibers respectively.

Yields exceed 90% in either case of SM 8 fibers and SM 4 fibers. Faults proceed from stripping process by 50% cleaving process by 30%, axial misalignment by 10%, and other miscellaneous process (supply, handling, reinforcement, etc.) by some 10%. When it comes to consumables such as acti-

ve parts, a clea-ing blade endures at least 300 times of breaking for one position (at least 12 points are available along a blade: which endures at least a total of 3600 time): similarly, a strippng blade and a discharging electrode have at least lifespans of 10000 times and 1000 times respectively. In addition, the lifespans of consumables were determined by means of SM 8-fiber ribbon.

Incidentally, a set of discharge electrodes is made up of fusion splicing and cleaning ones, which are unitized and replaceable together. Table 3 shows the characteristics regarding the performance explained before.

3.2 Operating Time

The splicing machine completes the cycle of processes in about four minutes. As shown in Figure 6, in reality, a following splice work overlaps a preceding reinforcement work, then a net time required for one splice is less than 3 minutes in real terms.

This machine is equipped with two sets

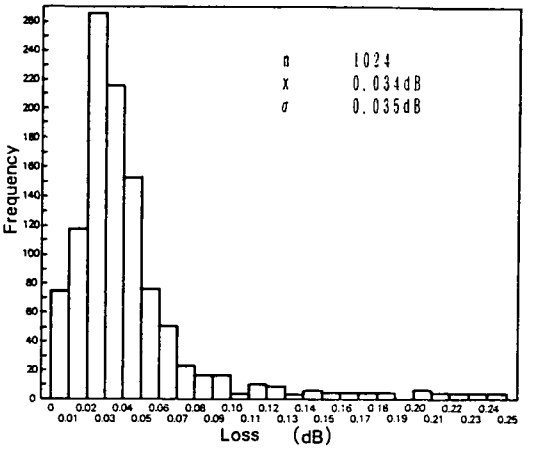


Fig. 10-1
Histogram of splice loss for SM8 fiber ribbon by S101 fusion splicer

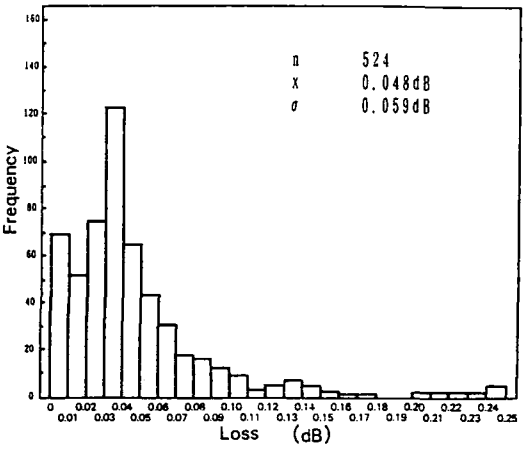


Fig. 10-2
Histogram of splice loss for SM4 fiber ribbon by S101 fusion splicer

Table 3 Performance

Items	SM8	SM4
Average splice loss (dB)	0.034	0.048
Standard deviation (dB)	0.035	0.059
Yield (%)	93.3	92.9
Cleaving life-span (times)	300 or more	—
Stripping life-span (times)	10000 or more	—
Electrode life-span (times)	1000 or more	—

Table 5 Characteristics of reinforced splice

Test items	Loss change (dB)
High temperature (80 ° C)	0.01 or less
Low temperature (-40° C)	0.07 or less
Damp heat (60 ° C, 95%RH)	0.02 or less
Heat-cycle (-30～60° C)	0.01 or less

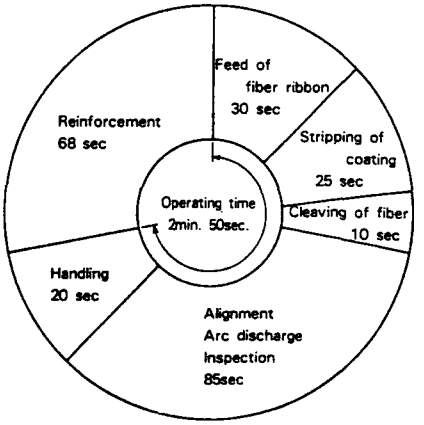


Fig. 11
Operating time of S101 fusion splicer

each of fiber cassette and reinforcing material
cassette. Therefore, it is practicable to preset following fiber ribbons for smooth operation. By extension, it can be done simultaneously that a spliced fiber ribbon is put in a closure, and following ribbons are preset during splice work ongoing in the main body. As the case stands, the new system curtails operating time greatly in comparison with conventional splicing machines. By way of trial, jointing work for a 800-fiber cable comprising SM 8-fiber ribbons was simulated, taking one day until the completion of splicing and housing works. Figure 11 shows Operating cycle time of fusion splice

3.3 Environmental Characteristics of Reinforcement

As shown in Table 5, the environmental characteristics of reinforcement is on a par level with what proceeds from sleeve reinforcement of thermal shrink, in a high /low temperature test, damp heat test, and heat cycle test.

4 Summary

We have completed a full automatic fusion splicer for splicing and reinforcing both SM 8 and 4-fiber ribbons. The performance measures up to a splice loss of 0.05 dB or less, tact time 3 min. or less, and yield of 90% or more.

We would like to conclude by thanking the staff at NTT Network Systems Development Center for their invaluable advices.

5. References

1) Y. Kato et al.:
"Single-mode Optical Fiber Ribbon Splicer"
Proceedings of IWCS, P386-390, (1987).
2) M. Matsumoto, T. Haibara and M. Kawase:
"Fully automatic mass-fusion splicer for singlemode optical fiber ribbon"
Proceedings of IWCS, P225-231, (1989).

Yuji SUGIYAMA

The Furukawa Electric
Co., Ltd.
6 Yawata-Kaigandori,
Ichihara, Chiba, 290
Japan



He was born in Mie, Japan, in 1961.
He received the B.E. degree in mechanical engineering from Waseda University in 1984.
He joined The Furukawa Electric Co., Ltd. in 1984.
He has been engaged in research and development of optical fiber splice technologies.

Seiryo MISHIMA

The Furukawa Electric
Co., Ltd.
6 Yawata-Kaigandori,
Ichihara, Chiba, 290
Japan



He was born in Kagoshima, Japan, in 1963. He received mechanical engineering from Narita College of aviation in 1983. He joined The Furukawa Electric Co., Ltd. in 1988.
He has been engaged in research and development of optical fiber splice technologies.

Yutaka SANSHIGE

The Furukawa Electric
Co., Ltd.
6 Yawata-Kaigandori,
Ichihara, Chiba, 290
Japan



He was born in Hiroshima, Japan, in 1965.
He received the B.E. degree in information engineering from Osaka Electro-Communication University in 1989. He joined The Furukawa Electric Co., Ltd. in 1989.
He has been engaged in research and development of optical fiber splice technologies.

Development of Compact Fusion Splicer for 4-Fiber Ribbon and Single Fiber

K.Ohzawa S.Toyoshige H.Taya I.Suzuki M.Yoshinuma

Fujikura Ltd.

ABSTRACT

This paper presents development of compact discharge fusion splicer for 4-fiber ribbon and single fiber. Recently, the demand of compact fusion splicer for emergency repair etc. is increased and the demand of fiber ribbon is also increased. Accordingly, we undertook development of the compact fusion splicer for fiber ribbon. This splicer is compact size and easy to carry compared with existent mass-fusion splicer. In order to obtain good splice result, the existent mass-fusion splicer's splice technology is applied to this splicer. This splicer's power supply is an internal NiCd battery which can be recharged. We spliced 4-fiber ribbon and single fiber by this splicer and good result has been obtained.

1. INTRODUCTION

Utilization of discharge fusion splicer is increased with diffusion of optical fiber. Since fusion splicer is used in various situations, many kind of splicers (for example, mass-fusion splicer, polarization maintaining optical fiber splicer, etc.) have been developed.

Recently, demand of optical fiber is increased, so it has been important how to construct many optical fiber cables efficiently and how to splice many optical fibers efficiently. Then, fiber ribbon has been diffused and demand of mass-fusion splicer is also increased with diffusion of fiber ribbon. Moreover, demand of compact fusion splicer for emergency repair for optical cables or splicing fibers in the buildings (for LAN etc.) is increased. A few compact fusion splicers for single fiber have already existed, but existent mass-fusion splicers are large size and high-cost because of their complicated fiber-monitoring system which can estimates splicing point. Accordingly, we have developed the compact fusion splicer for fiber ribbon.

On the occasion of development of this splicer, we took following things into consideration.

1 Small Size (easy to carry)
2 Light weight
3 Simple Design (easy to operation)
4 Low-cost
5 Low Splice Loss

2. Feature of the Compact Fusion Splicer

Figure 2-1 shows an appearance of compact fusion splicer. This splicer is attempted to be smaller, lighter and lower-cost compared with the existent mass-fusion splicer. Table 2-1 shows the size and weight of this compact splicer.

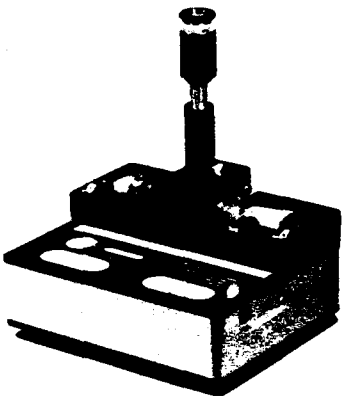


Figure 2-1 Appearance of Compact Fusion Splicer

SIZE	166×136×57 [mm] (except microscope)
WEIGHT	about 2kg

Table 2-1 The Size and Weight of This Splicer

This splicer's power supply is an internal NiCd battery. When the battery voltage becomes low, the splicer indicates "low battery" by lighting a LED. A battery charge circuit is also built in the splicer, and the battery can be charged by connecting AC/DC converter to the splicer. The internal battery can be charged for about 1 hour. We confirmed that 4-fiber ribbon could be spliced about 80 times per one charge, and single fiber could be spliced about 120 times.

This splicer has following optional parts. The fiber image can be observed with the optional CCD camera and monitor. The optional tube heater for the heat shrinking tube, which reinforces splicing point, and battery for the tube heater can be combined with the splicer.

Figure 2-2 shows a flow chart for a brief operation of this splicer. Cleaved fibers to be spliced are set on the splicer. We can observe the fiber ends by a microscope. There is a few graduations in the microscope. The fiber ends gap distance is set by manual operation with the microscope. After pushing the splice key on the splicer to start splicing, the fibers are fused by discharge heat and stuffed for constant distance automatically, and the fibers are spliced.

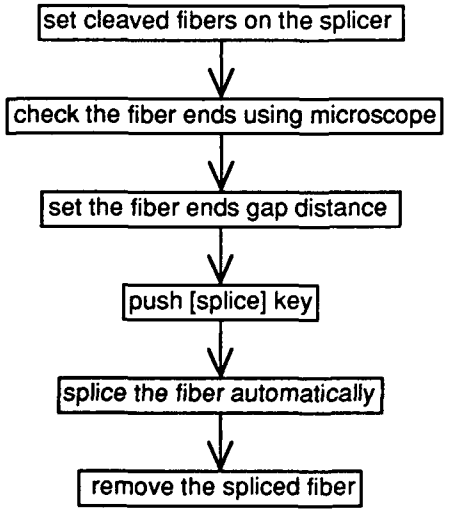


Figure 2-2 Flow Chart for Operation of This Splicer

3. PRINCIPLE OF SPLICING FIBER RIBBON

In order to obtain good splice result, the existent mass-fusion splicer's splice technology is applied to this compact fusion splicer.

The factor which affects splice loss very much is an axis offset between left and right fibers. Then, the both fibers to be spliced are set on each precisely machined V-grooves in the mass-fusion splicer[1]. (Refer to Figure 3-1.) However, small fiber axis offset remains even if the fibers are set on the V-groove. During the discharge heating for splice, surface tension is generated at the fiber surface, and the fiber axes are self-aligned due to this surface tension. In order to use this self-aligning due to this surface tension very much, the discharge heating is set to longer time in the mass-fusion splicer. This compact splicer also uses these methods.

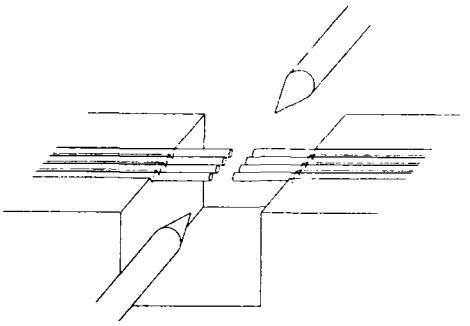


Figure 3-1 Setting Fiber ribbon on the Precisely Machined V-groove

When fiber ribbon is spliced by discharge heating, it is important to give uniform heat to each fibers of ribbon. If we dispose fiber ribbon as (A) in Figure 3-2, the out-side fibers are given stronger heat compared with in-side fibers. Then, there is an offset between the fiber ribbon level and the electrodes level as disposition (B) in the mass-fusion splicer[2][3]. In the disposition (B), the uniform discharge heat is obtained along the fiber row. The fiber ribbon set in this compact splicer is also disposed as (B).

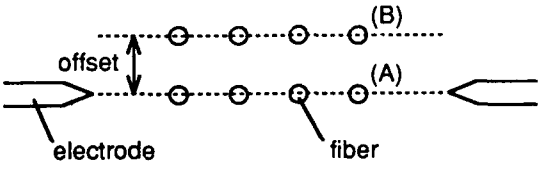


Figure 3-2 Position of Fibers between Electrodes

Usually, Horizontal distances between the electrode and fiber ribbon ((a) and (b) in Figure 3-3) are same in the existent mass-fusion splicer because the discharge heat distribution is symmetrical along the fiber row. But we have unsymmetrical discharge heat distribution in this compact fusion splicer. It can be conjectured that some material around the electrode affects to the discharge. To give an uniform heat to each fibers, we adjusted distance (a) and (b) adequately in this compact splicer.

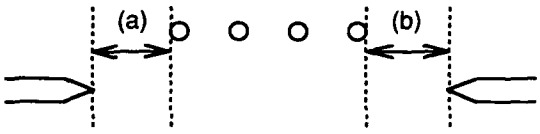


Figure 3-3 Horizontal Distances between Electrode and Fiber Ribbon

4. RESULT

Figure 4-1 shows single-mode (SM) 4-fiber ribbon splice loss at room temperature using this compact splicer. Figure 4-2 shows SM single fiber splice loss at room temperature. We obtained good result in both 4-fiber ribbon and single fiber. Figure 4-3 shows multi-mode (MM) single fiber splice loss at room temperature. We also obtained good result in splicing MM fibers.

Table 4-1 shows SM 4-fiber ribbon and SM single fiber splice loss result at high and low temperature (at 40 and 0 degrees centigrade). As shown in table 4-1, stable splice loss is obtained in spite of the temperature.

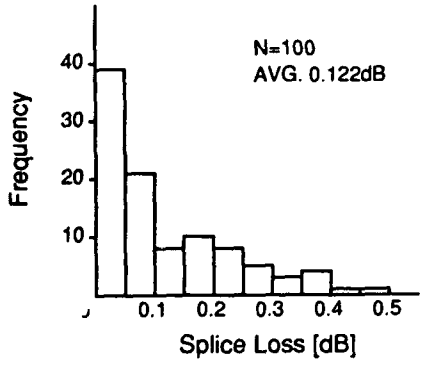


Figure 4-1 SM 4-Fiber Ribbon Splice Loss

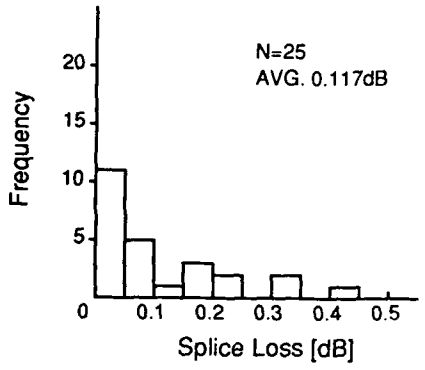


Figure 4-2 SM Single Fiber Splice Loss

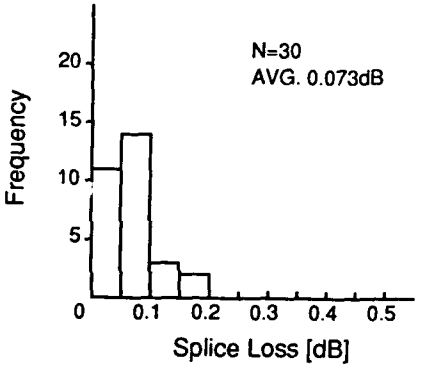


Figure 4-3 MM Single Fiber Splice Loss

	Temperature	N	Average Splice Loss
SM 4-Fiber Ribbon	0℃	40	0.135dB
	40℃	40	0.124dB
SM Single Fiber	0℃	10	0.144dB
	40℃	10	0.127dB

Table 4-1 Splice Loss at High and Low Temperature

Figure 4-4 shows SM 4-fiber ribbon splice loss with the frequency of splice from full-charged. The axis of ordinate shows an average splice loss of 4-fiber ribbon, and the axis of abscissa shows the frequency of splice from full-charged. As shown in Figure 4-4, stable splice loss can be obtained until about 90 times. Over 90 times, splice loss rises rapidly and we cannot obtain good splice. It can be conjectured that this rise of splice loss is caused by decrease of discharge power with drop of battery voltage. In this splice test, the splicer indicated "low battery" at 82 times. We can obtain good splice loss at least 80 times from full-charged.

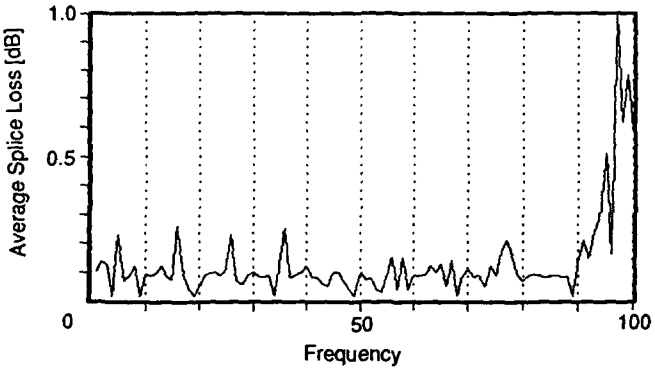


Figure 4-4 SM 4-Fiber Ribbon Splice Loss with the Frequency of Splice from Full-Charged

5. CONCLUSION

We developed compact fusion splicer for 4-fiber ribbon and single fiber. We spliced 4-fiber ribbon and single fiber using this compact splicer, and we obtained good result in various situation. We confirmed that this splicer was fully useful for emergency repair etc.

REFERENCES

(1) Y.Kato, A.Ishikura, T.Sano and S.Takashima, "Single-Mode Optical Fiber Ribbon Splicer", International Wire & Cable Symposium Proceedings, p.386-391, 1987

(2) M.Tachikura, "Fusion mass-splicings for optical fibers using electric discharges between two pairs of electrodes", APPLIED OPTICS, Vol.23, No.3, p.492-498, 1984

(3) M.Tachikura and N.Kashima, "Fusion Mass-Splices for Optical Fibers Using High-Frequency Discharge", JOURNAL OF LIGHTWAVE TECHNOLOGY, Vol.LT-2, No.1, 1984



Kohji Ohzawa

Optical System Research and Development Department
Fujikura Ltd.

1440, Mutsuzaki, Sakura,
Chiba, 285, JAPAN

Kohji Ohzawa was born in 1967. He received the B.E. degree in electronics from Kyushu University in 1990.

He joined Fujikura Ltd. in 1990 and has been engaged in the research and development of an optical fiber splicer.

Mr.Ohzawa is a member of the Institute of Electronics and Communication Engineers of Japan.



Isao Suzuki

Optical System Research and Development Department
Fujikura Ltd.

1440, Mutsuzaki, Sakura,
Chiba, 285, JAPAN

Isao Suzuki was born in 1955. He graduated in mechanical engineering from Tokyo University of Agriculture and Technology in 1978.

He joined the optical system research and development department in Fujikura Ltd. in 1984.

He is now an assistant chief of the Precision Instrument Section.



Shuichi Toyoshige

Optical System Research and Development Department
Fujikura Ltd.

1440, Mutsuzaki, Sakura,
Chiba, 285, JAPAN

Shuichi Toyoshige was born in 1960. He received the B.E. degree in mechanical engineering from Keio University, in 1984.

He joined Fujikura Ltd. in 1988 and has been engaged in the research and development of an optical fiber splice machine.



Mikio Yoshinuma

Optical System Research and Development Department
Fujikura Ltd.

1440, Mutsuzaki, Sakura,
Chiba, 285, JAPAN

Mikio Yoshinuma was born in 1947. He graduated in mechanical engineering from Chiba University in 1971.

After graduation, he joined Fujikura Ltd. and has been engaged in research and development on mechanical equipment and tools for communication wires, cables, and parts.

He is now a manager of the Precision Instrument Section.



Hiroyuki Taya

Optical System Research and Development Department
Fujikura Ltd.

1440, Mutsuzaki, Sakura,
Chiba, 285, JAPAN

Hiroyuki Taya was born in 1960. He received the B.E. and M.E. degrees in electrical engineering from Tokyo University of Agriculture and Technology in 1983 and 1985, respectively.

He joined Fujikura Ltd. in 1985 and has been engaged in the research and development of an optical fiber splice machine.

Mr. Taya is a member of the Institute of Electronics and Communication Engineers of Japan.

Situation and Influence of Standardization for fibres and cables

Michel de Vecchis

Alcatel Cable 30, Rue des Chasses 92111 CLICHY - FRANCE

Abstract : This paper presents the organization of standardization for optical fibres and cables and the relationships between the different bodies.It describes the achievements, the on-going works and remaining problems. Finally the possible consequences and the influence of standardization are discussed.

I. Introduction :

Few years after the first developments on optical fibres and cables, the need appeared for some standardization activity and during the late 70's, the first International Meetings for standardization of optical fibres and cables have been held. This activity has grown continuously and there are now several bodies and several publications dealing with this subject. The purpose of this paper is to review the situation, the main achievements, the predictable future and the main implications of this work.

II. Organisation of standardization

Standardization is done at different levels : national, regional (North America, Europe, Far East) and international. It is clear that the ultimate goal is to achieve an international standardization and that other levels are mainly concerned by the preparation of the International Standards and consequently this paper is mainly devoted to this level. However, this paper considers also the European level for two reasons :

- European Standardization is a first level of multinational discussions involving a large number of active countries in the field of optical fibres and cables.
- The recently agreed procedure of parallel voting between some International and European bodies recognizes this first level of consensus and may have some influence on the future development of works.

II.1.International level :

Standardization of optical fibres and cables is done in two organizations :

CCITT

International Telegraph and Telephone Consultative Committee (part of the I.T.U. International Telecommunication Union).
Secretariat : GENEVA (Switzerland)
Mainly concerned : Study Group VI
Study Group XV

IEC

International Electrotechnical Commission
Central Office : GENEVA (Switzerland)
Mainly concerned : T.C. 86

II.1.1. CCITT :

CCITT activities are dedicated to Public Telecommunications.
Members are Telecommunication Administrations and Operators, recognized scientific and industrial organizations. CCITT work is done by 4 years long Study Periods. "Questions" are adressed for a Study Period to the Study Group

and the result of the work published at the end of a Study Period as "Recommendation".

For the Study Period 1989 - 1992 CCITT is dealing with cable related subjects in Study Group VI and with transmission and system related subjects in Study Group XV.

The list of questions related to optical fibres is as follows :

From Study Group VI

07/VI Optical fibre cable installation
08/VI Optical fibre cable restoration
09/VI Optical fibre cable construction
10/VI Performance tests for optical fibre cables
11/VI Optical fibre cables inside buildings
12/VI Optical fibre cable distribution networks
13/VI Passive optical components

From Study Group XV

11/XV Characteristics and test methods for single - mode optical fibre cables
12/XV Characteristics and test methods for multimode optical fibre cables.
13/XV Characteristics for submarine optical fibre cables and systems.
14/XV Characteristics of optical cables for local networks.
15/XV Characteristics of line systems on optical fibre cables.
16/XV Characteristics of digital line systems for use in local networks, including narrow-band and broadband ISDN access.
18/XV Availability and reliability on line systems on optical fibres.
27/XV Terminology for transmission equipement, network and systems.
29/XV Characteristics of digital systems on optical fibre cables for the synchronous hierarchy.
31/XV Guide for the application of new technologies in local networks.

CCITT Work methods

Studies by CCITT are appointed to Study Groups (SG's) by the Plenary Assembly (PA). The Plenary Assembly exists of the 166 National Telecommunication Administrations. Nowadays there are 18 Study Groups. Each Study Group selects questions to be studied which have to be approved by the PA's.

Each question study is coordinated by a Special Rapporteur. This by means of sending out a questionnaire or a proposal of study.

The results of the study are published during the Study Period as white documents, delayed contributions or temporary-documents and final results are published in handbooks or recommendations.

At the end of a Study Period, the Plenary Assembly decides on :

- Approval of the Recommendations (Rec.)
- Publication of the books and independent Rec.
- Organization of the next Study Period and relevant rules.
- Approval of the Questions and assignement to the SG's.

II.1.2. I.E.C.

I.E.C. works on optical fibres and cables are done in the Sub Committee 86 A (SC 86 A) which belongs to the Technical Committee 86 (TC 86) : Fiber Optics. Some others TC's or SC's within the IEC can also have an impact on optical fibres and cables for example the SC 20C which deals with burning characteristics of cables or the SC 47 C which is in charge of optoelectronic components.

SC 86 A was inaugurated at the IEC Montreal meeting 1985 together with TC 86 "Fibre Optics" and SC 86 B "Fibre Optic interconnecting devices and passive components". Before 1985 international standardization of optical fibres and cables was done in IEC SC 46 E. The scope of SC 86 A comprises optical fibres and optical fibre cables, excluding image transmission types. The main activities in the past have referred to measurement and test methods for fibres and cables.

Within the TC 86 there are now three Subcommittees as a new SC 86 C on Sub Systems has been added and Working Groups (WG's) attached

to the TC or to the SC's. Some WG's of the TC 86 can be of interest for fibres and cables :

WG1-Terminology-Symbology
WG2-Safety
WG4-Calibration of measuring equipements

The SC 86 A was organized in three WG's :

WG1-A2, A2 and A4 fibres
(I.e. "short distance" fibres)
WG2-A1 and B fibres
(i.e. "long distance" fibres)
WG3-Cables

Since the last plenary meeting in Madrid (October 1991), the WG1 and WG2 have been merged in only one WG1 : Fibres, considering that most of the work specific to short distance fibres was done.

IEC work methods

The work is done within the WG's on subjects approved by the National Committees by voting on New Work Item Proposals. Either National contributions or Expert's contributions are used during this phase. The working groups present the result of their work as Committee Drafts (CD) documents.

The CD's are circulated for comments to National Committees. CD's and attached comments are reviewed during the Plenary meeting of the SC which decides if the document is ready for circulation as Draft International Standard (DIS).

A document approved for circulation as a DIS is sent to National Committees for voting yes or no. No more comments are permitted during voting on a DIS.

If accepted, the document is published as an International S' ndard.

II.2. European level

Several organizations are working on the standardization of optical fibres and cables, mainly :

CECC

CENELEC Electronic Components Committee
General Secretariat : Frankfurt (Germany)

Note : CENELEC is the European body in charge of European Standardization for Electrotechnical problems.

ETSI

European Telecommunication Standards Institute
Sophia Antipolis (France)

AECMA

European Association of Aerospatial Equipment Manufacturers : Paris (France)

Works are in progress in CECC, responsible for the European System of Quality Assessed Electronic Components and other organizations such as ETSI and AECMA which are concerned by specific categories of application.

Work in CECC is done in the WG 28 Fibres and Cables. A good cooperation has been established between CECC WG 28 and ETSI/TMI/WG1. Fibres and Cables, in the framework of the general agreement between CENELEC and ETSI. This cooperation is based on the subcontracting by CECC to ETSI of "functional and system related aspects" with the intention of establishing documents, accepted by both parties, concerning telecommunication cables, and intended to be published as EN (European Standard).

Recently, an agreement as been signed between CENELEC and IEC that offers the possibility for both parties to enter a document in a parallel voting procedure, the DIS being submitted as Draft EN and vice versa. After voting under this procedure, the main difference comes from the status of EN's whose applications are mandatory in European countries. Therefore it is (at least in theory) possible for a European country to cast two different votes on the Draft EN and the DIS.

III Main achievements

III.1. Documents published by the CCITT.

The outcome of the work of CCITT is published in handbooks or recommendations.

The S.G.VI has published two handbooks after the last Study Period :

- HOP : Handbook Qutside Plant technologies for Public Networks.

- HOF : Handbook construction, installation jointing and protection of Optical Fibre Cables.

Furthemore the L series of recommendations (on lightning protection, corrosion protection, preservation of wooden poles, ...) were extended and they are considering the case of optical cables.

The SG XV has published several recommendations which are of interest for optical fibres and cables :

G 651 (Characteristics of a 50/125 μm multimode graded index optical fibre cable)

G 652 (Characteristics of a single-mode optical fibre cable)

G 653 (Characteristics of a dispersion-shifted single-mode optical fibre cable)

G 654 (Characteristics of a 1550 nm wavelength loss - minimized single-mode optical fibre cable)

G 955 (Digital line systems based on the 1544 kbit/s erarchy on optical fibre cables)

G 956 (Digital line systems based on the 2048 kbit/s hierarchy on optical fibre cables)

III.2. Documents published by the IEC

Four documents on optical fibres and cables have been published. Since the beginning of the work they have been improved by the publication of amendments or new editions.

At the time of writing this paper, the situation is :

- Publication 793-1 - Optical fibres - Generic Specification - Fourth Edition - Publication planned : September 1992.

- Publication 793-2 - Optical fibres - Product Specification - Third Edition - Published June 1992.

- Publication 794-1 - Optical fibre cables - Generic Specification - Third Edition - Publication planned : November 1992.

- Publication 794-2 - Optical fibre cables - Product Specification - Second Edition - Published October 1989.

III.3. Documents published (or ready for publication) at European Level.

The CECC has prepared two documents which have been approved for publication as EN. They are now in process of publication.

EN 187000 - Generic Specification : Optical Fibre Cables

EN 188000 - Generic Specification : Optical Fibres.

ETSI has prepared four documents IETS (Interim European Telecom Standard). These documents according to the ETSI - CENELEC agreement will be considered by CECC in order to prepare the corresponding Draft EN that should be, according to the parallel voting agreement with IEC, introduced for voting as DIS. They are :

pr. I.ETS 300226 : Single mode optical fibre cables to be used in ducts and for directly buried application

pr. I.ETS 300227 : CCITT Recommendation G 652 - type single mode optical fibre.

pr. I.ETS 300228 : CCITT Recommendation G 653 - type single mode optical fibre.

pr. I.ETS 300229 : Single mode optical fibre cables to be used for aerial application.

III.4. Summary of the situation

From the above description it appears that the level of Generic Specifications (i.e. the collection of measurement methods) has been well covered by the different standardization bodies. A lot of work has also been done on the specification of products.

However, if we consider the different levels necessary to achieve a complete set of standardization (3 or 4 levels according to the bodies : Generic Spec - Sectional Spec - Family Spec - Detailed Spec) it appears that some works has still to be done.

IV Pending Issues

Even at the Generic level some issues have been discussed but they have not achieved for the moment a sufficient level of maturation.

The main items which are still under discussion for the generic specifications are :

- longitudinal uniformity of fibres
- characterization of primary coating
- reliability and life time of fibres
- standardization of ribbons : list of test methods and description of the methods.

For other levels of specifications some works have also been started concerning, for example , some common functional requirements for large categories of products. The pr I.ETS prepared by ETSI are an illustration of such a tendency.
These documents could likely become a good starting point for the preparation of family specifications concerning telecommunication products.

Some other important points are also presently in discussion :

- Quality assurance of optical fibres and cables : The work has been initiated by the CECC WG 28. IEC SG 86 A has expressed a strong interest but decided not to duplicate the work and to wait until the first results of the work on CECC. The WG 28 has decided to base in principle the quality assurance for fibres and cables on the Capability Approval and an Ad Hoc Working Group has been created to prepare a first Draft.

- Installation practices for optical cables.:

 This subject has been included in the scope of the WG 3 Cables of SC 86 A. However what is really needed and how to specify these installation practices are not, at least for the moment, totally clarified.

V Impact of standardization

Is Standard a blocking or a stimulating factor for technical progress ? The question has been discussed many times and the answer is not obvious.

If we restrict the debate to the case of optical fibres and cables it is, may be, easier to provide some answer. It has been said quite often that fibre optics technology evolves very quickly. So the risk for the standards of not being able to follow quickly enough the evolutions exists.

However the short history of optical standards shows an important evolution : the 4 th Edition of the IEC Publication 793-1 Generic Specification of Fibres is now ready for publication and every previous edition has been the subject of one or two amendments to follow the evolutions. Other IEC Standards have also been updated continuously.
On a similar way CCITT Recommendations are updated every 4 years.

Moreover the agreements on some key issues on Standards have certainly been a stimulating factor for the industry. The agreement on the dimensions of multimode fibres (50/125 µm) as

early as 1980 has been an important factor to limitate the proliferation of different unnecessary types of fibres and to promote the starting up of the industry.

So it seems that, due to the possibility of amendments and new editions of Standards supported by a continuous work of experts in Standard Committees, the standardization of optical fibres and cables had, up to now, very few negative impacts on the development of the Industry and has been, at several occasion a good help and support for this development.

VI Conclusion

The review of standardization activities for optical fibres and cables shows that a consistent work has been done since the late 70's and that it has been possible to follow the quick evolution of the technology. It still remains some important points to be solved.

To solve these points and to continue to follow the technological changes, that will be the challenge of standardization bodies for the next years.

Biography

Michel de VECCHIS - ALCATEL CABLE
30, Rue des Chasses - 92111 CLICHY - FRANCE



Michel de VECCHIS was born in 1946. He is graduated from Ecole Nationale Supérieure des Télécommunications (1969). He joined LTT in 1970 where he worked on microwave components. He started to work on fiber optics in 1974 and has been Technical Director of the Cable Division until the merging in 1986 of LTT cable activities with Les Cables de Lyon now Alcatel Cable. He is now Director of Technical International Marketing at Alcatel Cable Telecommunications Branch.

He is involved in International Standardization of optical fibers and cables (Chairman of CECC WG 28 and Secretary of IEC SC 86 A).

Development of Ribbon Loose Tube Cable for Optical Subscriber Loop

Yutaka KUROSAWA, Hiroyuki SAWANO,
Matsuhiro MIYAMOTO, Nobuyasu SATO

FUJIKURA Ltd.

Sakura-shi, Chiba-ken, 285 Japan

1.ABSTRACT

In order to achieve the construction of optical subscriber networks for Fiber To The Home(FTTH) in the future, it will be necessary to use high-count optical fiber cables.

In this paper, we attempted to attain higher density, short-time working for fiber fusion splice and easy identification with encasing ribbons in loose tubes. The sizes of tubes to be used for this purpose were investigated in respect of tube-to-ribbon clearance. An optimum structure of ribbon loose tube cable encasing high-count fiber was investigated. Ribbon loose tube cables were made experimentally based on the results of these investigations and evaluated for their transmission and mechanical characteristics.

2.INTRODUCTION

In recent year, optical fiber cable networks find extensive use in various applications, transmission of much more information has become necessary with requirements of increasing number of fibers and higher density for these cables. Increasing the number of fibers requires mass fusion splicing and easy identification of fiber. An example of the fiber structure that can satisfy such requirements is a ribbon fiber. In this paper, the number of fibers was increased by encasing plural ribbons in each loose tube, and an optimum structure for ribbon loose tube cables was designed without degrading transmission losses, mechanical and water penetration characteristics.

First, when determining the sizes of the loose tube in which to encase ribbons, several tubes were made on trial, which are different in tube-to-ribbon clearance and in fiber excess length. For each of these tubes, the minimum ribbon bend radius in the loose tube was calculated from the tube-to-ribbon clearance and fiber excess length, and its relationship with ribbon fiber loss increase was investigated to determine the permissible ribbon bend radius in the loose tube. Further, the low temperature contraction percentage in a cable structure was estimated, and an optimum tube-to-ribbon clearance was determined from the relationship between the minimum bend radius and the tube-to-ribbon clearance by investigating ribbon meandering caused at low temperature. Actually, these investigations were made on jelly-filled tubes each having either for 4-fiber or 12-fiber ribbons encased therein.

Next, the design of an optimum cable structure was determined from the ribbon curvature radius calculated from the stranding pitch, at which six tubes each containing four ribbons are stranded around a central member.

Finally, the ribbon tube cables (with up to 288 fibers) were made as a result of these investigations and evaluated for transmission and mechanical characteristics.

3.CABLE STRUCTURE

Optical fiber cables currently being in extensive use are roughly classified into two types: loose and tight. In terms of fibers encased in cables, there are two types of fiber unit: fiber bundle type and ribbon fiber type. The conventional loose tube cable encases plural single fibers in each tube as shown in FIG.1. Usually such cables are easy to be made, but cannot include more than about twelve fibers per tube at maximum. Therefore, these cables are used for low-fiber count with a compact structure, and an attempt to increase the number of fibers in a tube would give rise to such problems as "it is troublesome to identify individual fibers","working for fiber fusion splice has to be done many times, which is uneconomical", etc. Working time for fiber splice consists of preparation time for splicing and splicing time with fusion splicer, reinforcement time by heat-shrinkable tube. Working time for high count fiber splice with single fiber and 6-fiber ribbon, 12-fiber ribbon, 12-fiber ribbonization, respectively is shown in FIG.4. 12-fiber ribbonization is to apply

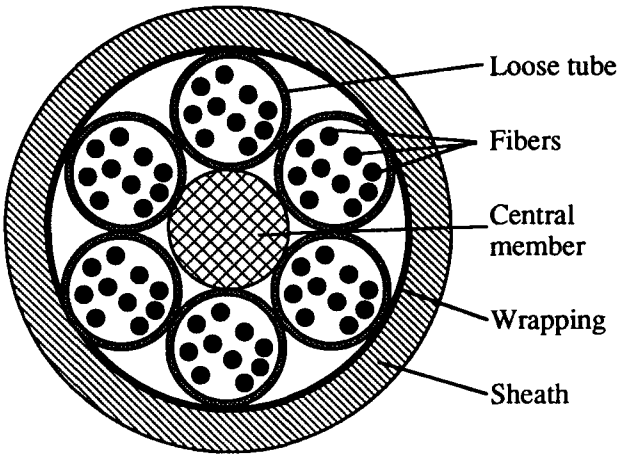


Fig.1 Fiber bundle loose tube cable structure

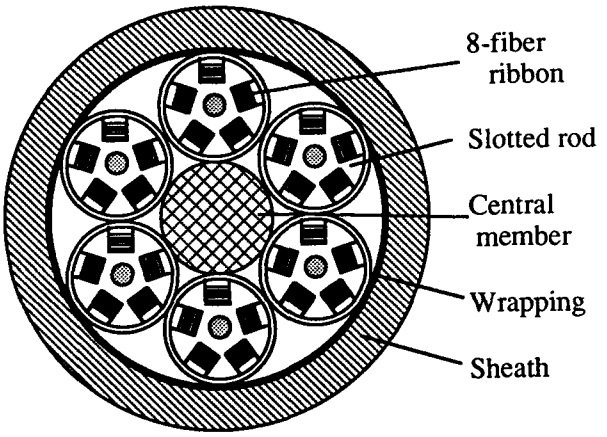


Fig.2 1000-fiber slotted core ribbon cable structure

the adhesive on the arranged twelve fibers to form the 12-fiber ribbon. Working time with 6-fiber ribbon and 12-fiber ribbonization are about half of that with single fiber. Moreover, working time with 12-fiber ribbon is about quarter of that with single fiber. Ribbon fiber unit is used extensively to avoid above problems. As a loose tube cable using ribbons, a high-count fiber cable is used extensively, which has multi-fiber ribbons encased in central core tube to provide as much as 200 fibers. With this type of loose tube cable, however, it would be difficult to attain a further increase of fiber-number. On the other hand, there is another loose tube cable in which cable cores constructed with two stranded layers of LAP pipes each having multi-fiber ribbons with Graded-Index fibers, but it has not reached the stage of practical application yet.[1] While, the tight type includes a slot type cable using ribbons. The slot type tight cable contain ribbons as shown in FIG.2, so it provides as much 1000 fibers with a compact structure.

In view of the foregoing, we made investigations to design a tube ribbon cable as shown in FIG.3, which is a six-tube type structure and enable a further increase more than 200 fibers. This cable contains multi-fiber ribbons, so individual fibers are easy to identify. Moreover, using ribbon fiber makes it possible to attain short-time working for fiber fusion splice as shown in FIG.4. Six such tubes are stranded into a cable, so a further increase in number of fibers becomes possible. In this paper, 96- and 288- fiber cables were designed by using 4- and 12- fiber ribbons, respectively. These cables were all sheathed with polyethylene and made very compact in structure with an outside diameter less than 20 mm.

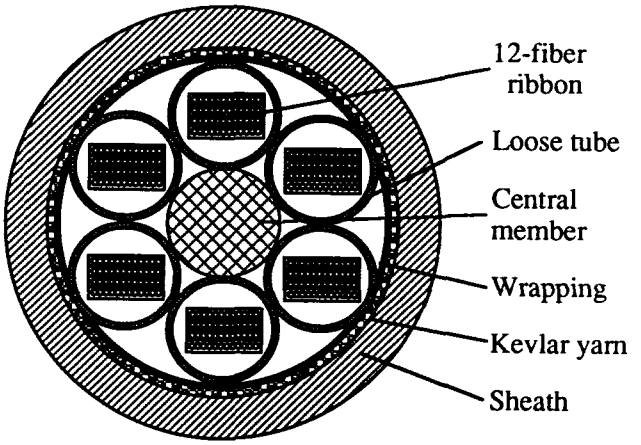


Fig.3 Developed ribbon loose tube cable structure

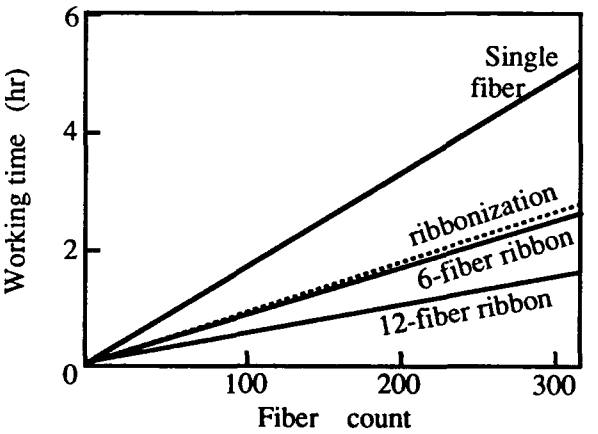


Fig.4 Working time for fiber splice at each of fiber type

4. CABLE DESIGN

(1) Optical Fiber Ribbon

The fiber used in this study was a single-mode fiber. It is a fiber in common use, its major characteristics are: MFD = 9.5±0.5 μm, λ = 1.10 to 1.28 μm, fiber diameter = 125μm, and dual coating O.D.=250μm.

Multi-fiber ribbons are classified into two types: edge-bonded and encapsulated, as shown in FIG.5. The encapsulated type is said to be higher in resistance to lateral pressure by a value corresponding to the coating thickness of the ribbon and is used in slot type cables. On the other hand, the edge-bonded type is frequently used in loose cables, whose structure gives compactness in total thickness of stacked ribbons. In this study, for the purpose of investigating loose cables, we used edge-bonded 12-fiber ribbons. At the same time, we investigated a loose tube having encapsulated 4-fiber ribbons encased therein for comparison.



Encapsulated type ribbon



Edge-bonded type ribbon

Fig. 5 Two types of 12-fiber ribbon

(2) Loose Tube Design

The tube structure used for investigation was a resin-made, jelly-filled loose tube having four 12-fiber ribbons encased therein, as shown in FIG.6. The resin used was a thermoplastic resin having heat resistance and high Young's modulus. The jelly was used as filling compound for loose tube cables.

The tube-to-ribbon clearance (C) and the fiber excess length (ε) are important parameters for determining the loose tube size. Here, the clearance (C) is defined as shown in FIG.6 and the fiber excess length (ε) is the ratio of the length of encased ribbon to the tube length. Assuming that L_T=tube length and L_R=ribbon fiber length, the fiber excess length is represented by (1),

$$\varepsilon = (L_R - L_T)/L_T \qquad (1)$$

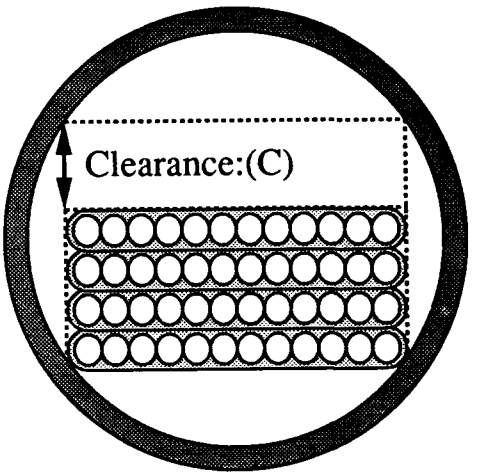


Fig.6 Loose tube encasing 12-fiber ribbon structure

The optical loss increase resulting from various stresses applied to the cable, e.g., when it is made low in temperature, is considered attributable to the occurrence of micro/macrobending of the fibers. First, tubes having different fiber excess lengths and tube-to-ribbon clearances were manufactured and measured for loss increase in them. Supposing that the ribbons bending in the tube along a sine curve owing to the excess length, resulting in such bending which causes ribbon loss increase, this bending is generally assumed to be able to be approximately represented as the minimum bend radius (R_{min}) by (2),[2][3][4]

$$R_{min} \cong C/8\varepsilon \qquad (2)$$

The relationship between Rmin calculated by (2) and the average loss increase in the ribbons of each tube is was investigated and given in FIG.7. As a result of this experiment, R_{min} can be approximately represented by (3) with the optical loss increase taken as α(dB/km, at1.55μm),

$$\alpha \cong 2.05 * 10^9 R_{min}^{-5.3} \qquad (3)$$

when the optical loss increase by micro/macrobending, resulting from the stress applied to the cable , is allowed to be less than 0.05 dB/km. Therefore, it is necessary that R_{min} be larger than 100mm in order to reduce the optical loss increase by micro/macrobending in the loose tube below 0.05dB/km.

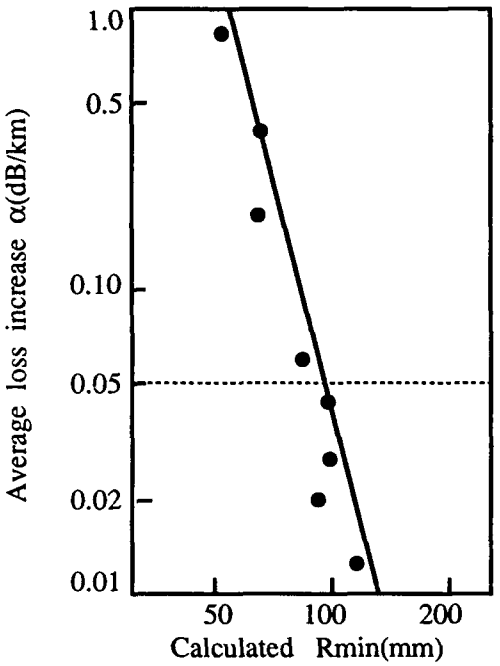


Fig.7 Relationship between calculated Rmin from excess length and average loss increase for ribbon fibers in the tube.

Next, a tube size, with which the loss increase is held at less than 0.05dB/km when the cable is stressed, could be calculated by setting a tube-to-ribbon clearance, which ensures a value of R_{min}>100mm even when the fiber in the tube undergo micro/macrobending as a result of stresses actually applied to the cable. In this case, the contraction of the cable at low temperature was assumed as the cable stress that causes micro/macrobending to the fibers. Supposing a ribbon loose tube cable as shown in FIG.3, the low-temperature contraction of the cable can be approximately estimated from the thermal expansion coefficient of the cable and ribbon fiber materials. For a cable having four 12-fiber ribbons encased in tubes as shown in FIG.3, its thermal expansion coefficient is estimated from the cross sectional area and Young's modulus of the central member. Namely, if the wall thickness of the tube is fixed and the tube size is in a conceivable range, the thermal expansion coefficient of the cable can be approximately calculated from the specification of the central member used for the cable. The central member used here was an FRP member of about 5 mm in diameter, commonly used for cable as shown in FIG.3. From the foregoing, the thermal expansion coefficient (β) of the cable was assumed to be equal to $1.8*10^{-5}$, $2.0*10^{-5}$ or $2.2*10^{-5}$ (1/°C). Hence, taking the temperature change of the cable when made low in temperature as " T", the contraction percentage (ΔL) of the cable can be approximated by (4),

$$\Delta L=\Delta T*\beta \qquad (4)$$

The fiber excess length caused in the ribbons in the tube under the low-temperature contraction of the cable is the sum of the value resulting from this contraction and the value produced in the stage of cable fabrication. Assuming that sine wave-like micro/macrobending in the ribbons is caused by this excess length, the following formula (5) for micro/macrobending can be derived by approximately from (2),

$$R_{min} \equiv C/8(\Delta L+\varepsilon) \qquad (5)$$

For temperature changes of 60°C, the tube-to-ribbon clearance (C) and minimum bending radius (R_{min}) were calculated by (4) and (5). As a result, FIG.8 was obtained. Taking also into consideration the permissible micro/macrobending (R_{min}) of more than 100 mm, needed to reduce the optical loss increase in the ribbons of the tube below 0.05 dB/km, the permissible tube-to-ribbon clearance for the tube under consideration, which has four 12-fiber ribbons therein, is considered sufficient for this type of tubes, provided that the tube-to-ribbon clearance is satisfied to be a value of 1.2mm at minimum.

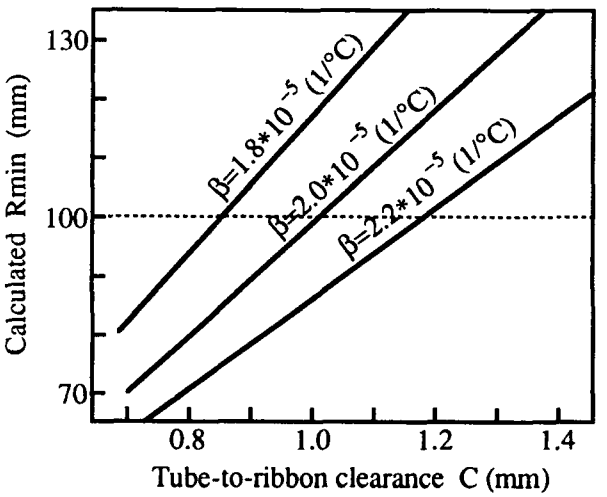


Fig.8 Relationship between tube-to-ribbon clearance and calculated Rmin about assumed β

(3) Cable Design

What is most important when designing a loose tube cable is to determine an optimum value of curvature ribbon radius for stranding in tubes, accordingly to minimize the fiber strains resulting from the ribbons being bent with the curvature radius of the tubes when stranded into a cable. As the long-term reliability of the optical cable is affected the residual strain of the fiber with the curvature radius for stranding. Here, the relationship between the ribbon bend in the tube and the tube stranding pitch was investigated. The curvature radius of the ribbons in the tube was estimated, using tubes, which satisfy the permissible tube-to-ribbon clearance derived in the preceding section and taking the stranding pitch as a parameter for the cable having a structure as shown in FIG.3. The curvature radius (ρ) of the ribbons when the tubes are stranded around the central member is approximated by (6),[5] with the tube diameter as "a" and the diameter of the central member as "b" ,

$$\rho \cong (a+b)/2+\{(p/2\pi)^2/(a+b)/2\} \qquad (6)$$

In addition, the minimum curvature radius when the cable under consideration is wound on a test or experimental reel was also calculated. The results are given in FIG.9. Here, the drum O.D. for cable tests was taken equal to 800 mm and 1000 mm, and the state of the cable not wound on the reel was take as "ρ_0". In general, at both the loose tube cable and the slot type cable, the curvature radius for the encased fibers (including the ribbon type) is experimentally required to be more than 1000 mm in terms of the residual strains affecting the long-term reliability. For cable performance tests, a curvature radius of more than 300 mm seems necessary because the cable is kept wound on the reel for just a short time. Taking these into account, a stranding pitch of more than 400 mm seems necessary in designing a ribbon type loose tube cable having a structure as shown in FIG.3.

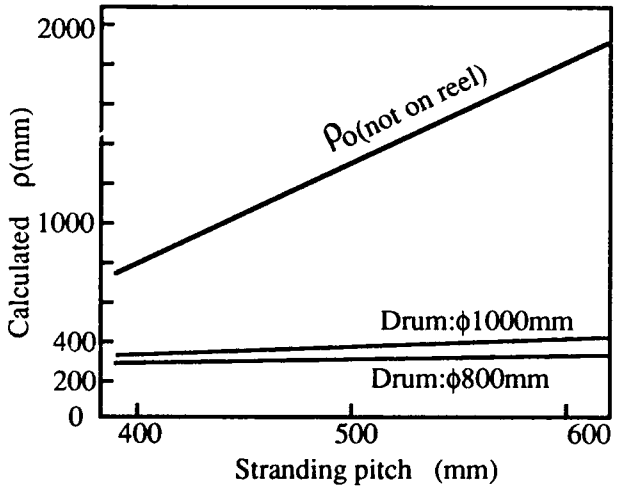


Fig. 9 Relationship between Stranding Pitch and calculated curvature radius

5. TRIAL MANUFACTURE OF CABLES AND THEIR EVALUATION

(1) Cable Structure

Based on the investigation results in the preceding section, cables having the structure of Table.1 were manufactured by using tubes each having either four 4-fiber or 12-fiber ribbons therein. In the following sections, the evaluation results are presented for only 12-fiber ribbon loose tube cable. The performance of 4-fiber ribbon loose tube cable was investigated and found to be equivalent or superior to that of 12-fiber ribbon loose tube cable.

Item	4-fiber ribbon	12-fiber ribbon
Fiber Number	96	288
Strand Pitch	500 mm	500 mm
Central Member	ϕ4mm(FRP)	ϕ5mm(FRP)
Diameter	16 mm	20 mm
Weight	170 kg/km	250 kg/km

Table. 1 Characteristics of experimental cable

(2) Optical Attenuation Increase in Cable Manufacturing Process

The change in optical attenuation increase in the cable manufacturing process is given in FIG. 10. As seen from this figure, the fibers exhibits a stable optical attenuation both after tubing and stranding. Therefore, the size and stranding pitch of the tubes can be said to be appropriate.

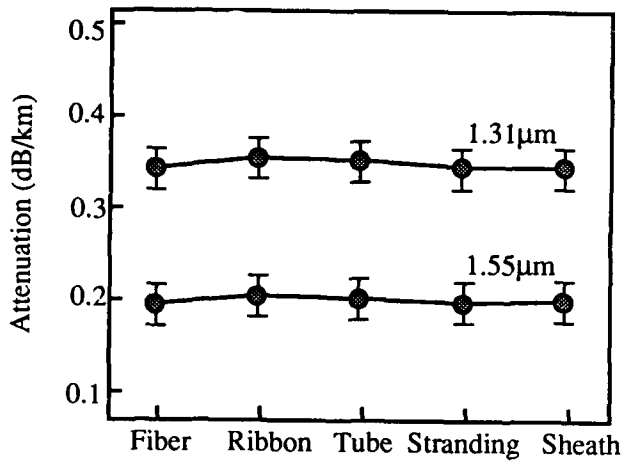


Fig. 10 Attenuation change in Cable Manufacturing Process

(3) Temperature Cycling Test

To predict the long-term reliability of optical attenuation for cables, we subjected cables to a heat cycle test. The temperature cycle pattern for this test and the obtained results are given in FIG.11. The change in attenuation at this test was stable and did not exhibit at low temperature. The micro/macrobending losses of the fibers, which seem to have been caused by cable contraction at low temperatures, were below 0.05 dB/km. Thus the test cables were superior in low-temperature characteristics.

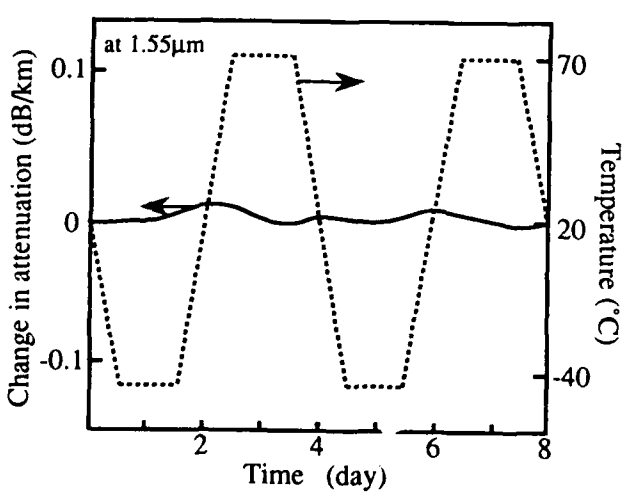


Fig. 11 Result of heat cycling test for the trail cable

(4) Mechanical Tests

The methods and requirements for mechanical tests made in this study as shown in Table.2. The results of the tensile and compression tests satisfied the requirements as shown in FIG.12,13, respectively.

Test item	Condition	Loss change
Tensile	Tensile load : 100m/300kg at1.55μm	During the test ≤0.05dB
Compression	Compressive load : 100mm/250kg at1.55μm	During the test ≤0.05dB

Table.2 Requirements of mechanical characteristics

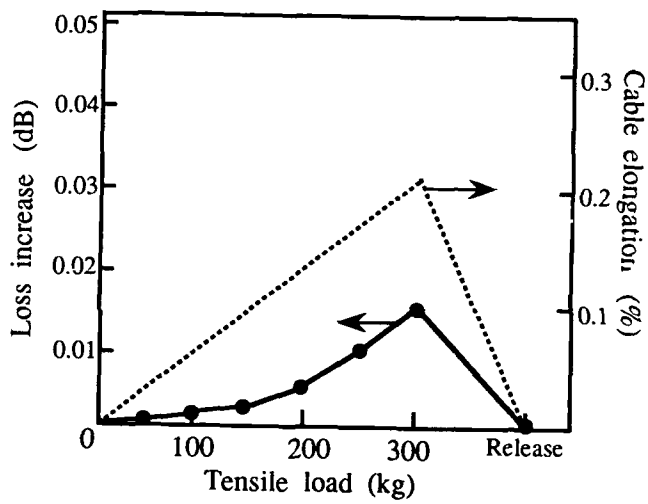


Fig.12 Result of tensile test for trail cable

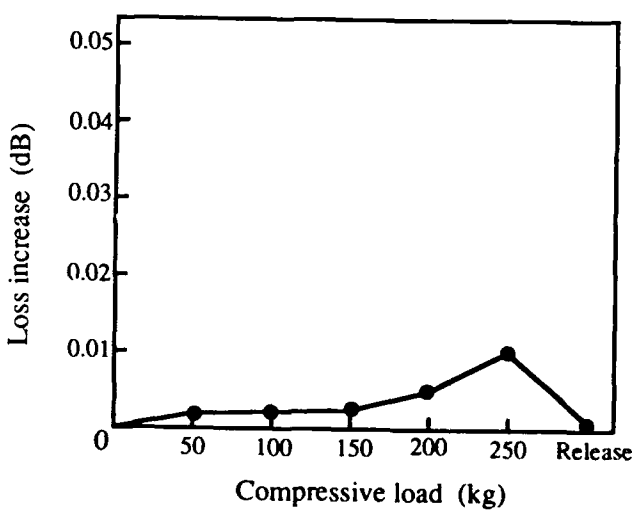


Fig.13 Result of compression test for trail cable

6. CONCLUSION

As described in the foregoing, we evaluated the design of a loose tube cable, which has multi-fiber ribbons encased in tubes, in terms of tube-to-ribbon clearance and the curvature radius of the ribbons in tubes when stranded into a cable, and actually made such cables. The obtained cables were superior in optical transmission losses, low temperature and mechanical characteristics. Using such theory made it possible to attain a further increase in number of fibers without degrading cable performance and economics the high-count loose cables equivalent to conventional fiber bundle loose tube cables, and to realize an efficient fusion splicing and a compact structure that are advantages of ribbon type cables.

7.Reference

[1] S.Tomita, M.Matsumoto, T.Yabuta, T,Uenoya,"Preliminary research into ultra high density and high count optical fiber cables" 40th IWCS, 1991.

[2] S.Hatano, Y.Katsuyama, T.Kokubun, K.Hogari,"Design and characteristics of multi-hundred-core optical-fiber cable for use in subscriber feeder",J.of Light Technology,Vol. LT-4, No.8, August 1986.

[3] D.Boscher, B.Missout, and P.Cheron,"Low-loss optical fiber cable design and manufacture", in Proc. 30th IWCS, 1981.

[4] S.Stueflotten, "Low temperature excess loss of loose tube fiber cables",Appl. Opt., vol.21, no.23, pp.4300-4307, 1982.

[5] Y.Katsuyama, H.Kobayashi, Y.Mitsunaga, K.Harada, Y.Ishida, "Bending property and allowable bending radius for unit-type optical cable', Trans. IECE Japan, vol.J-66B, no.2, 1983. (in Japanese)



Yutaka KUROSAWA

Opto-Electronics
Laboratory
Fujikura LTD.

1440 Mutsuzaki,
Sakura-shi, Chiba-ken
285 Japan

Mr. KUROSAWA was born in 1962. He joined Fujikura LTD. after his graduation from Saitama University with a B.C. Degree in 1985 and has been engaged in research and development of optical cables. He is now an engineer of Telecommunication Cable Material Section and a member of IEICE of Japan.



Hiroyuki SAWANO

Opto-Electronics
Laboratory
Fujikura LTD.

1440 Mutsuzaki,
Sakura-shi, Chiba-ken
285 Japan

Mr. SAWANO was born in 1955. He joined Fujikura LTD. after his graduation from Hokkaido University with a M.S. Degree in 1983 and has been engaged in research and development of optical cables. He is now an engineer of Telecommunication Cable Section and a member of IEICE of Japan.



Matsuhiro MIYAMOTO

Opto-Electronics
Laboratory
Fujikura LTD.

1440 Mutsuzaki,
Sakura-shi, Chiba-ken
285 Japan

Mr. MIYAMOTO was born in 1953. He joined Fujikura LTD. after his graduation from Tokyo Institute of Technology with a M.S. Degree in 1978 and has been engaged in design and research of optical fibers and cables. He is now a section chief of Telecommunication Cable Section and a member of IEICE of Japan.



Nobuyasu SATO

Opto-Electronics
Laboratory
Fujikura LTD.

1440 Mutsuzaki,
Sakura-shi, Chiba-ken
285 Japan

Mr. SATO was born in 1943. He joined Fujikura LTD. after his graduation from Tohoku University with a B.E. in 1966 and has been engaged in research and development of transmission cables. He is now the manager of Transmission Line Department and a member of IECE of Japan.

A FIBER-OPTIC CABLE FOR HOSTILE ENVIRONMENTS

K. Kathiresan, A. J. Panuska, J. W. Shea, W. H. Ficke, M. R. Santana, C. R. Taylor, and L. T. Carlton
AT&T Bell Laboratories and AT&T Network Cable Systems, Norcross, Georgia 30071

ABSTRACT

More stringent performance demands are being placed on fiber-optic cables to operate reliably for long periods of time in hostile environments. For example, underground steam pipe leaks or ruptures and subsequent failure of neighboring fiber-optic and copper cables are becoming increasingly common in the large cities of the U. S. due to aging steam systems. These occurrences are of major concern to most of the telecommunication operating companies. In general, the steam is superheated and is under high pressure and at high temperature. When a high pressure steam pipe ruptures, the fiber-optic cable is exposed to a high temperature, high moisture, and high velocity environment. It is estimated from field data that the maximum steam temperature to which the cables may be exposed when there is a steam pipe leak or break could be as high as 140°C (284°F). The duration of exposure could be as long as several months. Other hostile environments the fiber-optic cable may be exposed to are as follow : high temperature, petroleum products, chemicals, corrosion, hydrogen, lightning, rodents and insects, and shallow water. A new fiber-optic cable has been designed and developed to withstand and operate in the above mentioned hostile environments and is described in the paper.

INTRODUCTION

Optical fiber transmission systems have been maturing over the past two decades and are saturating the communication networks around the world. As they saturate, the systems are either encountering unforeseen hostile environments or proliferating into new applications with known hostile environments. The transmission media, the cables, are particularly vulnerable to exposure to these environments. The severity and significance of these commonly encountered outside plant hostile environments and a fiber-optic cable capable of surviving these environments are discussed below.

HOSTILE ENVIRONMENTS

Commonly encountered hostile environments in outside plant are as follow : steam, high temperature, petroleum products, chemicals, corrosion, hydrogen, lightning, rodents and insects, and shallow water. The severity and significance of these environments are expanded on below.

Steam

Underground steam pipe leaks or ruptures and subsequent failure of neighboring fiber-optic and copper cables are becoming common in over 40 large cities of the U. S. due to aging steam systems [1]. Such failures are of major concern to most of the telecommunication operating companies. In general, the steam in underground pipes is superheated and is under high pressure and at high temperature. The operating condition of the steam inside the pipes varies generally from 0.69 MPa (100 psig) to 2.76 MPa (400 psig). The corresponding minimum temperature (higher, if superheated) of the steam varies from 165°C (329°F) to 230°C (446°F). Field data and a thermodynamic modeling and analysis of a steam pipe rupture [2] indicate that the maximum steam temperature to which the cable are generally exposed when there is a steam pipe leak or rupture could be as high as 140°C (284°F). The duration of exposure could be as long as several months. Current standard commercial fiber-optic cables have been found to fail in such an environment, and several such failures have been documented by the telecommunication operating companies. The failures are not surprising since the cables were not designed for such an environment. The high temperature and high humidity conditions degrade or melt the cable materials leaving the fibers vulnerable to mechanical damage.

High Temperature

Fiber-optics transmission systems frequently encounter high temperature environments with moderate or low humidity. For example, it occurs in nuclear, coal and oil powered plants, ship engine rooms, aircraft engines, metal, chemical and petroleum processing plants, and smelting and heat processing facilities for metals and refractories.

Petroleum Products

Communication systems are frequently exposed to hostile fluids such as gasoline, diesel fuel, turbine fuel (JP-5, JP-6, etc.), hydraulic fluids, lubricating oils, etc. Quite frequently, processing facilities, airports, and aircraft and ship engines are some examples where such hostile fluid environments are found. Most of the current thermoplastic materials used in communication cables soften or may even dissolve in these high temperature hostile fluid environments.

Chemicals

In addition to petroleum based hostile fluids, communication systems may also be exposed to other hostile fluids/chemicals such as high concentrations of coolants, alcohol, chlorinated

organic and ketone based solvents, salt/sea water, acids, alkalis, and other chemicals.

Corrosion

As a result of combinations of some or all of the environments discussed above and/or natural contaminants, pollution and other sources, a high potential exists for corrosion problems in the outside plant.

Hydrogen

When metals corrode, the accompanying cathodic reaction can result in the generation of molecular hydrogen. The metals are often found in the outside plant either in the cable as a component or as a protective system such as metal ducts. Molecular hydrogen is known to cause a significant increase of attenuation in optical fibers.

Lightning

Lightning is a natural phenomenon which is very prevalent in the outside plant throughout the world. For example, almost the entire U. S. is susceptible to lightning strikes of differing magnitudes. When metals are used in outside plant cables, they attract lightning, significantly increasing the possibility of cable damage.

Rodents and Insects

Rodents and insects attack, like lightning, is another natural problem which is also very prevalent throughout the world. Some of the most common rodents which attack cables are gophers (Geomys Bursarius), wood rats (Newtoma Mexicana), squirrels and groundhogs. In the U. S., while squirrels and groundhogs are prevalent throughout, over 60% of the country is infested with gophers. Regarding insects, for example, in the Gulf coast areas of the U. S., the voracious Formosan termite (Coptotermes Formosanus) has attacked directly buried cables and underground cables.

Shallow Water

The potential for exposure of outside plant cables to shallow water is very high. One scenario is the possibility of flooding due to heavy rains. Other possibilities of flooding are underground installations where the water mains, aqueducts, or dikes could rupture and flood underground ducts. In other cases, the cable may have been deployed in known shallow water areas, for example, rivers, lakes, or bays.

FIBER-OPTIC CABLE FOR HOSTILE ENVIRONMENTS

A new fiber-optic cable has been designed and developed for application in the above hostile environments, individually or in combinations thereof. The original design intent was to develop a fiber-optic cable for underground steam leak problems, which also included the high temperature, petroleum products, chemicals, corrosion, and hydrogen capabilities. The cable's capability and application to the remaining environments, lightning, rodents and insects, and shallow water, are additional performance benefits of the cable design.

Cable Design

The hostile environment fiber-optic cable consists of the *core cable* and an *oversheathing* as shown in Figures 1 (isometric view) and 2 (cross-sectional view).

The key design concept of this cable is a seam-welded, corrugated copper barrier that keep all of the hostile environments except temperature from reaching the heart of the cable, called the *core cable*. Use of suitable materials for long-term 140°C (284°F) exposure for the core cable assures

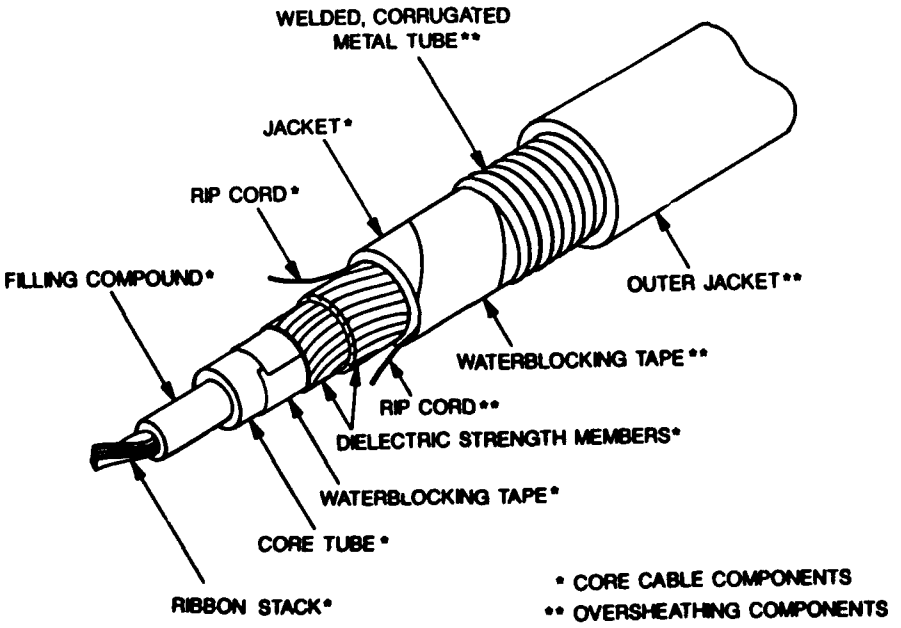


Figure 1. Isometric View of Hostile Environment Cable

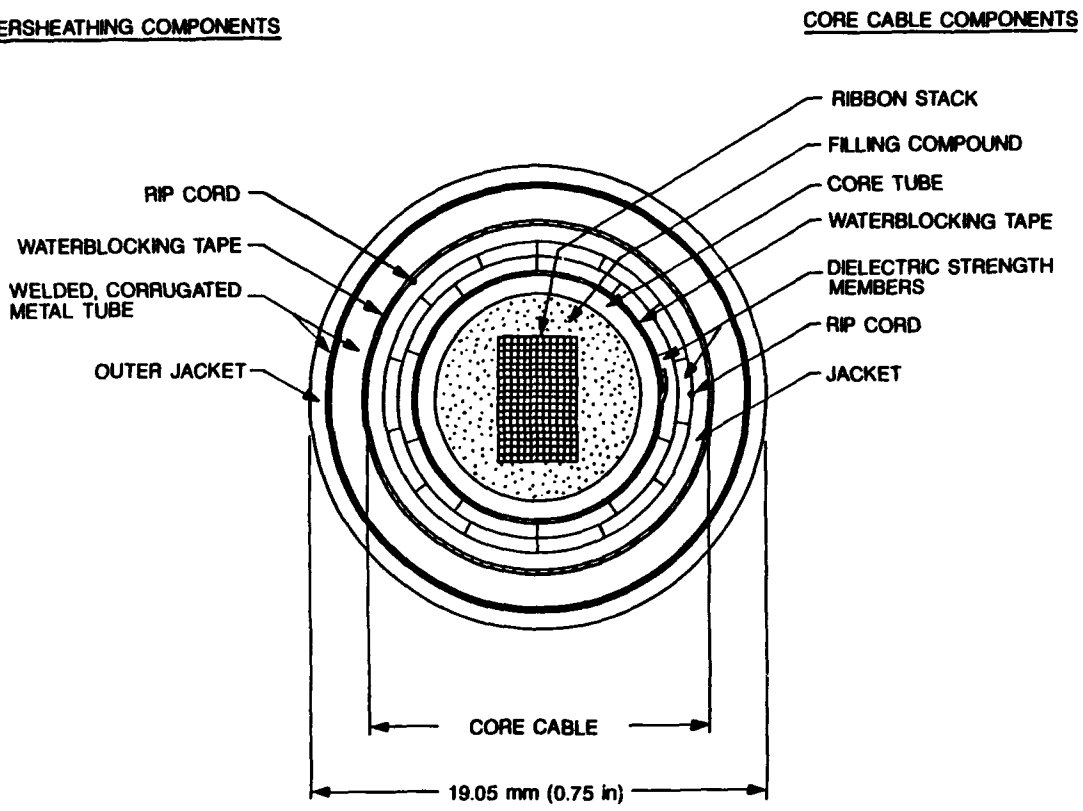


Figure 2. Cross-Sectional View of Hostile Environment Cable

the performance of the cable in the hostile environments. The core cable is a dielectric-crossply-sheathed cable [3]. It consists of a polyester core tube, which houses the fibers [4,5] in the form of bonded ribbons (1 to 18 12-fiber ribbons) [6], and filling compound. A waterblocking tape is wrapped longitudinally over the core tube. Two sets of fiber glass strength members and two polyester yarn rip cords are stranded over the waterblocking tape having opposite lays. A polyester jacket is then extruded completing the core cable construction. In the *oversheathing* operation, an aramid yarn rip cord is placed longitudinally over the core cable. Two waterblocking tapes are then wrapped helically over the core cable and rip cord. A strip of copper tape is then formed, welded, drawn and corrugated to provide a metallic barrier to the core cable. The cable is then completed by extruding a fluoropolymer or a high density polyethylene (HDPE) outer jacket. The outer diameter of the finished cable ranges from 16 to 19 mm (0.63 to 0.75 in.) depending on the number of fibers/ribbons in the cable.

The copper barrier and the selection and use of suitable thermoplastic materials for 140°C (284°F) long-term exposure [7] are the key design features which make the cable capable of performing in these hostile environments.

CABLE PERFORMANCE CHARACTERISTICS

The hostile environment cable was tested thoroughly, and the battery of tests included : the standard Bellcore Outside Plant tests [8], steam and high temperature tests, other hostile environment tests, underground installation tests, and cable-air installation system tests. Results of the tests are summarized below.

Standard Bellcore Tests

A cable with twelve 12-fiber ribbons (144 fibers) with depressed-clad fibers was manufactured to evaluate the performance. First, an attenuation test was conducted for the finished cable. The attenuation data at 1310 nm and 1550 nm wavelengths are presented in Figures 3 and 4.

The cable was then subjected to the following mechanical and environmental tests as specified by Bellcore for outside plant applications.

Mechanical Tests: The mechanical tests consist of low and high temperature cable bend, impact resistance, compressive strength, tensile strength of cable, cable twist, cable cyclic flexing, cable freezing, resistance to water penetration, and filling and flooding compound flow. During installation, at the ends and at mid-sheath entry points, the oversheathing portion of the cable may be removed and the core cable will be handled like any other cable. For this reason, the core cable was also subjected to the same set of mechanical tests, with the exception of tensile load and bend test, as the finished hostile environment cable. Test results for the finished cable and core cable are given in Tables I and II, respectively. Both cables meet and/or exceed the outside plant 1550 nm wavelength performance requirements. For example, in the compression test, the finished cable was subjected to a load of 880 N/cm

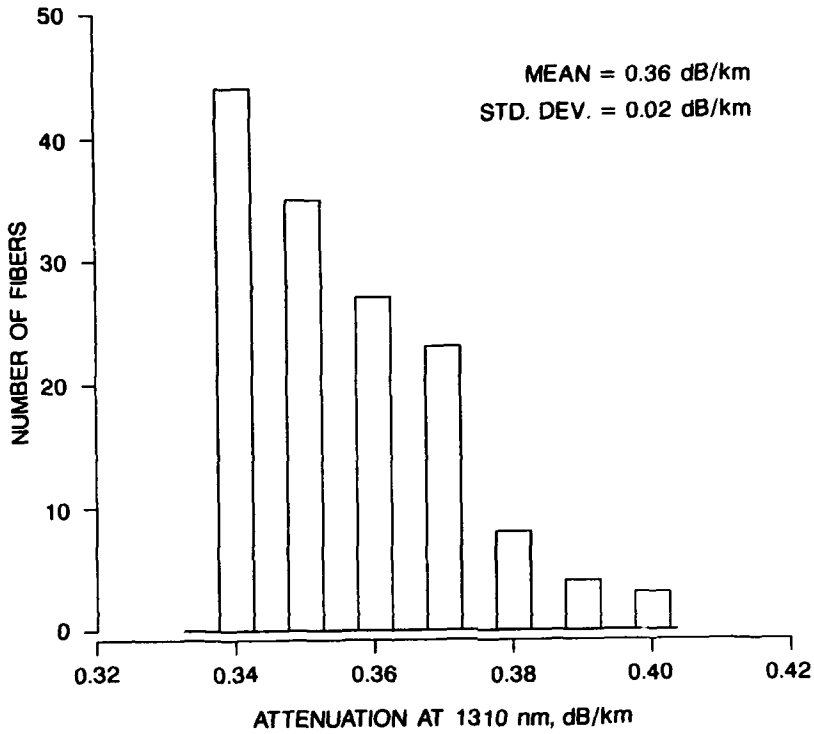


Figure 3. Hostile Environment Cable Attenuation Data at 1310 nm

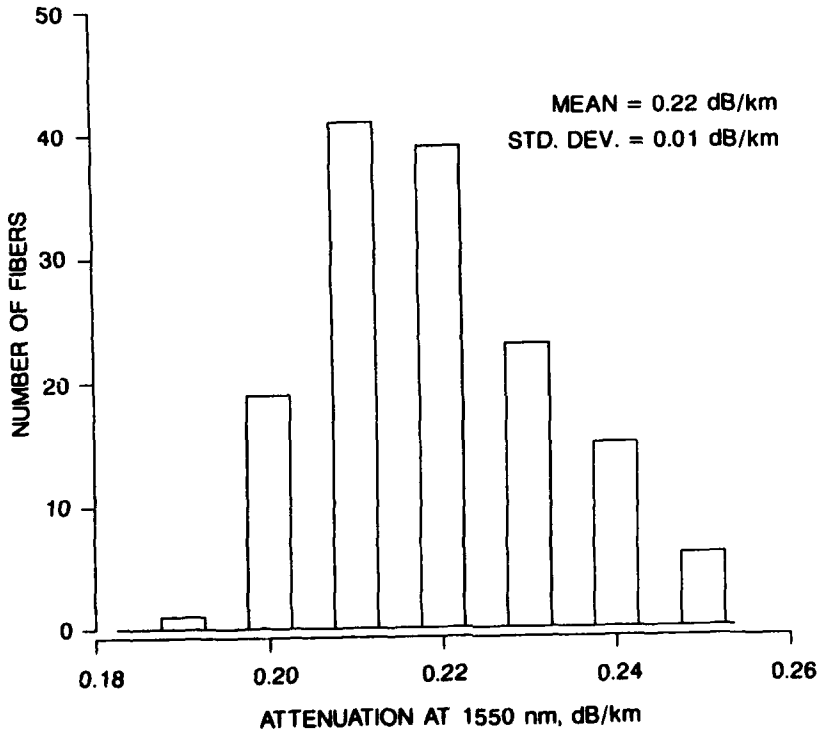


Figure 4. Hostile Environment Cable Attenuation Data at 1550 nm

TABLE I. MECHANICAL TEST RESULTS FOR FINISHED CABLE

EIA Fiber Optic Test Procedure	Bellcore TR-TSY-000020 Requirement	Laboratory Test Level	Cable Performance Δ Loss @ 1550 nm
EIA FOTP-25 Impact Test	5 kg Mass, 20 Impacts @ 30 Cycles/min. Avg.Δ Loss ≤ 0.20 dB	16.0 kg Mass 20 impacts @ 30 Cycles/min.	Avg. Δ Loss = 0.01 dB Max. Δ Loss = 0.01 dB No Visual Damage Observed @ 10 X Mag.
EIA FOTP-33 Tensile Load & Bend Test	2669 N Tensile Load, 1 hour duration, 560 mm Universal Sheave Dia. Avg.Δ Loss ≤ 0.10 dB	5338 N Tensile Load 2 hour duration, 400 mm Universal Sheave Dia.	Avg. Δ Loss = 0.00 dB Max. Δ Loss = 0.02 dB No Visual Damage Observed @ 10 X Mag.
EIA FOTP 37A High Temperature Bend Test	4 hours @ + 65°C, 4 Wraps on Mandrel Dia. ≤ 20 X Cable Dia. or 380 mm Avg.Δ Loss ≤ 0.20 dB	4 hours @ + 65°C, 4 Wraps on Mandrel Dia. = 200 mm	Avg. Δ Loss = 0.00 dB Max. Δ Loss = 0.01 dB No Visual Damage Observed @ 10 X Mag.
EIA FOTP-37A Low Temperature Bend Test	4 hours @ -30°C, 4 Wraps on Mandrel Dia. ≤ 20 X Cable Dia. or 380 mm Avg.Δ Loss ≤ 0.20 dB	4 hours @ -30°C, 4 Wraps on Mandrel Dia. = 200 mm	Avg. Δ Loss = 0.00 dB Max. Δ Loss = 0.01 dB No Visual Damage Observed @ 10 X Mag.
EIA FOTP-41 Compressive Loading Resistance Test	440 N/cm Compressive Load, 100 mm Compressive Plates, 10 minute Duration Avg.Δ Loss ≤ 0.10 dB	880 N/cm Compressive Load, 100 mm Compressive Plates, 1.5 hours Duration	Avg. Δ Loss = 0.00 dB Max. Δ Loss = 0.02 dB No Visual Damage Observed @ 10 X Mag.
EIA FOTP-85 Twist Test	10 Cycles Of: 180° CW Twist, 180° CCW Twist, L= 4 Meters Avg.Δ Loss ≤ 0.10 dB	10 Cycles Of: 180° CW Twist, 180° CCW Twist, L= 4 Meters	Avg. Δ Loss =-0.01 dB Max. Δ Loss = 0.01 dB No Visual Damage Observed @ 10 X Mag.
EIA FOTP-104 Cyclic Flexing Test	25 180° Flexes, Sheave Dia. ≤ 20 X Cable Dia., or 380 mm Avg.Δ Loss ≤ 0.10 dB	25 180° Flexes, Sheave Dia. = 350 mm	Avg. Δ Loss =-0.00 dB Max. Δ Loss = 0.04 dB No Visual Damage Observed @ 10 X Mag.
EIA FOTP-98A External Freezing Test	50 meters Test Length, Submerged in 1.2 m Dia. Tank of H_2O in an Environmental Chamber @ -10° C Until Frozen Avg.Δ Loss ≤ 0.10 dB	50 meters Test Length, Submerged in 1.2 m Dia. Tank of H_2O in an Environmental Chamber @ -10° C Until Frozen	Avg. Δ Loss =-0.00 dB Max. Δ Loss = 0.04 dB No Visual Damage Observed @ 10 X Mag.

(500 lbf/in.) for 1.5 hours instead of the required load of 440 N/cm (250 lbf/in.) for 10 minutes.

Environmental Tests: The environmental tests consist of temperature cycling, cable aging, color performance, and hydrogen in cable. Unlike the mechanical tests, the core cable by itself was not subjected to any environmental tests, since typically long length cables are used in environmental tests and long length core cable by itself is not intended to be deployed in the field.

The temperature cycling and cable aging tests were combined into a single test as shown in Figure 5. The required measurement points are labeled "M" in the figure. For temperature cycling, the change in attenuation requirement is that it shall not be greater than 0.20 dB/km, with 80% of the measured values no greater than 0.1 dB/km (first 3 "M" points). Similar requirement for aging cycle is that it shall not be greater than 0.4 dB/km, with 80% of the measured values no greater than 0.2 dB/km (remaining 2 "M" points). These change in attenuation requirements apply at 1550 nm wavelength. A 1.0 km (3280 ft) cable was used for the test. The results of the test for 1310 nm and 1550 nm wavelengths are given in Figures 6 and 7, respectively. The cable met and exceeded the above requirements at both wavelengths. Note

TABLE II. MECHANICAL TEST RESULTS FOR CORE CABLE

EIA Fiber Optic Test Procedure	Bellcore TR-TSY-000020 Requirement	Laboratory Test Level	Core Cable Performance Δ Loss @ 1550 nm
EIA FOTP-25 Impact Test	5 kg Mass, 20 Impacts @ 30 Cycles/min. Avg.Δ Loss ≤ 0.20 dB	16.0 kg Mass 20 impacts @ 30 Cycles/min.	Avg. Δ Loss = 0.01 dB Max. Δ Loss = 0.01 dB No Visual Damage Observed @ 10 X Mag.
EIA FOTP 37A High Temperature Bend Test	4 hours @ + 65°C, 4 Wraps on Mandrel Dia. ≤ 20 X Cable Dia. or 280 mm Avg.Δ Loss ≤ 0.20 dB	4 hours @ + 65°C, 4 Wraps on Mandrel Dia. = 280 mm	Avg. Δ Loss = -0.01 dB Max. Δ Loss = 0.00 dB No Visual Damage Observed @ 10 X Mag.
EIA FOTP-37A Low Temperature Bend Test	4 hours @ -30°C, 4 Wraps on Mandrel Dia. ≤ 20 X Cable Dia. or 280 mm Avg.Δ Loss ≤ 0.20 dB	4 hours @ -30°C, 4 Wraps on Mandrel Dia. = 280 mm	Avg. Δ Loss = 0.00 dB Max. Δ Loss = 0.01 dB No Visual Damage Observed @ 10 X Mag.
EIA FOTP-41 Compressive Loading Resistance Test	220 N/cm Compressive Load, 100 mm Compressive Plates, 10 minute Duration Avg.Δ Loss ≤ 0.10 dB	880 N/cm Compressive Load, 100 mm Compressive Plates, 1.5 hours Duration	Avg. Δ Loss = 0.00 dB Max. Δ Loss = 0.02 dB No Visual Damage Observed @ 10 X Mag.
EIA FOTP-85 Twist Test	10 Cycles Of: 180° CW Twist, 180° CCW Twist, L= 4 Meters Avg.Δ Loss ≤ 0.10 dB	10 Cycles Of: 180° CW Twist, 180° CCW Twist, L= 1 Meters	Avg. Δ Loss =0.00 dB Max. Δ Loss = 0.03 dB No Visual Damage Observed @ 10 X Mag.
EIA FOTP-104 Cyclic Flexing Test	25 180° Flexes, Sheave Dia. ≤ 20 X Cable Dia., or 285 mm Avg.Δ Loss ≤ 0.10 dB	25 180° Flexes, Sheave Dia. = 200 mm	Avg. Δ Loss =-0.00 dB Max. Δ Loss = 0.04 dB No Visual Damage Observed @ 10 X Mag.
EIA FOTP-98A External Freezing Test	50 meters Test Length, Submerged in 1.2 m Dia. Tank of H_2O in an Environmental Chamber @ -10° C Until Frozen Avg.Δ Loss ≤ 0.10 dB	50 meters Test Length, 1 m Exposed Core, Submerged in 1.2 m Dia. Tank of H_2O in an Environmental Chamber @ -10° C Until Frozen	Avg. Δ Loss =-0.00 dB Max. Δ Loss = 0.04 dB No Visual Damage Observed @ 10 X Mag.

that the cable was also exposed to -60°C (-76°F), which is not a requirement. The cable performed well at this temperature also.

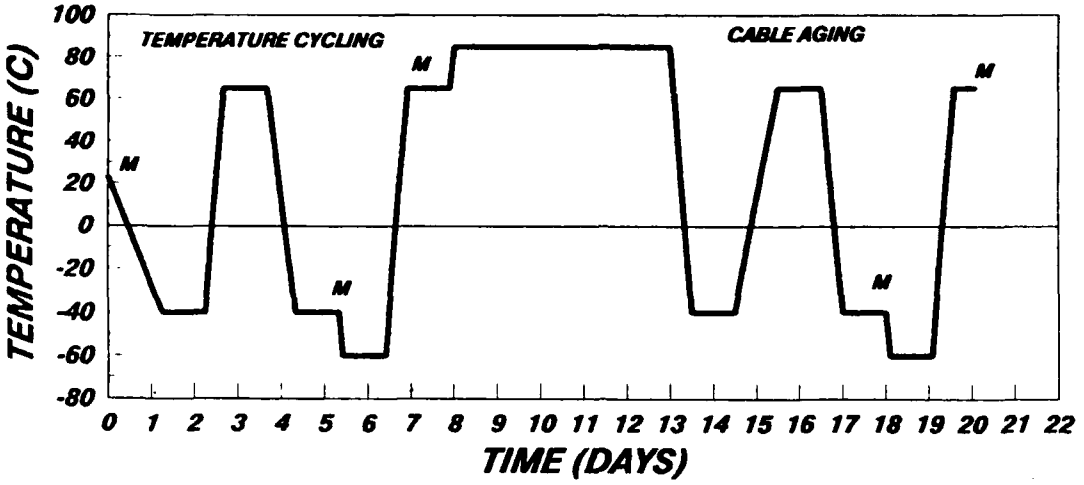
The cable also met the color performance requirement of no visual color change of the jacket marking, fiber color, or the unit color after the above temperature and aging cycle test.

For the hydrogen in cable test, a 200 m (650 ft) was used. In order to obtain sufficient measurement length, a 1600 m (5250 ft) path was created by splicing 8 fibers end to end, and two such paths were created. The cable passed the added loss requirement of ≤ 0.1 dB/km with a good margin, and the test result is presented in Table III.

Steam and High Temperature Tests

Due to the basic design concept of the metallic humidity barrier, the high temperature environment becomes a subset of the steam environment with ambient or no humidity. In other words, the core cable will experience only the temperature (and no humidity) even in a steam environment. Thus, the steam and high temperature environments are treated together for performance evaluation of the cable in these environments.

Several steam and high temperature tests were conducted to evaluate different critical components of the cable. These tests included : fiber strength evaluation for different high temperature conditions, fiber strength evaluation using Bellcore steam test (under development), Bellcore corrosion test (under development) for copper, outer jacket evaluation at high temperatures and high humidity conditions, and long-term cable aging at 140°C with attenuation measurements. Results of these tests are discussed below.



1. M = Required Measurement Point.
2. All temperature changes at a rate of 10 deg C/hour.

Figure 5. Cable Temperature and Aging Cycle

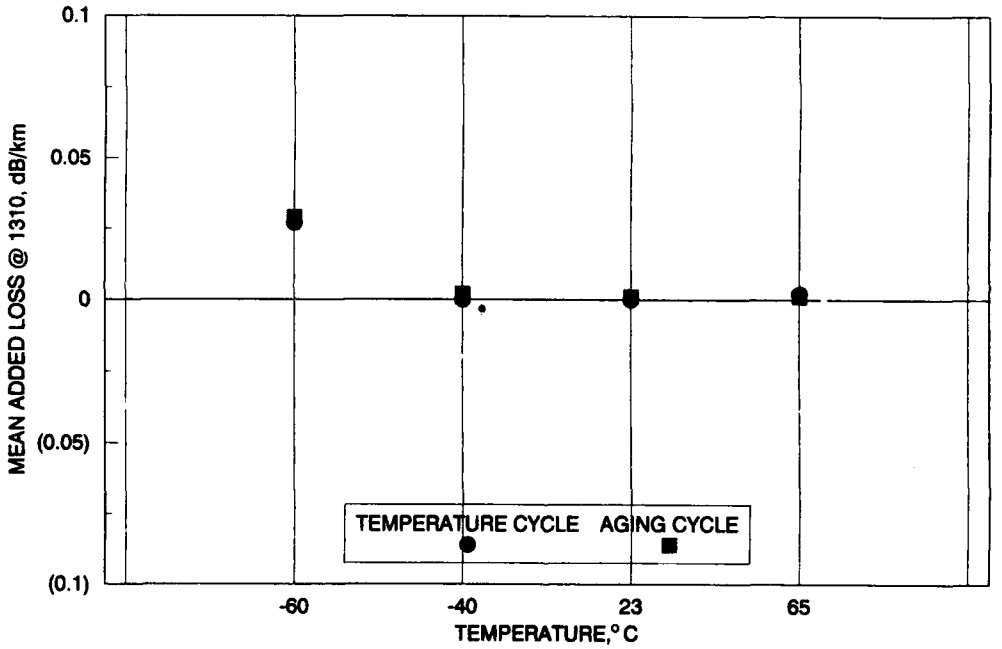


Figure 6. Cable Temperature and Aging Cycle Test Result at 1310 nm

TABLE III. HYDROGEN IN CABLE TEST RESULT

Fiber Path	Loss (dB/km) Before Test (1240 nm)	Loss (dB/km) After Test (1240 nm)	Δ Loss (dB/km) (1240 nm)
#1	1.02	1.01	-0.01
#2	2.12	2.12	0.00

Though this is a high temperature application, it was decided to use fibers and ribbons used in standard commercial applications with a maximum operational temperature of 65°C (149°F) [4,5,6] for the reason of compatibility with the rest of the network. Fibers were tested at 150°C (302°F) in air. The median strength values for 76 and 175 days of aging are given in Figure 8. The aged fiber strength values show that the fiber strength remained essentially unchanged. In order to simulate actual cable condition, fiber ribbons housed in the core tube with the filling compound were also tested. The samples were aged at 170°C (338°F) and 190°C (374°F). The median fiber strength results after aging at 170°C (338°F) for up to 171 days and at 190°C (374°F) for up to 106 days are also given in Figure 8. The figure shows that the fiber strength was not affected at 170°C (338°F) even after 171 days. At 190°C (374°F), median strength after 71 days is higher than the

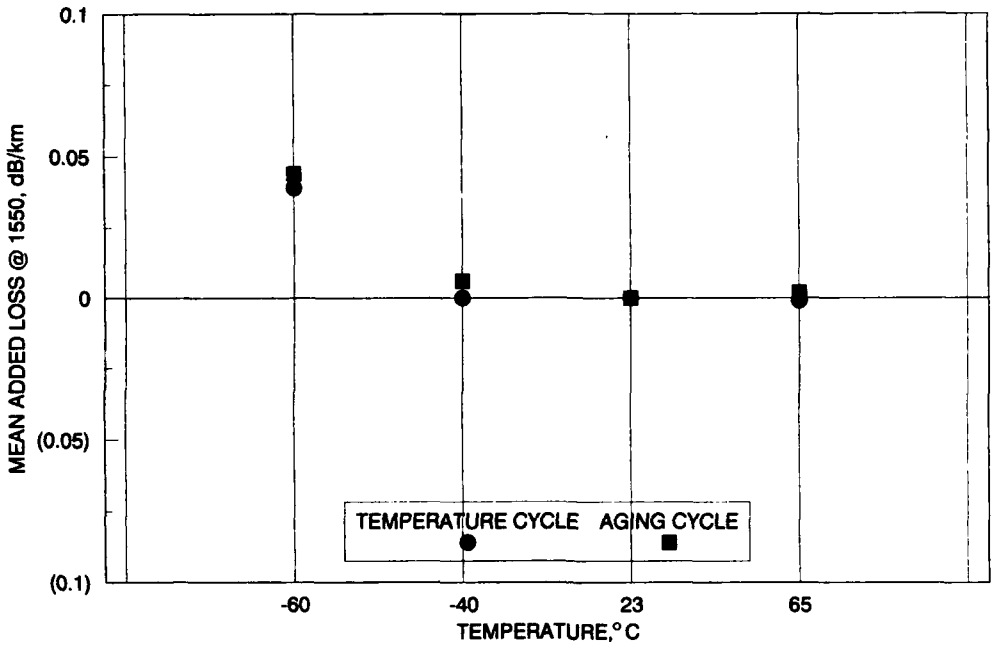


Figure 7. Cable Temperature and Aging Cycle Test Result at 1550 nm

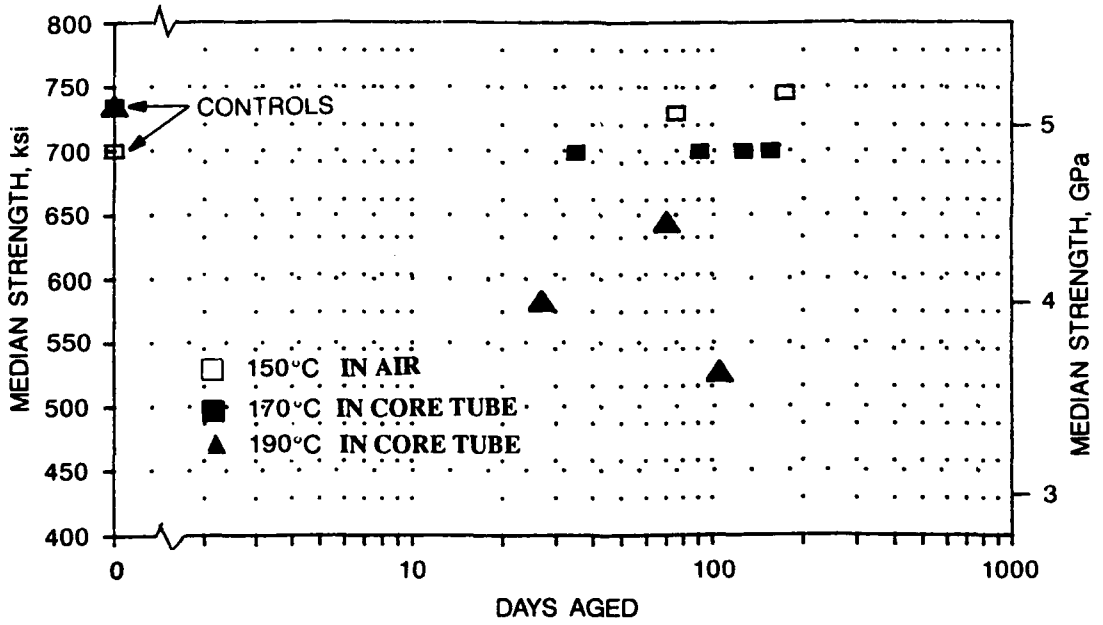


Figure 8. Strength Data of Fibers Exposed to High Temperatures

median strength after 27 days, suggesting that extrinsic factors like handling in the process of tensile testing are affecting fiber strength. In spite of the handling effect, the median strength after 106 days is 3.6 GPa (527 ksi). Note that the strength distribution is not intrinsic or real. Proctor, et al [9] did not observe any reduction in strength for uncoated fused silica fibers below 200°C (392°F).

In order to develop performance criteria for the design and development of steam resistant fiber optic cables, Bellcore is in the process of developing a new steam test [10]. In this test, cable samples, approximately 1.0 m (3.3 ft) long, were placed inside an autoclave, which generated 132°C (270°F) steam at 0.21 MPa (30 psi) pressure. Both sample ends were sealed to prevent ingress of moisture through the core of the cable. Initially, the cable ends were closed using epoxy and were subjected to the test. Cable samples were removed periodically for evaluation. Examinations by dissecting the samples showed that the closing of ends with epoxy was not effective at all, and there was significant moisture present inside the cable. However, median fiber strength values for up to 120 days shown in Figure 9, obtained by AT&T and Bellcore [10], showed only a slight drop (< 5%) in fiber strength. This means

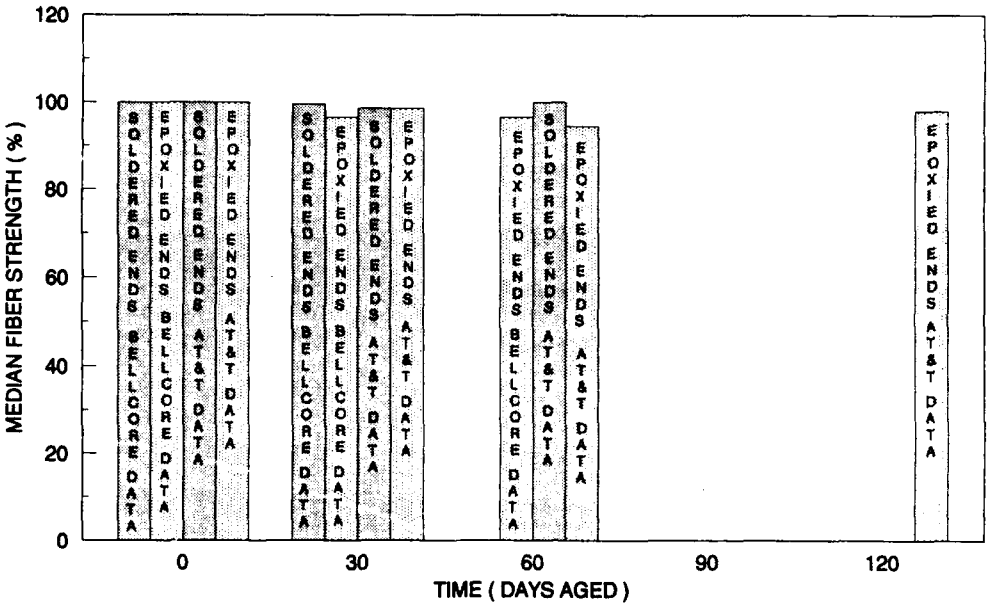


Figure 9. Strength Data of Fibers Exposed to Bellcore Steam Test

that even with practically non-closed ends, the performance of the fiber is excellent. The tests are being repeated with soldered ends and the results are given in Figure 9 for up to 60 days. In this case, there was no observable drop in strength at all.

Since the metallic humidity barrier is very susceptible to corrosion in steam environments, Bellcore is also in the process of developing a corrosion test [10]. This test consists of exposing cable samples to fine sand wet with 3.5% sodium chloride solution for 30 days at 135°C (275°F) in an autoclave. The samples were then examined for any cracks, perforations or pits. The cable samples had no measurable copper surface degradation showing excellent corrosion performance.

Unlike the components inside the metallic humidity barrier, the cable outer jacket will be exposed to very high humidity along with the temperature. Two approaches are possible for the selection of outer jacket material selection, and yet maintain the same performance levels of materials inside the copper humidity barrier. One approach would be to choose a HDPE, in which case the jacket will be a sacrificial member. The second approach is to choose a material from the fluoropolymer family. One such material was chosen and was subjected to aging conditions at different temperatures with and without water vapor concentration. The fluoropolymer jacket material showed only small changes in material elongation, indicating good performance when exposed to either steam or high temperature environments. These data are presented in Figure 10.

In order to simulate long-term exposure of cables to steam in the field, a test was devised wherein a small portion of a 1.0 km (3280 ft) cable, about 20 m (65 ft), is being to exposed to 140°C (284°F). The current plan is to conduct this long-term exposure for 6 months, and possibly a year. The change in attenuation values have been obtained for 30 days so far, and the results are presented in Table IV.

Other Hostile Environment Tests

The cable's performance characteristics in the other hostile environments are discussed next. The cable was not tested for all of these hostile environments. Whenever tested, the results are reported. Whenever not tested, rationales are provided to substantiate the capability of the cable to perform in such hostile environments.

Petroleum Products : - Typical hostile fluids requirements can be found in EIA/TIA Fiber Optic Test Procedure-12A or military cable specification [11]. In general, these requirements are met by using thermoset (radiation crosslinked or continuous vulcanization) materials. The copper barrier in the current cable design provides an excellent protection from these fluids by sealing them out of the core cable.

Chemicals : - As in the case of "petroleum products" above, the copper barrier also provides excellent protection from chemicals by sealing them out of the core cable.

Corrosion : - The cable's corrosion performance was already discussed under the steam and high temperature tests using the

TABLE IV. 140°C (284°F) LONG-TERM AGING TEST RESULTS

Number of Days	Added Loss, dB					
	1310 nm Wavelength			1550 nm Wavelength		
	Mean	Std. Dev.	Max.	Mean	Std. Dev.	Max.
5	0.00	0.02	0.04	0.00	0.01	0.04
30	0.00	0.01	0.03	0.00	0.01	0.03

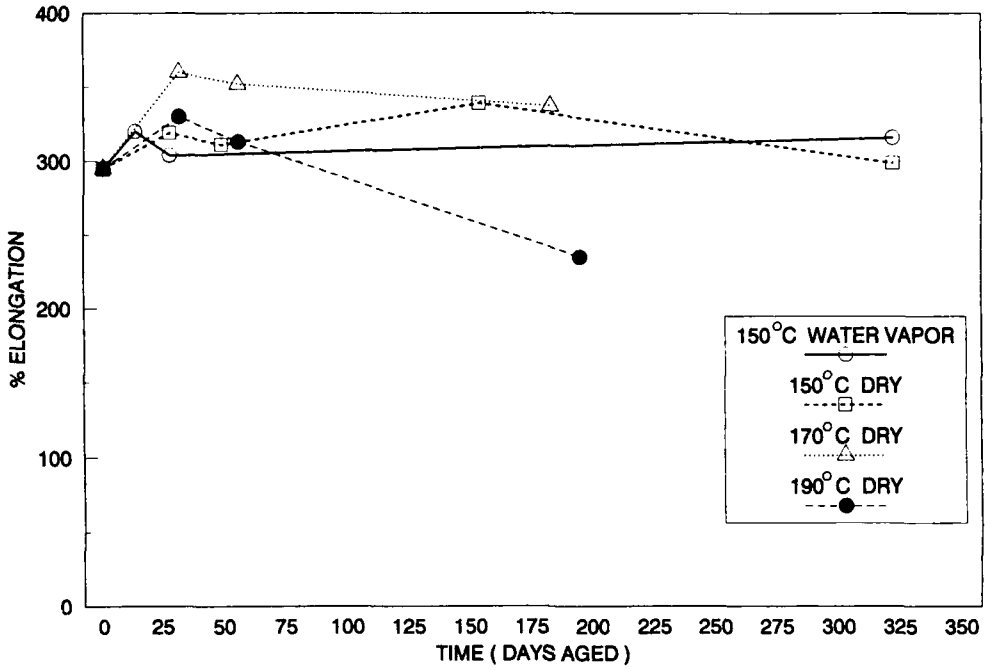


Figure 10. Elongation of Fluoropolymer Material Exposed to High Temperatures and High Humidity

Bellcore devised corrosion test, which is also considered to be a stringent test.

Hydrogen : - The copper barrier, once again, seals any hydrogen molecules out of the core cable and protects the fiber. In addition, since the core cable does not use any fluoro- and sulfone based polymers, no hydrofluoric or sulfuric/sulfonic acid is generated, which in turn could react with the metal to generate hydrogen. Also, among copper, stainless steel, low carbon steel, and aluminum, copper is known to be the best, and aluminum is the worst in terms of hydrogen generation. Also, note that the hydrogen in cable test result was presented above in the standard Bellcore tests section.

Lightning : - Bellcore requires [8] a lightning damage susceptibility test with a current of 105 kA. The cable was tested to a current of 225 kA. The cable passed the test making it one of the best in terms of lightning performance.

Rodents and Insects : - The Denver Wildlife Research Center of the U. S. Department of Agriculture, as a part of their research efforts, evaluate the performance of the cable exposed to one of the most aggressive rodents, the pocket gopher. They rate the cable from 0 (no damage) to 5 (cable severed). A rating of 2 (outer jacket penetrated) or below is considered good and an acceptable performance of the cable. The current cable has a rating of 1.8. No specific test was conducted for insects.

Shallow Water : - While this cable is not suitable for deep water applications like submarine cable, it can be used for shallow water applications where the water is a few hundred feet deep, a few thousand feet long and no boat traffic, and for locations where there is potential for flooding.

Underground Installation Tests

The cable was subjected to a set of underground installation tests. The tests conducted were : grip test, duct test, sheave test, ultimate strength test, luffing test, and figure 8 test. Results of the tests are summarized below.

Grip Test - The cable was first gripped using a Kellems® grip applied over the outer jacket for a length of 0.46 m (18 in.) as shown in Figure 11(a) and was subjected to a load of 2.9 kN (650 lbf). The cable was unable to hold the load because of the stretching of the copper tube and the outer jacket. A length of the outer jacket and the copper tube was then removed to expose the core cable. A Kellems® grip for the diameter range [illegible] to 16 mm (0.5 to 0.625 in.) was used to grip the core cable as shown in Figure 11(b). The cable was loaded to 5.3 kN (1,200 lbf)—twice the rated maximum load—and held at that load for several hours. The load was then increased to 11.1 kN (2,500 lbf) and held at that load for 30 minutes. The cable withstood the loads without any problems.

The gripping arrangement was then slightly modified to grip the core cable along with a short length of the outer jacket as shown in Figure 11(c). This arrangement provides a relatively smooth change in diameter at the leading end of the outer jacket. The cable was loaded to 11.1 kN (2,500 lbf) and held there for 90 minutes without any damage. From this test, it is recommended that the gripping method shown in Figure 11(c) be used in the field, though the method shown in Figure 11(b) can also be used if the outer jacket is taped to provide a smooth transition behind the grip.

Underground Duct Test - In this test, the cable was pulled through an underground duct system with a wall-to-wall duct length of about 150 m (500 ft). The duct system has a total of about 960° of bend. The duct is smooth-wall PVC with an

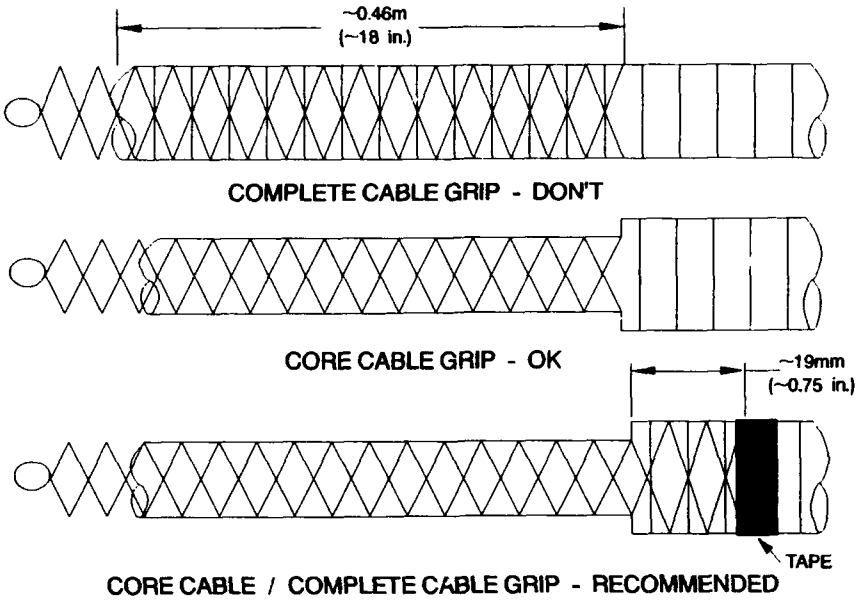


Figure 11. Cable Gripping Method for Underground Installation

inner diameter of about 31.8 mm (1.25 in.). The cable was pulled three times into the duct system, and no damage to the cable or fibers was observed. The loads during these three pulls ranged from 2.6 to 4.4 kN (580 to 1,000 lbf).

In a field trial at Boston [12], a 900 m (3000 ft) cable was installed successfully in a duct system where the first 660 m (2200 ft) had a 31.8 mm (1.25 in.) inner diameter duct and the remaining 240 m (800 ft) had a 25.4 mm (1.0 in.) inner diameter duct. The cable, however, is recommended to be installed in 31.8 mm (1.25 in.) inner diameter duct systems only.

Sheave Test - During the retrieval of the cable from the duct system after the underground duct tests, almost the entire cable length was pulled around two sheaves 0.6 m (24 in.) in diameter. In addition, a separate sheave test was conducted by pulling the cable over a 0.46 m (18 in.) sheave under a load of 3.3 kN (750 lbf). Neither cable nor fiber damage was observed.

Cable Ultimate-Strength Test - Using the grip method of Figure 11(c), both virgin cable and the cable section that had been subjected to the above sheave tests were loaded to failure in tension. The values had a wide range between 10.9 kN (2,400 lbf) and 16.7 kN (3,750 lbf). There was no significant strength difference between the virgin and sheave tested samples.

Luffing Test - Luffing is used to position a cable in its proper place in an underground manhole and requires the use of a split grip attached to the cable. In the test, the cable was first pulled about 1.2 m (4 ft) with a load of about 3.1 kN (700 lbf). Next, the cable was pulled about 0.6 m (2 ft) with a load of about 4.4 kN (1,000 lbf). In both cases, the cable performed well with no damage.

Figure 8 Test - Like other standard cables, the hostile environment cable was also placed in a figure 8 configuration during some of the above underground installation tests.

Cable-Air Installation System Tests

Though blowing-in of fibers using air pressure in small tubes has been in practice for several years, the use of such techniques to blow cables in duct systems [13] is gaining popularity in the past couple of years or so. The hostile environment cable was tested using one such technique and the results were as follows [14]. In a duct system with approximately 3000° of total angular turns, a 700 m (2300 ft) cable was blown-in 19.5 minutes, resulting in 36 m/min (118 ft/min). In the second test, a 915 m (3000 ft) cable was blown-in in a duct system with approximately 1500° total angular turns in 15.5 minute, yielding a speed of 59 m/min (194 ft/min). In both cases, the inner diameter of the smooth-walled duct was 31.8 mm (1.25 in.). The time required by the cable-air installation system to install a given length of cable is significantly lower when compared with the classical underground installation technique discussed above, offering a good potential for increased productivity.

In a field trial at Manhattan, New York, an 800 m (2600 ft) cable was installed in a 31.8 mm (1.25 in.) inner diameter smooth-walled duct system with approximately 1000° total angular turns in 13 minutes, yielding a speed of 62 m/min (200 ft/min) [15].

CONCLUSION

Commonly encountered outside plant hostile environments, their severity and significance, and a fiber-optic cable capable of surviving these environments were presented. The cable was subjected to a battery of standard Bellcore tests, hostile environment tests, and underground installation tests, and the results were also presented. The cable met and often exceeded the requirements with excellent margins.

ACKNOWLEDGEMENTS

The authors gratefully acknowledge the contributions of Messers J. J. Blee, H. C. Chandan, H. P. Debban, D. W. Gibson, A. L. Hale, N. E. Hardwick, III, J. T. Krause and N. W. Sollenberger, and several other members of AT&T Bell Laboratories and AT&T Network Cable Systems.

REFERENCES

1. Maddali, P. S. V., "Technical Presentation on Steam Problems", Presented to the Telecommunication Wire and Cable Standard Technical Advisory Committee, May, 1990, New Orleans, LA.
2. Hardwick, N. E., Kathiresan, K. and J. G. Hartley "Analyses of Fiber Optic Cable Design Conditions in the Vicinity of Steam Line - Ruptured and Pristine", Proceedings of the 41st International Wire and Cable Symposium, November 16-19, 1992, Reno, Nevada.
3. Arroyo, C. J., Jenkins, A. C., Patel, P.D., and Panuska, A. J., "A High Performance Nonmetallic Sheath for Lightguide Cables", Proceedings of the 36th International Wire and Cable Symposium, November, 1987, Arlington, VA, pp. 344-349.
4. Shea, J. W., Turnipseed, J. M., Taylor, C. R., Petisce, J. R., and Overton, B. J., "Characterization of Critical Parameters of Optical Fiber Coatings", Proceedings of the Materials Research Society, 1991, Boston, MA.
5. Cottingham, C. F., and Michie, M. M., "New Coatings Eliminate Fiber Surprise", *Telephone Engineer and* Management, November 15, 1991.
6. Jackson, K. W., Patel, P. D., Pearsall, M. L., and Lochkovic, G. A., "An Enhanced Ribbon Structure for High Fiber Count Cables in the Loop", Proceedings of the 38th International Wire and Cable Symposium, November, 1989, Atlanta, GA, pp.569-574.
7. Kathiresan, K., Panuska, A. J., Shea, J. W., Chandan, H. C., and Carlton, L. T., "A Steam Resistant Fiber-Optic Cable", Proceedings of the 8th Annual National Fiber Optics Engineers Conference, Vol. I, April 21-24, 1992, Washington, D. C.
8. Bellcore Technical Reference TR-000020, "Generic Requirements for Optical Fiber and Optical Fiber Cable", Issue 4, March, 1990.
9. Proctor, B. A., Whitney, I., and Johnson, J. W., "The Strength of Fused Silica", Proceedings of the Royal Society, Vol. 297A, 1966, pp. 534-557.
10. Yuce, H. H., Bellcore, Private Communication.
11. Military Specification MIL-C-85045E, "General Specification for Fiber Optics Cables (Metric)", May, 1992.
12. McCabe, B., New England Telephone Company, Private Communication.
13. Plumettaz, G., and Orr, R. E., "Fiber-Optic Cable Installation Method", Proceedings of 1992 ICC Transnational Technologies Meeting (Insulated Conductors Committee), Paper No. 19, July 20-24, 1992, Birmingham, England.
14. Orr, R. E., Sherman & Reilly, Inc., Private Communication.
15. Neville, P., New York Telephone Company, Private Communication.

Kris Kathiresan is a Distinguished Member of Technical Staff in the Fiber Optic Cable and Materials Development and Engineering Department at AT&T Bell Laboratories in Norcross, Georgia. He is responsible for the design and development of outside plant fiber-optic cables. Prior to his current assignment, he was responsible for the design and development of military and specialty fiber-optic cables. Dr. Kathiresan joined AT&T Bell Laboratories in 1985. He has a B. E. Hons in Mechanical Engineering from University of Madras, India, an M. E. in Aerospace Engineering from Indian Institute of Science, India, and a Ph. D. in Engineering Science and Mechanics from Georgia Institute of Technology, Atlanta, Georgia. Dr. Kathiresan is a Senior Member of AIAA and a Member of ASME. He is a registered Professional Engineer (Mechanical) in the States of Georgia and Florida.

Andrew J. Panuska is a Member of Technical Staff with AT&T Network Cable Systems in Norcross, Georgia. He received B. S. Degrees in Mechanical Engineering and Civil Engineering from the John Hopkins University. He joined AT&T in 1963 on the Ocean Cable Project and in 1969 was assigned to copper cable sheathing and jacketing. Since 1979, he has worked in the Fiber Optic Cable Development Department responsible for the development of fiber optic cable products and processes.

John W. Shea received a B.S. in Chemistry from King's College, Wilkes-Barre, PA and an M.S. in Physics from the University of Notre Dame. After 10 years as a resin chemist with Union Carbide Corporation, he joined AT&T Bell Laboratories in 1967. He has worked in the areas of printed circuit materials, injection molding, and extrusion. For the last several years he has been involved in optical fiber coatings and cable materials.

William H. Ficke is the Supervisor of the Fiber Optic Cable Qualification Laboratory in the Premises and Specialty Cable and Measurements Group at AT&T Bell Laboratories, Norcross, Georgia. He is responsible for the mechanical and environmental qualification and development testing for Outside Plant, Premises, Specialty, and Military Fiber Optic Cables. He joined AT&T in the Copper Cable Development Engineering Department in 1972. He has an AAS degree in Aeronautical Engineering from New York State University.

Manuel R. Santana is Supervisor of the Outside Plant Cable Group with research and development responsibility for fiber-optic cables used in the outside plant. He has been involved in research and product development in fiber-optic cable and he has been awarded nine patents and has twenty-five publications to his credit.

Mr. Santana joined AT&T Bell Laboratories in 1970, having received his B.S.E.E. from University of Hartford, and M.S.E.E. from Georgia Institute of Technology. He is a Senior Member of the IEEE.

Carl R. Taylor is currently Supervisor of the Materials Technology and Quality Group at AT&T's main Fiber Optics Manufacturing site in Atlanta. The group has the responsibility for the design and engineering of materials used in fiber optic cable and apparatus products as well as responsibility for the quality of all incoming materials and components. He has previously been Supervisor of the Plastics Engineering and Characterization Group in Atlanta, and Supervisor of the Polymer Materials Research, Engineering, and Applications Group in Murray Hill. Prior to joining Bell Laboratories in 1977, he earned a B. S. in Chemistry from the College of Wooster in Ohio and a Ph. D. in Physical Chemistry from the University of Wisconsin in Madison. His graduate work focussed on the physical and viscoelastic properties of polymers. He holds twelve patents and has authored/co-authored 25 publications.

Laurie T. Carlton is a Senior Product Planner with AT&T Network Cable Systems with product management responsibilities for a number of fiber optic cable products including the Hostile Environment Cable. Laurie has worked in the field of fiber optics for 12 years. Laurie started her career with Western Electric in 1980 as a development engineer for fiber optic connectors. Laurie received a BSEE degree from the Georgia Institute of Technology in 1980, and an MBA degree from the Georgia State University in 1985.

POLARIZATION MODE DISPERSION OF SINGLE MODE AND DISPERSION SHIFTED FIBERS

Y. TERASAWA , Y. KUBO , Y. SUETSUGU , S. TANAKA

SUMITOMO ELECTORIC INDUSTIES, LTD.

1 TAYA-CHO, SAKAE-KU, YOKOHAMA, 244 JAPAN

Abstract

The polarization mode dispersion (PMD) characteristics of single mode fiber and dispersion shifted fiber were measured. The dependency of polarization mode dispersion on fiber length was found to be proportional to the square root of the fiber length, as was known previously, and the temperature dependency was not detected from -20 °C to 60 °C and good stability was confirmed for fiber.

1.Introduction

In recent years, with the development of optical fiber amplifier technology, ultra-long length, high bit rate optical transmission over several thousand kilometers is becoming a possibility. At the same time, as an accompaniment to improvements in the manufacturing technology for optical fibers, it is anticipated that chromatic dispersion will be compensated by improving the controllability of chromatic dispersion and tuning the operating wavelength to the zero dispersion wavelength of the total system length.

However, due to the use of no-repeater systems, polarization mode dispersion, which has conventionally been ignored, must now be regarded as a problem. The reason is that polarization mode dispersion, which can be ignored with a repeater span interval of about 100 km, accumulates in a no-repeater system of several thousand kilometers. This has a harmful effect on the transmission signal.

Previously the relationship between core non-circularity and polarization mode dispersion was well known[1], but optical parameter except core non-circularity or environment dependency have not yet clarified. Correlations between polarization mode dispersion fiber parameters and changes in the value of polarization mode dispersion according to fiber state are described in this paper.

2. Theory

With ordinary axisymmetric single mode fiber, it is actually possible for two polarized modes to propagate in two directions orthogonally (in the x direction and the y direction) in the fiber cross section. If the fiber structure is truly axisymmetrical, and if the fiber is not under any stress, these two orthogonal polarized modes will exhibit exactly the same group delay, and thus no dispersion will arise. However, if birefringence arises due to stress resulting from non-circularity of the core, bending, twisting, pressure, or tension, group delay will appear between the two modes, giving rise to polarization mode dispersion.

A schematic diagram of our polarization mode dispersion measurement system is shown in Figure 1. The measurement principle is the same as that of the Michelson interferometer[1].

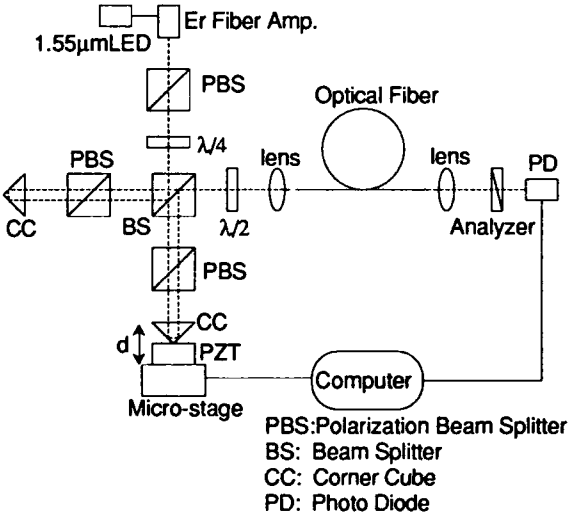


Figure 1 Schematic diagram of experimental set up

The polarization mode dispersion τ can be expressed with the following formula if the optical path difference $L_0 = 2d$ (d:movement of micro-stage) is obtained for the condition where the difference in group delay time between the two orthogonal polarized modes due to this interference pattern is zero.

$$\tau = L_0 / c = 2d / c \qquad \text{(c: velocity of light)}$$

3. Experimental Results

Measurement of polarization mode dispersion was performed using the measurement system shown in Figure 1 in order to study the correlations between various parameters.

3.1 Refractive index design

We compared the polarization mode dispersion of single mode fiber for conventional 1.3 μm use to that of dispersion shifted fiber. Representative parameters for each fiber are shown in Table 1. The profile of single mode fiber for 1.3 μm use is of the step index type, and its refractive index difference is 0.34 %. In contrast, dispersion shifted fiber is of the dual shape core type, and its refractive index difference has a peak value of 0.95 %.

Table 1 Representative parameters

Fiber	Profile	Δn	MFD	λ0
1.3μm SM		0.34%	9.5μm (@1.3μm)	1.3μm
DSF		0.95% (peak)	8.0μm (@1.55μm)	1.55μm

Figure 2 shows the polarization mode dispersion characteristics of the two fiber types. Fiber length dependency is also examined in the figure. Two samples of each type were measured using a fiber measurement length of 10 km. The same fibers were then divided into 1 km sections and measured again.

A comparison of the two types shows that dispersion shifted fiber has slightly greater polarization mode dispersion. The cause of this is considered to be a more complex profile resulting from a greater refractive index difference. The dependency of PMD with regard to length was found to be proportional to the square root of the length, as has been reported before[1][2][3].

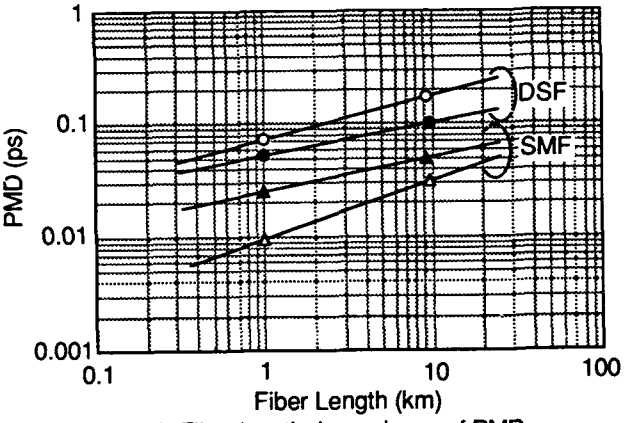


Figure 2 Fiber length dependence of PMD in single mode fiber (SMF) and dispersion shifted fiber (DSF)

3.2 Mode field diameter (MFD)

The correlation between PMD and MFD was studied for dispersion shifted fiber. MFD was varied from 7.3 to 8.7 μm, as stipulated in CCITT Recommendation G653. However, the result was that no particular correlation was discovered, as is indicated in Figure 3.

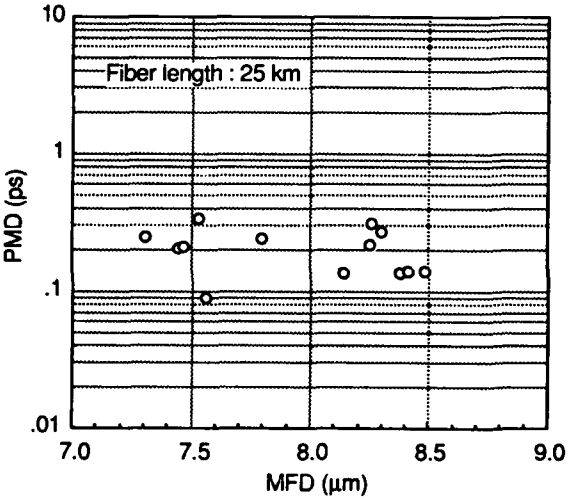


Figure 3 Relationship between PMD and MFD

3.3 Eccentricity

The correlation between PMD and eccentricity was studied for dispersion shifted fiber. The samples were selected at random from mass-produced dispersion shifted fibers. Figure 4 shows the results. No correlation to PMD was found for fibers with eccentricity of 0.7 μm and below.

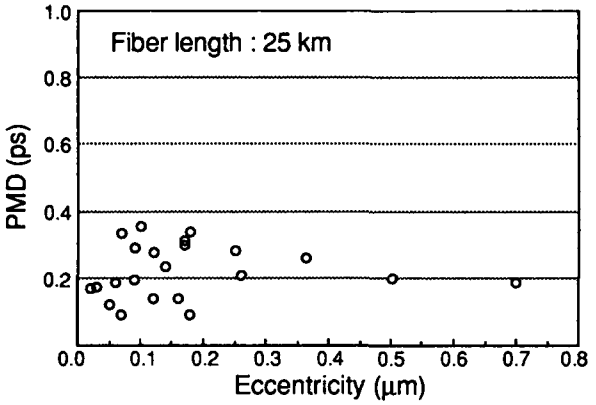


Figure 4 Relationship between PMD and eccentricity

4. Various experiments

To investigate PMD characteristics, various experiments were performed using single-mode and dispersion shifted fiber.

4.1 Spool tension

It might be considered that the value of polarization mode dispersion is determined by the external force added from the outside.

Thus, the dependency of PMD on spool tension was studied by varying the spool tension of a bobbin. The diameter of the bobbin was 280 mmϕ, and the sample fiber length was 10 km. Figure 6 shows the results of PMD measurement when the tension was varied from 40 to 100 g.

In addition to spool tension dependency, we examined the tension dependency using the bobbin wound sandpaper. The using bobbin diameter was 280mmϕ, wound sandpaper (#260) around. Then 400 m sample dispersion shifted fiber was wound around that bobbin at 200 g tension.

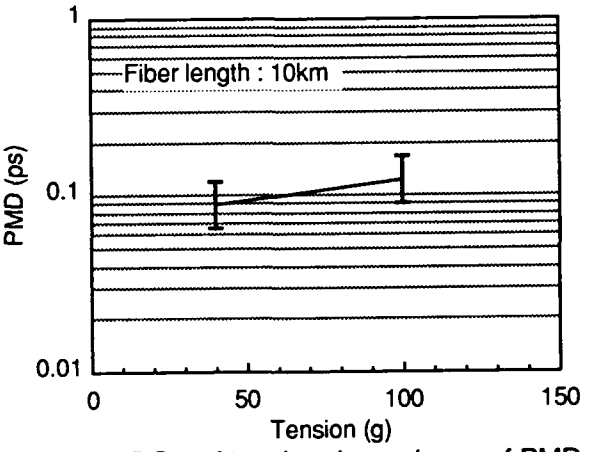


Figure 5 Spool tension dependence of PMD

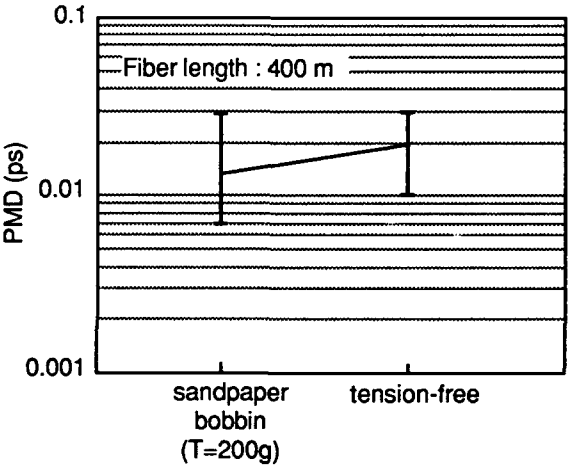


Figure 6 Result of sandpaper bobbin expriment

The attenuation in sandpaper spool state was 0.20 dB/km at 1.55 μm, and then loss was 0.76 dB/km in tension-free state. The results are shown in Figure 6.

There was no correlation between spool tension and PMD within the range of tension and sandpaper measured in the experiment, showing that there is no relationship between spool tension and PMD.

4.2 Splices

When fiber is used for long distance applications such as optical submarine cable, the use of fiber splices is an extremely important matter. For this reason, it might be considered that total polarization mode dispersion varies according to the axial directions of each of the fibers at the splice points.

To confirm this, polarization mode dispersion was measured while rotating two fibers (fiber A and B) in relation to the polarized axis (see Figure 7). The results are shown in Figure 8. Each fiber length was 10 km. It was found that there was splice angle at which polarization mode dispersion after splice was smaller than initial polarization mode dispersion. According to the experiment, it may be possible that PMD after splice is smaller than the sum of each fiber's PMD.

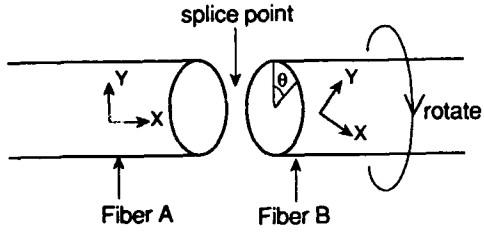


Figure 7 Experimental set up of splice

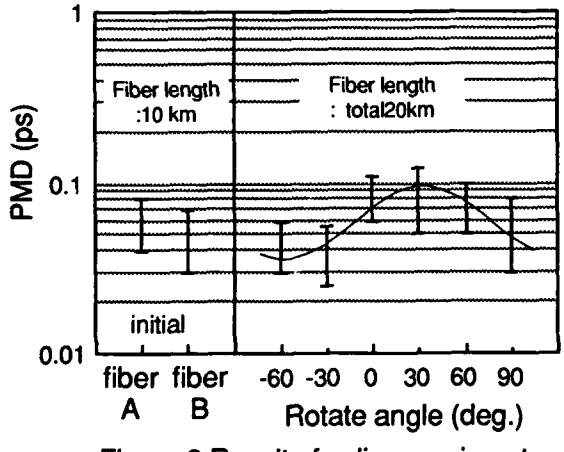


Figure 8 Result of splice expriment

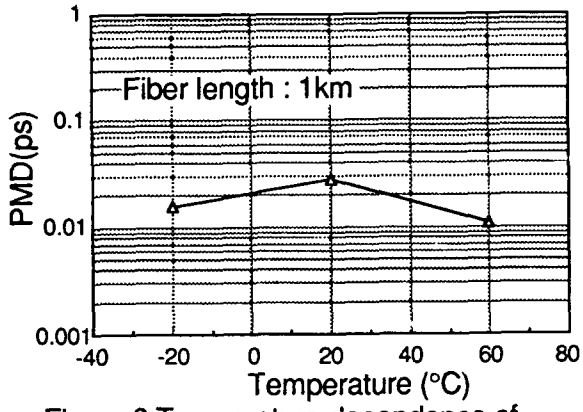


Figure 9 Temperature dependence of PMD in single mode fiber (SMF)

4.3 Temperature

When cables and the like will be exposed to outside environment, it is important to examine the temperature dependency of the fiber characteristics. Therefore, we studied the temperature dependency of polarization mode dispersion. The sample single mode fiber length was 1 km. Samples in a tension-free state were placed in a thermostatic chamber, and polarization mode dispersion was measured while varying the temperature from -20 °C to 60 °C. The results are shown in Figure 9. According to the experiment, temperature dependency of polarization mode dispersion was not detected from -20 °C to 60 °C and good stability was confirmed for the single mode fiber.

5. Conclusion

The polarization mode dispersion of optical fibers was studied, centering on dispersion shifted fiber. No clear correlation was found between polarization mode dispersion and optical parameters such as MFD. And the temperature dependency was not detected from -20 °C to 60 °C and good stability was confirmed for fiber.

Reference

[1] C.D.Poole, "Measurement of polarization mode dispersion in single-mode fibers with randam mode coupling", Opt.Lett.,vol.14,No.10,1989

[2] Y.Namihira, etal., "Fiber length dependence of polarization mode dispersion measurement in long-length optical fibers and installed optical cable", J.Opt.Comm., vol.12,1991

[3] M.Tsubokawa, etal., "A consideration of polarization dispersion determining from a Stokes parameter evaluation", J.LT.,vol.9,No.8,1991



Yoshiaki Terasawa

Sumitomo Electric
Industries, Ltd.

1, Taya-cho, Sakae-ku
Yokohama, Japan

Yoshiaki Terasawa was born in 1961 in Hokkaido, Japan. He received the B.S. and M.S. degree in applied physics from Hokkaido University in 1985 and 1987, respectively.
He joined Sumitomo Electric Industries, Ltd. in 1987 and engaged in research and development of optical fiber cable. Mr. Terasawa is a member of Communication R&D Development in Yokohama Research Laboratories.



Yoshiyuki Suetsugu

Sumitomo Electric
Industries, Ltd.

1, Taya-cho, Sakae-ku
Yokohama, Japan

Yoshiyuki Suetsugu was born in 1961 and received the B.S. degree from Tsukuba University in 1984.
He joined Sumitomo Electric Industries, Ltd. in 1984 and engaged in research and development of optical fiber cable. Mr. Suetsugu is a member of Institute of Electronics, Information and Communication Engineers of Japan.



Yuji Kubo

Sumitomo Electric
Industries, Ltd.

1, Taya-cho, Sakae-ku
Yokohama, Japan

Yuji Kubo was born in 1962 in Hokkaido, Japan. He received the B.S. and M.S. degree from Hokkaido University in 1985 and 1987, respectively.
He joined Sumitomo Electric Industries, Ltd. in 1987 and engaged in research and development of optical fibers in Fiber Optic Division. Mr. Kubo is a member of Institute of Electronics, Information and Communication Engineers of Japan.

Shigeru Tanaka

Sumitomo Electric
Industries, Ltd.

1, Taya-cho, Sakae-ku
Yokohama, Japan

Sigeru Tanaka was born in 1951 in Tokyo, Japan. He received the B.S. and M.S. degree from Tokyo University in 1974 and 1976, respectively.
He joined Sumitomo Electric Industries, Ltd. in 1976 and has been engaged in the design and characterization of optical fibers and fiber cables. He is a Chief Research Associate of Communication R&D Department. Mr. Tanaka is a member of Institute of Electronics, Information and Communication Engineers of Japan.

Fiber strain measurement in optical cables employing Brillouin gain analysis

M.Kamikatano H.Sawano M.Miyamoto N.Sato

Fujikura Ltd.

ABSTRACT

Brillouin scattering in optical fibers is one of the nonlinear phenomena in which an incident light interacts with an acoustic wave in the fiber and is scattered, shifted in frequency by an amount equal to a frequency that is intrinsic to the medium. Horiguchi et al.[1][2] suggested that optical fiber strains can be determined with high accuracy by measuring the Brillouin gain spectra using the pump probe method. Longitudinal strain distributions can also be measured by using a pulsed light.

In this study, we measured the Brillouin gain spectra using a continuous wave (cw) laser and made a basic evaluation of strains applied to optical fibers under various conditions, particularly for ribbon type cables.

INTRODUCTION

1) Principle

Brillouin scattering is a phenomenon in which an incident light propagating in a medium is scattered, shifted in frequency by an amount equal to a frequency that is intrinsic to the medium. For single-mode optical fibers, the frequency shift of the backward scattered light, ν_B, is expressed as shown below. The incident light is scattered by an acoustic wave (phonon), and its frequency changes(Doppler shift) by an amount equal to the intrinsic frequency, ν_B, of the fiber.

$$|\nu_B| = \frac{2nV_a}{\lambda} = \frac{2V_a}{(C/n)} \qquad (1)$$

$$V_a = \sqrt{\frac{E(1-\kappa)}{\rho(1+\kappa)(1-2\kappa)}} \qquad (2)$$

where Va, n, λ, c, ρ, E and κ are the acoustic wave velocity, refractive index, wavelength of the incident light, velocity of light, density, Young's modulus, and Poisson's ratio in fibers, respectively. For optical fibers, it has been shown that the amount of change in ν_B, $\Delta\nu_B$, is most susceptible to stress-induced strains applied to fibers, and is proportional to this strain if limited to a small value. Strain measurements can be made with a resolution of 10^{-4} and higher. Because the intensity of the Brillouin-scattered light in single-mode fibers is very low compared to the Brillouin gain spectra by the pump-probe method using frequency-variable lasers, which utilizes Brillouin light amplification, we used the pump-probe method to evaluate stress-induced strains applied to fibers.

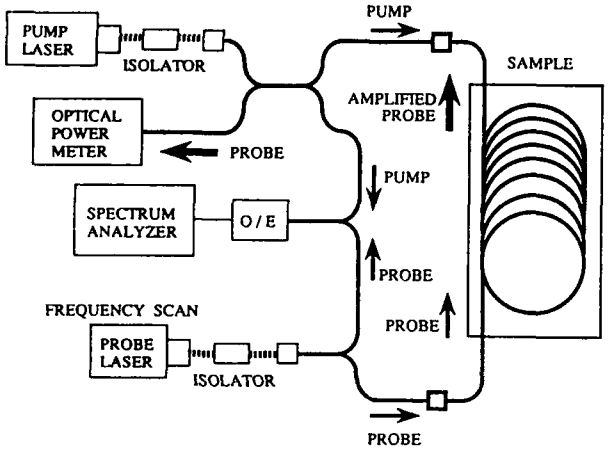
2) Measuring System

Fig.1 shows the measuring system. For both light sources, we used a frequency-variable, cw LD-excited YAG laser with a wavelength of 1319 nm and a spectrum width of 5 kHz. The input power into the fiber is of the order of 5 mW for the pump laser and 0.2 mW for the probe laser. The frequency of the probe laser is scanned until the difference between these two lasers frequencies becomes equal to the value of the Brillouin shift for the fiber medium . At that time, a probe laser light, starting at the opposite end of the fiber from the pump laser, is amplified to the maximum level. The amplified light is split by a fiber coupler and measured using an optical power meter. To determine the laser frequency difference, both laser lights are mixed by a fiber coupler and the beat frequency of the mixed iight is measured using a spectrum analyzer (bandwidth: 22 GHz). The bandwidth of the Brillouin gain observed with ordinary single-mode fibers is about 30-50 MHz in the 1.3 μm

region when the Brillouin shift, ν_B, is of the order of 13 GHz.

Longitudinal strain distributions can also be measured by using pulsed light as the light source. This method is called "BOTDA"[3] (Brillouin Optical-fiber Time Domain Analysis) However, the bandwidth of the Brillouin gain is narrow as described above, so the distance resolution is 10m or more, for measuring the fiber strain at an accuracy of about 10^{-4} . It is better to use cw light than pulsed light to estimate the strain of the short fiber or to estimate short range strain distribution. Therefore, we made measurements with the cw light only.

Fig.1 MEASUREMENT SYSTEM



MEASUREMENT

1) Fiber parameter dependence

To measure the tensile strain, it is necessary to know the value of ν_{Bo}, which is the Brillouin shift in the unstressed condition.

If we can obtain the value of ν_B from fiber parameters only, it is then very easy to predict the fiber strain under various conditions.

We have measured bundled fibers and ribbons, and we believe that they have no initial strain.

Fig.2 shows MFD dependence of ν_{Bo}. Fig.3 shows Δn dependence of ν_{Bo}.

The MFD dependence shows weakly positive correlation, and the Δn dependence shows weakly negative correlation, but each data vary widely

In formula (1), refractive index n, density ρ, etc., are major factors that determine the Brillouin shift, so possible causes for the lack of the relation with refractive index difference Δn are:

a. Residual strain at fiber drawing.
b. Δn measuring accuracy.
c. Stresses acting between fibers and coating material.

When we evaluate the fibers' strain, we have to measure the initial Brillouin shift of the light in the fibers.

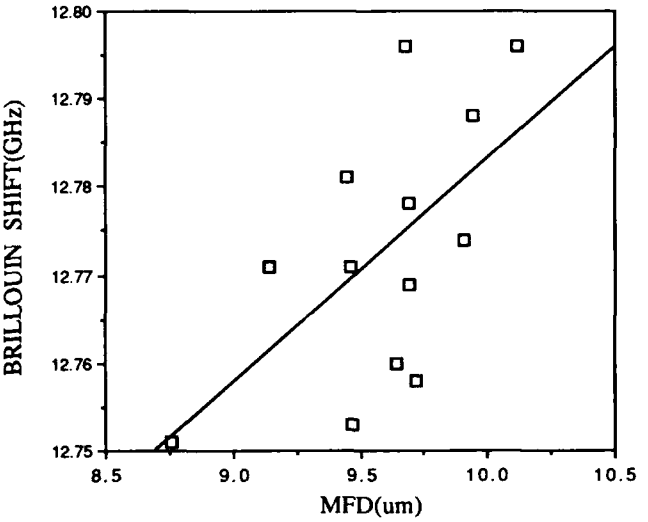


Fig.2 Brillouin shift MFD dependence

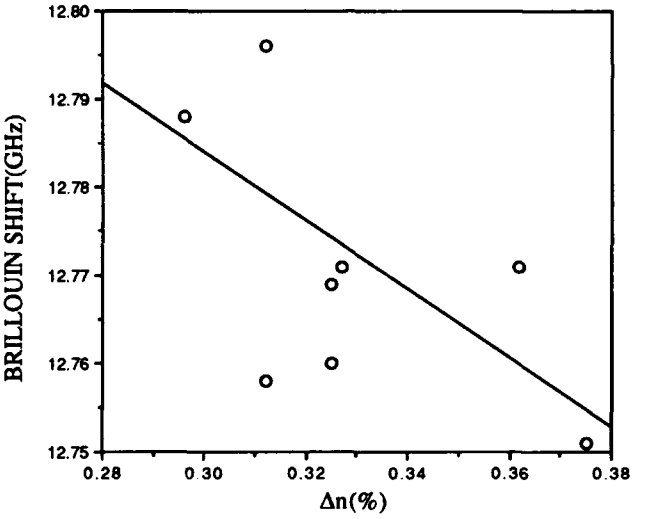


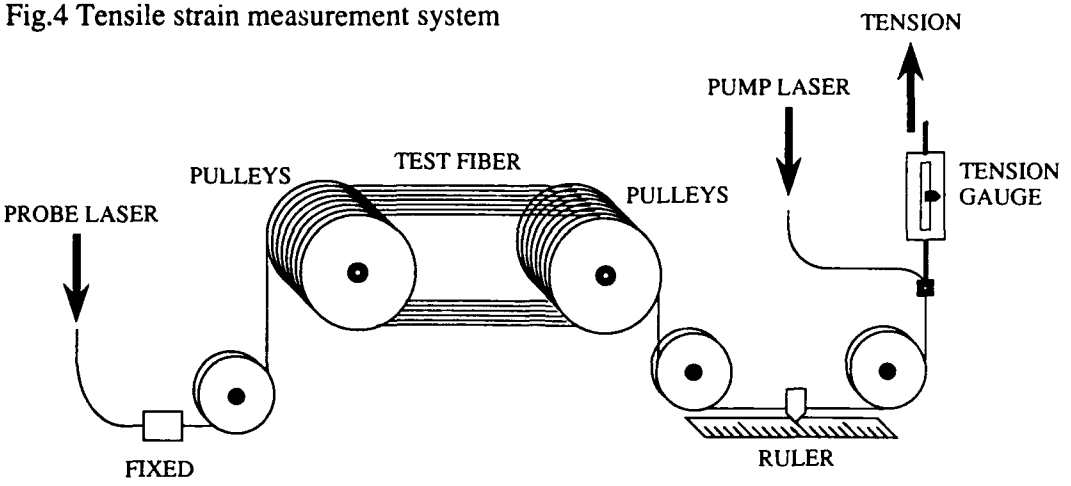
Fig.3 Brillouin shift Δn dependence

2)Tensile strain

Before cable measurement, it is necessary to obtain the fundamental data about the Brillouin shift between strain and tension

Fig. 4 shows the measuring system. Two kinds of samples were used: UV resin-coated single fibers and four-fiber ribbons. A 200 m long sample extended through pulleys was put under the tension by connecting a tension gauge to one end, with the other end fixed, and ΔL was measured using a ruler.

Fig.4 Tensile strain measurement system



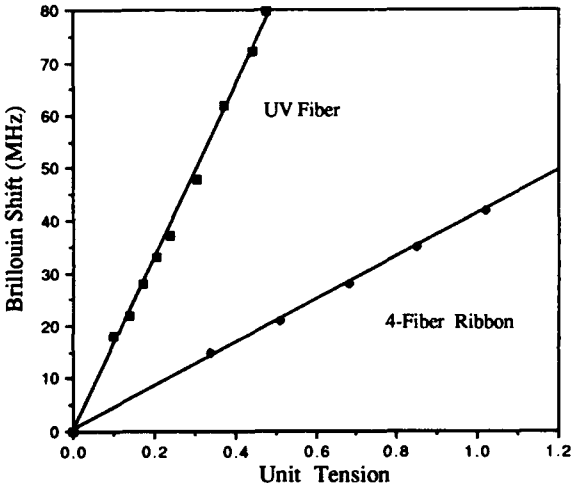


Fig.5 Tension Dependence on Brillouin Shift

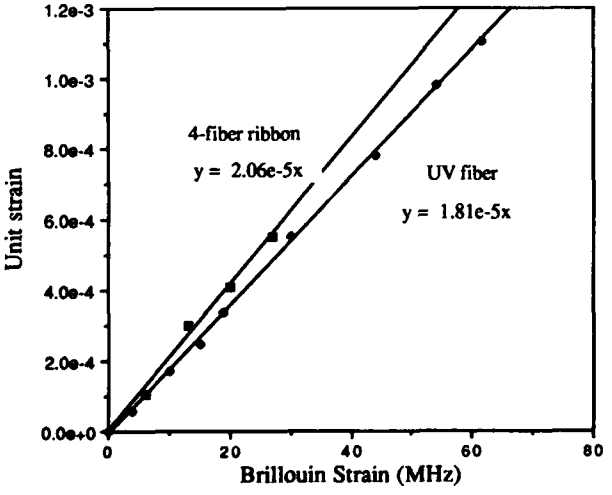


fig.6 Strain dependence on Brillouin shift

Fig.5 shows the relation between Brillouin shift and tension. UV mono-fiber's $\Delta\nu_B$ per unit tension is about 4-times larger than that of 4-fiber ribbon Fig.6 shows the relation between the Brillouin shift and strain. As can be seen from both figures, a good linearity was observed. For both kinds of samples, the strain dependence of the Brillouin shift was of the order of 2×10^{-5} per MHz. With a measuring accuracy of 1 MHz for the Brillouin shift, it is possible to measure strains with an accuracy of 2×10^{-5}.

3) Temperature characteristic

For optical fibers, there are two types of temperature dependence of the Brillouin shift: One is the temperature dependence of fibers themselves, and the other is the effect of the temperature dependence of coating material.

Table.1 shows the typical value of the Brillouin shift temperature dependence of three fibers.

Fig.7 shows the example data of these three type fibers.

With ordinary fibers and fiber ribbons, the thermal expansion coefficient of primary coated fibers is much lower than the coating materials (silica: 5×10^{-7} /°C, UV resin and silicone resin: about 10^{-4} /°C), so the Brillouin shift depends largely on the Young's modulus of the coating material and the coating thickness.

In special instances, an optical fiber like Fiber B, which has a lower Brillouin shift temperature dependence than the silica glass fiber, can also be made by using a cladding or coating material having a negative thermal expansion coefficient.

Table. 1 Temperature dependence

fiber A	1.0 to1.2	Silicone-coated, UV resin-coated
fiber B	0.6	Coated with a material having a low thermal expansion coefficient
Ribbon	1.3 to1.6	UV resin-coated, four-fiber

(MHz/°C)

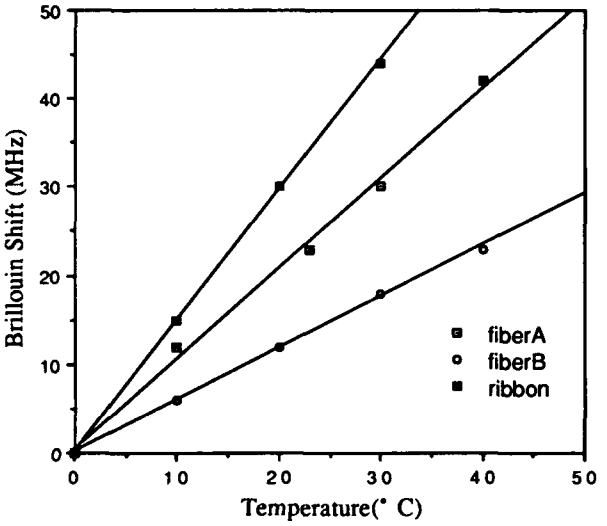


Fig.7 Brillouin shift Temperature dependence

4) Dependence on Lateral Pressure of fiber

The value directly obtainable from measurements of Brillouin shift is the acoustic velocity (phonon frequency). Therefore, it can be assumed that not only the tension applied to fibers but also some external forces like lateral pressure, water pressure, bending, etc., give rise to changes in the Brillouin shift and the form of spectra. Here, we made an attempt to measure changes in Brillouin gain spectra caused by the lateral pressure applied to fibers.

The sample was a UV resin-coated fiber of 400 μm in outside diameter and 125 μm glass fiber. Such fibers were laid over a plate loaded surface by placing another surface plate thereon.

As a result, no changes were observed in Brillouin gain spectra under loads up to 220 kg per 100 m (=22 g/cm). So it can be said that the influence of lateral pressure on Brillouin shift is not so severe.(see Fig.8)

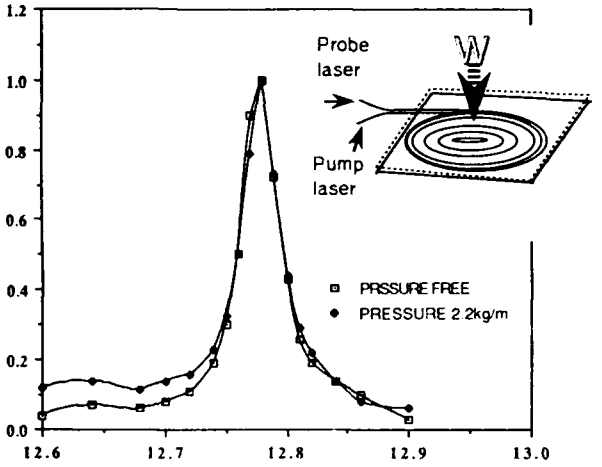


Fig.8 Brillouin spectrum Lateral Pressure dependence

5) Twisting characteristic of fiber ribbon

In this section, to estimate the accuracy of the Brillouin shift method, we measured the minute strain of twisted fiber ribbon.

Fig.9 shows the experimental set-up when a 50g initial tension was applied to a 8-fiber ribbon, which was then twisted with its two ends fixed.

Fig.10 shows the dependence on twisting pitch of the Brillouin shift of the edge fibers and middle fibers. It can be seen from this figure that the edge fibers gradually undergo tensile strain and have a good agreement with the calculated values from equation(3).

$$\varepsilon=\frac{L+\Delta L}{L}=\frac{N\sqrt{(\pi D)^2+(L/N)^2}}{L} \qquad (3)$$

Where ε, L, ΔL, N and D are the strain, total length, length change, pitch number and ribbon width.

The middle fibers undergo tensile relaxation though they initially exhibit virtually no change.

As a result, it can be said that fiber strain can be measured the order of 1MHz accuracy when the sample is longitudinally uniform as in this case.

Fig.9 Twisted ribbon Brillouin shift measurement

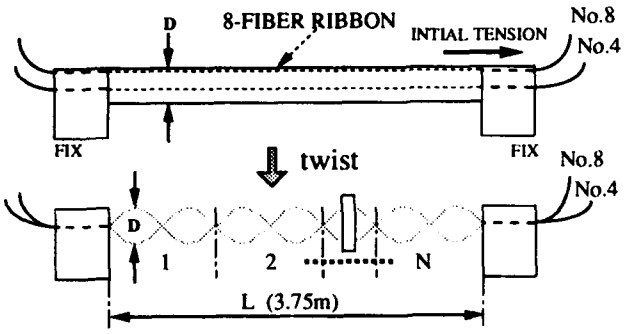
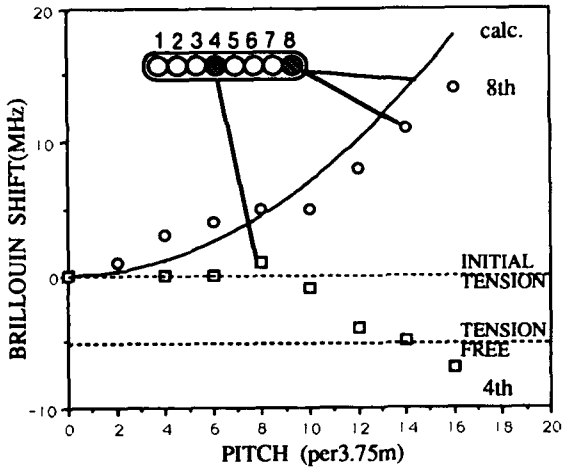


Fig.10 Twisted 8-fiber ribbon Brillouin shift



6) Brillouin gain spectrum of bent cable

As for the strains applied to drum-wound cables, a tensile strain and a compressive strain occur in a cyclic manner, so these strains cannot be measured by the phase shift method, as they counterbalance each other. When the Brillouin gain spectrum is measured, however, the spectrum shape, especially the spectrum linewidth will change and not be counterbalanced by the strain distribution[4].

Fig.11 shows the Brillouin spectra of a four-fiber ribbon itself, and Fig.12 shows the spectra of the same type ribbon in a cable which is wound on a drum. By comparing the spectra of the No.1 and No.4 fibers with the No.2 and No.3 fibers of the ribbon , it can be found that the peak Brillouin shift does not change largely, but the spectra of the edge fibers are broadened by 50 MHz or more when the cable is wound.

As a rough approximation, there is 0.1% strain distribution in this fiber, based on the strain dependence coefficient of the Brillouin shift M (=2.0E-5 / MHz).

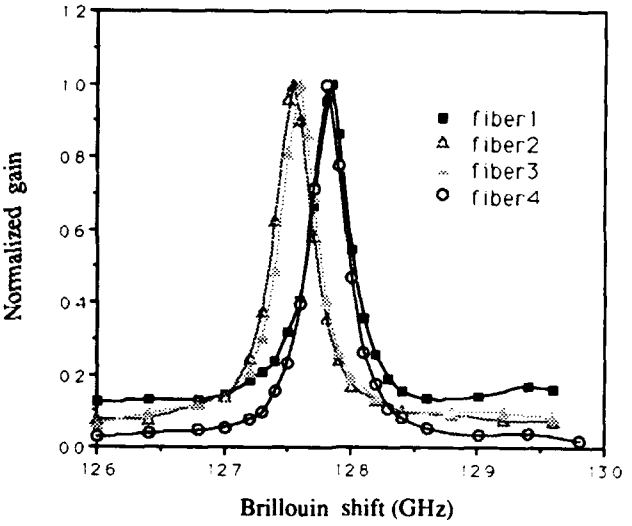


Fig.11 Brillouin spectra of 4-fiber ribbon

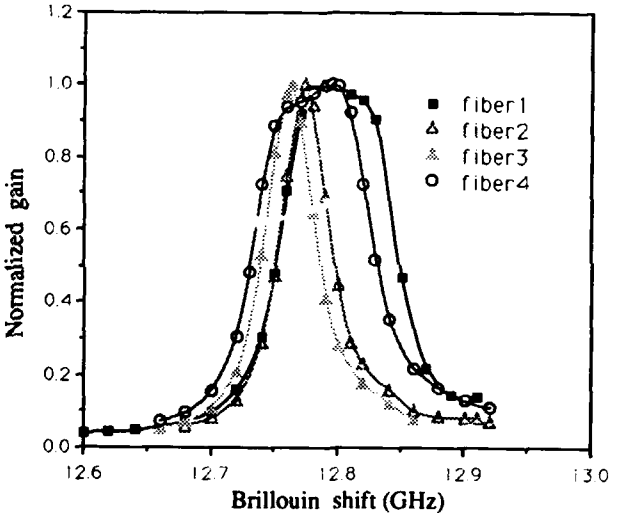


Fig.12 Brillouin spectra of 4-fiber ribbon in bent cable

Fig.13 shows the winding drum diameter dependency of the linewidth of 4-fiber ribbon in the same cable.

When the cable is laid straight, the linewidth of each fiber is almost the same. But when the cable is wound on a drum, the outer fibers' spectrum is broadened, and the inner fibers linewidth changes only slightly.

Fig.14 shows the same measurement for a 8-fiber-ribbon cable wound on a 1m diameter drum. For the outer fibers of the ribbon, the linewidth is broadened, but for the inner fibers, the linewidth change is small.

We were able to evaluate the strain distribution in bent fiber cables qualitatively. But to obtain more accurate strain distribution, we have to know the cyclic strain function of bent fiber cable. It is generally difficult determine, but we will investigate more deeply into this problem.

CONCLUSION

In this paper, we measured the Brillouin gain spectrum of fiber and fiber cable under various conditions. Using this method we can obtain highly accurate fiber strain measurements. We can also obtain information about the strain distribution of a fiber ribbon in a bent cable from its Brillouin gain spectrum lineshape.

REFERENCES

(1) N.Shibata Y.Azuma T.Horiguchi T.Tateda Opt. Lett., 13, 595(1988)

(2) T.Horiguchi T.Kurashima M.Tateda IEEE Photon Tech.Lett.,1,5,107-108(1989)

(3) T.Horiguchi T.Kurashima M.Tateda IEICE Japan,J73-B-I,2,pp144-152 1990

(4) T.Horiguchi T.Kurasima M.Tateda and K.Ishihara ECOC 509-512(1990)

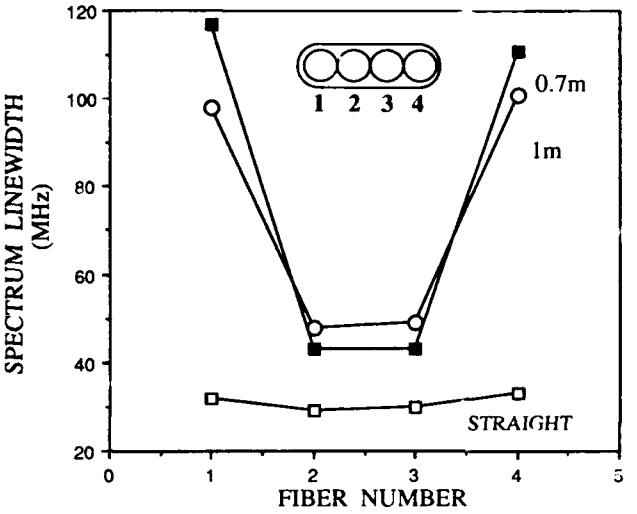


Fig.13 4-Fiber ribbon linewidth in drum-winding cable

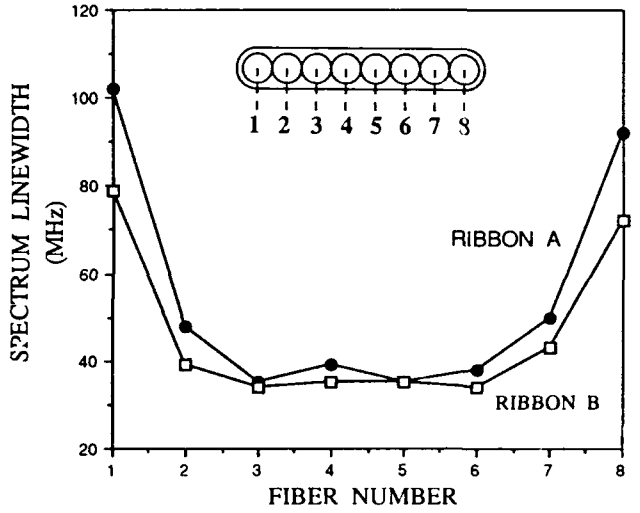


Fig.14 8-fiber ribbons linewidth in drum-winding cable



Mitsuru Kamikatano

Opto-Electronics
Laboratory
Fujikura LTD.

1440 Mutsuzaki,
Sakura-shi, Chiba-ken
285 Japan

Mr. Kamikatano was born in 1961. He joined Fujikura LTD. after his graduation from Tokyo University with a M.C. Degree in 1986 and has been engaged in research and development of optical cables. He is now an engineer of Telecommunication Cable Section and a member of IEICE of Japan.



Matsuhiro MIYAMOTO

Opto-Electronics
Laboratory
Fujikura LTD.

1440 Mutsuzaki,
Sakura-shi, Chiba-ken
285 Japan

Mr. MIYAMOTO was born in 1953. He joined Fujikura LTD. after his graduation from Tokyo Institute of Technology with a M.S. Degree in 1978 and has been engaged in design and research of optical fibers and cables. He is now a section chief of Telecommunication Cable Section and a member of IEICE of Japan.



Hiroyuki SAWANO

Opto-Electronics
Laboratory
Fujikura LTD.

1440 Mutsuzaki,
Sakura-shi, Chiba-ken
285 Japan

Mr. SAWANO was born in 1955. He joined Fujikura LTD. after his graduation from Hokkaido University with a M.S. Degree in 1983 and has been engaged in research and development of optical cables. He is now an engineer of Telecommunication Cable Section and a member of IEICE of Japan.



Nobuyasu SATO

Opto-Electronics
Laboratory
Fujikura LTD.

1440 Mutsuzaki,
Sakura-shi, Chiba-ken
285 Japan

Mr. SATO was born in 1943. He joined Fujikura LTD. after his graduation from Tohoku University with a B.E. in 1966 and has been engaged in research and development of transmission cables. He is now the manager of Transmission Line Department and a member of IECE of Japan.

THE DEVELOPMENT OF OPTICAL FIBER CABLE NETWORK AND OPTICAL FIBER CABLE INDUSTRY IN CHINA

Zhang You Kun, Tian He Chen, Xu Nai Ying

Chengdu Cable Plant of P & T Ministry, PRC

ABSTRACT

In China, optical fiber cables have now been used on most inter-office trunks of the local network,and entered the national and provincial toll network. In the Eighth Five Year Plan of 1991-1995,optical fiber cable in the subscriber's network and local area networks as well as the production of OPGW is at the research and experimental stage. Optical fiber cable industry of China has been developing on the basis of existing telecommunication cable industry and a few new optical fiber cable plants have been put into operation. The present paper reviews the development of optical fiber cable network and optical fiber cable industry of China. On the basis of investigations into the various kinds of optical fiber cable design and the domestic conditions, suggestions are made for the proper choice of cable design and the necessary tests to be made on these cables.

1. INTRODUCTION

At the time of founding of new China,the telecommunication network in China was extremely backward. The number of tele - phone set was less than 0.3 per 100 persons. No great progress was realized in the 50's to 70's years period. Telecommunication began to develop in the 80's, and the rate of development increased gradually. There are two reasons. Firstly,China began to adopt the reform and open policy in order to accelerate modernization, and in the course of modernization, People recognized the importance of telecommunications. Secondly, since the introduction of digital techniques and optical fiber techniques , their advantages were rapidly appreciated. In the large and medium sized cities throughout China, large capacity SPC exchange equipments and optical fiber inter-office trunks were introduced. Many provinces,especially those of coastal region, began to install optical fiber toll cables. The existing national toll network at that time, which is chiefly composed of open wire and symmetrical and coaxial cables, could no more satisfy the ever increasing demand. In the 90's, therefore, we began to accelerate the construction of national optical fiber toll cable network.

With the rapid advance of the digital technology, all kinds of informations including telephone can be transmitted, received, processed and stored digitally. Therefore, various kinds of non-telephone services such as data, facsimile, video - conference, etc. have appeared, and after a period of experimental work and field trials, optical fiber cables will gradually enter the subscriber's network.

2. DEVELOPMENT OF TELECOMMUNICATION NETWORK IN CHINA

The telecommunication networks in China are divided into two major groups, namely, the public network and proprietary network (military, railway,electric power, etc.).

We here chiefly discuss the public network.

After liberation, damaged pole lines were restored and rearranged to carry 3- and 12-channel carrier systems. In local networks, measures were taken to prolong the life of the then existing paper-insulated lead-sheathed cables. From late 50's to early 80's, carrier frequency quad toll cables, 2.6/9.5 mm and 1.2/4.4 mm coaxial cables as well as paper-insulated lead-sheathed local cables were manufactured by our own cable plants and installed in the toll and local networks.

The research and development of olefin - insulated local pair cables began in the early 70's, but due to the limitation of the necessary raw materials and manufacturing equipments available at that time, the products were not satisfactory until Chengdu Cable Plant (CDC) introduced in early 80's licenses from Essex and selected the necessary manufacturing equipments, testing instruments, and raw materials from different foreign suppliers. In the late 80's and early 90's, these cables have been produced by many cable plants in China.

The research and development of optical fiber and optical fiber cables began in the late 70's. In 1978, the first optical fiber inter-office junction cable were installed in Shanghai, using domestic products. The fibers are multi-mode fibers operating in the 850 nm wavelength region. In the early 80's, multi-mode fibers operating in the 1300 nm region were produced, but soon turned to the single mode fibers in the late 80's. Although a certain amount of multi-mode fiber cables were used on inter-office trunks, the optical fiber cables on toll routes are single mode. The optical fiber cables already installed are of three kinds, namely, domestic cables using domestic fibers, domestic cables using imported fibers, and imported cables. Due to the fact that domestic fibers are still somewhat inferior in tensile strength, and/or attenuation characteristics, these three kinds of cables are selected according to specific engineering requirements.

Besides wire transmission, the analog microwave systems carrying 600, 900 and 1800 channels were put into operation. The total length exceed ten thousand kilometers. Recently, digital microwave systems were also introduced.

TABLE 1 THE GROWTH OF THE TELECOMMUNICATION NETWORK OF CHINA

Wire or Cable	Unit	End of Year 1990	1991
Open Wire	1000 route-km	168	166
	1000 pair-km	680	672
Toll Symm.	1000 route-km	10.4	10.1
Cables	1000 sheath-km	18.6	18.3
2.6/9.5 Coax.	1000 sheath-km	6.5	6.6
1.2/4.4 Coax.	1000 sheath-km	5.2	5.5
Local Cu Cable	1000 sheath-km	137	165
Toll O.F.Cable	1000 sheath-km	3.3	6.5
Local O.F.Cable	1000 sheath-km	2.4	3.4

TABLE 2 THE GROWTH OF EXCHANGE CAPACITY AND THE AMOUNT OF TELEPHONE SET IN CHINA

Item	Unit	End of Year 1990	1991
Toll Exchange:			
Manual	1000 Lines	200	197
Elec.-Mech.	1000 Ch.-term.	9.8	10.3
SPC	1000 Ch.-term.	152	276
Local Exchange:			
Manual	Million Lines	0.3	0.3
Elec.-Mech.	Million Lines	4.0	4.4
SPC	Million Lines	3.6	5.7
PBX	Million Lines	7.4	8.5
Telephone Set:			
On Public Ex.	Million Sets	5.3	Total
On PBX	Million Sets	5.0	14.5

From 1980, when China began to adopt reform and open policy, the development of telecommunication speeded up. P & T Ministry of China suggested that in the two decades from 1980 to 2000, the telecommunication services be increased eight times.

Table 1 and Table 2 show the status of telecommunication equipments by the end of 1990. The Eighth Five Year Plan began from 1991, and the development of telecommunication is further accelerated. Table 1 and Table 2 show the growth. From the tables, it can be seen that the rate of increase of the SPC exchange and optical fiber cables were extremely high, and far exceeded the average rate of increase suggested by P & T Ministry for the two decades from 1980 to 2000. Nevertheless, due to the large population, the number of telephone sets per 100 inhabitants was still as low as 1.2 by the end of 1991. This means that there is a great potential need for the telecommunication equipments in China.

A study on the future development of optical fiber cable network and optical fiber cable industry is of prime importance. This will be discussed below.

3. AN ESTIMATION ON THE FUTURE DEVELOPMENT OF OPTICAL FIBER CABLE NETWORK

It can be seen from the previous paragraph, that optical fiber cables, apart from the inter-office trunks accompanying the growth of SPC exchanges, are entering the national and provincial toll routes at a quite rapid rate. We discuss here the development trends of optical fiber cables in the next decade.

3.1 Inter-office cables

The inter-office cables already installed are mostly single mode fiber cables(G.652) with a small portion of multimode fiber cables (G.651). The optical fiber cables to be installed in the future will be solely single mode optical fiber cables, conforming with the CCITT G.652 Recommendation. Most of the cables will operate on 140 Mbit/s, and a small part will operate on 34 Mbit/s at first stage and converted to 140 Mbit/s later on. In rare cases where the traffic is exceptionally high, 565 or 622 Mbit/s systems may be used. It is estimated that the maximum number of fiber in the cables will be 48. Most of the optical fiber cables used up to the present are of loose structure (loose tube or slotted core). The number of fibers in a loose tube or slot varies from 1 to 8. The cables have LAP sheath and are mostly jelly-filled. These cables are mostly installed in PE sub-ducts with 25-27 mm inside diameter. Three sub-ducts are preinstalled in a 90mm concrete duct. It is estimated that no great change will occur in the cable structure and installation practice.

3.2 Toll cables

The toll cables already installed are similar to those used in local network, except that the cables are armored for direct burial. The armor usually consists of longitudinally applied corrugated steel tape coated on both sides so that it is bonded to the PE outer jacket. The maximum number of fibers in toll cables is 24 and possibly will be increased to 48 also. It can be seen from Table 1, that in the year of 1991, more than three thousand kilometers of toll cables were put into operation. It is estmated that by the end of 1995, additional more than ten thousand kilometers of toll cable will be installed. Due to the fact that there are 160,000 kilometers of open wire pole line still existing, aerial optical fiber cables were also installed.Aerial toll cables are hung on messenger wires by means of cable rings. The installation expenses for aerial cables are much less than those for underground cables,and hence a considerable amount of aerial cables will be installed in the next decade. A possible way to increase the traffic carrying capability is the upgrading of the 140 Mbit/s system to 565 or 622 Mbit/s system. Therefore, the fibers used in the cables should comply with the requirements for these high bit rate systems. The exploitation of the 1550 nm wave length region is not anticipated, at least before

1995.

3.3 Cables in the subscriber's loop

In developed countries, optical fiber cables are entering the subscriber's loop. In China, however, copper cables are still used in the subscriber's loop and a considerable amount of copper cables will be installed in the near future. The use of 2B+D ISDN on copper cables to satisfy the needs of a part of subscribers is under experiment. For some special subscriber, however, there will be need for direct access to optical fiber. Therefore, medium size optical fiber cables for the subscriber's loop should also be taken into consideration, especially those that can be installed in the sub-ducts.

3.4 Optical fiber cables for LAN

In the past few years, large enterprises, factories, financial organizations and news agencies appeared in China and Local Area network(LAN) began to develop. The optical fiber cables used in LAN will be somewhat different from those used in the public network. For example, the cables should be easy to terminate and easy to branch, they should be thin and flexible, and indoor cables should be fire-retardant. The number of fibers varies from single to a few hundred fibers. The requirement for the attenuation is not so stringent. The multi - mode and tight buffer tube fibers may be required.

3.5 Optical Ground Wire (OPGW)

The optical ground wire is another important application of fiber-optic communication. In the past, the communication facilities used by the electric power transmission systems in China were microwave and carriers on the high tension transmission lines. Due to the fact that optical fibers are immune from the electro-magnetic inductions which are strong in the vicinity of the high tension lines, optical fibers become the most reliable transmission medium. The production of OPGW in China is yet in the experimental stage. As there is a great potential need, due attention should be paid to the design, manufacture and installation of OPGW.

4. THE DEVELOPMENT OF OPTICAL FIBER CABLE INDUSTRY IN CHINA

The development of optical fiber industry in China began in the late 70's. In the early stage, MCVD process was used to produce multi-mode fibers encapsulated in tight buffer tubes, operating in the 850nm wave length region, and later in the 1300 nm wave length region. The fibers were produced by research organizations, and cables are produced by existing cable plants, with some minor improvement made on the cabling machines in order to reduce the tensile force on fibers. The first domestic optical fiber cable was installed in Shanghai in 1978. In the 80's, foreign MCVD preform manufacturing equipments and fiber drawing towers were introduced for large scale production.The quality of the fibers improved, but, due to various factors, it remains not so satisfactory as expected, especially in the tensile strength of the fibers, the bandwidth of multi-mode fibers and the attenuation of the single mode fibers. VAD preform equipment was also introduced, but it works not so satisfactorily and were not put into regular production. According to rough estimate, the production capacity of fibers in China amounts to 200 thousand kilometers per year, but the actual fiber product in 1991 is estimated to be less than 20 thousand kilometers. To meet the urgent demand of the telecommunication network, many cable plants improved their equipments and/or ordered foreign equipments to produce optical fiber cable, using both domestic and imported fibers. As mentioned earlier, these cables are largely of loose type(loose tube or slotted core). A part of the optical fiber cable was im-

ported and used on important toll routes, e.g, on the Nanjing-Wuhan route. In 1990, a Joint Venture was founded and began regular production early this year. The fibers are manufactured by the PCVD process. It was reported that the quality of the fibers equals the imported ones. From now on, domestic optical fiber cables will increasingly be used on the national and provincial toll routes as well as in the local networks. On the Beijing-Wuhan-Guangzhou and Tianjing-Nanjing toll routes now under construction, the optical fiber cables are being produced by several cable plants, CDC being one of the large suppliers. These cable plants will, in the course of regular production, continously improve their cable design, technology, and test equipments. In these respects, IWCS Proceedings have given and will continue to give valuable help.

Recently,the fiber-bundle central core tube type cable was put on the market. There have been various comments on such cable. These will be discussed in the following paragraph.

5. THE FUTURE DEVELOPMENT OF OPTICAL FIBER CABLE INDUSTRY IN CHINA

On the basis of the discussion in the preceding paragraphs, the authors considered that in order to satisfy the growing demands, apart from the production of high quality fibers (discussions about the fiber production are beyond the scope of this article), the following points should be carefully studied by the optical fiber industry, in cooperation with the telecommunication administrations, who are responsible for the networks.

5.1 Fiber-bundle central core tube type cable vs. other type cables

The fiber-bundle central core tube type cable has certain advantages as compared with the loose construction cable. Amoung others, easy access to fibers and light weight for thr direct burial cables are the most important. Certain precautions, however, seem to be necessary during manufacture and installation.

Firstly, due to the fact that the core tube is placed along the cable axis, apart from the excess length of fibers in the core tube itself, no additional excess length can be obtained from twisting the tubes around the central member.According to Ref.(1),in the LXE cable of AT & T,the fiber excess length is about 0.15%. When the cable is pulled to the rated tensile load of 2700 N, the cable is elongated about by 0.33%. That is to say, the fibers in the cable will be elongated by 0.18 %. This elongation is equivalent to a stress level of about 30 kpsi, which constitutes 60% of the proof test strength. This seems to be somewhat too high for cables which are liable to be under high tensile load, e.g, for aerial cables and for pulling long length cables into ducts. In loose tube cables, due to the twist of the tubes around the central member, the following additionalexcess length ε is obtained (expressed in fraction):

$$\varepsilon = (1/2) \times (2\pi R/s)^2 \times [2\,\delta R/R - (\delta R/R)^2]$$

where R --(pitch diameter of loose tubes)/2
δR --(inside radius of loose tube)
-(equi.radius of fiber bundle)
S --length of twist

Figure 1 shows the additional excess length of fibers in loose tube cables as a function of twist length. It can be seen from the figure that with 100-140 mm twist length, sufficient additional excess length is obtained. The effective bending radius of the fibers Re as a result of twist can be calculated as follows:

$$Re = R + (s/2\pi)^2/R$$

The values of Re as a function of S are also shown in Fig. 1. When S lies in the

range 100-140 mm, Re will be in the range 117-228 mm, which is allowable for most fibers.

Secondly, due to the fact that the two diametrically opposite 1.6 mm strength members are extruded in the HDPE sheath. The thickness of the sheath at the strength members will be less than 1 mm. People doubt that under the condition of the installation practice used in China, this small thickness may be unable to maitain the sheath integrity.

In China, for the installation of direct burial cables, direct plowing is seldomly used, and manual trenching is the common practice. The cable is unrolled from the drum and placed in the form of figure"8" on special shelves. The shelves are then carried to appropriate locations for place - ment into the trench. Therefore, during installation, the cable is not liable to be damaged by the mechanical forces produced by the plowing operation, nor liable to be put under appreciable tensile load. but,due to the fact that the trenching and refilling operations are commonly done by local farmers, sheath damages by shovels or falling rocks during refilling operations are not infrequent. At road crossings, where the cable must go through protecting pipes, sheath damages at the pipe entrances often occur. These sheath damages have been positively confirmed by the experience in the installation of 1.2/4.4 mm coaxial toll cables. These coaxial cables have a aluminum sheath 1.4 mm thick and a PE outer jacket 2.0 mm thick. The sheath damages have been considered as a serious problem for a long time. For the detection and location of the sheath damage after installation, the insulation resistance between the sheath and ground is monitored, so that the sheatn damages can be repaired. Such repairs, however, sometimes prove to be unsatisfactory.

Ref(1) reported the experience with the LXE cable, with the sheath thickness increased to 3 mm, 3% sheath damage was reported. This needs further investigation.

TABLE 3 DIMENSION AND WEIGHT OF OPTICAL FIBER CABLES (8 - 48 FIBERS)

	LXE-ME Cable (At & T)	Loose-tube Cable Unarmored	Armored
O/s Dia.,mm	12.4	10.7	14.7
Wt., kg/km	156	130	268

From Table 3, it can be seen that in the viewpoint of cable dimension and weight , LXE-ME cable is better than the loose tube cable for direct burial use, but the case is reversed for duct use. It seems to us that deep investigations and some modifications may be necessary.

5.2 Subscriber optical fiber cable design

Although optical fiber cable will not enter the subscriber's loop in large quantities in the next few years, as discussed earlier, it is time for the optical fiber industry to consider this matter. For small size cable (e.g.,with less than 96 fibers), ordinary loose tube or slotted core cable can be used as well. When the number of fibers increases, however, the reduction of cable diameter will become essential. In metropolitan areas, where the underground ducts are congested, it will be economically advantageous if the subscriber's cable can be put into the sub-ducts.The adoption of fiber ribbons seems preferable. The fiber ribbons can be assembled into core tubes,slotted cores or special spacers(2,3,4). In the ordinary loose tube cables, the average cross-sectional area of the cable per fiber is approximately 3 sq.mm. If fiber ribbons, instead of individual fibers, are placed in the loose tubes, the cross-sectional area per fiber will be reduced to about 0.8 sq.mm and if fiber ribbons

are assembled in slots, this figure will be further reduced to 0.4 sq.mm per fiber. With the adoption of special spacers, the cross-sectional area per fiber may reach 0.2 sq.mm. In this case, the outside diameter of a 4000 fiber cable will be only 35 mm(4). The mass splicing is another advantage of the fiber ribbons, which results in the economy of time and cost of installation. Although fiber ribbons are not new, they are yet unfamilar to our country, and it is recommended that the optical fiber cable industry should begin their design and manufacture, and put into field trial.

5.3 LAN optical fiber cables

For the optical fiber cables used in the local area network(LAN), there are several peculiarities to be investigated and experimented by the optical fiber cable industry, apart from the selection of appropriate fiber for use. Firstly, the application of the tight secondary buffer coating of the fibers was not satisfactory at the early stage of production in the 80's, especially the microbending loss when lateral pressure is applied during cabling and installation. Secondly, fire-retardant shaeth materials have to be carefully selected and the extrusion process investigated. The single or dual fiber drop cables for aerial entrance to buildings also need investigation,because high tensile strength and small size are required.

Another type of cable which may be of interest to LAN is the air-blown fiber cable. For some special subscribers, the use of optical fibers in their premises is not very distant, but at present it is possibly not yet economical, and metallic symmetrical or coaxial cables are installed. To simplify the rearrangement in the near future, empty tubes may be provided in these metallic cables and optical fibers may be blown in at the time of need. This may be an economical solution(5). Similar condition exists in the entrance cable of the distribution network into large subscriber's premises. It seems that there is no difficulty for the provision of tubes in the metallic cables, but the cable plants should cooperate with the installation companies for the field trial of the air-blown techniques.

5.4 Non-metallic optical fiber cables

For cable routes which are in close proximity with high tension power transmission lines or electric railroads where,in case of fault, serious overvoltage will occur, non-metallic cables are preferred. These cables take maximum advantage of the induction-free characteristic of optical fibers. The same situation exist when the optical fiber cables go through districts where thunder storms are frequent. As the electrification of railroads and expansion of the high tension power transmission lines are in progress at a quite rapid rate in China, the optical fiber cable industry should accelerate the development of non-metallic cables.

The most promising material to be used as the tension bearing elements is fiber reenforced plastic(FRP). FRP is processed into the form of rods having a circular cross-section and used in place of metallic tension members both in the cable core and in the armor(6). The cross-section of the FRP rods, however, must be much larger than that of the metal wires, because the Young's modulus of FRP rod is only about one fourth that of steel wire(7).In order that the diameter increase will not seriously impair the flexibility of the cable, FRP rods having different cross-sections (oval,rectangular,etc.) were developed(7). This is specially important for indoor cables. Moreover, as there is no longer metallic moisture barriers in non-metallic cables, the sheath design should be more

careful to prevent the possibility of moisture penetration. The optical fiber cable industry in China should quickly get familiar with the non-metallic cable design and manufacture, especially in the processing of FRP rods.

5.5 Optical ground wire

Optical ground wires (OPGW) are usually installed on long spans, and in order to keep OPGW operate satisfactorily even under extreme climatic conditions, OPGW must be designed such that when OPGW is subjected to the largest possible tensile load, the strain in the fibers is still kept within allowable limits. Optical fibers along the wire axis may prove unsatisfactory in this respect. Experimetal OPGW of such type was manufactured in China, and fiber breakage did occur. Fibers placed in loose tubes or slots away from the wire axis may be more preferable, because the total excess length of the fibers may easily designed to be as large as 0.4-0.5%. Loose tube fibers in slots of aluminum core presented by AEG could be a suitable design (8), and the use of welded steel tubes as the loose tubes for fibers may be more suitable. As the manufacturing equipments for OPGW are partly different from those used for other optical fiber cables, the cable plants that manufacture power wire and cables may be more suitable.

5.6 Test for the fiber strain in optical fiber cables

For the sake of confirming that optical fiber cables satisfy the cable specifications, the manufacturer should perform various type approval tests besides the normal acceptance tests. Among others, the mechanical tests are the most important. Table 4 gives the tests usually performed. In China, a computer controlled mechanical performance test set was developed and improved for this purpose.

TABLE 4 MECHANICAL PERFORMANCE TESTS ON OPTICAL FIBER CABLES

Test Item	Specifications IEC	EIA*	Bellcore**	GB ***
Tensile Loading	794-1-E1	FOTP-33	5.1.4	7425.2
Compressive Loading	794-E3	FOTP-41	5.1.3	7425.3
Twist	794-1-E7	FOTP-85	5.1.5	7425.6
Repeated bend	794-1-E6	FOTP-104	5.1.6	7425.5
Impact	794-1-E4	FOTP-25	5.1.2	7425.4

* EIA Standard RS-455

** Bellcore TR-TSY-000020 Issue 4

***Chinese National Standard, 1987

Other tests are sometimes required, however, in order to ascertain that the cable will satisfy the installation and operation requirements. The fiber strain test is one of the important tests. As discussed earlier, by proper cable design, the strain on the fibers in the cable can be made to be far less than that of the cable. Tests are necessary to determine whether the design objective has been accomplished. The tensile loading test results listed in Table 4 do not clearly reveal the strain of fiber, because in these tests, only the fiber attenuation is monitored. The attenuation of the fiber in the cable under test depends upon many factors. For example, in the central core tube type cable, when the cable is put under tension, no noticeable attenuation change will be observed before the fiber breaks. As any possible strain existing in the fibers will more or less affect the life of the fibers, the determination of the strain on the fibers in the cable is essential. Articles have been published on such tests(9). Such tests were also performed in China, utilizing the computer controlled mechanical performance test set mentioned above.Fig.2

shows the schematic diagram of such a test. The strain on the fiber in the cable under test is calculated from change in propagation time in frequency domain(9,10).Fig.3 shows the test result of CDC on loose tube cables. From the figure, it can be seen that for cable strain below 0.3% (corresponding to 4.3 KN tensile load), the rate of increase of strain is less than that of the cable. The dotted line shows the theoretical result. The discrepancy between the theoretical and measured results may probably be explained by the fact that the fibers require some time to relax themselves in the loose tubes which is filled with jelly. The rate of application of the tensile load should probably be decreased. Further investigations are necessary. For the OPGW, such a test may be even more important.

5.7 Test for the fiber excess attenuation at low temperatures

China has a large territory and the climatic conditions varies widely from place to place. Optical fiber cables may encounter extreme temperatures, especially in the case of aerial cables. At low temperatures, the shrinkage of the cable may cause the macro-and micro-bending of the fibers. Although great care could be taken in the cable design, based on the knowledge of the linear expansion coefficient of various elements of the cable, precise results are often difficult to obtain. The more reliable and final way is by means of low temperature tests performed on the finished cables. Temperature controlled chambers of sufficient size is therefore necessary. Fig.4 shows the result of such a test performed in CDC on an 8-fiber loose structure cable. It can be seen from the figure that for temperatures below -30 deg.C, excess attenuation increases. While such a cable is well suitable for underground use elsewhere in our country, it should be further improved if it is to be used for aerial installations in the northern districts where the temperature in the winter may be as low as -50deg. C. For toll cables, which may exploit 1550 nm wavelength region, such a test will be even more important, as in this region the fibers are far more sensitive to bending than in the 1310 nm region. It is necessary for the cable manufacturer to get more experience in this respect.

5.8 Lightning protection of optical fiber cables

Although the optical fiber itself is immune to lightning discharges, the lightning protection of optical fiber cables is still necessary so long as metallic elements are incorporated in the cable. In the southern districts of China, lightning hazards on metallic toll cables are not rare. The metallic elements in optical fiber cables are usually the strength member, the water barrier, and the armor. For adequate lightning protection, how to connect these metallic elements in the joint closures is an open question. Some people advocate to insulate these metallic elements at the closures. The reason is to interrupt the addition of induced voltages in adjacent cable lengths. If necessary, metallic strand wire are placed directly above the cable to by-pass discharge current. Other people insist on connecting all the metallic element across the joint closure and ground them at regular intervals,just as what has been done with the metallic toll cables. Although the telecommunication administrations should be shiefly responsible for the lightning protection, the cable manufacturer should closely cooperate with them, as the lightning protection capability depends, in a certain extent, on the discharge current carrying capacity of the cable. The use of non-metallic cable is another possible solution for lightning protection. Although at present, it is often economically dis-

advantageous, it may be quite promising in the future.

5.9 The hydrogen source in optical fiber cables

It is well known that the attenuation and life of the fibers will be seriously affected by the presence of hydrogen. The chief sources of hydrogen are the metallic elements in the cable. These elements, in the presence of moisture, may generate hydrogen due to electrolysis. LAP sheaths are widely used in China, but the problem of hydrogen-generation has not been well studied, and potential risk may exist. A deep investigation may be necessary for the cable manufacturer.

6. CONCLUSION

In China, telecommunication is developing at an unprecedented rate. Optical fiber cables have been universely used in the inter-office trunks of the local network and are entering the toll network. The use of optical fiber cables in subscriber's and local area networks is at experimental stage. The optical fiber cable industry should take up the responsibility of supplying the various kinds of optical fiber cables. Several suggestions are presented by the authors. They are:

(1) The possible improvement of the optical fiber cables for the inter-office trunks and toll trunks, including the fiber-bundle central core tube type.

(2) The development of subscriber's cables and cables for the local area networks, including the premise cables and air-blown fiber cables.

(3) The improvement of the OPGW design.

(4) Several basic tests, including the fiber strain tests on fibers in the cable, low temperature test, lightning protection tests, and hydrogen tests.

By way of these efforts, the present optical fiber cable industry, through certain additional improvements in equipments and technology, will be able to meet the increasing demands.

ACKNOWLEDGEMENTS

The authors would like to express deep gratitude to Mr.Wang Shou Jia, Mr. Wang Xiang, Mr. Wang Tao, etc., engineers of the Chengdu Cable Plant, for their excellent work on the fiber strain measurement and the temperature dependence measurement of fiber excess attenuation on optical fiber cables. Acknowledgement is also due to the people who provide the statistical data on the outside plants, exchange equipments, and subscribers' telephone sets in China.

REFERENCES

(1) Liu Jian Ming: "A Brief Introduction on the Production and Testing of LXE-ME Optical Fiber Cable", Technical Information on Fiber and Fiber Products by AT & T (China) Beijing Office (In Chinese).

(2) Y.Kikuchi, H.Sawano, Y. Sato, K.Kobayashi, K. Okamura, H. Suzuki and N.Sato: "Cnaracteristics of One-Thousand- Fiber Water Proof Cable", IWCS Proc., 1990,pp. 197-202.

(3) Y.Yamazaki, H. Horima, H. Igarashi, K. Niikura:"Characteristics of Jelly-filled non-metallic Ribbon Fiber Slotted-core Cables", IWCS Proc., 1990,pp.190-195.

(4) S. Somita, M. Matsumoto, T. Yabuta,and T. Uenoya: "Preliminary Research into Ultra High Density and High Count Optical Fiber Cables", IWCS Proc., 1991,pp. 8-15.

(5) S.Konno, K. Kikuchi, A. Ona, G.Morikawa, K. Yamashita, M. Ryuto: "New Composite Cable Applying the Air Blown Fiber Techniques", IWCS Proc., 1989,pp. 344-350.

(6) Y. Kuwata, K. Niikura, H. Horima:"Development of FRP Armored Non-metallic Opti-

cal Cable and the Armoring Process", IWCS Proc., 1990,pp.44-50.

(7) Y.Kuwata, H.Horima, T.Ishii, S.Matsuno: "Development of Non-metallic Fiber Optic Cable for Indoor Use Applying Advanced FRP Forming Technology", IWCS Proc.,1991,pp. 38-43.

(8) H.G. Haag, G. Hog, P. E. Zamzow:"New Generation of Self Supporting Optical Fiber Cables", IWCS Proc., 1989,pp. 575-582.

(9) W. Wenski, B. Menze, J. Schulte :"Fiber Strain during Cable Pulling--An Important Factor in Cable Design", IWCS Proc., 1989, pp. 268-373.

(10) A. Bertholds, R. Bandliker: "Determination of the Individual Strain-optic coefficients in Single Mode Optical Fibers", J. Lightwave Technology, 6, 1988,p.17.

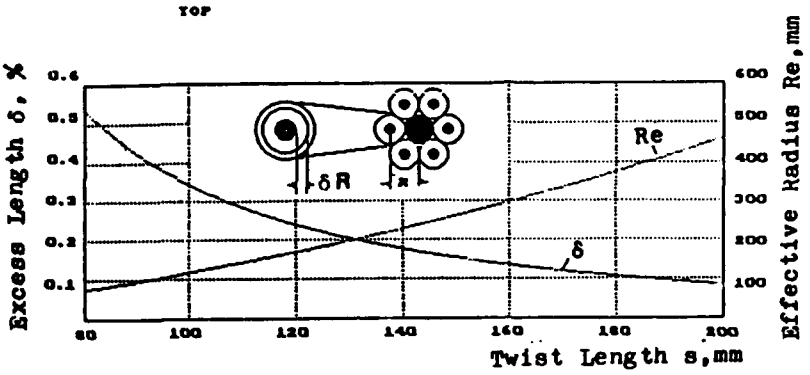
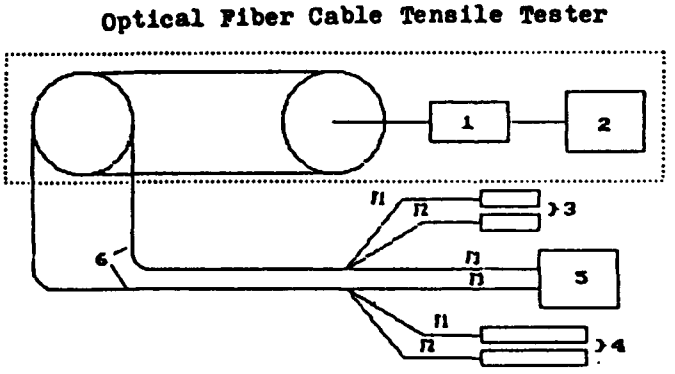


Fig.1 Excess Length and Effective Radius of Fibers in Loose Tube Optical Fiber Cables as a Function of Twist Length



1--Tensile Gauge
2--Power Drive
3--Optical Source
4--Optical Power Meter
5--Dispersion Measuring Set
6--Optical Fiber Cable under Test
F1-F3--Fiber No. 1-3

Fig.2 Schematic Diagram of Strain Measurement for fibers in optical cable

TOP

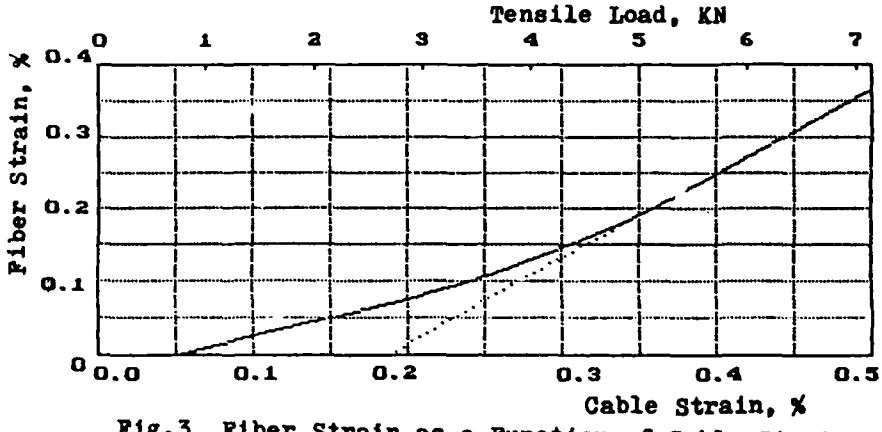


Fig.3 Fiber Strain as a Function of Cable Strain or Tensile Load on Cable

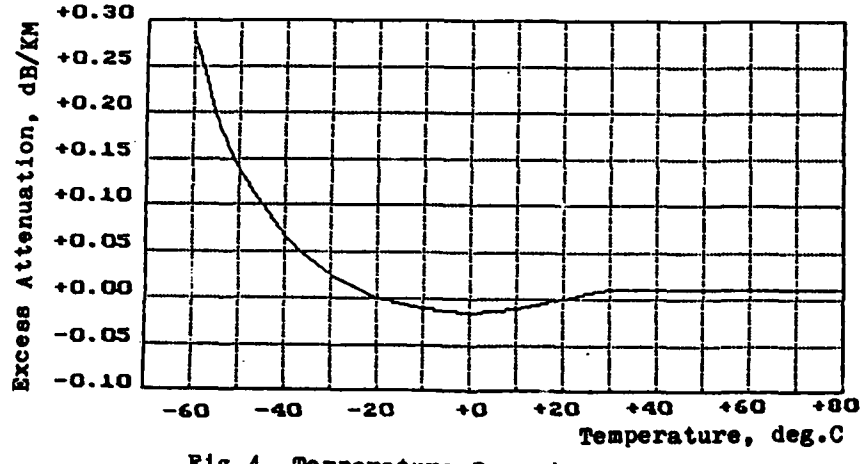


Fig.4 Temperature Dependence of Fiber Excess Loss in Cable



Zhang You Kun
Chengdu Cable Plant
Chengdu, Sichuan,
China

Madam Zhang You Kun graduated from Xian Jiao Tong University in 1960, majoring in electrical insulation and cable technology. After graduation, she joined the Chengdu Cable Plant and has been engaged in cable design and manufacturing technology. In 1981 she was promoted to Chief Engineer and is responsible for the technical development of new products. She is a senior engineering member of the Telecommunication Line Committee of China Institute of communication. In 1986, she was awarded the title of National Expert for her outstanding contributions in China.



Tian He Chen
Chengdu Cable Plant
Chengdu, Sichuan,
China

Mr. Tian He Chen was born in 1937 and was graduated from Electrical Engineering Department of Xian Jiao Tong University in 1961, majoring in electric insulation and cable technology. He joined Chengdu Cable Plant in the same year. He was engaged in the research, design and manufacture of telecommunication cables. He is now Deputy Chief Engineer, senior engineer of the Plant, and is in charge of the research and development of optical fiber cables and materials.



Xu Nai Ying
Chengdu Cable Plant
Chengdu, Sichuan,
China

Mr. Xu Nai Ying received his B.S. degree in 1946 in Electrical Engineering from Jiao Tong University in Shanghai, China. He has been engaged in the research and development work of metallic as well as optical fiber telecommunication cables in the Acedemy of Posts and Telecommunications of MPT (Beijing, 1956-1965) and the fifth Research Institute of MPT (Chengdu, 1965-1985, as Deputy Chief Engineer). He is now a Council Member of China Institute of communications(CIC) and Director of the Telecommunication Line Committee of CIC. He is also one of the Advisors of the Cheng du Cable Plant.

Investigations on a Radiation Hardened Multimode Fibre

M. Emmerich

Kabelwerk Oberspree GmbH
Berlin, Germany

Abstract

The results of investigations on a radiation hardened multimode fibre at steady state gamma and pulsed electron radiation are presented. The influence of the wavelength, the temperature, the launched power and the dose rate on the radiation induced losses is shown. Different cable constructions using these fibres are presented.

1. Introduction

Because of the various advantages of optical fibres, their application is of great interest under adverse environmental conditions like nuclear radiation too. The standard multimode fibres are very high sensitive against radiation. Because of typical induced loss of 70 dB/km at 1300 nm at a total dose of 10^4 rads these fibres are unsuitable for the use in data communication systems under radiation environment. It was necessary to develop a new radiation resistant fibre. The research was concentrated on a multimode fibre, because of the smaller problems when coupling different cable lengths by lens-connectors in comparison to single-mode ones. Under the same conditions this new fibre shows a loss increase of only 2 dB/km [1].
This paper is to investigate the influence on the radiation induced losses both at steady state and pulsed radiation dependent on the most important fibre-independent parameters like the total dose, the dose rate, the temperature, the wavelength and the launched power. The results allow to estimate the application of the fibre under dif-ferent environments. Additional to the measurements in the wavelength range between 600 nm and 1700 nm to find out the influence of wavelength on the radiation induced losses the other examinations were made at both typical wavelengths for multimode fibres 850 nm and 1300 nm.

2. Fibre Design

The research was made on a Ge-doped graded index multimode fibre with the dimensions 50/125 µm. Also other dimensions like 62.5/125 µm are possible. The typical optical values for this fibre are:

Attenuation at 850 nm	: 2.5 ± 0.1 dB/km
Attenuation at 1300 nm	: 0.9 ± 0.1 dB/km
Bandwidth at 850 nm	: 400 MHz·km
Bandwidth at 1300 nm	: 800 MHz·km
Numerical Aperture	: 0.20 ± 0.015

3. Steady State Gamma Radiation

For the steady state radiation a Co^{60} source with a maximum activity of 600 Ci and a dose rate of $3 \cdot 10^4$ rad/min at a spool diameter of 4 cm was used. The dosimetry was realised with a CAPINTEC Exposure/Exposure-Rate Meter Model 192. Fig.1 shows the experimental apparatus. The following dependencies of the radiation induced losses were measured :

* Wavelength in the range from 600 nm to 1700 nm
* Temperature between -50°C and +100°C
* Launched power from 0.01 µW to 650 µW
* Dose rate in the range from 1 rad/s to 157 rad/s with doses up to 10^8 rads.

3.1. Wavelength Dependence

Fig.2 shows the radiation response of the fibre at doses up to 10^6 rads for the wavelengths from 600 nm to 1700 nm. In the whole range the induced losses decrease continuously with increasing wavelength in contrast to P-codoped fibres, where the attenuation rises again at wavelengths greater than 1100 nm. Because of the limited dynamic range of the measurement equipment the investigations were made with 2 different fibre lengths. In the case of the short wavelengths the attenuation was measured on a fibre length of 1.02 m , with higher ones, where the induced losses are smaller it was performed at a 80 m fibre length. The larger launched power in the short fibre sample produces a lower value of loss in comparison to the results on the longer fibre at the same wavelength. This is due to the 'Photobleaching-Effect'. The curves of the spectral attenuation show that the application of this fibre is sensible only in the 2. optical window at 1300 nm or at higher wavelengths. For a total dose of 10^6 rads the induced loss at 850 nm was 331 dB/km, but at 1300 nm only 8.9 dB/km.

3.2. Temperature Dependence

For the use of this fibre under extreme environmental conditions, additional to the radiations at room temperature (RT), measurements were made at -50°C and 100°C. In Fig.3 and 4 the induced losses are presented at 1300 nm during and after irradiation. The values at -50°C are about 7 times higher than at RT and 100°C in spite of the absence of `Thermal Annealing`. At 100°C this annealing-effect was not visible any more. After removal from the radiation field only the -50°C curve shows a significant recovery.

3.3. Dependence on the Launched Power

These investigations were made to find out whether it is possible to reduce the losses during the irradiation by using the `Photobleaching-Effect`. Dependent on the wavelength the typical launched powers of LED's in communication systems are about 10 µW. At 850 nm a significant decrease of induced losses with increasing launched power becomes visible (Fig.5). For P > 20 µW an additional improvement couldn't be measured. In comparison no influence of the power of the light source in the range of 0.01 µW to 324 µW could be observed at 1300 nm. The fluctuation of the 324 µW curve is caused by drifting and instabilities of the laser diode used in this case in contrast to the LED-sources for the lower launched powers.
This shows that at the typical launched power of 10 µW effects a loss decrease by 'Photobleaching' for short wavelengths. To eliminate every influence of 'Photobleaching' on the attenuation measurements of the other parameters a launched power of 1 µW was used whole the time.

3.4 Dose Rate Dependence

For the different application fields of these fibres such as nuclear power techniques, medicine or military use, different dose rates occur, varying about several decimal places. To compare this influence on radiation induced losses, the attenuation of the fibre was measured for dose rates between 1 rad/s and 157 rad/s and total doses to 10^8 rads. The values of induced losses do not differ much when changing the dose rate at both wavelengths (Fig. 7,8). Above $3{\cdot}5{\cdot}10^5$ rads the attenuation reaches a saturation, independent of the dose rate. In the diagram 'Induced Loss/Dose Rate over Time' (Fig.9) the curves measured for the different dose rates coincide, but only below the 'saturation dose'. You can approximately calculate the attenuation as a function of the dose for any dose rates if you multiply the x- and y-axis by the interesting dose rate [2]. On the other hand measurements with -50°C show, both at 850 nm and 1300 nm, a stronger dependence on the dose rate during and after gamma radiation than at RT (Tab. 1).

Tab.1 Induced Losses [dB/km] in Dependence on Dose Rate and Temperature (Total Dose 10^4 rads)

Dose Rate	λ [nm]	Temperature 25°C	-50°C
1 rad/s	850	32.1	37.2
	1300	1.2	5.5
22 rad/s	850	43.7	119
	1300	2.3	13.7

4. Pulsed Electron Radiation

The fibre was exposed to pulsed electron radiation from 500 rads to 10^5 rads in a 20 ns pulse using a FEBETRON 705 equipment with an electron energy of 1.1 MeV to 2.3 MeV (Fig.10). Again radiation induced losses in dependence of the temperature, the launched power and the total dose were measured.

4.1 Dose Dependence

The fibre was irradiated with 500 rads, 10^4 rads and 10^5 rads at 25°C. Fig.11 and 12 show the dose dependence of the losses at 850 nm and 1300 nm. The attenuation recovers within 10 s for approximately more than 2 decimal places. This means that the attenuation on 1300 nm at a dose of 500 rads drops from 110 dB/km to 0.1 dB/km in this time.

4.2 Temperature Dependence

For an electron dose of 10 krads the influence of temperature at -50°C, 25°C and 100°C was measured. Significant differences in the recovery of attenuation become visible for both wavelengths. Fig. 13 shows the curves at 1300 nm. The increasing of attenuation of the 100°C-curve after $1 \cdot 10^{-2}$s is genuine. One reason for this reaction could be the conversion at high temperatures of short-lived fault centres (colour centres) within long-lived ones, which leads to this increase in attenuation. You can see the same behaviour on the recovery curve for the constant ray treatment (Fig.4), where also the 100°C measuring curve shows an increase in attenuation past irradiation.

4.3 Influence of Launched Power

At 850 nm as well as at 1300 nm the dependence of radiation induced losses from the launched power at -50°C, 25°C and 100°C with doses of 1 krads was examined. By varying the launched power between 1 µW and about 400 µW no influence on the attenuation by Photobleaching at both wavelengths was visible. Also at -50°C and 100°C no changes could be measured.

5. Cable Constructions

Especially for the radiation hardened multimode fibre different metal free cable constructions were developed. Fig.14 shows a cable, designed for mobile use, with high flexibility, low temperature dependence (less than 0.1 dB/km increase of attenuation in the range of -50°C to 70°C) and a permissible tensile strength of 2500 N. For indoor applications we use the cable type, shown in Fig.15, with 2 to 4 optical fibres. The jacket of this cable consists of a halogen free, flame retardent, low smoke material.
The cable in Fig.16 was developed for a special customer, who wanted to install a radiation resistant optical fibre cable in a hanging position over 1000 m in a storage for nuclear material. Therefore this cable was constructed for a high tensile strength of 8000 N.

6. Summary

A radiation hardened multimode fibre was examined under steady state gamma and pulsed electron radiation. The influence of fibre-independent properties like wavelength, launched power, temperature, dose rate and total dose were tested.
At 1300 nm the fibre shows a good resistance against radiation. During steady state irradiation the influence of temperature changes in the range between -50°C to 100°C, the variation of launched power between 0.01 uW and 324 uW and the dose rate from 1 rad/s to 157 rad/s on induced losses is very small.
While pulsed radiation with varying launched power no changes in the behaviour of the attenuation occured. However a significant dependence of the induced loss on the temperature was measured.
Cable types for different applications were presented.

7. Acknowledgement

The author thanks Dr. H. Henschel, Fraunhofer Institut INT Euskirchen, for arranging the radiation tests.

References

[1] M.Emmerich, U.Reinholz
"Strahlenresistenzuntersuchungen an Lichtwellenleitern für das 2. optische Fenster", Scientific Reports of the Militärtechnische Institut Königs Wusterhausen, 1989

[2] H. Büker, F.W. Häsing, St. Wanzek, Report of the 1991 Meeting of the Nuclear Effects Task Group, NATO Panel 4, RSG 12, Sept. 16-18, 1991, NRL Publication 218-6505

H. Henschel, to be published



Michael Emmerich (35) received his diploma in electrical engineering from the Technische Universität Dresden. 1982 he joined Kabelwerk Oberspree. He is engaged in the development of optical fibres cables and optical measurement techniques.

Figure 1

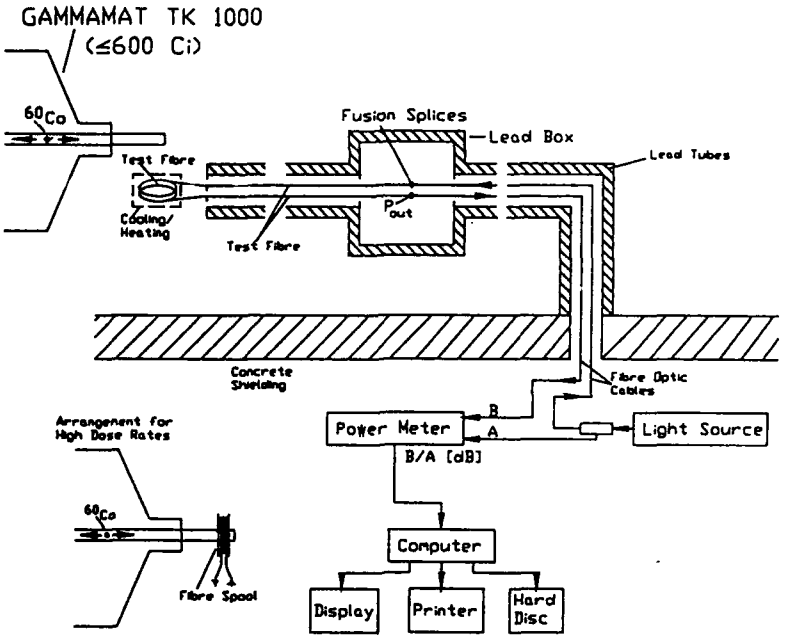
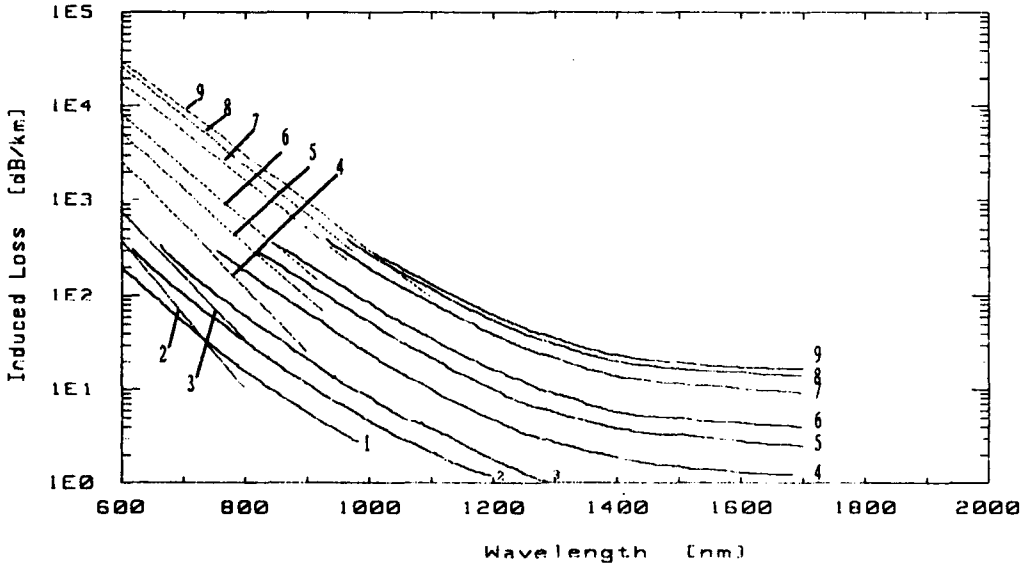


Figure 2: Wavelength Dependence of the Induced Loss



Dose Rate	$\dot{D}_\gamma$ =	22.12 rad(SiO_2)/s
Fibre Temperature	T =	23 °C
—— **Fibre Length**	L =	1.02 m
····· **Fibre Length**	L =	80 m

1	D_γ = 3 krad	2	D_γ = 6 krad	3	D_γ = 10 krad
4	D_γ = 30 krad	5	D_γ = 60 krad	6	D_γ = 100 krad
7	D_γ = 300 krad	8	D_γ = 600 krad	9	D_γ = 1 Mrad

Temperature Dependence at λ = 1300 nm
(Steady State Irradiation)

Figure 3: Radiation

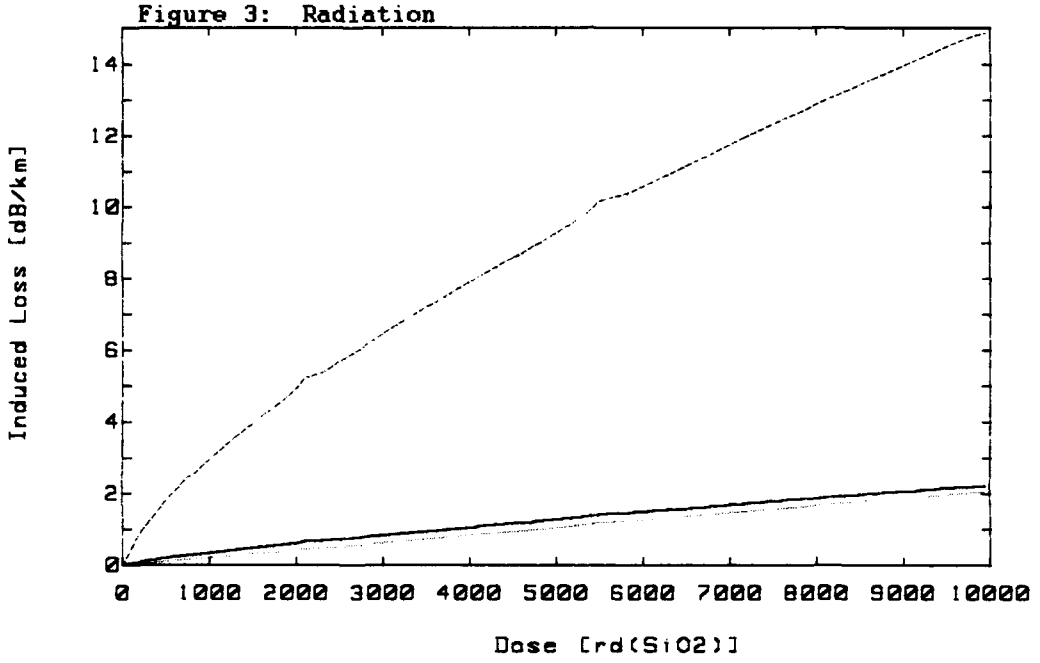
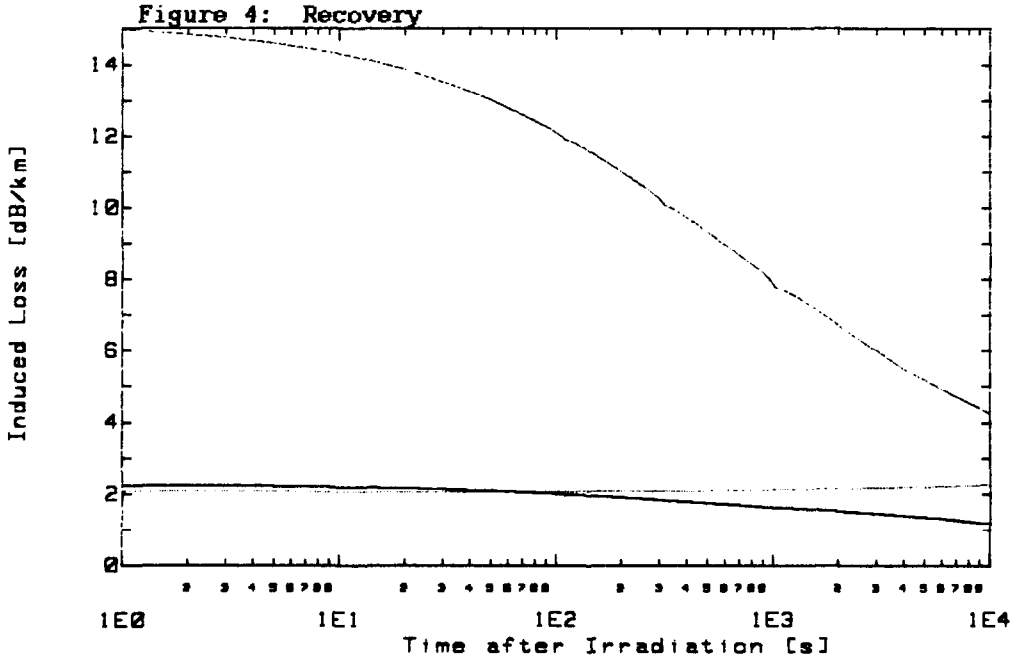


Figure 4: Recovery



Launched Power P = 1 µW
Dose Rate $\dot{D}_\gamma$ = 22.12 rad(SiO_2)/s

—— T = 23°C, ····· T = 100°C, ------ T = -50°C

Dependence on Launched Power
(Steady State Irradiation)

Figure 5: λ = 850 nm

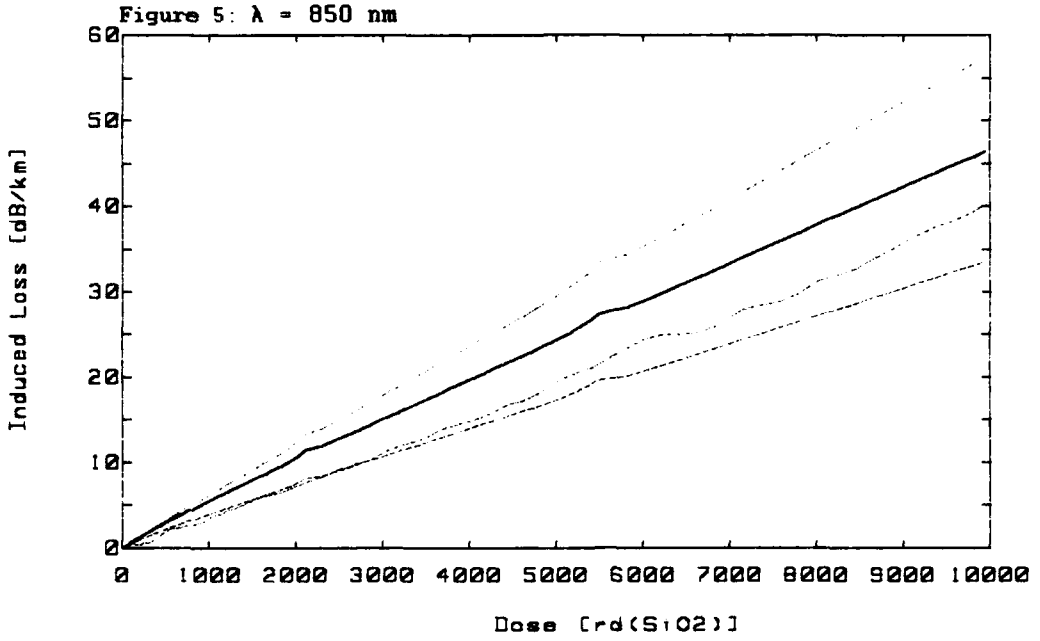
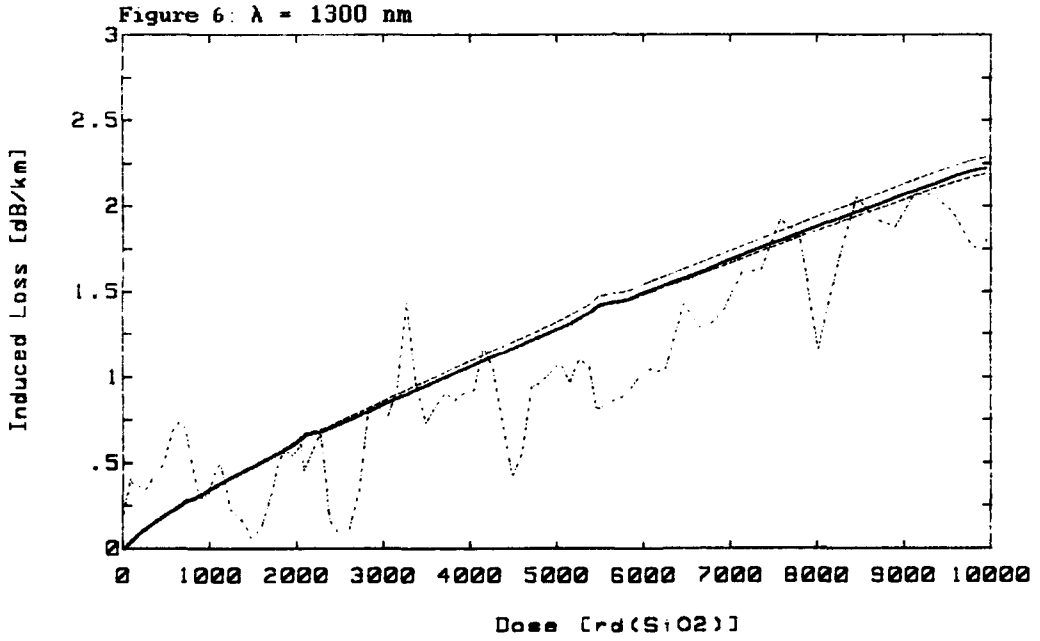


Figure 6: λ = 1300 nm



Dose Rate $\dot{D}\gamma$ = 22.12 rad(SiO_2)/s

Fibre Length L = 20 m

Fibre Temperature T = 23 °C

P = 0.01 µW, —— P = 1 µW, ····· P = 20,9 µW

P = 650 µW

Dependence on Dose Rate
(Steady State Irradiation)

Figure 7: λ = 850 nm

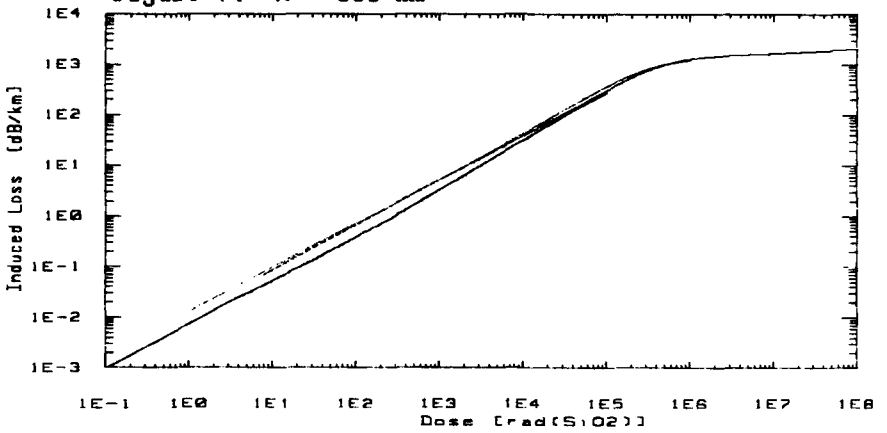


Figure 8: λ = 1300 nm

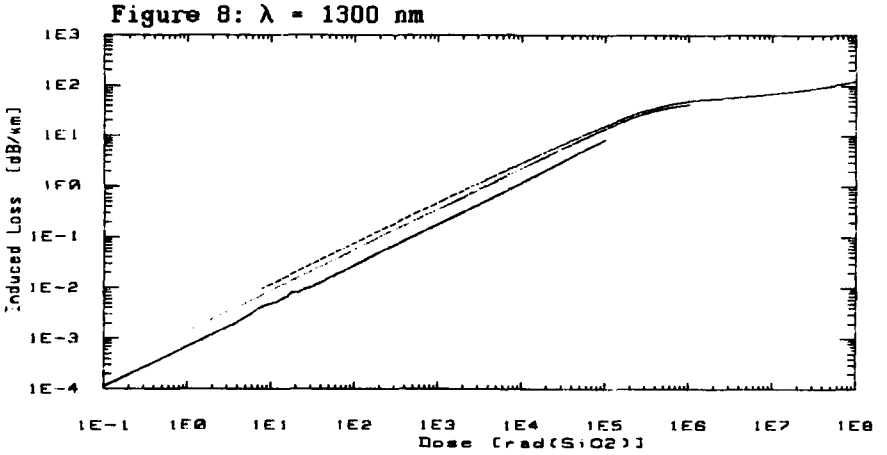
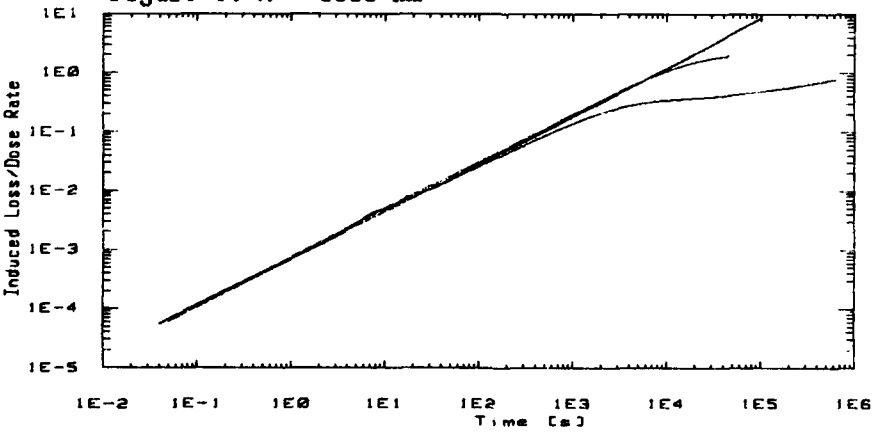


Figure 9: λ = 1300 nm

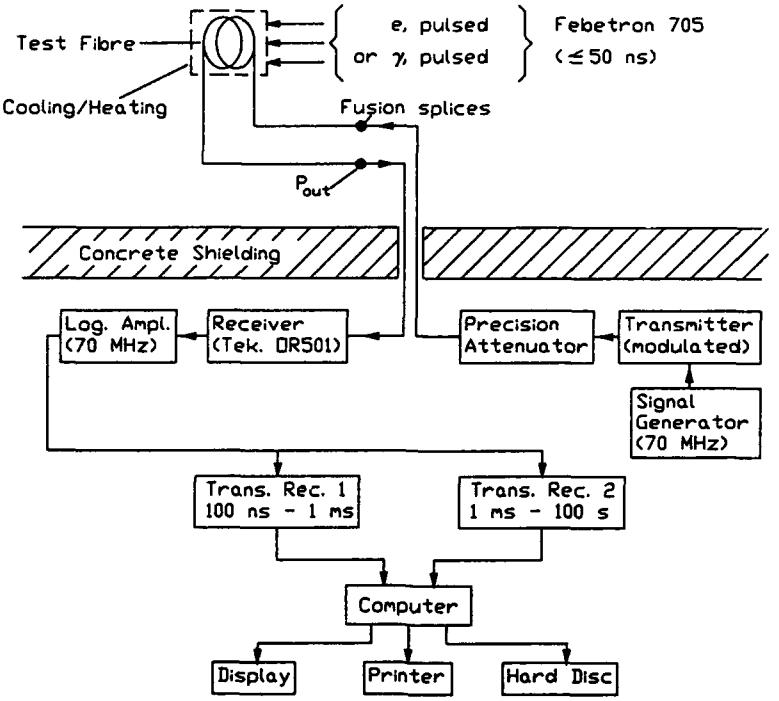


Launched Power P = 1 µW
Fibre Temperature T = 25 °C

——— $\dot{D}_\gamma$ = 1.007 rad/s

$\dot{D}_\gamma$ = 22.12 rad/s $\dot{D}_\gamma$ = 157 rad/s

Figure 10



Dose Dependence
(Pulsed Electron Radiation)

Figure 11: λ = 850 nm

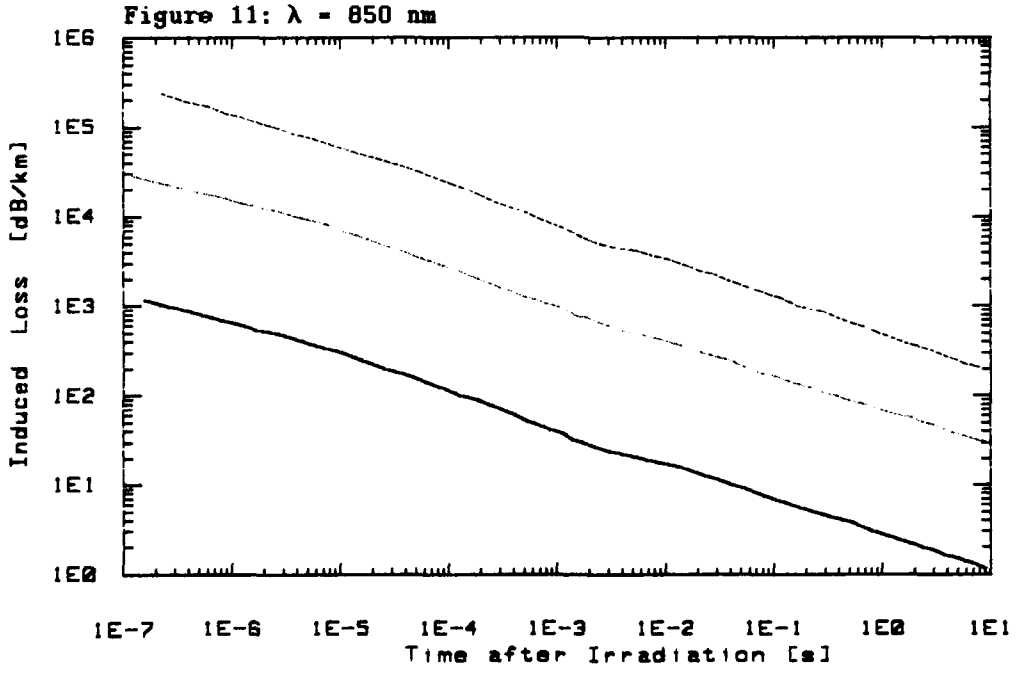
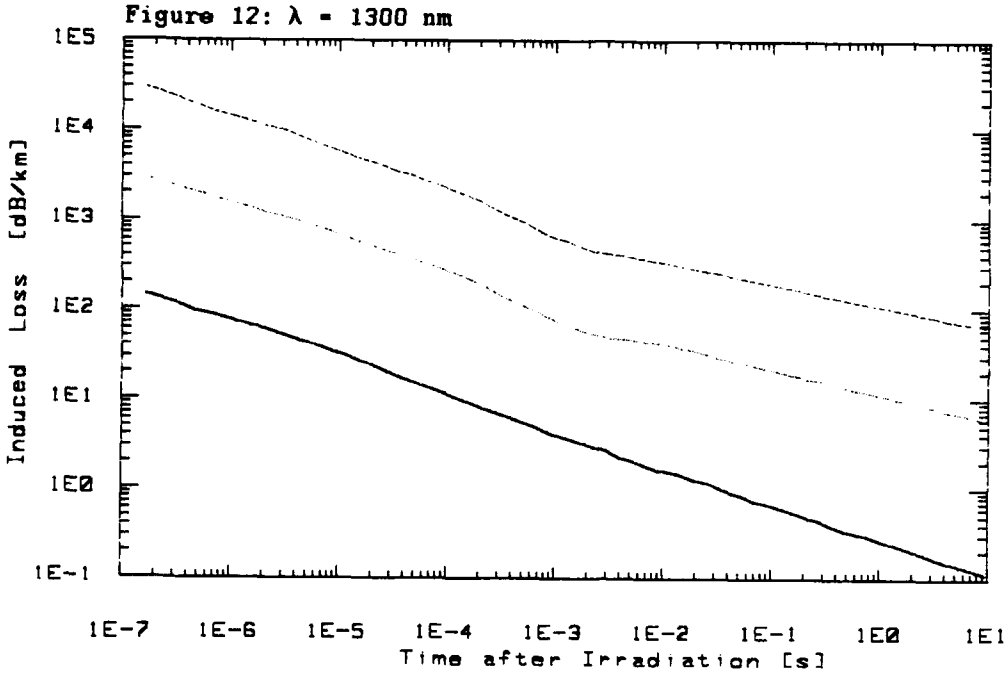


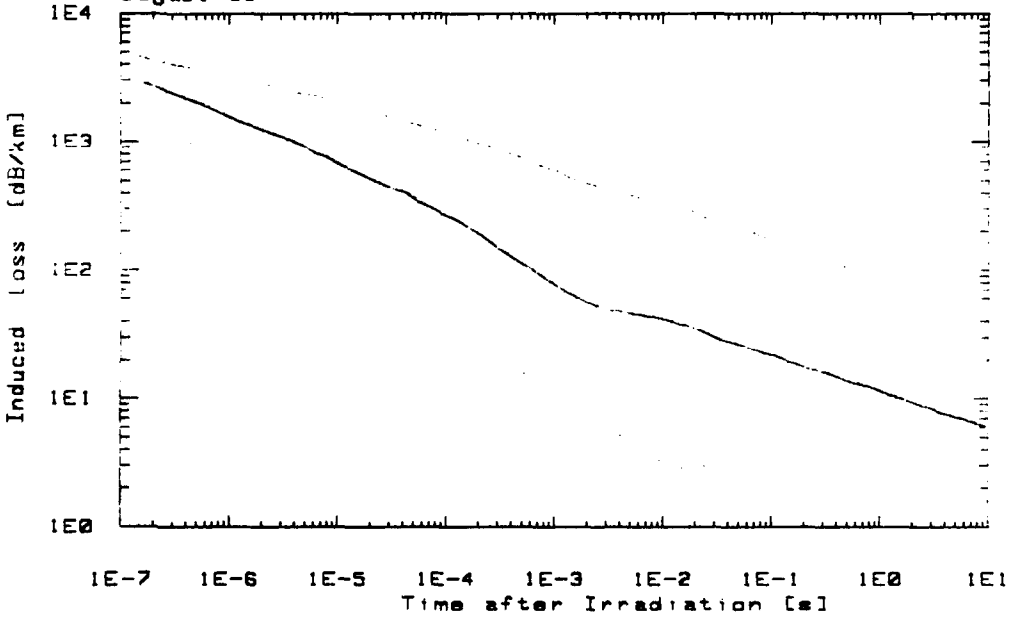
Figure 12: λ = 1300 nm



——— D_e = 500 rad(SiO_2)
····· D_e = 10^4 rad(SiO_2)
- - - - - D_e = 10^5 rad(SiO_2)

Temperature Dependence
(Pulsed Electron Radiation)

Figure 13



Electron Dose D_e = 10 krad
Launched Power P = 10 µW
····· T = -50 °C ——— T = 25 °C T = 100 °C

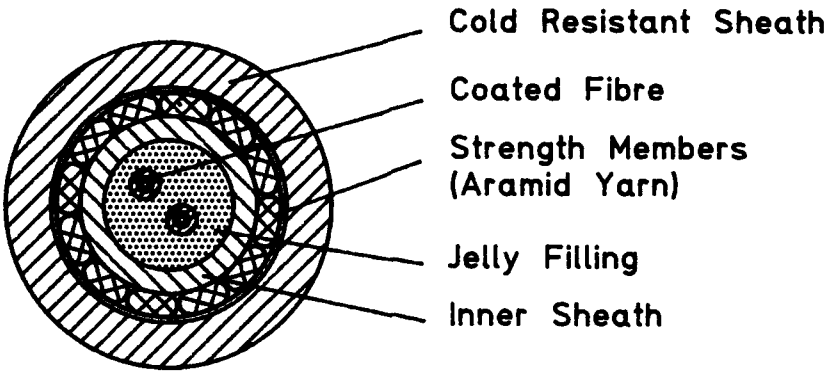


Fig. 14 Cable for Mobile Use

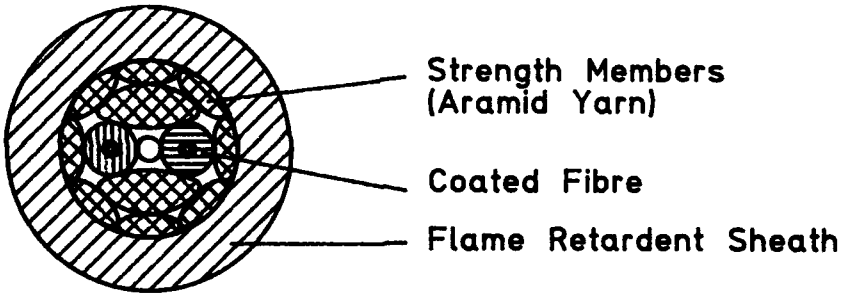


Fig. 15 Indoor Cable

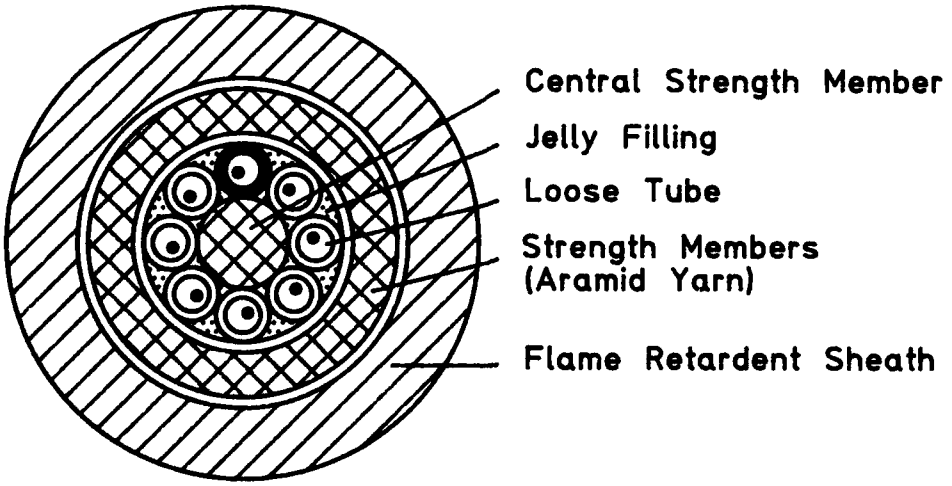


Fig. 16 Cable for High Tensile Performance

OPTICAL CABLE IDENTIFIER UTILIZING THE EXTERNAL PHOTOELASTIC POLARIZATION MODULATION

H.Nimura, A.Fujisaki, *K.Kinoshita

THE FURUKAWA ELECTRIC CO.,LTD
6 Yawatakaigan dori, Ichihara, Chiba, 290 Japan
Tel. +81-436-42-1773 Fax. +81-436-43-5805
***TOKYO ELECTRIC POWER COMPANY**
1-1-3 Utisaiwaityou, Chiyoda, Tokyo, 100 Japan
Tel. +81-3-3501-8111 Fax. +81-3-3596-8525

ABSTRACT:

Utilizing the External Photoelastic Polarization Modulation method, we have developed the optical cable identifier for several types of optical cables. This device can be used for distance of longer than 30km.

INTRODUCTION:

The high demand for optical cables has increased the number of construction works for optical cable installation, branching and root changing. And numbers of links are rapidly increasing in large cities where several optical cables are installed in many of single routes. However, because the optical cables have moved on of dielectric, there have been no means to correctly identify the optical cables and several accidents have occurred each year such as cutting other optical cables incorrectly. In order to eliminate these troubles, the need for an optical cable identifier have been mounting high. To meet this demand, we have developed an optical cable identifier utilizing External Photoelastic Polarization Modulation (EPPM) method.

OCI METHOD AND CONFIGURATION:

The optical cable identifier (OCI), we have developed, consists of a light source which emits the continuous wave light, polarization modulator utilizing EPPM, and optical signal receiver which detects polarization modulated signal with an analyzer.

Let us assume a work of optical cable identification in the way of a route connecting two offices (Fig.1). The light source is installed in office 1, and the receiver with a analyzer and O/E is in the office 2. By applying an ultrasonic wave signal from outside of the sheath of the optical cable with the polarization modulator, the state of polarization light passing through the optical cable is modulated at the work site. This signal is received in the office 2 and the cable is recognized whether the objective cable is or not. This is the system to identify the optical cable.

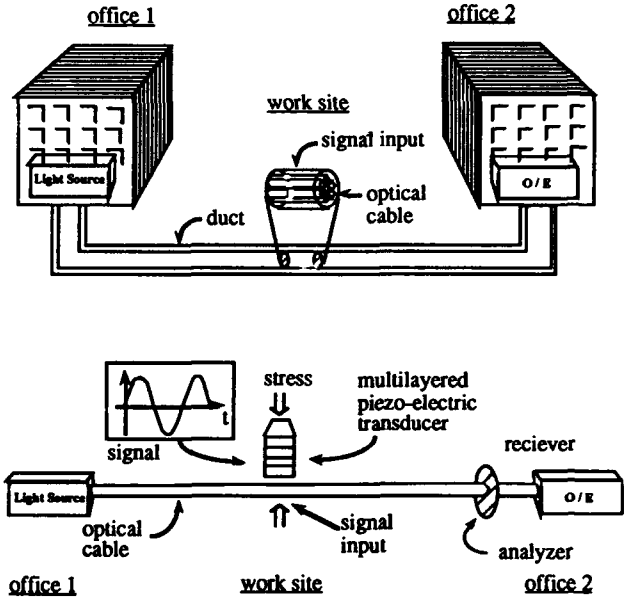
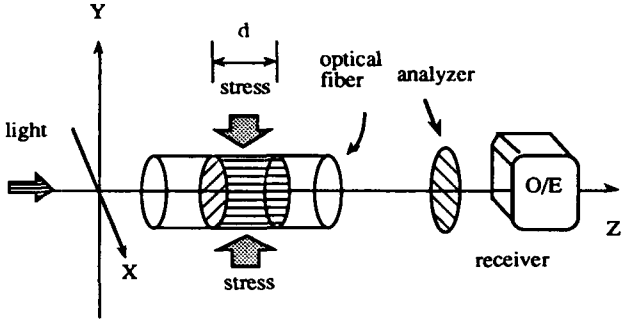


Fig 1. Configuration of optical cable identification.

MECHANISM OF EPPM:

Fig.2 shows the mechanism of the EPPM method in detail. When a stress signal is applied into the optical fiber from direction Y at the signal applying point, a index difference occurs between X and Y axes of the optical fiber, by the photoelastic effect. The index difference causes a phase difference between polarization X and Y axes of the light passing through the optical fiber. The signal light which is modulated in polarization phase and transmitted through the optical fiber and passes through the analyzer at

the receiver is converted into the intensity modulated optical signal. This signal is known to vary proportionate to the strength of stress and stress applying length (d) at the signal applying point.



$$\sigma(t) = m \sin(\omega t)$$

$$\phi_x - \phi_y = A d \sigma(t)$$

Fig 2. Schematic diagram of the EPPM method mechanism ; Stress $\sigma(t)$ modulates the phase difference $\phi_x - \phi_y$ between x - y axis of polarization of a light.

In order to stably operate the OCI, we have studied: (1) technique to avoid sound noise and cross talk which causes identification errors, (2) selecting of an ultrasonic transducer to generate larger photoelastic effect, (3) behavior of ultrasonic signal and influence of an optical fiber position inside the optical cable.

CROSS TALK AND SOUND NOISE:

Misidentification may happen if ultrasonic signal conducts to other adjoining cables. So, ultrasonic signal cross talk between adjoining cables should be small. However, it has been confirmed that cross talk is sufficiently small when ultrasonic signal frequency is greater than 20kHz. And if frequency band of ultrasonic signal and frequency band of audible sound is same, it causes uncomfortable noise. Frequency bandwidth of audible sound is from several hundred Hz to about 15kHz. So, it is necessary to use frequency of ultrasonic signal with higher than 20kHz.

ULTRASONIC TRANSDUCER:

Fig 3 shows the frequency characteristics of various vibrators (motor, voice coil and multilayered piezo electric transducer), audible sound noise and cross talk. However, the frequency bandwidth of signals, which are

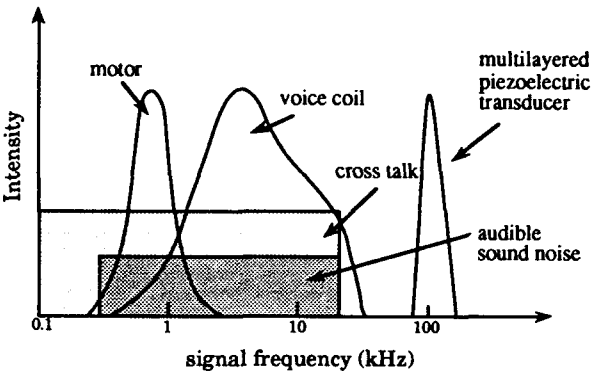


Fig3. Frequency bandwidth of various vibrators.

mechanically generated by motor and voice coil, exist in sound noise and cross talk bandwidth. So, we have utilized the multilayered piezoelectric transducer that resonance frequency is 102 kHz. In this transducer, we can use frequency bandwidth of lower than 120kHz that ultrasonic signal is not absorbed into optical cable sheath (polyethylene sheath). It can generate large stress signal because PZTs are multilayered with about a hundred layers. And it is so useful to drive because this transducer has low impedance. Fig 4 shows frequency characteristics of multilayered piezoelectric transducer. Fig 4 shows that resonance frequency of this transducer is around 102 kHz.

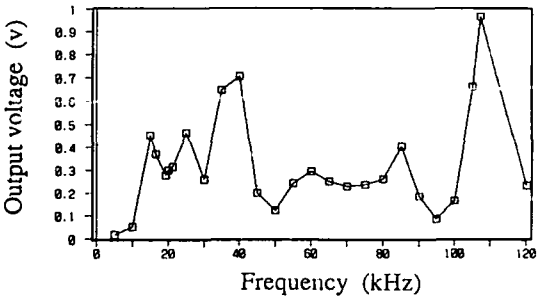


Fig 4. Frequency characteristics of multilayered piezoelectric transducer.

OPTICAL CABLE STRUCTURES:

We used two types of optical cable in this experiment. Fig.5 shows the structures of cables used in this experiment. TYPE-A optical cable consists of polyethylene sheath, 8 loose tubes which has 6 fibers, FRP strength member, and jelly. Type-B optical cable consists of polyethylene sheath, 6-slotted-rod which has 4 pieces of 2-fiber ribbons in a slot, FRP strength member, and jelly. Both type-A and type-B are

filled up with jelly compound. This element of jelly compound have great implications for transmission of ultrasonic signal.

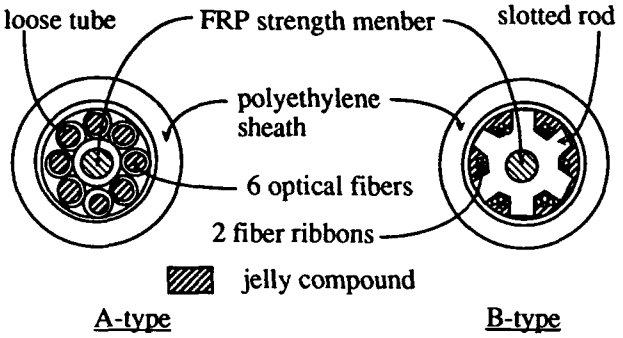


Fig.5 Optical cable structure.

Both Fig 6 and Fig 7 show the result of test that ultrasonic signal is applied into optical cable out of cable sheath from all directions. Fig 6 shows A-type optical cable and Fig 7 shows B-type optical cable. At both Figures, x axis shows the signal applying direction and y axis shows the SN ratio at the receiver side. As both types of optical cables, directions of signal application cause fluctuations of SN ratio at receiver. This is because of difference between ultrasonic signal applying direction and position. So, it become necessary to study the way that ultrasonic signal is conveyed in the optical cable.

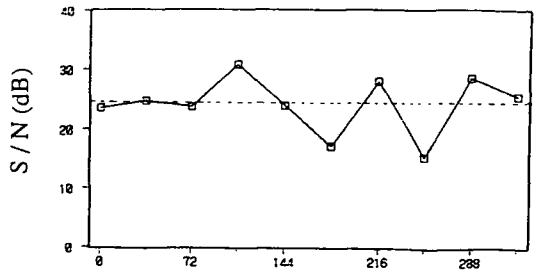


Fig 6. Relation between signal applying direction and SN ratio. (type-A)

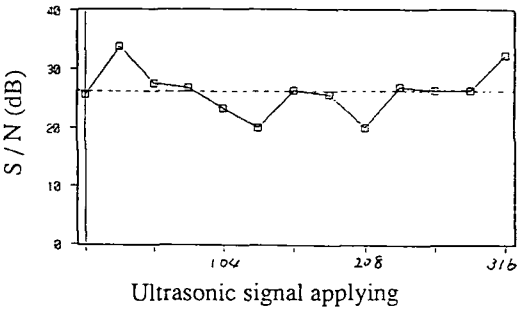


Fig 7 Relation between signal applying direction and SN ratio. (type-B)

TRANSMISSION OF ULTRASONIC SIGNAL:

When the way that ultrasonic signal is conveyed in the optical cable is considered, reflection and attenuation and directivity of ultrasonic signals are important. Let us assume a case that ultrasonic signal passes through the boundary surface which solid A is contacted with solid B. And solid B has extremely larger acoustic impedance than solid A. When ultrasonic signal inserts into solid B from solid A, signal is reflected and signal intensity decreases. However, as optical cables we used in this experiment, all gaps are filled up with jelly so that acoustic impedances are almost same value. So, attenuation can be ignored.

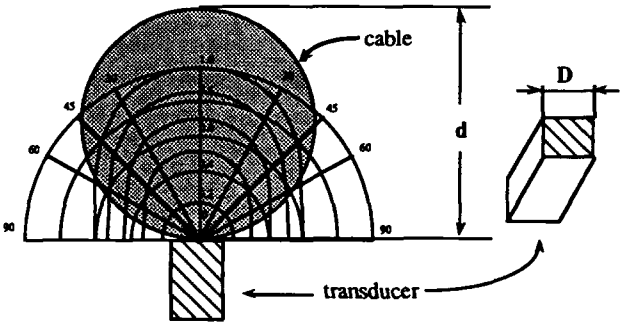


Fig 8.Transmission of ultrasonic signal in optical cable.

But directivity of 102 kHz ultrasonic signal is not able to ignore. When we would calculate directivity exponent of 102kHz ultrasonic signal from diameter of sound source D and wavelength of ultrasonic signal λ, and we had got directivity exponent about 0.5. When it is 0.5, the way of ultrasonic signal transmission is shown in Fig 8. Fig 8 shows that it is impossible to cover all the cable by only one transducer because the diameter of sound source D is smaller than the diameter of optical cable d.

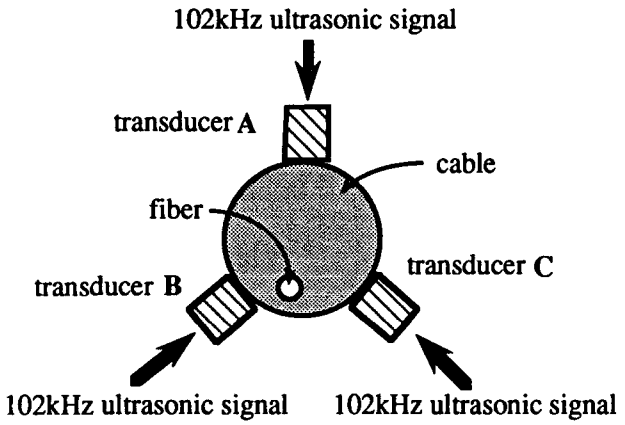


Fig 9. Signal applying structure.

So, we develop the method to apply ultrasonic signal from three directions at intervals of 120 degree. Fig 9 shows this structure. By this method, wherever the position of monitoring optical fiber is inside the optical cable, it become possible to identify at least one signal in the three signals at the receiver side. However, if all multilayered piezoelectric transducers are driven at the same time, the problem of interaction may happen and the fluctuation of ultrasonic signal intensity occurs inside the optical cable. So, we develop new technique as shown in Fig 10.

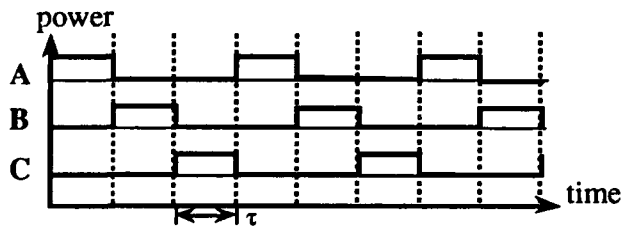


Fig 10. Signal applying timing.
(A , B , C : transducer)

At Fig 10, x axis shows drive timings of each multilayered piezoelectric transducer. Using this technique to drive each multilayered piezoelectric transducer alternately, we have solved the problem of interaction and it is also useful to decrease electrical power consumption

SPECIFICATIONS:

Fig 11 shows the relation between applied driving voltage of multilayered piezoelectric transducer and SN ratio at the receiver. And, Fig 12 shows the relation between receiving optical level and SN ratio. These are important factors to define the dynamic range of this OCI system. At Fig 11, x axis shows the driving voltage of multilayered piezoelectric transducer and y axis shows the SN ratio at the receiver. This figure shows that receiving SN ratio vary proportionate to applied driving voltage. And, in this OCI system, it is important to drive by battery. So, we decide to adopt 12V as driving voltage because 12V batteries are widely used.

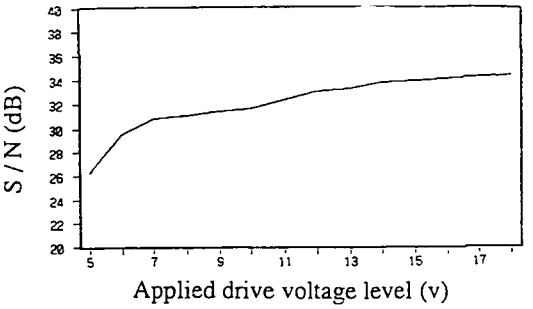


Fig 11. Relation between drive voltage of transducer and SN ratio at the receiver.

Taking the minimum receiving optical level into consideration, it is necessary to have more than 25 dB SN of ratio at the receiver side in order to identify the receiving signal. Fig 12 shows that minimum receiving optical level is -11 dBm.

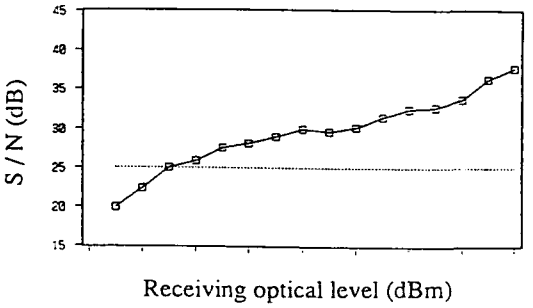


Fig 12. Relation between receiving optical level and SN ratio at the receiver.
(drive voltage: 12V)

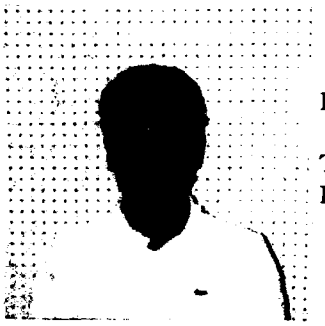
Our developed OCI system consists of high power light source unit capable of +4dBm output, receiver unit capable of minimum receiving optical level -11dBm, and transmission unit which is able to generate 102kHz and 24W ultrasonic wave. In this system, the dynamic range is realized 15 dB, that shows the possibility of long distance operation more than 30 km.

CONCLUSION:

We have developed OCI system utilizing the external photoelastic polarization modulation. Important developmental points are described here . (1) We have selected a multilayered piezoelectric transducer which has low impedance, high power and useful shape. (2) A position of an optical fiber in the cable significantly affected for transmission characteristics of the ultrasonic signal into the fiber. we have solved the problem by using a method to apply ultrasonic signal from several directions to stabilize the received intensity signal without influence of position inside the cable as shown in Fig.9. (3) The problem of cross talk and sound noise were solved by selecting an optimal frequency around 102kHz after studying the relationship between the signal frequency and cross talk.

REFERENCES:

1)H.NIMURA"EXTERNAL PHOTOELASTIC POLARIZATION MODULATION FOR OPTICAL FIBER DATA TRANSMISSION" ,40TH,IWCS,1991PP738-741

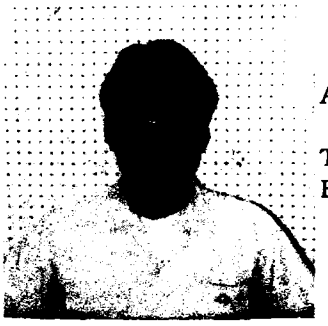


HIJIRI NIMURA

The Furukawa Electric Co.,Ltd.

Mr.Nimura received B.S.degree in physical engineering from Tohoku University in 1989 and joined The Furukawa Electric Co.,Ltd.

He has been engaged in optical transmission system research section.



AKIRA FUJISAKI

The Furukawa Electric Co.,Ltd.

Mr.Fujisaki received B.S.degree in electrical engineering from Waseda University in 1987 and joined The Furukawa Electric Co.,Ltd.

He has been engaged in optical transmission system research section.



KAZUTAKA KINOSHITA

The Tokyo Electric Power Company,Inc.

Mr.Kinoshita received B.S.degree in electrical engineering from Hiroshima University in 1976 and joined The Tokyo Electric Power Company,Inc.

He has been engaged in electronic telecommunication tusk section.

Optical cable with lateral pressure sensor

Shigeo SHIMIZU, Katsuaki SUZUKI, Atsuro TAKASE and Akihiro OTAKE

The Furukawa Electric Co.,Ltd.
2-6-1, Marunouchi, Chiyodaku, Tokyo, Japan

Abstract

An optical fiber cable is damaged by various lateral pressures. Then it is required to detect the location and degree of damage and to repair the cable immediately.

A new optical cable with lateral pressure sensor has been developed. It was found that the location of the cable deformation of 20% or more could be detected by measuring the bending loss of the optical fiber by optical time domain reflectmeter.

It is also found that the optical cable with lateral pressure sensor is expected to be applied in various optical composite cables.

1. Introduction

The optical cable is damaged by various lateral pressures. For example, the following situations may be supposed.

·The conduit cable is crushed when the conduit is destroyed.

·The direct buried cable is crushed when the land rises or sinks.

·The underwater cable is hooked by fishing net or anchor.

If the optical cable is heavily damaged, it must be immediately repaired. Therefore, from the viewpoint of maintenance of the cable line, it is important to detect the location and degree of the damage easily.

By making the optical cable easy to increase the loss structurally for the cable deformation caused by such a damage, it may be possible to detect the location and degree of the damage by measuring the optical fiber loss by the optical time domain reflectmeter. Accordingly, two types of optical cables incorporating sensing optical fibers and optical communication fibers were fabricated, and the performance of the sensing optical fiber and effects of the cable deformation on the optical communication fibers were investigated.

These optical cables with lateral pressure sensors may be applied in detection of the damage of not only the optical cables for communication but also the main body cable of optical composite cable.

2. Cable structure

Two types of optical cables and optical fibers were compared in order to investigate the effects of the cable structure. The cross-sectional structures of the optical cables are shown in Fig.1.

2.1 Optical fiber

As the sensing optical fiber, a 50/125 graded-index fiber and a single-mode fiber for 1.3 μ m band were compared in the detection sensitivity.

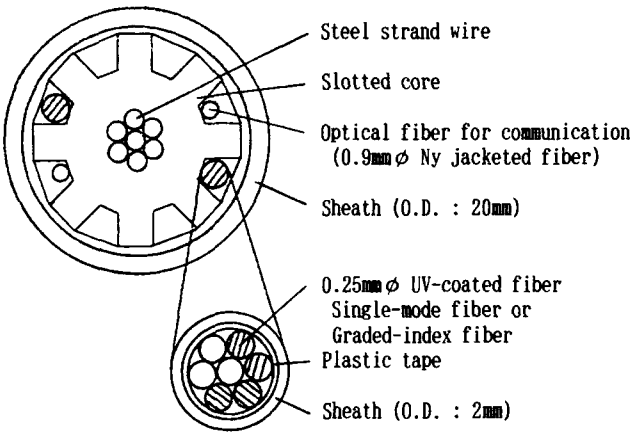
As the optical communication fiber, Nylon jacketed 50/125 graded-index fiber was used, and the effect of cable deformation on it was also investigated.

2.2 Optical cable type A

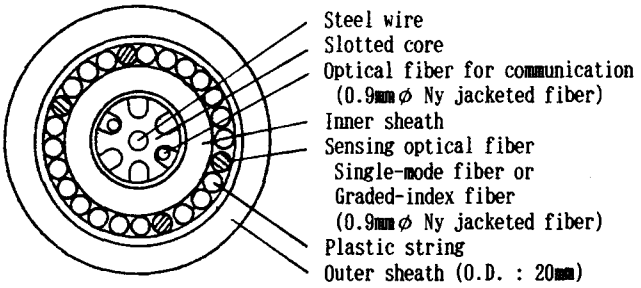
In this structure, the sensing optical unit and the optical communication fiber are accommodated in slots. The groove depth is 2mm. In order to make the sensing optical unit more susceptible to the stress of cable deformation than the optical communication fiber, it is composed of 0.25mm ϕ coated fibers stranded around a central core and sheathed with a thick wall to extend the outer diameter.

The graded-index fiber for communication was put in the adjacent slot.

The number and configuration of the



(a) Type A



(b) Type B

Fig.1 Cross-sectional structure of optical cable

sensing units are limited by the number of slots and the optical communication fibers.

2.3 Optical cable type B

The optical communication fibers are incorporated in the optical communication unit. It is disposed in the inner layer that is less affected by the cable deformation. While the sensing optical fibers are stranded in layers with plastic strings around it.

The sensing optical fiber is jacketed by Nylon with 0.9mm φ outer diameter. The diameter of the plastic string is 1.25mm φ.

This structure is free of designing because the number and configuration of the sensing optical fiber are not dependent on the dimension and structure of the optical communication unit.

3. Test and result

3.1 Test method

The optical cable was compressed with a flat plate of 50mm width at a compression rate of 1mm/min.. The deformation amount of optical cable, compression load, and loss increase of optical fiber were measured. The loss increase was measured by using LED and power meter at the wavelength of 1.3 μm and 1.55 μm for the 50/125 graded-index fiber and the single-mode fiber, respectively.

It was investigated that the shift of the relative position of the sensing optical fiber and the compression direction influenced on the detection performance.

The optical fibers were jointed as follows.

Type A : single-mode fibers and graded-index fibers in a sensing optical unit were formed in two-core loop, respectively.

Table 1 TEST RESULTS

	Optical cable type-A			Optical cable type-B		
	Sensing optical fiber		Optical communication fiber	Sensing optical fiber		Optical communication fiber
	SM fiber	GI fiber	GI fiber	SM fiber	GI fiber	GI fiber
Cable deformation at starting loss increase	12 %	13 %	21 %	17 %	16 %	22 %
Loss increase						
20% Deformed (Max.)	0.7 dB	1.3 dB	0 dB	0.6 dB	0.3 dB	0 dB
25% Deformed (Max.)	2.1 dB	2.4 dB	0.1 dB	4.4 dB	0.9 dB	0.03 dB
After removing lateral pressure	0 dB	0 dB	0 dB	0 dB	0 dB	0 dB

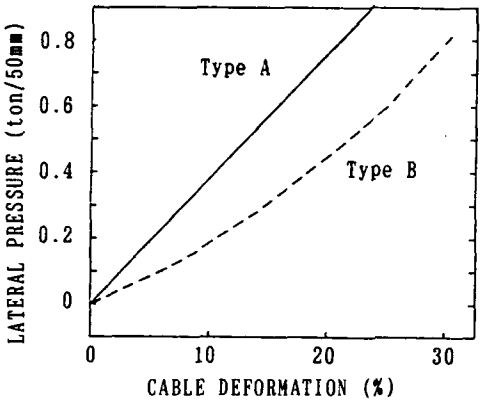


Fig.2 Optical cable deformation by lateral pressure

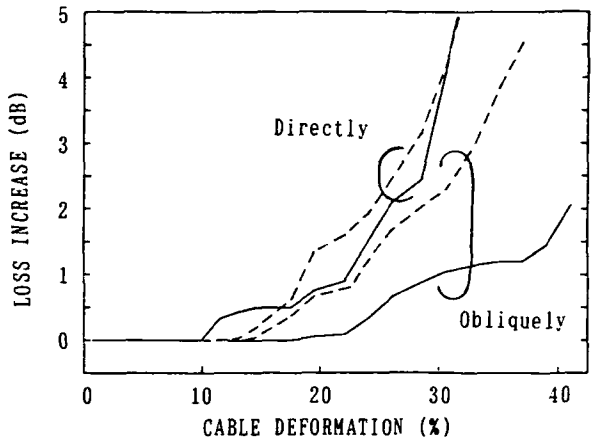


Fig.3 Loss increase of optical cable type A

Type B : single-mode fibers and graded-index fibers were disposed at the diagonal positions in the sectional area and formed in two-core loop, respectively.

3.2 Result

The results of measurements of loss increases of optical fibers are summarized in Table 1.

Fig.2 shows the optical cable deformations with lateral pressure.

Loss increases of the sensing optical fibers in optical cable type A and type B are shown in Figs.3 and 4, respectively.

Type A requires a relatively larger compressive load at a same cable deformation.

The cable deformation at which the loss of the sensing optical fiber began to increase was smaller in optical cable type A.

The loss of the optical cable type A slowly increased with respect to the cable deformation. While the loss of optical cable type B abruptly increased over the deformation of about 20% or more, and was greater than type A over the deformation of 25%.

In the single-mode fiber, when compressed directly, the loss increase is large, but when compressed obliquely, the loss increase was small. It shows the great dependence on the direction of compression.

In the graded-index fiber, whether compressed directly or obliquely, the difference of loss increase was relatively small. It shows that the dependence on the direction of compression is small.

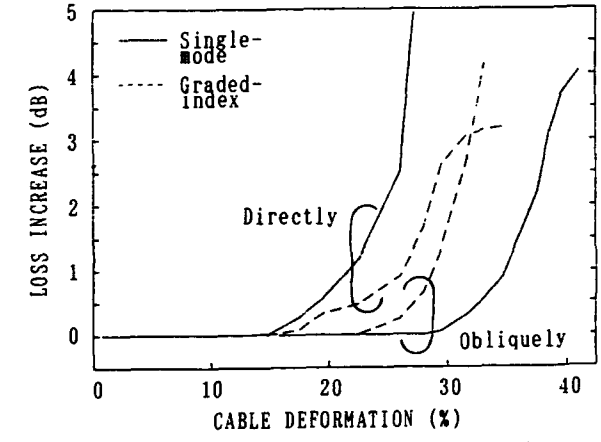


Fig.4 Loss increase of optical cable type B

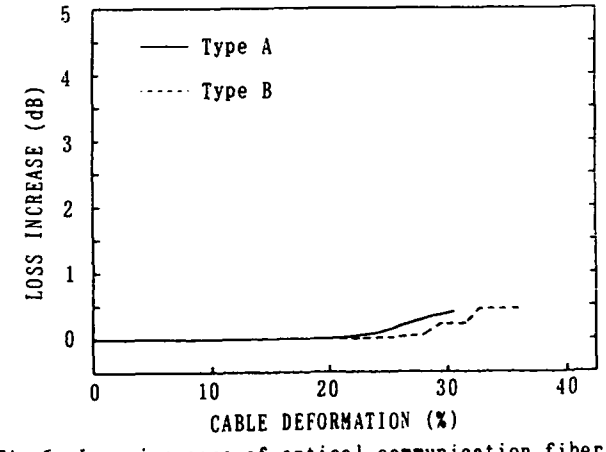


Fig.5 Loss increase of optical communication fiber

The cable deformation at which the loss of the optical communication fiber began to increase was similar on both cables.

The loss increase of the optical communication fiber was slight, as shown in Fig.5.

In both optical cables and both optical fibers for sensing and for communication, the residual losses after removing the lateral load were not observed.

These results are summarized as follows:

In the combination of cable type A and graded-index fiber, a moderate loss increase occurs at the cable deformation amount of about 12% or more. And the dependence of the sensitivity on the direction of compression is small. Therefore, it is easy to estimate the cable deformation from the loss increase amount.

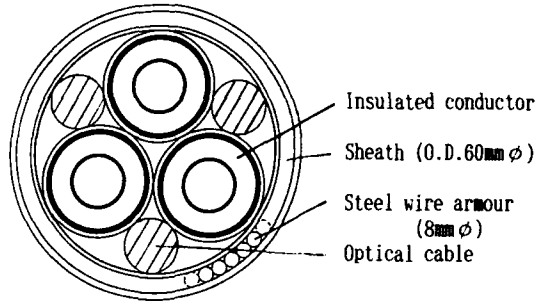
In the combination of optical cable type B and single-mode fiber, a loss increase suddenly occurs above deformation amount of 20%. It shows that the detection sensitivity is high. However, since the dependence of the sensitivity on the direction of compression is large, it is necessary to optimize the number of sensing optical fibers. It was thought that at least four fibers should be disposed at 45-degree intervals.

It was thought that the cable deformation of about 20% or more can be detected by using the optical time domain reflectmeter in both cable types.

4. Application

The optical cable with lateral pressure sensor may be used either alone or in combination with other cables so as to monitor the cable deformation by the lateral pressure. For example, when the submarine power cable is combined with this optical cable with lateral pressure sensor, it may be very useful for monitoring the power cable which has a high risk of being damaged by fishing net or anchor. In this case, the optical cable with the sensor may be composed of the optical communication fiber.

Accordingly, the submarine power cable was combined with the optical cable with lateral pressure, and the detection performance of lateral pressure deformation was investigated.



Cable O.D. 160mm φ

Fig.6 Optical composite power cable

4.1 Composite cable structure

The cross-sectional structure of the composite cable is shown in Fig.6. The optical cable with lateral pressure sensor was covered with 1.5mm thick lead in order to be water-proofed. Each one of the optical cables was stranded at three outside gaps of the power cable that was composed of three insulated conductors of 60mm in outside diameter. The outside diameter of the composite cable was 160mm.

4.2 Test method

While compressing the composite cable with a flat plate of 200mm width, the deformation amount of the composite cable, compressive load and loss increases of optical fibers were measured. At this time, the detection performance was investigated by compressing while shifting the compressing direction of the composite cable.

The losses of three optical cables inserted in the gaps were individually measured.

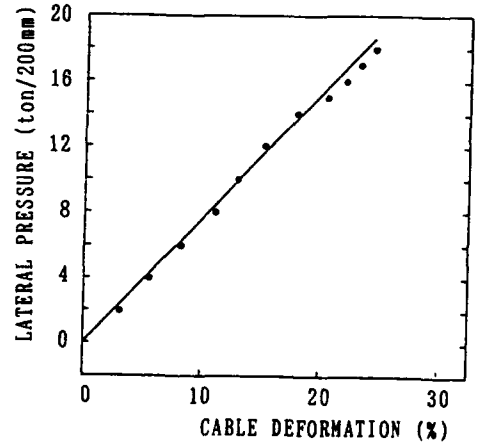


Fig.7 Composite cable deformation by lateral pressure

4.3 Result

The relation between the compression load and the composite cable deformation is shown in Fig.7. The composite cable deformation was nearly proportional to the compression load, and was about 25% at 18 ton/200mm.

The loss increase was observed typically in one of the three optical cables at one compression test. The loss increase of the other optical cables were very slight or none. It suggests a great dependence on the relative positions of the compression direction and the optical cables in the composite cable. Therefore, the most loss increase among them was plotted in a figure as the result of one compression.

Figs.8 and 9 show the results of the composite cable combined with the optical cable type A. In the single-mode fiber, large loss increases sometimes occurred, but those were small in most cases. On the other hand, the fluctuations of loss increases of graded-index fibers were relatively small. These results show the difference in the dependence on the compression direction between the optical fibers.

Figs.10 and 11 show the result of the composite cable combined with the optical cable type B. The loss increase of single-mode fiber was sharp over the deformation of about 20%. On the other hand, the loss increase of the graded-index fiber was smaller than that of the single-mode fiber, but fluctuations due to repetition were smaller. This result also seemed to be due to the difference in the dependence on the compression direction.

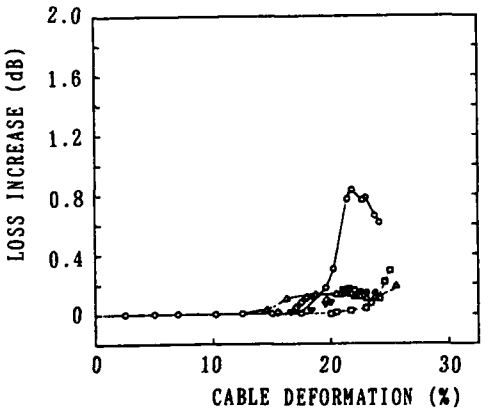


Fig.8 Loss increase of single-mode fiber in optical cable type A

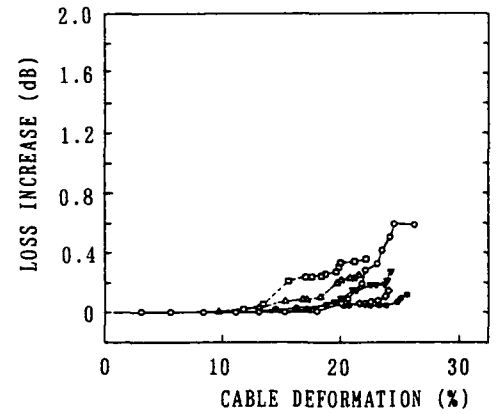


Fig.9 Loss increase of graded-index fiber in optical cable type A

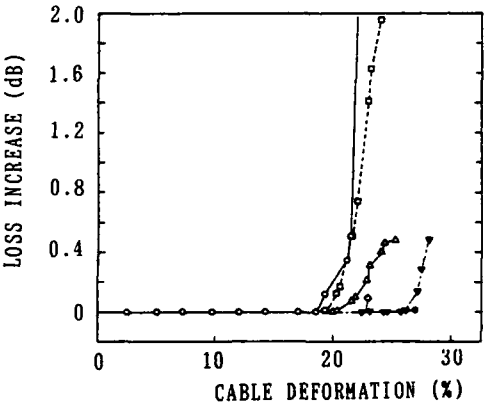


Fig.10 Loss increase of single-mode fiber in optical cable type B

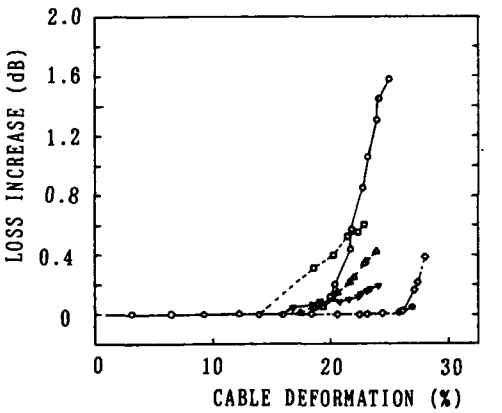


Fig.11 Loss increase of graded-index fiber in optical cable type B

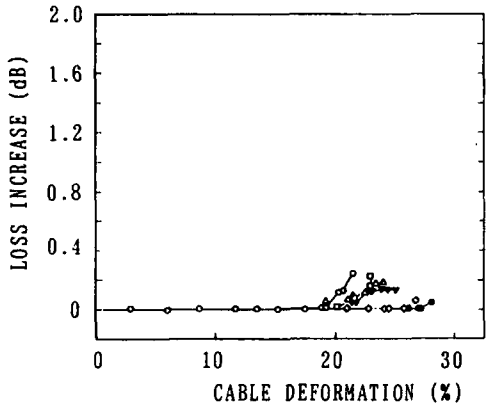


Fig.12 Loss increase of graded-index communication fiber in optical cable type B

It was found that the detection sensitivity of the optical cable type B is higher than that of type A.

The composite cable deformation at which the loss of the optical cable type A began to increase was smaller than the case of type B.

The result of optical communication fiber is shown in Fig.12. Loss increase was not observed at the deformation of less than 25% in type A. In type B, it was observed in most cases at deformation of 20%. There were no residual losses after removal of lateral pressure in both optical fibers for sensing and for communication.

5. Conclusion

The following conclusions were obtained.

In the combination of the optical cable type B and the single-mode fiber for 1.3 μ m band, when the loss was measured at wavelength of 1.55 μ m, a sharp loss increase took place at the cable deformation of about 20% or more, which shows that the detection sensitivity is large. However, since the dependence on the direction of compression is large, it is necessary to optimize the number of the sensing optical fibers.

In the combination of the optical cable type A and the graded-index fiber, a moderate loss increase occurred above at the cable deformation of 13%, and since the dependence on the direction of compression is relatively small, it seems to be easy to estimate the cable deformation amount from the loss increase.

Effects of optical cable deformation on optical communication fibers were slight.

The optical cable with lateral pressure sensor may be used not only alone as communication cable, but also in combination with other cable for the purpose of monitoring of the composite cable.



Shigeo SHIMIZU

The Furukawa Electric Co., Ltd.

6,Yawata-kaigandori, Ichihara,Chiba,290,Japan

Mr. Shimizu was born in 1957. He received B.S. degree in engineering from Nagoya University in 1980. He joined The Furukawa Electric Co., Ltd. and has been engaged in development of optical fibers and cables.

He is now a staff engineer of optical fiber transmission research section, and is a member of The Institute of Electronics, Information and Communication Engineers of Japan.



Atsuro TAKASE

The Furukawa Electric Co., Ltd.

2-6-1, Marunouchi, Chiyodaku, Tokyo,100, Japan

Mr. Takase graduated from Nagoya University in 1984 with the B.S. degree in electrical engineering. He then joined The Furukawa Electric Co., Ltd. and has been engaged in development and production of optical fiber cables.

He is now a staff engineer of Feeld Engineering Design Section, Tokyo head office.



Katsuaki SUZUKI

The Furukawa Electric Co., Ltd.

6,Yawata-kaigandori, Ichihara,Chiba,290,Japan

Mr. Suzuki was born in 1964. He graduated from Yamanashi University in 1987 with the B.S. degree in electric engineering. Then he joined The Furukawa Electric Co., Ltd. and has been engaged in development of optical fiber cables.

He is now a staff engineer of the Production Engineering Section of Optical Fiber and Telecommunication Division.



Akihiro OTAKE

The Furukawa Electric Co., Ltd.

6,Yawatakaigandori, Ichihara,Chiba,290,Japan

Mr. Otake graduated from Tohoku University and joined The Furukawa Electric Co., Ltd. in 1974. He has been engaged in research and development of optical fiber cables and those accessories.

He is now a manager of optical fiber transmission research section.

(His photo was late for printing)

A Real-Time Configuration Management System Using Two-Pin Optical Fiber Identification Devices for Optical Fiber Cable Networks

Katsuya YAMASHITA, Fumio OHTSUKI, and Yoshikazu YAMAMOTO

NTT Telecommunication Field Systems R&D Center
Nippon Telegraph and Telephone Corporation

ABSTRACT

For a more reliable and cost-effective configuration management system for line facilities, we propose using a new fiber identification (ID) module instead of the previously proposed EEPROM module. The new module consists of a matrix of resistors and switching diodes packaged into a two-pin single-in-line circuit device. The combination of two resistors is used as identification information, which is read by measuring forward and backward circuit impedances and calculating the value of each resistor. This method increases reliability by reducing the number of terminals required to one-third the number needed for the previous modules. A host computer and dedicated data transmitters for the new ID modules make up a data network and provide a reliable system module for managing network configuration. This management system module has a real-time data updating capability, which will contribute to realization of an integrated cable network operation system in the near future.

1. INTRODUCTION

To supply speedy, economical and reliable optical fiber communication services in the near future, a new integrated cable network operation system is required.[1,2] The principal reason such a system needed is that recovery from cable faults takes longer in optical fiber networks than in metallic networks, and the fault affects service quality much more because of the huge transmission capacity of a line. Another major reason is that the multi-dropping wiring used in metallic cables to effectively function with a limited number of twisted pairs is impossible in optical networks. Therefore, a line switching system for the optical network that operates in close cooperation with a correct configuration database is needed. Such a system is important in achieving effective use of cable infrastructure and quick response to service order requests.

The integrated cable network operation system under consideration will include automated and/or remote control functions for line test surveillance,[3] fiber switching,[4] and management of line configuration.[5] To effectively and reliably operate this integrated system, a highly reliable database is strongly required and a dedicated transmission network for transmission of operation signals or data among system modules is also required. In this paper, a real-time configuration management system module for attaining such a reliable database and dedicated transmission network are discussed. This management system has two key components. ID modules attached to fiber connectors and a data transmitter called LCTR. For the ID module, taking device reliability into account for practical use, a new ID module is proposed for use as the ID modules instead of the previously proposed EEPROM ID module.[5] Actual fabrication results of the new ID modules are described. LCTR transmits ID data to an operation center, and the data or control signals required by other cable network operation modules. This paper explains the basic concept of the integrated operation system and the behavior of the data transmission network within the system.

2. CONCEPT OF A LINE OPERATION SYSTEM

A block diagram of the new cable network operation system is shown in Fig. 1. The system consists of five system modules: a fiber test and surveillance system, fiber switching system, line configuration management system with data communication network, shared database, and supervisory operation platform with external communication function. The platform can supervise other system modules, which normally do their own tasks. For example, the test/surveillance system module does periodical tests on optical fibers under service and the configuration management system gathers fiber concatenation information using the data communication network to reflect the current configurations in the shared database. When an emergency or a service order occurs, an operator can interrupt the regular tasks. An example of how this integrated system behaves when a cable fault occurs is described below.

First, the platform commands the switching system module to switch faulty fibers to alternate fibers so as to minimize the line fault term. The alternative fiber routing is determined in advance according to line configuration information in the database. Then, the switching command is transmitted to switching equipment using the communication network of local controllers (LCTR), which are data transmitters in the

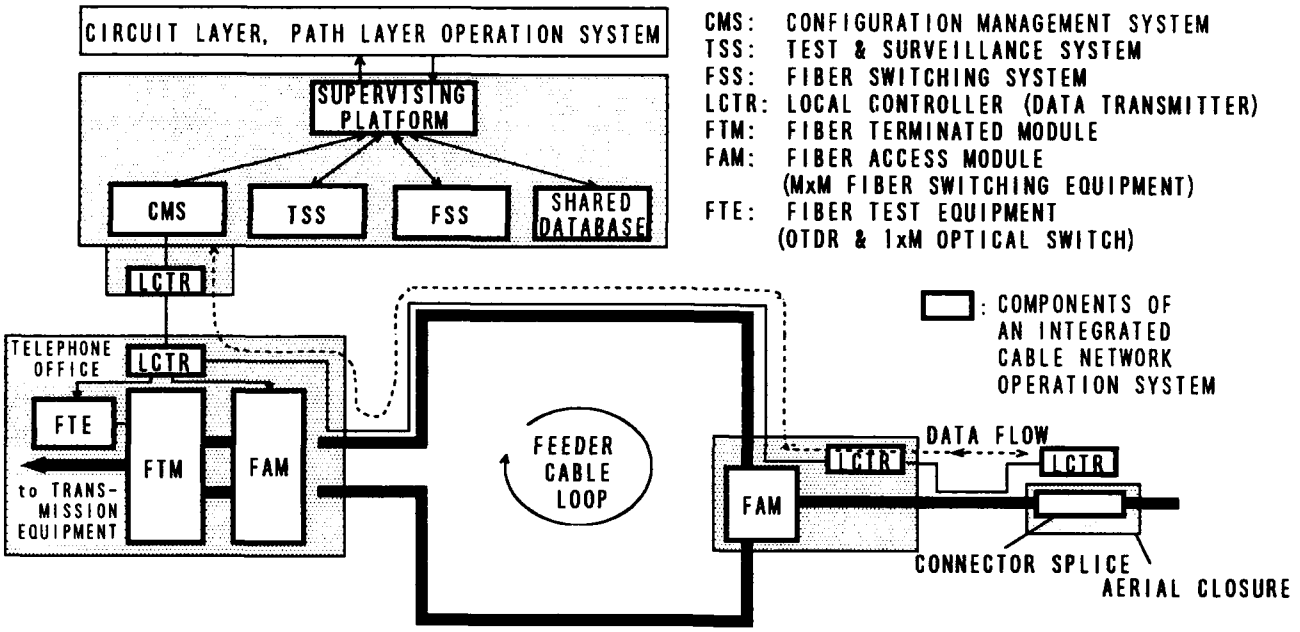


Fig.1 Basic configuration of an integrated cable network operation system

configuration management system. Afterwards, the platform commands a test and surveillance module to detect the cable fault location. According to the test results, the platform can send a cable repair order to a maintenance center. The faulty cable repair can be done at a suitable time. Thus, the integrated cable network operation system provides speedy communication recovery from cable faults and effective, economical repair planning.

This system requires reliable line configuration management. The line configuration databases of traditional metal networks are updated by manual keyboard operation, resulting in considerable updating delays with many errors that inevitably slow the response to customer requests. This fact severely restricts the realization of the integrated cable network operation system.

To avoid these defects of the conventional databases and to construct a reliable database, at the last symposium we proposed a novel line configuration management system with a real-time updating capability for fiber concatenation. The key components of the management system module are an ID module attached to an optical fiber connector and a local controller(LCTR) that serves as an ID data transmitter. LCTRs construct the data communication network. Physical line configuration or fiber concatenation, information is obtained by reading ID information from the ID modules of connected fiber pairs and by transmitting that information to the operation center over the LCTR network. A host computer in the configuration management module at the center can get the current fiber concatenation conditions and update the configuration database in real-time if connection changes are detected. The LCTR network controlled by the configuration management system can also bidirectionally transmit control signals or the data required in other system modules in the same way as for ID information. The key components of the configuration management system are described in detail below.

3. ID MODULES FOR OPTICAL CONNECTORS

There are two types of optical connectors in optical fiber networks. SC connectors interface optical fibers to communication equipment and are used indoors. MT connectors are used to join two optical fibers or optical fiber ribbons and are mainly used in fiber closures installed in the field. To cope with harsh physical conditions in the field, highly reliable physical characteristics are required, especially for the MT connectors. We call an SC connector with an ID module an SC-ID and an MT connector with an ID module an MT-ID in the following.

Most errors in line configuration databases of metal networks are related to concatenation information at distribution frames and free-access closures. Thus, ID modules should be installed in those parts. At least 8,000 ID codes are required for use in one fiber terminated module (FTM) at a telephone center, but about one hundred is sufficient for one closure for fiber access because of the low count distribution cable using multi-fiber ribbon. Therefore, required specifications of SC-ID and MT-ID differ; SC-ID needs more memory than MT-ID, and MT-ID needs more reliable physical characteristics than SC-ID. The ID module previously proposed consists of an EEPROM (Electrically Erasable and Programmable Read-Only-Memory) chip with a memory capacity of from 1 kbits to 16 kbits.

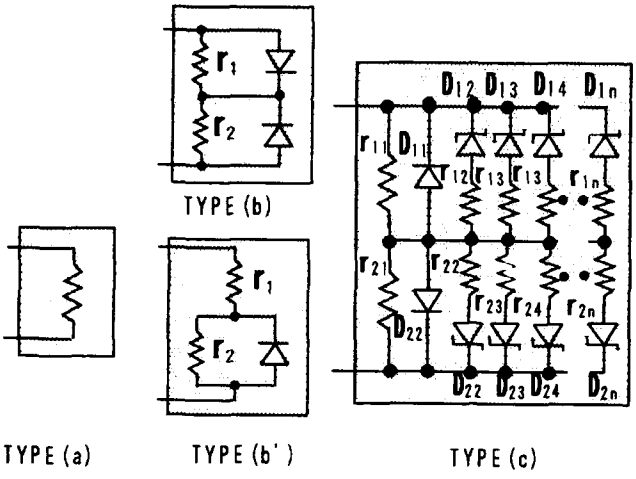


Fig.2 Three types of resistor and diode matrix ID modules

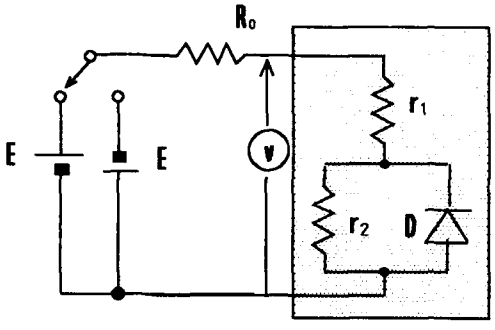


Fig.3 A resistance measurement circuit

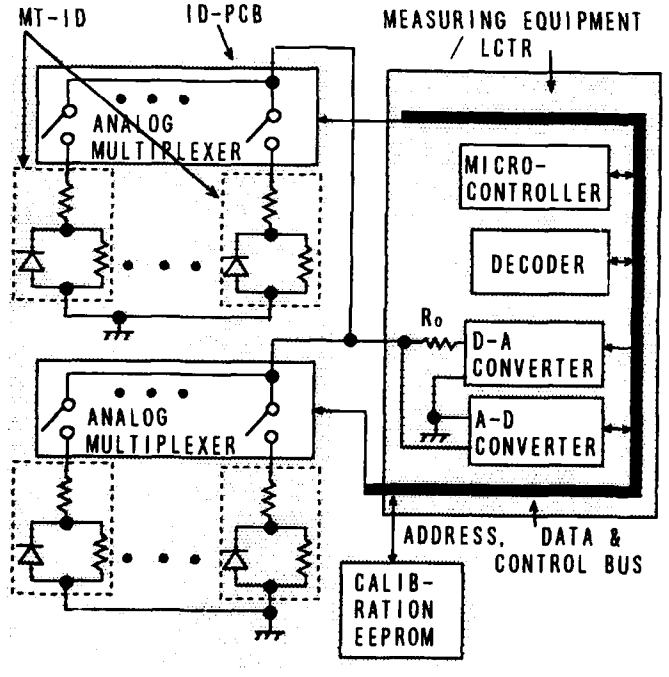


Fig.4 Block diagram for actual measurement of multiple ID module recognition

The reliability of the CMOS EEPROM itself is high, for example, several tenths of FIT or less in operation. However, the EEPROM requires four or more terminals, which indirectly affects ID module reliability. Soldering or poor contact faults increase with the number of terminals.

A new ID module with fewer terminals is investigated, especially for MT-ID. Here, unique resistor values are substituted for ID codes. The basic circuit types of this new ID module are shown in Fig. 2. Each type has only two terminals, one third the number of the previously reported EEPROM ID module. Type (a) in Fig. 2 consists of a single resistor, type (b) has two resistors and two diodes, type (b') has two resistors and one diode and type (c) has 2n resistors and 2n diodes. Type (a) requires a resistor value for each desired ID code number. This is a disadvantage because too many kinds of resistors are needed.

For type (b), the combination of the two resistors (r_1 and r_2) is the ID code. Using N values of resistors allows N^2 combinations. The number of combinations corresponds to the required number of ID codes and the number of required resistor values is the square root of the number of ID codes required. For example, 16 resistor values are necessary and sufficient for 256 ID codes. Two measurements are needed to read the two resistor values through two external terminals. Type (b') aims at higher reliability and lower cost than type (b). The resistor measuring setup of (b') is shown in Fig. 3. The resistor values can be estimated by applying forward and backward voltages (+E and -E) to the terminals (v_1 and v_2) and measuring the voltage difference between them as follows.

$$r_1 = v_{r1}R_o/d_{v2}, \quad (1)$$

$$r_2 = (v_1 d_{v2} - v_{r1} d_{v1})Ro/(d_{v1} d_{v2}), \quad (2)$$

where,

$$d_{v1}=E-v_1,\ d_{v2}=-E-v_2,\ v_{r1}=v_2-V_d,$$

R_o denotes power source resistance, and V_d denotes diode forward voltage drop. An empirical formula about V_d of a 1SS352 silicon switching diode is

$$V_d = 0.103\log_{10}((-E-v_2)/R_o)+0.94+a(T-25), \quad (3)$$

where, a is the temperature coefficient, -2.2×10^{-3} V/degree, and T is device temperature in degrees centigrade.

The type (c) module is the same as type (b), but with zener diodes and resistors added. N resistor values allows N^{2n} combinations, where 2n is the number of resistors in the module. This method requires 2n diodes, 2n measurements for 2n values of applied voltages. For example, when n=4, eight resistors, two diodes and six zener diodes are installed in the ID

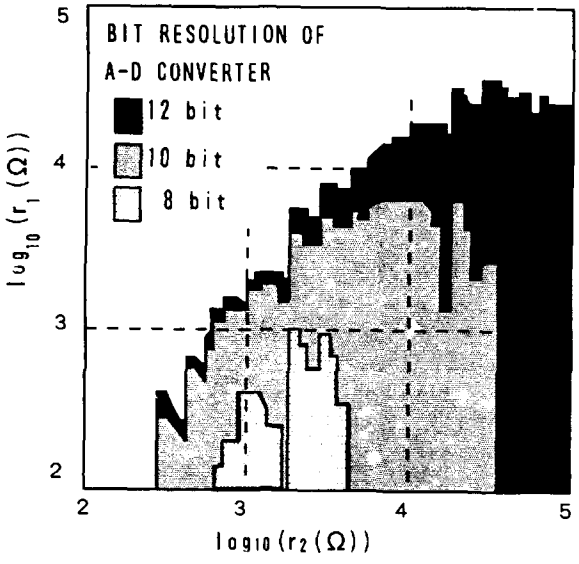


Fig.5 A recognizable area for E 24 series resistor combinations

$\delta E_1, \delta E_2, \delta v_1, \delta v_2$: bit error 1 LSB
$\delta R_1 = \delta R_2 = \delta R_0 = \delta R_{ON} = 0.01$
$R_0 = 1\ k\Omega$, $R_{ON} = 500\ \Omega$
r_1, r_2 : E 24 series



Fig.6 Prototype MT-ID connectors

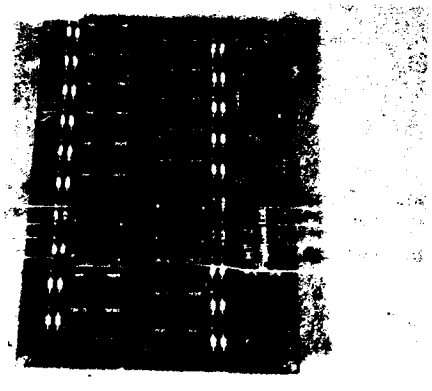


Fig.7 Prototype ID-PCB for 20 pairs of MT-ID

module, and only two resistor values are needed to attain 256 combination. However, considering the measurement error generated by the variance in zener diode V-I characteristics, the need for 2n measurements and the increased number of parts, type (c) is not necessarily better than type (b) or (b)'. Type (b') is employed as the prototype ID module circuit.

The block diagram for actual measurements is shown in Fig. 4. The measuring equipment block can be installed in the LCTR. An analog multiplexer is employed to select the ID module under measurement in a printed circuit board (ID-PCB), where many connectors with ID modules are attached. The measurement voltage is applied to the ID module terminals by a D-A converter through reference source resistance R_0 and the multiplexer, and voltage differences between ID module terminals are measured by an A-D converter. Two measurements with opposite voltage polarity are done. The multiplexer and the converters are fully controlled by a micro-controller (MCU) which recognizes ID codes after calculating resistor values and finding ID codes from an assignment table of ID codes and resistor values. By recognizing the ID codes of consecutive ports on the ID-PCB, connector concatenation is detected. LCTR can transmit connected pair information, i.e., line configuration information to the host computer of the configuration management system.

The actual limit number of the number of type (b') ID modules that can be recognized is evaluated. The limit is determined by resistance tolerance, converter error, on-resistance of analog multiplexer, and A-D converter resolution. Measurement error of r_1 and r_2 are given by

$$\delta r_1^2 = \left(\frac{\partial r_1}{\partial E_2}\right)^2 \delta E_2^2 + \left(\frac{\partial r_1}{\partial V_2}\right)^2 \delta V_2^2 + \left(\frac{\partial r_1}{\partial R_0}\right)^2 \delta R_0^2 + \left(\frac{\partial r_1}{\partial R_{on}}\right)^2 \delta R_{on}^2 + \delta r_{t1}^2 \quad (4)$$

$$\delta r_2^2 = \left(\frac{\partial r_2}{\partial E_2}\right)^2 \delta E_2^2 + \left(\frac{\partial r_2}{\partial V_2}\right)^2 \delta V_2^2 + \left(\frac{\partial r_2}{\partial R_0}\right)^2 \delta R_0^2 + \left(\frac{\partial r_2}{\partial R_{on}}\right)^2 \delta R_{on}^2 + \left(\frac{\partial r_2}{\partial r_1}\right)^2 \delta r_1^2 + \delta r_{t2}^2 \quad (5)$$

where, δE_1, δE_2, δV_1, δV_2 are the maximum measurement errors of an A-D converter, δr_{t1}, δr_{t2}, δV_1, δR_{on} are the maximum errors of resistors, r_1, r_2, R_0, and δR_{on} is the maximum on-resistance error of the analog multiplexers.

When the measured resistances are sorted in ascending order as $r_1[1]<r_1[2]<r_1[3]<....$, and $r_2[1]<r_2[2]<r_2[3]<....$, the recognition conditions are given by

$$r_j[i-1] + \delta r_j[i-1] < r_j[i] - \delta r_j[i] \quad (6)$$

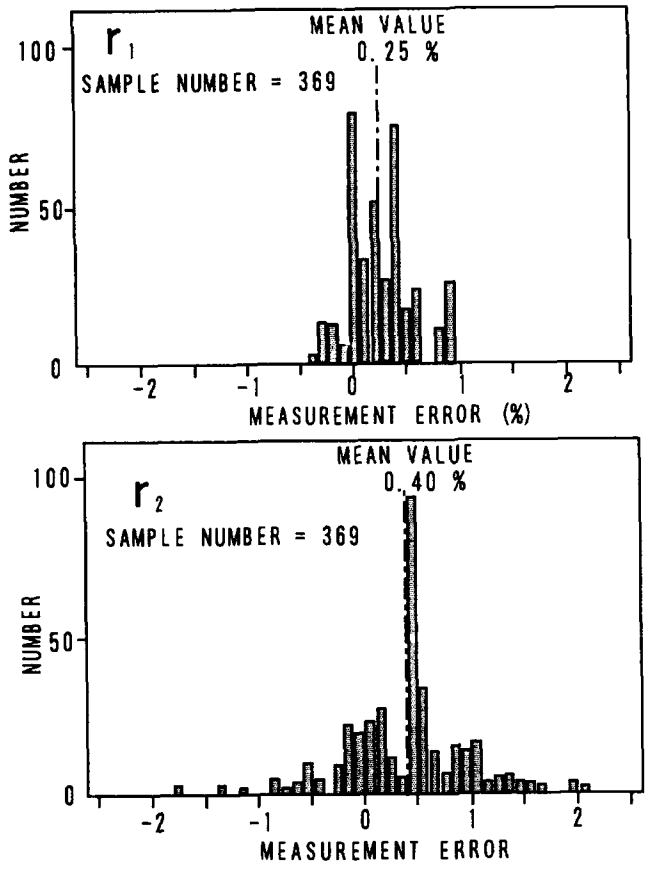


Fig.8 Histograms of measured resistance errors for r_1 and r_2

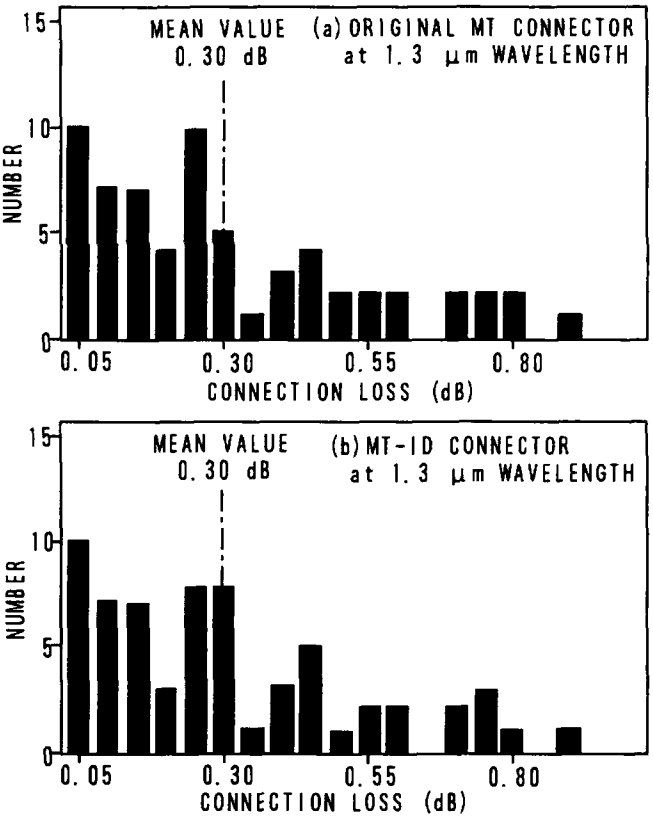


Fig.9 A connection loss histogram change caused by attaching ID modules to MT connectors

$$r_j[i] + \delta r_j[i] < r_j[i+1] + \delta r_j[i+1] \quad (7)$$

where j=1 for r_1 and j=2 for r_2. Calculated results are shown in Fig. 5, where all of the E 24 series are employed. The E 24 series is composed of rounded values of the theoretical numbers $10^{m/24}$ in which the exponent m is a whole positive or negative integer as defined in IEC 63. Examples of actual resistor values of the E 24 series are 1.0 k, 1.1 k, 1.2 k, 1.3 k, 1.5 k,..., 6.8 k, 7.5 k, 8.2 k, 9.1 k, 10.0 k ohms for resistor values from 1 k-ohms to 10 k-ohms. In the calculation, resistance tolerance is 1 %. To keep the error at 1 % for multiplexer on-resistance, each on-resistance must be calibrated. Therefore, an EEPROM for calibration should be installed on the ID-PCB, in which the calibrated on-resistance values for each channel are stored. According to Fig. 5, where the resistors range from 100 ohms to 100 k-ohms, about 2,500 resistor combinations can be recognized by using an A-D converter with 12-bit resolution. The calculated recognition number is enough for MT-ID, however, improvement is desired for large-scale application to SC-ID.

4. MT-ID EXPERIMENTAL RESULTS

Prototype MT-ID connectors are fabricated, in which the resistor range is from 13 k-ohms to 24 k-ohms of the E 24 series and 1% tolerance. A photograph of the MT-ID connector is shown in Fig. 6 and photograph of the ID-PCB is shown in Fig. 7. The resistor combination numbers 49, which corresponds to the number of IDs. Measured r_1 and r_2 values are shown in Fig. 8. The estimated errors are -0.4 to +1.0 % for r_1 and -1.8 to +2.1 % for r_2. In the E 24 series, the normalized resistor values that are nearest each other are 1.5 and 1.6 (15 k-ohms and 16 k-ohms for prototype ID modules), where there is a 3.2 % difference in resistor values. The absolute errors in experimental results are sufficiently less than 3.2 %. Therefore, 100 % recognition of resistor combinations is attained. Changes in optical loss of connectors before and after attaching the ID modules are also measured (Fig. 9). The mean connection loss does not changed at all.

5. LOCAL CONTROLLER (LCTR)

ID information is transmitted using an LCTR network. A block diagram of the LCTR is shown in Fig. 10. The LCTR has an optical bidirectional communication port, ID module interface, RS-232C serial communication interface and sensor coupling interface. The LCTR uses these interface ports for four functions:

(1) ID code recognition
(2) local fiber identification

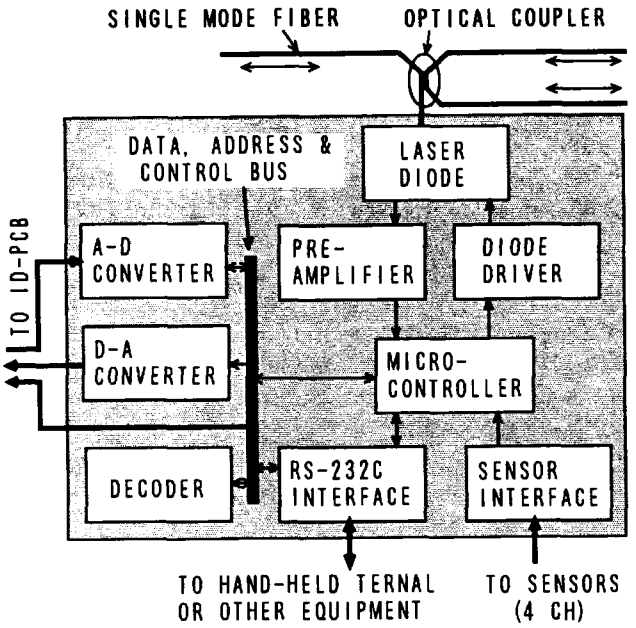


Fig.10 Block diagram of LCTR

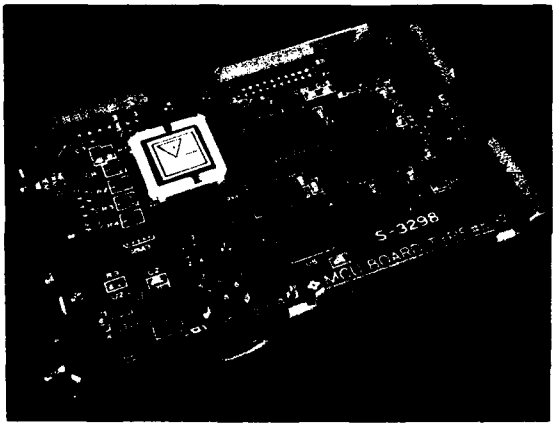


Fig.11 Prototype LCTR (inner chassis)

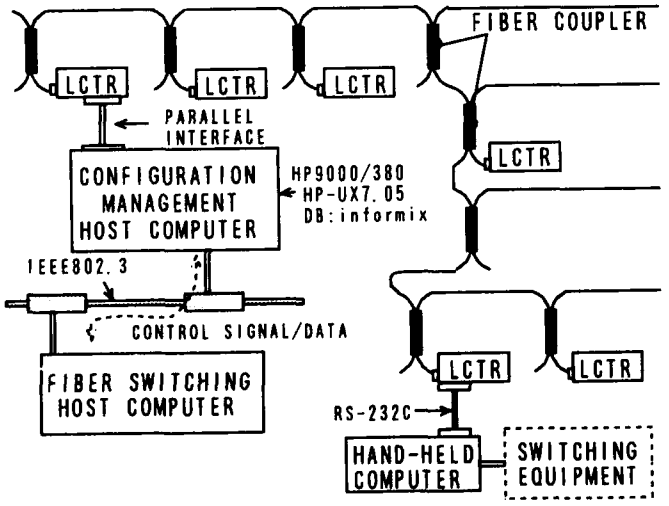


Fig.12 Experimental setup for LCTR network

(3) control signal transmission
(4) environmental sensing

The first function, ID code recognition, can be used at construction or service order operation and so on, where fiber connector concatenations are changed. After fiber concatenation changes using connectors with ID modules, the LCTR is connected to a dedicated communication line; a hand-held terminal is also connected to the LCTR. Power is supplied to the LCTR and the terminal by battery through a dc-dc converter. A field worker can operate the LCTR through the terminal. The LCTR controlled by the terminal automatically recognizes ID codes of all connectors and transmits that information to the host computer through the bidirectional optical communication port over a dedicated communication line. The host computer updates the related data of the line configuration database. LCTR is then disconnected from the line and taken back to a center.

The second function, local fiber identification, is subject to the same conditions as the first. It is realized by transmitting a query about line service status to the host computer using the LCTR and the terminal. The field worker can recognize the service status (in-service , to be dropped, out of order, and so on) of all connectors with ID modules. For visual recognition, a visible LED matrix is installed on the surface of the ID-PCB (Fig. 7). This function considerably reduces the time of local fiber identification in comparison with the conventional fiber bending identification technique. This status information contributes much more to reliable field operations than the conventional method. When the work is finished, the LCTR is taken back to a center.

The third function is control signal transmission, which helps fiber switching system module to transmit switching signals or data to remote fiber switching equipment. The host computer of the configuration management system is interrupted by the platform commands and transmits an arbitrary signal to the directed location.

The fourth function, environmental sensing, is used for detecting fiber closure open-shut status, measuring temperature, detecting water penetration, and so on.

A prototype LCTR matched to the new ID modules is shown in Fig. 11. Its basic functions and performance are listed in Table. 1. The ID interface is modified to be suitable for the MT-ID and visible LED matrix for local fiber identification. Communication performance is almost same as for the previous LCTR. The outer size is lager than that of the previous LCTR[5] because of the 12-bit A-D and 8-bit D-A converters for MT-ID recognition. Average power consumption is drastically reduced from 5 W to 1 W by using CMOS devices and implementing a shutdown mode.

Finally, the experimental setup shown in Fig. 12 for checking the LCTR network is fabricated and the above mentioned LCTR functions are confirmed.

TABLE 1. LCTR functions and performance

ID interface	ID-PCB (MT-ID) with LED matrix	
hand-held terminal interface		
signal	RS-232C	
rate	9600bps	
bidirectional communication		
light source/detector	one InGaAs LD	
signal	half duplex NRZ	
optical fiber	one SM-fiber	
bit rate	125 kbps	
optical dynamic range	22 dB	
bit error rate	$<10^{-7}$	
environmental sensing		
full scale	2V	
resolution	8 bit	
channels	4 CH	
size	110 x 70 x 22 mm	
power consumption	1.04 W	normal
	0.20 W	wait

6. CONCLUSION

The need for an integrated cable network operation system consisting of a number of system modules is described. To realize this system, a reliable database which reflects current line configurations is indispensable. The real-time configuration management system is one module of the cable network operation system, whose purpose is to realize a database that is more reliable than conventional databases concerning line configurations. When fiber concatenation changes, connectors having ID modules with dedicated data transmitters (LCTRs) provides automatic, reliable database updating. A new ID module consisting of a resistor and diode matrix is proposed to attain more physical reliability than the previously demonstrated ID modules using EEPROM. Tests of prototype connectors equipped with the new ID modules demonstrate successful ID code recognition. The functions and performance of the prototype LCTR matched with the new ID devices are tested, and LCTR use for each function in the field is clarified. In future, the actual reliability of MT-ID connectors and LCTR should be investigated under practical field conditions.

ACKNOWLEDGMENTS

The authors wish to thank Mr. Yutaka Wakui, Dr. Koushi Ishihara and Dr. Tadashi Haibara for their useful suggestions and encouragement throughout this work.

REFERENCES

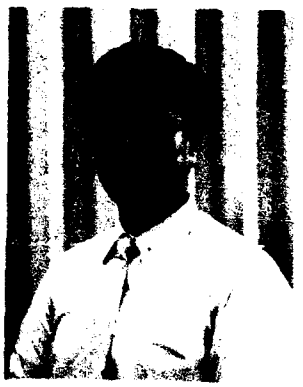
1. Y. Koyamada et al., "Basic Concepts of Fiber Optic Subscriber Loop Operation Systems," IEEE ICC'90, 341.1.1.-341.1.5.

2. Y. Yamamoto, H. Kobayashi, Y. Katsuyama, K. Yamashita and N. Kashima, "Effective Network Configuration for Optical Subscriber Loops," NTT R&D Vol. 41, No. 7, pp. 841-850, 1992. (in Japanese)

3. I. Sankawa, Y. Koyamada, S. Furukawa and T. Horiguchi, "Optical Fiber Line Surveillance System for Preventive Maintenance Based on Fiber Strain and Loss Monitor" IWCS Proc. 1992 (to be published).

4. T. Katagiri, Y. Koyamada, M. Tachikura and Y. Katsuyama, "Nonblocking 100x100 Optomechanical Matrix Switch for Subscriber Networks," IWCS Proc. 1991, pp.285-290.

5. K. Yamashita, F. Ohtsuki, M. Tateda and Y. Koyamada, "A Real-Time Configuration Management System for Line Facilities in Optical Fiber Networks," IWCS Proc. 1991, pp.793-799.



Katsuya Yamashita

NTT Telecommunication
Field Systems R&D Center

Tokai-mura, Ibaraki-ken,
319-11, Japan

Mr. Yamashita received the B.S.E.E. degree from Kumamoto University, Japan in 1975. After joining the Electrical Communications Laboratories, he researched submarine optical fiber cables and optical fiber measuring equipment. He is now a Senior Research Engineer, Supervisor, in the Telecommunication Field R&D Center, responsible for research and development of line configuration management systems in optical fiber networks. He is a member of the IEICE Japan.



Yoshikazu YAMAMOTO

NTT Telecommunication
Field Systems R&D Center

Tokai-mura, Ibaraki-ken,
319-11, Japan.

He received B.S., M.S. and Ph.D degrees from Kyoto University, Japan in 1969, 1971 and 1985. After joining the Electrical Communications Laboratories, he researched transmission quality evaluation and optimum line configuration of coaxial transmission lines, and optical network configuration and distribution. He is now a Senior Research Engineer, Supervisor, in the Telecommunication Field Systems R&D Center, responsible for research and development of line operation systems in optical fiber networks. He is a member of the IEICE Japan and IEEE.



Fumio Ohtsuki

NTT Telecommunication
Field Systems R&D Center

Tokai-mura, Ibaraki-ken,
319-11, Japan

Mr. Ohtsuki graduated from Mito Technical High School,Japan in 1967. After joining the Electrical Communications Laboratories, he researched protection of telecommunication lines against lightning surge, and electromagnetic compatibility. He is now a Senior Research Engineer in the Telecommunication Field R&D Center, responsible for optical fiber network media management. He is a member of the IEICE Japan.

INTELLIGENT BUILDING: DESIGN CONSIDERATION

Christopher Di Minico

Digital Equipment Corporation
Low End Networks and Communications

Summary

Building technologies, codes, standards and regulations have an enormous impact on the architect, the consulting engineer, the building owner and the building facility manager. Voice and data communication equipment standards, which now include Building Control Technologies, are recognized as an integral part of the structured wiring, and structured pathway standards. The Intelligent Building (IB) lacks such standards and guidelines. This paper presents an overview of the Intelligent Building concept primarily focusing on the Information Technology (IT) component. It additionally, proposes that a collection of existing and developing standards could provide the foundation for Intelligent Building designs.

Background

The Intelligent Building concept has been proposed in a variety of manifestations over the last decade, each failing to generate much consumer interest. The Intelligent Buildings are scattered about the world each promoting their uniqueness. Therein lies the problem. Unique, one-of-a-kind solutions are by definition not easily repeatable, scalable, or extensible. A contributing factor to the lack of acceptance of the Intelligent Building concept is the absence of a standards based Intelligent Building platform. The platform would define the basic elements, their inter-relationship, and their application. The platform would establish a framework for measuring the return on investments for building developers, owners and tenants.

Worth noting, but not directly addressed here, is the resistance to the Intelligent Building concept by the people involved with the building operations. Each element of the Intelligent Building concept includes a person. Historically, the telecommunication (Voice/PBX), data-communication (LAN/W .., and facility managers each have uniquely defined network hardware, software, and management strategies. The difficulty of integrating and establishing relationships between the individuals involved especially with-in an operating building, is enormous. Many of these people are protective of their individual responsibility and fear that integration of systems and services may result in lost jobs - as in 'lights-out' manufacturing. A standards based Intelligent Building definition could reduce the fear generated by misinformation and provide the basis for meaningful collaboration.

Intelligent Building Design Concept:

The Washington based Intelligent Building Institute (IBI) has already achieved some level of consensus towards an Intelligent Building definition. This definition will be used as the framework to relate the Intelligent Building concept with the relevant standards and potential applications. The Intelligent Building, as proposed by the IBI, is to provide a productive and cost effective environment through optimization of its four basic elements; the structure, the systems, the services, and the management as well as the inter-relationship between them.

1. STRUCTURE:

Structured Wiring and Structured Pathways for Intelligent Buildings:

The Electronic Industries Association (EIA) and the Telecommunications Industries Association (TIA) have developed a standard for telecommunications wiring for commercial buildings as specified in the EIA/TIA-568 Commercial Building Wiring Standard. Also EIA/TIA developed the EIA/TIA-569 Commercial Building Standard for Telecommunications Pathways & Spaces in recognition that the building wiring cannot be standardized without standardizing the building architecture into which the building wiring is installed.

An International version of the EIA/TIA-568 is under development by the ISO/JTC1 SC25 WG3. At Present the draft is out for ballot by the Working Group.

The stated goal of EIA/TIA-568 is to provide a uniform wiring system that supports multiproduct, multivendor environments. The related EIA/TIA-569 covers the pathways and spaces.

The EIA/TIA-568 and the EIA/TIA-569 have established inter-relationships among the core sections of the standards.

Comparison of Core Sections of EIA/TIA-568/569

EIA/TIA-568	EIA/TIA-569
4. Horizontal Wiring	4. Horizontal Pathways
5. Backbone Wiring	5. Backbone Pathways
6. Work Area	6. Work Station
7. Telecommunications Closet	7. Telecommunications Closet
8. Equipment Room	8. Equipment Room
9. Entrance Facilities	9. Entrance Facilities

Expanded OSI Reference Model: (Figure 1)

The concept proposed here is to expand the OSI Physical Layer to include Structured Wiring and Structured Pathways. It is not to imply a functional relationship within the framework of the OSI implementation but to establish a context for Intelligent Building design using the OSI reference model.

OSI Reference Model:

The International Standards Organization (ISO) initiated work in 1977 on the Open Systems Interconnection (OSI) to address the requirements of internetworking heterogeneous computer systems. The OSI reference model is an abstract description of interprocess communication structured in layers of smaller bsystems.

The Physical Layer provides the mechanical, electrical, functional, a procedural standards to access the physical media.

Figure 1

VII.	Application Layer
VI.	Presentation Layer
V.	Session Layer
IV.	Transport Layer
III.	Network Layer
II.	Data Link Layer
I. Physical Layer	EIA/TIA - 568 - Structured * Wiring ISO/IEC JTC1 SC25
Building Architecture Layer - EIA/TIA-569 *	

* Not within the OSI implementation.

Building Controls on Structured Wiring:

Most of the contending Building Automation Protocols physical layer requirements are satisfied by the EIA/TIA-568 specification for topology, media and connectors. Notable exceptions are the Master Slave/Token Passing (MS/TP) datalink implemented using the EIA-485 physical layer proposed by the American Society of Heating Refrigerating and Air-Conditioning Engineers (ASHRE). ASHRE SPC 135P BACnet: A Data Communication Protocol for Building Automation and Control Networks which specifies RS-485 implemented with 18 AWG shielded twisted pair.

The intelligence of the building control functionalities are becoming decentralized and moving closer to the controlled systems. The data communication interfaces for these 'smart' controllers are often RS-232, and RS-423 which can be provided by traditional data communication products such as terminal servers. The terminal server to 'smart' controller is accomplished in a star or radial wire distribution topology rather than a bus on 24 AWG unshielded or shielded twisted pair. This implementation is consistent with the passive infrastructure specified in EIA/TIA-568. These terminal servers often reside as modules in a network 'smart' hub.

2. MANAGEMENT

In recognition of the requirements for standardized application services and protocols for the exchange of management information across systems, ISO/IEC 7498-4 has provided a basic reference model for a standard management framework. The framework is to establish a management protocol that would transport management information between the individual layer standards. The management information is structured in a Management Information Base (MIB). The Abstract Syntax Notation One (ANS.1) is the ISO term for the data structures exchanged, along with the management information. Management products are available today that meet a sub-set of the ISO/IEC requirements.

Rather than presenting Intelligent Building Management in the abstract, a prototype of an integrated building management platform is presented (Figure 2).

Potential users of the integrated Building Management platform are:

- Building Facility Personnel
- Security Managers Personnel
- Real Estate Managers Personnel
- IT/Network Managers Personnel
- Finance Management Personnel

Intelligent Building Management can be characterized by functional areas as follows:

- Design/Configuration Management - is the area that concentrates on the design, storage, and presentation of the physical layout of managed objects. It also deals with the storage of the managed systems' and operating specifications.
 * physical representation of building infrastructure
 * physical and logical representation of the IT Network; both the passive cabling system and the active products.
 * interior layout (modular furniture, partitions, etc.)
- Real-time Building Management - is the area that consists of management and control of the dynamic building environment.
 * HVAC system
 * Security system
 * Lighting system
 * Fire/safety system
 * Environmental systems
- Administration Information Management - consist of the building operational information.
 * Faults, maintenance and repair logs
 * Systems and services usage and consumption
 * Asset identification

The core of the platform is an information repository which is common to the three functional management areas. The integrated repository ensures the consistency and integrity of the information shared by the management functions. The presentation of the data will be based on the user application accessing the information (Figure 3)..

- Physical Presentation
- Schematic Presentation
- Real-Time Graphics
- Text

3. SYSTEMS:

In OSI parlance a System is considered to be one or more autonomous computers, their associated software, peripherals, and users that are capable of information processing and/or transfer.

Based on the customers demand for interoperability, voice and data vendors have long provided end user service via standards based Systems (Networks) characterized typically by geographical span such as Local Area Networks (LANs), Metropolitan Area Networks (MANs) and Wide Area Networks (WANs).

The Building Control Vendors and end users are also responding with proposals for a standards based open protocol for Building Automation Systems. The Intelligent Building Institute has created an evaluation metric to review the leading contenders and have identified three implementations for further review:

- ASHRE 135P BACnet:
- ECHELON
- PWC (Public Works Canada)

Other protocols positioned as Intelligent Building contenders are:

- Firm-Neutral Data Transmission (FND)
- TRON

ASHRE 135P: BACnet: Data Communication Protocol for Building Automation

Purpose:

To define a data communication services and protocol for Computer Equipment used for monitoring and control of HVAC and other building systems.

To define an object-oriented representation of information communicated between such systems, to facilitate application development.

Scope:

- **Based on a 4 layer collapsed OSI Basic Reference Model (ISO 7498):**

BACnet Layers	Equivalent ISO Layers
BACnet Application Layer	(7) Application
BACnet Network Layer	(3) Network
ISO 8802-2 IEEE 802.2 MS/TP	(2) Data Link
ISO 8802-3 IEEE 802.3 ARCNET EIA-485	(1) Physical

Public Works Canada (PWC/SCP)

Public Works Canada has developed a Standard Communication Protocol (SCP) for Energy Management Control System (EMCS), and a related Gateway Specification for EMCS using PWC protocol. Developed by Universal Software Inc., under contract to Canadian Federal agency to provide a unified application interface; initial focus will be on the building energy management system with the capability for later extension to other building systems. The specification and the associated operator interface standard will become part of the government's National Master Specification for all new installations.

ECHELON LonTalk

LonTalk was developed by the Echelon Corporation. The protocol is implemented in silicon produced under license agreement with Echelon by Motorola. The protocol is advertised as following the ISO/OSI seven layer reference model.

FND

Firm-Neutral Data Transmission System in Public Buildings and Premises was developed by the Working Group on Mechanical and Electrical Engineering of the State and Municipal Office Administrations Office (AMEV) of the Federal Ministry for area Planning, Construction Industry and Municipal Construction, of Germany.

FND specifies a Standard Interface Adapter to be used by the control vendors. The interface establishes the point of integration for the proprietary vendors implementation.

TRON

The Real Time Operating Nuclei was initially developed at the University of Tokyo. Several TRON applications exist. M-TRON (macro-TRON) is currently under development for building automation. TRON is administered by the Tron association of Japan. Nippon Telegraph and Telephone (NTT) and the Japanese Ministry of International Trade and Industry (MITI) are primary supporters of TRON.

4. SERVICES

The promise of a standards based service independent communication network is still unfulfilled. Although Integrated Service Digital Network (ISDN) was championed as resolving the voice/data integration problem, it will not meet the demands of many services requiring high speed data transfer.

Broadband ISDN (B-ISDN), operating on a Synchronous Optical Network (SONET), providing bandwith on demand to end-users in the form Asynchronous Mode Transmission packets (ATM) is now positioned as the solution to the universal network problem. The network 'smart' hub environment with ATM switching providing multirate services supporting video, voice, and data applications is a popular future vision for the universal network. The future awaits.

Traditionally, Intelligent Building Service offerings have been positioned as Shared Tenant Services. The basic premise is that building owners would attract tenants by providing access to services that they would not be able to afford on their own.

These services, due to the lack of an integrated solution, are directly related to the Systems (Networks) employed. The services are typically broken into two distinct communication categories, telecommunications (PBX), and data communications. The list of unique services are exhaustive - only a sample will be provided below.

Telecommunication Services:

- Shared Tenant Services
- Message Center
- Computer Integrated Telephony (CIT)
- Modem pool
- FAX
- Voice mail

Data communications Services:

- Shared Tenant Services
- Encryption-system security
- Computer/Database services
- Video teleconferencing
- Employee Locator
- print servers
- file and information servers

Conclusion:

The structure, the management, the systems, and the services all of the elements of an Intelligent Building Concept have established standards or are developing standards that need to be applied collectively to provide the basic framework for Intelligent Building designs.

Author

Christopher Di Minico is an engineering supervisor for Digital Equipment Corporation's Low End Network and Communication group.

BS/BA, Electrical Engineering/Music, Northeastern University and University of Massachusetts respectively.

Acknowledgment

Digital Equipment Corporation's Building Intergration Services Intelligent Building Technology Team and the reviewers of this document.

Figure 2

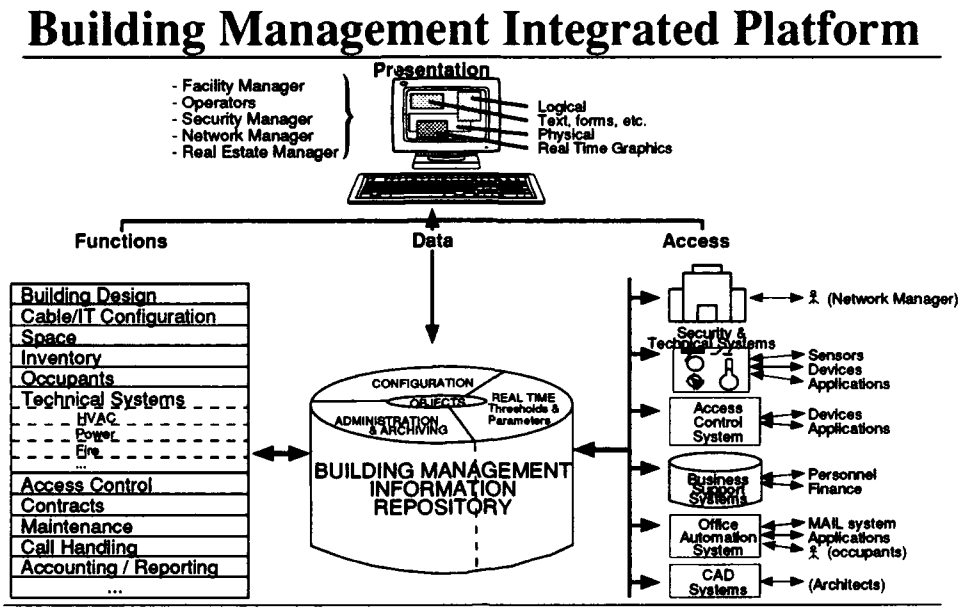
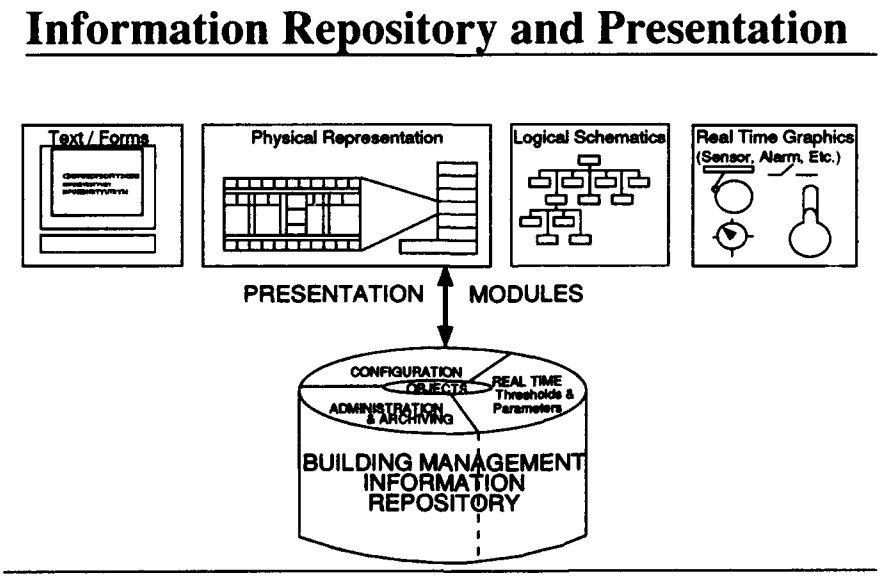


Figure 3



An 8-Fiber 3-State 2X2 High Speed Switch

H. Furukawa S. C. Yow Y. Nomura H. Yokosuka
Fujikura Ltd Opto-Electronics Lab
Chiba, Japan

Abstract

A high speed, 3-state (cross, bar and loop) 2X2 mechanical switch for 8-fiber optical fiber ribbons has been developed. This paper describes the concept of a 3-state switch and how it is realized in design. Next, the structure of the switch, namely the fiber connections, the driving mechanism and the switch block is described. Finally, the performance of the switch is reported.

1. Introduction

The introduction of optical fiber in the subscriber loop environment in the coming decades presents many challenging problems. Maintaining its economic viability through effective network utilization and management and providing service continuity of such networks in cable cuts are some of the challenges that must be faced. One means of meeting these challenges is the use of small, low cost, high speed switches aptly placed at various points on a network to route traffic to available or reserve line capacities. In this way, network capacities can be maximized and cable cuts can be handled by rerouting affected traffic[1]. Studies on 2-state (cross, bar), high speed mechanical switches have been done[2] and such switches have already been developed[3] and can be used for this purpose. However, network engineers have begun to demand for more flexibility in switches used in complex networks or subscribers network[4]. In particular, switches with a third state have found uses in these networks. We have built a switch with a third state - a 3-state (cross, bar and loop) 2X2 mechanical switch. The switch has a switching loss of less than 1.2dB and a switching time of less than 10ms. It can be used with up to 8 fibers or with an 8-fiber ribbon tape per port.

2. Concept

Fig. 1 illustrates the 3 states of the switch. The two 'traditional' states are the 'cross' and the 'bar' states while the third state that was added is the 'loop'. At first glance, it may seem that the 'loop' only serves to return the traffic to its origin and thus does not serve any purpose whatsoever. However, it really depends on where the switch is used, how it is used in conjunction with other switches in the network and the origins and destinations of the traffic entering and leaving each switch. The non-parallel lines on each side of the switch in the figure serve to emphasize this point.

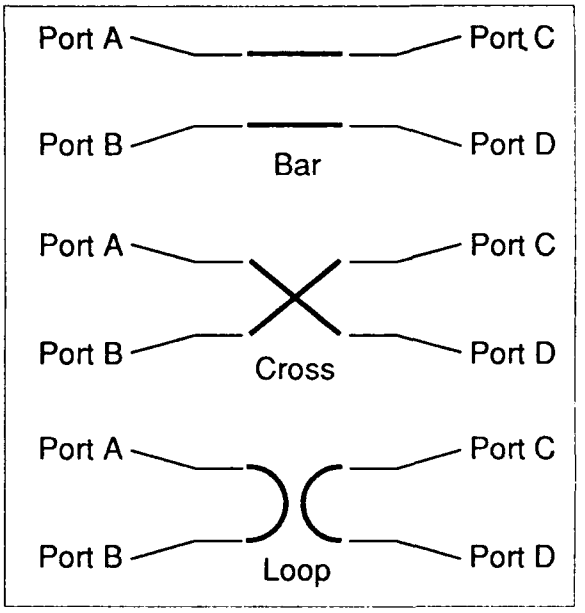


Figure 1. The 3 states of the switch

Fig. 2 shows schematically how the 3 states can be realized with fibers set inside two mating ferrules. As shown in the figure each of the ferrules has two switching positions, the lower or retracted position and the upper or extended position. Together these result in 3 combinations and hence the 3 switching states of the switch. One of the advantages of this arrangement is that the distance between the two switching positions of the ferrule is the smallest possible and is the spacing between the fibers set on the ferrule(250μm). The short distance over which the ferrules have to travel contributes in part to the high switching speed. Furthermore, if each ferrule is driven independently, then the switching time will be the same for either state the switch changes to. The

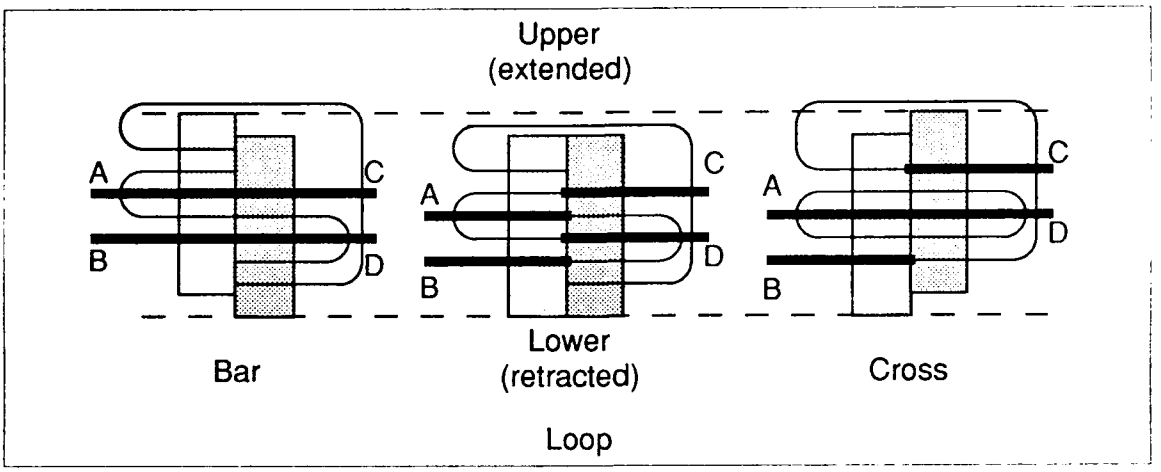


Figure 2. Realization of a 3-state switch using 2 ferrules mounted with fibers

switching time will be the same irregardless of whether one ferrule or both ferrules are switched.

3. Structure

The structure of the switch is shown in Fig. 3 and is similar in principle to the 2-state mechanical switch that we have developed[3]. The major components of the switch are the ferrules on which the fibers are set, the driving unit which switches the position of the ferrules and the switch block within which the ferrules and driving unit are contained. It differs from the 2-state switch in that both its ferrules are switchable and can be moved independently of one another. The switch is also built to accommodate up to eight fibers per port - hence the size of its ferrule is much larger than a 2-state switch for paired fibers.

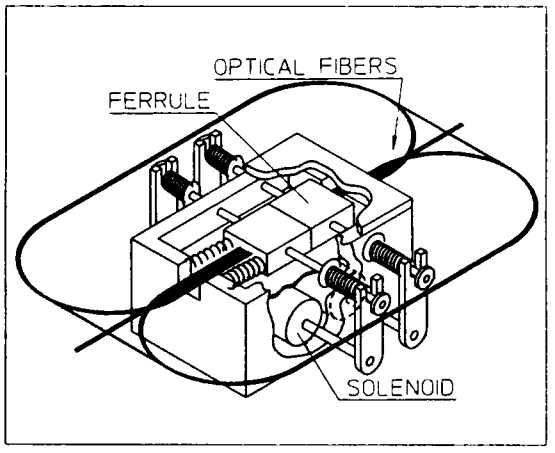


Figure 3. Structure of the switch

3.1 Ferrule

The fibers inside the switch terminate in a pair of mating ceramic ferrules. Connection between fibers takes place when the fibers in one ferrule is aligned with the appropriate fibers in the other ferrule (as is shown in fig. 2).

The ferrules in this switch consist of two parts - a base plate and top plate. The base consists of a series of V-grooves machined to a precise depth and at a precise interval of 250μm. The depth and intervals of the V-grooves have an accuracy of ±0.5μm. Fibers are mounted on the V-grooves and the top plate is used to fix the fibers firmly in position.

The base plate also has two elongated V-grooves on which alignment pins are mounted (see fig. 4). The sizes of the elongated V-grooves and the alignment pin are such that in the 'bar' state and the 'cross' state, the relative displacement of the two ferrules is exactly 250μm (which is exactly the spacing between fibers mounted on the ferrules). From the 'loop' state which is considered to be the home state, it is possible to switch to the other two states by moving one of the ferrules exactly 250 mm. Thus the optical performance in the 'bar' and 'cross' states are dependent on the accuracy of the elongated V-grooves.

The 'loop' state performance on the other hand depends on additional factors. Both the ferrules are machined together with one of their sides pressed firmly against the wall of the milling machine table. This is considered to be the reference line for measurements. The mating V grooves are formed through a single cutting action thereby ensuring that each V-groove is precisely positioned with respect to the reference wall.

Additionally, alignment pins are fixed in the interface

between the side of the ferrule and the side wall of the switch. This is to reduce the contact surface area thereby reducing friction. This leads to good repeatability of the switching loss. It is also possible to make fine adjustments by varying the outer diameter of the pin.

It can be seen that the loss performance of the switch depends heavily on how precisely the ferrules and V-grooves are machined.

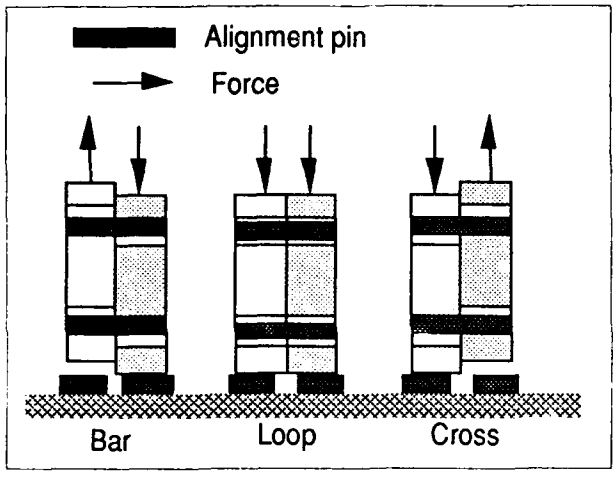


Figure 4. Alignment of the ferrules

3.2 Driving Unit

The driving unit is used to switch and hold the position of the ferrules (fig. 5). The ferrules are moved by push pins as represented by the arrows in figure 4. The push pins at the opposite sides of a ferrule are linked by rods and bearings to a single, high speed, fast response, latch-on type solenoid.

By linking the push pins together, the extension and retraction of the two push pins are synchronized. This eliminates the possibility that the extension of one push pin is faster than the retraction of the push pin on the opposite sides, which could damage the ferrule or slow down the switching motion of the ferrule.

The use of high speed, fast response solenoids contributes to the high switching speed of the switch. The latch-on feature of the solenoid enables the switch to maintain its switching state without consuming electrical energy. The bearings at the solenoid shaft stabilize the motion of the push pin which in turn contributes to a cleaner switching waveform.

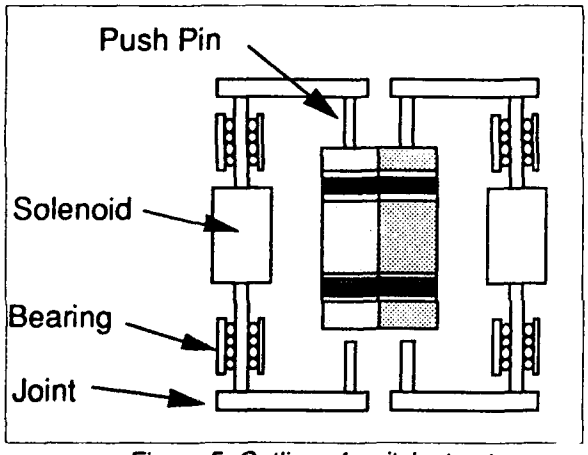


Figure 5. Outline of switch structure

3.3 Switch Block

The ferrules are enclosed within the switch block and immersed in a specially developed low viscosity index-matching oil. The solenoid and bearings are attached to the outer walls of the switch block. The push pins enter the switch block through diaphragms which prevent the leakage of index-matching oil.

The entire switch measures a compact 130(L) X 130(W) X 20(H) mm. It is designed such that individual switches can be easily stacked one on top of another without creating any dead space in between. The modular design of this switch can pave the way towards the development of high capacity 3-state switches, in line with the high density fiber cables being developed for use in subscriber networks.

4. Performance

The performance of the switch will be briefly reported here.

4.1 Connection Loss

Losses were measured using an LED light source of 1.31μm wavelength. The light is sent into one of the ports and the loss in power is measured at the corresponding output ports of each of the switch's states. The process is continued until losses through all combinations of ports are recorded. Fig. 6 shows the connection losses for each of the three positions of the switch. The average connection loss was 0.65 dB. There were no significant differences among the three states. We can therefore conclude that the new third state (loop) provides as good a connection as the any of the other states.

4.2 Switching Time

The switching time is defined as the interval between the electrical triggering of the switch and the attainment of new switch state. The switch is considered to have attained the new state when the light output at the appropriate port has stabilized. As can be seen in Fig.7 the switching time was less than 10ms. There were no significant differences among the three states. If the interruption to transmission signal is considered instead,

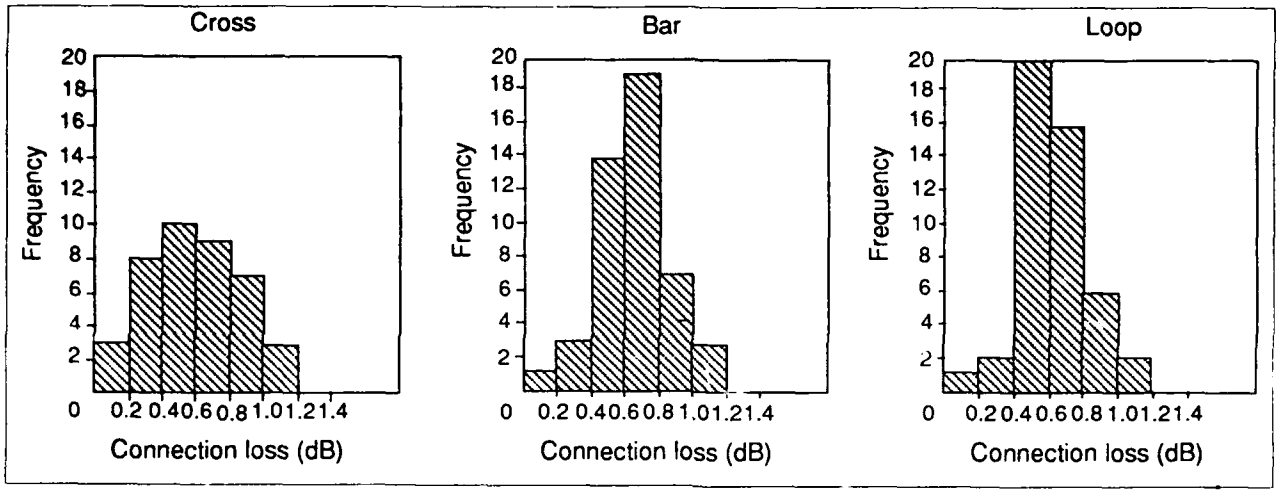


Figure 6. Connection Losses

the time would be much shorter. Fig. 8 shows the switching waveform.

(ms)

	Cross	Bar	Loop
Electrical triggering time	5.8	5.2	5.8
Switching time	3.2	4.0	2.6
Total time	9.0	9.2	8.4

Figure 7. Switching Time

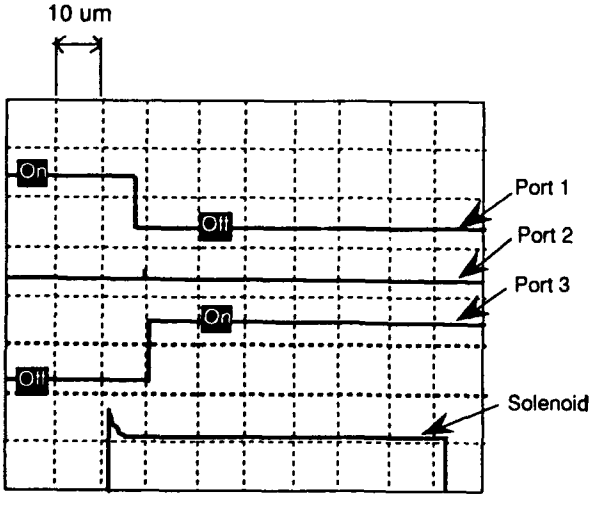


Figure 8. Switching Waveform

4.3 Return Loss

The use of index matching liquid has resulted in a high return loss of greater than 50dB at the mating faces of the ferrules. The return loss was measured using a 1.31μm light source and a coupling/branching filter. The output side of the switch was immersed in refractive-index matching oil to make it non-refractive.

5. Conclusions

A 8-fiber 3-state (cross, bar, loop) 2X2 high speed mechanical switch has been developed. It has a connection loss of less than 1.2dB and a fast switching time of less than 10ms. We believe the switch will give network designers and managers added flexibility and power to meet the challenges of the coming decades.

References

[1] Daniel Kidd, David Hiscoe. Getting to the source of network disasters. Telephony, p26-34, Oct 29, 1990.

[2] S.Nagasawa et al. A low-loss multifiber mechanical switch for 1.55μm zero–dispersion fibers. Trans. IEICE, Vol E73, P1147-1149, 1990.

[3] K.Jimbo Y.Nomura. A low-loss mutifiber mechanical switch. In Proceedings of 13th International Telecommunication Symposium, Vol II, p225-228, Taipei, Taiwan, Feb 1992.

[4] T. Uenoya. The "Optical Fiber Loop 21" Plan. In Technical Digest of 3rd Opto-electronics Conference (OEC '90) p268-271, Chiba, Japan, July 1990.



Yoshikazu Nomura
FUJIKURA LTD.
Opto-Electronics Lab.
1440 Mutsuzaki
Sakura City, Chiba
Japan

Yoshikazu Nomura was born in 1951. He graduated in mechanical engineering from Shinshu University.
He has been engaged in the research and development of telecommunication cables and accessories.
He is presently a manager in the Fiber and Cable Accessory Department.



Hiroshi Furukawa
FUJIKURA LTD.
Opto-Electronics Lab.
1440 Mutsuzaki
Sakura City, Chiba
Japan

Hiroshi Furukawa was born in 1959. He graduated from Chiba University in 1980.
He joined Fujikura and has been engaged in research and development in the Fiber and Cable Accessory Section.
Mr. Furukawa is a member of the IEICE of Japan.



Yow Sai Cheong
FUJIKURA LTD.
Opto-Electronics Lab.
1440 Mutsuzaki
Sakura City, Chiba
Japan

Yow Sai Cheong was born in Singapore in 1965. He graduated in mechanical engineering from the National University of Singapore in 1990.
He joined Fujikura in the same year and has since been involved in the research and development of telecommunication switching devices and connections.



Hiroshi Yokosuka
FUJIKURA LTD.
Opto-Electronics Lab.
1440 Mutsuzaki
Sakura City, Chiba
Japan

Hiroshi Yokosuka graduated in mechanical engineering from the Tokyo Metropolitan Technical Junior College in 1967.
He has been engaged in the development of telecommunication cables and accessories. He is presently the general manager of the Fiber and Cable Accessory Department.
Mr. Yokosuka is a member of the IEICE of Japan.

"Fiber Protective Coating Design for Evolving Telecommunication Applications"

H. C. Chandan, J. R. Petisce, J. W. Shea and C. R. Taylor
AT&T Bell Laboratories
Norcross, Georgia 30071

L. L. Blyler, D. Inniss, and L. Shepherd
AT&T Bell Laboratories
Murray Hill, New Jersey 07974

ABSTRACT

Today's evolving telecommunication and CATV applications for optical fibers are demanding higher performance in handling properties and reliability. In particular, the elevated temperature and humidity encountered in outdoor environments place added requirements on the fiber coating to maintain performance after long periods of exposure. These demands prompted us to generate a technology platform to understand critical coating properties which can effect field performance. Results are presented on strippability, fiber strength retention, solvent/solution resistance and aging/reliability testing.

Introduction

The performance requirements for UV cured acrylate coating systems have become more stringent since the late 1970's when these coating materials were introduced into optical fiber manufacture. Initial design requirements for UV cured optical fiber coatings focused on low temperature transmission loss[1] and fiber strength.[2] The late 1980's presented special end-use applications of optical fiber such as fiber-optic guided missiles and high temperature resistant aircraft cables which expanded or exceeded the performance limits of UV cured acrylate coatings.[3] In 1988, many of the first Fiber-to-the-Subscriber (FTTS) applications for several telephone companies occurred.[4] Coatings on optical fiber utilized in FTTS applications can undergo oxidative degradation due to high temperature exposure[5] or hydrolytic degradation due to simultaneous exposure to high temperature and high humidity.[6] Other applications of optical fiber which have been evolving in the 1990's include cable television (CATV) and long distance aerial installations which can expose optical fiber coatings to the same degradation mechanisms encountered in FTTS installations. The greater likelihood of more frequent handling of the coated optical fiber in the above applications prompted us to generate a technology platform containing a thorough understanding of the critical coating properties which can affect fiber handling in the field. This paper presents data and its interpretation related to the following critical coating properties: 1) strippability, 2) fiber strength retention, 3) solvent/solution resistance, and 4) aging/reliability. Some coating characterization tools previously developed have been utilized in this work.[7]

Strippability

In the evolving applications for optical fibers the ability to cleanly remove the coating from the glass for splicing and connectorization is critical. In order to provide a coating which can be removed with low force and will not leave residues which can interfere with splicing and connectorization, it is necessary to understand the coating properties which affect strippability. To clearly understand these effects, it is first necessary to distinguish between coating adhesion and coating strippability.

A method of measuring adhesion of coatings to glass fiber[8] has been employed and is illustrated in Figure 1. A one centimeter gauge length of coated fiber is bonded to a rigid tab (glass slide, hard cardboard, etc.) using a rigid adhesive (i.e., cyanoacrylate). The fiber is not encapsulated by the adhesive. The coating is then severed at the edge of the tab. The sample is mounted in an Instron and the force required to pull the glass from the coating is measured. The sample fails in shear on the primary coating/glass interface and represents an adhesive failure at that interface. The method for measuring strip force for optical fibers is defined by EIA-FOTP-178. The need to distinguish strip force from adhesion is shown in Figure 2 where a fiber with a very high strip force (> 1 lb) has a low pullout force and in fact delaminates when exposed to high humidity, even at room temperature. Even after the fiber coating is delaminated from the glass, the strip force remains relatively high. As a further illustration (Figure 3), a study of 160 fibers of widely varying adhesion as measured by pullout force showed essentially no variation in strip force.

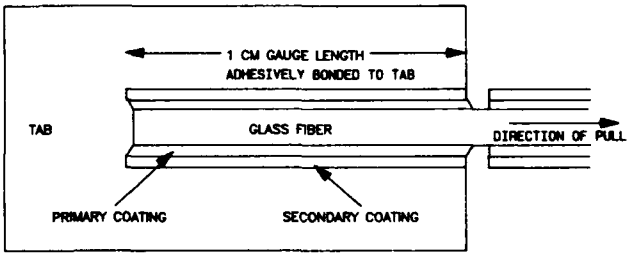


FIGURE 1. SCHEMATIC OF COATING ADHESION TEST

With this background, the effect of coating properties on strippability can now be examined. Figure 4 shows the failure mode of three different coatings during strip force testing. In Case 1 the coating shreds away from the fiber as the sample is stripped, resulting in a low, uniform strip force. In Case 2 the coating tends to "accordion", creating a high strip force followed by a cracking of the coating and a drop in strip force. This alternate behavior between the "accordion" and "shredding" modes continues resulting in a jagged force/time curve until the coating comes off. In Case 3 the coating "accordions" over the whole length resulting in a low force followed by an increasing level of force as the coating is stripped.

The relative behavior of these three coatings is determined by the behavior of the high modulus secondary coating with only minor contributions from the low modulus primary. An example of the dominant behavior of the secondary coating is shown in Figure 5. Two different secondary coatings were used with the same primary coating to prepare fibers. Secondary coating 2 had a lower elongation (11%) than secondary coating 1 (33%).

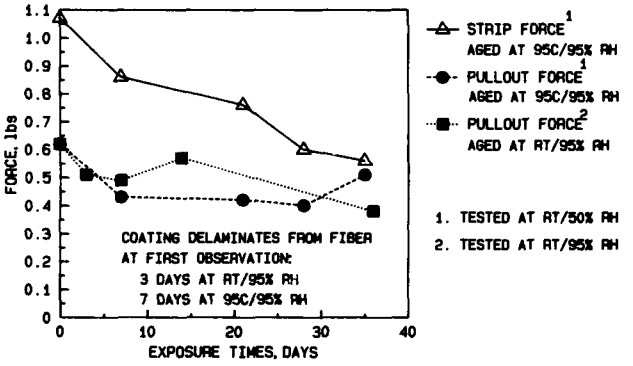


FIGURE 2. PULLOUT AND STRIP FORCE OF COATING D

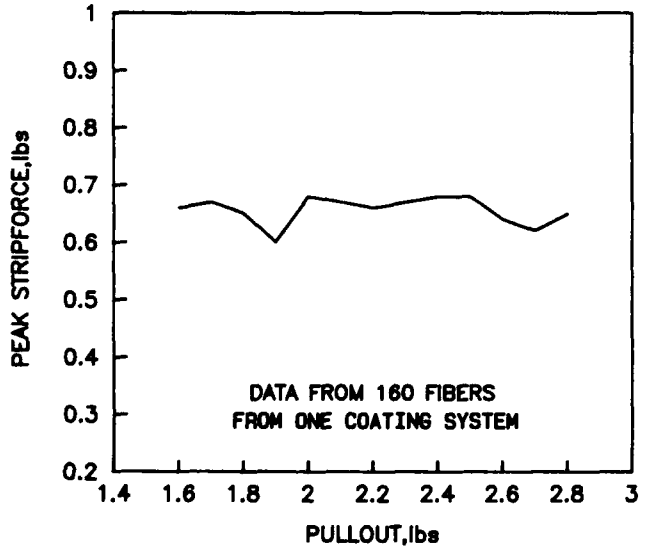


FIGURE 3. STRIPPABILITY VERSUS PULLOUT COMMERCIAL OPTICAL FIBER

Adhesion (pullout force) and strip force were measured over a range of cures. While both coating systems showed the same adhesion behavior, as measured by pullout, a 50% reduction in the force required to strip the coating was observed for the lower elongation secondary.

One other aspect of strippability of fibers is the presence of coating residues on the glass after stripping. These residues, if they persist after the usual alcohol wipe, can interfere with mass fusion splicing or with insertion of the fiber into the precision ferrules used in many splices and connectors. To evaluate this behavior, precision ferrules can be used to detect the presence of residues by fiber insertion following coating removal which includes an alcohol wipe. In general, few problems have been found in evaluation of most commercially available fibers as manufactured. This is demonstrated in Figures 6 and 7 which show microscope photographs of unaged fibers and fiber ribbons following stripping of the coating and alcohol cleaning, respectively. Coating residues are present in all cases after stripping. For the fibers the residues are gone after alcohol wiping. For the ribbons some evidence of residue after alcohol wiping is seen. This can be caused by wiping multiple fibers at one time, leaving residues in the

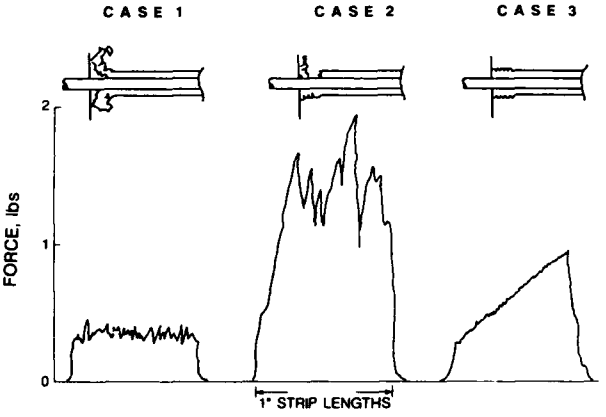


FIGURE 4. STRIPFORCE TRACES FOR VARIOUS COATINGS

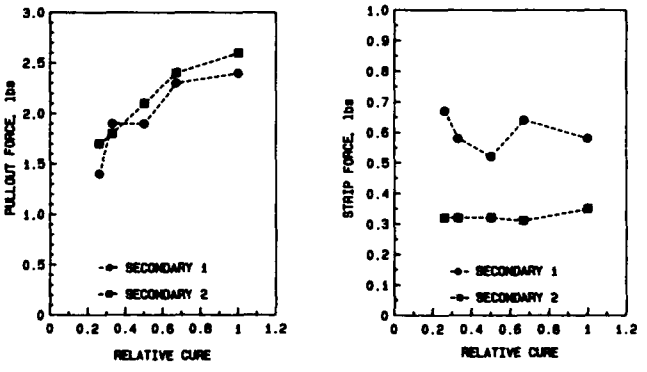


FIGURE 5. COMPARISON OF PULLOUT AND STRIP FORCE USING TWO DIFFERENT SECONDARY COATINGS OVER THE SAME PRIMARY COATING

difficult to reach area between the fibers. Continued wiping results in complete residue removal. This result points out the necessity for careful fiber cleaning in all cases but particularly when using ribbons, since any residues may interfere in fiber alignment during mass fusion splicing.

Fiber Strength Retention

A basic requirement for the reliability of any fiber installation is to maintain uninterrupted low loss transmission. Since glass can weaken over time due to flaw growth under stress, considerable engineering effort has gone into characterizing the static fatigue behavior of glass and controlling the stress levels applied to the glass fibers in cables and installations. FTTS and CATV applications have created additional concerns about fiber reliability due to increased environmental exposure, potential stress conditions, and handling. Recently, considerable attention has been focused on the profound influence coatings can have on fiber strength retention in elevated temperature/humidity environments. Yuce, et.al.,[9,10] have reported results on two coated fibers, one of which caused significant corrosion of the glass surface to produce a surface roughness (as measured by Atomic Force Microscopy, AFM) that was shown to correlate with a strength reduction. Similarly, Kennedy, et.al.,[11] compared three commercially available fibers and also show that strength degradation was accompanied by increased surface roughness. Evidence presented by Inniss, et.al.,[12] suggests that coating ingredients or contaminants which produce either a basic environment (e.g., a Lewis base that interacts with water to produce hydroxyl ions) or ionic environment can corrode the glass surface to produce surface roughness and a strength reduction.

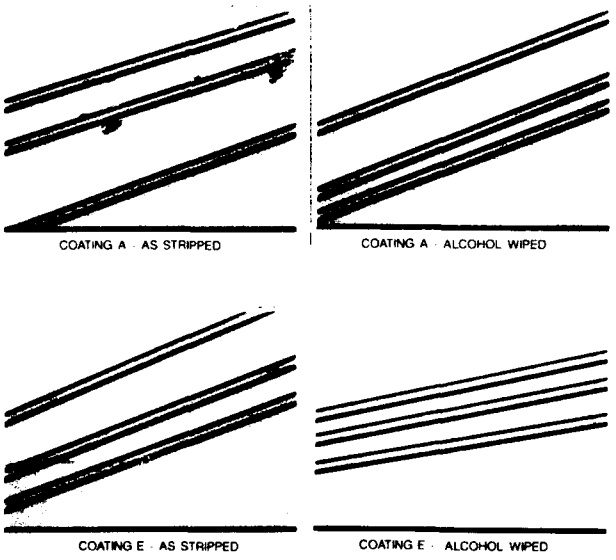


FIGURE 6. STRIPPING RESIDUES - UNAGED FIBERS

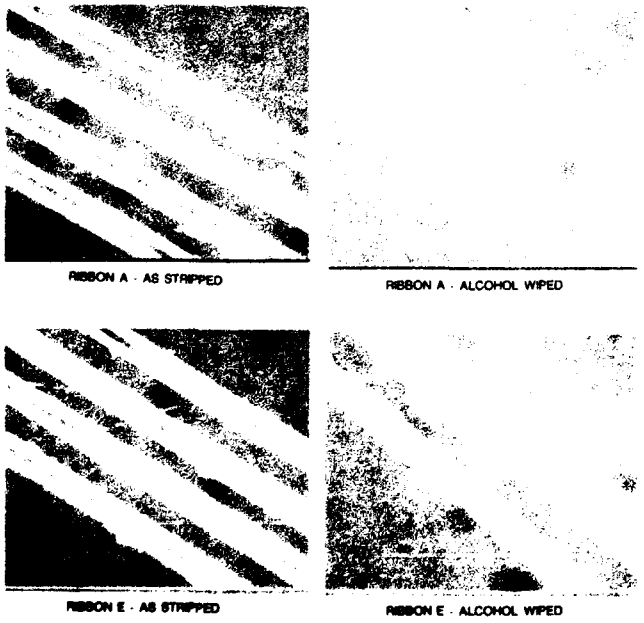


FIGURE 7. FIBER RIBBON STRIPPING

We have examined the effects of a small amount of a potentially corrosive component in base polymer primary/secondary coating formulations and have results on the role that coating to glass adhesion plays in retarding corrosion/strength reduction. The primary/secondary formulations used to make fiber are listed in Table I.

TABLE I

Experimental Primary/Secondary Coatings

Fiber Code	Primary/Secondary Formulations	Primary Adhesion Promoter	Potentially Corrosive Ingredient
W	Base Polymers	#1	No
X	Base Polymers	#2	No
Y	Base Polymers	#1	Yes
Z	Base Polymers	#2	Yes

The different adhesion promoters used in the primary coating both give adequate adhesion under ambient conditions but adhesion promoter #1 maintains a high quality coating-glass interface under elevated temperature/high humidity conditions whereas adhesion promoter #2 shows a substantial degradation of the interface at elevated temperature/high humidity. This is shown by the microscope photographs of the coating-glass interface in Figure 8. For adhesion promoter #2, the pullout level is maintained but the quality of the interface degrades giving a multitude of microscopic pockets where moisture and corrosive materials can concentrate. Adhesion promoter #1 on the other hand maintains the integrity of the interface even under more severe aging conditions. To evaluate the effects of adhesion promoters and corrosive materials, strength tests were carried out on fibers aged at 85°C/85% RH according to EIA/TIA-455-

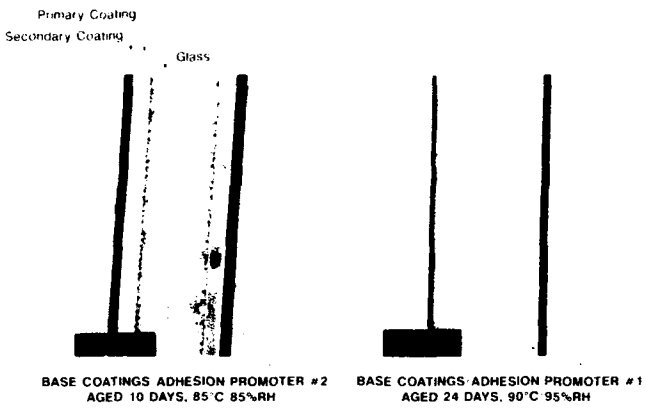


FIGURE 8. A COMPARISON OF COATING TO GLASS INTERFACE QUALITY AFTER ELEVATED TEMPERATURE/HUMIDITY EXPOSURE

28B using a gauge length of 50 cm and a strain rate of 2.5%/minute. The benefits of a high quality coating-glass interface are shown in Figure 9 where the strength after aging at 85°C in 85% RH is reduced only slightly for fiber W with adhesion promoter #1 whereas fiber X with adhesion promoter #2 shows approximately 15% reduction. The benefits of the high quality coating-glass interface are even more evident in fibers Y and Z where a potentially corrosive ingredient has been added. The effects of the corrosive ingredient are not eliminated by a high quality interface but the effects are reduced by approximately 50%. AFM was performed on the glass surface of fiber Z and is shown in Figure 10. The surface is rough, but in addition to the roughness there are pitted regions which match the size of the microscopic pockets that have formed at the coating-glass interface. In this region the glass is more

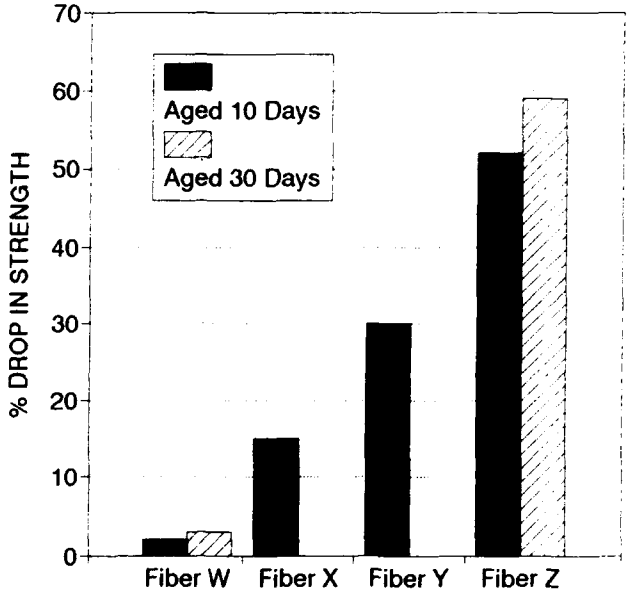


FIGURE 9. STRENGTH REDUCTIONS FOR FIBERS AGED AT 85 DEG C AND 85 % RH. COATING DESIGNATIONS INDICATED IN TABLE 1.

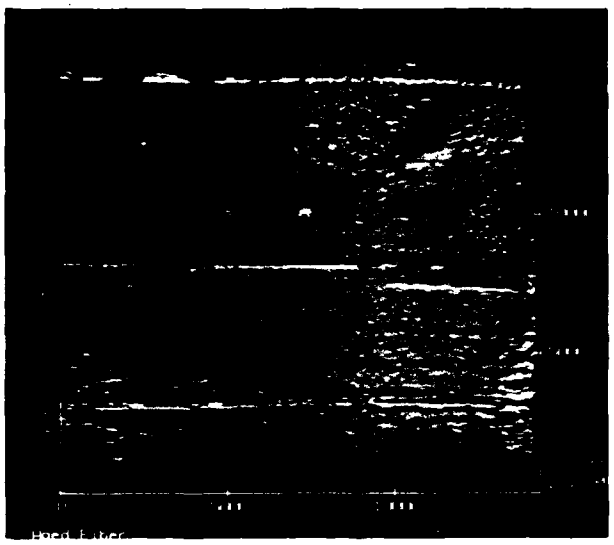


FIGURE 10. AFM OF GLASS SURFACE - FIBER Z. AGED 10 DAYS AT 85°C/85%RH

highly corroded, reflecting the tendency to collect moisture and corrosive components in delaminated regions.

The results shown in Figure 9 illustrate the need to maintain high quality coatings for good strength retention, which includes maintaining high purity levels to avoid potentially corrosive contaminants and maintaining good coating adhesion.

Solvent and Solution Resistance

As new optical fiber applications evolve in the subscriber loop, the fibers may be exposed to a wider variety of solvents and solutions including petroleum distillates in wasp sprays, chlorinated solvents, alcohols, bleach, and ammonia. An assessment must be made of the likelihood of fiber contact with a solvent and the coated fiber must be tested for resistance to these materials using procedures that duplicate field use, e.g., spraying with a wasp spray and cleaning fibers with alcohol. One approach to defining the solvent resistance of coating materials is to evaluate polymer/solvent interactions through the determination of polymer swelling over a wide range of solvents.

Sheets of both a primary and a secondary coating material, approximately 8 mils thick, were fully cured using a Fusion Systems "D" Lamp. Samples were die cut from the sheets, length was measured using a vernier accurate to .01 mm, then placed in a Petri dish, and covered with solvent. The cover was placed on the Petri dish and the dish wrapped in aluminum foil to retard solvent evaporation. Since volatile solvents can rapidly escape from the sheet samples if they are removed for weighing or measuring, sample lengths were measured at various times in the Petri dish. Solvent was added if necessary following each measurement and the dishes re-wrapped in foil. Volume changes were calculated from length changes assuming isotropic swelling of the coating.

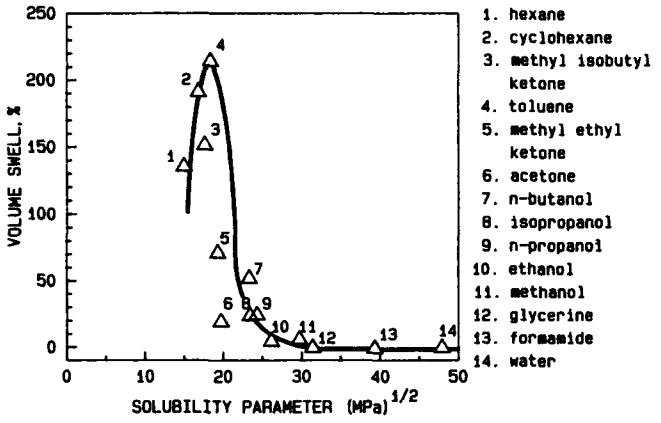


FIGURE 11. EFFECT OF SOLUBILITY PARAMETER ON SWELLING OF PRIMARY COATING SHEETS

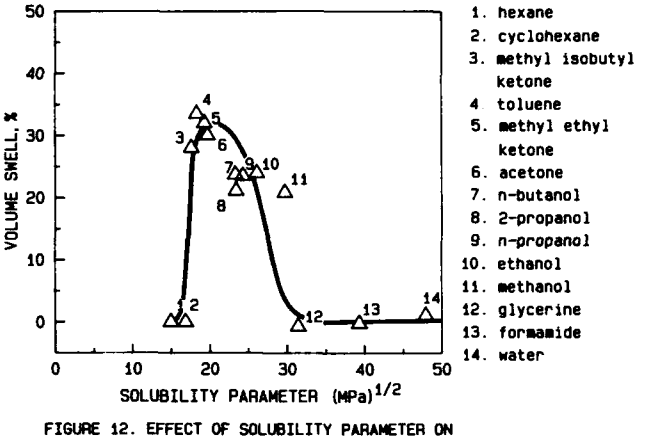


FIGURE 12. EFFECT OF SOLUBILITY PARAMETER ON SWELLING OF SECONDARY COATING SHEETS

The volume increase as a result of swelling of the primary coating as a function of solubility parameter, δ, (which is a measure of the solvent polarity) is shown in Figure 11 and for the secondary coating in Figure 12. The shapes of the curves reveal a maximum that can be shown to correspond to the point where the solvent solubility parameter matches that of the coating. The general shape of the curves can be derived from the Flory-Huggins equation and is expressed by the following equation[13]

$$\ln(1-\phi_2)+\phi_2+\chi\phi_2^2+\frac{\rho V_1}{M_c}\phi_2^{1/3}=0 \quad . \qquad (1)$$

Where ϕ_2 is the volume fraction of crosslinked polymer, ρ is the polymer density, V_1 is the molar volume of the solvent, and M_c is the molecular weight between crosslinks. χ is the well known polymer-solvent interaction parameter which depends on the molecular properties of the polymer-solvent combination. For the primary coating in the region of high swelling and neglecting contributions from chain free ends, Equation (1) can be simplified by expanding the logarithm and neglecting second order terms to yield:

$$\frac{\rho V_1}{M_c} \cong \left[\frac{1}{2}-\chi\right]\phi_2^{5/3} \qquad (2)$$

The interaction parameter can be calculated from solubility parameters by the following semiempirical equation,

$$\chi=\frac{V_1}{RT}(\delta_1-\delta_2)^2+\chi_s \qquad (3)$$

where δ_1 and δ_2 are the solubility parameters for solvent and polymer, respectively, and χ_s is the entropy contribution which is roughly equal to 0.34. From Equations (2) and (3), the volume swelling ratio (SR) of a crosslinked polymer by a solvent can be calculated as:

$$SR=\frac{V}{V_o}=\frac{1}{\phi_2}\cong\left[\frac{M_c}{\rho RT}\left[\frac{0.16RT}{V_1}-(\delta_1-\delta_2)^2\right]\right]^{3/5} \qquad (4)$$

where V_o is the original volume of the coating and V is the swollen volume. From this equation, the maximum in swelling ratio can be seen to occur when:

$$\delta_1 \text{ (solvent)} = \delta_2 \text{ (coating)} \quad . \qquad (5)$$

The amount of swelling that occurs at the maximum point is determined by the crosslink density of the primary coating as measured by the molecular weight between crosslinks, M_c. The maximum for the primary coating is seen to occur at the value of δ for toluene which has $\delta = 18$ and molar volume of 106 cm^3/mole. From Equation (4) we calculate M_c = 4700 g/mole. This can be compared to mechanical data through an equation (also neglecting chain free ends) that relates shear modulus of the primary coating to M_c by:

$$G=\frac{\rho RT}{M_c} \qquad (6)$$

The shear modulus as measured by dynamic mechanical methods for the primary coating in Figure 11 is 4.0 x 10^6 dynes/cm^2 and ρ = 1.0 which yields an M_c of 6200 g/mole in fairly good agreement with the M_c obtained from swelling. A similar calculation is not done for the secondary coating because it is densely crosslinked and the approximate equations used above do not apply. The positions and magnitudes of the points of maximum swelling of the primary and secondary coatings on the solubility parameter curves will determine whether and how much the coating will interact with various solvents. Referring to Figures 11 and 12, we can assess the general behavior of these coatings in solvents, some of which may be encountered in the field. For example, gasoline and petroleum distillates, essentially hydrocarbon materials,

would be expected to swell the primary coating significantly while the isopropanol used to clean fibers would have a much smaller effect. For the secondary coating the results are somewhat different with aliphatic hydrocarbons having no swelling effect while alcohol gives substantial swelling. The results in Figures 11 and 12 form the basis for understanding the behavior of coated fiber in various solvents or solutions. Since all polymer coatings will absorb solvents in some region of the solubility parameter spectrum, the challenge is to design primary/secondary coating composites that work together to provide the required level of solvent/solution resistance.

A particularly important area for solvent resistance performance of coatings is that of cleaning fluids used to remove cable filling compounds during splicing/connectorization operations and in some cases to enter ribbons. For these applications the rate of penetration of the cleaning solvent into the secondary coating plays a key role in coating design and solvent selection. Isopropanol is typically used as a general cleaning solvent and ethanol is used for special applications. The rate of swelling of the secondary coating in three alcohols is shown in Figure 13.

Ethanol begins to swell the material very rapidly while n-propanol shows little effect for approximately 2 hours and then rapidly swells. Isopropanol shows no initial swelling and then swells at a much lower rate than the linear alcohols. The final swollen volume of the coating is essentially the same for all three alcohols. In previous work on swelling of poly (methyl methacrylate) (PMMA) films, the effective cross-section of a molecule was more significant in determining penetration rates than the molecular volume.[14] The difference in the behavior of the materials is related to molecular size and shape of the solvent molecules. Table II shows the size characteristics of the alcohol molecules.

TABLE II

	Effective Molecular Shape	Molecular Cross Section For Penetration Angstrom^2
Ethanol	Cylindrical	42.4
n-Propanol	Cylindrical	45.9
Isopropanol	Spherical	54.5

Since isopropanol is an almost spherical molecule while ethanol and n-propanol are more elliptical in shape, the effective comparison is the spherical cross-section of isopropanol (54.5) versus the cylindrical cross sections of ethanol (42.4) and n-propanol (45.9). Based on this, the anticipated rate of swelling should be ethanol>n-propanol>isopropanol, as observed.

These results indicate that isopropanol is the preferred cleaning solvent for this set of coating materials since it

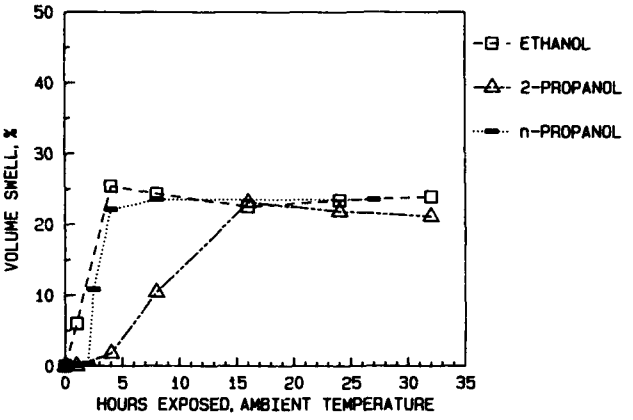


FIGURE 13. SHEET SWELLING OF A SECONDARY COATING IN 2-PROPANOL, n-PROPANOL AND ETHANOL (95%)

will not penetrate the secondary coating during cleaning operations. Ethanol can be used but procedures should require a one hour time limit on exposure. None of these solvents should be used when they will remain in contact with the fiber for many hours.

Aging and Reliability

Many of the new evolving applications for optical fibers involve exposure in outdoor equipment where the fibers will be subjected to elevated temperatures and/or humidity for long time periods. Temperatures inside telecommunications equipment can be as high as 68°C in Yuma, Arizona, while temperatures of 40°C at relative humidities over 70% are seen in Miami, Florida. Under these conditions the urethane/acrylate systems used in fiber optic coatings can degrade thermally (oxidation) or through attack by water (hydrolysis).

The degradation of the coating materials can effect fiber performance in several ways:

1. Yellowing/Darkening - Changes in the coating color on aging can result in the loss of color code identification of the fibers.
2. Loss of Physical Properties - Coating degradation can result in lowered strip force and tenacious residues after coating removal, added susceptibility to microbending loss, and less resistance to damage from handling.
3. Loss of Adhesion - The coating can delaminate from the fiber resulting in handling problems and exposure of the glass surface to attack by water.

In order to design coatings for resistance to oxidation, we utilize accelerated testing at a temperature of 125°C. We have based this choice on a typical activation energy of 70 kJ/mole for urethane/acrylate materials. Based on the Arrhenius function,

$$\ln (t_2/t_1) = \frac{E_a}{R}\left[\frac{1}{T_2} - \frac{1}{T_1}\right] \quad (7)$$

where t_2 and t_1 are aging times at temperatures T_2 and T_1 in degrees Kelvin, respectively, E_a is the activation energy, and R is the gas constant, we can calculate that 35 days at 125°C roughly simulates 30 years at 40°C. Although this test does not give an accurate determination of lifetime, it has been very useful in comparing candidate coating materials for oxidative stability.

In the case of hydrolytic aging, both temperature and humidity must be considered. Typically, the time to degradation can be expressed as

$$t \propto \frac{\exp - (E_a/RT)}{[H_2O]} \quad (8)$$

which can be expressed as

$$\ln t = - E_a/RT - \ln [H_2O] + C \quad (9)$$

where E_a is the activation energy for hydrolysis, C is a constant and $[H_2O]$ is the water concentration. Equations of this form have been previously used to describe the time/temperature dependence of degradation of polybutylene terephthalate.[15,16] Using a typical activation energy of ~ 40 kJ/mole to describe the behavior of urethane/acrylate systems in hydrolysis, we calculate that 77 days of aging at 95°C/95% RH roughly simulates 30 years at 40°C and 70% RH. As with the oxidative test described above, this test method is very useful for comparative coating design.

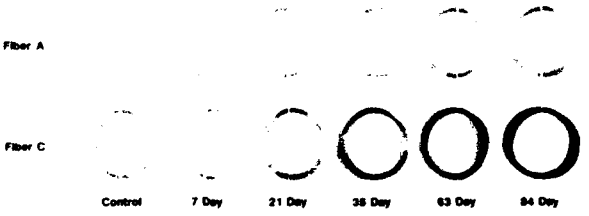


FIGURE 14. EFFECT OF AGING AT 95°C/95%RH ON COLOR OF OPTICAL FIBER COATINGS

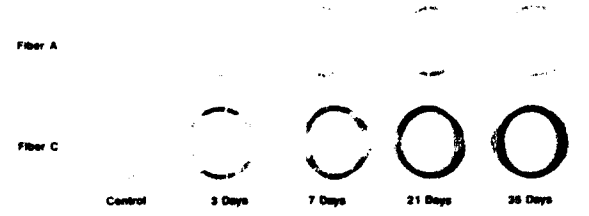


FIGURE 15. EFFECT OF AGING AT 125°C ON COLOR OF OPTICAL FIBER COATINGS

Using these accelerated tests, we compared the color changes of two coatings exposed to these conditions as shown in Figures 14 and 15. Coating C shows much more severe color changes than Coating A. Significant problems in fiber identification may occur with Coating C in outdoor applications.

The effect on physical properties under these same exposure conditions is shown in Figures 16 and 17. Coatings B and C show major changes in both strip force and adhesion after aging at 95°C/95% RH. In fact, degradation is so severe after ~ 35 days that adjacent coils of Fiber B stuck to each other, and could not be separated for testing. The same occurred with Fiber C. Evaluation of the strippability of several fibers after aging showed that no problem exists in the formation of tenacious residues after aging at 125°C for all coatings tested (Coatings A, C and E) exhibiting no problems on ferrule insertion. After aging at 95°C/95% RH, Coatings A and E stripped easily (Figure 18). However, Coating C had severe residues after stripping and small tenacious residue areas after wiping (Figure 19) such that ferrule insertion was no longer possible.

Delamination behavior of the coatings was examined by exposing fibers at 95% RH and temperatures ranging from RT to 95°C (Figure 20). A wide range of behavior was observed. Coating A exhibited no delamination even after 200 days at 95°C/95% RH. Coating F delaminated within 30 days at 60°C/95% RH, and Coating D delaminated in three days at RT/95% RH. Delamination as observed in

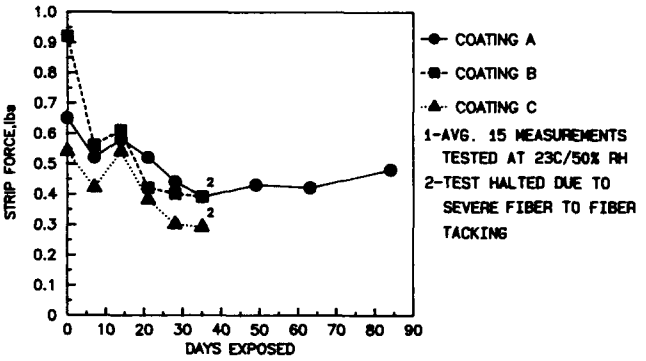


FIGURE 16. EFFECT OF AGING ON MECHANICAL STRIPFORCE FOR DUAL COATED FIBER AGED AT 95C/95% RH

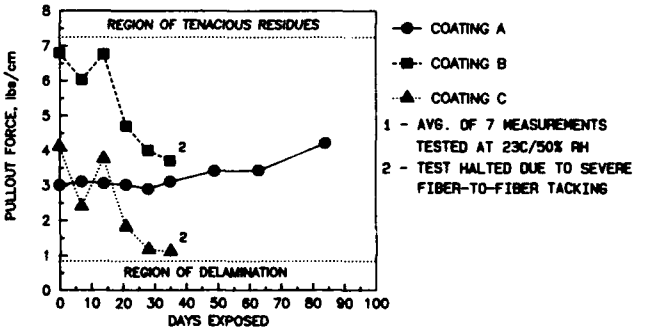


FIGURE 17. EFFECT OF AGING ON PULLOUT FORCE FOR DUAL COATED FIBER AGED AT 95C/95% RH

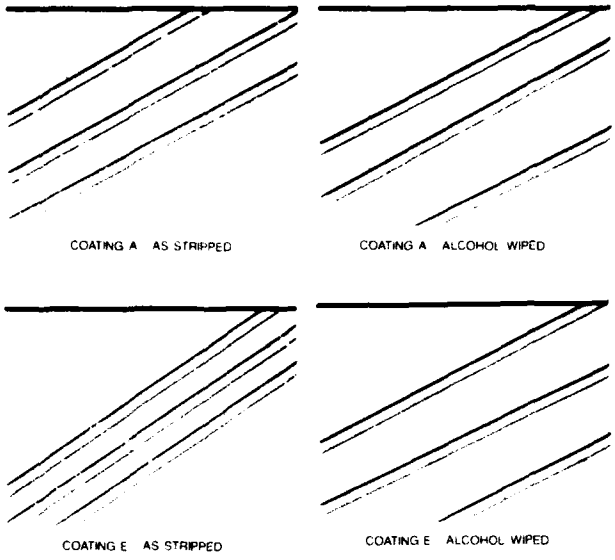


FIGURE 18. STRIPPING RESIDUES - HYDROLYTICALLY STABLE FIBERS AGED 84 DAYS AT 95°C/95%RH

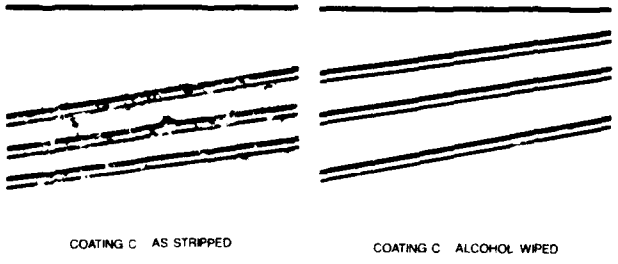


FIGURE 19. STRIPPING RESIDUES - HYDROLYTICALLY STABLE FIBERS AGED 84 DAYS AT 95°C/95%RH

Fibers D and F can result in glass strength degradation and handling problems since the coating comes off the fiber easily.

Degradation of optical fiber coatings in installations where elevated temperatures and humidity are encountered can result in loss of colored fiber identification, coating removal problems, and delamination of the coating from the glass. Accelerated aging tests can be used to design coatings that age well and minimize the chances of problems occurring.

Summary

As fiber optic applications continue to evolve, fibers are subjected to ever increasing performance demands. Coated fibers are required to provide uninterrupted low transmission loss while being exposed to elevated temperatures and humidity, increased solvent exposure, and increased handling during installation and rearrangement. The fibers must remain identifiable, retain strength, maintain adhesion of the coating to the glass, and resist the solvents and solutions that are used. To design coatings for

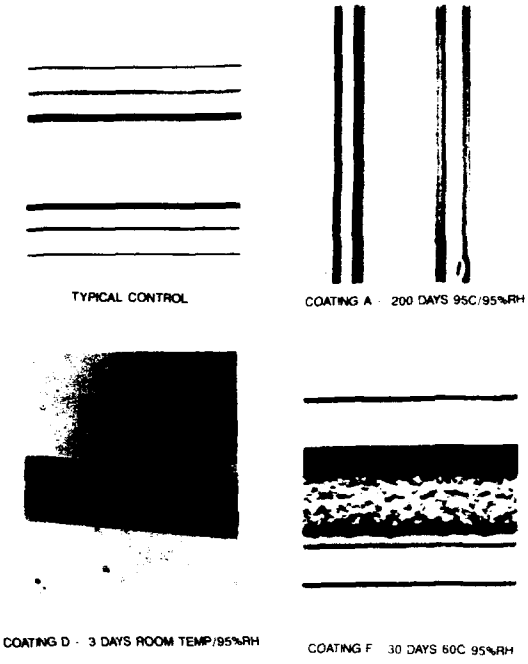


FIGURE 20. RELATIVE DELAMINATION BEHAVIOR OF THREE OPTICAL FIBERS

this level of performance, we utilize results from accelerated tests to select the coating candidates that will give the desired performance. We have presented techniques for evaluation of coating performance in the critical areas of strippability, strength retention, solvent and solution resistance, and aging and reliability.

ACKNOWLEDGMENT

The authors gratefully acknowledge contributions to this work from D. L. Brownlow, M. P. Green, M. C. Pirz, X. Quan, and D. A. Simoff of AT&T Bell Laboratories, Murray Hill, New Jersey, D. J. Harper, AT&T Network Cable Systems and C. H. Plagianis and B. Dritschler, Atlanta, Georgia.

REFERENCES

1. a) D. Gloge, Bell System Technical Journal, 54, 245, 1975. b) L. L. Blyler and C. J. Aloisio, *ACS Symposium*, Series No. 285, Applied Polymer Science, 907, 1985.
2. a) L. L. Blyler, F. V. DiMarcello and R. G. Huff, *ACS Symposium Series*, Polymers for High Technology, 410, 1987. b) L. L. Blyler and F. V. DiMarcello, *Encyclopedia of Physical Science and Technology*, 9, 647, 1987.
3. G. Kar, *Proceedings of the Optical Fiber Conference*, TUG1, 1988.

4. G. S. Cobb, W. H. Bensel, J. B. Haber, and M. M. Dixit, *Proceedings of the 38th International Wire and Cable Symposium*, 149, 1989.

5. D. A. Simoff, M. G. Chan, J. T. Chapin, and B. J. Overton, *Poly Engineering Science*, Vol. 29, 1177, 1989.

6. D. S. Szum, C. P. Chawla, T. E. Bishop, K. P. Murray, and J. M. Zimmerman, *Proceedings of the 39th International Wire and Cable Symposium*, 703, 1990.

7. J. W. Shea, J. M. Turnipseed, C. R. Taylor, J. R. Petisce, and B. J. Overton, *Mat. Res. Soc. Proc., 244, 85, 1992.*

8. B. J. Overton and C. R. Taylor, *Proceedings of SPE ANTEC*, April 18-21, 392, 1988.

9. H. H. Yuce, J. P. Varachi, Jr., J. P. Kilmer, C. R. Kurkjian and M. J. Mathewson, *Optical Fiber Communication Conference, Post-Deadline Papers, Optical Society of America*, Washington, D.C., PD-21, 1992.

10. H. H. Yuce, A. D. Hasse, P. L. Key and M. J. Andrejco, *Proceedings of the 37th International Wire and Cable Symposium* 732, 1988.

11. M. T. Kennedy, E. Cuellar and D. R. Roberts, *SPIE Proceedings*, 152, 1991.

12. D. Inniss, D. L. Brownlow and C. R. Kurkjian, *J. Am. Ceram. Soc.* 75, 364, 1992.

13. F. Rodriguez, *Principles of Polymer Systems*, 3rd Edition, Hemisphere Publishing Corporation, 1989.

14. J. S. Paponu, et.al., *J. App. Poly. Science*, 39, 803, 1990.

15. R. J. Gardner, J. R. Martin, *J. App. Poly. Sci.*, 25, 2353, 1980.

16. W. F. H. Borman, *Poly. Eng. Sci.*, Mid-October, Vol. 22, No. 14, 1982.



600 Mountain Avenue
P.O. Box 636 Murray Hill, NJ 07974-0636

Lee L. Blyler, Jr. attended Princeton University where he received his BSE in Chemical Engineering in 1961, MSE in the Polymer Materials Program in 1962 and Ph.D. in Aerospace and Mechanical Sciences in 1966. He joined AT&T Bell Laboratories in 1965 where he is currently Supervisor of the Plastics Applied Research, Properties and Processing Group. His research interests include physical properties and characterization of polymers, polymer melt rheology and processing, and polymer applications in lightwave technology and undersea cable systems. He has published over 60 papers in these areas and holds 15 patents, most of which involve lightwave technology.



2000 N.E. Expressway
Norcross, GA 30071

Harish C. Chandan is a Member of Technical Staff at AT&T Bell Laboratories, Norcross, Georgia which he joined in 1977. His current activities include mechanical reliability and processing of optical fibers. Dr. Chandan holds a Ph.D. from Penn State University in Ceramics Science. He is active in the Fiber Reliability Working Group in the Electronic Industries Association. He is a member of American Ceramic Society.



600 Mountain Avenue
P.O. Box 636 Murray Hill, NJ 07974-0636

Daryl Inniss is a Member of the Technical Staff of the Optical Fiber Research Department. He joined AT&T Bell Laboratories in 1988 and began his career working on the chemical mechanism which leads to fracture of silica optical fibers. He has also developed a "Hermetic Splice Overcoating" technique which can be used to hermetically seal the spliced region of hermetic fiber. Dr. Inniss was educated at Princeton University, Princeton, NJ, where he received an AB in Chemistry in 1983. He subsequently attended the University of California at Los Angeles and received a Ph.D. in Chemistry in 1988. He was the recipient of a Graduate Opportunity Fellowship and a Proctor and Gamble Graduate Fellowship at UCLA.



2000 N.E Expressway
Norcross, GA 30071

James R. Petisce is a Member of Technical Staff in the Materials Engineering Department at AT&T Bell Laboratories in Norcross, Georgia. After receiving a BA/MA in Chemistry from Boston University in 1980, he received a Ph.D. in Organic Chemistry from Northwestern University (Evanston, IL.) in 1984. Since joining Bell Laboratories in 1984, he has worked on the design and development of optical fiber coatings, bonded ribbon matrix materials, UV curable adhesives, index matching compounds, optical fiber color codings, and polyimide optical fiber coatings. His present responsibilities include design and development of materials for optical fiber and cable.



600 Mountain Avenue
P.O. Box 636 Murray
Hill, NJ 07974-0636

Lloyd Shepherd is Supervisor of the Plastics Chemistry Research and Engineering Group at AT&T Bell Laboratories in Murray Hill, New Jersey. He received his B.S. degree in Chemistry and his Ph.D. in Polymer Science from the University of Akron, Akron, Ohio. He joined Bell Laboratories in 1974 where he has been engaged in conducting chemical research on engineering polymer materials and processes. His research interests include polymer synthesis and stabilization, kinetics and mechanisms of polymer reactions, composite materials, and polymer applications in telecommunication cable systems. He has published numerous papers and holds several patents in these areas.



2000 N.E. Expressway
Norcross, GA 30071

John W. Shea received a B.S. in Chemistry from King's College, Wilkes-Barre, PA and on M.S. in Physics from the University of Notre Dame. After 10 years as a resin chemist with Union Carbide Corp., he joined AT&T Bell Laboratories in 1967. He has worked in the areas of printed circuit materials, injection molding, and extrusion. For the last several years he has been involved in optical fiber coatings and cable materials.



2000 N.E. Expressway
Norcross, GA 30071

Carl R. Taylor is currently Supervisor of the Materials Technology and Quality Group at AT&T's main Fiber Optic Manufacturing site in Atlanta. The group has responsibility for the design and engineering of materials used in fiber optic cable and apparatus products as well as responsibility for the quality of all incoming materials and components. He has previously been Supervisor of the Plastics Engineering and Characterization Group in Atlanta and Supervisor of the Polymer Materials Research, Engineering, and Applications Group at AT&T Bell Laboratories in Murray Hill, NJ. Prior to joining AT&T Bell Laboratories in 1977, he earned a B.S. in Chemistry from the College of Wooster in Ohio and a Ph.D. in Physical Chemistry from the University of Wisconsin in Madison. His graduate work focused on the physical and viscoelastic properties of polymers. He holds twelve patents and has authored or co-authored 25 publications.

Application of FT-IR to the cure degree measurement of UV curable optical fiber coating

A. Mizutani D. Saitho S. Endo N. Yoshioka

SUMITOMO ELECTRIC INDUSTRIES, LTD.
1. Taya-cho, Sakae-ku, Yokohama, Japan

Abstract

Detailed study on FT-IR ATR(Attenuated Total Reflectance)method for the cure degree measurement demonstrated that ATR gave better sensitivity and reproducibility than conventional extraction and/or modulus measurement. Depth dependence of cure degree along the radial direction of fiber coating showed that ATR surface measurement of 250μm coated fiber represented the cure degree of entire coating, even though measured portion had only a few microns thin layer at the surface.

ATR technique can be used for the cure degree measurement of thin UV inked layer as a further application.

Introduction

UV curable coating systems are widely used for the protective coating of the optical fiber with very fast polymerization process. The properties of the cured coating, that must protect the glass fiber from mechanical and chemical attacks, strongly depend on the cure degree.

Therefore, several techniques for measuring the cure degree of optical fiber coating have been proposed and evaluated. (1) Among those, the methods measuring the amount of extractives and/or elastic modulus of the coating have been well known for determining the cure degree of coating, although these methods take a rather long time for sample preparations and measurement, and only give insufficient accuracy. In the actual manufacturing, there has been an urgent requirement for more convenient and accurate method to determine the cure degree of optical fiber coating.

FT-IR ATR method gives us useful information about the fiber coating without complicated sample pretreatment, (2) and the potentiality of applying this method to the cure degree measurement has been demonstrated in the previous study. (1) It can, however, measure only a few micron layer of the outer surface. To clarify the relation between the cure degrees at the coating surface and the inner portion, we examined the depth dependence of the cure degree of thin film samples.

Then, we applied FT-IR ATR method to the actual 250μm coated fiber and compared the results with the conventional extraction and modulus measurements. Furthermore, the application to the cure degree measurement of very thin UV ink layer of colored fiber was studied as well.

Experimental

In the curing process of the UV curable resin, the double bond in the acrylate group is converted to the three dimensional network through the crosslinking reaction. The double bond content decreases with increasing the cross linking reaction. IR method measures the residual unreacted double bond content through the IR absorbance spectrum. In this study, We used the peak area ratio of the double bond peak at around 810cm^{-1} to the constant peak that was not affected by the cross linking reaction, as a parameter.

The ratio decreases with the increase of the cure degree. We used FT-IR spectrometer (model FTS-40, Bio-Rad, USA), 45° ZnSe crystal for ATR, and IR microscope (model UMA-300, Bio-Rad, USA) for measuring double bond content at the inner portion of the fiber coating with 10～20μm thickness sliced coating. With the conveyer type UV irradiator, we prepared 30μm thickness film samples which had the same thickness as the secondary layer of the fiber coating, and put them on the ZnSe crystal directly. For the actual fibers, 20～30 fiber peaces were put

together on the crystal in the manner that each fiber was aligned side by side. In addition, the tensile modulus and extractives measurements were conducted to ensure the sensitivity of the FT-IR method. For the tensile modulus measurement, we took specimens by peeling the coating material from the actual fibers. The fiber coating was extracted by MEK (Methyl-Ethyl-Ketone) for the extractives measurement. The actual fiber samples were manufactured with changing the fiber drawing speed and UV irradiation conditions.

Result and Discussion

Fiber coating The UV dose dependences of the unreacted double bond content at the UV irradiated surface and opposite side of the 30μm thickness film samples are shown in Fig.1. Both UV dose dependences show almost similar values and the same tendency that the unreacted double bond content decreased with increasing the UV dose rate. Since the 30μm film samples had the same thickness as the secondary layer of 250μm coated fiber, we anticipated there was no major difference of the residual unreacted double bond content, that should represent the cure degree, between the outer surface of the fiber coating and the boundary portion near the primary layer.

Then, we confirmed this through the measurement results for the actual fiber shown in Fig.2.

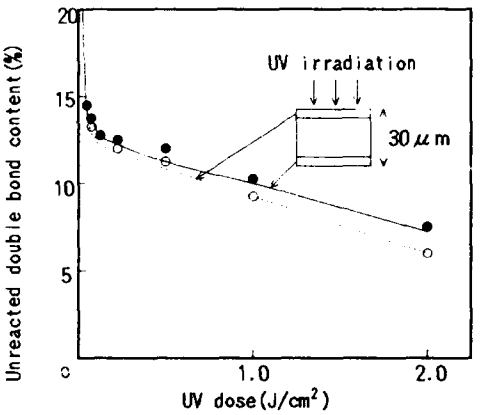


Fig1. UV dose dependence of unreacted double bond content at both sides of sheet samples measured by ATR

The surface unreacted double bond content of the actual fiber coating measured by ATR method are almost the same as those of the inner portion measured by IR microscope with the similar UV dose dependence, and the difference is small enough to evaluate the cure degree of the fiber coating.

These results indicate that the cure degree measured by FT-IR ATR method can represent that of the entire coating and FT-IR ATR method can be used as a characterization method of the cure degree of the fiber coating.

Fig.3. (A) and (B) show the comparison between the FT-IR ATR method and conventional tensile modulus and extractives measurements. The result measured by FT-IR ATR method well correlates with the conventional methods with the better sensitivity.

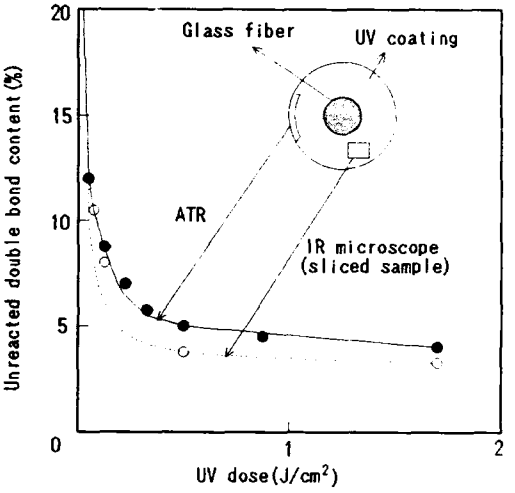


Fig.2 UV dose dependence of unreacted double bond content at the outer surface and the inner portion of fiber coatings measured by ATR and IR microscope

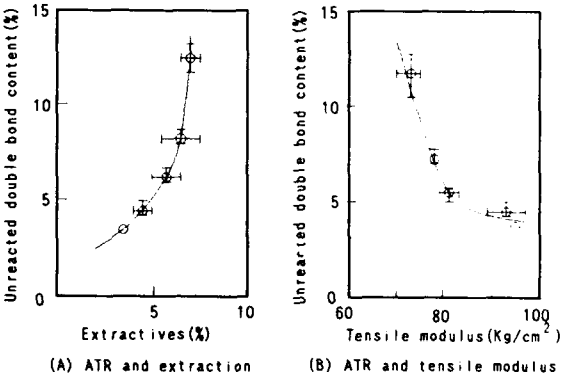


Fig.3 Comparison of cure degree measurments

FT-IR ATR method doesn't need the complicated sample pretreatment such as a humidity control in the tensile modulus measurement and it takes only around a score of minute which is fairly shorter than the extractives measurement. We think that FT-IR ATR is suitable to the actual manufacturing for the evaluation of the cure degree of the fiber coating.

Colored fiber UV curable inking is now popularly used for the identification purpose, and conventional methods can't be applied to the cure degree measurement of the very thin ink layer because they measure total properties including both the ink and the coating. We also applied FT-IR ATR technique to the ink layer of the UV ink colored fiber. As shown in Fig. 4, cured ink films of the 5～10μm thickness show the similar UV dose dependence of the unreacted double bond content to the fiber coating in the way double bond content decreased with increasing the UV dose. The measurement results of the actual colored fibers show the similar UV dose dependence to the film samples with good reproducibility as the fiber coating, shown in Fig. 5.

Consequently, FT-IR ATR method can be applicable to the evaluation of the cure degree at the ink layer of the UV curable ink colored fiber with no influences of the fiber coating.

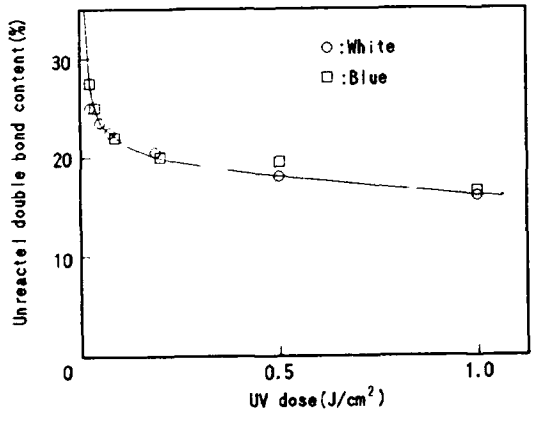


Fig. 4 UV dose dependence of unreacted double bond content of the cured UV ink film measured by ATR

Conclusion

We examined the FT-IR ATR method as a measurement tool of the cure degree. The results of the fiber coating measured by FT-IR ATR method showed the rational UV dose dependence with better sensitivity and reproducibility than the conventional tensile modulus and extraction measurement. The simple measurement procedure of FT-IR ATR provides us the easy and convenient in-process evaluation method of the cure degree and suitable tool to the actual manufacturing. Furthermore, we confirmed FT-IR ATR method to be applicable to the cure degree measurement of the UV curable ink coloring layer which has been difficult to be accurately evaluated by conventional method due to its thin thickness and composite system with the fiber coating.

Reference

(1) R. A. Frantz, I. M. Pliez, S. R. Schmid, Proceedings of the 40 th Interrational Wire and Cable Symposium, November 1991, p. 134.

(2) Y. Lin, J. Hsiao, D. Fann, S. Wang, K. Chen, Proceedings of the 40 th International Wire and Cable Symposium, November 1991, p. 504.

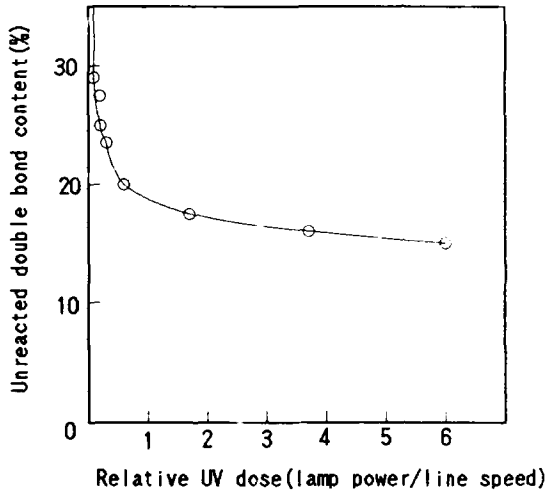


Fig. 5 UV dose dependence of unreacted double bond content of the UV curable ink colored fiber(white)



Akihiko Mizutani

Akihiko Mizutani received a M.S. degree from Nagoya University in 1985 and directly joined Sumitomo Electric Industries, Ltd. He has been engaged in development of manufacturing optical fiber.



Naoki Yosioka

Naoki Yoshioka received a M.S. degree from Osaka University in 1975. He joined Sumitomo Electric Industries, Ltd. in 1975, and has been engaged in research and development of optical fiber fabrication. He is a manager of fiber optics production engineering section.



Daisuke Saitoh

Daisuke Saitoh received the B.E. degree in engineering from Keio University in 1991 and joined Sumitomo Electric Industries, Ltd. He is an engineer of the Fiber Optics Production Engineering Section.



Shigeki Endo

Shigeki Endo received the B.S. degree for Electrical Engineering from Waseda University in 1976. He joined Sumitomo Electric Industries, Ltd, and worked on the production engineering of 9.5 and 4.4 coaxial cable. Thereafter he has been engaged in the development of manufacturing optical fiber. He is an assistant manager of fiber optics production engineering section of fiber optics division.

VINYL ETHERS, A NEW MATERIAL TECHNOLOGY FOR ULTRA-VIOLET CURABLE OPTICAL FIBER COATINGS

G. David Green and James R. Snyder
Allied - Signal Inc.
Morristown, New Jersey

Alvin C. Levy and Raymond J. Kovac
Alvin C. Levy & Associates, Inc.
Norcross, Georgia

Paul R. Foy
Fiber Optic Materials Research Program
Rutgers University
Piscataway, New Jersey

ABSTRACT

Ultra-violet (UV) curable materials based on acrylate chemistry are widely used as coatings for optical fibers. These materials are useful because they are easy to adapt to the fiber coating process. Over the years much effort has been directed at improving properties, especially the low temperature mechanical properties of primary coatings and the environmental stability of coatings in general. More recently, as draw speeds have increased, a need has developed for materials that cure at faster rates than available with acrylate technology. This paper discusses a new UV cure technology as applied to coatings for optical fiber. These new materials are based on crosslinking through a vinyl ether linkage as opposed to an acrylate linkage. Data are presented which show how these new compounds compare with acrylates in terms of physical properties and cure rate. In addition some limited results of fiber coating studies are presented.

INTRODUCTION

Glass optical fibers require protective coatings[1] to protect the fiber from physical damage and to buffer the fiber from "microbending" induced optical loss. In order to accomplish these ends, two coatings are frequently applied to the fiber; a low modulus primary coating for microbending protection, and a stiff secondary coating for mechanical protection. The coatings are applied to the fiber in-line during fiber drawing. These coatings, like other materials used in the manufacture of telecommunications cable, must be functional over a broad temperature range (i.e. -40 ^{o}C to 80 ^{o}C) for periods of from 20 to 40 years.

Ultra-violet (UV) curable materials based on acrylate chemistry have been widely used as coating materials because they can be applied and cured at high draw rates. Although these compounds have proven extremely functional, the state of fiber drawing technology may soon require higher cure rate capability than is available with acrylate chemistry. In addition, it is often difficult to obtain low glass transition temperature (Tg) primary coatings with acrylates.

The subject of this paper is UV curable coatings based on vinyl ether rather than acrylate chemistry. Vinyl ether coatings differ chemically from acrylate coatings primarily in the reactive group through which crosslinking takes place. The balance of the chemistry is very similar to that of acrylate materials. For example, the chemistry of the oligomers in terms of the molecular building blocks between the reactive groups can be the same for both types of coatings. However, this difference in the reactive group has a number of profound beneficial effects on coating properties. These new coatings offer significant advantages with respect to cure speed and ease of obtaining low modulus primary coatings at -40 ^{o}C. This paper discusses the general principles of vinyl ether chemistry, physical properties generally associated with fiber performance, coating stability, limited results from studies of coated fiber and finally plans for future work.

VINYL ETHER CHEMISTRY

CURING OF VINYL ETHERS

The major difference between acrylates and vinyl ethers is their cure mechanism. Acrylates cure radically while vinyl ethers cure cationically. This difference manifests itself primarily in cure speed, cure dose, resin matrix effects during curing, susceptibility to impurities, and dark cure.

The key component of a cationic curing system is an acid generating photoinitiator. The best known classes of photoacid initiators are diaryl iodonium salts and triaryl sulfonium salts. These materials liberate strong acids upon UV or EB irradiation. This strong acid is capable of catalyzing cationic polymerization reactions.[2,3]

The high reactivity of vinyl ethers in cationic polymerization is a consequence of the electron rich nature of the carbon-carbon double bond. Resonance structures may be drawn which illustrate the stabilization of the resulting carbocation (Eq 1).

$$R^+ + CH_2=CH\text{-}O\text{-}R' \rightarrow R\text{-}CH_2\text{-}CH^+\text{-}O\text{-}R \leftrightarrow R\text{-}CH_2\text{-}CH=O^+\text{-}R' \quad (1)$$

Differential photocalorimetry (DPC) is a convenient method to illustrate the high reactivity of vinyl ethers relative to other photoinitiated systems. DPC measures the heat evolved by the UV induced polymerization reaction. Figure 1 shows conversion as a function of time for triethyleneglycol divinyl ether (DVE-3). A triacrylate monomer (trimethylopropane triacrylate) and a bis cycloaliphatic epoxy monomer, 3,4-epoxycyclohexylmethyl-3'4'-epoxycyclohexane carboxylate (BCE) are also shown for comparison. The vinyl ether reached high conversion in less than 30 seconds. The acrylate showed the next highest polymerization rate. The cycloaliphatic epoxy monomer showed the slowest polymerization rate of these three systems by DPC. The divinyl ether monomer also reached the highest conversion under these conditions.[4] The high conversion of the vinyl ether may be attributed to its high reactivity and also the relatively low Tg of the resulting polymer, which will minimize the effect of matrix vitrification.

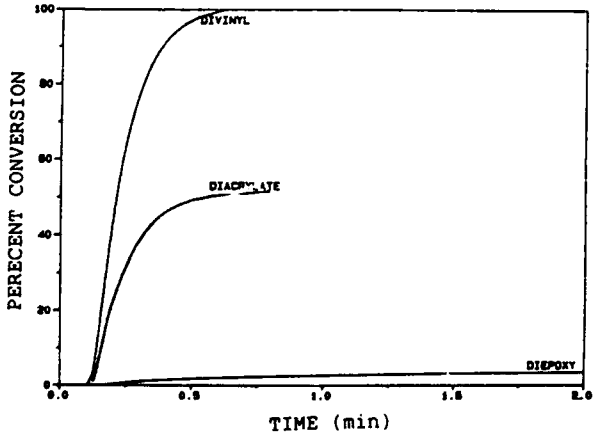
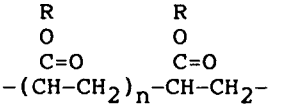


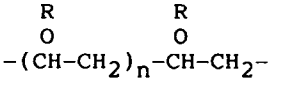
FIGURE 1. Percent Cure Versus Time, 0.7 second, 60 uW/cm^2 UV exposure @ 35 ^oC. Conversion has been corrected based on literature values of polymerization enthalpy. (Ref. 4; [a]triethyleneglycol divinyl ether; [b]trimethylolpropane triacrylate; [c]3,4-epoxycyclohexylmethyl-3'4'-epoxycyclohexane carboxylate).

VINYL ETHER FUNCTIONALIZED MONOMERS AND OLIGOMERS

In principle it is possible to produce vinyl ether based formulations in which the oligomeric spacers are identical to those in acrylate formulations. While the same general trends in coating properties may be expected within each series, significant differences may be observed in the vinyl ether and acrylate based systems. One reason for the difference in properties is the difference in the structures in the newly formed polymer chains. Acrylates produce a C-C backbone with pendant ester groups while vinyl ethers produce a C-C backbone with pendant ether groups. Even if the substituent (R) was the same in both polymers, different properties would be expected. The acrylate backbone is generally rigid, while more flexibility is expected in a polyvinyl ether backbone.[5,6] The vinyl ether terminated coatings would therefore be expected to have lower Tg and higher flexibility.



Polyacrylate



Polyvinyl ether

Vinyl Ether Terminated Ester Monomers

Vinyl Ether terminated esters are a versatile class of materials that may be prepared by the reaction of hydroxyvinyl ether monomers with carboxylic derivatives. Multifunctional carboxylic acid derivatives may be used to produce multifunctional vinyl ether products (Eq 2).[5,7]

$$R\text{-}(CO\text{-}X)_n + n\ HO\text{-}R'\text{-}O\text{-}CH=CH_2 \rightarrow R\text{-}(COO\text{-}R'\text{-}O\text{-}CH=CH_2)_n + HX \quad (2)$$

Vinyl Ether Terminated Urethane Oligomers Vinyl ether terminated urethanes are a class of compounds that may be prepared from hydroxyvinyl ether precursors. These materials are prepared by the reaction of hydroxyvinyl ethers with compounds containing isocyanate groups.[8] The alcohol group of the hydroxyvinyl ether reacts with the isocyanate to form the desired urethane linkage (Eq 3).

$$R\text{-}(NCO)_n + n\ HO\text{-}R'\text{-}O\text{-}CH{=}CH_2 \rightarrow R\text{-}(NHCOO\text{-}R'\text{-}O\text{-}CH{=}CH_2)n \quad (3)$$

There are a wide variety of urethane prepolymers that can be used to form vinyl ether terminated urethane oligomers. The prepolymers are formed by reacting an excess of a diisocyanate with an oligomeric polyol. Polyethers and hydroxy terminated polyesters are the most commonly used polyols. The resulting prepolymers have unreacted terminal isocyanate groups which are then end-capped with hydroxyvinyl ether.

CURE PROPERTIES OF VINYL ETHER COATINGS

As described above, the cure of vinyl ether (VE) coatings is cationically initiated. Typically full cure requires a dose of from about 0.25 to 0.5 J/cm^2. This value compares with exposure requirements for acrylates of 0.5 to 1.0 J/cm^2 for secondary coatings and higher for primary coatings. Examples of vinyl ether cure behavior are given in Figures 2 and 3 where the tensile modulus of the primary and secondary vinyl ether coatings respectively are shown as a function of cure dose. Curing for all studies unless otherwise noted was done with a Fusion Systems H bulb (6 inch, 300 watt/inch) under a nitrogen blanket. The cure dose was measured with a UVPS compact radiometer.

As can be seen, full cure of the vinyl ether primary coating is attained at a dose of only about 0.3 joules/cm^2. Full cure of the secondary coating requires a dose of approximately 0.6 joules/cm^2. Other vinyl ether secondary coatings have been cured at doses of about 0.25 joules/cm^2.

PHYSICAL PROPERTIES OF COATINGS

The property ranges for a number of vinyl ether coatings are shown in Table I. Data for the acrylate coatings given in Table 2 were taken from reference 9 and are not meant to represent the limits of acrylate technology.

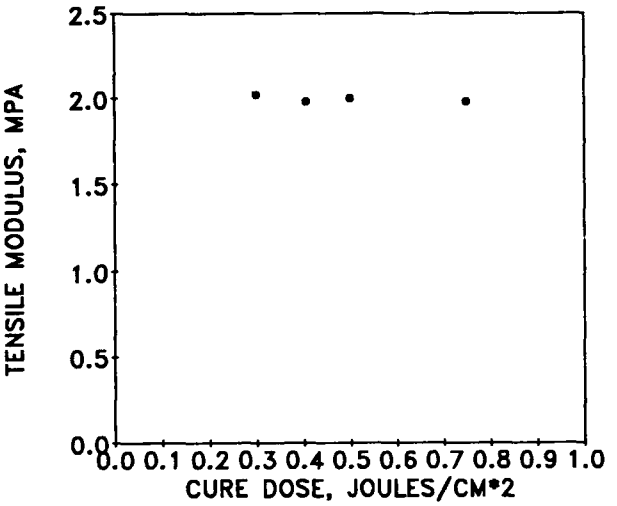


FIGURE 2. Modulus Versus Cure Dose, Vinyl Ether Primary Coating @ 25 °C, 50% RH

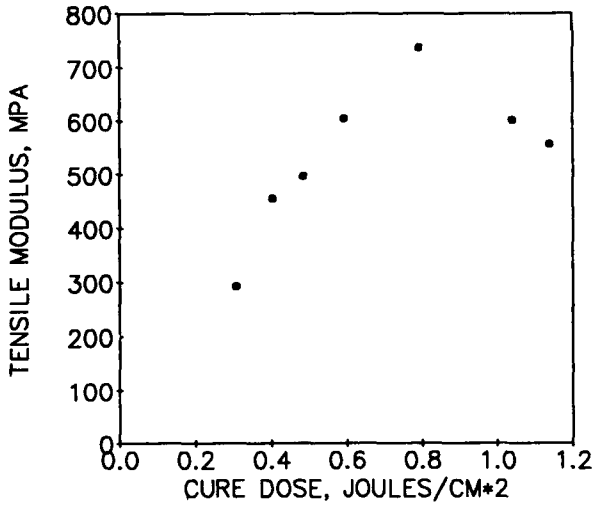


FIGURE 3. Modulus Versus Cure Dose, Vinyl Ether Secondary Coating @ 25 °C, 50% RH

TENSILE PROPERTIES

These data indicate that the tensile properties at 25 ^{o}C of vinyl ethers are similar to those of acrylate compounds. However, because properties such as modulus can vary greatly with humidity, it is difficult to make precise comparisons unless humidity conditions are identical. Further discussion of the effect of humidity on tensile properties may be found in the Environmental Stability section.

MECHANICAL ANALYSES

With respect to glass transition temperature, one would expect lower Tgs for vinyl ethers than for acrylates. As previously stated, the ether linkage in vinyl ethers is inherently more flexible than the ester linkage found in acrylates. Therefore, primary coatings with very low glass transition temperatures as shown in Table I are relatively easy to obtain with vinyl ether technology. As a further explanation of the Tg data, the Tg for the DMA data corresponds to the maximum in Tan Delta. For the TMA data, the Tg is based on an extrapolation of the expansion data.

The limited coefficient of expansion data indicates that the two types of coatings are comparable in that respect. Likewise, the viscosity ranges of vinyl ethers and the acrylates are similar.

WATER ABSORPTION

The water absorption data show that the vinyl ethers coatings developed to date are generally lower in that property than typical acrylate compounds. This difference is potentially important since the brittle fatigue failure of glass is accelerated by the presence of moisture. Other properties such as modulus are also dependent on the level of water present in the coating. (See the Environmental Stability section below.)

TABLE I
VINYL ETHER PROPERTY RANGE

PROPERTY	PRIMARY COATING	SECONDARY COATING
Tensile @ 50% RH, 25 C (0.5 J/cm^2 cure dose)		
Modulus, MPa	1.5 - 2.0	325 - 750
Break Strength, MPa	1.5 - 1.7	16 - 34
Elongation, %	50 - 150	16 - 26
Glass Trans. Temp., C @ 1% RH		
by DMA @ 4 Hertz		
Knee of Curve	-37 - -19	42 - 50
Tan Delta Max.	-25 - -4	65 - 67
by TMA (1% RH)	-45 - -23	34 - 70
Coefficient of Expansion @ 1% RH, in/(in x ^{o}C) x 10^{-6}		
below Tg	a	26 - 34
above Tg	580 - 595	279 - 285
Viscosity @ 25 C, poise	60 - 100	45 - 90
Water Absorption, %	1.3 - 2.1	1.6 - 2.5

a. Insufficient range below Tg to determine

TABLE II
PROPERTIES OF ACRYLATE COATINGS

PROPERTY	PRIMARY COATING	SECONDARY COATING
Tensile @ 50% RH, 25 C		
Modulus, MPa	2.1 - 2.8	600 - 1035
Break Strength, MPa	1.9 - 4.1	25 - 38
Elongation, %	125 - 200	16 - 30
Glass Trans. Temp., C by TMA	-32 - +10	50 - 60
Coefficient of Expansion by TMA, in/in/ ^{o}C x 10^{-6}		
below Tg	80 - 200	10 - 210
above Tg	280 - 420	190 - 910
Viscosity @ 25 C, cps	87 - 105	50 - 130
Water Absorption, %	2.6 - 8.0	2.5 - 5.7

ENVIRONMENTAL STABILITY

The environmental stability data consists of the determination of modulus as a function of relative humidity and thermal stability data.

HUMIDITY EFFECTS

The modulus versus humidity data are given in Figures 4 and 5. As can be seen from Figure 4, the tensile modulus is strongly dependent on the moisture content for both vinyl ether and acrylate secondary coatings. Figure 5 indicates a similar effect with primary coatings, but to a lesser degree. The smaller influence with the primary coatings is likely related to a lower solubility of water in the primary coating relative to the secondary coating. Although not shown, increasing humidity decreases break strength and increases elongation. Based on these data, one can see that it is extremely important to specify the humidity when citing tensile properties.

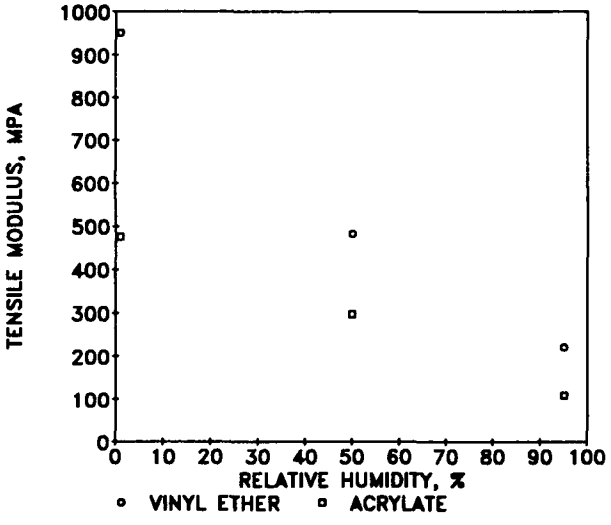


FIGURE 4. Modulus Versus Relative Humid., Secondary Coatings @ 25 °C

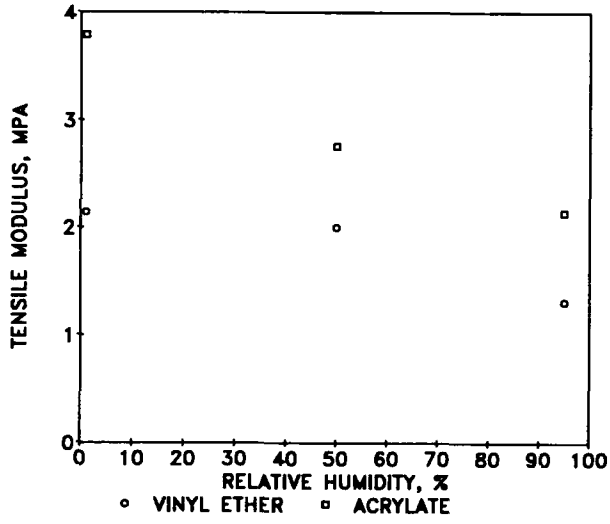


FIGURE 5. Modulus Versus Relative Humid., Primary Coatings @ 25 °C

THERMAL STABILITY

In terms of thermal stability, both primary and secondary vinyl ether coatings were evaluated with respect to hydrogen generation, oxidation onset temperature, weight loss, and mechanical stability.

HYDROGEN GENERATION

The hydrogen generation after aging for 48 hours at 100 °C for the various vinyl ether coatings are shown in Table III. These data are higher than those reported for acrylates in reference 9 (0.2 - 0.6 ul/g for primary coatings and 0.5 - 1.5 for secondary coatings aged 24 hours at 80 °C). However, because the aging conditions are different for the vinyl ether and acrylates coatings, direct comparisons are not valid.

OXIDATION ONSET AND WEIGHT LOSS

The Oxidation Onset and Weight Loss data are also given in Table III. As a point of reference, commercial primary and secondary acrylate coatings exhibited Oxidation Onset temperatures of 240 °C and 279 °C respectively, and 7 day Weight Loss at 125 °C of 7.4 % and 3.7 % respectively. It should also be particularly noted that there was no discoloration of coatings B and D after 7 days at 125 °C. Color changes for the acrylate coatings were intermediate between the ranges observed for the vinyl ether coatings. Since, performance in these tests is very much dependent on stabilization packages, work in this area is continuing.

TABLE III
THERMAL STABILITY DATA

PROPERTY	PRIMARY COATING A	PRIMARY COATING B	SECONDARY C	SECONDARY D
Hydrogen Generation, ul/g (48 hours @ 100 °C)	1.8	1.9	4.8	3.0
Onset of Oxidation, (TGA @ 5 C/min., air)				
Temperature, C	262	270	248	258
Wt. Loss at Onset, %	7.4	2.1	4.4	3.2
Weight Loss @ 125 C, % by wt.				
1 day	5.4	2.4	2.8	2.5
7 day	8.0	3.8	4.4	3.7
Discoloration, 7 days @ 125 °C	Yellow	none	L.Yel	none

MECHANICAL STABILITY

The glass transition temperatures for vinyl ether coatings A and C were also measured after aging for 21 days at 80 °C. The increases in the Tg for the primary and secondary coatings relative to the unaged materials were 5 °C and 1 °C respectively.

FIBER COATING STUDY

In order to evaluate coating process variables, fiber coating experiments were conducted at Rutgers University at the Fiber Optics Materials Research Program Laboratories. The fiber was drawn from high quality glass rods as opposed to optical quality preforms. The coatings were applied in-line with drawing using separate applicators for the primary and secondary coatings. One Fusion Systems curing unit was located between the two coating applicators and a second curing unit between the secondary coating station and the tractor unit. Each station had one 10 inch long 300 watt/inch D bulb for a total power of 3000 watts. In the first experiment, vinyl ether coatings were drawn at rates from 1 m/sec up to the limit of the draw tower equipment, 3 m/sec. The bare glass fiber, primary coated fiber, and total coated fiber diameters were 125, 200, and 250 microns respectively. No problems were encountered with curing of the coating or stability of the applied coatings.

The residual tack of the coated fibers were examined at intervals from one hour to two weeks after coating. The method of examination was to see if the fiber would freely unwind under a one meter length of its own weight. No problems were encountered, although occasionally a slightly greater force than the weight of the fiber was required for the 3 m/sec samples.

In a second experiment, the same vinyl ether coatings and a set of commercial acrylate coatings were used to coat fiber drawn from a high quality synthetic silica rod (Suprasil from Heraeus Amersil, Inc.). The purpose of this test was to obtain fiber for a long length strength evaluation. The draw rate was 1 m/sec. The other conditions were as described above.

The long length strength evaluation is not currently complete and will be reported at a later date. However, samples of both coated fiber types were evaluated for onset of oxidation as described in the Environmental Stability section. The onset temperature for both the vinyl ether and the acrylate coated fiber were found to be 265 °C.

CONCLUSIONS

At the time of the publication cut-off date, work was continuing in the areas of formulation and stabilization of vinyl ether coatings. However, even in the absence of completion of the study some conclusions can be made.

- The first conclusion is that a major improvement in cure rate can be expected with coatings based on vinyl ether chemistry relative to those based on acrylate chemistry.

- Secondly, lower primary coating glass transition temperatures can be obtained with vinyl ether based materials than with compounds based on acrylate chemistry.

- With respect to other physical properties, both vinyl ether and acrylate coatings are similar in behavior.

Hydrogen generation is an area where improvement may be necessary. That work is still in progress as are studies on thermal hydrolytic stability and fiber strength. Coating of fiber drawn from optical quality preforms are also planned for Rutgers University.

REFERENCES

1. L. L. Blyler, Jr., and C. J. Aloisio in R. W. Tess and G. W. Poele, eds., Applied Polymer Science, 2nd ed., The American Chemical Society, Washington, D. C., 1984, Chapt. 38.

2. For a review see: J. V. Crivello, Adv. Polym. Sci., 62, 1 (1984).

3. D. R. McKean, U. Schaedeli, and S. A. MacDonald, J. Polym. Sci., Polym. Chem. Ed. 27, 3927 (1989).

4. S. R. Sauerbrumm and D. C. Armbruster, RadTech '90: Conf. Proc., p. 303, RadTech International, Northbrook, IL (1990).

5. S. C. Lapin and J. R. Snyder, RadTech '90: Conf. Proc., p. 410, RadTech International, Northbrook, IL (1990).

6. R. J. Brautigam, S. C. Lapin, and J. R. Snyder, RadTech '90: Conf. Proc., p. 99, RadTech International, Northbrook, IL (1990).

7. S. C. Lapin and S. A. Munk, U.S. Patent 4,749,807 (1988).

8. S. C. Lapin, RadTech 88: Conf. Proc., p. 395, RadTech International, Northbrook, IL (1988).

9. DeSoto, Inc., Desolite*, March, 1987.

*Registered Trademark of DeSoto, Inc.



G. David Green received his Ph.D. in organic chemistry from the University of Arizona. Since joining Allied-Signal in 1986, he has been involved in synthetic polymer research. His experience includes the development of barrier coatings for fibrous substrates, radiation effects on polymer substrates, high temperature thermosetting resins and more recently radiation curable coatings. He has over 15 publications and presentations on topics ranging from nonlinear optical effects in polymers to radiation curable resins for stereolithography.



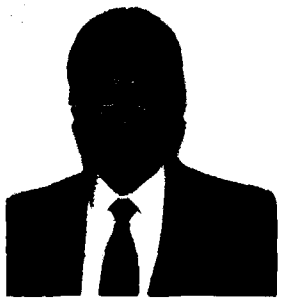
James R. Snyder received his B.S. from the University of Illinois - Urbana/Champaign. Since 1988, he has been a research chemist at the Allied-Signal corporate laboratory in Chicago. His experience has been primarily in material research and product development, especially within cationic polymerizable systems. Mr. Snyder has seven patents and publications in conjunction with this work.



Alvin C. Levy received his Ph.D. in physical chemistry from the Georgia Institute of Technology. Since 1987 he has been president of Alvin C. Levy & Associates, a R&D laboratory specializing in the development of adhesives, coatings and sealants. His prior work experience includes product development with AT&T Bell Laboratories and E.I. Du Pont. Dr. Levy holds patents on coatings for optical fiber and filling compounds for both copper and optical fiber cable.



Paul R. Foy is the Laboratory Supervisor of the Fiber Optic Materials Research Program at Rutgers University in Piscataway, New Jersey. He received a Bachelor of Science Degree in Ceramic Engineering from Rutgers University in 1982. Mr. Foy worked for AFG Industries as a Production Engineer in their Float Glass Operation until 1986. Since that time, Mr. Foy has been involved in the research and development of fiber optic materials for Rutgers University. He has continued his education by completing a Masters Degree in Ceramic Engineering in 1990 and is presently pursuing a PhD in ceramic Enginnering from Rutgers University.



Raymond J. Kovac is a research engineer with Alvin C. Levy & Associates. He received his B.S. in Chemical Engineering from Drexel University. He has experience in R&D, manufacturing, product development and process economics. He worked previously for the Georgia Tech Research Institute, Witco, and AMAX.

THE EFFECT OF DRAWING RATE ON MECHANICAL PROPERTIES OF UV CURABLE POLYURETHANE ACRYLATE COATINGS FOR OPTICAL FIBER

T. Ukachi, A. Aoyama, Y. Naito, and K. Igarashi

Tokyo Research Laboratory Japan Synthetic Rubber Co., Ltd.
3-5-1 Higashiyurigaoka Asao-Ku, Kawasaki 215, Japan

Abstract

The effect of draw tower rate on the mechanical film properties of ultraviolet (UV) curable polyurethane acrylates is investigated. In a tandem dual coating system, the surface temperature of the fiber, after being coated and cured with a primary layer, was measured as a function of draw rate and fiber cooling distance. It was found that the secondary layer is coated and cured at rather high temperatures and that the mechanical properties of the secondary coating are strongly affected by the curing temperature. Some secondary coatings show drastic change in their Young's modulus: typically from 80 kg/mm^2 to 220 kg/mm^2 without any corresponding changes in degree of cure as measured by gel fraction. The relationship between cured film properties of coatings and the microstructure of polyurethane acrylate is discussed as a function of curing temperature (drawing rate).

Introduction

In the past decade, optical fiber telecommunication networks have developed rapidly both in quality and quantity. As the fiber to the home becomes reality, optical fibers will be used under various, rather severe conditions. Relatively fragile optical glass fibers are generally coated with organic buffer layers to prevent mechanical, chemical and weathering damage. Ultraviolet (UV) curable polyurethane acrylates have been widely used to protect optical fibers because of their well balanced mechanical properties and good chemical and weathering resistance. In addition to these properties, the fast cure rate of UV curable coatings results in high productivity of optical fibers. A tandem dual coating system has been employed to obtain high productivity and optimum coating performance. Depending upon the design of the fibers, the dual coatings generally consist of a soft inner (primary) coating and a hard outer (secondary) one. A glass fiber drawn from a rod of fused silica mounted at the top of the draw tower is coated by pulling the fiber through two coating cups. The first and the second coating cups contain the liquid primary and secondary coatings, respecyively (see figure 1). The primary coating is cured as it pass the curing chamber mounted between the first and second coating cups and the secondary coating is cured as it passes the second curing unit. As the coated fiber passes through the first UV curing unit, the temperature of the coating increases rapidly from the radiation emitted by the UV lamp in addition to the heat of polymerization released during the curing process of the primary layer. Even at fast drawing speed, it is rather difficult to keep the fiber at ambient temperature after being cured with the primary layer in the dual coating system. Hence, the secondary layer is processed at rather high temperatures.

On the other hand, the excellent mechanical properties of polyurethane acrylate coatings result from their microscopic structure: so called bulk state "hard and soft" segment phase separation.[1] Since this phase separation is typically an endothermic process, the mechanical film properties of these coatings are highly affected by the temperature of the coatings during curing.[2] An additional problem when the coating temperature is high is the potential for bubble formation in the coating due to vaporization of the coating.[3]

It is, therefore, important to know the coating temperature during curing and how the draw rate affects cured film properties. In this paper, we report the measurement of the temperature of optical fibers during drawing and how the curing temperature, or, drawing rate may affect the properties of coatings.

Experimental

1) Sample Preparation

Two secondary coatings, H-1 and H-2, and one primary coating, S-1, are employed for this study. Table 1 lists the typical liquid and cured film properties of these coatings. Using our experimental draw tower, illustrated in figure 1, fibers were prepared using the three different coatings, changing the draw rate and the "cooling distance" which is defined as the fiber travels prior to entering the secondary coating application cup. Fiber was drawn from a fused silica

rod to a diameter of 125 μm and cooled to ambient temperature as it passed through a cooling unit. The outer diameter of the primary and secondary layer was controlled to 175 μm and 220 μm ± 5 μm, respectively. Each respective single UV curing unit is equipped with a 3.5 kw metal-halide lamp. The temperature of the liquid secondary coating was thermostatically controlled to the desired temperature which varied from 40 °C to 80 °C.

2) Temperature Measurements of the Fiber Surface

During drawing the temperature at the surface of the primary layer was measured using a radiation thermometer as illustrated schematically in figure 2. Temperature of the surface of the fiber during running is detected by thermocouple 1 placed close to the fiber surface. The gap between the themocouple and the surface of the coating is adjusted to less than 0.4 mm. The copper heat-block of the thermometer was heated to reach an equilibrium state between the thermocouple 1 and 2 which indicates the temperature of the heat-block. After reaching the equilibrium temperature, the recording of thermocouple 2 represents the temperature of the surface of the coating. The response time of this radiation thermometer is less than 0.3 sec and the accuracy of the measurement of the temperature is better than ± 0.5 °C.

3) Evaluation of the coatings

For the following experiments, specimens were prepared by carefully scraping off the dual layered coatings from the glass fibers. In order to evaluate the tensile properties, such as Young's modulus, the specimen was clamped in a tensile testing machine with a gauge length of 25 mm and extended at a rate of 1 mm/min. The cross section of each specimen was determined by measuring the cross sectional area under a microscope after the fracture.

Table 1. Liquid and Cured Film Properties of Coatings S-1, H-1, and H-2.

	S-1	H-1	H-2
Viscosity at 25 °C cps	3500	6700	6000
Young's Modulus kg/mm^2	0.10	150	152
Tensile Strength kg/mm^2	0.27	6.5	6.0
Tensile Elongation %	190	10	8
Gel Fraction %	90	95	95

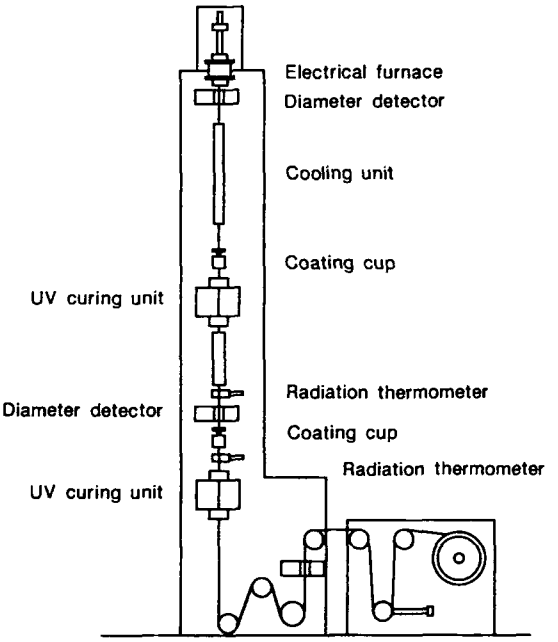


Figure 1. Schematical drawing of the experimental draw tower. The hight of the draw tower is 8 meter.

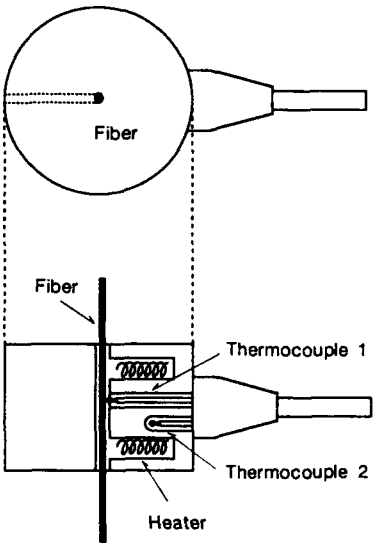


Figure 2. Schematical drawing of the radiation thermometer. Thermocouple 1 is placed in the vicinity of the surface of the running fiber. After a thermal equilibrium is reached between thermocouples 1 and 2, temperature of thermocouple 2 represents the temperature of the fiber surface.

For the evaluation of the dynamic mechanical response of the coatings, twelve dual coated fibers, 6 mm in length, were bundled in a linear array and were mechanically bended at a rate of 10 Hz with a heating rate of 2 °C/min. Temperature dependence of loss tangent (tan δ) for the twelve bound fibers was measured and evaluated by neglecting the effect of the existence of the glass fiber core because the glass itself showed no significant change in loss tangent at this temperature range, -100 °C to 200 °C.

The extent of cure of coatings was estimated by measuring the methylethylketone (MEK) unextractable content (gel fraction). A specimen was extracted by refluxing in MEK for a period of 12 hours and the remaining film was dried to obtain the percent unextractables. Swelling ratio was also measured on the coatings in tetrahydrofuran (THF) to evaluate the extent of the crosslinking density of coatings. The coated fiber, 20 mm in length was soaked in THF for 24 hours at 23 °C. The swelling ratio of the coating was determined by the ratio of the length of the swollen coating and that of the original one.

Results and Discussion

The surface temperature of the fiber coated with a primary layer was measured and is plotted in figure 3 as a function of the draw rate and the cooling distance travelled by the fiber. At the slowest draw rate, 60 m/min, a temperature as high as 200 °C was measured at the surface of the primary layer as the fiber just exited the first UV curing unit. Even when a faster draw rate, 540 m/min, was employed, the surface temperature of the coating varied from 120 °C to 40 °C as a function of the cooling distance. Considering the thermal properties of polyurethane acrylates, this wide temperature change, 120 °C to 40 °C, is sufficient to significantly affect the properties of the secondary layer. The mechanical properties of cured polyurethane acrylates are derived from the microscopic phase separation structure. The microstructure can be expected to be affected by the thermal conditions, such as temperature of coating. In order to clarify the affect of curing temperature on the properties of coatings, the secondary layer was applied of varying distances from the first UV curing unit (varying degree of cooling). The temperature of coating cup 2 was also controlled to maintain the same temperature which corresponds to the temperature of the fiber as controlled by the location of the cup. At a constant draw rate of 60 m/min, several fibers were prepared using secondary coatings H-1 and H-2. By changing the cooling distance of the primary coating, the curing temperature of the secondary coatings were varied. Figure 4 and 5 show Young's modulus and gel fraction of the coatings, H-1 and H-2, as a function of the curing temperature, respectively. In coating H-1, a drastic change was found on Young's modulus without any significant change on gel fractions. Young's modulus measured for the coating cured at 80 °C was two times larger than that measured at 40 °C. But no significant change both in Young's modulus and gel fractions was seen on the coating H-2. Note that the coatings H-1 and H-2 show almost the same mechanical properties tested on sheet samples as listed in Table 1. MEK unextractables represent the extent of reaction of acrylic groups of a coating but does not show how the reaction takes place. Despite the same degree of cure as measured by gel fraction, the higher Young's modulus obtained at high temperature curing might be explained by the difference in the manner of the curing.

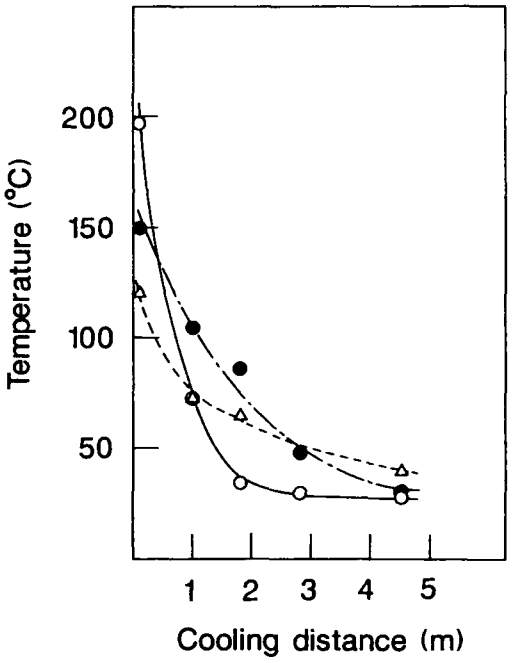


Figure 3. The surface temperature of the fiber coated with a primary layer is plotted as a function of the draw rate and the cooling distance of the fiber. The cooling distance is measured from the exit of the first UV curing unit to the position of the radiation thermometer.

Open circle :drawing rate of 60 m/min
Closed circle:drawing rate of 240 m/min
Open triangle:drawing rate of 540 m/min

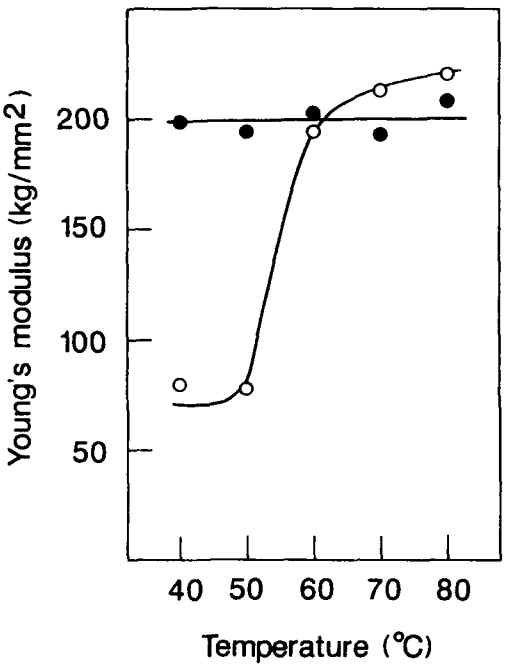


Figure 4. Young's modulus of the coatings H-1 and H-2 drawn at a rate of 60 m/min. are plotted as a function of the curing temperature. Open and closed circles show coatings H-1 and H-2, respectively.

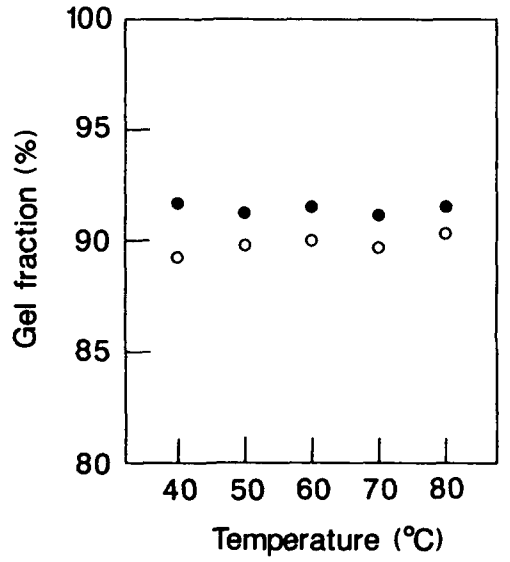


Figure 5. Gel fractions of the coatings H-1 and H-2 are plotted as a function of the curing temperature. Open and closed circles show coatings H-1 and H-2, respectively.

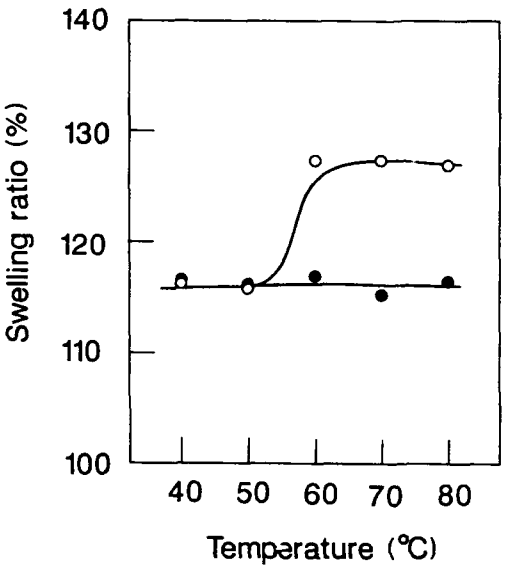


Figure 6. The dependence of the curing temperature to the swelling ratio of coatings H-1 and H-2. Open and closed circles show coatings H-1and H-2, respectively.

The results of the measurements of swelling of coatings, H-1 and H-2, prepared at several different temperatures are also shown in figure 6. For the temperature dependence of swelling ratio, a drastic change is found only on coating H-1. As expected from the data of Young's modulus, no change was found on that of coating H-2. The swelling ratio is inversely proportional to the crosslink density of the coatings. Thus the higher swelling ratio seen on coating H-1 cured at high temperature indicates the lower crosslink density of the coatings comparing to that cured at lower temperature. This swelling behavior of coating H-1 seems to be inconsistent with the results of the measurements of Young's modulus. The coating, H-1, cured at higher temperature shows higher Young's modulus in spite of the rather small extent of crosslink density and the same degree of cure, gel fraction, compared to the coating cured at low temperature.

Figure 7-a and 7-b show the temperature dependence of the loss tangent for coating H-1 cured at 80 °C and 40 °C, respectively. A peak observed around 100 °C is assigned to be a hydrogen bonding between urethane linkages.[4] On the other hand a peak around 150 °C is believed to originate from the carbon-carbon linkages of crosslinked polymer network. In figure 7-a, coating H-1, cured at 80 °C, shows twin peaks around 100 and 150 °C. In figure 7-b, coating H-1 cured at 40 °C, shows a single peak at 150 °C. This suggests that the hydrogen bonding between urethane linkages disappeared in coating H-1 cured at 40 °C. The higher Young's modulus of

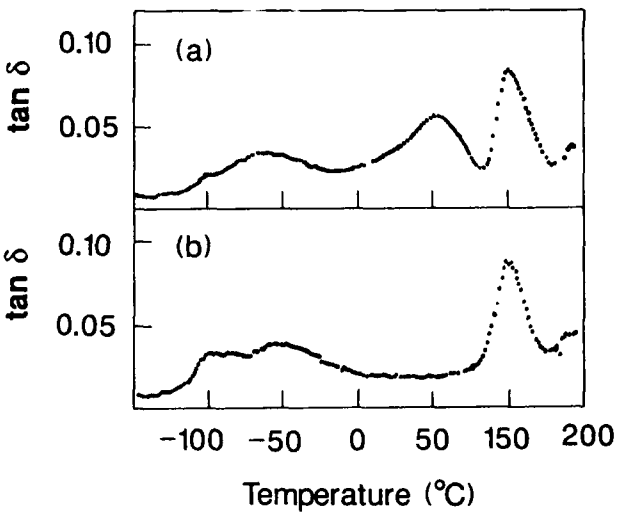


Figure 7. The temperature dependence of the loss tangents (tan δ) of coating H-1 cured at 80 °C and 40 °C are shown in figure 7-(a) and 7-(b), respectively. A peak observed around 100 °C is assigned to a hydrogen bonding between urethane linkages and a peak around 150 °C is to the carbon-carbon linkages of crosslinked polymer network.

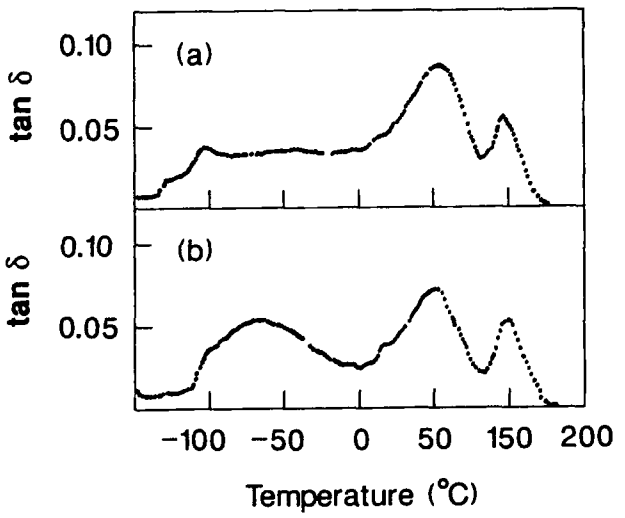


Figure 8. The temperature dependence of the loss tangents (tan δ) of coating H-2 cured at 80 °C and 40 °C are shown in figure 8-(a) and 8-(b), respectively.

H-1, cured at a high temperature, is considered to be derived from the hydrogen bonding in the polymer network. Since the hydrogen bonding gives additional pseudo crosslinking in a polymer network consisted of carbon-carbon chemical linkages. Although the effective crosslinking density increased by the additional hydrogen bonding, this could not be detected by the swelling test because hydrogen bonding easily disappeared in THF. As shown in figure 8-a and 8-b, twin peaks are observed on coating H-2 both cured at 40 °C and 80 °C. It is consistent that the same magnitude of Young's modulus was obtained in both cases of coating H-2.

It was found that coating H-1 varied in polymer structure, in this case the existence of hydrogen bonding, with a change in curing temperature. The coating composition or each component of coating may strongly influence the change in polymer structure created during curing. Considering the coating process on the drawing tower, liquid resin is extruded from a very thin slit at the coating cup. Therefore, the coating resin may be exposed to very high shear rate. At a 240 m/min drawing rate, the shear rate reaches an order of magnitude of 10^5 sec^{-1}. When the coating resin is exposed to rather high shear rate and high temperature, certain orientation of the polymer takes place during the coating and curing process. That is, a certain microstructure is possibly created and imparts particular effects to the properties of coatings.

The design of polymers for coatings are based on the data obtained from samples coated and cured under laboratory conditions, slow shear rate coating and ambient temperature curing. Taking into account shear rate and curing temperature affects mentioned above, it is important to evaluate coatings under actual drawing conditions even at the early stage of development of coatings.

Conclusion

We report here a novel method for measuring the surface temperature of fiber immediately after being coated and cured with an ultraviolet (UV) curable polyurethane acrylate primary layer. A secondary layer was found to be coated and cured at rather high temperature and consequently the mechanical properties of secondary coatings were strongly affected by the curing temperature which corresponds to the rate of drawing. The high temperature coating and curing causes the change of the microscopic structure of polymer network. In this case, the existence of hydrogen bonding between urethane linkages results in a drastic change in mechanical properties of coatings. It is therefore very important to pay attention to the curing temperature in terms of drawing rate and cooling distance in order to obtain better coatings. Also it is important to evaluate the coatings under actual drawing tower in order to design the better coatings.

Acknowledgment

The authors acknowledge to Dr. G. Pasternack for his helpful discussion.

References

1) J. H. Saunders and K. C. Frisch edited. "Polyurethanes: Chemistry and Technology", Robert E. Krieger Publishing Co., Inc. Fl, 1983.
D. C. Allport and W. H. Janes edited, "Block Copolymers" Applied Science Publishers Ltd. England, 1973.
2) M. Ando, T Uryu, J. Appl. Polym. Sci., **35** 397 (1988).
3) K. Kobayashi, K. Tsurusaki, Y. Sato, and S. Araki, Proc. **40th** IWCS, 126, (1991).
4) C. LI. R. M. Nagarajan, C. C. Chiang, and S. L. Cooper, Polym. Eng. Sci., **26** 1442 (1986).



Takashi Ukachi received his BE degree in biophysics and bioengineering from Osaka University, Osaka, Japan in 1976. He started his professional carrier at Tokyo Research Laboratory of Japan Synthetic Rubber Co., Ltd. where he has been engaged in research on development of new functional polymers for electrical and optical uses. His current research interests include the development of optics relating polymeric materials and their applications.



Akira Aoyama received the BE degree in chemical engineering from Tokyo Agriculture and Technology University, Tokyo, Japan in 1990 and joined Tokyo Research Laboratory of Japan Synthetic Rubber Co., Ltd. He is a member of Radiation Curable Material Development division.



Yuji Naito graduated in Chemical Engineering Course of Sagamidai Technical High School in 1971 and joined Tokyo Research Laboratory of Japan Synthetic Rubber Co., Ltd. He has been engaged in research and development on plastics and rubber. He is now a chief engineer of Radiation Curable Material Development division.



Katsutoshi Igarashi received his BE degree in chemical engineering from Hokkaido University, Hokkaido, Japan in 1969 and joined Japan Synthetic Rubber Co., Ltd. He is currently a general manager of Radiation Curable Material Development division.

DIFFERENTIAL QUANTITATIVE DETERMINATION OF THE EXTENT OF THE RADIATION CURE OF BOTH THE PRIMARY AND THE SECONDARY COMPONENT FOR DOUBLE COATED FIBRES

Josef L. Jostan°, Ronald G. Sommer*, Michael Hoffart*

° DAIMLER BENZ AG Research Center, Wilhelm Runge Str. 11, 7900 Ulm, Germany

* KABEL RHEYDT AG (formerly AEG KABEL AG), 4050 Mönchengladbach 2, Germany

SUMMARY

A degree of coating cure near 100 % minimizes variations in coating properties both at fibre manufacture and with aging. Reported is a method to determine simultaneously, but independently, the degrees of cure of both the primary and secondary for a radiation cured dual coating. Retained monomers are solvent extracted with acetonitrile from a short length of dual coated fibre, separated with HPLC (High Pressure/Performance Liquid Chromatography), and the retention-time ordered UV absorption at 205 nm peaks recorded. The peak heights of one or more monomers for both primary and secondary converted by calibration curves to percent values of retained monomers represent the degrees of cure. Changes in degrees of cure with fibre draw speed and fibre aging were studied.

INTRODUCTION

Radiation curing dual coatings for optical fibres are commonly based on some modified-urethane acrylate system. The uncured liquid coatings, one for the primary and one for the secondary, are each composed of several components. These include the base unsaturated prepolymer resin (oligomer) itself, one or more reactive monomers, photo-initiator, synergistic materials, and stabilizers. The monomers may differ between the primary and secondary in several ways: in chemical compositions, in the number of types present, and in their proportions/1/. This composition difference contributes to the desired difference in physical characteristics on curing of having around the fibre a soft and elastic primary which is then surrounded by a hard and mechanically strong secondary.

The curing proceeds under UV irradiation as a radical based polymerization in which the monomers react with the unsaturated oligomer converting the liquid coating to a crosslinked solid body structure. For any such heterogeneous system, whether the primary or the secondary, the chemical reaction is not 100% complete within a limited time and a certain proportion of each of the monomers remain unreacted and are retained within the polymerized body.

The crosslink density of each of the polymeric fibre coating layers in the dual coating, or the degree of cure of each, is related to the respective proportions of retained monomers. Variations in physical and mechanical properties of the as-made cured dual coating correspond in turn to variations in these crosslink densities /2,3/. Additionally aging performance through diffusion out, extraction by surrounding fluids, or later curing over the fibre lifetime, of the retained monomers is dependent on the initial degrees of cure.

In the past various methods, many indirect in nature, to evaluate the degree of hardness of a resin coating have been put forward: mechanical or surface property tests such as strip force, surface tackiness, and color shade of the coating /4,5/; chemical and physical characterization tests such as Fourier Transform Infrared (FTIR) spectroscopy /6/, Differential Photocalorimetry (DPC) /7/, Evaporation Rate Analysis (ERA) , and dielectric measurements /8/; and weight loss extraction tests such as with methyl ethyl ketone (MEK) to determine the total proportion of soluble components remaining after coating cure. Frantz, Plitz, and Schmid /9/ evaluated some of these techniques and concluded that solvent extraction, FTIR, DPC, and ERA offered promise of providing sensitive and reproducible measures of the extent of cure.

However, several of the above methods are not directly applicable to a coated fibre and require a separate test probe preparation. Some are relatively unspecific, as is, for example, weight loss by MEK extraction. All retained and soluble components, monomers, as well as stabilizers and photo-initiators whose content is irrevelant to crosslink density, are included.

The above described methods do not allow simultaneous and independent determinations of the cures of both primary and secondary in a dual coating directly from a coated fibre sample.

The goal of the degree of cure test method development reported here was a direct and simultaneous quantification of retained monomers' contents for UV cured double fibre coatings. The result of this effort was a technique combining solvent extraction with chromatographic separation and the subsequent detection of the eluted components in the UV spectral region.

EXTRACTION

The solubility of the components of the dual fibre coating in an organic solvent reduces with increasing molecular weight. Low molecular weight components dissolve, higher weight components only become colloidally suspended, and completely crosslinked macromolecules do not dissolve. As the total thickness of the dual coating on conventional fibre is only nominally 60 micrometers, solvent penetration of the full coating depth with dissolution of all low molecular weight retained monomers, photo-initiators and their photolysis products, synergistic materials, and stabilizers occurs readily. Acetonitrile (ACN) is the preferred solvent. It is an especially good solvent for the retained monomers. It mixes with water due to its high dielectric constant and thus subsequently functions well as a constituent of the mobile phase in the chromatographic separation step which is performed with a elution mixture of water and ACN in the ratio of 1:1. Moreover it is highly transparent in the UV spectral region in which detection of the separated components is made.

Essentially full and reproducible extraction from dual coated fibre with ACN at room temperature was experimentally found to occur in 15 to 20 hours. The extraction of the secondary comes to a plateau in monomer content in several hours, but the extraction of the secondary covered primary is much slower to do so.

To implement the quantitative determination of retained monomers' contents within an UV-cured acrylate double coating an 150 mm length of the dual coated optical fibre is cut into 5 to 8 mm long pieces. An 150 mm length with a nominal glass diameter of 125 micrometers and a nominal outer coated diameter of 250 micrometers contains on the order of 6.1 mg of double coating. These pieces are immersed in 0.10 ml of ACN within a sealable microglass bottle (an autosampler vial, of a 10 mm diameter, of an approx. volume of 3 ml). After standing more than 16 hours at room temperature, e.g. overnight, 0.005 ml of the solution is used for the HLPC separation and the proportionality analysis described below.

HPLC SEPARATION, UV DETECTION OF MONOMERS

The mass of the material solvent extracted from a short length of coated fibre is minute and consists of, as previously stated, a mixture of several components of which only the retained monomers' proportions are of interest.

High Performance/Pressure Liquid Chromatography (HPLC) which quickly separates components with a high level of selectivity through their varied retention times as they exchange between a stationary phase (the packed column) and the mobile phase (the elution mixture) suits this situation well.

Once separated into retention-time ordered components, spectralphotometric detection in the UV region at a wavelength of 205 nm gives a peak for each retained monomer at its characteristic retention-time for which the peak height (the peak area could also be used) is proportional to the retained momomer's content.

The apparatus used is schematically illustrated in Figure 1. From the reservoir (1) is pumped (2) an uniform pressure smoothed, pulse free stream (4) of elution mixture. A safety valve (3) is situated at the point of highest possible pressure. The mobile phase streams through an entrance chamber (6) into the packed column (7) with a manometer at point (5) to measure the pressure. After leaving the packed column the now separated components are seen at the detector (8) and the resulting chromatogram recorded with a printer plotter (9).

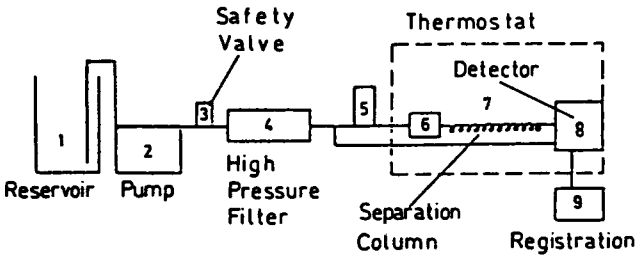


Fig. 1: Schematic of HPLC Apparatus

To implement the chromatographic separation 0.005 ml of the previously prepared ACN extraction of the dual fiber coating is introduced into the HLPC with a water and ACN mixture in a fixed 1:1 ratio as the elution fluid. The flow speed is 1.5 ml/min.

PEAK ASSIGNMENTS

For each and every coating, primary or secondary, a HPLC retention-time peak assignment and a proportionality calibration must be made for at least one constituent monomer in order to determine quantitative degree of cure.

If the monomers' compositions are known and these monomers are separately available, a retention-time HPLC peak can be unequivocally assigned to each compound. If additionally the proportions of these monomers to each other and the total monomers' proportion of each liquid resin coating are known, calibration can be done directly. Simply performing several HPLC runs with the individual monomers or mixtures under similar conditions to the ACN extraction, HPLC separation, and UV region detection procedure outlined above for coated fibre are sufficient. In practice having this level of information is not to be expected as commercial coatings are generally proprietary in nature.

The more commonly implemented procedure for HPLC peak assignment is thus to compare the HPLC chromatograms of the individual as-delivered uncured liquid coatings in ACN solution with those of ACN extracts from partially to nearly completely crosslinked coating layers made by the UV irradiation of thin films of the liquid coatings on glass plates.

One or more monomer retention-time peaks can then be assigned, for example, as illustrated in Figure 2 for a primary: Monomer P1 at 1.3 minutes retention-time and Monomer P2 at 3.6 minutes retention-time. These retention-times are for a fixed apparatus and fixed test procedure. They will vary slightly in time from sample to sample and day to day due to variations in temperature of elution mixture, aging of the packed column, and so forth.

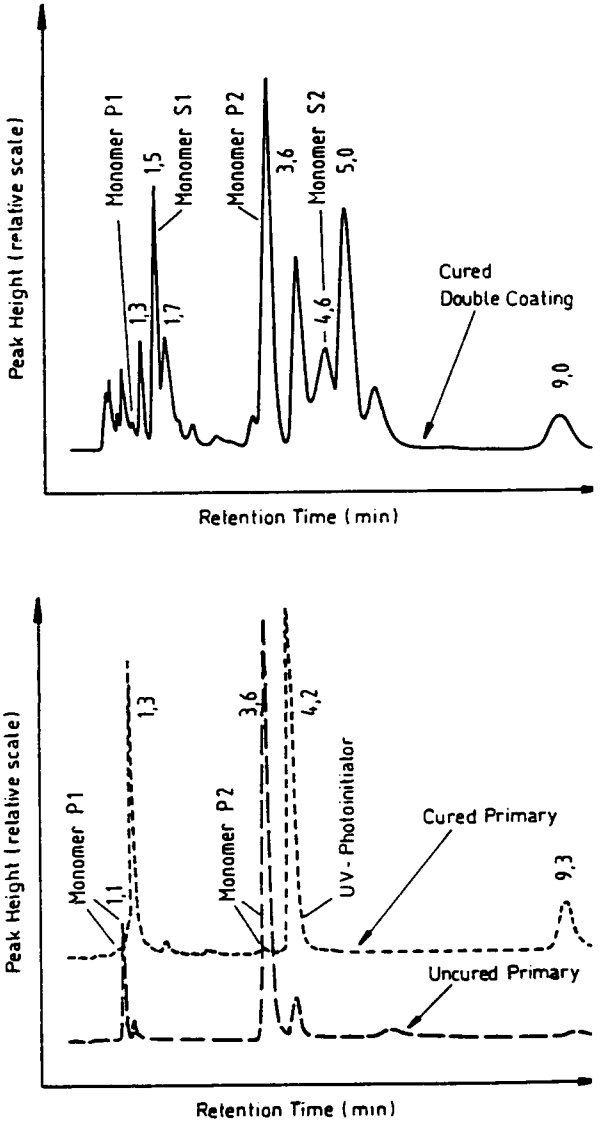


Fig. 2: HPLC Chromatograms
P1 = Monomer 1 of Primary, S1 = Monomer 1 of Secondary, and so forth

There are additional peaks evident in the chromatograms (Figure 2) from other low molecular weight materials such as photo-initiators and stabilizers. The oligomer does not appear here. The monomers' peaks are identifiable through the comparisons of the chromatogram for uncured material to those for cured material as with UV-irradiation they

progressively shrink with degree of cure from being major peaks to being minor peaks. At the same time a peak for a material such as a photo-initiator switchs from being a minor to a major peak. For a primary or secondary containing more than one monomer, which occurs in most cases, then the monomer for each in the highest proportion which stands the most alone in the chromatogram for the dual coating is best used to judge the degree of cure of each coating layer. (See again Figure 2.)

CALIBRATION OF MONOMERS' PROPORTIONS

Calibration curves are generated for each monomer of interest. As previously stated an 150 mm long piece of coated fibre contains on the order of 6.1 mg of cured coating. For the situation of a primary to secondary thickness ratio of 1:1, or in other words, when each coating is approx. 30 micrometers thick, then the primary portion of this 6.1 mg is 2.5 mg and the secondary portion is 3.6 mg. Therefore, to a good first approximation, the height of each individual monomer's peak seen in HPLC by dissolving, respectively, 2.5 mg of liquid primary coating and 3.6 mg of liquid secondary coating in 0.10 ml of ACN can be assigned a value of 100% retention. By the appropriate dilution 10, 1, and 0.1 % points then can be obtained with which a linear log peak height against log monomer concentration calibration curve can be made for each monomer. On performance of a degree of cure test for a dual coating each monomer's peak height is converted to a percent retained monomer content through application of these curves. The result is degree of cure in terms of content of monomers which were left behind unreacted. A value of less than 1 % for each monomer indicates absolutely full and complete cure for a 30 micrometer thick coating layer.

New calibration curves are not necessary for a within 20% variation (thicker or thinner) from the nominal 30 micrometers.

The per cent retained monomers' values just need to be multiplied with the ratio of 30 over the actual thickness in micrometer.

The precision and reproducibility of this HPLC test for degree of cure was determined through repeated analyses of one dual coated fibre. For retained monomers' contents between 0.03 and 0.90 %, the variance was found to be between 8.5 and 10 %. For retained monomers' contents above 3 %, the analysis precision is plus or minus 5 %.

APPLICATION EXAMPLES

The two following examples illustrate the usefulness of the HPLC cure test method described in this paper.

An experiment was performed to see the effect of changing only draw speed with all other parameters held constant on the degrees of cure of primary and secondary for a dual coating system. Figure 3 shows the increase in retained Monomer P1 and retained Monomer S2 contents as draw speed increases. That is, the degrees of cure decrease with increasing speed. These data indicate , for example, either increased UV-curing lamp power or a faster curing dual coating system is necessary.

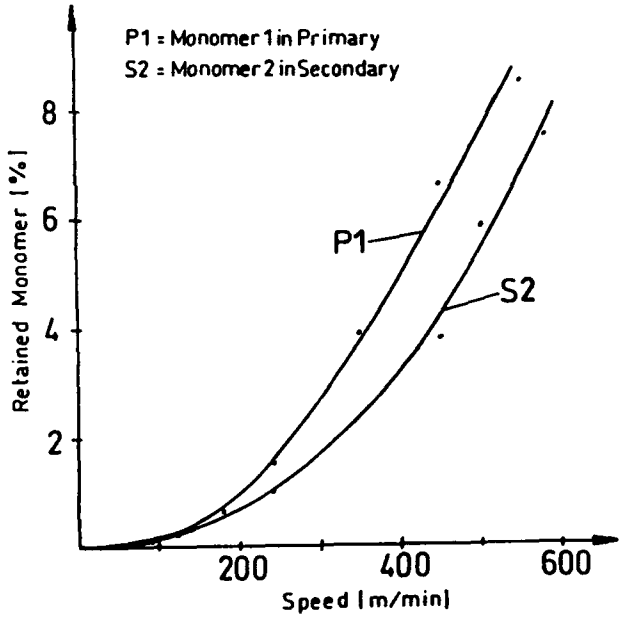


Fig. 3: Decrease in P1 and S2 with increasing draw speed

An additional experiment was performed which illustrates the change in retained monomers' contents with time when the dual coating is not fully cured at the time of manufacture. A fibre sample drawn at a 450 m/min draw speed for the previously described experiment was allowed to age on the shelf under room conditions. Figure 4 shows the decrease in both Monomer P1 and Monomer S2 contents over 100 days. The change for the primary is more dramatic than for

that of the secondary. These changes in contents can be taken to be representative of what is similarly occurring with respect to the contents of the other retained monomers. Some decrease occurs through diffusion out of especially the more volatile monomers. A significant part of the decrease is through delayed polymerization. Thus the degrees of cure increase. One expects therefore physical properties to have altered.

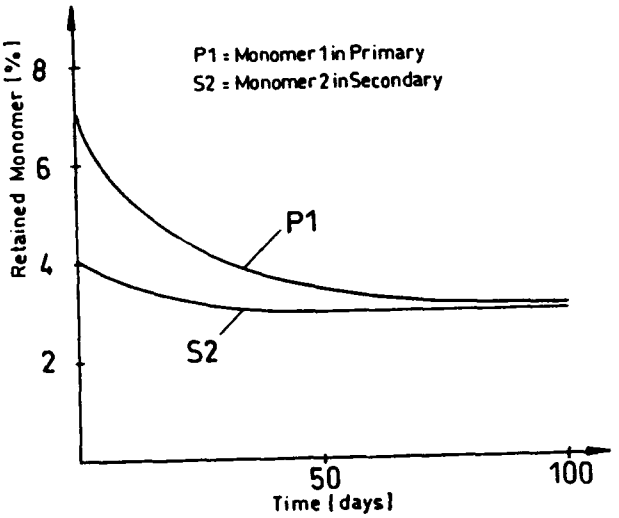


Fig. 4: Decrease in P1 and S2 with storage age under room conditions

CONCLUSION

An accurate and reproducible method has been successfully developed to simultaneously, but independently, determine the degrees of cure of the primary and the secondary for dual coating fiber. The degrees of cure are reported in terms of the percents of original monomers' contents retained unreacted in the respective polymerized bodies.

The described procedure consists of solvent extraction of retained monomers with acetonitrile followed be HPLC separation with retention-time ordered UV absorption at 205 nm peaks recorded. By means of readily generated calibration curves, the peak heights convert to quantitative values for retained monomers' contents.

The reported technique, as illustrated in the two application examples, is an useful tool for evaluating processing parameter changes, new dual coatings, and physical and mechanical property changes with aging.

The underlying strengths of the technique: solvent extraction, chromatographic separation of components, and specific to a species quantification of contents, may make it suitable for adaptation to testing diffusion of primary monomers into the secondary (repeated short time extractions), inking effects, or enviromental exposure effects.

REFERENCES

1. M. Köhler, 'Chemische Aspekte der radikalischen UV-Härtung', Kontakte (Merck, Darmstadt) 1988 (3), pp. 12-18.

2. J.M. Martin, 'Contributions of Dual Coat Cured Coatings to Optical Fiber Strength and Durability', RADCURE Europe '87 Conference Proceedings, Munich, May 1987.

3. H.H. Yuce, I.M. Plitz, R.A. Franz, and M. Andrejco, 'The Effects of Coating Cure on the Mechanical Characteristics of Optical Fibers', Proceedings of the 39th International Wire and Cable Symposium, November, 1990, pp. 715-721.

4. G. Pasternak, D.G. Anderson, R.W. Johnson, A.F. Leo, and O.R. Cutler, 'Property Measurements of Acrylate Based Radiation Curable Coatings', RADCURE '86 Conference Proceedings, September 1986, p. 17-1.

5. B.L. Brann, Test Methods for Measuring Degree of Cure in Radiation Curable Coating', Journal of Radiation Curing, 12 (7), 1985, pp. 4-10.

6. J.M. Jilian, A.M. Millon, 'Quality Control Testing of UV-Curable Coatings Using FTIR', Journal of Coatings Technology, 60, 1988, p. 89.

7. D.D. (Ziem) Le, 'Monitoring UV-Photopolymerization in Real-Time. Effects of Curing Parameters On Cure-Rate & Extent', Journal of Radiation Curing, 12 (4), 1985, pp. 2-6, 8.

8. K. Venkataswamy and R. Waack, 'Rapid Cure Monitoring by Microdielectrometry', Plastics Engineering, February, 1983, p. 43.

9. R.A. Frantz, I.M. Plitz, S.R. Schmid, 'Evaluation of Techniques for Determining the Extent of Cures of Optical Fiber Coatings', Proceedings of the 40th International Wire and Cable Symposium, November 1991, pp. 134-140.



Josef L. Jostan
DAIMLER-BENZ AG Research Center
Ulm, Germany

Dr. Josef L. Jostan (54) studied chemistry at the University of Munich (Dipl. Chem. 1962, Dr. rer. nat. 1965). On completion of his doctoral studies he joined the AEG Research Institute-Ulm which became in 1989 the Daimler-Benz Research Center AG Ulm. He is the head of the Chemical Technologies Department within the Microelectronics and Optoelectronics Division.



Michael Hoffart
KABEL RHEYDT AG (formerly AEG KABEL AG)
Mönchengladbach, Germany

Michael Hoffart (36) is General Manager of the Optical Fibre Plant. He received his Dipl.-Ing. degree from the Bergische University, Wuppertal in 1983. He joined AEG KABEL on graduation and has been engaged in the fields of optical measurement techniques and telecommunication cables.



Ronald G. Sommer
KABEL RHEYDT AG (formerly AEG KABEL AG)
Mönchengladbach, Germany

Dr. Ronald G. Sommer (48) is Manager for Optical Fibre Development. He received a Ph.D. in Physical Chemistry from the University of Iowa in 1974. He has since continually worked in the area of optical fibres, joining AEG KABEL in 1987 after prior employment in the USA and the U.K.

A Study of Hermetically Coated Optical Fiber

T.Zushi *S.Nakahara *T.Takeda T.Kaide *H.Tanaka

MITSUBISHI CABLE INDUSTRIES, LTD.
8 Nishinocho , Higashimukaijima , Amagasaki , Hyogo , 660 Japan
* 4-3 Ikejiri , Itami , Hyogo , 664 Japan

ABSTRACT

Our experimental results revealed for the first time that the hermetic properties of carbon coated optical fiber strongly depend on the roughness of the carbon layer which is affected by the CVD reaction temperature. To obtain a good hydrogen resistance, the maximum surface roughness was 0.97nm. Further a 400Å thickness of carbon layer was necessary to prevent hydrogen permeation. To obtain a satisfactory tensile strength after 80℃ water immersion, only the thickness of the carbon layer of over 180Å was necessary. There is no roughness dependence of the carbon surface. We also investigated carbon coating for large core fiber. It has a satisfactory water resisting property and a high fatigue index.

1.Introduction

Hermetically coated optical fiber (HCF) are characterized by excellent hydrogen and water resitance.(1,2) As these characteristics mostly depend on the quality of the carbon layer deposited around the fiber, it is important to clarify the conditions to obtain good quality. We have conducted experiments to study the relationship between the Chemical Vapor Deposition (CVD) reaction temperature, to deposit the carbon layer, and the quality of the carbon layer as well as hydrogen and water resistance of the resulting fibers.
A study was also conducted on application of carbon coating to large core fiber, used for laser beam transmission and other purposes.

2. Experiment

2-1. Experimental Apparatus.

Figure 1 shows the typical manufacturing process of this fiber. After drawing the glass fiber, a thin carbon layer is coated on the surface of the glass by CVD reaction and after then, the UV curable resin is coated by usual manner.

The apparatus is provided with non-contact type measurement unit for measuring the thickness of the carbon layer, with a view to utilizing measurment results in stabilizing the characteristics of the carbon deposition.

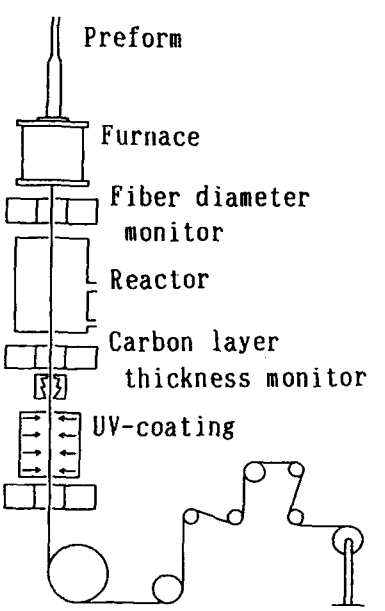


Fig.1 Manufacturing Process of HCF.

2-2. Experimental Conditions.

Table 1 shows the experimental conditions where the test fiber was made. The drawing rate of the fiber and the flow rate of material gas were kept constant and only the reaction temperature of the carbon deposition was changed.

2-3. Procedure.

1) Thickness of the Carbon Layer

After completely covering a sample fiber with epoxy resin, an extremely thin piece of the fiber was obtain with a dianond cutter. Then the thickness of the carbon layer was measured using a Transmission Electron Microscope (TEM). An example of a typical measurement result is shown in Fig.2.

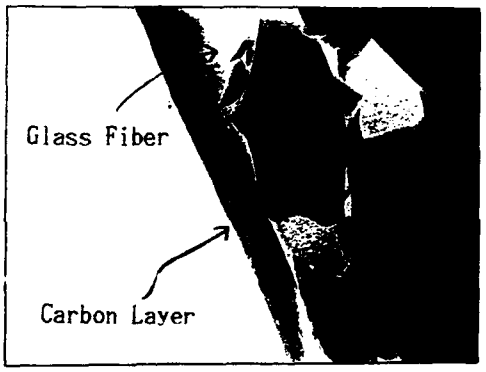


Fig.2 TEM Image of the Carbon Layer.

2) Tensile Strength.

The tensile strength of the resulting fiber was measured with a span of 10m and a strain rate of 50%/min.,using 20 samples.

3) Dynamic Fatigue Characteristic.

Dynamic fatigue tests were conducted at a range of strain rates (0.5, 1.0 ,10 and 50 %/min), so that the dynamic fatigue behavior of the resulting fiber could be characterized.

4) Hydrogen Resistance.

Sample fibers, 1000m in length, were allowed to stand in a chamber with the hydrogen gas pressure at 3atm and the optical loss increase at 1.24μm was measured at certain time intervals.

5) Observation of the Carbon Surface.

The structure of the carbon sureface was observed with a Scanning Tunnelling Microscope (STM). Using this system, the Ra value was calculated to determine surface roughness. An example of an observation result is illustrated in Fig.3.

Table 1 Manufacturing conditions and results of HCFs.

No.	Conditions			Results									
	Flow rate of material gas	Drowing rate	Reaction Temperature	Thickness of carbon layer	Tensile strength Kg			Tensile strength (after 80℃ water immersion) Kg			n value	H_2 ※ resistance	Roughness (Ra)
	cc/min	m/min	℃	Å	max	min	ave	max	min	ave	—	dB/Km	nm
1	—	250	—	—	6.2	3.8	5.5	5.0	3.2	3.9	32	16.2	—
2	600	250	1290	180	6.2	6.0	6.1	6.3	6.1	6.2	210	6.5	0.40
3	600	250	1350	240	6.1	5.9	6.1	6.1	5.8	6.0	180	6.7	0.62
4	600	250	1400	400	6.2	6.1	6.1	6.2	5.9	6.1	250	0	0.97
5	600	250	1480	450	6.3	5.9	6.2	6.2	6.0	6.1	290	4.8	1.11
6	600	250	1550	520	6.3	6.2	6.2	6.2	5.9	6.0	290	8.1	1.21
7	600	250	1630	550	6.2	6.1	6.2	6.3	6.0	6.1	220	9.5	1.54
8	600	250	1720	580	6.2	6.0	6.1	6.2	6.0	6.1	150	9.9	1.73

※ after 300Hr

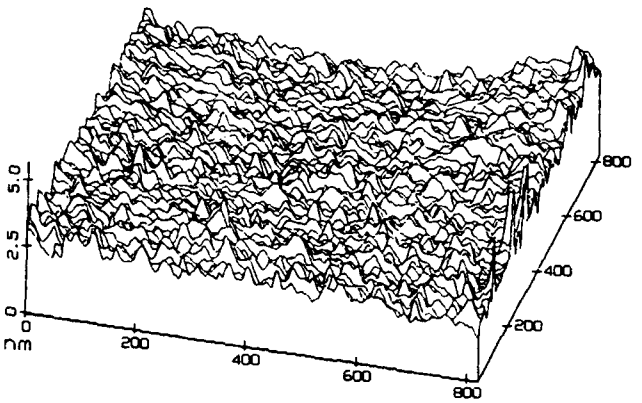


Fig.3 A Typical STM Image of the Carbon Surface.

3. Results.

3-1. Tensile Strength.

Measurement results show that any of the HCFs manufactured the during experiment had a tensile strength exceeding 6Kg. Figure 4 shows the Weibull plot for sample No.4. This figure indicates that the sample dose not have any portion with a low tensile strength.

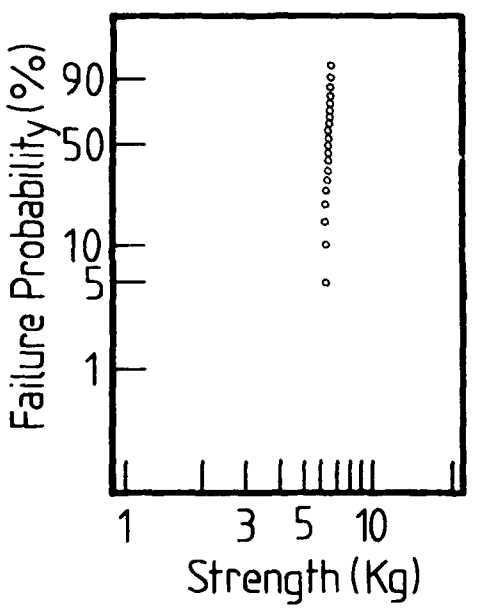


Fig.4 Weibull Plot of Tensile Strength of HCF (sample No.4).

3-2. Test on Hydrogen Resisting Property.

A test on the hydrogen resisting property, conducted during the present study, revealed the following;

1) In the range of reaction temperatures between 1290 and 1350℃ a satisfactory hydrogen resisting property cannot be obtained because the thickness of carbon layer is insufficient.

2) In the range of reaction temperatures between 1400 and 1720℃ the hydrogen resisting property becomes less favorable, though the thickness of the carbon layer increases with rising reaction temperature. This fact shows that the hydrogen resisting property is influenced greatly not only the thickness of the carbon layer, but also by the quality of the deposited carbon.

3-3. Water Resisting Property.

During the present study it was found that a satisfactory water resisting property can be obtained when the thickness of the carbon layer is approx. 180Å. In this respect, the water resisting property is different from the hydrogen resisting property, which depends not only the thickness of the carbon layer, but also on the quality of the carbon deposited, as previously mentioned.

3-4. Observation of the Carbon Surface.

During the present study the surface structure of the deposited carbon layer was observed via STM. Observation results are shown in Fig.5. This figure indicates that the unevennes of the surface roughness becomes greater with increasing reaction temperature.

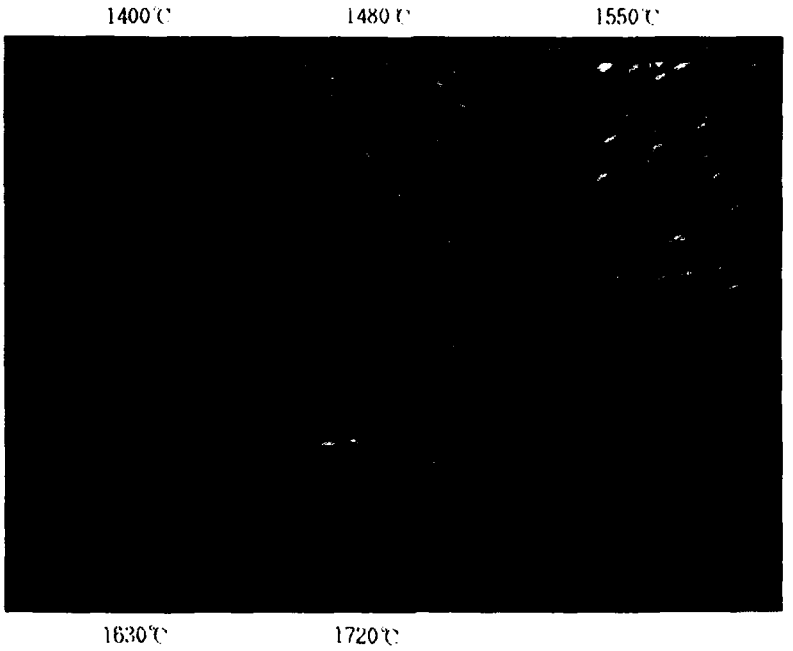


Fig.5 STM Image of the Carbon Surface.

4. Discussion.

A satisfactory hydrogen resisting property cannot be obtained with a fiber having a 180 or 240Å thickness carbon layer manufactured at a low reaction temperature because the layer is too thin. Figure 6 shows the relationship between the roughness of the carbon layer and the hydrogen resisting property for the fiber having a carbon layer with a thickness of 400Å or more. This figure shows that the hydrogen resisting property becomes less favorable with an increase in surface roughness. This deterioration of the hydrogen resisting property is due to the fact that the CVD reaction progresses more rapidly than a lower reaction temperature . Because of the rapid carbon deposition, the carbon layer may have become rough, causing the permeation of hydrogen gas through the carbon grain boundary.

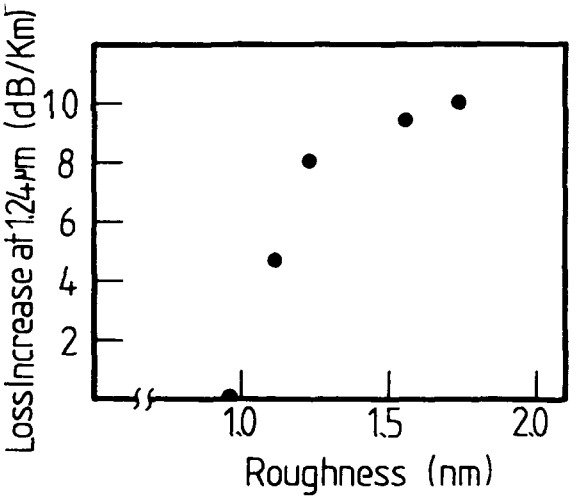


Fig.6 Relationship between Roughness of the Carbon Surface and Loss Increase at 1.24μm.

5. Large Core Hermetically Coated Optical Fiber.

5-1. Experimental Apparatus.

The apparatus shown in Fig.1 was used to manufacture two kind of large core HCFs (core / fiber diameter = 200/250,400/450).

5-2. Results.

Figure 7 shows the Weibull plot of the resulting HCFs, for conditions before and after 80℃ water immersion. Figure 8 shows the results of the dynamic fatigue characteristics for 250 μm HCFs. These results indicate that large HCFs have a satisfactory water resisting property. The fatigue index of this HCF is very high, though the initial strength somewhat decreases as a result of carbon coating.

Future studies will be conducted with the gole of increasing the fatigue index and the tensile strength.

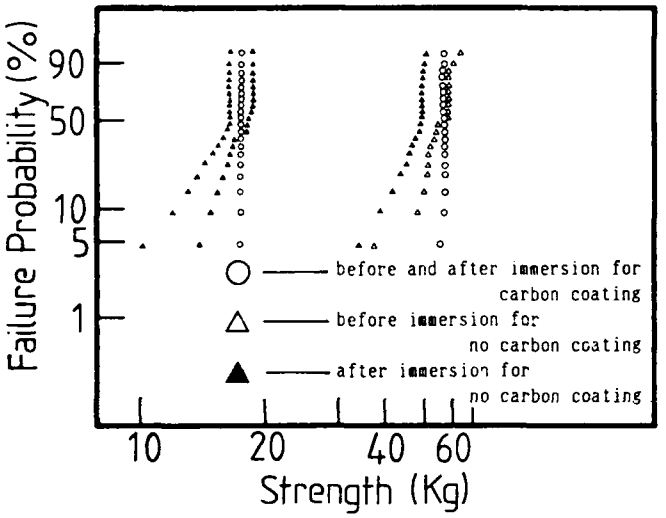


Fig.7 Weibull Plot of Tensile Strength of Large Core HCFs before and after 80℃ Water Immersion.

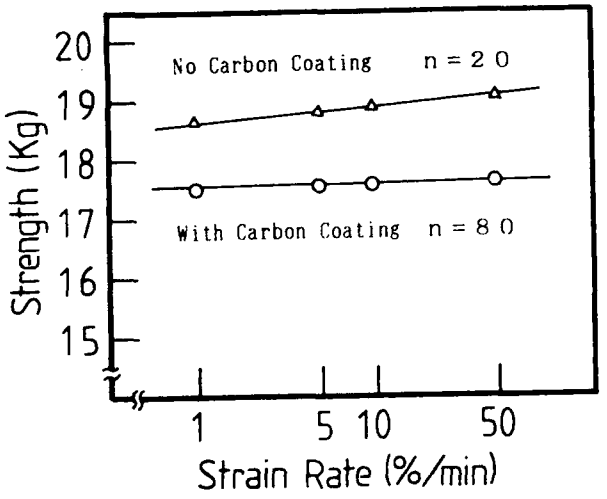


Fig.8 Dynamic Fatigue Characteristic for Large Core HCF.

6. Conclusion.

The experimental results revealed the following;

1) The roughness of the carbon surface increases with reaction temperature during carbon deposition.

2) A satisfactory hydrogen resisting property can be obtained if the minimum thickness of the carbon layer is 400Å and the maximum Ra is 0.97nm.

3) A satisfactory water resisting property can be obtained, regardless of surface roughness, if the thickness of the carbon layer is 180Å or more.

4) An examination of large core HCF revealed that the fiber has a satisfactory water resisting property and a high fatigue index.

< Reference >

(1) R.G.Huff et al.,OFC '88 THU2 (1988)

(2) N.Yoshizawa et al.,Electron. Lett.,25, p1429(1989)



T.Zushi

8 Nisninocho Higashimukaijima,
Amagasaki , Hyogo , Japan

T.Zushi joined Mitsubishi Cable Industries, Ltd. after received a B.E. Degree in Synthetic Chemistry from Okayama University in 1985. He is a chemist of Materials Research Department and a member of the Institute of Electronics and Communication Engineers of Japan.



T.Kaide

8 Nisninocho Higashimukaijima,
Amagasaki , Hyogo , Japan

T.Kaide, senior research engineer of Materials Research Department,is engaged in development of communication cable and electric wire. He graduated from Hyogo High School in 1958 and joined Mitsubishi Cable Industries, Ltd.



S.Nakahara

4-3 Ikejiri
Itami , Hyogo , Japan

S. Nakahara, engineer of Electronics & Communication Research Department,is engaged in development of optical fiber cable. He graduated Osaka Railway High School in 1970 and joined Mitsubishi Cable Industries, Ltd.



H.Tanaka

4-3 Ikejiri
Itami , Hyogo , Japan

H.Tanaka is deputy manager of Electronics & Communication Research Department. He received M.S. degree in Electricl Engineering from Osaka University in 1971. He is a member of the Institute of Electronics and Communication Engineers of Japan.



T.Takeda

4-3 Ikejiri
Itami , Hyogo , Japan

T.Takeda, engineer of Electronics & Communication Research Department, is engaged in development of optical fiber cable. He joined Mitsubishi Cable Industries, Ltd. after graduated Osaka Institute of Tchnology in 1989.

THE EFFECTS OF AGING ON OPTICAL FIBERS WITH INCOMPLETELY CURED COATINGS

Rolf A. Frantz*, Irene M. Plitz**, Hakan H. Yuce*, and Osman S. Gebizlioglu**

*Bellcore, Morristown, NJ; **Bellcore, Red Bank, NJ

ABSTRACT

Polymer coatings are applied to optical fibers as protection against mechanical and environmental stresses. Inadequately cured coatings may affect the chemical environment at the glass surface by permitting mobile ionic species and/or contaminants to diffuse to the glass/coating interface. Subsequent interactions with minute flaws on the glass surface can adversely affect long-term reliability. To investigate these effects, we conducted stress-free aging of sample fibers using two different polyurethane acrylate coatings, each with two extents of cure. Fibers were aged at 85°C in an 85% relative humidity environment, in deionized water, and in a dry oven. We measured changes in the residual coating cure, fiber strength, and coating strip force and glass transition temperature after various aging intervals. One day of wet aging was enough to prevent any further curing. The initial extent of cure did not affect the changes in fiber strength during aging, but it did influence the changes in strip force. Both strength and strip force were more affected by the deionized water environment.

INTRODUCTION

As protection against mechanically- and environmentally-induced stresses, polymeric coatings are applied to glass optical fibers and cured in-line during the drawing process. These coatings can affect the local chemical environment at the glass surface[1,2]; the nature and degree of such effects will vary with the extent of cure of the coating. Inadequately cured coatings may contain mobile ionic species and/or contaminants that can diffuse to the glass surface. Coatings that are somewhat permeable can still act to partially encapsulate atmospheric moisture and contaminants at the coating/glass interface. Since the glass surface is the location of most strength-reducing flaws, moisture and other chemical contaminants can adversely affect long-term fiber reliability through their interactions with these minute flaws. In addition, changes in the undercured coatings themselves may contribute to changes in the mechanical characteristics of the coating/glass composite.

To quantify these effects, we investigated how different extents of cure affected the stress-free aging of optical fibers. We used two polyurethane acrylate single-coat coatings: Desolite® 950-008, a hard, high-modulus coating, and Desolite® 950-133, a soft, low-modulus coating. For each coating, we drew fibers nominally 125 μm in diameter from a common fire-polished fused silica rod. All fibers were coated in-line to a nominal overall diameter of 250 μm. Different extents of cure were obtained by varying the draw speed and the lamp power.[3] The initial extent of cure of each coating was characterized using a variety of techniques; we also measured mechanical characteristics such as strength and strip force.[3,4] The fibers selected for this aging investigation were those described in [4] as 950-008 fibers #3 and #4 (higher and lower extents of cure, respectively) and 950-133 fibers #1 (higher cure) and #2 (lower cure). Samples of all four fibers were subjected to three aging conditions, all at 85°C: (i) an 85% relative humidity (RH) environment; (ii) deionized water of pH 7; and (iii) a dry (<30%RH) oven. Samples were aged under stress-free conditions for one day and one week in all environments and also for one month and three months at 85% RH and in deionized water. We used differential photocalorimetry (DPC) to measure the residual curing of the coatings after aging. The coating glass transition temperature, T_g, and the mechanical loss factor were measured using dynamic mechanical thermal analysis (DMTA). Fiber strength was determined using two-point bending in 23°C deionized water,[5-7] and the force required to strip the coating off the fiber was measured.

We first summarize the initial characteristics of the fibe samples and describe the aging conditions. We then describe the results of the various tests on the aged fibers. We next discuss correlations among the test results and conclude with a brief summary of our results.

FIBER CHARACTERIZATION AND AGING

The characteristics of the unaged fibers were reported in [4]. We have summarized the most important results in Table 1. Specific details on the various tests are given in [4].

Table 1. Initial Characterization of Test Fibers

	950-008 #3	950-008 #4	950-133 #1	950-133 #2
DPC Residual Cure Reaction*	3.7 J/g	7.5 J/g	<1 J/g	6.7 J/g
Extractables (FOTP-10)	6.21%	9.24%	6.25%	9.28%
Strip Force (FOTP-178)	5.66N	6.32N	3.35N	2.42N
Tensile Strength (FOTP-28B)	3834 MPa	3758 MPa	4454 MPa	4447 MPa

*A corrected DPC cell constant was used to calculate these values.

All of the aging was done under stress-free conditions. Several loose coils of each fiber were placed in a forced-circulation temperature/humidity chamber with the ends of the individual fiber strands outside the chamber to prevent moisture from entering at the exposed glass-coating interface. The chamber

® Registered trademark of DSM Desotech Inc.

temperature was maintained at 85±0.5°C; the humidity was maintained at 85±4% using deionized water of pH 7.0±0.3. Similar loose coils were immersed in recirculating tanks with precision heaters to maintain the temperature at 85±0.1°C. Deionized water was used with a resistivity of 18MΩ-cm and a pH of 7.0±0.3. The fiber ends were again kept outside the water tank. Finally, smaller coils were aged in a convection oven at 85±2°C; previous measurements in this oven indicated an ambient relative humidity of <30% at 85°C.

DIFFERENTIAL PHOTOCALORIMETRY

A detailed description of the DPC test procedure was published previously.[8] Briefly, 12-15 mg samples of the aged fibers were cut into short lengths that fit into standard thermal analysis pans. A small amount of mineral oil was used to enhance thermal conductivity between the fiber lengths and the pan. Each sample was exposed to ultraviolet light in the DPC instrument and the exothermic heat generated by its residual curing reaction was measured. The analysis of each curve included compensation for external heating of the sample by infrared radiation from the light source.

The samples aged at 85°C/85% RH and in 85°C deionized water showed no residual coating cure during DPC. This was true for all samples after all aging intervals. These and other results are discussed in detail later.

DPC tests of the dry-aged samples did generate exothermic curves. The size of the residual exotherm depended upon the coating tested, its initial extent of cure, and the duration of the aging, as shown in Table 2. After one day of aging, fiber 133 #1, which had a high initial extent of coating cure, had a less pronounced exotherm than the other fibers. The shape of the curve suggests that 3.6 J/g is artificially high; the baseline could not be adjusted to compensate fully for infrared heating. A more typical exotherm, for fiber 008 #4 after one day of aging, is shown in Figure 1; the baseline compensation for infrared heating is also shown. Seven days of aging was long enough that only fiber 008 #4, whose initial extent of coating cure was quite low, showed a residual exotherm; however, the curves were difficult to read and the value for the exotherm is only approximate.

Table 2. Residual Exotherm for Dry-Aged Fibers

	008 #3	008 #4	133 #1	133 #2
Aged 1 Day	2.2 J/g	6.3 J/g	<1 to 3.6 J/g	3.4 J/g
Aged 7 Days	—	≈0.5 J/g	—	—

FIBER STRENGTH

Fiber strength was measured using a two-point bending apparatus, consisting of two parallel platens, one fixed and one moving, between which a fiber loop is bent until it breaks. The moving platen is driven by a computer-controlled stepper motor; the rate of closure can be varied so that the maximum stress in the fiber changes at a constant rate. When fiber failure is detected by an acoustic transducer, the computer stops the moving platen and records the platen separation. The failure stress is calculated from this separation, the fiber dimensions, and the elastic modulus of the glass. Because the effective gage length is small, the probability of measuring a fiber sample containing a large flaw is also small, and the test results tend to be uniform and unimodal. The bending tests were conducted at a stress rate of 6 MPa/sec with the fiber loops immersed in 23°C deionized water with a pH of 7.0±0.3.

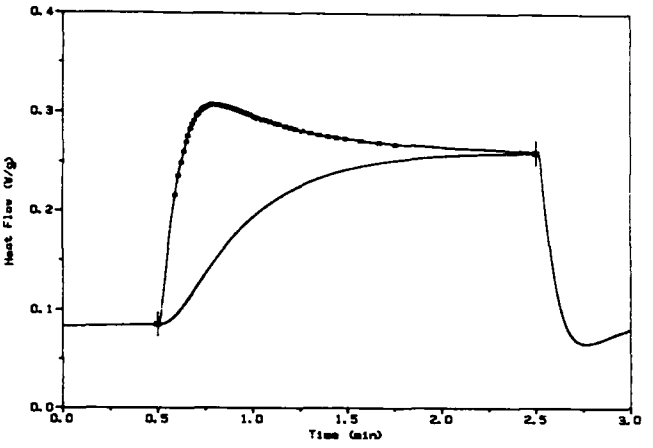


Figure 1. Residual Cure of Fiber 008 #4 after One Day of 85°C Dry Aging

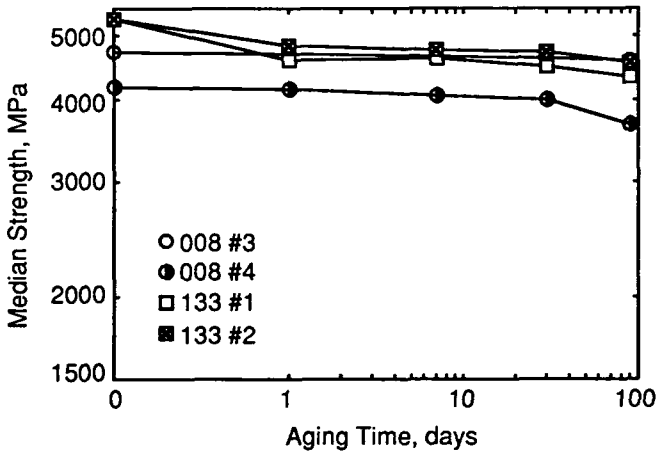


Figure 2. Strength Degradation during Aging at 85°C/85% RH

The effects of aging at 85°C/85% RH on the strength of all four fibers are shown in Figure 2. Fiber 008 #3 (higher cure coating) was hardly affected, losing less than 3% of its strength after 90 days. Fiber 008 #4 behaved similarly for the first 30 days of aging, losing about 4% of its strength; between 30 and 90 days, however, a significant additional loss of strength occurred, for a total strength decrease of about 12%. For fibers 133 #1 and #2, the greatest loss of strength occurred in the first day, about 13% for #1 (higher cure) and 9% for #2. Thereafter, the rate of loss was slower and roughly constant for both fibers; the final decrease in strength was about 18% for fiber #1 and almost 14% for #2.

The results for the fibers aged in 85°C deionized water are given in Figure 3. Both fiber 008 #3 and #4 showed a slow decrease in strength, about 32% for #3 and almost 27% for #4. The rate of decrease was essentially constant over time. Fibers 133 #1 and #2 showed a much larger decrease in strength, about 63% for #1 and 59% for #2. Also, the rate of decrease was not constant, as both fibers lost about 50% of their strength in the first week of aging.

STRIP FORCE

Strip force tests were performed in accordance with FOTP-178.[9] The force required to strip the coating was measured using a commercial stripping tool mounted in a screw-driven universal tensile testing machine. A gage length of 3 cm and a stripping speed of 50 cm/min were used.

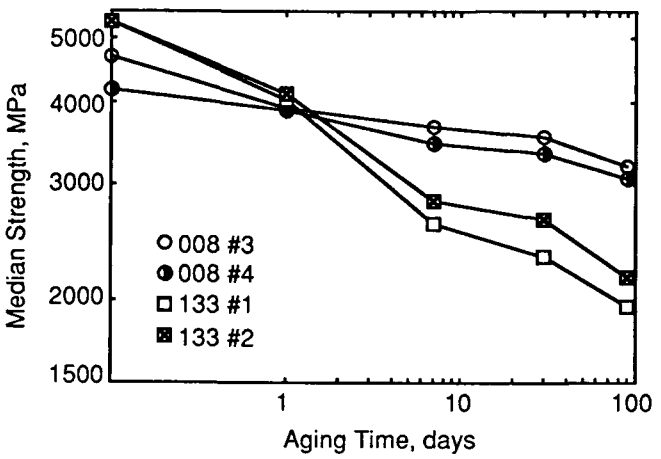


Figure 3. Strength Degradation during Aging in 85°C Deionized Water

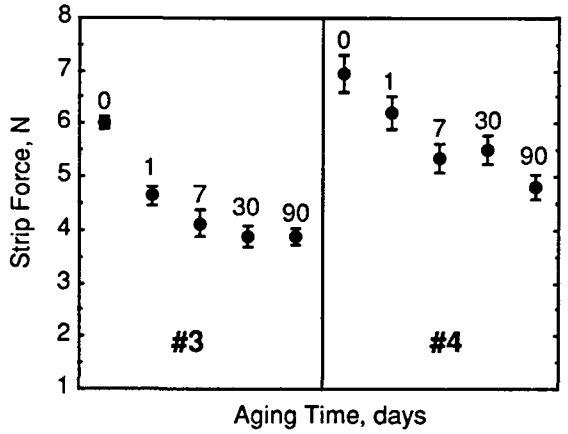


Figure 4. Strip Force for 008-Coated Fibers after RH Aging

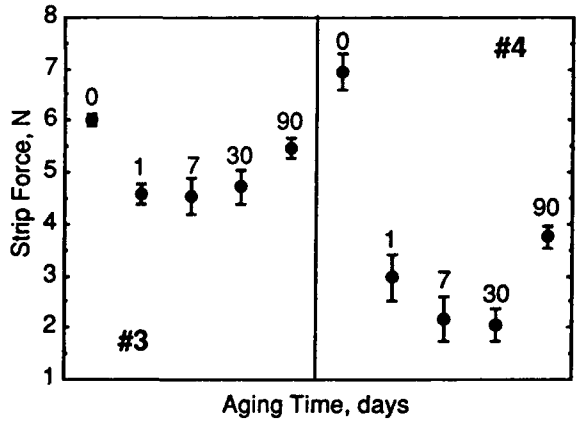


Figure 5. Strip Force for 008-Coated Fibers after Deionized-Water Aging

The results for 008-coated fibers #3 and #4 aged at 85°C/85% RH are shown in Figure 4. The strip force for the unaged samples was higher for lower cure coating #4 than for higher cure coating #3. This is consistent with our previous results (Table 1), although the values are 6-10% higher than measured earlier. For both samples, strip force decreased with aging time, to about 65% of its initial value for coating #3 and to about 70% of its initial value for coating #4. The

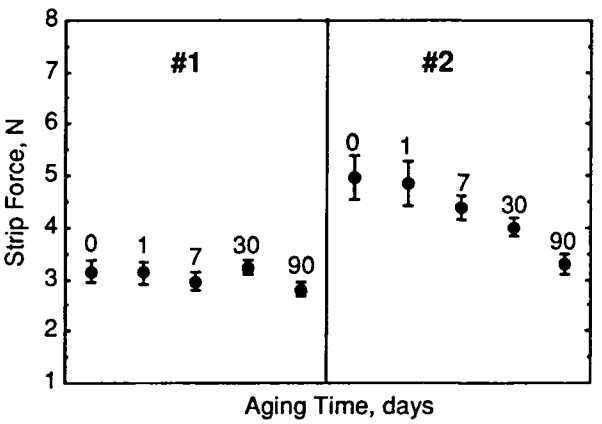


Figure 6. Strip Force for 133-Coated Fibers after RH Aging

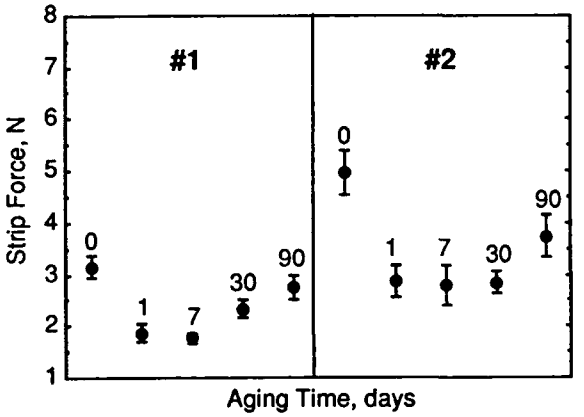


Figure 7. Strip Force for 133-Coated Fibers after Deionized Water Aging

scatter in the data was less for coating #3 than for #4. For both samples, the rate of decrease slowed as aging progressed.

The data for 008-coated fibers #3 and #4 aged in 85°C deionized water are shown in Figure 5. The values for lower cure coating #4 fell well below those for higher cure #3 after one day of aging; they also had a greater scatter. Strip force initially decreased about 25% for #3 and over 70% for #4. In both cases, however, strip force eventually increased, to over 90% and to 55% of the unaged values, respectively.

The results for 133-coated fibers #1 and #2 are shown in Figures 6 and 7 for RH and deionized water aging, respectively. The strip force for unaged higher cure fiber #1 was unchanged from our earlier measurements; however, the value for unaged fiber #2 doubled. The behavior during RH aging was similar to the 008 fibers in several ways: lower cure coating #2 had higher strip forces than #1; strip force decreased with aging, by about 10% for coating #1 and about 30% for #2; and the data for fiber #2 showed more scatter than for #1. However, both 133-coated fibers (especially higher cure #1) were less affected by the RH environment. Also, the rate of change of strip force for fiber 133 #2 increased rather than decreased during aging.

In deionized water, the strip force initially decreased by about 45% for coating #1 and 55% for #2. In both cases, the strip force eventually increased during aging, to about 85% and 75% of the unaged values, respectively. Although the magnitudes of the changes are different, these results are qualitatively similar to those for the 008-coated fibers.

OTHER CHARACTERISTICS

We measured the weight loss of 133-coated fibers immersed in 80°C deionized water for one day and longer. Fiber lengths were conditioned at 23±2°C, 50±5% RH before and after aging. The weight loss was 2% for fiber #1 and 1% for fiber #2 after one day; it increased more slowly thereafter.

Typical mean values for the diameters of unaged fibers and of fibers aged at 85% RH and in deionized water are given in Table 3. Shrinkage of the coatings ranged from <1% to 7% during 90 days of aging at 85% RH. All fibers exhibited greater changes during deionized-water aging than during RH aging: after 90 days, the shrinkage ranged from 6% to 11%.

Table 3. Diameter Shrinkage of 008- and 133-Coated Fibers during Aging

	Fiber as Drawn	90 Days at 85°C/85%RH	90 Days in 85°C Deionized Water
008 #3	262 μm	245 μm	239 μm
008 #4	261 μm	239 μm	232 μm
133 #1	240 μm	239 μm	225 μm
133 #2	230 μm	222 μm	215 μm

Dynamic mechanical thermal analysis (DMTA) was performed on the unaged and several of the aged fiber samples. A parallel array of 2.5-cm-long fiber pieces in a special fiber clamp[10] was subjected to single-cantilever bending with a small oscillatory strain at 1, 10 and 30 Hz over the temperature range -135°C to +125°C. The glass transition temperature (T_g) and loss tangent (tan δ, the ratio of the loss modulus to the storage modulus) of the coating were measured. Changes in these parameters indicate changes in the extent of cure and/or degradation of the coating. The results for fiber 008 #3 are shown in Table 4. Fiber 008 #4 was similarly affected by both 85°C deionized-water aging and 85°C/85% RH aging.

Table 4. Changes in T_g and tan δ for Fiber 008 #3 Due to Aging

	Unaged Condition	1 Day 85% Dry	30 Days at 85°C/85% RH	30 Days in 85°C Deionized Water
T_g	70°C	74°C	74°C	75°C
tan δ	0.090	0.088	0.079	0.079

DISCUSSION

The lack of a residual exotherm for fibers aged at 85% RH and in deionized water indicates that no additional curing occurs. This means either that the curing reaction was completed via thermal aging or that no further reaction was possible because one or more reactants were absent. Completion of the reaction in less than one day of thermal aging is unlikely for fibers with low initial extents of cure; also, exotherms were obtained for samples dry-aged for one day. It is more likely that one or more reactants were extracted from the incompletely cured coating by water or humidity in the aging environment.

Fiber 008 #4 lost about 4% of its initial coating weight when aged in 80°C deionized water for one day or longer.[4] Fiber 008 #3 lost about 3% of its initial coating weight. Similarly-aged 133-coated fibers experienced weight losses of about 2% for fiber #2 and about 1% for fiber #1. A study of the weight changes in polyurethane acrylate coatings aged in 25°C water showed that fully cured coatings gained weight in the first few hours due to water absorption, followed by weight losses of up to 4% after 28 days.[11] The higher aging temperatures and incomplete extents of cure in the present tests accelerate these changes. Recent work[12] indicates that the photoinitiator in such coatings is susceptible to extraction by water; high humidity has this solvent effect to a lesser degree. Extraction of unreacted photoinitiator would account for both the weight losses and the shrinkages in diameter, and would prevent any further curing reaction in wet-aged samples. When these coatings were aged in a dry environment, however, no extraction occurred. Residual curing was thermally stimulated, as observed with UV curable polyurethane acrylate splice adhesives.[13] Exothermic evidence of residual curing disappeared over several days of dry aging; the coating with the lowest overall extent of cure (008 #4) maintained the highest residual cure reaction for the longest time (Table 2).

The greater weight losses experienced by the 008-coated fibers are consistent with the greater shrinkage measured for these fibers (Table 3). These changes were largest for lower cure fiber #4, consistent with the large amount of photoinitiator available for extraction from this coating. Greater shrinkage was also experienced by all fibers during deionized water aging than during RH aging, indicating that deionized water had a stronger solvent action than the high humidity environment.

The DMTA results (Table 4) offer additional evidence of this effect, as T_g showed a greater change after aging in deionized water than after RH aging. A decrease in tan δ together with an increase in T_g, as seen for all three aging environments, typically indicates an increase in the extent of cure, as the crosslink density increases and the material becomes more elastic. Since extraction of photoinitiator in the wet environments prevented further curing from occurring, the observed changes at first seem contradictory. However, after extraction, crosslinked material represents a greater fraction of the remaining coating. These higher *proportional* extents of cure are thus consistent with the changes in weight, diameter, and residual cure.

The strength data (Figures 2 and 3) reflect the differences in the properties of the two coatings, different initial extents of cure, and different aging environments. The 133-coated fibers experienced twice the strength degradation, on average, of the 008-coated fibers; one-half to two-thirds of the degradation occurred in the first few days in either aging environment. The results are consistent with the differences in the properties of the 008 and 133 coating materials (Table 5). The higher crosslink density of the 008 coating makes it stiffer, stronger, and less affected by changes in temperature and humidity. At comparable but still incomplete extents of cure, 008 coatings have higher crosslink densities than 133 coatings, thus hindering the extraction of unreacted material from the crosslinked matrix and to some degree slowing the permeation of water or humidity through the coating.

Table 5. Properties of Fully-Cured 008 and 133 Coatings

	008 Coating	133 Coating
Tensile Modulus, MPa	655	28
Tensile Strength, MPa	26	9
Expansion Coefficient Ratio Above T_g/Below T_g	2:1	4:1
Modulus Change, 25°C to -40°C	2:1	30:1
Glass Adhesion Ratio 50% RH/95% RH	3:1	5:1

The strength differences for fibers with the same coating were similar throughout the aging. Even after 90 days of RH aging, fiber 008 #4 was less than 10% below its extrapolated value relative to 008 #3. Degradation in strength is essentially independent of extent of cure, at least for these coatings, and the effects of different extents of coating cure on fiber strength can be completely determined by testing unaged fibers.

The median strength of all fibers decreased with increasing aging time. The degradations for each of the four coated fibers during deionized water aging were from two to ten times larger than for the same fiber during RH aging. This effect is similar to the greater shrinkage experienced by all fibers in the deionized water environment. The results are also consistent with previous predictions and experimental findings regarding the effects of local chemistry on the surface degradation of the glass.[14,16] The coating hinders the diffusion of the outside environment toward, and reaction products away from, the glass surface; it can also directly influence the chemical environment at the glass surface through reaction by-products and dissolved materials.[1,2] Since the water and RH aging environments were both generated using pH-neutral deionized water, differences in strength between otherwise-identical fibers are traceable to the different degradation products introduced at the glass surface by the differences in chemical composition between the coatings. The degradation is both more rapid and more pronounced in deionized water because of its stronger solvent action.

The strip force data (Figures 4-7) also reflect differences in the two coatings, their initial extents of cure, and the aging environments. Strip forces measured for 133-coated samples were generally lower than those for 008-coated samples with a similar aging history and comparable extent of cure. This was noted previously for samples with no wet preconditioning or aging.[4] (The present higher values for the unaged samples likely reflect a sensitivity to storage in an uncontrolled environment between the tests.) For both the 008 and 133 coatings, the strip force for unaged samples was higher for the fiber with the lower extent of coating cure. The lower cure coatings buckled into accordion folds when stripped, rather than sliding off as a smooth tube; this same behavior was noted previously for unaged, unconditioned samples.[4] Higher strip forces were measured for the lower cure coatings during RH aging. However, during deionized water aging the strip forces for each lower cure coating were comparable to or lower than those for the corresponding higher cure coating. This is evidence that the aggressive deionized water environment penetrates the coatings, leading to entrapped-water effects that dominate extent-of-cure effects.

Lower extents of cure enhance the differences between the deionized water and RH environment effects. The strip forces for higher cure coating 008 #3 in the RH environment were comparable to those in deionized water during much of the aging. Even after 90 days of RH aging, however, the strip force for lower cure coating 008 #4 was higher than that for the same fiber aged in deionized water. The differences in strip force for higher cure coating 133 #1 between the two environments were about two-thirds of the differences for coating 133 #2 until the very end of the aging period. Ninety days of RH aging were again required before the strip force for coating 133 #2 became comparable to that for samples aged in deionized water.

Strip force incorporates the effects of coating adhesion to glass, friction, and coating stiffness and cohesion. The different behaviors just cited are due to the different stripping mechanisms that result from different coating cures. A small amount of water at the coating/glass interface lubricates the mechanical slippage of a smooth tube of coating off the glass. The buckling mechanism, however, involves radial forces that pull the coating off the glass. The deionized water environment soon introduces enough water into the coating to affect both stripping mechanisms. The RH environment introduces water more slowly, and the sliding friction is affected more quickly than the less water-sensitive buckling mechanism.

Aging in deionized water caused an initial decrease in strip force for all four fibers, followed by a gradual (smaller) increase. The overall decrease suggests that the coating structure may be unravelling, which may result from the loss of water-soluble components (e.g., photoinitiator) and the disentanglement of crosslinks. The eventual increase is likely due to the shrinkage of the coating, which increases its mechanical grip on the fiber and hence the friction component of the strip force.

SUMMARY

We tested fibers with two different coatings, each with two extents of cure, to determine the effects of the extent of cure on aging behavior. Aging in deionized water or at 85% RH extracted unreacted photoinitiator from the coating, preventing further curing. Extraction also caused shrinkage and weight loss in both coatings. The strength degradations depended on the coating properties, including differences in chemical composition, and on the aging environment; they were largely independent of the extent of cure. Strip force, however, did show a dependence on the extent of cure: longer aging times at 85% RH were required to weaken the strip forces for the lower cure coatings. Strength and strip force were both more affected by the more severe deionized-water environment.

ACKNOWLEDGEMENTS

We gratefully acknowledge the work of Matt Andrejco in drawing the test fibers.

REFERENCES

1. Krause, J. T., *Journal of Non-Crystalline Solids*, Volumes 38 & 39, 1980, p. 497.

2. Yuce, H. H., Kurkjian, C. R., and Matthewson, M. J., submitted to the *Journal of the American Ceramics Society*, 1992.

3. Yuce, H. H., Plitz, I. M., Frantz, R. A., and Andrejco, M., *Proceedings of the 39th International Wire and Cable Symposium*, November 1990, p. 715.

4. Frantz, R. A., Plitz, I. M., and Schmid, S. R., *Proceedings of the 40th International Wire and Cable Symposium*, November 1991, p. 134.

5. Matthewson, M. J., Kurkjian, C. R., and Gulati, S. T., *Journal of the American Ceramics Society*, Volume 69, Number 11, 1986, p. 815.

6. Yuce, H. H., Melczer, M. E., and Key, P. L., *Proceedings of the 7th International Conference on Integrated Optics*, 1989, p. 44.

7. France, P. W., et. al., *Journal of Materials Science*, Volume 15, 1980, p. 825.

8. Plitz, I. M., and Frantz, R. A., *RadTech '92 North American UV/EB Conference Proceedings*, April 1992, p. 308.

9. Fiber Optic Test Procedures are available by number from the Telecommunications Industries Association, Eye Street, N.W., Washington, DC 20006.

10. Gebizlioglu, et al., to be published

11. Chawla, C. P., Bishop, T. E., Szum, D. M. and Murray, K. P., *Optical Engineering*, Volume 30, Number 6, June 1991, p. 763.

12. Julian, J. and Chawla, C. P., *RadTech '92 North American UV/EB Conference Proceedings*, April 1992, p. 315.

13. Frantz, R. A., Reith, L. A., and Plitz, I. M., *Proceedings of the 41st International Wire and Cable Symposium*, November 1992, in press.

14. Kurkjian, C. R., Krause, J. T., and Paek, U. C., *Journal of Physics*, (Les Ulis, Fr.), Volume 43, Number 12, 1982, p. C9-585.

15. Robinson, R. S., and Yuce, H. H., *Journal of the American Ceramics Society*, Volume 74, Number 4, 1991, p. 814.

16. Yuce, H. H., et al., *Optical Fiber Conference (OFC)*, 1992, post-deadline paper PD21.



Rolf A. Frantz is a Distinguished Member of Technical Staff in the Fiber Distribution and Reliability Research Group at Bellcore. He holds BS and MEng degrees from Cornell University. After receiving his PhD from Brown University, he joined Bell Labs where he worked in a variety of assignments. His principal responsibilities focused on dielectric materials, an area in which he continued to work when he joined Bellcore in 1983. For the last four years, he has been concerned with the applications and reliability of materials used in manufacturing optical fibers and fiber assemblies.



Hakan H. Yuce is a Member of Technical Staff in the Fiber Distribution and Reliability Research Group at Bellcore. He has a BS degree from the Technical University in Istanbul, an MS from MIT (both in Mechanical Engineering), and a PhD in Mechanical Engineering and Materials Science from Stanford University. Since he joined Bellcore in 1987, his research has focused on the long-term mechanical reliability of optical fibers and interconnections. He provides technical input and support to Bellcore organizations responsible for generic requirements and provides analyses and consultations in response to field failures and reliability problems. He is also active in standards development, both within TIA/EIA working groups and under IEC auspices in the international arena.



Irene M. Plitz is a Member of Technical Staff in Bellcore's Plastics and Rubber Research Group. She received her BS in chemistry from Morgan State University in 1970 and joined Bell Laboratories in that same year. She came to Bellcore in 1984 and since then her efforts have focused on chemical and structural analyses of polymers. Her special interests have been polymers used as optical fiber coatings, for cabling materials, and in fiber splices, connectors, couplers and similar components.



Osman S. Gebizlioglu is a Member of Technical Staff in Bellcore's Plastics and Rubber Research Group. He holds BS and MS degrees in chemical engineering from the Middle East Technical University in Ankara, Turkey. After receiving his PhD in the Polymer Materials Program at Princeton University, he was appointed a Monsanto Postdoctoral Fellow in the Department of Mechanical Engineering at MIT. There he investigated the physics of toughening glassy polymers and deformation mechanisms in glassy polymers blended with rubbers. Since he joined Bellcore in 1987, his research has focused on polymers used in optical fibers and fiber cables, particularly in harsh service environments.

DEVELOPMENT OF CO-EXTRUDED POLYETHYLENE/POLYAMIDE 12 INSECT RESISTANT TELECOMMUNICATIONS CABLE

Mr P. Boes* Mr P. Latoszynski* Mr J. Rachcoff** Ms M. Styzinski***

* Telecom Australia, Melbourne Australia
** MM Cables Communication Products, Melbourne Australia
*** ICI Australia, Melbourne Australia

ABSTRACT

Telecommunications cables used in the Australian network have historically been subject to attack by subterranean insects resulting in significant damage to cable sheath. As a result of extensive investigations the most successful solution to the problem has been the extrusion of a protective polyamide jacket over conventional polyethylene sheathed cable. This system, however, still retained some inherent technical and economic disadvantages. The development of a co-extruded polyethylene / polyamide 12 cable construction, where the sheath and jacket are integrally bonded, overcame these deficiencies. This paper describes the processes of the development from innovative material and cable manufacture to assessment of cable performance .

INTRODUCTION

The Australian environment imposes a host of challenges to the design and effective performance of external telecommunications cable installations. Environmental factors, in many instances quite unique to Australia, that impinge on the cable performance range from the wide climatic extremes to varied geological barriers and attack from both indigenous and introduced flora and fauna.

One such challenge focuses on the protection of external telecommunications cable from subterranean insect attack. Telecommunications cables used in Australia, both in rural and metropolitan installations, have historically been subject to attack by termites and ants, resulting in cable sheath damage exemplified by Figure 1.



(a) (b)

Figure 1. Termite Damage to Telecommunications Cable (a) Lead Sheath (b) Polyethylene Sheath

Numerous approaches to solving the problem of termite attack had been investigated ranging from soil and cable impregnation with chemicals (insecticides and repellents) to the development and evaluation of materials considered resistant to the attack mechanisms[1,2].

The majority of the approaches, however, were found to be technically and/or environmentally unacceptable. Through a systematic elimination of potential candidate materials, based on processing inadequacies, high costs and failure under field evaluation, the polyamides 11 and 12 proved to be the only materials which were resistant to termite attack and suitable for use in cable construction, specifically as a thin (0.35 mm), unblemished outer jacket over standard design cables.

This system has been used in the Australian network for many years and has markedly reduced the incidence of cable damage due to termite attack. However, it too has some inherent technical and economic disadvantages:

a) the cable jacket is prone to creasing (Figure 2) when subjected to severe bending either through unwinding from cable drums or during installation. Such surface blemishes are initiation points for insect attack and also sites that can catch and promote tearing of the jacket during cable laying.
b) the cost of cable is considerably higher due to the need to extrude the additional covering of polyamide, plus the high cost of the fully imported polyamide 12 raw material.



Figure 2. Typical Creasing of Polyamide Jacket

It was considered that the provision of a high strength bond between the underlying polyethylene sheath and the polyamide jacket may be the solution to these inadequacies.

This paper describes the development of such a cable construction in which the bond is achieved through the chemical modification of the polyethylene sheathing material and the use of a two-layer co-extrusion sheathing process. This system both promotes adhesion and reduces process and material costs.

PERFORMANCE CRITERIA

The success of the development was dependent on the conformance, of both the materials and finished cable, to stringent performance criteria which were identified at the start of the project.

Materials Parameters

The materials selected were required to exhibit:

- good adhesion between the sheath and jacket (minimum 1.5 N/mm width bond strength)
- long term environmental stability comparable to that of current sheath and jacket materials
- acceptable processing characteristics
- satisfactory shelf life
- minimal cost increases

Cable Parameters

The finished cable was required to exhibit:

- uniform circumferential bond between the sheath and jacket (minimum bond strength of 1.5 N/mm width)
- retention of bond strength under a variety of environmental conditions
 - 30 days immersion in water at 60°C
 - 30 days immersion in petrol at 23°C
 - 30 days in air oven at 80°C
- acceptable cable finish ie. smooth gloss finish and no propensity to crease
- compatibility with current jointing practices
- termite and ant resistance

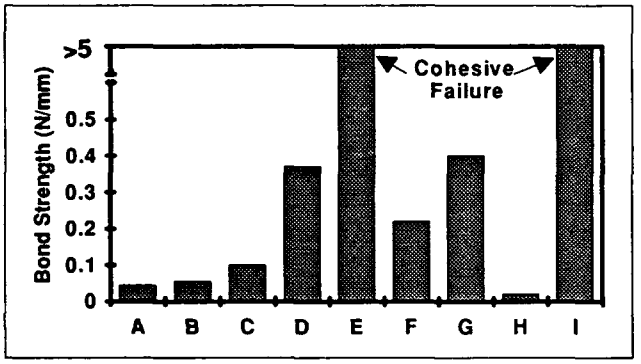
MATERIAL DEVELOPMENT

The major obstacle in achieving an integral bond between polyethylenes and polyamides lies in the materials' incompatibility due to polarity differences. This incompatibility has in part been overcome in the packaging industry where the adhesion of dissimilar multi-layer films is achieved by co-extrusion of tie-layers between the incompatible materials.

The cost of using such tie-layer technology in the cable manufacturing industry, however, is prohibitive. A simpler and more cost effective solution was to incorporate an additive of appropriate polarity into one of the existing materials (either the polyamide or polyethylene) which would enable it to bond to the other without compromising the physical

properties, stability, processability or surface finish of either. As the polyamide 12 has proven insect resistance, it was considered prudent not to interfere with its formulation, but rather to modify the polyethylene layer beneath.

Various formulations of polyethylene based materials containing unsaturated acids or anhydrides[3] were trialed in the laboratory. The critical parameter of bond strength, measured using the standard 180° peel test[4], was initially assessed on blow moulded co-extruded bottles having wall thicknesses of the polyamide and polyethylene consistent with that found on cables. This enabled the determination of the most suitable adhesive component (Figure 3) and respective concentration required to produce a minimum bond strength of 1.5 N/mm width.



A: 0.006% Maleic Anhydride B: 0.008% Maleic Anhydride
C: 0.010% Maleic Hydride D: 0.012% Maleic Anhydride
E: 0.400% Maleic Anhydride
F: 0.008% Maleic Anhydride + 12.74% Butyl Acrylate
G: 0.010% Maleic Anhydride + 12.74% Butyl Acrylate
H: 4.95% Acrylic Acid I: 8.25% Acrylic Acid

Figure 3. Peel Strength Variations With Different Additive Components and Concentrations

During the fine tuning stage greater flexibility and reproducibility in sample preparation was obtained using an Otto Bruger Heat Sealer, an apparatus commonly used for testing sealing properties of packaging films. The polyamide and the modified polyethylene compounds were each extruded into tapes of appropriate thickness. Then laminates of aluminium / modified polyethylene / polyamide were formed on the heat sealer using various control parameters such as polymer temperature, contact time prior to quenching and contact pressure.

This method proved to be more representative of extrusion conditions used during cable manufacture. It demonstrated that the polyethylene / polyamide bond strength improved as temperature and pre-quench time was increased but deteriorated if the contact pressure was too high.

The modified polyethylene also adhered well to uncoated aluminium which raised the as yet unexplored opportunity of using uncoated aluminium as the moisture barrier in a one pass cable manufacturing process. At present the aluminium moisture barrier used for Australian cables is pre-coated with a layer of ethylene-ethyl acrylate copolymer to ensure adhesion to the polyethylene sheath.

In addition to the bond strength tests, accelerated thermal ageing tests were performed on the modified polyethylene to compare its long term stability with that of current sheathing materials. Results of Oxidation Induction Time (OIT)[5] measurements (Figure 4) and tensile tests[6] on the aged specimens indicated similar performance for both the modified and unmodified polyethylene sheath resins.

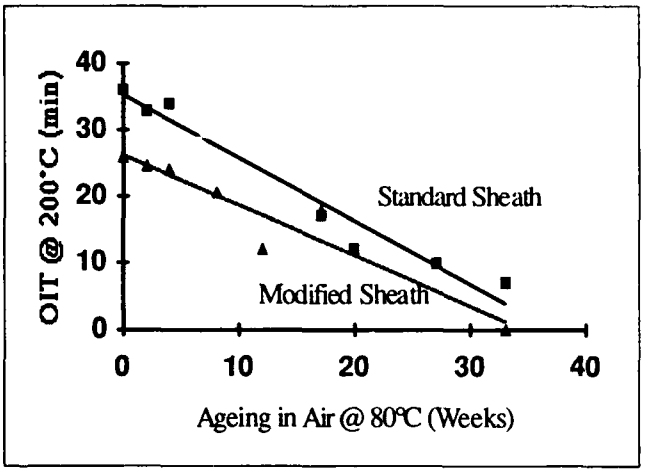


Figure 4. Comparison of Ageing Characteristics of Standard and Modified Polyethylene Sheath Materials

The durability of the bond, tested by ageing the laminates in the prescribed environments, also proved satisfactory with retention of bond strength at an acceptable level after exposure. Finally, the shelf life of the modified compound was found to be satisfactory through regular adhesion tests over a 2 year period.

The version of the modified polyethylene compound which performed best was ICI COEX 500. This grade was ultimately used in the cable manufacturing trials.

CABLE MANUFACTURE

The manufacturing development occurred through a number of stages to examine and optimise the processing variables. This was carried out in conjunction with the material development programme.

The first experimental cables were manufactured on a standard co-extrusion line consisting of a 3½ inch main extruder used for the inner polyethylene sheath and a 1 inch vertical extruder used for the extrusion of the outer polyamide 12 jacket. The vertical extruder fed the polyamide melt directly into the head of the main polyethylene extruder and the two materials made first contact in the head and then extruded through a common die. Both materials were processed with standard temperature profiles recommended by the material suppliers.

During the initial trials it was considered important that the melt temperatures of both materials be kept as close as possible to facilitate the transfer of bonding agent between the inner polyethylene and outer polyamide to maximise the bond strength. These early trials, however, met with little success due to difficulties caused by exudation of the active ingredient from the polyethylene. This problem lead to further polyethylene reformulation.

These early stages of cable development did, however, highlight three equipment / processing problems:

- the polyamide jacket exhibited melt joins
- the vertical extruder had output pressure limitations which resulted in extruder cut outs during cable manufacture
- variations in polyamide jacket thickness

These challenges were overcome by:

- altering the tooling design
- adapting a 2 inch extruder for the polyamide to the line.
- placement of a gear pump in the neck between the extruder and the head where the two materials meet. This enabled an increase in the polyamide output with the ability to withstand high extrusion pressures in the die. It also minimised variations in the polyamide output allowing the jacket to be extruded at 0.2 mm thicknesses with more confidence. This resulted in an overall reduced polyamide usage.

The co-extruded cables produced with the new extruder set up showed a marked improvement in the polyethylene / polyamide bond strength, with bond strengths up to 2.5 N/mm width being attained. It was also noted that the bond between the materials varied around the circumference of the cable which was primarily due to inconsistent extrusion pressures resulting from an oval shape of the cable core.

To further optimise the manufacturing process an experimental matrix was designed to assess the parameters which most effect the bonding (Table 1). Cables co-extruded with the improved polyethylene formulation, COEX 500, exhibited improved bond strengths which conformed to all the bond strength performance criteria.

Run No.	Variable			
	A	B	C	D
1	H	L	L	L
2	H	L	H	H
3	H	H	L	H
4	H	H	H	L
5	L	L	L	H
6	L	L	H	L
7	L	H	L	L
8	L	H	H	H

Variables
A Extrusion Head Pressure
B Polyethylene melt temperature
C Nylon melt temperature
D Line Speed

H = High
L = Low

Table 1. Experimental Matrix for Optimisation of Process Parameters

Bond strength evaluation on the completed cables manufactured in these optimisation trials (Figure 5) indicated that:

- changes to the polyethylene and polyamide melt temperatures, within the processing window, had minimal effect on bond strength on the finished cable. In addition it was noted that

high melt temperature runs produced an unsatisfactory surface finish on the polyamide with defects such as sharp lumps and pimples.

- variations in the extrusion head pressure and the line speed had the greatest effect on the bond strength. The line speed has a direct effect on the time that the polyethylene and polyamide melts are in contact prior to being cooled.

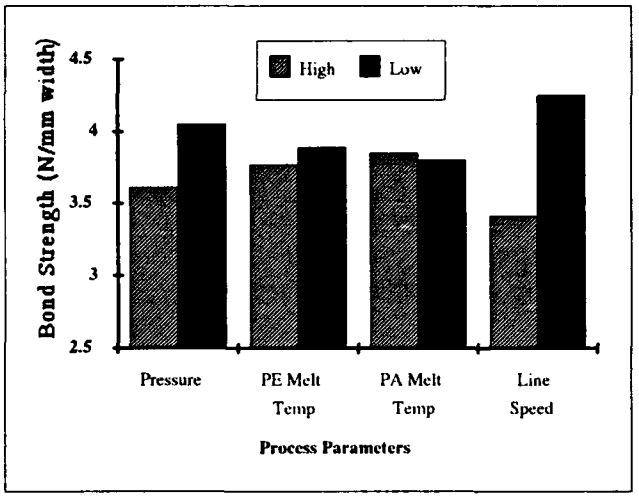


Figure 5. Effect of Process Parameter Variation on Bond Strength

Successful optimisation of both the material modifications and the processing conditions lead to production of cables for laboratory and field evaluation. The bond strength between the polyethylene sheath and the polyamide 12 jacket achieved was in excess of 4.0 N/mm width which is well above the specification requirements.



(a) (b)

Figure 6. Scanning Electron Micrographs (x50) of Sheath / Jacket Interface (a) Co-extruded Cable (b) Two Pass Extruded Cable

Micrographs of the sheath / jacket interface (Figure 6) further confirmed that a uniform integral bond exists whereas in the two pass extrusion previously practiced it is clearly evident that no bonding occurs.

CABLE PERFORMANCE EVALUATION

Crucial to the successful implementation of the newly developed cable into the network is its comparative performance to that of the conventional polyamide jacketed cable in the areas of factory handling, storage, field installation and overall long term field performance.

The quality and long term performance of the conventional polyamide jacketed cable is primarily dependent on the smoothness and thickness of the jacket and its ease of removal during joint installation. In the case of the co-extruded cable the long term performance will depend, in addition to the surface finish requirements, more on the bonding quality of the polyethylene to the polyamide and the sealing quality of the various cable joints to the outer polyamide jacket.

In order to evaluate the performance of the co-extruded cable against that of conventional cable a number of Telecom specified tests were carried out. These included:

- Environmental Ageing[4]
- Cable Bending[7]
- Cable Jointing Compatibility[8,9,10]

Environmental Ageing Results

Evaluation of the cables exposed to the specified accelerated environmental ageing conditions indicated that bond strength was retained at an acceptable level under all conditions (Figure 7). Extended long term laboratory tests indicate this performance will be maintained in the field situation. Field evaluation of termite resistance is still in progress, but it is expected to be satisfactory, on the basis of previous experience.

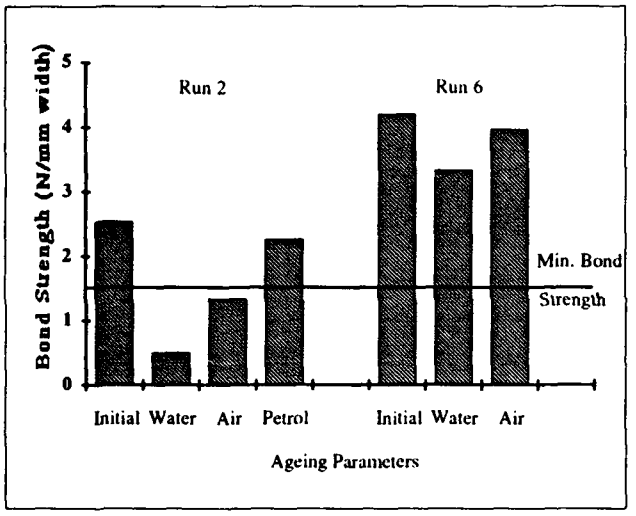


Figure 7. Degree of Bond Strength Retention After Environmental Exposure

Cable Bending

The purpose of this test is to ensure that the cable jacket does not crease or delaminate when subjected to specified bending conditions that may be likely to occur during installation. The test involves subjecting, both unaged and heat aged, cable to two forward and reverse 360 degree cycles of bending around a mandrel of a diameter 30 times the cable diameter. To accentuate the bending force the cables were also tested around mandrels 10 and 15 times the diameter of the cable. All samples passed with no evidence of creasing, delamination or any other defects.

Cable Joint Compatibility

The Australian network utilises a variety of jointing techniques for both copper and optical fibre cable. Jointing practices associated with the conventional polyamide jacketed cables rely on the removal of the jacket at the cable entry ports. This is done in order to prevent any moisture, formed in the void between the polyamide jacket and the polyethylene sheath along the cable length, entering the cable joint. In the case of the co-extruded cable this process cannot occur as the polyethylene and polyamide are bonded. As the polyamide jacket cannot be removed, its compatibility with current jointing practices needed to be investigated, particularly under conditions considered to simulate expected field situations.

The three cable joints, commonly used within the network, involved in the test were:

a) In-Line Joints - An unpressurised joint used primarily for rural, direct buried filled cable installation and repair. Its operating environment may include temperature ranges from -10°C to 40°C, humidity extremes and immersion in highly alkaline water for extended periods of time.
b) Openable Distribution Joints - An unpressurised joint used in urban and rural areas for jointing filled distribution cable in pits and manholes exposed to similar operating environments to that of in-line joints.
c) Pressurised Closures - Used for jointing both air core and jelly filled cables in manholes. These joints are exposed to similar environments to that of the other joints described.

In the case of the In-line and Openable Distribution joints heat shrinkable plastic tubing is used to seal the cable entry ports. In this process the hot melt adhesive, coated onto the inner surface of the tubing, adheres directly onto the polyethylene sheath. However, with the co-extruded cable the thermo-shrink tubing will be required to adhere to the polyamide jacket surface.

To determine joint compatibility with the co-extruded cable both the in-line and distribution joints were subjected to a testing programme including:

- Thermo-shrink Sleeve Peel Strength
- Flexure test
- Alkaline resistance
- Head of water
- Heat ageing
- Thermal cycling
- Insulation withstand voltage
- Axial pull out strength

In the case of the pressurised closures, where butyl rubber is used to seal the entry ports, a slightly different testing programme was carried out including:

- Tightness test
- Thermal ageing
- Temperature cycling
- Head of water
- Tension test
- Pressurisation test
- Bending test

The results indicated that the co-extruded cable performed similarly to the conventional polyethylene / polyamide cable in all the cable joint compatibility tests and met all specification requirements.

CONCLUSION

The refinement of specific material compositions and cable manufacturing procedures has resulted in development of an innovative telecommunications cable construction, based on a co-extruded modified polyethylene / polyamide 12 cable design, which has proved to be technically and economically superior to insect resistant cable designs previously used.

ACKNOWLEDGMENTS

The authors wish to acknowledge the assistance and co-operation of all parties involved in the development, in particular ICI (Australia) and MM Cables Communication Products. The permission of the Director of Research, Telecom Research Laboratories and Group Managing Director of Commercial and Consumer Business, Telecom Australia to publish and present this paper is also acknowledged.

REFERENCES

1 R.A.Clarke and G.Flatau, "Development of Nylon Jacketed Insect Resistant Cable", 21st. IWCS, USA, 1972.
2 H.J.Ruddell, "Development of an Insect Resistant Telecommunications Cable for the Australian Environment", Telecommunication Journal of Australia, Vol. 35, No.2, 1985.
3 Australian Patent Application No. 606285
4 Telecom Australia Specification, Attachment LC1, "Specification for Polyethylene Sheath, Polyethylene Jacket and Lead Sheath for External Telecommunications Cables", Issue 10, 1992.
5 R.Ashby, "Developments in the Study of Oxidative Thermal Stability of Polyolefins by Differential Thermal Analysis", PIT III, 25.1, 1982.
6 Australian Standard 1049-1986, "Telecommunication Cables-Insulation and Sheath-Polyethylene", Appendix C.
7 Telecom Australia Specification, Attachment LC2, "Insect Resistant Jacket for Telecommunications Cable", Issue 11, 1992.
8 Telecom Australia Schedule MS5105, Specification D1340 Issue b, "Heat Shrink Tubing for Moisture Barrier Cable Joint Closure Kits".
9 Telecom Australia Schedule MS5053, "Distribution Cable Jointing Materials and Accessories".
10 Telecom Australia Schedule MS5069, "Universal Joint Closures and Accessories".

AUTHORS

Paul Boes

Access Product Group
Commercial and Consumer Business
Telecom Australia
6/242 Exhibition Street
Melbourne VIC 3000
AUSTRALIA



Paul Boes joined Telecom Australia in 1986 after graduating with a B.E. degree in communications engineering from the Royal Melbourne Institute of Technology in the same year. He is currently Principal Engineer in the Access Product Group, Commercial and Consumer Business, responsible for the development, implementation and technical management of copper and optical fibre cable in the Telecom Australia Customer Access Network.

Maria Styzinski

Plastics Technical Centre
ICI Australia
Stanford Street
Ascot Vale, VIC. 3032
AUSTRALIA



Maria Styzinski completed an honours degree in Applied Science (Chemistry) at the University of Melbourne in 1987. She then joined ICI Australia's polymer research team as a research scientist. Since 1989, when she took on the role of Wire and Cable Technical Service Officer with the Speciality Plastic's Division of ICI Plastics, Maria has been responsible for responding to the technical needs of the Wire and Cable market in Australia.

Peter Latoszynski

Telecom Research
Laboratories
Telecom Australia
770 Blackburn Road
Clayton, Vic 3168
AUSTRALIA



Peter Latoszynski is an Applied Science Graduate of Footscray Institute of Technology (1975) and also gained post graduate qualifications in Analytical Chemistry from the Royal Melbourne Institute of Technology in 1980. Peter joined the Telecom Australia Research laboratories in 1972 and has held a variety of technical positions prior to specialising in polymer technology. He is currently Principal Polymer Chemist responsible for network materials stabilisation, new cable materials and electro-active polymers.

John Rachcoff

MM Cables-Communication
Products
71 Whiteside Road
Clayton, Vic 3168
AUSTRALIA



John Rachcoff graduated from the University of Melbourne in 1989 with a Bachelor of Science (Chemistry). He joined MM Cables Communication Products as a works chemist in the technical department and is engaged in the processing/development of new materials for use in telecommunication cables.

ON THE DEVELOPMENT OF AN ARAMID YARN WITH WATER-BLOCKING PROPERTIES

O. Grabandt, S. Willemsen and J.H. v. Leeuwen

AKZO Fibers, Arami, P.O. Box 9300,
6800 SB Arnhem, The Netherlands

Abstract

Twaron[R] aramid fibers with water-blocking capability in Optical Fiber Cables have been developed. By using water-in-oil emulsions of super-absorbing polymers, easy application of these emulsions on the aramid fibers is possible. The water-blocking capability of these finished fibers is superior compared to fibers treated with conventional methods.

Introduction

Optical fiber protection

Optical Fiber Cable (OFC) designs have to anticipate and counteract all possible deteriorating influences on the light guiding properties of the optical fiber. Since optical glass fibers are used as signal guides due to their low light-attenuation properties, the problem of the mechanical and chemical vulnerability of the optical glass fiber has to be solved by the OFC construction.

Mechanical forces acting on the optical fiber can be eliminated by including linear strength members of high modulus material in the OFC design. Aramid fibers posess a unique combination of mechanical properties, such as low weight, high strength, high modulus, non-corossive, which make them ideally suited for application as linear strength member material. Presently, the application of Twaron[R] aramid fibers in aerial and duct-in OFC's for this purpose is recognised as highly advantageous.

A second major problem in OFC design is the sensitivity of the OFC and in particular of the optical glass fiber to water. Water contact with the optical fiber will inevitably lead to optical signal attenuation hereby rendering a strongly reduced lifetime of the OFC. In addition water penetrated into the OFC can lead to mechanical damage of the OFC after exposure to freezing temperatures.

The two main sources of water contact are splices and damaged OFC outer-shields. An OFC design therefore has to incorporate an effective water repelling/blocking mechanism. The traditional solution to this problem was to use gas-pressurized OFC's. Production and maintenance costs of the gas-pressurized OFC's have led to the development of alternative solutions. Optical fibers are embedded in petroleum jells. The petroleum jells are also added to shields incorporated in the OFC design. The choice of petroleum jell is difficult since the chemical and physical (mechanical) properties of the jell have to be optimized due to its direct contact with the optical fibers. Although water absorbing powders were used in other bulk applications, incorporating these powders in OFC designs has been a major innovation. These powders have a water-blocking effect in the OFC design. Upon water contact the powder increases in volume by absorbing the water to form a gel. This effectively blocks the water from further diffusion into the OFC. The water-blocking effect of water-absorbing components such as these powders in OFC's is referred to as longitudinal water-tightness.

Traditional approaches

Several variations of the powder application approach are practiced. The powder can be integrated in the OFC by application in the interstitial areas in the OFC. A more appropriate solution is the impregnation of fibers or tapes around the OFC core hereby shielding the optical fiber. Although this solution represents the state-of-art several drawbacks can be stated. During production of the impregnated fiber/tape the amount of water-absorbing powder which sticks to the fiber/tape is difficult to control. In addition in each subsequent process step some of the powder will be removed from the fiber/tape by mechanical action. Since the powder is usually applied in a seperate process the economic consequences of powder application can be severe. The most important drawback

of the powder method is the resulting inhomogeneous distribution of the powder along the tape/fiber. The result of such an inhomogeneous distribution is a strongly reduced water-blocking capability of the fiber/tape in the final OFC construction. This can only be counteracted by adding more water-blocking fiber/tape in the OFC design making the OFC unnecessary expensive. The application of SAP's from suspension is also cumbersome since the SAP forms high viscosity solutions. The low SAP concentrations which are needed to keep the viscosity acceptable results in the use of an appreciable amount of solvent which has to be removed in the drying process step.

Our approach

In this work we present a new approach to solve the mechanical-load as well as the water-sensitivity problem. Twaron^{R} aramid fibers are finished in the final production process step with a water-in-oil emulsion containing super-absorbing-polymers (SAP). This finish is evenly distributed along the aramid fiber leading to a homogeneous coating of the fiber with the SAP. Thus treated aramid fibers can be applied in the OFC design as linear strength members. A tight-buffered OFC design in which the SAP containing aramid fibers are stranded around the cable core including the optical fibers, results in excellent water shielding of the optical fibers. Due to the integration of the application of the SAP in the fiber production process as well as the reduction of SAP containing fibers in the OFC due to the homogeneous distribution of the SAP along the aramid fibers, a cost-effective solution to the mechanical-load as well as the water-sensitivity problem of the optical fibers in an OFC has been developed.

How to evaluate the water-blocking properties

The experiments described in this work are performed using Akzo's aramid fiber Twaron^{R}. The intermediate modulus type as well as the high modulus type are included.

Two tests are used in order to evaluate the water-absorbing properties of the aramid fibers : the swelling test and the longitudinal water-tightness test.

The swelling test measures the amount of water which is physically adsorbed on the fiber. A small amount of fibers (10 gr.) is submerged in demineralized water (20°C, 1 min.). The fibers are subsequently filtered and spin-dried (2800 rpm, rotor diameter 24 cm). The weight of the fibers is determined directly after spin drying. The physically adsorbed water is removed in a hot air oven (105°C) and the fibers are weighed again. The weight loss (%) is calculated relative to the hot-air dried fibers. The weight loss is called the swelling value.



Fig. 1. A sample tube containing a bundle aramid fibers ready for use in the water-tightness test.

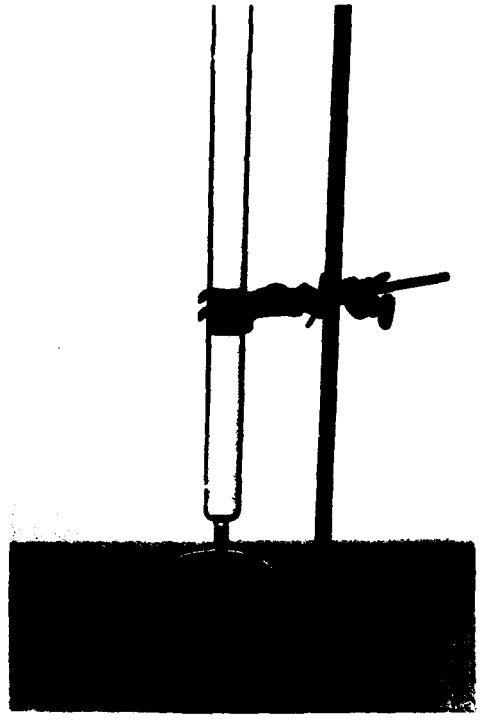


Fig. 2. The water-tightness test set-up.

Since the desired property of the aramid fibers is longitudinal water-blocking, a special test, measuring longitudinal water-tightness, was developed. It consists of a small test tube (length 5 cm, PVC) mounted beneath a water column (1 meter). The inner diameter of the PVC test tube is 5 mm and contains aramid fibers with total linear density of 16.8 g/m. The characteristic water-blocking time (through-flow time) is measured starting from application of the water column on the test tube to appearance of the first water droplets at the air exposed end of the test tube. The test tube filled with aramid fibers is shown in fig. 1. The set-up consisting of water column and test tube is illustrated in fig. 2.

Development results

Hydrofobic aramid fibers

The first experiments in attempting to create a water repelling/blocking aramid fiber concerned the application of hydrofobic finishes on the fibers. Finishes consisting of waxes, polydimethylsiloxanes, polybutenes or fluoro-carbon compounds were evaluated. The water repellency of fibers can be demonstrated by placing water droplets on a spool. High water repellency is recognised by the fact that the water droplets do not penetrate the fiber package on the spool but can be shaken off. Fibers finished with polybutene and in particular fluoro-carbon compounds showed high water repellency according to this test. The expected water blocking properties of these water repelling fibers were however disappointing. The characteristic result of the water-tightness test of water repelling fibers amounts to 1.5 min. compared to 0.8 min. for the unfinished fiber. The through-flow time is only slightly larger compared to the unfinished fibers. In addition to the marginally improved water-tightness it was observed that the hydrofobic fibers presented processing problems due to deposit formation on yarn guides resulting in filament breakage and loss of strength. Therefore a different approach to water blocking aramid fibers was attempted. It must be stated that hydrofobic aramid fiber show good anti-ballistic properties by strongly increased bullet penetration resistance demonstrating serendipity within research.

Hydrofillic aramid fibers

The use of super-absorbing polymers (SAP) in OFC's shows high potential. By impregnating the aramid fibers, which are inserted in the OFC, with SAP's paradoxically a hydrofillic fiber is obtained. We use SAP's in order to make hydrofillic water-blocking aramid fibers but are able to circumvent the problems stated above (see Introduction) by application of the SAP on the fiber from water-in-oil emulsions. Suitable monomers are dissolved in water. After addition of a non-polar solvent and emulsifier a water-in-oil emulsion is created containing the monomers in the water phase. Polymerization then takes place in the water phase. The result is an emulsion containing high concentration SAP but with still relatively low viscosity. The viscosity of the emulsion can be optimized for the preferred application technique (kiss-roll) by diluting with a non-polar solvent.

Several SAP emulsions have been tested on their suitability for water-blocking applications i.e. poly(potassium)acrylate (compound A), (sodium)acrylate/acrylamid copolymer (B), terpolymer of acrylamid, carboxylate and sulphate groups containing monomers (C), polyacrylamid copolymers (D, E). All SAP emulsions are commercially obtained.

Proof of principle. The proof of principle is demonstrated in table 1. The emulsions A, B and C contain approximately 30% SAP. The viscosity amounted to 200-800 mm^2/s (25°C). After application on the fiber and drying, finished fibers were obtained with 0.5% - 2.0% SAP. Compound C clearly demonstrates a time dependence in the water-tightness test on the amount of SAP. The swelling and through-flow value of the unfinished fiber are included. All SAP finished fibers clearly show a tremendous increase in through-flow time compared to the unfinished fiber. The swelling value of C-finished fibers is correspondingly increased compared to the unfinished fiber.

Production considerations. In order to lower the viscosity and increase the stability of emulsions parafinnic hydrocarbons and substituted sorbitantrioleates were added. Emulsion compositions containing 4% - 11% SAP and approx. 5% stabilizer have been applied using a kiss-roll. No reduction in through-flow time is observed. The addition of 10% stabilizer in the emulsion composition resulted in 4X - 10X increase in time span before solid material could be observed in the unstirred emulsions showing the beneficial effect of a stabilizer in a SAP emulsion for a production environment.

Mechanical properties. Static charging of the fibers can lead to reduction of the tensile strength due to damage of isolated filaments. The stabilizers used appeared to have an anti-static effect as well. Compositions without stabilizer show a 10% - 15% reduction in tensile strength. Inclusion of a stabilizer (approx. 10%) leads to a tensile strength equal to the unfinished fi-

ber. In addition the modulus remained at the level of the unfinished fiber.

Moisture sensitivity. Special attention has been given to the moisture sensitivity of the SAP-finished fibers. Emulsions of compounds C, D and E (25% - 30% SAP) were applied on the fiber (1.5% SAP, 0.8% stabilizer). The fibers were analyzed on moisture content directly after production resulting in 1.5% - 2.5% moisture. The moisture content was determined again after 4 weeks conditioning (20°C, 65% rel. humidity). The moisture content of the SAP-finished fibers appeared to be equal to the unfinished fiber : 3.0% - 3.5%. It is concluded that the SAP-finished fibers are not hygroscopic.

Comparison with suspension application. A general comparison of the water-in-oil SAP emulsion method with the suspension method is made by using the method described in patent application EP-A 0351100. This patent descibes the application of a SAP an aramid fiber from suspension. In our laboratory suspension finished fibers containing 0.6%, 0.9% and 1.3% SAP were prepared by this suspension method and analyzed. The swelling values range between 40 and 50. The observed through-flow times are 7 min., 15 min. and 15 hours respectively. Although this constitutes an increased water-blocking capability it is concluded that our water-in-oil emulsion method leads to a superior water-blocking capability of the SAP-finished aramid fibers. The water-tightness test has been performed upto 17 days on samples finished with diluted, stabilized water-in-oil SAP emulsions without sample failure.

Table 1. Swelling test and water-tightness test results of high modulus aramid fiber finished with super-absorbing polymers as well as unfinished fiber.

SAP	% finish	through-flow time	swelling value
A	0.5	>4 days	-
B	0.5	>4 days	-
C	0.5	18 hours	-
C	1.0	>4 days	183
C	2.0	>4 days	295
-	-	<1 min.	19

The mechanism by which the SAP application from water-in-oil emulsion leads to better water-tightness results compared to application from suspension has been partly solved. It is assumed that the distribution of the SAP along the aramid fibers is a key factor. The electron microscopy pictures of unfinished and SAP-finished (from water-in-oil emulsion) fibers are shown in fig. 3 and fig. 4. It is clearly visible that the SAP-finished fiber contains a homogenous coating of water-blocking SAP. A less homogeneous distribution of the SAP along the fiber might easily lead to a decreased water-blocking capability.

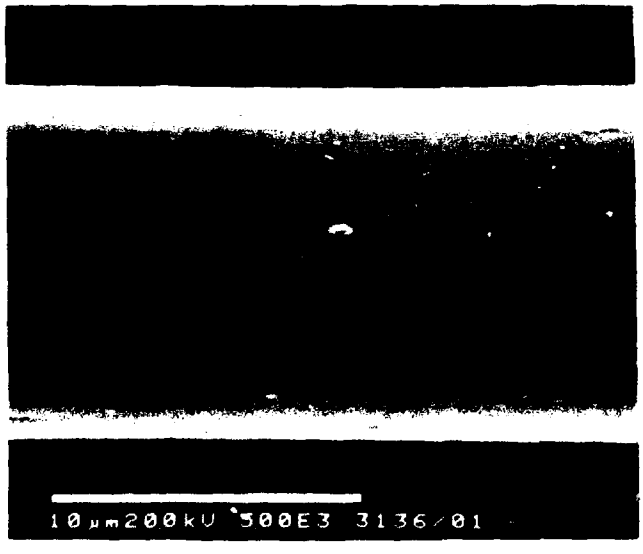


Fig. 3. Electron microscopy photo of unfinished high modulus aramid fiber.

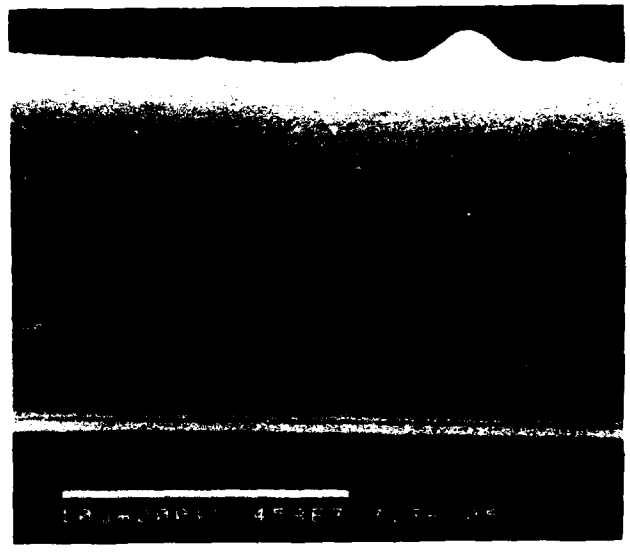


Fig. 4. Electron microscopy photo of SAP-finished high modulus aramid fiber.

Temperature effects in further processing. The SAP finished aramid fibers can be applied in the OFC by means of a stranding apparatus. The aramid fibers are wound around the optical fiber containing core. Subsequently a shield is extruded around the cable. In this process the SAP-finished aramid fibers are exposed to elevated temperatures. The through-flow times of SAP-finished fibers (from water-in-oil emulsions) after several heat-treatments have been evaluated. The following heat-treatments have been given: 1 min./200°C, 5 min./200°C, 1 week/60°C amd 1 day/-25°C. The water-tightness test has been performed at room temperature. No loss in through-flow time is observed, therefore it is concluded that the water-blocking capability is not affected by the heat treatments. In addition the through-flow time has been measured at 60°C after a heat treatment of 1 week/60°C. The experimental set-up is shown in fig.5. The water-tightness test is placed inside a hot-air oven. Again the SAP-finished aramid fibers show no reduction in through-flow time at this elevated temperature.

Presently patent applications have been filed covering the constitution of the SAP finishes, the application method by water-in-oil emulsions, the implementation in the production process and the application of the SAP-finished aramid fibers in an OFC (EP-A 0482703).

Conclusions

1. Excellent water-blocking capabilities of Twaron^{R} aramid fibers are obtained after application of a finish consisting of super-absorbing polymers (SAP).
2. The SAP finish has no adverse effect on the mechanical properties of the aramid fibers.
3. The SAP-finished aramid fibers have good processing properties.
4. SAP-finished production fibers have been shipped to several leading manufacturers. Construction of OFC's containing these fibers has already successfully been demonstrated.

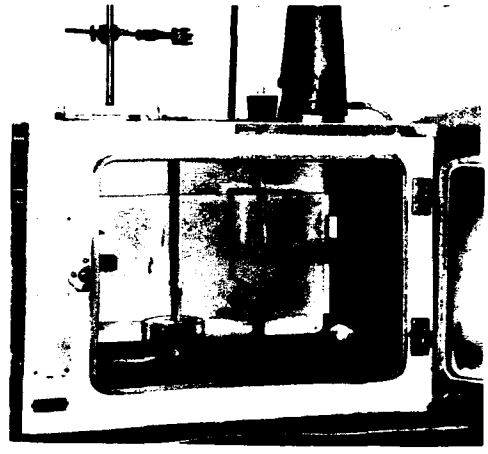


Fig. 5. The water-tightness test set-up at elevated temperatures.



Dr. O. Grabandt (1957) received his Ph.D. in physical chemistry from the University of Amsterdam. He joined Akzo Research Laboratories in 1988 and worked on carbon and aramid fibers. Presently (1992) he is an end use development engineer at Akzo Arami.



S. Willemsen (1943) joined Akzo Research in 1965 as a technician in plastics research. After the conclusion of his evening study in chemical engineering (1980) at the PBNA Institute of Arnhem (Netherlands) he was appointed researcher of finishes, with special emphasis on finishes for Twaron aramid fibers. The base patent for water-blocking aramid is in his name.



Ir. J.H. van Leeuwen (1941) moved after 5 years of experience in applied physics within Akzo to a group studying the possibilities of industrial fibers in New Applications. Since 8 years he is involved in product and end use development for Twaron aramid fibers. Since 1990 he is Technical Marketing Manager for Twaron in Ropes/Cables-OFC and Mechanical Rubber Goods applications.

EVALUATION OF ANTIOXIDANT UNIFORMITY IN POLYETHYLENE INSULATIONS

Y. Gau - Union Carbide Corporation
E.D. Nelson - AT&T Bell Laboratories, GA
K.D. Dye - AT&T Network Systems, AZ

Abstract

Polyethylene insulations contain stabilizers to control oxidation which occurs in the various phases of the conversion process from the base resins to the compounds, to the single wires, to the cables, and in end-use applications. In addition to using the right types and having a proper level, a uniform distribution of the stabilizers within the polyethylene insulations is critical to achieve a good long term performance of the wire insulations.

To study the effect of antioxidant uniformity on the performance of the cables, samples with various degrees of mixing in solid, and cellular polyethylene insulations were produced, and made into wires. The antioxidant uniformity within the compounds and along the wires was characterized by oxidative induction time. HPLC data on the compounds were also collected. It was found that with the current compounding practices and technology, good uniformity of antioxidants exists as determined by oxidative induction time. The achieved level of mixing of the stabilizers within the polyethylene insulations is sufficient to prevent any localized oxidation. The evidence suggests that failures observed on wire insulations are caused by mechanisms other than antioxidant uniformity.

Introduction

Polyethylene was introduced in the 50's for telephone wire insulation, and has remained the material of choice for this application. Low density polyethylene (LDPE) was initially used and provided electrical and mechanical properties suitable for most cable construction. In the 70's, medium and high density polyethylene (MDPE and HDPE), which have better resistance to petroleum base cable fillers and improved mechanical properties displaced LDPE and allowed for changes in cable designs. HDPE is mainly used in North America and Latin America, while MDPE is preferred in Europe, England and the Far East.

As with other plastic materials, polyethylene compounds are susceptible to oxidation.[1] The oxidation reactions can occur in the various phases of the conversion process: production of the compounds, manufacturing of the single wires, cabling, and in end use applications. To control oxidation and provide the desired protection, stabilizers are incorporated into the compounds. In addition to an adequate stabilizer level, a uniform distribution of the antioxidants within the insulation compounds is critical to achieve consistent performance along the wire. This is particularly important with difficult to disperse additives, especially those that are relatively insoluble in polyethylene. The study focused on characterization by oxidation induction time of the antioxidant distribution in polyethylene pellets and along wires made from the pellets.

The stabilization package for the HDPE insulation compounds has evolved over the years to include a primary antioxidant with a metal deactivator. The current antioxidant package generally used in the US consists of a phenolic antioxidant, Irganox 1010 (AO) and a combination antioxidant/metal deactivator, Irganox 1024 (MD).[2] Much work has been done to define the mechanisms leading to failure of the insulation in pedestal environment.[3,4,5,6] Nevertheless, questions on how well the antioxidants are distributed along the wire have until now not been clearly addressed.

Sample Preparation

The tested solid and cellular HDPE insulation samples were formulated with the antioxidant (AO) and the metal deactivator (MD), and with a blowing agent for the cellular compound. They were prepared in a pilot plant scale compounding line equipped with a 30 lb batch mixer discharging into an extruder for pelletization. The batch, discharged into the extruder prior to pelletizing, is called the "pig". Pellet samples were collected at the exit of the pelletizer/dryer. The experiment was designed with two levels of mixing of the stabilizers for both the solid and cellular insulation compounds: High Intensity Mixing and Low Intensity Mixing.

The level of mixing was controlled by the sequence and time of addition of the antioxidants into the batch mixer. The mixing cycle time was kept constant for the solid and cellular insulation compounds, and was controlled by the discharge melt temperature out of the batch mixer. For instance in High Intensity Mixing, all ingredients were added at the beginning of the cycle while in Low Intensity

Mixing, the antioxidants saw only a portion of the total mixing cycle time. A small "pig" sample was also collected at the feed throat of the extruder after the discharge of the batch out of the mixer. The objective was to determine if any reduction in the level of antioxidants occurred through the pelletizing process. Moreover, the solid and cellular samples were converted into 26 gauge solid and foam skin wires to evaluate the antioxidant uniformity along them and the effects of this coating process on the final level of stabilizer.

Testing

Since isothermal analyses have been extensively used to study oxidation stability of plastic materials, the oxidation induction time technique (OIT) was selected to characterize the distribution of antioxidants in the samples.[6] OIT also provides a quick way to check the quality of the stabilization package in the insulation compounds. In the study, the OIT test was run according to the procedure spelled out in ASTM D 4565.

- Use a Dupont analyzer and a 5 to 7 mg sample in an aluminum pan.

- Switch to oxygen immediately upon reaching the selected isothermal temperature (200°C in the majority of the tests), and maintain a flow of oxygen of 200 mL/min.

OIT values were determined for the "pig", pellets and wire insulation samples. The OIT values were measured as the time from start of the isothermal phase to the beginning of the exothermal decomposition, Figure 1. Duplicate samples were submitted to five labs for testing. Preparation of pellet samples was standardized to assure that the center portion of pellets was tested; outer surfaces were shaved and discarded. One of the involved labs performed a comparison of pellet testing methods by collecting OIT data from pressed and shaved samples at 200 and at 220°C. The pressed samples were punched out from 10 mil films compression molded at 150°C. Wire insulation was sampled at one foot intervals and tested with and without the conductor. Antioxidant level in "pig" and pellet samples was also measured in two labs by HPLC, according to the method of Fech and Dewitt.[7]

Results

Antioxidant Levels - For this study, the measured antioxidant levels in the solid and cellular compounds by HPLC were generally lower than the targeted values by weight check but they fell within acceptable limits considering the sensitivity of the HPLC method to the sample extraction method. Table 1 gives the HPLC results expressed as % of weight added. Within the scattering of the data, they did not appear to be affected by the level of mixing in the compounds. Moreover, the pellet samples contained about the same level of antioxidants as the "pig" samples indicating that little or no consumption of antioxidants took place in the pelletizing extruder. This conclusion was further supported by the OIT measurements.

OIT Of Pellet Samples - Tables 2 and 3 list the OIT data from the five labs on the solid and foam compounds respectively. Figures 2 and 3 show these data graphically for the solid and cellular pellets. Within a given set of data, the standard deviation was less than 10%. For a given lab, there were no significant differences in OIT values on the pellet between the High Intensity Mixing and Low Intensity Mixing. OIT values on the "pig" and pellets also fell within the same range, particularly when the measured levels of antioxidants were comparable. In the round robin tests, variations in average OIT among the five labs involved were noticeable. For the solid samples, the average OIT ranged from 165 to 208 minutes, while on the cellular samples they ranged from 179 to 220 minutes. No attempt was made to reconcile the differences in OIT since there has been an industry working group addressing this concern, looking into a proposed test method to reduce lab to lab variability.

OIT Of Shaved Pellets vs. Molded Samples - The data shown in Tables 4 and 5 are for the solid and cellular insulation compounds respectively. Within each set of five values, the OIT of molded samples gave lower variations than those from the shaved pellets. More data would be required to confirm the advantages of molded samples over shaving from pellet in OIT testing. The ASTM procedure D 4565 recommends cold compression of the insulation compounds into thin film before punching out the sample. This does not appear to be practical nor necessary for tests in aluminum pan.

OIT At High Temperatures - OIT measurements at 220°C were also performed in Lab 1. The samples with High Intensity Mixing showed a 5 to 10% higher OIT than those with Low Intensity Mixing in both the solid and cellular insulation compounds, Table 6 and 7. This increase however, came from a very low 25 to 30 minutes OIT. It made the absolute difference rather small, and stay within the experimental error, of the order of 3 to 5 minutes. On the other hand the OIT at 200°C ran almost 10 times longer. With OIT data generated at a number of selected temperatures, an Arrhenius plot of the logarithm of OIT as a function of the reciprocal absolute temperature could be made. Within a limited range of temperatures the resulting plot is normally linear. This allows extrapolation of OIT to a number of temperatures. The error is usually small unless a different degradation mechanism occurs during the test in which case there is a change in the slope of the line. This approach is not appropriate to extrapolate to use temperatures which are at solid phase temperatures.

OIT Along Solid And Foam Skin Wire - OIT data were collected on the wire insulation at one foot intervals. On the solid wire with the conductor out or conductor in (Table 8, Figure 4), the OIT values fell within the same range of those of pellets (see Table 2) of about 200 minutes. They were also quite close to one another within each set of data. The results concurred with a previous study linking the small reduction in the level of the antioxidants to the lower ratio of copper to polyethylene in the solid than in the foam insulation.[4] In addition, the OIT from the Low Intensity Mixing was comparable to the OIT from the High Intensity Mixing.

On the foam skin wire with conductor out (Table 9, Figure 5), the OIT values on the wire were about 15% lower than those of the pellets (See Table 3). This has been brought about by a depletion during processing in the level of antioxidants resulting from chemical reactions among the additives in the compound. In contrast with conductor in, the OIT dropped to one fourth of those of the pellet. The mechanisms leading to the lower OIT values on foam skin wire with conductor in have been the object of many investigations.[4,8] The proposed mechanism involves the interaction of the MD and the blowing agent in the presence of copper which reduces the level and effectiveness of this antioxidant.

On both the solid and the foam skin wires, no significant differences were observed between the OIT from the High Intensity and Low Intensity Mixing. It appears that with the developed compounding technology used in this study and in our manufacturing process, the mixing intensity achieved in the mixer and pelletizing extruder was more than adequate to provide a uniform distribution of antioxidants in the produced compounds and along the wires.

Conclusions

OIT data on the solid and cellular compounds, and on the solid and foam skin wires at High Intensity and Low Intensity Mixing show that with the developed compounding technology, good uniformity of antioxidants is achieved in the pellets and along the wires. The results suggest that failures observed on telecommunication cables are caused by factors other than antioxidant uniformity in polyethylene insulation. The small variations in OIT values within each set of data also appeared to validate the suitability of OIT testing as a quality control tool for a quick check on the level of stabilizers in polyethylene insulation compounds when calibrated for a given stabilization package in a particular compound. The differences in OIT among the various labs confirm that more work needs to be done in standardizing the test equipment and procedure. This will be particularly critical if OIT values are included in the product and cable specifications.

Acknowledgements

The authors would like to thank T. Caulkins, N.D. Wilson, Union Carbide, and C. Duffy, S. kelly, AT&T for generating the OIT data, A. Dewitt, Union Carbide for the HPLC work, and Dr. T.S. Dougherty, AT&T-NS Phoenix, for manufacturing the insulated wires.

References

1.) J.B. Howard, "Stabilization Problems With Low Density Polyethylene Insulation," Proceedings Of The 21st International Wire And Cable Symposium (IWCS), 329 (1972).

2.) M.G. Chan, "High Density Polyethylene For PIC Insulation: Oxidative Stability," Proceedings Of The 23rd IWCS, 34-41 (1974).

3.) D.D. O'Rell, A. Patel, "Oxidative Stability Studies On Cellular High Density Polyethylene Insulation For Communication Wire," Proceedings Of The 24th IWCS, 231-236 (1975).

4.) M.G. Chan, V.J. Kuck,F.C. Schilling, K.D. Dye, L.D. Loan, "Stabilization Of Foamed Polyethylene Communication Cable Over Copper Conductors," International Conference On Advances In The Stabilization And Degradation Of Polymers, 11-21 (1991).

5.) G.D. Brown, L.E. Davis, "Evaluation Of Materials For Improved Life Expectancy Of Foam Skin Insulation," Proceedings Of The 36th IWCS, 734-743 (1987).

6.) G.D. Brown, "Performance Of HDPE Insulation Antioxidants In Filled Telephone Cable Applications," Proceedings Of The 36th IWCS, 337-343 (1987).

7.) J. Fech, A. Dewitt, "Copper Inhibitor And Antioxidant Levels In HDPE: Their Measurement By High Performance Liquid Chromatography And Relation To Insulation Life," Proceeding Of the 29th IWCS, 327-330 (1980).

8.) M.G. Chan, H.M. Gilroy, L. Johnson, W.M. Martin, "Copper Deactivators For Polyolefin Insulation," Proceedings Of The 27th IWCS, 99-106 (1978).

TABLE 1: ANTIOXIDANT LEVEL* BY HPLC IN SOLID AND CELLULAR HDPE COMPOUNDS IN PERCENT OF WEIGHT ADDED

1.1: SOLID INSULATION

	AO		MD	
SAMPLES CONDITIONS	LAB 1	LAB 2	LAB 1	LAB 2
LOW MIXING "PIG"	88	86	89	84
LOW MIXING PELLET	86	84	87	84
HIGH MIXING "PIG"	92	90	89	97
HIGH MIXING PELLET	100	89	103	84

1.2: FOAM INSULATION

	AO		MD	
SAMPLES CONDITIONS	LAB 1	LAB 2	LAB 1	LAB 2
LOW MIXING "PIG"	76	82	81	97
LOW MIXING PELLET	79	92	81	94
HIGH MIXING "PIG"	86	88	92	100
HIGH MIXING PELLET	88	86	94	86

* Duplicate Analysis

TABLE 2: SOLID INSULATION -- OXIDATION INDUCTION TIME (MINUTES) OF SHAVED PELLETS ISOTHERMAL TEMPERATURE = 200°C

	LOW MIXING "PIG"	HIGH MIXING "PIG"	LOW MIXING PELLET	HIGH MIXING PELLET
LAB 1	208	207	186	180
	201	202	194	184
	217	200	197	209
	186	209	200	169
	168	202	205	190
MEAN	196	204	197	186
SD*	19.3	3.7	7.2	14.8
LAB 2	179	191	181	185
	188	194	171	187
	187	178	186	190
	191	191	183	182
		192	167	193
MEAN	186	189	178	187
SD	5.1	6.4	8.2	4.3
LAB 3	219	205	169	203
	208	204	194	196
	204	203	205	203
	202	210	200	213
	207	220	197	195
MEAN	208	208	193	202
SD	6.6	7.0	14.0	7.2
LAB 4	181	180	174	188
	182	182	189	196
	181	193	180	195
		190	170	179
		176	213	167
MEAN	181	184	185	185
SD	0.6	7.1	17.1	12.1
LAB 5	178	184	164	161
	178	180	169	168
MEAN	178	182	167	165
SD	0.3	2.8	3.7	5.3

* Standard Deviation

TABLE 3:FOAM INSULATION -- OXIDATION INDUCTION TIME (MINUTES) OF SHAVED PELLETS ISOTHERMAL TEMPERATURE = 200°C

	LOW MIXING "PIG"	HIGH MIXING "PIG"	LOW MIXING PELLET	HIGH MIXING PELLET
LAB 1	195	192	229	227
	218	203	209	220
	197	207	219	219
	229	228	240	227
	211	240	240	232
		184	200	
			235	
MEAN	210	209	224	225
SD*	14.3	21.2	16.0	5.4
LAB 2	205	214	193	212
	187	206	200	204
	194	204	196	205
	191	210	215	208
	186	196	209	207
MEAN	193	206	203	207
SD	7.6	6.8	9.2	3.1
LAB 3	206	235	235	233
	208	223	229	222
	194	213	202	239
	182	214	217	207
	219	218	220	196
MEAN	202	221	221	219
SD	14.2	9.0	12.6	17.9
LAB 4	188	197	189	194
	202	197	208	226
	218	204	212	206
	189	208	207	217
	195	212	206	221
	190	212		216
	203			
MEAN	198	205	204	213
SD	10.8	6.9	8.9	11.6
LAB 5	181	185	177	186
	183	188	181	183
MEAN	182	187	179	184
SD	1.8	2.3	2.7	2.0

* Standard Deviation

TABLE 4: SOLID INSULATION -- OXIDATION INDUCTION TIME (MINUTES) OF SHAVED PELLET VS PRESSING

ISOTHERMAL TEMPERATURE = 200°C

LOW MIXING "PIG"	*	208	201	217	186	168
	**	201	195	181	198	193
HIGH MIXING "PIG"	*	207	202	200	209	202
	**	199	179	199	194	202
LOW MIXING PELLET	*	186	194	197	200	205
	**	193	198	195	201	201
HIGH MIXING PELLET	*	180	184	209	169	190
	**	183	190	208	194	208

TABLE 5: FOAM INSULATION -- OXIDATION INDUCTION TIME (MINUTES) OF SHAVED PELLET VS PRESSING

LOW MIXING "PIG"	*	195	218	197	229	211
	**	199	214	217	220	
HIGH MIXING "PIG"	*	192	203	207	228	>240
	*	184				
	**	222	216	222	222	225
LOW MIXING PELLET	*	229	209	215	>240	>240
	*	200	235			
	**	211	207	224	234	209
HIGH MIXING PELLET	*	227	220	219	227	232
	**	210	211	214	202	228

* FROM SHAVED PELLETS

** FROM PRESSING

TABLE 6: SOLID INSULATION -- OXIDATION INDUCTION TIME (MINUTES) AT ISOTHERMAL TEMPERATURE OF 220°C

LOW MIXING "PIG"	28	28	28
HIGH MIXING "PIG"	29	31	33
LOW MIXING PELLET	27	27	27
HIGH MIXING PELLET	29	29	30

TABLE 7: FOAM INSULATION -- OXIDATION INDUCTION TIME (MINUTES) AT ISOTHERMAL TEMPERATURE OF 220°C

LOW MIXING "PIG"	26	29	30
HIGH MIXING "PIG"	30	28	30
LOW MIXING PELLET	29	26	30
HIGH MIXING PELLET	33	33	33

TABLE 8: OXIDATION INDUCTION TIME (MINUTES) ALONG SOLID INSULATION WIRE

	LAB 1		LAB 2		LAB 3	
	CONDUCTOR OUT		CONDUCTOR IN		CONDUCTOR IN	
	HIGH MIXING	LOW MIXING	HIGH MIXING	LOW MIXING	HIGH MIXING	LOW MIXING
	212	192	168	186	178	172
	203	197	174	170	179	186
	219	200	174	177	179	188
	203	200	181	181		188
	212	196	184	173		
	205	197	188	159		
	204	200	186	173		
	209	199	179	167		
	205	202	175	168		
	213	197	181	173		
MEAN	208	198	179	173	179	184
SD*	5.3	2.8	6.2	8.3	0.6	7.7

* Standard Deviation

TABLE 9: OXIDATION INDUCTION TIME (MINUTES) ALONG FOAM/SKIN INSULATION WIRE

	LAB 1				LAB 2		LAB 3			
	HIGH MIXING		LOW MIXING		HIGH MIXING	LOW MIXING	HIGH MIXING		LOW MIXING	
	COND. OUT	COND. IN	COND. OUT	COND. IN	COND. OUT	COND. OUT	COND. OUT	COND. IN	COND. OUT	IN
	197	53	194	49	155	164	188	55	188	51
	172	57	182	52	147	166	188	57	189	53
	200	55	188	53	171	168	192	59	190	54
	197	52	176	54	153	160	200	60	196	
	200	65	151	48	179	195	220		211	
	205	51	193	51	156	174				
	192	63	194	61	177	153				
	202	67	203	54	188	186				
	201	56	187	45	157	163				
	203	63	182	48	159	175				
					178	173				
MEAN	197	58	185	52	165	171	198	58	195	53
SD*	9.5	5.7	14.1	4.5	13.5	11.9	13.4	2.2	9.6	1.5

* Standard Deviation

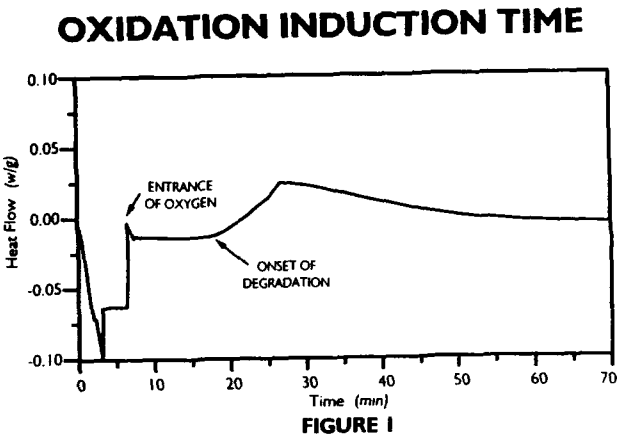


FIGURE 1

FIGURE 2

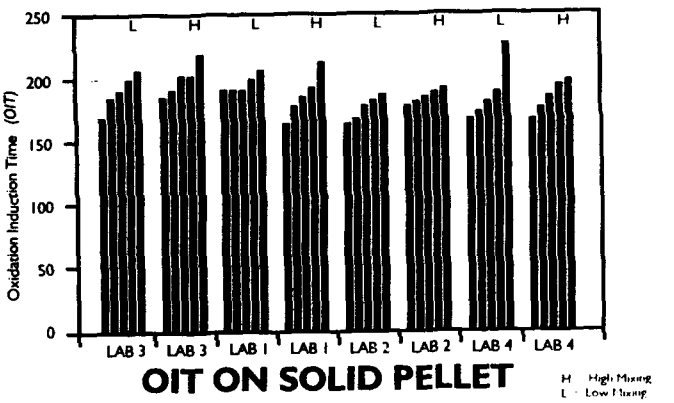


FIGURE 3

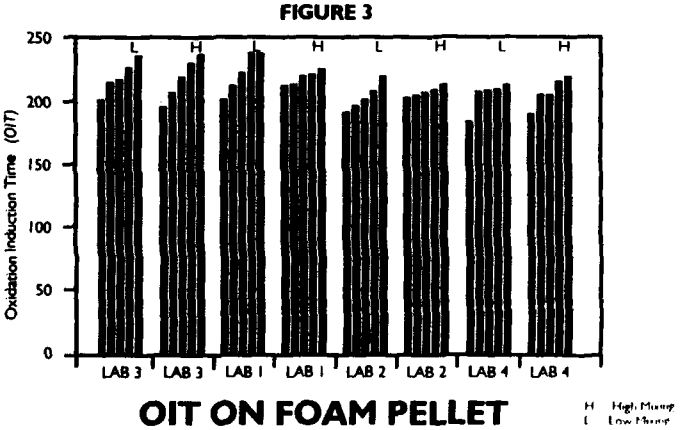
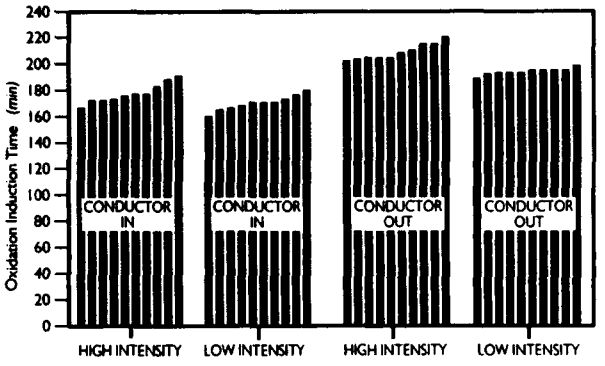
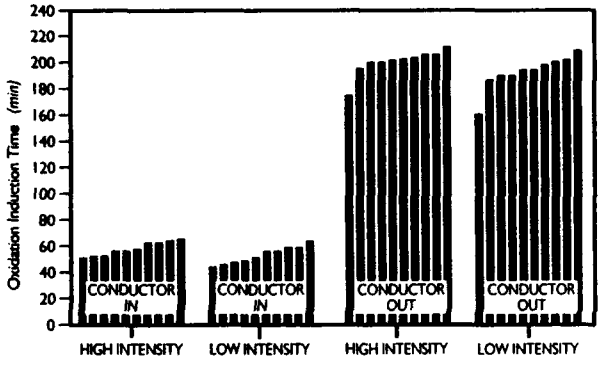


FIGURE 4



OIT ALONG SOLID INSULATED WIRE

FIGURE 5



OIT ALONG FOAM-SKIN WIRE



Yimsan Gau joined Union Carbide in 1979 and is currently a Senior Development Scientist. He has been involved in solids handling, polymer processing and product development. A native of Cambodia, Yimsan obtained his undergraduate degrees from the French Naval Academy in 1969 and the U.S. Naval Post Graduate School in 1975, and his Ph.D. in Mechanical Engineering/Corrosion in 1979 from the University of California at Berkeley.



Karen D. Dye graduated from New Mexico Institute of Mining and Technology in 1982 with a B.S. in Chemistry. She joined AT&T Network Systems (Phoenix Works) in 1985, where she is an Engineer in the Materials Laboratory. She is involved in analysis of raw materials, final product evaluations, and development work. Her area of special interest is analytical methods development.



E.D. Nelson has been with AT&T Bell Laboratories for 25 years. He is currently a member of the Chemistry Group in the Materials Engineering Department. He received a B.S. degree in Chemistry from St. Francis College and a M.S. degree in Engineering Science from the Newark College of Engineering. His interests include fire and smoke properties as well as oxidative stability of polymeric materials.

INVESTIGATION OF FACTORS AFFECTING LONG TERM HEAT STABILITY OF POLYOLEFIN INSULATION RESINS

Koksal Tonyali

Quantum Chemical Corporaton
11530 Northlake Drive, MSN-43G2
Cincinnati, OH 45249

ABSTRACT

Cracking of polyolefin telephone insulations has been observed in the field over the last two decades. Depletion of stabilizers from the insulations has been identified as a major cause for these failures. A study was initiated in our laboratories to elucidate the antioxidant extraction mechanism and thereby develop an improved additive package. Oxidative induction time (OIT) measurements and high performance liquid chromatography (HPLC) techniques were utilized to characterize the stabilizer level in polyethylene. The stabilizer depletion mechanism was observed to be dependent on the chemical structure, the thermal stability of the antioxidant system, and the chemical composition of the filling compound. The stabilizer extraction process is identified to include several steps; first, initial plasticization or the swelling of the insulation resin by the filling compound, and then either the diffusion of the stabilizer molecules or the dissolution of the stabilizer by a component of the filling compound. These processes result in outward migration of antioxidants from the insulation into the filling compound due to low compatibility of stabilizers with polyethylene and the chemical potential difference between the insulation and the filling compound. A new stabilizer system has been developed to reduce the extraction of the additives. Furthermore, a synergistic effect was observed when the proposed stabilizer was used in the presence of the current known antioxidants for polyolefin telephone insulation resins.

INTRODUCTION

Foam-skin high density polyethylene (HDPE) insulations have been found to be susceptible to thermal oxidation and cracking [1-11]. Environmental factors such as heat, light, oxygen and physical stress are known to accelerate this deterioration. Installations in the southern U.S.A., e.g., Arizona, have experienced cable failures in the field [1]. The degradation of the material has been related to the depletion of the antioxidants from the insulations. As a result of this observation, the stabilizer levels incorporated into the HDPE resins have been increased to prevent cracking.

A combination of a phenolic type primary antioxidant and a metal deactivator is commonly used to protect polyolefin compositions used to insulate copper conductors [5,12]. A stabilizer formulation containing pentaerythrityl tetrakis[3(3',5'-di-t-butyl-4'-hydroxy phenyl) propionate] (AO-1) and N,N'-bis[3,(3',5'-di-t-butyl-4' hydroxy phenyl) propionyl]hydrazine (AO-2) was demonstrated to be the most effective.

Absorption of moisture by the telephone insulations results in poor communication quality, such as cross-talk [12]. To prevent or minimize this problem, various water-blocking filling compounds are forced under pressure into the cable cores to fill the voids and interstices therein. The water-blocking agents are usually hydrocarbons of heavy oil or waxy compounds. While these cable fillers have generally proven to be effective water repelling agents, they have a tendency to extract stabilizers from the insulation materials [1-12]. There is a significant decrease in the stabilizer protection level after exposure to the water-blocking agents for a period of time. The use of water repelling agents in a cable construction leads to premature failure although the oxidative heat stability of the insulation may have been adequate initially.

A comparative study [12] concluded that heat aging in the presence of petrolatum reduced the stability of solid polyethylene by 35 percent and of cellular (foamed) polyethylene by 10-40 percent. The choice of the stabilizer package, i.e., a primary antioxidant and a metal-deactivator, is therefore even more critical where the insulated conductor is used in conjuction with a water-blocking cable filler. After evaluating numerous primary antioxidant/metal deactivator combinations, Brown [5] suggested that the AO-1/AO-2 combination was the most effective system when incorporated at high levels.

In this paper, the current knowledge of the insulation aging is reviewed and the requirements for a good stabilizer package are defined. The extraction mechanisms for the individual stabilizer components are discussed. A new antioxidant system, which imparts superior oxidative stability to polyethylene insulation resins in the presence of cable filler compounds, is proposed.

EXPERIMENTAL

The high density polyethylene (HDPE) used in this work was a hexene copolymer with a melt index of 0.70 g/10 min. and a density of 0.947 g/cc. The antioxidants used for the extraction studies were:

AO-1: Pentaerythrityl tetrakis[3(3',5'-di-t-butyl-4'-hydroxyphenyl)propionate] - a primary antioxidant;

AO-2: N,N'-bis[3,(3',5'-di-t-butyl-4'-hydroxyphenyl)propionyl] hydrazine - a metal deactivator;

AO-3: A proprietary stabilizer - a primary antioxidant; and

AO-4: 2,2'-Thiodiethyl-bis[3-(3,5-di-t-butyl-4-hydroxyphenyl) propionate] - a primary antioxidant.

These antioxidants will be designated as AO-1, AO-2, AO-3 and AO-4 for simplicity.

The HDPE reactor powders were first dry-blended with the antioxidants in a high speed mixer (Henschel mixer) at 1500 rpm for 5 minutes. The dry blends were then melt-mixed in a twin screw extruder (Leistritz LSM 30.34) at 230°C. The screw speed was set at 250 rpm with an output rate of 7 kg/h. The polymer strands were pelletized after cooling with water. The pellets were extruded into 0.5 mm thick films using a Brabender laboratory-scale extruder.

The films were aged at 70°C in a number of filling compounds, namely, a mineral oil (Penreco - Drakeol 35), a petroleum jelly (Penreco - PE/PJ cable filler - 4585) and a non-petrolatum cable filler (Penreco FW cable filler - 4495). Approximately, 0.5 g of films were aged in 8 g of the cable fillers.

The oxidative induction times (OIT) of aged and unaged samples were measured at 200°C using DuPont 2910 DSC. The OIT measurement procedure employed was as follows: Set initial temperature at 60°C, purge with nitrogen for 5 minutes, ramp temperature at a rate of 20°C/min to 200°C, hold temperature isothermally for 5 minutes, switch to oxygen gas (oxygen and nitrogen flow rate = 50 ml/min), and conclude the test when exothermic signal is observed.

The pellets with various stabilizer formulations were compression molded into 1.8 mm thick plaques at 170°C under 70 MPa. The plaques were water cooled to room temperature and stored for 2 days. Type IV tensile bars per ASTM D-638 were cut and aged at 70°C in the filling compound, Penreco FW cable filler, for 28 days. These tensile bars were then aged further at 110°C for 56 days in an air circulated oven. The mechanical properties of the aged and unaged specimens were evaluated at 5 cm/min using an Instron tensile tester at room temperature. The percent property retention was calculated after the aging process.

High performance liquid chromatography (HPLC) analysis was performed using a similar technique employed by Dye et. al. [7]. The stabilizer extraction was carried out in a microwave oven.

RESULTS AND DISCUSSION

Polymers designed for long term applications require stabilizers which have not only a high stabilizer efficiency but also sufficient ability to remain in the resin during its service life. Thermal stability of polymers is a function of the molecular structure of the polymer and the additives present. A suitable stabilizer must be non-volatile and resistant to extraction, and must have sufficient mobility to diffuse within the polymer matrix [13]. The stabilizer effectiveness is decreased considerably in the absence of these properties.

The properties of the most commonly used stabilizers, AO-1 and AO-2, in the telecommunications industry are shown in Table I [14]. These antioxidants are non-volatile, i.e., high molecular weight, and stable at high temperatures. The solubility values in hexane are also included in Table I. Mineral oils and cable filler compounds are comprised of low molecular weight hydrocarbons higher than that of hexane. Thus, it is assumed that the antioxidants will exhibit similar solubility in cable filling compounds. The solubility is known to increase with increasing temperature [15]. Generally, cable aging is performed at 70°C which enhances the solubility of the stabilizers in the filling compounds leading to extensive antioxidant depletion from the insulation.

A rough estimate indicates that a telephone cable construction contains approximately equal weight amounts of the HDPE insulation

and the filling compound. A calculation using the data in Table I shows that 2000 ppm of AO-1 in the insulation could be dissolved and extracted even at room temperature. Increasing the testing time or the performance temperature will aid the extraction process. However, AO-1 is known to be less extraction resistant than AO-2, probably due to the lower solubility of AO-2 in mineral oils [5,7].

The solubility level of the stabilizers in polyethylenes is also important for stability efficiency since the polymer must hold the antioxidants. The solubility of AO-1 and AO-2 in polyethylene are relatively low [16,17]. The solubility of AO-1 is 0.06 weight% at 60°C. The incompatibility and insolubility of antioxidants in polymers cause rapid depletion of the stabilizer molecules at high temperatures. AO-1 and AO-2 are reported to migrate readily at 70°C in the absence of the filling compounds [16]. AO-2 is almost insoluble in filling compounds (Table I). Thus, the mechanism of migration of AO-2 molecules at high temperatures may be attributed to the diffusion as a result of the incompatibility of the stabilizer with polyethylene.

Low molecular weight hydrocarbons, such as hexane, mineral oil and petroleum jelly, swell and plasticize polyethylenes [15,18]. The presence of low molecular weight molecules in a polymer has a profound effect on the physical properties of resins [18]. It is expected that the amorphous component of a semicrystalline polymer, e.g., polyethylene, absorbs most of the sorbed solvent [15].

HDPE tensile specimens were aged in the filling compound, Penreco FW cable filler, at 70°C for 28 days. The mechanical properties were measured at room temperature before and after aging. The results are presented in Figure 1. The yield stress decreased while the ultimate elongation increased significantly, indicating that the HDPE was plasticized when aged in the filling compound. It is believed that the antioxidant molecules become highly mobile [15] in this plasticized medium, leading to higher diffusion or migration rates from the insulation into the filling compounds. AO-1 will be expected to have higher extraction levels since it is more soluble in the filling compound compared to AO-2. Thus AO-1 is first dissolved by the penetrating mineral oil and then migrates out of the insulation. This process may be similar to leaching.

The solubility data of Moisan [17] indicate that 0.059% AO-1 is the equilibrium solubility value for a polyethylene/AO-1 system. The equilibrium solubility of AO-1 is 0.3% in hexane, i.e., mineral oil or filling compounds, at room temperature (Table I). Thus, the filling compound will dissolve AO-1 as soon as it diffuses into polyethylene. The thermodynamics of a solution [19] suggests that a stabilizer concentration gradient exists between the mineral oil swollen insulation and the external filling compound. Migration of stabilizer will take place to equalize the concentration. However, it is also likely that the filling compound may hold more stabilizer than the insulation since its limiting solubility level is higher. Published data [7], as well as our unpublished observations, support this mechanism.

Stabilizers may be added to the cable filling compounds to prevent the insulation cracking due to the antioxidant depletion. Antioxidant addition may extend the insulation performance but may not totally eliminate failures. AO-2 is not soluble in the filling compound and, thus, the incorporation of AO-2 into the cable filler may not be effective. Therefore, the decision to add stabilizers other than those in the insulation to the filling compound must be made carefully since these additives could migrate into the insulation to equilibrate the chemical potential [19]. The incorporation of stabilizers into filling compounds other than those in the insulation does not necessarily eliminate the failure of the insulation although some improvement in stabilization may be observed. Furthermore, most of the sorbed antioxidants could leach out of the insulation with the filling compound during the desorption process once the cable is exposed to air.

The effect of the addition of the stabilizers to the filling compounds on the oxidative induction times (OIT) were studied in Figure 2 using various antioxidants. OIT is often utilized to characterize the degradation of the insulation [5-9]. However, OIT method only determines the presence of the antioxidants in the polymer. Films with AO-1 and AO-2 were aged in the filling compound, Penreco FW cable filler with 0.6% stabilizer, at 70°C for 14 days. The OIT retention is shown in Figure 2. The retention of the OIT values is higher with the samples exposed to the filling compound containing AO-4 compared to AO-1, AO-2. AO-4 is known to be more soluble in the polymer and cable filler [14,16] and, thus, it is expected to migrate into the film at higher levels and at a faster rate. The results in Figure 2 suggests that AO-4 is absorbed by the film. The filling compound with AO-2 had the least effect on OIT since its solubility and compatibility are low. The OIT retention values, however, do not indicate

the exact efficiency of the stabilizer. Some stabilizers may exhibit high OIT values although they are less effective in protecting the polymer.

Cracking of telephone insulations has been observed to occur in air exposed parts above ground, e.g., pedestals. It was reported earlier that filling compounds swell and plasticize the insulation. It is believed that the sorbed filling compound in the insulation permeates out together with the stabilizer when the cable is spliced and exposed to air. This process further reduces the antioxidant level in the insulation. The sorption-desorption process may generate changes in the polymer morphology and reorganization of the crystalline structure [15]. Such changes may create defects or channels which enhance the stabilizer migration and ultimate cracking of the insulation.

The antioxidant depletion in telephone insulations and PIC cracking have led the industry to specify higher levels of stabilizers in the HDPE resins. However, incorporating higher levels of stabilizers has the disadvantage of deteriorating the mechanical properties of the resin, since high loadings of antioxidants are incompatible with polyolefins.

There are two potential solutions to prevent cracking in polyolefin insulations: 1) The elimination of the aggressive component of the filling compound which swells or plasticizes the polymer, or 2) A new stabilizer package that is extraction resistant to filling compounds. Here, the latter solution will be discussed further.

A Proposed Stabilizer Package

A suitable stabilizer package for telephone insulation exposed to cable filling compound must have the following characteristics: a) little or no solubility in filling compounds and b) a slow diffusion or low mobility of the stabilizer molecules at high temperatures.

A proprietary antioxidant (AO-3) exhibiting such properties with a solubility of 0.01% or less in the filling compounds was used to stabilize three HDPE formulations, SF1, SF2 and SF3. The formulations were prepared with compositions [0.2% AO-1 + 0.2% AO-2], [0.1% AO-1 + 0.2% AO-2 + 0.1% AO-3] and [0.2% AO-1 + 0.2% AO-3], respectively. The material was formed into 0.5 mm thick films and aged at 70°C in the unstabilized mineral oil (Drakeol 35). Oxidative induction times (OIT) were measured after various aging times. The data is illustrated in Figure 3.

The OIT results depicted in Figure 3 indicate that a sudden drop is initially observed with the aging time up to 5 days, followed by a constant rate of change in OIT. Similar data have been published in previous studies [5,6,9]. The magnitude of the initial rapid reduction in OIT is greater in SF1 compared to that of SF3.

A surprisingly high OIT value was noticed for unaged SF2 samples compared to SF1 and SF3 (Figure 3). A synergistic effect was obtained in OIT when AO-3 was compounded with AO-1 and AO-2. However, the synergy was almost absent after 5 days of aging. It is believed that most of the stabilizer extraction occurs during the initial days of the aging at which swelling and plasticization of the resin also take place [18]. The swelling enhances the mobility of the stabilizer additives and thus the migration and/or diffusion rate of the stabilizer molecules. It was discussed earlier that the extraction mechanism for AO-1 was due to the migration of the dissolved AO-1 molecules by the sorbed filling compound in the insulation, i.e., leaching effect, whereas AO-2 depleted due to the increased mobility (diffusion constant) of the AO-2 molecules in the plasticized insulation. Thus, it is expected that AO-1 will be extracted faster since it is more soluble and mobile in the swelling agent. The faster initial drop rate in OIT (Figure 3) support this explanation. Therefore, the synergistic effect in SF2 is lost once AO-1 is extracted from the polymer. Figure 3 also illustrates that the OIT values for SF2 and SF3 are 2 to 3 times higher than that of SF1 after the 28 day aging indicating that AO-3 is less extractable by the mineral oil.

The films from SF1, SF2 and SF3 were also aged in the unstabilized filling compound, Penreco FW cable filler, at 70°C for 16 and 28 days. The OIT results are presented in Figure 4. It is clear that AO-3 is more extraction resistant. The additive levels of the 28 day aged samples were analysed utilizing HPLC. The data in Table II implies that almost all of AO-1 migrated out of the sample while the retention values of AO-2 and AO-3 were 20% and 50%, respectively.

The 1.8 mm thick ASTM type IV tensile specimens were prepared from the formulations, SF1 and SF2, and aged in Penreco FW cable filler for 28 days. These cable filler aged specimens were then placed in an air circulated oven for 56 days at 110°C. The retention of the mechanical properties is shown in Figure 5. The data indicate that the formulation with AO-3 (SF2) is superior to that of AO-1 (SF1) in improving the heat stability. These new stabilizer formulations have been extruded onto copper conductors, and are

currently being evaluated in long-term pedestal aging tests.

CONCLUSIONS

1. The filling compounds swell and plasticize polyolefin insulations.

2. The swelling creates a mobile medium where the diffusion and/or migration of the antioxidant molecules are facilitated.

3. It is believed that AO-2 diffuses out of the insulation since it is compatible with the polymer at low levels, and the diffusion rate is increased due to the plasticization of the insulation caused by the sorbed filling compound component.

4. AO-1 is highly soluble in the filling compound compared to the polyethylene insulation. Thus, the sorbed component of the filling compound dissolves and leaches AO-1.

5. A new stabilizer package has been developed. This system is insoluble in cable filling compounds and resists extraction. The initial evaluation shows that the heat stability is superior to the current stabilizer packages.

REFERENCES

1. T.N. Bowmer, Proceed. 37th Int. Wire Cable Symp., 475, 1988.

2. L.E. Davis, Proceed. 37th Int. Wire Cable Symp., 484, 1988.

3. W. Englehart and R. Hayes, 35th Int. Wire Cable Symp., 252, 1986.

4. L.P. Beltz, Proceed. 38th Int. Wire Cable Symp., 123, 1989.

5. G.D. Brown, Proceed. 36th Int. Wire Cable Symp., 337, 1987.

6. G.D. Brown and L.E. Davis, 36th Int. Wire Cable Symp., 734, 1987.

7. K.D. Dye, V.J. Kuck, F.C. Schilling, M.G. Chan, and L.D. Loan, Proceed. 38th Int. Wire Cable Symp., 98, 1989.

8. T.N. Bowmer, E.P. Hjorth, R.J. Miner, and O.S. Gebizlioglu, Proceed. 37th Int. Wire Cable Symp., 490, 1988.

9. T.N. Bowmer, R.J. Miner, I.M. Plitz, J.N. D'Amico, and L.M. Hore, Proceed. 39th Int. Wire Cable Symp., 316, 1990.

10. K. Dawes, T.A. Hunter, and C.M. Chan, Proceed. 39th Int. Wire Cable Symp., 328, 1990.

11. T.N. Bowmer, R.J. Miner, and R.C. Coker, Proceed. 39th Int. Wire Cable Symp., 335, 1990.

12. Plastics Additives Handbook, Ed. R. Gachter and H. Muller, Hanser Publishers, 1987.

13. Photodegradation, Photo-oxidation and Photostabilization of Polymers, B. Ranby and J. Rabek, Wiley, London, 1975.

14. Antioxidants for Polyolefins, Ciba-Geigy Catalog, 1987.

15. C.E. Rogers, Chapter 15 - Polymer Films as Coatings in "Surfaces and Coatings related to Paper and Wood", Syracuse University Press, Syracuse - New York, 1967.

16. B.L. Board and H.J. Rudell, Proceed. 31th Int. Wire Cable Symp., 300, 1982.

17. J.Y. Moisan, Plast. in Telecommun., 2nd Int. Conf., 26.1, 1978.

18. C. Gieniewski and L.L. Blyler Jr., Proceed. 30th Int. Wire Cable Symp., 270, 1981.

19. Physical Chemistry of Macromolecules, C. Tanford, Wiley, New York - London - Sydney, 1961.

Table I: Properties of Stabilizers

PROPERTY	AO-1	AO-2
DENSITY (g/cc)	1.15	1.11
MOLECULAR WEIGHT	1178	553
MELT TEMPERATURE (C)	110-125	224-229
TEMPERATURE AT 1% WEIGHT LOSS	310	240
SOLUBILITY IN HEXANE AT 20 C	0.3	<0.01%

Table II: HPLC Analysis of Stabilizers

SAMPLE	AO-1 (ppm)	AO-2 (ppm)	AO-3 (ppm)
SF1	15	430	--
SF2	0	405	477
SF3	--	415	1172

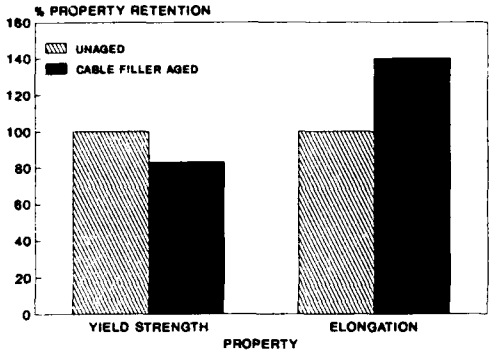


Figure 1. Property Retention After Aging in a Cable Filler

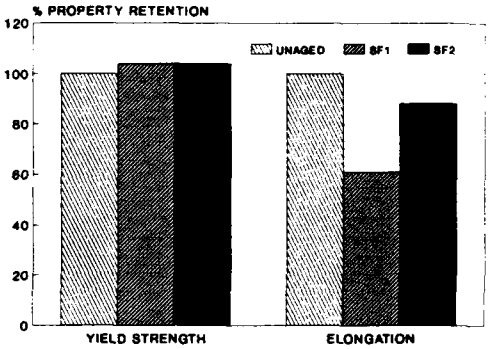


Figure 5. Property Retention After Oven Aging the Filling Compound Exposed Tensile Specimens

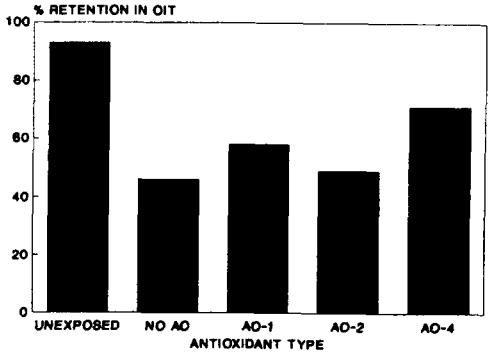


Figure 2. The Effect of Stabilized Filling Compounds on OIT

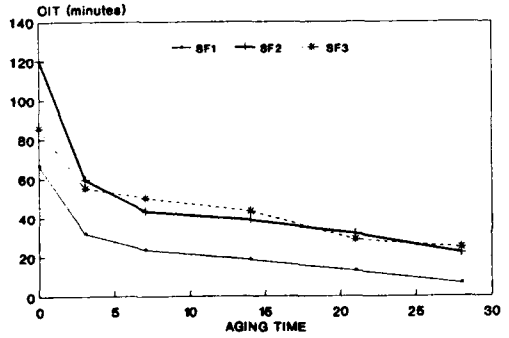


Figure 3. The Effect of Aging Time on OIT

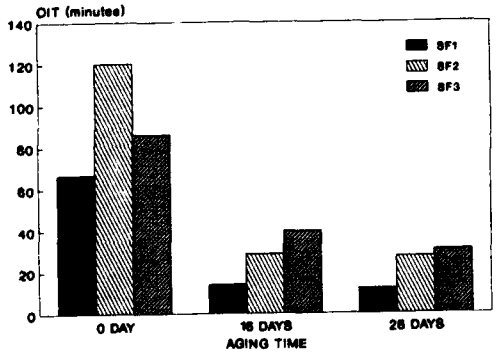


Figure 4. OIT Results of Cable Filling Compound Aged Films



Koksal Tonyali receieved a B.Sc. degree in Polymer Science and Technology from University of Manchester Institute of Science and Technology, and his M.S. and Ph.D. degrees in Polymer Science and Engineering from Case Western Reserve University in 1985 and 1986, respectively. He worked on radiation effects on polymers as a postdoctoral research associate at Washington State University before joining Quantum Chemical Corporation in 1988. He is currently a member of the Wire and Cable Product Development Group at Quantum. His research interests include environmental effects on polymers, fracture mechanics and environmental stress cracking, structure-property relationships in materials, blends and alloys, polymer pocessing, and reactive processing.

REMEDIAL STRATEGIES FOR POLYOLEFIN INSULATIONS IN OUTSIDE PLANT

Trevor N. Bowmer and Joseph N. D'Amico

Bellcore

Red Bank, New Jersey 07701

ABSTRACT

There is 1.3 million miles of buried cable containing ~350 million miles of polyolefin insulated conductors (PIC) installed in the outside plant of the Regional Bell Operating Companies of the USA. Cracked PIC insulations have caused recurring problems over the last 25 years in aboveground closures. This paper discusses various proactive remedial actions available for installed outside plant to extend PIC insulation lifetime and reduce the effects of thermal oxidative degradation. For example, airtight closures can increase insulation lifetimes sixfold or temperatures inside typical outside plant closures can be reduced by 20-25°F and thereby double field lifetimes of PIC insulations. Both laboratory aging studies and field trial results will be used to determine the quantitative effects of airtight sealing of plant, temperature reduction, solvent cleaning and other plant practices on the stability of PIC insulations.

INTRODUCTION

The seven Regional Bell Operating Companies (RBOCs) in the USA have $160+ billion dollars invested in the outside plant of their networks and spend ~$20 billion dollars annually to upgrade and maintain this plant. A significant fraction of this plant is the 1.3 million miles of buried cable containing ~350 million miles of polyolefin insulated conductors (PIC) [1].

These PIC cables are subjected to a variety of field conditions with the aboveground open-access pedestal environment being one of the worst; e.g., temperatures as high as 150°F were recorded in pedestals in Arizona. Over the last 25 years, several episodes of insulation failure in pedestals were attributed to the thermal oxidation of the polyolefin insulation[2-11]. During the 1980s, the discovery of cracked insulations in the latest foam-skin design of high density polyethylene (HDPE) insulations initiated extensive studies on the thermal oxidative degradation of polyethylene insulations[5,6,8,9,12-17] as well as on the appropriate thermal stability tests[12,14,16-20] for new PIC cable products. Although improved thermal stability requirements[21] for PIC insulations will ensure that the new PIC cable products are adequate for the field environments, these new requirements will not affect the 350 million miles of wire already installed. Therefore remedial action strategies are essential to maximize the useful lifetime of the copper plant until optical fiber transmission becomes universal.

This paper will discuss various proactive remedial actions available for installed outside plant to extend polyolefin insulation lifetime and reduce the effects of thermal oxidative degradation. Both laboratory aging studies and field trial results will be used to determine the efficacy of airtight sealing of plant, temperature reduction by closure modification, solvent cleaning and other plant practices.

EXPERIMENTAL

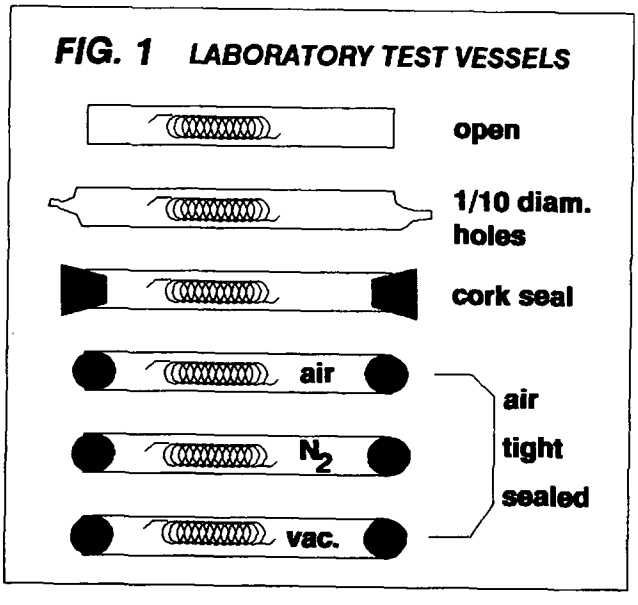
Oxidative Induction Time (OIT) Analysis : The OIT value for an insulation is defined as the elapsed time at a specified temperature in oxygen before the exothermic oxidation reaction is observed[22-25]. The OIT value is known to be proportional to stabilizer content and insulation lifetime for a given insulation and stabilizer package[20,22]. The insulation is typically stripped from the copper wire and analyzed in aluminum pans with a Du Pont 1090 calorimeter at 200°C.

Aging Tests : Samples were wound in tight coils and aged in laboratory pedestals heated to temperatures between 60 and 110°C. Other coiled samples were aged in forced-air ovens at temperatures between 60 and 100°C. The test apparatus and procedure for both pedestal tests and oven tests are detailed elsewhere[19-21].

Sealed Plant Experiments : Insulated wire samples were collected in Mobile, Alabama, from 1984 vintage cables installed into both open-access pedestals and pedestals containing secondary airtight enclosures. The secondary enclosure, consisting of a plastic shroud with an airtight seal at the cable entry point, isolated the exposed wireworks (splices, connections, etc..) from the environment. Cable #1 was a 25 pair filled cable containing 24 AWG wire insulated with foam-skin HDPE. Cable #2 was a 50-pair filled cable with 22AWG wire insulated with foam-skin HDPE. Four or

six insulated wires were sampled from four pedestal closures on each cable run and their residual stability was measured by OIT analysis.

Laboratory aging tests were performed using copper wires (26AWG) insulated with foam-skin HDPE from a standard commercial cable. A blue/white pair was selected from the cable and pre-aged in a forced-air oven until the OIT-values of the insulations were low; i.e., 2-4 mins. These insulated wire samples were aged in ovens and pedestals as tightly wrapped coils. Different plant closure designs were simulated using glass tubes sealed to varying degrees as illustrated in Figure 1.



Closure Cooling Field Trial : Commercial cables were selected for a field trial in Mesa, Arizona, to include:

- different cable vintages (1987,1989 & 1991)
- different insulation types (solid & foam-skin HDPEs)
- different insulation stabilizer packages
- filling compounds with different stabilizer packages.

Standard green metal pedestals (6x6x48 inch) were either used "as received" from Champion Metal Products, painted tan or white, or protected with a white vented aluminum cover. The experimental details of the reflective paints, pedestal covers, thermocouple placements used at the site are given elsewhere[17]. For each closure, a 3-4 foot section of cable was cut and the outer black jacket, metallic shields and the mylar core wraps were removed from one end for about 2 feet. To simulate typical open-access outside plant, a prepared cable piece was placed in each closure with the exposed insulated wires in the top section of the closure and the sheathed cable end buried in gravel at the bottom of the closure. The exposed insulated wires were fanned out and looped over the plastic bracket supplied with each pedestal. Samples were taken after 56 and 153 days field exposure and the insulation stability measured by OIT analysis.

Solvent Cleaning of Insulated Wires : Fifty insulated wires were selected from a 1989 vintage PIC cable for the solvent cleaning experiments. Fourteen solvents were chosen to cover a broad range of solubility parameters[26] (i.e., δ values of 6.6 to 23.4 $(cal/cm^3)^{1/2}$). The wires (30-35 cm) were placed in a sealed glass jar with 500-800 ml of solvent and shaken vigorously for 2-5 minutes. After 30 minutes, the jars were opened and the "cleaned" wires were removed and allowed to air-dry at room temperature. After a visual and tactile inspection, a rating between 1 and 10 was given for cleaning efficiency.

1-3 = poor solvent, insulations still greasy
4-7 = 40-70% of filling compound removed (still greasy to touch)
8-10 = no filling compound detected

For each set of wires, the white/slate and blue/black pairs were selected and the OIT values for these insulations were measured at 200°C. These OIT values were then compared to reference OIT values measured on insulations simply wiped with a clean dry paper towel.

RESULTS AND DISCUSSIONS

Figure 2 illustrates the options and decision process for determining the most appropriate remedial action for a company's outside plant. Field survey data combined with laboratory test results can predict the average percentage of PIC insulations susceptible to thermal oxidation cracking for a given geographic region and closure type[6,8]. Based on these predictions and the associated maintenance/repair costs, various actions can be contemplated including :

- No Action
- Modify Physical Plant
- Improve Plant Practice
- Cable/Wire Replacement

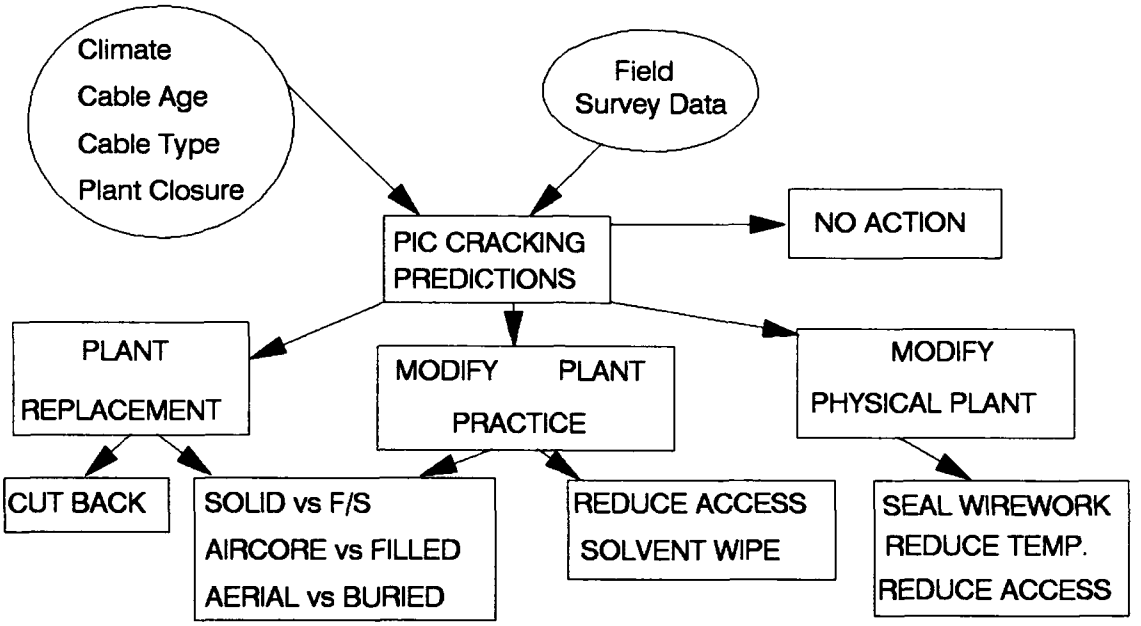
The laboratory and field data relevant to these remedial options shall be discussed below.

Cracked Insulations and the No Action Option

In the mid-1980s, annular cracks were found in foam-skin insulations in aboveground closures where cable jackets are removed to permit connections and splices. These cracked insulations produced unacceptable noise and crosstalk problems. OIT values were measured for insulations gathered from around the USA and we concluded that the probability an insulation was cracked or was vulnerable to oxidation increased as the

FIG. 2

DECISION CHART FOR REMEDIAL ACTION STRATEGY



(i) exposure temperature increased,
(ii) insulation thickness or wire gauge decreased,
(iii) field exposure (i.e., cable age) increased and
(iv) physical stress on the insulation increased.

Our field survey data (summarized elsewhere[6,8]) can be combined with laboratory aging tests to predict the average percentage of cracked insulations to be expected for a given geographic region. For example, Figure 3 plots the percentage of cracked insulations in aboveground closures for a typical RBOC located between 30° and 40° north latitude that has ~60% of its 300,000 cable miles and ~40% of its 70 million wire miles as buried plant. This RBOC would have about 1.5 million aboveground closures. Figure 3 shows four possible scenarios -

- Curve A - If all future PIC insulations have 1980-85 stabilizer levels.
- Curve B - If all future PIC insulations have 1989-90 stabilizer levels.
- Curve C - If all future cables (after 1992) meet the requirements of Bellcore TR-000421[21].
- Curve D - If proactive remedial actions proposed in this memorandum are implemented for 1-2% of the PIC plant per year.

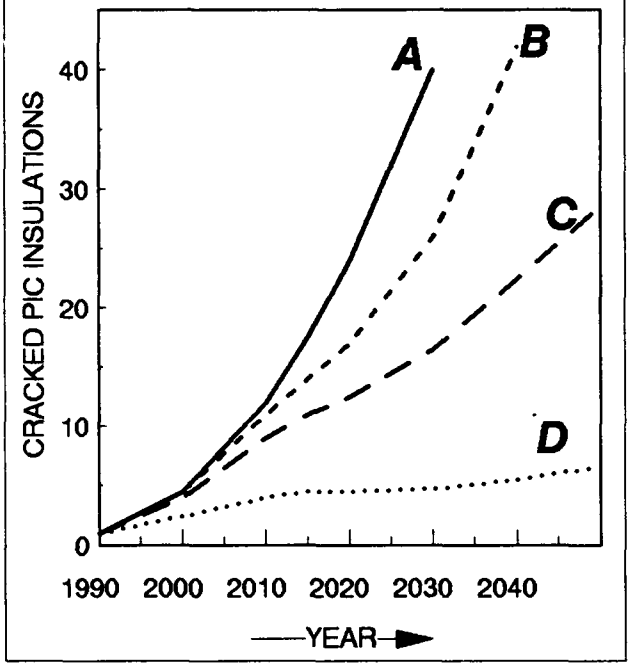
Between 1985 and 1992, many manufacturers enhanced their stabilizer packages for insulations and filling compounds. However, this improved stability will not have an impact on installed PIC insulations until after the year 2010. For this representative RBOC, insulations that crack between the present and 2010 were installed before any significant increases in stabilizer levels occurred (i.e., before 1986). The improvements represented by curve D in Figure 3 depend on the extent & rate of proactive remedial actions and the particular actions selected.

The first option ("No Option") is to use routine repair/maintenance procedures to control any PIC insulation cracking problems. Two factors may encourage a RBOC to follow the "No Action" option. First, RBOCs with their network mostly in the cooler parts of the country will not experience significant PIC insulation cracking until 2010-2020. Secondly, the strategic business plans of a RBOC may entail rapid deployment of fiber to the customer and therefore complete removal of the copper network before significant cracking problems develop.

Figure 3 predictions assumed that the total amount of buried copper cable will peak during 1990-1995 and begin to decline at ~2%/year. There is debate over the rates at which fiber cable will penetrate the local loop and how fast the copper plant will be replaced or removed. If all copper

FIG. 3

CRACKED PIC INSULATION PREDICTIONS



cable is replaced before 2020, then the cracked foam-skin PIC insulation problems could be ignored by all companies expect those with plant in the hottest climates (i.e., zones 4 and 5 as defined in references 6,8). However, we consider that copper cables will probably remain active in the network much longer than 2020; particularly in the distribution plant nearest to the customer. It will then become more critical to ensure that these copper wire links in the network do not become the weak links in delivering the latest telecommunications services.

Physical Plant Modifications

Airtight sealing of the plant and temperature reduction strategies for aboveground closures are the two most efficient remedial actions available to extend the useful lifetime of currently installed PIC insulations.

Airtight sealing of plant : Field samples showed a marked improvement in insulation stability for wireworks sealed in an airtight secondary closures relative to open-access closures. The OIT values of field insulations sampled from inside airtight closures were 3-4 times larger than the values found for insulations from open-access pedestals. Insulations from cable #1 showed OIT values of 9± 1 min in the open access environment while the OIT values for the insulations from inside pedestals using the airtight closures were 23.5± 1 min. Insulations from cable #2 showed similar results with OIT values of 2.5± 0.5 minutes from open access sites and 10± 2 mins from sealed closures. The initial OIT of the insulation when installed was not known and therefore to determine the quantitative improvement in stability, laboratory experiments were performed with the test vessels shown in Figure 1.

Both pedestal and oven tests showed that the tighter the seal, the larger was the time-to-crack value (t_c) for the insulations. The insulation's lifetime increased because sealing the insulations reduced both stabilizer loss by evaporation and oxygen access to the polyethylene insulation. Insulations are known to crack only if (a) all the

TABLE 1. SEALED PLANT AGING RESULTS

(ped. = pedestal test at 90°C , oven = oven test at 80°C)

TEST VESSEL	LABORATORY TEST	STABILITY FACTOR $\{t_c/t_c(\text{no tube})\}$	EQUIVALENT PLANT CLOSURE OR PRACTICE
no tube	ped./oven	1.0	free-breathing
open tube	ped.	1.0	open access
open tube	oven	1.2	pedestals
tube (1/4" hole)	oven	2.6	plastic & metal bags
tube (1/10" hole)	ped.	2.8	
tube (1/10" hole)	oven	4.0	flood covers
non-airtight seal (corked & taped)	oven	4-6	encapsulated plant
sealed in air	oven	>15	airtight secondary closures
sealed in air	ped.	>32	
seal in nitrogen	oven	>15	sheathed/buried cable
sealed in vacuum	oven	>15	
sealed in vacuum	ped.	>32	

TABLE 2. PROS & CONS OF VARIOUS SEALED PLANT PRACTICES

CLOSURE/PRACTICE	MAJOR ADVANTAGE(S)	MAJOR DISADVANTAGE(S)
• open access pedestals (free breathing)	• easy access for repair, modification, ... • moisture & volatile pollutants easily flushed out	• exposed to environment (e.g. climate, pollutants, vandalism)
• plastic wrappings/bags • metallic mesh bags	• easy installation and re-entry • inexpensive	• mechanical weakness • stabilizer migration into plastic • potential for metal corrosion or electrical grounding/shorting problems
• environmentally sealed closures (e.g., flood covers)	• sealed from environment • flood protection	• any trapped moisture and/or environmental contaminants are retained near wireworks
• secondary closures (e.g., airtight shrouds)	• airtight closure - excludes environment	• can be expensive • re-entry difficult
• encapsulated plant	• sealed from air and environment • excludes water	• stabilizer extracted by oil-based urethane • re-entry difficult and messy
• sheathed/buried cable	• isolated from environment	• inaccessible

stabilizers are lost or reacted, (b) enough oxygen is present to cause oxidation of the polyethylene and (c) the insulations are physically stressed[6,8,10,19,20].

The laboratory results showed that the lifetime of insulations can be increased by 4-6 times with non-airtight seals and by 15+ times with airtight seals. These test vessels were chosen to simulate various plant closures and practices. Table 1 lists the test vessel, relative time-to-crack values (t_c) for insulations in the laboratory tests and the equivalent plant closure/practice. If thermal oxidative degradation is the rate determining step in the deterioration of polyethylene insulations, then insulations inside metallic mesh and plastic wrappings/bags should survive 2-3 times longer than in open access pedestals. Plastic pedestals and flood covers that are used to protect wireworks in flood-prone areas may increase the lifetime before cracking by 2-4 times. During a flood, these closures act on the bell jar principle by creating an air pocket that restricts water entry into the top half of the pedestal where the exposed wires, splices, etc.. are located. Some flood closure designs will also trap heat under sun exposure and the anticipated benefit of flood-type closures may be reduced markedly by increased temperatures inside the closure.

Sealing the plant in encapsulants (e.g., oil-based urethane materials) effectively isolates the wireworks from the environment and increases the insulation stability greater than six times. Similarly, a secondary enclosure with an airtight seal should have a stability increase factor of more than six since the wireworks are enclosed inside an impermeable membrane. These predictions are consistent with other reported studies of encapsulated splices[27] and cable sheaths[6,8] that have shown high and/or stable OIT values after long term aging.

However, each of the various sealed plant practices have their own advantages and disadvantages, see Table 2. For example, in open-access pedestals, moisture and pollutants can move easily from the outside environment into the pedestal and may accelerate the degradation of the wireworks. Conversely, these pollutants can also be readily flushed out of the pedestal because of the same rapid exchange between the environment and the wireworks. In sealed plant, the rates of both the entrance and removal of pollutants are reduced since the air exchange with the environment is limited. Insulations that are truly isolated from the outside environment should remain protected from the effects of weather, moisture, polluted air, etc.. while antioxidant stabilizers are retained. Problems will occur if the seals are initially imperfect or degrade with time, so that leaks develop. Fluctuations in outside temperature and humidity may then act as a pump and accumulate water and pollutants inside the plant. Retaining trapped moisture and/or pollutants inside a closure adjacent to the wireworks will accelerate degradation of the plant.

In encapsulated plant, stabilizers are readily extracted from insulations by the oil-based urethane encapsulants as shown by a 40-60% reduction in OIT values of the insulations[27,28]. However, these low OIT values of encapsulated insulations

were unchanged after long term aging in the field or laboratory[27,8]. The initial stabilizer loss at the time of encapsulation was compensated by enhanced long term stability. Burying the encapsulated splices would further isolate the outside plant from the environment, particularly the high temperatures found in some aboveground pedestals. Such out-of-sight plant will reduce any thermal oxidative problems at the expense of easy access for maintenance or repair work.

The adoption of any of the plant closures or practices listed in Table 2 will involve compromises between labor/material costs and improved plant reliability. The enhanced thermal oxidative stability of polyethylene insulations is only one factor to be considered to maintain a reliable, long-lived network.

Temperature Reduction Strategies : High temperature is the major environmental factor in the degradation of PIC insulations in aboveground closures[2-8,16,17,29]. At a New Jersey test site, we found that convective cooling, internal venting, thermal insulation and light/heat reflective coatings[17] could significantly reduce internal closure temperatures. The most promising modifications were field trialed in a hot southwestern location at Mesa, Arizona. Well-characterized cable samples were installed in these modified closures and the insulation stability, closure temperature and climate data were tracked.

The temperature reductions achieved in the mild climate of New Jersey were matched in the hot, harsh summer climate of Arizona and the stabilizer loss from the insulations were significantly retarded by the pedestal cooling strategies. Temperature reductions of 20-25°F were achieved by painting pedestals lighter colors or using vented covers. Fifty-to-hundred percent increases in PIC insulation lifetime were possible with such 20-25°F reductions.

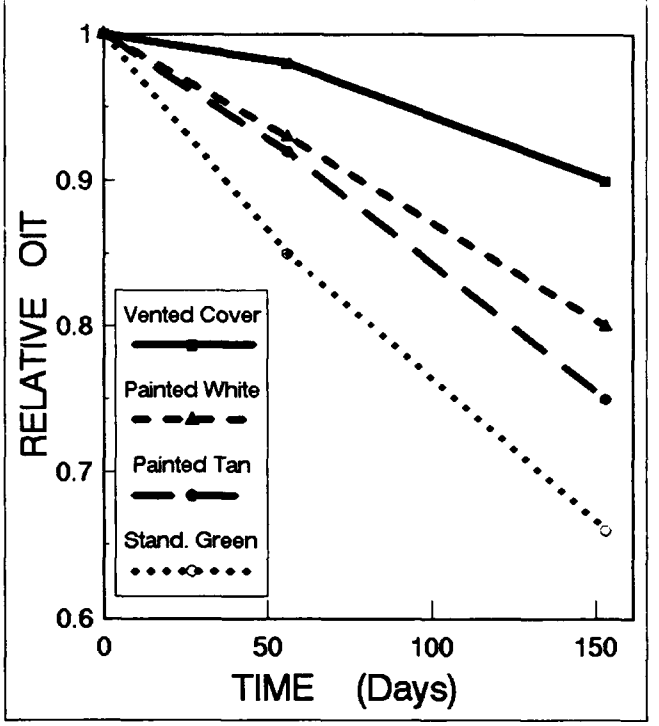
Figure 4 shows the stability decay curves for foam-skin HDPE PIC insulations from a 1991 cable exposed in standard green metal pedestals, pedestal painted white or tan, and pedestals covered with a vented cover. The lower the wireworks temperature, the greater was the stability of the insulation after any given exposure time. The insulation was most stable in pedestals with white vented covers, and least stable in the standard green pedestals. Relative to green standard pedestals, white and tan painted pedestals increased the stability of the insulations in proportion to the temperature decrease inside the closure. Similar behavior was found for all cable vintages and Figure 5 shows the linear relationship between insulation stability (OIT value) and average wireworks temperature for test insulations from 1987, 1989 and 1991 vintage cables.

The temperature/stability relationship found from these Mesa samples agreed with our laboratory aging results[17,20] and the theory that PIC insulation degradation in the field is primarily a thermal oxidation process. Activation

FIG. 4

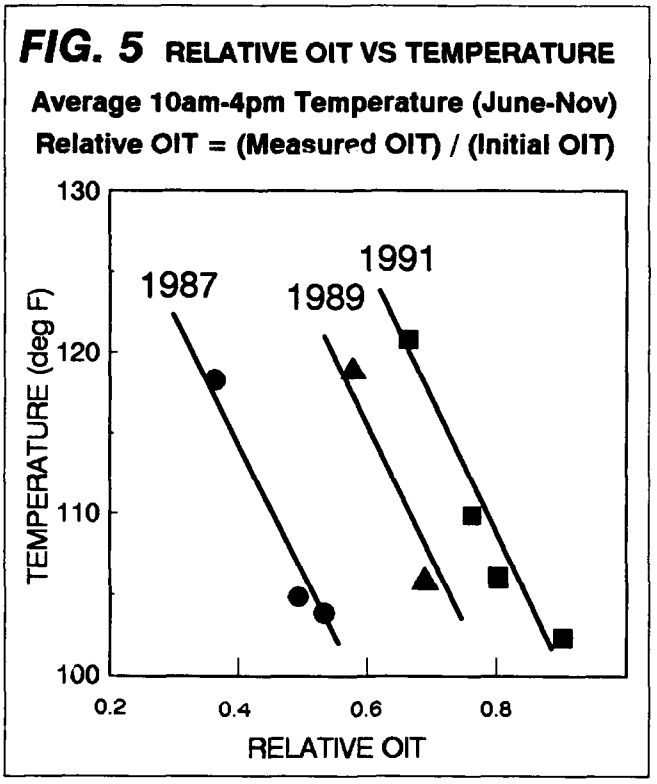
LOSS OF PIC STABILITY IN PEDESTALS

Relative OIT = Measured OIT/Initial OIT



energies between 38 and 46 kcal/mole for the oxidation of polyethylene insulations were calculated from the slopes of Arrhenius plots {i.e., (Temperature, °K)$^{-1}$ vs. Ln(time-to-crack) } reported in earlier papers[19,20]. The data for these Arrhenius plots was obtained from laboratory aging of insulations in heated pedestals (@60-110°C) following pedestal test procedures outlined in Bellcore document TR-NWT-000421[21]. The Arrhenius plots were curved implying that the activation energy changes with temperature; e.g., 44-46kcal/mole at 80-100°C and 38-40 kcal/mole below 60°C. Using the temperatures measured in our field closures, **THEORETICAL** lifetime enhancement factors for the various pedestal modifications can be calculated from the Arrhenius relationship.

Although none of the insulations in our Mesa trial cracked, **FIELD** lifetime enhancement factors were calculated from the decay times to reach a specified value of the RELATIVE OIT. Decay times and lifetime ratios for 20, 40 and 60 percent OIT reductions for our three cable vintages were calculated. For example, compare the decay times for the same insulations from the 1991 cable in green and white pedestals in Figure 4. The OIT value for these insulation decreased by 20% to a RELATIVE OIT value of 0.8 after only 80 days in the green standard pedestal; whereas, the insulations in the white pedestals survived until



155 days before the same 20% reduction was observed. Therefore the lifetime ratio for insulations in white painted pedestals compared to green standard pedestals is 155÷ 80 ≃ 1.9 which is defined as the lifetime enhancement factor.

Using data from all the Mesa samples, average **FIELD** lifetime enhancement factors were determined and are listed in Table 3 along with the **THEORETICAL** predictions from the laboratory aging data (Arrhenius plots). The Arrhenius predictions and the Mesa field trial results agree within experimental error.

TABLE 3. LIFETIME ENHANCEMENT FACTORS

PEDESTAL (Color & Cover)	ENHANCEMENT FACTOR	
	FIELD	THEORETICAL
Standard Green -		
painted Tan	**1.5± 0.1**	**1.3-1.5**
painted White	**1.6± 0.3**	**1.4-1.8**
with White Vented Cover	**2.1± 0.5**	**1.6-2.2**

Besides protecting outside plant against thermal oxidation, numerous design and performance factors need to be considered for selection of the best closure in a particular location. Additional requirements include physical robustness, fire resistance, security, flood resistance, compatibility with other outside plant hardware, friendliness to craftspersons and suitable electrical properties[30]. Closures need to be evaluated for all these properties before procurement/installation decisions.

This discussion has focussed on simple inexpensive modifications that can be made to currently installed and/or future outside plant closures in the network. The conclusions for PIC insulations in pedestals can be extended to other hardware items and different aboveground closures. For instance, in El Paso (Texas), the reliability of some remote switches was increased by changing the color of the cabinets. Trouble reports ceased after brown aboveground cabinets were painted white[31].

There are more sophisticated techniques for cooling outside plant and equipment such as solar-powered cooling fans, solar-powered heat exchanges and thermal insulations based on PCM (Phase-Change-Materials) technology[32-34]. The cost/benefit analysis of these techniques may make them too expensive for the copper cable pedestal plant. However, these strategies may become cost competitive for large equipment cabinets containing remote switches and for aboveground closures used in FITL (Fiber-In-The-Loop) deployments. The equipment and installation costs for FITL components are such that more expensive cooling strategies may become attractive to ensure network reliability and increased lifetime of the outside plant components.

Plant Practice Modification Options :

A second class of options is not to purchase any new hardware but to treat the vulnerable wireworks under field conditions. Suggestions for plant practice modifications include (1) antioxidant sprays to coat vulnerable insulations and minimize further oxidative degradation, and (2) solvent cleaning to remove filling compound that can extract stabilizers from insulations.

Sprays and Surface Treatments : Sprays were successfully tested for low density polyethylene insulations in the 1970s[35]. Table 4 shows an example of a 1968 vintage insulation that was sprayed during the 1970s. The antioxidant did prevent insulation cracking but the insulation OIT value did not increase. The sprayed coating provided an airtight seal to inhibit any further oxidation and crack development. No re-stabilization of the insulation occurred, since beneath the coating the PIC insulation had an OIT value of only 0.6 mins.

Urethane coatings and phenolic-type varnish sprays were reported[15] to reduce the effects of thermal oxidation on not only low-density polyethylene insulations but also high-density polyethylene (solid and foam-skin designs). Disadvantages of the spray include the careful preparation and application procedures generally required to ensure that an effective coating is applied and adheres to the

TABLE 4. FIELD SAMPLES - SPRAYED INSULATIONS
(From pedestal in Layton, Iowa)
(*) LDPE = Low-Density Polyethylene

SAMPLE (*) Cables placed in 1968	OIT (200°C) (mins)
Solid LDPE (Spray coated, 1970s)	2.5
Solid LDPE (Coating removed)	0.6
Solid LDPE CRACKED (Not spray coated)	0.8

insulation. The resulting sprayed wires adhere together and make it difficult for any craftperson to work with the wire bundle. After drying and aging, the coating can become brittle and later craft activity will crack the coating and insulation degradation will continue.

In filled cables, these problems are exacerbated by the need to remove thoroughly all filling compound before spraying. Good adhesion between the antioxidant spray and the insulation usually requires minimal filling compound be present on the insulation surface. The most efficient cleaning procedure requires solvents that may extract stabilizers from the insulations and create a disposal problem.

Filling Compounds and Solvent Cleaning of Wires : As a protective barrier, the filling compound excludes or reduces oxygen access, water penetration and environmental contamination, all of which can initiate or accelerate degradation of the insulation. Conversely, stabilizers are more soluble in filling compounds than in insulations and therefore stabilizers are readily extracted from insulations into the filling compounds[12-14,19]. A poorly stabilized filling compound may even initiate oxidation and deplete stabilizers intended to protect the insulation. Finally, typical filling compounds are greasy and messy to handle. A well stabilized filling compound (i.e., $OIT_{190°C}$ value of 150+ mins) will not significantly extract stabilizers from insulations and should act as a barrier to oxygen and thereby reduce oxidation of the polyethylene insulation. Conversely, a poorly stabilized filling compound (i.e., $OIT_{190°C}$ value below 20 minutes), would not only extract stabilizer from the insulation, but also would be vulnerable to oxidation itself leading to premature oxidation of the insulation and reaction of stabilizers intended to protect the HDPE insulation.

Removal of filling compound may or may not be a improvement to the thermal stability of the insulation. Removal of a well stabilized filling compound may expose an insulation to accelerated degradation whereas removal of a weakly stabilized filling compound may extend the insulation's lifetime. The cleaning procedure (e.g., solvent used) may also affect the outcome of filling compound removal. The competing effects of filling compounds is clearly illustrated in Table 5 where laboratory aging results are shown for two sample sets -

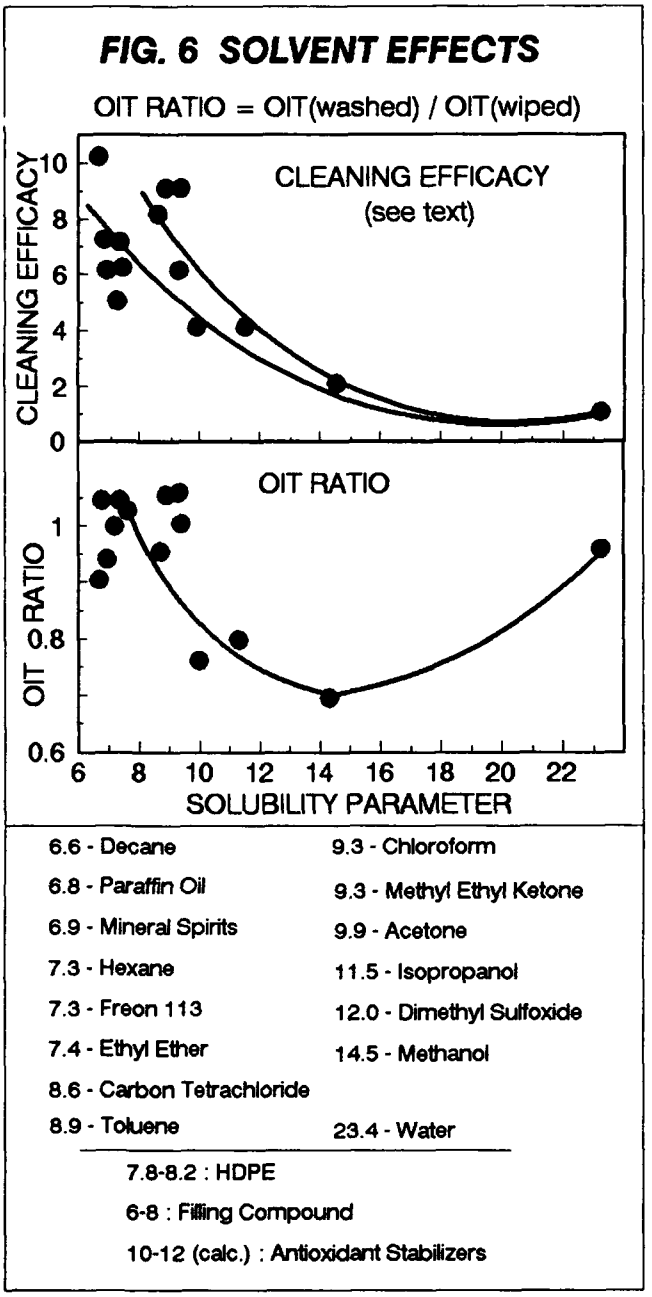
(A) foam-skin HDPE insulated wires removed from a filled commercial cable and
(B) foam-skin HDPE insulated wires that were never cabled or exposed to filling compound.

TABLE 5. EFFECTS OF FILLING COMPOUND

SAMPLE	INSULATION TIME-TO-CRACK	
	90°C Pedestal	80°C Oven
(A1) Wiped with dry cloth	65-70 days	200-250 days
(A2) Coated with filling compound	150-190 days	600 days
(B1) "As received"	> 350 days	> 900 days
(B2) Preaged in filling compound	60-65 days	300 days

Aging results for samples A1 and A2 showed that retaining a thick coating of filling compound increased the insulation lifetime by 2-3 times. In contrast, samples B1 and B2 illustrated how effectively stabilizer can be extracted from insulation by filling compound. The insulations that were never exposed to filling compounds survived at least 5 times longer in the laboratory aging tests. Beltz[15] has reported on increased insulation lifetimes after solvent (i.e., 3M Scotchcast 4413 solvent blend) cleaning of filling compound from PIC cable insulations. In contrast, Hershkowitz and Hore[27] reported 10% lower stabilizer levels for insulations that were cleaned with solvents prior to encapsulation in splices. Hershkowitz and Hore[27] tested Type-B cleaning fluids, gasoline and perchloroethylene-type cleaners as representative of solvents and fluids that PIC insulations may be exposed to in the field.

We examined fourteen different solvents and measured their cleaning efficacy and their effect on stability of the insulation. Two general trends were apparent from Figure 6 where the cleaning efficiencies and OIT ratios are plotted as a function of solubility parameters (δs). One, the closer the $\delta_{solvent}$ was to the δ_{HDPE} or to the $\delta_{filling\ compound}$, the better the insulations were cleaned. Two, the closer the $\delta_{solvent}$ was to $\delta_{stabilizers}$, the more stabilizer was extracted from the insulation, and the greater was the reduction in OIT (i.e., lower OIT ratio). Alcohols and some polar



solvents extracted stabilizers from and reduced OIT value of the insulations more easily than other solvents. The most promising solvents had δ-values of 7-9 $(cal/cm^3)^{1/2}$ and extracted less than 5-10% of the stabilizers from the PIC insulations. After washing with some solvents (e.g., toluene) a small 5% increase in OIT was found compared to the wiped insulation. Apparently, a small amount of filling compound remained adsorbed on the insulation after wiping and reduced the OIT value of the insulation. The toluene wash must have removed the last vestiges of filling compound and thereby increased the measured OIT of the insulation.

If 95+ % of the filling compound can be removed from the insulation than the long term stability of the insulation should be improved. The major problems of this cleaning process were (a) leaving significant amounts of filling compound on the insulation and (b) extracting significant fractions of the insulation stabilizers. Any filling compound that remained may act as an initiator for oxidation since the stabilizer in the filling compound was depleted by the solvent cleaning.

A generic statement that cleaning the insulations will enhance thermal stability is incomplete. Given appropriate solvents or cleaners and the correct procedures, the removal of filling compounds may be able to enhance the long term thermal stability of PIC insulations. The correct implementation of any such cleaning practice may be difficult and the problems of solvent/cleaner disposal have not been addressed. Environmental codes, safety concerns, fire risks and other regulations may play a major consideration in the feasibility of any solvent cleaning practice. Since many scenarios are possible in which the stability of insulations may be enhanced, degraded or remain unaffected by filling compound removal, we do not recommend a generic cleaning practice be implemented at this time.

Cable Replacement

The more drastic option for cracked or vulnerable PIC insulations is cable replacement. One may cutback into the sheathed cable in the lower section of a closure and expose insulations that were protected by the jacket and sheaths. OIT analysis of field samples showed a large increase in OIT values if the insulated wires were enclosed by the jacket[6,8]. Table 6 lists data from cables installed up to 27 years ago that illustrate the protective effect of the jacket.

Removal of the exposed insulated wires and resplicing from insulated wires should double the lifetime of the insulations. Of course, the splice/connections will be much lower in the pedestal, more difficult to access, as well as more susceptible to other environmental hazards (e.g., water penetration from floods). The new splice could be encapsulated and buried below ground level to minimize thermal oxidative degradation of the insulations.

Another variation on the cable replacement theme is to cut out the cable section with cracked or vulnerable PIC insulations and replace that 3-6 foot section with new more stable insulations, such as solid high-density polyethylene insulations[36].

TABLE 6. FIELD SAMPLES - JACKET EFFECT

LOCATION #8 = Yuma pedestal #1,3 = Iowa pedestals	INSULATION SAMPLE	OIT (mins)
Cable 8A placed 1983		
#8 - Exposed	**Foam-skin HDPE**	**1.0**
#8 - Under Jacket	**Foam-skin HDPE**	**4.0**
Cable 1A placed 1965		
#1 - Exposed	**Solid LDPE (Cracked)**	**0.4**
#1 - Under Jacket	**Solid LDPE**	**11.5**
Cable 3A placed 1965		
#3 - Exposed	**Solid LDPE (Cracked)**	**0.4**
#3 - Under Jacket	**Solid LDPE**	**11**

CONCLUSIONS

We have discussed the various remedial strategies available for installed PIC insulations to maximize the service life of these insulations with respect to thermal oxidative degradation.

Using routine repair/maintenance procedures to control any problems arising from PIC insulation cracking is a reasonable short term policy. This "No Action" option does entail some long term risk depending on the replacement rate of copper technology by optical fiber technology, the geographic location, and the strategic plan of the individual telecommunications company.

Airtight closure systems can increase insulation lifetimes sixfold or more. However, an imperfect seal can result in accumulation of water and pollutants inside the closure and thereby cause *more* degradation problems than in a standard open-access, free-breathing closure.

Temperatures inside typical outside plant closures can be reduced by 20-25°F by convective cooling, internal venting, thermal insulation or light/heat reflective coatings strategies and thereby increase field lifetimes of PIC insulations. Pedestals painted white or protected with vented covers were found to *extend PIC insulation lifetime by 50-100%* as compared to the conventional green pedestals.

Removal of filling compounds by solvent cleaning or other means may either enhance, degrade or leave unaffected the thermal stability of PIC insulations. Filling compounds may both protect insulations from oxidation as well as reduce insulation stability by stabilizer extraction. The cleaning ability of any particular solvent needs to be balanced with its tendency to extract stabilizers from insulations. In addition labor costs, safety and disposal concerns will determine if filling compound removal is economically sensible.

There are various proactive remedial actions that can be used to extend the useful life of the 350+ million miles of copper wires in the USA telecommunications network. Use of the procedures and plant modifications discussed in this memorandum should help minimize any future field problems caused by thermal oxidative cracking of PIC insulations.

ACKNOWLEDGEMENTS

Various people in the regional telephone companies assisted in gathering samples, preparing field trial sites and supplying information & advice on outside plant questions. In particular, we thank J. Blaszczynski, D. Wilmont and D. Whitley of BellSouth Services, and R.E. Coker, R. Whinery, C. Will, D. Ensle, A. Perry, R. Munson, R. Trevizo, W. Kerr and C. Frederick of U S WEST Communications.

REFERENCES

1. Federal Communications Commission - "Statistics of Communications Common Carriers - 1990-91 Edition" U.S. Government (1991)
2. J.B. Howard, *Proceed. 21st Int. Wire and Cable Symp.*, p329 (1972).
3. H.M. Gilroy, *Proceed. 23rd Int. Wire and Cable Symp.*, p42 (1974).
4. B.D. Gesner, J.W. Shea and F.R. Wight; *Proceed. 22nd Int. Wire and Cable Symp.*, p7 (1973).
5. B. Havens, *Outside Plant*, p19 (Jan-Feb 1988).
6. T.N. Bowmer, *Proceed. 37th Int. Wire and Cable Symp.*, p475 (1988).
7. L.D. Loan, *Proceedings Golden Jubilee Conference on Polyethylenes 1933-83*, (June 1983) London.
8. T.N. Bowmer, P.C. Warren and E.E. Hershkowitz; *Plastics and Rubber Processing and Applications*, **14**, p15 (1990) and references cited therein.
9. M.G. Chan, H.M. Gilroy and W.M. Martin; *SPE RETEC* US Army Communications Electronics Command, Fort Monmouth NJ (1984)
10. G.A. Schmidt, *Proceed. 22nd Int. Wire and Cable Symp.*, p11 (1973).
11. G.A. Schmidt, *Proceed. 26th Int. Wire and Cable Symp.*, p161 (1977).
12. L.E. Davis, *Proceed. 36th Int. Wire and Cable Symp.*, p475 (1987).

13. G.D. Brown, *Proceed. 36th Int. Wire and Cable Symp.*, p337 (1987).
14. G.D. Brown and L.E. Davis, *Proceed. 36th Int. Wire and Cable Symp.*, p734 (1987).
15. L.P. Beltz, *Proceed. 38th Int. Wire and Cable Symp.*, p123 (1989) and *TE&M Magazine* p60 (Sept 1st - 1990).
16. T.N. Bowmer, R.J. Miner and R.E. Coker; *Proceed. 39th Int. Wire and Cable Symp.*, p335 (1990).
17. J.N. D'Amico and T.N. Bowmer; *Proceed. 40th Int. Wire and Cable Symp.*, p476 (1991).
18. K.D. Dye, V.J. Kuck, F.C. Schilling, M.G. Chan and L.D. Loan; *Proceed. 38th Int. Wire and Cable Symp.*, p98 (1989).
19. T.N. Bowmer, E.P. Hjorth, R.J. Miner and O.S. Gebizlioglu; *Proceed. 37th Int. Wire and Cable Symp.*, p490 (1988).
20. T.N. Bowmer, R.J. Miner, I.M. Plitz, J.N. D'Amico and L.M. Hore; *Proceed. 39th Int. Wire and Cable Symp.*, p316 (1990) and references cited therein.
21. Bellcore Technical Requirements - *TR-NWT-000421* - "*Generic Requirements for Metallic Telecommunications Cable*", Issue 3, Sept. 1991.
22. W.L. Hawkins, M.G. Chan and G.L. Link; *Polymer Engineering & Science;* **11(5)**, p377 (1971).
23. American Society of Testing and Materials (ASTM), *ASTM Method D3895* - "*Oxidative Induction Time of Polyolefins by Thermal Analysis*", (1986)
24. ASTM Method D4565 Section 17 - "*Oxidative Induction Time Test Procedure For Polyolefin Insulations*" This method was revised by ICEA Working Party #646 and a revised procedure is currently being balloted within the ASTM. (August 1992).
25. V.J. Kuck, *Proceedings of the International Conference on "Plastics in Telecommunications"*, - September 1992 (London), in press.
26. *Polymer Handbook (3rd Edition)* - p VII-519 - (Eds. J. Brandrup and E.H. Immergut) John Wiley (1989).
27. L.M. Hore and Hershkowitz; *Proceed. 39th Int. Wire and Cable Symp.*, p479 (1990).
28. E.P. Hjorth, private communication.
29. E.A. Capadona and D. LaPointe, *Outside Plant*, p22 (July - 1988).
30. Bellcore TR-NWT-000013 - " Generic Requirements for Pedestal Terminal Closures" (Issue 2, Oct. 1990)
31. T. Mercuez - private communication
32. J.R. McKay, *Proceed. Int. Telecommunications Energy Conference, INTELEC* (Oct. 1989) Florence, Italy .
33. J.R. McKay, "*Use of Air to Air Heat Exchanger to Reduce Peak Temperatures in Outdoor Cabinets*", private communication (Oct. 1989).
34. R.C. Estes, "*The Effect of Thermal Capacitance and Phase Change on Outside Plant Enclosures*", private communication and
R.K. Prudhow and L. Doukas, *Proceed. INTELEC Conference (Orlando, Florida)*, paper 25-6, p589 (Oct. 1990)
35. F.R. Wight, *Proceed. 28th Int. Wire and Cable Symp.*, p112 (1979).
36. T.N. Bowmer, unpublished results - Solid HDPE insulations will survive 2-4 times longer in aging tests than foam-skin HDPE insulations with the same concentration and type of antioxidant stabilizers.



Trevor Bowmer is a member of the Plastics and Rubber Research Group in Bellcore. He received his Ph.D. in chemistry from the University of Queensland, Australia, where he studied radiation chemistry of polymers. Joining Bell laboratories in 1980, he investigated radiation cured systems and lithographic materials. In 1984, he came to his present position where his interests include degradation mechanisms and characterization of polymeric materials used in telecommunications applications.



Joe D'Amico has worked on engineering and materials issues affecting all types of telecommunications and power cables in his 25 year career. He first worked with communications cable at Western Electric before joining General Cable Company in 1967. There as senior research physicist, he investigated the structure and composition of all types of telecommunications wire, cable and optical fiber as well as electrical power cables. Since 1985 he has worked at Bellcore, initially as a Quality Assurance Engineer and since 1989, as a member of the Plastics and Rubber Research Group in Red Bank, New Jersey. Joe is a graduate of Seton Hall University. He received his MS degree from Fairleigh Dickinson University.

SHORT AND LONG TERM BEHAVIOUR OF HALOGEN FREE FIRE RETARDANT CABLE MATERIALS IN DIFFERENT ENVIRONMENTS

Lars Grüner-Nielsen Peter Hasløv Niels H. Skovgaard

NKT Elektronik A/S
NKT Alle 85, 2605 Broendby, Denmark

Abstract

Short term properties of 7 different halogen free fire retardant materials from 4 suppliers have been evaluated. Testing of long term reliability is reported for the first time. 4 of the 7 materials have been selected for long term reliability testing. The short term test program has included tensile testing, flame spread and smoke generation. The processability has been judged as well. Accelerated long term ageing tests have been performed in different environments such as air, water, salt water, oil and UV-light. On the basis of the accelerated test results life time predictions have been made.

Introduction

Since the introduction of halogen free fire retardant (HFFR) materials for cable application in the early eighties[1, 2], there has been an increasing use of HFFR cables. A lot of papers have been published since then mainly dealing with the short term properties of HFFR materials, but to our knowledge no papers have been published about the long term reliability of these materials.

Examination of the long term reliability of HFFR materials is of special importance because practical long term experience does not yet exist for these materials, i.e. cables in service for 20 to 30 years. This is opposite to well established materials as e.g. PVC, which have proven their reliability through their practical use throughout many years. For new materials like HFFR materials the only quick method to simulate long lifetimes is to conduct accelerated ageing experiments.

The purpose of the enclosed work has been to study what can be achieved today with such materials regarding both short term properties and long term reliability. For this purpose we have made a comparative experimental study of different commercially available materials.

Application of HFFR cables

In the last 5 to 10 years HFFR cables have found use for more and more applications because of the superior performance of the HFFR cables in the event of fire. HFFR materials are flame retarded and in addition they generate very little dense smoke[3]. The corrosivity of the smoke is very low as well.

This has led to applications of HFFR cables in crowded areas such as hotels, banks, office buildings, underground railways and ships[4] where smoke emission in a fire situation is a major concern. Other applications, where especially the low corrosivity of the smoke is a driving force, are computer installations and telephone exchanges. Many European countries and for example Australia[5] now install HFFR cables only for all new telephone exchange installations.

Another driving force for HFFR materials especially in Europe is the general concern for the environment. Many, especially among the "green organisations", have considered primarily PVC as an ecologically bad material[6, 7]. HFFR materials could for many applications be an alternative to PVC.

Examples on HFFR cables.

On fig. 1 to 3 are shown 3 examples of HFFR optical fibre cables manufactured by NKT.

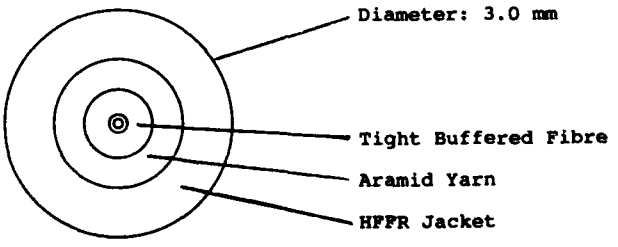


Fig.1. Single fibre optical cable.

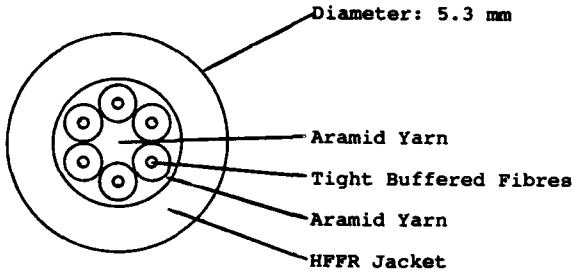


Fig. 2. 6 fibre light duty optical cable.

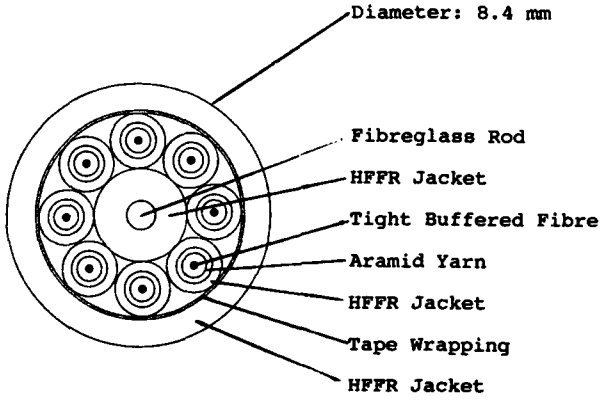


Fig. 3. 8 fibre break out optical cable.

Fire performance data for the cables are shown in table 1.

Property	Test method	Result
Flame spread	UL 1666	Pass, UL listed, type OFNR
	IEC 332-3-C	Pass
Smoke density	IEC 1034	Light transmission min. 50 %
Smoke corrosivity	IEC 754-1	max. 0.3 %
	IEC 754-2	pH > 4.3 Conductivity < 100 µS
Smoke toxicity	NES 713	max. 3.0

Table 1. Properties of optical HFFR cables.

Short term properties

7 materials designated A to G from 4 different suppliers labelled I to IV were selected for comparison. All materials are commercially available. They are all thermoplastic polyolefin based compounds, which don't require any cross-linking.

Based on the preliminary experimental results 4 materials have been chosen for the full test program.

The manufacturers do not give very much information about the chemical composition of their compounds, but the compounds from supplier I are to our best knowledge based on magnesium-dihydroxide, while the compounds from supplier II, III and IV are based on aluminiumtrihydrate as the filler giving the compounds their flame retarding properties.

An overview of the results of the preliminary examination of the 7 materials is given in table 2. With all 7 materials single fibre cables with a design as shown in fig. 1 have been manufactured. All measurements except the limiting oxygen index (LOI) have been performed on samples taken from the produced cables.

Tensile strength above 10 N/mm² and elongation at break above 150 % will satisfy most specifications for optical cable jacket materials. It is seen, that all materials except C fulfil this requirement. E is however somewhat marginal with respect to the elongation at break.

The usual requirement for hot pressure is max. 50 % indentation. All materials are below, but C is quite close to the limit.

The examination of processability is described in detail in next chapter.

The LOI has been measured in two ways. Strictly as prescribed by the ASTM standard and with a proprietary modification of the ASTM method. The modified method has shown to give LOI's with much better correlation to actual cable fire tests. Compound E is a good example, it has a very high LOI when measured according to ASTM, but fails the IEC 332-1 fire test.

All materials evolve very little smoke, when tested according to the IEC 1034-1 and -2 test method.

Based on the above results we have chosen material A, B, D and F for the full test program.

Property	Test method	Unit							
Material			A	B	C	D	E	F	G
Supplier			I	I	I	II	II	III	IV
Tensile strength	IEC 811-1-1-9	N/mm²	11.7	15.7	7.8	16.1	13.5	13.1	15.8
Elongation at break	IEC 811-1-1-9	%	180	280	540	210	150	190	230
Hot pressure, 80°C, 6 h	IEC 811-3-1-8	%	28	10	47	3	nm	32	12
Cold bend, - 25°C	IEC 811-1-4-8.2		pass	pass	pass	pass	nm	pass	pass
Processability			good	good	good	poor	poor	fair	fair
LOI	ASTM D 2863	%	41	38	32	45	44	38	26
LOI - modified	D 2863-modified	%	37	29	26	31	24	33	23
Flame spread	IEC 332-1		pass	pass	pass	pass	fail	pass	fail
Flame spread	IEC 332-3-C		pass	pass	nm	pass	nm	pass	nm
Smoke density; min. transmission	IEC 1034	%	93	94	93	91		94	80

nm: not measured

Table 2. Main result of preliminary examination.

Material E and G have been excluded due to bad fire retardation. Material C has been excluded because of low tensile strength and bad hot pressure performance. Material C has also been considered to have too low fire retardant properties for many applications.

The choice of material D is questionable due to the poor processability, but it has been regarded as important to have materials from at least 3 suppliers in our test program.

Processability

One of the main problems with HFFR materials has turned out to be the extrusion of the materials[8,9,10]. This is mainly caused by the high viscosity of the melt due to the high content of inorganic fillers and low processing temperatures. The processing temperature has to be kept low to avoid liberation of water from the fillers.

Supplier II to IV generally recommend to avoid high shear rates. They recommend use of single flight screws with a deep metering zone and a low compression of the order of 1.2:1. The material temperature should be kept in the range of 160 to 180°C (Supplier IV allows up to 200°C). Supplier I on the contrary recommends use of screws with a shallow metering zone and a compression ratio of 2:1 to 3:1. Both single flight and barrier mixing screws are proposed. The material temperature should be kept in the range 200 to 230°C.

To compare the processability of the 7 materials we have made extrusion trials on a 30 mm 25D extruder. Two types of screws have been used: A single flight screw with a compression ratio of 2.0:1 and a barrier mixing screw with a compression ratio of 1.8:1. The results are summarised in table 3. Column 6 shows the set-point temperature of the die. Column 7 shows the difference between the material temperature measured just after it leaves the die and the die set-point temperature. This figure should be as low as possible in order to avoid overheating and degradation of the material.

Column 8 shows the specific energy consumption (SEC) by the screw. SEC is the power put into the screw divided by the output. This number, which normally tends to become a constant at high screw speeds, is a measure of the energy put into the material by the screw. For high viscosity materials as HFFR materials the SEC should be kept as low as possible in order to keep the temperature increase of the material as low as possible.

It is seen, when comparing materials from the same supplier, that materials with high flame resistance are more difficult to process than materials with low flame resistance both when looking at SEC and temperature increase. (A, B, C and D, E).

It is remarkable that material A shows better performance with a barrier mixing screw than with a single flight screw.

Mat.	Sup.	Screw	Screw speed	Out-put	Die temp. set.	Mat. temp. incr.	Spec. energy cons.	N B
			RPM	l/h	°C	°C	W·h/l	
A	I	S, 2.0:1	70	7.4	180	33	280	
A	I	B, 1.8:1	51	7.5	180	25	250	
B	I	B, 1.8:1	48	7.2	180	20	130	
C	I	S, 2.0:1	50	5.8	180	15	190	*
D	II	S, 2.0:1	39	4.3	140	24	410	
E	II	S, 2.0:1	64	5.8	140	17	340	*
F	III	S, 2.0:1	58	7.2	155	19	270	
G	IV	S, 2.0:1	47	5.8	180	22	260	*

NB! The 3 materials marked with * were run with a set of tooling with higher back pressure than the others.

Table 3. Results of extrusion trial on a 30 mm extruder.

In a comparative classification of the processability of the materials A, B and C must be judged as good, especially because they have a large margin for temperature increase. F and G are fair.

D and E must be judged as poor because of high SEC and relatively high temperature increase and small margin for temperature increase. For material D it was not possible to pass the shown output of 4.3 l/h, before the material temperature became too high and the material began to degrade. This is at least 3 times less than the output, which can be achieved with some of the other materials.

LONG TERM AGEING TESTS

Test methodology

The basic method to determine the lifetime of plastic materials at different temperatures is for example described in IEC 216[11]. The principle is to determine the time to failure at a few elevated temperatures. From these data the time to failure at the service temperature is extrapolated. This extrapolation is normally done by assuming that the degradation process follows an Arrhenius relationship[11].

The basic procedure to determine the time to failure has been to monitor tensile strength and elongation at break as a function of time. Tensile strength and elongation at break have been measured according to IEC 811-1-1-9[12]. In all cases 3 fold measurements have been performed. We have chosen to consider a tensile strength below 5 N/mm² and an elongation at break below 100 % as failure criteria.

Single fibre optical cables with a design as shown on fig. 1 were produced with jacket made of material A, B, D and F respectively. All ageing tests except UV ageing have been performed on these cable samples. The ageing has been performed on the complete cable, except at temperatures above 80°C, where it has been necessary to make the ageing on the jacket alone because the jacket otherwise would stick to the aramid yarns and in this way make it impossible to remove the jacket for measurement.

The basic aim with the test program, reported below, has been to determine the life time of the materials at the operating temperature for the cables (for optical cables typically 20°C or less) in different typical environments. The chosen conditions are:

1. Dry air
2. Tap water, which had a pH of 7
3. Water with a pH of 4
4. NaCl solution, 3.5 %
5. Vaseline
6. ASTM Oil No. 2
7. Antarox CO-630 solution, 10 %
8. UV-ageing.

1 simulates normal indoor use, 2 and 3 buried outdoor applications, 4 offshore applications, 5 application for vaseline filled cables, 6 and 7 resistance to chemicals and 8 exposure to sunlight.

Air ageing.

Ageing has been performed at 80, 95 and 120°C. The results are summarized in table 4 for all temperatures.

Temperature		80°C	95°C	120°C
Time		4000 h	3400 h	1900 h
Change in tensile strength N/mm²	A	11.7 → 12.4	11.7 → 12.5	11.7 → 12.7
	B	15.7 → 14.3	15.7 → 16.7	15.7 → 18.3
	D	16.1 → 19.7	16.1 → 17.1	16.1 → 20.5
	F	13.1 → 15.7	13.1 → 16.5	13.1 → 19.5
Change in elongation at break %	A	180 → 110	180 → 120	180 → 90
	B	280 → 120	280 → 180	280 → 170
	D	210 → 140	210 → 190	210 → 130
	F	190 → 130	190 → 140	190 → 130

Table 4. Change in tensile strength and elongation at break during ageing in air.

As an example of a full sequence the change in tensile strength (TS) and elongation at break (EB) for the 4 materials at 95°C have been plotted in fig. 4 and 5.

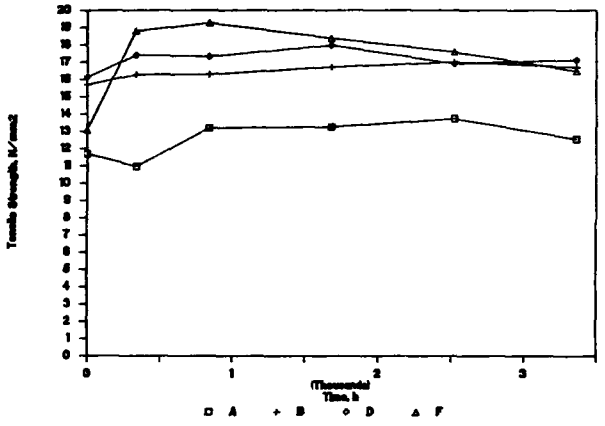


Fig. 4. Change in tensile strength in air at 95°C.

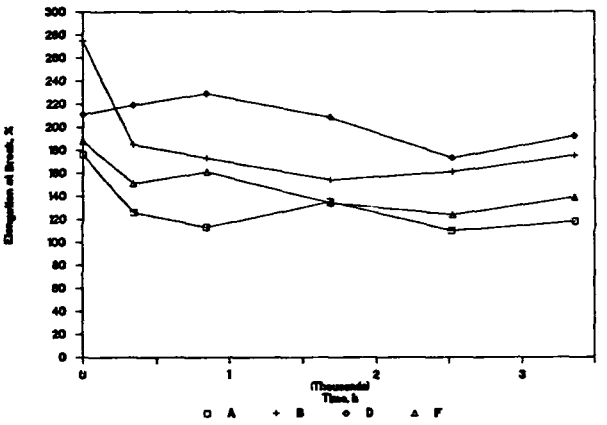


Fig. 5. Change in elongation at break in air at 95°C.

The overall picture is the same at 80, 95 and 120°C. After a certain time TS and EB stabilize at a certain level. The stabilization time is shortest at the high temperatures.

During none of the air oven ageing experiments the jacket material has been ruined. The increased tensile strength and the reduced elongation at break especially at 95 and 120°C can probably be explained as effects of cross-linking or perhaps improved wetting of the filler particles resulting in improved interfacial strength between filler and polymer. Actually, it looks as if the mechanical properties of the materials are improved by ageing at 95-120°C while a certain degradation takes place at 80°C.

Because of the unusual temperature dependence of the degradation in the temperature range investigated it is not possible to predict life time at lower temperatures using the normal Arrhenius approach. That is, as we have not been able to reach a failure even after 1900 h at 120°C, in itself a strong indication of long lifetimes, we cannot predict the lifetime at 20°C with the commonly accepted Arrhenius technique. However in practice it has shown that the degradation rate doubles for every 10 degrees temperature rise for many plastic materials.

Using the above assumption a life time of min. 4000 h at 80°C corresponds to min. 30 years at 20°C.

Wet ageing in tap water pH 7.

TS and EB have been monitored after ageing in tap water pH 7 at 20, 50, 65, 80 and 95°C. An overview of the results are given in table 5. In table 6 is given the result of weight increase measurements at 20 °C.

Temperature		20°C	50°C	65°C	80°C	95°C
Time		5000 h	5000 h	5000 h	5000 h	5000 h
Change in tensile strength N/mm²	A	11.7 → 8.9	11.7 → 7.4	11.7 → 6.7	11.7 → 6.4	11.7 → 5.5
	B	15.7 → 12.5	15.7 → 12.6	15.7 → 12.9	15.7 → 13.5	15.7 → 11.9
	D	16.1 → 15.4	16.1 → 14.9	16.1 → 14.8	16.1 → 14.8	16.1 → 14.9
	F	13.1 → 11.0	13.1 → 11.3	13.1 → 11.5	13.1 → 13.0	13.1 → 11.3
Change in elongation at break %	A	180 → 140	180 → 160	180 → 110	180 → 130	180 → 62
	B	280 → 310	280 → 310	280 → 300	280 → 210	280 → 180
	D	210 → 180	210 → 180	210 → 180	210 → 170	210 → 170
	F	190 → 210	190 → 190	190 → 170	190 → 130	190 → 90

Table 5. Change in tensile strength and elongation at break after ageing in tap water pH 7.

Material	Weight inc.; %	Saturation time; h
A	5	1300
B	2	800
D	0.5	1000
F	3	700

Table 6. Weight increase at 20°C in tap water pH 7.

A, which has the highest tendency to absorb water, also shows the highest degradation rate in water, pH 7, while D, which hardly absorbs water, is stable in water up to 95°C for at least 5000 hours. Also B and F fit in this picture.

Because of the limited knowledge of the chemical composition of the materials it is difficult to judge the degradation mechanism. The tensile properties measured indicate that the degradation mechanisms are quite different in dry and wet environment. The relation between water absorption and degradation rate, however, indicates that the amount of water in the polymer is important. The water probably diffuses along boundaries between filler and polymer, thereby reducing interfacial strength. The dry ageing is probably dominated by oxidation reactions in which cross-linking and chain scission act simultaneously.

If an elongation of 100% is chosen as the lowest acceptable value, we obtain a minimum lifetime of 5000 hours at 80°C corresponding to 36 years at 20°C assuming a doubling of the lifetime for each 10°C temperature decrease. If special attention has to be given to water resistance D should be chosen if the other properties are acceptable.

Wet ageing, pH 4.

Temperature		20°C	80°C
Time		5000 h	5000 h
Change in tensile strength N/mm²	A	11.7 → 6.6	11.7 → 3.5
	B	15.7 → 10.6	15.7 → 11.0
	D	16.1 → 15.5	16.1 → 12.7
	F	13.1 → 9.7	13.1 → 8.3
Change in elongation at break %	A	180 → 160	180 → 190
	B	280 → 400	280 → 240
	D	210 → 190	210 → 170
	F	190 → 190	190 → 110

Table 7. Change in tensile strength and elongation at break during ageing in water pH 4.

Material	Weight inc.; %	Saturation time; h
A	-2.5	1800
B	1	1500
D	0.3	1000
F	3	2000

Table 8. Weight increase in water at 20°C and pH 4.

Compound A seems to be degraded by the acid. This material loses weight due to degradation products being washed out by the water and it loses its strength totally at 80°C while the elongation at break increases.

The other three materials all show a reduction of strength compared to the experiments in water at pH 7.

The time to reach the chosen failure point for TS of 5 N/mm² for A at 80°C is 2000 h, which with the previously used calculation method corresponds to a lifetime at 20°C of 15 years.

Wet ageing in NaCl solution, 3.5%.

Temperature		20°C	80°C
Time		5000 h	5000 h
Change in tensile strength N/mm²	A	11.7 → 9.0	11.7 → 5.7
	B	15.7 → 12.5	15.7 → 13.9
	D	16.1 → 16.3	16.1 → 15.7
	F	13.1 → 11.2	13.1 → 12.1
Change in elongation at break %	A	180 → 160	180 → 140
	B	280 → 310	280 → 220
	D	210 → 180	210 → 160
	F	190 → 210	190 → 160

Table 9. Change in tensile strength and elongation at break during ageing in NaCl solution, 3.5 %.

Material	Weight inc.; %	Saturation time; h
A	0.8	700
B	0.6	1000
D	0.2	1110
F	1.1	1500

Table 10. Weight increase at 20°C in NaCl solution 3.5 %.

The observed weight changes were all 3-5 times lower than in water at pH 7, because the osmotic pressure reduces the water absorption of the materials.

The changes in tensile properties were all nearly identical to what was observed at pH 7.

Thus, salt water is no particular threat to these materials.

Ageing in vaseline.

Ageing has been performed in a commonly used cable vaseline for optical cables.

Temperature		20°C	80°C
Time		3400 h	1300 h
Change in tensile strength N/mm²	A	11.7 → 8.1	11.7 → 5.2
	B	15.7 → 11.9	15.7 → 8.9
	D	16.1 → 14.1	16.1 → 13.3
	F	13.1 → 12.1	13.1 → 3.1
Change in elongation at break %	A	180 → 110	180 → 80
	B	280 → 130	280 → 180
	D	210 → 140	210 → 140
	F	190 → 170	190 → 100

Table 11. Change in tensile strength and elongation at break during ageing in vaseline.

Material	Weight inc.; %	Saturation time; h
A	2	800
B	4	3000
D	9	3000
F	3	3000

Table 12. Weight increase at 20°C in vaseline.

Ageing at 20°C results in decreased TS and EB for all materials, while at 80°C TS decreases a lot except for D although this material absorbs the highest amount of vaseline.

As in water compound A and F are the most sensitive, although the weight increases are the lowest. This may be due to extraction of material.

The possible reactions occurring are absorption, extraction, migration of low molecular weight components e.g. stabilizers and oxidation.

The tendency to stress cracking has been tested as well. Cable samples have been wound around mandrels with a diameter of 9 mm (3 times the cable diameter) and stored in vaseline at 20°C in 2600 h followed by 1300 h at 50°C. No tendency to stress cracking have been observed.

It is not advisable to use these materials in contact with vaseline without further experimental evidence. Compound D is the most promising candidate.

Ageing in ASTM OIL No. 2.

Temperature		20°C	80°C
Time		3400 h	1300 h
Change in tensile strength N/mm²	A	11.7 → 6.9	11.7 → 1.6
	B	15.7 → 13.1	15.7 → 6.4
	D	16.1 → 14.0	16.1 → 12.7
	F	13.1 → 9.3	13.1 → 1.2
Change in elongation at break %	A	180 → 170	180 → 90
	B	280 → 250	280 → 210
	D	210 → 150	210 → 220
	F	190 → 190	190 → 170

Table 13. Change in tensile strength and elongation at break during ageing in ASTM oil No. 2.

Material	Weight in. 20°C; %	Sat. time 20°C; h	Weight in. 80°C; % *)	Sat. time 80°C; h
A	> 13	> 3400	50	150
B	8	2400	20	300
D	7	600	30	150
F	> 12	> 3400	70	200

*) Measured on plaques.

Table 14. Weight increase in ASTM oil No. 2.

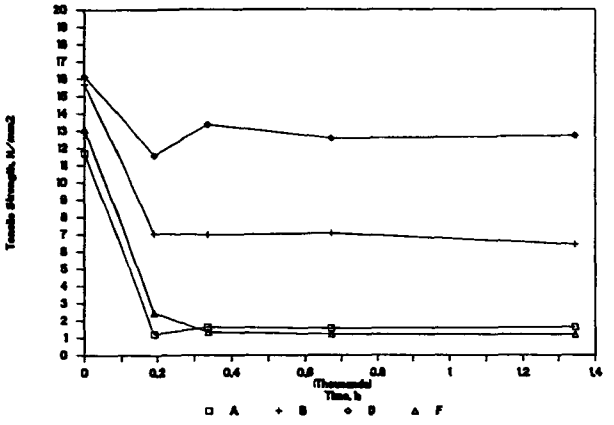


Fig 6. Change in tensile strength at 80°C in ASTM oil No. 2.

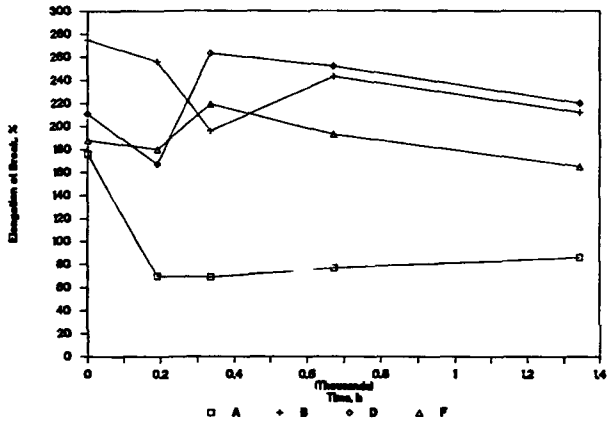


Fig 7. Change in elongation at break at 80°C in ASTM oil No. 2.

Fast degradation of A and F, and to some degree also B is observed. Again D shows remarkably good resistance and lowest absorption. In all cases very high absorption values are seen.

The tendency to stress cracking has been tested as well. Cable samples have been wound around mandrels with a diameter of 9 mm and stored at 20°C for 2600 h followed by 1300 h at 50°C. No observations of stress cracking have been made on sample B,D and F, whereas A cracked after 1000 h at 50°C.

In general, contact with oil should be avoided, but D and maybe B could be tested in more detail.

Wet ageing in Antarox CO-630 solution, 10%.

The tendency to stress cracking has been tested. Cable samples have been wound around mandrels with a diameter of 9 mm and stored in a 10% Antarox CO-630 solution at 20°C. No observations of stress cracking have been seen after 2600 h.

Change in TS and EB and weight increase after ageing at 20°C have been monitored as well. The results are seen in table 15 and 16.

Temperature		20°C
Time		3400 h
Change in tensile strength N/mm²	A	11.7 → 8.1
	B	15.7 → 11.0
	D	16.1 → 14.5
	F	13.1 → 9.3
Change in elongation at break %	A	180 → 200
	B	280 → 400
	D	210 → 170
	F	190 → 260

Table 15. Change in tensile strength and elongation at break during ageing in Antarox CO-630 solution, 10 %.

Material	Weight inc.; %	Saturation time; h
A	2	1300
B	> 2	>3400
D	0.3	1000
F	2	1300

Table 16. Weight increase at 20°C in Antarox CO-630 solution 10 %.

The reductions in TS and EB are similar to those found after ageing in water pH 7. However, F seems to have a somewhat higher decrease in TS and an increase in EB.

UV ageing.

UV ageing in a QUV accelerated weathering tester[12] has been performed. The apparatus was equipped with UVA 340 lamps. The test cycle was 20 h UV irradiation at 60°C followed by 4 h of water condensation at 50°C. This test corresponds in our experience to a 50 times acceleration when comparing with North-European outdoor exposure. Like always such acceleration factors must be used with caution, because they can vary from one material to the other.

The test was for all materials performed on uncoloured plaques. UV-stabilizer was added per the suppliers recommendation. That is no UV-stabilizer for A and D, 0.5 % UV-stabilizer for B. Material F has been tested both with 0.5 % UV-stabilizer and without as the supplier mentions both alternatives. The result of the test is seen on fig. 8 and 9.

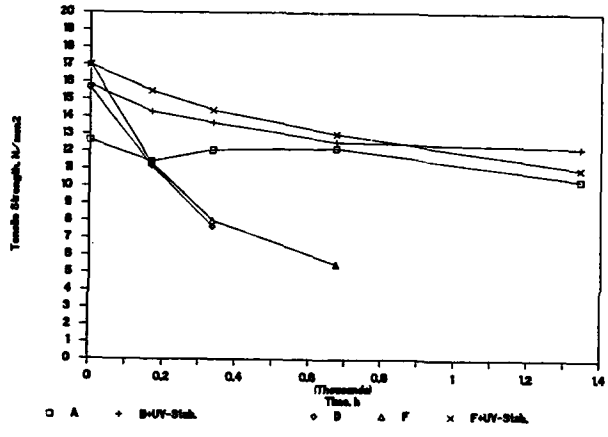


Fig. 8. Change in Tensile strength after UV ageing in QUV apparatus.

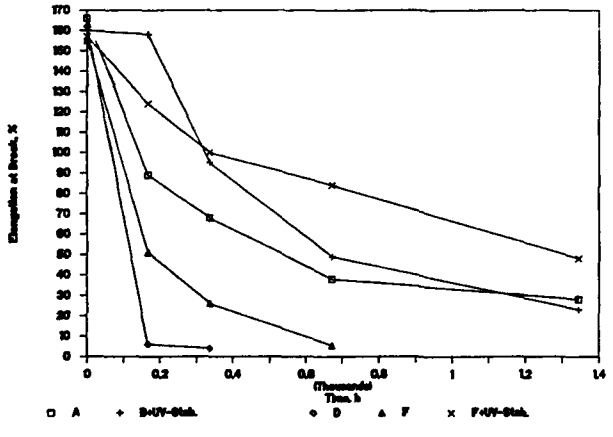


Fig. 9. Change in elongation at break after UV ageing in QUV apparatus.

The time to failure (in all cases EB below 100 %) is summarized in table 17.

Material	Time to failure in QUV in h	Estimated life-time in North Europe in years
A	150	1
B + UV-stabilizer	300	1.5
D	< 70	<0.5
F	100	0.5
F + UV-stabilizer	350	2

Table 17. Results of UV ageing test.

Our test shows a good effect of the UV stabilizer, the UV resistance of F has been improved 6-7 times in this way. The UV resistance of D could perhaps also be improved by addition of an UV-stabilizer.

Permanent outdoor applications should be avoided for all the tested types. A positive effect from pigmentation has previously been observed and should be expected, especially from carbon black.

To make HFFR materials suitable for outdoor use better UV-stabilization systems[10] as well as addition of carbon black as commonly done with polyethylene should be considered.

Conclusion

HFFR materials exist today with good fire performance as well as mechanical properties. The processability vary a great deal from material to material. The conventional ASTM LOI measurement gives on HFFR materials poor correlation to actual cable fire test, while a modified LOI measurement method gives much better correlation to actual cable fire tests.

For the first time long term reliability of HFFR material has been verified as well.

All 4 tested material indicated lifetimes of min. 30 years in dry air at 20°.

In water all 4 materials showed a lifetime of min. 30 years if pH is close to 7. Salt water (3.5 % NaCl solution) was no problem either. In acid water (pH around 4) one material (A) had only an estimated lifetime of 15 years while the other 3 demonstrated the same performance as for pH 7. Due to very slow degradation it was not possible to use the normal Arrhenius approach neither in air nor in water.

Vaseline could be a problem for several of the materials. More testing is necessary before use of HFFR material in contact with vaseline can be recommended.

Permanent contact with oil should be avoided, but two of the compounds (D and B) may after further testing turn out to be acceptable for contact with oils.

None of the compounds should be used in outdoor applications with exposure to sunlight without further protection.

Acknowledgement

The authors would like to thank Liselotte Lorenzen, who has performed all the ageing tests with great care. We also thank Keld Venø Poulsen from NKT Power Cables for his advise and support throughout this work. Finally we would like to thank the Danish Environmental Protection Agency, which partly has sponsored this work under a government program for development of cleaner technologies in a project entitled: "Alternatives to PVC in Cables and Associated Building Installations".

References

1. Briker H.; "Brandsichere Kabel". Bulletin des Schweizerischen Elektrotechnischen Vereins, Vol. 69, pp 67-71. January 1978.

2. Mayer H.A. and Hög, G.; "New Generation of Non Halogenated, Flame Retardant Compounds and Cables". Proceedings of the 29th IWCS, pp 253-262. 1980.

3. Fujimura S., Nakayame K. and Morii A.; "Smoke-Generating Properties of Flame-Retardant Cables". Proceeding of the Twenty-First Symposium on Electrical Insulating Materials pp 287-290. IEEE Japan 1988.

4. Pownall J.A.; "Reduction of Fire Hazards Due to the Cables Fitted to Warships". Proceeding of the 36th IWCS, pp 598-603 1987.

5. Colla L., Adams D.J. and Grubits S.; "Axe Exchange Cable Fire Performance Testing". Proceedings of the 37th IWCS, pp 656-664. 1988.

6. "Dokumentation des PVC Hearing: Gefährden PVC-Produkte die Umwelt?". Stadt Bielefeld, Umweltdezernat und Presseamt, Germany. 1986.

7. "Ausstieg aus der PVC-Nutzung, Möglichkeiten und Hindernisse im öffentlichen Bau- und Beschaffungswesen". Aktionskonferenz Nordsee e.V., Bremen, Germany. 1990.

8. Artingstall S., Taylor J. and Pyle A.J. ; "Recent Advances in Thermoplastic, Zero Halogen, Low Smoke, Fire Retardant Cable Compound Technology". Proceedings of the 36th IWCS, pp 254-264. 1987.

9. Ramachandran S., Jow J., Keogh J. and Nesgood, P.J.; "Improved Processability in Reduced Emission Wire and Cable Materials for the Telecommunication Industry. Proceedings of the 39th IWCS, pp 655-660. 1990.

10. Sawyer D.N., Preston J. and Taylor J.A.; Recent Developments in Low Smoke, Zero Halogen Fire Retardant Compounds for the Wire and Cable Industry. Special Meeting of the Insulated Conductors Committee of the IEEE at Birmingham, UK. July 1992.

11. IEC 216 part 1 to 5, "Guide for the determination of thermal endurance properties of electrical insulating materials. 1990.

12. IEC 811-1-1-9, "Common test methods for insulating and sheathing materials of electric cables - Test for determining the mechanical properties". 1985.

13. ASTM G 53-88, "Standard Practice for Operating Light and Water-Exposure Apparatus (Fluorescent UV-Condensation Type) for Exposure of Nonmetallic Materials". 1988.



Lars Grüner-Nielsen

NKT Elektronik A/S
NKT Alle 85
2605 Broendby
Denmark

Lars Grüner Nielsen was born in Denmark in 1959. He received his M.Sc. degree in Electrical Engineering in 1983. The same year he joined NKT's R. & D. department for optical cables. Since then he has been working in different areas of optical cables including: Design, testing and process development. He is now section manager responsible for design and development of optical data cables.



Peter Hasløv

NKT Elektronik A/S
NKT Alle 85
2605 Broendby
Denmark

Peter Hasløv (M.Sc. Chem. Eng.) graduated from DTH in 1974 with polymer technology as special subject. After 13 years in the plastics industry, he joined NKT Elektronik in 1987 and is responsible for selecting, testing and processing polymers for telecommunication cables. He is also engaged in lifetime estimation of optical fibres.



Niels H. Skovgaard

NKT Elektronik A/S
NKT Alle 85
2605 Broendby
Denmark

Niels H. Skovgaard was born in Copenhagen, Denmark in 1952. He received his M.Sc. degree in Mechanical Enginnering in 1981. From 1981 he worked as researcher at The Techinical University of Denmark. In 1984 he joined NKT working with research and development of optical fibre cables. Since 1986 he has been manager of the cable design and development department of NKT Elektronik A/S.

SHIPBOARD HARDENED FIBER OPTIC CABLES UTILIZING THERMOSET JACKETS

Authors

Harold J. Russell III
Mail Stop 138-328
GE Aerospace
199 Borton Landing Road
Moorestown, NJ 08057-3075

Michael Connaughton
Brand-Rex Company
1600 West Main Street
Willimantic, CT 06226-1128

Eli J. Joseph
Mail Stop 138-227
GE Aerospace
199 Borton Landing Road
Moorestown, NJ 08057-3075

Larry Rogers (PMS 400B3B)
Naval Sea Systems Command
Department of the Navy
National Center 2, Room 10E24
Washington, DC 20362-5101

Abstract

During the 1980's, the AEGIS Shipbuilding Program developed replacements for both multiconductor and radio frequency (RF) Mil-Spec cables. These new cables included low smoke, low toxicity and flame retardant materials. Cable specifications called for cross-linked (thermoset) jackets to provide ruggedness, durability and the ability to withstand higher temperatures to retard flame spread. Now that system data rate requirements are driven to use optical fibers as the necessary transmission medium, the same rugged shipboard hardened jacketing system that has proved successful for Navy copper cables is proposed for fiber optic cables. This will ensure that fiber optic cables will maintain the overall system integrity previously baselined for power, control, and signal cables.

Introduction

Today, as data communication systems become faster and more complex, the need for greater information capacity becomes increasingly important. Because of inherent problems associated with copper paths at high data rates (e.g., limited bandwidth, crosstalk and attenuation), optical fiber was selected as the proposed solution. The effectiveness of optical fiber systems is well established in the commercial industry and is gaining wider acceptance in military applications. Such is the case in the AEGIS Program.

General Electric's Government Electronic Systems Division (GESD), formerly RCA, in Moorestown, NJ, has proposed incorporation of the first fiber optic local area network (LAN) in the AEGIS Combat System Tactical Graphics LAN. GE/GESD is the AEGIS Combat System Engineering Agent and is ultimately responsible for Combat System integrity when equipment is installed on the Navy's *Ticonderoga*-class cruisers and *Arleigh Burke*-class destroyers. Engineering analysis performed on the Tactical Graphics and review of system requirements showed that an optical data transmission LAN would be required; hence the requirement for fiber optic cable.

Shipboard fiber optic cable posed a unique problem for cable manufacturers because of the Navy's requirement for a Low-Smoke/Low-Toxicity (LS/LT) thermoset jacket. The processes used to manufacture a thermoset jacketed cable suitable for shipboard use historically have severely degraded the performance of the optical fibers. However, allowance to use thermoplastic jacket materials could jeopardize the ruggedness of the cable and could cause unforeseen system installation/integrity problems.

Cables installed on AEGIS-class ships must be durable enough to withstand the harsh installation techniques used at the shipyards and exposure to various environmental elements. Those affiliated with new ship construction or overhaul procedures are familiar with the stringent environments to which cables are exposed. Shipboard cables must be capable of enduring abrasive and sharp metal edges upon installation, severe weather, and exposure to high-temperature solvents and oils. During exposure to fire, these cables must be self-extinguishing and not emit dark smoke or toxic fumes. Over the past decade, copper cables were developed that meet these requirements.

Cable Development Background

Copper

In the early 1980s, an effort began in the AEGIS Shipbuilding Program office (PMS 400) to develop replacements for polyvinyl chloride (PVC) jacketed multiconductor cables specified in MIL-C-915. These new cables included material having LS/LT and flame retardant attributes. The first cables were designed to be lighter in weight, have lower smoke and toxicity generation when burned, and inhibit the propagation of fire. The results of this successful cable development is now referred to as the Advanced Marine Cable (AMC) design, which is contained in MIL-C-24640.

MIL-C-24640 cables were primarily designed for signal/control applications and did not include conductor sizes greater than 14 AWG. Many of the MIL-C-915 constructions were still needed for power applications, and changes to overall diameters would greatly hamper interchangeability and termination hardware. It was decided that the jacket material approved for MIL-C-24640 would be extended to power cables in MIL-C-915. These new cables were listed in a separate military specification, MIL-C-24643, so as not to confuse the LS/LT jacket material cables with PVC jacket material cables.

Having successfully developed these cable specifications (MIL-C-24640 and MIL-C-24643), the Navy implemented a program to introduce the cables in AEGIS-class ships. The program to phase in LS/LT jacketed multiconductor cables was initiated on USS *Vincennes* (CG 49) and was to be completed on USS *Lake Champlain* (CG 57).[1]

Since the design and development of LS/LT cables were addressed and handled successfully, PMS 400 funded a study to conduct a survey and define cables that did not use the new LS/LT jacketing system on AEGIS ships. This study was in direct response to a Department of the Navy directive that required the removal of all PVC from surface vessels.[2] The study revealed that approximately 23 percent, roughly 160,000 feet of cable used in the AEGIS Combat System was the flexible RF type that did not utilize the new LS/LT jacketing material. Almost all of these cables were procured to MIL-C-17.[3] It appeared feasible that techniques used in developing AMC cables could be applied to flexible RF cables.

An RF cable development program was initiated and RCA generated procurement specifications drawings 6322493 and 6262065. These two cable specifications were used to establish the criteria for cables interconnecting High and Low Level Serial interfaces, respectively, for MIL-STD-1397 Naval Tactical Data System equipment used in AEGIS ships.

Many different types of MIL-C-17 PVC jacketed, flexible RF cable constructions were reviewed for replacement. Therefore, work toward creating a general-requirements RF cable specification was initiated. The general specification contents were based on electrical performance requirements that were patterned after MIL-C-17, and the physical, mechanical, and environmental parameters patterned after MIL-C-24640. The specification was delivered as NAVSEA 6323050 and contains all criteria and test procedures for the family of RF cables used in the AEGIS Combat System today. Individual cable construction details are presently defined in separate "satellite" drawings that reference applicable test requirements, which are listed in the General Specification drawing. Recent completion of this program set the Navy benchmark for RF cable design.

Fiber Optic

In 1987, while Navy copper cable specifications were being upgraded, the AEGIS community generated a general specification for fiber optic cable, PMS-400-XYZ. This specification incorporated many of the physical and mechanical test requirements contained in MIL-C-24640. After a few years of development, PMS-400-XYZ was not adopted because of lack of system requirements to use optical data transmission. Without planned incorporation of an optical-based system into AEGIS, final cable development was left up to the discretion of the cable industry.

During the same time, the Naval Sea Systems Command Office (NAVSEA 56ZC) was generating fiber optic component specifications for the Navy. PMS-400-XYZ requirements were incorporated into DOD-C-85045C. However, requirements for a thermoset jacket were relaxed to the point where a thermoplastic jacketed fiber optic cable was allowed. DOD-C-85045C, which was intended to be a Tri-Service document, evolved into a Navy specification, MIL-C-0085045D. Again, the lack of optical-based systems in the Navy resulted in no approved supplier being listed on the Qualified Parts List (QPL) for fiber optic cables designed to this specification.

NAVSEA 6710781 Development

In support of the Tactical Graphics program, GE/GESD generated procurement documentation that defined the criteria for fiber optic cables in the same manner as those for LS/LT RF cables. A general specification for fiber optic cable was developed to contain common requirements. Individual procurement drawings referencing the general requirements were created similar to that of a military specification and its slash sheets.

The general requirements specification, NAVSEA 6710781, was based on NAVSEA 6323050 for mechanical and environmental performance, and PMS-400-XYZ for optical performance. Test parameters contained in the RF cable specifications were used to the fullest extent practical to allay the concern of putting optical fiber on Navy ships.

NAVSEA 6710781 specifies an electrically nonconductive fiber optic cable construction that uses jacket material that is cross-linked and environmentally stable, and possesses low smoke, low halogen and low fire hazard characteristics. Cables built to this specification are suitable for Naval shipboard applications, and are therefore waterblocked. All temperature requirements specified in MIL-E-16400, including Range 1 (−54 °C to +65 °C operating), for all environments, were met by this specification.

Program Development Objectives

There were four primary objectives in the initial phases of the development program. These objectives allowed Brand-Rex Company to focus on successfully developing a fiber optic cable that would be superior to those currently available in industry. These objectives were:

1. Developing a thermoset jacket that had little to no effect on attenuation.
2. LS/LT flame retardant material.
3. Tough, environmentally benign, waterblocked cable that had a minimum amount of cost impact.
4. Termination intermatability.

Thermoset Jackets. Cross-linking is a technique by which polyolefin thermoplastic materials are transformed into thermoset materials. Cross-linking allows individual polymer chains in the material to form a high three-dimensional network of molecules, thereby increasing the size of the molecule chains. The primary benefit is that the jacket mate-

rial is capable of exhibiting its intrinsic physical properties over a higher temperature range and also will not fuel a fire by liquefying. Other benefits also are gained by cross-linking: improved cut-through resistance and solvent resistance. The attributes of polyolefin thermoset jacketed cables for Navy shipboard use have been well documented over the past few years. MIL-C-24640, MIL-C-24643, and NAVSEA 6323050 all require the same type of thermoset jackets.

A particular problem in the PMS-400-XYZ cable was encountered when electron beam cross-linking occurred to transform the jacket into a thermoset material — the optical fibers in the cable were degraded. Brand Rex knew of this phenomenon and worked toward controlling their manufacturing process and selecting materials and components that would be less susceptible to the effects of electron beam cross-linking.

LS/LT Flame Retardant Material. Controlling smoke and toxicity levels during a fire is a major concern on Navy ships. Since the Navy had specified LS/LT requirements back in the early 1980s, it was apparent that these new fiber optic cables also had to meet that requirement. Specifying retardation of flame propagation attributes, along with LS/LT characteristics, has made these cables compatible with MIL-C-24640, MIL-C-24643, and NAVSEA 6323050 requirements.

The smoke test specified in UL 910 was selected over other test techniques. This test requires measuring the optical density of a burning cable in a confined area. Toxicity tests were performed to NES 713 specifications. This test allows measuring the toxicity/halogens levels expelled while a cable burns.

Fiber optic cables developed for the AEGIS Program had to be self extinguishing. The flame propagation test invoked was IEEE 383. This test is used to determine the ability of the cable to resist the propagation of a fire exposed at the bottom of its length. This ability to control flame spread will help contain a fire within a compartment, thereby allowing conventional firefighting techniques to be successful.

Tough Environmentally Benign Cable. There were many proposals over the past few years to include optical-based systems on Navy ships. Few have been accepted. Reluctance still exists to install "glass" on Navy vessels. To address this concern, fiber optic cables have to meet or surpass the requirements of their copper counterparts. Mechanical and environmental tests from existing copper cable specifications were adopted to preclude a compromise in overall performance. The goal was not to relax any requirements; in fact, some requirements were made more stringent. This would ensure that fiber optic technology is ready for the installation rigors and environments found on Navy ships.

Production cost for this type of fiber optic cable was a major concern. In a defense industry climate where decreased spending is the accepted business practice, fiber optic cables built to NAVSEA 6710781 had to be comparable with other available shipboard fiber optic cable designs. Even though the requirements contained in NAVSEA 6710781 were more stringent than any other Navy specification (hence better cable performance) the cable cost/performance ratio had to be calculated so that the gain in performance would outweigh any increases in cost.

Termination Intermatability. A major advantage of fiber optic systems over copper path systems is the reduced amount of different parts needed to create the system. A decrease in the amount of different part numbers has a cost/time savings ripple effect in the logistics and system maintenance. In copper systems, hundreds of different qualified cables are available, and with each different cable, there usually is a unique set of termination hardware, i.e., connectors and backshells. Fiber optic systems require only a few cable configurations (single mode or multimode) and number of transmission members (4-fiber, 8-fiber, etc.) are the varying characteristics. Methods had already been adopted to terminate Navy ruggedized fiber optic cables. They are: MIL-C-28876 heavy-duty connector, MIL-C-83522 light duty connector, or MIL-S-24623 splice. Therefore, any new cable design would have to be compatible with the existing termination hardware.

Program Implementation

With program objectives clearly defined, the focus shifted to a suitable cable design. The primary concern was whether an optical fiber was available that could withstand the cross-linking process. A fiber is usually received, along with a description of its optical performance. An important parameter for a multimode fiber is its attenuation. Prior testing showed that cross-linking by electron beam increases fiber attenuation beyond acceptable levels.[4] It was now believed that with advances in optical fiber technology and by carefully organizing the manufacturing processes, it was possible to manufacture a fiber optic cable using a cross-linked jacket with limited increases in attenuation. After a thorough analysis of available cross-linking processes, two were deemed viable: irradiation by electron beam and heat activated curing. It was decided by Brand Rex that electron beam curing would be the preferred method. A test plan was initiated to manufacture an 8-fiber cable. This cable would contain a mix of optical fibers from different suppliers.

Fiber Testing

An experiment was conducted using various optical fibers in an electron beam cross-linked jacketed cable to develop a cable that would meet NAVSEA 6710781. The objective was to prove the viability of the cable, as well as to gain comparative data for the different fiber types. Four different types of fiber were used in the cable:

- 62.5/125 graded index fiber from Supplier A.
- 62.5/125 graded index fiber from Supplier B.
- 62.5/125 graded index standard-grade fiber from Supplier C.
- Single-mode standard grade fiber from Supplier D.

Two of each of the fibers were assembled together in the cable, as shown in Figure 1.

Attenuation of each fiber was tested after each operation and tracked through the manufacturing process to determine the effect each operation had on the optical fibers.

It was expected that cross-linking by electron beam would have the most significant effect on the fibers' optical transmission characteristics. Optical fibers show a gradual recovery from the induced effects of radiation exposure. Therefore, measurements were planned at intervals immediately before and after cross-linking, then at 24 hours, five days, 28 days, and 12 weeks after cross-linking.[5]

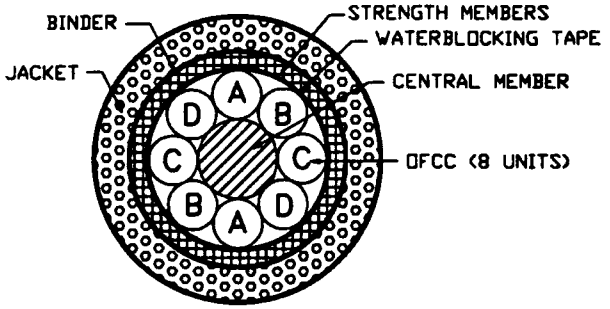


Fig. 1 Cross-section of eight-fiber test cable

The incoming fiber, post optical fiber cable component (OFCC) construction, and post-cable assembly measurements were made by using a Textronix TFP2 Fibermaster OTDR at 850 nm and 1300 nm for multimode fibers and at 1310 nm and 1550 nm for single mode fibers. The post-jacket, post-curing, and 24-hour measurements were made using a Textronix OF150 at 820 nm and a Tektronix OF152 at 1300 nm for the multimode fibers. No single mode measurements were made at these steps. All remaining measurements were made using the Photon Kinetics Model 2500 fiber optic test bench.

Results

As can be seen in Table I, all fibers had increases in attenuation through the jacketing operation. However, these increases were anticipated and acceptable. A dramatic change was noticed immediately following cross-linking. Vendors A and B retained acceptable losses at the 1300 nm window, but only Vendor B had a value that could be considered usable at the 850 nm window. Vendor C was rendered effectively useless after the operation.

After 28 days, fibers from all three vendors recovered to 2.0 dB/km or less at 1300 nm. Only Vendor B met the additional requirement of less than 1.0 dB/km change from incoming values.

An additional measurement was made at 12 weeks to allow the fibers additional time to heal. Vendor A showed improvement at the 850 nm window, but the attenuation was still unacceptably high. Vendor B values are close to commercial cable values at the 850 nm window at this point. Vendor C showed significant decreases in attenuation over the extended time.

Since single-mode (Supplier D) measurements were unable to be obtained during the intermediate manufacturing process, no values or conclusions were included in this report.

Optical Test Summary

Optical fibers manufactured by Supplier B retained their optical performance after electron beam curing of the cable jacket material. The long-term effects at the 1300 nm window were negligible, and the 850 nm window performance was within 0.6 dB/km of commercial grade "FDDI fiber."

Vendor A performed well at the 1300 nm window only, and Vendor C had marginal results.

TABLE I FIBER TEST RESULTS SHOWING DIFFERENCES BETWEEN MULTIMODE FIBER TYPES

Vendor	Wavelength NM	Incoming	Post OFCC	Post Cable	Post Jacket	Post Cure	24 Hours	5 Days	28 Days	12 Weeks
A	850	3.2	3.2	3.5	4.2	14.1	17.8	30.5	41.9	18.4
	1300	0.8	0.7	0.9	Note 2	1.2	1.3	1.7	2.0	1.3
A	850	3.2	3.3	Note 1	4.2	14.6	17.2	16.7	41.3	16.8
	1300	0.8	0.8		Note 2	1.1	1.3	1.5	1.9	1.2
B	850	2.7	2.8	2.8	3.5	7.1	5.9	8.7	6.4	4.1
	1300	0.5	0.6	0.6	Note 2	1.8	1.3	1.1	1.1	0.9
B	850	2.7	2.7	2.8	3.2	7.6	5.9	8.6	7.7	3.9
	1300	0.5	0.6	0.6	Note 2	1.9	1.4	0.9	0.9	0.7
C	850	3.0	3.4	3.7	4.2	25.0	25.0	32.2	8.9	9.1
	1300	0.6	0.9	1.2	Note 2	15.2	17.3	3.4	1.7	1.5
C	850	3.0	3.4	3.7	3.9	25.0	24.0	37.3	12.5	9.1
	1300	0.6	0.9	1.2	Note 2	15.6	16.2	3.2	1.6	1.5

Note 1: No end was available for test at this step.
Note 2: Because of interface problem, 1300 nm measurements were not made at post jacket.
Note 3: Post jacket/post cure/24-hour measurements were made using a wavelength of 820 nm.
Note 4: No values or conclusions were included from Supplier D (single-mode measurements.)

For dual window, multimode fibers assembled in a cable jacketed with cross-linked, electron-beam curing material, Vendor B's product was the only one that successfully demonstrated satisfactory results.

Cable Design

By organizing the cabling process to limit the number of operations, the likelihood of a mishandled fiber is reduced. Processes are in place to eliminate strain on an optical fiber during cabling. Once contained in a completed cable, the cable construction ideally absorbs all stresses applied to the cable without affecting the fiber. This process is followed for all fiber optic cables to ensure a strain-free fiber.

NAVSEA 6710781 allows for several cable constructions, but a 4-fiber multimode OFCC cable construction was the first utilized (NAVSEA 6710782 Cable, Fiber Optic, Multimode, 4-Fiber), as shown in Figure 2. NAVSEA 6710782 uses individual optical fibers (62.5/125) that are built-up with a color-coded buffer to 900 micrometers in diameter. Aramid yarn is then pulled in over the buffered fiber, and then jacketed to form the OFCC, as shown in Figure 3. The OFCCs are cabled along with strength members and waterblocking tapes prior to jacketing for overall protection, as shown in Figure 4. It is this finished cable that is exposed to cross-linking. After cross-linking, the total change in cable attenuation is specified not to exceed 1 dB/km, at an operating wavelength of 1300 nm, measured against received optical fiber values.

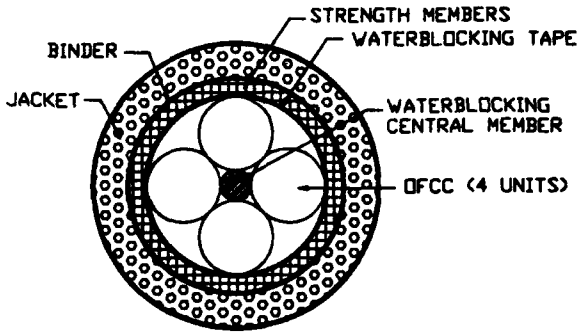


Fig. 2 Cross-section of four- fiber multimode cable

Test Requirements

The following is a sample of some of the more rigorous environmental and mechanical tests performed on fiber optic cables built to NAVSEA 6710781.

Fluid Immersion

In a shipboard environment, it is not uncommon for cables to come in contact with high-temperature fluids such as lubricants. When cables are exposed to high-temperature fluids, it is important that they continue to perform their intended function. The requirement in NAVSEA 6710782 specifies a test for a cable jacket's ability to withstand 24 hours of exposure to common shipboard solvents at elevated temperatures without degrading the tensile strength and elongation of the jacket by more than 50 percent. The fluids and test temperatures are those recommended by the National Electrical Manufacturers Association (NEMA). The test temperatures can also be found in MIL-C-24640, MIL-C-24643, and NAVSEA drawing 6323050.

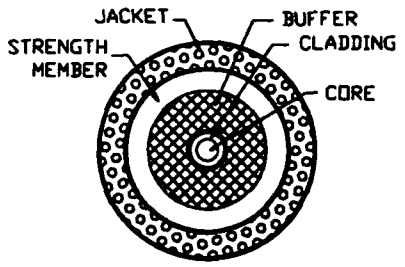


Fig. 3 Cross-section of optical fiber cable component



Fig. 4 NAVSEA 6710782 cable

Cable Abrasion Resistance

There are two cable abrasion resistance test requirements: scraping abrasion and cable-to-cable abrasion. These two tests are considered very important, since a torn cable jacket during installation would require either the cable to be repaired or a new cable to be installed.

The first test is a scraping abrasion resistance check. A cable can be exposed to many sharp edges during installation. Therefore, a cable jacket's ability to withstand repeated scraping without exposing the core components must be verified. The same test requirement is specified in Mil-C-17F. The cable jacket has to withstand a minimum of 750 scraping cycles. The second test is a cable-to-cable abrasion resistance check. This tests the cable's ability to be installed in crowded cableways where the cable-to-cable abrasion is along the cable's length. The cable jackets must withstand a minimum 500 cycles of scraping abrasion without exposing any cable core components.

Low Temperature Cold Bend

This requirement invokes a test to verify the cable's ability to be deployed at a reduced temperature of −54 °C and still operate. Since these cables can withstand extremely low temperatures and still perform their intended function, they are recommended for topside use. In fact, cables built to this specification are the only Navy fiber optic cables that meet the Range 1 temperature extremes per MIL-E-16400. A specimen is considered to have failed this test if the jacket reveals any surface damage, e.g., splitting or cracking, or if any of the optical fibers show more than 0.5 dB change in attenuation.

Halogen Content

In commercial fiber optic cables, halogens (most commonly fluorine and chlorine) are used in jacket materials as flame retardants. However, when burned, they create a dark, toxic smoke. During the Falkland Islands War, HMS *Sheffield* was hit with a missile. The resultant smoke and fire was responsible for many of the deaths of the crew members, which could be attributed to halogens contained in the PVC jacketed cables. This led to the British and U.S. Navy requirements of zero/low halogen jacketed cables. A specimen from the NAVSEA 6710782 is considered to have failed this test when there is more than 0.2 percent halogen found by weight.

Conclusion

The initial program goals were achieved. The same rugged shipboard hardened jacketing system that has proved successful for Navy shipboard copper cable has been successfully applied to fiber optic cables. The test performed on fiber optic cables built to NAVSEA 6710782 ensures that the cross-linking process provides little to no degradation of cable optical characteristics. With the stringent test requirements and tight process control invoked at Brand Rex Company, the AEGIS Program can be assured of a quality product. Now a fiber optic cable has been designed, manufactured, and tested which meets or exceeds the currently used copper specifications and is eminently suited to shipboard applications.

Footnotes:

1. Department of the Navy, Naval Sea Systems Command, Letter of Direction, 4460, 400G31/622 dated 26 March 1985. Request for ECP, to Implement Low-Smoke, Low-Toxicity Cables.
2. Department of the Navy, AEGIS Policy and Guidance Paper, 85-07, dated 26 March 1985, Introduction of Low-Smoke, Low-Toxicity Electrical Cable on AEGIS Cruisers.
3. "Development and Application of Low-Smoke, Flame Retardant Flexible RF Cable," Anthony R. Fedor, International Wire and Cable Symposium, 1989.
4. "Advanced Fiber Optic Cable Design for Shipboard Applications," Giovanni Tomasi, MFOC '88-West, 1988.
5. "Irradiation of Fiber Optics in the SCC Tunnel," C. E. Dickey, Document SSCL-261, March 1990.

Acknowledgment

The authors wish to thank Mr. Mark Joseph for his contribution to this program. Also, thanks to Mr. Bill Wood and Mr. Joe Gauvin for their patience and dedication during production and development of this program.

Biographies

Hal Russell is a member of the engineering staff at General Electric's Government Electronic Systems Division (GESD), where he has been employed since 1986. He has spent the last six years on the AEGIS Program, which provides the U.S. Navy surface fleets with antiair, antisurface, and antisubmarine warfare state-of-the-art defense technology. He is currently with the Advanced Ship Design & Special Projects group. He holds a BA degree in Physics from Rutgers University in New Jersey, and is currently working toward an MSEE degree at Drexel University in Pennsylvania.



Eli Joseph joined the engineering staff at GE/GESD in 1983. He has been working on the AEGIS Program for his entire GE career as well, particularly involved with AEGIS Weapon System Specification Standards and Qualifications. He received his BA degree in Industrial Engineering from State University of New York.



Michael Connaughton is a product engineer for fiber optic products at Brand Rex Company. He is a 1990 graduate of Wentworth Institute of Technology, where he received a BS degree in Engineering Technology. He is also a member of the Optical Society of America.



RECENT AND FUTURE DEVELOPMENTS IN CABLE TECHNOLOGY IN THE UK ROYAL NAVY

T Dawson

UK Ministry of Defence, Bath, England

Summary

The requirements for cabling in UK Royal Navy (RN) Warships in the immediate future are being made increasingly stringent as greater knowledge and experience is gained and cable technology advances. To achieve current goals some fundamental rethinking of construction techniques or installation practices seem inevitable and this combined with decreasing demands is placing considerable strain on the development process. A review of the history of the current situation is combined with an analysis of the future trends and movements in technology to indicate how future requirements may be achieved.

Developments in Copper Cabling

Background

In the last 20 years there have been in excess of 2000 shipboard fires, of which some 10% were significant and all of which were accidents not directly caused by cable equipment. Whatever the cause, the effect upon the cable equipment adjacent to the fire material has been consistent, extensive burning of insulation materials, loss of continuity as well as smoke and chemical emission damage. In many instances the consequential damage to electrical equipment was greater than that directly attributable to the fire. While the immediate loss of life as a result of these incidents was fortunately not very great, probably as a result of good fortune and well trained crew members, the loss of ships either completely or from an operational pool could have had disastrous consequences. Therefore the political will, and hence some financial provision, was placed firmly behind a program of work to remove the perceived problem.

Environment for Development

Before addressing the developments and attempting to look into the future it is worth explaining some of the constraints which are imposed by RN Ship Construction Techniques as far as one is able within this forum. While some of these may be common to other activities and nations there are one or two which have limited the extent of permissable change.

Compatibility. R N Ships have a design life of 25 years or greater and therefore a decision has to be made whether or not changes to cable equipments are to be applied retrospectively. A policy decision to employ new material where possible at refit opportunities within the normal constraints of cost and timescale lead to a compatibility constraint. New items have to be compatible with old.

Size and Weight. The constant demand to reduce space and limit the top-weight effects of ships cabling was a constraint which is easily achieved using modern materials.

Cable Installation Techniques. This was a constraint which was initially overlooked with some expensive results. Ship "electricians" have for years been a highly skilled team of workmen who have developed their own methods of installing cable equipments within fairly broad prescribed methodologies.

Cable Joining Techniques. The preferred and authorised way of jointing and terminating cables on RN Ships is by the use of crimping backed up with insulation and cable sheath repair by taping or sleeving. New cables had to allow this well established technique to be continued.

Glanding Techniques. The use of various glanding techniques, pre-formed bulkhead penetrators, multi-transit glands, etc, was well established and viable alternatives were not available. Therefore new cables and materials had to be compatible with these items.

Cable and Wire Development

Existing Technology. Prior to 1982 all cables fitted to RN Warships were constructed using PVC, EPR, CSP, Silicon Rubber and similar cable materials. These cables were designed for use in conjunction with particular glanding processes but many were variants of commercial design. They were purchased against specifications which were produced in collusion with the British Cable Industry. These documents spelt out in great detail the methods of construction required, the material specifications to be used in the make-up of the cables and the tests to be applied during production and on the final product. Director

General Ships (DGS) Specifications 211[1], 212[2], 213[3], 214[4]). A few of the products, because of their unusual nature and the lack of a commercial application, required the manufacturer to undergo qualification approval. However, outside of these few specials, because of the detailed nature of the specifications any manufacturer could supply cables to these specifications and in all cases the end products would be extremely similar. As a result, installers would be familiar with the cable, wherever it was manufactured, and all ancillary equipment could be developed to meet the common product standard.

Motivation. While the resultant cable equipment was generally satisfactory, despite one or two isolated problems, in the latter part of the 1970s there was some pressure to improve the make-up of these old cables to reduce the effect of fire on the materials used. However, obtaining funds to make the potential step change required was difficult. At that time the noxious and corrosive properties of the smoke from burning PVC insulated cables and the dense smoke from other traditional materials had been experienced on a number of occasions.

As a result of the Falklands Campaign, there was even greater experience of the problem, and because of the high profile of the effects, considerable political will, and some finance, went behind the drive to reduce the toxic and smoke emissions from cables exposed to fire and high temperatures.

Development. The work which had been ticking over for years came into prominence and a programme of development was established in conjunction with British Cable Manufacturers to write specifications for Low Fire Hazard Cables and to search for suitable materials to meet these specifications. However, at that time an important philosophical change was made in the style of the specifications. Because they would no longer be based on established commercial practice, it was no longer possible to define in precise detail the make-up of the various products.

Therefore, it was agreed that performance specifications would be written which would allow each manufacturer to choose suitable techniques and materials within some overall constraints. However, it would also be necessary for any manufacturer to prove that his product met the relevant specifications and thus earn a certificate of qualification approval.

Specification Development

At this time the definition of these new cables was altered to be Limited fire Hazard Cables (LFH) which enabled a progressive improvement to be established without semantic problems. The initial specifications were written to cover four main areas:

- the sheath material,
- conductor insulation,
- small cables with thin-wall insulation and
- larger cables where the thickness of the insulation was not a significant factor.

The actual specifications for these aspects are respectively:

- NES 518[5] to cover the Sheath Material, this has successfully been converted into Def-Stan 61-12 Part 31[6].
- Def-Stan 61-12 Part 18[7] for the insulated conductors and equipment wires,
- NES 525[8] for cables having thin-wall insulation and up to 2.5mm^2 csa conductors,
- NES 526[9] for cables over 2.5 mm^2 csa conductors and normal insulation.

These specifications are of two types, as shown, the Naval Engineering Standard (NES) and the tri-service Defence Standard (Def-Stan). There is a general policy that the former should whenever possible develop into the latter, but to amalgamate without losing essential individual requirements is not easy. Standardisation people by definition are unwilling to accept that ships are different from aircraft and tanks. (It is significant that the ultimate development route leads through British Standards (BS) to European Standards and hence to International Standards. This will take many years to achieve).

The noteworthy aspects of the standards for sheath material and conductor insulation are contained in the actual limiting requirements for the materials and the test methods to be applied to ensure that the requirements are met. The most significant of these are summarised in Tables 1 and 2. (Where tests to a British Standard (BS) are quoted the NES will contain much more detail of the test parameters to be used).

Table 1 shows the relevant test figures for NES 518[5] which also apply to Def-Stan 61-12 Part 31[6].

Table 2 shows test figures applicable to equipment wires to Def-Stan 12 Part 18[7]. This is a tri-service document and requires careful application to determine what is acceptable for naval use, eg the document allows the use of either single strand or multiple strand conductors whereas for Navy use only multiple strands are now permissible.

Note that the nature of these standards does not allow a direct comparison between them. They are, however, equally stringent and based upon the common LFH philosophy.

TEST PARAMETER	LIMITS	TEST METHOD
Tensile Strength	8 N/mm² minimum	Test on dumb-bell
Elongation at break	200 % minimum	Test on dumb-bell
Elongation at yield	120 % minimum	Test on dumb-bell
Tear resistance	5 N/mm minimum	Test on dumb-bell
Thermal endurance	40,000 hrs at 85 °C	BS 5691[10]
Accelerated ageing	Agreed each time	BS 6469[11]
Critical Oxygen index	29 minimum	NES 714[12]
Temperature Index	250 °C minimum	NES 715[13]
Toxicity Index	5 maximum	NES 713[14]
Halogen content	Negative for all halogens	Lassaigne test
Smoke Index	20 maximum	NES 711[15]
Resistance to fluids	Tensile strength 60% Elongation at break 60% Volume Swell 10-50% dependant on fluid.	28 days soak in fuel oil, hydraulic fluid, lubricating oil and water at various temperatures
Ozone resist.	No cracks	BS 6469
Cold elongation	20% minimum elongation	BS 6469
Heat Shock	No cracks	BS 6469
Hot Set Test	Max el. 175% Max perm. el. 25%	BS 6469. 200 °C, 0.2 N/mm²
Insulation Resistance	0.1 MΩ Km	

Ambient Temp range -30°C to +105° C

NES 518. Requirements for Limited Fire Hazard Sheathing for Electric Cables' includes the acceptance test limits shown.

TABLE 1

TEST PARAMETER	LIMITS	TEST METHOD
Thermal Endurance	40,000 hrs at 85 °C	BS 5691
Dry Spark test	Pass	BS G230[16] 5 kv or 8 kv
High Voltage Immersion test	Pass	BS G230 at 2.5 kv
Insulation resistance.	0.1 MΩ minimum	BS G230 Wood's Metal
Surface Resistance		BS G230
Dielectric Constant	> 4 at 1 KHz	BS G230
Dry Spark Test	Pass at 1 KV	BS G230
Critical Oxygen index	29 minimum	NES 714
Temperature Index	250 °C minimum	NES 715
Toxicity Index	0.2 max for 1m of size 22 wire (was 1.5)	NES 713
Hydrochloric Acid Gas Concentration	10 cm³ / metre	NES 713
Smoke Index	12 max for 1m of wire	NES 711
Resistance to fluids	2.5 KV test after 7 days Pass.	7 days soak in fuel oil, hydraulic fluid, lubricating oil and water at various temperatures.
Resistance to solder heat	Max 1 mm retraction	Stripped end immersed in molten solder.
Flammability Test	Pass	BS G230 5 or 12 seconds in flame

Ambient Temp range -30°C to +105° C

Def - Stan 61-12 Part 18. insulated conductors and equipment wires includes the acceptance figures shown.

TABLE 2

Cable Development

The physical cable development was influenced by two overriding factors. These were the ability of manufacturers to meet the requirements and agree the test limits and methods and the potential cost of the resultant product.

Test Limits and Methods. While many of the elements are common to standard cable standards, great debate and argument centred upon the fire hazard characteristics of the specified materials. Flammability, toxicity index, smoke index, oxygen index, temperature index, mechanical strength and resistance to fluids are the particular areas where difficulties and compromises have had to be made. In addition to the actual stated figures there has been continuous debate about which test methods should be used within the specification. The current end result has been as a result of compromise and one or two "executive decisions".

Cost. While it has been accepted that the required gains were unlikely to be achieved without significant per unit length cost penalties, some limit had to be applied. The original figure dreamed up was "less than 50% increase in cost" and this has now been achieved.

Many of the parameters were not easily reached. The requirement for zero halogen sheath material in conjunction with all of the other limiting requirements was a particular example. However, because the standards were so new they could be developed in parallel with various involved manufacturers development exercises. The process was double edged from the manufacturers point of view. Whilst those involved initially were having to commit themselves to a certain element of "private venture" work, they were able to influence the standards to whatever their materials seemed able to achieve.

Current Position

The actual make up of each manufacturers material is a closely guarded secret and therefore any company not involved at the outset and later wishing to seek approval has the disadvantage that the specifications will now never be relaxed. Just the opposite, there are constant moves to tighten the requirements, especially with regard to toxicity and smoke generation.

From the users point of view we are now in the situation where the specifications are good, but further tightening is not out of order. We have a good system for approving manufacturers to the various standards. We are aligning more and more with National and International Specifications where this means no reduction in our standards. But our requirements in terms of quantity for shipboard cables are diminishing and therefore fewer manufacturers are capable of, or interested in manufacturing cables or becoming qualification approved.

Therefore our only hope is that more and more commercial bodies (and military organisations) recognise the validity and worth of using cables to our standards in hazardous environments. This added demand will encourage a larger manufacturing base and hence maintain both the availability of the cables and a competitive market.

It is worth noting perhaps that in comparison to the Naval Cable specifications used throughout countries of the NATO alliance the UK specifications are better defined and considerably more stringent thus leading to superior performance cables.

Aspects Overlooked and Lessons Learnt

One important aspect which was overlooked initially was the effect that the dramatic changes in materials would have on the installation process. The initial change required training of operatives in new techniques especially because of the increased strength and rigidity of the insulation and sheath. This was overlooked on the initial introduction with some disastrous results.

The second aspect which was overlooked was the difference between cables from different manufacturers as a direct result of using performance specifications. While the "important" parameters were defined those factors which are of greatest consequence to the installer, familiarity and feel, could not be defined. Therefore, installers were occasionally caught unawares by the differences between notionally identical cables from different manufacturers. This problem still exists but is lessened by awareness and experience by the installers.

Further Developments

Harsh Environments. Having covered the bulk of the cable requirements with the developments to date the next stage was to produce cables for use in the exceptionally intolerant environmental conditions found in particular areas. Generally in the past such cables have been Silicon Rubber Insulated and Low Smoke CSP sheathed giving them a thermal endurance of 40,000 hours at 95°C conductor temperature. To raise these to modern standards a new standard NES 527[17] was prepared for Silicon insulated cables with a LFH sheath to Def-Stan 61-12 Part 31. This was relatively painless but only one company is so far approved to this standard.

The Final Step. However, everything which has gone so far has only been the practice heats in the race to the ultimate requirement, a fire survival cable which can be used in all circumstances. The standard for such cables (NES 528[18] is now in draft form and the significant

requirements are as follows

Sheath material:	LFH type with toxicity index less than 5, fire survival at 750°C for 3 hours (1100°C for 20 mins), zero halogen, fluid resistant as previously defined.
Insulation:	To meet LFH and fire survival requirements.
Cable:	Resistance to fire test as specified in BS 6387[20]. Fire, spray drench and mechanical shock followed by electrical tests combined to assess fire survivability.

This is seen as the ultimate development in cable technology for the UK Royal Navy and should provide the materials for the fleets of the next century. If it is as successful as hoped, and can be satisfactorily developed and manufactured there is likely to be a special form produced which will also survive ionising radiation. This later variant, however, will have a very limited and specialised usage which may either make it impossibly expensive because of low usage or not a practical proposition for any cable manufacturer. The Navy may rule the waves but these days it has to be accepted that it has very little influence on cable manufacturers when times are hard and demand is low. Additionally, such extreme requirements require careful justification from both engineering and operational viewpoints.

Potential Contenders. Of course there are cables in existence which might come close to meeting some or even most of these requirements. Mineral insulated cables are a strong contender but they would introduce a considerable weight penalty if used throughout a ship and also pose conductor size constraints. However, their use, with stainless steel jackets, is well established for particular applications. There are also a number of established materials which could be used in a cable to meet the requirements. It is hoped that combining these will provide the required result thus eliminating the need for any new material development. It is just a pity that halogen free PTFE is not possible!

Alternative Solution. Just in case none of these product developments come to fruition there is also a continuous review of ships wiring requirements and methods to see if any new radical approaches are possible. To date very little progress has been made in these respects. The UK RN now places the design responsibility for new ships with industry and this is by nature very conservative. The timescale from concept to order and build is also very long so any new techniques will not be used for many years.

Standardisation of Fibre Optic Cabling

For signal wiring, fibre optics is a strong contender. Previously this was only being considered for use in particular projects and consequently there was some proliferation in types and sizes and little standardisation. The production of a standard NES 1009[19] has brought this situation under control and allowed the greater potential and quality use of FO for ships cabling. This standard has also ensured that the sheath of FO cable is thick enough to allow easy handling and installation as well as being made of true LFH material in accordance with the standard for cable sheaths. However, progress is still restrained by the need for find suitable compatible methods of installation, glanding, redundancy, repair and terminations.

The first step that must be made is to increase the potential survivability of FO cables which is, in theory, considerably less than copper equivalents. This increase can be assisted by multiple redundancy but the limiting factor is likely to be the skill level and complexity of repair of a fibre vis-a-vis a copper cable. The fastest method of repair is possibly complete replacement, but this is made more difficult when the cables pass through glanding systems. Therefore some line repair facility will be required and assessing and developing the ability to do this in real shipboard conditions is likely to take considerable time and effort.

All fibre optic cable will be of the tight buffered, tight tube, silica cored type. The use of blown fibre technology has been considered and is currently being assessed, but the problem with glanding and watertight integrity are as yet unsolved.

Glanding of FO cabling is another area where there is no obvious solution. Watertight and pressure tight bulkhead and hull hlands will be required and as yet little experience of successful design for RN use is apparent.

Jointing and installation will remain an area where high levels of quality assurance will be required as well as cleaner and better defined conditions for carrying out the work.

None of these aspects are impossible but until more shipboard fibres are installed the experience available to solve the problems will remain limited and unsure. The option remains that FO ship cabling could be installed with the associated system installation instead of in readiness for the installation. This will limit the number and extent of joints and should not be any more difficult to achieve than many other equipments. It is however, a complete change in philosophy and may require some radical rethinking of some of the ship design features.

Underwater Cabling Developments

The processes used for underwater cables, glanding and connections have for a long time followed a different development path to inboard equipments. Clearly cable equipments completely and permanently submerged do not need to be Fire survival or even LFH and therefore Polyethylene has formed the primary material for such work. This has the advantage that it is easily mounded and sealed and resistant to sea water. Its mechanical strength, certainly against abrasion and sharp edges has its detractors but these factors can be overcome in the design of the installation.

The off-shore oil industry uses both polyethylene and the much tougher polyurethane cables but our experience has precluded the latter. While much of the design work for these systems is well established, jointing, repair and installation techniques still need some development if only to reduce the size and space requirements. There is also a constant search for new ways of passing connections, and this includes Fibre Optics, through watertight and pressure tight interfaces with the sea. With the limited resources now available it seems probable that developments in commercial sub-sea components will form the basis for the next generation of equipment.

Conclusion

Demand for improved environmental factors on ships has played a major role in raising the standards of cable equipment used throughout the Navy. As a result, the UK MOD has specified and hence driven the development of new cable types in advance of most other organisations. However, these changes have caused problems in the traditionally based ship construction industry which, with the benefit of hindsight, could have been prevented by publicity and training. These shortcomings are now understood and for the next generation, these basic requirements will be met.

If the new developments are to be commercially viable it is important that as many users as possible understand, and where necessary, utilise the quoted new specifications, or their international derivatives, for installations requiring Limited Fire Hazard or Flexible Fire Survival cables. Our primary purpose must be to encourage greater general usage of these types of cables and consequently encourage more manufacturers to seek qualification approval against the various standards. This will result in a safer environment for many people, not just in the armed services, at a competitive and acceptable price.

(C) British Crown Copyright 1992/MOD

Published and Reproduced with the permission of the Controller of Her Britannic Majesty's Stationary Office.

References:

1. DGS Specification 211. Cables, Electrical, Silicone Insulated for General Services.
2. DGS Specification 212. Cables, Electrical, Ethylene Propylene Rubber Insulated and Chlorosulphonated Polythene Insulated for General Services.
3. DGS Specification 213. Cables, Electrical, Polyvinyl Chloride Insulated, Polytetrafluoroethylene Insulated, Rubber Insulated and Mineral Insulated for General services.
4. Cables, electrical, Miscellaneous, for Special Services.
5. Naval Engineering Standard 518 (NES 518). Requirements for Limited Fire Hazard Sheathing for Electric Cables.
6. Defence Standard (Def-Stan) 61-12 Part 31. Wires, Cords and Cables, Electrical. Sheaths Limited Fire Hazard.
7. Defence Standard (Def-Stan) 61-12 Part 18. Wires, Cords and Cables. Equipment Wires. Limited Fire Hazard.
8. Naval Engineering Standard 525 (NES 525). Requirements for Electric Cables, Thin-Wall Insulated, Limited Fire Hazard.
9. Naval Engineering Standard 526 (NES 526). Requirements for Cables Electric, Rubber Insulated, Limited Fire Hazard Sheathed for General Services.
10. British Standard BS 5691. Determination of Thermal Endurance Properties of Electrical Insulating Materials.
11. British Standard BS 6469. Methods of Test for Insulation and Sheaths of Electric Cables.
12. Naval Engineering Standard 714 (NES 714). Determination of the Critical Oxygen Index of Combustion Products of Small Specimens of Material.
13. Naval Engineering Standard 715 (NES 715). Determination of the Temperature Index of Combustion Products of Small Speciments of Material.
14. Naval Engineering Standard 713 (NES 713). Determination of the Toxicity Index of Combustion Products of Small Specimens of Material.
15. Naval Engineering Standard 711 (NES 711). Determination of the Smoke Index of Combustion Products of Small Specimens of Materials.
16. British Standard BS G230. General Requirements for Aircraft Electrical Cables.
17. Naval Engineering Standard 527 (NES 527). Requirements for Cables Electric, High Temperature Zones and Limited Fire Hazard Sheathed.
18. Naval Engineering Standard 528 (NES 528). Requirements for Cables Electric, Thin-Wall Insulated, Fire Survival, High Temperature Zones and Limited Fire hazard Sheathed. (Draft).
19. Naval Engineering Standard 1009 (NES 1009). Requirements for the Application of Fibre Optics in Ships.

Author:
Trevor Dawson BSc. MIEE. C Eng.
UK Ministry of Defence.
Room 102, B Block.
Foxhill.
BATH. BA1 5RG
ENGLAND.

Trevor Dawson is a Chartered Electrical Engineer who has been employed throughout his career in varied areas of the UK MOD (Navy). Although an Electronics expert by profession he is currently employed to manage the ongoing development of Cable Equipment for the Royal Navy which will serve into the next century. He sees the major requirement of this current post as the need to maintain development and commercial interest in the light of a reducing quantity of demand.



IMPLEMENTING THE CANADA-UNITED STATES FREE-TRADE AGREEMENT: HARMONIZING FIRE REQUIREMENTS FOR CABLES

Stanley Kaufman

AT&T Bell Laboratories
AT&T Network Cable Systems
Norcross, Georgia 30071, U.S.A.

ABSTRACT

As part of the implementation of the Canada-United States Free-Trade Agreement, the electrical codes in the United States and Canada have been harmonized with regard to fire resistance requirements and marking of communications cables. A cable substitution hierarchy has been introduced into the Canadian Electrical Code. The (U. S.) National Electrical Code has a new cable marking to indicate cables that have passed the Canadian FT-4 vertical tray fire test.

INTRODUCTION

The Canada-United States Free-Trade Agreement[1] stipulates that the United States and Canada shall not maintain or introduce standards which create unnecessary obstacles to trade between the countries. It states (Chapter 6):

> "The two governments will endeavour to make their respective standards-related measures more compatible to reduce the obstacles to trade and the costs of exporting which arise from having to meet different standards."

In order to implement the Free-Trade Agreement as it relates to trade in electrical equipment (including cables), the National Fire Protection Association, which issues the National Electrical Code®,[2] (NEC) and the Canadian Standards Association, which issues the Canadian Electrical Code[3] (CEC), formed the Binational Correlating Committee on Electrical Codes. The co-chairmen of the committee are Richard Biermann, who is chairman of the NEC Correlating Committee, and Roy Hicks, who is chairman of the Committee on the CEC.

The Binational Correlating Committee is working to identify parts of the two electrical codes which are hindrance to free trade. The first area identified for action was requirements for communications and optical fiber cables. In order to prepare proposals for changing the two codes a working group was needed. The Insulated Cable Engineers Association (ICEA) already had a working group which was attempting to harmonize the Underwriters Laboratories and Canadian Standards Association standards for communications cables. However, the prospects for harmonizing the UL and CSA standards was limited by differences mandated by the differences in the two electrical codes. Hence, the scope of the working group was expanded to propose changes in the codes, and membership of the working group, originally composed of cable manufacturers exclusively, was expanded to include members of Panel 16 of the NEC Committee and Subcommittee 60 of the CEC. Panel 16 and Subcommittee 60 are responsible for communications wiring regulations in the NEC and CEC respectively.

While the Canadian Electrical Code is revised continuously, the National Electrical Code is revised every three years. The deadline for proposals for the 1993 NEC was November 9, 1990. The working group prepared its proposals and the Binational Correlating Committee submitted them for the 1993 NEC. Proposals for the CEC were submitted in late 1990. All of these proposals were accepted and incorporated into the 1993 NEC and the 1994 CEC. The differences between the 1990 NEC and 1990 CEC requirements are primarily in fire resistance requirements. Hence, this paper will begin by reviewing the fire resistance requirements for communications and optical fiber cables in the *1990 NEC* and *1990 CEC*.

NEC FIRE RATINGS:

The 1990 NEC fire rating hierarchy[4][5][6][7] for communications cable is illustrated in Figure 1. At the bottom of the hierarchy are cables with a low level of fire resistance and deemed suitable for use in very limited applications, primarily in one- and two-family residences. These cables are labeled CMX. Next on the hierarchy are general purpose building cables which may be used anywhere in a building except in a riser shaft or on a plenum. These cables are labeled CM and may substitute for CMX cable. Riser cables, labeled CMR, are suitable for use in risers and may substitute for CM and CMX cables. At the top of the hierarchy are plenum cables; they are marked CMP and may substitute for CMR, CM and CMX cables. A typical application for a plenum cable is within a hung ceiling area used for air handling.

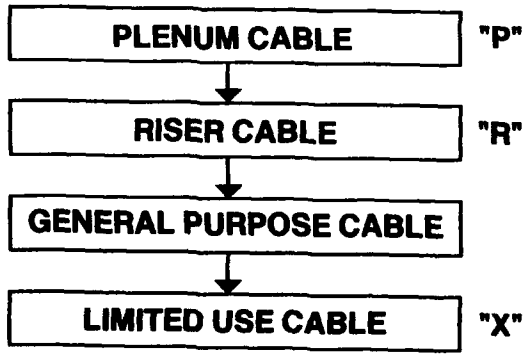


Figure 1. 1990 NEC Fire Rating Hierarchy

APPLICATION	CABLE MARKING	FIRE TEST
Plenum	MPP, CMP, OFNP, OFCP	UL-910
Riser	MPR, CMR, OFNR, OFCR	UL-1666
General Purpose	MP, CM, OFN, OFC	UL-1581/IEEE 383 or FT-4
Residential	CMX	VW-1

Figure 2. 1990 NEC Fire Hierarchy, Cable Markings and Fire Tests

Figure 2 shows the 1990 NEC hierarchy with the associated fire tests for each rating and the required markings for multipurpose cables (MP), communications cables (CM), nonconductive optical fiber cables (OFN) and conductive optical fiber cables (OFC). As we move up in fire resistance ratings, the severity of the associated fire test increases. The VW-1 test[8] for CMX cable is a low-energy Bunsen burner type test. The vertical tray test and for CM cables has two versions, the U. S. version contained in IEEE standard 383[9][10] or UL standard 1581,[11] and the Canadian version,[12][13] widely known as FT-4 test. Recognizing that the FT-4 test is more severe than the U. S. vertical tray test is an important fact to be utilized when the U. S. and Canadian hierarchies are interweaved. The riser test[10][14][15] for CMR cable is a large scale vertical test which simulates cables in a riser shaft. At the top of the hierarchy, the plenum test[10][16][17] is the most severe fire test; unlike any of the other tests, plenum cables have a requirement for low smoke emissions.

CEC FIRE RATINGS

The 1990 CEC fire rating hierarchy is shown in Figure 3. Cables used in combustible buildings are required to pass the FT-1 test,[18] and be marked FT-1. The FT-1 test is a Bunsen burner type test similar to the VW-1 test but somewhat less severe. Cables used in noncombustible buildings must pass the Canadian vertical tray test and be marked FT-4. Under the CEC, these cables may be used anywhere in a noncombustible building, including risers and plenums. In some provinces cables used in plenums are required to pass the same set of requirements as plenum cables in the U. S. and be marked FT-6. Canada has no formal substitution hierarchy; informally, cables labeled FT-6 are permitted to substitute for cables labeled FT-4 and FT-1, and cables labeled FT-4 are permitted to substitute for cables labeled FT-1.

APPLICATION	CABLE MARKING
Plenums (in some provinces)	FT-6
Noncombustible Buildings	FT-4
Combustible Buildings	FT-1

Figure 3. Informal Canadian Fire Rating Hierarchy

UL-910/FT-6 Plenum Test

UL-1666 Riser Test

FT-4 Canadian Vertical Tray Test

UL-1581/IEEE 383 U.S. Vertical Tray Test

UL VW-1 Vertical Wire Test

FT-1 Canadian Vertical Wire Test

Figure 4. Combined Hierarchy of Canadian and U.S. Fire Tests

HARMONIZATION OF NEC AND CEC FIRE RATINGS

The working group agreed that the UL 1666 fire test for riser cables was more severe than the FT-4 vertical tray test and the FT-4 vertical tray test was more severe than the U. S. vertical test. It also agreed that the VW-1 test was more severe than the FT-1 test. Consequently, the rank ordering of U. S. and Canadian fire tests as shown in Figure 4 was agreed upon.

Having recognized that the Canadian vertical tray test (FT-4) is more severe than the U. S. vertical tray test (UL 1581/IEEE 383), it was proposed that the general purpose listing category be divided into two subcategories with different markings. General purpose communication cables that passed the more stringent Canadian FT-4 test would be marked CMG, and be suitable for use in noncombustible buildings in Canada, whereas those that only passed the U. S. vertical tray test would continue to be marked CM and would be suitable for use in combustible buildings only in Canada.

The new fire resistance hierarchy for the 1993 NEC is shown in Figure 5. The only change from the 1990 NEC is to split the general purpose category.

The new fire resistance hierarchy for Canada is shown in Figure 6. There are several major changes. First, a substitution hierarchy based on the hierarchy of fire tests has been established. Second, cable markings are changed; cables previously marked FT-6 will be marked with the suffix "P" for plenum, e.g. CMP; cables previously marked FT-4 will be marked with the suffix "G" for general purpose, e.g. CMG; cables previously marked FT-1 will be marked with the suffix "H" for house, e.g. CMH. Third, recognizing that cables rated CMX pass a somewhat more severe test than cables rated CMH, CMX cables will be permitted to substitute for CMH cables.

APPLICATION	CABLE MARKING	FIRE TEST
Plenum	MPP, CMP, OFNP, OFCP	UL-910
Riser	MPR, CMR, OFNR, OFCR	UL-1666
General Purpose	MPG, CMG, OFNG, OFCG	FT-4
General Purpose	MP, CM, OFN, OFC	UL-1581/IEEE 383
Residential	CMX	VW-1

Figure 5. 1993 NEC Fire Hierarchy, Cable Markings and Fire Tests

APPLICATION	CABLE MARKING	FIRE TEST
General Purpose-Nonconbustible Buildings and Plenums (in some provinces)	MPP, CMP, OFNP, OFCP	UL-910/FT-6
General Purpose-Noncombustible Buildings	MPR, CMR, OFNR, OFCR	UL-1666
General Purpose-Noncombustible Buildings	MPG, CMG, OFNG, OFCG	FT-4
Combustible Buildings	MP, CM, OFN, OFC	UL-1581/IEEE 383
Combustible Buildings	CMX	VW-1
Combustible Buildings	CMH, OFNH, OFCH	FT-1

Figure 6. 1994 CEC Fire Hierarchy, Cable Markings and Fire Tests

U.S.	CANADIAN
MPP, CMP, OFNP, OFCP	MPP, CMP, OFNP, OFCP
MPR, CMR, OFNR, OFCR	MPR, CMR, OFNR, OFCR
MPG, CMG, OFNG, OFCG	MPG, CMG, OFNG, OFCG
MP, CM, OFN, OFC	MP, CM, OFN, OFC
CMX	CMX
	CMH, OFNH, OFCH

Figure 7. Cable Markings for the 1993 NEC and 1994 CEC

SUMMARY

Figure 7 shows the cable markings for the 1993 NEC and 1994 CEC for communications cables (CM), multipurpose cables (MP), nonconductive optical fiber cables (OFN) and conductive optical fiber cables (OFC). These markings harmonize cable markings for communications cables in the U. S. and Canada. With the exception of cables marked with the suffix "H", all markings will be identical.

The new cable substitution charts for the 1993 National Electrical Code are shown in Figures 8 and 9.

FUTURE CHANGES

Having just published the 1993 National Electrical Code in September of 1992, it's time to ask "What's next?" (The deadline for proposals for the 1996 National Electrical Code is November 5, 1993.) Proposals for Code changes often arise from an effort to improve the Code and make it more user friendly. One way to decide what parts need improvement is to determine which parts generate many requests for interpretation by the staff of the National Fire Protection Association.

The cable substitution chart, Figure 8, generated many requests for interpretation even before the addition of MPG and CMG cables. There are several possibilities for simplification. Contrast the substitution chart for metallic cables (Figure 8) with the chart for optical fiber cables. One difference that is immediately obvious is that there are only three levels of fire resistance in the substitution hierarchy for optical fiber cables whereas there are four levels for the metallic cables, except for fire alarm cables. One simplification is to eliminate "X" rated cables.

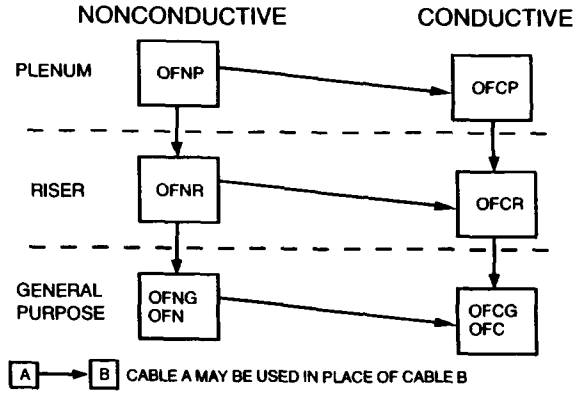


Figure 8. Cable Substitution Chart for Optical Fiber Cables in the 1993 NEC

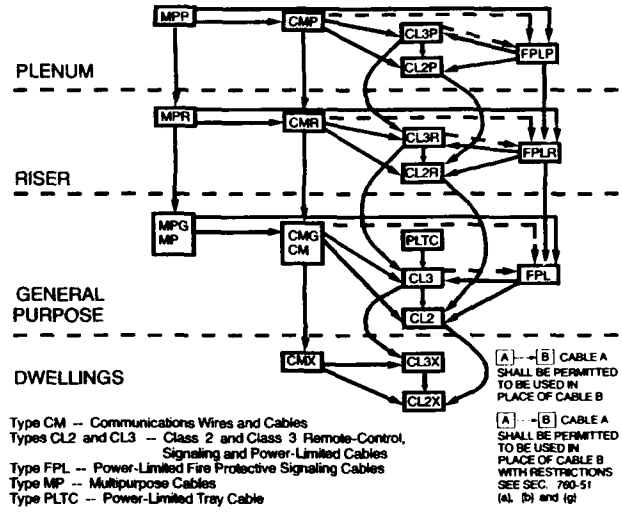


Figure 9. Cable Substitution Chart for Metallic Cables in the 1993 NEC

Another complication is the conditional substitution of communications cables for fire alarm cables. Multiconductor communications cables that meet the stranding and gauge requirements for fire alarm use in sections 760-51(a) and (b) may be used in place of fire alarm cable, and may also be listed as multipurpose cables. An electrical inspector cannot readily determine if a communications cable is suitable for use with fire alarm circuits. Enforcement of the Code would be simplified if only multipurpose cables were permitted to substitute for fire alarm cables. A further opportunity for simplification is to eliminate fire alarm cables and require the use of multipurpose cables for fire alarm circuits.

If these changes were adopted, i.e., elimination of "X" rated cables and fire alarm cables, and requiring the use of multipurpose cables for fire alarm applications, then the simplified cable substitution chart shown in Figure 10 would ensue.

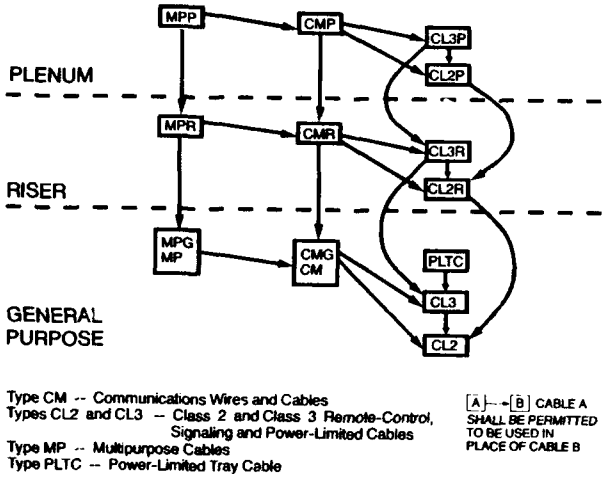


Figure 10. Simplified Cable Substitution Chart

ACKNOWLEDGEMENTS

The Code changes described in this paper were drafted by the ICEA Working Group co-chaired by Eric Gouldson of Northern Telecom and Arthur Fine of AT&T Bell Labs.

REFERENCES

1. Canada-United States Free-Trade Agreement, Final Text, December 9, 1987.
2. ANSI/NFPA Standard 70, *National Electrical Code®: 1990*, 1990, National Fire Protection Association, Batterymarch Park, Quincy, MA.
3. CSA Standard C22.1-1990, *Canadian Electrical Code, Part I*, Canadian Standards Association, Rexdale, Ontario.
4. Stanley Kaufman, "The 1990 National Electrical Code - Its Impact on the Communications Industry," *IAEI NEWS*, Jan/Feb 1990, p. 34.
5. Stanley Kaufman, "Fiber Optic Building Cables - The 1987 National Electrical Code Requirements," *Fiber Optics Magazine*, Jan/Feb 1988, p. 27.
6. Reference 2, Section 800-53(e).
7. Reference 2, Section 770-53(d).
8. Reference Standard for Electrical Wires, Cables, and Flexible Cords, UL 1581, First Edition, Section 1060, Underwriters Laboratories, Northbrook, Illinois.
9. IEEE Standard for Type Test of Class IE Electric Cables, Field Splices, and Connections for Nuclear Power Generating Stations, IEEE Std. 383-1974, The Institute of Electrical and Electronics Engineers, New York, New York, 1974.
10. Stanley Kaufman, "Fire Tests and Fire-Resistant Telecommunications Cables," *Fire Journal*, Nov. 1985, p. 33.
11. Reference 8, Section 1160.
12. Test Methods for Electrical Wires and Cables, Section 4.11.4 Vertical Flame Test - Cables in Cabletroughs, C22.2 No. 0.3-M-1985, Canadian Standards Association, Rexdale, Ontario.
13. Reference 8, Section 1164.
14. S. Kaufman, J. L. Williams, E. E. Smith, L. J. Przybyla, "Large Scale Fire Tests of Building Riser Cables," *Journal of Fire Sciences*, Vol. 1, No. 1, Jan./Feb. 1983, p. 54.
15. Standard Test for Flame Propagation Height of Electrical and Optical-Fiber Cable Installer Vertically in Shafts, ANSI/UL 1666-1986, Underwriters Laboratories, Northbrook, Illinois.
16. UL-910, Standard for Test Method for Fire and Smoke Characteristics of Cables Used in Air-Handling Spaces, Underwriters Laboratories, Northbrook, Illinois.
17. J. R. Beyreis, J. W. Skjordahl, S. Kaufman, M. M. Yocum, "A Test Method for Measuring and Classifying the Flame Spreading and Smoke Generating Characteristics of Communications Cable," *Proceedings of the Twenty-Fifth International Wire and Cable Symposium*, 1976, U. S. Army Electronics Command, Fort Monmouth, New Jersey, p. 291.
18. Reference 12, Section 4.11.1, "Vertical Test."

Stanley Kaufman is the Supervisor of the Chemistry, Environmental, Health and Safety Group in AT&T Bell Laboratories and AT&T Network Cable Systems in Norcross, Georgia. He is also the Environment and Safety Officer for AT&T Network Cable Systems global operations. He is a member of National Electrical Code Panel 16 which is responsible for Communications Wiring and is also a member of the Binational Correlation Committee on Electrical Codes. Dr. Kaufman has a B.S. in Physics from the City College of New York and a Ph.D. in Chemistry from Brown University.



NEW UNREPEATERED CABLE DESIGN TESTING METHODOLOGY AND RESULTS

S.C. Beech I.R. Doble J.R. Ford C.J. Rochester

STC Submarine Systems, Southampton
(part of the Northern Telecom Group)

ABSTRACT

A cable has been developed specifically for unrepeatered submarine telecommunication systems. The design process has been previously reported at the 1990 IWCS ref(1). For connection of cable section lengths and system repair a joint has been developed based on the proven STC repeatered cable jointing technology. Prototype and qualification cables and joints have been manufactured and their performance verified by an extensive test programme. Land based testing has been used to determine the performance envelope and prove that the in service performance limits can be achieved. A beach ploughing trial and sea trials have demonstrated that cable systems can be deployed and recovered using both conventional cable ships and converted flat back type vessels. This paper details the cable design, testing methodology and the results of the comprehensive programme of qualification testing. The test programme has proved that the cable and joints developed meet the required performance criteria for unrepeatered systems.

INTRODUCTION

The recent advances in low loss fibres, high power stable laser sources and very sensitive detectors at 1550 nm have made it possible for systems to operate over distances greater than 300 km without using underwater amplifiers. This has enabled many routes that previously could only have only linked with a repeatered system to be traversed by a single unrepeatered cable span. The cables traditionally used for unrepeatered links have been designed for long haul transoceanic repeatered systems. They have a very high cable strength, high hydrostatic pressure resistance and the ability to conduct high voltage electrical power to the submerged regenerators. These design features are not germane to unrepeatered systems and a more economical cable has, therefore, been developed for this application.

PERFORMANCE REQUIREMENTS

The fibres need to be adequately protected from the tensile and compressive forces experienced during laying and recovery operations. Fibre survival probability also needs to be guaranteed over the system lifetime of 25 years. Damage to the fibre by tensile elongation during deployment can be prevented by a high cable tensile strength and optimum selection of the fibre proof strain. Residual strain after deployment is also reduced by a high tensile strength. This reduces the probability of fibre failure by static fatigue.

Low fibre loss is essential for long distances to be spanned, particularly in coastal festoons where total cost can be reduced considerably through a reduction in the number of land based terminal stations. Low fibre loss has to be maintained during laying and recovery operations, and throughout the system lifetime. In addition to high tensile strength, preventing excessive elongation, a pressure tube must isolate the fibres from the hydrostatic pressure on the sea bed.

Hydrogen gas, causes an increase in attenuation when in contact with optical fibres, ref(2). It can be generated within the cable structure, or externally, as a by-product of metallic corrosion, organic degradation or magneto hydrodynamic effects. The polymeric materials may also outgas dissolved hydrogen or produce it by degradation. The fibres must, therefore, be protected by a suitable hydrogen barrier such as a welded metal tube. A copper tube 0.4 mm thick will reduce any loss increment from external hydrogen to less than 0.0003 dB/Km ref (1). None of the materials within the tube must significantly outgas hydrogen.

The only electrical requirement for unrepeatered cable is for the conduction of a low power 25 Hz toning signal for fault location if the cable becomes damaged in service.

The core must be insulated from sea water with an outer sheath that will also provide protection from abrasion, impact, tearing and stripping forces. A high rigidity material will increase the cable's torsional stiffness reducing the amount of twist under tension caused by strand generated torque.

In water depths of less than 1 km there is a risk of cable damage by external hazards such as fishing, ships' anchors or rocks. This can be significantly reduced by cable burial to depths greater than 0.5 metres into the sea bed. The cable then lies below the sea bed volume disturbed by the majority of hazards. Cable with a density of 2.2 to 2.5 kg/m3, higher than that of sea bed materials, will remain buried. High density surface laid cables will, in the majority of circumstances, self bury reducing the risk from external hazard damage. A higher density cable also has a greater stability to sea bed currents and therefore has a reduced risk from abrasion. Where the cable cannot be buried and there is a significant risk of damage, additional armour protection is required to increase the cable's density and strength.

The cost of transportation of the cable from the factory to the point of installation can be minimised by loading it on drums or in containers and sending it by conventional freight transport. The cables must therefore have a low diameter to maximise the length capable of being carried in each load.

The cable must have good handling properties when used with standard cable laying equipment on either conventional or non conventional cable laying vessels. This will give the system provider the freedom to select the most appropriate installation and maintenance solution for each particular project.

DESIGN DESCRIPTION

Figure 1 shows a telescopic view of the core cable design. The fibres are equally spaced around a high tensile steel kingwire at the centre of the cable and are embedded in elastomer to form a fibre package. This maintains a low optical loss by holding the fibres firmly and reliably in position. The package construction has been used with great success in many thousands of kilometres of STC repeatered optical cable systems now in service and there is no measurable loss difference between the fibre bought in and manufactured cable other than for splices.

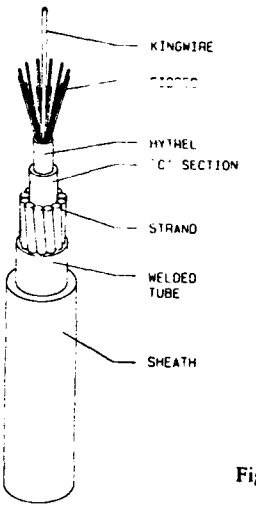


Fig.1

The fibre package is encased in a fully closed C section mild steel pressure tube. The interstitial gap between the package and the inside of the tube is filled with a high viscosity waterblocking compound to prevent water penetration if the cable becomes damaged. The internal diameter of the tube and all the materials within it are the same as used in the proven repeatered cable design. The fibres are therefore in exactly the same environment as in the repeatered cable producing a similarly low loss and high reliability construction.

Around the pressure tube is a unilayer of high tensile steel strand that provides the majority of the cable strength and is sufficient to maintain a cable strain on deployment or recovery below 0.5% to the maximum design water depth of 4 km. The strand lay length is optimised to minimise twist under tension but maintain cable flexibility. The interstices between the strand wires are fully water blocked to prevent axial water penetration if the cable becomes damaged.

A welded copper tube is formed tightly around the strand to act as a hydrogen barrier by preventing any external hydrogen from diffusing into the fibres, thus causing an increase in loss. All the materials within the hydrogen barrier have an insignificant hydrogen outgassing potential. This will ensure that there is a minimal loss increment due to hydrogen over the 25 year system lifetime. The copper tube is formed tightly to hold the strand for effective tensile load transfer when the cable is gripped. The tube increases the torsional stiffness of the cable, reducing the cable twist generated under tension. It also conducts a 25 Hz toning signal used for fault location.

The copper cladding is insulated from the sea water by a layer of high density polyethylene. This insulates the cable electrically from the sea for conduction of a toning signal. It also provides protection from handling damage.

The risk of damage in service is dependent on factors such as water depth, sea bed condition and marine activity. Three cables have therefore been developed with different levels of protection to suit the environment into which they are to be deployed. For any application the most cost effective solution that will reduce the risk of cable damage can be chosen.

For burial in shallow water and surface laying at depths where the risk from damage is low a steel tape protected (STP) cable has been developed. An overlapped corrugated steel tape and a high density polyethylene sheath are wrapped around the core cable. The tape is corrugated to provide an effective barrier against impact and abrasion whilst maintaining cable flexibility for ease of handling.

In shallow water where there are medium hazards from for example small fishing vessels a C65, 3.2mm, single wire armoured (SWA) cable has been developed. These wires will provide adequate impact and tensile strength that will protect the cable core from fairly severe impact and abrasion. The additional weight of the armour wires increases the cable density. This improves the self burial properties and makes it more stable in the sea bed currents reducing abrasion damage.

Where the risk from hazards such as fishing activity is much higher an A65, 7.6mm, heavy wire armoured (HWA) cable has been developed. This has a much more substantial layer of armour wires that significantly increase the impact resistance, density, stability and self burial properties.

The basic characteristics of the cable range are:-

	STP	SWA	HWA	
Outside Dia.	17.5	27.7	36.3	mm
Minimum UTS	43	120	275	kN
Min. bend rad.	0.5	0.5	0.75	m
Wt in water	2.45	9.81	25.2	kN/km

JOINT DESIGN

The unrepeatered cable joint design for the range of cables available adopts many of the jointing features of the proven repeatered submarine cable joint. The only significant deviation is a move away from the traditional injection moulded polyethylene joint insulation to a heatshrink joint encapsulation approach.

Prototype and qualification samples of all cable types with the corresponding joints have now been manufactured and a rigorous test programme undertaken to verify product performance.

QUALIFICATION OF THE PRODUCT

The philosophy towards product qualification of submarine cable systems has been proven on numerous cable and joint designs from analogue to the present iteration of the fibre optic design. Three basic stages are involved which together form the platform for high system reliability and installation confidence. The three stages are:

Prototype manufacture and test
Qualification manufacture and test
Sea trial verification

Stages 1 and 2 involve a comprehensive series of land based tests designed to explore the extremes of anticipated cable system storage, handling, transportation, deployment, recovery, repair and in service conditions. The tests also explore the ultimate performance limits of the cable system.

Optical monitoring at the system wavelength of 1550nm is the key performance parameter of the majority of tests. Optical loss changes of less than or equal to 0.05dB per fibre path are permitted.

Prototype Stage

This stage is used to verify that the chosen design of cable and joint meet the performance requirements of the qualification tests. On successful completion of these tests the design will be finalised and full system qualification undertaken.

For the new unrepeatered cable design 20 prototype test samples were manufactured in both steel tape protected and single wire armoured cable. Although not reported here all testing was successfully completed.

Qualification stage

Following the completion of the cable and joint design from stage 1, stage 2 involved the manufacture under full production conditions of 40 samples. Each test was completed on an STP or SWA cable sample and (*) denotes where the appropriate joint has also been tested. The qualification testing performed falls into three categories:

1.0 **Handling and storage**

TEST	PURPOSE
1.1 Turnover Test (*) 1.2 Coiling Test 1.3 Cable Drumming	To simulate worst case cable bend radii during factory handling.
1.4 Static Crush	To simulate worst case cable crush during storage.
1.5 Impact Resistance	To simulate objects falling onto the cable (maximum impact energy 20 Joules)
1.6 Bump and vibration (Joint only)	To simulate joint handling and movement.
1.7 Temperature Cycling (*) (See Fig.2)	To Explore extreme storage conditions -40°C to +60°C.

2.0 **Shipboard**

TEST	PURPOSE
2.1 Linear Cable Engine (L.C.E.)(*)	To demonstrate the dynamic and static operation at maximum depth and recovery tensions of L.C.E..
2.2 Torsion (*)	To Simulate the worst case twist generated in a cable tank (1 turn/5 metres).
2.3 Snatch Test (Joint Only)	To simulate the snatch loading of a joint coming out of a cable tank.
2.4 Round the sheave (RTS) 2 metre diameter (Joint Only)	To simulate the worst case recovery tensions over the bow sheave (STP 31kN, SWA 90kN).
2.5 Fatigue (*)	To simulate worst case tensions when repairing the cable (50 hour duration).
2.6 Tensile (*) Figs 3&4	To simulate extreme tension conditions in recovery or repair.

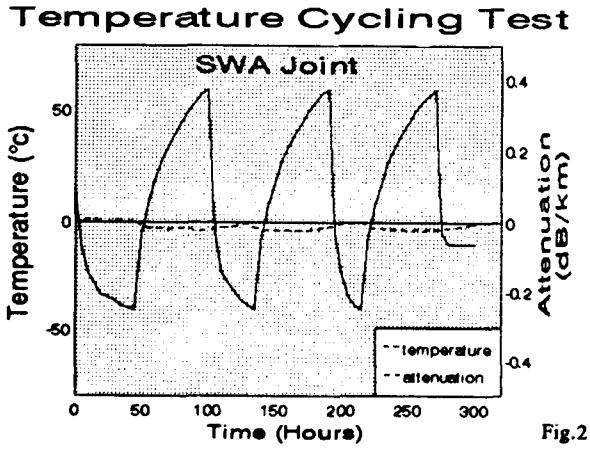


Fig.2

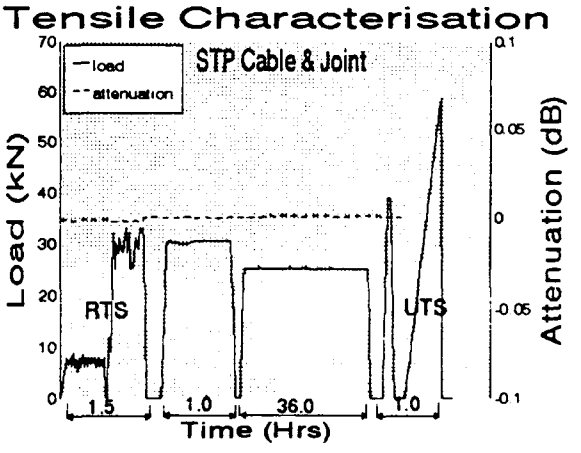


Fig.3

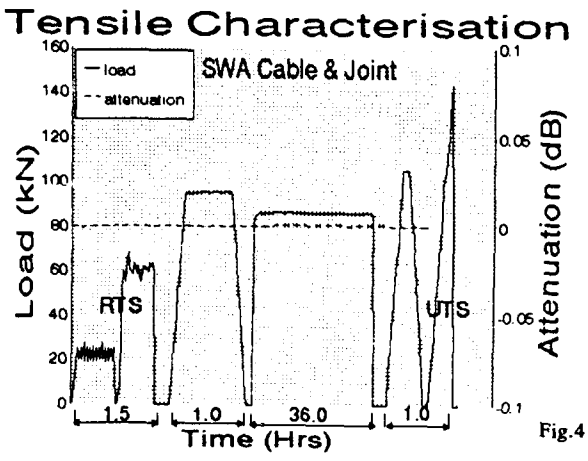


Fig.4

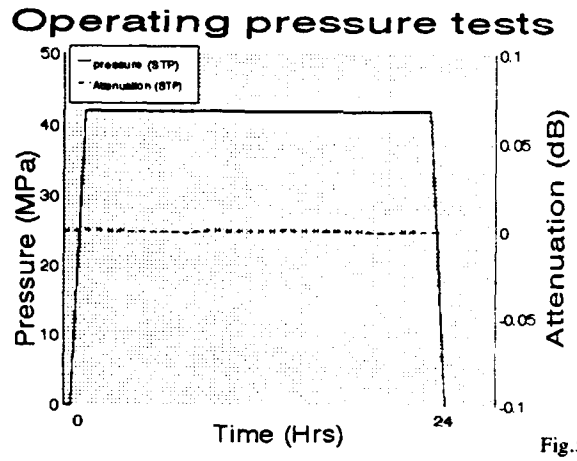


Fig.5

2.7 Cable Stopper	To demonstrate that a cable stopper can hold, during worst case conditions (STP 31kN, SWA 90kN)
2.8 Grapnel	To simulate recovery from the sea bed.
2.9 Block End Seal	To simulate buoying off, tensile and R.T.S. performance.
2.10 Bend/Flex	To demonstrate handling around a 1.8m diameter sheave
2.11 Elongation /Rotation	To demonstrate that cable strain gap, optical signal and cable geometry is acceptable during three loading cycles up to maximum service tension

3.0 Sea Bed

TEST	PURPOSE
3.1 Water blocking	To demonstrate that the cable effectively prevents water ingress at maximum sea bed pressures for 14 days (STP 41MPa,SWA 20MPa).
3.2 Corrosion (Joint Only)	To demonstrate that jointing components withstand a simulated 25 year life. (18months, 50°C).
3.3 Pressure Resistance See Fig 5.	To demonstrate that the cable system can withstand maximum sea bed pressure.
3.4 Hydrogen Evolution /Ageing	To demonstrate that over a simulated 25 years no material compatibility issues exist. Optical loss associated with any hydrogen evolution shall be within 0.005 dB/Km.

First sea trial

The first sea trial took place in August 1991 using a conventional cable ship. A mini system comprising of steel tape protected cables and three joints was deployed and recovered in a 20 metre water depth. Continuous optical monitoring was carried out with an OTDR and a 1550 nm laser and detector. The system was deployed with a payout tension of 1.5 tonnes to simulate deployment to the maximum design depth of 4 km. A diver inspection was then completed which showed that the system was lying satisfactorily on the sea bed. A bow to stern transfer was carried out and the system was recovered at a tension of 2.5 tonnes, representative of tensions at the maximum design depth.

The cable handled very well throughout the trial proving that it can withstand the 4 km water depth deployment and recovery tensions without any degradation in optical or mechanical performance.

Beach ploughing trials

Beach ploughing trials were completed, consisting of the ploughing in of lengths of STP cable containing STP joints to a depth of 0.7m. Fibre loops were optically monitored for fibre loss and strain throughout both trials. After plough manoeuvring trials the cable and joints were buried and subsequently peeled out, the peel-out

technique simulating the action of a holding grapnel. During the trials there were no optical loss anomalies measured and cable strains were well within acceptable limits. On examination the cable and joints showed no sign of damage, proving that they are robust and can be readily handled through a plough.

Shore end and ploughing trials

A second sea trial was completed using a flatback type vessel, specially converted for cable laying. A mini system of STP and SWA cables was assembled and subjected to shore end landing, deployment (including ploughing) and recovery operations.

The cable was transported by air, sea and land and was then off drummed into temporary creels in a warehouse adjacent to the quay. It was then assembled, tested and loaded onto the ship. During the trial optical monitoring was carried out on four fibre loops using a high stability 1550 nm loss measuring set, an optical length measuring set and two high resolution OTDR's. The SWA armoured cable shore end was deployed onto a beach. The plough was deployed and ploughing of SWA cable commenced 0.6 metres into the sea bed. Two STP/SWA transition joints and lengths of both STP and SWA cables were ploughed in. At the end of the deployment the plough was recovered and the system was inspected by divers. It was verified that the cable was laying flat on the sea bed at the shore end and was completely buried where ploughing had been carried out. The system was then recovered by peeling out the cable at a speed of 1 km/hr. During the trial there was no measurable change in the optical performance of the cable, demonstrating that a shore end can be landed and that both STP and SWA cables and joints can be ploughed into the sea bed successfully.

A65 deployment trial

A trial was conducted on a conventional cable ship in order to prove that the A65 cable can be deployed and recovered. An 800 metre length of A65 cable was loaded from a drum on the quayside into the ships main tank. The cable was then deployed in 200 metres of water, held briefly and then recovered. During the trial the mechanical performance and handling of the cable were found to be satisfactory.

FIRST COMMERCIAL CABLE SYSTEMS

The first commercial system to use this new cable design is already under construction. It is a coastal festoon in the Gulf of Thailand comprising 11 links and over 1100 km of cable. The system will be fully operational by mid 1993.

CONCLUSION

This paper has described the design of the range of cables developed specifically for unrepeatered telecommunications systems. The rigorous test programme involving land based testing and sea trials has been described and the results have proved that the design principles were sound and that the new cables will meet the performance requirements for unrepeatered systems.

REFERENCES

(1) Rochester C.J. et al.

"Cable Design For Unrepeatered Single Span Systems"

Proc of the IWCS, 1990, p 29 - 36

(2) Worthington P., Russell J.N.

"The design and manufacture of submarine optical cables in the UK"

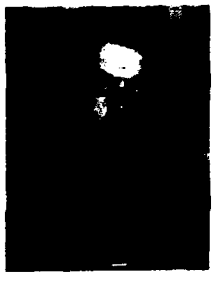
Proc of Sub optic, 1986,



Christopher Rochester
STC Submarine Systems
West Bay Road
Western Docks
Southampton
S09 4YE
United Kingdom

Dr Christopher Rochester is a Principal Engineer in the Cable Engineering Development Group at STC Submarine Systems.

He received a BSc in Chemistry and a PhD in Materials Science at the University of Sheffield. He started work at TSL on the development of doped silica glass preforms for optical fibre manufacture. Since 1988 he has worked for STC as a development project manager on high strength splicing, DOD and unrepeatered cables.



Ian Doble
STC Submarine Systems
West Bay Road
Western Docks
Southampton
S09 4YE
United Kingdom

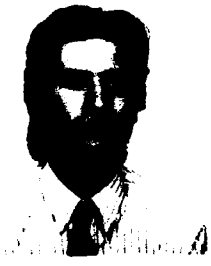
Ian Doble joined STC Submarine systems in 1987 where he is now Principal Engineer. He received a BSc in Physics from Southampton University in 1982.

As well as being involved with many aspects of cable and joint development within STC he has been responsible for the design and qualification of the unrepeatered cable joint.

John Ford
STC Submarine Systems
West Bay Road
Western Docks
Southampton
S09 4YE
United Kingdom

Dr. John Ford is responsible for the qualification testing and material selection for the unrepeatered cable design.

He obtained his first degree in Physics from Nottingham university in 1984. He then went on to study Polymer Science at Reading University. In 1988 he joined the Technical department of STC completing his PhD in 1991.



Craig Beech
STC Submarine Systems
West Bay Road
Western Docks
Southampton
S09 4YE
United Kingdom

Craig Beech was born in Burton-upon-Trent, England in 1969. He graduated from Reading University with a B.Eng in Mechanical Engineering in 1990.

Since joining STC in 1991 he has been working as part of the development and qualification team for unrepeatered submarine systems.

THE APPLICATION OF ELECTRIC STRESS ANALYSIS AND BREAKDOWN STATISTICS TO INSPECTION CRITERIA FOR SUBMARINE CABLE SYSTEMS

J. Bishop* A.E. Davies+

* STC Submarine Systems (Part of Northern Telecom Europe.) Southampton. UK

+University of Southampton Southampton. UK

ABSTRACT

Inspection standards for submarine cable systems were established in 1954 prior to the first transatlantic link being installed, to screen out defects likely to cause electrical breakdown. Despite various small modifications to the standard, the procedure for evaluating the level of voids and inclusions in the insulation has remained the same. The work outlined here provides the basis for updating the inspection procedure by the application of electric stress analysis (PE2D) to determine the levels of stress caused by the presence of defects within a polyethylene dielectric, and breakdown statistics for cable joints and terminations to determine the stress / time characteristics likely to cause HV breakdown. Rules can be established to limit void and inclusion sizes for given areas in a the bulk insulation.

1. INTRODUCTION

Long haul fibre optic submarine cables require power to enable the in-line signal regenerators to function. This is provided by a DC supply at voltages of up to 10 kV, The system is expected to last for 25 years in the sea-bed environment. Confidence in the system for these timescales can only be attained by high voltage testing to levels far in excess of service conditions. Low density polyethylene (LDPE) has been chosen as the insulation for these systems because of it's good electrical properties as well as it's excellent environmental resistance. Inclusions and voids need to be restricted as far as possible to prevent these defective areas becoming sites of excessive electrical stress and causing premature failure in the system. The part of the system that is subjected to the higher risk from this type of contamination are joints and terminations, because of the extra exposure to possible airborne contaminants during the moulding stage. Amalgamations resulting from this process also introduce regions of possible electrical and mechanical weakness.

The level of defects in a joint or termination can be detected by X-ray radiography on the completed moulding which is then assessed by examining the photographic plate. Voids and inclusions up to 0.1 mm can be detected in this way. The X-ray camera is rotated around the joint and photographs are taken at fixed angles around the moulding. This method of assessing the integrity of the moulding has been applied to many thousands of miles of cable in service which have run largely free of trouble for the desired service life. However the method of assessing the contamination is becoming further and further removed from the systems for which the standards were established - early analogue systems powered by AC supply. This is particularly poignant, because of the predicted increase in system voltages that will occur as a result of the introduction of optically amplified systems.

This work has enabled controlled HV (DC) breakdowns and Weibull analysis to forecast an electric stress below which a joint is unlikely to breakdown (powered at 10 kV DC for a period of 25 years). Electric Stress Analysis of the effect that the presence of various defect sizes, shapes, and positions have on the computed electric stress has enabled a set of rules to be established and has ultimately resulted in a fundamental change to the inspection standards.

2. ELECTRICAL BREAKDOWN ANALYSIS

Breakdown data was obtained for 3 different High Voltage tests - ramp to breakdown (74 mouldings broken down); 100 kV/ 9 days (22 mouldings broken down - 28 mouldings survived), and mouldings aged at service voltages for long periods (3 broken down during first 6 months, the remainder are still on test after approximately 4 years). The 3 sets of results were analysed using Weibull statistics.(see Figure 1).

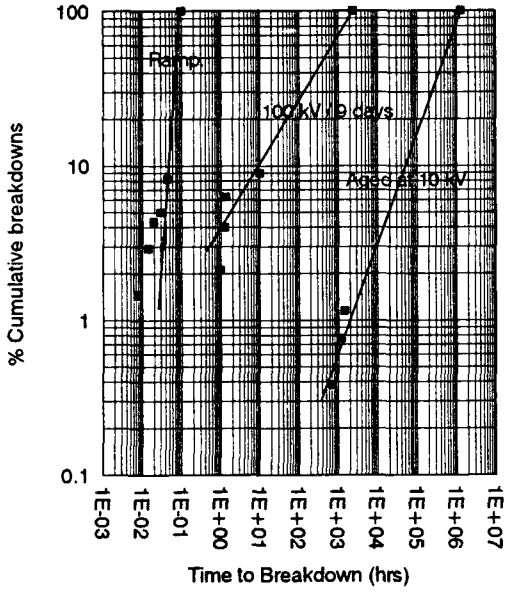


FIGURE 1 Weibull graphs for Ramp, 100kV/9 day and breakdowns at service voltages.

Taking the characteristic breakdown (63%) from each of the sets of results has enabled a plot of log time Vs log stress to be obtained. Using $\log_{10}$ enables the standard formula due to Peek[1] for life prediction to be employed:-

$$tV^n = k \quad \ldots\ldots\ldots\ldots\ldots (1)$$

$$\log t + n \log V = \log k. \quad \ldots\ldots (2)$$

where t = time, v = voltage, n and k are constants, the graph having a slope of n (see figure 2).

The results thus generated did obey closely the formula, giving an overall value for n of 6.3. The main aim of this work was to determine a level of electric stress below which breakdown would not be predicted to occur. This data suggests that after 25 years a stress below 6 kV mm^{-1} would survive at a constant voltage of 10 kV. In conjunction with the results from the computational analysis on uncontaminated mouldings, it is thus possible to calculate a stress enhancement ratio caused by the presence of given defects.

The connection between factory based tests and the service-type data ensures that the results obtained here are representative of the fibre optic systems that are currently in operation.

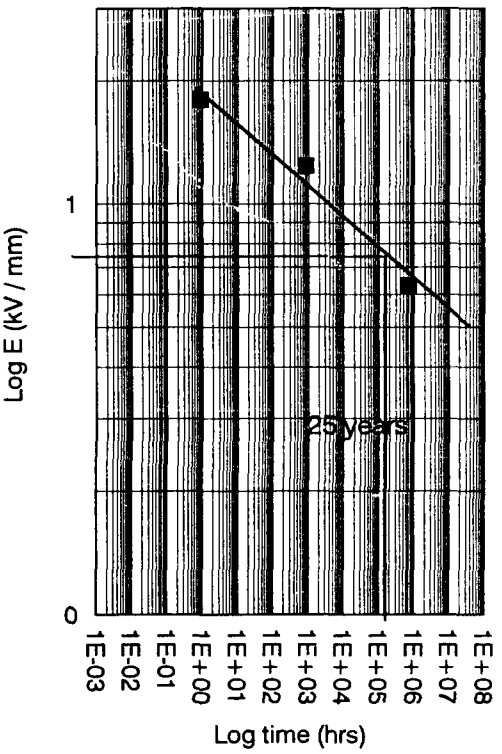


FIGURE 2 Stress vs Time graph based on 63% characteristic values.

While it would be possible to adjust the factory based tests on the strength of this data - by using an n value of 6.3, further work is in progress to generate experimental and controlled breakdown data to support this work.

A number of other valuable results can be obtained from this data. Application of confidence limits to the breakdown results show that a secondary distribution can be found from the ramp tests. The secondary distribution corresponds to the mouldings that breakdown at

the lowest voltages. These can be considered to be the sub-standard mouldings, and it is reasonable to assume that the breakdowns at service voltages belong to this category (because they are few in number and have occurred at short time spans). Once the sub-standard mouldings have been removed, it is predicted that the first breakdown from the main distribution of mouldings in service will take place well after the 25 year service life has been completed.

While there is no absolute way of determining the percentage of service mouldings in the secondary distribution, it can now be assumed to be very small, as no breakdowns have been found with these mouldings for several years. Furthermore, the incidence of service failures on more recently installed systems is now minimal, as a result of over-engineering in the final product.

It is also apparent that the type of breakdowns that occur under low electric stresses display more similarities to the breakdowns that are found during ramp testing than to an ageing test. This would indicate that a qualification HV test needs a ramp test element as well as an ageing aspect to give a high level of confidence in the fact that a system will not breakdown at any time during the life.

3. CONTROLLED ELECTRICAL BREAKDOWNS.

To establish a relationship between breakdown voltage and theoretical values, it was necessary to introduce carefully controlled defects into sections of cable and carrying out breakdowns on the cable samples, and then determining the resultant stress increase. Needles with 0.01mm tip radius were gently pushed into warmed sections of tail-tube (to minimise the mechanical stresses from the introduction of the needle). The needle penetration depth was measured before any voltage was applied. DC voltage was applied at a ramp rate of 10 kV min^{-1} across the insulation until breakdown (or flashover) occurred. The breakdown site was examined using microscopy to ensure that the needle penetration depth was correct. The geometry of the tail tube and the needle penetration depth were simulated using a finite element package (PE2D), which has been developed to solve electromagnetic problems. By changing the terminology and parameters, the package can be used to evaluate electric stress problems[2]. A relationship between the theoretical electric stress - at the tip of the needle was calculated using the wall thickness of the insulant. A good correlation between the computed stress and the experimental breakdowns was found (see Figure 3)

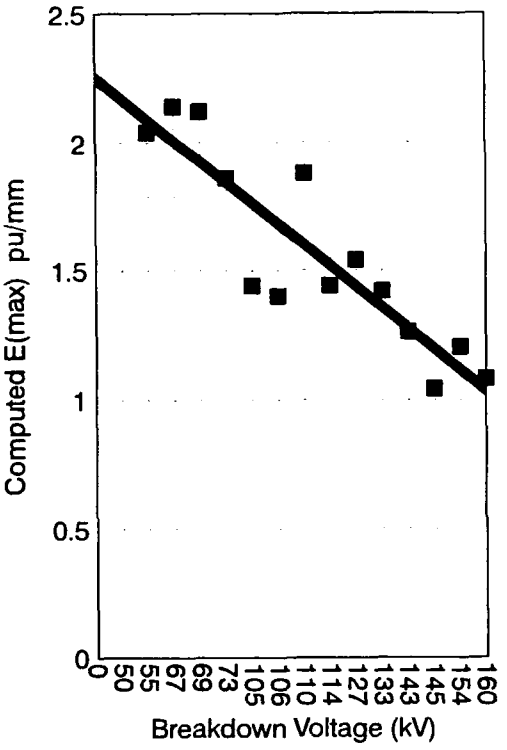


FIGURE 3 Plot of Actual breakdown stress Vs computed breakdown stress

4. ELECTRIC STRESS ANALYSIS.

A number of calculations were carried out simulating sections of a termination with no contamination. The computer was set up using axisymmetry about the y-axis in a divergent field. 1 per unit voltage was applied to the inner conductor and 0 per unit voltage to the outer surface. The stress along various lines across the insulation was calculated, and measured as a per unit per millimetre value (pu mm^{-1}). This can then be converted into

absolute stress by multiplication of the system voltage giving E in kV mm^{-1}

The model was then applied to smaller sections of the moulding but with defects in various positions in the insulation. Because axisymmetry was used the defect was modelled as being continuous and circular about the y-axis. This is a feasible modification since the X-ray diagnostic equipment is unable to accurately place the radial position of a defect. Inclusions were taken as being conducting and having sharp edges to assume the worst possible case. For modelling purposes a dry air void was assumed.

Five principal variables were taken:-

a) The size of the defect,

b) The depth of the defect in the insulation

c) The area of the moulding where the defect occurs.

d) The angle of the defect to the conductor

e) The influence of another defect nearby.

Taking the stress caused by the defect and dividing by the stress occurring in the same position of uncontaminated insulation enables a value for stress enhancement to be obtained for various contaminants, and quantitative limits for defects and sizes can be set based on the stress enhancement. A summary of the stress enhancement caused by some important defects is given in Figure 4.

The analysis did not prove to be very sensitive to the size of voids, and it was necessary to take account of a known key factor in breakdowns caused by voids - partial discharge activity. This work had been done previously[3] and the calculations resulting from this work were close to that previously established. A more important factor in this type of breakdown is the phenomenon of space charge injection, but as yet, the equipment to analyse space charge (Pressure Wave Propagation Technique)[4] is not suitably developed for quantitative results to be available, although progress is being made.

Inner Conductor	Tail Tube.	Joint body.
Stress in uncontaminated sample (pu/mm)	0.48	0.19
Stress in sample with 0.5 mm protrusion (pu/mm)	1.10	0.26
Stress enhancement	2.30	1.31
Outer Conductor		
Stress in undamaged sample (pu/mm)	0.25	-
Stress in sample with 0.5mm incision (pu/mm)	0.83	-
Stress enhancement	3.32	-

FIGURE 4 The effect of protrusions on the inner conductor and incisions to the outer conductor on electric stress

5. RESULTS AND DISCUSSION.

A number of rules as to the limits on defect sizes, positions, effect of two close contaminants have become clear, which had not been included in the previous inspection standard:

a) Contamination has a severe and unacceptable effect on the stress on or near the inner conductor. In regions of relatively high stress (such as the tail tube), very strict limits need to be imposed on the defect size. Contaminants and surface damage to the outer conductor also cause equally high levels of stress enhancement and great caution needs to be taken with the outer surface. It is important to ensure that incisions on the outside of a moulding do not have sharp edges, causing the outer surface to be the most highly stressed region of the moulding. Unlike damage to the inner conductor, steps can be taken to reduce the stress caused by such damage. Removal of the incision to leave a tapered smooth profile results in a much reduced level of electric stress on the surface. Damage

should be seen as being as dangerous as protrusions - protruding in from the outer conductor. Figures 5 and 6 indicate the stress caused by a damage to the outer conductor before and after the incision has been dressed out. Figures 5a and 6a show the equipotentials and a flux line A-B. Figures 5b and 6b represent the stress plots along the flux line.

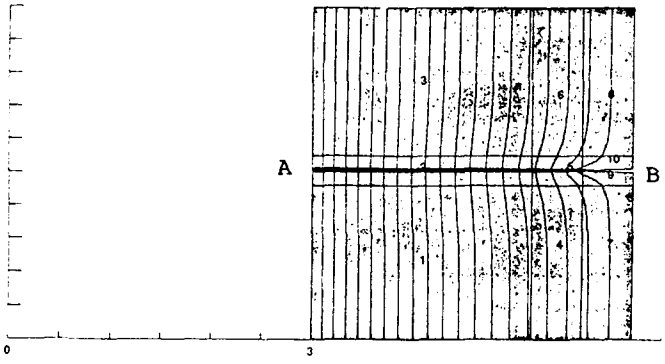


FIGURE 5a Equipotentials and flux for incision on outer surface of tail cable.

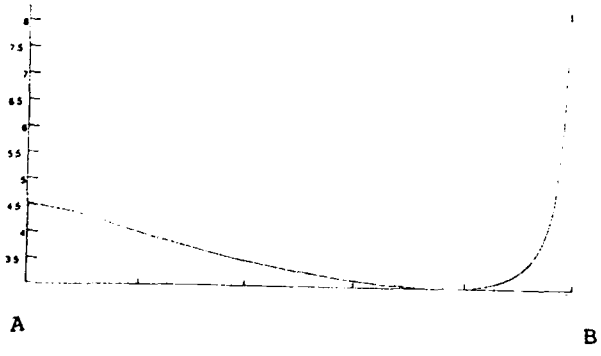


FIGURE 5b Stress distribution along flux line A-B vs E (pu mm^{-1}) for incision on outer surface of tail cable.

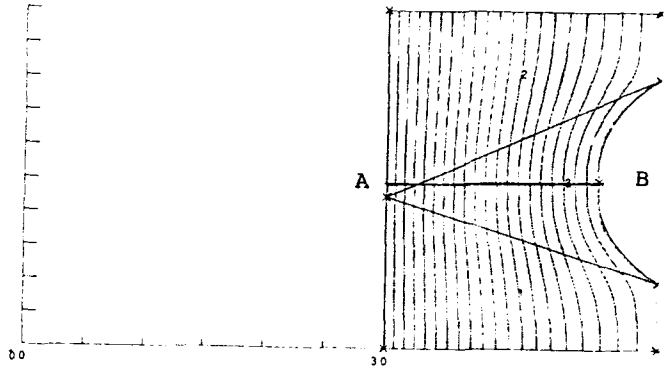


FIGURE 6a Equipotentials and flux for 'dressed out' damage to outer surface of tail cable.

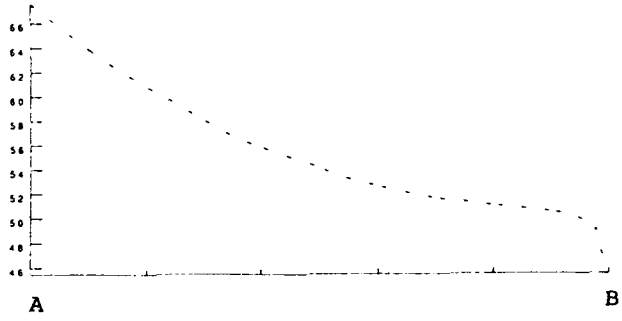


FIGURE 6b Stress distribution for 'dressed out' damage to tail cable.

b) Increased stress occurs in an area around each defect. If another defect is in this area then a synergistic effect exists which increases the stress in both defects. This area has been found to be 6 x the length of the larger of the two defects. The stress increase is noticed for any two defect types (e.g. a void near an inclusion etc.)

c) In the bulk insulation relatively large defects are acceptable - up to 1.5 mm in some regions

d) Defects running perpendicular to the equipotentials are far more deleterious to the insulation than defects of the same size, but lying parallel to the equipotentials

A number of other factors need to be considered when establishing such a standard - which can not be modelled in this way. Analytical work on mouldings[5] has shown that the most common breakdown path occur through amalgamation zones. This can be either as a result of poor amalgamation arising from irregular crystallisation from the melt or because contamination enters the mould and is swept along the amalgamation causing an easy breakdown path.

A further key factor is that the method of X-raying involves rotating the camera around the joint and taking shots at fixed angles. This enables most defects to be detected but does not help in quantifying the size. If a protrusion occurs exactly in-between two shots then the size of the protrusion that could be hidden by the cylindrical nature of the moulding varies between 0.2 mm and 0.45 mm - depending on the radial diameter of the section of the steel joint casing in question. This gives further justification to restrict the size of defects on the inner conductor.

6. CONCLUSIONS.

The use of electric stress analysis to determine the level of electric stress caused by the presence of a given defect correlates closely with experimental breakdown results. This forms the basis of a powerful method for applying computational results to genuine breakdown data, by the application of Weibull analysis. The method can subsequently be applied to minimise the breakdowns caused by the presence of visible contaminants in the moulded regions of a joint. However, as not all DC breakdown mechanisms are fully understood, this work can only be seen as a starting point for more experimental work examining the significance of other phenomena - such as space charge effects.

The results of applying Weibull analysis to breakdown statistics for a large number of joints under different stresses has generated some important initial findings concerning the levels of HV testing. It appears that the levels to which mouldings are tested to are generally excessive, especially in the simulation of ageing. However, considerable experimental work to evaluate the effects of ageing and ramp testing is required before the accepted practices can be changed.

Reassessment of the 1954 inspection standard has taken place as a result of this work and has removed many aspects which can not be justified by current understanding. The emphasis has changed to protecting the outer conductor from damage and reducing the acceptable individual defect size near the inner conductor and around amalgamations.

This analysis has been applied to a specific joint/termination design. If the design were to be significantly changed it would have different breakdown characteristics, and different regions of high stress. Comprehensive breakdown data would be needed before this method could be applied to the modified joint design.

References.

1. F.W Peek, Gen. Elec. Review 18 1915 1050-57

2. Biddlecome, Diserens, Riley, Simpkin. PE2D User Guide (Version 6).1981

3. Ford. Internal communication 1988

4. Chapeau, Alquier, Lewiner. IEEE Trans EI 21 1986, 405-11

5. Bishop, Doble, Chan, Dissado, Wolfe, Davies. Proc. IWCS 1991 634-41

Acknowledgements:

The support of the Teaching Company Scheme is greatly appreciated.

The Teaching Company is jointly funded by the DTI and an industrial company (STC) to give an academic understanding of an industrial issue.

Development Of An Alternate Undersea Armored Cable Protective Coating Compound

W. B. Wargotz

AT&T Bell Laboratories
Holmdel, New Jersey 07733

ABSTRACT

This paper reports on the results of a material and process development, cable trials and cable qualification regimen which has resulted in the introduction of a cost competitive and a more environmentally acceptable alternate to coal tar in armored cable coating formulations.

Alternate hot melt synthetic amorphous polymers to replace asphalt as well as natural extender oils to replace coal tar were evaluated in this materials study.

Employing the guidelines of the Product Realization Process two concurrent developments, both a materials investigation and equipment-process change, were introduced in the manufacture of undersea armored cables. These developments proceeded simultaneously and the PRP appeared to accelerate the development cycle.

1. INTRODUCTION

Undersea cable system designers and cable manufacturers have been concerned with the ongoing use of coal tar and coal tar pitch in armored cable application. The coal tar oil is employed in blends with asphalt as a cable "slushing" material between armored wire interstices, as a saturant between textile bedding separating armored wires, and as the exterior coating on the textile serving over armored wires.

These cable slushing compounds afford corrosion protection to the armor wires (galvanized steel) surrounding the cable core by providing a moisture imperious coating. Figure 1 is a representation of a Single Armored (SA) fiber-optic undersea communication cable highlighting features where armor wires and textile bedding are coated with slushing compound. The slushing compound is also employed as the outer protective coating on the final textile serving covering the armor wires. Slushing compounds have been cost effective and employed universally in the protection of armor in underwater power and communication cables.

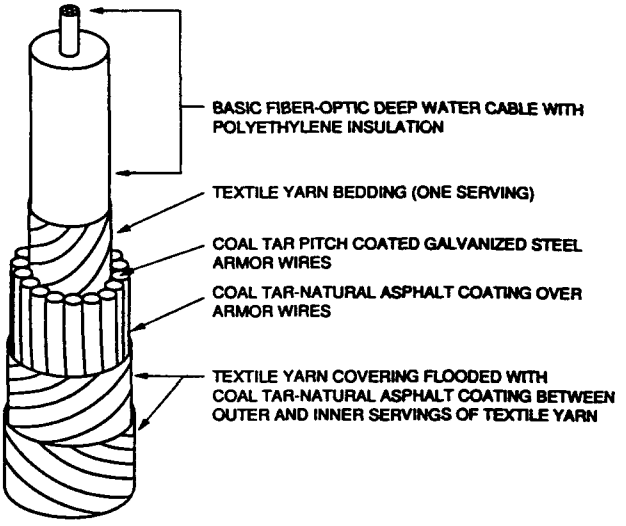


Figure I: Armored Fiber-Optic Ocean Cable

It has been recognized that prolonged contact with refined coal tar oil without prudent practices, engineering controls and protective equipment can lead to adverse health effects. It is to the cable industry benefit to assure the use of materials that are of the least possible hazard with respect to human health and the environment.

An alternate undersea armored cable coating compound has been developed that is both cost competitive and more environmentally acceptable in the factory environment and in shipboard handling than the coal tar compound employed to precoat galvanized steel armor wire and the present coal tar asphalt slushing compound. This material is a blend of a more benign pine tar oil with natural asphalt.

This development was conducted under the guidance of the **Product Realization Process**.

2. DEVELOPMENT-PRODUCT REALIZATION PROCESS (PRP)

PRP manages a project by establishing requirements and milestones. A cross-functional team effort through use of Product Definition Teams (PDT) and Product Implementation Teams (PIT), can ease entry to manufacture.

TABLE I
GENERAL PROPERTIES OF CANDIDATE CABLE SLUSHING COMPOUND

- Hot melt material, low viscosity at application temperature <350°F.
- Compatible with metallic (noncorrosive) and plastic components of cable structure.
- Anti blocking under creep load.
- Easily applied and removed in factory or field repair.
- Low volatiles.
- Impervious to marine exposure (waterproof) and marine organism attack.
- Heat stability processing and recycle.
- Oxidative and ultraviolet stability of a coating.
- Comply with acceptable environmental and occupational use and exposure regulations.
- Coating flexible at ambient and 5°C.

2.1 Product Definition Team (PDT)

A PDT was assembled with members of the undersea cable design/materials, cable manufacturer, quality control and engineering and construction organizations to examine options for replacement of the existing coal tar formulation with a material that would function in both the cable manufacturing environment and shipboard storage and deployment. The PDT recommended that replacement of coal tar in the cable manufacturing operation be conducted within two concurrent independent developments. These were: 1) equipment development and 2) materials development. Based upon discussions within the PDT a list of the general (Table I) requirements for candidate cable slushing compounds were developed.

2.2 Product Implementation Team (PIT)

A PIT was assembled incorporating members of the PDT and expanded to incorporate additional personnel from the cable manufacturer involved in materials testing and development engineering. The responsibility of the PIT was to focus on the material of choice for a armor cable protective coating and assess the performance of trial cables. A **plan of work** was formatted with milestones for program management.

In the assessment of trial development cables subjective and non subjective testing was conducted in the presence of design and material engineers and shipboard deployment personnel.

3. MATERIALS DEVELOPMENT

One of the major considerations in development of the material requirements (Table I) was the perception that an improvement in the hardness, i.e. stiffer compound would result in diminished creep of the outer protective coating layer under the weight of cable coils in storage. The concern was the binding ("blocking") of the coating between stacked cable coils. Another major consideration in materials development was to assure penetrability of the cable slushing compound into the interstices of the textile outer and inner rovings. Penetrability provides a degree of waterproofing and would diminish contact of the marine environment with the armored wires. It is believed that the coal tar addition to the asphalt provides a solvent that permits some degree of saturation of the textile with asphalt.

There were two material options available that the PDT felt would reduce the development cycle for an alternate material. These were:

1. Modify an existing synthetic thermoplastic flooding compound. This type of material alone or plasticized is employed as a moisture vapor barrier and corrosion inhibitor between layers of metal and plastic. In addition, these materials are employed as a water blocking compound between insulated conductors in terrestrial cables.
2. Replace the natural asphalt cable slushing compound "plasticizer", coal tar oil. with a environmentally and occupationally acceptable, material that would be impervious to marine exposure and organism attack.

3.1 Thermoplastic Flooding Compounds As Cable Slushing

3.1.1 Amorphous Polyolefins

Amorphous polyolefins are tacky synthetic thermoplastic compounds employed as hot melt sealants. In mixtures with asphalt they have been employed as a binder resin for non woven polyester for house roofing. A feasibility study was conducted to examine the properties of selected candidate developmental and commercial amorphous polyolefins alone or in formulations with asphalt compared to coal tar-asphalt. The data are presented for amorphous polyolefins alone (Table II) and those in blends with asphalt (Table III).

TABLE II
PROPERTY COMPARISON OF AMORPHOUS POLYOLEFINS

Test	Sample		
	Coal Tar Asphalt	Amorphous Polyolefin #1	Amorphous Polyolefin #2
Ring & Ball Softening Point,°C	53	100	108
Needle Penetration Hardness,0.1 mm	49	20	15
Viscosity at 150°C, Thermosel cps	234	406	488

A property comparison was made between candidate amorphous polyolefins (propylene copolymers # 1 and # 2) and coal-tar asphalt cable slushing, Table II. Viscosity/temperature data was generated comparing the viscosity behavior of coal-tar asphalt blend with typical cable waterproofing compounds (amorphous polypropylene-1) and candidate, amorphous polyolefin-2, Figure II. The amorphous polyolefins

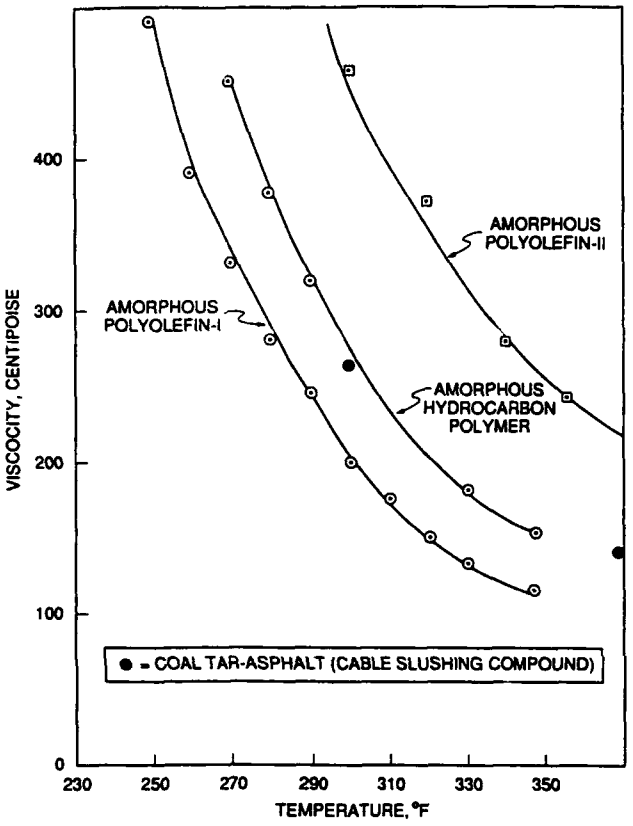


Figure II:
Viscosity vs. temperature for candidate armor cable coating compounds

offer attractive features i.e. synthetic reproducible material, low odor and less hazards associated with use in the workplace and disposal, stiffer and less tacky then coal tar-asphalt to improve handling of a textile coated cable during shipboard loading and deployment. However, based upon the following considerations further work was discontinued:

1. The amorphous polyolefins viscosity were higher than desired.
2. Thermal stabilizer additives would be required to process stabilize the amorphous polyolefins during exposure to 240-300° F for lengthy periods during cable armoring.
3. Questions as to whether the inner and outer textile yarn coverings would be saturated with resin to provide a waterproof coating.

3.1.2 Amorphous Polyolefins Blended With Asphalt

From the data in Table III it is apparent that the melt viscosity of amorphous polyolefins blends with asphalt, as expected, are notably higher than coal tar-asphalt. One possible candidate blend, AP-A, was reformulated with a hydrocarbon extender oil, to prepare a material with a lower melt viscosity, AP-A-HC-1 (Table III). There was concern with the phase separation of the oil and possible sorption by the polyethylene dielectric with some compromise in the reliability of the undersea cable. Further work with asphalt blends was discontinued based upon the same considerations as enumerated above, Table II, for amorphous polyolefins alone.

TABLE III
AMORPHOUS POLYOLEFIN - ASPHALT
BLEND CHARACTERIZATION
Property Comparison

MATERIAL	MELT** VISCOSITY (cps)	NEEDLE*** PENETRATION (0.1 mn)	RING BALL SOFTENING POINT (°F)
AP*-A-HC-1	3050	19	175
AP-A-HC-2	23825	1	248
AP- A	32750	1	218
COAL TAR - ASPHALT	875	55	137
ASPHALT	15800	0	198

* AP = Amorphous Polyolefin, A = Asphalt, HC = Hydrocarbon Oil
** determined at 150°C.
*** determined at 25°C.

3.2 Pine Tar Oil-Natural Asphalt Cable Slushing Compound

Pine tar oil is employed extensively in the automotive tire and rubber molding industry as a tackifier in compounding. Pine tar oil is derived from the destructive distillation of pine tar stumps and bark. It is a low cost material with a density of ~ 0.975.

With the knowledge that natural asphalt is partially oxidized and pine tar oil contains polar constituents, it was anticipated that mixtures of these materials would be compatible and a possible replacement cable slushing compound blend could be developed. Blends of pine tar oil with natural asphalt were prepared. The objective of this program was to prepare a blend with the properties comparable to coal tar-natural asphalt.

The comparative physical and chemical properties of coal tar-asphalt and a candidate pine tar oil blend with asphalt are found in Table IV.

3.2.1 Comparative Physical/Chemical Properties

The data presented in Table IV suggests that a candidate pine tar oil asphalt blend resulted in less weight loss on heating, and no significant change in the softening point or penetration of the candidate cable slushing compound compared to the presently employed coal tar mixture. Comparable heat stability data on softening point and penetration is beneficial in that it suggests that the pine tar blend material would store well during shutdown/turnaround and extended cable armoring production.

TABLE IV
COMPARATIVE PHYSICAL PROPERTY DATA

COAL TAR - NATURAL ASPHALT AND CANDIDATE PINE TAR-

NATURAL ASPHALT CABLE SLUSHING COMPOUND

Property	Test	Result	
		Coal Tar	Pine Tar
Viscosity Thermosel, cps	190°/375°F	125	188
	150°C/302°F	250	438
Heat Stability at 325°F			
Softening Pt.°F	Original	115	122
	4 hrs.	117	120
	24 hrs.	132	130
Penetration (0.1mm)	Original	90	86
	4 hrs	76	75
	24 hrs	40	27-68
Weight loss on Heating, %	5 hrs. at 325°F	1.4	0.7
Corrosion of Copper	Copper Wire	NCT	NCT*

NCT = No Apparent Corrosion or Tarnishing

Before examining the performance of the candidate pine tar oil-asphalt blend in a cable armoring trial it was imperative that the environmental sensitivity be determined for pine tar oil and its blend with asphalt compared to coal tar. In addition, the undersea cable polyethylene insulation propensity to environmental stress crack in contact with pine tar as well as its blend with asphalt needed to be determined.

It was demonstrated that the pine tar oil-asphalt blend was not a environmental stress crack agent to polyethylene cable dielectric material. In addition, it was observed in immersion testing that pine tar oil has a lower affinity for polyethylene than coal tar.

3.3 Bacterial Assay

The environmental and occupational aspects associated with substitution of pine tar oil for coal tar oil were examined in a bacterial assay test. Both literature review[1] and assay testing[2,3] suggested that pine tar oil is less occupationally sensitive than coal tar oil in asphalt formulation.

3.4 Summary - Raw Material Development

The raw material development work established:

1. Pine tar oil can be substituted for coal tar in natural asphalt to prepare a material with comparable cable slushing properties.
2. Incorporation of pine tar results in a more environmentally and occupationally acceptable cable slushing material than a composition with coal tar.

4. FABRICATION OF SA CABLE WITH PINE TAR-ASPHALT BLEND

Standard armoring practices were employed in producing a 10 kilometer length of SA (single armored) fiber-optic undersea cable (Figure I) with pine tar-asphalt blend substituted for coal tar-asphalt as cable slushing. Adjustments in melt viscosity were made by slightly raising the temperature of application. No significant difficulties were experienced in the fabrication of this length of cable.

4.1 Cable Qualification Testing

A Cable Qualification Test Plan was approved by the Product Implementation Team (Table V).

TABLE V
CABLE QUALIFICATION TEST PLAN

CABLE QUALIFICATION TESTS	
TEST	DESCRIPTION
SLUSHING CMP'D COVERAGE	Dissect Cable -coverage on yarn bedding -coverage on wires -sorption by PE insulation -(determined by extraction)
CABLE DAMAGE	Contamination of insulation by adherent slushing compound after storage. Compliance with the molding requirements. Examine for heat/pressure affects.
MECHANICAL	1. Each development cable and control cable tested Tension - Rotation - Elongation 2. Temperature/Flexure (5°C) followed by dissection and examination
HANDLING	Cable storage tank removal unloading and shipboard loading

Table VI is a summary of the visual observations on slushing compound coverage on the structural components of the dissected cable prepared with pine tar compared to a comparable cable prepared with coal tar. The subjective observation method revealed little difference in coverage exhibited by either cable employing the same method of application. The presence of cable slushing on the deepwater core (Figure 1) arose from random separation of the first textile yarn permitting penetration of the cable slushing and slight discoloration. Adjustments were

TABLE VI
CABLE SLUSHING COMPOUND COVERAGE

	Asphalt Blend	
	Coal Tar	Pine Tar
2nd Textile Yarn Layer(outside)	B	B
1st Textile Yarn Layer	B	A
Armor Wire, Inner Surface	B	A
Armor Wire, Outer Surface	B	B
Textile Yarn, Bedding Outer Surface	A	A
Textile Yarn, Bedding Inner Surface	C	B
Deepwater PE Insulated Cable Core	C	C-B

A - Heavy Tar
B - Medium Tar
C - Light Tar
D - No Tar

made in the later fabrication of armored cables that eliminated yarn separation.

In this initial trial the presence of random discoloration was of concern as to its effect on the reliability of cable integrations (i.e. molding of splices between cable lengths).

4.1.1 Adsorption of Cable Slushing On Polyethylene Dielectric Surface

There was no significant differences in the surface extractables from a control armored cable which did not have surface discoloration and that from the trial cables above. This result suggested surface discoloration with no sorption during fabrication.

4.1.2 Molding Trials On Environmentally Exposed Armored Cables

An aging study (Table VII) was conducted to determine if the candidate cable slushing coating hardered during aging by separation or sorption of pine tar and/or the surface discoloration compromised the reliability of cable splices.

1. The aged cable samples were dissected and the deepwater cable core recovered. It was observed that the outer layers of the textile roving were more difficult to remove than was observed with unaged cable. The pine tar blend was flexible after aging and did not embrittle. The coal tar blend was more brittle after aging.
2. The recoved deepwater polyethylene insulated cable cores were joined to cable splice boxes. The moldings were prepared in two different molding machines and tested.

TABLE VII
ENVIRONMENTAL EXPOSURE OF ARMORED CABLE

	TEMPERATURE CYCLING
Start Temperature	=50°C for 100 hours
Cycle 1	=3°C for 100 hours
Cycle 2	=50°C for 100 hours
Cycle 3	=3°C for 100 hours
Cycle 4	=50°C for 100 hours
Cycle 5	=3°C for 100 hours
Cycle 6	=50°C for 100 hours

Test conducted were:

- An x-ray analysis for inclusions i.e. particulates
- Microtome samples were prepared encompassing the overmolding interfacial area and the recovered specimens tensile tested.
- Heat shrink testing.

All tests were satisfactory and meet requirements.

4.1.3 Low Temperature Flexibility As part of the cable qualification test plan (Table V) low temperature flexing of the armored cable was required. The purpose of this test was to ascertain any differences in the low temperature performance of the coal tar -asphalt and pine tar -asphalt adhering to the textile bedding and armored wires. After conditioning cable samples for 24 hours at 40° F ± 8° F the coal tar and pine tar-asphalt cables were flexed 50 cycles on a 36 inch radius, Figure III. After flex testing the samples were dissected and following subjective observation noted.

- The coal tar-asphalt cable slushing on the armor wire textile coverings **was brittle.** Upon pulling the textile off the armored wires the coal tar-asphalt coating failed adhesively exposing bare armor wires with the cable slushing adhering to the textile. The armored wires could be readily separated from the brittle cable slushing between the interstices of the armor strands.
- The pine tar-asphalt cable sample was dissected. This mix adhered to the textile bedding, was not brittle and pulled away from the armor wires leaving the wires bare. In separating the armor wires cohesive failure of the adherent coating occurred between interstices of the galvanized steel armor.

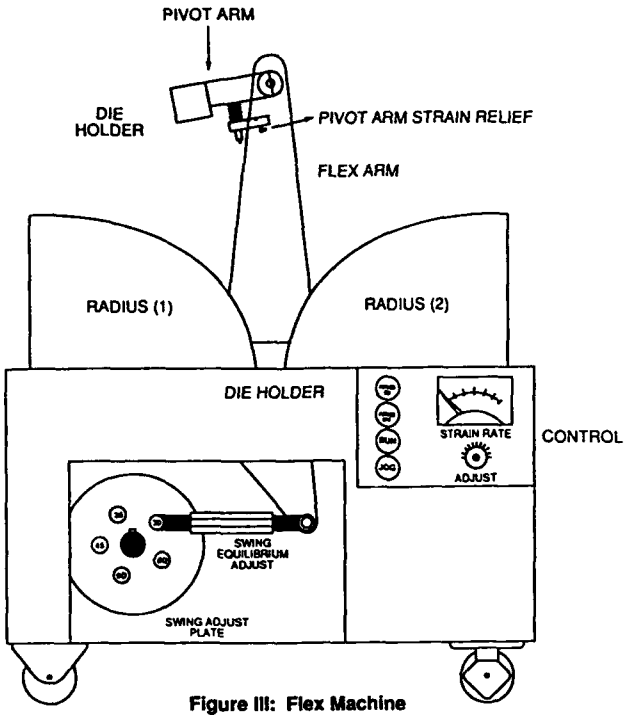


Figure III: Flex Machine

The results of the low temperature flex testing suggest that the pine tar blend is a better low performance coating than the coal tar blend and would retain its flexibility as a coating at low temperature and be less prone to embrittlement. This could be important if the armored cable is torqued during deployment or on the ocean bottom.

4.1.4 Mechanical Testing

Sample lengths of both the coal tar and pine tar -asphalt cable slushed armored cables were submitted for Tensile-Rotation-Elongation testing. The purpose for performing these test was to determine if the method of application of cable slushing compound or material affected the cable rotation (torque) during shipboard deployment. The apparatus employed in test is found in Figure IV The test results are found in Table VIII. The data revealed no significant difference among the specimens. The reproducibility of the test is demonstrated by the correspondence of the replicate data on coal tar-asphalt coated armor cables tested six months apart.

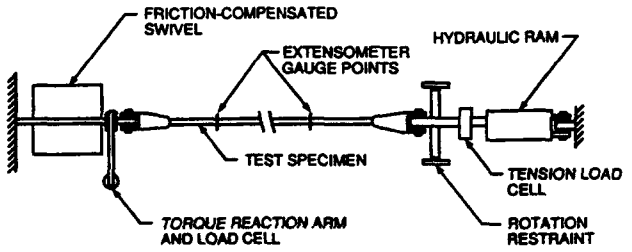


Figure IV: Apparatus Used for Measurement of Cable Elongation, Torque, and Rotation

TABLE VIII
TABLE SUMMARY OF TEST RESULTS

Load Cycle	Tension pounds	Cable Rotation, degrees per foot	
		Coal Tar-Asphalt	Pine Tar-Asphalt
1	32,000	28.8 (30.7*)	29.3
	400	3.6 (4.2)	4.1
10	32,000	29.7 (31.4)	30.8
	400	4.3 (4.8)	5.1
11	50,000	59.8 (61.5)	63.0
	400	15.6 (18.0)	19.1
20	50,000	64.4 (66.4)	72.4
	400	20.4 (22.0)	30.4

* Six month earlier data

4.1.5 Assessment of Cable Slushing Outer Coating of SA Cable

After three month storage (coiled in holding tanks) the 10 km cable was shipboard loaded. The shipboard loading was event free (no "blocking") and little if any smearing observed during transfer over slides and capstans during cable shipboard loading. These observation suggest that the ~3 months storage (ambient) did not result in creep and "blocking" of the armored cable external coating of pine tar-asphalt textile between coils of staked cable. (Table V)

4.1.6 Pine Tar-Asphalt Process Stability

Samples of the pine tar-asphalt mix were withdrawn during the application of the cable slushing in processing the 10 km armored cable. These samples were tested to ascertain the processing stability . The results, Table IX, indicate that the pine tar-asphalt blend increases in stiffness and viscosity. These effects did not appear to compromise the ability to process the coating during the fabrication of the length of armored cable.

TABLE IX
PROCESS STABILITY PINE TAR - ASPHALT BLEND

		Hours Exposed				
	Original	24	48	120	150	175
Softening Point °F	122	132	133	130	134	135
Penetration (0.1 mn)	80	47	42	44	39	38
Wt. Loss % 5 hrs at 325°F	0.9	.671	.443	.341	.370	.449

4.2 Summary - Blend Of Pine Tar Oil - Asphalt As An Armored Cable Slushing Compound

Observations and data generated during cable processing and cable qualification follow:

1. There are no significant processing and physical property behavior that suggests instability in use of pine tar-asphalt as a cable slushing material.
2. There is the suggestion that the low temperature performance of the pine tar-asphalt would be an improvement over present cable slushing material.
3. Cable qualification results are comparable to those exhibited by coal tar-natural asphalt applied to armored cable in a similar process.
4. Shipboard handling of pine tar-asphalt externally coated armored cables are comparable to present coal tar-asphalt coated armored cables.
5. The pine tar oil-asphalt blend is an environmentally acceptable alternate to coal tar oil in armored cable coating formulations.

5. CONCLUSION

Employing the Product Realization Process (PRP) applied to two concurrent developments, equipment and material, appeared to accelerate the development cycle.

An alternate undersea armored cable coating compound has been developed that is both cost competitive and less hazardous in the factory environment and in shipboard handling as the present coal tar-natural asphalt cable slushing material. This material is a blend of a more benign pine tar, a naval store, with natural asphalt.

Cable qualification testing on both development and production cables demonstrated comparable mechanical, physical and handling characteristics as presently fabricated cables.

6. ACKNOWLEDGEMENT

This development would not been completed without the cooperation and effort of people and organizations.

We appreciate the cooperation of many individuals at Simplex Wire and Cable Corporation who were instrumental in providing facilities for conducting cable trials and assisting in analyses of material performance and cable qualification.

The support of the AT&T/ International Construction and Engineering personnel in contributing and moving this development forward is appreciated.

Especial thanks are given to L. Brooks of the Industrial Hygiene organization at AT&T-Bell Laboratories in shepherding the toxicological characterization of the cable slushing materials.

The rapid response of the material suppliers in providing testing, materials and meeting commitments is acknowledged.

REFERENCES

[1] Hazardous Substances Data Bank (HSDB) on-line computer database. U.S. Department of Health and Human Services. National Institutes of Health. National Library of Medicine.

[2] Ames, B.N., J. McCann, and E. Yamasaki. 1975. *Mutation Research :31:347-364.*

[3] Maron, D.M. and B.N. Ames. 1983. *Mutation Research :113:173-215.*



Bernard Wargotz's work experience includes supervising and conducting research and development in the chemical industry on new polymers. He has contributed, as manager and member of technical staff, toward the design, material investigations and process development both in communication and power wire and cable, as well as interconnection/ electronic assembly technology.

His Bachelor and Master of Science Degrees were received from the University of Michigan and his PhD from the University of Rochester. He is a Distinguished Member of Technical Staff at AT&T Bell Laboratories and is presently concerned with design, materials and processes related to the development of undersea fiber-optic cable systems.

He is the recipient of 10 patents and authored over thirty publications.

THE FLEXIBLE TUBULAR SPLICE. - A TECHNIQUE FOR MANUFACTURING VERY LONG CONTINOUS SUBMARINE FIBRE OPTIC CABLE, WITHOUT DIAMETER INCREASE AT THE SPLICE.

Jørn Wardeberg
Kaj Nyaas

ALCATEL KABEL NORGE AS
Østre Aker vei 33, N-0509 Oslo, Norway

ABSTRACT

The reported cable jointing technique enables the manufacturing of very long continuous submarine cables with no visible joint boxes as the reported joint is flexible and has the same nominal diameter as the rest of the cable. In addition, its optical, electrical, mechanical and thermal properties are identical to any other section of the cable.

The major advantage of the technique is that no extra precautions are required during cable handling, deployment or burial.

The tubular splice has been utilised in both 6 and 12 fibre cables for international submarine projects.

The typical optical splice loss is 0.07 dB.

1. INTRODUCTION

Traditionally, the manufactured continous length of fibre optical cables has been limited due to material, manufacturing facilities and various processing restrictions. Thus to make up very long cables, shorter sections have to be jointed together after manufacturing.

In the manufacturing stages prior to the final armouring of the cable, there is also the risk of damage to the cable core which would also require jointing.

Up to now, both production related limitations and cable repair have required the use of traditional cable joint boxes. These joint boxes have been in the form of voluminous metal enclosures, which have restricted cable manufacture, handling and deployment.

In order to manufacture very long, continuous lengths of optical submarine cable, a technique has been developed for splicing the cable core, including the optical fibres, which avoids the use of traditional joint boxes. The technique is based on a pressure balanced polycarbonate tube with the same diameter as the fibre optical cable core, onto which the slotted core element is mechanically terminated in both ends. The optical fibre splices are positioned inside the tube, protected from mechanical and chemical exposure.

All fibres are spliced with equal excess lengths, enabling very high cable elongation without any tension being transferred to the fibre splices. As the fibres cannot be coiled as in a traditional joint box, all fibres must be successfully spliced the first time and with identical lengths.

The tubular splice design can also accomodate electrical conductors. Depending on the actual cable design, any conductors are jointed either inside or outside the tube.

The tubular splicing process is carried out in the armouring machine. The armouring wires are applied directly over the polycarbonate tube, thus giving a continuous armour over the joint which has a diameter identical to the rest of the cable.

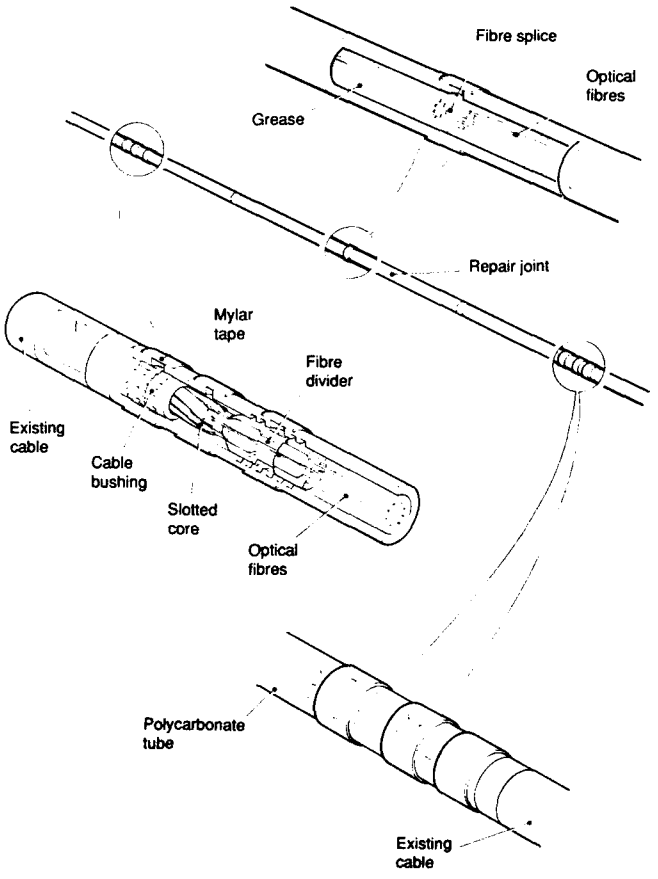
Once armoured, the splice exhibits identical mechanical, thermal, electrical and optical transmission characteristics to any other cable section. No special precautions are required during the armouring or any subsequent manufacturing processes such as outer protection extrusion. In addition, no special precautions are required during the succeding cable handling, deployment, laying, burial or eventual retrieval.

The tubular joint is developed for a slotted core cable design, with an FRP central strength member.

2. TUBULAR JOINT DESIGN

Mechanical design.

The tubular joint is based on a polycarbonate tube, onto which the central fibre reinforced plastic (FRP) element of the optical fibre cable is mechanically terminated at both ends. This is shown in figur 1.



Figur 1. Tubular splice design.

The overall length of the polycarbonate tube is 1500 mm, dictated by the optical fibre lengths required to perform the fusion splicing. The outer diameter is 12 mm, conforming with the submarine cable inner sheath diameter and with the FRP axial tension properties.

The polycarbonate tube transfers the axial loads beween the jointed FRP elements and protects the optical fibres and the fibre splices from chemical and mechanical exposure.

The mechanical termination between the polycarbonate tube and the parent cable is implemented by two pairs of stainless steel bushings. The inner pair, denoted fibre divider, is attached to the central FRP element. A number of radial slots, equal to the number of slots in the slotted core element, ensures that the optical fibres can pass freely from the slotted core to the fibre splicing area.

The fibre divider is in turn attached to the polycarbonate tube using a resin, thus tranfering the axial load between the polycarbonate tube and the FRP element.

The outer pair of stainless steel bushings, denoted cable bushings, ensure rotational stability beween the cable inner sheath and the polycarbonate tube.

The slotted core element with the optical fibres is free to move with respect to the cable bushing.

The tube is filled with a cable filling compound for hydrostatic pressure performance and fibre protection.

Optical fibre splicing

The optical fibres are individually spliced, tensile tested and recoated prior to positioning the polycarbonate tube over the fibre dividers and the spliced fibres.

The design of the tubular joint permits only a limited excess fibre length to be coiled inside the tube, and hence imposes stringent demands on the fibre splicing process: All fibres must be cleaved to the exact same length, and all individual fibre stripping, cleaving, fusion splicing, tension testing and recoating must meet their respective specifications the first time. Otherwise the complete splicing procedure must start from the beginning again.

The only way to avoid restarting the splicing procedure is to allow multiple splices on one fibre. This would however, influence the power budget and might exceed the specified splice loss.

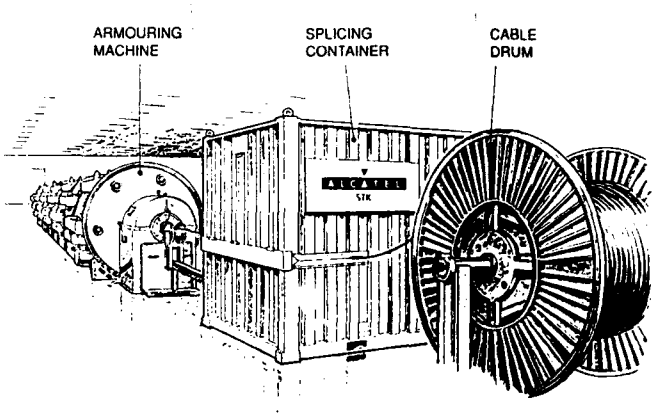
In order to ensure that no axial loads are transferred to the optical fibres or their splices during the armouring process or during the cable operational life time, the spliced fibres are given an excess length of 0.5 % relative to the polycarbonate tube.

The typical optical loss of the spliced fibres is 0.07 dB at 1550 nm. No additional optical loss has been observed due to the assembly of the tubular joint, nor subsequent manufacturing or installation.

The fibre splicing process is carried out using commercially available splicing equipment. The tubular splice has been employed both for single mode carbon coated hermetic fibres and single mode standard fibre.

3. ASSEMBLY

The tubular joint is assembled in the cable armouring process. For the purpose of establishing adequate working conditions during the critical fibre splicing, all jointing work is performed in a separate container, in which the environment is carefully controlled. This is depicted in figure 2.



Figur 2. Assembly of the tubular joint in the armouring line

The assembly of the tubular splice is performed in the following four phases:

* slide the polycarbonate tube over one of the cable ends and attach the fibre divider to the FRP elements.
* cleave the optical fibres to exact lengths and fusion splice.
* position the polycarbonate tube over the spliced fibres. Attach cable bushings and fibre dividers to polycarbonate tube using epoxy resin.
* fill all polycarbonate tube voids with filling compound and seal all filling and venting holes.

In order to cut the fibres to correct and identical lengths and to protect the spliced fibres during the work, a special jig has been developed. The jig also ensures that no tension is transferred to the spliced fibres during positioning of the polycarbonate tube.

A special tool has also been developed to carefully force the cable bushings into the polycarbonate tube.

Special attention is required to protect the fibres when fixing the fibre divider and the cable bushing to the polycarbonate tube. Any resin directly on the fibres would prevent their free movement, and potentially inflict fibre breakage once the splice is exposed to axial or radial load.

The resin used for mechanical fixing has been selected for maximum shear strength, minimum hardening time, hardening temperature and viscosity. Correct viscosity enables the resin to fix the polycarbonate tube and bushings without wetting the optical fibres.

Once the tubular splice has been assembled all voids are filled with a cable filling compound. Finally, all filling holes and venting holes are sealed using a resin and a tape.

The polycarbonate tube is transparent, thus enabling the operators to visually inspect the spliced fibres during the assembly operations.

The remaining joint assembly stages depend on the cable design. If the cable contains copper conductors outside of the inner sheath for cable electroding purposes, these will be jointed and insulated outside the polycarbonate tube. Any bedding is replaced outside the tube.

Dictated by the resin hardening time, the cable armouring process can now continue. Single or multiple armour can be applied directly on to the tubular joint, forming an integrated and continuous cable joint.

A complete tubular splice on a cable containing 6 fibres can presently be completed within approximately 8 hours.

4. QUALIFICATION TESTING

The tubular splice has been qualified for use in submarine cables supplied to the Norwegian Telecom and other customers internationally. The qualification tests were performed on jointed and armoured (single armour) submarine cable. The tests are shown in Table 1.

Table 1. Qualification Tests.

Test	Condition
Tensile loading	60 kN
Compressive loading	7,5 kN Exposed section: 10 cm
Impact	Energy: 75 Nm Radius of curvature: 50 mm
Temperature Cycling	-40 °C - +70 °C 10 cycles
Hydrostatic pressure	100 bar Duration: 24 hours
Flexibility	Bend radius: 75 cm 100 cycles Tension: 500 N Room temperature
Torsion	40° pr. 10 m Tension: 30 kN

The tubular jointing technique has been successfully employed for several international submarine cables during 1992. The cables have contained 6 and 12 fibres respectively.

5. CONCLUSIONS

The design, assembly and test specifications of the tubular joint have been described.

The tubular joint technique enables the production of very long continuous fibre optic submarine cable lengths with no visible joint boxes. The diameter of the cable remains the same over the whole length, also at the joints, and the armouring is continous across the joints.

Testing of cables with the tubular joint has shown that single and double armoured submarine cables can be jointed with this technique such that the jointed cable has the same axial or radial mechanical properties, flexibility, optical fibre reliability or thermal properties, as the parent cable.

Manufacturing experience has fully proven this jointing technique to be viable.

Installation experience has shown that with the tubular joint, no special attention is required when cable joints are passing through cable ways, linear engines, ploughs or jetting machines during loading, laying and burial.

Acknowledgements

The authors wish to thank Arne Berg of Optoplan for his contributions to the development work.

Jørn Wardeberg
Alcatel Kabel Norge AS
Østre Aker vei 33
P.O. Box 130, Økern
N-0509 Oslo
Norway



Jørn Wardeberg graduated from the Technical University in Trondheim (Norway) in 1981 with a degree in physics. He joined Alcatel Kabel Norge AS in 1987 as project manager, and is currently responsible for optical cables jointing.

Kaj Nyaas
Alcatel Kabel Norge AS
Østre Aker vei 33
P.O. Box 130, Økern
N-0509 Oslo
Norway



Kaj Nyaas has a background as a telephone exchange installer at STK, but has been working with development of splicing technology for fibres in the Communication Cable Division of STK (now Alcatel Kabel) since 1983.

A New Cable Family for the Optical Fiber Subscriber Network

Peter Delage, Reinhard Girbig, Georg Hög, Michael Hoffart,
Herbert Moers, Peter E. Zamzow

KABEL RHEYDT AG (former AEG KABEL), Bonnenbroicher Str. 2-14, 4050
Mönchengladbach 2, Germany

Abstract

Fiber optics in the local network has been iscussed in conjunction with broadband ISDN for everal years. For such a network the rchitecture, a cable familiy on the basis of ptical fiber ribbon technology and the needed ccessories will be presented. Constructions, ests and first field trials with the new echnology will be reported.

. Introduction

A new optimized optical fiber cable family ıith ribbons will be presented. The cable family ın the local network cable level is constructed ıith equal basic elements. The solution is a l-fibre-ribbon technique in encapsulated :onstruction with UV-coloured single mode fibers. :orresponding to the network architecture the :able types are designed in a way that leads to an economic production and is easy to handle. The ıasic elements of the ribbons are constructed in :ube technique with 4-20 fibers per unit. The :able family is constructed with few units. A main :able with 200 fibers will have an outer diameter less than 21 mm. In the distribution level these ıasic units are single sheathed and bonded to flat :able units up to 5 units. In thus a cable of 100 Fibers is possible. These units can be branched ıithout splicing and fed to the building. For the drop cable a single element with in general 4 Fibers is proposed. If applicable the cables are ıreconnctorized.

Additional an estimation for the splicing :echnique and mounting construction for this cable Family will be presented. The experiences in a Field test with the Deutsche Bundespost TELEKOM in Nürnberg with more than 200 subscribers as the First stage of this concept were positive.

:. Network Architecture

For a long time the introduction of the ptical fiber technique into the subscriber access etwork has been discussed world wide to be done s large scale introduction. /1//2//3//4//5/.

ut since that time only overlay-networks were ealized, for example the so called VBN-network in ermany. From cost aspects such a network is not ıpplicable for a full coverage.

Therefore other strategies are required for the introduction of the optical fiber technique into the local network.
For this reason networks are searched as close as possible to the subscriber (OPAL 93 in Germany), which allow telephone-, data-, small-band-ISDN services and optional CATV for the mass of subscribers as well as broadband services PMBX (2Mbit/s) for a number of subscribers. Later on there must be the chance to extend such a network to a broadband ISDN network for a great number of subscribers. As the necessary investments must be obtained by the today realized services an optimized course of investments has to be found. This network must be aquivalent from the costs as the existing copper network.

For such networks estimations have been done as FTTC, FTTH and FTTB. (Fig. 1).

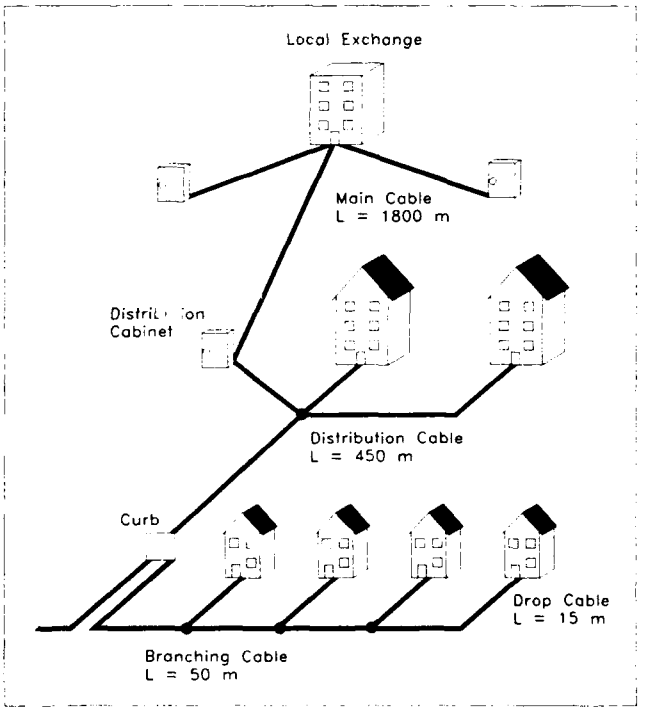


Fig. 1 Basic Network Structure with Optical Fiber Cables

The greatest costs for the whole network are the system components, such like optical transmitters and receivers.
Therefore the employment of optical splitters (up to 1x16 or 1x32) makes sense for reducing these costs. This means for the main cable area low fibre count cables, which are laid normally into ducts. For this case it is very simple to upgrade the existing network with optical fibers. The branching cables behind the distribution cabinet (see Fig. 1) have more fibers. These branching cables lead to greater buildings (more than 10-20 subscribers) or to curbs. Behind these curbs and in the buildings normally copper cables (symmetrical or coaxial) are used. Today' strategies use in most cases the structure of the existing copper local network. Concerning the better transmission properties of the optical fiber the density of the local exchanges can be reduced. The cable lengths will be increased for example from 2 km to 10 km.
In this case the costs for local exchanges and installation in the main cable area are clearly reduced.
For these considerations cable constructions with optical fibers in ribbons might be useful.

3. Cable Design

3.1 Fiber

The single-mode fibers which are employed in subscriber network cables are optimized for a wavelength range around 1310 nm, with zero disperion in this wavelength region, but additionally perform well at 1550 nm. The fiber are germanium doped without phosphorus. The fibers profile is a "matched cladding" type. The nominal mode field diameter is 9.3 µm.

The low intrinsic attenuation of fibers with tight geometrical tolerances guarantee very good transmission characteristics in ribbon cables. The geometry of the single-mode fibers used in the experiment expressed as average values with 1 σ are:

outer glass diameter:	125 µm ± 0.5 µm
mode field diameter :	9.3 µm ± 0.13 µm
core/clad excentricity:	0.4 µm ± 0.1 µm
coating diameter :	245 µm ± 3.3 µm

For their employment in fiber ribbons the fibers are UV-coloured. For this 12 colours are available (Fig. 2).

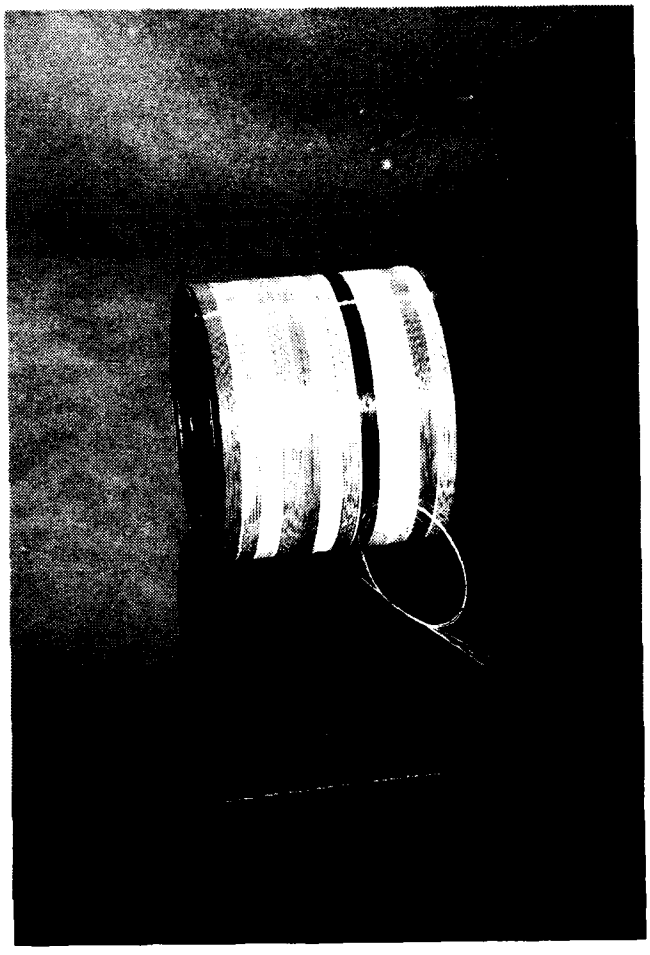


Fig. 2. Model Spool with 12 Fiber Colours

The UV-colouring ensures that the good regularity and the narrow tolerances of the fibers will be maintained. The thickness of colour coating is around 5 µm. Because of the UV-colouring the fibers in the ribbon structure have very good separability characteristics.

3.2 Ribbons

The ribbon used in this cable construction is of the so-called type "encapsulated". Here the UV-coloured fibers are fully surrounded by a special UV-acrylate-coating (Fig. 3).

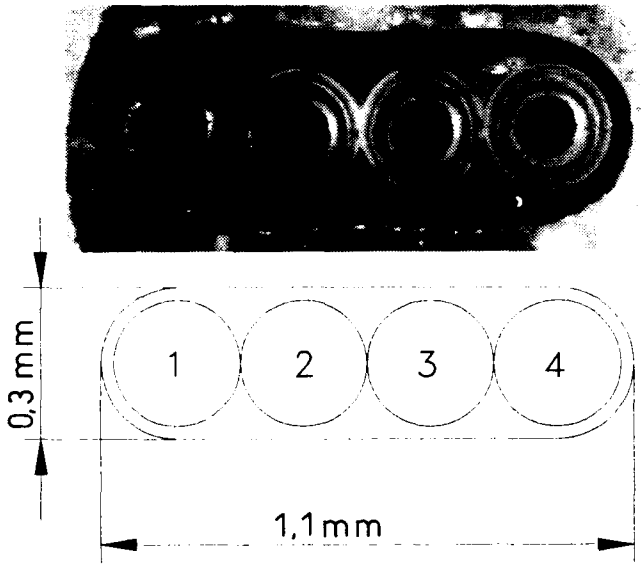


Fig. 3 Ribbon Endcut

The height of the ribbon of 300 µm has been chosen in order to minimize the cable diameter.

The ribbons are produced in a horizontally installed machine in which the forming of the fiber ribbon is carried out in a vertical coating tower. By means of a special construction of the coating die for the UV-acrylate-coating very good geometric tolerances are achieved.

Geometry of the ribbons employed in the test cables:

height: 286 µm + 5 µm 1)
width : 1042 µm + 15 µm 1)
1) tolerances 1σ - values
planarity: typically < 10 um
In general nominal targets should be :
height: 300 µm ± 50 µm
width : 1100 µm ± 100 µm

The ribbon is constructed with four different UV-curing coatings: the primary- and secondary coating of the fibers, the colour coating and the ribbon coating to encapsulate. The compatibility of the four different coatings is most important for the microbending sensitivity of the singlemode fibers in ribbon structure.

In order to quantify the microbending sensitivity of the ribboned fibers microbending attenuation measurements have been made according to CECC /6/. The ribbon is wound onto a spool with a diameter of 0.3 m on sand-paper of the quality PSA-grade 40 um-mineral A10. The winding power is in total 3.2 cN over the entire ribbon. The microbending attenuation is calculated by the following formula:

microbending sensitivity = a * R/T
where a (dB/km) = Increase in attenuation caused by microbendings
R (m) = spool radius
T (N) = winding tension

The ribbons employed in the test cables were under 0.5 dB/km/N/m with regard to their microbending sensitivity. With these low values a very good cabling of the ribbons is guaranteed.

3.3 Ribbon-Unit

The second step for manufacturing an optical fiber ribbon cable is the production of the basic element, the so-called ribbon tube. This tube has an outer diameter of 4.5 mm for the 4 fiber ribbon (Fig. 4).

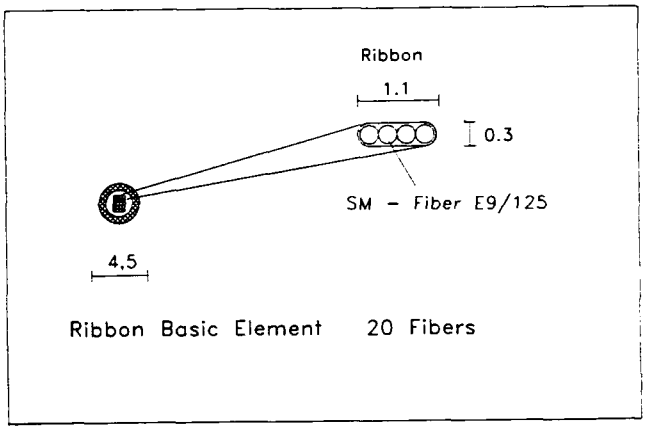


Fig. 4 Ribbon Basic Element with 20 Fibers

For the tube a material as it is known from the conventional loose tube technique (filling compound, tube material) is used. The thixotropic filling compound makes the tube watertight and decouples the ribbon mechanically from the inner layer of the tube material.
The high strength of the tube material (polyester, polyamid or polycarbonat) with a thickness around 0.7 mm is a good protection for the ribbon against the stresses occuring in longitudinal and transverse direction in the finished cable and also during cabling. These stresses are absorbed by this basic element in a wide range so the optical transmission quality of the optical fiber in the ribbon is not influenced by that.

This ribbon-unit gives good package density combined with sufficient mechanical decoupling of fibers and the rest of cable. For a 20 fiber ribbon-unit (5 ribbons in one unit) the density is 0,8 mm² per fibre.

3.4 Cable construction

The above mentioned ribbon-unit will be used for the following members of the new cable family.

- Cable with central ribbon unit

Low count optical fiber ribbon cables (4...20 OF) can favourably produced with a central core, in order to achieve a cable diameter of 8mm with limited production costs. Dependent on the arrangement of the ribbon tube in the centre of the cable in case of high tensions and elongation of the cable this construction type does not have any microbending effects and by that no considerable additional attenuation arises on the occassion of these conditions. However, the optical fibers are joined in the stresses depending on the cable elongation. But the fiber elongation resulting from these stresses is in an uncritical range (about 0.2%). Above the central ribbon tube, strength members made of glas or aramide rowings are arranged adapted to the corresponding tension forces. As outer protection sheath the conventional laminated aluminium polyethylene sheath or a simple polyethylene sheath is applied.
Fig. 5 shows cable construction with 4 up to 20 fibers.

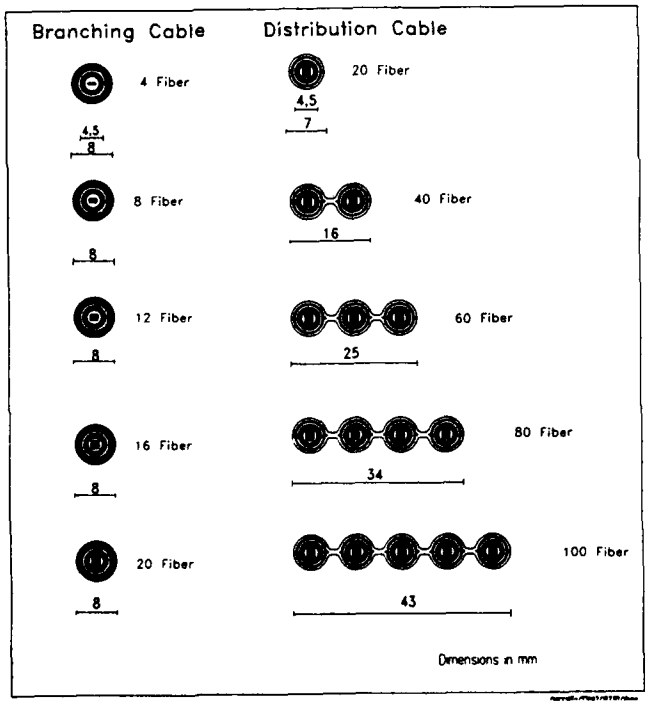


Fig. 5 Ribbon Cable Construction with Central Tube

- Flat cable

This cable type represents a new cable for the direct subscriber termination. By this it is possible to connect the subscriber to the existing network without splicing (FTTH) cost of a single cable.

A flat cable construction allows to remove separate optical transmission elements without opening the whole cable or to have to connect again the transmission elements to the continuing telecommunication line. The presented construction consists of basic elements: ribbon tube, tension members and a PE-outer sheath. This basic elements are separately connected by webs.

With these webs it is possible to take out the individual element from the cable without affecting the cable in its qualities. In order to protect the individual element against mechanical stress, tension members are integrated in the PE-sheath of the single element. They protect these single cable element of the whole cable for the laying and mounting to the subscriber. At the complete cable special compression protection members at the edges of the cable protect this flat cable and allow to lay the cable along greater distances (Fig.6).

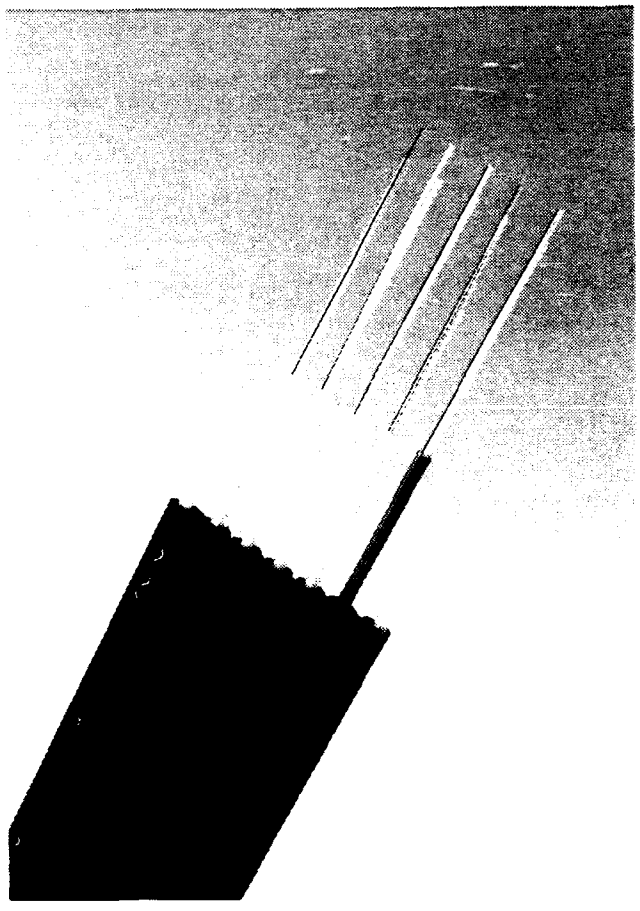


Fig. 6 Flat Cable with Ribbons

- Cable with stranded ribbon tube

Highcount optical fiber ribbon cables (80...200 OF) will be constructed with tubes of 20 optical fibers per tube, stranded in a single layer around a central strength member (steel wire or FRP-rod).

By this an optical fiber cable with a minimum outer diameter and low cable weight can be obtained according to the customer demands for subscriber cables. For high mechanical stresses the cable is protected in addition to the central strength member with tension members under the outer sheath of the cable. The multiple sheath of the ribbon cable consists of these tension members, optional an aluminium foil as moisture barrier and the PE outer sheath. For the watertigthness the interstices in the cable core are filled with petrojelly and the sealing of the tension members is obtained by a swelling tape. By the stranding of the ribbon tubes and the resulting flexibility of the ribbon stack in the cable this construction is able to withstand cable elongation without ribbon strain (fiber elongation). Fig. 7 shows an optical fiber cable (80 fibers) with basic units of 20 fibers.

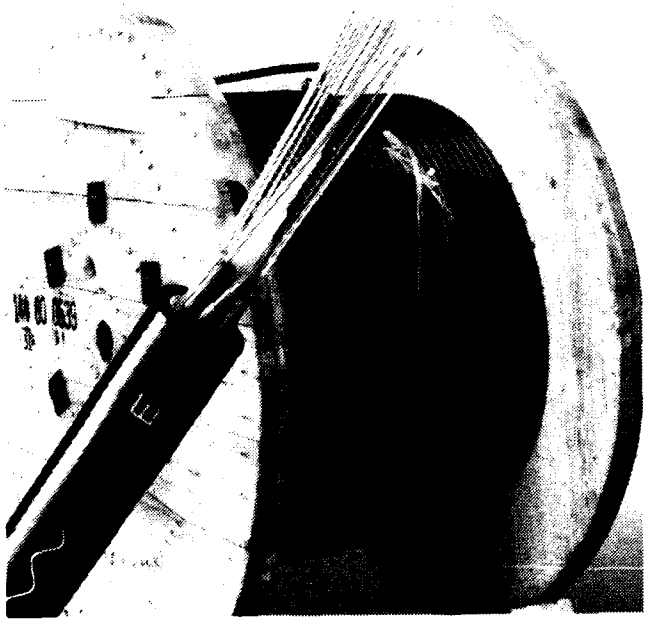


Fig. 7 80-Fiber Main Cable with 4-Fiber Ribbons

3.5 Characteristics

Cable constructions with ribbon technology for the subscriber loop must fullfil the mechanical and optical demands in this area.
As basis for this for example the technical specifications of the Deutsche Bundespost Telekom for optical fiber cables in the local network can be taken /7/. The main test criterions required are the following:

- temperature behaviour between -20°C and +60°C,
 with $a \leq 0{,}1$ dB/km
- tensile stress up to 2-times of the kilometric cable weight
 with $a \leq 0{,}1$ dB/km
- bending test with 15-times of the cable diameter,
 with $a < 0{,}1$ dB measured length
- longitudinal watertightness for 1 m cable during 72 h with 1 m water heigth

In Fig. 8 the measured results for the three cable constructions are concluded. They show that the ribbon cables meet all requirements which are required from today' optical fiber cable for the local network.

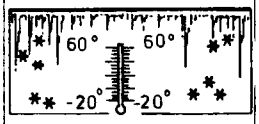
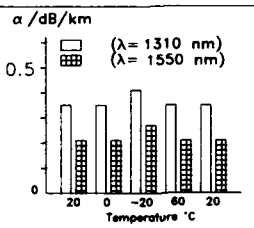
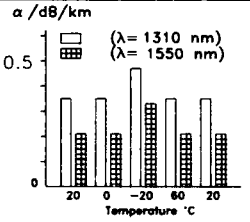
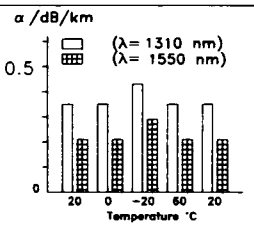
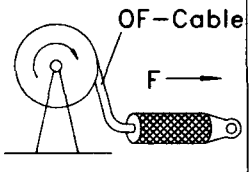
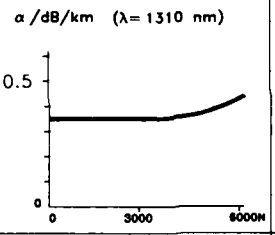
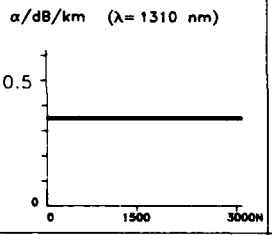
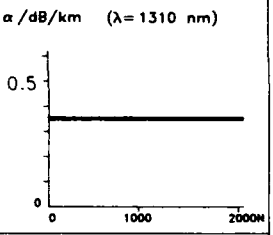
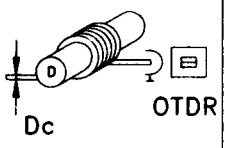
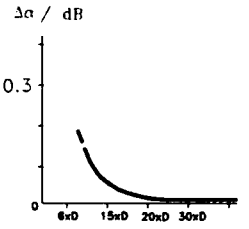
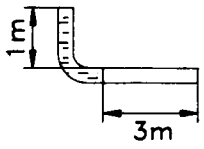
New Cable Family for FITL			 15 mm 80-Fiber Cable	 8 mm 20-Fiber Cable	 65 mm 20-Fiber Cable
Performance	Parameter	Range	Results on 2km Lengths		
Cable Type			Stranded Tube	Central Tube	Flat-Cable
Temperature Cycling 	Tempera-ture Linger Time/Step	-20°C.. +60°C 24 h			
Tension 	Force	2x Weight/km			
Bending 	Mandrel Diameter	5 Times 15xDc	no additional loss		no additional loss
Waterblocking 	Water Pressure Time	0,1bar 72 h	no penetration	no penetration	no penetration

Fig. 8 Test Results on Various Ribbon Cable Constructions

In all test cables the ribbons were unstranded in the tubes. Better test results, especially bending behaviour, might be achieved with a pre-stranded ribbon stack. This is important for future aspects, when ribbons with more fibers than only four should be used.

4. Installation Technique

4.1 Connection technique

The connection technique for the represented new cable family does not considerably differ from the conncetion technique for standard cables. For permanent fix connection fusion splices are used, detachable connections are realized with connectors /8/.
Based on the fusion splice equipment for single fibers splice units have been developed which are able to melt fiber ribbons with up to 12 fibers at the same time. The average splice attenuation for a 4-fiber ribbon is about 0.02 dB (σ = 0.02 dB) in case of identical fibers. The splice time excluding the time for the fiber preparation is about 1 min for a 4-fiber ribbon. The whole time including the fiber preparation is about 10 min. Depending on the manual skill of the installation staff time can be gained.

A connection between fiber ribbon and single fibers is also possible so that a cable of the new family can be spliced to existing cable systems with standard cables with the same equipment.

An alternative to the fusion splice connection is the use of connectors. They are favourably employed where cables pre-terminated in the factory have to be quickly connected in the field without special tools. Naturally, the insertion loss is higher with connectors than with fusion splices. Average values for 4-fiber or 8-fiber ribbons are about 0.35 dB.

4.2 Joint boxes

In order to protect the splices and connectors joint boxes are used. Concerning the Deutsche Bundespost Telekom thermoplastic jointing closures for the buried cable connections proved to be good. They are easy to handle, watertight, pressure-resistant and available in different sizes for cable connection and cable distribution. Within the closures the fibers and splices are arranged in splice boxes consisting of plastic which have been introduced by the Deutsche Bundespost as standard.

For logistic reasons these joint and splice boxes should also be used for the new cables. For all circular cable constructions the closures can be taken over without change. Concerning the flat-cables modifications of the sealing bodies are necessary. Up to three flat-cables are practicable because of sealing problems. Figure 9 shows an open closure for the connection of round ribbon cable to a standard cable with loose tubes.

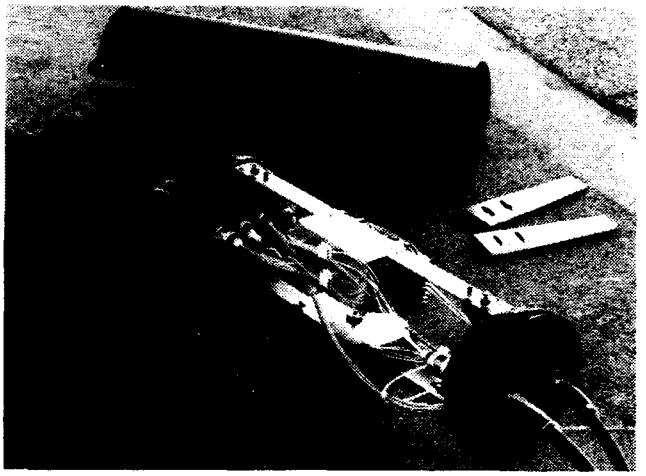


Fig. 9 Open Closure with Fiber Ribbons Spliced to Single Fibers

The standard splice box can also be used for ribbons, only the splice holders for the splice protection have to be modified.

4.3 Distribution technique

At the subscriber end of the network a great number of cable distributions have to be realised in the case of FTTH. In order to minimize the installation costs the flat-cable has been developed. At the subscriber end it combines the distribution and the drop cable and makes it possible to install without joint boxes at few mounting efforts up to the house. At the junction point of the house only a simple branch is to be mounted which serves as tension member and bending protection.
Although the optical fiber flat-cable is developed for the branch to the house without joint box it may be necessary to make a connection to the installed cable later on. For this case a cable branch has been developed which allows a connection at a very small space (Figure 10); by this the size of the manhole can be reduced to 1 m x 1 m.

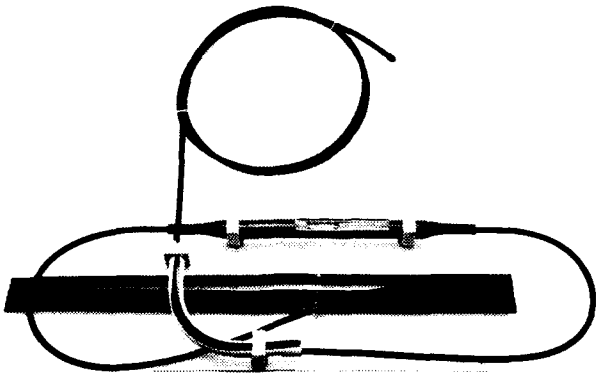


Fig. 10 Flat Cable Branch with Drop Cable

The connection of the fibers can be made by fusion splices or connectors. For the protection and integration serves a slim cylindrical body which is sealed by a shrunk-on tube. Possibly necessary additional fiber lengths for more splicing will be taken from the cable.

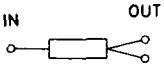
4.4 Splitter installation

The high demands on the return loss - ≥ 60 dB - and mechanical longterm stablility at the moment are only met by taper couplers. Therefore the necessary optical splitters are connected in cascade by single coupler elements (Fig.11).

Specifications for SM-Taper-Couplers
for 1310 nm and 1550 nm

Temperature Range : - 40° ... + 85° C
Return-Loss : > 60 dB on all Ports
Bandpass : ± 10 nm within both Wavelengths

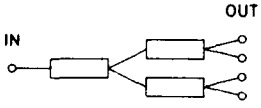
Type: 1 : 2



Insertion-Loss / Port:
typ. : - 3.4 dB
max. : - 3.7 dB

Uniformity:
max. : 0.4 dB

Type: 1 : 4



Insertion-Loss / Port:
typ. : - 7.0 dB
max. : - 7.6 dB

Uniformity:
max. : 0.8 dB

Fig. 11 Single Mode Taper-Coupler Specification

This connection in cascade is executed in the factory in standard splice boxes, that means at the road works only complete splitter components are installed. Depending on the employment the splitters can also be applicated together with plugs as an installation unit. In this case also the complete unit would be pre-terminated and measured in the factory a 1:2 coupler shows Fig. 12.

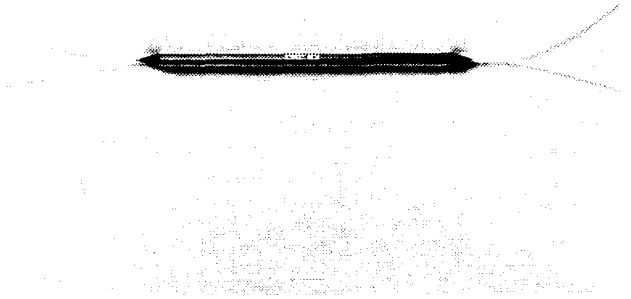


Fig. 12 Single Mode Taper-Coupler (2x2)

The standard measuring technique of optical fiber networks is the backscatter method by which the defects can be discovered as well as the attenuation can be measured. Using optical splitters in the networks this technique can no longer be applied without restriction. At that time all over the world procedures and methods are searched for which allow the use of OTDR also in networks with optical splitters.

4.5 Termination

By the use of connectors for the connection of optical fiber ribbons it is possible to reduce the mounting efforts in the field. This will be obtained by cables pre-terminated in the factory. Especially for drop cables this technique is suitable as normally only few standard lengths are necessary, for example 5 m, 10 m, 30 m. By that in addition the stock-keeping will be simplified very much. A cable overlength can simply be layed down in the hole in front of the lead-in.

From the part of the network the cables are equipped with ribbon connectors, from the part of the house with the connectors specified by the system (Fig.13).

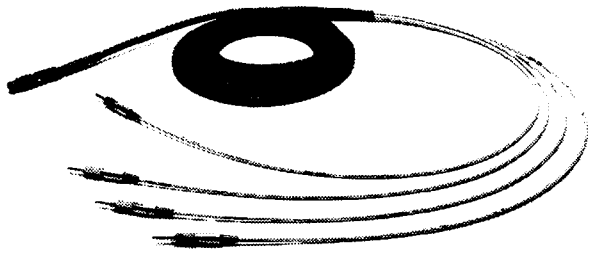


Fig. 13 Pre-Terminated Drop Cable with MT and DIN Plugs

4.6 Laying techniques

The presented cable constructions with circular cross-section can be installed with all usual laying techniques that means they can be layed into open trenches or in ducts. In duct systems they can be installed by air-pressure.

The flat-cables are predestinated for a laying in an open trench because of their rectangular cross-section. But due to the high flexibility it is also possible to shape them to circular forms along their longitudinal axis during the installation and pull them into the ducts.

As the laying of the flat-cable differs from the usual and well-known laying techniques in the following the laying of a flat-cable in an open trench will be described. After the excavation of the trench the cable will be unwinded from the delivery drum and layed in the trench beginning at the distribution point along the houses to be connected. By that an additional cable length must be taken into consideration by which the distance of the last house to be connected must be added from the distribution point to the ditch. Subsequently the cable elements for the subscriber, also with an additional cable length, are separated from the flat-cable. This can be made with a double-bladed knife or by tearing up by hand. By tearing up by hand it must be taken care of the single elements not to be bended. At the distribution point the cable element is protected against bending and against high tensile forces by a simple arrangement.

For the further laying of the single elements to the house the weel-known techniques can be used.

5. Fields trails results

5.1 OPAL 6

In co-operation with the DBPT within the scope of the FAST consortium the pilot project OPAL 6 has been carried out. The project is concerned in innovative and low-cost optical fiber systems, which allow the supplying of the customer with a complete offer of services. This passive network has been planned for 200 customers and contains the two alternatives FTTH (fiber to the home) and FTTC (fiber to the curb). The demands for an economical use of optical transmission technique by an employment of the optical fiber ribbons in the cable and the splice-free installation technique by the special optical flat cable have been taken into consideration. With FTTH each customer receives three optical fibers whereby two fibers are used for the dialog service and one fiber supplies cable television.

The connections of the double passive star network are distributed by taper couplers and work by a distribution factor of 1/32.

6. Outlook

The calculation of various network architectures for the telecommunication of different services has shown that solution methods can be found which reduce the costs. One of the most important points is that the employment of optical fibers is advantageous all along the area if greater switching centers are concentrated.

On the other hand this causes a multiple of cable lengths to the subscriber. It has been calculated that the average subscriber length increases from 2 km to 10 km.

By using their topology and passive optical componentens (**splitter**) the number of fibers in the cable will decrease. It can be expected that the number of fibers in the main cables will obviously be under 50 fibers and in the distribution area not more than 200 fibers per cable will exist. From the curb point or the building point the fiber number to the subscriber

will be around 10 and less. Regarding the services and the technique it seems to be useful to supply all buildings in the future with 4-fiber basic elements.
The efforts for the managing of such an installation with ribbon elements may be cost-reducing.
In the future it will be surely of great importance to supply hybrid cables from the curb point (double copper cores combined with optical fibers in a proportion of copper/OF = 5/1), as necessarily the laying costs and the saving of material at the cable will reduce the costs.
Besides the development of pure optical fiber cables the hybrid cables will become more important in the future, because the existing copper networks should be integrated into the new conceptions with optical fibers.

7. References

/1/ Tetsuya Miki:
How to opticalize Subscriber loop networks, NTT Transmission Systems Laboratories, 1991

/2/ Haag, Hög, Zamzow:
Optical fibre and System Considerations for a broadband subscriber network, International Wire and Cable Symposium Proceedings, 1985 pp. 355-363

/3/ Haag, Hög, Zamzow:
Optical fibre cables for subscriber loop, Journal of Lightwave Technology, Vol. 7, No 11, 1989 pp. 1667 - 1674

/4/ H. Schüßler:
A Combined Subscriber Network with Optical Fibers for Telephone and Broadband Distribution in Suburban Areas-Economical Considerations
Fibre to the Home, Proceedings of a congress, Munich 1990

/5/ H.G. Zielinski/H. Moers/D. Knodel:
Proposal for an Economical Fully Covering Installation of Fiberoptic Cables in the Subscriber Loop
Fibre to the Home, Proceedings of a congress, Munich 1990

/6/ Draft CECC Pr.EN 188000 Issue 1, January 1992 Method 306

/7/ Technische Lieferbedingungen
Außenkabel für Fernmeldelinien TL-Nr. 6015-3005 der Deutschen Bundespost Telekom

/8/ F. Ashiya, T. Satake and S. Nagasawa,
"Development of Multifibre Connectors and their Application", 9th EFOC/LAN 91, London 1991, pp. 304 - 308



Peter Delage
KABEL RHEYDT AG (former AEG KABEL)
Mönchengladbach, Germany

Peter Delage (35) is head of the Development Group for Special Optical Cables. After getting his Dipl.-Ing.-Degree he joined AEG KABEL in 1983 in the Development Group for Optical Fibre Cables. Since 1986 he covers his present position.



Reinhard Girbig
KABEL RHEYDT AG (former AEG KABEL)
Mönchengladbach, Germany

Reinhard Girbig (38) is head of the Development Group for Optical Fiber Cable Installation Technique. He received his Dipl.-Ing.-degree from the "Ruhr-University Bochum" in 1982 and joined AEG KABEL in 1987. Working as a development engineer in the fiber optics area he was responsible for the technical aspects of OTDR measurement. Since 1991 he covers his present position.



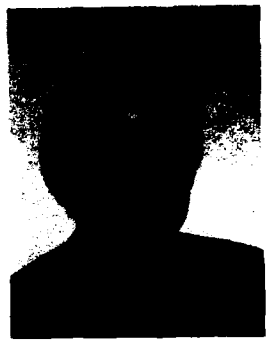
Georg Hög
KABEL RHEYDT AG (former AEG KABEL)
Mönchengladbach, Germany

Georg Hög (42) is head of the Development Group for Optical Fibre Cables. He reached his Dipl.-Ing.-Degree from the University of Aachen and joined AEG KABEL in 1977. After being engaged in the development of symmetrical telecommunications cables he got the responsibility for this group in 1980. Since 1985 he covers his present position.



Michael Hoffart
KABEL RHEYDT AG (former AEG KABEL)
Mönchengladbach, Germany

Michael Hoffart (36) is General Manager of the Optical Fibre Plant. He received his Dipl.-Ing.-Degree from the "Bergische University" Wuppertal in 1983. He joined AEG KABEL on graduation and has been engaged in the field of optical measurement technique and telecommunication cables.



Peter E. Zamzow
KABEL RHEYDT AG (former AEG KABEL)
Mönchengladbach, Germany

Peter E. Zamzow (52) is director of the Telecommunicaton Development Division. After finishing his postgraduate studies in telecommunications in Munich and Graz as Dipl.-Ing. he joined AEG KABEL in 1970. He has been engaged in development and production of telecommunication cables. In 1980 he became head of the fiber optic division at AEG KABEL and in 1982 he was nominated as a senior engineer. Since 1985 he has covered his present position.

Herbert Moers
KABEL RHEYDT AG (former AEG KABEL)
Mönchengladbach, Germany

Herbert Moers (35) is responsible for the Sales Department for Telecom Assemblies. He received his Dipl.-Ing.-Degree from the University in Hamburg in 1981. After being engaged in the development of optical fibre systems he got his present position in 1991.

Fabrication and Evaluation of 40-Fiber Array.

Ryuichi MATSUOKA, Yasuhiro SHINDO, Noboru OKADA, Nobukazu KUME

The Furukawa Electric Co., Ltd. 6, Yawatakaigandori, Ichihara, Chiba, 290, Japan

1. ABSTRACT

Recently, optical parallel transmission systems between equipment such as computers have been studied in various fields from the viewpoint of transmitting and processing large volumes of information.

The delay time difference (skew) of signals between optical fibers becomes an important factor in optical parallel transmission, requiring the skew to be minimized for transmission of larger volumes of information. In this respect, ribbon fiber is most suitable for use in optical parallel transmission because the physical length of individual optical fibers may be equalized.

In this study, We fabricated 40-fiber ribbon arrays available for the optical parallel transmission, and evaluated them mainly about skew.

2. FABRICATION OF 40-FIBER ARRAY

A cross section of 40-fiber ribbon array is shown in Fig. 1. Forty single mode (SM) optical fibers are arranged in a row, and the dimensions of this ribbon array are 10.4mm in width and 0.4mm in thickness. The manufacturing process of 40-fiber ribbon array comprises two steps: the first step of bonding ten SM optical fibers into a 10-fiber ribbon array, and the second step of binding four 10-fiber ribbons to compose a 40-fiber ribbon array.

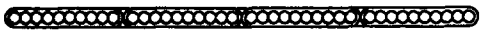


Fig. 1 Sectional View of 40-Fiber Ribbon Array.

In fabrication of 10-fiber ribbon array, difference in strain may occur in the individual optical fibers due to difference or fluctuation of supply back tension or the like. Furthermore, the sectional shape of ribbon fiber may have structural non-uniformity, such as curve, uneven thickness of coating, and misalignment of cores. These structural non-uniformity may affect the skew of the ribbon fiber, and so should be minimized as possible. Similarly, in the manufacture of 40-fiber ribbon array, the supplied 10-fiber ribbons must be stabilized, and the bind shape between 10-fiber ribbons must be made uniform.

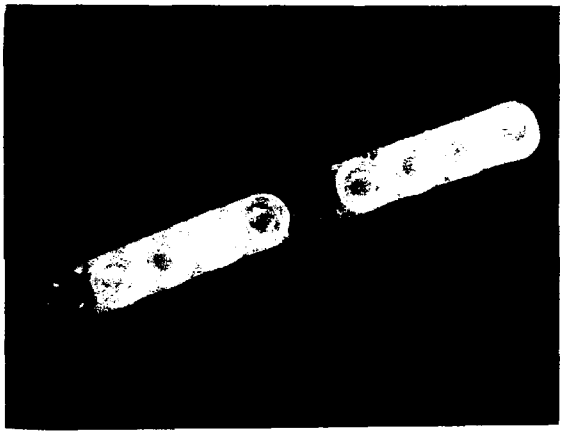


Photo 1 10-Fiber Ribbon Array

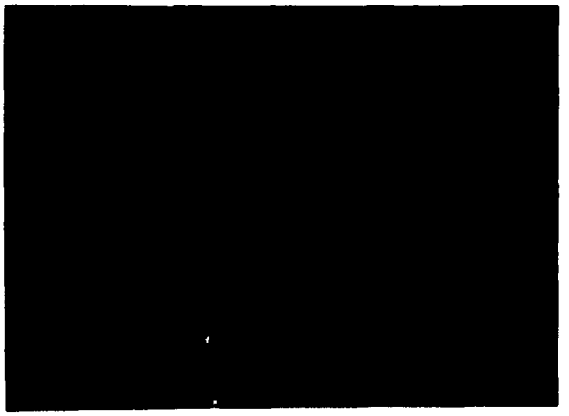


Photo 2 40-Fiber Ribbon Array

Photo 1 and Photo 2 show the sectional views of the 10-fiber and 40-fiber ribbon array. Evaluation of attenuation, temperature cycling, and mechanical stability of the 40-fiber array brought satisfactory results as compared with the conventional ribbon fibers.

3. SKEW FACTOR ANALYSIS

The following three factors can be listed as the causes for skew which occurs with ribbon fiber:

1. Difference in signal propagation time caused by fiber parameter deviation.
2. Difference in residual distortion during ribbon fiber manufacture.
3. Difference in Physical length caused by structural non-uniformity of ribbon fiber.

3.1 Skew Caused by Fiber Parameter Deviation.

Using optical fiber parameters, the fiber delay time t can be given as

$$ct=\frac{d\beta}{dk}\fallingdotseq N_2\left(1+\Delta\frac{d(vb)}{dv}\right) \qquad (1)$$

where β is a propagation constant, v is a normalized frequency, N is a group refractive index, and Δ is the relative index difference. b is a normalized variable of β and can be written as

$$b=\frac{\beta^2-k^2n_2^2}{k^2n_1^2-k^2n_2^2} \qquad (2)$$

where n_1 and n_2 are refractive indexes of single mode (SM) optical fiber core and cladding. In SM optical fibers, v can be obtained from the cutoff wavelength λ_c, normalized cutoff frequency v_c (=2.405) and operating wavelength λ, and the relation between v and b can be obtained from a dispersion curve. Therefore, skews in SM ribbon fibers are determined from deviation of the Δ values and cutoff wavelength λ_c of individual cores in ribbon fibers.

3.2 Skew by Residual Distortion of Ribbon Fiber.

Residual strain differences between cores are caused by difference of supply back tensions of uncoated fibers during the manufacture of ribbon fiber. the effect of the residual strain differences on skew of ribbon fiber must be taken into consideration.

The delay time t in optical fiber in the length of L applied with strain ε are given as

$$t=\frac{NL}{c}\frac{1+\kappa\varepsilon}{1+\varepsilon} \qquad (3)$$

where κ is a photo-elasticity coefficient. The skew Δt between cores in ribbon fiber of length L applied with strain ε_1 and ε_2 ($\ll 1$) can be given as

$$\Delta t=(\kappa-1)(\varepsilon_1-\varepsilon_2)\frac{NL}{c} \qquad (4)$$

3.3 Skew by Structural Non-uniformity of Ribbon Fiber.

Physical length of optical fibers wound on a bobbin or drum differ due to strain applied to cores if ribbon fiber has curves or misalignment. If the structural non-uniformity of ribbon fibers enlarges, the effect on skew cannot be ignored. The value of skew caused by structural non-uniformity of ribbon fiber is calculated from the diameter r of a take-up bobbin and the misalignment dimension d of the ribbon fiber. The physical length difference ΔL caused between optical fibers when ribbon fiber is wound on a bobbin for the length L can be given as

$$\Delta L=2\pi d\times\frac{L}{2\pi r}=\frac{dL}{r} \qquad (5)$$

The skew Δt between cores can be written as follows if the photo-elastic effects are taken into consideration:

$$\Delta t=\Delta L\times\frac{\kappa N}{c}=\frac{\kappa dLN}{cr} \qquad (6)$$

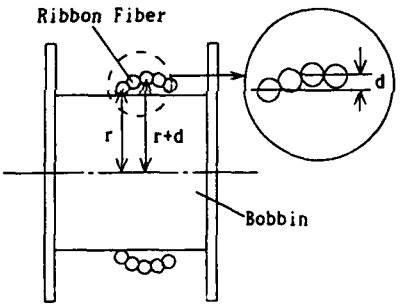


Fig. 2 Physical Length Difference Caused by the Structural Non-uniformity of Ribbon Fiber.

4. SKEW MEASURING METHOD

Fundamentally, the ribbon fiber skew is measured by a method similar to that applied to measuring chromatic dispersions of SM optical fibers. Utilizing the apparatus for measuring chromatic dispersions, instead of changing of wavelength, fibers to be measured are changed in succession to obtain relative skews among fibers. The apparatus for measuring skew by phase shift method is shown in Fig. 3. The light sinusoidally modulated is driven into a core of the ribbon fiber, and the light emitted from the fiber is converted into an electrical signal by a photodetecor. The phase angle difference of this output light to reference signal is measured on each core of the ribbon fiber, and gives the delay time difference from the reference signal.

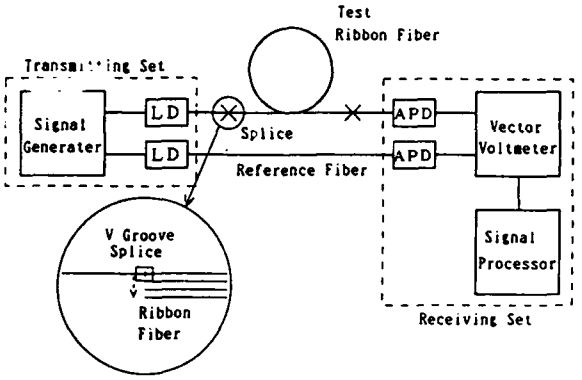


Figure 3 Apparatus for Measuring Skew by Phase Shift Method.

5. SKEW OF 40-FIBER ARRAY

The skew was measured in the 10-fiber and 40-fiber array. In this paper, the unit of skew is standardized in the value of the delay time per 100m (ns/100m).

5.1 10-Fiber Array

Figure 4 shows the result of measuring skew of 10-fiber ribbon. In the diagram, the axis of abscissas denotes the core wire number of the ribbon fiber, and the axis of ordinates indicates the difference of the delay time per unit length from that of the core wire No.1. The length of the 10-fiber ribbon was 1000m, and the skew was measured in the wound state on the bobbin of 280mm in diameter. To clarify the factors for causing skew, optical fibers of a single preform were applied in all cores in the 10-fiber ribbon. Accordingly, the factors for causing skew were limited to the residual strain in fabrication , or the difference in physical length due to structural non-uniformity of ribbon fibers. In Fig.4, in the 10-fiber array, it was observed that the delay time tends to become smaller as going from the core wire of both edge toward the central. The maximum value of measuring skew was 0.120 ns/100m.

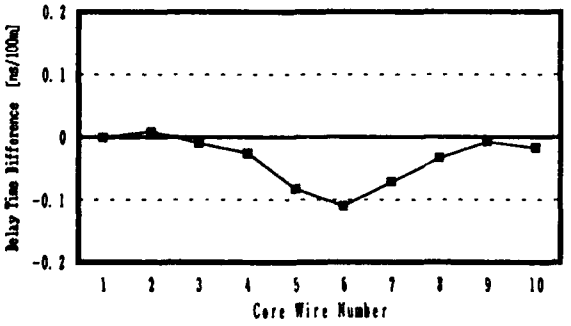


Figure 4 Skew of 10-Fiber Ribbon Array

5.2 40-Fiber ARRAY

Figure 5 shows the result of measuring skew of 40-fiber ribbon array fabricated from the 10-fiber ribbon mentioned above. As compared with the measurement in 10-fiber array indicated by interrupted line, the tendency of the delay time in the 10-fiber ribbon was almost inverted in magnitude. This is because the face and back side to the wound bobbin of the 10-fiber ribbon were reversed when fabricating the 40-fiber ribbon, and therefore the magnitude of the strain applied to the core wire in the 40-fiber array wound on a bobbin was varied. It was also observed that the delay times tend to become larger in the core closer to the bind between 10-fiber ribbon. This is because the non-uniformity of the bind shape had the section of 40-fiber ribbon slightly curved, thereby causing a difference in the physical length due to the corresponding strain when wound on a bobbin.

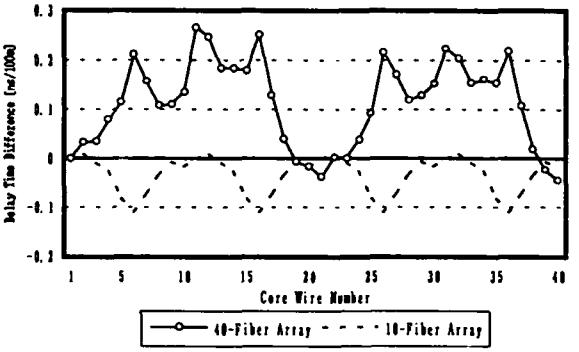


Figure 5 Skew of 40-Fiber ribbon array

5.3 Effects of Fiber Parameter

To evaluate the effects of fiber parameters on the skew, 10-fiber ribbon composed of optical fibers in several preforms were separately fabricated. Table 1 shows the relative index difference Δ and cut-off wavelength λc of optical fibers for composing the 10-fiber ribbon. The result of measuring skew in the 10-fiber ribbon wound up on a bobbin of 280mm in diameter was shown in Fig.6, but the results also include the effects of the structural non-uniformity of the ribbon fiber as mentioned above.

Table 1 Fiber Parameters for Composing the 10-Fiber Ribbon.

No. 1			No. 2		
Fiber Number	λc [μm]	Δ [%]	Fiber Number	λc [μm]	Δ [%]
1～4, 6	1.246	0.38	1	1.228	0.36
5, 7, 8	1.258	0.35	2～4	1.278	0.37
9, 10	1.248	0.36	5, 7～10	1.280	0.35
			6	1.278	0.34

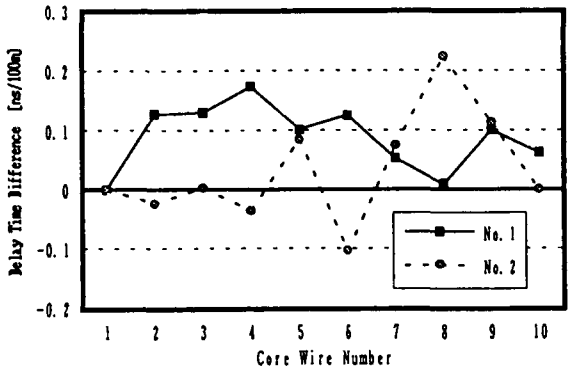


Figure 6 Skew of 10-Fiber Ribbon Array.
(Those fiber parameters are given in Table 1)

In the state of the cable fabricated from the 40-fiber ribbon, the skew was measured again. The cable was in flat structure, and measured in the state wound up on a drum of 1200mm in diameter, and so it is expected that the skew due to structural non-uniformity of the ribbon fiber would be 1/4 or less. The results of measurement are shown in Fig. 7 and Fig. 8 in comparison with the values of the delay time difference calculated by using Formula (1) and the fiber parameter in Table 1. The values of measuring skew of both 10-fiber array nearly reflect the parameter of the constituent optical fiber in ribbon. That is, since the relative index difference Δ and the cut-off wavelength λ_c determine the signal propagation time of optical fiber, the skew of the ribbon fiber can be limited by controlling them.

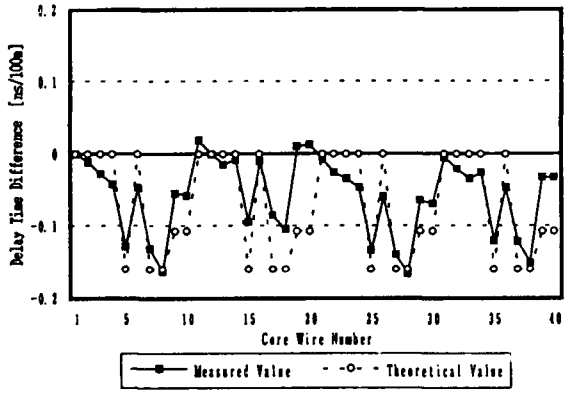


Figure 7 Measured and Theoretical Value of Skew of 40-fiber Ribbon No. 1.

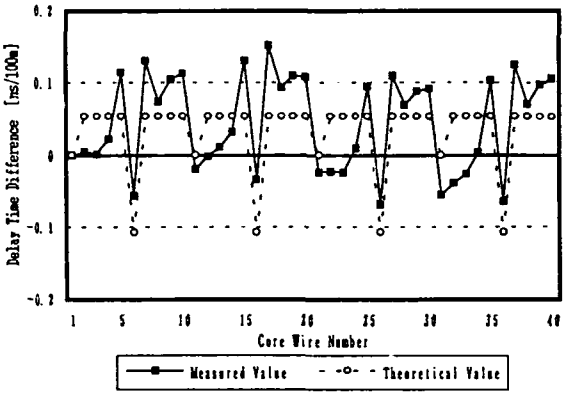


Figure 8 Measured and Theoretical Value of Skew of 40-fiber Ribbon No. 2.

6. SUMMARY

The 40-fiber ribbon array was fabricated for the purpose of applying to the optical parallel transmission, and its performance including the skew were evaluated.

1) The attenuation, temperature cycling, and mechanical stability of the 40-fiber array were equal to those of conventional ribbon fibers.
2) The sectional structure of the 40-fiber array contribute the measurement of skew in the bobbin wound state. To minimize the skew, it is necessary to reduce this structural non-uniformity.
3) The relative index difference Δ and cut-off wavelength λ_c of the SM fiber determine the signal propagation time, and therefore the skew of the ribbon fiber may be limited by controlling the fiber parameters composing the ribbon fiber.



Ryuichi Matsuoka

The Furukawa Electric Co., Ltd.

6, Yawatakaigandori, Ichihara, Chiba, 290, Japan

Mr. Matsuoka was born in 1965. He received B.E. degree in Electronics from Osaka University in 1989 and joined The Furukawa Electric Co., Ltd. in 1991. He has been engaged in development of optical fibers and cables.

He is a member of The Institute of Electronics, Information and Communication Engineers of Japan.



Nobukazu Kume

The Furukawa Electric Co., Ltd.

6-1, Marunouchi 2-chome Chiyoda-ku, Tokyo 100, Japan

Mr. Kume was born in 1956. He received B.E. degree in electronic and communication engineering from Waseda University in 1980 and joined The Furukawa Electric Co., Ltd. He has been engaged in network integration engineering.

He is a member of The Institute of Electronics, Information and Communication Engineers of Japan.



Yasuhiro Shindo

The Furukawa Electric Co., Ltd.

6, Yawatakaigandori, Ichihara, Chiba, 290, Japan

Mr. Shindo was born in 1966. He received B.E. degree in Electrical engineering from Kyusyu University in 1991 and joined The Furukawa Electric Co., Ltd. He has been engaged in production engineering of optical fibers.



Noboru Okada

The Furukawa Electric Co., Ltd.

6, Yawatakaigandori, Ichihara, Chiba, 290, Japan

Mr. Okada was born in 1967. He received B.S. degree in physics from Sizuoka University in 1991 and joined The Furukawa Electric Co., Ltd. He has been engaged in production engineering of optical cables.

A STUDY ON SELF-SUPPORTING OPTICAL FIBER CABLE WITH FOUR FIBER RIBBONS

H. Sawano, S. Saito, M. Miyamoto

Fujikura Ltd.

ABSTRACT

A new optical fiber aerial cable in figure-eight fashion was designed based upon slotted rod units with four-fiber ribbons and the reverse lay technique. In designing aerial optical fiber cables, it is important to reduce the stresses added to the optical fibers. The adopted technique for reducing the above stresses is to add excess fiber length by the reverse lay stranding method. In this cable, the stress added to the optical cable is absorbed by the slip of the optical fiber units circumferentially on the central member. A one-hundred-fiber cable with four-fiber ribbons was made. It was clarified that the fiber elongation of the cable designed on the basis of the above concept was 1/4 of the cable elongation and this cable was subjected to several mechanical and environmental tests, consequently, it was verified that the cables had sufficient cable strength and reliability.

1. Introduction

It has become popular to use optical fibers in the transmission lines, because of their large transmission capacity. In Japan, one-thousand-fiber water proof cable was developed and has been used in practical subscriber networks[1),2)]. With the increase of the application of optical fibers to subscriber networks, several types of the distribution cables such as helically slotted-core cable using four-fiber ribbons[3)], reverse-lay slotted-core cable using two-fiber ribbons[4)] and others were developed and have been introduced to subscriber networks.

Distribution cables are generally installed on poles as well as ducts. In the case of aerial distribution optical fiber cables, stresses due to installation stretching, temperature change,and wind and snow are added to the optical fibers in the cable. These stresses degrade the life time of the optical fibers, so many structures of the aerial cables are designed and tested extensively[5),6),7),8)].

In this paper, we show a new structure of a aerial cable based upon the slotted rod units and reverse-lay technique.

2. Design criteria

Cables that are used in the subscriber network should satisfy the following requirements:

1) high fiber count,
2) easy installation,
3) rapid cable joining capability,
4) mid-span access capability.

In order to realize the above requirements, it is known to use the slotted rod cable using four-fiber ribbons.

Moreover, in designing the aerial cable, span between poles, sag of the cable and wind pressure must be determined. We adopted these values as follows:

Span between poles	45m,
Wind pressure	110kgf/m^2,
Sag(at 35°C)	70cm.

From the view point of the life time of the optical fiber, the maximum cable elongation is set below 0.2%.

This value assures that the fiber failure probability is less than ten Fits/fiber /100km for twenty years[9)].

3.Cable design

There are two major concepts for protecting the optical fiber from stretching forces. One is suppressing the cable elongation by enlarging the cable modulus or adopting the optimum cable shape[8),10)], the other is including the excess fiber length in the cable design to relieve fiber stretching force[5),6),7)].

3-1. Excess fiber length

To give the excess fiber length, it is popular to use the loose tube structure. In this method, the excess fiber length is determined by the lay length(s), the stranding radius of the loose tube(R), the tube inner radius(Ri) and the radius of coated fiber. Assuming that the fibers in an unstressed cable are in the axes of the tubes, the excess fiber length (ε) can be calculated by Eq.(1):

$$\varepsilon=2\pi^2\delta R/s^2(2R-\delta R) \qquad (1)$$

This time, we have tried to get the excess fiber length by other method and investigated the effect on fiber relaxation. The adopted technique is the combination of the unit reverse lay method. Assuming that the rotation angle of the optical units as a function of cable length can be expressed as a sine function, the excess fiber length can be calculated by Eq.(2):

$$\varepsilon=(\pi R\vartheta)^2/s^2 \qquad (2)$$

wherein we assume the stranding radius of the optical unit is much smaller than the lay length (s is larger than 20R).

3-2. Fiber elongation in the trial cable

The optical units are fastened to the central member by wrapping tapes or other materials, so not all the fiber excess length can contribute to the stress relaxation. The factors that dominate the stress relaxation are the reverse lay angle, the reverse lay length and the friction between the optical units and the central member. Fig.1 shows the schematic diagram of the newly designed optical cable. The reverse lay angle of the optical units along the cable axis is shown in Fig.2. The solid curve shows the lay angle of the optical units in an unstressed cable. When the cable is stretched, the optical units are also elongated, however, the elongation of the optical units will be smaller than that of the optical cable because the optical units slip in the cable. Assuming that the slip of the optical units occurs only circumferentially on the central member, the lay angle can be shown as the broken curve in Fig.2. In addition, regarding the curves that show the lay angles as a combination of the catenary curves with alternatively changing the directions to opposite side. With above assumption, the relationship between the cable elongation and the optical unit elongation can be expressed by Eq.(3)[11].

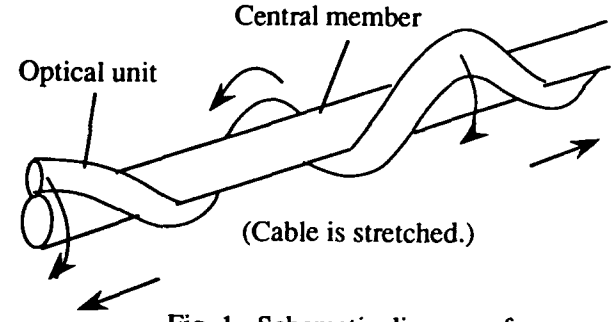


Fig. 1 Schematic diagram of the newly designed cable.

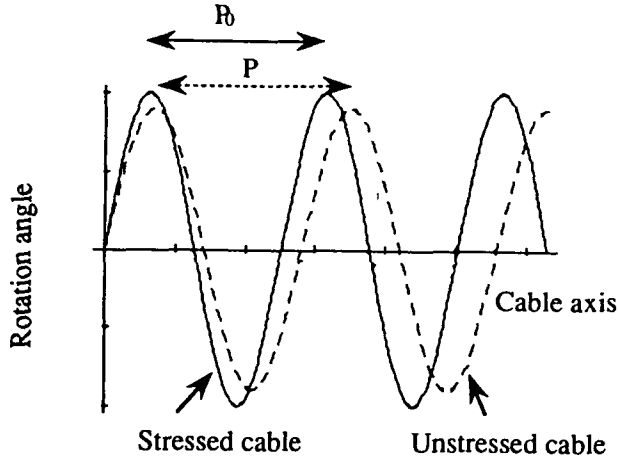


Fig. 2 Rotation angle of the unstressed cable and the stressed cable.

$$A\varepsilon_u^3-B\varepsilon_u^2=C \qquad (3)$$

$$A=p_o^2+2(r_o\vartheta)^2/3$$
$$B=p_o^2\varepsilon_s-2(r_o\vartheta)^2/3$$
$$C=\{f^2p_o^4(1+\varepsilon_s)^3\}/\{24(EA)^2\}$$

where ε_u=Unit elongation
ε_s=Cable elongation
p_o=Reverse lay length in an unstressed cable
r_o=Stranding radius of the optical units
ϑ=Reverse lay angle (radian)
f=Friction force between the optical units and the central member
E=Young's modulus of the unit
A=Area of the unit

In Eq(3), friction force between the optical units and the central member is the drawing force of the optical units during being pulled out of the cable.

Fig.3 shows the relationship between the cable elongation and the fiber elongation. In the calculations, the stranding radius of the optical units is 4.3mm, the fiction between the optical units and the central member is 8kgf/m and EA is 100000kgf. The fiber elongation under those conditions is estimated at 0.07% when the cable elongation is 0.2%.

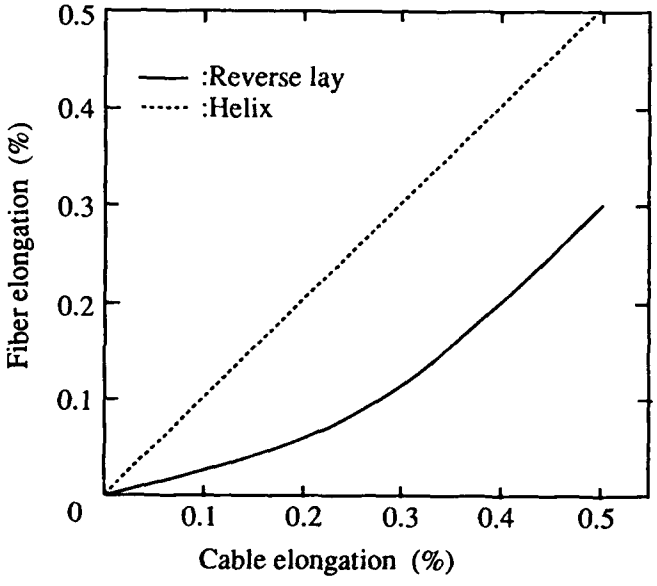


Fig. 3 Relationship between fiber elongation and cable elongation.

3-3. Suspension wire

EA of the suspension wire must satisfy the following relation[10].

$$EA > Wl^2/\{p(24ql^2+64d_0)^{1/2}\} \quad (4)$$

$$W=\{W_0^2+(hP_w)^2\}^{1/2}$$
$$p=\varepsilon_s-\alpha(t-t_0')$$
$$q=\varepsilon_s-\alpha(t_0-t_0')$$

where E=Young's modulus of the suspension wire (18000kgf/mm^2)
A=Area of the suspension wire
W=Effective cable weight
W_0=Cable weight
h=Cable height
P_w=Wind pressure(110kgf/m^2)
l=Span between poles
d_0=Sag of the cable in the stable state(70cm)
α=Linear expansion coefficient
ε_s=Allowable cable elongation
t=Temperature in deployed cable
t_0=Temperature in the stable state(35°C)
t_0'=Temperature in cable manufacturing (20°C)

Herein, the stable state means that the cable temperature is 35°C, the sag of the cable is 70cm and there is no wind. Considering the design criteria, the EA/W was calculated as a function of the span between poles. The result is shown in Fig.4. When the cable weight and height are 0.3kg/m and 25mm, respectively, seven suspension wires of 1mm diameter each satisfy the above condition.

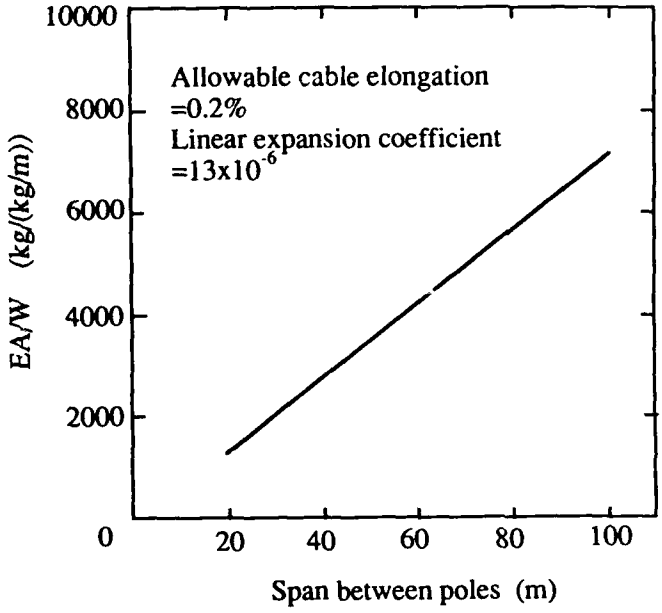


Fig. 4 Relationship between EA/W and pole span.

4. Cable structure

Fig.5 shows the newly designed one-hundred-fiber aerial cable. The optical unit consists of a slotted rod with a four-fiber ribbon in each slot These units are stranded on a central member in the reverse lay fashion. The water proofing is achieved by jelly compound in the slots and water swellable materials outside of the units. The diameters of the optical units and cable core are 5mm and 15.5mm. Considering the mid span access, the reverse lay length and angle are 500mm and 2π, respectively. From these values, the unit excess length is calculated as 0.7% using Eq.(2).

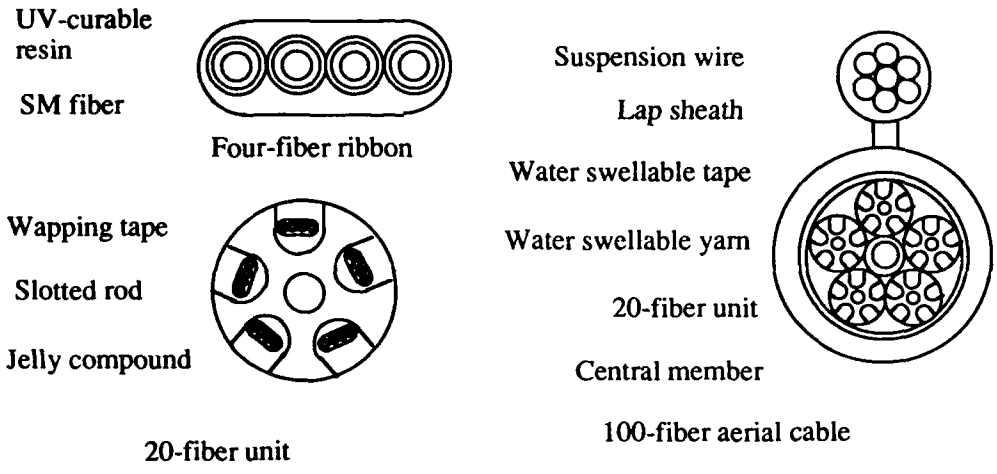


Fig. 5 Structure of the newly designed aerial cable.

5. Cable performance

5-1. Stretching test

Fig. 6 shows the result of the stretching test. The fiber elongation is as small as 1/4 of the cable elongation. This result shows that the reverse lay method has the expected relaxation effect.

5-2. Loss stability

Fig.7 shows the losses in the cable manufaturing process and after installation. The loss change through cable manufacturing process was less than 0.02dB/km in both 1.3μm and 1.55μm wavelength or no loss increase was observed after cable installation.
Fig.8 shows the result of the cyclic temperature test. Through the temperature change between -40°C and 70°C, the loss change was less than 0.05dB/km in 1.55μm wavelength.
Fig.9 shows the loss histogram of the deployed cable. The maximum loss of the cable was 0.24dB/km after one year deployment.

5-3. Mechanical properties

The result of the mechanical tests are listed in table1. Bending, stretching, crush, vibration, impact and squeezing tests are performed. During these mechanical tests, no degradation of the transmission characteristics or injury was observed.

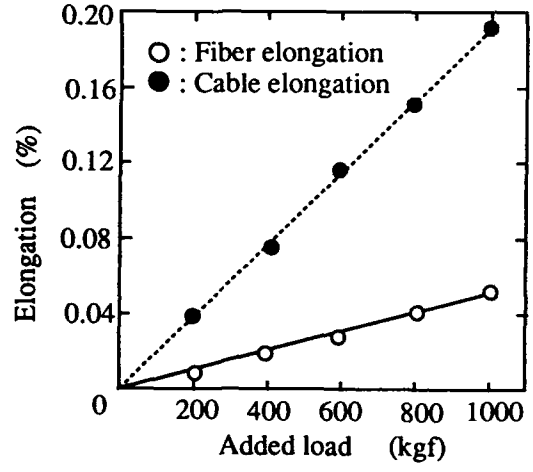


Fig. 6 Result of cable stretching test.

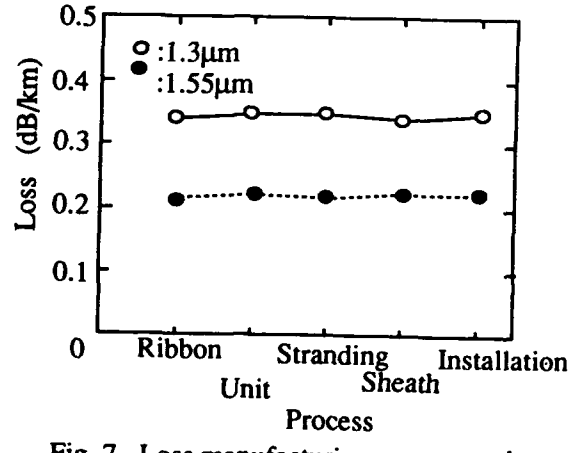


Fig. 7 Loss manufacturing process and after installation.

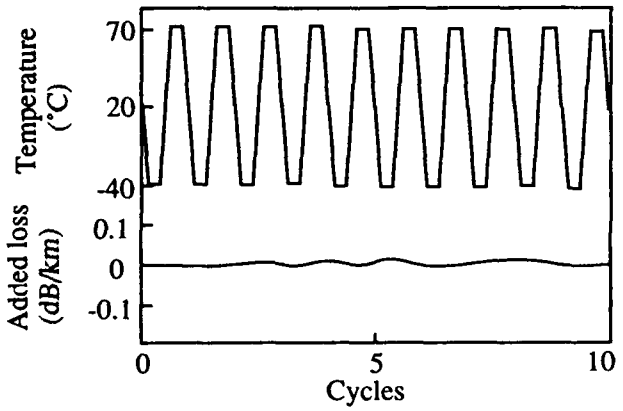


Fig. 8 Temperature chracteristics of the optical loss.

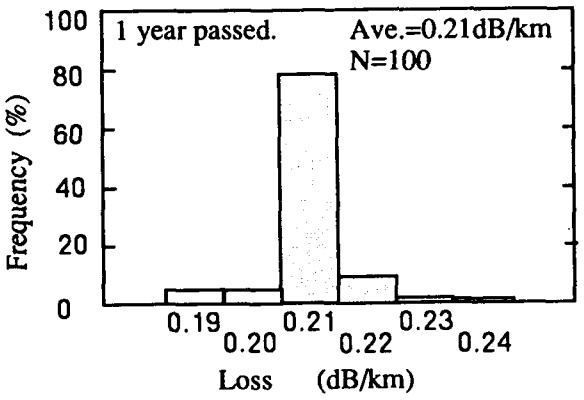


Fig. 9 Loss histogram of the deployed cable.

Table 1 Mechnical propertyies of the newly designed one-hundred-fiber aerial cable

Item	Condition	Result
Bending	R=200mm, 1turn	less than 0.01dB/turn
Stretching	up to 0.2% elongation	less than 0.01dB/100m
Crush	up to 2500N/50mm of lateral force	less than 0.01dB/50mm
Vibration	10Hz, 5mm of amplitude, 1 million times	less than 0.01dB/m
Impact	1kg, 1m height	less than 0.01dB
Squeezing	R=200mm, up to 0.2% elongation	less than 0.01dB/100m

6. Conclusion

A new optical fiber aerial cable was designed based upon the slotted rod unit and the reverse lay technique. The difficulty in designing this cable is to determine the optimum reveres lay length and the reverse lay angle of the units in order to suppress the fiber elongation. By using the reverse lay technique, we made a water proof aerial cable that consisted of slotted rod units with four fiber ribbons and could limit the fiber elongation to 1/4 of the cable elongation. This cable was subjected to several mechanical and environmental tests, and consequently, it was verified that the cables had sufficient strength and reliability.

Acknowledgment

Authors would like to express their sincere appreciation to Dr. Inada for his helpful discussions and encouragement and other members who engaged in this work.

References

1) S. Tomita, F. Ashiya and M. Kawase,"1000-fiber *water blocking cable*', *Trans.* IEICE, Vol. E73, No. 9, 1990.
2) Y. Kikuchi, H. Sawano, Y. Sato, K. Kobayashi, k. Okamura, H. Suzuki and N. Sato,"Characteristics of one-thousand-fiber water proof cable", 39th IWCS 1990.
3) F. Ashiya, k. Hogari and K. Omoto,"A water-blocking optical fiber system for subscriber networks", NTT REVIEW Vol. 3, No. 1,1991.
4) N. Okada, A. Mogi, N. Misono, T. Hayakawa, M. Miyazaki, M. Kurokawa and K. Niijima, " A SZ slot ribbon fiber cable for subscriber network", 38th IWCS 1989
5) N. Okada, A. Mogi, I. Okada, N. Misono and H. Suzuki,"Characteristics of loose tube type optical fiber cable", Spring national convention record, IEICE, 1989.
6) T. Hayano, H. Sawano, Y. Kikuchi, n. Misono, H. Suzuki and N. Sato,"Characteristics of self-supporting optical fiber cable", Autumn national convention record, IEICE, 1989.
7) H. Ishii, N. Misono, Y. Sugawara, T. Hayakawa, S. Suzuki and K. Fujii,"SZ-cabled metal-free optical cable for long span aerial application", 37th IWCS, 1988.
8) S. Tomita, H. Shinohara and M. Kawase,"Suppression of galloping osillation due to

wind for a self-supporting cable", Trans. IEICE, Vol. J70-C, No.7, 1987.
9) Y. Mitsunaga, Y. Katsuyama and Y. Ishida,"Reliability assuarance for long-length optical fiber based on proof testing", Electronics Letters, Vol. 17, 1981.
10) Y. Sugawara and H. Shinohara,"Design of a self-supporting optical fiber cable", Trans. IECE Vol. J65-B, No. 1, 1982.
11) H. Shinohara, S. Tomita and M. Kawase,"Design of self-supporting optical fiber cable with SZ twisting structure", Trans. IEICE, Vol. J70-C, No. 6, 1987.



HIROYUKI SAWANO

Opto-Electronics
Laboratory
Fujikura LTD.

1440 Mutsuzaki,
Sakura-shi, Chiba-ken,
285, Japan

Mr. SAWANO was born in 1955. He joined Fujikura LTD. after his graduation from Hokkaido University with a M.S. Degree in 1983 and he has been engaged in research and development of the optical cables. He is now an engineer of Telecommunication Cable Section and a member of IEICE of Japan.

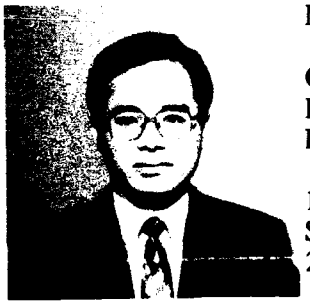


SUSUMU SAITO

Opto-Electronics
Laboratory
Fujikura LTD.

1440 Mutsuzaki,
Sakura-shi, Chiba-ken,
285, Japan

Mr. SAITO was born in 1964. He joined Fujikura LTD. after his graduation from Sophia University with a B.S. Degree in 1987 and he has been engaged in research and development of the optical fibers and cables. He is now an engineer of Telecommunication Cable Section.



MATSUHIRO MIYAMOTO

Opto-Electronics
Laboratory
Fujikura LTD.

1440 Mutsuzaki,
Sakura-shi, Chiba-ken,
285, Japan

Mr. MIYAMOTO was born in 1953. He joined Fujikura LTD. after his graduation from the Tokyo Institute of Technology University with a M.S. Degree in 1978 and he has been engaged in research and development of the optical cables. He is now a Section Chief of Telecommunication Cable Section and a member of IEICE of Japan.

Optical Fiber Ribbon Containing High Strength Splices for Long Span Submarine Cable

H. Ishikawa , I. Fujita , Y. Kitayama , K. Osaka , S. Tanaka

Sumitomo Electric Industries, Ltd.
1, Taya-cho, Sakae-ku, Yokohama, 244, Japan

Abstract

The applicability of the high strength splice and restoration coating technique to optical-fiber ribbon was examined. The optical-fiber ribbon containing spliced fibers could be used in the submarine cables with the slotted rod spacer and ribbon type structure, in order to obtain the continuous long length cable by splicing the shorter fibers. The high strength splice and restoration coating technique has already been accomplished and used in practical submarine cables. However, the applicability of this technique to fiber ribbon manufacturing has not been studied.

We manufactured 4-fiber ribbons with spliced fibers (250μmϕ coated fibers) and examined their reliability and properties in the slotted rod spacer type cable. The test results showed sufficient performance for practical use.

1. Introduction

Recently, the demands for optical telecommunication service are becoming greater and getting various. In the field of fiber-optic submarine cables for the domestic trunk networks, a high-count, high- density cable is becoming increasingly required for large capacity transmission.

In 1989, Yoshizawa et al. (NTT Japan) proposed a one-hundred-fiber submarine cable with a slotted rod spacer and fiber-ribbon type structure for the first time in the world [1]. This type of submarine cable would be used for non-repeated system used in shallow sea. The slotted rod spacer and fiber-ribbon type structure is used commonly for terrestrial cables in Japan. From the aspects of manufacturing and handling, it is the most suitable structure for high-count,high-density fiber-optic cables.

This study has aimed to develop the manufacturing technique of fiber ribbon which would be used in this type of submarine cable.

On the other hand, in the field of the fiber-optic submarine cables, high strength splicing with restoration coating is commonly used [2,3] . This is because the optical submarine cables require high strength fibers and continuous long cable length. Thus the fibers for submarine cables must be exposed to a high level screening test and the survived fibers shorter than the full span length of cable should be spliced together in order to obtain the required length.

In the case of the new structure submarine cables, 4-fiber ribbons are required. Thus the spliced fibers should be arranged closely side by side with other fibers to be made into a ribbon. Hence there is a possibility of loss increase caused by the influence of neighboring fibers. This is because the restoration coating diameter should be slightly larger than that of original fiber coating layer. Moreover, the spliced portions in the ribbons should experience cabling process and finally be stuffed into a slot tightly. This might cause the degradation of transmission properties.

From these reasons, we focused on the examination of the influences of ribbon and cable manufacturing process on splice loss properties.

In this paper, the high strength splicing and restoration coating technique will be described. After that, we refer to the examination and manufacturing test performed on the spliced fibers.

Throughout the experiments, the spliced fibers showed sufficient performance for practical use and we confirmed the applicability of our high strength splice and restoration coating technique to the submarine cables.

2. High strength splicing

2.1 Splicing properties

The degradation of fiber tensile strength in spliced portion is caused by the mechanical damages on the glass fiber surface. Thus for the high strength splicing, it is essentially important to protect the fiber surface from the mechanical damages. In order to protect the fiber surface the thin film coating method has been developed and used in our study [4,5]. This technique is to cover the bare fiber portion in order to avoid the damages. The thin film coating is made with UV curable resin and the thickness of the film is about 5μm.

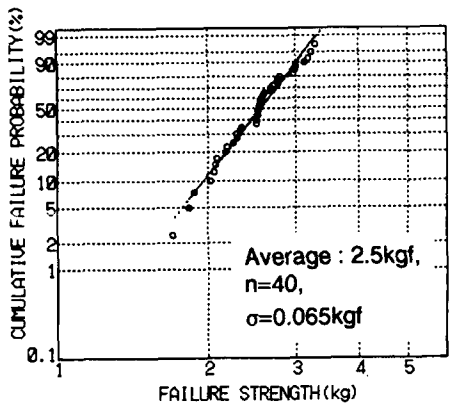


Fig. 1 Tensile strength distribution of high strength splice

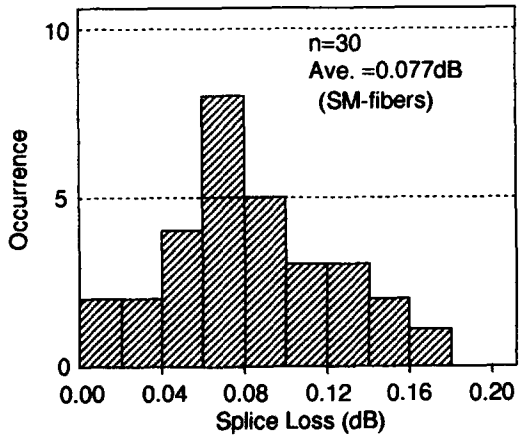


Fig. 2 Splice loss distribution of high strength splice

Fig. 1 shows the tensile strength distribution of high strength splices. The average tensile strength was 2.5kgf. Fig. 2 shows the splice loss distribution. The average splice loss was 0.077 dB/splice in our experiments. These splicing tests were carried out on Ge-doped silica core single-mode fibers of which the mode field diameters at the wavelength of 1.3μm were 9.4μm in average.

2.2 Restoration coating

Every spliced portion was restored with UV curable resin up to almost the same diameter as the original fiber coating layer. Fig. 3 demonstrates the schematic structure of the restored spliced portion. The length and diameter of restoration coating were about 24mm and 265μmϕ, respectively.

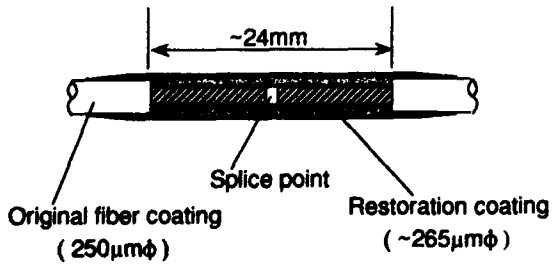


Fig. 3 Restoration coating structure

The reliability and mechanical properties of the restored spliced portions were examined and reported in references [4], [5] . The spliced fibers showed sufficient performances on the tests.

3. 4-fiber ribbon with spliced fibers

3.1 Ribbon structure

Fig. 4 shows the cross section of the 4-fiber ribbon with 250μmϕ UV curable resin coated fibers manufactured in our experiments and the perspective view of the spliced portion in the ribbon. It has the same structure as that of the 4-fiber ribbon which are used in the terrestrial fiber-optic cables. The thickness and width of the ribbon were 0.4mm and 1.1mm, respectively.

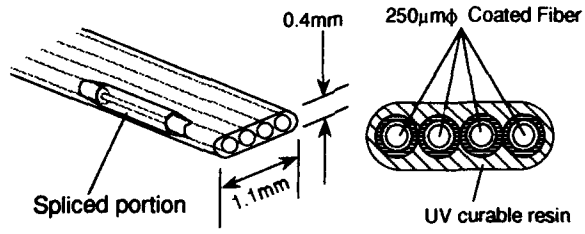


Fig. 4 Ribbon structure

3.2 Properties of ribbon with spliced fibers

First, the ribbon manufacturing test was carried out to confirm the basic properties of spliced fibers in the ribbon. The Ge-doped silica core single-mode fibbers were used. The fiber parameters were as follows ; the mode field diameter at λ=1.3μm was 9.4μm ; the effective cut-off wavelength was 1.25μm ; fiber diameter was 125μm ; coating layer diameter was 250μm. The fiber coating was composed with UV curable resin and it had the double layered structure.

Fig. 5 describes the composition of the experimentally manufactured ribbon. The #1 and #3 fibers of the ribbon were divided into eight parts and each of them contained ten serial splices. Thus these fibers contained eighty splices in all. For the #2 and #4 fibers, non-spliced fibers were used.

Table 1 shows the splice loss and transmission loss change in the spliced and non-spliced fibers due to ribboning process. The splice losses were measured with OTDR at the wavelength of 1.55μm. In the OTDR traces of #1 and #3 fibers, eight steps appeared corresponding to the ten serial splices and derived the average splice losses of ten serial splices from the

height of the steps. The measurements were made from both direction. The transmission loss measurements of non-spliced fibers were also done with OTDR.

As shown by table 1, the difference of splice losses between before and after the ribboning was only 0.01dB/splice in average. Taking into account the accuracy of the measurement it can be concluded that the ribboning process causes no splice loss changes.

The transmission loss changes in non-spliced fibers were 0.07 and 0.04 dB/km in #2 and #4 fibers, respectively. Assuming that these transmission loss changes were caused by the neighboring fibers' spliced portions, the influence of one splice was less than 0.002dB. Considering the practical use of spliced fibers in submarine cables, the spliced portions would be contained at the interval of about longer than ten kilometers. Thus it can be concluded that the influences of spliced portions on neighboring fibers are negligibly small.

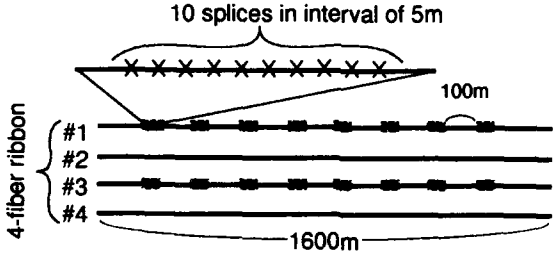


Fig. 5 Manufactured ribbon composition

Table 1 Splice loss and transmission loss changes due to ribboning process
(measured with OTDR at the wavelength of 1.55μm)

	Fiber #	Before ribboning	After ribboning	unit
Spliced fibers	#1	0.097	0.087	dB/splice
	#3	0.066	0.076	
non-spliced fibers*	#2	0.193	0.271	dB/km
	#4	0.195	0.240	

* : #2 and #4 fibers are neighbored by 160 and 80 splices in total 1600m, respectively.

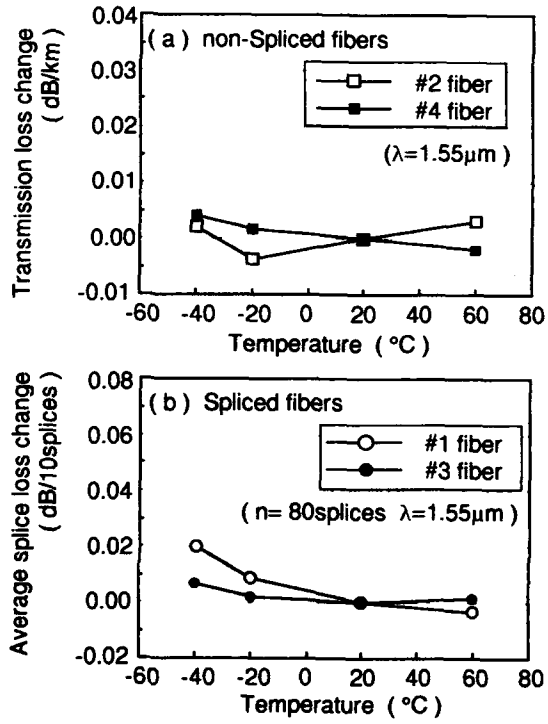
3.3 Reliability tests on fiber-ribbon with spliced fibers

Basic reliability tests were performed on the ribbon manufactured as described above. The samples for each test were prepared by dividing the ribbon, shown in Fig. 5, into eight parts including ten splices in each #1 and #3 fibers.

3.3.1 Temperature dependence of transmission properties

The temperature dependencies of transmission loss and splice loss were measured on both non-spliced and spliced fibers. The loss changes were monitored continuously at the wavelength of 1.55μm. The loss changes in non-spliced fibers were fairly small as indicated by Fig.6 (a). Thus the observed loss changes in the spliced fibers can be regarded as the splice loss changes due to temperature alternation.

Fig. 6 (b) shows the temperature dependence of splice losses in #1 and #3 fibers. The maximum splice loss changes observed at -40°C were only 0.02dB/10splices in #1 fiber. Considering the under sea condition in which environmental temperature is approximately 0°C, the test result means that the ribbon with spliced fibers had sufficient property for practical use.



Figs. 6 Temperature dependence of transmission loss and splice loss of 4-fiber ribbon with spliced fibers

3.3.2 Long-term thermal cycling test

A long-term thermal cycling test was also performed on the ribbon. The thermal cycles were conducted between -40°C and 80°C and the holding time were 2 hours for each temperature step. The ribbon was exposed to the thermal cycling for 40 cycles (approximately 12 days).

Fig. 7 shows the test result. The upper half shows the #1 and lower half shows the #3 fiber. The ordinate was indicated by the splice loss change per ten splices because of the same reason as described above.

There were splice loss changes due to temperature changes approximately equivalent to the previously described test result. However, any degradation of splice loss caused by the long-term thermal cycling were not observed in both #1 and #3 fibers. Thus it was confirmed that the manufactured ribbon with spliced fibers had enough reliability against the thermal cycling.

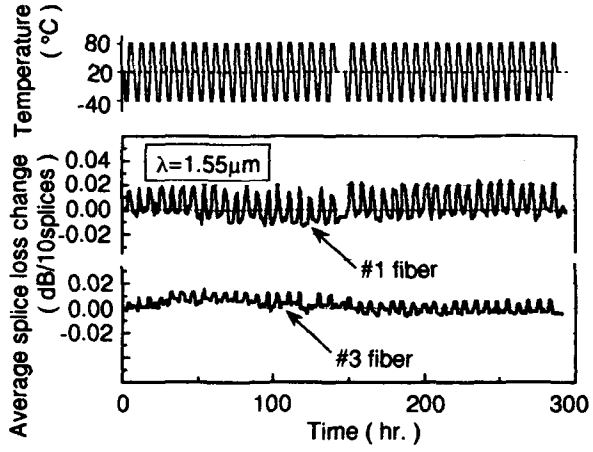


Fig. 7 Long- term thermal cycling test result on 4-fiber ribbon with spliced fibers

4. Cable manufacturing

Succeeding to the preliminary tests on the ribbon with spliced fibers, cable manufacturing were carried out. In order to examine the applicability of the ribbon with spliced fibers to slotted rod spacer type cable, the terrestrial cable structure and test conditions were applied.

4.1 Cable structure

Fig. 8 shows the cross section of manufactured cable schematically. It had the same structure as the one-hundred-fiber terrestrial cable. The cable outer diameter was 15mmϕ and the length was about 1km. Five 4-fiber ribbons were inserted into one of the slots tightly. The ribbons had the same structure as described in section 3.1.

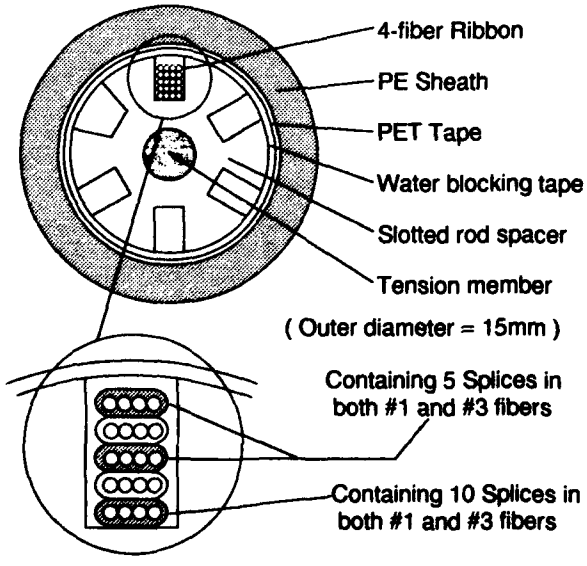


Fig. 8 Manufactured cable structure

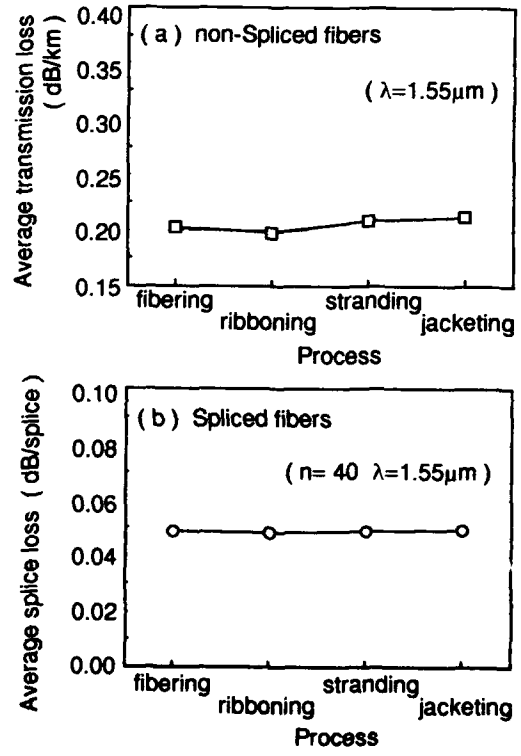
As indicated in Fig. 8, the first and the third ribbons contained five serial splices in #1 and #3 fibers severally. The bottom ribbon contained ten splices in each of #1 and #3 fibers. The second and the fourth ribbon were composed of non-spliced fibers. Forty splices were contained in the manufactured cable in total.

4.2 Transmission loss changes during cabling process

During the cabling process, the splice losses at the wavelength of 1.55μm were measured with OTDR by the same method as described in section 3.2.

Figs. 9 (a) and (b) show the transmission loss changes of non-spliced fibers which are neighboring the spliced fibers and the average splice loss changes due to cabling process, respectively. The average splice loss before ribboning was 0.049dB/splice and the splice loss changes during the cabling process were about 0.002dB/splice. Moreover, the maximum transmission loss changes in non-spliced fibers were as small as 0.015dB/km. This transmission loss change was comparable to the case of terrestrial cable manufacturing.

From these test results, it can be concluded that the cabling process causes no significant degradation of splice loss properties in the ribbon. Furthermore, the non-spliced fibers neighboring the spliced portions are not affected by the restoration coatings.



Figs. 9 Transmission loss and splice loss changes due to cabling process

4.3 Properties of cable with spliced fibers

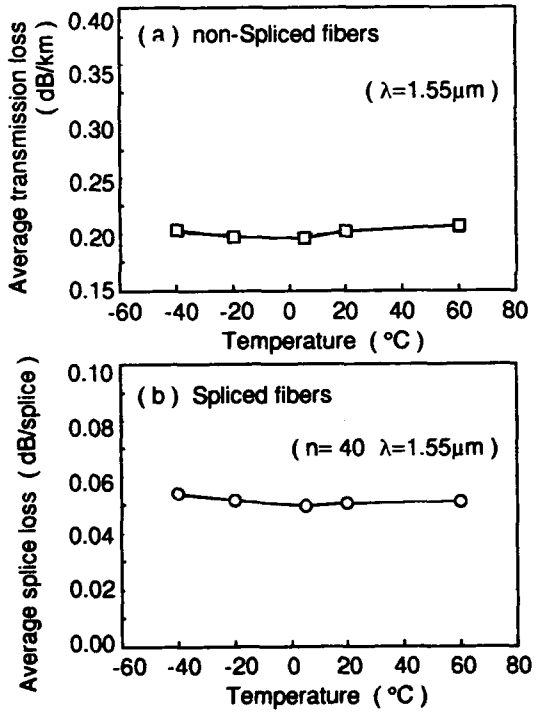
4.3.1 Temperature dependence of transmission properties

Figs. 10 (a) and (b) show the temperature dependence of transmission loss of the non-spliced fibers neighboring spliced fibers and splice loss, respectively. The measurements were carried out with OTDR by the same method as described in section 3.2 at the wavelength of 1.55μm.

The average splice loss at 20°C was 0.051dB/splice. The maximum splice loss change observed at -40 °C was only 0.015dB/splice. This result was comparable to that of the same examination performed on the spliced fibers before ribboning.

The maximum transmission loss change in non-spliced fibers due to temperature alternation between -40°C and 60°C were less than 0.015dB/km.

Therefore, it was confirmed that the cable manufacturing process had no influence on temperature dependence of splice loss.



Figs. 10 Temperature dependence of transmission loss and splice loss of manufactured cable

4.3.2 Installation simulation test

In order to simulate an installation, a pulling and squeezing test was performed on the manufactured cable. Fig. 11 shows the test system schematically. The system and test condition were chosen to equally to those of the terrestrial cable provisionally.

The 150m long sample cable, in which 2 splices were contained , was stretched between two poles. The cable tension was monitored by a tension meter at the one end of the tested cable. A movable truck with three curved guides moved from one end of the test cable to the other end squeezing the cable. As shown in the figure, the optical fiber cable was subjected to three bends. The bending radius of the cable was 250mm. During the squeezing, the test cable was loaded with a tension of 2,000N. This tension caused approximately 0.2% elongation on the cable.

The transmission loss changes were monitored at the wavelength of 1.55μm.

During the squeezing, there were no observable transmission loss changes for both spliced and non-spliced fibers. After the squeezing, no loss increase remained.

Throughout this test, it was confirmed that the performance of the manufactured cable during installation simulation was equal to that of the cables using non-spliced fibers.

5. Conclusion

The applicability of high strength arc fusion splice and restoration coating technique to fiber-ribbon manufacturing wa examined. The manufactured 4-fiber ribbon with spliced fibers showed no splice loss changes caused by ribboning process and its performances on reliability tests were sufficient for practical use in slotted rod spacer and ribbon type cable.

The cable manufacturing test with the ribbon containing spliced fibers was also conducted. The transmission loss properties of both spliced and non-spliced fibers were not affected by the existence of spliced portions during cabling process. The manufactured cable was shown to meet the severe environmental condition including wide temperature range from -40°C to 60°C. The installation simulation test result was also sufficient for practical use.

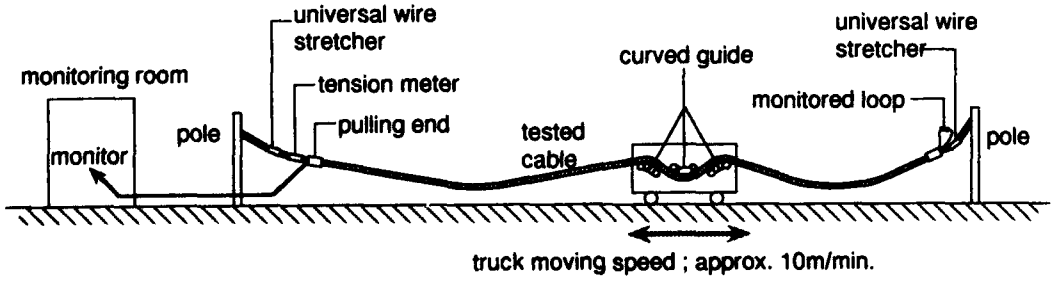


Fig. 11 Installation simulation system

Throughout this study, it was confirmed that the high strength splice and restoration coating technique will promise the stable production of slotted rod core type submarine cables.

reference

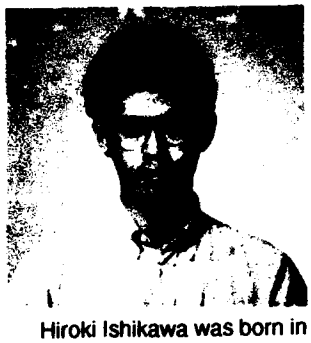
[1] N. Yoshizawa, Y. Miyajima, and Y. Katsuyama, "A One-hundred-fiber submarine cable composed of hermetically coated fiber ribbons inserted into slots", Proc. of the 38th IWCS, p. 603, (1989)

[2] Y. Miyajima, et al., "Long-length fiber containing high strength splices", Electron Lett., vol. 17, No. 18, p. 670, (1981)

[3] T. Kakii, et al., "New reinforcement method of fusion spliced fiber for long length cable manufacturing", OFC '82, paper THAA4, (1982)

[4] K. Osaka, T. Yanagi, Y. Asano, "Development of a field-usable, high-strength splicing technique for 1.55μm dispersion shifted fibers", Proc. of 37th IWCS, p. 546, (1988)

[5] T. Kakii, Y. Suetsugu, S. Tanaka, "High strength splice with restoration coat of optical fiber for cabling", Proc. of 34th IWCS, p. 275, (1985)



Hiroki Ishikawa

Sumitomo Electric
Industries, Ltd.
1, Taya-cho, Sakae-ku,
Yokohama, Japan

Hiroki Ishikawa was born in 1965 and received his M.E. degree in applied physics from Tohoku University in 1990.

He joined Sumitomo Electric Industries, Ltd. in 1990 and he has been engaged in the research and development of fiber-optic cables. Mr. Ishikawa is a member of Communication R&D Dept. in Yokohama Research Labs.



Isamu Fujita

Sumitomo Electric
Industries, Ltd.
1, Taya-cho, Sakae-ku,
Yokohama, Japan

Isamu Fujita was born in 1965 and received his M.E. degree in mechanical engineering from Tokyo University in 1990.

He joined Sumitomo Electric Industries, Ltd. in 1990 and he has been engaged in the research and development of fusion splicing technologies for optical fibers. He is a member of Optomechatronics Systems R&D Dept. in Yokohama Research Labs. and a member of Japan Society of Mechanical Engineers



Yoshinobu Kitayama

Sumitomo Electric
Industries, Ltd.
1, Taya-cho, Sakae-ku,
Yokohama, Japan

Yoshinobu Kitayama was born in 1957 and received his M.E. degree in Electrical Engineering from Kyoto University in 1982.

He joined Sumitomo Electric Industries, Ltd. in 1982 and he has been engaged in the design and characterization of optical fibers and fiber-optic cables. Mr. Kitayama is a senior engineer of Communication R&D Dept. in Yokohama Research Labs. and a member of the institute of Electronics, Information and Communication Engineers of Japan.



Keiji Osaka

Sumitomo Electric
Industries, Ltd.
1, Taya-cho, Sakae-ku,
Yokohama, Japan

Keiji Osaka was born in 1955 and received his M.E. degree in precision mechanical engineering from Kyoto University in 1981.

He joined Sumitomo Electric Industries, Ltd. in 1981 and he has been engaged in research and development of high NA optical fiber fabrication and fusion splicing technologies for optical fibers. He is a senior engineer of Optomechatoronics Systems R&D Dept. in Yokohama Research Labs. and a member of the institute of Electronics, Information and Communication Engineers of Japan.

Shigeru Tanaka

Sumitomo Electric
Industries, Ltd.
1, Taya-cho, Sakae-ku,
Yokohama, Japan

Shigeru Tanaka was born in 1951 and received the M.E. degree and Ph. D degree from Tokyo University in 1976 and 1989, respectively.

He joined Sumitomo Electric Industries, Ltd. in 1976 and he has been engaged in the design and characterization of optical fibers and fiber-optic cables. Dr. Tanaka is a chief researcher of the Communication R&D Dept. and a member of the institute of Electronics, Information and Communication Engineers of Japan.

Newly developed, small diameter optical link cord using compound glass fiber

Tatsuhiko Machida Masahiko Saegusa Norio Sugiyama

SHOWA ELECTRIC WIRE & CABLE CO.,LTD

Abstruct

lewly developed optical link cord is featured by ıin compound glass optical fiber with an adhesive, ıin, hard primary corting. Connecterizing can be ıde over the primary coat without exposing side ırface of glass fiber. Tough resins are selected ı order to reduce the coating diameter down to .5mm. The cord consist of two such thin optical ibers , twisted, reinforced with aramide yarn and ›vered with PVC sheath. The cross section of which ıs been reduced to 42% of that of conventional one. ıe cord is also characterized by high workability ıd reliability in connecterizing while keeping ›tical and mechanical characteristics equivalent › those of conventional ones.

Introduction

)emand for optical fibers are increasing lately ›r links of short to intermediate distance. It is ıid essential for those links , reflecting the reater use of optical cords in the field, to have ıinner cords with high connectibility because of he high amount of connections to be made per ystem. Newly coating design of compound glass iber, fertured by thin, hard and adhesive primary ›ating to the fiber, is developed. The use of ıich enables drastic reduction of cord diameter, ıly 65% of thatof conventional cord design, ithout affecting adversely to optical and echanical characteristics. Another unique ıaracteristics of the new coating design, which enables connecterizing over primary coat, has introduced a newly developed, crimping type connecter, thus, contributing to high mechanical reliability and simplification of connecterizing.

Fiber & cord design

The conventional compound glass fiber has core and cladding diameters of 200 and 250 μm respectively, and covered with silicone and polyamid coatings. the setting of a crimping type connecter to such an optical fiber requires removing of all coatings of glass fiber and fixing of connecter firmly on the exposed glass fiber. The method involves an inherent problem as to reliability because the crimping is made directly on the glass. New coating design of optical fiber was developed using ultra-violet curing resign both in order to reduce the coating diameter and to improve the performances of connecterizing. Tough resins are selected both for primary and secondary coatinga so as to reach a small coating diameter down to 0.5mm. On the other hand in order to reduce the connecterizing over primary coat, the resin for sufficient adhension to glass fiber, high processibility and stability all of them with as thin a thickness as 15 μm.The constructional comparision Fig 1,2 and Table 1.

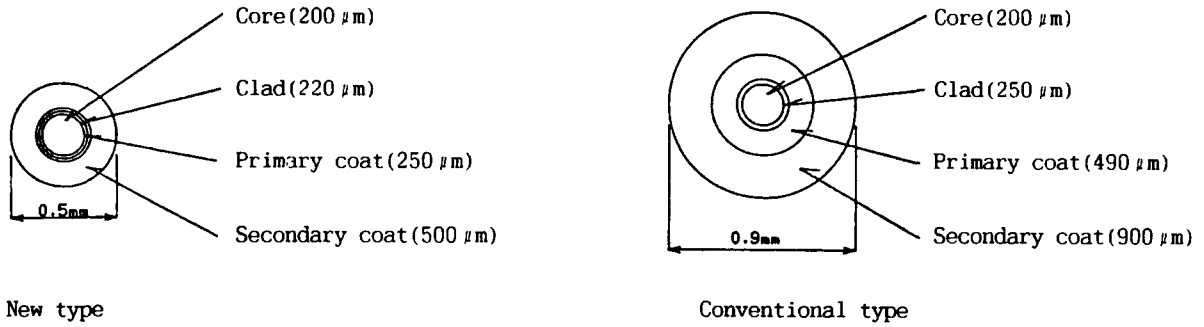


Fig.1 Optical Fiber

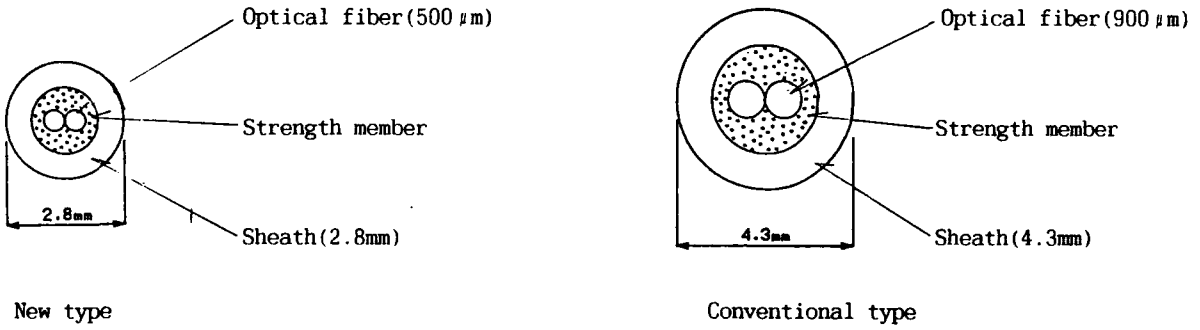


Fig.2 Optical Fiber Cord

Table.1 CONSTRUCTION OF CORD

Item		New type	Conventional type
Core	Material	Compound glass	Compound glass
	Diameter	200 μm	200 μm
Cladding	Material	Compound glass	Compound glass
	Diameter	220 μm	250 μm
Primary coat	Material	Epoxy acrilate	Silicone
	Diameter	250 μm	490 μm
Secondary coat	Material	Urethane acrilate	Polyamid
	Diameter	0.5 mm	0.9 mm
Number of fibers		2	2
Strength Member		Aramide yarn	Aramide yarn
Sheath		PVC	PVC
Diameter		2.8 mm	4.3 mm
Numerical Aperture		0.5	0.5

Optical characteristics

Attenuation spectral of thin compound glass fiber is shown in Fig 3. (It is measured by 0.4 launching NA) The relationship between attenuation and distance is shown in Fig 4.

Also, it is important to grasp the relationship between bandwidth and distance for the design of high spped communication system arising in FA,OA fields. Dispersion of multi mode optical fiber depend almost on mode dispersion. An empirical formura of the relationship between bandwidth and distance can be obtained from Fig.5 . The formura shown below indicates the fiber has little mode conversion because the exponential coefficient is nearly 1.

$$f(L)_{\text{at } 0.85\mu m} = 14.0 \cdot L^{-0.93}$$

This compound glass fiber has an excellent temperature characteristics because not only both of core and clad consists of compound glass, but also the primary coating has low linear expansion coefficient. The temperature characteristics of attenuation of optical fiber cord is shown in Fig 6.

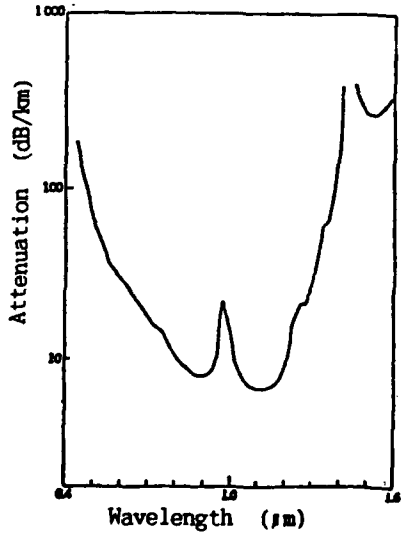


Fig 3. Attenuation Spectral

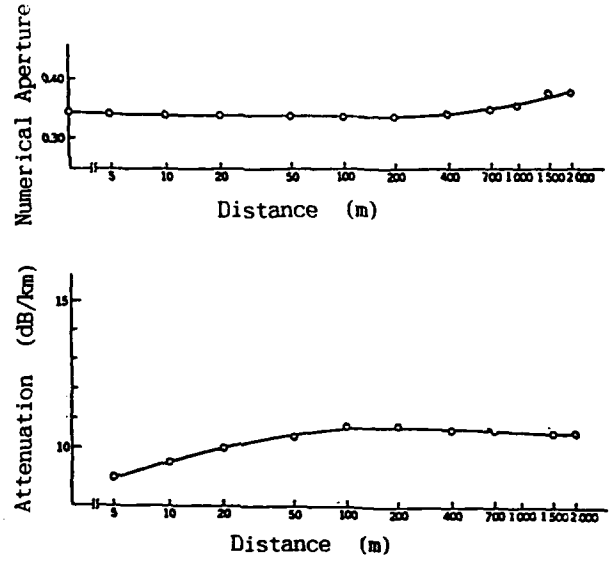


Fig 4. Relationship between attenuation, NA and distance

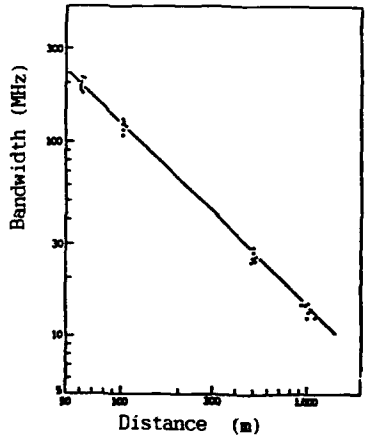


Fig 5. Relationship between bandwidth and distance

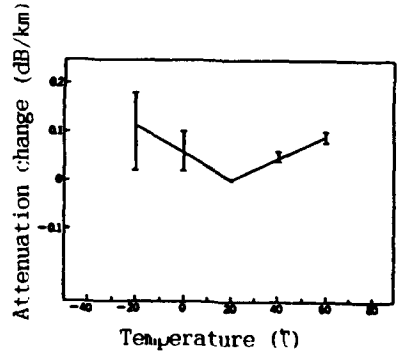
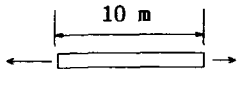
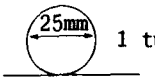
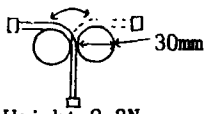
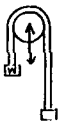
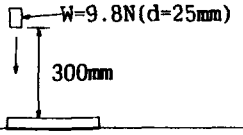
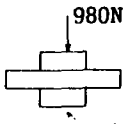


Fig 6. Temperature characteristics

Mechanical characteristics

Mechanical characteristics of optical fiber cord are shown in table 2.

Table 2. Mechanical characteristics of optical fiber cord

Item	Test condition	Test result
Tensile Performance	 Tension: 490 N	No fiber breakage
Bending	 1 turn	No fiber breakage
Repeat bending	 Weight:9.8N Bending times:100000	No fiber breakage
Squeezing	 Squeezing times:100000	No fiber breakage
Torsion	 Torsion times :500000	No fiber breakage
Impact		No fiber breakage
Crush	 Flate plate 50mm width	No fiber breakage

Conclusions

New coating design of compound glass fiber, featured by thin, hard and adhesive primary coating to the fiber, is developed. The use of which enables drastic reduction of of cord diameter, resulting in 42% of reduction rate compared with conventional cord design , without affecting adversely to optical and mechanical characteristics of cord. The use of the fiber of new coating design creates a new connecting system. Because connections are possible without adhesive primary coating, the crimping and elastic keeping type connectors become easy to make with the use of the fiber of new coating design, and the mechanical reliability of connecting section improves at the same time .



Tatsuhiko machida graduated from CHIBA INSTITUTE OF TECHNOLOGY in 1988. Then he joined SHOWA ELECTRIC WIRE & CABLE CO.,LTD. and has been engaged in development of optical fiber cable. He is now an Engineering of Optical Fiber Cable Sec., Optics & Communications Engineering Dept. at SHOWA ELECTRIC WIRE & CABLE CO.,LTD.



Norio Sugiyama graduated from KEIO UNIVERSITY in 1963. Then he joined SHOWA ELECTRIC WIRE & CABLE CO.,LTD. He is now a General Manager Optics & Communications Engineering Dept.
Information Communication Div
Mr.Sugiyama is a member of IEICE of Japan.



Masahiko Saegusa graduated from YOHAMA UNIVERSITY in 1976. Then he joined SHOWA ELECTRIC WIRE & CABLE CO.,LTD. and has been engaged in development of optical fiber cable. He is now an Manager, Optical Fiber Cable Sec. Optics & Communications Engineering Dept at SHOWA ELECTRIC WIRE & CABLE CO.,LTD.
Mr.Saegusa is a member of IEICE of Japan.

Extendable Optical Fibre Curled-Cord

Heinz W. Brückner, Georg Franken, Daljit S. Parmar

Kroschu-Kabelwerke, Kromberg & Schubert GmbH u. Co
Wiegenkamp 21, 4292 Rhede, Germany

Abstract

An extendable optical fibre curled-cord, as state of art in the copper technology, is developed to transmit optical signals from transportable systems. To avoid certain problems arising due to small curled-cord diameters, e.g. irreversible attenuation increase, a special optical cord design was selected. This design enabled us to reduce the curl diameter down to 20 mm with an insertion loss less than 2 dB.

Introduction

An extendable optical fibre curled-cord was developed to provide flexible connection, transmitting optical signals from portable and transportable equipment, e.g. patch panels, Robotarms or medicinal apparatus.
The manufactured curled-cord can be extended several times to its curled length and retracts back to its orginal length after the load is removed. The cord is assembled with special optical fibre connectors compatible to standard connectors. A special design of the cord enabled us to manufacture curled-cord with spiral diameter to 20 mm and an insertion loss of 0.5 dB to 1.5 dB with multimode gradient profile, 50/125 µm fibre.

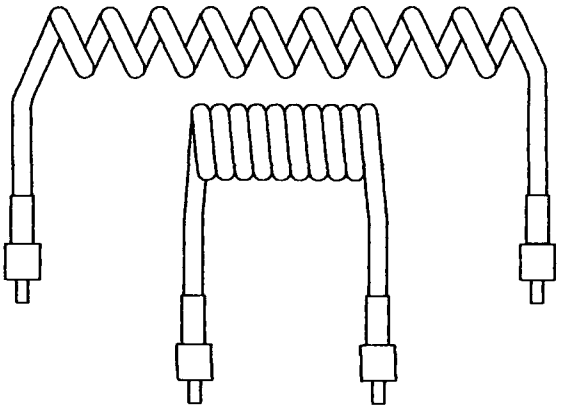


Figure 1: Connectorized extendable optical fibre curled-cord

Theoretical Aspects

The propagation of light in a multimode fibre takes place due to the total internal reflection. Light rays injected into the core at an angle (acceptance angle) are totally reflected whenever they encounter the core/cladding boundary. All the light rays, whose angle of acceptance is lower than the critical angle of total reflection, would be reflected down the length of the fibre.
The angle of acceptance at the core/cladding boundary increases when the fibre is bent. This increase of angle

causes more number of rays (modes) not reflecting into the core but, in contrary, coupled into the cladding and hence loss of transmission.

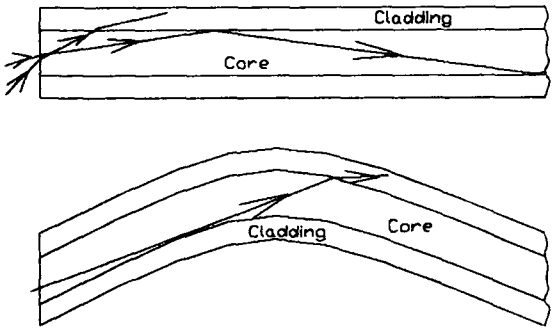


Figure 2: Propagation of light in a bent fibre

All the optical fibre cables are subjected to bends partly due to the installation of cable and partly the fibre undergoes microbends due to the excess length of the fibre in the loose tube (buckling of the fibre). This phenomena causes distribution of modes within the fibre after a transmission section of considerable length in such a way that only about 70% of the propagating modes, in reality, are propagated whereby the rest of the modes are coupled out into the cladding. This behaviour of propagation is termed as EMD -Equilibrium Mode Distribution. To avoid the influence of microbending to its lowest possible, a bend radius of at least 15 times the cable outer diameter has been fixed for standard optical fibre cables.

Besides EMD, another important effect is caused due to the high order modes. These modes propagate at an angle near to the critical angle and have to travel relatively longer path than the lower order modes. This results into higher attenuation and hence low order modes are preferred for transmission.

Because of mircobending and high attenuation in the outer region of the core, an optical fibre, after a certain length, so called couple length, has mode and intensity distribution around the central axis in the form of a Gaussian distribution.

If an optical fibre is wound several times in a narrow diameter (less than 8 times outer diameter), the high order modes would be coupled into the cladding. This would increase the fibre attenuation , specially with lower spiral diameter. At the same time the light intensity would also concentrate around the axis. The minimum multi bend radius for a fibre lies around 4 mm and that for a cable-cord of diameter 4 mm lies at 60 mm. To achieve an acceptable attenuation at a smaller spiral diameter (curl diameter) for an optical fibre curled-cord, a suitable curled-cord design has to be selected.

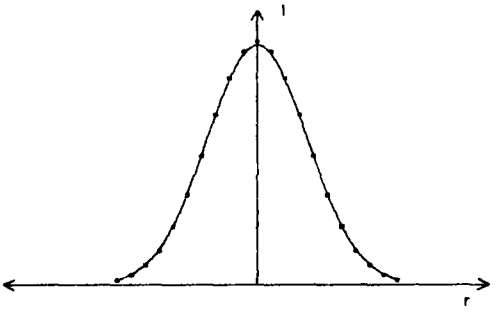


Figure 3: Mode distribution in a fibre

It should be taken into consideration that the influence of cord-design or

fibre jacketing do not total specify the minimum bend radius.

Cord-Design

The cord-design has been suited to the special requirements of the curled-cord, as described above.
To allow enough space for the fibre movement, a gel filled Nylon loose tube design of large diameter was selected. This enables the fibre not to undergo buckling in case the cord is bent to smaller diameter. This made us possible to curl the cord to lower winding diameters without experencing substancial losses through microbending.
The optical fibre curled-cord is so designed that the transmission-losses and attenuation-change remain within limits when the curled-cord is extended and retracted. The wall thickness of the tube at 0.8 mm is selected so that enough tensile strength and retractability of the cord is guaranteed.

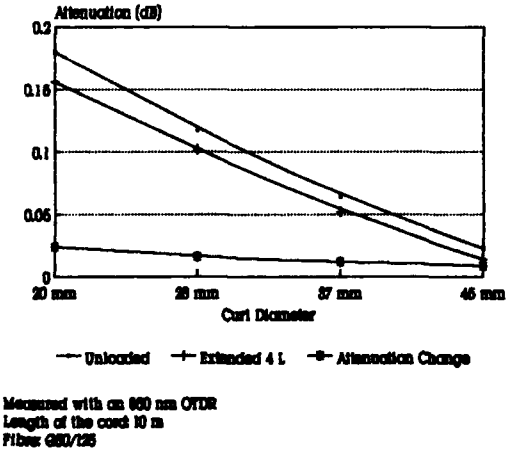


Figure 4: Attenuation change under load as a function of various curl diameter

The design allows the curled-cord to extend four times its original length without any substantial change to practically no change of attenuation. After the load is released, the cord retracts back to its original length. The attenuation change is below 0.1 dB for a 10 m cord.
The necessary load to extend the cord is presented in figure 5.
It can be seen that the load to extend the designed cord and the stretching force is higher than used by standard copper-curled-cords. This is a result of the material of construction used and the wall thickness of the Nylon-tube. It proved unsuitabel to use aramidyarn or any other material as tension-elements.

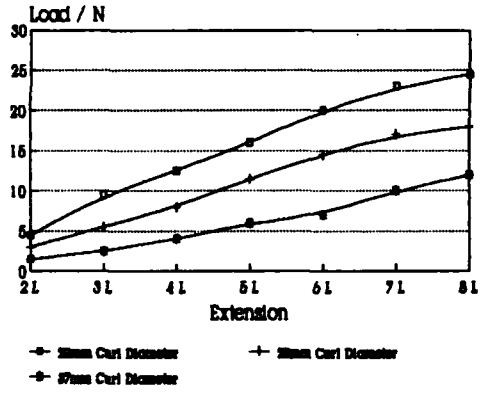


Figure 5: Extension force of curled cord

Curled-cord Assembly

For easy handling, the curled-cord has to be assembled with connectors. We decided for the most used connectors of the type F-SMA and BFOC/2.5. To assemble this

connector, a suitable fitting is required. The standard way of crimping the connector with the tension elements in the cord is not possible in this case. The connector, instead, is adhered to the elements and then crimped to the jacket. Various investigations and test results showed that this combination had enough tensile strength. This tensile strength is greater than the load needed for irreversible deformation of the curled-cord.

The insertion loss of the curled-cord assembly was measured during various launching conditions.

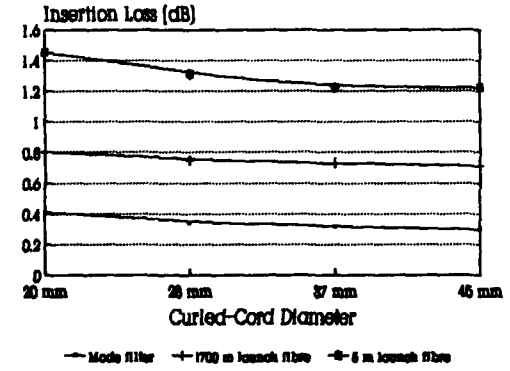


Figure 6: Insertion loss

The measured values, as shown in Fig. 5, are highly dependant on the launching conditions. These results confirm the theory that launching with low order modes alone (EMD) causes practically no attenuation change due to microbending. Only high order modes react to the microbending. The measurements also show that the total launching (UMD), i.e. coupling directly with LED or via a short cablelength, brings the insertion loss to about 2 dB. For the optical transmission over short lengths, this value is low enough. If the curled-cord is used to couple on a longer section, the insertion loss of 2 dB appears to be very high. Since in this case the concentration of modes occurs on the low order modes, the coupling in the section would be suitable and right in the beginning of the section an equilibrium mode distribution would take place. The total attenuation of such a system would not be higher than in case of direct coupling.

Conclusions

A compact and space saving robust optical fibre curled-cord assembled with special connectors has been designed and manufactured successfully using single mode as well as multimode fibres. The advantages of conventional copper curled-cords have been transferred to the fibre technology. Using a unique design of the cord, it was possible to achieve mechanically flexible and easy handling connections. Application in the field of transmitting optical signals from portable and transportable equipment, e.g. patch panels, Robotarms, medicinal equipment etc. are possible.

Acknowledgements

The authors wish their sincere appreciation to Mr. H. Dillge, Mr. K.H. Kremers and Mr. W. Schwarz for constructive assistance in designing, manufacturing and testing of the cord.



Heinz W.Brückner is head of the Product R&D Department of the Kroschu Kabelwerke. He studied Electrical Engineering at the Ruhr University of Bochum, Germany and received his Dipl.-Ing. Degree in the year 1977. He is specialized in the field of Opto-Electronics and cable systems for the automotive applications. Since 1986, he is member of the senior executive staff of the Kromberg & Schubert GmbH u. Co group.



Georg Franken studied Electrical Engineering at the Ruhr University of Bochum, Germany and received his Dipl.-Ing. degree in the year 1989. He joined the R&D Department of Kroschu Kabelwerke in 1988 to work on his Dissertation. After successfully completing the project, he joined the Kroschu Kabelwerke as a Development Engineer where he is engaged in the development of fibre optics and fibre optic applications.



Daljit S. Parmar is head of Production of the Kroschu Kabelwerke. He received his B.Tech. in Chemical Engineering from the University of Madras, India in 1968 and M.Sc. in Process Engineering from the University of Bradford, UK in 1970. He holds a Ph.D. in Engineering Managment from the Kennedy-Western University, California State Education. He has specialized in the field of Cable Technology and has more than 20 years experience in the process development and production of a wide variety of wire and cables. since 1986, he is member of the senior executive staff of the Kromberg & Schubert GmbH u. Co group.

FAILURE RATE AS THE TRUE PARAMETER OF OPTICAL FIBRE RELIABILITY

J G Titchmarsh

BNR Europe, Harlow, UK

Summary

For the user concerned about reliability against fibre fracture, the parameter of interest is not strength but failure rate. Using the standard fracture mechanics and Weibull statistical description of flaw growth it is shown that failure rate may increase, stay constant, or even decrease during exposure to constant tensile stress. Proof tested fibre is shown normally to be used under conditions which give a constant failure rate, so that its reliability, or 'perceived strength', is as high at the end of its life as at the start.

Introduction

The Nature of Fibre Strength

Experience has shown the reliability against fibre fracture of installed optical systems to be high, but from the nature of the failure mechanism there is a natural perception that the passage of time and the application of any tensile load must always make a fibre less reliable. It is the purpose of this paper to show that this is not normally the situation.

The analysis does not introduce any new model of fibre failure. It uses the fracture mechanics power law model of crack growth and the Weibull probability description of strength[1,2], which are the common currency of reliability calculations for installed fibre systems, but it extends this analysis to give a fresh perspective on practical problems.

Fibre stretches elastically under tension, but fails suddenly and catastrophically when the stress is sufficient to cause rapid bond rupture. Although this bond strength is constant, flaws in the structure, usually due to surface damage or contamination, cause local stress intensification. This stress intensification is dependent on flaw size, so that the applied stress which will cause immediate failure is variable, depending on the distribution of flaw sizes. Unless the fibre has a perfect hermetic coating there is a further complication. Even if an applied tensile stress is insufficient to cause immediate failure, in the presence of moisture it causes the flaws to grow, an effect known as static fatigue. All the time the flaws are under tension they are weakening and given long enough will eventually fail.

Flaw Weakening and Lifetime

If the stress required to cause immediate failure is σ_i, then the fracture mechanics analysis[1,2] shows that a lower service stress, σ_s, will cause failure after time, t_s, according to the following relationship:

$$\sigma_s^n t_s = B\sigma_i^{n-2} \qquad (1)$$

where n and B are the standard fatigue parameters. σ_i is usually referred to as the inert strength, because it is the strength which would be measured under moisture free, or inert, conditions.

In this equation t_s is clearly the lifetime of the flaw under the service stress σ_s.

If the flaw is subjected to a succession of different stresses then analysis[3] shows that failure will occur when

$$\sigma_1^n t_1 + \sigma_2^n t_2 + \ldots + \sigma_j^n t_j = B\sigma_i^{n-2} \qquad (2)$$

The term $\sigma^n t$ is thus seen to give a measure of crack weakening and $B\sigma_i^{n-2}$ the total amount of crack weakening to which a flaw may be subjected after which it will then fail.

Proof Testing and Service Conditions

Because we cannot measure the location and size of the particular flaws in a given fibre, we have to make use of our knowledge of statistical information gained from sample strength testing and the parameters of the proof test routinely applied to production fibre.

The simplest analysis is to use the fact that the proof test removes all flaws above a certain size. Reliability calculations offering a guarantee of survival may then be performed. These are based on equations 1 and 2, and arrange that the service conditions of stress, humidity and temperature just allow this largest possible flaw to survive to the end of the required lifetime.

Because of uncertainties in the fatigue parameter B and the fact that finite proof test unloading rates seriously reduce the minimum strength[3], it is usually impossible to offer a such a guarantee of survival. It would require either too low a service stress or a proof test giving too low a length yield. However, by only asking for a high, say 99%, survival probability, rather than 100%, satisfactory solutions can be found. The proof test not only provides a minimum strength, but generally depletes the population of flaws in a range well above the minimum strength. With some additional knowledge, such as proof test length yield[4], the probability of finding a flaw of any given size may be calculated. If the service survival probability required is 99%, then the size of flaw corresponding to a probability of occurrence of 1% is calculated, and the service conditions arranged just to allow this flaw to survive.

Strength, Reliability and Time

In the case of the guarantee based on the largest flaw surviving proof testing, there is a very clear meaning to strength and reliability in terms of the calculated lifetime. Below this time there is no chance of failure, while once it is exceeded this guarantee can no longer hold. As service proceeds this maximum sized flaw is getting weaker and the time for which the stress can be applied, without chance of failure, is getting correspondingly shorter. Additional stresses, before or during service, have the effect of further reducing the lifetime.

Making the change to a low, rather than a zero probability of failure, does not otherwise alter the calculations. Conditions are arranged so that a starting flaw size, corresponding to the selected probability of occurrence, is arranged just to fail at the end of the service period. The same concepts and behaviour of lifetime, strength and reliability would appear to follow.

Now consider these questions. If a cable supplier normally provides a warranty based on a calculated fibre failure probability of 1% over 25 years, how would this change if the cable was not a new one but had already been in service for 10 years? If an installed cable is exposed to severe strains outside the warranty conditions and the fibre survives, how should the warranty terms be changed?

In terms of the preceding analysis of strength, reliability and lifetime it might seem obvious that the answers must reflect a decrease in reliability. Following through the conventional analysis discussed, the author found that normally the reliability was unchanged. In seeking to explain this result it was realised that the parameter being calculated, a failure probability over a given period, was a failure rate and that the underlying question related to the way this behaved as a function of time under stress. The most appropriate treatment was thus one which calculated failure rate directly, rather than strength or time to failure. This paper presents the results of such an analysis.

Calculation of Fibre Failure Rate

In calculating failure rate we start with the conventional basic description of the cumulative failure probability, Φ, in terms of the inert strength, σ_i, fitted to a two parameter Weibull distribution

$$1-\Phi(\sigma_i) = \exp -\left(\frac{\sigma_i}{\sigma_0}\right)^m \qquad (3)$$

where σ_0 = position parameter
m = slope parameter

This may now be combined with equation (1) to eliminate σ_i and give the corresponding distribution of times to failure under static strain.

$$1-\Phi(t_s) = \exp -\left(\frac{t_s}{t_0}\right)^{\frac{m}{n-2}} \qquad (4)$$

where

$$t_0 = B\frac{\sigma_0^{n-2}}{\sigma_s^n} \qquad (5)$$

This again is a standard result, of the original Weibull form, but with the exponent m changed to m/(n-2).

What we wish to calculate is the failure rate. This parameter is defined by the statement that the probability that a fibre which has survived to time t_s will

fail during the next small time interval δt_s, is the failure rate multiplied by δt_s. It has the dimensions of failure probability per unit time and is obviously related to $d\Phi/dt_s$.

Differentiating equation (4) with respect to time gives

$$\frac{d\Phi}{dt_s} = \frac{m}{n-2}\left(\frac{t_s}{t_0}\right)^{\frac{m}{n-2}-1}\frac{1}{t_0}\exp-\left(\frac{t_s}{t_0}\right)^{\frac{m}{n-2}} \quad (6)$$

At this point it is necessary to recall exactly what the failure probability Φ means. The particular fibre under consideration will either have failed or not. Φ is the fraction (or percentage) which would have failed if a large number of fibres, N, from the same strength distribution had been subjected to the same stress. $N.d\Phi/dt_s.\delta t_s$ is the number of failures occurring in this distribution between times t_s and $t_s+\delta t_s$. From the definition of failure rate, this is also given by the product of the number of fibres surviving to time t_s, failure rate and δt_s. The number of fibres surviving to time t_s is $N(1-\Phi)$ and thus

$$N(1-\Phi).\textit{Failure rate}.\delta t_s = N\frac{d\Phi}{dt_s}\delta t_s \quad (7)$$

Substituting for Φ and $d\Phi/dt_s$ and rearranging gives

$$\textit{Failure rate} = \frac{m}{n-2}\left(\frac{t_s}{t_0}\right)^{\frac{m}{n-2}-1}\frac{1}{t_0} \quad (8)$$

Examination of the equations (4) and (8) shows that although the cumulative failure probability Φ always increases with time, the failure rate may increase, decrease or even be constant with time, depending on whether the exponent $m/(n-2)-1$ is greater than, less than or equal to zero.

Discussion

General Form of Failure Rate in Actual Fibre

Weibull plots are generated from dynamic tensile tests, often on a gauge length of 20 metres. A plot is constructed in Fig.1. to show typical features of interest to this analysis. At high failure probabilities the Weibull plot shows a high m value, typically >30. This is labelled region I and corresponds to the high strength seen in very short fibre lengths. At low failure probabilities a much lower slope is seen, with an m value typically <10. This is region II and

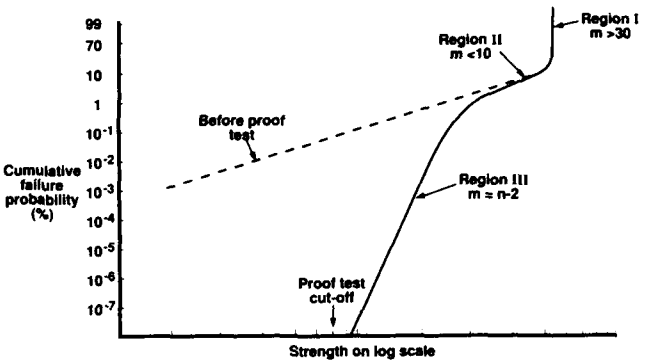


Fig. 1 Typical features of inert strength distribution

takes its character from the infrequently occurring larger flaws. Finally, the lower end of region II is modified by proof testing. This not only truncates the strength as discussed earlier but also modifies the Weibull slope above the truncation point to give region III. Flaws in this region are those which grew from a very narrow range of smaller initial sizes under the influence of the proof test. The Weibull slope, which is a measure of spread, approaches a value dependent only on the form of the growth law and turns out[3] to be n-2.

The value of n is normally measured in the range 15 to 30 and, for the purpose of performing reliability calculations, is taken to be single valued for any particular set of conditions. It is often taken to have the same value for proof test and service conditions [4]. This simplifying assumption has been followed here and a value of n=20 used.

Failure Rate Variation with Increasing Time

The failure rate is initially zero, because of the removal of flaws below the cut-off level of the proof test, but in this example is only at times below about a day and just off the scale.

The next failures are those corresponding to region III. Here m=n-2 and the exponent $m/(n-2)-1$ is exactly zero, denoting a constant failure rate.

At longer times the failures are those of region II where m<10, $m/(n-2)-1\leq 0$ and the failure rate decreases with time.

Finally region I failures occur where m>30 and the failure rate increases with time. These features are illustrated in Fig.2.

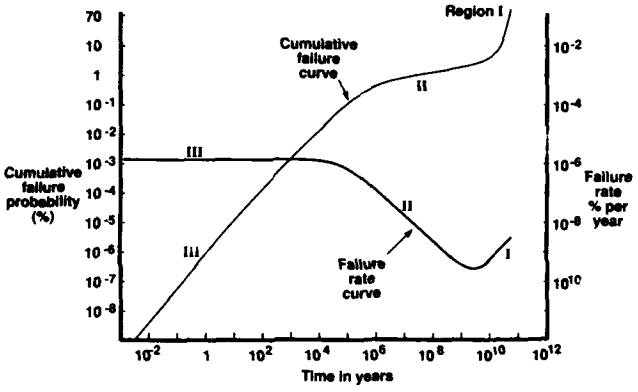


Fig. 2 Weibull distribution of failure times, t_s, and corresponding failure rate

Failure Rate variation with Fibre Length and Stress

Increasing the stress level applied to the fibre will decrease the times at which the transitions between the regions occur and increase the level of the failure rate. When fibre is in cable the stress is normally determined by the cable strain condition. The curves for three different strain levels, e_s, on the same fibre are shown in Fig.3.

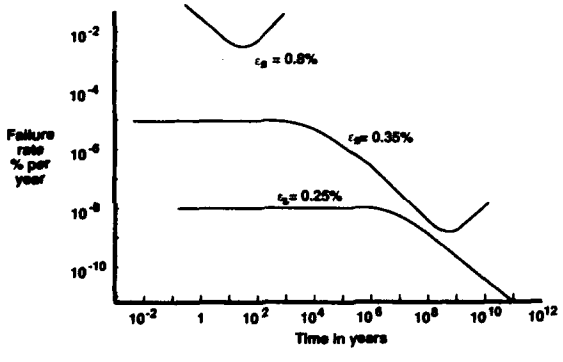


Fig. 3 Effect of strain level, ε_s, on failure rate

Increasing the length of fibre under stress in the system has the effect of shifting the original Weibull strength plot upwards vertically and gives a corresponding upward shift to the failure rate curve.

The particular points in time, at which the transitions from one region of failure rate to the next is made, are thus highly dependent on the parameters chosen or imposed for the system under consideration. One very general observation is worth making however.

In most cases involving more than a short total length at risk, say more than 1 km, the system designer sets an upper limit to the strain conditions by consideration of the proof test level of the fibre involved. In other words, they arrange for the fibre to operate over its design lifetime, typically 25 years, in the region where fibre strength is determined by the proof test, i.e. region III which gives constant failure probability.

Effect of Proof Test on Failure Rate

The effect of the proof test is now seen to be to depress the early failure level of region II. It is most easily thought of as doing it by removing some of the original larger flaws. Alternatively, bearing in mind that these curves represent a probable, not an actual, distribution, if no breaks occur the proof test improves the predicted strength by showing the larger flaws did not exist.

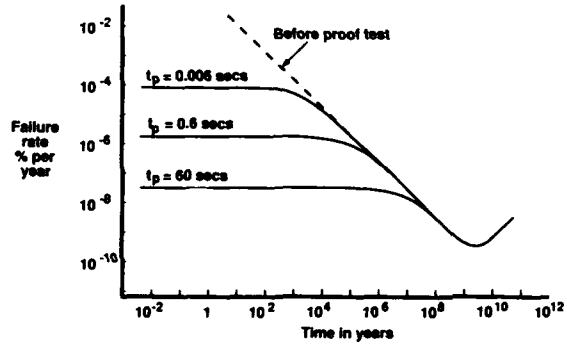


Fig. 4 Effect of proof test time, t_p, on failure rate

Fig.4 shows the effect of different proof test times. The failure rate for the non-proof tested fibre shows a decrease with

ne. The effect of the proof test may
is also be seen as giving an accelerated
ogress down this curve before the fibre
used. The amount of progress down the
rve may be increased by longer proof
st times, as in the example, or more
actically by higher proof test strain.

fect of Unbudgeted Strains

ere is rightly a concern to avoid
budgeted strains in manufacture,
stallation or service. It should now be
ear, however, that the effect of any
nsile strain, whether it be proof test,
rvice or unbudgeted, is simply to take
e fibre along the failure rate curve.
e rate of progress will depend on the
rain level, but the path followed will
the same. Provided that the strain has
t taken the fibre into the region of
creasing failure rate, there should be
concern that a fibre which has survived
unbudgeted strain is now unfit for
rvice. The reason for trying to avoid
budgeted strains should be to avoid
eakage during such strains, not a
rceived increased risk once the strain
is been removed.

lationship to Standard Reliability
alysis

ne concept of fibre reliability
ffectively increasing with time under
ress as shown by a decreasing failure
ate, can seem difficult to reconcile with
model of accelerating crack growth.
ost people are, however, familiar with
ne idea of `infant mortality', that
ystems may show early failures due to
aulty components but that these decrease
ith time. Viewing a fibre as a `system'
f cracks, a decreasing fibre failure rate
s just an example of infant mortality.
ystems may be given a `burn-in', an
nitial period of operation to allow such
ailures to occur before release for
ervice. The fibre proof test is seen to
e a form of accelerated `burn-in' to
educe service failure rates to an
ceptable level.

ne fibre proof test is most simply
derstood physically as strengthening the
ibre by removing the larger flaws[5], but
nis could be misleading. Whether breaks
o actually occur in any particular fibre
ill depend on the particular flaws
resent in that fibre, but simply knowing
hat the fibre has been subjected to a
roof test changes our prediction of its
trength. This is a generally true in the
hole analysis: the results do not depend
n changes being demonstrated by breaks
ut simply say how the prediction of
ailure varies with time and other
parameters. Indeed, failure rate itself is defined in terms of the probability of future failure for a particular fibre which has not yet had any break, and so the fact that this changes with time is clearly not conditional on breaks being demonstrated in that fibre.

The use of failure, or hazard, rate is a standard concept in the general field of reliability analysis. This is also the case for the sequence of `infant mortality', constant failure rate and `wearout' giving rise to the `bathtub' failure rate curve, and the use of the Weibull slope parameter to characterise these different regions[6]. However, there are two features of the analysis of fibre reliability in this paper which may be of interest to the wider community of reliability engineers. Firstly, the sequence of failure rate slopes is unusual in starting with constant failure rate and then going into decreasing failure rate, for which `infant mortality' is then an inappropriate name. Secondly, there is a natural temptation to think of the different regions of the `bathtub' curve as arising from different failure mechanisms. This may be true in any particular case, but the analysis in this paper shows that all three failure rate characteristics can arise from a single mechanism obeying the same decay characteristic. Whether it is increasing decreasing or constant failure rate simply depends on the distribution of the failure mechanism.

Limitations of This Analysis

This is a theoretical analysis, with the author being unaware of any useful evidence from field data. This is the familiar penalty of success in this field with engineers achieving a very low level of installed fibre failures.

The author has taken the view that introducing the new idea of failure rate is best done in terms of the common currency of reliability calculations which are still based on a velocity given by AK_I^n, where n is constant, and the Weibull distribution. Extension of this analysis to crack growth models based on an exponential dependence of crack velocity on stress intensity factor, or on an n value which is not constant, cannot be attempted here.

The feature of exactly constant failure rate is felt to arise from two conditions:

(i) a crack growth law which is strongly dependent on stress, so that service failures arise from such a narrow band of the original flaw distribution that they have an essentially constant density of flaw sizes

(ii) the assumption of a single growth law under all circumstances.

The degree to which departures from constant failure rate are seen or predicted by other models will then depend on the degree of departure from these conditions.

Conclusions

Using the standard assumptions and model of flaw size distribution based on Weibull statistics and a velocity $v = AK_I^n$, it follows that the failure rate of a fibre does not inevitably increase with time under tensile stress. The normal sequence for proof tested fibre is an initial period of constant failure rate extending at least over the design lifetime, followed by decreasing failure rate and only finally a period of increasing failure rate. Unbudgeted strains in manufacture, installation or service will only make the fibre less reliable if they accelerate this progress so that they take it into the region of increasing failure rate.

References

1. J E Ritter jr, `Engineering Design and Fatigue Failure of Brittle Materials', Fracture Mechanics of Ceramics, Bradt, Hasselman and Lange eds., vol.4, pp.667-686, Plenum Press, New York, 1978.

2. D Kalish, B K Tariyal and H C Chandan, `Effect of Moisture on the Strength of Optical Fibers', pp.331-341, 27th International Wire and Cable Symposium, November 14-16, 1978.

3. E R Fuller jr, S M Wiederhorn, J E Ritter jr and P B Oates, `Proof Testing of Ceramics: Part 2 Theory', J. Mat. Sci, vol.15, pp.2282-2295, 1980.

4. Y Mitsunaga, Y Katsuyama, H Kobayashi and Y Ishida, `Failure Prediction for Long Length Optical Fiber based on Proof Testing', J. Appl. Phys., vol.53, no.7, pp.4847-4853, July 1982.

5. J G Titchmarsh, `The Theory and Practice of Fibre Proof Testing', Proceedings of Fibre Optics '90, 24-26 April, 1990, SPIE Vol. 1314, pp134-143

6. N R Mann, R E Schafer and N D Singpurwalla, `Methods for Statistical Analysis of Reliability and Life Data', John Wiley and Sons, 1974, Chapter 4.



Jim Titchmarsh was born in Colchester, England, in 1942. He obtained a BSc in Physics from Bristol University in 1964. Obtaining an MSc in Solid State Electronics at Manchester University in 1966 he joined BNR Europe (then STL) to work on thin film deposition. After a period spent on plasma panel displays he has spent the rest of his career working on various aspects of optical fibres, concentrating recently on avionic cable and on fibre reliability.

Development of a Dual Layer Core Loose Tube Fiber Optic Cable and Its Tensile Window Analysis

Omid Daneshvar, Joseph Hill, Yasuhide Miyazaki

AT&T Fitel Company
201 Adamson Industrial Blvd.
Carrollton, Georgia 30117
(404) 834-6382

ABSTRACT

A fiber optic cable with 18 loose tubes stranded in two layers was developed for high fiber count applications in feeder and distribution areas. Environmental and mechanical testing was conducted in accordance with Bellcore's TR-TSY-000020 and appropriate Fiber Optic Test Procedures (FOTP) for this cable, and it met or exceeded all of the requirements. During tensile testing of the product, it was noticed that the outer layer core had much more tensile window than the inner layer. In order to investigate this discrepancy further, several cables were manufactured for tensile window analysis. Since the conventional formula was not adequate for predicting the tensile performance, a model was developed. The model was verified experimentally.

INTRODUCTION

As more optical subscriber systems are being deployed, higher fiber count optical fiber cables in a more compact design are desired. In addition, the accessibility to fibers at various points along the length of the cable is an important concern. Fiber counts as high as 216 are commonly installed for feeder applications, and many of these cables are installed in ducts where cable diameter becomes very critical. In order to meet these requirements, a dual layer core cable was designed, manufactured, and evaluated for environmental and mechanical characteristics. The cable had 18 buffer tubes stranded in two layers; 6 tubes stranded around a dielectric or steel central member in the first layer, and 12 tubes stranded around the inner layer in the second layer. To achieve a maximum fiber count of 216, 12 fibers were put in each tube. The dual layer design was chosen to make the cable compact. Also the Reverse Oscillating Lay (ROL) stranding method was chosen for ease of mid span accessibility of the fibers. During the initial evaluation, it was found out that in order to pass water penetration test consistently, the amount of gap between the inner layer tubes had to be increased, so flooding compound could penetrate inside the inner tubes and central member. Also some inconsistencies were noticed when lay length of the outer layer was measured. This variation was due to the inner layer core twisting during stranding of the outer layer tubes. To prevent the inner core from twisting, an anti-torsion device was designed and installed. During long length tensile testing, it was noticed that the outer layer has a much larger tensile window than the inner layer core. This had been observed previously when testing large diameter cables.

This paper explains the design of this dual layer cable, and proposes a model for calculating the tensile window of the outer layer core. The formula has been tested experimentally with cables having different lay lengths and central member diameters.

CABLE MANUFACTURE

The 216 fiber dual layer cable cross section is shown in Figure 1. The cable is composed of 6 tubes stranded in an ROL fashion around a dielectric or steel central member. Each tube is fully filled and contains 12 fibers. A binder thread is applied over the inner core to keep the tubes intact for further processing. An additional 12

buffer tubes are stranded around the inner tubes in an ROL method, and binder thread is again applied. The core is flooded during the jacketing process and one layer of aramid yarn is applied over the core before medium density polyethylene (MDPE) jacket is applied. The cable has the same diameter as a 144 fiber cable, a cable in which 12 buffer tubes are stranded in one layer around a central member.

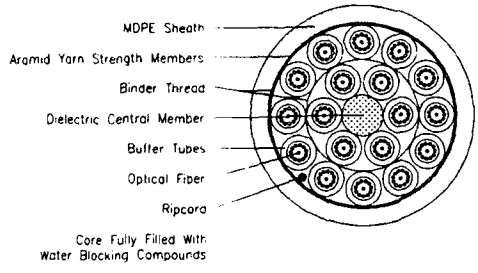


Figure 1: Dual Layer Loose Tube Cable

Cable Design Theory

The cable was designed to have a maximum of 216 fibers while at the same time, maintaining a small diameter. The maximum diameter of the cable was designed to be 19.0 mm. With this diameter, a cross sectional area of about 50 percent of the cross sectional area of the inner diameter of a 1 inch subduct could be achieved. This small diameter was achieved by having the tubes in two layers. The lay length of the inner layer was chosen so the bending strain of the fibers would not exceed 20 % of the proof stress level. In the case of fibers proof tested at 50 kpsi this equals to a maximum bending strain of 0.1%, as calculated by Equation 1 below.

$$\epsilon_b = \frac{\frac{1}{2} * FGD}{\frac{1}{2 * (COD+TOD)} * \left((COD+TOD)^2 + \frac{LL^2}{\pi^2}\right)} \quad (1)$$

where ϵ_b = Bending Strain
FGD = Glass Diameter, mm
COD = Central Member Diameter, mm
TOD = Tube Outer Diameter, mm
LL = Stranding Lay Length, mm

The outer layer lay length was also chosen by considering the same design parameters. A larger than usual central member was chosen for the dielectric version because of the extra torsional modulus needed for a two pass stranding operation. Also, due to concerns about water penetration for dual layer core, the inner layer core gap size was designed to be larger than that of a standard cable for a better penetration of the flooding compound inside the core and central member. Tensile strength of the cable was increased by adding a layer of aramid yarn over the core. The amount of yarn was chosen to allow installation load of up to 2700 N, as shown in Equation 2.

$$\epsilon_c = \frac{P}{\Sigma EA} \quad (2)$$

where ϵ_c = Cable Strain
P = Load, kg
E = Young's Modulus, kg
A = Cross sectional area, mm^2

Manufacturing

There were some processing issues when manufacturing this cable design. The inner layer core was the same as a standard cable core with the exception of the larger core gap, so standard processing conditions could be utilized. For the outer layer, however, there were additional concerns. One concern was the high frictional forces on the outer tubes when they are stranded over the inner layer. This can cause significant problems in keeping the lay length accurate and consistent. In order to overcome this potential problem, we determined that it was imperative to have a strander with a very quick reversal speed when stranding the outer layer of this cable design. In addition, an anti-torsional device was developed and installed, which held the inner core intact when the outer layer of tubes were being stranded. Using this apparatus, we were able to achieve both consistent and accurate lay lengths. The lay length of the binder thread was also reduced to keep the tube positions intact.

RESULTS

The cable was tested to Bellcore and REA standards for both mechanical and environmental performance. The cables were tested in accordance with applicable EIA and Bellcore standard test methods.

Impact, crush, twist, and flex testing was performed. Because of the initial concerns, water penetration testing was also performed several

times. In each case, the cable exceeded industry standards for performance. We found that the maximum water penetration at any location of the cable was less than 10 percent of the allowable penetration. In addition, drip testing was performed at both 65 and 80 degrees Celsius. Because of the large number of tubes in this cable designs, there are many more chances for failure of this test. In actual testing, we found no problems. Table 1 summarizes the requirements and the actual performance of the cable tested.

Tensile Testing

For testing, we used mechanical methods for measuring the cable strain, and time-of-flight technique for measuring fiber strain. We measured the cable, and found that there was a difference in actual and theoretical fiber strain between the inner and outer layers although both layers were designed to give the same fiber strain. A graph of the results is shown in Figure 2.

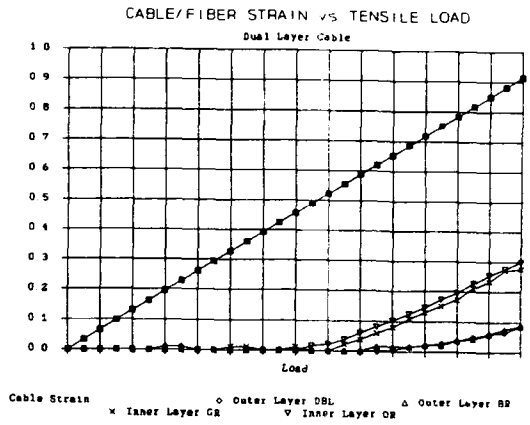


Figure 2:Cable/Fiber Stress-Strain Curve

In order to investigate the cause of this discrepancy, 4 cables were manufactured with different lay length to central member ratio. Also since this discrepancy had been noticed for large cables before which usually have 12 fibers per tube, a tube with 6 fibers and a tube with 12 fibers were put in the 4 trial cables to investigate the effect of number of fibers per tube to the actual tensile window. In order to keep the same fiber to tube ratio for all the cables, two long buffer tubes, one with 6 fibers and the other one with 12 fibers, were manufactured and cut in four different pieces and used in the cables.

Test	Requirement	Actual	Method
Impact	25 impacts, 4 kg, 0.20 dB	50 impacts, 8 kg, 0.06 dB	EIA-455-25A
Compression	220 N/cm, 10 min, 0.10 dB	220 N/cm, 0.01 dB	EIA-455-41
Twist	10 twists, 0.10 dB	100 twists, 0.03 dB	EIA-455-85
Flex	25 cycles, 0.10 dB	1000 cycles, 0.07 dB	EIA-455-104
Temperature Bend	-30/60 C, 0.20 dB	-40/70 C, 0.03 dB	EIA-455-37
Cable Freeze	0.10 dB	0.00 dB	EIA-455-98A
Compound Flow	65 and 80 C, 24 hrs	No Drip	EIA-455-82A
Water Penetration	1 m, 1 hours	10 cm max	EIA-455-81
Temperature Cycling	-40/65 C, 0.20 dB/km max, 80 % < 0.10 dB/km	-40/70 C, 97 % < 0.10 dB/km, 100 % < 0.20	EIA-455-3A
Cable Aging	85 C/120 hours, 0.40 dB/km max, 80 % < 0.20 dB/km	85 C/120 hours, -40/70 C, 100 % < 0.20 dB/km	EIA-455-3A

Table 1

The following cables were manufactured:

Cable 1: 6 position cable, LL/CM = 25.7
Cable 2: 8 position cable, LL/CM = 18.3
Cable 3: 10 position cable, LL/CM = 14.8
Cable 4: 12 position cable, LL/CM = 12.6

According to the theoretical calculation using the conventional helix formula shown in Equation 3, a 0.2% difference in the tensile window between the 6 and 12 fibers per tube (F/T) should be obtained.

$$\varepsilon_t = \frac{\pi^2 * W}{LL^2} * (TOD + COD - \frac{W}{2}) \quad (3)$$

where ϵ_t = Tensile Window
TOD = Tube Outer Diameter, mm
LL = Stranded Lay Length, mm
COD = Central Member Diameter, mm
W = Free Space (Tube ID - Fiber Bundle Diameter)

When fiber to tube ratio measurements performed, it was noticed that fibers in the 6 F/T tube were about 0.1% shorter than the fibers in the 12 F/T tube. This would change the difference in the tensile window to 0.1%. Two hundred meters of each cable was used to perform the long length tensile testing. Fiber strain for two fibers from each tube, and cable strain were monitored during the test. Figures 3, 4, 5 and 6 show the results of the tests.

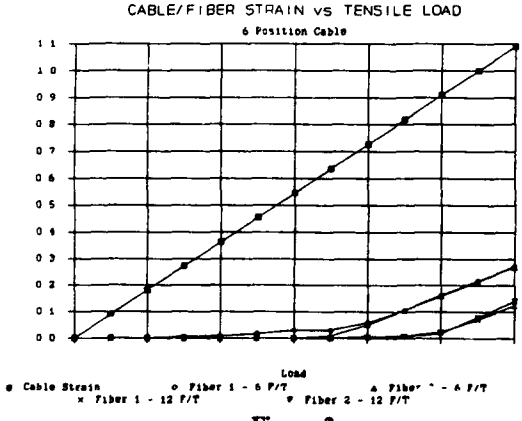


Figure 3

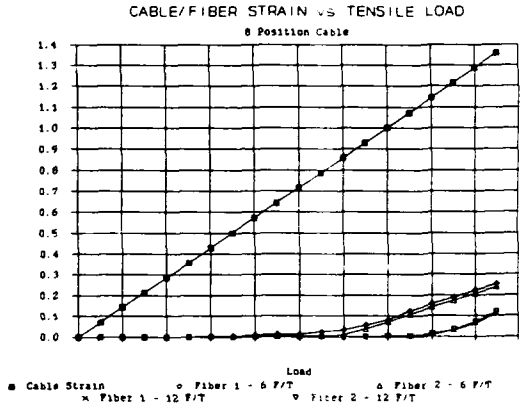


Figure 4

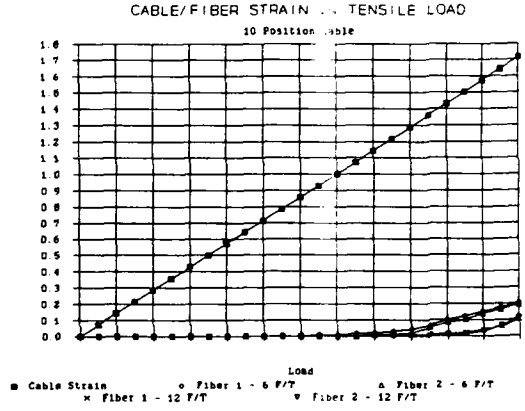


Figure 5

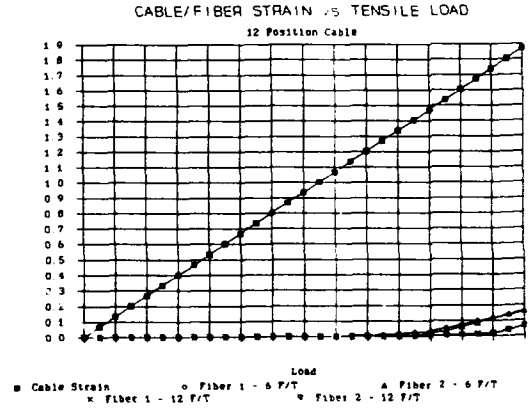


Figure 6

As expected, the lower the ratio of lay length to the central member diameter, the higher the discrepancy between the theoretical and measured tensile window. The measured tensile window difference between the fibers in two different tubes were exactly the same as the theoretical difference, so it was concluded that number of fibers per tube did not contribute to the discrepancy. A curve was generated correlating the difference between the actual and calculated window to the ratio of lay length to central member, shown in Figure 7. In addition, other cables which were not used in generating this curve were tested. Their data points were plotted to verify the accuracy of this model. The graph demonstrates that the curve was a good estimate for predicting the actual tensile window of those cables.

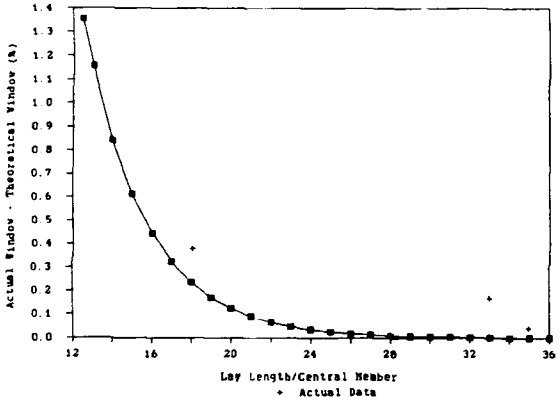


Figure 7: Correlation Between Lay Length to Central Member Ratio and Tensile Window

CONCLUSION

A loose tube compact cable with fiber counts of up to 216 was successfully developed. This has been achieved by an understanding of the factors resulting in the variation in the lay length of the second layer, and the tensile window of that layer. This work has given insight to the tensile window characteristics of large loose tube cables. For these cables, the actual tensile window was larger than the calculated value using the conventional helix formula, and was related to the tube lay lengths and size of the central member which tubes were stranded around. A model showing this relationship was presented, and verified. Although further work is required to establish in detail the exact reason for this relationship and how this relationship can be used to accurately predict the window characteristics of the cables, this model can be used as an estimate for the actual tensile performance of loose tube cables.

Acknowledgements

The authors would like to acknowledge Mr. Todd Pepple and Mr. Kevin Priest for their valuable assistance in manufacturing and testing the cables.



Omid Daneshvar is Research and Development Manager at the AT&T Fitel Company. He holds B. S. and M. S. degrees in Electrical Engineering from Georgia Institute of Technology. He joined AT&T Fitel in 1985 and has since had responsibilities in the development of fiber optic cables and measurement systems. Mr. Daneshvar is a member of the Optical Society of America.



Joseph A. Hill is Product Development Engineer at the AT&T Fitel Company. He received a B. S. in Ceramic Engineering from Clemson University in 1989. Since joining AT&T Fitel in 1990, he has held responsibilities for material and product development of fiber optic cables. Mr. Hill is a member of the American Ceramic Society (ACrS) and the National Institute of Ceramic Engineers (NICE).



Yasuhide Miyazaki is Product Engineering Supervisor at the AT&T Fitel Company. He received a B. S. degree in Mechanical Engineering from Kyusyu University in Fukuoka, Japan in 1984. Since joining the Furukawa Electric Company in 1984, he has had responsibilities for product and process engineering of fiber optic cables at both Furukawa Electric Company and AT&T Fitel Company.

DEGRADATION STUDY FOR STRESSED OPTICAL FIBRES IN WATER. NEW WORST CASE LIFE TIME ESTIMATION MODEL.

Peter Hasløv Knud Bundgaard Jensen Niels H. Skovgaard

NKT Elektronik A/S
NKT Alle 85, 2605 Broendby, Denmark

ABSTRACT

Simultaneously determined results from zero stress ageing and static fatigue measurements in water at 65, 80, and 95°C have been combined into a worst case fibre lifetime model which shows good agreement between predicted and observed failure times. The model shows that the lifetime in a wet environment of the largest crack at normal service strain (0.1%) is nearly identical to the lifetime of the pristine fibre and that the initial strength and the stress corrosion exponent are of minor importance for the lifetime.

Furthermore, it is shown that degradation in a water saturated jelly-filled cable is significantly slower than when fibres are directly immersed in water.

1. INTRODUCTION.

The traditional lifetime estimates for optical fibres in cables are based on the classical model of stress enhanced corrosion describing the growth of cracks under the influence of stress [1], [2]. For typical loose buffered optical fibre cables the predicted lifetimes of the fibres are enormous. However, for buried cables without a metallic moisture barrier, the inherent assumption of a constant environment is not fulfilled. The cables are saturated with water (100 % R.H.) after a short time, typically a few years. Several authors have found characteristic transitions in static fatigue experiments for fibres in water leading to shorter lifetime than predicted from the classical model [3], [4]. In [5], [6] and [7] the transition is explained by a combination of the conventional stress corrosion theory with an ageing of fibres in water under zero stress.

The aim of the present work is to further investigate the practical aspects of a lifetime model combining the two ageing mechanisms.

2. ZERO STRESS AGEING EXPERIMENT.

The fibres were aged in loose 20 cm coils in glass vessels filled with deionized water buffered to a pH value of 7. The strength σ_f of the fibres was measured at ambient conditions 24 hours after leaving the water in an Alwetron Tensile Tester with a strain rate of 10 %/min. For our standard dual UV-acrylate coated fibre the strength as a function of storage time at temperatures 65 °C, 80 °C and 95 °C is shown on fig. 1.

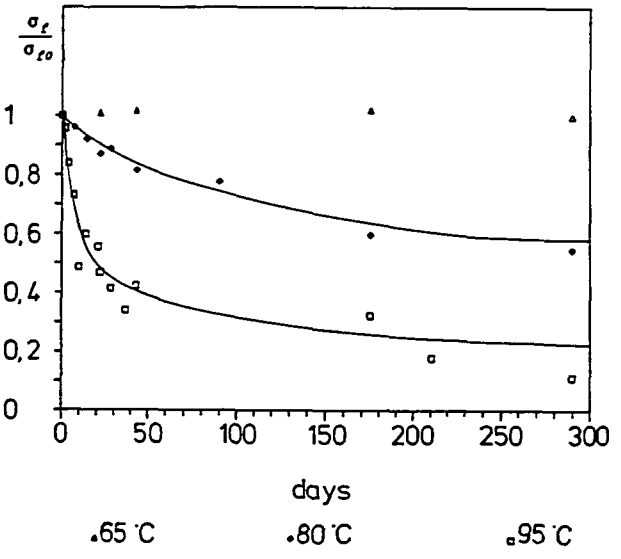


Fig.1 Medium strength of fibres as a function of storage time in water.

To the measured points are fitted

$$\sigma_f = \frac{\sigma_{f0}}{(1+\frac{t}{\tau})^p} \qquad (1)$$

with fitting parameters p = 0.33 and τ equal to 3 days and 60 days for 95 °C and 80 °C respectively. At 65°C, no degradation of strength has yet been observed. σ_{f0} is the measured strength at the time t = 0.

3. STATIC FATIGUE MEASUREMENTS.

The fibres were wound on glass mandrels and stored in the same glass vessels used for zero stress ageing. For each mandrel size the median time to failure is shown on fig. 2 as a function of the strain. The curves show a steep slope and correspondingly short lifetime at high strains in agreement with an n-value close to 20. This observation of a "knee" has been made by several authors [3], [4], [5], [6] and [7]. The arrows indicate that no failure has been observed yet.

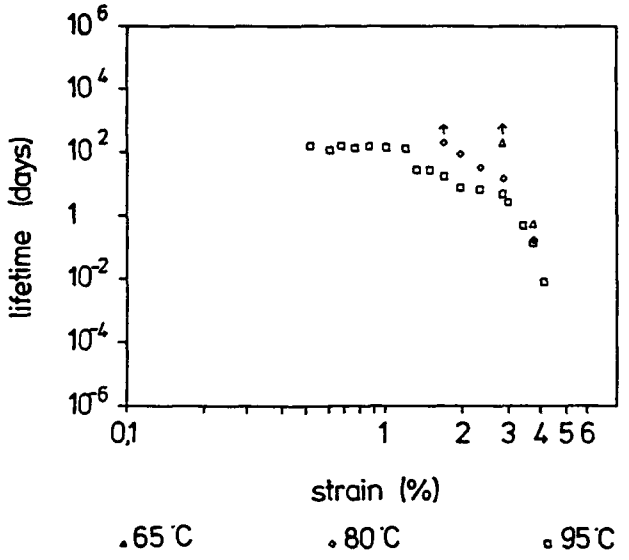


Fig.2 Medium time to failure as a function of strain for fibres wound on mandrels stored in water.

4. A COMBINED MODEL FOR THE STATIC FATIGUE OF PRISTINE FIBRES IN WATER.

A model will be set up which takes into account simultaneous degradation by zero stress ageing and stress corrosion. First stress corrosion alone is considered.

4.1 Stress corrosion

The classical model of stress corrosion [1], [2] gives a rate of strength degradation

$$\frac{d\sigma}{dt} = -\frac{1}{B} * \frac{1}{n-2} * \sigma_s^{\,n} * \sigma^{3-n} \qquad (2)$$

where
σ is the strength at the time t
σ_s is the static stress
n is the stress corrosion exponent
B is a constant containing material and process parameters.

(2) is straight forward solved

$$\sigma_i^{\,n-2} - \sigma^{n-2} = \frac{1}{B} * \sigma_s^{\,n} * t \qquad (3)$$

where σ_i is the initial strength of the fibre.

The lifetime t_s at the static load σ_s is found from (3) by substituting $\sigma = \sigma_s$.

$$t_s = \frac{B}{\sigma_s^{\,n}} * (\sigma_i^{\,n-2} - \sigma_s^{\,n-2}) \qquad (4)$$

In most static fatigue experiments where the right term in the bracket is much smaller than the left term (4) is reduced to

$$t_s = B * \frac{\sigma_i^{\,n-2}}{\sigma_s^{\,n}} \qquad (5)$$

In a log t_s vs. log σ_s graph this is a straight line with a slope of -n, that crosses a vertical line through σ_s = 1 GPa in log $B*\sigma_i^{n-2}$ (fig. 3).

This is the generally accepted empirical relationship for static fatigue of optical fibres in an ambient environment. The lifetime of pristine fibres can be predicted without a specific knowledge of the initial strength in the actual environment, only $B*\sigma_i^{n-2}$ is needed. This parameter is determined from the experimental line.

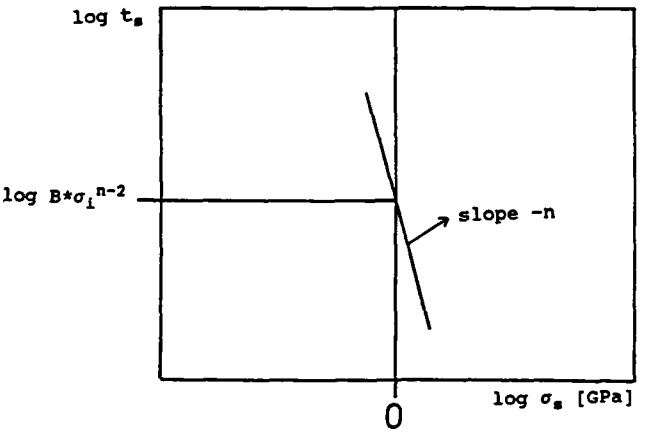


Fig.3 Static fatigue graph. t_s is the lifetime of the fibre at the static load σ_s.

4.2 A combined model for the static fatigue of fibres in water

The simultaneous effect of zero stress ageing and stress corrosion on strength degradation is expressed by

$$\frac{d\sigma}{dt} = \left(\frac{d\sigma}{dt}\right)_{zerostress} - \frac{1}{B} * \frac{1}{n-2} * \sigma_s^{\,n} * \sigma^{3-n} \qquad (6)$$

One inherent assumption is that stress corrosion always takes place at rates corresponding to high n-values and is the dominant mechanism at high stress levels compared to the fibre strength. This is justified by [8] which shows that fibres with big flaws undergo stress corrosion with n-values close to 20. [9] demonstrates that bare fibres pre-aged in water show static fatigue at high stress levels corresponding to even higher n-values.

The rate of zero stress degradation for the actual fibre is given by the fit (1). σ_f and σ_{f0} have been measured by dynamic strength measurements, and they are related to the spontaneous strengths σ and σ_{i0} by the classical relations [2]:

$$\sigma_f^{\,n+1} = (n+1) * B * \sigma^{n-2} * \dot{\sigma} \qquad (7)$$

$$\sigma_{f0}^{\,n+1} = (n+1) * B * \sigma_{io}^{\,n-2} * \dot{\sigma} \qquad (8)$$

where $\dot{\sigma}$ is the loading rate. Combining (7) and (8) gives

$$\frac{\sigma}{\sigma_{i0}} = \left(\frac{\sigma_f}{\sigma_{f0}}\right)^{\frac{n+1}{n-2}} \quad (9)$$

Substitution of (9) in (1) gives

$$\frac{\sigma}{\sigma_{i0}} = \left(1+\frac{t}{\tau}\right)^{x} \quad (10)$$

with

$$x = -\frac{n+1}{n-2} * p \quad (11)$$

The rate of strength degradation by zero stress ageing is found from the derivative of (10)

$$\left(\frac{d\sigma}{dt}\right)_{zerostress} = \sigma_{i0} * \frac{x}{\tau} * \left(1+\frac{t}{\tau}\right)^{x-1}$$

or

$$\left(\frac{d\sigma}{dt}\right)_{zerostress} = \sigma_{i0} * \frac{x}{\tau} * \left(\frac{\sigma}{\sigma_{i0}}\right)^{\frac{x-1}{x}} \quad (12)$$

Substitution of (12) in (6) gives

$$\frac{d\left(\frac{\sigma}{\sigma_i}\right)}{dt} = \frac{\sigma_{i0}}{\sigma_i} * \frac{x}{\tau} * \left(\frac{\sigma}{\sigma_{i0}}\right)^{\frac{x-1}{x}} - \frac{1}{B*\sigma_i^{n-2}} * \frac{1}{n-2} * \sigma_s^{n} * \left(\frac{\sigma}{\sigma_i}\right)^{3-n} \quad (13)$$

It should be noted that the scaling parameter σ_{i0} for zero stress ageing is the initial strength of a pristine fibre, while σ_i is the initial strength of the actual fibre.

For a pristine fibre (13) is reduced to

$$\frac{d\left(\frac{\sigma}{\sigma_i}\right)}{dt} = \frac{x}{\tau} * \left(\frac{\sigma}{\sigma_i}\right)^{\frac{x-1}{x}} - \frac{1}{B*\sigma_i^{n-2}*(n-2)} * \sigma_s^{n} * \left(\frac{\sigma}{\sigma_i}\right)^{3-n} \quad (14)$$

The differential equation (14) has to be solved numerically. The result of the calculation for fibres in 95 °C and 80 °C water is shown on fig. 4 with the experimental points from fig. 2. Also shown are results of static fatigue experiments in normal ambient environment.

The basic parameters for the calculation are written in the table in fig. 4. The n-value has been chosen equal to 20. As σ_i has been chosen 7 GPa which represents typical σ_i values measured in normal ambient environments for fused silica fibres [10]. The most important parameters τ and $B*\sigma_i^{n-2}$ have been found as previously described. It should be noticed that the lifetime calculated from (14) is little affected by the exact value of σ_i.

5. STATIC FATIGUE OF NON-PRISTINE FIBRES

5.1 Static fatigue of a pre-aged fibre

We have used the zero stress ageing mechanism to create low strength fibres with a narrow distribution of strength.

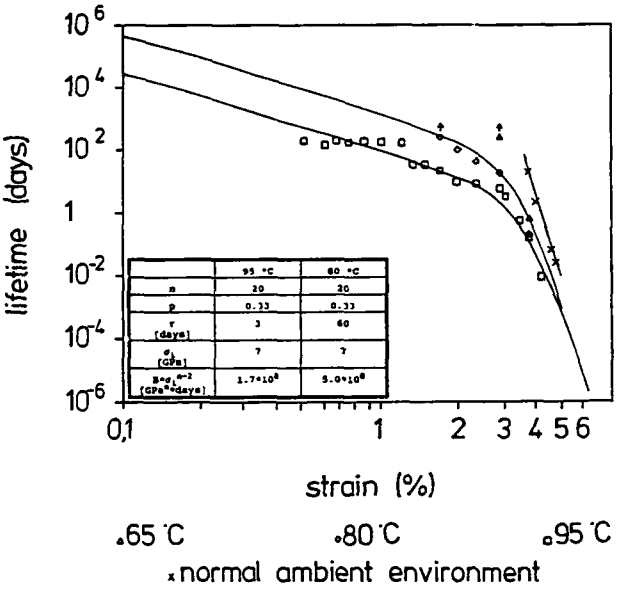


Fig.4 Calculated lifetime curves and experimental data.

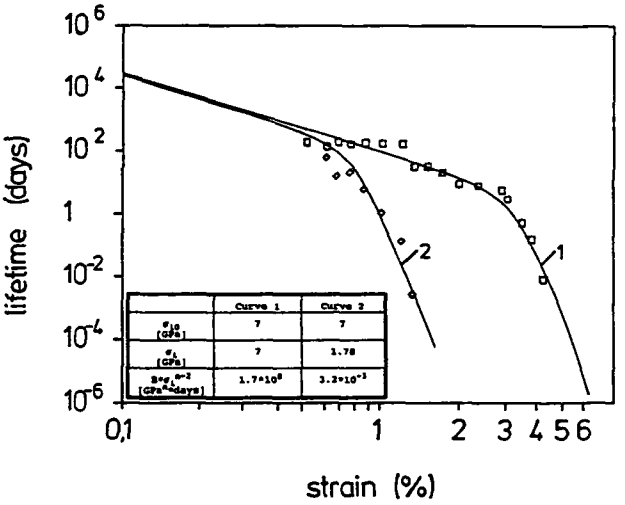


Fig.5 Calculated and measured static fatigue of a pristine fibre and a pre-aged fibre at 95 °C.

For fibres presoaked in water at 80 and 95°C at zero stress static fatigue experiments have been carried out at the same temperatures. The results are shown on fig 5 and 6 together with the results obtained at the same temperatures for the pristine fibre.

Also shown are 80 and 95°C lifetime graphs that have been calculated according to equation (13) using the parameters shown in the two tables.

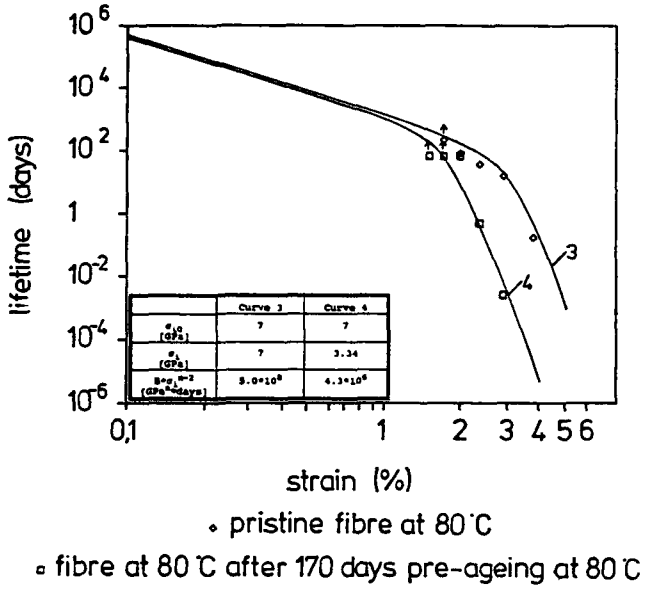


Fig.6 Calculated and measured static fatigue of a pristine fibre and a pre-aged fibre at 80 °C.

The most significant parameter for curves 2 and 4 is $B*\sigma_i^{n-2}$ which has been found using the method of section 4 assuming a constant n-value of 20. σ_i has been found from the horizontal shift illustrated in fig. 7.

At both temperatures there is good correlation between calculated and experimental data. Of special importance is the fact that the experiments verify the delay of the "knee" for lower strength fibres as predicted by the model.

At 95°C, in the low stress region with ageing times above 200 days the experimental values deviate from the predicted curve. A nearly horizontal curve is observed as opposed to the calculated slope of -2.4. A microscopic investigation of these fibres (aged for app. 200 days at 95°C) showed that the outer coating had cracked all along the fibre. In this way the chemical environment has been disturbed and access of water to the fibre surface was facilitated. We believe this is the reason for the deviation and that it is caused by the very high test temperature.

5.2 Static fatigue of a proof tested fibre

For the worst flaw in a proof tested fibre the initial strength is $\sigma_i = \sigma_p$, where σ_p is the proof test stress.

The basic static fatigue parameters for a 1 % proof tested fibre in water at 95 °C are written in the table in fig. 8.

The result of the calculation is also shown on fig. 8. It is seen that at low static strains near 0.1 % the lifetime of the worst flaw is very close to the lifetime of a pristine fibre. Consequently the exact knowledge of the classical stress corrosion parameters n, B and σ_{io} is not important. For fibres in wet environments at high temperatures the zero stress ageing predominates at stress levels normally used in optical cables.

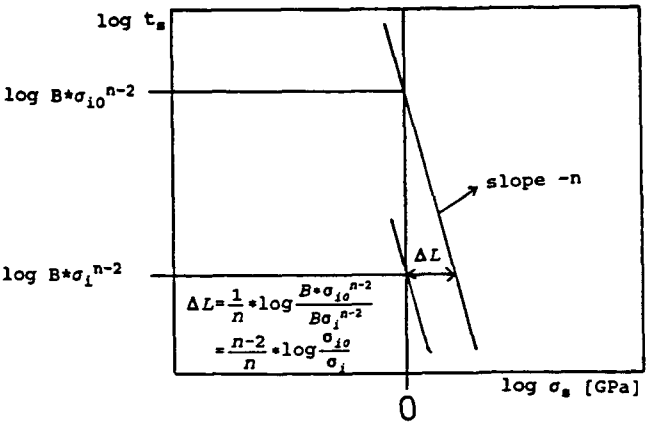


Fig.7 Static fatigue graph for a pristine and a pre-aged fibre. Calculation principle.

6. FIBRE DEGRADATION IN HUMID CABLE ENVIRONMENT.

In order to investigate the degradation of fibres in water saturated cables the following test was set up.

1. A metal free slotted core cable with two fibres with different dual acrylate coatings, A and B, was stored in 65°C water for 21 weeks in a nearly stress-free state. The tensile strength was measured regularly as in section 2 (fig. 9).

2. The same fibres were tested at 65°C as in section 2 directly immersed in water. These results are also shown on fig.9.

3. The static fatigue behaviour of the same fibres at 80°C was tested at strains from 1.7 to 3.5% with the fibres wound around mandrels made of the slotted core material and embedded in filling compound. Around this sample a heat shrinkable PE tube was mounted and the whole assembly was placed under water in such a manner that water could not penetrate from the ends. Fibre breaks were observed when light transmission was disturbed.
The results are shown on fig 10 together with static fatigue curves using the normal mandrel method (section 3).

The protective effect of the actual cable environment (filling compound) is clearly demonstrated by the tests (fibre A, fig. 10), and the importance of the zero stress ageing is also underlined. Fibre A, which ages much faster than B at zero stress also has much shorter failure times in the static fatigue plot (the "knee" occurring around 100 times faster).

SUMMARY.

An empirical model has been developed which predicts the failure times of stressed dual acrylate coated fibres in water. The predicted lifetimes are in good agreement with the observed values. It is shown that exact knowledge of σ_i, B, and n is unimportant whereas the time factor τ for the zero stress ageing is essential for the lifetime.
It has been shown that the time factor is strongly dependent on not only temperature but also the physical-chemical environment. Coating type is important but it is also worth noting that the cable environment can have a preserving effect on the fibres even when the cable is fully saturated with water.

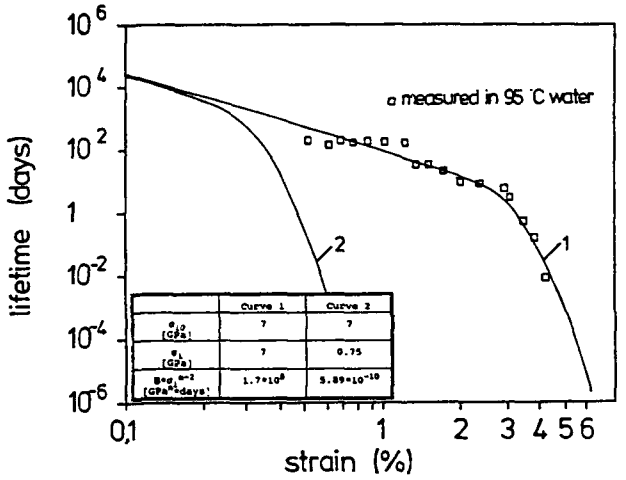


Fig.8 Calculated static fatigue for a pristine fibre (1) and a 1% proof tested fibre (2) in water at 95 °C.

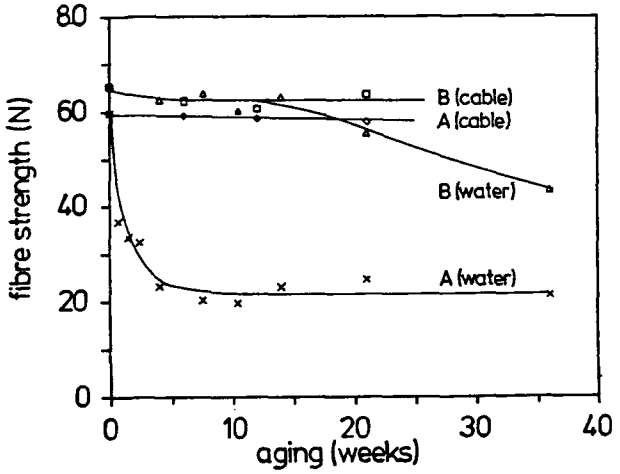


Fig.9 Medium strength of fibres A and B as a function of storage time in water at 65 °C.

References:

1. R.J. Charles: Static Fatigue of Glass. J. Appl. Phys. 29 (1958), 1554 - 60.
2. A.G. Evans, S.M. Wiederhorn: Proof testing of ceramic materials - an analytical basis for failure prediction, Int. J. Fract. 10 (1974), 379.
3. C. Chandan, D. Kalish: Temperature Dependence of Static Fatigue of Optical Fibres. Journal of the American Ceramic Society, Vol. 65, No. 3, March 1982.
4. J. Krause, C. Shute: Temperature Dependence of the Transition in Static Fatigue of Fused Silica Optical Fibre, Adv. Cer. Mat., 3 (2), 118 - 121 (1988).
5. P.W. France et al., BTRL: Strength and fatigue of multicomponent optical glass fibres. J. Mat. Sc. 18 (1983), 785 - 792.
6. M.J. Matthewson, C.R. Kurkjian, Bell Labs.: Environmental Effects and Static Fatigue of Silica Fibre. J. Am. Ceram. Soc., 71 (3), 177 - 83 (1988).
7. W. Griffioen, W. Ahn, A.T. De Boer, G. Segers: Stress- induced and stress - free ageing of optical fibres in water. Proc. of IWCS (1991), 673 - 678.
8. S.P. Craig, W.J. Duncan, P.W. France, J.E. Snodgrass, BTRL: The strength and fatigue of large flaws in silica fibre. Proc. ECOC 8, 1982, 205 - 208.
9. J.T. Krause, Bell Labs.: Zero stress strength reduction and transitions in static fatigue of fused silica fibre lightguides. Journal of Non-crystalline Solids, 38 & 39 (1980), 497 - 502.
10. J. Bjorkman, T. Svensson: Quick-Access to Fracture Statistics at Ultra-Wide-Range Tensile Test of Optical Fibres. Proc. IWCS, 1990, 373 - 378.

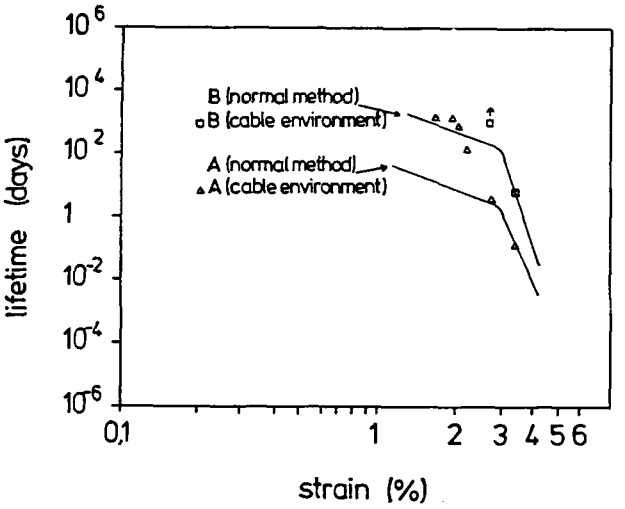


Fig.10 Static fatigue of fibres A and B in cable environment and in water at pH7.



Peter Hasløv

NKT Elektronik A/S
NKT Alle 85
2605 Broendby
Denmark

Peter Hasløv (M.Sc. Chem. Eng.) graduated from DTH in 1974 with polymer technology as special subject. After 13 years in the plastics industry, he joined NKT Elektronik in 1987 and is responsible for selecting, testing and processing polymers for telecommunication cables. He is also engaged in lifetime estimation of optical fibres.



Knud Bundgaard Jensen

NKT Elektronik A/S
NKT Alle 85
2605 Broendby
Denmark

Knud Bundgaard Jensen was born in Copenhagen, Denmark in 1944. He received his M.Sc. degree in Electrical Engineering in 1968. The same year he joined NKT's electrotechnical laboratory. From 1975 he worked with research and development of optical fibres. Since 1986 he has been working with development of optical fibre cables.



Niels H. Skovgaard

NKT Elektronik A/S
NKT Alle 85
2605 Broendby
Denmark

Niels H. Skovgaard was born in Copenhagen, Denmark in 1952. He received his M.Sc. degree in Mechanical Engineering in 1981. From 1981 he worked as researcher at The Technical University of Denmark. In 1984 he joined NKT working with research and development of optical fibre cables. Since 1986 he has been manager of the cable design and development department of NKT Elektronik A/S.

Design and qualification of optical fiber coating for ribbon fiber

N. Akasaka, W. Katsurashima, T. Nonaka, T. Hattori, Y. Matsuda,

Sumitomo Electric Industries, Ltd., Yokohama, JAPAN

ABSTRACT

This paper presents the design considerations for ribbon fiber which is used advantageously for high count cable design and reduction in splicing time, and also the qualification of the present ribbon fiber which has been introduced.

1. INTRODUCTION

Towards the 21st century, the construction of all fiber optic subscriber networks has been started to develop to distribute more informative and instructive services to every home(1). In order to apply optical fibers widely to these new subscriber networks, their cost reduction, improvement of quality and long term reliability are more desired. From such a viewpoint, ribbon fibers have been advantageously used for high-count cable designs and reduction in splicing time. Considering a slotted core ribbon cable design introduced in Japan(2), in order to satisfy a variety of required properties such as optical transmission characteristics, handling for splicing or connecting and long term reliability, the ribbon fiber technology should be completed by summarizing not only a lot of other elemental technologies but that of only drawn fiber(3). For this technology, this paper presents design considerations for coating materials of ribbon fiber which have been developed.

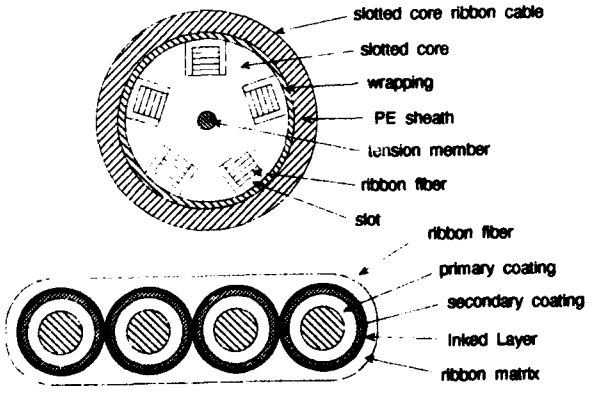


FIG.1
Structures of a slotted core ribbon cable and ribbon fiber

2. COATING DESIGN CONSIDERATIONS FOR RIBBON FIBER

2-1 Optical transmission characteristics.

(1) Anti-lateral force performance

Since a slotted core ribbon cable design is based on tight structure as shown in FIG.1 and accordingly ribbon fibers are tightly placed in a slotted core under some tension, the ribbon fibers are subject to stresses from the slotted core and each other. Therefore, it is necessary to design the coating system which is resistant to lateral forces.

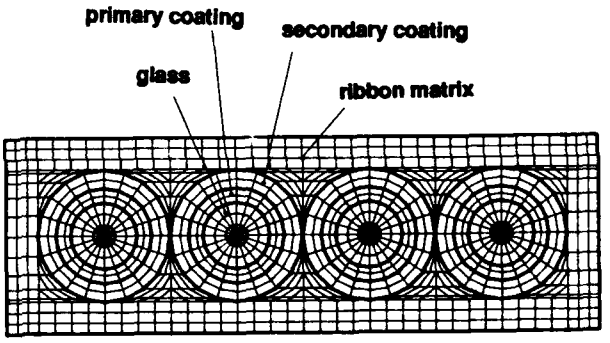


FIG.2 Calculation model of FEM analysis

At first, stress analysis of ribbon fiber by finite element method(FEM) was performed as a function of Young's modulus or thickness of each coating materials. The calculation model used in this analysis is shown in FIG.2 and the results of the calculation are represented in FIGs.3,4 and 5. FIG.3 shows the stress analysis of ribbon fibers providing a variety of the modulus of the primary coating materials as a function of the primary coating diameter. It has been found that for 250μm diameter fiber there is an optimum primary diameter between 190μm and 210μm. FIGs.4 and 5 show the same analysis as functions of moduli of the secondary and the ribbon matrix materials respectively. Anti-lateral force performance is expected to be significantly improved by increasing the modulus of the secondary coating or the ribbon matrix material and by decreasing the modulus of the primary coating material.

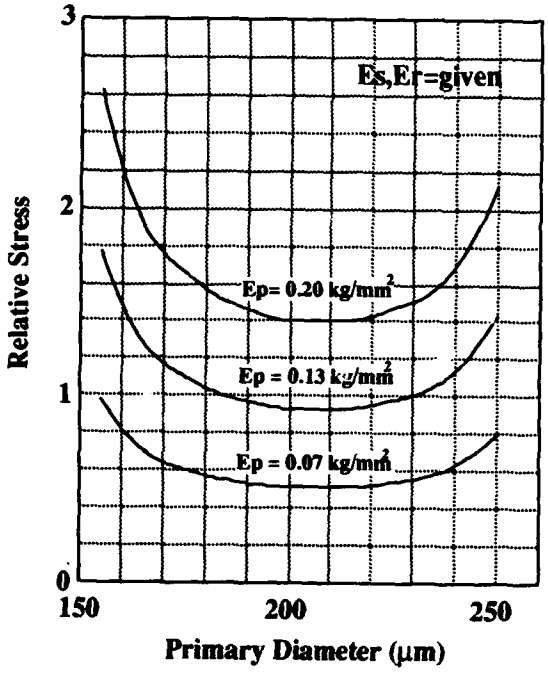


FIG.3 Stress analysis of ribbon fiber providing three kinds of moduli of the primary coating material as a function of the primary diameter

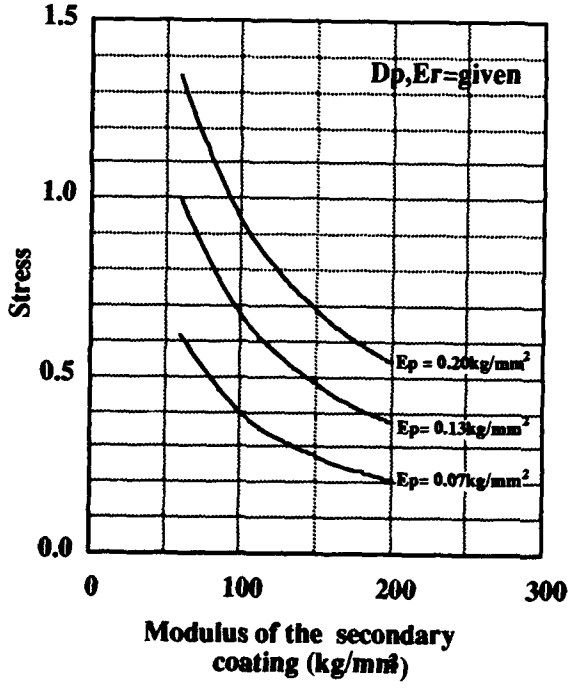


FIG.4 Stress analysis of ribbon fiber providing three kinds of moduli of the primary coating material as a function of moduli of the secondary coating

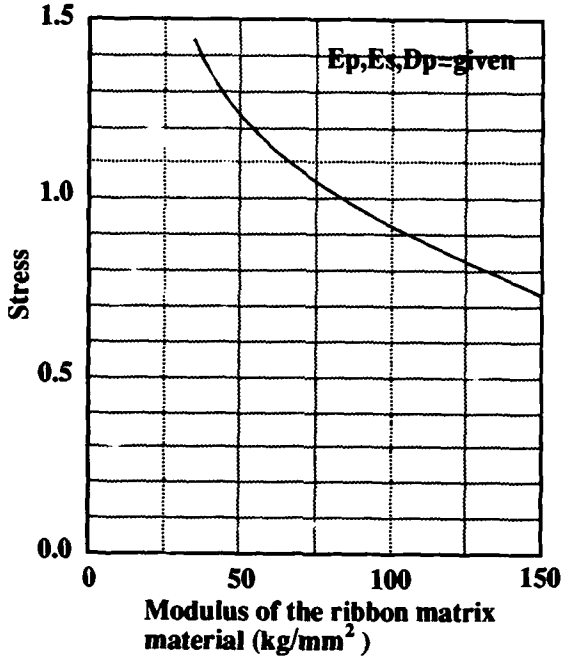


FIG.5 Stress analysis of ribbon fiber providing three kinds of moduli of the primary coating material as a function of moduli of the secondary coating

Next, on basis of above stress analysis, ribbon fibers were prepared in combination with the primary, secondary and ribbon matrix materials shown in TABLE 1. These were investigated on the anti-lateral force performance. Generally metal plate test illustrated in FIG.6 has been used as criteria for anti-lateral force performance. However this test seems to be suitable for the simulation of the collapse of cable with a relatively high stress, so that it is inadequate to evaluate the lateral force experienced by the ribbon fibers during cable making. We have developed "bobbin winding test" which is suitable for the evaluation of anti-lateral force performance for delicate fibers. This test is illustrated in FIG.7. A ribbon fiber is wound in one layer under some tension on a bobbin wrapped with a #250 sand paper and is measured with OTDR. Two experimental ribbon fibers characterized in TABLE 1 were measured.

TABLE 1 Properties of 4C-ribbon fibers for the test

Modulus (kg/mm^2)	Ⓐ Ⓑ Ⓒ Ⓓ				Ⓔ Ⓕ Ⓖ Ⓗ			
Primary	0.13	0.07	0.13	0.07	0.13	0.07	0.13	0.07
Secondary	60		150		60		150	
Ribbon	60				150			

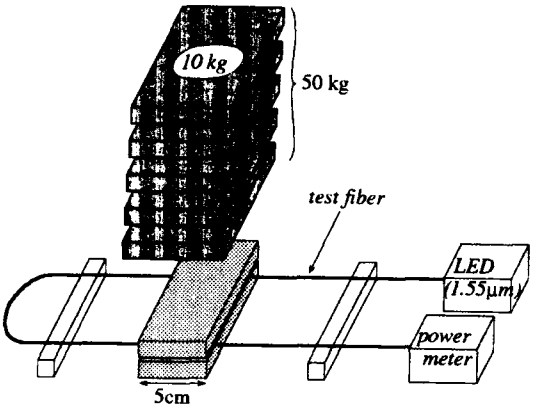


FIG.6 Illustration of metal plate test

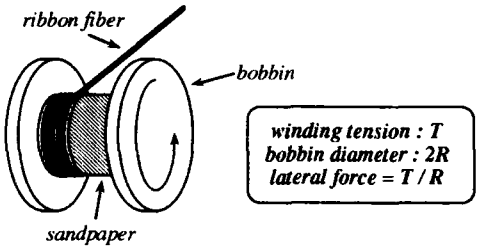


FIG.7
Illustration of bobbin winding test

From this test, it has been found that added losses for the fibers with the primary coating material of the lower modulus were able to be reduced to about one third. On the other hand, using the secondary coating or ribbon matrix material of higher modulus was not effective than expected by the calculation. A slotted core ribbon cable was fabricated as a trial test using ribbon fibers with an optimum coating structure and the same effect of the lower primary coating material was proved as in the bobbin winding test results. According to a series of test results, the lowest primary coating material has been started to develop.

(2) Temperature characteristics

For the slotted core ribbon cable, it is necessary to pay the attention to temperature characteristics not only at low temperatures but at high temperatures. At the low temperature, it has been considered that the cause for the added transmission losses is fiber buckling due to the force generated by the increases in the modulus of coatings and differences in expansion coefficient between the coating and glass fiber. Low temperature characteristics dose not have serious problems if the coatings are used with low modulus at low temperatures.

Also, it has been known that low temperature characteristics become worse due to the presence of bubbles in the coatings(4). In this problem, many experiments were made with various bubbles densities and coating designs, and it has been found that there is little effect of the presence of bubbles in the secondary coating on optical transmission characteristics however the presence of more than allowed bubbles in the primary coating causes the added loss. It was also proved that the more bubbles exist therein or the larger the primary coating diameter is, the more significantly added losses at low temperatures increase. At present the bubble free drawing technology has been established by the investigation of coating device designs. And also for the worse, a bubble detection in-line sensor has been being developed.

At high temperatures, since the slotted core made of HDPE expands with heat, the ribbon fibers are pressed to the slotted core and moduli of coating materials become small accordingly, the anti-lateral force characteristics are getting worse and added losses are likely to occur rather than at low temperatures. In order to simulate this phenomenon, the bobbin winding test without sand paper is also performed. A ribbon fiber is wound on a bobbin, afterward the bobbin is put in a constant temperature chamber and the transmission loss is monitored keeping high temperature. The same ribbon fibers as shown in TABLE 1 are tested. The added losses at 60°C have been reduced to about one third by the ribbon fiber with the lower primary coating material. Also using higher modulus materials, the effect of loss reduction corresponding to differences of modulus at high temperatures has been achieved. However, in general, higher modulus at high temperatures leads to the great increase of modulus at low temperature. So in consequence, there is an allowable limit of its modulus.

(3) Surface friction

Remaining distortion of ribbon fibers in a slotted core or bending distortion of fiber during cable making and installing are the important performance factors related to not only the stability of transmission characteristics but long term reliability of glass breakage. Several ribbon fibers are tightly placed in a slotted core with some distortion. If a tack of exists on the surfaces of ribbon fibers or the ribbon matrix material with significantly high friction is used, tacking occurs between adjacent ribbon fibers, resulting in hard controllability of ribbon fiber length in the slot, and larger bending distortion is applied to the fiber than designed when the cable is bent into a relatively small radius, resulting in apprehension of long term reliability of glass breakage. Accordingly, the ribbon matrix material should be cured in the inert atmosphere without oxygen and it is necessary to use the lowest frictional material as for as the winding condition of the ribbon fiber might no change.

2-2 Handling properties for mass fusion splicing or connecting

(1) Strippability of coating materials

A ribbon fiber has the advantage of mass fusion splicing. It aims at reduction in splicing time. To enable this splicing, all coating of ribbon fiber should be easily removed at once. After removal, there should not be any tenacious residues on the glass. On the other hand, if the adhesion is too poor, every fiber in ribbon can move easily during mass fusion splicing operation, resulting in "irregularity of fiber arrangement" illustrated in FIG.8 and ribbon fibers cannot be mass-spliced.

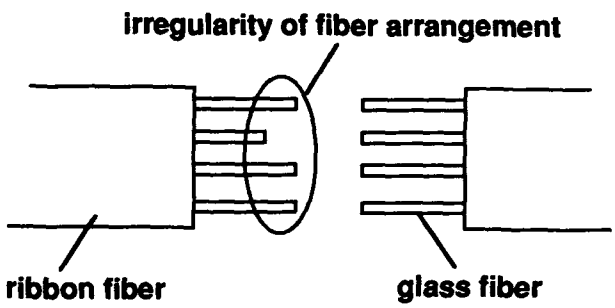


FIG.8 Illustration of irregularity of fiber arrangement in ribbon

Therefore, it has been found that there is suitable adhesion between the primary coating material and glass for ribbon fiber. We have much investigated the properties which play a major role in facility of mass fusion splicing and then it has been found that modulus and peel strength of the primary coating material. Peeling strength is defined as a force of pulling and peeling the primary coating film from a glass plate. The results are shown in FIG.9. As can be seen, it has been found that there exist the regions which satisfy both opposite properties when subjected to various operating environments such as high temperature, high humidity and filling compound immersion. For example, when the fiber is subject to high humidity condition, the interface between the primary coating and the glass is varying as shown in FIG.10 and the adhesion force is reduced. The effect of aging for 120days at 60°C and 95% relative humidity(RH) and filling compound immersion at 85°C on the stripping force of drawn fiber and ribbon fiber is shown in FIG.11. Long term reliability in these properties has been confirmed.

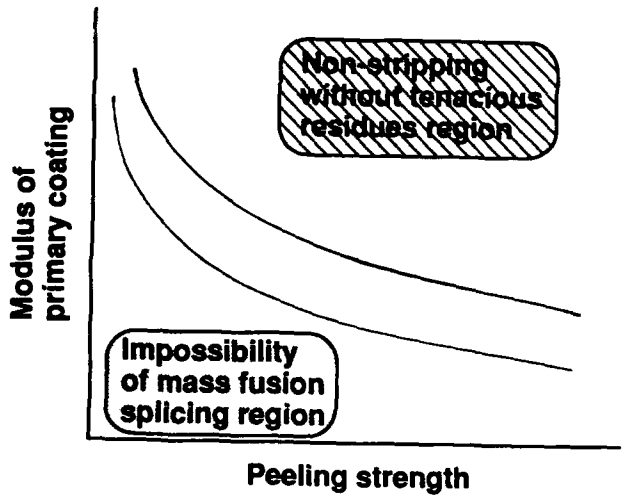


FIG.9 Relationship between peeling strength and modulus of primary coating for mass fusion splicing

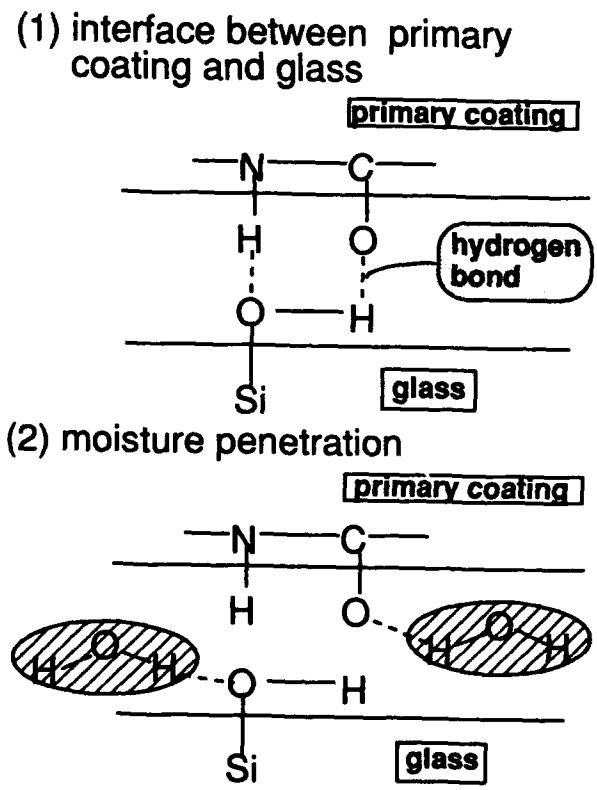


FIG.10 Interface between primary coating and glass at moisture penetration

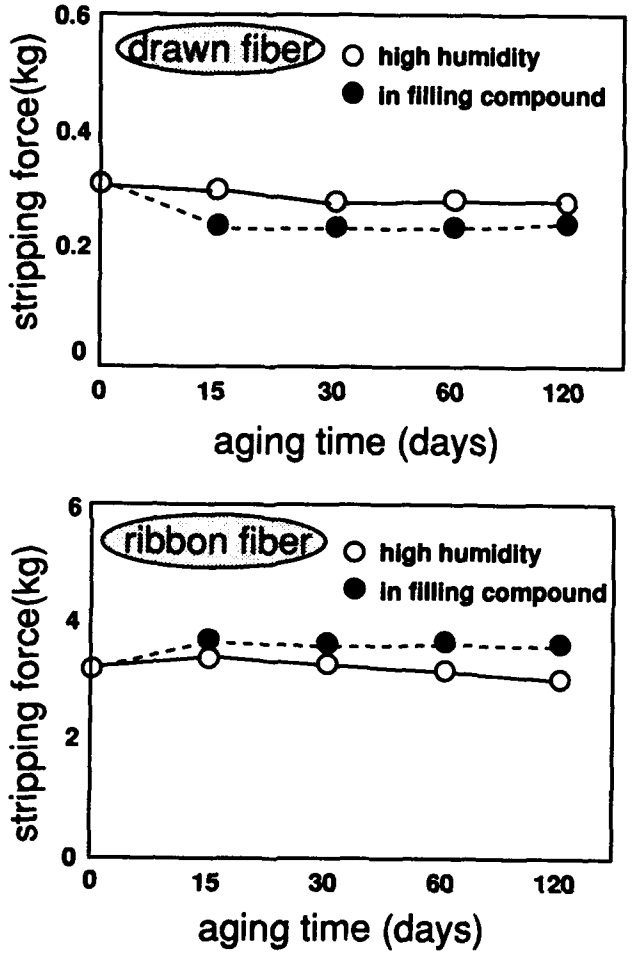


FIG.11 Long term reliability of stripping force for drawn and ribbon fibers under high humidity and filling compound immersion

(2) Separability of ribbon matrix material from inked fibers

According to the cable installed situation, the ribbon fiber is uni-spliced or connected in the field without mass fusion splicing. If the ribbon fiber is manufactured using inked fibers without an appropriate treatment, inked fibers would adhere strongly to the ribbon matrix material and they could hardly separate from each other. When each inked fibers are forced to separate from the ribbon matrix material in order to uni-splice, ink may stick to the ribbon matrix material and the function for identification may be useless. As the means of solving this problem, the method of using UV curable ink added a release agent has been introduced to reduce adhesion to the ribbon matrix material. In selecting the release agent, needless to say, the performance of ribbon fiber should not be deteriorated.

Wrong selection of this agent may cause many problems such as irregularity of inked fiber surface, reduction in curing speed, poor adhesion to the secondary coating and so forth. Nevertheless, according to the storage condition of drawn fibers before inking, adhesion of ink to the drawn fiber may be poor even with this treatment. Therefore, in order to improve this property, further, some methods shown in TABLE 2 have been being developed.

	Enhanced adhesion between ink and secondary coating	Reduced adhesion between ribbon matrix and secondary coating
Drawing in the presence of very few oxygen	○	—
Corona discharge on the surface of the secondary coating before inking	○	—
UV radiation on the surface of the secondary coating before inking	○	—
Ribbon matrix material with release agent	—	○
More than release agent in UV-ink	—	○

TABLE 2 Improvement of separability of ribbon matrix material from inked fiber

2-3 Long term reliability

Considering the circumstance to which a cable is exposed and the cable design, long term reliability in the performance of ribbon fiber used in the cable must be assured. As for circumstance, service temperatures are evaluated in the range of -40°C to 85°C, with high humidity or filling compound immersion depending on cable waterproof structures.

(1) Good compatibility with filling compound

The performance of the coated fiber may be deteriorated due to contact with filling compound. In particular, adhesion between the primary coating and glass fiber is reduced because part of based oil included in filling compound penetrate into the coatings and arrive at the interface of the primary coating and the glass. Of course, this problem is responsible for not only the coating materials but filling compounds. As reported at the previous IWCS, the based oil with high molecular weight should be used for filling compound(5). It is desired that coating material should not be influenced by any filling compounds. As a result of the experiment on the interface of filling compound penetration, the suitable coating system has been found to select the adhesion promoter against oils and to minimize the swelling of oils in consideration of the cross linking density or oligomer compositions of the coating materials.

(2) Moisture resistance

For a cable structure with PE sheath and swelling material, moisture penetrates through the sheath into the cable. Though water generated by heat cycling condition is absorbed into the swelling material, the humidity of inner cable may become significantly high. Therefore long term reliability of ribbon fiber should be estimated under high humidity. The important evaluated properties are the change of adhesion to each materials or the primary coating material and glass fiber and optical transmission characteristics. In very small voids somewhere at each interfaces, and then blistering may occur at any interfaces, resulting in microbending loss. Accordingly the selection of coating materials must be carefully considered. Our ribbon fiber exhibits the absence of change for 90days at 60°C and 95%RH on optical transmission characteristics.

3. CONCLUSION

In order to meet all requirements desired for ribbon fibers, with design considerations of all coating materials which the ribbon fiber is made of and reliability can be obtained. Further, in future the ribbon fiber which can stand severer environments should be developed.

REFERENCE

(1) T.Uenoya "The optical fiber loop21 plan" OEC'90(1990)

(2) M.Kawase et al "Loop-Network Configuration For Subscriber Loops and Single-mode Optical Fiber Cable Technologies Suitable For Mid-Span Access" 37th IWCS(1988)

(3) J.Thamas Chapin et al. US Pat. 4962992(1990)

(4) N.Yoshizawa et al. "Low Temperature Characteristics of UV-Curable Resin Coated Optical Fiber" J. of Lightwave Technology VOL.LT-3, No.4, 779, August, (1985)

(5) T.Hattori et al. "Optimal design of jelly compound for optical cable" 37th IWCS(1988)



Nobuhiro Akasaka

Sumitomo Electric
Industries, Ltd.
1, Taya-cho, Sakae-ku,
Yokohama, Japan

Nobuhiro Akasaka received his M.S. degree in Chemical Engineering from Tokyo University in 1983. He joined Sumitomo Electric Industries Ltd. in 1983, and has been engaged in research and development of optical fiber and cables. He is a senior engineer of Transmission Media R&D Department, Yokohama Research Laboratories.



Tomoyuki Hattori

Sumitomo Electric
Industries, Ltd.
1, Taya-cho, Sakae-ku,
Yokohama, Japan

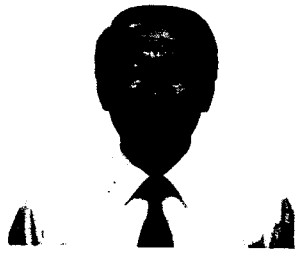
Tomoyuki Hattori received his M.S. degree in Chemistry from Kyoto University in 1987. He joined Sumitomo Electric Industries Ltd. in 1987,and has been engaged in research and development of optical fiber and cables. He is a member of Transmission Media R&D Department in Yokohama Research Laboratories.



Wataru Katsurashima

Sumitomo Electric
Industries, Ltd.
1, Taya-cho, Sakae-ku,
Yokohama, Japan

Wataru Katsurashima graduated from Tokyo University in 1987. He joined Sumitomo Electric Industries Ltd. in 1987, and has been engaged in optical fiber and cables. He is a member of Institute of Elestronics and Communication Engineers of Japan.



Yasuo Matsuda

Sumitomo Electric
Industries, Ltd.
1, Taya-cho, Sakae-ku,
Yokohama, Japan

Yasuo Matsuda received his M.S. degree in Chemistry from Kyoto University in 1978. He joined Sumitomo Electric Industries Ltd. in 1978 ,and has been engaged in research and development of optical fiber and cables. He is a chief research associate of Transmission Media R&D Department in Yokohama Research Laboratories.



Tsuyoshi Nonaka

Sumitomo Electric
Industries, Ltd.
1, Taya-cho, Sakae-ku,
Yokohama, Japan

Tsuyoshi Nonaka received his M.S. degree in Chemistry from Kyoto University in 1986. He joined Sumitomo Electric Industries Ltd. in 1986 ,and has been engaged in research and development of optical fiber and cables. He is a member of Transmission Media R&D Department in Yokohama Research Laboratories.

Effects of waterproofing compounds on the long term reliability of polymeric coated optical fibers

J.M. Hsiao, S.I. Wang, K.Y. Chen, T.C.Chang, D.M. Fann, Y.-c., Lin

OSP
Telecommunication Laboratories, M.O.C.
P.O.Box 71, Chung-Li, Taiwan, R.O.C.

ABSTRACT

Two types of optical fibers and three filling jelly compounds are combined to conduct an accelerated aging test at 50°, 70°, and 100°C to study the effect of jelly compounds on the long term reliability of optical fiber. The performance of fibers are evaluated by measuring the changes of fiber strength, color, weight , coating strippability, and bending resistance upon aging in jellies. When thermally aged, the fibers showed a weight loss, an increase of strength and strip force. However, when aged in jelly compounds, they showed as a weight gain, a deduction of fiber strength, and an increase of strip force that was still lower that induced by thermal aging. In addition, aging in jelly at elevated temperatures cause the deterioration of coating that reduces the coating buffer effect to result in a decrease of bending resistance of higher bending attenuation.

INTRODUCTION

Optical communication has essentially taken most of the load from telecommunication. From trans-ocean to fiber to the home, optical fiber is one of the most important transmission medium today. However, it has been recognized that optical fiber is extremely susceptible to water or moisture which cause the deterioration of fiber strength and the increase of transmission loss[1]. To protect optical fiber cable from water penetration, filling the cable with Jelly type compounds is the choice of solution. It has the advantage of low cost in contrast to the high cost of gas maintenance system and more reliable comparing to that of dry type system which is implemented with superabsorbents as the water blocking materials. Therefore, jelly immersed fibers is the inevitable choice for user and the reality that the fiber will be affected by the jelly compounds becomes conceivable if compatibility problem arises between the fiber coating and jelly compounds. Especially, different types of fiber coatings used by the fiber manufacture which then combined with diversified jelly compounds by cable manufacturer to make commercial cables. This leaves the end-user always uncertain whether the cables they bought will be as reliable as they expects. Some previous studies did show that improper coating composition may affect the fiber performance[2] such as the tensile strength, and water resistance, the impact of improper jelly to the overall performance of a polymer coated fiber was not yet well-understood and addressed. However, we found by occasion that the fiber in a jelly filled cable which has stored for 2.5 years showed apparent deterioration in its strength and appearance. As a result, a systematic in-situ characterization of the jelly effects on the long term reliability of optical fibers seems necessary and worth to take in the hope to ensure the reliability requirements as specified is adequate to screen out the unqualified cables.

EXPERIMENTAL

Materials:

Samples of fibers designated as U-fiber and V-fiber are commercial available. Three jelly compounds designated as JF, JC, and JT are also commercial available and obtained from cable manufacturers. Both fibers are single mode fiber (125 μm) coated with dual coatings in a diameter ca. 250 μm.

Aging:

U-fiber and V-fiber were cut to numbers of SAMPLES at a length of ca.2000 m which were loosely wound as circles (diameter = 300 mm) and placed in containers with the ends of fibers outside the containers. The samples were aged at 50°, 70°, and 100°C with one group in air and the other group immersed in jelly compounds (U-fiber in JF, V-fiber in JC or JT). Sample of fibers were removed from aging at period of time and the change of weight, tensile strength, strip force, and bending loss were measured.

Weight changes:

Samples of fibers were weighed by a micro balance before and after aging.

Tensile strength:

Minimum of 25 specimens for each sample were measured in a Universal Testing Machine using a gage length of 500 mm and a strain rate of 20mm/min in a laboratory ambient environments of 23°C and relative humidity of 60%.

Strip force:

Minimum of 10 specimens of each sample were measured in a customized stripping tensile testing machine mounted with a commercial stripping tool (0.18/0.30). The gage length is 100 mm and stripping length is 30 mm with a stripping rate of 500mm/min. Strip force were collected through out the stripping process. Each sample datum was taken from the median of 10 tested specimens.

Bending (macrobending) loss:

The attenuation of each sample (ca. 1000 m) was measured in a commercial spectrum meter scanned from 1000 nm to 1600 nm using cut-back method. First, the ends of a loosely winding sample (diameter=300 mm) was coupled to the input and output of a spectrum meter and the power output (P_0) was measured. Second, taking the middle part of the testing fiber without disturbing the input and output coupling and winding the fiber on the outside of a glass mandrel (diameter=30, 40, 50 mm) for 5 or 10 turns. The power reading was then taken as (P_i) according to each specified mandrel diameter and number of turns. Finally, cut the fiber back to a length of 2 m and reconnect it to the detecting position. Obtain a short-length power (P_f) as the reference. Attenuation (A_i) of each bend condition was then calculated as: $A_i = 10 \log (P_f/P_i)$ i= 0, 1, 2, ...

RESULTS AND DISCUSSION

Thermal aging in air

Fig. 1 showed the changes of the median strength of U-fiber and V-fiber upon aging in air at 50°, 70°, 100°C and 25°C. Before aging, U-fiber appears stronger than V-fiber and it remains true after 120 days of aging. The extent of thermal effect on the strength of two tested fibers showed quite distinct . An increase of strength occurred on V-fiber when aged at 70° and 100°C while little strength variation was observed on U-fiber. This fact was consistent to the observation of color changes. V-fibers became yellowish when they were aged to 14 days at 70°C and 100°C, but U-fiber remained as look-alike as beginning. However, prolonged aging beyond 60 days resulted an adverse drop of the progressive rising strength to a level that near that of the unaged samples (except for those aged at 100°C). Similar aging time effect can be seen in the strip force change profiles (Fig 8, 9, 10). Both fibers showed a significant increase of stripping force which peak up at the aging of 30 days but dropped and stayed at a level thereafter. Also, the weight change versus aging time as shown in Fig.2 indicated a maximum weight loss for both fiber at the day 14 of aging which corresponding to the onset of the increasing strength and strip force and the observable color changes of V-fibers. Yet, the prolonged aging produced no more additional weight loss. This indicates the weight loss during the initial thermal aging may be attributed to the evaporation of volatile materials from fiber coatings including moisture. Considering the moisture that residents inside the coating is a stress corrosion agent that may cause the reduction of fiber strength[3], removing such agent as done by the thermal aging can result in an increase of fiber strength, especially, as evident by the substantial increase of V-fiber upon aging. The thermal aging can also enhance the post-curing of fiber coatings to become harder and shrinking. As a result, the strip force increases substantially as evident on both fibers. However, the prolonged aging apparently caused more serious effects on the coatings. The yellowish color implies oxidative degradation may have occurred on V-fiber and the strip force have dropped from the peak value because the coating became more brittle. Aging at 50°C and 70°C has similar effects on fibers while at 100°C is different due to a complete different degradation mechanism exerting on the fiber coatings. U-fiber showed less susceptible to the thermal effect compared to V-fiber.

Aging in Jelly compounds

Weight changes

Fig. 3 and Fig 4 showed the weight changes of V-fiber aged in JC and JT compounds and U-fiber aged in JF jelly respectively. Substantial amount of JT and JC jellies were absorbed by V-fiber and JF jelly by U-fiber when they were aged at 100°C. The absorption became saturated after 30 days of aging. On the other hand, those aged at 50° and 70°C showed no weight loss or a weight loss comparable to those aged thermally. This weight loss is attributed to the extraction of low molecular weight substance from coating by jelly oils when fibers were aged at 50° and 70°C. At 100°C, the coating property was seriously deteriorated by the combination of excessive heat and jelly oil that the coating became soaking with the oils coming from jellies[4]. The result is a weight gain of fiber. The absorption of jelly compounds by coating apparently is govern by mechanisms that is temperature dependent.

Strength changes

Fig. 5, 6, 7 showed the changes of median fiber strength for V-fiber aged in JT and JC and U-fiber in JF jelly compounds. In contrast to the thermal aging, jelly immersed aging all gave a deduction of strength at a definite fashion when aging reached 30 days. Some scatter points, although, remained showing an increase as represented by U-fiber(in JF jelly) aged 50°C and V-fibers(in JC jelly) at 50° and 70°C, they were limited on the initial aging stage where the thermal effect was considered remaining effective. At 100°C, the strength of V-fiber dropped by 19% and 17% when aged in JT and JC jellies while U-fiber dropped by only 6% in JF jelly. The onset time of these significant deductions of strength coincided with the aging time where the weight gain became saturated. At this point,

the coating is soaked with jelly oil and its original structure and property apparently had deteriorated as shown by a dynamic mechanical thermal analysis in a previous study[4]. In the meantime, Aging at 50° and 70°C also showed a deduction of strength even though there were no weight gain but a weight loss. Considering that, at these temperatures, weight loss is due to the extraction of low molecular weight substance from coating by jelly oil ,and the residual stress corrosive agents such as moisture (inside the coating) is unlikely extracted by jelly oil because it is against the hydrophobic nature of jelly oils, it can be anticipated that stress corrosive agents remains inside coatings and is effective enough to cause the deduction of fiber strength. In addition, other corrosive agents that originally residing in jelly may access the fiber glass via the jelly extraction process. Improper jelly can become dangerous to the strength reliability of optical fiber.

Strip force changes

Fig. 8, 9 showed the strip force changes of V-fiber aged in JC and JF jellies. Fig.10 showed U-fiber in JF jelly. When aged at 50° and 70°C, all fibers showed an increase of strip force but not as much as those thermally aged. The maximum also occurred at the day 30 of aging and thereafter started dropping. Since the strip force relies on the adhesion between the glass and coating and the inherent properties of coating, any factor that changes above condition may have effect on the strip force. First, the thermal effect resulting in the post-cure and shrinkage of coating as described above has a positive effect on the increase of strip force. The strip force then gradually decreases due to the prolonged oxidative aging. This fact remains true even the fibers are aged in jelly. However, the penetration of jelly oil into and out of fiber coating may exert an adverse effect on the strip force due to the plasticizing effect by the oils. As a result, lower strip force is expected when the fibers are aged in jelly. Such jelly softening effect is also temperatures dependent. Unlike the thermal aging where the strip force changes showed nearly the same for the three aging temperatures, the aging at 50°C of V-fiber in JF jelly gave a rather low value that near the unaged sample. This indicates the softening effect is much effective at this temperature while it become less effective when the temperature increase where the thermal effect dominates again. As shown in Fig. 11 where the difference of strip force between thermally aged and jelly aged fibers ($S.F._{thermal}$- $S.F._{jelly}$) is plotted versus aging times, the profile of 50°C aging deviates from that of the other two aging temperatures. Due to the excessive absorption of JT jelly oil by V-fiber and JF jelly oil by U-fiber when aged at 100°C that the diameter of these fibers became too big to be inserted into the stripping tool, the strip force of these two fibers were not able to measure.

Macrobending loss

Fig. 12 and 13 showed the macrobending loss spectrum of unaged and aged V-fiber (100°C, 60 days in jelly JC and JT). Fig. 12 represented a macrobending produced from winding the fiber in a glass mandrel (diameter=40 mm) for 5 turns and Fig.13 for 10 turns. More turns results more loss at wavelength beyond 1500 nm and is shown as a typical macrobending loss. Without bending, the unaged and aged fibers (in both jelly) showed similar attenuation. Upon bending, more loss was observed for aged fibers compared to that of unaged fibers. As evident by the changes of fiber strength and strip force, the jelly aged effect has caused a deterioration of coating that the fiber became less buffered and more sensitive to bending. U-fiber also showed a similar attenuation changes. As shown in Fig. 14 where the unaged and aged fiber (in JF jelly for 60 days) was compared, substantial loss was induced by the bending . However, U-fiber showed less loss when compared to that of V-fiber at the same bending condition. It requires a 30 mm diameter of mandrel to achieve a loss that can be easily produced by a 40 mm diameter mandrel for the aged V-fiber. This is also consistent to the fact that U-fiber is less deteriorated as shown by a less change of strength and less susceptible to the jelly aging.

CONCLUSION

The effect of jelly filling compounds on the long term reliability of optical fiber as shown by the accelerated aging results can be serious if the fiber coating and jelly compounds was not well-compatible. Under elevated temperature aging in jelly, V-fiber showed a deduction of fiber strength of 19% and U-fiber showed a 6% of drop. Yet, the absorption of jelly by the coating of U-fiber is no less than that by the V-fiber, it is not the absorbing amount of jelly but is the interaction between the jelly compound and coating governs the reliability of optical fiber. Traditional compatibility examine method for coating and jelly that only measuring the weight gain is not sufficient to guarantee the long term reliability. Accelerated aging test in jelly can offer as the additional proved method to ensure the fiber long term reliability. The changes of strip force and macrobending loss induced by the jelly aging effect are also the indications of the fiber long term performance. Then can also served as the index of fiber reliability. In short, improper jelly compound can be dangerous to the long term reliability of fibers. It can cause the deterioration of fiber coating to result in the deduction of fiber strength, the decrease of bending resistance, and the difficulty of stripping.

REFERENCE

1)C. Kurkjian, J. Krause, M.J. Mathewson *J. Lightwave Technol.* 7(9), 1360, (1989)

2)(a) J.Toler, G. Kar *ANTEC*, 372 (1988)
(b) H. H. Yuce, I.M. Plitz, R.A. Frantz, M Andrejco *Proceed. 39th IWCS, 715* (1990)

3)H.H.Yuce, A.D. Hasse. *Proceed. 37th IWCS*, 732 (1988)

4)Y.-C. Lin, J.M. Hsiao, D.M. Fann, S. I. Wang,K. Y. Chen. *Proceed. 40th IWCS*, 504 (1991)

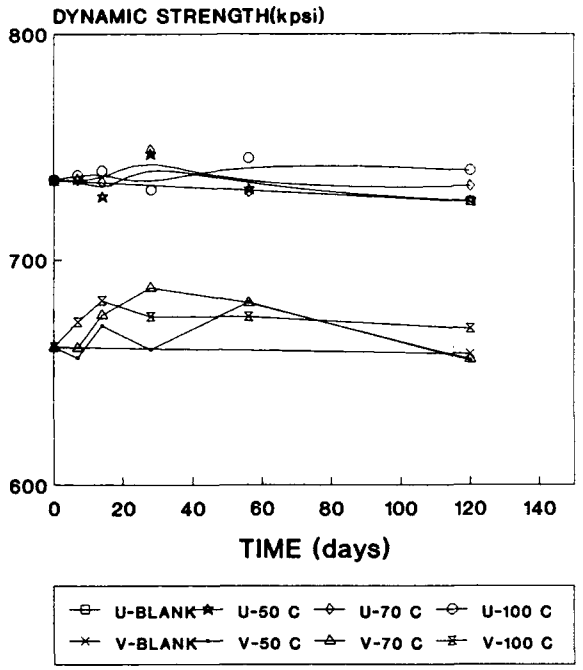


Fig.1 Median strength changes of U and V-fiber from thermal aging

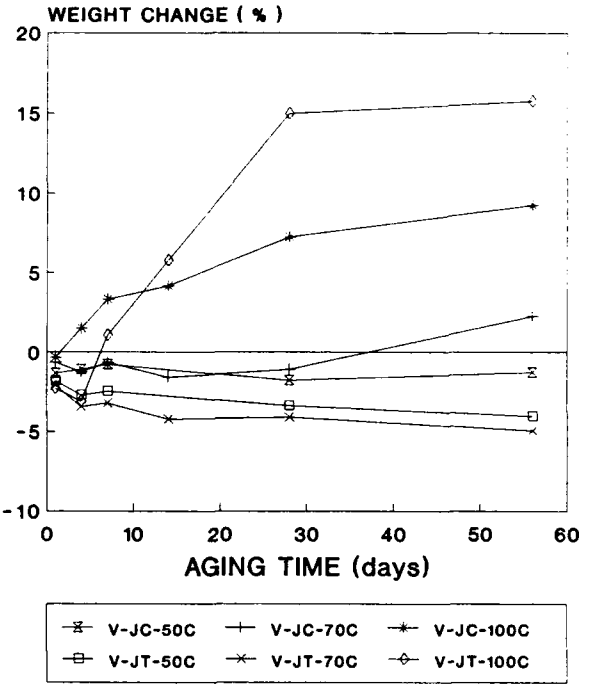


Fig. 3 Weight changes of V-fiber aged in JC and JT jellies

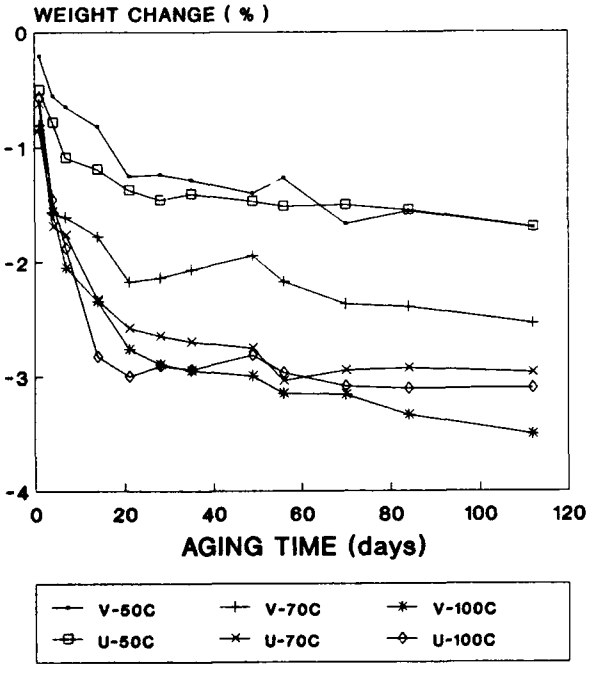


Fig.2 Weight changes of U and V fiber from thermal aging

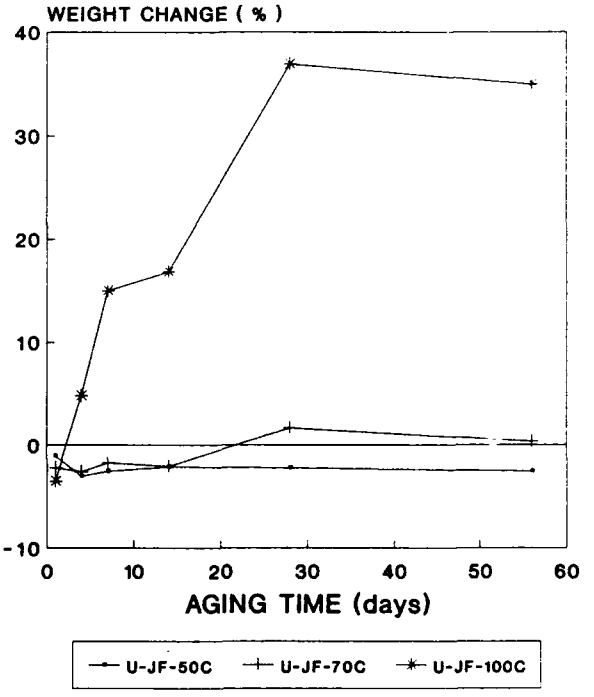


Fig. 4 Weight changes of U-fiber aged in JF jelly

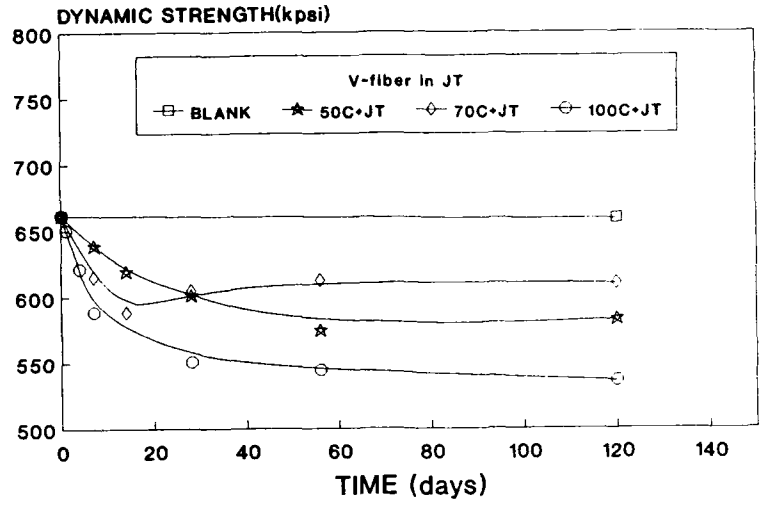


Fig. 5 Strength changes of V-fiber aged in JT jelly

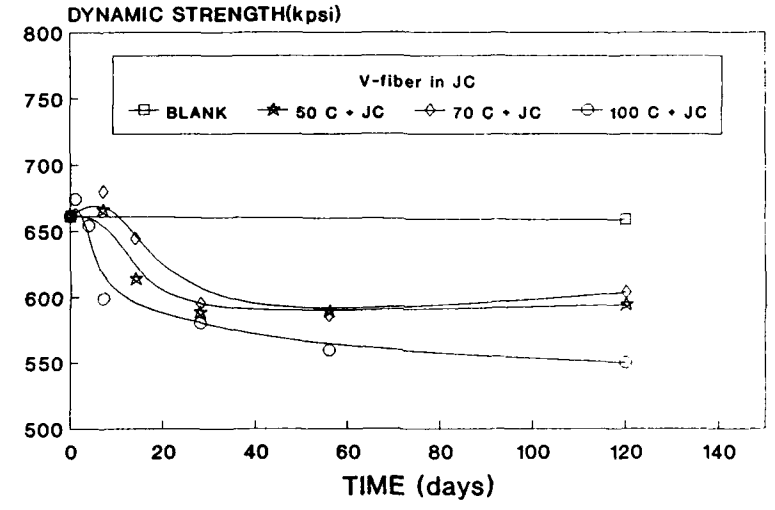


Fig. 6 Strength changes of V-fiber aged in JC jelly

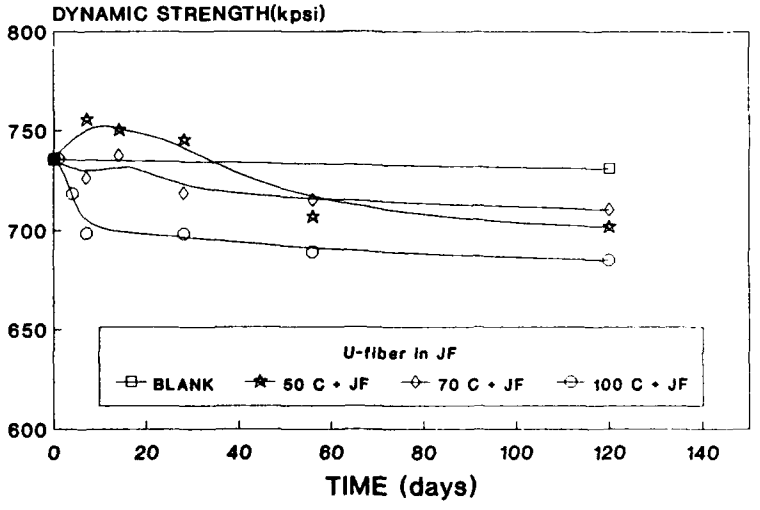


Fig.7 Strength changes of U-fiber aged in JF jelly

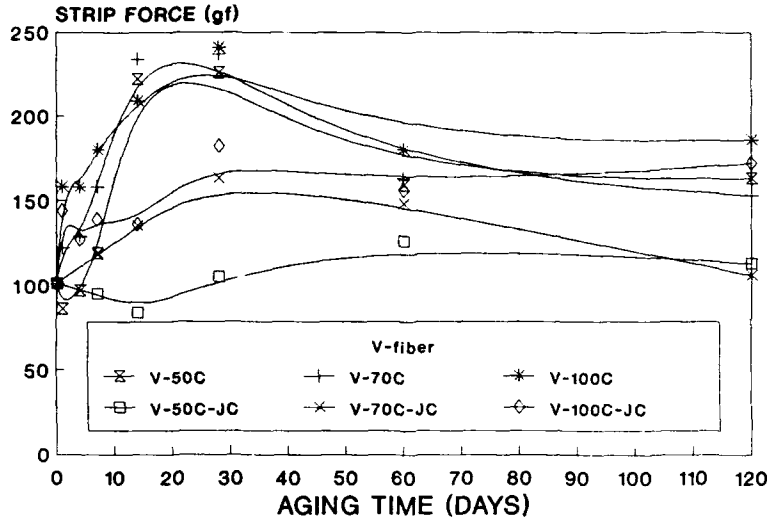


Fig. 8 Strip force changes of V-fiber aged thermally in air and JC-jelly

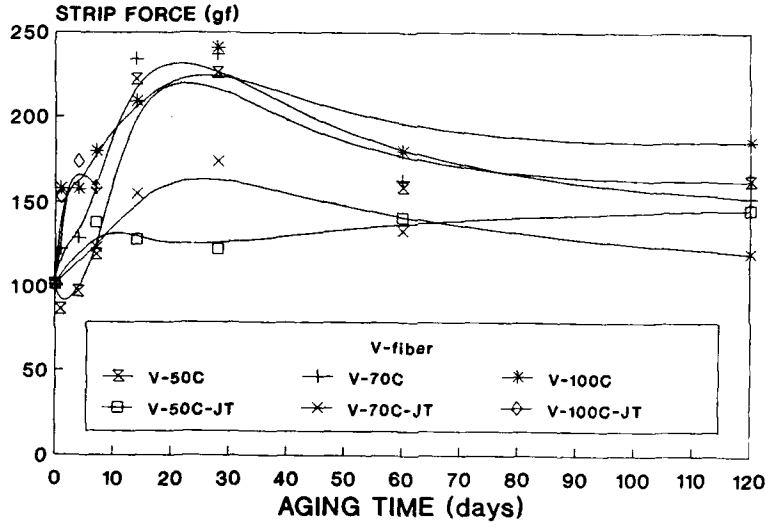


Fig.9 Strip force changes of V-fiber aged thermally in air and JT-jelly

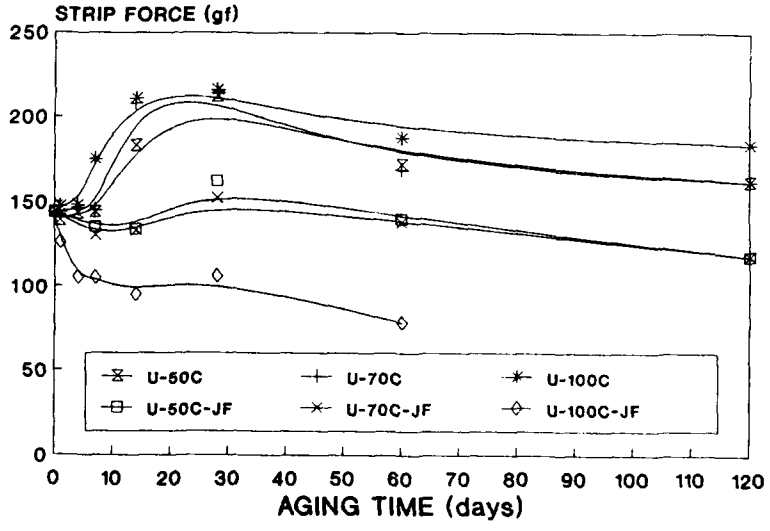


Fig.10 Strip force changes of U-fiber aged thermally in air and JF-jelly

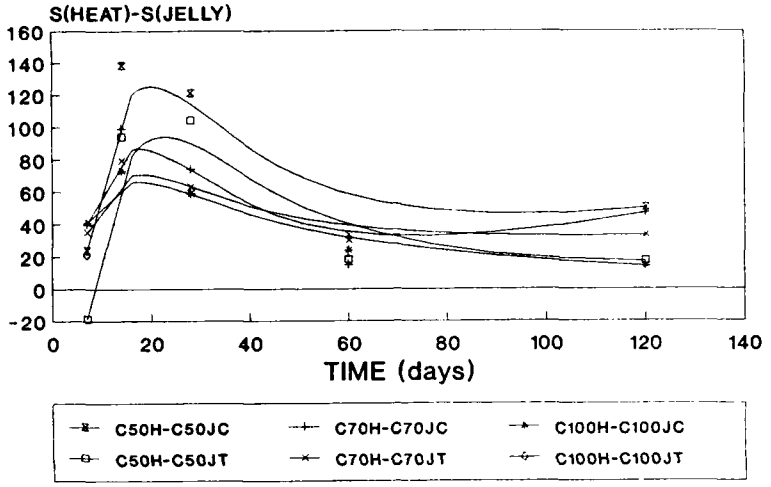


Fig.11 Difference of strip force of V-fiver between thermally aged and jelly aged effects

Fig.12 Macrobending loss of V−fiber in JC & JT

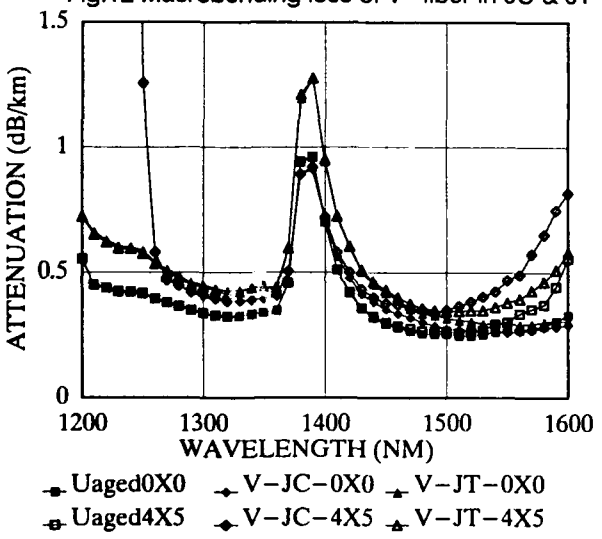


Fig.13 Macrobening loss of V−fiber in JC & JT

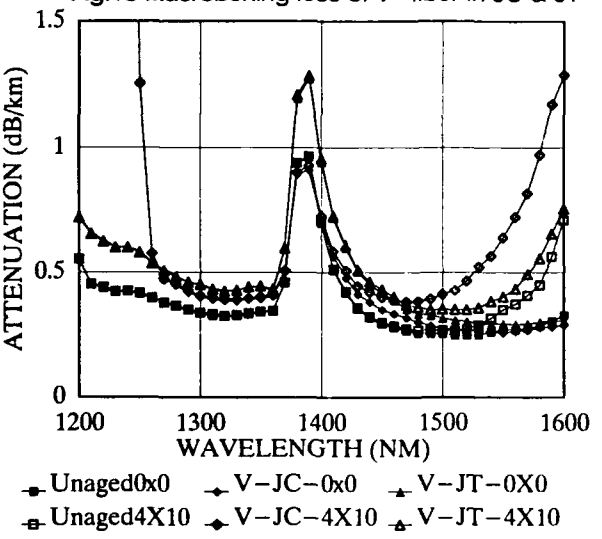
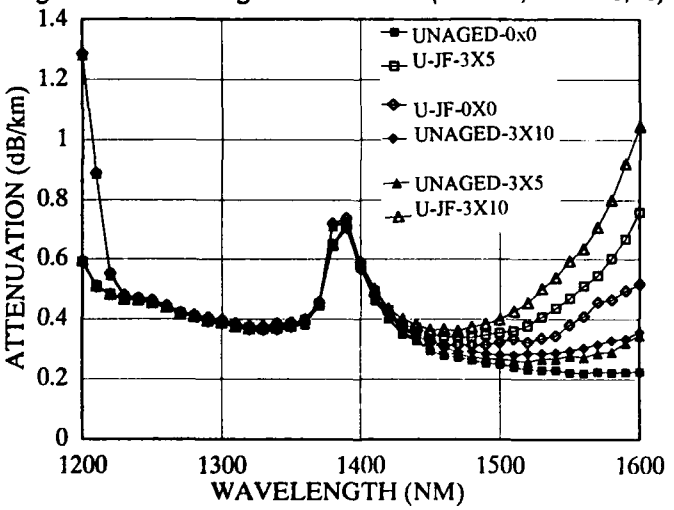


Fig.14 Macrobending loss of U−fiber (d=3cm, turns=5,10)



ASPECTS OF THERMO-OXIDATIVE AND HYDROLYTIC DEGRADATION IN OPTICAL FIBER CABLE MATRIX MATERIALS

T. Bishop, C. Chawla, D. Szum, and E. Poklacki

DSM Desotech Inc., Elgin Illinois

Abstract

Some UV-cured materials have been observed to exhibit color changes with time, especially at elevated temperature, humidity or UV exposure. While this may be an indication of oxidation, its relationship to more serious forms of degradation, such as crosslinking, bond order changes, chain scission, or depolymerization, has not been definitively established for these materials. This paper examines various aging phenomena in model fiber matrix materials. The cured films were aged at 125°C in an oven and at 120°C/100% RH in a pressure vessel. Changes in color were measured using a Macbeth colorimeter. Thermo-oxidative and hydrolytic stability were measured by dynamic mechanical analysis and weight loss. The data revealed that compositions which yellow may or may not mechanically degrade. It was therefore concluded that the degree of yellowness after aging is unreliable when used as the sole indicator of these materials' thermo-oxidative and hydrolytic stability.

Introduction

The use of radiation curable polymers as protective coatings for silica glass fibers and as binder materials in optical fiber ribbons is well established. These materials offer performance advantages over other technologies in processing speed, low added attenuation over temperature and humidity extremes, controlled strippability for fiber splicing, as well as mechanical protection of the glass.

As this technology advances into fiber optic ribbons, reliability of the ribbon matrix materials and lifetime prediction under adverse environments have increased in importance due to the replacement costs involved. In "Fiber to the Home" architecture, the cost for a buried drop-line to each residential subscriber is estimated to be between $100 - $200. [1] Coating requirements for these demanding applications have been reviewed by Kar. [2]

Major areas of study in the area of environmental degradation of the organic polymer have included: thermal and oxidative aging [3,4], hydrolytic aging [5,6], and stabilization using antioxidants. [7,8] The tendency of the polymer and/or its additives to discolor or yellow upon accelerated aging is one of the effects noted in environmental degradation. While excessive yellowing can prevent differentiation of the colored fibers within the ribbon, moderate yellowing does not necessarily hinder fiber identification. [9] The mechanisms and subsequent results of various types of environmental aging have been documented. [10] In UV curable systems, the mechanism of yellowing is complicated by the presence of UV sensitive species, i.e. the photoinitiator, stabilizers, etc. It is difficult to distinguish yellowing due to the degradation of the polymer versus possible degradation of additives, which can form strongly colored quinoids. In the former case, significant mechanical property changes will be observed. In the latter, the color may change, but no significant mechanical property changes may be noted. It is important therefore to establish whether yellowing is a reliable indicator of polymer degradation, or if more rigorous methods are required.

The focus of this paper will be mechanical property changes and color changes of the matrix materials after exposure to high temperature and high temperature/high humidity environmental conditions. In moist environments, the organic coating preserves fiber strength by serving as a temporary barrier to the passage of water to the glass/coating interface. However, it has been found that in immersion conditions in 23°C water, equilibrium absorption is generally reached within a 1 to 24 hour period. [11] The presence of this water may have a deleterious effect on the polymer by causing hydrolysis. The effects of hydrolysis on a polymer coating have been published, [5,12] and are characterized by a loss in crosslink density. Detection of this crosslink density loss in a polymer coating can be done with a rheometer via Dynamic Mechanical Analysis (DMA). This method generates an equilibrium modulus value (E_0) which is directly proportional to crosslink density. [13] If a coating hydrolyzes, bonds will break and a net decrease in E_0 will be seen when comparing DMA curves before and after aging.

Color changes will be quantified in this paper by using a colorimeter to measure the color in an FMC-2 color space before and after aging. In this method, ΔE values are calculated via the colorimeter software, and these results will be compared with DMA changes after aging.

Experimental

Oligomer Preparation

In the synthesis of the oligomers for the model compositions, special care was taken so that no excess reagents were left unreacted. Exact stoichiometry was used and the mole ratio of HEA:diisocyanate:polyol in each oligomer was identical. The same apparatus was employed throughout: a 1000 ml, 4-neck flask fitted with a teflon paddle stirrer, a thermometer, a reflux condenser, and a gas inlet tube. In each oligomer, titration showed that all of the NCO groups had reacted.

Coating Preparation

The coating formulations A through F (Table I) were prepared by weighing the components into a lined steel can, heating to 60°C in an oven, and mixing with a spatula. The coatings were centrifuged prior to curing to remove air bubbles.

Table I. Compositions of Coatings A Through F

COMPONENT	A	B	C	D	E	F
OLIGOMER 1	70	-	-	-	-	-
OLIGOMER 2	-	70	-	-	-	-
OLIGOMER 3	-	-	70	-	-	-
OLIGOMER 4	-	-	-	70	70	69.5
HDDA	22	22	22	22	22	22
IBOA	5	5	5	5	5	5
HPK	3	3	3	3	-	3
BDMB	-	-	-	-	3	-
STABILIZER	-	-	-	-	-	0.5

HDDA is 1,6-hexanediol diacrylate.
IBOA is isobornyl acrylate.
HPK is 1-hydroxycyclohexyl phenyl ketone.
BDMB is 2-benzyl-2-dimethylamino-1-(4-morpholinophenyl)-butanone-1.
Stabilizer is 4,4' di(α,α-dimethylbenzyl) diphenylamine

Film Preparation

Coatings A through F were drawn down on cleaned 23 cm x 30 cm glass plates using a Pacific Scientific Automatic Drawdown Apparatus. A 75 micrometer Bird draw down bar was used. These films were then cured at a dose of 1.0J/cm^2 using a "D" lamp in a Fusion Systems Curing Unit (Model K523/2) under the N_2 blanket with a flow rate of 230 liters/minute. The dose was measured by an International Light Inc. Light Bug IL 390.

Film Aging

Cured films were aged at 1) 125°C and 2) 120°C/100%RH for a period of seven days. The former condition provided the thermo-oxidative aging environment and it was conducted in a convection oven. The latter condition provided the hydrolytic aging environment and it was carried out in an electric pressure steam sterilizer [12].

Dynamic Mechanical Analysis

A Rheometrics Solids Analyzer RSA II was used to run the dynamic mechanical analysis on the aged and unaged samples. The sample dimensions were 12 mm X 23 mm. The frequency was set at 1.0 radian/second. Before starting a sweep, the sample was preheated to 80°C for a minimum of five minutes in the dry nitrogen atmosphere of the rheometer's environmental chamber to remove water that may be present and which could act as a plasticizer.

Color Measurement

Color measurement data was obtained from a Macbeth Series 1500 Color Measurement System (Model 2020). The colorimeter was calibrated and set to the following parameters:

Illuminant: D for primary and secondary illuminant
Color Difference: FMC-2
Mode:2, COL
Area of Measurement: Large Area View
Specular Component: Excluded (SCE)
UV Filter: Included
Background: White Calibration Standard

Each 3 cm x 3 cm sample square was placed in the viewport using the white calibration standard as a background. Color change was measured after aging versus each sample's respective control.

Weight Change Measurement

The weight change samples for 125°C and 120°C/100%RH were 3 cm x 3 cm. They were preconditioned at 60°C for 1 hour before aging, cooled in the desiccator for 15 minutes, and weighed. After aging at 125°C, the samples were cooled in the desiccator for 15 minutes before reweighing to determine the weight loss. The samples from 120°C/100%RH aging were conditioned at 60°C for 1 hour and then cooled in the desiccator for 15 minutes before reweighing.

Results and Discussion

The initial dynamic mechanical and color data for the six model matrix materials in the cured state are given in Table II.

TABLE II. Initial Data for Model Compositions

Composition	Description	$E'_{1000MPa}$ (°C)	E'_{100MPa} (°C)	E_o (MPa)	Observed Color
A	IPDI/Polyester /HPK	-18.0	22.0	16.0	colorless
B	TDI/Polyester /HPK	-20.0	17.0	17.0	colorless
C	TDI/Polyether /HPK	-20.0	13.0	15.0	colorless
D	IPDI/Polyether /HPK	-23.0	15.5	14.0	colorless
E	IPDI/Polyether /BDMB	-23.0	14.5	13.0	lt. yellow
F	IPDI/Polyether /HPK/stab	-23.0	14.5	14.0	colorless

It can be seen from the rheological data that all six compositions are very similar mechanically. The DMA temperature sweep plot of composition A is shown in Figure 1 and is representative of all six compositions. These compositions are characterized by shallow E' slopes resulting in broad tan δ peaks. This indicates that the compositions have broad glass transition ranges.

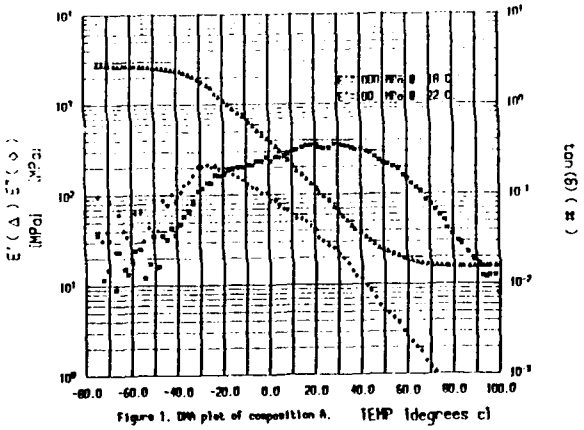


Figure 1. DMA plot of composition A.

Table III shows the quantities obtained from each color reading. The value for X, Y, and Z are measured three-dimensional coordinates in the FMC-2 color space. The quantities ΔRG, ΔYB, ΔC, ΔL, and ΔE are calculated quantities which represent deviations from the unaged control.

TABLE III.
Colorimeter Data for Composition A
Aged for 7 Days at 125°

Parameter	Description	Unaged Control	Aged Sample
X	blue	81	79
Y	red	83	82
Z	yellow	95	87
ΔRG	red-green	NA	3
ΔYB	yellow-blue	NA	7
ΔC	color	NA	8
ΔL	lightness	NA	-2
ΔE	total color	NA	8

For ΔRG, a positive number indicates that the material reddened; for ΔYB, a positive number indicates that the material yellowed. For ΔL, a negative number indicates that the material darkened. Delta C is the square root of the sum of the squares of ΔRG and ΔYB. Delta E is the square root of the sum of the squares of ΔRG, ΔYB, and ΔL. The following results will only include ΔE since it represents the total color deviation from the control. Delta E values less than 1 indicate a color difference which cannot be detected by the naked eye. Higher ΔE values indicate larger deviations from the original color.

The data for the model matrix materials after exposure to 125°C for 7 days are given in Table IV. The data for 120°C/100%RH 7-day exposure are given are Table V. The E_o change data and color change data are shown graphically in Figures 2-5.

TABLE IV.
125°C, 7-Day Data for Model Compositions

Composition	ΔWt. (%)	$\Delta E'_{1000MPa}$ (°C)	$\Delta E'_{100MPa}$ (°C)	ΔE_o (%)	ΔE (Color)	Observed Color
A	-3.5	0	+1.5	-20	+8	pale yellow
B	-3.2	0	+4.5	-24	+22	lt. yellow
C	-5.3	0	+6.5	-37	+33	med. yellow
D	-36.6	+76.0	+61.5	-14	+79	amber
E	-30.2	+54.0	+44.5	-32	+68	amber
F	-2.2	-1.0	+1.0	-7	+9	pale yellow

TABLE V.
120°C/100%RH, 7-Day Data for Model Compositions

Composition	ΔWt. (%)	$\Delta E'_{1000MPa}$ (°C)	$\Delta E'_{100MPa}$ (°C)	ΔE_o (%)	ΔE (Color)	Observed Color
A	-30.7	+39.0	+21.0	-68	+5	colorless
B	-32.9	+36.0	+25.0	-67	+43	med. yellow
C	-3.0	-5.0	-4.5	-45	+14	lt. yellow
D	-2.5	0	0	-14	+2	colorless
E	-0.6	+1.5	0	-8	+4	lt. yellow
F	-2.2	0	+0.5	-7	+2	colorless

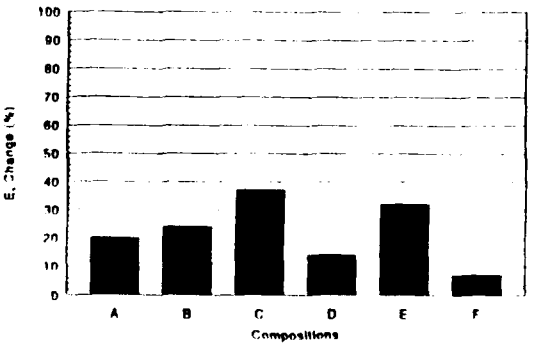


Figure 2. E_o change after 7 days, 125°C

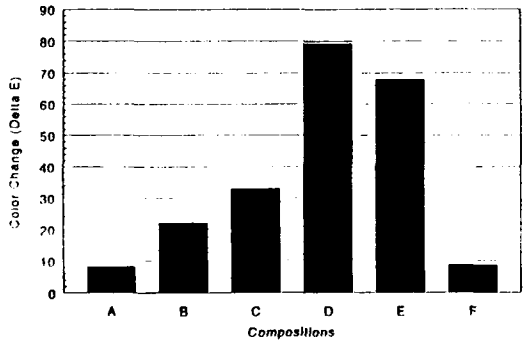


Figure 3. Color change after 7 days, 125°C.

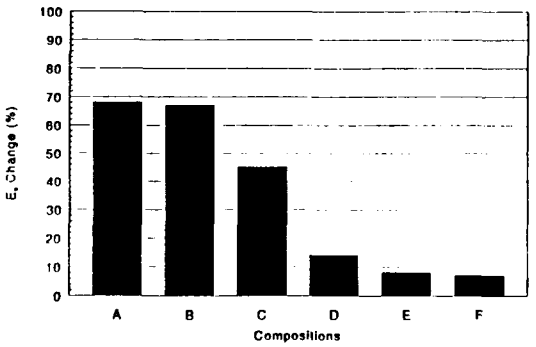


Figure 4. E_o change after 7 days, 120°C/100%RH.

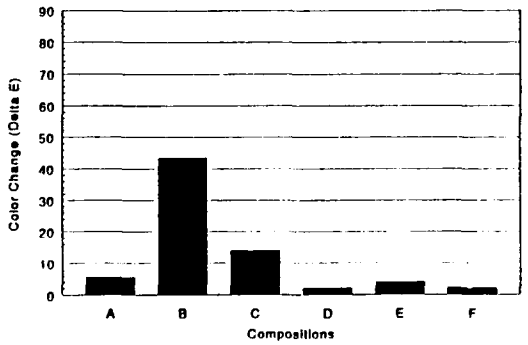


Figure 5. Color change after 7 days, 120°C/100%RH.

First of all, with respect to the 125°C data, it can be seen that there is some correlation between cured film stability and color change. Compositions D and E, which have the greatest weight loss and temperature shift, also have the largest color change. In addition, compositions A and F, which have a minimal weight loss and temperature shift, also have a minimal color change. This correlation is found to be deficient, however, when the E_o values are examined. As stated previously, the E_o values are critically important in that they indicate the material's cross-link density. Major decreases in E_o are signs of bond breakage and decomposition. After one week at 125°C, material C experiences the greatest reduction in E_o, but its color change is only midrange. In addition, material D shows the greatest color change, but its E_o change is the second lowest.

Secondly, with respect to the 120°C/100%RH data, there is even less correlation between cured film stability and color change. Composition B, which has the highest weight loss and second highest E_o change, has the largest color change. But composition A, which has a comparable weight loss, temperature shift, and E_o change, has practically no color change.

While it does appear that a significant yellowing of the cured material can be indicative of major weight losses, temperature shifts, or E_o reductions, this is not always the case. Composition C darkened considerably after 125°C exposure but had a minimal weight loss and temperature shift. Also, composition D darkened greatly at 125°C but had a low E_o change.

It also appears to be the case that other factors influence the amount of color change on aging. Aromatic materials are well known to yellow due to the formation of species with highly conjugated double bonds. Compositions A and B after 120°C/100%RH exposure both show a similar weight loss, temperature shift, and E_o reduction, but the aromatic material B exhibits much greater yellowing than the aliphatic material A.

Conclusions

There is some correlation between stability and yellowing in UV-cured materials. The correlation is weak, however, and the degree of yellowing has been found to be a poor indicator of the material's mechanical and gravimetric stability in accelerated thermo-oxidative and hydrolytic environments. Other factors which influence yellowing, such as the material's aromatic or aliphatic nature, must also be considered.

Acknowledgements

The authors wish to acknowledge Jennifer Chapman, Roger Salvesen, and Carrie Westbury for their aid in the preparation and testing of the samples.

References

[1] P. W. Shumate, "Special Broadband Needs of the Outside Plant," Proceedings of Broadband '89 FOC/LAN, (1989).

[2] G. Kar, "Progress in Optical Fiber Coatings," Proceedings of OFC '88, (1988).

[3] D. Simoff, M. Chan, J. Chapin, and B. Overton, "Thermo-oxidative Aging of a Primary Lightguide Coating in Films and Dual-Coated Fibers," Proceedings of ANTEC '88, 586-589 (1988).

[4] J. Flynn, "Lifetime Prediction for Polymeric Materials from Thermal Analytical Experiments," Proceedings of

ANTEC '88, 930-932 (1988).

[5] D. Szum, C. Chawla, T. Bishop, K. Murray, J. Zimmerman, "Water Sensitivity and Its Relationship to Stability in Optical Fiber Coatings," Proceedings of IWCS '90, 703-714 (1990).

[6] C. F. Cottingham and M. M. Michie, "New Coatings Eliminate 'Fiber Surprise'," Telephone Engineer & Management, November 15, 54-58 (1991).

[7] I. P. Heyward, M. G. Chan, and A. G. Ludwick, "Effects of Antioxidants on the Thermooxidative Stabilities of Ultraviolet Cured Coatings," ACS Symposium Series (Polym. Stab. Degrad.), (1985).

[8] M. G. Chan, I. P. Heyward, D. A. Simoff, P. M. Pruitt, "The Stabilization of UV Curable Coatings for Optical Fibers," Proceedings of the Fourth International Conference on Plastics in Telecommunications, London, U.K. (1986).

[9] D. Szum and R. Salvesen, "A New Method for Measuring the Contribution of UV Cured Coatings towards Color Changes upon Aging of UV Cured Inks," Proceedings of the Sixth International Conference on Plastics in Telecommunications, London, U.K. (1992).

[10] J. I. Kroschwitz et al ed. Encyclopedia of Polymer Science and Engineering, Vol. 4, 630-696, John Wiley & Sons, New York (1986).

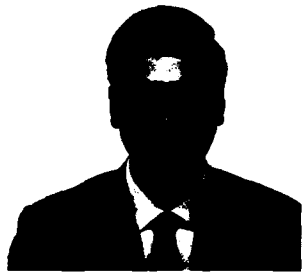
[11] C. Chawla, T. Bishop, D. Szum, K. Murray, "New Test Method for Determining, the Water Sensitivity of Optical Fiber Coatings," Optical Engineering Journal, Volume 30 No. 6, 763-766 (1991).

[12] T. Bishop and D. Szum, "A New Test Method for Measuring Hydrolytic Stability of UV Curable Coatings," Proceeding of Radtech Europe '91, 124-132 (1991).

[13] L. E. Nielsen, Mechanical Properties of Polymers and Composites, Vol. 1, Marcel Dekker Inc., New York, 176 (1974).



Timothy E. Bishop is a senior research chemist at DSM Desotech Inc. He received his BS in chemistry from Illinois State University in 1980. He has been engaged in developing UV curable coatings primarily for optical fiber since 1981. 1122 St. Charles St., Elgin, IL 60120.



Chander P. Chawla received his Ph.D. in polymer science from the University of Southern Mississippi in May 1990. He obtained a master's degree in polymer science and technology from the Indian Institute of Technology, New Delhi, in 1984, and a master's degree in chemistry from the University of Delhi, New Delhi, in 1982. He has been working in the area of fiber optic coatings since October 1989. He is currently a senior research chemist in the optical fiber coatings group of DSM Desotech Inc. 1122 St. Charles St., Elgin, IL 60120.



David M. Szum received an MS in chemistry from the University of Illinois at Chicago in 1989. He is currently a research chemist for DSM Desotech Inc. He has been engaged in research and development of coatings for optical fibers since 1989. 1122 St. Charles St., Elgin, IL 60120.



Erwin S. Poklacki received his Ph.D. in Organic Chemistry from Northwestern University in 1961, after receiving his bachelor's degree from Loyola University of Chicago in 1957. He has been working in polymer chemistry in synthetic rubber, plastics and coatings. He is currently a senior research associate in the Optical Fiber Materials Group of DSM Desotech Inc. 1122 St. Charles St., Elgin, IL 60120.

THE L^4 SPLICE - A NEW MECHANICAL OWG SPLICE

L. Finzel, L. Mendat, G. Boscher

Siemens AG / RXS Schrumpftechnik-Garnituren GmbH
Munich / Hagen, Germany

ABSTRACT

In the immediate future, the extension of the fiber optic telecommunications network will demand a splicing method to achieve optimal values of attenuation with a minimum of cost and material. To fill this need, a novel crimp splice has been developed which offers high quality and reliable joining technique for single-mode and multimode fibers. It can be installed on site using a simple work station. Practice oriented field trials have proven the field suitability of this splice. Due to its easy handling, this new splicing method is rapidly accepted by the installing craftsmen.

This paper details the L^4 Splice dealing specifically with its design, function, and preferred fields of application.

FEATURES OF THE L^4 SPLICE

The L^4 Splice (Fig. 1) is designed to rapidly join single-mode and multimode optical fibers with a coating diameter of 250 µm under field conditions. It is based on a non-positive joining technique which guarantees reliability and long life expectancy. The low demand of fiber length and very easy assembly open up new prospects for the application of this novel mechanical joining method.

Unlike conventional mechanical connectors, optical fiber ends no longer require preparation when using our newly developed splice. There is no further need for adhesive or grinding. Fiber ends are simply cut to length by means of a conventional cleaver and are then inserted into the single-fiber splice. The optical fibers are optimally aligned and joined through a crimping principle which causes plastic deformations of integrated fish joints of the inner and outer U-profile of the splice to fix the fiber ends (Fig. 2).

Its compact size makes it possible to organize up to twelve splices in one splice tray.

In addition to the usual connection of single-mode or multimode fibers in joining and distribution closures, this splice can also be employed in the branching area of passive optical networks (PON). If branch splices must be made in pre-existing cable networks, a simple splicing technique is preferable.

Existing fusion splicers take up significant room and additional lengths of fiber for splicing. The present looping method used when employing conventional splicing techniques requires very long closures, which can sometimes be difficult to house in distribution cabinets or manholes due to lack of space. The L^4 Splice requires only a minimum of fiber length and can thus be installed in conventional closures.

It provides an ideal joining device for all jumpering and distribution points in the fiber optic cable network as it is easy and quick to assemble. It can also be used as a fast and reliable repair splice, and its space-saving design allows this splice to be used as an inexpensive choice in customer premise applications.

FUNCTIONAL PRINCIPLE OF THE L^4 SPLICE

The tolerances observed during the manufacture of optical fibers guarantee a sufficiently accurate centering of the fiber cores through the cladding glass. The alignment of the optical fibers to be joined can be done very easily. The two fiber ends - and thus also the fiber cores - are aligned via their outer diameter in a continuous V-groove which constitutes the heart of the splice.

This unique splice measures approximately 31 mm in length and is of almost square outer dimensions (width 4 mm x heigth 5 mm). It consists of two U-shaped metal profiles which have been perfectly bonded at the factory.

This mechanical splice works on a clamping principle: two U-shaped profiles made of identical metal are inserted into each other so that the optical fiber is fixed between them. A high-precision V-groove is pressed into the outer U-profile forcing an absolutely accurate fiber alignment.

The V-groove is funnel-shaped at its ends both to accomodate the coating and to facilitate the insertion of the fiber. The bottom side of the inner U-profile is plane so that fiber guidance is absolutely accurate. The optical fibers are thus largely protected against environmental and accidental mechanical strain.

The fiber ends are fixed within the splice by plastic deformations of integrated fish joints of the inner and outer profiles simultaneously. The resulting elastic spring force fixes the fiber ends in an aging-resistant way even at high tensile forces.

The outer fish joints only serve to keep the inner and outer part together (Fig. 3).

A metal-only construction guarantees a long life expectancy and reliability. The selection of corrosion-proof material allows for chemical resistance and temperature independence. The stable mechanical construction also serves as "kink-protection" and ensures easy and vibration-safe handling and storing.

The splice has been pre-loaded with index matching gel at the factory. Since its refraction index has been adapted to the core glass, the gel guarantees good insertion losses in addition to high return losses and excellent long-term stability.

SPLICING PROCEDURE WITH THE L^4 SPLICE

Splicing optical fibers is extraordinarily easy using the L^4 Splice. A common stripper is used to remove the coating from the fiber. The cladding area is cleaned of dirt or coating remnants with an alcohol-soaked cleaning tissue. Cleaving of the fibers can be done with any customary cleaver, however a bare fiber length of approximately 6 to 7 mm should protrude under the coating. The cleaving length can be sufficiently observed through a simple optical mark. The prepared fiber is then inserted into one end of the splice. The funnel-shaped ports at both ends of the splice allow the fiber to be inserted easily.

The fiber can easily be pushed forward between the U-profiles until the fiber end is located in the splicing area. The funnel-shaped V-groove facilitates insertion. On each end of the inner U-profile there is a recess for taking up the coating. This graduation puts a stop to the coating end. The coating can not be pushed beyond the recess and the fiber ends will thus be spliced in the plane part of the inner U-profile.

After preparing the second fiber end accordingly, this one is also inserted into the splice. A low splice attenuation can be obtained, if both fiber ends are positioned as closely as possible. To achieve this, the second fiber end should be kept under axial tension. It is therefore advisable to hold the fiber in a loop and to support it by hand.

Crimping the fish joints to their provided stop concludes the splicing procedure. The optical fibers to be joined are thus optimally aligned and mechanically strain-relieved (Fig. 3).

During the crimping procedure, the optical fiber in the cladding area is pressed into the V-groove. The fibers are fixed within the splice by the elastic spring force of the legs of the U-profiles which are activated during the crimping procedure.

SPLICING WITH THE WORK STATION

The work station serves to prepare the fiber ends for splicing. This is done in individual steps, including the removal of the coating and cleaving of the fiber ends. The prepared fiber ends are then inserted into the splice, which has previously been mounted to the work station. A stop incorporated into the splice ensures that all preset assembly parameters are observed. The fiber ends are then fixed during a final crimping procedure: a movable formed piece is lowered to permanently shape the inner U-profile (Fig. 4).

RESULTS OF INSTALLATIONS PERFORMED WITH THE L^4 SPLICE

Tests carried out in laboratories and in the field according to Bellcore TR-TY-000765 have shown that the obtained values of attenuation scattered only slightly. This guarantees a sound repeatibility of the splice results (Fig. 5). The insertion losses were measured with single-mode fibers at 1300 and 1550 nm, but showed no considerable deviations. The return loss exceeds 40 dB. The splice shows constant behavior in climatic and vibration tests as well as during storage in water and ice.

Without great technical effort, this novel splice offers a quick and reliable splicing method for a wide range of applications, such as repair, branch-off, termination, and distribution.

PROSPECTS FOR THE L^4 SPLICE

In addition to the above areas of application, the splice also offers optimal features for jumpering points where flexibility is demanded. All incoming and outgoing fibers can be joined in a reliable, easy, and cost-conscious way, according to requirements. The present concepts of fiber optic overlay networks shows that frequent jumpering will become essential at cable termination racks, terminal boxes, and cross connecting facilities. Therefore, a handy and easy to install splice is one of the indispensable prerequisites for a flexible fiber optic overlay network.

In feeder cable networks, this splice offers the advantage of minimum fiber splicing length. Therefore, looping is possible while retaining the existing cable accessories. Productivity can be enormously increased by automatic splicing procedures of pre-magazined splices; one of the future goals.

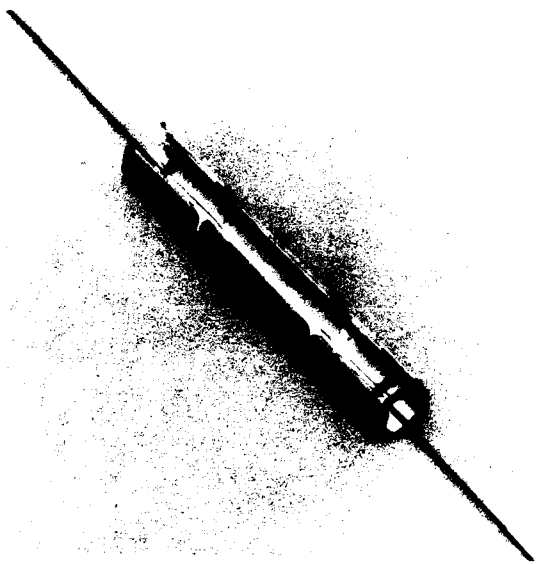


Fig. 1: L^4 Splice: General view

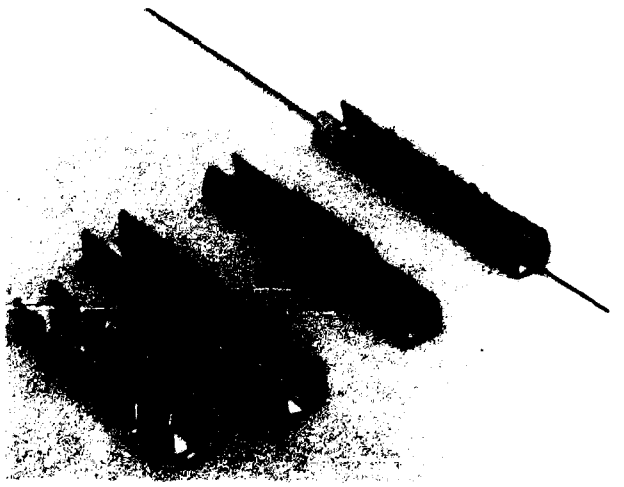


Fig. 2: L^4 Splice: Components

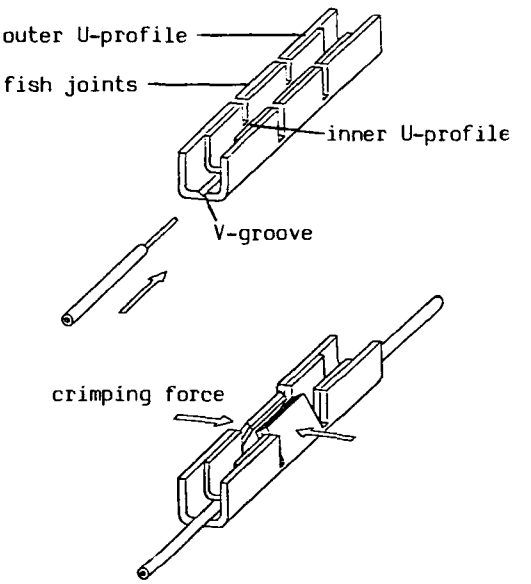


Fig. 3: Schematic splice procedure

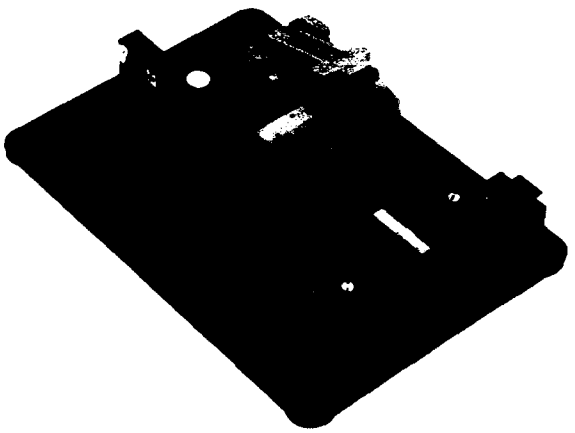


Fig. 4: Work station

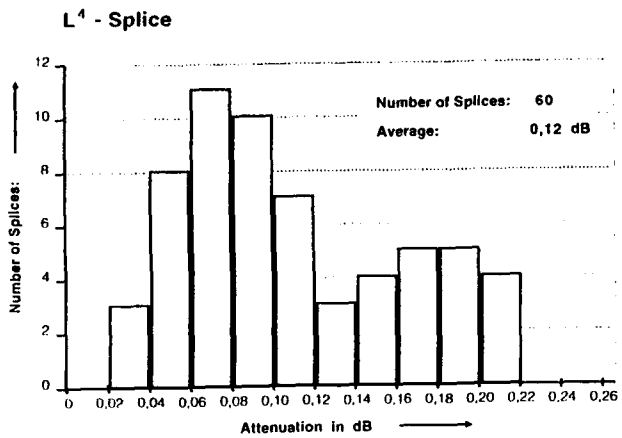


Fig. 5: frequency distribution of the splice loss



Leonard R. Mendat has been working for RXS Schrumpftechnik-Garnituren GmbH as Manager of Sales and Marketing for North America since 1989. Over the last 20 years he has been involved with outside plant telecommunication sales, marketing and product development.



Lothar Finzel received his diploma degree in mechanical engineering from the Technical University of West Berlin in 1984. Since then he has been employed at Siemens AG, Munich, where he at first worked on copper cables. Since 1987 he has been responsible for the development of mechanical splicing equipment for fiber optic cables.



Georg Boscher received his diploma degree in physics from the University of Munich, Germany in 1967. He joined Siemens AG and worked for several departments. In 1970 he became responsible for the development and testing of accessories in the Telecommunications Cable Division. Since 1985 he has been working as a deputy director and head of Marketing and Management of RXS Schrumpftechnik-Garnituren GmbH, a fully-owned subsidiary of Siemens AG. RXS manufactures and markets accessories for the telecommunications and power industries.

UNIVERSAL JOINTING FOR OPTICAL FIBRE UNDERSEA CABLES

C A Gould D J Tibbetts

BT Labs, Martlesham Heath, Ipswich, Suffolk, UK

ABSTRACT

This paper describes a Universal Jointing technology for optical undersea cables. A common joint housing is designed to mechanically terminate cable ends, provide safe storage for fibres and fibre splices and provide electrical continuity and insulation for the cable conductor. A cascaded ferrule assembly, specially adapted to each cable type fits into the common housing and grips all essential cable elements and isolates the fibres from any mechanical strain. An essential part of this jointing system is a set of equipment to assemble the joint; including fibre splicing, polyethylene moulding and ferrule pressing. The jointing system accommodates both lightweight and armoured cable types. A test regime, to prove the jointing system can meet all operational requirements is discussed, and sample results presented.

1. BACKGROUND

In 1986, the TAT-8 transatlantic cable system was a major milestone in optical fibre undersea cable technology insofar that American, British and French cable suppliers each provided a different cable structure to an undersea branching unit in the eastern Atlantic sector. At that time cable maintenance relied upon three different jointing methods used by the three maintenance authorities involved, AT&T, BT and France Telecom. In 1992, with the advent of TAT-9, a three supplier five landing point system, the complexity of maintenance became a major problem. This problem was solved by the concept of Universal Jointing which allows any ship from any maintenance depot to sail to repair any cable or repeater fault anywhere in the entire system.

2. INTRODUCTION

From October 1989, representatives from AT&T-USA, BT-UK, and Submarcom-France, met several times to discuss the technical and commercial feasibility of combining their jointing technologies to produce a common Universal Jointing system. Because of the three AT&T undersea branching units used on TAT 9 it was a great advantage to extend the jointing capability to the coupling of the repeater housing. All the parties of the consortium had an established cable jointing technology mainly based on the cable types produced by their domestic supplier. After careful consideration of the best features of these jointing equipments, items were chosen to give an effective tripartite technical solution.

Thus, by providing a single common jointing system, the cost of system maintenance can be reduced. The Universal jointing solution increases technological capability, improves system configuration flexibility, operator utilisation and reduces capital and recurring expenditure of cable stock and joint consumables.

3. ADVANTAGES OF UNIVERSAL JOINTING

The key feature of the Universal Joint is that it allows any cable from any supplier to be connected to it independently of the cable connected to the other side. The critical development is the cascaded ferrule assembly which enables the following technical and commercial advantages:

a. Shipboard installation or repair joint
b. Repair possible from any cableship.
c. Single set of unified joint equipment.
d. Commonality of jointer training.
e. Reduced jointer requalification.
f. Independance from original supplier.
g. Easy accommodation of new cables.
h. Suitable for repeater termination.
i. Ability to mix suppliers' cables.
j. Suitable for land or beach joint.

4. THE UNIVERSAL JOINT DESIGN

The majority of transoceanic undersea optical fibre cables are similar in generic design, but vary in detail. They comprise a fine piano wire around which are laid the optical transmission fibres, generally protected by some soft polymer.

This fibre package is central within a steel wire strand structure for tensile strength in combination with a copper tube for hydrostatic pressure resistance. All the metallic components are in contact to give a parallel DC power feed path for the series fed repeaters. Because of the resultant high system voltage the cable is insulated with polyethylene, and generally to a diameter of about an inch to ease shipboard handling. The Universal Joint has been designed to accommodate all these features and is shown in figure 1.

For applications in continental shelf areas or where trawl fishing or anchor damage is prevalent, additional steel wire armour protection is added to the cable. This is typically in the form of one or two long lay helical wire layers creating considerable extra strength against breakage. A typical shallow water armoured Universal Joint that reinstates the strength of the cable is shown in the figure 2.

5. CASCADED FERRULE ASSEMBLY

The ideal joint terminates all the elements of the cable so effectively that the discontinuity of the joint maintains original cable performance. In order to achieve this, each of the layers of the cable construction must be dealt with in such a way that each of them maintains its original purpose and is restrained from relative movement. The cascade ferrule assembly achieves this and is engineered specifically for each particular cable structure. The essence of the technique is to systematically secure every element of a given cable structure in a series of up to four cascaded clamp elements. They may be used to either prevent relative movement, through solid clamping, or control it, through for example sliding mechanisms, so that the design characteristics of the cable are mirrored. This ensures that the performance characteristics of the cable are maintained rather than compromised to produce an easier joint design. This cascaded ferrule assembly is constructed independently of the other cable to which it is to be eventually joined. Thus the destiny of the cable end need not be determined when it is terminated.

The strand strength is held by a crimped ferrule body with a hardened central insert to prevent crushing of the optical fibre package. The mechanics of the ferrule and its construction method are modified to suit the cable design and will secure a one, two or three wire layer strand to full dynamic fatigue and static strength performance. Copper, aluminium and steel power feed tubes are clamped as well as the fibre package and kingwire. In some cables the fibre package or kingwire exhibit a differential movement within the cable structure, possibly giving rise to kingwire or fibre buckling and transmission loss during subsequent reduction of the load or cable twist. The cascaded ferrule assembly is the only solution known which prevents this particular problem occurring.

6. THE COMMON COMPONENTS

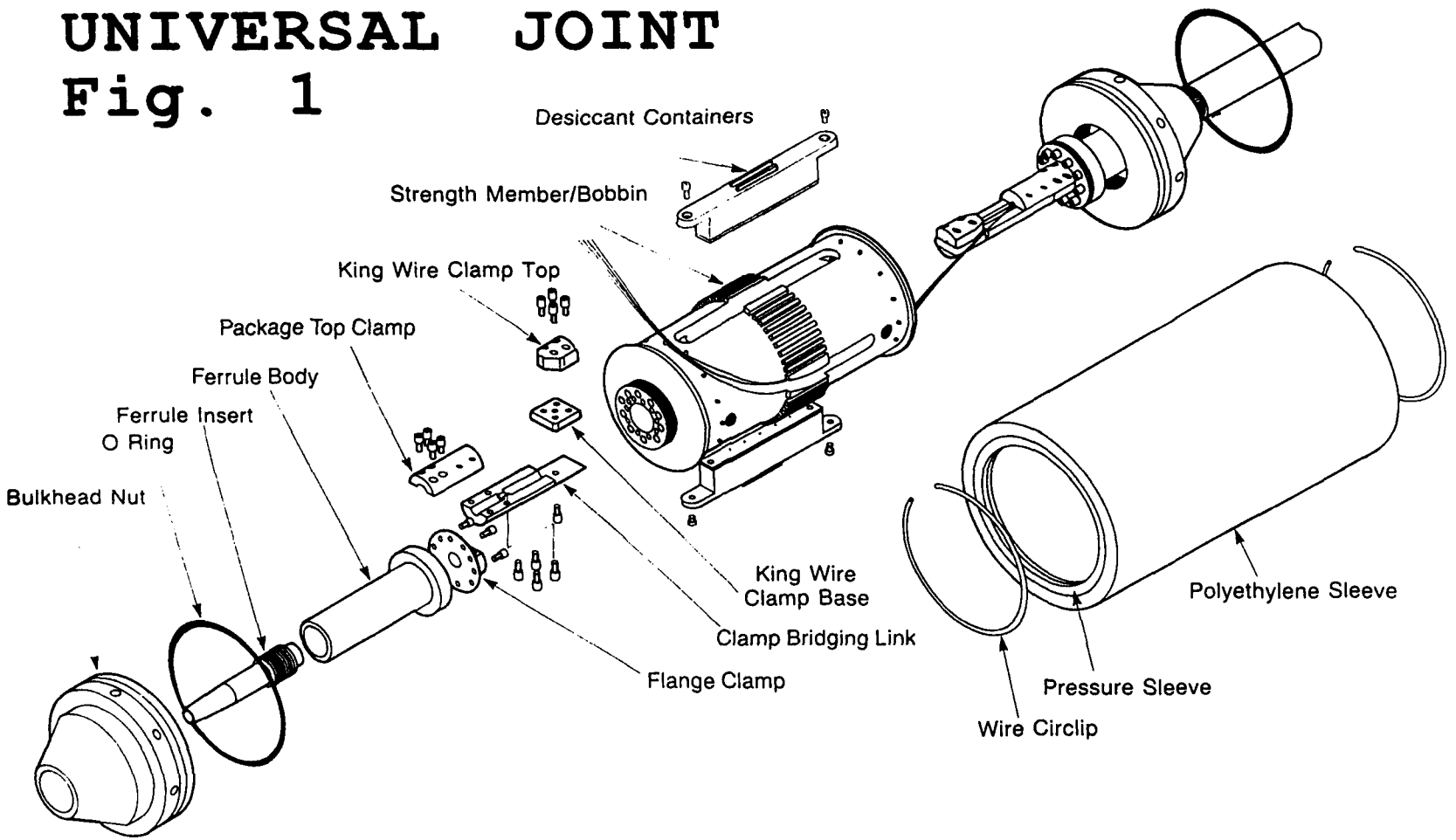
The design is based upon compatible components common to any joint or coupling, so that any chosen combination of two cascaded ferrule assembly cable ends can be assembled to create a joint. One of the novel parts of the design is the single central strength member or bobbin which provides mechanical integrity in tension, compression and torsion as well as the storage for sufficient fibre for repeat attempts at splicing, should they be necessary. The bobbin coupled with bulkhead nuts and a polyethylene covered steel tube provide the hydrostatic pressure resistance. The splicing arrangement will accommodate 40 or more splice positions with attenuators if needed. The polyethylene insulant is hot injection moulded to the parent cable with allowance for low, medium or high density extrudates with or without carbon black. Jointing between identical and differing suppliers' cable types is then possible. Single double or rock armour external wire protection layers are similarly accommodated in a unified armour press based on a cone and collet system.

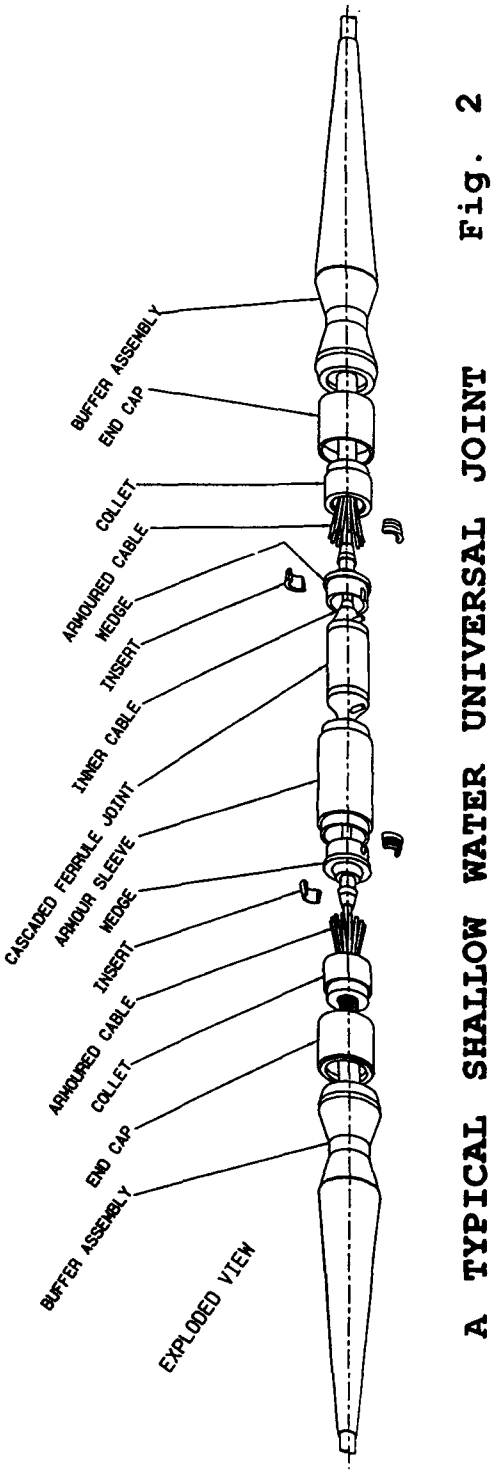
Independent cable end preparation confers a very powerful capability. Each cable end is prepared using a set of specific cascaded ferrule components together with a set of common components. Provided it is suitably protected it can then be stored until its final destination is decided. Having been assembled into a joint it is also possible to disassemble and connect to a different cable.

7. THE MODULAR APPROACH TO TESTING

The cascaded ferrule assembly is the only sub-assembly specific to a particular manufacturer's cable design. The same applies to the pigtail termination, where the cable is connected to a repeater housing. Each armour wire structure has its particular set of cone and collet clamps. The only dependence between any two cables or pigtail is the fibre splicing and the polyethylene reinstatement moulding. If a new cable system includes a cable type or one not already included in the universal joint

A TYPICAL DEEP SEA UNIVERSAL JOINT
Fig. 1





A TYPICAL SHALLOW WATER UNIVERSAL JOINT Fig. 2

list of qualified combinations, specific modification of the joint cascaded ferrule assembly would be required. Checks would be required on fibre types and the polyethylene and a limited re-qualification of fibre splices and the moulding would be needed.

Qualification of the constituent elements can be done separately. The test modules indicate that the kingwire or fibre type can be changed within the cable structure, or the grade of polyethylene insulant or sheath. The implication of these changes to materials is that requalification is only necessary to solely address the changed aspect, since the mechanical performance of the cable structure or the joint or coupler will be unaffected. This individual application of design, development, construction and testing is termed modularity. A consequence of this is that much testing work, time and cost can be saved. An example is that many of the coupler tests are common to the joint tests and thus need not be duplicated. Testing experience has shown that like to like cable qualification tests need not be done provided that the worst case unlike cable interconnections are tested.

Finally a modified joint would need to be constructed and tested to qualify it on any new type of cable. The range of qualification testing would not need to be as great as the original testing as aspects like hydrostatic pressure resistance, bump and vibration performance and plough compatibility have already been established.

8. MARINE PERFORMANCE OF THE DESIGN

The Universal Joint concept and implemention is designed to be suitable for shipboard and factory jointing. The shipboard capability has to safely withstand the rigours of handling associated with installation, recovery and repair with no change to the existing nations' cableships.

The Universal Jointing system has no special requirements in respect of temperature, humidity, air flow, cleanliness, vibration or power resources in terms of electricity, water or air supplies that are not commonly available on most cableships. All the tools and equipment for the Universal Jointing system are capable of transportation in a standard container of dimensions 40 foot by 8 foot by 8 foot. The system can therefore be easily transported to specialist jointing locations.

All current and proposed variants of the joints are ploughable, using known sea ploughs, insofar that no rigid dimension exceeds 40 inches in length or 5.5 inches in diameter. Based on demonstrated achievements to date, the target for construction for a lightweight joint is within a 12 hour shift. The Universal Jointing system has sufficient commonality and flexibility such that a cable end can be tested, capped and laid as a shore end earth seal or buoyed off, and then later used to construct a joint into any of the qualified cable variants.

The qualification work described below ensures maximum marine operating conditions worldwide in respect of deep ocean depths, temperature variation and tensile performance. This 100 manyear project has come to fruition to set a world standard in marine performance and operational flexibility.

9. QUALIFICATION TESTS

Based upon individual operational experience in the field, each of the contributors to the universal joint has collectively created a qualification test specification. Each specification has been critically reviewed with regard to suitability of tests and the applied range of values. It is the combined knowledge of these technical experts that the resultant proposed list of tests is deemed necessary and sufficient to assess the various products independently against all currently known or anticipated failure mechanisms. The range of tests evaluates both the joint or coupler mechanically, the fibres for transmission performance and the insulant and sheath for electrical properties.

Each variant of the joint or coupler which has been qualified complies with submerged plant specification requirements for the systems for which it is specified, in respect of:

a) Pressure resistance to 5 nm water depth
b) DC power feed at 2 amps and 10 kV, resistance less than 0.1 ohms.
c) Design Life of 25 years in regard to transmission loss, high voltage life performance and marine corrosion.
d) Thermal range 0-35°C operationally and -20 to +40°C for storage.
e) Mechanical handling demonstrated with a range of tensile tests, flexure test and torsion test as well as passage through and around simulated ship laying and recovery equipment, on a 3 metre diameter sheave with angles of lap of 90 and 135 degrees.
f) Tensile fatigue has been demonstrated for a duration of 48 hours, which represents three times the joint construction time plus an allowance for system test time.
g) Demonstration of bump and vibration capability.
h) Transmission loss through any variant of interconnection joint has been demonstrated to be better than 0.05 dB per splice of any fibre path, where characteristic cable losses are not incurred.
i) No tests are required for any cable compatibility problems that are not joint related and are therefore contained within the devlopment brief of each cable supplier.

10. CONCLUSION

The Universal Jointing system has been developed by a consortium of AT&T, BT and Alcatel Cables for a number of international optical fibre undersea cable systems. This enabling piece of technology allows a large variety of cables to be terminated in a common jointing technology. The Universal Jointing system is a powerful enabler for all undersea cable repair maintenance authorities worldwide to have a unified and flexible repair policy. This provides a more cost effective solution than existing technologies based solely on equipment from cable suppliers. This development has been successfully deployed in TAT 9 and a variety of other undersea cable systems which are now operational. The Universal Joint solution is now being seen by many of the world's cable suppliers as a World Standard to which there is a driving commercial need to establish compatability.

ACKNOWLEDGEMENTS

The TAT 9 owners are acknowleged for their vision and support in being the first to adopt Universal Jointing.

The valuable technical expertise and cooperation of the undersea systems engineers at AT&T Bell Labs, BT Labs and Alcatel Cables has enabled the concept to come to fruition.

The coordination and support of BT (Marine) Ltd has enabled the commercial exploitation of the product range worldwide.

AUTOBIOGRAPHY

Tony Gould joined BT at Dollis Hill, London in 1972 after receiving a BSc (Eng) at Leeds University. He has been involved in many aspects of cable design and development. Having initiated the concept of Universal Jointing he now leads the team to engineer the development for commercial systems.



David Tibbetts joined BT at Martlesham Heath in 1987 after reading a B Eng (Hons) from Oxford polytechnic and earlier experience as a production engineer. He has been involved in a diversity of cable and jointing aspects, most recently on specific design and development of additional Universal jointing products.



Optical Fiber Stresses Produced During Storage in Splice Organizers

P. B. Grimado, L. A. Reith and A. Pellegrino

Bellcore, Morristown, New Jersey, USA

ABSTRACT

Reliability of optical fibers requires that in-service mechanical tensile stress be much lower than the fiber proof stress. When fibers are looped for storage in splice tray organizers, large tensile stresses can be introduced in the vicinity of the splice through a twisting moment or torsion. The fibers that have experienced these high stress levels are coated with a polyester elastomer to an overall diameter of 900 μm and are used with splices that directly grip the bare fiber without strain relief. To quantify the stresses produced in the fibers at these potentially vulnerable splice points, a series of torsion tests in concert with analyses were conducted. The analyses required the development of a large displacement, three-dimensional finite element model. Torsion tests of straight lengths of partially stripped fibers showed that decoupling of the coating occurs at the coating/bare fiber interface, increasing the effective stripped length and reducing the torsional moment transmitted to the bare fiber. The results of the finite element model are in good agreement with experiments. The model also indicates that the torsional test criteria produce stresses consistent with spliced-fiber storage stresses and therefore can be used to assess the sensitivity of splices in splice tray organizer assemblies.

1. Introduction

In the past few years, a number of mechanical fiber failures have been reported [1]. Most of these failures have occurred in the vicinity of a splice. This area is particularly vulnerable because the protective coatings are removed and the bare fibers are handled directly. In handling and stripping, microscopic surface flaws can be introduced which can precipitate failure under relatively low stresses. Many of the reported failures displayed a fracture surface in the form of a conical spiral that resembles the failure mode of a piece of chalk when exposed to a torsional moment [2]. Consequently, if not solely responsible, a torsional stress component was at least significantly present. These failures have generally appeared in splices that directly grip the glass fiber. Fibers with a 900 mm tightly-buffered polyester elastomer coating were particularly susceptible to these failures because of the coating's relatively large stiffness. A torsional moment is applied to the spliced fiber whenever the splice assembly is secured in a splice-tray organizer and the excess fiber is stored [1]. Basic information on the susceptibility of splices to torsion was obtained through a series of static and dynamic torsion tests and reported in [1]. These tests simulated a splice arranged in a organizer assembly while a controlled twist was applied as shown in Fig. 1. The number of twists required to produce failure was recorded for fibers with different coating materials and coating thickness. Since the geometry of the fiber undergoing the test is complicated, the stress at failure is not easily computed. To analyze this test method, which gives rise to large displacements, a nonlinear, 3-dimensional, finite element model was developed.

In this paper a brief description of the finite element model is given in Section 2. In Section 3, the results of torsion tests on straight optical fibers with partially stripped lengths are presented. The finite element model is used to analyze the stress state of the fiber when exposed to the torsional test procedure shown in Fig. 1. This state of stress is then compared to the expected long-term storage stress in a typical splice tray organizer in Section 4. Finally, Section 5 includes a summary and conclusions.

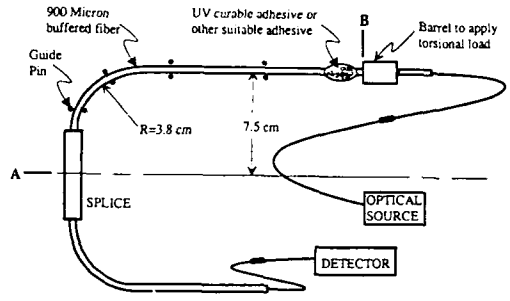


FIG. 1 : TORSION TEST APPARATUS

2. Three-Dimensional Finite Element Model

The optical fiber is considered an elastica with small deformations and large displacements. Initial configurations with curvature are constructed with a series of straight-beam elements oriented end-to-end to approximate the curve. A single beam element, Fig. 2, has 2 nodes, one at each end, and 6 degrees of freedom per node, 3 displacements and 3 rotations. The nodal forces consist of an axial force, 2 shear forces, a torsional moment and 2 bending moments.

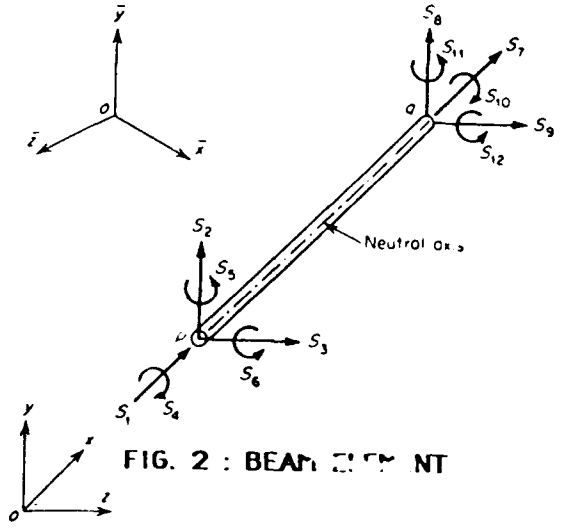


FIG. 2 : BEAM ELEMENT

Representing the nodal displacements in terms of polynomials:

$$u(x) = u_A (x_B - x)/L + u_B (x - x_A)/L$$
$$\omega(x) = \omega_A (x_B - x)/L + \omega_B (x - x_A)/L$$
$$w(x) = w_A \varphi_1(x) + w_B \varphi_2(x) + \phi_{zA} \varphi_3(x) + \phi_{zB} \varphi_4(x)$$
$$v(x) = v_A \varphi_1(x) + v_B \varphi_2(x) + \phi_{yA} \varphi_3(x) + \phi_{yB} \varphi_4(x)$$

where

$$\varphi_1(x) = 1 - 3(x - x_A)^2/L^2 + 2(x - x_A)^3/L^3$$
$$\varphi_2(x) = 1 - 3(x_B - x)^2/L^2 + 2(x_B - x)^3/L^3$$
$$\varphi_3(x) = (x - x_A) - 2(x - x_A)^2/L + (x - x_A)^3/L^2$$
$$\varphi_4(x) = -(x_B - x) - 2(x_B - x)^2/L + (x_B - x)^3/L^2,$$

u(x) is the axial displacement, w(x) and v(x) are the transverse deflections in the y and z directions, ω(x) is the angular twist, ϕ_y and ϕ_z are the angular rotations in the y and z directions, respectively, L is the length of the beam element and subscripts A and B designate parameter values evaluated at element nodes. These displacements are used to form the total energy expression of the beam element [3,4]. Equilibrium of the beam element is established by determining the nodal displacements that minimize the energy. This leads to 12 equations for the 12 unknown nodal displacements in local coordinates:

$$[K_l][u_l] = [F_l] + [P_l] + [F_l^{rt}] \qquad (1)$$

where $[K_l]$ is the local beam stiffness matrix [3,4], $[u_l]$ is the nodal displacement vector, $[F_l]$ and $[P_l]$ are the applied force and nodal reaction force vectors, respectively, and $[F_l^{rt}]$ is the rotational force vector required to correct for shrinking or lengthening of the element in the presence of a rigid body rotation [5]. When forming shapes using many elements at different orientations, all nodal displacements and forces are referenced to a fixed common system called the global coordinate system. The matrix equation for the beam element is reached using a transformation of the stiffness matrix [4]:

$$[K_g] = [\lambda]^T [K_l][\lambda]$$

where $[\lambda]$ is the transformation matrix and the superscript T specifies the transpose of the matrix. Consequently, eq. (1) in the global system is written as:

$$[K_g][u_g] = [F_g] + [P_g] + [F_g^{rt}]$$

The reaction forces at the internal nodes cancel when assembling an entire structure and therefore the matrix equation for the whole structure is:

$$[K][u] = [F] + [F^{rt}] \qquad (2)$$

where $[K]$ is the global stiffness of the whole structure, $[u]$ is the global nodal displacement vector, $[F]$ is the global applied force vector and $[F^{rt}]$ is the rotational load vector for the whole structure.

Equation (2) can be used whenever the displacements are small. However, when the motion is large, such that the geometric shape of the structure changes considerably during a load application, it is necessary to apply the load gradually and compute incremental displacements. At each incremental load application, the global stiffness is re-evaluated to compensate for the changed geometry. This results in the following equation for treating these geometric non-linearities:

$$[K_{n-1}][\delta u_n] = [F_n] + [F_{n-1}^{rt}] - [S_{n-1}]$$

where $[K_{n-1}]$ is the global stiffness of the structure after n-1 incremental load applications, $[S_{n-1}] = \sum_{i=1}^{n-1} [K_i][\delta u_i]$ is the matrix of cumulative internal nodal resisting forces and $[\delta u_n] = [u_n - u_{n-1}]$ is the incremental change in displacement from the previous load application.

For the optical fiber configurations considered, an additional nonlinearity occurs because of the restricted motion of the fiber within a splice tray organizer or the displacement constraints provided by the rigid guides shown in the torsional test apparatus of Fig. 1. Hence, this finite element program checks the location of each node at every incremental load cycle for contact with any rigid constraint. When contact is indicated, the affected nodes are fixed and the calculation is repeated. Subsequent incremental load cycles then require at least two iterations. The first iteration is performed to check the status of the nodes in contact with the barrier. This calculation is carried out with the affected nodes free. If continued barrier contact is indicated, the cycle is repeated with the nodes fixed; otherwise the results are accepted.

3. Torsion Tests on Straight Optical Fibers

Torsion tests were performed on commercial 125 μm diameter fibers. The fibers had an inner, multi-layer, protective acrylate coating with a thickness of approximately 187.5 μm and a tightly buffered 200 μm thick overlay. The overall diameter was therefore nominally 900 μm. A 23 cm (9 in) gage length was used for all tests. Since coating materials exhibit nonlinear behavior, unstripped fibers were twisted to quantify this attribute for inclusion in the finite element model. The torque versus twist per unit length data obtained from these tests were approximated by 5 linear segments in the model. Figure 3 is a plot of the experimental data and the finite element model. Good agreement between model and experiment is seen, indicating that the nonlinear properties of the coating have been modeled correctly.

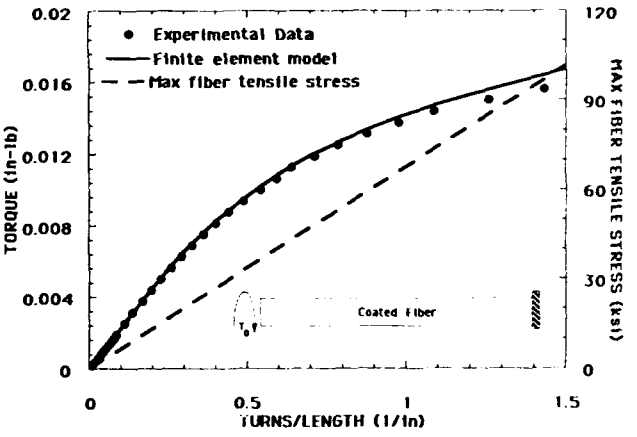


FIG. 3 : TORSION OF TIGHTLY BUFFERED 900 micron UNSTRIPPED POLYESTER ELASTOMER COATED FIBER

Torsion tests were also conducted on configurations that simulate a grip splice entry condition. One end of the fiber was stripped, and the splice gripping mechanism was simulated by using an epoxy adhesive to adhesive to attach a glass or copper capillary tube to the end of the stripped length [6]. Stripped sections of 35 mm, 15 mm and 2 mm were examined. Test data are plotted in Fig. 4 with the finite element model results. Notice that the model predicts a much stiffer response for all 3 cases because it is assumed that the glass fiber and layers of coating twist in unison. This is apparently valid for torsion of unstripped fiber but not true when a portion of the coating is stripped off. It is known that an abrupt cross-sectional change produces a shear stress distribution between the glass fiber and coating [7]. This shear stress is developed to allow a redistribution of the torque between the coating and glass. It is expected that the maximum shear stress occurs at the point of abrupt cross-section change and decays rapidly with distance. The first layer of coating,

an acrylate polymer that adheres to the glass, is typically compliant. Therefore it appears reasonable to expect that in the vicinity of the maximum shear, a decoupling of the glass and coating occurs. Under this condition, the torsional stiffness decreases and the fiber behaves as though the stripped length has increased.

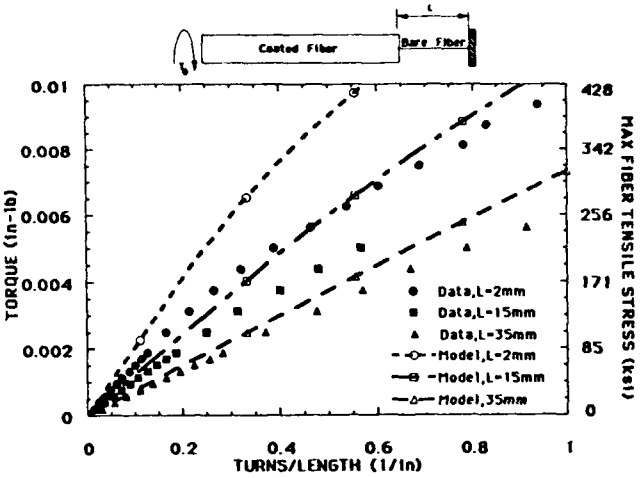


FIG. 4 : TORSION OF TIGHTLY BUFFERED 900 micron STRIPPED POLYESTER ELASTOMER COATED FIBER

Using elementary strength of materials [2], an equation for estimating the effective stripped length is obtained in the form:

$$(L_g)_{eff} = \frac{(GJ)_g L\{1/(GJ)_0 - 1/(GJ)_T\}}{\{1-(GJ)_g/(GJ)_T\}} \qquad (3)$$

where $(L_g)_{eff}$ is the effective stripped fiber length, L is the total length of stripped and unstripped fiber, $(GJ)_g$ is the torsional stiffness of bare glass fiber, $(GJ)_0$ is the elastic torsional stiffness of the partially stripped fiber from Fig. 4, and $(GJ)_T$ is the elastic torsional stiffness of the unstripped fiber from Fig. 3. Using eq. (3), the effective stripped length is found to increase an average amount of 5.8 mm (0.228 in) for the 3 sets of partially stripped fibers tested. The test data indicate that this effect takes place at low torque. Therefore, for all practical considerations, it can be taken to occur instantaneously. The fact that the effective stripped length increased the same for the 3 cases tested explains why the shortest stripped length (2 mm) shows the largest discrepancy with the model, because this represents a larger percentage of the original length of bare fiber.

It is not possible to observe this effect visually. However to check this hypothesis, a second series of torsion tests were conducted. For these tests an epoxy adhesive was placed at the edge of the stripped section to prevent large relative twists between the glass and coating at the critical cross-section. This technique enforces the requirement that the glass fiber and coating move in unison. The experimental data and finite element model results are in excellent agreement, as shown in Fig. 5. It is therefore concluded that in the vicinity of the strip point the coating experiences a significant relative twist with respect to the glass. This reduces the contribution of the coating to the torsional stiffness and effectively lengthens the bare fiber region. For a given twist, a compliant inner primary coating can be effective in reducing the torque and therefore the stress transmitted to the bare glass fiber in partially stripped fibers. Taking into account this effective increase in stripped length, the finite element model produces the results shown plotted in Fig. 6. The model and experimental data are now in good agreement.

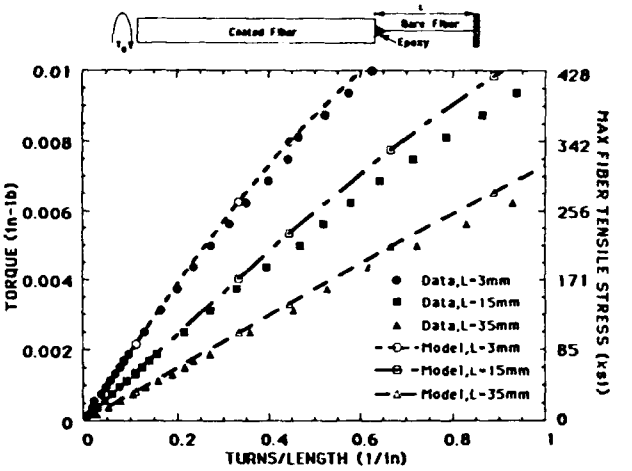


FIG. 5 : TORSION OF TIGHTLY BUFFERED 900 micron POLYESTER ELASTOMER COATED FIBER WITH EPOXY AT STRIP POINT

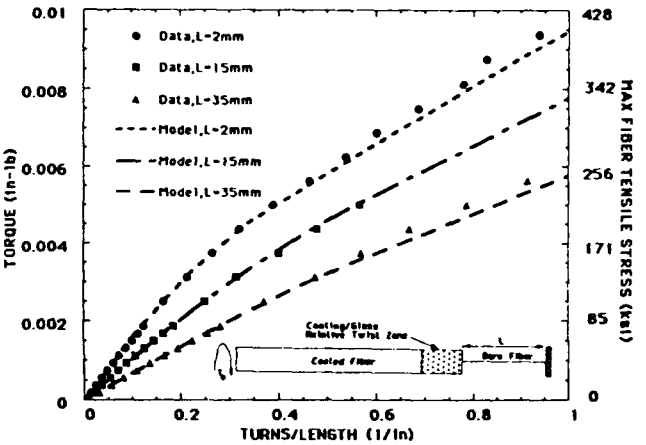


FIG. 6 : TORSION OF TIGHTLY BUFFERED 900 micron POLYESTER ELASTOMER COATED FIBER WIYH RELATIVE TWIST CORRECTION

4. Calculation of Stresses in Spliced Fibers

The test apparatus shown in Fig. 1 is used to assess the susceptibility of fibers contained in splice tray organizers to torsional loads. Torsional loading occurs when the splices are placed in organizers and the excess fiber is coiled for storage.

Computer simulations of the fiber under the torsional testing of the fixture of Fig. 1 were conducted using the finite element model discussed in Section 2. Because of their greater vulnerability, the computer simulations were performed with the 900 μm tightly buffered polyester elastomer coating. The arrangement of the fiber in the fixture was modeled assuming an elliptical bend and discrete rigid guide posts, as shown in Fig. 7. A total of 30 elements was used; of these, 14 elements were used to approximate the elliptical portion. The end of the fiber in the elliptical section was assumed to have a stripped section 3 mm long, typical of grip splices, and rigidly held at one end. In splices of this type, a 7 mm length of coated fiber is generally found to be loosely held in an oversized 100 μm clearance opening. This provides some bending strain relief. In the computer simulations, the finite element representing this coated fiber segment was allowed to translate only to the extent of the clearance, 100 μm. From the discussion of Section 3, the length of bare fiber was effectively increased. This mechanism was incorporated in the computer simulations by using a lower effective torsional rigidity for the element affected.

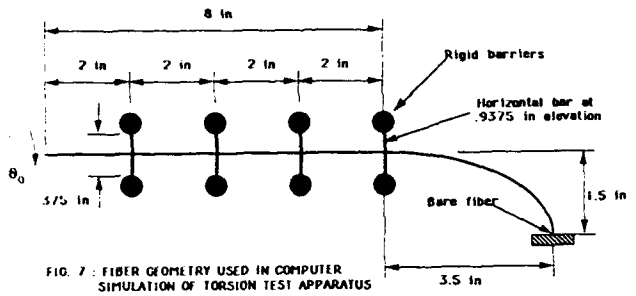


FIG. 7 : FIBER GEOMETRY USED IN COMPUTER SIMULATION OF TORSION TEST APPARATUS

Comparisons of the deflected mode shapes obtained by the model with those given in the torsional test apparatus are shown in Figs. 8(A-C). Despite some differences in initial fiber position and the elliptical approximation of the curved fiber segment, good agreement between model and test was achieved. The maximum fiber tensile stress at the splice predicted by the model is plotted against the number of end rotations in Fig. 9. The craftsperson preparing the splice is required not to degrade the tensile strength of the fiber below 200 ksi. The model therefore predicts that more than 4 rotations are needed for failure. In all of the tests conducted, more than 4 rotations were required to produce fiber failures, agreeing with results of the model.

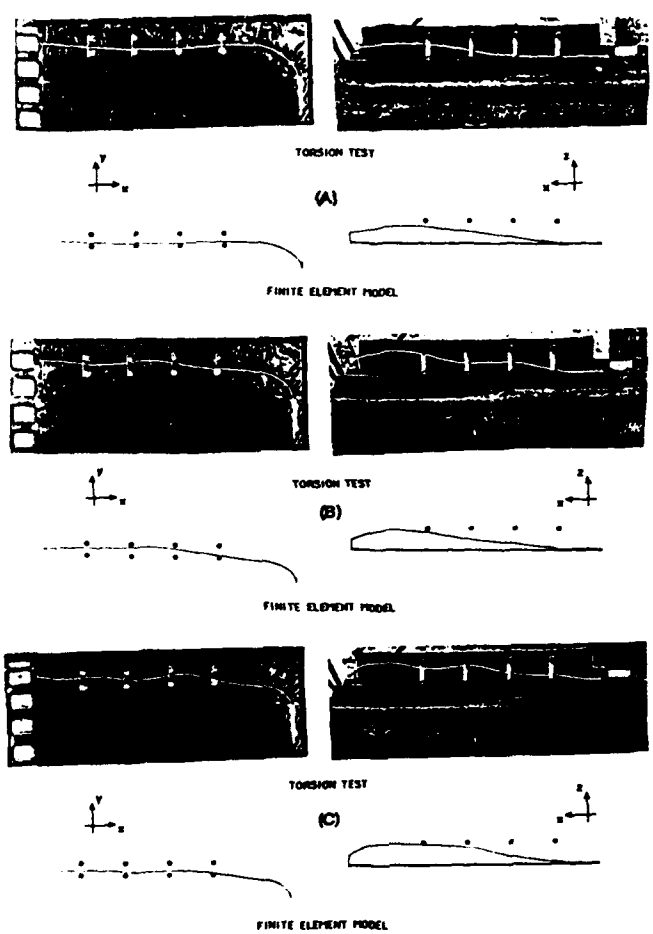


FIG.8 : DEFLECTED SHAPE FOR TORSION TEST AND MODEL (A) 1 TWIST, (B) 2 TWISTS, (C) 3 TWISTS

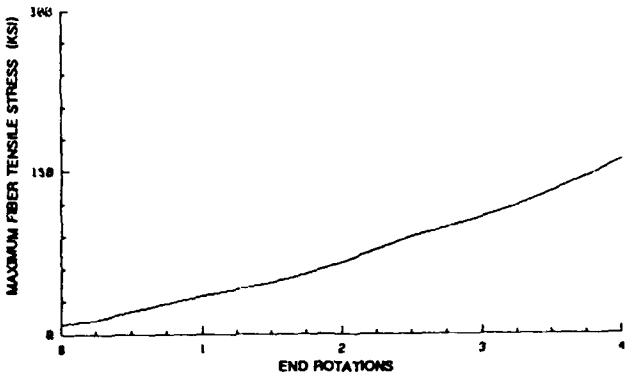


FIG.9 : MAXIMUM PRINCIPAL FIBER TENSILE STRESS AT SPLICE VERSUS NUMBER OF END ROTATIONS

To put these computed stress levels in perspective, consider estimating the expected storage fiber stress in a typical splice tray. A minimum of 60 cm (23.6 in) of excess fiber is stipulated when fiber is stored in an organizer assembly [8]. Organizers are generally sized to allow 15 cm (6 in) diameter loops to be formed and therefore at least two loops are generally incorporated. The formation of each loop produces a 2π twist in the fiber. The fiber loops are held in equilibrium only by end forces and moments and therefore the twist per unit length of fiber is a constant [9]. Hence, for calculating the torque, the fiber can be treated as a straight length. Since the splices considered do not provide torsional strain relief, the resulting torque is transmitted directly to the 3 mm bare-glass segment that lies just before the splice's gripping mechanism. Again, from strength of materials [2], the torque in a partially stripped fiber can be expressed in terms of the applied twist as:

$$T_0 = \left(\frac{\theta_0}{L}\right)\left\{\frac{(GJ)_g L}{L_g + (GJ)_g L_c/(GJ)_T}\right\} \qquad (4)$$

where T_0 is the torque in the fiber, θ_0/L=.65 is the twist angle per unit length after forming 2 loops, $(GJ)_g$=252x10^{-6} lb-in^2 is the torsional stiffness of the bare glass fiber and $(GJ)_T$=3617x10^{-6} lb-in^2 is the elastic torsional stiffness of the coated fiber. From eq. (4), the torque transmitted to the bare fiber is T_0=1.83x10^{-3} lb-in. This corresponds to a maximum shear stress of τ_{max}=74 ksi. In addition to torsion, a bending moment is also transmitted to the bare fiber at the splice when forming the fiber storage loop; but in this instance there is some intrinsic strain relief. The 7 mm coated length of fiber in the body of the splice is constrained and cannot translate more than the 100 µm clearance hole permits. For bending about the y and z axes, the normal stress on the perimeter of the fiber is given by [2]:

$$\sigma = \frac{E_g D_g}{2(EI)_g}\{M_z \cos\theta - M_y \sin\theta\} \qquad (5)$$

where σ is the normal stress in the bare fiber, E_g=10.25x10^3 ksi is Young's modulus of the glass fiber, D_g=4.92x10^{-3} in is the diameter of the glass fiber, $(EI)_g$=287x10^{-6} lb-in^2 is the flexural rigidity, M_z and M_y are the bending moments about the z and y axes, respectively, and the angle θ locates the stress points on the circumference of the fiber. The bending moments appearing in eq. (5) are computed from the end deflections and rotations of the 3 mm bare fiber segment contained in the splice through equations:

$$M_y = \frac{6(EI)_g}{L_g^2}\Delta_y + \frac{4(EI)_g}{L_g}\Phi_y$$
$$M_z = -\frac{6(EI)_g}{L_g^2}\Delta_z + \frac{4(EI)_g}{L_g}\Phi_z \qquad (6)$$

where L_g=0.118 in (3 mm) is the length of bare fiber in the splice $\Delta_y=\Delta_z$= - 0.002 in (50 μm) are the maximum end deflections allowed by the clearance opening, and Φ_z= - Φ_y=2(0.002 in)/(0.275 in)=2(50 μm)/(7 mm) are the maximum allowed end rotations assuming a rigid body motion. Equation (6) quantifies the bending moments: M_z= - M_y=3.18x110^{-4} in-lb. From eq. (5), the maximum tensile stress occurs when θ=45° and assumes the value σ_{max}=40 ksi. Using Mohr's circle [9], the maximum principal tensile stress expected in the looped fiber due to combined bending and torsion is 97 ksi. From Fig. 9 it is seen that approximately 3 rotations are required to induce this level of stress when the spliced fiber is subjected to the torsion test of Fig. 1.

5. Summary and Conclusions

Experiments and analyses were conducted to quantify torsional stresses in spliced optical fibers that are stored and arranged in splice-tray organizer assemblies. Tightly buffered optical fibers that are coated to an overall 900 μm diameter with a relatively stiff polyester elastomer and contained in a grip-type splice were considered because of their apparent greater vulnerability. To analyze a torsional test method a 3-dimensional finite element model was developed. This model can treat material nonlinearities and large displacements.

A series of pure torsion tests on straight fibers with different lengths of stripped coating were conducted. These tests were used to characterize the nonlinear properties of the coating and to assess the sensitivity of the stripped fiber length to the torsional stress transmitted to the bare glass fiber. The nonlinear material property of the coating determined in these tests was incorporated in the finite element model. The torsional stresses imparted to the bare fiber are inversely proportional to the length of stripped fiber for a given twist per unit length. It was also found that a significant relative twisting takes place between the glass fiber and coating at the point where the coating is stripped off. This has the effect of increasing the effective length of stripped fiber and ultimately results in reducing the torsional stresses transmitted to the bare glass fiber. The assumption usually made in analyzing this stress state is that the coating and glass fiber twist in unison, but at least for straight lengths combining stripped and unstripped fiber, this is not valid. A more accurate and less conservative calculation of the torsional stress should account for an increase in the effective stripped length. The region over which the coating moves relative to the glass fiber was found to be 5.8 mm (0. 228 in).

The deflected modes of the spliced fiber predicted by the finite element model are in good agreement with actual observed modes in the torsional test apparatus. The model predicts that in a dynamic test environment more than 4 twists are required for failure. This agrees with actual test results; where more than 4 twists were necessary to cause failure. It is also indicated that the stress levels transmitted to the spliced fiber in the torsional test apparatus are consistent with expected spliced fiber storage stresses and therefore can be used as a tool for assessing the issue of splice sensitivity to torsional stresses.

REFERENCES

1 S. Leopold, G. Kiss, A Pellegrino, N. Cehlot, "Torsional Criteria Development for Optical Fiber Splices," NFOEC,1991.
2. F. R. Shanley, *Strength of Materials*, McGraw-Hill,1957.
3. K. Bathe, E. L. Wilson, *"Numerical Methods in Finite Element Analysis,"* Prentice-Hall,1976.
4. J. S. Przemieniecki, *"Theory of Matrix Structural Analysis,"* McGraw-Hill, 1968.
5. ANSYS, Engineering Analysis System, Theoretical Manual.
6 S. P. Timoshenko, J. M. Goodier, *"Theory of Elasticity,"* McGraw-Hill, 1951.
7 L. A. Reith, J. P. Varachi, H. H. Yuce, "Analysis of Torsional Fiber Failures," IWCS Proc. pp 517 - 520, 1991
8. ———,*"Generic Requirements for Optical Fibers and Optical Fiber Cables,"* TR-TSY-000020, Issue 4, Bellcore, March 1989.
9 A. E. H. Love, *"A Treatise on the Mathematical Theory of Elasticity,"* Dover, 4th Edition, 1944.
10. W. Flugge, *"Handbook of Engineering Mechanics,"* McGraw-Hill, 1962.



Philip B. Grimado, B.S. (Civil Engineering, 1961), City University of New York; M. S. (1962) and Ph. D. (1968) in Applied Mechanics, Columbia University. He joined AT&T Bell Laboratories in 1968 as a member of technical staff. His research efforts were devoted to vulnerability studies of antiballistic missile systems, fire risk analyses of telecommunications equipment and methods for optimal control of environmental equipment. In 1983 he joined Bellcore where he has been involved in developing placement strategies for fiber optic cables and in mechanical reliability issues of optic fibers.



Leslie A. Reith received a B. A. degree from New York University in 1975, the M.Phil. degree from The City University of New York in 1979, and Ph. D. from The University of Texas at Austin in 1981, all in physics. In 1981 she joined AT&T Bell Laboratories as a member of Technical Staff. In 1984 she subsequently joined Bellcore, where she is presently a member of the Fiber Distribution and Reliability Research group in Morristown, N. J. Her recent research interests at Bellcore include reliability issues related to optical splices. She is an APS and IEEE member.

Anthony Pellegrino, B.S. (Management Science, 1976), Fairleigh Dickinson University; M.S. (Industrial Engineering), 1978), Rutgers University; M.B.A. (Industrial Management, 1981), Fairleigh Dickinson University. Tony joined AT&T-Technologies (Western Electric) in 1966 and transferred to Bellcore in 1984. He has been working as a Member of Technical Staff in the Optical Connectors and Splicing Technology Group since 1985. He is responsible for analyzing and developing criteria for splicing systems.

MECHANICAL RELIABILITY OF MULTI-FIBER FUSION SPLICES

H. H. Yuce, J. P. Varachi*, Jr, A. Pellegrino*, and P. L. Key***
Bellcore
**Morristown, NJ; **Red Bank, NJ*

T. Wei
GTE Laboratories Inc., Waltham, MA

ABSTRACT

In this paper we examine the effects of mass-fusion splicing techniques on the long-term reliability of fibers. As part of this work, we consider the effect of some of the variables in the mass-fusion splicing process that can affect the strength of the fiber. Specifically, we measured the tensile strength of the splices with and without plastic protection sleeves. Tensile strength measurements alone may not be sufficient to provide all the information needed for understanding the failure mechanisms and for assuring the mechanical integrity of mass-fusion splices. Therefore we also examined the effects of aging in different environments on the mechanical reliability of the splices.

INTRODUCTION

The mechanical reliability of optical fibers has been of major interest since their introduction into the telephone network. Initial work in this area concentrated on the strength of long lengths of fiber since the first telecommunications application of fiber optics was long-distance transmission. Optical cables for this application contain long lengths of fiber with relatively few splices, some of which are prefabricated in the factory. As the use of fibers spreads through the telecommunications plant, shorter cables containing numerous field splices are becoming more common. New, low- cost designs of all components are necessary to meet the requirements of high quality, large-scale production and installation. Since splicing is labor-intensive, highly-efficient fiber splicing techniques are indispensable for cost saving and for reducing construction time. Since a large number of fiber splices are required for high-count optical fiber cables, mass-fusion splicing techniques have been developed for joining multi-fibers quickly and economically.

The preparation of multiple-fiber fusion splices involves several steps which may damage the fiber. This includes removing the cable structure, stripping the coating, cleaning the stripped fiber, cleaving the fiber, splicing, fiber recoating and/or installation of the splice supporting structure (i.e., the splice protector). Many of these steps expose the glass surface to mechanical damage and the degradation effects of the environment. In a recent paper [1], we examined reliability issues for single-fiber fusion splices. In this paper, we examine the effects of mass-fusion splicing techniques on the strength of the fibers. As part of this work, we consider the effect of some of the variables in the mass-fusion splicing process that can affect the strength of the fiber. Specifically, we measured the tensile strength of fusion splices with and without plastic protection sleeves. Also, individual fiber strengths of the mass-fusion-spliced, 12-fiber ribbons were measured to determine the effect of a fiber's position in the ribbon during splicing. The tensile strengths of splices were also tested after aging at high temperature and humidity (85 °C and 85% RH) and at 85 °C in deionized water. In total, nearly 2,700 fusion splices were made and tested for this study.

EXPERIMENTAL PROCEDURE

The objective of this work was to characterize the strength reduction that takes places during the mass-fusion splice operation. A commercial 12-fiber ribbon, representative of current production, was obtained from a vendor. The individual fibers were 125-μm glass, coated with a UV-cured urethane acrylate to an overall diameter of 250 μm. The same procedure was used to prepare all ribbon fiber ends for the fusion step. This included stripping the coating with a thermo-mechanical multi-fiber stripper. The blade of the tool was cleaned regularly. The stripped ends were wiped clean by using a Q-tip dipped in ethyl alcohol, and the fiber ends were cleaved using a multi-fiber cleaving tool. The blades of the cleaving tool were also cleaned regularly. After cleaving, each fiber in a ribbon was placed cleaved-end-to-cleaved-end on a V-groove alignment plate (Figure 1) and mass-fusion spliced with an electric arc. All splices were made using the same commercial arc-fusion splicer to eliminate splicing machine variability. Two-thirds of the splices made in this study had a heat-shrunk, plastic protection sleeve installed over the stripped and spliced area as per manufacturers' instructions; the other third were prepared without the sleeve. Sleeves were obtained from two different sources; the sleeves are designated herein as sleeves 1 and 2. Figure 2 shows the structure of a typical protection sleeve. It is usually composed of 3 elements: a heat-shrink tube, a hot-melt adhesive tube, and a tension member. The protection sleeve is located over the spliced ends of the fiber and fixed in place by heating.

To determine whether the fusion conditions for every fiber were uniform during mass-fusion, the tensile strength of individual fibers in the ribbon were tested. We also measured the strength of the mass-fusion-spliced fiber ribbon with and without protection sleeves. The failure strength for our experiments was defined as the load at which the first breakage occurred in the spliced fibers in the ribbon. The tensile strength of the spliced samples was measured on a screw-driven universal tensile testing machine at a strain rate of 5% per minute in a test environment of 22 °C and 50% RH. Samples were gripped on 2-in. (5-cm) diameter capstans covered with a soft elastomeric sleeve and were secured with masking tape. A gage length between capstans of 20 in. (50 cm) was used and 61 samples were tested for each condition.

Spliced fiber ribbons were tested both in the as-spliced condition and after aging at high temperature and humidity (85 °C and 85% RH) and at 85 °C in deionized water. The samples were conditioned in the test environment a minimum of 24 hours before being tested. In addition, samples of unspliced, as-received fibers separated from the ribbon structure were tested to serve as a base-line for our study. The variables considered in this work were:

Sleeve	1, 2
Splice type	sleeved, unsleeved
Aging Conditions	85 °C - deionized water 85 °C - 85% RH
Aging Time	1 day, 1 week, 1 month, 3 months, 6 months

RESULTS AND DISCUSSION

Figure 3 shows the failure strength distribution of individual fibers in the mass-fusion spliced 12-fiber ribbons. Failure strength did not depend on the position of the fibers in the ribbon. This shows that the thermal distribution of the arc during the splicing operation does not affect the strength distribution. The average failure strength for the individual fibers was 102,000 psi (pounds per square inch). The strength of optical fibers normally can be fit to a Weibull distribution with a very steep slope that is characteristic of a narrow distribution of strengths. However, the strengths for both unaged and aged mass-fusion-spliced fibers showed (Figures 4-6) very broad distributions. The effect of fusion splicing on the tensile strength of ribbon fibers is summarized in Table 1.

Several observations about mass-fusion splicing are apparent. First, the splicing operation (stripping, cleaning, cleaving and fusing) is the cause of the largest deterioration in strength; for example, from 780,000 psi tensile strength as-received to 102,000 psi as-spliced. Examination of the fractures indicated that failure always occurred in the region adjacent to the fusion zone. Thus, the low strength observed is the result of damage to the exposed glass surface during the preparation of the fiber ends (stripping, cleaning, and cleaving) and during the mass-fusion operation (possibly abrasion in the V-grooves). This result agrees with the very few field failures [2] that have been experienced with mass-fusion splices. The use of a heat-shrink plastic protection sleeve increases the measured strength of the splice significantly in the unaged condition. This indicates that the load is carried across the weak splice(s) by the sleeve and that the measured strength is not a true indicator of the fiber strength.

Aging at 85 °C in deionized water or in high humidity has little effect on the strength of unsleeved splices. The flaws introduced into these fibers during the preparation and splicing operations are so large that the in size increase caused by the corrosive aging environment is insignificant. However, aging in either deionized water or high humidity may cause large decreases in the strength of splices with a heat-shrink plastic sleeve, as the splices with Sleeve 2 did. The aging environment rapidly destroyed the ability of Sleeve 2 to carry the load so that the measured strength of the aged sleeved samples approached the strength of the unsleeved splices. As shown in Table 1 and Figures 5 and 6, fibers spliced with Sleeve 1 showed less effect due to aging.

The results of this study, like that of our earlier one [1], show that the splicing operation, especially ribbon-fiber-end preparation, is very deleterious to the strength of the fiber. It is suggested that heat-shrink plastic sleeves provide an initial strengthening effect, but this may be rapidly lost, depending upon the sleeve design, when the splices are exposed to moisture. In addition, it is important to design splice enclosures to minimize stresses on the splice and to protect them from the service environment.

CONCLUSIONS

As a result of this study, several observations about mass-fusion splicing are apparent. First, the splicing operation (stripping, cleaning, cleaving and fusing) is the cause of the largest deterioration in strength. The use of a heat-shrink plastic protection sleeve increases the measured strength of the splice significantly in the unaged condition, but this effect can be lost rapidly when the splices are exposed to moisture.

In summary, multi-fiber splicing will become increasingly important for subscriber distribution. We have shown that the mechanical reliability of mass fusion splices is sensitive to the splicing practices and the effectiveness of each splice design in protecting the fibers from hostile environments and high stress.

REFERENCES

1. H. H. Yuce et al., *Proc. of 39th Int. Wire and Cable Symposium*, 400 (1990).
2. H. H. Yuce, unpublished.

Table 1 - Effect of Fusion Splicing on Fiber Strength

Fiber Condition	Aging Condition	Median Strength, psi		
		Unsleeved	Sleeved	
			Sleeve 1	Sleeve 2
Unstripped, unspliced	Unaged	780,000	-	-
Stripped, spliced	Unaged	102,00	523,000	569,000
Stripped, spliced	1 day, 85 °C, 85% RH	99,000	526,000	482,000
Stripped, spliced	1 week, 85 °C, 85% RH	91,000	505,000	362,000
Stripped, spliced	1 month, 85 °C, 85% RH	85,000	476,000	134,000
Stripped, spliced	3 months, 85 °C, 85% RH	67,000	481,000	135,000
Stripped, spliced	6 months, 85 °C, 85% RH	72,000	469,000	111,000
Stripped, spliced	1 day, 85 °C, deionized water	82,000	495,000	402,000
Stripped, spliced	1 week, 85 °C, deionized water	69,000	464,000	164,000
Stripped, spliced	1 month, 85 °C, deionized water	76,000	450,000	97,000
Stripped, spliced	3 months, 85 °C, deionized water	70,000	420,000	105,000
Stripped, spliced	6 months, 85 °C, deionized water	73,000	429,000	109,000

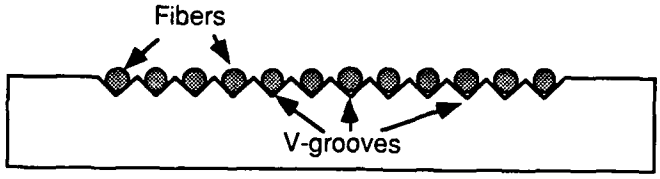
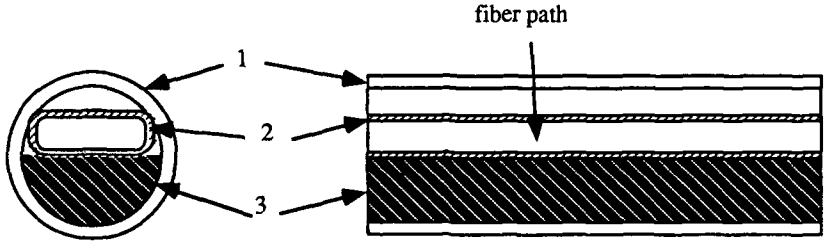


Figure 1 - V-groove alignment plate



1: heat-shrink tube
2: hot-melt adhesive tube
3: tension member

Figure 2 - The structure of a typical protection sleeve for reinforcement

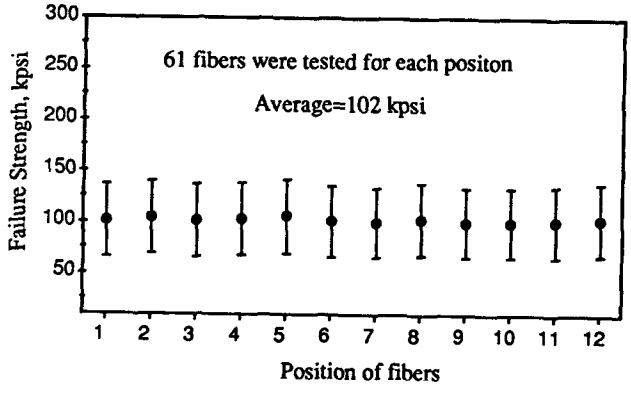


Figure 3 - Failure strength of fiber at each grove position

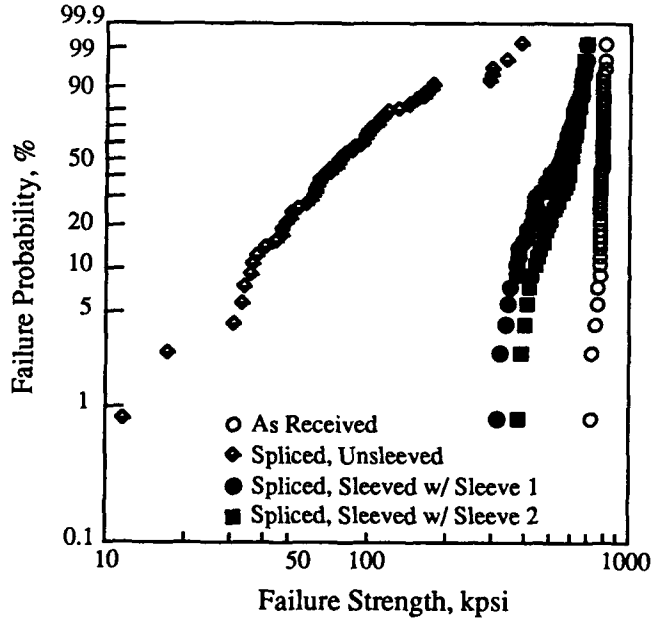


Figure 4 - Effect of mass-fusion splicing on strength of optical fibers

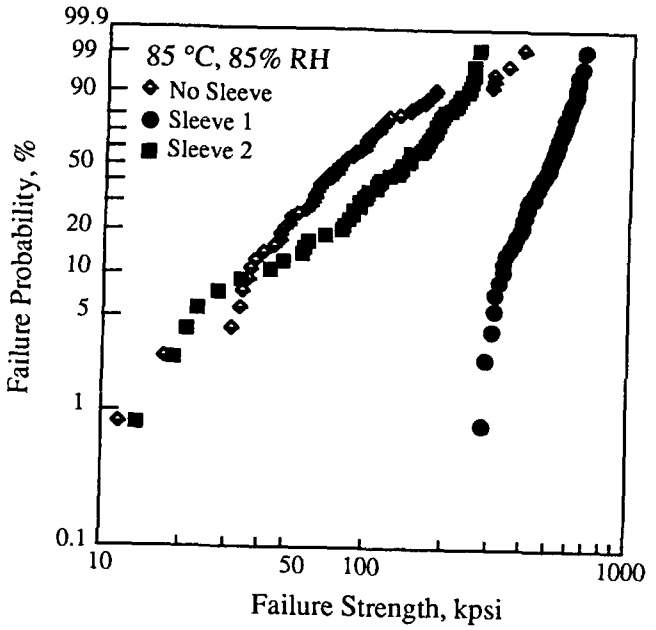


Figure 5 - Effect of aging at 85 °C, 85% RH for 1 month on strength of mass-fusion splices in optical fibers without and with plastic protection sleeves

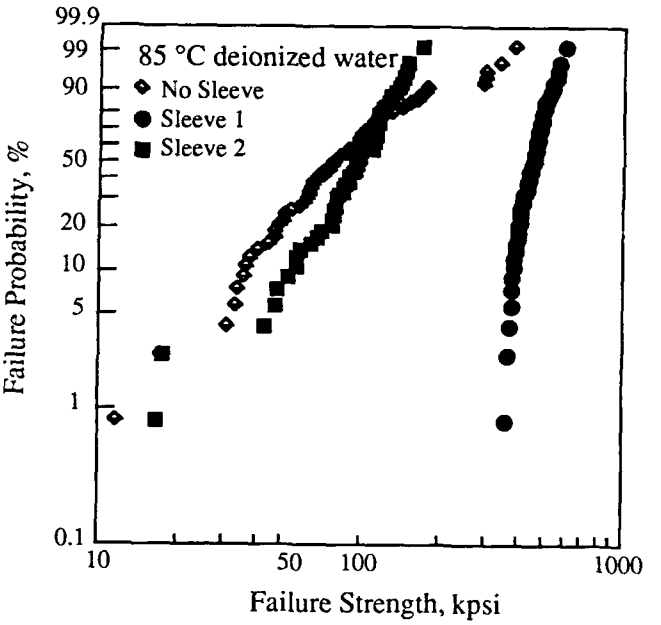
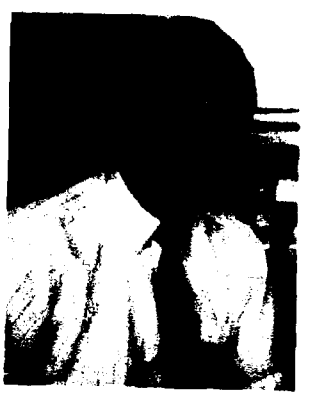


Figure 6 - Effect of aging in 85 °C deionized water for 1 month on strength of mass-fusion splices in optical fibers without and with plastic protection sleeves





Hakan H. Yuce is a member of technical staff in the "Fiber Distribution and Reliability Research" group at Bellcore. He leads a research program dealing with long-term mechanical reliability of optical fibers and interconnections. Hakan provides technical input and support to organizations responsible for generic requirements and responds to clients' immediate needs related to consultation on reliability and field failures. He also plays a active role in the establishment of U.S. and international standards within TIA and IEC regarding optical fiber test procedures to assure reliability. Hakan has a B.S. degree in Mechanical Engineering from Technical University of Istanbul, an M.S. in Mechanical Engineering from M.I.T.and a Ph.D degree in Mechanical Engineering and Material Science from Stanford University.

John Varachi is Director of Fiber Distribution and Reliability Research, at Bellcore. He is responsible for research in the areas of optical fiber and fiber-optic component reliability and new low-cost installation methods for fiber-in-the-loop deployment. He is an active participant in industry standards related to fiber-optic component reliability at the national and international level within TIA and IEC. Previously, John was a Member of Technical Staff in the Loop Transmission Division at Bell Laboratories where he was involved in systems engineering and physical design. John received Bachelor of Science and Master of Science degrees in Mechanical Engineering from Fairleigh Dickinson University and The Polytechnic Institute of New York and is a registered Professional Engineer in the State of New Jersey.



Anthony Pellegrino is a member of technical staff at Bellcore's Morristown Research Facilities. He is responsible for developing generic requirements for optical fiber splicing systems, performing analysis testing of mechanical and fusion splicing systems and fiber closures. Tony started his career at Western Electric, Kearny Works in 1966. In 1974 he was transferred to Purchased Product Engineer (Western Electric) where he was responsible for designing Public Telephone Enclosures and Central Office Lighting Equipment. At divestiture he was transferred to Bellcore. Tony is actively involved in EIA/TIA. He is also an Engineer Duty Officer in Naval Reserve. Tony has a B.S. degree in Management Science from Fairleigh Dickenson University, a M.S. in Industrial Engineering from Rutgers University and a MBA in industrial Management from Fairleigh Dickenson University.



P. Leland Key is Director of Metals and Glass Research at Bellcore in Red Bank, New Jersey. After receiving a PhD in Materials Science from the University of California at Berkeley, Mr. Key joined Bell Labs where he conducted research on the mechanical behavior of materials. In 1983, he joined Bellcore where is responsible for metals research.



T. (Mike) Wei is a Research Supervisor - Network Quality and Reliability at GTE Laboratories Incorporated, Waltham, MA, responsible for operations support and component reliability activities. He received the B.S. degree in physics from National Tsing Hua University, Hsinchu, Taiwan; and the Ph.D. degree in physics from University of Pennsylvania, USA. He is a member of the APS, IEEE, OSA, and SPIE. He has over 50 technical publications and holds two U.S. patents.

FIBER COATING AND TIGHT BUFFER DEGRADATION INDUCED BY INDEX-MATCHING GELS AND ADHESIVES

Rolf A. Frantz*, Leslie A. Reith*, and Irene M. Plitz**

*Bellcore, Morristown, NJ; **Bellcore, Red Bank, NJ

ABSTRACT

Optical fiber coatings (and tight-buffer layers) protect glass fibers from mechanical and environmental stresses that would otherwise cause failure. However, if the coating's integrity or its bond to the glass degrades, water or other environmental agents and/or mechanical wear mechanisms can attack the glass surface. Some fiber coatings have been shown to split and delaminate during aging in some common buffer tube gels. A similar aging condition exists when fibers are exposed to index-matching gels or incompletely cured adhesives in splices. We therefore conducted accelerated aging tests to evaluate the reliability of fiber coatings in such splice environments. Tests using three dual-coated fibers and three tight-buffered fibers in conjunction with two common index-matching gels resulted in only two cases of minor swelling and only one case where significant swelling and cracking occurred. Although the same fibers experienced a variety of degradations when exposed to uncured samples of three common splice adhesives, even a modest cure of the adhesives was sufficient to eliminate these interactions.

INTRODUCTION

Optical fibers are typically protected from environmental and mechanical stresses by polymeric coatings applied during the fiber drawing process. Supplemental protection against harsh environments or for applications involving significant fiber handling is often provided by tight-buffer layers applied in a subsequent manufacturing operation. However, if either the integrity of the coating (and the buffer, if present) or its bond to the glass surface is degraded, the anticipated protection is compromised. Water (humidity) or other agents present in the environment can reach the glass surface and attack it, reducing the fiber's strength and fatigue resistance. If mechanical stress or chemical attack opens the coating and/or buffer, the glass fiber can be exposed to abrasion and other wear degradation mechanisms. In previous work[1], we have shown that some commonly-used buffer tube gels can cause splitting and delamination of some fiber coatings during aging. In optical fiber splices, the cut ends of the fiber coatings and tight buffer layers may be immersed in index-matching gels or in splicing adhesives that have not been completely cured. In such situations, splitting and delamination similar to that experienced in buffer tube gels might be expected to occur in the coating and/or tight buffer layers. To investigate these potential adverse effects on the reliability of optical fiber splices and connectors, we performed a series of compatibility aging tests using three 250 µm-diameter coated fibers and three 900 µm-diameter tight-buffered fibers in conjunction with two index-matching gels and three UV-curable splice adhesives. All of the fibers, gels and adhesives used are commercially available products.

In the following section, we describe the preparation of the test fibers and how they were immersed in the gel or adhesive. We then describe the tests involving the gels and the adhesives, including the analyses used to characterize these materials chemically, and our observations and measurements of any degradation. Finally, we discuss the implications of our observations and how they relate to the reliability of actual field splices and connections.

SAMPLE PREPARATION

Six fibers were tested in combination with two gels and three UV-curable adhesives. Three of the fibers had polyurethane acrylate coatings from different manufacturers, all 250 µm in diameter; these are identified as fibers X, Y and Z. The other three fibers had additional tight buffer coatings 900 µm in diameter made of polyvinyl chloride (PVC), thermoplastic elastomer (TPE), or nylon. The nylon-buffered fiber had an intermediate silicone-based coating 400 µm in diameter. The ends of all fiber lengths were mechanically stripped back 0.15 - 0.30 cm before insertion into the gel or adhesive to simulate the actual end conditions in a mechanical splice.

Three series of tests were performed. In the first, about 3.5 cm of both ends of three fiber lengths of each type were immersed in each gel. The samples were aged in covered petri dishes to minimize the evaporation of volatile oils at elevated temperatures. In the second test, the uncured adhesives were poured into small graduated cylinders; one end of each of six lengths of each fiber type was immersed about 0.6 cm in each adhesive. The cylinders were capped with aluminum foil to minimize evaporation. In the third test, each partially-cured adhesive sample was prepared by spreading a thin layer of adhesive on one end of a microscope slide. Three lengths of each test fiber were immersed in each adhesive to a length of about 1.5-2 cm. The assemblies were exposed either to a curing dose just sufficient to form a flexible bond between the fiber and the glass or to a higher dose that rigidized this bond.

TESTING IN GELS

Gel Characterization

The two gels were analyzed using Fourier transform infrared (FTIR) spectroscopy to identify their generic chemical compositions and size exclusion chromatography to determine their molecular weight distributions.

The FTIR spectra were obtained by spreading thin films of the gels on KBr crystals which were inserted in a Nicolet 10-DX FTIR spectrometer. The spectrum for gel #1 showed that it is primarily a paraffin oil-based grease with a silicate additive. The latter is probably fumed silica, which is often added to such gels to improve their viscosity properties. The spectrum for gel #2 showed that it is phenylmethyl siloxane.

Molecular weight distributions were determined with a Waters liquid chromatography system using 100Å and 500Å ultrastyragel columns with toluene as the mobile phase. Alkanes from C-12 to C-40 were used as molecular weight standards. Molecular weight averages M_n for the two gels are given in Table 1. Multiple M_n values for adhesives A and B represent the average numbers for the multiple peaks in the molecular weight distribution.

Table 1. AVERAGE MOLECULAR WEIGHTS OF GELS AND ADHESIVES

GEL or ADHESIVE	MOLECULAR WEIGHT M_n
Gel #1	400
Gel #2	1300
Adhesive A	1000, 2500
Adhesive B	500, 1000, 2300
Adhesive C	> 2500

Aging Tests

All six fiber types were aged in each of the two gels at 50°C. The fibers were inspected under a 240/500X stereo microscope after 1, 2, 3, 5, 7, and 10 days, 2 weeks, 3 weeks, and 4 weeks. The samples were then aged for an additional week at 85°C. No noticeable degradation occurred during the entire test for the PVC or TPE tight buffered fibers or for fibers X and Z of the 250 µm coated fibers.

When the 900 µm nylon-buffered fibers were stripped, 0.03 -0.10 cm of the urethane acrylate and silicone inner coatings typically protruded beyond the nylon buffer. By the end of the fourth week, the inner coatings had elongated slightly in both gels and protruded approximately 0.12-0.25 cm. Additional aging at 85°C did not measurably worsen this effect, indicating that a steady state condition had been reached.

Fiber Y showed no noticeable effects during the 50°C aging in either gel. However, the coating did swell and crack during the final week of aging in gel #1 at 85°C. In order to determine whether the swelling was due to the effects of cumulative aging or whether it was a threshold effect that only occurred at higher temperatures, we aged new samples at 85°C. Cracks developed during the first day and grew rapidly, indicating a temperature threshold effect. Figure 1 is a photograph of a typical coating crack.

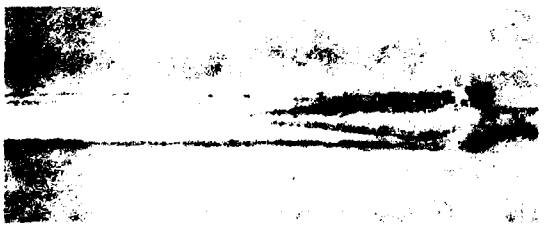


Figure 1. TYPICAL COATING CRACK AFTER IMMERSION IN GEL

To determine the threshold temperature, we aged a number of new samples of fiber Y at intermediate temperatures. Samples were aged for 10 days at 60°C or 24 days at 65°C with no sign of any deterioration. The 60°C samples were then aged at 70°C. After 17 more days, two small cracks finally appeared. New samples placed at 75°C, however, quickly developed cracks in the outer primary. As shown in Figure 2, these cracks rapidly propagated along the fiber.

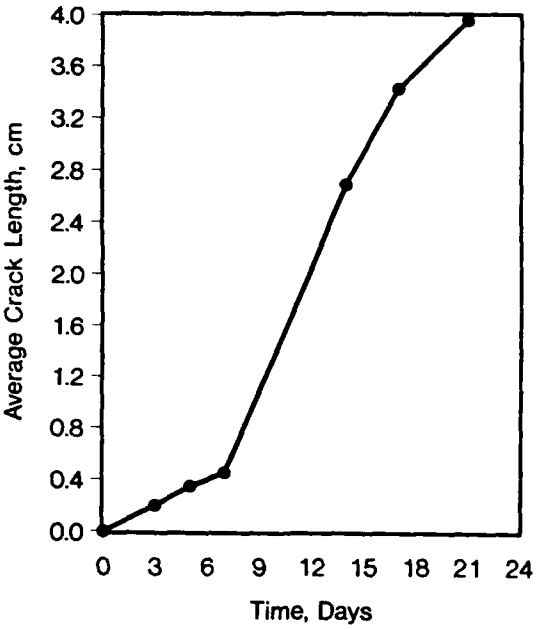


Figure 2. 75°C Aging of Fiber Y in Gel #1

TESTING IN ADHESIVES

Adhesives Characterization

The adhesives were characterized using FTIR spectroscopy and size exclusion chromatography in the same manner as was done for the gels. The FTIR spectra showed that all three adhesives were urethane-based acrylates — the same basic chemistry as the fiber coatings used in our tests. The molecular weight averages for the three adhesives are shown in Table 1.

Aging Tests

Adhesive A

All six fibers were aged in adhesive A at 50°C and were inspected (again using the 240/500X stereo microscope) after 1, 3, 5, 7, and 10 days, and 2, 3, and 4 weeks. The 900 µm tight buffered fibers were then aged for an additional week at 85°C. The PVC and TPE buffered fibers developed a yellow/brown discoloration of the buffer during the first few days. The discoloration became more pronounced as the aging continued, but there was no swelling, splitting, or cracking. The nylon-buffered fibers showed a slight elongation of the inner silicone and primary coatings similar to that seen in the gels. The additional aging at 85°C did not appreciably worsen any of these degradations.

All of the 250 µm fibers, however, did show signs of serious deterioration during the test period. Fiber X started to develop cracks by the third day. By the end of the fourth week, the coating on the immersed ends of two samples had peeled off when they were gently wiped for inspection. Three other samples had cracks more than 2.5 cm long, while only one coating end was still intact. The average crack length over time is plotted in Figure 3.

The coating on Fiber Y began to soften and delaminate after only three days and delaminated along the entire length of all samples by the end of the second week. The test was terminated at that point.

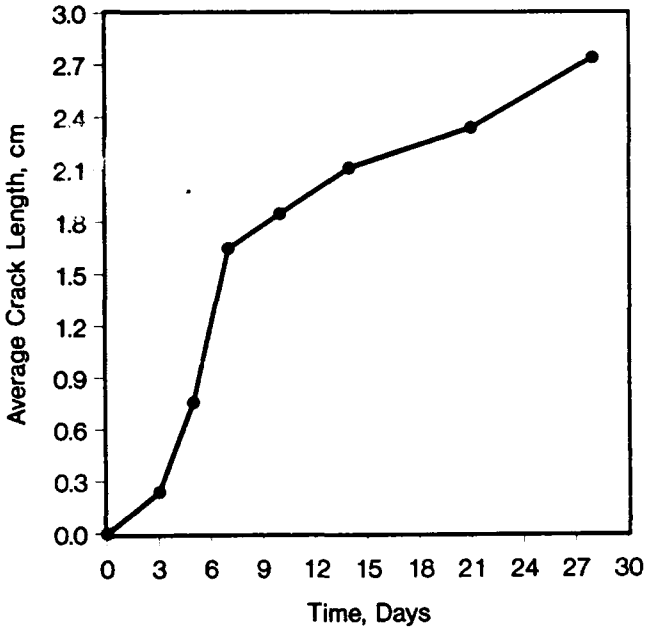


Figure 3. 50°C Aging of Fiber X in Adhesive A

Fiber Z began to show a slight flaring of the coating at the immersed ends after three days. After three weeks, the coating was clearly swelling, but no cracks developed until the fourth week, at which time one small crack was observed.

Adhesive B

All six fibers were aged in adhesive B at 50°C. The 900 µm tight buffered fibers were inspected after 1, 3, 5, 7, and 10 days and 2, 3, and 4 weeks. They were then aged at 85°C for one additional week. The PVC and TPE buffer layers again showed yellow/brown discoloration after only one day, but there were no other noticeable effects during the entire test. The nylon-buffered fiber again showed some elongation (0.03 -0.10 cm) of the inner silicone and primary coatings by the end of the test. Again, the 85°C aging did not significantly increase this elongation.

The 250 µm fibers did show significant deterioration, however. Cracks started to develop in the coating on the Fiber X samples by the third day. After four weeks of aging, all the samples had cracks longer than 2.5 cm. The average crack length as a function of time is shown in Figure 4.

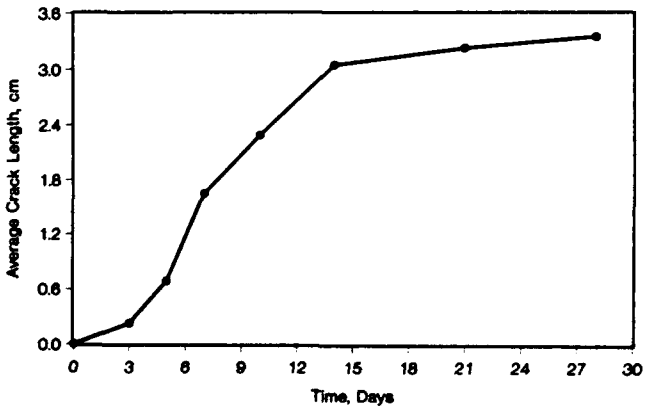


Figure 4. 50°C Aging of Fiber X in Adhesive B

The coating on the fiber Y samples began to delaminate by the third day. The coating had softened and delaminated along the entire length of all six samples by the end of two weeks. The test was terminated at that time.

One of the six samples of fiber Z developed a crack in the coating by the third day. By the end of the test, two fibers had lost a section of the coating during gentle wiping prior to the periodic inspection. Three other samples had cracks about 1.5 cm long.

Adhesive C

Five fibers were aged in adhesive C — all three 900 µm-diameter tight buffered fibers and 250 µm-diameter fibers Y and Z. All were aged at 50°C and inspected at the same intervals as the other adhesive tests. After one week, the TPE and nylon buffered fibers showed no change from their initial state. The PVC buffer, however, began to plasticize after one week, i.e., it softened and would stretch when wiped, then slowly relax. The primary coating appeared to lose its adhesion to the glass fiber. By the second week of the test, the TPE buffered fiber began to show similar effects. After four weeks, these degradations stabilized, affecting about 3 cm of the TPE buffer and about 5 cm of the PVC buffer. The nylon buffered fiber remained unaffected throughout the test.

Fiber Y showed rapid deterioration. Delamination began during the first day. By the end of the second week, all six fibers had delaminated along their entire length. The test was terminated at this point.

Fiber Z also deteriorated rapidly. After only one day, about 1.2 cm of coating stripped off all six fibers during gentle wiping. By the end of the first week, three of the coatings had stripped back almost 2.5 cm and were no longer in contact with the adhesive. The test was discontinued at this point.

Aging in Partially Cured Adhesives

A second set of aging tests was conducted by partially curing the adhesives. These tests simulated a more realistic scenario, where the UV adhesives would be cured enough to tack the fibers in place but still receive much lower curing doses than recommended by the manufacturers.

Four samples each of fibers Y and Z and of the nylon tight buffered fiber were tested in adhesives A and B. Fibers Y and Z were also tested in adhesive C.

Thin films of each adhesive were deposited on glass slides, just thick enough for the coated fibers to be immersed at one end. As before, about 0.3 cm of coating was removed before immersion. The adhesives were then partially cured to "low" and "high" levels. These doses were selected empirically and varied with the curing speeds of the different adhesives. Since curing is a volume-dependent phenomenon, the thicker layers of adhesive necessary to immerse the 900 µm fibers required higher doses for both cure levels than the layers in which the 250 µm fibers were immersed. Cure doses for the various combinations of adhesive and fiber are given in Table 2.

Table 2. PARTIAL CURE DOSES FOR ADHESIVES (mJ/cm²)

	250 µm FIBERS		900 µm FIBERS	
ADHESIVE	Low Dose	High Dose	Low Dose	High Dose
A	130	165	325	450
B	20	28	60	150
C	13	23	—	—

Typical doses recommended by the manufacturers for complete curing of all three adhesives are greater than 3000 mJ/cm^2. However, the properties of completely cured adhesives are approached asymptotically with increasing dose, and the manufacturer's recommendations are conservative to ensure complete cure. The fact that these low doses were adequate to form reasonably strong bonds between the fibers and the glass slides indicates that significant curing occurred.

The test samples were aged at 50°C and were examined after intervals as in the other tests. No noticeable degradation occurred for any fibers in either adhesive A or B. Fiber Y also showed no reaction in adhesive C. Fiber Z showed a limited reaction with adhesive C: two of the eight immersed fibers developed 0.03-0.1 cm-long cracks which stopped growing after 3 weeks of aging. By that time significant changes were observed that indicated additional curing had occurred in all three adhesives.

Adhesives A and B skinned over during the UV exposure, but remained somewhat liquid at the fiber-adhesive interface. The adhesives continued to cure slowly during aging, becoming firm by the end of the test. Their surfaces became rippled and dimpled. Adhesive C had a more uniform consistency after the UV exposure. The surface was soft and tacky; touching it with a probe caused dimples which disappeared quickly or slowly for the low or high partial cure level, respectively. As aging progressed, the tackiness disappeared; all samples became firmer and the dimples took longer to disappear.

DISCUSSION

In view of the differences between index-matching gels #1 and #2, it is not surprising that the only degradation reaction found to occur involved gel #1. This gel is composed of hydrocarbon-based oils of relatively low molecular weight — only slightly greater than those found in [1] to cause delamination and cracking of some fiber coatings. Gel #2 is essentially inert in contact with the fiber coatings and buffers, which is consistent with the fact that it is derived from silicone-based oils of higher molecular weight. The fact that only one of the three coatings tested showed any interaction is consistent with our previous results. The difference in behavior is traceable to the significant differences that may exist between coatings that nonetheless are members of the urethane acrylate family. Interactions may have occurred with the inner coatings on the tight buffered fibers, but these were not visible externally due to the constraining nature of the buffers. This shows the protective value of these buffering layers,which can provide an additional "line of defense" for the glass fiber against chemical attack.

The interaction between gel #1 and fiber Y clearly has an initiation threshold between 70° and 75°C. This temperature represents a realistic service stress level for splices, since it can be reached in pedestals and in outdoor equipment cabinets with active electronics.[2] An aging test at a continuous tempera ure of 75°C or above should be considered to assess the cor itibility of fiber coatings with any index-matching gel or s ce adhesive expected to see service in this typical field environment.

The changes seen in the nylon tight buffered fibers are not a cause for concern. The swelling of the inner coating layers is quite small. Also, this swelling stabilized after a relatively short period of aging; even additional aging at 85°C did not cause further degradation.

The issue of fiber/gel compatibility can be put into perspective by one last item of data. We examined the index-matching gels from seven commercially available splices. In all cases, they were similar to gel #2 (silicone oil-based, relatively high molecular weight). Since these represent the overwhelming majority of splices used in the field, the likelihood of fiber coating degradation is minimal.

It was expected that all three uncured adhesives would induce degradation reactions in all three fibers. Both the fiber coatings and the adhesives are urethane acrylate formulations, and this similarity in chemistry means that the uncured adhesives can act as solvents for the fiber coatings. The plasticizing of the PVC and TPE tight buffers by uncured adhesive C is a potential problem, since these physical changes may also indicate an increased susceptibility to other types of chemical or mechanical attack. However, any reaction with an uncured adhesive is extremely unlikely to occur in the field, since the adhesive must be at least partially cured during the splice assembly to provide the mechanical integrity necessary for handling and storage of a splice in an organizer.

Our attention therefore focussed on determining what level of cure was sufficient to eliminate the reactions we observed in the uncured adhesives. Provided the bond between the fiber and the splice sleeve is strong enough to resist at least modest pull-out forces on the fiber, the splice assembler may accept the splice even though only a partial curing of the adhesive has occurred. We therefore experimented with different curing doses until we found an appropriate dose for each adhesive that just held the immersed fiber samples in place (the "low dose" in Table 2). We also determined a second dose (the "high dose" listed in Table 2) which provided a rigid bond between the fiber samples and the glass slides on which they were mounted. As described in the previous section, no reactions occurred with either fiber Y or Z in either adhesive A or B at either cure dose, even after prolonged high-temperature aging. Very small cracks did develop in the coating on fiber Z when aged in partially cured adhesive C. However, these are not a serious concern because they are so small and because they stopped growing after 2—3 weeks. Thermally-stimulated curing occurred in all three adhesives, as evidenced by the changes observed in the samples during the aging test. At higher temperatures, the higher thermal acceleration of the crack growth is offset by the higher rate of thermal curing, while at lower temperatures the lower rate of thermal curing is compensated by the lower acceleration of the crack growth. Any curing dose that results in reasonable bond strength provides sufficient curing of these adhesives to eliminate any problems of chemical interaction.

SUMMARY

Aging tests on a variety of 250 μm coated and 900 μm tight buffered fibers in two index-matching gels and three UV-curable splice adhesives have shown that only limited compatibility problems exist. Only one fiber showed a significant reaction with one of the gels, and a check of seven widely-used commercial splices indicated that the gel in question was not used in any of them. While uncured adhesives did attack fiber coatings due to their similar chemical formulations, UV curing doses of 10% or less of the manufacturer's recommendations were sufficient to eliminate the problem. Since doses of at least this amount are required to ensure adequate mechanical integrity of completed splices, such chemical attack is extremely unlikely to occur in the field. Nonetheless, where chemical incompatibility is suspected (such as fiber Y with gel #1), an accelerated aging test should be performed to ensure that no interactions occur that adversely affect splice reliability.

REFERENCES

1. Frantz, R. A., and Plitz, I. M., "Fiber coating interactions with buffer tube gels", *Optical Engineering*, Volume 30, Number 6, June 1991, p. 767.

2. Bowmer, T. N., Miner, R. J., and Coker, R. C., "Field Temperatures in Outside Plant", *Proceedings of the 39th International Wire and Cable Symposium*, November 1990, p. 335.



Rolf A. Frantz is a Distinguished Member of Technical Staff in the Fiber Distribution and Reliability Research Group at Bellcore. He holds BS and MEng degrees from Cornell University. After receiving his PhD from Brown University, he joined Bell Labs where he worked in a variety of assignments. His principal responsibilities focused on dielectric materials, an area in which he continued to work when he joined Bellcore in 1983. For the last four years he has been concerned with the applications and reliability of materials used in manufacturing optical fibers and fiber assemblies such as splices.



Leslie A. Reith received a BA degree from New York University in 1975, the MPhil degree from the City University of New York in 1979, and the PhD degree from the University of Texas at Austin in 1981, all in physics. In 1981, she joined Bell Laboratories as a Member of Technical Staff. In 1984, she subsequently joined Bellcore, where she is presently a member of the Fiber Distribution and Reliability Research Group. Her recent research interests include reliability issues related to optical splices. She is an APS and IEEE member.



Irene M. Plitz is a Member of Technical Staff in Bellcore's Plastics and Rubber Research Group. She received her BS in chemistry from Morgan State University in 1970 and joined Bell Laboratories in that same year. She came to Bellcore in 1984 and since then her efforts have focused on chemical and structural analyses of polymers. Her special interests have been polymers used as optical fiber coatings, for cabling materials, and in fiber splices, connectors, couplers and similar components.

TESTING OF 4- AND 8-FIBER RIBBON STRIPPABILITY

Gregory A. Mills

Siecor Corporation
PO Box 489
Hickory, NC 28503-0489

ABSTRACT

The strip performance of a fiber optic ribbon is determined by two factors: first, the construction of the ribbon, which includes fiber type, fiber coating, fiber coloring, ribbon matrix material(s) and processing parameters; and second, the test method. This paper will deal only with the test method. The strip force of a particular ribbon is affected by the stripping speed, clamping force, strip tool temperature and strip length of that ribbon. Another aspect of ribbon stripping that should be considered is the cleanliness of the fibers after stripping.

4-fiber and 8-fiber ribbons of similar construction (Figure 1) and processing were made to test the effects of the above variables on strip performance. The data confirms the hypothesis that all factors do affect strip performance of a ribbon. In general, a higher strip speed, a longer strip length and a higher clamp force increase peak strip force, but a higher strip temperature decreases peak strip force. As for fiber cleanliness, higher strip speed and higher clamp force result in better fiber cleanliness rating, but a longer strip length and higher tool temperature result in a worse fiber cleanliness rating. Samples that are stripped manually (by hand) have an improved fiber cleanliness rating compared to samples stripped by machine.

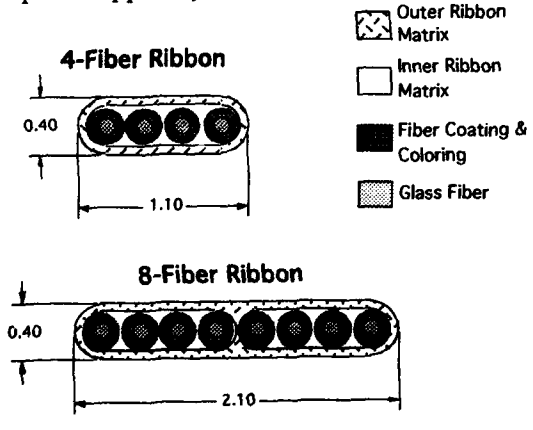


Figure 1: 4- and 8-Fiber Ribbon Construction

NOMENCLATURE

Strip Force:	the peak force required to strip a fiber ribbon in newtons
Strip Speed:	the speed in cm/mm the ribbon is pulled
Strip Temp.:	the temperature in degrees Celsius of the strip tool
Clamp Force:	force applied to the heated strip tool low: less than 1 newton medium: approximately 20 newtons high: approximately 80 newtons
Fiber Cleanliness:	a rating given to the stripped ribbon based on how clean the fibers are after stripping.

5.0 = Heavy Residue	fiber will not wipe clean with alcohol
4.0 = H. Medium Residue	3+ alcohol wipes will clean fibers
3.0 = S. Medium Residue	2 alcohol wipes will clean fibers
2.0 = Slight Residue	1 alcohol wipe will clean fibers
1.0 = No Visible Residue	

INTRODUCTION

With the increased use of optical fiber ribbons for high fiber count cables, it is important to determine the physical properties (attributes) of a ribbon. One very important attribute of an optical fiber ribbon is the ability to remove the fiber coating and ribbon matrix to expose the glass fibers (or ribbon stripping), for effective multi-fiber fusion splicing.

For individual fibers, strip force is specified by some customers and by regional, national and

international telephone regulating organizations (example: Bellcore in the U.S.A.). For example, there is TIA/FOTP 178 which specifies the test method for a single fiber. Presently there is no standard method for evaluating the strippability of a fiber ribbon. This paper is intended to provoke thought and provide information for a possible standard ribbon strippability test method.

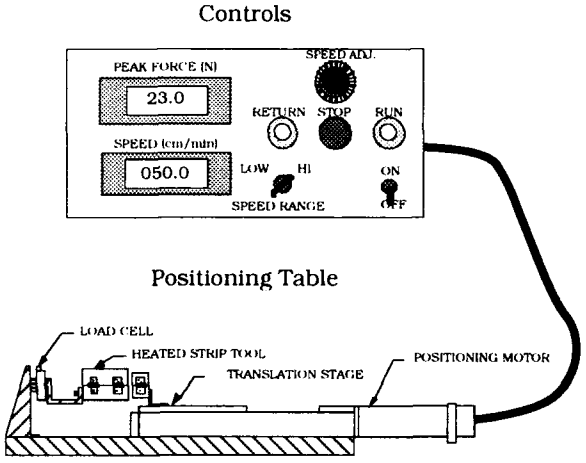


Figure 2: Strip Force Test Bench

Experimental Setup

A schematic of the ribbon strip tester is shown in Figure 2. A ribbon sample is placed in the ribbon holder with a measured amount of ribbon to be stripped. The heated strip tool is closed and the appropriate clamping force is applied. After a 10 to 15 second heat time, the run button is pushed and the positioning motor moves the translation stage at the preset speed, pulling the stripped ribbon out of the heated strip tool. While the ribbon is being pulled out of the strip tool, an analog peak force indicator records the peak strip force. The main parameters that affect the peak strip force of a particular ribbon are the ribbon length, strip tool temperature, stripping speed and clamping force. To determine the effects of the above mentioned variables, a 4-fiber and 8-fiber ribbon of similar construction were chosen for testing, and a test matrix was performed that included all possible combinations of the following settings (Table 1):

Strip Speed	Strip Length	Clamp Force	Tool Temp.
5 cm/min	5±0.5 mm	low	90±5°C
50 cm/min	15±0.5 mm	medium (med)	120±5°C
100 cm/min	30±0.5 mm	high (hi)	
200 cm/min			

Table 1: Strip Force Matrix

Making all possible combinations of the above yields 72 different setups for each 4-and 8-fiber ribbon. At each setup, 4 measurements were made, the average was taken as the result for that setup, and no data points were eliminated.

Results and Discussion

In comparing strip force within a parameter (i.e.: clamp force), the average of all data for the sub-parameters (i.e.: low, med, hi) was used and a t-test was performed at a 99% confidence interval to test for significant differences. This is a widely used method in design of experiments and results in an efficient and accurate use of data.[1&2] Table 2 contains the average strip force data, calculated t-values (t-cal.) and the critical t-values (t-critical). Values for t-cal. are determined by equation 1. For all cases, the calculated t-value is greater than the critical t-value for 4- and 8-fiber ribbons. This indicates the differences in average strip force are significant and not due to random error at a 99% confidence interval. Also interesting to note is that the average peak strip force of the 4-fiber ribbon is almost exactly one half that of the 8-fiber ribbon peak strip force (10.6 N vs. 21.1 N).

$$t\text{-cal} = \frac{|X_1 - X_2|}{S/\sqrt{n}} \qquad \text{Eq. 1}$$

Where: Xi = data average
S = Standard Deviation
S(4-fiber ribbon)=0.94 N
S(8-fiber ribbon)=1.54 N
n = Sample Size

Parameter		4-Fiber Ribbon		8-Fiber Ribbon			
		Force	t-cal.	Force	t-cal.	t-critical	n
Clamp Force	low	8.5	NA	13.6	NA	NA	96
	med	11.3	28.5	20.4	43.1	2.58	96
	hi	12.0	7.5	29.2	56.5	2.58	96
Strip Length (mm)	5	5.6	NA	10.5	NA	NA	96
	15	9.8	44.0	19.1	54.5	2.58	96
	30	16.4	68.3	33.6	92.6	2.58	96
STRIP TEMP.	90°C	11.8	NA	23.3	NA	NA	144
	120°C	9.4	30.6	18.9	34.3	2.58	144
Strip Speed (cm/min)	5	7.6	NA	13.9	NA	NA	72
	50	9.8	20.2	20.9	38.7	2.58	72
	100	11.2	12.4	23.4	13.6	2.58	72
	200	13.8	23.3	26.0	14.0	2.58	72

Table 2: Strip Force Results in Newtons for 4- and 8-Fiber Ribbons.

Although all differences are statistically significant at the 99% confidence interval, the magnitude of the difference is the real issue. If the change from one setting to another setting (i.e.: low, med, & hi clamp force) has a very low impact on the final strip force (i.e.: less than 5%), then it could be argued that any of these settings are acceptable. This is not the case; the 3 smallest changes are 6.4%, 10.8% and 11.8% and the average change within each parameter is 38.2%. These changes, besides being statistically significant, are quite large.

In both the 4- and 8-fiber ribbon, strip length has the largest effect on peak strip force. Increasing the strip length from 5 mm to 15 mm increases the force by ~80%; from 15 mm to 30 mm the force increases by ~75%. This is an average effect of .43 N/mm for 4-fiber ribbons and .93 N/mm for 8-fiber ribbons (note: 8-fiber ribbon force is approximately twice that of 4-fiber ribbon). The effect of strip tool temperature is also the same for 4- and 8-fiber ribbons. An increase in strip temperature of 30 °C results in about a 20% drop in strip force for both ribbon types.

The effect of clamp force on the strip force of a 4-fiber ribbon is large (32% increase) when a medium clamp force is applied as compared to a low clamp force, but only a small increase in strip force is measured when a high clamp force is applied (6% increase). For the 8-fiber ribbon the strip force increases 50% for the medium clamp force and 44% for the high clamp force. One would expect both ribbons to behave similarly for this parameter (more like the 8-fiber ribbon); that is, increasing clamp force should cause the strip force to increase until it approaches the break strength of the glass fibers.

Strip force for both ribbons increases with increasing strip speed. There is a large increase in strip force when the speed increases from 5 cm/min to 50 cm/min (30% for 4-fiber and 50% for 8-fiber ribbons). At higher speeds the force continues to increase, but at a decreasing rate (Figure 3). This indicates that if strip speed continues to increase, at some point the strip force will level out. Also, as the strip speed approaches zero, it approaches a minimum strip force. Again, 8-fiber ribbon strip force is approximately twice that of 4-fiber ribbon.

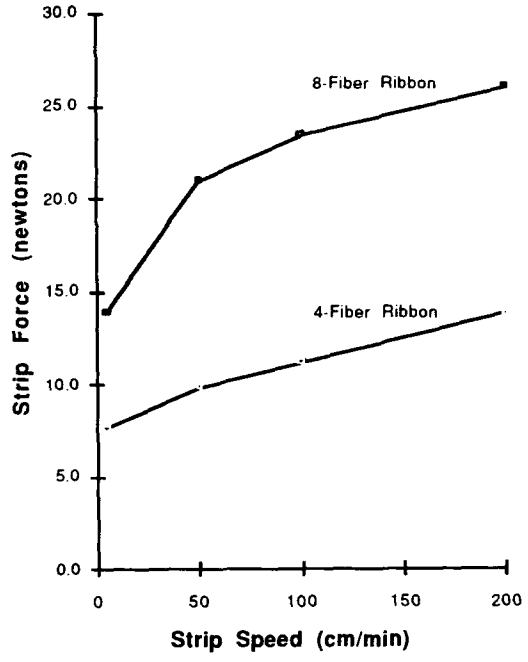


Figure 3: Strip Force vs Strip Speed for Different types Ribbons

The cleanliness of a ribbon after stripping is mainly controlled by the clamping force (see Table 3). A low clamp force always yields unacceptable results (cleanliness ratings > 4.0), for both 4- and 8-fiber ribbons. On 4-fiber ribbons, the ratings improve significantly for all parameters when the clamp force is increased to a medium level. At a high clamp force the 4-fiber ribbons show only a moderate improvement over the medium clamp force. The 8-fiber ribbon shows only a slight improvement with the medium clamp force, but with the high clamp force, the rating improve significantly for all parameters. Strip length slightly affects fiber cleanliness at a high clamp force, has no effect at low clamp force, and has a larger effect at medium clamp force. Strip speed has no effect on fiber cleanliness. The stripping temperature has a small effect on the fiber cleanliness rating; 90°C yields cleaner fibers than does 120°C. Overall, the main parameter that affects fiber cleanliness is clamp force.

Parameter		4-Fiber Ribbon Clamp Force			8-Fiber Ribbon Clamp Force		
		LOW	MED.	HIGH	LOW	MED.	HIGH
Strip Length (mm)	5	4.3	1.7	1.7	5.0	2.7	2.0
	15	5.0	2.6	2.0	5.0	4.6	2.2
	30	5.0	3.4	2.6	5.0	5.0	2.1
Strip Speed (cm/min)	5	4.7	2.7	2.8	5.0	4.3	2.3
	50	4.6	2.5	2.0	5.0	4.2	2.0
	100	4.8	2.3	1.8	5.0	4.1	2.1
	200	5.0	2.8	1.8	5.0	3.8	2.0
Strip Temp.	90°C	4.5	2.2	1.9	5.0	4.0	2.0
	120°C	5.0	3.0	2.5	5.0	4.2	2.4

Table 3: Fiber Cleanliness of Machine Stripped Ribbons

After all the machine stripping was completed for this experiment, the ribbons were stripped by hand using the exact same strip tool. The estimate strip speed of hand stripping (by this operator) is in the range of 1000 - 1500 cm/min and the clamp force is close to high setting. All these samples (except one) have cleanliness ratings of 2 or less (Table 4). These ratings are very close to the machine ratings at the high clamp force.

Temp. °C	Length mm	Ribbon Type	Fiber Cleanliness
90	5	4-FIBER	1.0
90	15	4-FIBER	1.0
90	30	4-FIBER	2.0
120	5	4-FIBER	1.0
120	15	4-FIBER	2.0
120	30	4-FIBER	2.0
90	5	8-FIBER	2.0
90	15	8-FIBER	2.0
90	30	8-FIBER	2.0
120	5	8-FIBER	2.0
120	15	8-FIBER	2.0
120	30	8-FIBER	3.0

Table 4: Fiber Cleanliness of Hand Stripped Ribbons

Conclusions

The strip force of a particular ribbon is affected by clamp force, strip length, strip temperature and strip speed. Fiber cleanliness is mainly affected by clamp force, but strip speed and strip temperature are also important in obtaining clean fibers. In order to develop a standard test for ribbon strippability these machine parameters (and maybe more) need to be specified. By setting a standard method, suppliers and manufactures will have a better understanding of what the customers' requirements are for ribbon strippability.

Acknowledgement

The author would like to thank Robert Ashley Herring for his diligent work in collection of all the data.

References

1. R.E. Walpole and R.H. Myers, Probability and Statistics for Engineers and Scientists, Macmillan Publishing Co., 1985.

2. C.D. Hendrix, Statistical Process Control, Handout Notes, 1990



Gregory A. Mills graduated from North Carolina State University in 1984 with Bachelor of Science degrees in Chemical Engineering and Textile Chemistry. He has worked in the fiber optic industry since 1985. Greg joined Siecor in 1989 where he was initially involved in engineering support to tight buffer cable manufacturing. Presently he is involved in the development of ribbon cables.

MINIATURE OPTICAL FILTER

S.Yodo, I.Ohta, H.Hayakawa, A.Hasemi, M.Shimizu

THE FURUKAWA ELECTRIC CO., LTD.

ABSTRACT

A miniature optical filter that can be directly connected with a FC-type connector has been developed. It is composed of two elements, that is, a ferrule and a housing.

In fabrication, a bare fiber was inserted in the ferrule and was fixed by adhesive. Next, both fiber ends were polished, and a slit was formed at a central region of the ferrule. A filter chip that was a dielectric multi-layered thin-film filter on a glass substrate, was inserted into the slit and the ferrule was assembled with a housing.

The device assembly was adopted a plug-receptacle type, and the device size was only 10 mm in diameter and 40 mm in length.

As the result, the average insertion loss was 0.9 dB, and good performances of the mechanical tests were obtained.

This device is not only applicable to other optical filters, such as LWPF and so on, but also applicable to an optical attenuator.

1. INTRODUCTION

With optical communications systems increasingly diversifying and more sophisticating in their function, advances are being made in studies and practical application of wavelength-division multiplexing systems. For the systems, wavelength-selective filters are essential devices to eliminate extraneous light. The paper will describe about optical fiber devises as wavelength-selective filters, to which filter embedded technology has been conventionally applied.

The devices with embedded filters are literally passive devices, in which a filter having the specific characteristics is formed onto a glass chip (filter chip) which is then embedded in the fiber, and followings can be mentioned as their features

(1) Fewer components mean easier assembly, and lower cost and higher reliability than previous micro-optic devices.

(2) Superior connection with optical fibers.

(3) The technique of forming of a slit in a single optical fiber fixed to a substrate assures that, unlike the case of butt joints between two optical fibers, there is no eccentricity loss, resulting in lower-loss devices.

(4) Depending on filter characteristics, it is possible to obtain devices with such functions as wavelength separation or polarization separation

For an instance, optical fiber with embedded filter is a very simple case of the application of this technology. However, the optical fibers require a certain space when they are set in an equipment, because pigtails have to be drawn out from them.

Consequently, the development was made on a plug-type miniature filter that further enhanced handling characteristics and capable of directly interfit to a connector, with the application of filter-embedded technology. The paper will report the results of the development.

2. Structure and Manufactureing Method of Developed Plug-Type Miniature Filter.

Fig.1 shows the structure of the miniature filter.

The filter is composed of two elements, a housing and a special ferrule. The latter have ZrO2 parts at both ends of it, and small holes for injecting adhesive in its center part.

The ferrule is fixed with adhesive after an optical fiber is penetrated through its inside and then the both ends of the optical fiber are polished (R20- PC polish). A slit is formed on its center part by a dicing saw and a dielectric multi-layered thin-film filter chip is inserted and fixed to the slit. Additionally, at this time, we used a standard single-mode fiber and SWPF (short wavelength pass filter) that is usually used for single mode transmission. Also filter chip insertion angle was selected 8 to prevent reflective light and the slit width was set at 35 um. Besides those terms, one end of

the housing is a plug type and the other end is receptacle type. The size of the filter is as small as 10 mm in diameter and 40 mm in length.
The manufacturing processes of the filter are as follows.

(1) Fixing the fiber
(2) Polishing
(3) Slit forming
(4) Inserting and fixing the filter chip
(5) Assembling

3. Characteristics of The Filter

The wavelength characteristic of the filter is shown in Fig. 2. The figure clearly proves that filter transmits 1.31 um wavelength with about 20 %. loss and shuts off 1.55 um wavelength, reflecting faithfully the characteristics of used filter chip.
As for the insertion loss, the radiation loss value α due to a gap between optical fibers can be calculated by Equation (1), when single-mode fibers are butt spliced one another.

$$\alpha = 10\log\left(1+\left(\frac{\lambda S}{2\pi n\omega^2}\right)^2\right) \quad [\mathrm{dB}] \qquad (1)$$

where:

λ is the wavelength
S is the gap between optical fibers
n is the index of refraction
ω is the mode field radius

According to the equation, the radiation loss is about 0.2 dB at the slit width of 35 um. The value of the insertion loss at the filter embedded element is expected to be about 0.4 dB. The additional losses are the increase loss due to the tolerance of the slit, the absorption loss of adhesive and so on. When splicing loss at both ends of the ferrule element is added to the above loss values, the total insertion loss is expected to be about 1 dB. The average insertion loss of this filter was 0.9 dB (at 1.31 um), showing that nearly expected result was obtained. The value of the insertion loss was also over 50 dB, a favorable figure, at the 1.55 um. The amount of reflective attenuation is more than 25 dB, showing that reflection at the both ends of the PC connector are more dominant. From this, it is expected that the reflection at the filter is very small.

4. Reliability

Heat cycle test, vibration test and impact test were conducted to test the reliability of the sample. The test results are shown in Table 1. The favorable result of a loss fluctuation range of -0.1 dB was obtained at both vibration and impact test. The loss fluctuation range of less than 0.4 dB was obtained at the heat cycle test. But the result can be considered reasonable, because loss fluctuation of three parts, two splicing points of a connector and the filter, is added to the original loss fluctuation.

5. Practical Application

The following are some examples of practical application of the miniature filter that was developed this time.

(1) Full-reflective edge:
Full-reflective edge is obtained by making gold deposit on one end of the special ferrule. As for its practical use, it is applied to a reference measurement of return loss of various optical devices.
(2) Anti-reflective edge:
Anti-reflective edge is obtained by oblique angle polish of one end of the special ferrule and is used for anti-reflective treatment of 2x2 couplers.

6. Summary

Development was made on a miniature filter that embedded a filter chip in a single mode fiber. The filter obtained favorable results at both initial characteristic test and reliability test.
It is possible to apply the filter not only to other filters (such as LWPF) but also to light attenuation devices. The filter also makes it possible to realize other structure such as plug-plug type, receptacle-receptacle type.

References

1) Kiyomatsu et al. 1990. Proc. Fall Conf. of IECE B-695.(in Japanese).
2) Matsumoto et al. 1991. Proc. Spring Conf. of IECE B-894.(in Japanese).
3) Yanagawa, H. et al. 1988. Electronics Letters vol. 24, No10:596.
4) Marcuse,D. 1977. Bell Syst. Tech. J. vol. 56:703.

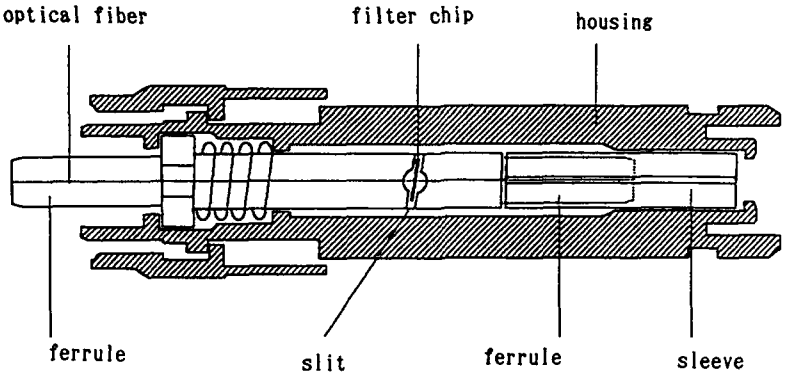


Fig.1 Schematic diagram of miniature optical filter.

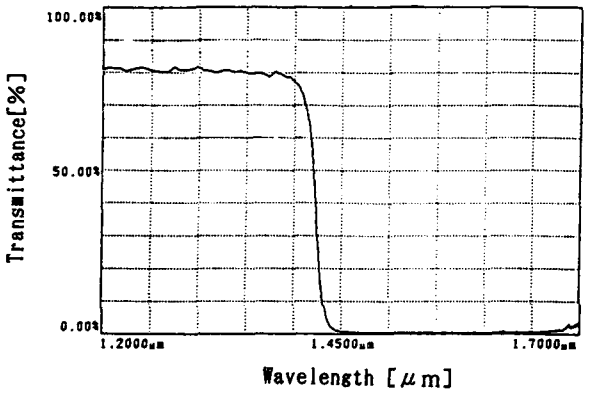


Fig.2 Wavelength characteristics of a miniature optical filter

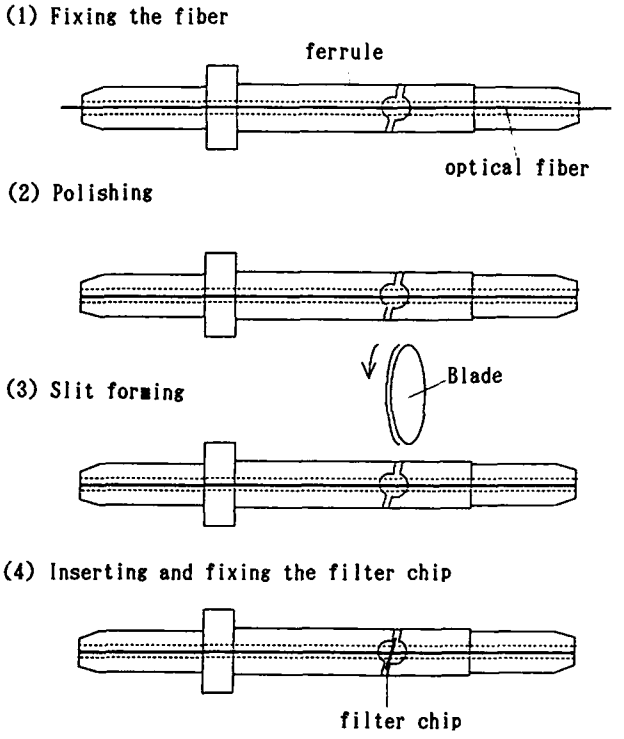


Fig.3 Process for fabricating a miniature optical filter

Table 1 The result of reliability test.

Test	Condition	Result
Impact	980N, 6msec, 10times	Loss variation: ≦0.1[dB]
Vibration	10~55Hz/min, 1.5mm, 6hr	No physical damage
Heat cycle	-30~70℃/6hr, 20cycle	Loss variation: ≦0.4[dB]

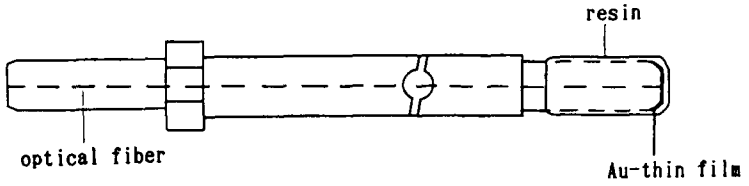


Fig.4 Structure of ferrule for full-reflective

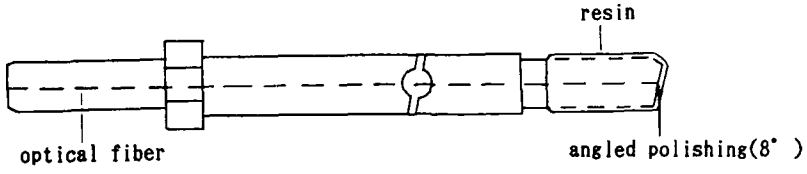


Fig.5 Structure of ferrule for anti-reflective

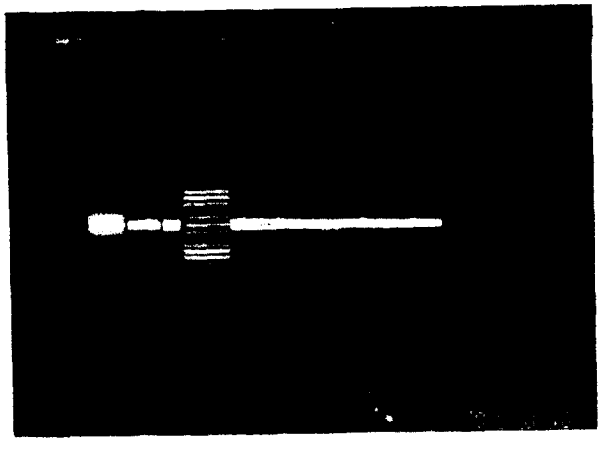


photo.1 Miniature full-reflective edge
(Anti-reflective edge)

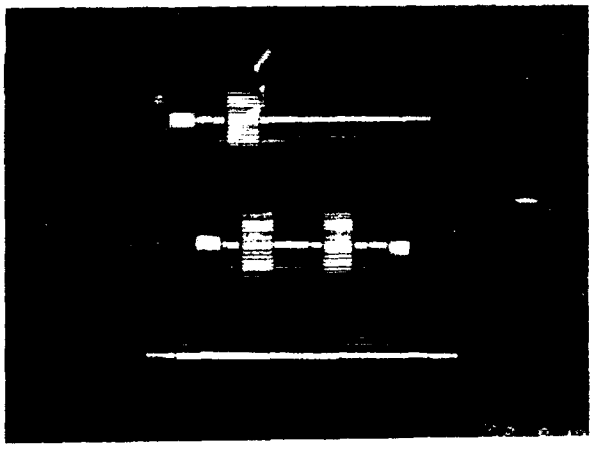


photo.2 Miniature optical filter
(from top :plug-receptacle type
plug-plug type
receptacle-receptacle type)

Shigehito YODO

The Furukawa Electric
Co., Ltd.
6 Yawata-Kaigandori,
Ichihara,Chiba,290
Japan



He was born in Yamagata, Japan, in 1965. He received the B.E. degree in electrical engineering from Yamagata University in 1989. He joined The Furukawa Electric Co., Ltd. in 1989.
He has been engaged in research and development of fiber optics device & equipment.

Hirokazu HAYAKAWA

The Furukawa Electric
Co., Ltd.
6 Yawata-Kaigandori,
Ichihara,Chiba,290
Japan



He was born in Tokyo, Japan, in 1963. He received the B.S. degree in Physics from Chiba University in 1985. He joined The Furukawa Electric Co., Ltd. in 1985.
He has been engaged in research and development of fiber optics device & equipment.

Masanobu SHIMIZU

The Furukawa Electric
Co., Ltd.
6 Yawata-Kaigandori,
Ichihara,Chiba,290
Japan



He was born in Ehime, Japan, in 1951. He received the B.E., M.E. degrees in mechanical engineering from Kyoto University in 1974 and 1976, respectively. He joined The Furukawa Electric Co., Ltd. in 1976.
He has been engaged in research and development of fiber optics device & equipment.

Ikuo OHTA

The Furukawa Electric
Co., Ltd.
6 Yawata-Kaigandori,
Ichihara,Chiba,290
Japan



He was born in Kagoshima, Japan, in 1967. He received the B.E. degree in chemical engineering from Tokyo University in 1990. He joined The Furukawa Electric Co., Ltd. in 1990.
He has been engaged in research and development of fiber optics device & equipment.

Akio HASEMI

The Furukawa Electric
Co., Ltd.
6 Yawata-Kaigandori,
Ichihara,Chiba,290
Japan



He was born in Chiba, Japan, in 1955. He received the B.E. degree in chemical engineering from Chiba University in 1979. He joined The Furukawa Electric Co., Ltd. in 1992.
He has been engaged in research and development of fiber optics device & equipment.

NOVEL SPIRAL-AIR SYSTEM FOR OPTICAL FIBER AND CABLE INSTALLATION

K. Horii*1, K. Ohsumi*2, Y. Tomita*3, T. Hamade*4, Y. Shimo*4 and Y. Matsumae*1

*1 Shirayuri Women's College, Tokyo, Japan
*2 Toa Kikai Kogyo Co.,Ltd., Yamaguchi, Japan
*3 Kyushu Institute of Technology, Fukuoka, Japan
*4 NTT, Ishikawa, Japan

Abstract

A new installation technology using spiral airflow to control turbulence has been enabled optical fibers and cables to be installed in conduits 6~150 mm in diameter over distances much longer than achieved with conventional systems. With this new system, a 2 mm optical fiber has been successfully blown through a 1500 meter, 6 mm diameter tube coiled in a drum. In the process of laying a 12 mm optical cable, a 10 mm pulling rope was passed through a 1200 meter, 80mm diameter conduit. The spiral generator constructed with a single device, or combination of devices, each consisting of a conical cylinder with an annular slit, produces a highly focussed, stable airflow which increases the drag force on the fiber and reduces scraping against the conduit, enabling installation over long distances.

1. Introduction

To keep up with today's high-speed, high-volume information transfer needs, optical cable and fiber installation technology must be reliable, efficient and easy to use. Thus, the motivation in developing this new spiral airflow installation technology was:

1) To efficiently install optical fibers over long distances, taking into account the specific characteristics of optical fiber.
2) To enable the installation of additional cables in existing conduits.

2. Installation Trial

Experiments were conducted in order to test the technique's performance and to study the installation effects on fiber and cable.

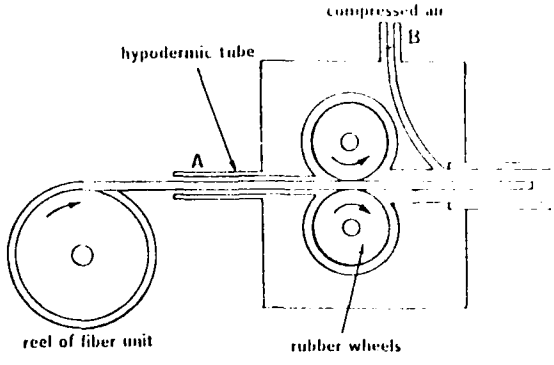


Fig.1 Conventional System

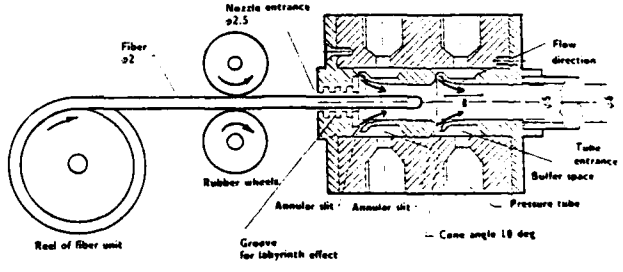


Fig.2 New System

2.1. Optical Fiber Installation in Tubes

At present, the only device available for optical fiber installation is the one developed by BT[1,2]. As illustrated in Fig.1, the conventional system is designed with a pair of rubber wheels inside the device's pressurized metal block. The optical fiber is fed through a hypodermic needle with these wheels, and then blown into the tube by compressed air. Since the airflow in the block is not controlled, back presure develops requiring the seal to withstand the resulting back flow as well as fiber friction. The wheels help to minimize the fiber scraping caused by turbulence and the friction of the

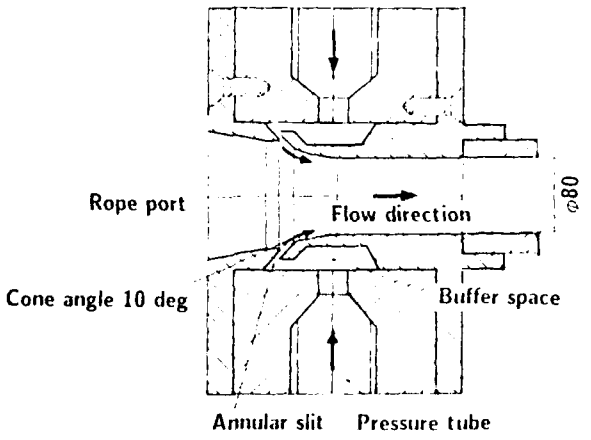


Fig.3 Spiral Nozzle

fiber against the seal. However in order to accomplish this, the wheels must be placed inside the pressure block, otherwise the fiber would scrape against the tube wall.

In the new system as shown in Fig.2, fluid dynamic control and an improved sealing method enable the wheels to be installed outside the pressure block thereby simplifying the new device and making it more efficient. The wheels lead the fiber into the Coanda spiral unit[3], then the fiber is blown with a spiral airflow. The inherent characteristics of the fluid dynamic control achieved with a spiral flow help to overcome the major drawbacks of the conventional system. The back flow is prevented by the Coanda effect, and even if back pressure develops (i.e., when installing over long distances), the labyrinth effect seals against this flow without the friction problems of the conventional mechanical sealing method (hypodermic needle). The result is a highly efficient process for installing optical fiber.

Experiments with long, 6 mm-diameter tubes, coiled and varied to lengths 1000 and 1500 meters, were performed to test the passage of a 2 mm-diameter optical fiber weighing 2.0 g/m. Airflow was generated by both the spiral-flow device and a simple constant-diameter turbulent-flow entrance conventional device. The pressure in the tube was raised to 800 KPa-gage and average pipe flow velocities of 47 m/s and 30 m/s respectively, developed at the tube outlets, corresponding to pipe-diameter Reynolds numbers of 1.9×10^4 and 1.2×10^4.

With the normal turbulent flow, the fibers did not blow through, but rather scraped, and became trapped inside the tube. In contrast, using the spiral flow device, a fiber was easily blown through a 6 mm-diameter rolled tube over distances of 1500 meters. Based on the average of 10 measurements, it took only 30 minutes to install fibers in 1000-meter tubes, and 90 minutes for the 1500-meter tubes.

2.2. Multiple Cable installation Over Long Distances

Multiple cable installation technology should be developed from the viewpoint of more effectively utilizing existing conduits. A conventional multiple installation system, which can only install additional cables over a maximum 250 meters, is not satisfactory for installing cables through a long conduit. Using the new spiral airflow technology, cables have been installed in existing conduit 1200 meters long.

The conventional cable installation method using compressed air involves four steps:

(1) Purging water and mud,
(2) Blowing a lead rope,
(3) Installing a pulling rope,
(4) Installing a cable with the pulling rope.

There are several drawbacks of this conventional method. In step (1) the water and mud cannot be purged completely, thus the installation process is rarely smooth. To accomplish step (2), a pig (or parachute) is attached to the end of the lead rope and blown through the conduit (with the nozzle sealed at its entrance) by a large quantity of compressed air. Unfortunately, this process limits the installation distances, often causes the rope to violently fly out of the conduit due to the extremely high air pressure developing in the sealed conduit and may cause the lead rope to entangle with the existing cables making additional installation impossible.

With the new spiral flow installation nozzle as shown in Fig.3, water and mud are purged completely, the pulling rope can be installed without a lead rope (thus eliminating step (2), above), and the pulling rope does not become entangled with the existing cables.

Experiments with 80 mm-diameter conduit over distances of 1122 meters were performed to test water removal and the passage of a flat tape (width, 12 mm; thickness, 2 mm; weight, 17g/m) to pull additional 12 mm diameter cables. Airflow was generated by either the spiral flow device or a simple constant-diameter turbulent-flow entrance device. The pressure of spiral nozzle tube was raised to 500 KPa-gage, and an average pipe flow velocity of 16 m/s developed, corresponding to a pipe diameter Reynolds number of 8.5×10^4.

The spiral flow pushed the rope through the pipe much faster than the conventional turbulent flow did. Passing a rope through the conduit in only 6 minutes. In contrast, installation was unsuccessful using the conventional turbulent flow which is only capable of installing flat tape over distances of up to 100 meters.



Fiber Motion in Turbulence Fiber Motion in Spiral Flow

Fig.4 Rope and Fiber Motion



Turbulence Spiral flow

Fig.5 Radial Fluctuation Visualization

3. Spiral Air Flow — Installation Efficiency and Control

Installation efficiency is determined by the drag force of the airflow on the fiber or rope and the friction of the fiber/rope against the inner conduit wall. A greater net force, i.e., a large drag force and a small friction force, results in higher installation efficiency.

These forces are dependent on the location in the conduit. In the first part of the conduit, the airflow velocity is low and the drag force is small, therefore the friction must be reduced to increase efficiency. The highly stable, sharply focused spiral airflow positions the fiber/rope to the center axis[4], thereby decreasing contact with the conduit wall and increasing the drag force.

In the latter part of the conduit, the higher velocity airflow increases the drag force enough that even if the fiber or rope does scrape against the conduit, the installation process is not affected. Therefore, improving efficiency is dependent on the airflow control in the first part of the conduit; the spiral flow breakdown in the latter part of the conduit does not influence the installation efficiency.

Purging stagnant water and mud from the conduit is an important task when installing multiple cables. A simple turbulent airflow cannot completely clear out all of the water and mud. Although various modifications of conventional methods have been tried without success, the spiral flow has proven to work perfectly, completely purging all water and mud.

Visualization during testing has revealed that this ordered airflow blows the fluid and debris in a spiral motion up toward the top of the conduit, and as it drops down toward the center axis, it is purged out by the main axial flow. Thus the characteristic spiral motion of the airflow is the key element in complete purging.

4. Fiber and Rope Motion in Both Flows

To study the influence of instability on fiber motion, both the turbulent and the spiral flow were tested.

Figure 4 shows the fiber and rope motions at a mean air velocity 15 m/s. The spiral-flow device focuses and orients the fiber near the axis, greatly reducing its friction against the tubes walls[5]. However, in the turbulent tube flow, the fiber undergoes irregular transverse vibrations, forming a wave which scrapes against the tube walls and fails to blow through.

By visualizing the rope motion, it could be seen that the spiral flow caused the rope to rotate around the axis, and form a sine curve with the same pitch when viewed from the side of the conduit. In turbulent flow, the rope exhibited an intense vibration phenomenon towards the radius of the conduit which appeared to be a self-induced vibration. Looking at the photograph of the side of the conduit, a sawtooth waveform was clearly observed.

To gain more insight into the success of the spiral-flow device, both turbulence measurements and flow visualization were carried out. Figure 5 shows jet-flow structure sequence pictures taken at 1/60 second intervals visualized with a laser sheet placed parallel to and through the jet axis. The spiral-flow jet was tightly formed and stable, while the normal turbulent jet's velocity fluctuated.

Fluid instability causes fiber vibration in the conduit's radial direction and leads to an increase in the friction between the fiber/rope and the conduit.

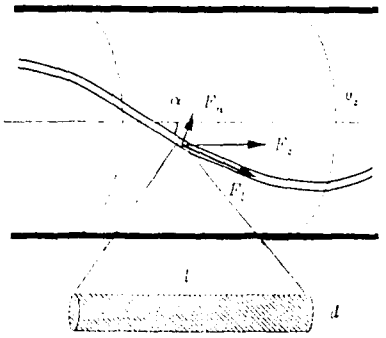


Fig.6 Force Acting on Rope

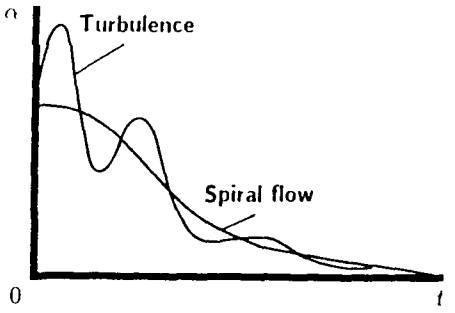


Fig.7 Numerical Approximation of α for t

5. The Net Force for Installation

The installation efficiency is determined by the drag force and the friction force. The drag force arises from the friction between the fluid and the fiber or rope, and is the motive force for blowing the fiber or rope through the conduit. The friction between the conduit wall and the fiber or rope impairs installation.

This friction is particularly important in the first part of the conduit where the drag force is small. For successful installation, the friction must also be small. To examine the fiber or rope vibration in the first part of conduit which decreases efficiency, the ability to position the fiber or rope to the conduit center due to the oscillation caused by the fluctuating velocity has been analyzed. The following assumptions were made:

(1) Only the force due to the axial velocity is considered; the others are ignored.

(2) The axial velocity, from the experimental results, is given by

$$v_z = \overline{v_z} + B\sin\omega t \tag{1}$$

The force acting on the normal line of the fiber or rope: (as shown in Fig.6), and the acceleration are obtained as follows:

$$F_n = \frac{C_D}{2}\rho v_z^2 ld\sin^2\alpha = H_D v_z^2 \sin^2\alpha \tag{2}$$

$$a_n = \frac{1}{s}\frac{d}{dt}\left(s^2\frac{d\alpha}{dt}\right) \tag{3}$$

The equation of motion from Eqs.(2) and (3) is given as

$$\frac{d^2\alpha}{dt^2} = \frac{H_D}{m_s} v_z^2 \sin^2\alpha \tag{4}$$

Equation (4) is expressed by substituting Eq.(1) into Eq.(4) as,

$$\frac{d^2\alpha}{dt^2} = \frac{H_D}{m_s}\sin^2\alpha(v_z + B\sin\omega t)^2 \tag{5}$$

Equation (5) is rearranged as,

$$\alpha = \arcsin\left\{C_0\exp\left[-\frac{H_D}{m_s}\left(\frac{v_z^2 t^2}{2} - \frac{\overline{v_z}B}{\omega^2}\sin\omega t\right)\right]\right\} \tag{6}$$

The numerical approximation of α for t is shown in Fig.7.

Equation (6) indicates that the spiral flow tends to position the fiber or rope to the conduit center with less vibration than turbulent flow thereby reducing contact with conduit wall and resulting in highly efficient installation. This approximation was in agreement with the observed results.

6. Conclusion

A high performance apparatus for installing optical fiber and cable has been developed. With this apparatus, a 2 mm-diameter optical fiber was blown through a 6mm-diameter rolled tube over a distance of 1500 meters, which is longer than the 700 meters achieved by the best conventional techniques. In the process of laying a 12 mm-diameter optical cable, a 10 mm-diameter pulling rope was passed through a 1200 meter, 80 mm-diameter conduit. Furthermore, with the new system, the conduit is completely purged, fewer operational steps are required, the same device can be used for all steps, and the cable replacement technique is easy and safe. This efficient installation is achieved by the ordered structure of a spiral flow and the Coanda effect.

References

1) Hornung,S., Cassidy,S.A., Yennadhiou,P. and Reeve,H.M., 1986, "The Blown Fiber Cable", *IEEE Journal of Sel Areas Communication*, Vol.4, No.5, pp.679-685.

2) Cassidy,S.A. and Reeve,M.H., 1983, "A radically new approach to the installation of optical fibers using the viscous drag of air", *Proceeding of the ECOC*.

3) Horii,K., 1988, US.PAT. No.4,721,126, UK.PAT. No.2,180,957.

4) Horii,K., 1990, "Using Spiral Flow for Optical Cord Passing", *Mechanical Engineering - ASME*, Vol.112, No.8, pp.68-69.

5) Horii,K. et al., 1991, "Focusing Phenomenon and Stability of Spiral-Flow Jet", *Transactions of the Japan Society for Aeronautical and Space Science*, Vol.33, No.102, pp.141-153.



Kiyoshi Horii

Shirayuri Women's College, 1-25 Midorigaoka, Chofu-shi, Tokyo 182 Japan.

Kiyoshi Horii is a professor at Shirayuri Women's College and received his Ph D. in Chemical Enginering from Waseda University in 1975. His research interests include the theory and applications of fluid mechanics. He has developed a nozzle for generating a focused, stable spiral flow and applied it to various industrial areas. Kiyoshi Horii is a member of ASME, APS, IEICE and the Japan Aerospace and Science Society. He is also the vice-chairman of ASME-Japan.



Yuji Tomita

Kyushu Institute of Technology, 1-1 Sensui-cho, Tobata-ku, Kitakyushu-shi, 804 Japan

Yuji Tomita is a professor at Kyushu Institute of Technology (K.I.T.) and head of the Thermal Engineering Laboratory. He received his Ph D. Degrees in Mechanical Engineering from Tokyo University in 1970. His research interests are in the areas of pneumatic transport of solids and hydraulic capsule transport. While at K.I.T., he has worked on various aspects of gas-solid two-phase flow and established a new model for the hydraulic capsule transport. Yuji Tomita is a member of JSME, and the Society of Powder Technology, Japan.



Yukio Shimo

NTT Hokuriku Network Technical Center, 4-1 Dewa-machi, Kanazawa-shi, Ishikawa 920 Japan.

Yukio Shimo joined NTT in 1965 after graduating from Hokuriku Technical High School. He has been engaged in research and development of safe cable installation and sightseeing guide system using FM. He is now chief of cable setting section and a member of IEICE.



Kakuji Ohsumi

Toa Kikai Kogyo Co.,Ltd., 1-49 Chofuohgi-machi, Shimonoseki-shi, Yamaguchi, 752 Japan

Kakuji Ohsumi is president of Toa Kikai Kogyo Co.,Ltd.(TKK). He has been with the TKK group since 1950 after receiving his B.Sc. in Mechamcal Engineering from Yamaguchi University. He has worked on many aspects of machine construction and developed highly efficient operating systems for manhole construction and optical cable installation.



Toshiharu Hamade

NTT Hokuriku Technical Support Center, 4-1 Dewa-machi, Kanazawa, Ishikawa 920 Japan.

Toshiharu Hamade joined NTT in 1969 after graduating from Toyama Technical College. His research interests are in the area of cable installation over long distances. He has developed a sealing method for preventing the flow of N_2 gas-filler out from cable connection point. He is now chief of general constructing section and a member of IEICE.



Yuji Matsumae

Shirayuri Women's College, 1-25 Midorigaoka, Chofu-shi, Tokyo 182 Japan.

Yuji Matsumae is a lecturer at Shirayuri Women's College. He received his Ph D. from Waseda University in 1991. His research interests are in the area of fluid mechanics and computer science. Currently he is working on the characteristics of new nozzle developed by Dr.Horii, using a UNIX workstation to simulate the new nozzle's spiral structure generation. Yuji Matsumae is a member of the Institute of Electronics, Information and Communication Engineers and the Japan Aerospace and Science Society.

AN ALL DIELECTRIC FIBER OPTIC CABLE MONITORING SYSTEM

David Vokey, Ken Sontag, Jim Ritchie*

Norscan Instruments Ltd., 7 Terracon Place, Winnipeg, MB, Canada R2J 4B3
*** Manitoba Telephone System, 489 Empress St., Winnipeg, MB, Canada R3C 3V6**

ABSTRACT

A fiber optic cable monitoring system has been developed for use on all dielectric cables.

Operating over a single mode fiber, the system monitors and provides early warning of microbending and macrobending optical loss increases which are the result of changes in or damage to the cable structure.

Using a special moisture detection tape and digitally coded electronic sensors coupled to the monitoring fiber, the system uniquely identifies and monitors individual splice closures.

The first of such systems was deployed on a 95.5 km intra-provincial fiber optic cable route in Manitoba Canada.

INTRODUCTION

Cable monitoring systems, which provide early warning of cable damage or leaking splice closures have been previously reported[1,2]. These monitoring systems provide splice closure monitoring and/or sheath damage detection by operating over metallic elements such as a copper pair or cable armor.

For certain fiber optic cable applications, such as inclusion in overhead power transmission static wires, or when suspended below or with phase conductors on transmission towers, fiber optic cables are constructed using non-conductive all-dielectric strength members and protective sheaths. As a result, cable and splice monitoring methods, which require a metallic electrical conductor element can not be applied.

In an effort to provide optical loss and moisture monitoring OTDR techniques have been proposed[3]. However, in practical applications, OTDR methods require optical switching equipment to time share the system, operate only over spare fibers, do not work with optical coupler power splitting or WDM arrangements. Additionally, to detect water penetration into a splice closure, the OTDR technique requires a special moisture sensitive fiber bending device to induce a macrobend loss which must then be located.

An optical monitoring system was developed to continuously monitor the performance of selected single mode fibers and to relate that performance to the overall cable condition. Additionally, a novel splice moisture sensor was designed to uniquely identify and monitor the condition of the splice closures.

FIBER LOSS MECHANISMS

As shown in Figure 1, microbending related loss increases, which are caused by high frequency mechanical bend perturbations with radii in the nanometer range, are relatively independent of wavelength over the optical spectrum from 1300 to 1550 nm.

Microbending loss increases can usually be attributed to temperature dependent cable and/or coating problems, external forces which crush the cable structure or excessive tensile stain which forces the fiber against the sides of the buffer tube or strength elements.

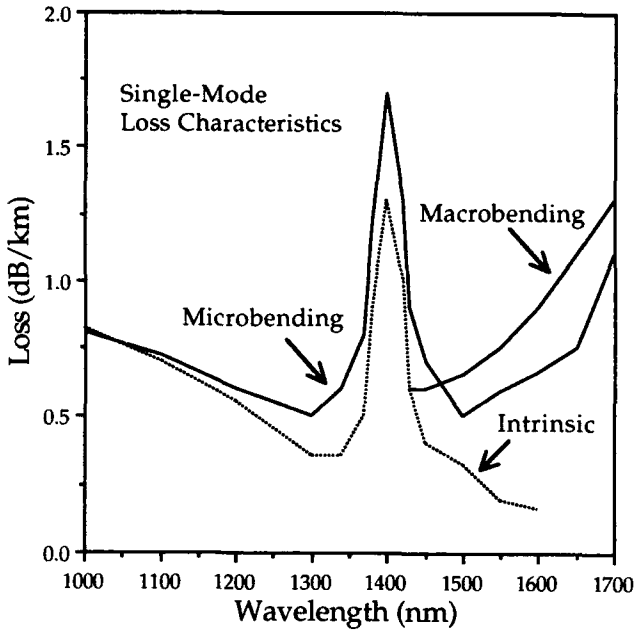


Figure 1: Single-Mode Loss Mechanisms

Loss increases, which occur predominantly at longer wavelengths, including 1550 nm, are caused by macrobending and are usually the result of a tightening of the fiber bend radius below acceptable limits.

Macrobending losses can occur inside of a splice closure if movement occurs or is caused which forces the fiber into a tighter bend.

Macrobending loss can also occur in the cable if the structure shifts through thermal or tensile loading. The differential movement of the cable sheath and/or strength members can cause a pull- back which buckles the fiber elements into a tighter radius.

This problem is most evident at the cable ends, especially at splice points, where the mechanical continuity is interrupted and coupling of the sheath and fiber elements to the antibuckling members is weakest.

DESIGN OBJECTIVES

In developing an optical monitoring system several design criteria were identified:

- Single mode fiber should be monitored for both microbending and macrobending losses to provide insight into loss mechanism.
- Splice closures should be monitored with a digitally coded sensor and moisture detection tape.
- The optical attenuation measurement system should have a wide dynamic range with high stability.
- Where no spare fiber is available, the system should operate over a "working" fiber without interference.
- The system design should allow simultaneous monitoring of several cable systems.
- The optical monitoring system should be plug-in compatible with an existing 2000 Cable Monitoring System (CMS) in use by several major telcos in Canada.

SYSTEM DESCRIPTION

To meet the outlined requirements, it was decided to use a dual wavelength modulated laser source. The basic monitoring system is shown in Figure 2. At the transmitter end, lasers were chosen with operating wavelengths of 1300 and 1550 nm. The dual wavelength source provides a critical look at the fiber loss characteristics at both operating windows. By observing loss increases at both wavelengths, an estimate of microbending and macrobending losses can be made.

Digitally coded sensor units are placed in the splice closures to detect any water ingress. In the alarm state, the sensors modulate the monitoring optical signal at 10 baud.

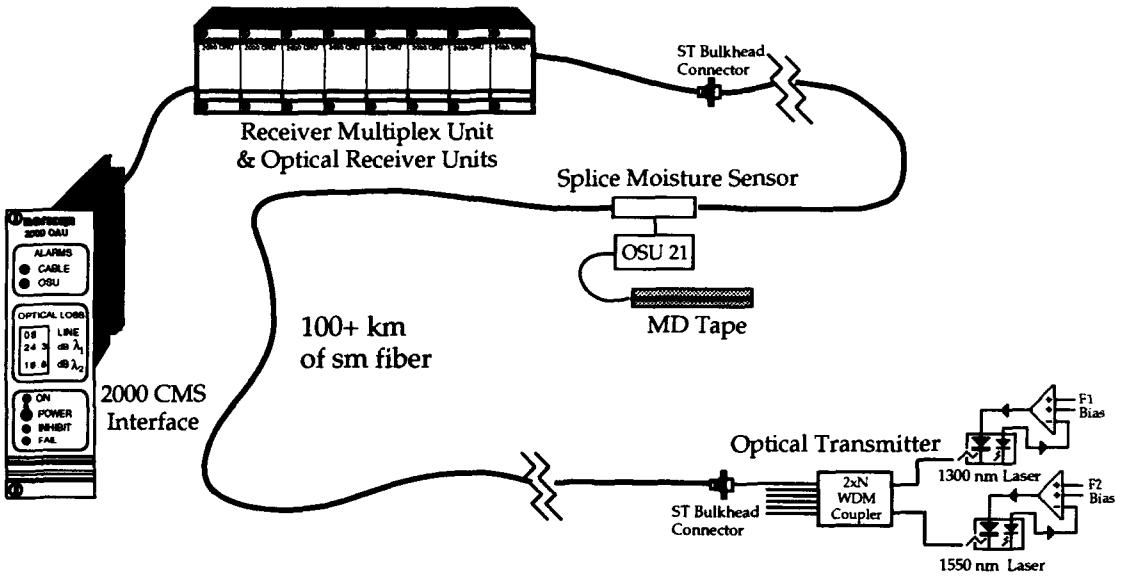


Figure 2: Basic Components of the Fiber Optic Cable Monitoring System

The optical receiver separates the detected optical signal into 1300 nm and 1550 nm components which are amplified and detected to provide power level signals.

Sensor alarm signals are derived from the amplifier outputs, detected, regenerated and forwarded to the 2000 CMS for decoding.

Optical Transmitter

The transmitter unit is rack mounted in the end office and consists of a stabilized power supply, modulators and laser drivers. A block diagram of the transmitter is shown in Figure 3.

To make efficient use of the 1300 and 1550 nm lasers, a 2x8 coupler is used to allow monitoring of up to 8 cable systems originating from the same office.

A feedback loop from the monitor photodiode is used to control the laser drive current so that the average output power is constant.

The 1300 and 1550 nm lasers are modulated at 20 k Hz and 30 k Hz respectively.

Optical transmitter specifications:

- Laser 1 ... $\lambda_1 = 1300 + - 20$ nm
 Po ≥ -8 dBm
 Modulation F1=20 k Hz
- Laser 2 ... $\lambda_2 = 1550 + - 30$ nm
 Po ≥ -8 dBm
 Modulation F2=30 k Hz
- Optical power stability 0.01 %
- Optical power at each output port .. ≥ -18 dBm

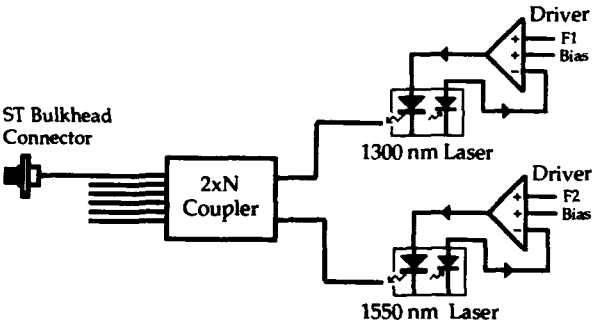


Figure 3: Basic Circuit of the Transmitter

Optical Receiver

The optical receiver, as shown in Figure 4, uses a InGaAs photodiode in a transimpedance amplifier configuration with an operational spectral range from 800 to 1800 nm.

The signals from the pre-amp are separated into F1 (20 k Hz) and F2 (30 k Hz) components, amplified and detected to give received power levels for 1300 nm and 1550 nm respectively. A lowpass section filters and detects any splice sensor alarm signals.

Up to 8 optical receivers can be mounted in the receiver multiplex shelf. The signals from all installed receivers are scanned and forwarded in digital format to the 2000 CMS for processing, display and alarm forwarding.

Optical receiver specifications:

- Spectral Range 800 to 1800 nm
- Measuring Range 0 to -65 dBm
- Resolution 0.1 dBm
- Accuracy +- 0.2 dB

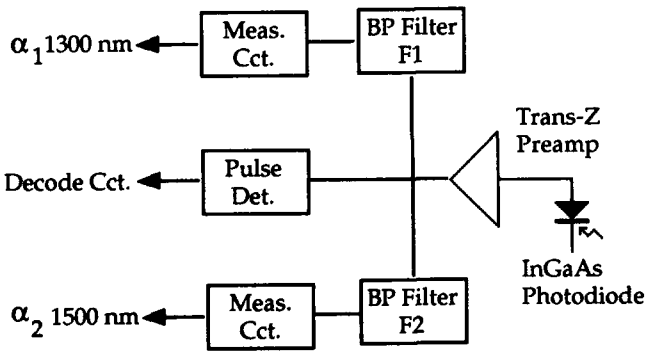


Figure 4: Block Diagram of the Optical Receiver

Splice Moisture Sensor

A novel approach was taken to the problem of monitoring the splice closures for moisture. It was desirable to place a device in the closure that would not only detect the presence of moisture but also transmit back to the receiver a digitally coded message providing the exact location of the wet splice. To accomplish this task, the problem of a power source for the sensor electronics had to be resolved. Assuming that no conductor would be available to carry power from the office equipment, it was obvious that the power would have to be generated at the splice location. It was decided that the splice located moisture sensor and power source would have to meet the following performance requirements:

- The power source and electronics must be capable of long term storage (20 yrs. or more).
- Upon detecting moisture, the sensor should activate and transmit an alarm signal for several hours.
- Low voltage, μ watt digital circuits driving a low power electro-optic modulator should be used.

The sensor, as detailed in Figure 5, was designed using microwatt digital circuits and a low power longitudinal offset modulator. When activated, the sensor pulses the electro-optic modulator with a 16 bit 10 baud drive current which amplitude modulates the optical signal.

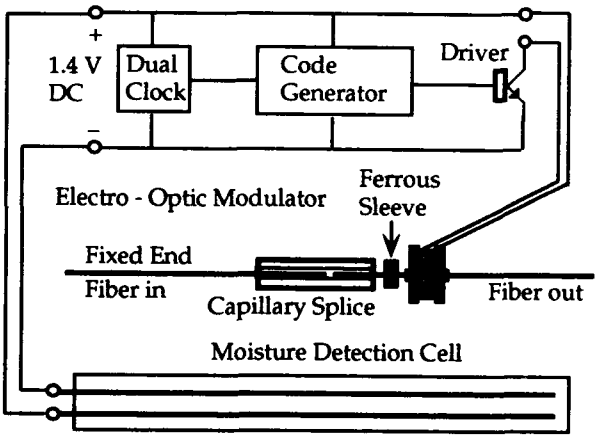


Figure 5: Moisture Detection Cell and Sensor Circuits

A special moisture detection tape operates as a water activated storage cell to power the sensor. The detection tape, as shown in Figure 6, is constructed with a strip of copper and a strip of magnesium separated by a porous insulator and a water soluble ionizing solid. When water comes into contact with the tape, an electrolyte is created and the tape becomes a voltaic cell to drive the sensor circuits. The cell develops approximately 2.5 V DC which is well above the 1.5 V required to power the sensor circuit.

The overall cell reaction is

$$Mg + Cu^{2+} \text{------>} Mg^{2+} + Cu \quad (1)$$

During testing, moisture sensors operated for periods of several hours with as little as a few cm of damp tape. In the dry state, the tape is inert and has excellent storage life.

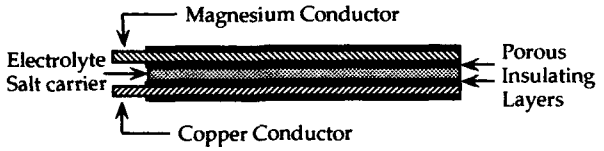


Figure 6: Construction of Water Activated Detection Cell

Monitoring a Working Fiber

When a spare fiber is not available, the monitoring system can be configured as shown in Figure 7. Wave Division Multiplex couplers with wavelength isolation of 16 dB or more are used at the ends of each span to separate the fiber monitoring system at 1550 nm from the transmission system at 1300 nm.

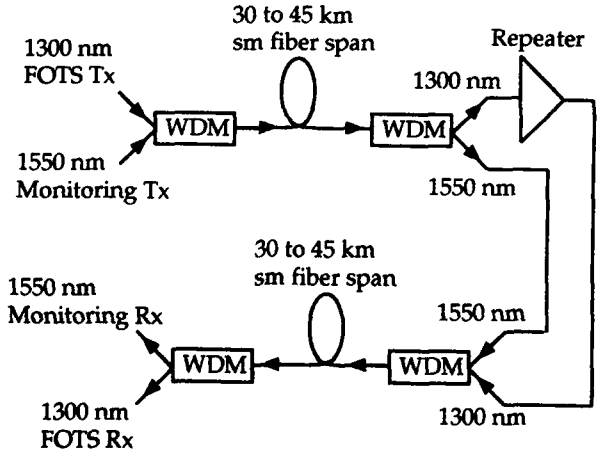


Figure 7: Monitoring at 1550 nm on a "Working" Fiber

The monitoring system continuously measures the optical performance of the fiber at 1550 nm where macrobending and microbending problems are more readily detected. Warning of loss increases are reported well in advance of transmission system degradation.

FIELD TRIAL

The first optical cable monitoring system was placed on a Manitoba Telephone System intra-provincial trunking route extending a distance of 95.5 km.

The cable construction, as shown in Figure 8, is a 6 to 12 tight buffered fiber, fully-filled design protected with a flooded double GP sheath (double layers of corrugated 0.15 mm coated steel tape and PE jacket). The cable and splice closures are direct buried at a depth of 72 inches.

For the initial tests, a spare fiber was selected and the optical transmitter and receiver equipment placed in the Headingly and Portage La Prairie central office locations respectively. A data line was connected via modem at the receiver equipment site to allow dial-up monitoring of the system and cable performance. As of this writing, the installation was in the completion stage.

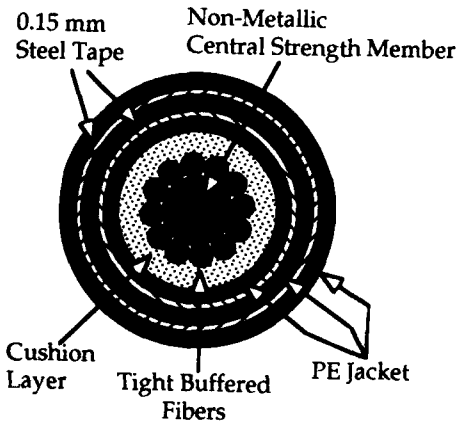


Figure 8: Typical Lay Up of 6 to 12 SM Fiber Cable

CONCLUSIONS

A fiber optic cable monitoring system has been developed to monitor the cable structure and splice closures for damage or moisture ingress.

Unlike other monitoring systems in current use, the new method does not require metallic conductors to provide an electrical path to monitor the structure or power splice located sensing devices. Additionally, OTDR techniques, which have also been proposed in recent literature, are not used thus avoiding the limitations and difficulties that they impose.

The first system of this design was deployed on a Manitoba Telephone System intra-provincial fiber cable route in 1992.

REFERENCES

1. Vokey, David E., "A Means For Monitoring and Protecting Outside Cable Plant For Moisture", Proceedings of the 29th International Wire and Cable Symposium, pp.452-56, November 18-20, 1980.

2. Sontag K., Ross A., "A Fiber Optic Cable Monitoring System", Proceedings of the 35th International Wire and Cable Symposium, pp.449-54, November 18-20, 1986.

3. Sawano H., et al, "Optical Fiber Cable with Submersion Sensor Fiber", Proceedings of the 36th International Wire and Cable Symposium, pp.284-90, November 17-19, 1987.



David Vokey works as a consultant for Norscan Instrument Ltd. He graduated from the The Manitoba Institute of Technology in 1969 with a Dip. of Tech in Electronic Technology, the University of Manitoba with a Bachelor of Science Degree in Electrical Engineering in 1973 and a Master of Engineering Degree in 1984. Prior to consulting for Norscan, he worked for Canada Wire and Cable as the Manager of Design and Development and for Siecor Corp. as the Manager of Cable Development with R&D. He is a member of IEEE and an associate member of the Association of Professional Engineers of Manitoba.



Ken Sontag is a Senior Engineer with Norscan Instruments Ltd. He graduated from the University of Manitoba with a Bachelor of Science Degree in Electrical Engineering in 1974. Prior to joining Norscan, he worked with Transport Canada in the telecommunications industry with responsibility for the design of communications, navigation and control systems. He is a member of the Association of Professional Engineers of Manitoba and the Association of Professional Engineers of Ontario.

Jim Ritchie began his career with the Manitoba Telephone system in 1973. He worked for 15 years as a cable splicer responsible for splicing and maintaining VF and F/O cables. Since 1983, he has been with Outside Plant Fibre Optics Standards as a Specialist responsible for evaluation, standardization and support of all outside plant F/O material, systems and equipment.

INSTALLATION OF SUBMARINE FIBEROPTIC CABLES IN RUGGED COASTAL TERRAIN

Svend Hopland and Albert Klykken *

Norwegian Telecom

Cables Division, Oslo
Submarine Cable Installation Group, Bodø *

ABSTRACT

We have described a concept for installation of fiberoptic submarine cables in rugged terrain. Multibeam echosounder surveys along cable route corridors have provided detailed terrain models and topograpy maps which are used to find optimal cable routes as well as to determine detailed laying programs for the cables. Laying angles for different cable types have been found by performing a towing experiment. An ROV-survey of laid cables have shown that the laying program must be closely followed in order to avoid cable suspensions or overlength on laid cables.

1. INTRODUCTION

Today, fiberoptic submarine cables are widely used in telecommunications. Cables are beeing installed between countries and continents, and telecom operators are installing submarine cable in the national networks.

A critical part of an fiberoptic submarine cable installation is the initial laying of the cable on the sea bottom. Fiberoptic submarine cables are vulnerable to damage and it is of great importance that the cable is properly laid on the sea bottom during the installation.

During laying of a light fiberoptic cable, excess cable length can easily be payed out, which may result in cable loops on the sea bottom. Such loops could be tightened during laying, resulting in a cable fault. However, loops can be left open, and in this case we can not detect any subsequent fiber attenuation increase. Nevertheless, the risk for a later cable fault is substantially increased. Attacks on or attempts to move the cable at several kilometers distance from an open loop may tighten the loop and cause a cable fault.

Also, insufficient cable length could be payed out, which may result in significant cable suspensions in rugged terrain making the cable vulnerable to future attacks. In addition, large suspensions could result in high point loads on the cable, which may, combined with cable movements due to sea currents, cause the cable to deteriorate over time.

Ideally, during laying only the exact amount of cable nescessary to cover the bottom profile should be payed out, and the laid cable should genarally form a straight line following perfectly the bottom terrain along a predetermined route. In our experience, with a light fiberoptic cable and a varying bottom topography, this is a difficult task. In this paper, we will describe an installation concept which allows a nearly perfect match of the cable to the sea bottom topography along a predetermined route.

2. SUBMARINE CABLE AND MARINE ENVIRONMENT

Norwegian Telecom is installing submarine cable along the Norwegian coast as parts of our junction and trunk network. The network connects population centra along the coast, and consist partly of land cable and partly of submarine cable. The submarine cables are used for crossing fjords, passing along fjords and elsewhere to connect parts of landbased cable.

Our submarine cable constructions are light armoured (LA) with one layer of armour, or heavy armoured (HA) with two layers of armour[1]. The cables have outer sheets consisting of a high density polyethylene with a smooth outer surface. Cable parameters are shown in Table 1.

Cable type	Weight in water (kg/m)	Outer diameter (mm)	Outer sheat
LA	1.0	25	HDPE
HA1	1.8	33	HDPE
HA2	2.1	36	HDPE

Table 1: Submarine cable parameters.

Our submarine cables are free from built-in mechanical tensions. Coiling tests are performed in the factory and on the cable ship to ensure that the cables are mechanically "dead". Only cables with perfect coiling properties are installed.

The individual submarine cable lengths are typically between 2 and 30 km. The maximum sea depth may vary between 20 and 1300 m. However, maximum depths of 150-700 m are most frequently encountered. Nearly 100 % of the cables are laid directly on the surface with no additional protective burial.

The sea bottom topography along the Norwegian coast is generally rugged and rocky. Near the landing points of a cable route, the bottom may be very steep and rocky. Elsewhere along a proposed cable route we may find underwater mountain formations, sharp and high ridges, valleys and troughs, but also parts of flat bottom consisting of soft clay or sand.

3. INSTALLATION METHOD

3.1 Cable route

A basic element in our installation concept is the provision of a detailed terrain model/topography map of the sea bed in a sufficiently broad corridor along the proposed cable route. This is accomplished by performing a comprehensive multibeam echosounder survey (MBE) along the proposed cable route. In a single MBE scan, data are collected from up to 60 single beams in a swathe covering a corridor of up to 7.4 times the sea depth. From these data, a high density digital terrain model is established. Subsequently, sofisticated data processing provides topography maps of the route corridors with a depth accuracy of 1-2 meters.

The topography maps are carefully studied in order to find the optimal cable route between the landing points. Here, our intention is to "hide" the cable in terrain formations and to avoid passing over high ridges and the steepest slopes. However, terrain slopes of 30-60 degrees can be frequently encountered and sometimes almost vertical walls must be passed.

Having determined the optimal cable route on the sea bottom, the vertical bottom profile is established. We also determine the surface line which the cable ship shall follow during laying of the cable. This line is the horizontal projection of the cable route, except in the regions where a change in course takes place. Here, we make a surface position compensation in order to place the cable in correct position on the sea bottom. An example of part of a horizontal and vertical profile of a cable route is shown in Figure 1.

3.2 Cable laying

During laying, it is necessary to deploy cable slack in order to match the terrain on which the cable is laid. If the terrain forms a constant slope and the cable assumes a straight line configuration from the cable ship down to the bottom, the slack to be payed out can be expressed as [2]:

$$(1) \qquad \frac{V}{Vc} = \frac{\sin \alpha + \sin \beta}{\sin (\alpha + \beta)}$$

where V is the speed of the cable ship, Vc is the payout rate of the cable, α is the angle between the cable and horizontal and β is angle between the bottom and the horisontal. For downhill laying β

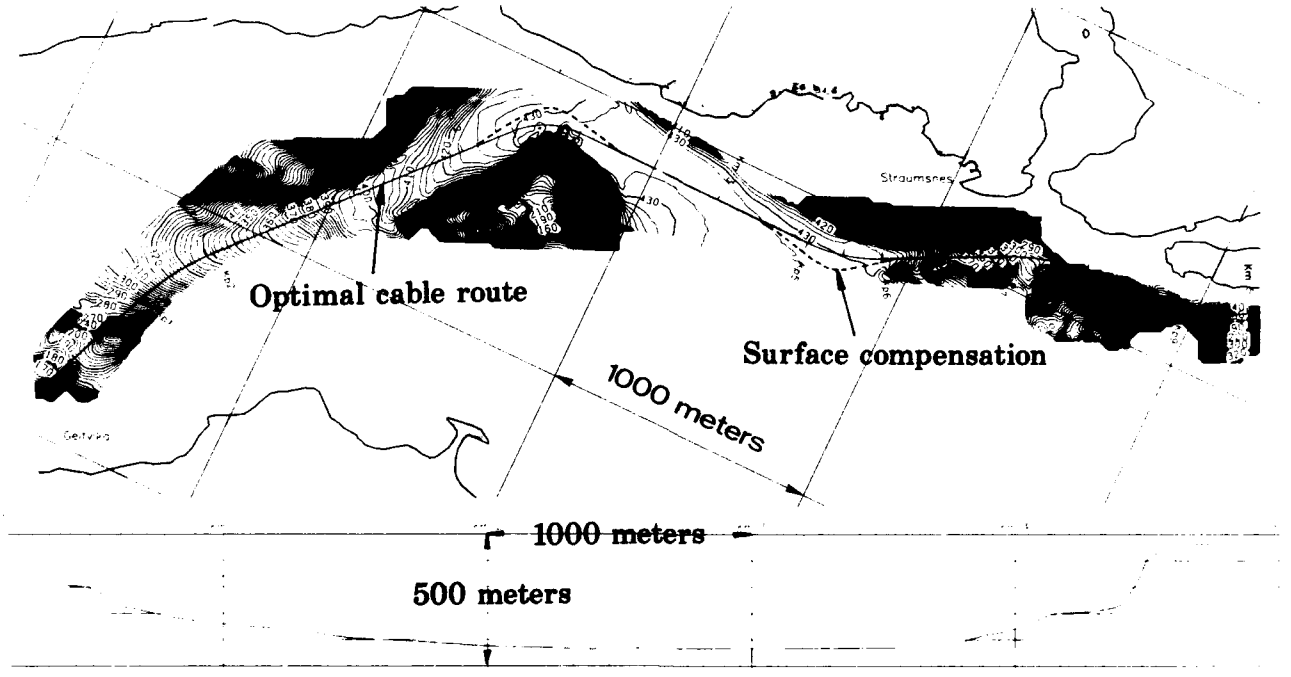


Figure 1: Example of horizontal and vertical profile of part of a cable route.

is positive, and for uphill laying β is negative. In addition, for uphill laying, $|\beta|$ must not exceed the laying angle α in order to avoid cable suspensions.

For laying on flat bottom, the payout rate equals the ship speed and the slack is zero.

The laying angle α for steady laying of the cable is approximately given by [2]:

$$\alpha = \frac{H}{V} \qquad (2)$$

where H is the hydrodynamic constant of the cable.

The necessary slack increases as the terrain slopes and laying angle increases. Substantial slack have to be payed out or hauled in as the terrain becomes rugged.

In a practical case, the terrain slope varies continously throughout the cable route. When the terrain becomes rugged, the variations in bottom slope β can be rapid and significant. We have used our digital terrain model of the cable route corridor to precalculate an exact laying program for each cable route. Basically, for all surface positions during laying, the cable length from the ship down to the sea bottom and fitting exactly the bottom profile for the desired cable route backwards to the starting point, are calculated. Here we assume a straight line cable configuration from the ship down to the bottom as shown in Figure 2. Instantanous slack values for all ship positions are derived. This is carried out for different laying angles and in both laying directions.

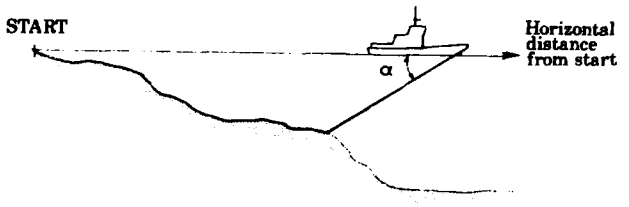


Figure 2: Geometry for calculation of laying program.

Several factors are considered before a final laying program is selected. The laying angle is kept constant throughout the cable route, and is chosen according to the results of the towing experiment described later in chapter 4. Different laying angles are used for different cable types. The cable route topography is studied to find the optimal laying direction. For reasons described later in chapter 5, the laying direction giving the minimum uphill slope, is preferred. In most cases, the reqiurements for laying angle α to be higher than the uphill slope β, is satisfied. Otherwise, special procedures must be followed.

Sea currents and wind may sometimes be significant along the Norwegian coast, but can be minimized by a proper timing of the laying operation.

The laying program and the surface line to be followed during laying, are fed into a computer which continously controls the laying of the cable. Readings of actual ship position, cable length deployed, ship speed and cable payout rate are continously compared with the precalculated values and any deviations from the precalculated laying program are corrected.

4. TOWING EXPERIMENT

When performing steady laying, the cable should in theory form a straight line configuration from the ship down to the bottom[2] with an angle given by Equation (2). To check the validity of this assumption and to determine laying angles for our cables, a towing experiment was performed.

Cable lengths of approximately 300 meters of LA and HA2 type (Table 1) were towed after the ship. 4 minitransponders were mounted on each cable with intervals of 75 meters. Using a high precision underwater navigation system, the positions of the transponders relative to the ship were continously monitored during towing. The transponders were small and light compared with the cables and should not affect the towed cable geometries.

In Figure 3 is showed towed cable geometries at five different times approximately 3 minutes apart in a 15 minutes interval of steady towing of the LA cable and the HA2 cable. The average ship speed in the 15 minutes interval was 2.1 and 1.4 knots for the LA and HA2 cable, respectively. All readings of cable geometries during steady towing showed curves with straight lines or nearly straight lines. This suggest that the straight line approximation is valid for steady laying of our cables.

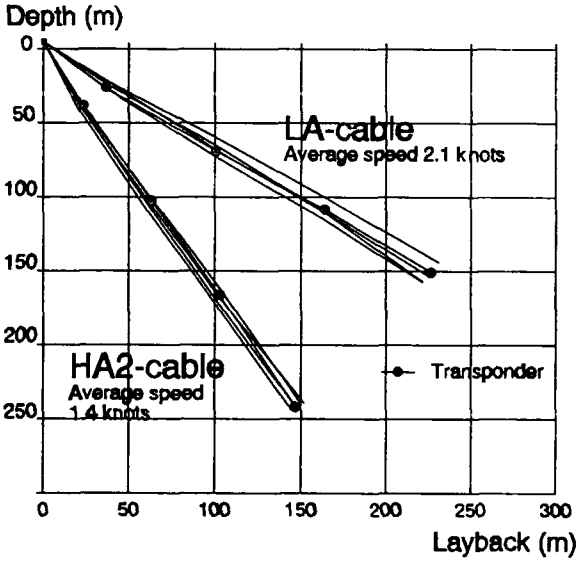


Figure 3: Examples of cable towing geometries.

In Figure 4 is shown the average towing angle versus average towing speed for LA and HA2 cable. We observe that the towing angle for HA2 cable is approximately 10 degrees higher than for LA cable at all towing speeds.

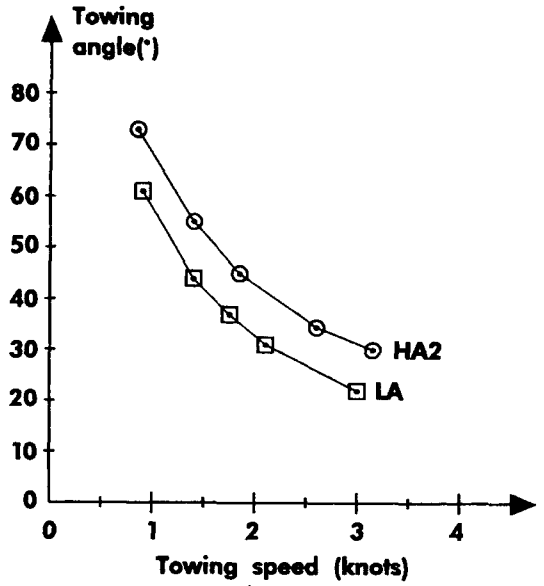


Figure 4: Towing angle versus towing speed.

The cable laying speed is usually 1.5-2.0 knots. At a laying speed of 2.2 knots, the towing angles are approximately 30 degrees and 40 degrees for LA cable and HA2 cable, respectively. These values are selected as the basic laying angles for LA and HA2 cables.

5. INVESTIGATION OF INSTALLED CABLES

In order to investigate our laying concept we have performed a comprehensive ROV-survey of 4 different cable routes. The total examined length was approximately 30 km with maximum sea depths of 300-600 m. The routes contained a variety of steep and rocky downhill and uphill slopes including almost vertical walls as well as flat bottom. A cable tracker was used to locate the cable in areas where it had disappeared in the soft clay. Throughout the cable routes we have determined cable positions and cable configurations.

During laying of these cables, manual correction of ship's course, and ship speed and cable payout rate was performed to fit the laying program. Therefore, deviations from the laying program was experienced in short periods. We have correlated the actual cable positions cable configurations on the sea bottom with the laying program and have reached some important conclusions which are summarized in the following:

With this method the cable can be placed close to the desired position on the sea bed. On the investigated cables, the accuracy in bottom position was typically 10-30 meters. In regions where a change in ship's course was made, the accuracy could be less if not correct compensation was made on the surface. The survey observations suggest that an accuracy which is fully adequate to place the cable in the terrain formations, can be obtained. In Figure 5 is shown the predetermined cable route, cable ship route and actual laid cable positions for one of the surveyed cables. Laid cable configurations are also indicated.

None-perfect cable configurations on the bottom were found at positions corresponding well with expected positions according to "incidents" on the cable ship on the surface. This conforms to the assumption of a straigth line cable configuration from the ship down to the sea bed.

When the touch-down point of cable is in a downhill slope (laying downhill), some deviation from the

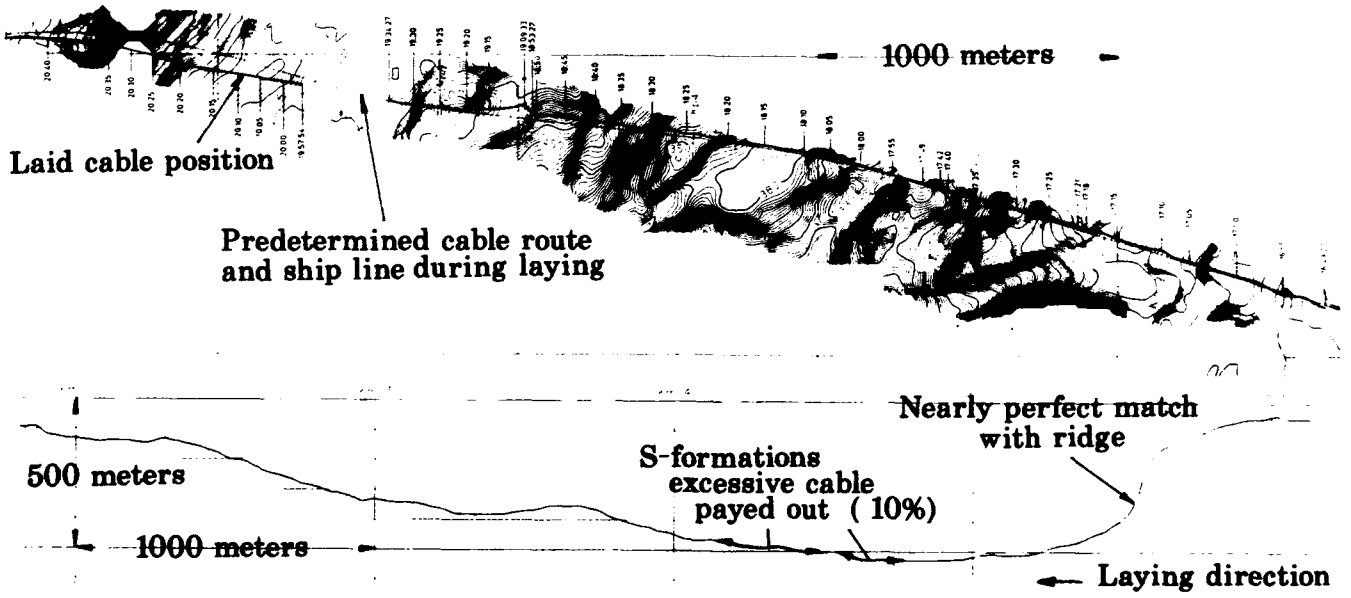


Figure 5: ROV-surveyed cable route.

payout program can be tolerated without any affects on the laid cable configuration. Due to weight and low friction against the bottom, the cable tends to be tensioned and consequently forms a straight line. Obviously, in steeper rocky slopes the cable can not fill in small bottom irregularities and hence short regions with suspended cable cannot be avoided.

However, to avoid significant cable suspentions when laying downhill, sufficient cable length must have been deployed at the end of the downhill slope. In our experience, when high steep slopes or walls are passed, only a few tens of meters insufficient cable length may result in large cable suspensions.

If excessive cable length have been payed out at the end of a downhill slope, the laid cable still forms a straight line; but the laying angle have increased. From this point onward we may change to a slightly different laying program with an new laying angle, or we may carefully adjust back to the initial laying program.

When laying cable on flat bottom, we have found that it is important that the payout program is closely followed. We have observed that only a 10 % excessive cable payout rate during a short time period have resulted in significant S-formations on the cable.

When laying the cable in an uphill slope it is very important that the laying program is critically followed. Due to cable weight, low friction against the bottom and terrain topography details, excessive cable length may move along the bottom slope and accumulate in small areas and eventually cause large S-formations or loops. We have registered that only a few excessive cable meters may cause such problems. As a consequence, the laying direction giving the minimum uphill slope is preferred.

In summary, these observations suggest that any corrections to the laying program during laying should be performed automatically by the computer.

6. NAVIGATIONAL ACCURACIES

Our installation concept is dependant on the use of high accuracy navigational equipment for the maritime operations. We have used the Global Positioning System (GPS) in the differential mode or alternatively landbased transponder systems as navigational aids for the multibeam echosounder survey and the cable laying operation. In addition, for the ROV-survey of laid cables and the towing experiment, high precision underwater navigation systems were used. All systems have positional accuracies of better than $\pm$ 5 meters.

7. CONCLUSIONS

We have described a concept for installation of fiberoptic submarine cables in rugged terrain. A key element is the use of detailed terrain models and topography maps of cable route corridors provided by performing comprehensive multibeam echosounder surveys along the cable routes. These models/maps are used to find the optimal cable route between the landing points as well as calculating detailed laying programs for the cable laying operations. We have performed a towing experiment to determine laying angles for our submarine cables. The towing experiment has also shown that a straight line cable configuration can be assumed during steady laying of the cables. We have surveyed a number of installed cables and determined their position and as laid configuration on the sea bottom. The survey results have shown that the cable can placed with good accuracy on the sea bottom. Furthermore, we have found that the laying program must be closely followed in order to avoid cable suspensions or overlength on the laid cable. Automatic correction to the laying program during laying is reqiured.

8. ACKNOWLEGDEMENT

The authors would like to thank the crew on our cable ship "Nordkabel" for performing continously enthusiastic field work. Also thanks to Emil Marhaug, Norwegian Telecom for indispensable assistance in the field.

9. REFERENCES

1. S. Hopland: "Measurements of low hydrogen levels in installed open fiberoptic submarine cables": ICWS 1991, pp. 742-748.

2. E. E. Zajac: "Dynamics and kinematics of the laying and recovery of submarine cable": Bell System Technical Journal, Sept. 1957, pp. 1129-1207.



Svend Hopland
Norwegian Telecom,
Cable Division,
Munch's gate 5B,
N-0130 Oslo, Norway

Svend Hopland graduated from the Norwegian Institute of Technology in 1985 with a Ph. D. on optical fibers. In 1986 he joined Norwegian Telecom, Cables Division. He is presently a senior engineer on fiberoptic cables.



Albert Klykken
Norwegian Telecom,
Submarine Cable
Installation Group,
8000 Bodø, Norway

Albert Klykken joined Norwegian Telecom in 1976. In 1986 he graduated from Gjøvik Collage of Engineering. He is presently technical engineer on Norwegian Telecom's cableship "Nordkabel".

CHARACTERIZATION AND DEVELOPMENT OF FOAM-SKIN POLYETHYLENE INSULATION RESINS

Koksal Tonyali and Priya L. Fernando

Quantum Chemical Corporation
11530 Northlake Drive
Cincinnati, OH 45249

ABSTRACT

Foam-skin insulation resins are coextruded onto conductors at high line speeds up to 8000 feet/minute. High line speeds impose very strict processability requirements on high density polyethylene (HDPE) resins. An acceptable resin must exhibit high melt strength and a smooth surface (no melt fracture or rough surface) with low shrinkback properties at these high shear rates. In coextruded foam-skin constructions, interfacial instability between the layers has been identified as a cause of surface roughness. The insulation resins are also required to exhibit excellent environmental stress crack resistance (ESCR). In this work, these material parameters were evaluated using low and high shear rate rheology, shrinkback test and an ESCR test based on linear elastic fracture mechanics. Structure-property relationships were developed for HDPE and these concepts were applied in new resins to optimize performance.

INTRODUCTION

Wire coating involves an extrusion coating process to manufacture a solid insulation single or a coextrusion process to form a multilayer (foam-skin) insulation. High density polyethylene (HDPE) is usually the material of choice for insulating telephone singles.

High extrusion speeds up to 8000 ft/min impose strict property requirements on polyethylene. A quality insulation resin is expected to exhibit good processability with smooth surfaces, excellent environmental stress crack resistance (ESCR) and low shrinkback.

Commodity polyethylene resins exhibit melt fracture at high shear rates experienced in the wire extrusion coating process. The elimination of melt fracture or rough surface in foam-skin insulations has been studied [1,2] by modifying the molecular weight (MWt) and the molecular weight distribution (MWtD) of the polymer. It has been concluded that rough surface formation was not entirely controlled by MWt (or MWtD) of the polymer [1,2].

During the wire coating process, the molten polymer molecules are extended or oriented considerably under the influence of high stresses. Chain orientation introduces residual stresses and strains in insulations upon cooling from the melt [3,4]. The relaxation of these stresses leads to the retraction of the insulation, described as **"shrinkback"** exposing the conductor. The shrinkback behavior is attributed to the viscoelastic relaxation of the oriented molecules [1,3]. Rough surfaces and high shrinkback result in poor quality telephone insulations which lead to cross-talk and installation difficulties.

Environmental stress crack resistance (ESCR) of the resins is also important to protect the conductors from aggressive environments such as surface active agents, hydrocarbons, oils, etc. Cable manufacturers often require the resin manufacturers to include a minimum specification on ESCR.

The purpose of this paper is to discuss insulation resin requirements and efforts to tailor HDPE's with a balance of properties for communications cable applications. Individual property requirements are studied using the knowledge of structure-property relationships. The elimination of undesirable properties, such as rough surfaces and high shrinkback, is discussed. The development of a superior insulation resin is undertaken based on this fundamental knowledge.

EXPERIMENTAL

The characteristics of the HDPE resins employed in this study are presented in Table I. All resins were made using the same catalyst system except Resin E to study the effect of structural parameters on physical properties. Using the same catalyst system allowed varying only one

structural parameter of a resin at a time while the other variables were kept constant.

Environmental Stress Crack Resistance (ESCR) Test

ESCR of the resins was evaluated using the 3-point bend test described elsewhere [5]. Plaques were compression-molded at 170°C under 100,000 psi for 10 minutes, and then water-cooled to room temperature. Six millimeter thick 3-point bend specimens with a span of 60 mm and a width of 10 mm were cut from the plaques. A sharp notch with a depth of 2.5 mm was introduced to each specimen using a sharp fly-cutter blade. The failure times were determined in a 10% Igepal solution at 30°C under a constant bending load of 3.9 kg.

Low Shear Rheology

Rheological properties were measured using a Rheometrics Mechanical Spectrometer - Model RMS-605 operated in the oscillatory mode with 20% strain at 190°C. The frequency ranged from 0.01 to 400 rad/s with a parallel plate geometry of 25 mm diameter. The data are expressed as complex viscosity or modulus as a function of frequency.

High Shear Rheology

Melt fracture or melt instability was detected at 190°C using a Rosand Twin Barrel Advanced Rheometer System equipped with a capillary die (L/D= 16). The results were corrected for end effects. The data were presented as a plot of shear stress (or viscosity) vs shear rate. The critical shear rate for melt fracture or instability was obtained from the graphs.

Shrinkback Measurements

Shrinkback level was determined by evaluating insulated wires from commercial and laboratory wire coating lines. Six inch insulated wire specimens were placed on a felt surface in an air circulated oven at 115°C for 24 hours. The insulation relaxed during the heat treatment exposing the copper wire. The extent of shrinkage, i.e., the total length of bare copper wire, was measured in 1/64 inch units.

RESULTS AND DISCUSSION

The resin properties of HDPE are controlled by the structural parameters such as molecular weight (MWt), molecular weight distribution (MWtD), density, comonomer content, and comonomer branch distribution [6]. The influence of these parameters on properties is illustrated in Table II. Resins can be tailor-made to provide the necessary property balance required for specific applications by careful selection of structural parameters. For instance, ESCR, elongation and melt viscosity of a polyethylene may be increased by increasing the high molecular weight fraction of the molecular weight distribution. However, increasing MWt has a negative effect on processibility. Improving the processibility by broadening the molecular weight distribution of the resin usually sacrifices the mechanical properties (Table II). Thus a compromise is needed to obtain the optimum property balance. The resin requirements for communications cable applications are discussed below with the fundamental understanding of the influence of structural parameters.

Environmental Stress Crack Resistance

Bent strip ESCR test [7] is often employed to evaluate the ESCR of wire and cable resins. A recent paper discusses the major drawbacks of this method [5]. A novel technique based on linear elastic fracture mechanics concept was utilized to rank the materials in this report [5]. Failure times for Resins A to D using the 3-point bend test were measured and presented in Figure 1. The values at the top of the bars indicate the densities of the resins. Resins A through D have the melt indicies of 0.40, 0.35, 0.70 and 0.70, respectively. All resins were made using the same catalyst system. Resin A was further modified using a post-reactor modification process to obtain Resin B. Figure 1 illustrates the influence of structural parameters on the ESCR property. Lowering the molecular weight from 110,000 to 94,000 (Resin A and Resin C) reduces the ESCR while decreasing the density improves the ESCR (Resin C and Resin D).

The 3-point bend test succesfully differentiated the inherent property differences in resins [5]. The differences between Resin A and Resin B were not apparent by the bent strip test. Figure 1 indicates the usefullness of the 3-point bend ESCR test in ranking resins.

Similarly other physical properties of wire and cable resins can be improved by varying the density and the melt index of the resin for a given system. A comparison of Resins B, C and D is presented in Figure 2. Mechanical properties were measured using ASTM type IV specimens according to the method D-638.

Processability of Resins

Rheological measurements at low and high shear rates are useful in characterizing the flow properties of a resin. The processability requirements for telephone insulation resins are very stringent due to the high extrusion speeds or extremely high shear rates in the wire coating process. The laboratory tests performed at much lower shear rates can only differentiate the materials on a relative basis.

Polymer melt flow in the extrusion die becomes disrupted at the onset of flow instability. Flow instability causes melt fracture or rough surfaces of the insulation during extrusion. Usually it is difficult to quantify or predict the onset of melt fracture. Barnett [8] defined a melt fracture number (MFN) for a specific processing equipment. It was argued that MFN is proportional to the viscosity of the resin and the shear rate, and is inversely proportional to the molecular weight distribution of the resin. MFN usually remains constant, but the critical shear rate changes upon varying viscosity, MWt and MWtD.

Barnett's argument [8] was applied to the resins in Table I. The plots of shear stress vs shear rate in Figure 3 illustrate the melt fracture phenomenon. Resin A begins to show a decrease in shear stress **"melt instability"** at a critical shear rate of 2000 1/s. This resin shows melt fracture at an extrusion line speed of 5000 ft/min. Resins C and D with a lower melt viscosity (Table I) showed no melt fracture in Figure 3. Correspondingly, Resins C and D exhibited smooth insulation surfaces above 6500 ft/min on commercial wire lines.

Resin B processed well at 6000-6500 ft/min line speeds while exhibiting shear modification [9]. The critical shear rate of Resin B for melt fracture was determined by the laboratory test to be 3000 1/s compared to 2000 1/s of Resin A.

In **"single layer"** solid insulation applications, the surface roughness is due to the melt fracture of the resin. Melt fracture may be prevented by resin modification or adjusting the structural parameters. However, no correlation was seen between the critical shear rate and the formation of rough surfaces in coextruded foam-skin insulations. Previous studies showed that the quality of the foam-skin insulation is not dependent entirely on the molecular weight and molecular weight distribution of the resins [2,10].

In some cases it was observed through light microscopy analysis that the skin thickness in foam-skin insulations was non-uniform. A schematic drawing is shown in Figure 4. The interface between the foamable resin and the skin resin was wavy although the insulation surface was smooth. Further, at extreme conditions rough surfaces were observed on the insulation surface when the magnitude of waviness increased. However, a smooth surface resulted when the same skin resin was coated onto conductors as a single layer. Therefore, the formation of rough surfaces was seen to be dependent on the characteristics of both the foamable and the solid resin components.

Surface roughness in coextruded foam-skin insulations was successfully eliminated by matching the viscosities of the foamable and the solid resin at high shear rates, i.e, at 6500 ft/min line speed. Selecting a foamable resin (Resin D) and a solid resin (Resin B), both with a viscosity of 2900 P at a shear rate of 1000 1/s, resulted in a smooth insulation surface and a uniform skin thickness. However, increasing the melt viscosity of the skin resin to 3200 P and above at 1000 1/s introduced a rough surface to the insulation. Skin resins with vicosities between 2900 and 3200 P at a shear rate of 1000 1/s indicated only wavy interface between the foam and skin layers. All of these insulation resins showed no rough surface when they were coated as a single solid layer onto a 26 AWG copper conductor at 6500 ft/min, i.e, without the foamable resin.

A recent paper [11] discusses the melt instability in coextruded films. It is proposed that interfacial flow instability at the melt interface is responsible for the interface waviness. We speculate that similar interfacial instability also led to a non-uniform skin thickness in coextruded foam-skin insulations. Based on the melt flow instability phenomenon [11 and references therein], it is suggested here that the foamed melt layer molecules relax faster than the skin polymer molecules. The higher mobility of the foamable melt results in regions of relaxed molecules leading to non-uniform foam or skin thickness. This phenomenon may be analagous to the changes in dimensions (thicker thickness, shorter length) of an uniaxially oriented article when it is annealed at temperatures close to its melting point.

The formation of a wavy interface between the foam and the skin is due to the non-uniform relaxation of the molecules. Thus matching the viscosity of both the foamable and the skin resins would eliminate the interfacial instability leading to a smooth interface because of uniform relaxation of the polymer molecules. Furthermore, small increases in the viscosity of the skin

layer would introduce a wavy interface, although the foam-skin insulation surface is smooth. However, a rough insulation surface would be generated if the viscosity differences between the foamable and the skin resins is too large (Figure 4). The size of the wavy structures could become very large compared to the dimensions of the insulation thickness.

A large melt viscosity difference between the resins in a coextruded foam-solid construction seems to affect the surface quality of the insulation as well as the skin thickness uniformity. However, further work on melt behavior of the resins is needed to gain full understanding of rough surface formation.

Rough surface formation in foam-skin insulations was accompanied with lower tensile elongation values (as much as 50 percent) since localized deformation occurred in the thinner solid sections of the insulation. As a result of this non-uniformity, a break-up of the foam underneath the solid insulation was also observed. Further, variations in the capacitance seen with this insulation may also be the result of this irregularity.

Shrinkback

Molten polymers exhibit time dependent elastic behavior. The melts are subjected to high shear rates during wire coating. As a result the polymer chains are elongated or oriented along the flow direction. The chain orientation causes built-in stresses in the insulation upon cooling the melt. Such residual stresses lead to shrinkback causing difficulties during installation and performance deficiencies [1,3,4]. The residual stresses and the molecular orientation can be controlled by the molecular weight and molecular weight distribution of the polymers, and the cooling conditions during extrusion.

One approach to prevent shrinkback problems is to modify the polymer molecules which relax faster than the time scale of the fabrication process. Molecular relaxation processes may be studied by employing low shear rate dynamic rheology tests [12]. Dynamic complex viscosity vs frequency plots are shown in Figure 4 for Resins A, B, D and E. Resins A, B and E are commercial resins while Resin D is a developmental resin. Resin A is a high molecular weight polymer (Table I) and, thus, it exhibits higher melt viscosities at all frequencies compared to Resin D.

Resin B shows shear modification [1,9] leading to lower shrinkback values. This polymer behaves in a similar manner as a high molecular weight resin at low shear rates (low frequencies), while it demonstrates shear thinning at high shear rates (high frequencies). The shrinkback values for Resins A, B, D and E were measured to be 9"/64, 6"/64, 4"/64, and 3"/64, respectively. The samples were prepared using a 26 AWG solid insulated copper conductor coated at 3200 ft/min line speed on a laboratory extruder. The shrinkback value is higher in Resin A, as expected, since the molecular weight is higher than those of Resins D and E (Table I), and it does not show any shear thinning effect at high frequencies (Figure 5).

The relaxation of the molecules with longer chain length is difficult due to the lower mobility of the chains [12]. The molecular weight of Resin A was lowered to increase the chain mobility (Resin D) and hence, the shrinkback was reduced from 9"/64 to 4"/64. Resin D was also coated onto a 26 AWG copper conductor on a commercial wire line at a line speed of 6500 ft/min. The resulting insulations showed less than 1"/64 shrinkback. The lower shrinkback value may be partly due to the good control of the cooling process on commercial wire lines.

The relaxation process of polymers can be predicted using dynamic rheology data [12]. A plot of elastic modulus as a function of frequency is presented in Figure 6 for resins A and D. Resin A exhibits higher viscosities (Figure 5) and elastic moduli (Figure 6) at all frequencies compared to Resin D. Higher viscosity values are attributed to the presence of longer polymer chains in Resin A. Thus it is expected that the molecules of Resin D relax faster than those of Resin A. Higher elastic modulus and melt viscosity values indicate the presence of longer molecular weight species in Resin A leading to longer relaxation times. Lower viscosity of Resin D supports the observation of low shrinkback values.

CONCLUSIONS

The key resin property requirements for communications cable applications were studied. The results may be summarized as follows:

1. Resin D was optimized for communications cable insulations using the knowledge of structure-property relationships.

2. ESCR of HDPE's may be evaluated using a novel 3-point bend test based on fracture mechanics concepts to differentiate inherent resin properties.

3. Melt fracture and shrinkback may be prevented by modifying the molecular weight and the molecular weight distribution.

4. Rough surface formation in foam-skin insulations is attributed to interfacial instability between the foamable and the solid resin during the coextrusion process.

ACKNOWLEDGMENTS

We thank S. Chang, H. Mavridis, D. Roberts and R.N. Shroff of Quantum Chemical Corporation for their valuable discussions.

REFERENCES

1. L.Wild, M. Goekbora and C.D. Lee, Proceed. Int. Conf. on Electrical and Electronic Materials, **2**, 46 (1990).

2. Y.S. Kim and J.Y. Hah, Proceed. 40th Int. Wire Cable Symp., 492 (1991).

3. C.R. Taylor, H.M. Dillow and C.J. Aloisio, Proceed. 31st Int. Wire Cable Symp., 350 (1982).

4. S.R. Barnes, O.C.A. Hill, M.K.R. Vyas and R. Sutehall, Plast. in Telecommu., 4th Int. Conf., 10.1, 1986.

5. K. Tonyali and P.L. Fernando, SPE Annual Technical Conf. Proceed., 2200 (1991).

6. Encyclopedia of Chemical Technology, 3rd Ed., Vol. 16, p421, Wiley, 1981.

7. Bell ESCR Test, ASTM D-1693 Method.

8. S.M. Barnett, Polym. Eng. Sci., **7**, 168 (1967).

9. B. Maxwell, E.J. Dormier, F.P. Smith and P.P. Tong, Polym. Eng. Sci., **22**, 280 (1980).

10. Z.Y. Xi, Proceed. 39th Int. Wire Cable Symp., 59 (1990).

11. R.N. Shroff and H. Mavridis, Plast. Technol., February Issue, 54 (1991).

12. J.D. Ferry, Viscoelastic Properties of Polymers, 3rd Ed., Wiley, New York, 1980.

Table I. Characteristics of High Density Polyethylenes

PROPERTY	RESIN A	RESIN B	RESIN C	RESIN D	RESIN E
DENSITY (g/cc)	0.946	0.946	0.946	0.944	0.944
MELT INDEX (g/10 min)	0.40	0.35	0.70	0.70	0.70
Mw	110,000	115,000	94,000	95,000	111,000
Mw/Mn	9.2	11.0	8.8	8.9	11.5
VISCOSITY (P) AT 1000 1/s	3400	2950	2850	2900	3000
SHRINKBACK (1/64 in)	9	6	---	4	3

--- Mn and Mw are number and weight average molecular weights, respectively.

Table II. The Influence of Structural Parameters on Resin Properties

PROPERTY*	INCREASING DENSITY	INCREASING MWt	BROADENING MWtD
ESCR	-	+	+
TOUGHNESS	-	+	-
STIFFNESS	+	...	...
YIELD STRESS	+	...	...
ELONGATION	-	+	...
MELT VISCOSITY	+	+	-
PROCESSABILITY	...	-	+

* + and - denote increasing and decreasing, respectively.

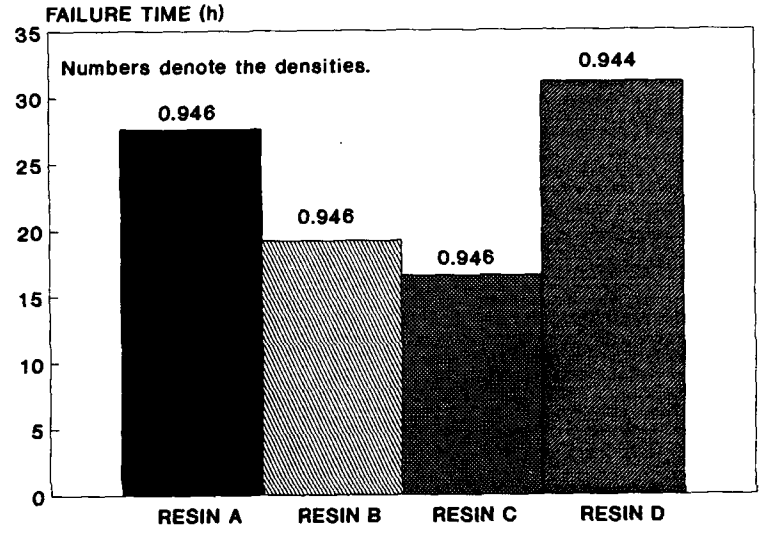


Figure 1. ESCR Failure Times for HDPE Resins

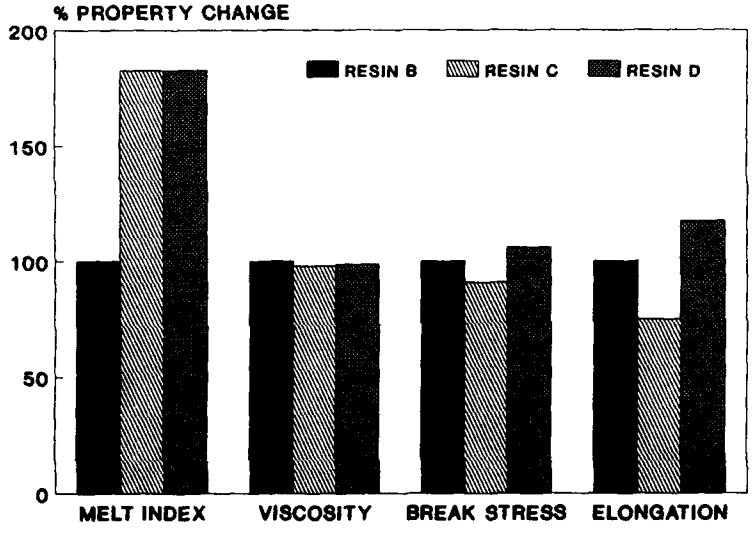


Figure 2. Effect of Melt Index and Density on Properties

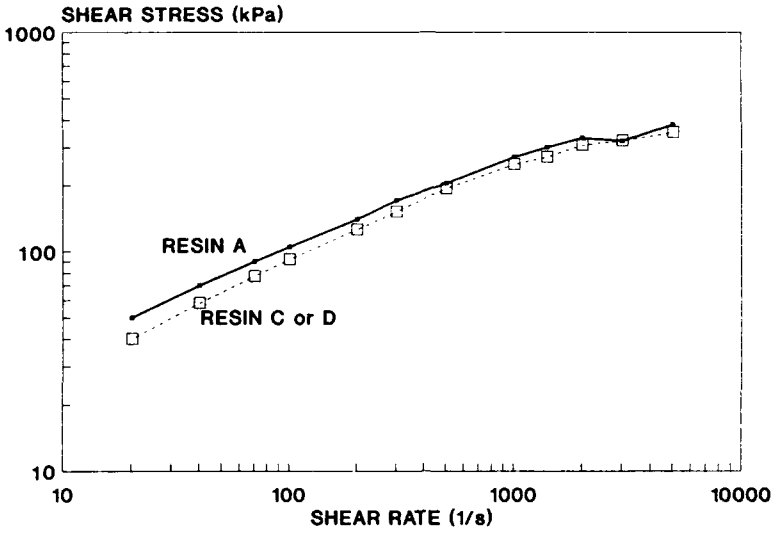


Figure 3. Determination of Melt Flow Instability Point

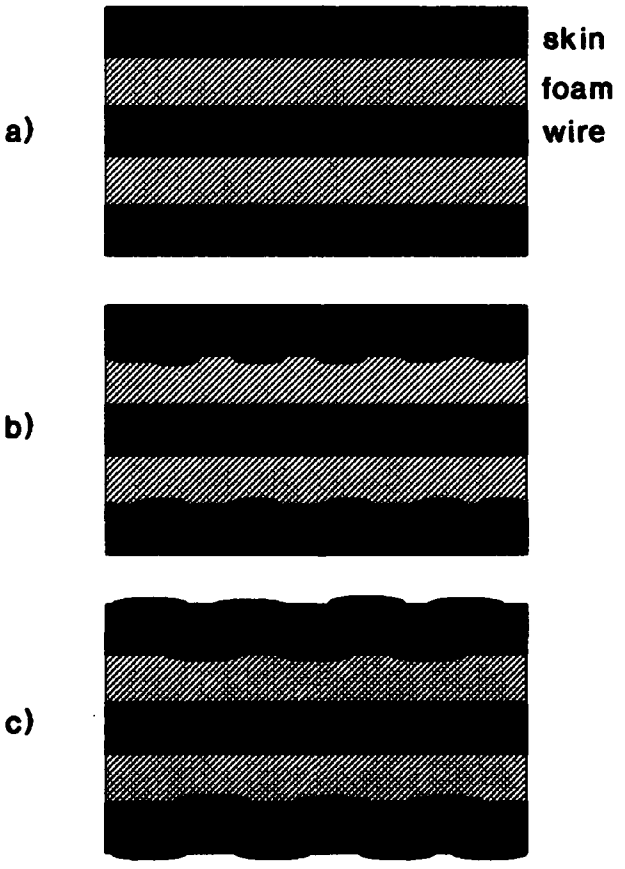


Figure 4. Interfacial Instability in Foam-Skin Insulations: Viscosity difference: a) zero, b) small and c) large

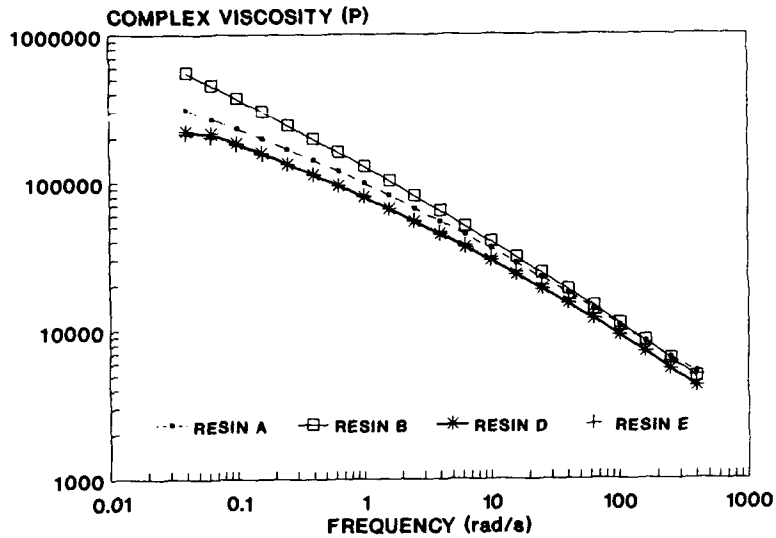


Figure 5. Low Shear Rheology Data for HDPE Resins

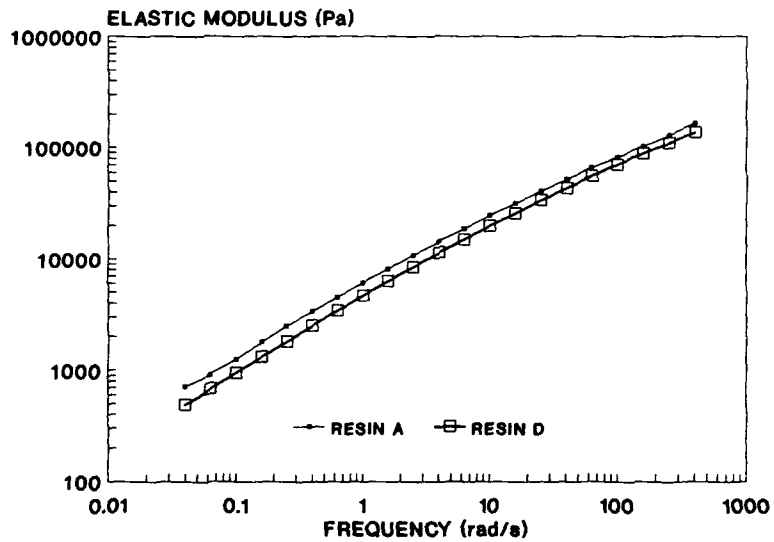


Figure 6. Elastic Modulus of Resins at Low Shear Rates



Koksal Tonyali receieved a B.Sc. degree in Polymer Science and Technology from University of Manchester Institute of Science and Technology, and his M.S. and Ph.D. degrees in Polymer Science and Engineering from Case Western Reserve University in 1985 and 1986, respectively. He worked on radiation effects on polymers as a postdoctoral research associate at Washington State University before joining Quantum Chemical Corporation in 1988. He is currently a member of the Wire and Cable Product Development Group at Quantum. His research interests include environmental effects on polymers, fracture mechanics and environmental stress cracking, structure-property relationships in materials, blends and alloys, polymer pocessing, and reactive processing.



Priya Fernando joined Quantum Chemical Corporation in 1980, and has worked in research and development of Wire and Cable Resins since 1989. As a research manager in the Applied Research Department he is responsible for directing new product development efforts and technical service activities for Quantum Specialty Polymers. He received his B.Sc. in Mechanical Engineering and Ph.D. in Polymer Engineering from Imperial College, University of London in 1976 and 1980, respectively. His current areas of research interest include developing structure-property relations of polyolefins with an emphasis on failure mechanisms. He has authored eight technical papers. He is a member of the Society of Plastics Engineers and the Institute of City and Guilds.

HIGHLY EXPANDABLE COMPOUND AND PROCESSING TECHNIQUES FOR COAXIAL CABLE

S. Hashimoto, T. Sakamoto, Y. Moritani, J. Hakozaki

Nippon Unicar Co., Ltd.
Kawasaki, Japan

Abstract

Conventional expanded insulation for ultra-low loss coaxial cable is usually produced by using a gas injection system which can make the insulation layer expand to over 70% and reduce the dielectric constant to less than 1.30. Recently, requests to produce the same type of cables via a chemical expansion method have increased since environmental problems related to fuluorocarbon gas source have arisen. We have developed a new expandable compound with a 70% expansion rate using a chemical blowing system without any environmental problems by optimizing the selection of base resins and chemical blowing agents, and also by establishing appropriate processing conditions to achieve the desired expansion. Cables using this new insulation material have been commercialized for field applications.

1. Introduction

For more than 20 years coaxial cables with 50% expanded polyethylene insulation have been manufactured primarily using the chemical blowing systems. On the other hand, for ultra-low loss cable, highly expanded insulation with over 70% rate had to be made utilizing direct gas injection, since in general the development of chemically expandable polyethylene over 70% was too difficult. We have undertaken this challenge in recognition of the needs of some wire and cables makers who do not have gas injection systems or who are hesitant to install new gas injection systems due to their high investment cost and difficult processing techniques, and also because of the recent serious concerns about the use of fluorocarbon gasses.

We have succeeded in the development of a specially designed compound and the establishment of the processing conditions for a chemical blowing system to obtain a 70% expansion rate. At present, the ultra-low loss coaxial cables using this material have been commercialized for field applications, although the size of the cables has been limited to those smaller than 7C-HFL.

In order to achieve this expansion rate, the basic factors focused on were: the rheological properties of base resins; the selection of blowing agents to minimize the dissipation factor; and also the processing conditions to optimize the characteristics of the compound.

2. Development of Materials

2.1 Selection of Base Resins

Our conventional compound for 50% expansion by chemical method was used as a basic reference. The base resin used in this compound, however, was too low in density to be suitable for a 70% expanded insulation, so a new base resin modified with a higher density type was studied. Rheologically, a high melt tension in the resin is required for a high expansion rate, and thus the modification was controlled to minimize the decrease of melt tension. Table 1 shows the optimum base resin selected.

Table 1 Selection of Base Resins

Base Resin Type	New Resin	Conventional
Expansion Rate (Aimed%)	70	50
Basic Properties		
Melt Index (g/10min)	2.2	2.0
Density (g/cc)	0.928	0.918
Melt Tension*1 (g)	7.8	8.2

*1: 190℃

2.2 Selection of Chemical Blowing Agents

From the relationship between gas volume and expansion rate, the ideal gas volume to obtain the 70% expansion rate was estimated. Fig. 1 shows that about twice as much gas volume for 70% expansion rate is needed compared to that required for 50% expansion rate. The chemical blowing agents which generate the most gas volume after thermal decomposition with a minimum content in the compound are desirable to minimize the increase of dissipation factor of the compound.

Table 2 shows that a combination of different types of blowing agents is optimal for the 70% expansion rate with very fine cell structure and low dissipation factor. Very fine cell structure is necessary to get a high expansion rate by preventing cell-breakage before cooling, and it is also necessary to maintain the core hardness which is represented by the deformation of the expanded core shown in Table 2.

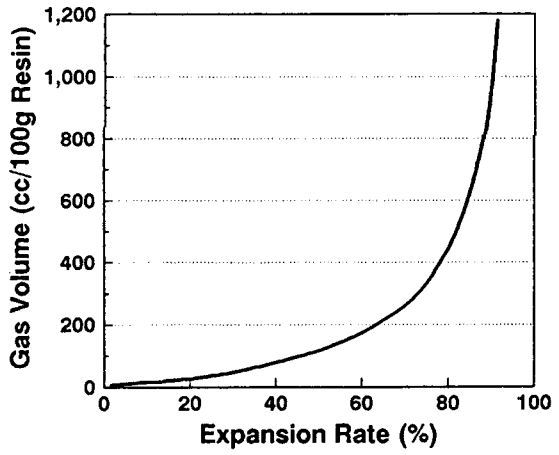


Fig. 1 Relationship between Expansion Rate and needed Gas Volume

2.3 Compound Properties

The highly expandable formulation was optimized through the selection of base resins, blowing agents and some amount of other additives such as antioxidants. Besides the study of the composition, careful compounding conditons for good dispersion of the blowing agent and for prevention of pre-blow during the mixing process were also established.

The properties of the compound developed for 70% expansion rate are shown in Table 3.

Table 3 Properties of 70% Expandable Material

Items	Unit	Values
Base Resin Properties		
Melt Index	g/10min	2.5
Density	g/cc	0.928
Foamed Properties		
Tensile Strength	kg/cm^2	60
Elongation	%	350
Dielectric Constant (1MHz)		1.3
Dissipation Factor (1MHz)		$4x10^{-4}$
Volume Resistivity	Ω-cm	$10^{16}<$

Table 2 Selection of Chemical Blowing Agents

Blowing Agents*1	Expansion Rate (Max.%)	Cell Structure	Deformation*2 of Expanded Core (%)	Tanδ*3 $x10^{-4}$
A	68	Coarse	0.8	6.5
B	70	Fine	0.5	3.4
C	65	Very Fine	0.2	5.5
A + C	72	Very Fine	0.3	4.3

*1: A, B : Hydrazide type C : Azo type
*2: 1 kg loading for 30min. at 23℃. *3: 1 MHz

2.4 Adhesive Materials for Conductor Pre-coating

In order to achieve a perfectly round insulation, and to make the handling of cable joint operation easy, it is necessary to pre-coat the inner conductor with a solid thin film to obtain moderate adhesion between the conductor and the expanded insulation. Since the type of material for precoating and its thickness on the conductor affect the electrical properties of the insulation, a material with thin-coating characteristics and a low dissipation factor was selected. Table 4 shows that LLDPE is suitable for this application.

Table 4 Selection of Precoating Materials

Resins	Adhesion to Conductor	Adhesion to Insulation	Tanδ *3 x10^{-4}	Processing Property*4
LDPE	Moderate	Strong	1	Fair
LLDPE	Moderate	Strong	0.1	Good
EEA*1	Moderate	Moderate	90	Fair
EAA*2	Strong	Poor	50	Fair

*1: Comonomer 15%, *2: Comonomer 7%, *3: 1MHz
*4: Thin-coating Characteristics

3. Processing Techniques for 70% Expansion

As well as optimizing the compound composition, the establishment of the processing conditions to achieve the 70% expansion rate is also very important. Key factors to control are follows;

1. Conductor preheating
2. Extrusion conditions to get the stable out-put and line-speed
3. Die design to get the optimum melt pressure
4. Temperature control of the cooling trough

These factors are related to each other, and they must be properly controlled to obtain good performance of the compound. In paticular, a highly expanded core before cooling is very sensitive to diameter fluctuations in the longitudinal direction, so, the out put and the line speed should be closely controlled for stable operation to prevent structural return loss or spikes in the final cable.

Extrusion temperature control is another critical factor to obtain uniform cell structure. Since a highly expanded core is also easily flattened if the cooling conditions are inadequate, gradual temperature decrease for cooling process starting from the hot water in the No.1 cooling trough is desirable for getting a round core.

Typical processing conditions are shown in Table 5. Cell structure was analyzed by using an Image Analyzer attached with a micro-computer, and Fig.2 shows a typical 70% expanded cross-section and a histogram analyzing the cell size distribution.

4. Characteristics of the Cable

Table 6 shows the foam and electrical properties of typical coaxial cables for CATV insulated with the new compound with 70% chemical expansion, compared to those for 50% by chemical and 75% by gas injection method. The frequency dependance of attenuation constants of the chemically expanded cable used the new compound is essentially the same as that of the gas injected system.

Fig. 3 illustrates a cross-section of 7C-HFL cable insulation using the new compound viewed through an optical microscope. The cell structure is excellent and equal to those made by gas inection system.

Table 5 Typical Extrusion Temperature and Expansion Properties

Temperature*1 (℃)	Expansion Rate (%)	Cell Structure
155	65	Fine
158	68	Fine
160	70	Fine
163	70	Fine
165	66	Coarse

*1: Resin temperature at die exit
*2: Extrusion conditions
Extruder : 50mmφ Test machine
Screw : L/D=24, C.R=3.4, 30rpm
Take-up speed: 12 m/min
Cu conductor : 1.8 mmφ
Core diamter : 7.3 mmφ
Temperature profile of cooling troughs: 90-75-60-20℃

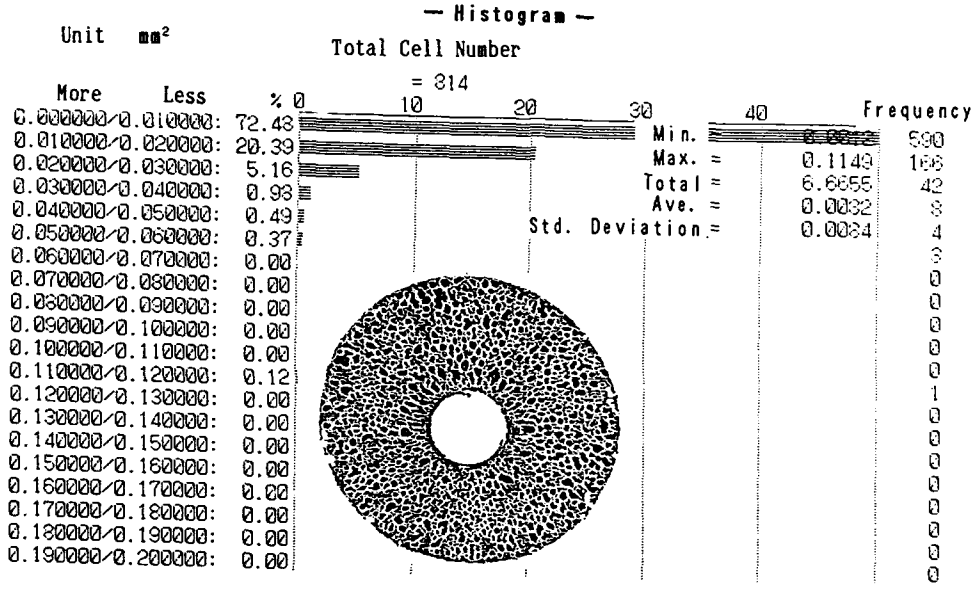


Fig. 2 70% Expanded Cross-section and Histogram for Cell Size Distribution

Table 6 Characteristics of Coaxial Cables*1

Cable No.	Cable A	Cable B	Cable C*2
Expansion System	Chemical	Chemical	Gas Injc.
Expansion Rate (Aimed%)	70	50	75
Foamed Properties			
Blown Density (g/cc)	0.27	0.40	0.25
Expansion Rate (%)	72	52	75
Deformation*3 (%)	0.3	0.2	0.2
Electrical Properties			
Core Diameter (mm)	7.2-7.3	7.2-7.3	7.2-7.3
Capacitance (PF/m)	51-52	54-55	50-51
Impedance (Ω)	76	78	74
10 MHz	11	13	11
90 MHz	38	40	37
220 MHz	57	63	58
450 MHz	86	94	85

*1: Cable Structure : 7C-HFL Type
Inner Conductor - 1.8mmφ Cu
Outer Conductor - Al Laminate Tape (0.2mmt)
*2: Commercial Cable of Gas Injected Insulation
*3: Core only tested under 1kg loading for 30min at 23℃

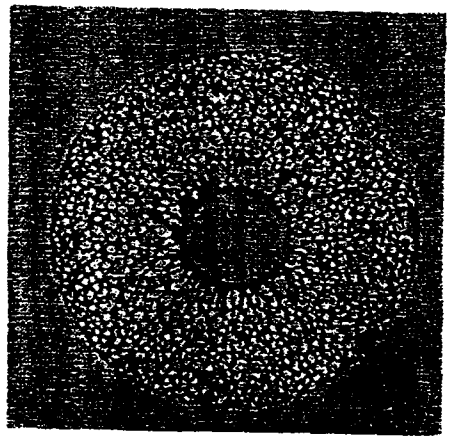


Fig. 3 72% Expanded Cross-section of 7C-HFL Cable insulated with the New Compound

5. Conclusions

A polyethylene based compound expandable to a 70% rate by utilizing a chemical expansion system was developed through the selection of a suitable base resin and a composite blowing agent with different chemical structures.

The establishment of suitable processing conditions of the compound was very important in achieving the desired expansion ability of the compound.

6. Acknowledgements

The authers wish to thank Mr. Y. Sagara, Mr. M. Yasunari, Mr. Takahashi for their many helpful hints concerning the compouding process.

7. References

1) R.H.Hansen, "Production of Fine Cells in the Extrusion of Foams", SPE Journal, 18, No.1, 77, 1962

2) B.H.Madock, "Extrusion of Cellular Polyethylene for CATV Coaxial Cable", 17th International Wire & Cable Symposium, 1969

3) F.Suzuki, et al. "Microcoaxial Cables Insulated with Highly Expandable 27th International Wire & Cable Symposium, 1978



Jun-ichi Hakozaki

Nippon Unicar Co., Ltd.
8-1 Ukishima-cho
Kawasaki 210, Japan

Dr. Hakozaki received B.S. and Ph. D. degree in chemistry all from Tokyo Kyoiku University in 1954 and 1968, respectively. He joined Nippon Unicar Co., Ltd. in 1966 Where he was engaged in manufacturing technology and products development. Since 1985 he consecutively held Plant Manager and General Manager Research and Development Division, and is now a technical advisor of Polyethylene Division. Dr. Hakozaki is a senior member of Society of Plastics Engineers and a member of The Society of Polymer Science, Japan.



Satoshi Hashimoto

Polymer Research
Laboratory
Nippon Unicar Co., Ltd
8-1 Ukishima-cho
Kawasaki 210, Japan

Mr. Hashimoto received a B.S. and M.S. degree in Applied Chemical Engineering from Hokkaido University in 1963 and 1965. He joined Nippon Uicar Co., Ltd. in 1968, where he has been engaged in research and development on wire and cable materials and other application of polyethylene and is now senior research Engineer of Polymer Research Laboratory.



Toshio Sakamoto

Polymer Research
Laboratory
Nippon Unicar Co., Ltd.
8-1 Ukishima-cho
Kawasaki 210, Japan

Mr. Sakamoto graduated from High School in Aomori Prefecture in 1959. He joined Nippon Unicar Co., Ltd. in 1962, where he has been engaged in research and development on wire and cable materials, especially in development on processing techniques in extrusion, and is now a member of Polymer Research Laboraotry.



Yasuharu Moritani

Polymer Research
Laboraotry
Nippon Unicar Co., Ltd.
8-1 Ukishima-cho
Kawasaki 210, Japan

Mr. Moritani received B.S. degree of Industrial Chemical Engineering from Kyoto University in 1961. He joined Nippon Unicar Co., Ltd. in 1966 where he has been engaged in research and development on wire and cable materials and other specialties of polyethylene. In 1992, he was assigned a deputy manager of Polymer Research Laboratory. Mr. Moritani is a member of IEEE and a member of the Institute of Electrical Engineers of Japan.

INTERACTIVE MANUFACTURING & COSTING SYSTEM (I_MACS) FOR MULTI-PAIR TELECOMMUNICATION CABLES

M. J. Khan

Saudi Cable Company
Tele-Cable Division, Jeddah, Saudi Arabia

ABSTRACT

A fully integrated telephone cable manufacturing and price / costing system has been developed for a modern telecommunications cable manufacturing facility. The black box concept implemented on PC based LAN, integrates Sales/Marketing, Technical, Material planning, Cost accounting and Quality control departments. A versatile cable coding structure has been described to handle virtually all cable constructions that exist in the International and National standards of different countries and PT&T administrations. The total concept has been implemented thru vigorous application of formula based computation and algorithms developed in modular plug-in modules. Once the system is initialized with the basic cable design, process and machine parameters, it then can generate the manufacturing information by evaluating the item code of a cable, that is entered by the user. Thus absolutely no or minimum user data entry is required and high degree of accuracy and information integration achieved.

INTRODUCTION

Fierce competition both at domestic and international fronts is among the factors leading to a new commitment by the manufacturing companies to respond faster to market demands, most competitively with high degree of reliable and quality products. This competition in the present day world market sets an ever- increasing pressure on the management of a manufacturing unit to optimize product design, reduce scrap and increase operational efficiency etc. and finally produce a quality product at reduced costs.

Actions are generated in a cable manufacturing industry by either customer's inquiry or order. In case of a customer's inquiry, sales, technical/design engineering and planning departments are involved to quote Price and Delivery schedule of the cables requested. In case, an order is placed the cables got to be manufactured according to the agreed (contract) technical specification/design and quality tests requirements. These actions are carried out starting from the design engineering to planning, process, quality control and final inspection until the cables are transferred to shipping department/customer. Various information and documents are thus needed to complete the customer order. In this paper, efforts have been made to computerize the customer order processing from an initial customer's inquiry and preparation of quotation to manufacturing the cables after placement of the order in accordance with the agreed technical specifications and quality test requirements etc.

The system offers a unique opportunity to Management to instantly retrieve information such as no. of quotations made during a week/month/year and orders received during the same period, materials costs, materials to sales price ratios, raw material requirement (by weight and dimensions) for particular cable types (tenders) besides, machine/operating efficiencies and various other manufacturing and accounting reports.

I_MACS CONCEPT

The majority of CIM based systems are either ready-made packages bought from software houses which require to be tailored to a manufacturing unit's requirement, where as others are built in-house to perform various tasks in each department and partly integrated. These systems are generally based on huge data bases, developed thru years of data entry for each product and new products that are developed from time to time as a result of R & D and for products of specific customer's specifications and test requirements. The data based CIM systems are generally developed taking into consideration known standards, customer's specifications and the manufacturing capabilities (existing machinery layout). However, as the market expands (from domestic to international arena) and cables to various specifications are to be produced, the CIM software would need to be upgraded and/or modified to meet the demand of non-standard products. In the process, several bottlenecks got to be resolved adversely affecting the overall productivity and responses to the end users. In some cases, the bottlenecks could not be

resolved due to limitation of the system bought/developed and hence the information are to be prepared manually or manually prepared information are to be entered into the computer to get a desired report. Also constant improvements in product design, materials usage, it's type and application and/or change in plant machinery lay-out may require to replace / update the existing data. These changes which are normal in a cable manufacturing plant further leads to modification of the CIM software. Thus initially a well purchased/developed system may turn into a semi-manual system as the market trends changes with more and more non-standard products that are to be offered to satisfy possibly all inquiries from customers.

The Interactive Manufacturing and Costing System (I_MACS) described in this paper is developed keeping in view the difficulties usually encountered with a typical data based system particularly those which have been purchased as ready made package and needed adaptation to user's requirements. The I_MACS is being developed based on a black box concept which is driven by product identification code(s). As the system is initialized, it then requires minimum data entry for any (new) cables type(s) that are to be manufactured according to an unknown customer's specification. Fig. 1 shows the black box concept accessible by various departments of a typical telephone cable manufacturing plant. It consists of a main module FCE (Formula Computation Engine) and a number of sub-modules pertaining to each department. Each department access the FCE after log-in and password authorization using any of the following (access) keys.

- Customer's Inquiry no.
- Product Item Code (and/or Computer no.)
- Mill Order no. (Sales Order no.)

The FCE is a formula based module which computes the cable dimensions and material weights. The black box interprets the access keys, computes the cable dimensional data and bill of materials of pre-selected cable type(s) and size(s) of an inquiry or Sales order and make available these information to the sub-module(s) of the calling department. Once the material types, weights (Kg/Km) and cable dimensions at each stage are computed, further analyses are done by the designated module(s) of the black box pertaining to a certain department. Typical reports that a department would like to generate are shown in Fig.1. These reports can be viewed and/or printed in a matter of less than few seconds, however, the important thing is that no output of a report or cable construction (i.e. cable design and material weights etc.) are saved by the computer. The system uses FCE repeatedly for items (cable types & sizes) as selected by the user to generate particular analyses (reports).

PRODUCT DESIGNATION CODE (ITEM CODE)

The I_MACS has been envisaged with absolutely no data entry or minimum possible entries by the user. It is a product code and menu-driven system offering multiple options and features to select from. It was therefore essential to evolve a universal coding structure that simulates almost all known national and international standards as well as deviations from standard specifications that would be necessary for manufacturing reasons to comply with some quality test requirements and inspection clauses of a customer's specifications.

The cable construction of the telephone cable taking into account all possible variations in materials and design parameters meeting a variety of specifications has been defined by an item code structure for finished cable and semi-finished WIP (work-in-process).

The finished cable item code consists of two parts namely;

- Item code or cable designation code (alphabetical)
- Computer no. (numerical)

The alphabetical part of the item code comprises of three parts; the first part is made of four fixed alphabet positions and describes the cable design; the second part made of unlimited alphabet locations, each is defined for a material type and can be applied in any sequence, the 3rd. part is numerical which represents the cable size (pair count, pair and diameter of conductor). Each alphabet of the item code defines a material and it's sequences of application as shown in Fig. 2. As can be seen, the first four alphabet positions (1 to 4) describes conductor type, insulation material type, mutual capacitance (finished cable) and stranding process type. These alphabets as selected from each stage of operation and it's sequence will give the stage-wise cable construction. Thus the first four alphabets make the cable upto assembled core. The subsequent alphabets, each defining materials for screening, sheathing and armouring can be applied in any sequence, depending upon customer's specifications. The default setting of the alphabets defining a finished cable item code with cable description is shown in the example in Fig.2. The WIP codes have been developed in a similiar way which identify the semi-finished product at each production stage. The 2nd. part of the finished cable item code is a numerical number. For each cable construction, a six digit sequential numerical number is assigned (automatically generated) by the computer. This computer number is unique and without any nomenclature (definition).

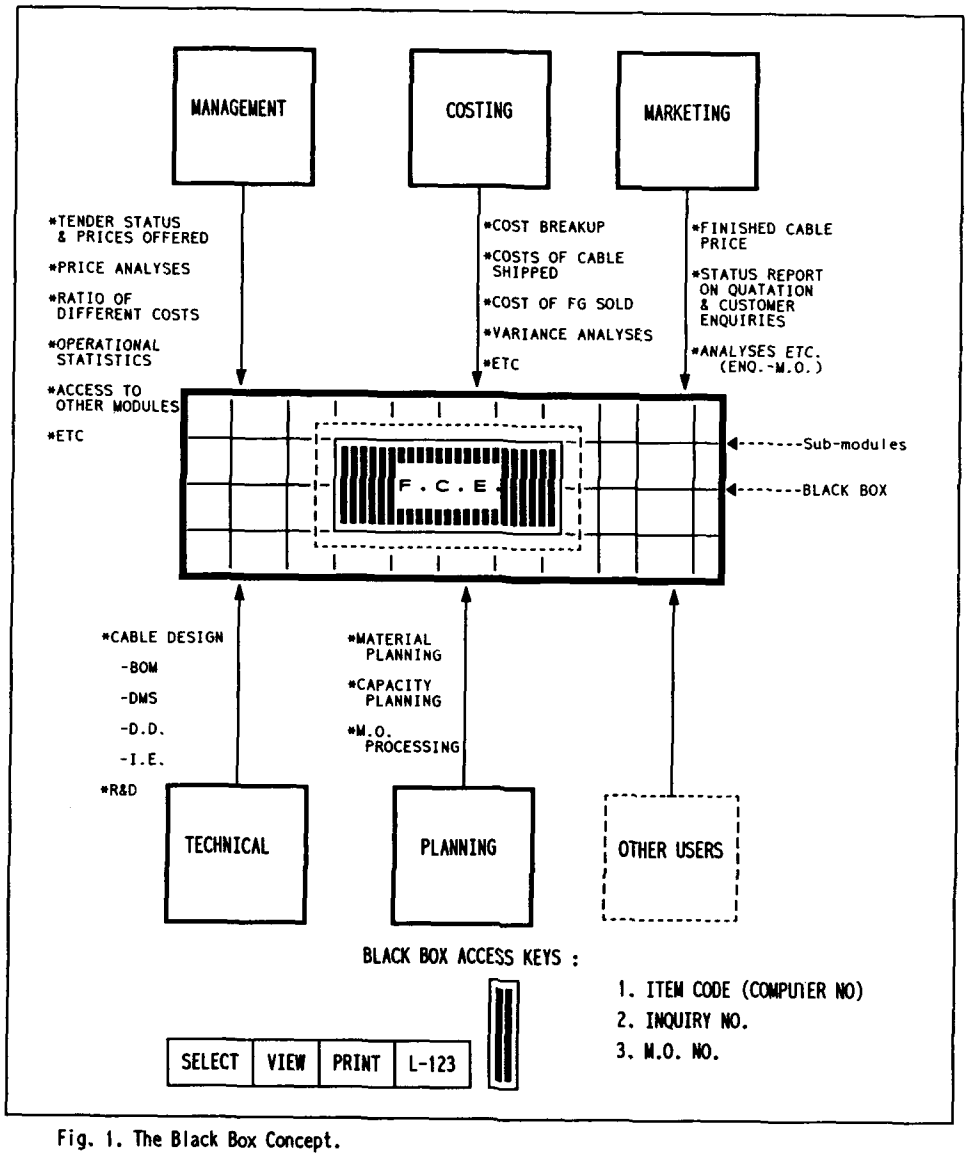


Fig. 1. The Black Box Concept.

The above cable item code structure offer almost unlimited flexibility with respect to defining a cable construction complying with a particular specification taking into account manufacturing and process limitations of a cable plant. Some examples of these item code designations are given in table 1 which demonstrate it's application to a number of known standards for telephone cables.

STANDARD AND NON-STANDARD CABLE CONSTRUCTIONS

For cable manufacturers, the standard cable constructions are those of their own country's utilities (PT&T and Telecom organizations). For instance, for North American manufacturers, the standard products are those complying with REA specifications, UL standards, and various cable specification of Telecom utilities etc. For these manufacturers, VDE standards and French specifications which are based on quad cable construction are non-standard. The I_MACS concept is based on first initializing the system with standard cables of the company (usually those products, listed in it's catalogs/leaflets). Then any new cable(s) specified in customer's inquiries are to be designed and deviations from standard recorded. The deviations (if any) in a cable construction are recorded by I_MACS by assigning a five digit computer number called as computer deviation no. The deviation numbers are not only used for new cable types but also for standard cables where a different material type or it's application and/or test requirements are requested. The deviation no. as shown

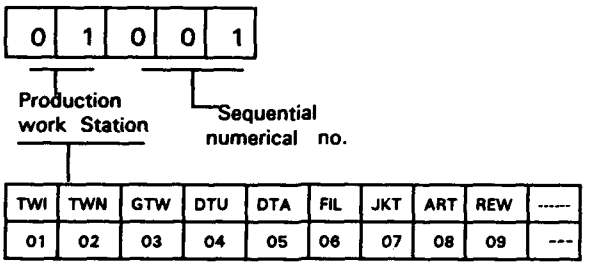
TABLE – 1

CABLE ITEM CODES AND CONSTRUCTIONAL VARIATIONS

CABLE SIZE : 300 x 2 x 0.40 (example)

ITEM CODE	COMP. NO.	CABLE CONSTRUCTIONAL VARIATIONS	SPECIFICATION
PENRAL	100101	F/Skin ins., Filled, 10 pairs based S/unit,Al.screen & PE sheath, Low Capacitance : 42 nF/Km	IEC 708-2
PENCAL	100102	F/Skin ins., Filled, but 12,13,25 pairs S/unit,Al.screen & PE sheath, Low Capacitance : 42 nF/Km	IEC 708-2
PENQAL	100103	F/Skin ins., Filled, 5 quads based S/unit, Al.screen,PE sheath, Low Capacitance : 42 nF/Km	IEC 708-2
PETRAL	100104	F/Skin, Filled, 10 pairs based S/unit,Al.screen & PE sheath, High Capacitance : 55 nF/Km	IEC 708-2
PUTRAL	100105	PE solid ins. Un-Filled , Al. screen & PE sheath, High Capacitance : 55 nF/Km	IEC 708-3
PUTRALO	100106	PE solid ins., Un-Filled,Al.screen, PE sheath Self-Supporting Cable, Hig Cap. : 55 nF/Km	IEC 708-4
PENRALGL	100107	F/Skin ins., Filled,Al. screen , double galv. steel tape armoured, PE sheath, Low Cap. : 42 nF/Km.	IEC 708-2
PASCAL	100201	PE solid ins., Filled, 12,13; 25 pairs S/unit, Corr. Al., screen, PE sheath, Hig Cap. : 52 nF/Km.	REA PE-39
PASCAZL	100202	PE solid ins., Filled, 12,13,25 pairs S/unit, Corr. Al., screen, Corr. steel tape, PE sheath, Hig Cap. : 52 nF/Km	REA PE-39
PESCAL	100203	F/Skin ins., Filled, 12,13,25 pairs s/unit, Corr. Al. screen, PE Sehath, High Capacitance : 52 nF/Km	REA PE-89
PUSCAL	100204	PE solid ins., Un-Filled, 12,13,25 pairs S/unit, Corr. Al. screen, PE sheath, High Cap. : 52 nF/Km	REA PE-23
PUSCALO	100205	PE solid ins., Un-Filled, 12,13,25 pairs S/unit, Corr. Al. screen, PE sheath, S.S.Cable, High Cap. : 52 nF/Km	REA PE-38
PIXRAL	100301	PE Foam., Filled, 10 pair based s/unit, Al. Screen, PE sheath, High Cap. : 56 nF/Km	CW 1128C
PYXCAL	100302	Cellular Foam ins., Un-Filled, 12 13 & 25 pairs S/unit, Al. Screen, PE sheath, High Capacitance : 52 nF/Km	CW 1224 B
PUTQAL	100401	PE solid ins., Un-Filled, 14 quad based S/unit, Al. Screen with continuity wire & PE sheath, High Cap. : 52.5 nF/Km.	L123(French)
PAXQALGL	100501	PE solid ins., Filled, 5 quads based S/unit, Al. Screen, Double GST armour & PE sheath , High Cap. : 50 nF/Km.	VDE 816

below, consists of two parts, the first part consists of 2 digits which represent the production work station and the second part is a sequential numerical number assigned to a certain deviation in cable design.



The production work stations are also codified, abbreviated as follows (example);

TWI - Tandem drawing and wire insulation line
TWN - Twinner for pairs (spare pairs)
GTW - Group twinning (10,12,13,25pairs & quad conventional, X-stranding or S-Z stranding)
DTU - Drum twister (unit maker 50,100 pairs)
DTA - Drum twister (core assembly)
FIL - Filling line (filling process can also be in DTA or JKT lines)
JKT - Tandem (filling), screening, (corrugated armouring) and jacketing lines.
ART - Tape armouring line
REW - Rewinding line
--- - Etc.

The standard cable constructions to various specifications are shown in table 1. The cable description of first item code PENRAL with computer no. 100101 is as follows;

"Plain annealed solid copper conductor, Foam-skin insulated, paired, unit type, filled (based on 10 pairs cross-stranded basic sub-unit), polymer coated aluminum tape screen, LDPE sheathed, low capacitance (42 nF/Km), local telephone cable to IEC 708-2".

Say this cable and others with similar construction is standard for a company "ABC", which has established the design and process parameters and the company supplied hundreds of Km to it's customer(s). The longitudinal water penetration test requirement for this

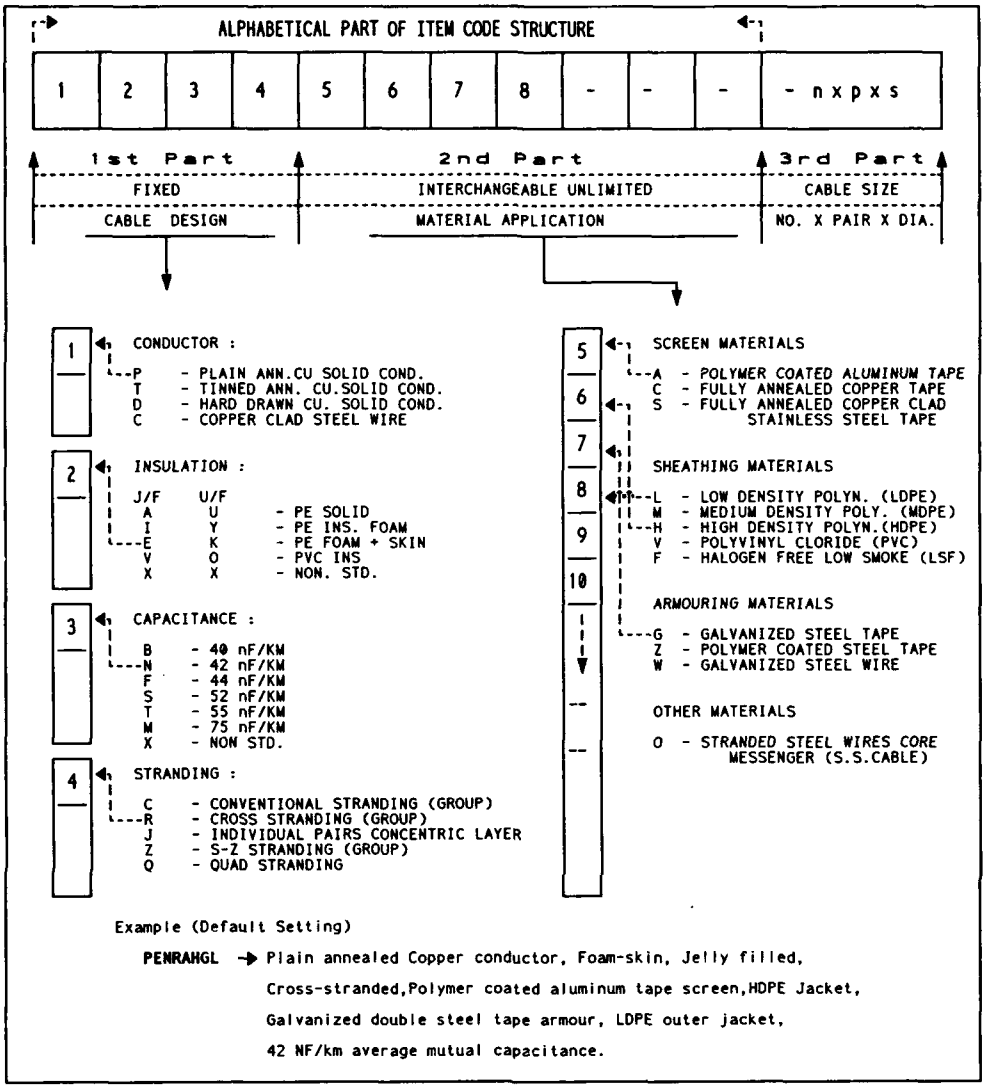


Fig. 2. Item Code Structure - Cable Design and Material Definitions

cable per IEC 708-2 is 24 hours on a 3 meter cable length (T-type test method). A specific customer may want the same cable meeting the W.P. test for 14 days on a one meter cable length (L-type test method). Now for the company "ABC" with normal process parameters and materials, it may not be possible to produce a fully water tight cable meeting the 14 days longitudinal W.P. test requirement, unless introducing in the cable design special water blocking (swellable) tapes or yarn. With a water blocking tape application over the polyester wrapped core (replacing the standard flooding compound) is a deviation against ABC's standard cable construction and will be recorded with a deviation number as shown in example 1 of Fig. 3.

In example 1 of Fig.3., there is only one deviation in the cable construction substituting water blocking tape for standard material of flooding compound and assign a new computer no. 100153 with a deviation no. 07001. The first two digits in this deviation no. 07 indicates the stage of operation or work station. In this case the W.B tape to be applied longitudinally over the polyester tape in tandem with aluminum tape screening and LDPE extrusion in the sheathing line. Example 2. is with two deviations for material type and jacket thickness and example 3. is with four deviations in the cable for number of spare pairs (4 pairs instead of 2 pairs) basic unit construction (12,13,25 pairs instead of standard 10 pairs subunit), corrugated polymer coated aluminum tape screening (instead of plain tape) and 2.3 mm jacket thickness (instead of standard 1.5 mm). The item code in example 4. is without any deviation although HDPE sheathing material is substituted for standard LDPE. Since this material variation is shown with in the item

STANDARD ITEM CODE : PENRAL- 300X2X0.40
COMPUTER NO : 100101

#	ITEM CODE	COMP.NO.	DEV.NO.	DESC(DEV.)	STD(DEFAULT)	DEVIATION
1.	PENRAL-300X2X0.40	100153	07001	MATERIAL	FLD. COMPOUND	W.B. TAPE
2.	PENRAL-300X2X0.40	100154	07001	MATERIAL	FLD. COMPOUND	W.B. TAPE
			07002	JKT-THK	1.5	2.0
3.	PENCAL-300X2X0.40	100155	02001	SPARE PAIR	2	4
			03001	CONSTRUCTION	10 PAIRS	25 PAIRS
			07003	MATERIAL	PLAIN AL. TAPE	CORRUG. AL. TAPE
			07004	JKT-THK	1.5	2.3
4.	PENRAH-300X2X0.40	100156	NOT REQ'D		LDPE	HDPE

Fig. 3. Example of Deviations from Standard Cable Construction.

code designation (alphabet "H" instead of "L"), therefore there is no need to record this variation with a deviation. The most important thing to note is that each cable is with different computer no. which is unique. The deviation no. 07001 is repeated two times in example 1 & 2, representing the same variation from standard however, the system records it only one time and retrieves it thru it's dictionary tracking system which is linked with the unique computer number.

I_MACS INITIALIZATION AND OPERATION

The I_MACS software has been developed for a multi-user environment and implemented on PC based Novell local area network as shown in Fig. 4.

In order to retrieve various information (departmental as well as management reports and analyses, examples of typical reports shown in Fig. 1), the system needs to be first initialized for standard known products. This means to codify the standard products i.e. for each cable type, an item code (alphabetical part) is to be built which defines the basic cable construction, material types, and it's sequence of application. The item code construction is generally made by a cable design engineer who is able to make it in a matter of few minutes (based on item code definitions per fig.2), once the cable specification are read and it's requirements understood. The item codes for each cable size are then entered one by one in the I_MACS. The item code entry module is shown in Fig. 5(a). Each alphabet of the item code is validated

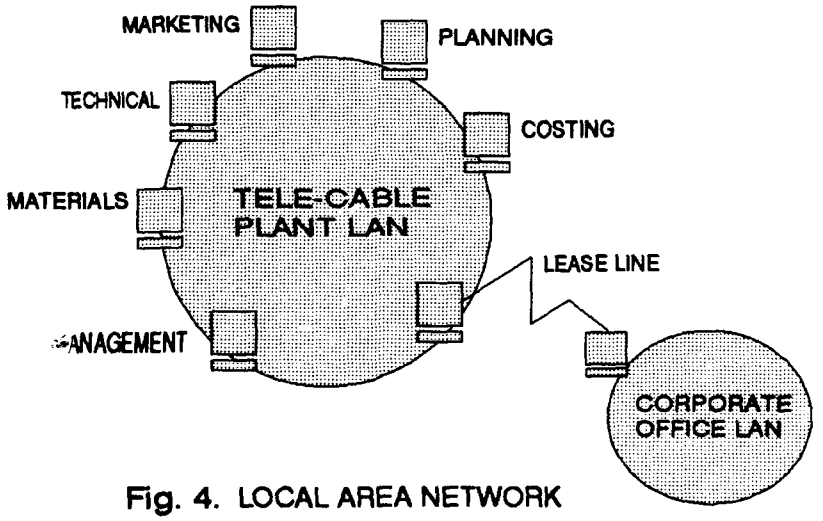


Fig. 4. LOCAL AREA NETWORK

(A) ENTER ITEM CODE

P	E	N	R	A	L					2400X2X0.40

POP-UP HELP

P - PLAIN ANN.CU.
T - TINNED ANN.CU.
D - HARD DRAWN
C - CLAD HARD DRAWN

(B) MASTER ITEM FILE

TAG	COMP. NO.	CODE	STD	RMKS
-	100098	PENRAL-050X2X0.40	S	STD'92
-	100099	PENRAL-100X2X0.40	S	STD'92
-	100100	PENRAL-200X2X0.40	S	STD'92
-	100101	PENRAL-300X2X0.40	S	STD'92
-	100120	PENRAL-2400X2X0.40	S	STD'92

FIG. 5. I_MACS Initialization for Standard Products.

against the item code structure and "help" window pops-up incase a wrong alphabet is entered or help is needed by the user. After the item codes for standard products are entered, all the items simultaneously appear in the master item file with computer number assigned to each item code as shown in Fig. 5(b) and the system initialization is completed for all standard products.

For a customer's inquiry, Sales would either quote the standard product if it is established from customer's inquiry or offer exactly as per customer's requirements. In both cases, Sales enter the BOQ (Bill Of Quantity) i.e. cable size and sheathed KM (SKM) in I_MACS Sales entry module as shown in Fig. 6(a). As the BOQ is entered, item code computer numbers pops-up in a window showing the standard cable and non-standard cables of the same size that might have been previously quoted. A further explosion of the selected computer numbers will show exactly the previously quoted customer's inquiry no., company name and date of quotation made for each inquiry. If none of the previous items are selected by the Sales and wish to comply with customer's specification requirements, a message in the remarks column "To be designed" is selected for technical (design engineering) department.

The Sales Master Inquiry File is shown in Fig. 6(b) which gives the latest update on the customer's inquiries. As the inquiry numbers are scrolled, the BOQ associated with the inquiry also appear in the Bill of Quantity Files. In Fig. 6(b), the inquiry no. E1345-R01 has been shown with it's BOQ. As seen in the BOQ screen, the 3rd. item being left to technical department to design the cable per customer's specifications requirements.

The technical cable design module is shown in Fig. 7(a). As can be seen, the BOQ of Sales inquiry no. E1345-R01 is displayed where only one item (size 300 x 2 x 0.4) per Sales request to be designed according to customer's specification. All what is needed by the deign engineer, to enter an item code after his/her study of the customer's specification. In this case, he/she enters PENCAL, the routing of machine-layout appears instantly with raw materials of a standard cable (item code : PENCAL - 300 x 2 x 0.4 comp. no. 100102). Now the design engineer has the total flexibility to delete, add, replace and/or modify any material type, it's application and materials thicknesses etc. The materials modified/replaced to meet customer's specification requirements at twining (TWN), stranding (GTW) and jacket extrusion (JKT) stage of processes are shown with computer deviation numbers against the standard materials and cable construction (default values) in Fig. 7(b). After the necessary modifications is made in the standard cable construction, a new computer no. (100155) is assigned sequentially by the computer. The designer has the option to view/print the bill of materials for the newly designed cable while still working in the temporary design file. After satisfaction over the correctness of modifications made, the new cable is formally released (release is made with pass-word authorization) to Master Item File as shown in Fig. 7(c). The master item file holds the total products (cable type & size) of a company (both standard and non-standard). In Fig. 7(c), the items of inquiry E1345-R01 have been added to the existing product data base. The master item file can be scrolled and the description of deviation(s) in the cable construction (if any) appear simultaneously as shown. Thus one can know instantly the type of cable offered to a customer. The cable type originally requested by Sales for design has a number of deviations and it may not be possible to manufacture due to machine limitation for instance, in this case the company may not have the corrugating machine to offer corrugated aluminum tape screen and hence the remarks "CONSULT TECHNICAL" appear in the remarks column of master item file for this item. The design operation of I_MACS is completed once the requested product is designed and the corresponding item code with the assigned computer number is released. The information are instantly available to Sales in their Inquiry Master File.

COSTING & MANUFACTURING INFORMATION

The status of an inquiry and existing products listing (standard & non standard) can be viewed by any one connected to the LAN. The items of an inquiry or the

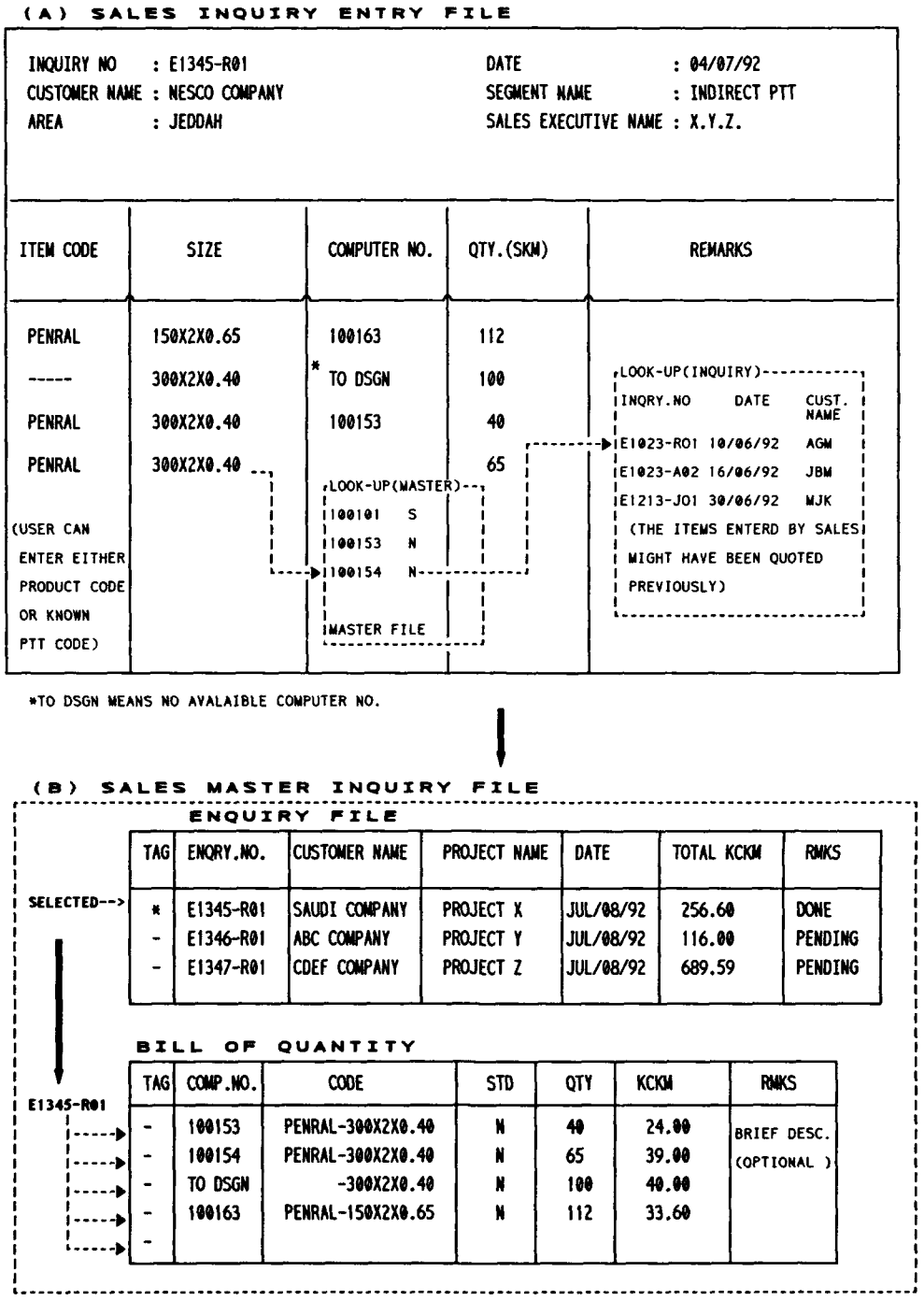


Fig. 6. User Interface for Sales Department

Master Item File are tagged (selected) to generate a particular information. The sequence of operation to generate the manufacturing cost and final prices of the items in the inquiry no. E 1345-R01 is as follows;

The black box computes the bill of materials, for each size and dimensional data from inlet drawing copper conductor diameter to the outside finished cable diameter. The in-process reels sizes, the batch lengths at each production stage are determined and machine hours per Km computed. These information along with the machine rates ($/Km), raw material prices ($/Kg), direct / indirect labour costs ($/Km) and factory overhead etc. will give the manufacturing cost and thus final prices of the selected products (inquiry) are displayed. Further options in respect of analyses of what price to be quoted

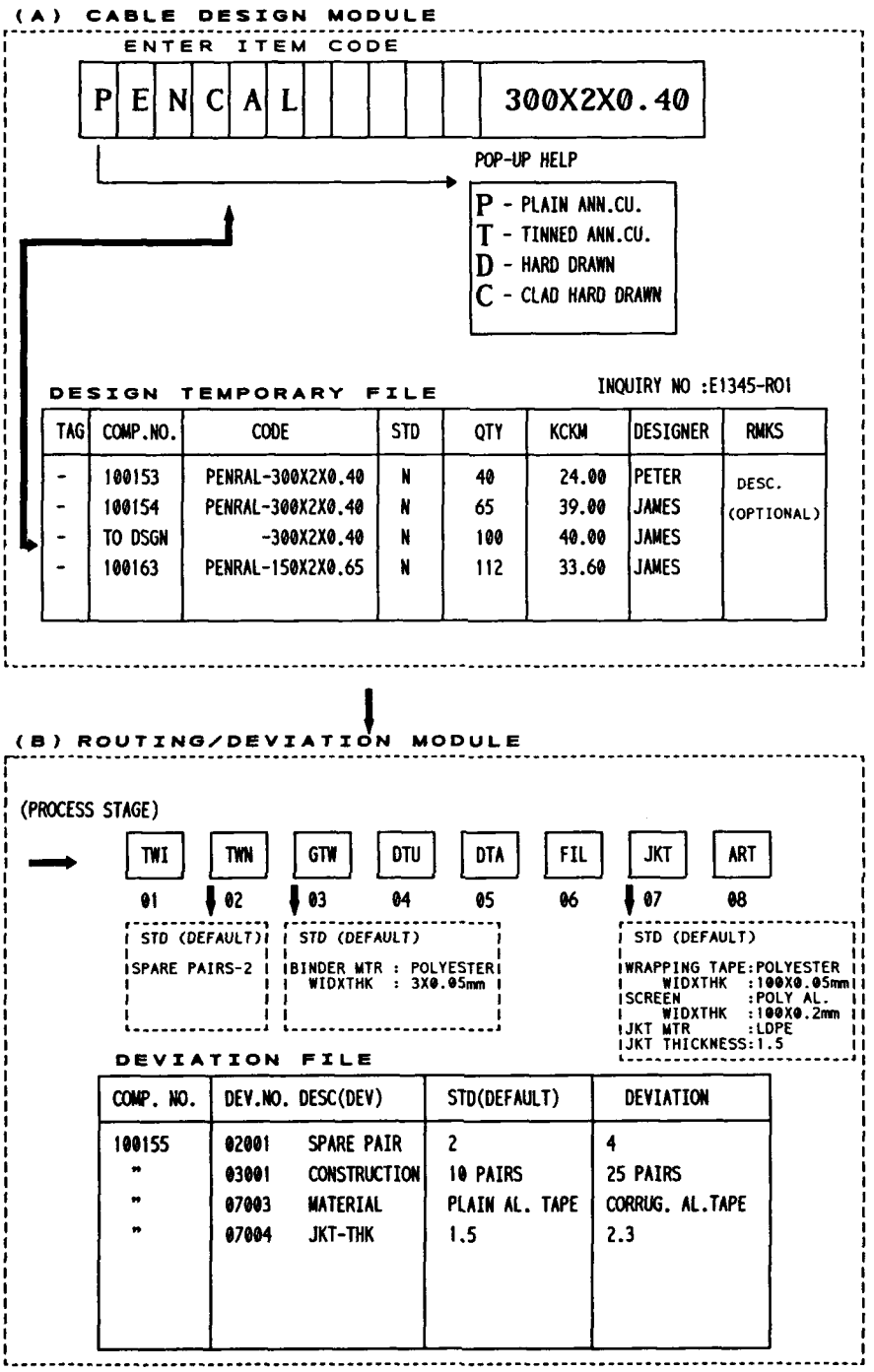


FIG.7 Design Engineering Entry/Output Module For NON-STD Products.

to customer is provided to the Sales/Marketing department. The main manufacturing information that I_MACS generate are; mill order (M.O), work order (W.O), design manufacturing specification (DMS which is the cable design parameters as it will be produced at the shop floor at each production machine) and manufacturing layout (machine routing, reel sizes (pay-off/take-up sizes), wire/assembled core/cable length in each bobbin/reel, industrial engineering standard i.e. machine hours) besides raw material weights and widths of various tapes etc.

The typical reports/data that each department can generate out of the computed information by the I_MACS are shown in Fig.1.

(C) MASTER ITEM FILE WITH DEVIATION VIEW FILE

MASTER ITEM FILE

TAG	COMP. NO.	CODE	STD	RMKS
-	100101	PENRAL-300X2X0.40	S	-
-	100153	PENRAL-300X2X0.40	N	-
-	100154	PENRAL-300X2X0.40	N	-
-	100155	PENCAL-300X2X0.40	N	* CONSULT TECHNICAL
-	100163	PENRAL-150X2X0.65	N	-

* MANUFACTURE IMPOSSIBLE

DEVIATION FILE

COMP. NO.	DEV.NO.	DESC(DEV)	STD(DEFAULT)	DEVIATION
100153	07001	MATERIAL	FLD. COMPOUND	W.B. TAPE
100154	07001	MATERIAL	FLD. COMPOUND	W.B. TAPE
"	07002	JKT-THK	1.5	2.0
100155	02001	SPARE PAIR	2	4
"	03001	CONSTRUCTION	10 PAIRS	25 PAIRS
"	07003	MATERIAL	PLAIN AL. TAPE	CORRUG. AL.TAPE
"	07004	JKT-THK	1.5	2.3
100163	07001	JKT-THK	1.5	2.0

FIG. 7. Design Engineering Entry/Output Module For NON-STD Products.

CONTINUATION OF WORK

The work on some I_MACS modules is in progress. This includes capacity planning module, shop floor actual production data retrieval module and final quality control (inspection) data. Besides, connecting the tele-cable LAN to wide area network to provide information to the corporate office over a dedicated lease line.

CONCLUSION

A user friendly single instruction driven computerized manufacturing and costing system implemented on PC based LAN integrates the information between the various departments responsible for cable design, planning, manufacturing, quality control, costing and sales. The key objective of promptly responding to customer's inquiries for cable requirements (tenders) is achieved i.e. quoting price and delivery, maintaining accurate manufacturing data and tracibility of various documents from sales to production and finished goods manufactured. The system after implementation can be fine tuned by replacing the design and process parameters by practical data obtained thru SPC and other established procedures implemented on the production shop floor. The system thus generates as close as possible the materials and operational cost variances. The system though uses a common dbase language does not have large data base, mostly generates the manufacturing and costing dated by itteratively computing the cable design/process parameters. The proposed item code structure (cable designation codes) has been tested for a number of cable types complying to known National and International standards as well as other telephone cable constructions for specific application with special material requirements.

ACKNOWLEDGMENTS

The author wishes to thank the Management of Saudi Cable Co. particularly the President, Mr. M.N. Joukhdar and Mr. M.H. Kutbi, V.P. Tele-cable division for their continuous support to this project. Special appreciation is extended to Mr. P. Gary for hard-coding and development of I_MACS software and finally thanks to Mr. S.Faheemudin for typing the manuscript.



M. Javed Khan received his BS degree from the University of Pashawar, Pakistan in 1974 and M.A.Sc. degree from the University of Windsor, Ontario, Canada in 1980, both in electrical engineering. He worked with Phillips cables as cable design engineer before joining Saudi Cable Company late in 1982. He is presently responsible for design engineering and quality control departments of telecommunication cable plant of Saudi Cable Company.

The Development of a Cost Effective, Environmentally Friendly Method for Lagging Wire and Cable Shipping Reels

Joseph A. Hill — AT&T Fitel
Christopher E. Hall — Sonoco Products Company
Karl B. Shields — C&S Associates

Introduction

A new, flexible lagging material has been developed which is designed to provide thermal and mechanical protection during the shipment of fiber optic telecommunication cable. It is manufactured with an extruded, water resistant board comprised of post industrial recycled paper and plastic sandwiched in between a treated outer sheet of non-woven polypropylene and an inner sheet of polypropylene foam. This paper will examine the stated goals and anticipated benefits of using this new, flexible lagging in lieu of traditional lagging materials. We will review the development of this product to its current construction and examine the rationale at critical decision points. We will discuss test methods and data which support this new product as a viable, cost effective alternative to current thermal and mechanical lagging methods. Finally, we will present data which supports the effectiveness of this material in the field.

Background

The need for a product which adequately protects fiber optic cable against impact, compression and abrasion combined with the concern over recycling and disposal issues led Sonoco Products Company's Baker Division, C&S Associates, and AT&T Fitel to begin field testing a new lagging material with Bell Atlantic in June of 1991.

The new lagging material contains over 80% post industrial waste paper and plastic by weight and can be recycled. This is a positive for both domestic and export shipments since the use of recycled material reduces the tonnage of packaging entering the waste stream. In addition, on export cable shipments, most countries require treatment of wood products (reels and lagging) with Copper Napthenate, which is classified as a hazardous material by the EPA. The use of this new material, which does not require such treatment eliminates the need for treated wood lagging, minimizing the customer's cost of handling and disposal overseas.

The product significantly improves the labor efficiency and the overall cost effectiveness of the lagging process. Due to the modified application process at the cable manufacturer, which entails laying the material directly on the cable surface and then strapping the material on the loaded reel, the potentially hazardous practice of nailing wood lags onto the reels is eliminated. This process modification also significantly reduces lagging time. Time savings ranging from 34% on a 42" diameter reel to 64% on an 88" diameter reel were documented at a number of major fiber optic cable manufacturers when utilizing a specially designed portable payoff stand.

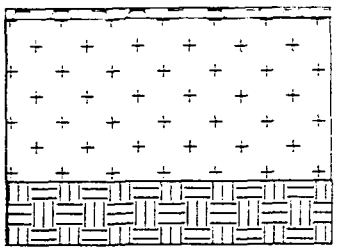
Field operators also report significantly improved labor efficiency in handling the new lagging material. Prior to switching to this material, the tools required to handle lagging removal in the field were hammers and crowbars, since the wood lagging was normally nailed and strapped onto the reels. Field operators are now able to use pliers to remove the strapping applied at the cable manufacturer and tape and scissors or plastic banding to reapply the material in the field after testing the cable.

Additional cost savings are gained through lower package weight and more efficient storage. The new lagging material consistently weighs 70-80% less than traditional wood lagging on both wooden and steel reels ranging in size from 32" to 96" in diameter. Storage space has been reduced by up to 50% due to the ability to pyramid stack the rolls of material versus the palletizing required for wood lagging.

From an aesthetics standpoint, the product does not warp or discolor like wood. Also, the treated outer sheet of Typar allows for custom printing of logos and handling instructions.

This new lagging material is particularly well suited as a replacement for traditional wood lagging given the current political climate surrounding packaging in this country. Legislators in 1992 continue the trend of aggressively pursuing the development of bills which will strictly mandate recycled content and disposal methods for both industrial and consumer packaging. (A prime example is House Bill HR 3865, which would require every package used in the U.S. to meet one of three standards: 1) Contain 25% recycled material (escalating to 50% by 2001); or 2) Be reusable 5 times; or 3) Use between 15 and 20% less material than the same or similar package used for the same product five years before.)

The necessary infrastructure is in place to handle reclamation of this product from the end users and a key part of the manufacturer's commitment in providing this material to the industry is to actively coordinate such a reclamation effort.



Cross-section of lagging material

Development Process

Rationalize Choice of Materials

Typar: 10.0 mil thick, polypropylene coated Typar was chosen over other outer sheet materials due to a variety of superior physical characteristics. A nonwoven, spunbonded, continuous filament polypropylene, it combines a low basis weight of 2.6 oz/yd^2 with high tensile and tear strength in all directions due to uniform stress distribution. Unlike woven fabrics, it will not ravel or fray and can be slit with a clean edge. The material is temperature resistant as well, with a melt temperature in excess of 165° C (330° F). A UV inhibitor coating provides exceptional resistance to extended exposure in the field.

The material is inert to most acids, alkalis, and salts. Like all polypropylenes, it does have a tendency to swell when exposed to some hydrocarbons and chlorinated solvents. The material is insoluble at room temperature, shows excellent resistance to environmental stress cracking, and is hydrophobic. The material also provides an excellent surface for printing logos and handling instructions.

Edgeboard: The core board is a critical element in providing the mechanical protection to the cable. A wide variety of core boards were tested prior to the selection of Edgeboard, with a broad criteria of adequate impact and compression strength, moisture resistance, and cost effectiveness. One hundred percent poly boards were tested and met all requirements, but were not cost competitive against standard wood lagging. One hundred percent kraft paper boards were cost competitive but did not resist moisture over extended exposure causing severe delamination both of the board itself and from the foam and typar layers.

The core board is produced through a patented extrusion process by Sonoco Products Company. The process allows the manufacturer to combine post industrial and consumer poly and paper through a shredder that feeds into an extrusion line. The blend of poly and paper is then wrapped inside a kraft paper outer layer to provide additional strength and stiffness. These boards are cut to length and delivered to the converting line after curing for a minimum 24 hour period. A positive feature of the patented technology is that the manufacturer can take the reclaimed lagging material from end users in the wire and cable industry and shred it into new raw material for the core board. As noted under the heading "Finished Product Evaluation," this product meets or exceeds industry thermal protection criteria allowing cable manufacturers the option of eliminating thermal wrap.

Cycle testing was completed on samples of both the core board and the lagging material to determine the effect of repeated soakings and drying on the integrity of the product.

Five pieces measuring .160"x3.0"x6.0" were completely immersed in 68° F water and left to soak. After 24 hours, the product was air dried for 24 hours in 72° F environment. This cycle of soak/dry is intended to demonstrate performance of both the core board and the lagging material in extremely wet field conditions.

After removing from soaking and prior to air drying, the material was measured for

indicate moisture absorption. Prior to initiating a new cycle the material was visually checked for delamination and flexed to determine any loss of rigidity, two characteristics deemed essential for effective cable protection. After three complete cycles there was no significant change in board thickness (less than 5% variation) and no visual evidence of delamination or loss of rigidity.

Foam: A 1/16" thick low density polypropylene foam was chosen for the internal face of the lagging which rests directly on the cable surface. The two primary functions of this layer are to provide cushioning from impact and compression and to enhance the thermal protection of the overall wrap. The material used has a density rating of 0.7 lbs/ft^2 and a water absorption rate of .0003 lbs/ft^2 area, making it virtually hydrophobic. Thermal conductivity and resistance characteristics were tested by the manufacturer under ASTM-C-177 *Steady State Thermal Transmission Properties by Means of the Guarded Hot Plate*. The product exhibits a thermal conductivity rate of 0.27 BTU/hr ft^2/F/in and a thermal resistance rate (R factor) of 3.7 (1") Hr/ft^2/F/BTU. The material has a melt point of 160° C (320° F) as determined by ASTM-D-789 *Test Method for Determination of Relative Viscosity Melting Point and Moisture Content.*

Adhesives: The product is bonded with a sprayed hot melt adhesive. The criteria used to evaluate adhesives was successful, consistent application of uniform quantities of material across the slats on a high speed converting line and a product which demonstrated superior resistance to extreme environmental conditions. Testing to quantify the performance of the adhesive at temperature and moisture extremes was completed by the manufacturer during June 1992.

Typar and polyethylene foam were bonded to the core board in a laboratory environment and allowed to cure for 24 hours. After cure the testing was conducted on six samples as follows:

First, six samples were placed in an oven for 72 hours at +60° C (158° F). Two were visually checked for adhesion after heating. Four of the six samples were then cooled to -30°C (-20° F) for 24 hours. Two samples were soaked for 24 hours after the initial heating.

After the -30° C cycle, those samples were flexed and a visual inspection made to check for a sufficient bond before peel testing. After the cycles of +70° C, -30° C and the water soak, two samples were peeled and checked for substrate destruction.

After the +70° C cycle, the samples, when peeled, showed kraft destruction, indicating a strong bond between the adhesive, the core board, the top sheet and the foam. Samples were flexed after the -30° C cycle without any delamination and peeling and showed slight poly destruct indicating a strong bond to the adhesive. The water soak showed no delamination of the lagging material and no degradation of the core board.

In summary, the adhesive met our expectations under cycles that represented extreme environments which the material could encounter after being in the field for approximately one year.

Payoff Stand Development

In August, 1991, we determined that projected efficiency gains in the lagging department of the cable manufacturer could only be met with the installation of a mechanical payoff stand. We contacted three automated payoff stand manufacturers for quotes and concepts. The equipment proved to be far too sophisticated for our needs. In response, Baker generated an in-house request to engineering for concepts and costs on a simple "A" frame stand with the capability to effectively dispense the lagging material. An initial prototype was developed for AT&T Fitel with two roll capability. Delivery was made in December, 1991.

In February, 1992, we met with AT&T Fitel lagging department personnel for recommended modifications. A third pintle was added to allow for three roll capability and new, locking rollers were installed on the base of the stand for improved mobility in the shop. As of June, 1992, this second generation Payoff stand is in service at AT&T Fitel and other major fiber optic cable manufacturers.

Testing of Product

Finished Product Evaluation

After the performance of the individual lagging components was determined, the finished product was tested to determine the level of protection it gives. The lagging material was tested for both mechanical and environmental performance. Because there are no industry standard tests for the mechanical performance of lagging materials, we chose to evaluate its performance by

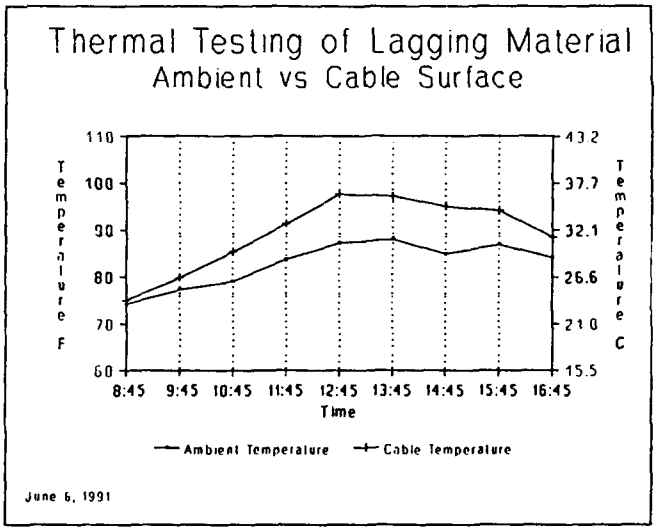
we chose to evaluate its performance by comparing a cable's optical performance when tested with and without the presence of the lagging material. We chose to perform impact and compression testing, as they are the most severe mechanical tests and most closely simulate actual reel handling conditions. For testing, twelve fibers were monitored by connecting them to an LED operating at 1440 Nm and a power meter through two, thirteen channel optical switches. A reference fiber was also used for monitoring the light source power variation. The testing was conducted in accordance with EIA-455-25A, *Impact Testing of Fiber Optic Cables and Cable Assemblies*. Cable samples were impacted 25 times using a 4 kilogram mass dropped for 150 mm. There was no increase in attenuation or cable damage when tested either with or without the use of the lagging material.

The impact of the lagging material was also tested per ASTM D 3029-84. The test equipment consisted of a drop hammer mass capable of delivering an impact of 0 to 18.1 Newton-meters onto a 1.27 cm (0.5 inch) hemispherical die. The failure criteria during impact testing was originally considered to be visual damage to the lagging. Using this criteria, the impact strength of the lagging was rated at 14.1 Newton-meters. We retested the lagging on top of a cable, and changed the failure criteria to cable damage. We tested to 18.1 Newton-meters using this particular apparatus. There is no standard test method for impact testing of lagging, but it was apparent that the use of lagging greatly decreases damage to the surface of the cable due to impact.

The product was also tested for compression resistance. The testing was performed in accordance with EIA-455-41 *Compression Loading Resistance of Fiber Optic Cable*. Several samples were tested with and without the protection of lagging material, the cable was able to withstand approximately 20 percent more load while maintaining equivalent performance. In addition, the lagging alone was compressed to the machine limit of 32,000 kg/m^2, and exhibited no damage.

The lagging was tested for thermal protection per REA Specification PE-90, *Filled Fiber Optic Cable*, and Bellcore TR-TSY-000020, Issue 4, *Generic Requirements for Optical Fiber and Optical Fiber Cable*. The REA test procedure required two cable samples to be placed against an insulating material. A thermocouple is attached to the surface of each cable, and one of the samples is covered with the thermal barrier under test. A radiant heat source capable of heating the uncovered cable surface to 70° C (160° F) is used to simulate solar radiation. The source is turned on until the temperature of the samples stabilizes. The difference in temperature between the jacket with the thermal wrap and the bare cable sample must be greater than or equal to 17° C (31° F). This test was performed using the lagging material as a thermal wrap, and the uncovered sample had a temperature of 76.7° C (170° F) while the covered sample had a temperature of 52.9° C (127° F). The temperature difference of 23.9° C (43° F) easily met the requirement.

The thermal protection was also tested using Bellcore requirements. A thermocouple was attached to the surface of a cable on a reel, and lagging was placed over the cable. The cable was placed outdoors in direct sunlight on June 6, 1991, from 8:45 AM to 4:45 PM. Each hour, the cable surface temperature and the ambient temperature were measured. Bellcore requires that the cable surface temperature be no greater than 10° C (18° F) above the ambient temperature under maximum solar radiation. The maximum difference during our test was 5.8° C (10.4° F). The graph below shows the ambient and cable surface temperatures during the test.



Results

Since June, 1991, there has been a demonstrated success in the field. No cable damage has been reported on either domestic or export shipments of over 200 steel and wood reels lagged with this new material. Having fully evaluated other mechanical/thermal lagging materials available today, Bell Atlantic feels there is no other cost effective lagging option which

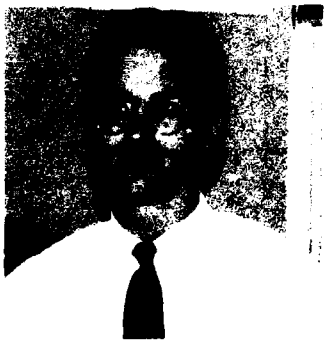
1) meets industry mechanical and thermal performance criteria, 2) is recyclable, 3) is made of recycled material and 4) does not add to the domestic waste stream.

Bell Atlantic has enjoyed such success with this product that they will be authorizing all of their suppliers to use it exclusively on shipments of fiber optic cable effective January, 1993.



Joseph A. Hill
AT&T Fitel
201 Adamson Ind. Blvd.
Carrollton, GA 30117

Joseph A. Hill received a B.S. degree in Ceramic Engineering in 1989 from Clemson University. He joined the AT&T Fitel Company in 1990, where he currently holds the position of Product Development Engineer. He is a member of the American Ceramic Society (ACrS) and the National Institute of Ceramic Engineers (NICE).



Christopher E. Hall
Sonoco Products Co.
P. O. Box 668
Hartselle, AL 35640

Christopher E. Hall is the Marketing Services Manager for Sonoco Products Company, Baker Division. He has product management responsibilities for the lagging material. Mr. Hall graduated from Boston Univ. in 1984.



Karl B. Shields
C&S Associates
P. O. Box 839
Coraopolis, PA 15108

Karl B. Shields is the President of C&S Associates, the designer and manufacturer of the lagging material. His company holds the design patents on the product.

MOISTURE PERMEABILITY OF STEAM RESISTANT TELEPHONE CABLES

Joseph N. D'Amico and Osman S. Gebizlioglu

Bellcore
Red Bank, New Jersey 07701 U.S.A.

ABSTRACT

Some fiber optic and copper subterranean telecommunications cables in major cities are degrading prematurely or have been destroyed by leaking utility steam. To develop generic requirements for steam resistant cables, we have constructed an apparatus to measure the moisture permeation of cable sheaths in a steam environment.

We have tested fiber optic and copper cables in this apparatus. We found that a cable sheath constructed with a sealed metal shield will prevent moisture permeation to the cable core. Moreover, we discovered that all the optical cable samples with sealed shields contained about one gram of moisture per seven foot length. A maximum allowable moisture content requirement may be necessary to prevent the degradation of cable core materials resulting from this intrinsic trapped water vapor.

INTRODUCTION

Many of the nation's larger cities distribute utility steam to provide buildings with space heating and cooling. In some cities many of the steam mains are now old and often corroded. They regularly leak and, at times, even break. The defective pipes may not be repaired promptly by the steam utility unless the condition is deemed dangerous. Consequently, it has become necessary for the telephone companies to consider the utilization of steam resistant fiber optic and copper cables. The effectiveness of such cable designs relies on preventing moisture entry into the cable core at steam temperatures and in limiting its internal exposure to dry heat. In this report we present an evaluation of the moisture permeability of prototype steam resistant cables.

We have constructed an apparatus to measure the moisture permeation into fiber optic and copper cables in a steam environment. This test unit exposes the three foot long mid-section of a seven foot long cable to saturated steam. The water vapor permeating through the cable sheath into the core is collected by the dry nitrogen carrier gas. The heated gas carries the moisture first to condensers and then into tubes filled with desiccants where any remaining water vapor is removed from the gas stream. The total quantity of the captured moisture is then determined gravimetrically. (Should the cable core be filled and restrictive to gas flow, components of the core, such as the central strength member in an optical cable, can be removed to provide a flow channel.)

The first part of this paper describes the apparatus while the second presents results obtained on current and newly-designed steam resistant cables. Finally, we suggest generic requirements for steam resistant cables.

PART I

TEST APPARATUS

We designed and built a test unit to place a cable section (fiber optic or copper) in a saturated steam environment. A seven foot sample is positioned longitudinally at the centerline of a three foot long steam tube. The cable extends out through the ends of the steam chamber, through an air gap and into the carrier gas entry and exit chambers, respectively. Seals around the cable at the chambers' entry and exit ports prevent the escape of either steam or nitrogen into the atmosphere (Figure 1). Dry nitrogen with monitored pressure and flow rate passes through a molecular sieve drier and into the cable entry chamber from which it transits the cable core to the exit chamber. From there the carrier gas flows through the condenser/absorber moisture collector where the absorbed water is removed.

Equipment Detail

The Steam Chamber

Figure 2 shows the steam chamber consisting of a three foot long, six inch diameter iron pipe with flanges welded to each end. The test sample enters and exits the steam chamber through stainless steel collets which are bolted to the chamber end plates and flanges. The collets confine a

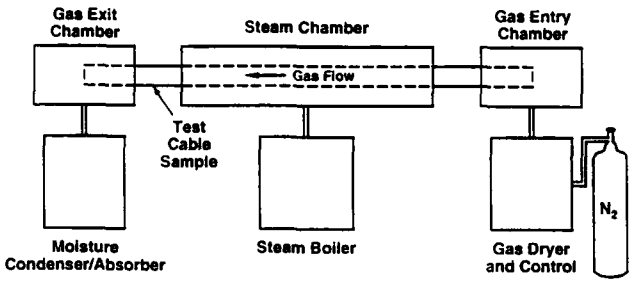


Figure 1 - Steam Resistance Moisture Permeation Cable Tester

graphite impregnated graphite yarn rope to form a broad compression seal on the cable sheath. Two viewing ports permit cable observation in the steam environment while gauges display the temperature and steam pressure. Up to five thermocouples positioned along the internal top, bottom and sides of the chamber provide continuous input to a data logger.† The steam chamber is equipped with pressure relief devices for safety.

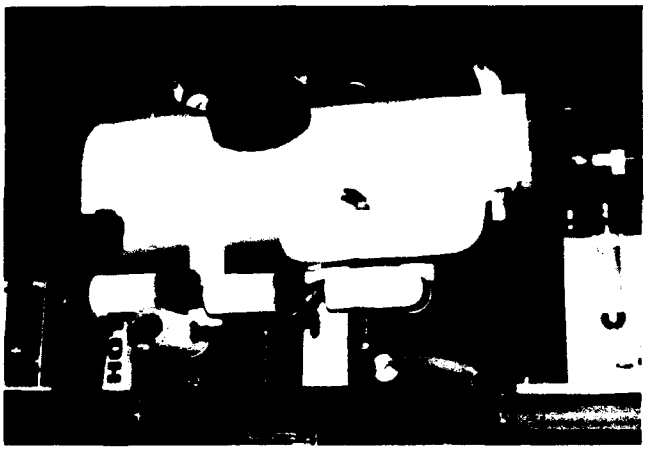


FIGURE 2 - Steam Test Chamber

Steam, with its temperature and pressure precisely controlled, is generated for continuous operation by an electric boiler‡. The saturated steam envelops the test cable providing the environment required for moisture permeation.

The Carrier Gas Entry:

We use dry nitrogen (zero grade) as the carrier gas and control its flow rate with a precision low flow rate regulator at 100 ml/min. and 15 psig. At the gas entry control panel, the gas passes through a molecular sieve drier, a flowmeter and is then directed to either the cable gas entry chamber or a bypass for supply cylinder gas moisture analysis, shown in Figure 3. The carrier gas pressure and temperature are



FIGURE 3 - Carrier Gas Entry Control and Temperature Datalogger

monitored in the cable entry chamber. The temperature is continuously recorded because any significant increase in the carrier gas temperature indicates steam leakage into the cable core.

Gas Collection and Moisture Detection

The carrier gas exits the test sample into a six inch diameter one foot long cylinder similar to the gas entry chamber. The exit chamber, however, is electrically heated to prevent

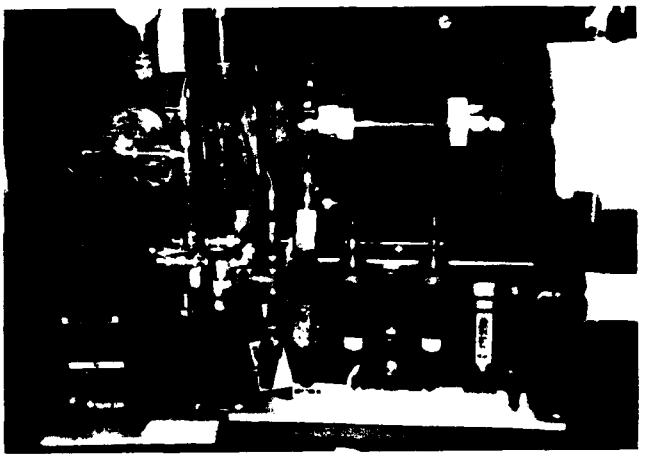


FIGURE 4 - Carrier Gas Exit Chamber and Moisture Removal Apparatus

premature moisture condensation from the carrier gas. (At 55 °C the nitrogen can hold ten times the moisture that it can at room temperature.) The temperature and pressure in this

† Ungrounded type K thermocouples with one sixteenth inch stainless steel sheath manufactured by Omega Engineering, Inc., Stamford, CT. Model 50 datalogger, manufactured by Electronic Controls Design, Inc., Milwaukee OR.

‡ Manufactured by Sussman Electric Boilers, New York City, NY; Model MB6L (Max. steam rate, 18 lbs/hr; max. pressure, 90 psig)

chamber are monitored by a thermometer & thermocouple and guage, and the gas flow rate via a rotameter, respectively. The gas pressure drops from the carrier gas entry chamber to the exit chamber because of the resistance of the cable core to gas flow. This steady state pressure drop may change as the temperature rises since the flow channel may be altered by material expansion or melting and/or filling compound flow or degradation.

The nitrogen gas carrying moisture passes through air cooled condensers to either of two clear plastic collectors followed by a dual series of desiccant columns which remove any absorbed moisture. The total amount of water collected by condensation in these collectors and by absorption in the desiccant columns gives the moisture removed from the cable core. This quantity represents the initial moisture content of the cable from the cable drying operation and the amount of moisture permeated through the cable sheath during steam exposure. The efficiency of the condensers is monitored by two thermocouples located in the gas stream. (Figure 4)

Theory of Operation

In designing the test, we had to consider the moisture carrying ability of the gas. If the flow rate were too slow, moisture could permeate the cable sheath faster than the gas could remove it; if it were too fast, the thermal profile of the cable core would be altered and the accuracy of the experiment compromised.

The initial drying stage is carried out at room temperature. This stage involves the surface evaporation of water from the cable core components. The transfer rate of water from the cable core surfaces to the carrier gas depends on the carrier gas density, viscosity, flow rate and the diffusivity of water vapor into the carrier gas. During the later steam exposure stage, water vapor from the outer surface of the cable sheath diffuses into the cable core and raises its temperature. Thus, most of the water vapor transfer to the carrier gas takes place at elevated temperatures where the gas can hold more moisture than it can at room temperature.

The carrier gas flow rate in the cable core determines the transfer rate of water vapor into the carrier gas stream. This transfer rate of is commonly expressed in terms of two dimensionless numbers[1,2]; namely, Reynolds Number: Re, and Schmidt Number: Sc. These dimensionless numbers arise from non-dimensionalizing (mass, momentum, and energy) conservation equations for evaporation into a carrier gas flow in a cylindrical tube[2]. The Reynolds number expresses the relative strength of bulk flow to the viscosity-dominated laminar flow, and it is given as follows:

$$Re = (d\ U_a\ \rho)/\mu$$

where d, U_a, ρ, and μ are tube diameter, carrier gas linear velocity, gas density, and gas viscosity, respectively. The Schmidt Number expresses the relative importance of viscosity- dominated flow to the mass diffusion, and it is defined as:

$$Sc = \mu/(\rho\ D_{water\text{-}nitrogen})$$

where $D_{water\text{-}nitrogen}$ is the diffusion coefficient of water vapor in the carrier gas. The mass transfer rate, j_D, is expressed as function of these two numbers,

$$j_D = C(Re)^n(Sc)^m$$

where C, n and m are constants.

To calculate Re and Sc for this cable drying experiment, the following parameters are used:

Gas flow rate, Q = 100 ml min^{-1}

pressure, P = 29.7 psia

density = 0.001122 gm ml^{-1} at 25 °C [3]

viscosity, μ = 0.01750 cp at 25 °C [4]
(cp = centipoise, 1 poise = 1 gm cm^{-1} sec^{-1})

The Diffusion Coefficient[5], $D_{Water\text{-}Nitrogen}$, 25 °C = 0.256 cm^2 sec^{-1}

For a cable sheath of 2-inch inner diameter, with no internal obstruction, the linear velocity, U_a, is calculated from the gas flow rate, Q as follows,

$$U_a = Q/((\pi d^2)/4)$$

Then, we compute the following values for the Reynolds and Schmidt Numbers:

$$Re = 2.68 \quad \text{and} \quad Sc = 0.61$$

For all Re < 2100, the gas flow is laminar with a parabolic velocity profile, i.e., the maximum gas velocity occurs at the centerline of the cable with parallel streamlines. A value of 0.61 for Sc indicates that water vapor transport takes place by diffusion into the carrier gas. If the gas flow with the same volumetric rate is forced into a smaller cable cross sectional area, e.g., 10% of the original internal cross-sectional area, then the linear velocity and Re increase to 0.82 cm sec^{-1} and 26.8, respectively. However, this change is not large enough to change the overall transport rate significantly. This latter case may also represent the situation for drying a fiber optic cable with a removed central strength member.

During steam exposure, the cable core temperature rises. Consequently, the carrier gas viscosity and the water vapor diffusivity increase while the gas density decreases. Thus, the Reynolds and Schmidt Numbers may increase indicating a faster water removal rate from the cable core. The overall temperature of the test cable is not significantly lowered by the carrier gas in the cable core since the mass of the gas is

small in comparison with that of the cable. Moreover, the heating capacity of the steam boiler is very large when compared to the energy removed by the carrier gas.

PART II

EXPERIMENTAL

Sample Cables

We tested four fiber optic cables:

A. A standard (non-steam resistant) cable containing a central strength member (removed for the test) and six buffer tubes with optical fibers. The filled cable core was covered with polyimide yarn and sheathed with a polyolefin jacket.

B. A steam resistant optical cable with a welded metal shield. The filled cable core also consisted of a central strength member (not removed) surrounded by six buffer tubes containing optical fibers. The metal shield was covered with a polyimide reinforced polyolefin jacket.

C. A steam resistant cable with a welded metal shield and a fluorocarbon jacket. This filled cable contained water blocking tapes, a single core tube and optical fibers.

D. A steam resistant cable with an overlapped polymer coated steel shield and nylon jacket. This filled cable core consisted of a central strength member and six optical fiber buffer tubes wrapped in a polyimide yarn.

We also tested two 600 pair steam resistant copper conductor cables:

I. A standard "Steampeth" cable with pulp insulated conductors, an overlapped steel shield and a medium density polyethylene jacket.

II. A special cable manufactured with fluorocarbon insulated conductors, an overlapped steel shield and a crosslinked jacket of modified polyethylene.

Test Procedure

The cables were placed in the steam resistance moisture permeation cable tester, pressurized with nitrogen to 15 psig, and static tested for leaks. Meanwhile a moisture determination of the carrier gas itself was made to assure its dryness. The actual test for optical cables began with a four day purge of the cable's inherent moisture at room temperature. Following this drying period, the test cable was exposed to five psig pressure saturated steam (108.5 °C) for one week and twenty five psig pressure steam (130.5 °C) for a second week. Cables with a low melting temperature (< 130 °C) jacket were tested at a lower steam pressure for the second week. (Figure 5)

RESULTS

Fiber Optic Cables

All the optical cables that we tested showed about one gram of initial moisture per seven foot section. Steam exposure of initially dried cables with welded metal shields demonstrated the effectiveness of those shields in preventing water entry into the cable core. For Cable "A", a standard loose tube type optical cable without a metallic shield, we measured a water permeation rate of 13.5 mg hr^{-1} $inch^{-1}$ (of cable outside diameter) in five psig pressure steam, as indicated in Table 1. At that rate, a cable with a five percent internal void space could conceivably become filled with water in less than twenty four days.

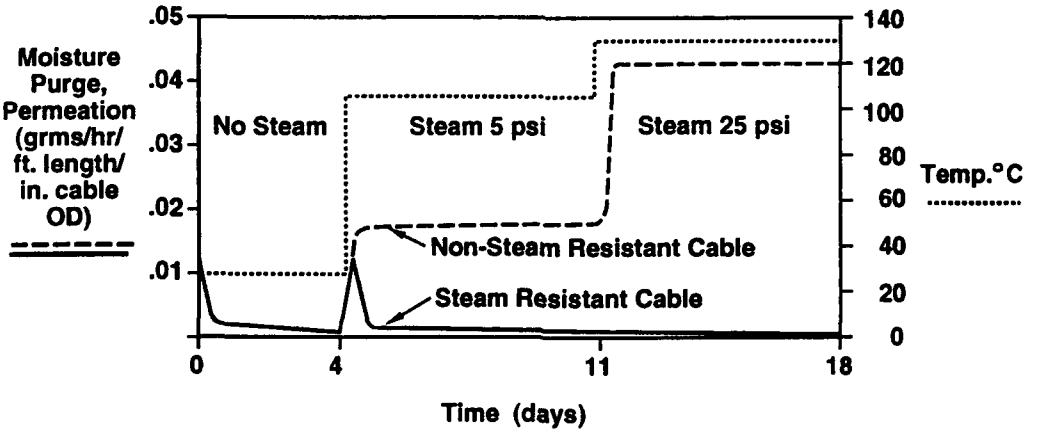


FIGURE 5 - Typical Moisture Purge - Permeation Data Plot

Optical Cable Sample	Initial Moisture At Room Temp.	Removed (grams) At 108.5 °C
"A"	1.30	*
"B"	1.34	1.23
"C"	1.15	0.68
"D"	0.82	*

* Initial moisture undeterminable due to steam penetration of the cable sheath.

FIBER OPTIC CABLES
Inherent Moisture Content (gms./7 ft. sample)

TABLE 1

Copper Cables

The two copper conductor cables that we tested did not show significant resistance to steam. So-called "Steampeth" cables, in fact, were never designed for continuous operation in steam. Moisture permeation through the Steampeth sheath averaged 12.7 mg per linear cable foot/inch of cable diameter for each hour of steam exposure (5 psig pressure, 108.5 °C). The electrical transmission characteristics of this cable would quickly degrade under that condition. The moisture permeation rate of this cable doubled in steam at 15 psig pressure. At 126 °C the semi-molten cable jacket was forced into the shield overlap by the steam pressure somewhat reducing moisture permeation. This condition would not be realized in the field where the pressure of the unconfined steam would be dissipated into the surroundings. At 128 °C, the jacket finally melted, steam penetrated directly into the cable core and ruptured the jacket outside the steam chamber.

We tested two samples of Cable II with its core of fluorocarbon insulated copper conductors. Its jacket is a filled modified crosslinked polyethylene which, like Cable I, was bonded by a thermoplastic polymer to an overlapped steel shield. This jacket quickly separated from the shield when the cable was tested in 108.5 °C steam. The moisture permeation rate of Cable II was approximately three times that of Cable I (Table 2). While the cable jacket did not melt, it ballooned from the 15 psig internal nitrogen gas pressure. One of the test samples ruptured under the carrier gas induced hoop stress after only two days in steam at 5 psig pressure. (A similar cable sheath had failed under central office air pressure during a 1991 field trial in New York City.)

DISCUSSION

Steam resistant optical cable designs proposed by major cable manufacturers usually incorporate standard optical cable core components in a sealed cable sheath. It is fabricated to form the major barrier to steam penetration into the cable core. This barrier consists of two resistances-in-series to steam flow: The outer one is the cable jacket, while the inner one is the sealed metal shield. Since all polymers become increasingly permeable to water vapor at elevated temperatures[6,7], the jacket's resistance to steam will decrease drastically during steam exposure. Thus, a polymer cable jacket cannot be relied on as a steam barrier. Our results on sample cables showed that the sealed metallic shield is the key component that prevents steam from entering the cable core. Nevertheless, a cable jacket is an essential part of the cable sheath, as it thermally and electrically insulates the metallic shield. It also provides protection during cable installation and acts as an impediment to water migration to penetrations in the metal shield.

Cable Sample	Moisture Permeation Rate In Steam ^ At 108.5 °C (5 psig)	At 130.5 °C (25 psig)	Shield	Jacket Material
Fiber Cables				
"A"	0.013	Jkt. Failure	None	Polyolefin
"B"	0.0	0.0	Welded Metal	Polyolefin
"C"	0.0	0.0	Welded Metal	Fluorocarbon
"D"	*	*	Overlapped Steel	Nylon
Copper Cables		At 115 °C (10 psig)		
I	0.013	0.018	Overlapped Steel	MDPE
II	0.035	0.045 to >0.064	Overlapped Steel	XLPE

^ Moisture permeation rate in grams/foot length/inch cable outer diameter
* Moisture undeterminable due to cable core blockage.

FIBER OPTIC AND COPPER CABLES
Moisture Permeation Rate In Steam
(All cables, except "A", are of steam resistant design.)

TABLE 2

Moisture readily permeated all the cable jackets that we tested in steam, (Table 2). Moisture did not penetrate into the core of fiber optic Cables "B" or "C", both of which have welded metal shields. However, Cable "C" exhibited water droplets between the fluorocarbon polymer jacket and the welded metal shield. The MDPE jacket on another cable melted and dripped to the floor of the test chamber, (Figure 6). Drippings from this cable literally had to be chiseled from the surface of the test chamber. A cable in the field with such a jacket would be very difficult to remove from its duct for repair or replacement. These observations also suggest that a cable jacket be well bonded to the shield at steam temperatures to prevent the formation and migration of water droplets on the shield surface.

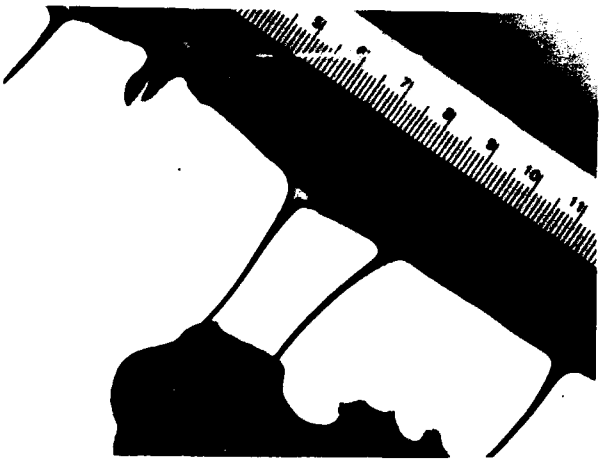


FIGURE 6 - Optical Cable after Steam Exposure - MDPE Jacket Melted

While a sealed metal shield provides an effective barrier to steam, it also serves to trap volatile products from core components (filling compounds, core/buffer tubes, and coatings). Our tests showed that all vendor cables contained about a gram of initial moisture in a 7-ft section. This quantity of trapped water may pose two major reliability risks: 1) Water in the core will vaporize as its temperature rises when the cable sheath comes in contact with steam. Hot water vapor causes some core/buffer tube materials to degrade by hydrolysis. 2) One gram of hot water vapor upon contact with certain metals may be catalytically converted to about one liter of hydrogen. Hydrogen trapped in the cable core could cause transmission loss if absorbed into the glass fiber. Our tests to date have indicated that the first risk factor may be significant enough to establish a maximum allowable initial moisture content for steam resistant optical cables.

While those fiber optic cables that were impervious to moisture penetration had welded metal shields, it is conceivable that other methods could be used to so seal the shield. In this paper we discuss the effectiveness of the metal shield in restricting or preventing water transmission to the cable core; we do not mention their projected longevity. These cables are expected to function for a long time in a harsh environment, one which often contains corrosive salts. There may even be nearby DC electrical sources, such as an electrified subway rail line, which can lead to stray electrical currents in the shield. These currents are known to accelerate shield corrosion.

It is absolutely essential to keep moisture from entering the core of an optical fiber cable since once it is present, it cannot be easily removed. Unlike optical cables, copper conductor cables used in underground ducts are usually unfilled. They rely on the central office dry gas (or air) purge to keep them dry. Consequently, these metallic cables will tolerate a very low rate of moisture permeation provided that it does not occur over an extended cable length.

CONCLUSION

Telephone cables, both fiber optic and copper conductor, are expected to operate for many years, even when they may be located in the harsh environment of escaping utility steam. Such speciality cables must have a heat resistant core and a moisture impermeable sheath. The cable core itself must not contain moisture which upon heating will form steam. The shield metal should not only resist corrosion in steam but also it should not catalytically generate hydrogen from heated moisture present within the cable core. Polymer cable jackets alone are unable to prevent moisture permeation to the cable core, but in conjunction with a sealed metal shield, reliable steam resistant cable sheaths can satisfy the application.

Cables designed to be steam resistant can be measured for moisture permeation in a steam environment with apparatus such as that described in this paper. Moisture ingress and initially contained moisture are only two of the several special parameters which the designers and purchasers of steam resistant cables must take into account. Bellcore Technical Advisory TA NWT-001322, Issue 1, "Steam Resistant Optical Cable", is expected to be issued during the fourth quarter of 1992. It will provide Bellcore's Clients and the industry with Bellcore's view as to the technical requirements needed to assure the quality of a steam resistant optical cable.

ACKNOWLEDGEMENTS

The authors thank Robert J. Wasilewski and Lawrence B. Green for their mechanical designs and Grant F. Apgar and Frank J. Garriel for constructing the cable tester.

REFERENCES

1. T.K. Sherwood, R.L.Pigford,, C.R. Wilke,, "Mass Transfer", Mc-Graw Hill, New York, 1975, p 201.
2. R.B. Bird, W.E. Stewart, E.N. Lightfoot, "Transport Phenomena" Wiley-Interscience, 1960, p 555, 647.
3. CRC Handbook of Chemistry and Physics, 67th Ed., 1986, p. F-10, CRC Press, Inc., Boca Raton, Florida.
4. Chemical Engineers' Handbook, R.H. Perry and C.H. Chilton, Eds., Fifth Ed., Mc-Graw Hill, New York, 1973, p 3-211.
5. R.C. Reid, J.M. Prausnitz, T.K. Sherwood, "Properties of Gases and Liquids", Mc-Graw Hill, New York, 1977, p 559.
6. Polymer Handbook, J. Brandrup and E.H. Immergut, Eds., 2nd Ed., Wiley-Interscience, New York, 1975, p III-229.
7. Friesen, H. W. and Windeler, A. S., "Moisture Permeation and Its Effect On Communications Cable", Proc. 15th. Annual Wire and Cable Symposium, Dec. 1966.



Joe D'Amico has worked on engineering and materials issues affecting all types of telecommunications and power cables in his 25 year career. He first worked with communications cable at Western Electric before joining General Cable Company in 1967. There as senior research physicist, he investigated the structure and composition of all types of telecommunications wire, cable and optical fiber as well as electrical power cables. Since 1985 he has worked at Bellcore, initially as a Quality Assurance Engineer and since 1989, as a member of the Plastics and Rubber Research Group in Red Bank, New Jersey. Joe is a graduate of Seton Hall University. He received his MS degree from Fairleigh Dickinson University.



Osman S. Gebizlioglu is a Member of Technical Staff in Bellcore's Plastics and Rubber Research Group. He holds BS and MS degrees in chemical engineering from the Middle East Technical University, Ankara, Turkey. After receiving his Ph.D in the Polymer Materials Program at Princeton University, he was a Monsanto Postdoctoral Fellow in the Mechanical Engineering Department of MIT where he investigated the physics of toughening glassy polymers. Since he joined Bellcore in 1987, he has focussed his research on polymers used in optical fiber cables, particularly in harsh environments.

THE REMOVAL OF COPPER PAIRS OF DISTRIBUTION CABLES TO CREATE PATHS FOR PLACING FIBER CABLES

P. R. Briggs, Jr., L. M. Slavin, E. E. Hershkowitz, S. A. Khan*, J. P. Varachi, Jr.

Bellcore, Morristown, N. J.
*Bellcore, Red Bank, N. J.

Abstract

One of the methods under investigation by Bellcore to facilitate the installation of fiber cables in established residential areas with buried plant, in order to accomplish a Fiber-in-the-Loop (FITL) upgrade, involves the re-use of existing cable paths in the ground. As a first step in determining the feasibility of such an approach, tests were performed aimed at removing the copper conductors, or "cores", from typical telephone distribution cables. The ability to pull out the cores of such cables would allow the use of the resultant pathway for placing fiber-optic media. Various techniques were investigated, including that of pumping lubricant into the interstices of air-core cables, and elevating the temperature of waterproof cables in order to soften or melt the filling compound. Outdoor tests performed on buried lengths of 100-pair air-core and filled cables resulted in the successful removal of copper cores of up to 200 ft., with indications of greater possible lengths. Fiber cables of 1/2-in. diameter were inserted into several of the cavities created.

Introduction

The telephone local loop is undergoing a major evolution in the form of Fiber-in-the-Loop (FITL), for which mass deployment is expected to begin by the middle of this decade, or sooner. Although initial implementation will tend to be in growth (new construction) areas, there will be applications in areas requiring replacement of degrading copper facilities. Eventually there will also be a need to upgrade other areas in order to obtain the various long-term benefits of the fiber-optic based technology. Such replacements and upgrades will require installation of new, relatively small diameter, fiber distribution cables in existing residential areas with buried plant. Major concerns in these endeavors include the minimization of restoration expenses and damage avoidance to other buried utilities. One technique under investigation by Bellcore involves the re-use of existing cable paths in the ground. As a first step in determining the feasibility of such an approach, laboratory and field experiments have been performed to remove the copper conductors, or "cores", from typical shielded telephone distribution cables. The ability to remove the cores of such cables between existing curbside pedestals would allow the use of the resultant cavity to place fiber-optic media.

Although the removal of copper pairs from cables has been done in the past, it was generally done on a sporadic basis for larger (retired) cables embedded in underground conduit. For a given length, the removal of the core of a distribution cable along a residential street is expected to be more difficult because of the relatively low tensile strength of the typically smaller size cables, and the greater degree of undulations associated with direct-buried installations. In addition, newer direct-buried cables contain waterproof filling compound, which would significantly increase the force required to remove the core. Thus, the present investigation is intended to address this relatively difficult case, and to eventually develop a well-understood, routine process.

The cables of interest are typically of two general types -- air-core and waterproof ("filled"). Cables buried in recent years have been primarily of the waterproof construction. In this case, a filling compound is used to block the flow of water along the interior of the cable in order to minimize cable degradation and transmission problems. However, in the early years of buried plant construction, air-core cables were often used for this application. Many present-day copper rehabilitation projects are associated with replacing degraded buried air-core cables.

Both air-core and waterproof cables contain bundles of twisted 19- to 26-gauge copper pairs -- ranging in size from 25 pairs to many hundreds of pairs. The conductor insulation is "plastic" (e.g., polyethylene), and there is a loose dielectric (plastic) core wrap around the spiraled copper bundles. The sheath is of several possible constructions, including a corrugated aluminum shield and an outer black polyethylene jacket. In addition, cables can include a second metallic (steel) shield and an inner polyethylene jacket within the shield(s). Furthermore, a variety of overlaying outer layers are available to provide added mechanical protection against gophers, corrosion, etc. For waterproof versions, the cores have been filled with various types of petroleum-based compounds, with a flooding material placed between the shields and the outer jacket. Figure 1 illustrates the generic construction of the cables of interest.

Although the most direct means of creating an available cavity would appear to be the removal of the twisted

copper pairs, leaving the metal shield as structural support, the strengths of the bonds between the various layers will determine at which interface slippage will actually occur. For example, it is possible that the core and shield as a unit will pull out of the outer jacket, or even that the entire cable will pull out of the soil. The method of grasping and securing the cable core or shield, as well as the preparation used to facilitate the core removal process, will be factors in determining which (if any) components will be removed.

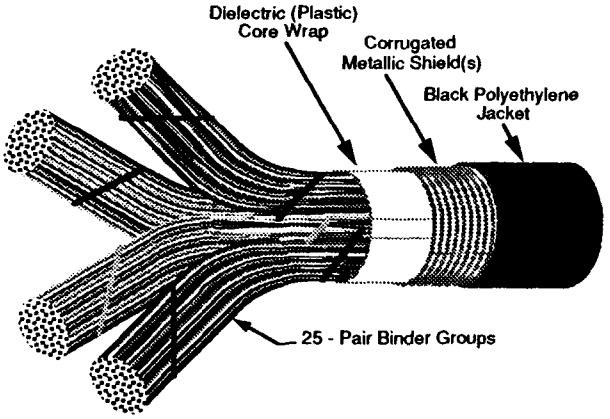


Figure 1. Typical Distribution Cable Construction

Distribution cables in the relatively small size range of 100- to 200-pairs are commonly used along the branch portions of distribution routes, between pedestals. It is anticipated that the removal of any practical lengths of core -- i.e., on the order of 100 feet or more -- in actual buried situations (including undulations along the original trench or, possibly, other discrete route bends) will not be easy. Therefore, two basic methods have been investigated to reduce the frictional drag or viscous forces between the core and the sheath.

For air-core cables, a significant fraction of the core consists of voids through which it is possible to pump fluids, such as lubricants, in an attempt to reduce the drag forces on the core. For waterproof cables, the adhesion between the core and the sheath is significantly greater than for air-core cables. However, the petroleum-based filling materials have relatively low melting points (e.g., typically less than 200°F), and lower softening temperatures. Thus, elevating the temperature of the cable in the vicinity of the shield should lead to a reduction of the drag forces on the core. For example, applying a heavy electric current to the shield of a buried (non-working, disconnected) cable, analogous to an electric welder connected to a frozen water pipe to accomplish thawing, would elevate the temperature immediately adjacent to the shield.

Preliminary Laboratory Experiments

As a preliminary step, a series of laboratory experiments were performed on short (10 ft.) test samples subjected to various lubricants and temperatures. The results were used to guide the selection of materials and methods for application to longer lengths of buried cables in the more difficult (and costly) outdoor buried tests. The preliminary laboratory experiments were performed on air-core and waterproof cables, representing those of a major manufacturer of telephone cable (the most likely manufacturer to be encountered for the present application). The cables tested included 50-, 100-, or 300-pairs of 24- or 26-gauge copper conductors.

For example, the results illustrated in Figure 2 apply to a 100-pair, 24-gauge waterproof cable filled with an extended thermoplastic rubber (ETPR) filling compound. Both the peak force required to initiate core slippage and the steady force required to maintain movement are indicated. (Data corresponding to a second attempt on the same sample, following release of the pulling force for the first attempt, is also shown.) Three separate 10 ft. cable samples were tested at different temperatures: ambient room temperature ("reference"), 140°F, and 195°F. It is evident that there is a dramatic reduction in the required removal force at 195°F -- to approximately one-third that at ambient conditions. There was no apparent benefit in heating to only 140°F. These results are consistent with separate laboratory experiments in which samples of the ETPR compound were subjected to rheological testing using a parallel plate geometry in a dynamic mode. As indicated in Figure 3, the viscosity of the filling material dramatically decreases by more than an order of magnitude as the temperature increases from 140°F to above 175°F.

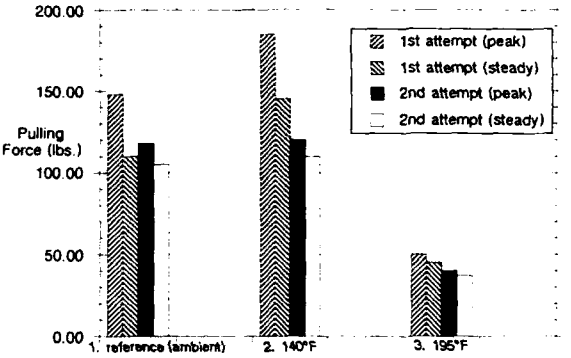


Figure 2. Preliminary Laboratory Experiments, 10 ft. Samples (100-pair, 24-gauge ETPR-filled Cable)

Outdoor Buried Tests

The outdoor tests were performed on various lengths of 100-pair, 24-gauge air-core or filled cable, buried at a 30-in. depth in 12-in. wide straight trenches. The ends of the cables were gradually brought to the surface over a 10 ft. distance to minimize the effects of discrete bends when pulling the cable cores via a surface winch. This arrangement conveniently allowed the use of available equipment and in-line spring gauges for force

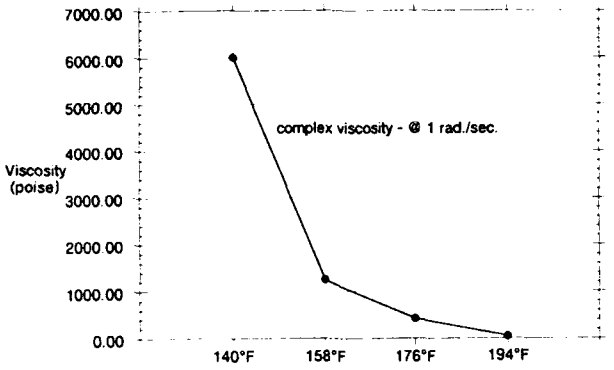


Figure 3. Viscosity as a Function of Temperature, ETPR Filling Compound

measurement. The geometry also simulates the procedure of digging a small pit at the pulling end, and using equipment that can be lowered into the pit in order to provide a straight horizontal pull. A "core-connection" was formed at the pulling end of the cable to facilitate the removal of the copper pairs from the sheath, and a line was attached to the trailing end of the copper pairs, to be pulled into the cavity as the core is removed. For each sample, several tests were performed to determine the peak force required to cause the copper pairs to begin to pull out of the sheath.

Air-Core Cable

The air-core design contained a single (aluminum) shield and (outer) polyethylene jacket. The corresponding outer diameter is 0.86 inches. Two lengths of nominally 100 ft. each, and one length of 300 ft., were buried. Figure 4 illustrates the results of a number of tests performed on the three buried cable samples. The "reference" case refers to a 100 ft. length of non-lubricated cable. The corresponding peak tensile force required to cause slippage of the core was initially as high as 2000 lbs. due to the damaged sheath condition at the far end of the cable. Once the local damaged section was removed, the required peak forces dropped to only 1000 lbs. The breaking strength of the 100 copper pairs is calculated to be 2200 lbs.

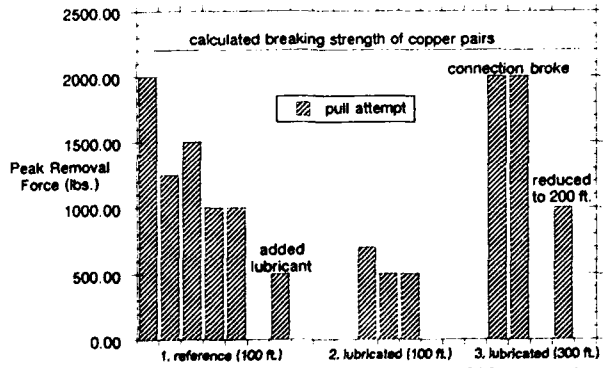


Figure 4. Outdoor Buried Tests, 100 ft. - 300 ft. Lengths (100-pair, 24-gauge Air-core Cable)

The second 100 ft. sample was filled with a liquid lubricant (i.e., a silicone emulsion), using the technique illustrated in Figure 5. A pump injected the lubricant at approximately 40 psi pressure, enabling the liquid to reach the opposite end within 10 minutes. The pump was then disconnected, and a line attached to the trailing end of the copper pairs to be pulled into the sheath. Subsequent repetitive attempts to cause the core to slip in the sheath, when pulled at the core connection, indicated peak removal forces of 500 - 700 lbs. -- or approximately half of the force required in the non-lubricated reference sample. To further verify the benefit of the lubricant, a test was performed on the original reference sample following the addition of the lubricant, resulting in a 500 lb. removal force.

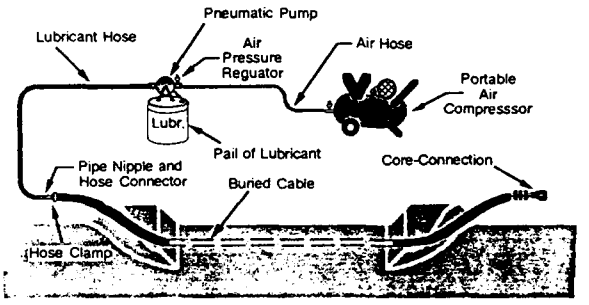


Figure 5. Technique Used for Inserting Lubricant into Air-Core Cable

The third cable sample, 300 ft. long, was filled with the same lubricant as the previous (second) 100 ft. sample. In this case, however, it was apparent that there was a break somewhere along the length of the sheath since the lubricant did not exit from the opposite end during the pumping operation, in spite of the large volume of lubricant introduced into the cable core. The first two attempts to create movement of the core failed as the core connection broke at approximately 2000 lbs. Since it was recognized that the cable was likely damaged and crushed at the break in the sheath, inhibiting the core removal, the cable was cut at the 100 ft. point, and the test repeated on the remaining 200 ft. length. As a result, the core was removed with a tensile load of approximately 1000 lbs. This is twice the load required for the lubricated 100 ft. samples.

A 1/2-in. diameter fiber-optic cable, which could contain on the order of 100 fibers, was subsequently inserted into the 100 ft. cavity of the second sample, illustrating a possible implementation for a FITL upgrade process.

Waterproof Cable

The sheaths of the waterproof cables tested contained a double shield -- aluminum (inner) and steel (outer) -- with a polyethylene jacket. Two types of filling compound were represented, depending upon the cable vintage. The earlier version, 0.96-in. diameter, contains

a petrolatum -- or petroleum jelly (PJ) -- filling compound, with an asphalt flooding material between the outer jacket and the shields. The more recent version, 0.98-in. diameter, contains the ETPR filling compound, with a polybutene flooding material. Samples nominally 75 ft. and 150 ft. in length were tested, some following a heating operation via the use of a portable gasoline-powered DC electric welder (Figure 6). The welder was used to provide 200 amps along the metallic shields of the buried cables. A heavy (4/0) stranded copper conductor served as a return lead to the welder.

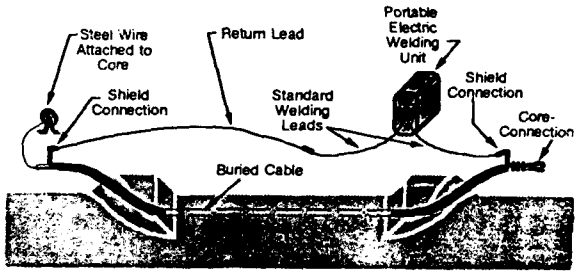


Figure 6. Technique for Heating Cable Using Electric Welder

Figure 7 illustrates the test results. For the reference (non-heated) 75 ft. PJ-filled cable, two attempts were made to pull the twisted pairs out of the cable. Although the first attempt failed, with the connection breaking at 2000 lbs. peak force, the second succeeded, at approximately the same force level. A subsequent test on a duplicate length sample, following heating to approximately 180°F, allowed the removal of the entire core *plus the metallic shields* at a level of approximately 600 lbs. force -- or less than one-third of that at the ambient conditions. The slippage along the shield-jacket interface was facilitated by the melting of the asphalt flooding compound. Subsequent tests, however, on a longer length (150 ft.) of heated PJ-filled cable were unsuccessful. The first 2 attempts failed at relatively low force levels as the high current introduced into the shield caused sparking at one of the shield connections to the welding leads. This is believed to have been caused by an improper electrical connection to the shields, causing arcing, weakening the copper pairs locally, and resulting in the core connections breaking at 1200 and 1500 lbs., successively. This test was therefore repeated, during which new core connections were made and the welder connected to both shields simultaneously in order to prevent this problem. Although the arcing did not occur, the attempts to remove the core were unsuccessful; the connections broke at approximately 2000 lbs.

For the ETPR-filled cable, the test on the (non-heated) 150 ft. reference sample failed to remove the core. However, following heating of the same sample with the welder for approximately 1 hour, the entire core was successfully pulled out at 1500 lbs. This test was successfully repeated on 2 other 150 ft. samples, following heating for more than 1.5 hours to a temperature of approximately 185°F. The results indicate peak force levels of the same magnitude.

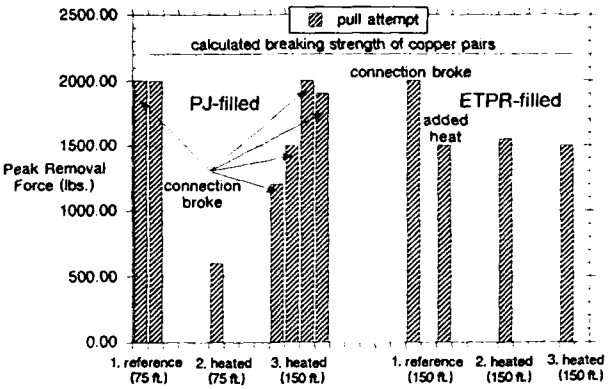


Figure 7. Outdoor Buried Tests, 75 ft. - 150 ft. Lengths (100-pair, 24-gauge Filled Cable)

Due to the excessive temperatures achieved at the exposed ends of the cables, fusing of the conductor insulation tends to occur in these areas, resulting in locally rigid segments when the cable cools. This suggests that if the core is not successfully removed the first time the cable is heated, subsequent attempts may be affected. This effect may account for the lack of success in removing the 150 ft. core of the PJ-filled cable.

A 150 ft. continuous length of 1/2-in. diameter fiber-optic cable was subsequently inserted into the 2 adjacent (end-to-end) 75 ft. long cavities of the PJ-filled samples.

Early Field Experience

In order to verify the feasibility of the general strategy in a realistic environment, an attempt was made to remove the copper pairs of a non-working 300 ft. length of 200-pair, 24-gauge cable buried approximately 20 years ago by a local regional Bell operating company (RBOC). Specifically, since this was an air-core design cable, the technique of pumping lubricant into the core in order to facilitate the core removal process was determined to be applicable. Although the 300 ft. cable represents a greater length than that removed for the buried tests on the 100-pair cables, the higher strength of the 200-pair cable would normally tend to allow success at greater lengths.

Applying the same procedures for inserting lubricant into the core as described previously, the 300 ft. cavity was successfully filled, without incident, with 4 gallons of a silicone emulsion following 45 minutes of pumping at a pressure of 40-50 psi.

A core-connection was then formed at the same end of the cable, allowing the copper pairs to be pulled by a winch system mounted on an RBOC truck. (Since a

local pit was not dug, the pulling angle was not optimized.) In this case, several attempts at applying loads of up to 4000 lbs. failed to cause the core to slip in the sheath, resulting in broken connections at the pulling end.

An inspection of the cable indicated a spiral-wound corrugated core wrap, which was unlike the samples tested during the laboratory experiments and outdoor tests. This particular RBOC cable was manufactured by a different vendor than that of the cable samples previously investigated in detail, for which the plastic core wrap between the copper pairs and the sheath had a smooth surface and a longitudinal slit along the cable length. A subsequent laboratory experiment performed on a short sample of the RBOC cable, after filling the interior with lubricant, resulted in a required removal force several times greater than that of unlubricated lengths of the previously tested air-core cables. The greater force is apparently due to a tendency for the spiral-wound corrugated wrap to effectively grab the core, preventing core slippage within the wrap, coupled with the corrugations being imbedded in the inner polyethylene jacket of the particular cable design used in this installation.

This experience illustrates that the specific details of the cable design are an important factor in determining the feasibility of the techniques investigated. Fortunately, the most common cables to be encountered in actual practice correspond to those with the less problematic construction, representing the (historically) most prolific vendor for the RBOCs.

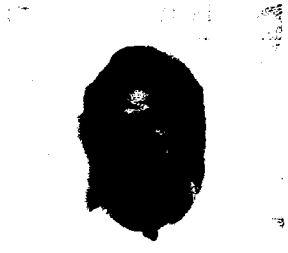
Summary

As a first step in determining the feasibility of using existing buried cables to facilitate a FITL upgrade, laboratory experiments and outdoor tests have been performed aimed at removing the copper conductors, or "cores", from typical telephone distribution cables. The ability to remove the cores of such cables between existing curbside pedestals would allow the possible use of the resultant pathway to place fiber-optic media. The successful removal of the core of a copper cable depends upon the condition of the sheath, as well as the details of the cable construction (as originally specified by the particular cable manufacturer).

Outdoor tests were performed on various lengths of buried 100-pair air-core and filled cables. Waterproof cables filled with petroleum jelly (PJ) as well as extended thermoplastic rubber (ETPR) filling compound were tested. The use of a silicone emulsion as an internal lubricant in an air-core cable reduced the peak required pulling forces to half that required for a non-lubricated sample, allowing the successful removal of copper cores of up to 200 ft., with indications of greater possible lengths. Similarly, heating waterproof cables, allowing the filling and/or flooding compounds to soften or melt, reduced the required core removal force for a PJ-filled cable to less than one-third that of an unheated sample, and repeatedly allowed removal of 150 ft. core lengths of ETPR-filled cable which was otherwise not possible. The heating operation was accomplished by applying an electric welder to the shield of the cable. Fiber cables of 1/2-in. diameter were inserted into several of the cavities created. In general, the results clearly indicate that the successful removal of the copper core is dependent upon the sheath being undamaged.

At the request of a regional Bell operating company, an early field test was carried out at on a non-working 300 ft. length of buried 200-pair air-core cable. Although the general procedure for adding lubricant to the cable core was demonstrated to be practical, the core removal was not successful -- primarily due to the specific construction of the particular cable involved. This illustrates that the cable design details are a major factor in determining the feasibility of the present approach. Fortunately, the most common cables to be encountered in actual practice in the Bell operating companies correspond to those with less problematic construction.

Future efforts will investigate methods for re-use of the created cavities, including expansion and/or "cleaning" of the cavity -- especially for filled cables in which the re-solidified residue may inhibit the later insertion of a fiber cable. In order to be adapted into a viable system to be utilized by the RBOCs, it will also be necessary to develop or define methods for maintaining customer service while performing this operation on "working" cables (assuming there are no previously abandoned, non-working cables along the route), and to determine appropriate equipment and procedures for practical application in the field.



Paul R. Briggs, Jr.
Bellcore
445 South Street
Morristown, NJ 07962

Paul R. Briggs, Jr. has a degree in Mechanical Engineering from Delaware Valley Institute. Paul is a Member of the Technical Staff of the Fiber Distribution & Reliability Research group at Bellcore. From 1967 to 1983, he worked on outside plant apparatus and central office equipment design and installation methods for Bell Laboratories. In 1984, Paul transferred to Bellcore's Applied Research Area to investigate fiber-optic apparatus and installation methods for Fiber-in-the-Loop.



Lawrence M. Slavin
Bellcore
445 South Street
Morristown, NJ 07962

Lawrence M. Slavin received the BSME degree from The Cooper Union for the Advancement of Science and Art in 1961, and the MSME and Ph.D. in Mechanical Engineering degrees from New York University in 1963 and 1969, respectively. From 1961 through 1989 Larry was engaged in a wide variety of projects, including software development, analytical mechanics studies, and design and development of outside plant and loop electronics systems. He joined Bellcore in 1989 as a member of the Fiber Distribution & Reliability Research group, responsible for investigating methods for installing fiber media in existing areas to facilitate Fiber-in-the-Loop upgrades.



John P. Varachi, Jr.
Bellcore
445 South Street
Morristown, NJ 07962

John Varachi is Director of Fiber Distribution and Reliability Research, at Bellcore. He is responsible for research in the areas of optical fiber and fiber-optic component reliability and new low-cost installation methods for fiber-in-the-loop deployment. He is an active participant in industry standards related to fiber-optic component reliability at the national and international level within TIA and IEC. Previously, John was a Member of Technical Staff in the Loop Transmission Division at Bell Laboratories where he was involved in systems engineering and physical design. John received Bachelor of Science and Master of Science degrees in Mechanical Engineering from Fairleigh Dickinson University and The Polytechnic Institute of New York and is a registered Professional Engineer in the State of New Jersey.

A HIGH PRODUCTIVITY, LOW SMOKE, ZERO HALOGEN COMPOUND FOR SHEATHING POWER AND TELECOMMUNICATION CABLES

Dr Jack Taylor, Mr Joe Preston, Mr Dudley Sawyer & Miss Lai Ping Cheng

Lindsay & Williams Limited, Columbine Street,
Manchester, M11 2LH England

SUMMARY

The development of a new zero halogen, low smoke, fire retardant cable jacketing compound is described. This new material displays good mechanical and thermomechanical properties. As a low smoke, zero halogen material, the generation of acidic fumes and smoke is minimal. The material is also judged to produce very little toxic emission when burned. The compound has been shown to pass a standard vertical tray fire test for a typical power cable design.

One of the main advantages offered by this new material over earlier products is that its melt viscosity is significantly lower. This leads to a lower power requirement for the extruder and hence a lower melt temperature at higher screw speeds. This in turn leads to significantly higher output on any given screw design and hence lower production costs.

INTRODUCTION

It is now almost 10 years since the first zero halogen low smoke fire retardant compounds were reported at the International Wire & Cable Symposium[1]. Since that time there have been a number of major disasters around the world[2,3,4] which have highlighted and emphasised the need for materials with improved performance in a fire.

The beneficial fire properties offered by zero halogen low smoke fire retardant cables are widely accepted around the world. Cables for installation in areas where smoke and acidic or toxic fumes present particular problems. There are, many national specifications covering the performance of zero halogen low smoke fire retardant cables[5-10] along with many military[11-14], utility[15], telecom[16-17] and mass transit[18] authority specifications (the references provided are not designed to provide a comprehensive list but serve to indicate the diversity of cable types and applications utilising zero halogen, low smoke, fire retardant materials).

The first generation of these improved materials[1] possessed excellent fire and smoke properties, but were mechanically weak and were slow to process when compared to the PVC compounds which they were replacing. The second generation materials i.e. compound S300 were first reported at the IWCS[19] five years ago, and offered products whose mechanical and electrical properties were similar to those of PVC jacketing compounds. Since that time, cable manufacturers have been pressing for compounds with similar mechanical and electrical properties, but with significantly faster processing speeds. This paper describes the development and properties of a new sheathing material designated S500, which possesses good mechanicals and can be processsed at speeds similar to those of PVC compounds.

MECHANICAL PROPERTIES

There are several European specifications[5-10] covering the performance of zero halogen low smoke fire retardant cable jacketing materials. Figure 1 shows some of the properties of compound S300 compared to those of the new compound S500. Both compounds S300 and S500 meet the requirements of many of the above specifications. As can be seen, compound S500 has approximately 50% higher tear strength than the standard S300, whilst possessing a significantly lower SG and melt viscosity.

THERMOMECHANICAL PROPERTIES

Low Temperature Performance

Figure 2 shows the elongation at break of standard dumbells at various temperatures. These results would indicate that compound S500 should be satisfactory at temperatures down to -40°C. This is a significant improvement over the performance of the standard S300.

High Temperature Performance

The results of hot pressure[20] and hot deformation tests[20] are presented in Figure 3.

	S300	S500
UNAGED		
TENSILE STRENGTH	15 MPa(2175psi)	12.6MPa(1820psi)
ELONGATION	150%	212 %
AFTER 7 DAYS AT 80 °C (176 °F)		
TENSILE STRENGTH	16MPa(2320psi)	13.1MPa(1900psi)
RETENSION OF TENSILE	107%	104 %
ELONGATION	145%	180 %
RETENSION OF ELONGN	98%	85 %
LOSS OF MASS	0.004mg/cm2	0.005mg/cm2
AFTER 7 DAYS AT 100 °C (212 °F)		
TENSILE STRENGTH	19MPa(2755psi)	14.3MPa(2075psi)
RETENSION OF TENSILE	127%	112 %
ELONGATION	112%	174 %
RETENSION OF ELONGN	75%	82 %
LOSS OF MASS	0.04%	0.04mg/cm2
AFTER 10 DAYS AT 100 °C (212 °F)		
TENSILE STRENGTH	17.2MPa(2495psi)	14.6MPa(2115psi)
RETENSION OF TENSILE	85%	116 %
ELONGATION	134%	170 %
RETENSION OF ELONGN	89%	80 %
LOSS OF MASS	0.07mg/cm2	0.08mg/cm2
AFTER 7 DAYS AT 121 °C (250 °F)		
TENSILE STRENGTH	17.6MPa(2552psi)	15.0MPa(2180psi)
RETENSION OF TENSILE	117%	119 %
ELONGATION	114%	144 %
RETENSION OF ELONGN	76%	68 %
LOSS OF MASS	0.17mg/cm2	0.15mg/cm2
SPECTIFIC GRAVITY	1.57	1.46
HARDNESS(SHORE A)	96	95
TEAR	4 N/mm	6.5N/mm
MOONEY VISCOSITY (ML1+4,140°C)	50	37

FIGURE 1
MECHANICAL PROPERTIES AND AGEING

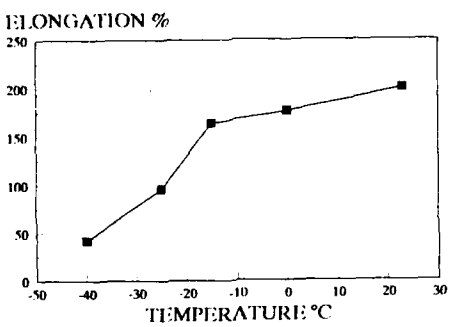


FIGURE 2
S500 - COLD ELONGATION

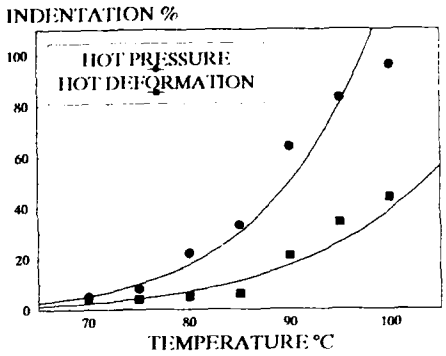


FIGURE 3
S500 - HOT PRESSURE AND HOT DEFORMATION

	S500	PVC
BS 6425:PART1:1990	ZERO	20.5%
VDE 0472:PART 813		
pH	6.3	2.4
CONDUCTIVITY	13 μS/cm	4500 μS/cm
MIL C 24643	0.01 %	20.0%

FIGURE 4
S500 -ACID GAS EVOLUTION

	CONCENTRATION PPM	INDICES
CO2	2,500.00	0.38
CO	10.00	0.14
HCHO	0.00	0.00
HF	0.00	0.00
HCl	0.00	0.00
HBr	0.00	0.00
HCN	0.00	0.00
NOx	3.00	0.55
CH2CHCN	0.25	0.03
NH3	0.00	0.00
H2S	0.00	0.00
SO2	0.00	0.00
COCl2	0.00	0.00
C6H5OH	0.00	0.00
TOXICITY INDEX		1.10

FIGURE 7
S500 -TOXICITY INDEX

In both cases, the S500 compound gave slightly higher penetration and deformation values than the standard S300 but despite this the values obtained for the hot pressure test at 22% penetration are still significantly below the usual specification requirement of 50% maximum penetration and therefore must be regarded as perfectly acceptable.

ACID GAS EVOLUTION

There are a number of test methods available to measure the acidity of the fumes evolved from burning cable materials. Generally zero halogen low smoke fire retardant materials perform well in these tests and compound S500 is no exception. Figure 4 shows the results obtained using several recognised test procedures, along with data from a typical PVC compound for comparison. As can be seen, compound S500 generates no chloride ion and only minor amounts of acidic species whereas the combustion of the PVC compound results in the formation of solutions which are quite acidic.

SMOKE GENERATION

Small Scale Material Tests

The NBS Smoke Chamber is the basis for the ASTM E662 : 1983 test method. The results presented in Figure 5 show the performance of compound S500 compared to that of a typical PVC compound. In this case the PVC compound generates smoke at a very much faster rate than compound S500. The PVC compound also generates a much greater quantity of smoke leading to a far greater degree of obscuration than that of the S500 compound.

Smoke Test on Cable

A low voltage power cable[5] was tested in the 3 metre cube smoke chamber as described by the appropriate specification[5]. The results presented in Figure 6 show a broadly similar picture to the small scale material test in that the compound S500 generated only very low levels of smoke, and at a very much lower rate of smoke generation than the PVC compound.

TOXICITY

Compound S500 has been tested to the UK Navy NES713[21] and the results presented in Figure 7. The UK Navy requires a maximum value of Toxicity Index of 5[11] whilst that of S500 was only 1.1. The results also serve to highlight the zero halogen nature of the material.

FIRE PROPERTIES

The results of small scale material tests are presented in Figure 8, and clearly demonstrate the fire retardant nature of S500. Low voltage power cables[5] jacketed with compound S500 have been subjected to a vertical tray burn test[22].

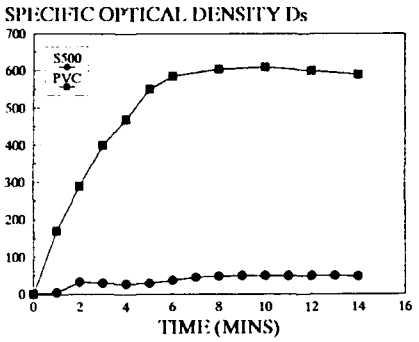


FIGURE 5
ASTM E662 SMOKE GENERATION

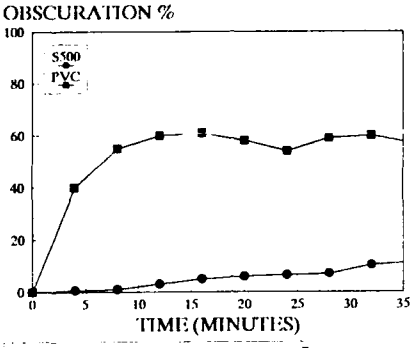


FIGURE 6
3 METRE CUBE SMOKE TEST

	S500 RESULT
OXYGEN INDEX	35
FLAMMABILITY TEMP	255°C

FIGURE 8
S500 - SMALL SCALE FIRE TESTS

In this test, any non-metallic portions of the cable are regarded as potential fuel. The 3m high cable ladder was loaded with sufficient cables in a defined manner, such that the volume of non-metallic materials was 1.5 litres per vertical metre of ladder. A 70, 000 Btu flame was applied for the specified 20 minute period after which time the char damaged to the cable jacket was limited to less than 1.5 metres from the flame. This falls well within the allowable parameters of the test method.

PROCESSING

Screw Design

The cable industry utilises several different types of materials; the processing of which has been optimised over several decades. It was of interest therefore to examine the extrusion characteristics of S500 on a number of different screw designs. For this work[23], a 48mm 24 L/D extruder was used, which could be fitted with screws which normally are used for (a) flexible PVC, (b) rigid PVC and (c) zero halogen, low smoke, fire retardant compounds[24]. In this series of experiments, the characteristics of the standard low smoke zero halogen compound S300 were compared to those of the new S500 compound, and the results are presented in Figures 9 - 14.

Figures 9 - 11 show that on each screw design compound S500 requires significantly less screw torque than S300. This is due to the reduced melt viscosity of compound S500. Figures 12 and 13 show the screw torque of each compound on the different screw designs. Here it is clear that the screw designed for low smoke zero halogen fire retardant compounds requires lower torque than each of the other screw designs for a given compound.

Figure 14 shows the volumetric outputs obtained from each screw design on both compounds.

It is reasonable to consider the extruder to be a volumetric pump and so it is not surprising to find similar volume outputs for each material on a given screw design. Again the screw specially designed for low smoke compounds gave the highest output. Indeed, for this latter screw rotating at 25 rpm (i.e. 15 litres/hour) the flexible PVC screw wuld need to achieve 40 rpm whilst the rigid PVC screw would need to be in excess of 50 rpm.

PRODUCTIVITY IMPROVEMENTS

In a further series of experiments[25,26] on somewhat larger extruders, similar results have been obtained. For these experiments, screws whose designs have been optimised for low smoke zero halogen fire retardant compounds were

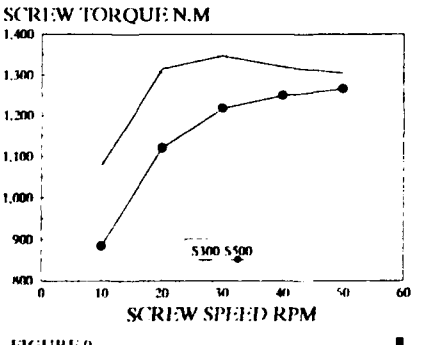


FIGURE 9
EXTRUSION TRIAL 48MM, 24L/D EXTRUDER
FLEXIBLE PVC SCREW

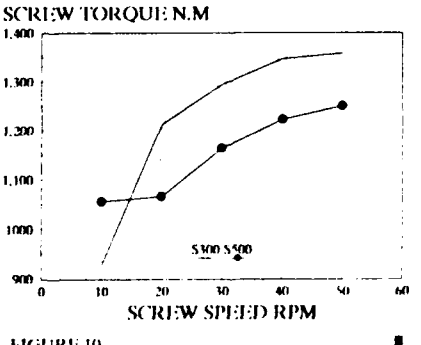


FIGURE 10
EXTRUSION TRIAL 48MM, 24L/D EXTRUDER
RIGID PVC SCREW

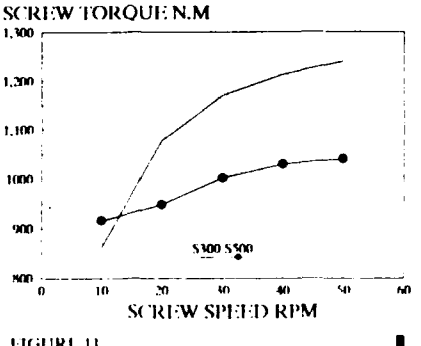


FIGURE 11
EXTRUSION TRIAL 48MM, 24L/D EXTRUDER
MEGOLON SCREW

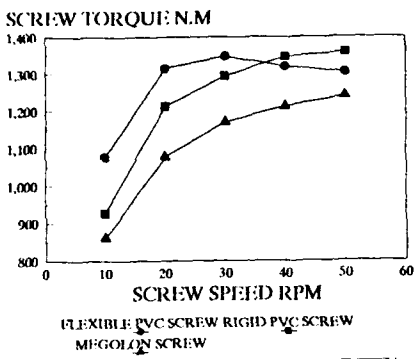


FIGURE 12
EXTRUSION TRIALS 48MM 24L/D EXTRUDER
COMPOUND S300

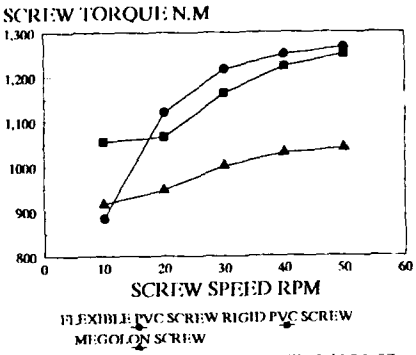


FIGURE 13
EXTRUSION TRIALS 48MM 24L/D EXTRUDER
COMPOUND S500

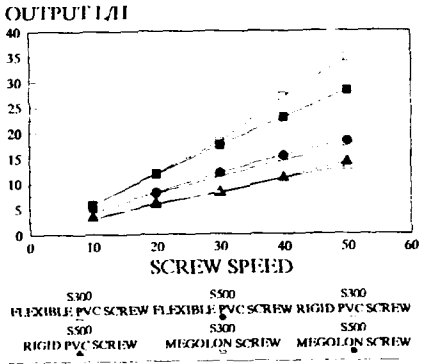


FIGURE 14
EXTRUSION TRIALS 48MM 24L/D EXTRUDER
VOLUMETRIC OUTPUT

employed[24,26].

Figures 15 and 16 again demonstrate that on a given screw design, the S500 compound requires less torque than the S300 compound. This reduced power demand results in slower rise in melt temperature as the screw is accelerated.

If the speed of extrusion is limited by the maximum melt temperature of approx 175°C, then the screw speed at which this temperature is reached is significantly higher for S500 than for S300. This is clearly demonstrated by Figures 17 and 18.

This increase in screw speed provides a very significant increase in output.

By examining the data presented in Figures 17 - 19 it is possible to estimate the improvements in productivity afforded by compound S500. These are summarised in Figure 20, and demonstrate that compound S500 can provide up to almost 50% increase in productivity over S300. Whilst the results from the 150mm extruder are not quite as good as from the 120mm; nevertheless the manufacturer of the extrusion equipment feels that further significant output improvements can be gained by utilising a more appropriate crosshead and/or a slightly different screw design[27].

EFFECT OF EXTRUSION STYLES ON SHRINKAGE

S500 is a polyolefinic material and can therefore be oriented by increasing the drawdown ratio during extrusion. Figures 21 and 22 demonstrate clearly that increased drawdown can lead to increased shrinkage. It should be emphasised that these results have been obtained on dumbell samples rather than measuring sheath retraction. The authors feel that dumbell shrinkage is a more sensitive measure. The results in Figures 21 and 22 clearly show that even after 7 days at 100°C, the shrinkage is acceptable providing the drawdown ratio is kept low. For most purposes a drawdown ratio of 1.5: gives adequate performance.

CONCLUSIONS

1. The properties of a new thermoplastic low smoke zero halogen compound S500, have been described, and can satisfy a number of existing specifications.

2. S500 can provide improvements in productivity of almost 50% over the standard zero halogen compounds.

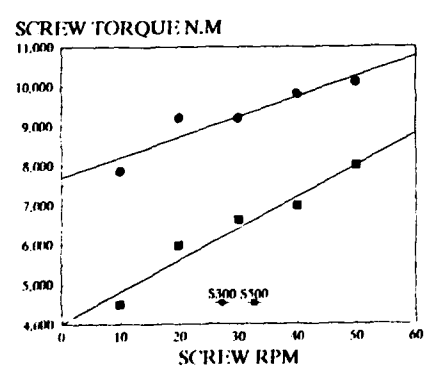


FIGURE 15
EXTRUSION TRIALS 120MM 18L/D EXTRUDER
SCREW TORQUE

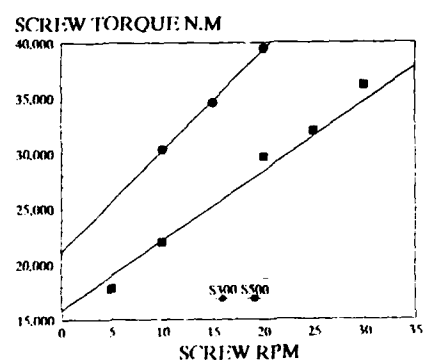


FIGURE 16
EXTRUSION TRIALS 150MM 24L/D EXTRUDER
SCREW TORQUE

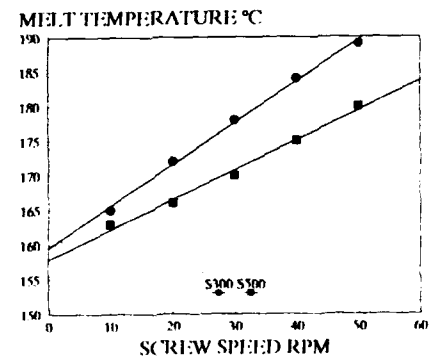


FIGURE 17
EXTRUSION TRIALS 120MM 18L/D EXTRUDER
MELT TEMPERATURE

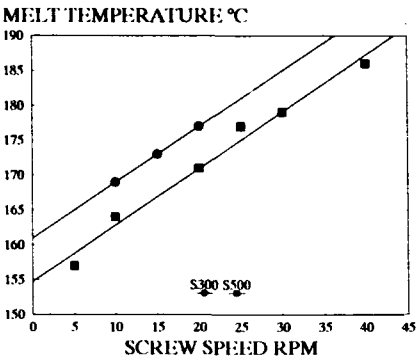


FIGURE 18
EXTRUSION TRIALS 150MM 24L/D EXTRUDER
MELT TEMPERATURE

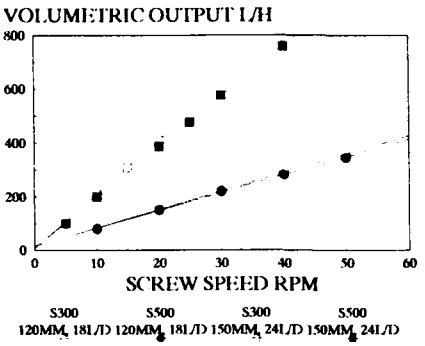


FIGURE 19
EXTRUSION TRIALS
VOLUMETRIC OUTPUTS

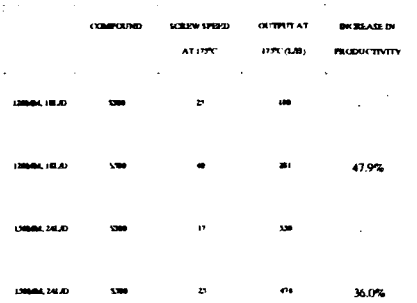


FIGURE 20
S500 - PRODUCTIVITY GAINS

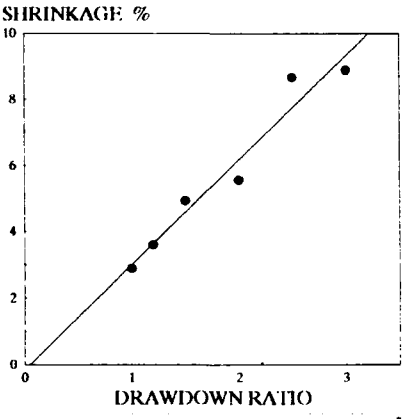


FIGURE 21
S500 - DUMBELL SHRINKAGE AFTER 2 HOURS AT 100°C

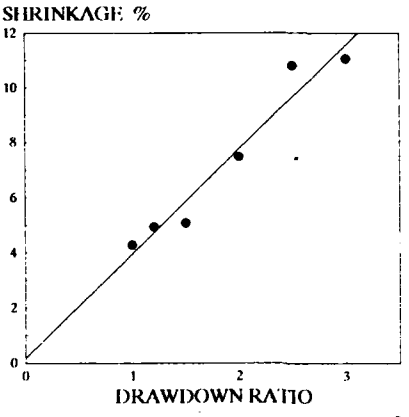


FIGURE 22
S500 - DUMBELL SHRINKAGE AFTER 168 HRS AT 100°C

3. S500 can be processed on screws designed to process PVC compounds although speeds may be limited.

REFERENCES

1. H A Mayer et al : "A New Generation of Non-Halogenated, Flame Retardant Compounds & Cables", IWCS, November 1980
2. Falklands Conflict 1982
3. Kings Cross Fire 1987
4. Hinsdale Telephone Exchange Fire
5. BS6724 : "Armoured Cables for Electricity Supply having Thermosetting Insulation with Low Emission of Smoke and Corrosive Gases when Affected by Fire", 1990
6. NFC 32323 : "Cables Rigides 0.6/1KV Sans Halogenes a compartement au feu ameliare, de Categorie C1, a isolation symthetique reticulee avec gaine de Protection Synthentique Extrudee", 1988
7. VDE 0207 : Part 23 : Isolier - und Mantel Mischungen fur Kabel und Isolierte Leitungen - Halogen Freie Isolier Mischungen", 1989
8. VDE 0207 : Part 24 : "Isolier-und Mantel Mischungen fur Kabel und Isolierte Leitungen - Halogen Freie Manten Mischungen", 1989
9. CEI 20-11 : "Prove Sui Materiali Elastici e Termoplastici dei Cavi per Energia", 1987
10. NEMKO 184.1 : "Halogen Free Cables with Voltage Rating 0.6/1.0KV", 1987
11. Def Standard 61-12 Part 31, "Sheaths - Limited Fire Hazard", 1990
12. MIL-C-24643 : Cable, Electric, General Purpose, Lightweight, for Shipboard Use, General Specification for"
13. Royal Australian Navy : Technical Report 2/88, "Requirements for Low Fire Hazard Electric Cables", 1988
14. VG 95219 : Parts 50-63 : "Kabel, Halogen Frei", 1987
15. CEGB E/TSS/EX5/5061; "Power Station Cabling; 6/11KV, Extruded Solid Insulation Cables (excluding PVC materials)
16. CW1600; British Telecom
17. CNET CM26
18. London Underground Ltd; SE569
19. J A Taylor et al : "Recent Advances in Low Smoke Zero Halogen Fire Retardant Compounds", IWCS, November 1987
20. BS6469 : 1984; "Insulation and Sheaths of Electric Cables"
21. NES 713
22. BS4066 : Part 3, 1986, "Tests on Electric Cables under Fire Conditions"

23. The authors would like to express their thanks to Dr Daljit Parmar, Kromberg & Schubert GmbH
24. MEGOLON Screw : Design Copywright Lindsay & Williams Ltd
25. The authors would like to express their thanks to Mr David Dickson & Mr Sigurd Soedring of Irish Cable & Wire
26. The authors would like to express their thanks to Mr Ulrich Hochstrasse, and Marc Pahud of Nokia Maillefer SA, Ecublens Switzerland

27. Screw Q15 : Proprietary Design - Nokia Maillefer SA
28. Personal Communication : H Jaun, Nokia Maillefer SA
29. Screw Design Aline : Proprietary Design - Nokia Maillefer SA



Jack Taylor began his working life as a Laboratory Technician examining fibre-reinforced polymers. He gained his BSc (Hons) and PhD degrees in chemistry at the University of Salford, subsequently joining Akzo Chemie UK where he worked on the synthesis of novel halogenated flame-retardants and evaluation of PVC stabiliser systems. Dr Taylor was Product Manager for the Megolon range of halogen-free, fire-retardant cable compounds until 1988 when he was appointed Sales Manager for all of Lindsay & Williams cable products, which in addition to the Megolon range include semi-conductive cable tapes, insulating cable tapes and an extensive range of self-amalgamating tapes and putty's.



Lai Ping Cheng studied 'A' levels in both Mathematics and Chemistry at Central Manchester Colleges prior to joining Lindsay & Williams Ltd in 1990 as a Quality Control Inspector for the Megolon range of compounds. In 1991 she transferred to the development section where she has been instrumental in the development of the latest Megolon range of low-smoke, halogen-free, fire-retardant compounds. She is currently studying Polymer Science & Technology at Manchester Polytechnic with a view to attaining BSc (Hons).



Joe Preston joined Lindsay & Williams Ltd in 1970 as a Laboratory Assistant following 2½ years experience in the Plastics Industry. He studied chemistry at the North Trafford College of Technology. In 1977 he became responsible for the Quality Control function at Lindsay & Williams. He transferred his efforts in 1982 to Development, working on specialised cable tapes, and in more recent years, the Megolon range of low-smoke, halogen-free, fire-retardant compounds. In 1991 he was appointed Technical Manager of Lindsay & Williams, responsible for all development and quality control functions.



Dudley Sawyer joined Lindsay & Williams Ltd in January 1991 to work on the development of new zero-halogen, flame-retardant extrusion compounds for the electrical cable industry. He gained BSc (Hons) in Chemistry at the University of Manchester and he has extensive experience of the cable industry having previously spent 21 years with BICC Cables from 1969 - 1990, progressing from Assistant Chemist in the Wire and General Cables Division to Senior Materials Technologist.

TECHNIQUES TO CHARACTERIZE THE CORROSIVITY OF CABLE FIRE-PRODUCTS

Fun L. Chu

Factory Mutual Research Corporation 1151 Boston-Providence Turnpike, Norwood, MA 02062

Abstract

Two standardized techniques have been developed to characterize the corrosivity of cable fire-products. Technique I assesses the immediate corrosion due to condensing fire-products on a surface, and Technique II assesses the long term post-fire corrosion due to contaminated aqueous solution in contact with a surface.

Using these techniques, the nonthermal hazard and a consistent corrosivity order has been found for the fire products of five cables. The extent of nonthermal hazard is consistent with the chemistry of the cable insulation materials. A correlation between corrosion rate (Å/min) and contaminant surface density (μg/sq. cm.) is also obtained by the combined application of Technique II and the ion-selective electrode analytical technique. The critical chloride level is found to be 3.2 $\mu g/cm^2$, below which nonthermal hazard (corrosion damage) by chloride is not expected.

Introduction

When cables are exposed to heat in a fire, products are generated which can cause damage due to 1) smoke deposition, and 2) corrosion of mechanical, electrical or electronic parts and chemical attack on the building itself. Damage due to smoke and corrosive products on surfaces away from the fire origin is defined as nonthermal damage. The characterization of smoke and corrosivity of fire-products is thus needed for the prediction of the extent and nature of property damage.

Presently, most existing cable standards classify cables on the basis of fire propagation and heat release rate. Cable fire products responsible for nonthermal damage (corrosion) are seldom considered. Thus little work for the characterization of cable fire-products corrosivity has been reported in this area. This presentation describes the techniques that are being developed at the Factory Mutual Research Corporation (FMRC).

Since cable fire-products contaminate surfaces in the form of hot flowing mixtures or in the form of condensate, the assessment of nonthermal damage is conducted through two approaches: 1) quantification of the corrosion rate of a probe due to the effect of hot flowing fire-products coming in contact with a metal surface, by Technique I, and 2) quantification of the corrosion rate of a probe exposed to aqueous solution (known volume) contaminated with fire-products by Technique II.

Experimental

1) Technique I. In this technique, materials are burnt in the FMRC Ignition, Pyrolysis-Combustion-Flame-Spread (IPCFS) Apparatus. Fire-products generated are channeled through a small Pyrex tube of 1.0 in (.025 m) I.D. and targeted towards a highly sensitive atmospheric corrosion probe (Figure 1a), placed 1 in. (.025 m) above the

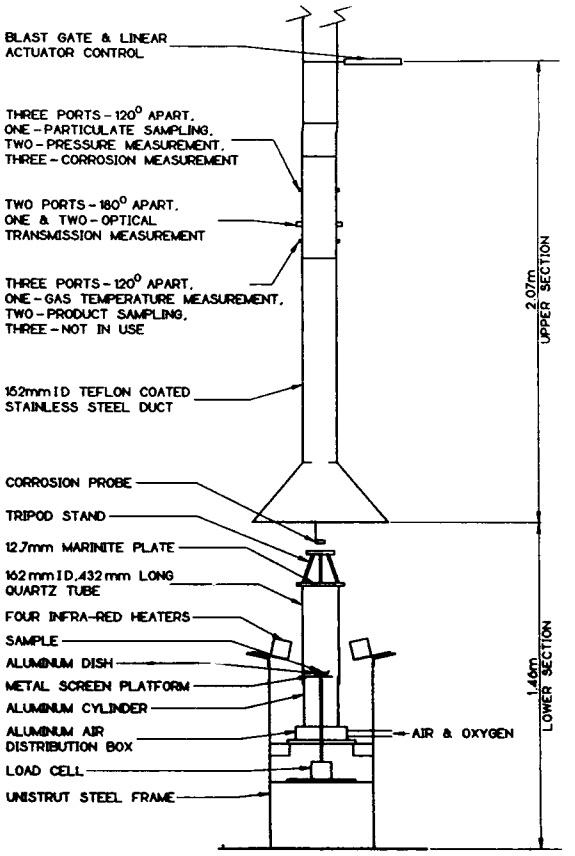


Figure 1a. IPCFS Apparatus Adopted with Corrosion Measurements.

Pyrex tube. This arrangement maximizes direct contact and hence the chemical interaction between the hot flowing fire-products and the metal probe. The probe consists of a reference side and a measuring side, both made up of the same element. The reference side is protected from corrosion attack by a "hemifil" coating. The surface temperature of the probe is kept below 60° C by circulating cold water. Corrosion on the probe is monitored by a Rohrback Casasco Corrosometer. A microcomputer system connected to the corrosometer measures corrosion by the change in electrical resistance of the probe. When corrosive fire-products (anions) react with the probe surface, chemical compounds are formed between the metal and anions in the presence of moisture via electrolytic processes. This results in reduced conductivity and increased electrical resistance of the probe. The corrosometer circuit converts this change directly to a linear readout in units of Å. The extent of corrosion damage resulting from the hot flowing fire-products is quantified in terms of corrosion rate, R, such that

$$R = D/t \qquad (1)$$

where R = corrosion rate; units mil/hr or Å/hr,
D = metal thinning; corrosometer readout, units mil or Å; and
t = time of exposure to corrosive environment, unit min, hr etc.

2) Technique II. Here, fire-products generated are first sampled onto an adsorptive medium. The adsorptive medium used is a Whatman circular filter paper (5.5 cm I.D.). The filter paper is mounted on a tripod stand placed over the Pyrex tube (Figure 1b). Approximately 30 sec. after the start of the pyrolysis, the collection of fire-products on filter paper begins. The first filter paper is exposed to flowing fire-products for 1 min, after which it is replaced by a second, and this procedure is repeated. In the experiments, the filter papers are prewetted to enhance the adsorption capacity for hydrophilic compounds such as hydrochloric acid (HCℓ). Usually 6-8 samples of contaminated filter paper are collected for each test. Water-soluble fire-products adsorbed on the filter papers are desorbed by extraction in 50 ml (c.c.) of distilled water. The nonthermal hazard of this solution is gauged by the corrosion rate of a mild

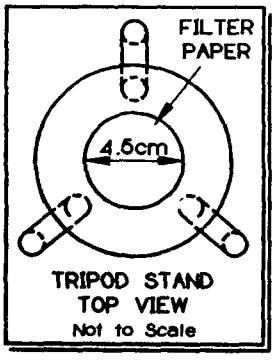


Figure 1b. Tripod Stand.

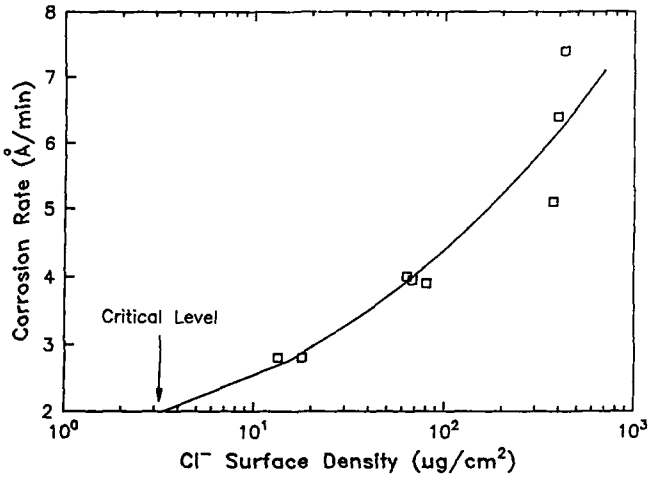


Figure 2. Correlation Between Chloride Level and Corrosion Rate.

steel probe exposed to the solution, whose rate is determined by the corrosometer described above. The corrosivity of each sample is computed according to Equation 1.

Concentrations of ions of interest present in the extracted samples are determined by the ion-selective electrode (ISE) technique (1). The activity (concentration) of a specific ion, e.g., Cℓ, is measured in terms of its potential by a voltmeter; and the potentials of known chloride standard solutions are obtained similarly. A calibration graph of potential (mv) vs. concentration (µg/ml) is prepared. From this plot, the quantity of chloride ions (µg) present is estimated, which with the effective area for ion adsorption, yields the ionic surface density (µg/cm^2). By correlating the ionic surface density with the corresponding corrosion damage for some pure PVC polymer samples, the critical chloride level for nonthermal damage can be determined (Figure 2).

Results and Discussion

Fire-products from five cables designated as C1-C5 have been examined. Among them C1 and C2 are chlorinated cables, C3 is fluorinated and C4 and C5 are non-chlorinated cables. Corrosion hazards of fire-products follow the order C5 < C4 < C2 < C1 < C3 (Table I). This order is con-

Table I

Indication of Cable Fire-Products Corrosivity

Cable Sample	Possible Corrosive Chemicals Involved	MOD (m^2/g)	Corrosion Rate (mil/hr per g of mass loss)	
			Technique I	Technique II
C1	HCℓ	0.32	1.0×10^{-4}	6.5×10^{-3}
C2	HCℓ	1.10	3.4×10^{-4}	1.9×10^{-3}
C3	HF	0.76	6.0×10^{-4}	3.2×10^{-3}
C4	--	0.42	0.4×10^{-4}	1.2×10^{-3}
C5	--	0.87	0.2×10^{-4}	1.0×10^{-3}

Note: MOD Mass Optical Density

sistent with the chemistry of the cable insulation materials. Repeatability and consistency of the data suggest the possibility of adapting the corrosivity tests to current and future cable standards.

A correlation between ionic surface density ($\mu g/cm^2$) and corrosion rate (mil/hr) established for various chlorinated fire-products (Figure 2) indicates the critical chloride surface density 3.2 $\mu g/cm^2$; this value agrees with findings by Reagor (2) and Rislund (3). At or below this level, Chloride is reported to present no corrosion hazard. Chloride contamination levels of various fire-products are indicated in Table II. The data obtained are consistent with previous findings such that chloride levels of 40 $\mu g/cm^2$ and above correspond to surfaces heavily contaminated from PVC fires.[2,3]

Table II

Correlation Between Chloride Level and Corrosion Rate

Sample	Chloride Level ($\mu g/cm^2$)	Corrosion Rate (A/min)
* PE(25%Cl), 1st collection	63.25	4.0
* PE(25%Cl), last collection	17.75	2.8
* PVC, 1st collection	80.55	3.9
* PVC, last collection	13.26	2.8
-- PVC, 1st collection	392.93	6.4
-- PVC, 2nd collection	429.78	7.4
-- PVC, 3rd collection	372.10	5.1
-- PVC, last collection	67.73	4.0

Note:
* denotes Chloride ions extracted from dry surface
-- denotes Chloride ions extracted from prewetted surface
All samples are collected from fire products of pure polymer powders

Conclusion

With the development of standardized corrosivity techniques for fire-products, the assessment of corrosion hazards of various materials is made possible in tests at laboratory as well as at full-scale. Samples tested have included fire-products from cables, cables with coatings, and from chlorinated pure polymers as well as decomposed Halon products.

References

1. Skoong, D.A. & West, D.M. "Principles of Instrumental Analysis", 2nd Edition, Chapter 18, Saunders College, Philadelphia, PA.

2. Reagor, B.T., "Smoke Corrosivity: Generation, Impart, Detection and Protection". Colloquium on Smoke Corrosivity, Nov. 7-8, 1991, Baltimore, MD.

3. Rislund, E., "Reduction of Corrosion Losses Due to PVC Fires", Materials Performance, p. 44, April, 1979.

The Author

Fun L. Chu received her Ph.D. in analytical chemistry at the University of Massachusetts in 1989. In the same year, she joined the Factory Mutual Research Corporation, Norwood, MA as a Senior Research Scientist. Her research work involves the design and development of analytical methods for the analysis of fire products; the quantification of corrosion damage due to fire products; and the application of these techniques to assess the impact of nonthermal damage on various properties.

QUANTITATIVE DETERMINATION OF A THIOESTER ANTIOXIDANT IN CABLE FILLING COMPOUNDS BASED ON FOURIER TRANSFORM-INFRARED SPECTROSCOPY AND CORRELATION TO OXIDATION INDUCTION TIME.

W. J. Thalman, A. Eckard, A. Debska

Witco Corporation, Sonneborn Division, 100 Bauer Drive, Oakland, N.J. 07436

ABSTRACT

An FTIR method has been developed to quantify the concentration of a Thioester Antioxidant in Extended Thermoplastic Rubber (ETPR) and Polyethylene Petroleum Jelly (PE/PJ) Cable Filling Compounds. The precision of the method has been established using statistical analysis.

To better understand the relationship between the antioxidant concentration of a Cable Filler and the oxidative stability of the material using Differential Scanning Calorimetry (DSC), an extensive study was undertaken to correlate measured concentrations of antioxidant to the Cable Filler's Oxidation Induction Time (OIT). The antioxidant concentration was found to be linearly proportional to OIT in the range of interest.

Although the OIT performance test is an indicator of the level of antioxidant in Cable Filling compounds, the FTIR method is an analytical tool that can determine precisely, directly and quickly the actual concentration of antioxidant in Cable Fillers. This method is also suitable for use in quality assurance programs.

INTRODUCTION

Historically, the Oxidation Induction Time has been used as a Quality Assurance indicator for Cable Filling Compounds. Alternate methodologies have been investigated in the past. These include complicated extraction processes as well as High Performance Liquid Chromatography (HPLC). The resulting methods could not readily quantify the antioxidant content in Cable Fillers. Additionally, the methods did not exhibit satisfactory repeatability or analysis time was prohibitively long to allow the method(s) to be used as a routine test. A quantitative FTIR method which readily monitors the concentration of antioxidant is proving to be a valuable tool for investigating Cable Filler performance.

PROCEDURE

FTIR Sample Preparation

A thin film KBr transmission cell equipped with Luer Loks® and a 0.5mm insert, a suitable syringe, and the Cable Filler sample, are preheated to 110°C. 10cc of the molten Cable Filler sample is injected through the cell. This both washes out the residue of the previous sample and introduces the new one. The sample and cell are left face up to equilibrate to room temperature and to prevent the Cable Filler from exiting the Luer Loks®, subsequently causing voids in the sample. Disassembling the transmission cell should be avoided, as this may change the path length and necessitate recalibration. After the sample in the cell has cooled and set, inspect the cell. If there are obvious voids, reheat the cell, and reintroduce the sample.

FTIR Settings

A Mattson Polaris single beam FTIR was used for this procedure. Typical data handling software for the integration and plotting was also used. The spectra was produced using 16 scans with a resolution of 4 and a signal to gain of 1.

OIT Sample Preparation

The Cable Filler sample is melted at a temperature of 110°C and thoroughly mixed. A portion of this molten mixture is poured on a room temperature surface in order to cast a film. After this layer solidifies an OIT sample is cut from the layer using a razor blade.

OIT Settings

A Perkin Elmer DSC7 instrument and a modified ASTM D 3895-80 procedure using 50 ml/min gas flows, were used for the OIT analysis. The OIT sample size is 4 ± 0.25 mg placed in a pre-oxidized open copper pan. (To pre-oxidize the copper pan, it is held in a bunsen burner 2-3 seconds until the pan glows. This procedure is repeated twice.) The isothermal temperature is 190°C, with a temperature rate from ambient to isothermal of 10°C/min. There is an equilibrium time of 2 minutes at the isothermal temperature after which the oxygen flow is started. The recorder used is a Perkin Elmer GP2, displaying heat flow vs. time

DISCUSSION AND RESULTS

FTIR Spectra of ETPR and PE/PJ Cable Fillers

Figure 1 is the FTIR absorbance spectrum of a sample of ETPR Cable Filler and Figure 2 is the FTIR absorbance spectrum of a sample of PE/PJ Cable Filler; both Cable Fillers contain thioester antioxidant (Thiodiethylene bis(3,5-di-tert-butyl-4-hydroxyhydrocinnamate)). At a 0.5mm film thickness, a portion of each spectrum is off scale, but the area of interest is in the proper range. The carbonyl peak is readily visible at 1744cm^{-1}. There are no interferences

from other components in either the ETPR or PE/PJ Cable Filler so the carbonyl peak can be used for quantification of the thioester antioxidant.

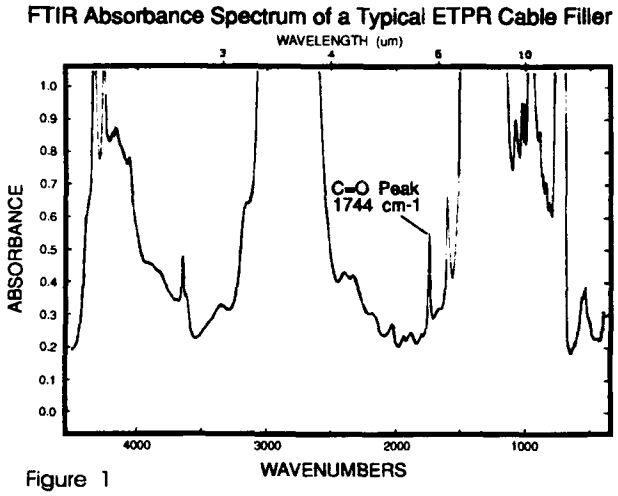


Figure 1

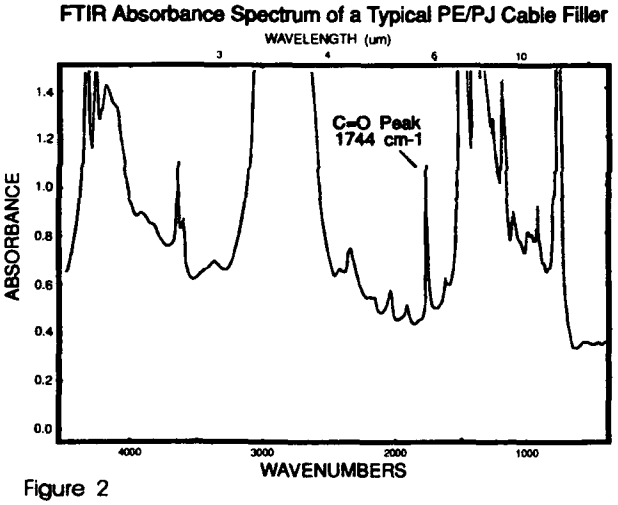


Figure 2

Calibration Standards

Cable Filler standards containing a known thioester antioxidant concentration were analyzed via the FTIR method. Figure 3 is an overlay of the carbonyl (C=O, 1744cm^{-1}) peaks associated with the various concentrations of standards. The peak area associated with the carbonyl (C=O) group in the thioester antioxidant was used to produce both linear and quadratic calibration curves.

The linear curve is accurate for the range of 0.2 to 1.6 wgt% thioester antioxidant and the quadratic curve is accurate to 2.5 wgt%. The quadratic calibration curve takes into account the nonlinear relationship between antioxidant concentration and the peak area when the carbonyl's FTIR absorbance became greater than 1.2.

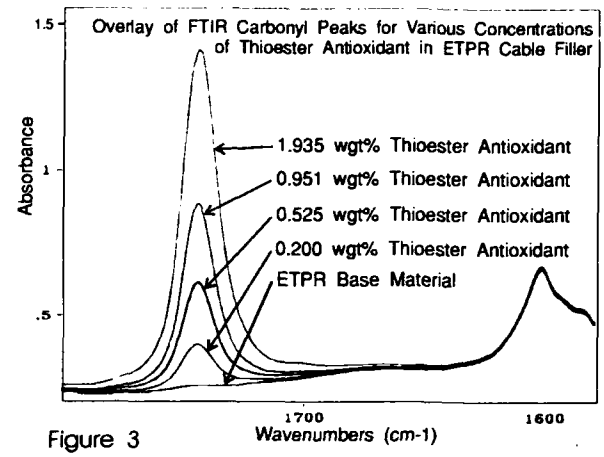


Figure 3

The Cable Filler base material was found to have a constant, residual absorbance in the part of the spectrum where the carbonyl peak appears. This residual carbonyl peak area was taken into account when calculating both calibration curves. The data in Figure 3 was used to produce a quadratic calibration curve having a correlation coefficient of 0.99967. This calibration curve is pictured in Figure 4.

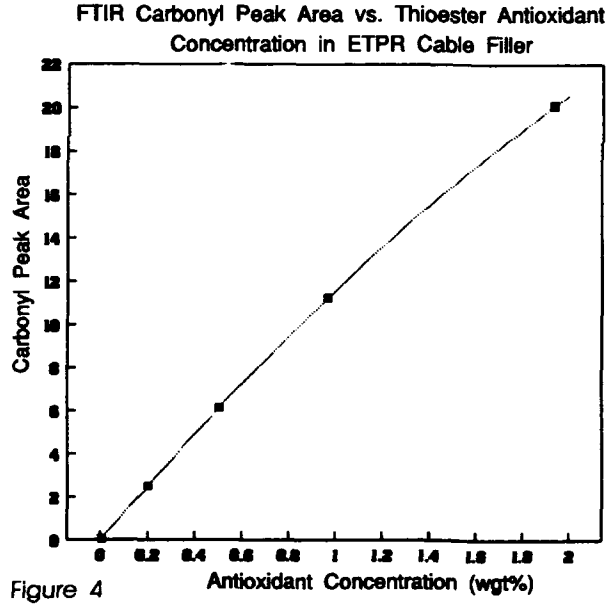


Figure 4

Repeatability of FTIR Method

A single sample of Cable Filler was analyzed several times over a 7 month period. For each analysis, the sample was injected into the 0.5mm path length FTIR sample cell. The FTIR method repeatedly verified this sample to contain thioester antioxidant in the range of 0.432 to 0.439 wgt% antioxidant when using the linear calibration curve based on the carbonyl peak area. Using this data a standard deviation of 0.0025 wgt% is calculated; the precision of the analysis on a single sample appears to be 0.005 at the 95% confidence limit.

This demonstrates both the consistency of the method, and that the sample preparation is adequate for obtaining repeatable results.

Accuracy of FTIR Method

Samples containing a known concentration in the range of 0.2 to 1.6 wgt% thioester antioxidant in Cable Filler base material were analyzed via the FTIR method using the linear calibration curve based on the carbonyl peak area. The average difference is less than 2% between the known antioxidant concentration, and the concentration predicted by the FTIR method.

Repeatability of OIT

In order to minimize local variations of antioxidant concentration, a Cable Filler sample preparation procedure was followed (see Procedure section). Using this procedure, a series of 10 measurements on a representative sample resulted in a standard deviation of 2.80 minutes.

In contrast to the specified procedure, when the same Cable Filler material was sampled without melting, only partially melting or melting but not mixing, the results of OIT testing had a much broader range. A series of 19 measurements resulted in a standard deviation of 21.2 minutes. The specified sample preparation significantly reduces the range of OIT values, as evidenced by the reduction in the standard deviation.

Antioxidant Concentration vs OIT

The OIT of a Cable Filling compound has long been used as a performance indicator of the material. OIT testing has demonstrated that increased levels of antioxidant have increased the performance of the Cable Filling compound. A correlation between antioxidant concentration and OIT performance is a significant step in the ability to improve Cable Filler materials.

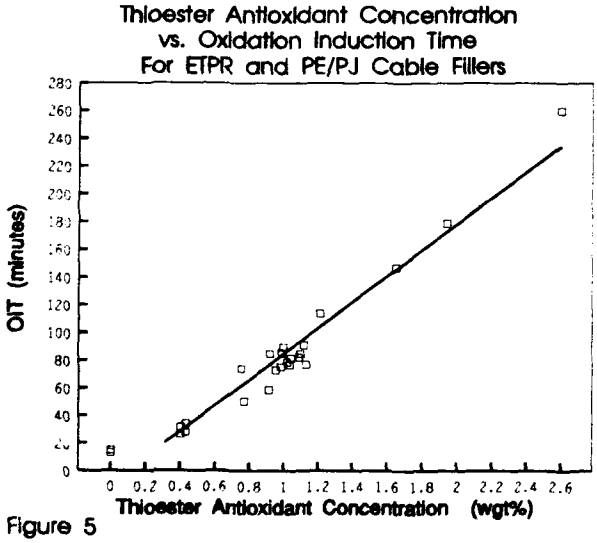


Figure 5

Samples of ETPR and PE/PJ Cable Fillers, containing thioester antioxidant, have been analyzed for their antioxidant concentration, via FTIR, and their Oxidation Induction Time. Figure 5 demonstrates the linear relationship between the antioxidant concentration and OIT within the range of practical interest.

The OIT data represented in Figure 5 was analyzed via the modified ASTM D 3895-80 procedure using 50 ml/min gas flows. Selected representative samples from this data were also analyzed via the modified ASTM procedure using 200 ml/min gas flows. No statistical difference in OIT measurements were found between these two sets of data.

CONCLUSIONS

An FTIR spectroscopic method has been developed that directly quantifies the antioxidant concentration in ETPR and PE/PJ Cable Filling Compounds, which is critical to the performance of the finished telecommunications cable.

The repeatability and accuracy of this method is satisfactory for the concentration of thioester antioxidant in the range of 0.2 to 1.6 wgt%.

The FTIR analysis method may also be viable for Quality Assurance in cable filler production.

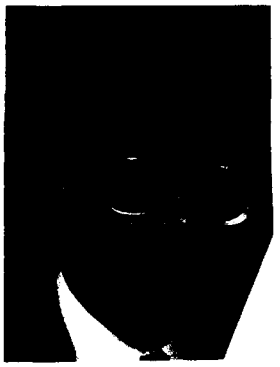
It has been verified that the antioxidant concentration linearly correlates to the Oxidation Induction Time (OIT) of Cable Fillers.

Future Work

Future work will focus on migration of antioxidants into and out of filling compounds and the effects of differing antioxidants and stabilizers on the thermal stability of the filler and insulation as reflected in OIT measurement.

Acknowledgements

We would like to thank J. Weaver and K. Blair for their assistance with the statistical analysis aspects of this paper, T. Roessing for providing Cable Filler materials, and also A. Stratton, R. Morawek, M. Papazoglou and B. Isbitsky for their suggestions with the manuscript.



Dr. Alan D. Eckard has received his B.S. degree from Rensselaer Polytechnic Institute and his Ph.D. in physical chemistry from the University of Liverpool, England. After research fellowships at Keele University (UK) and the University of Toronto, Dr. Eckard has been involved in development and application of industrial lubricants, coatings and surface treatment chemicals with several international manufacturers of these products for the past 19 years. He is currently Manager of Research for the Sonneborn Division of Witco Corporation at their research center in Oakland, NJ.



Dr. Anna Debska-Chwaja has received Masters degrees in Chemical Engineering and Petroleum Technology and a Ph.D. degree in Petroleum Engineering. She was trained and worked in Poland, Romania, Italy, and France. She is a member of ACS and STLE and is currently employed by the Sonneborn Division of Witco Corporation as a Research Scientist specializing in solid hydrocarbons, lubricants, cable fillers and tribology. Dr. Debska is the author of 30 publications and 5 patents.



Willian J. Thalman has received his Masters degree in Chemistry from Montclair State College and is nearing completion of his Ph.D. degree in Physical Chemistry at Rutgers University. Mr. Thalman has been involved in the pilot development of hydrogenation and sulfonation technologies and is currently investigating methods to improve cable filler performance. He is employed as a Chemist for the Sonneborn Division of Witco Corporation at their research center in Oakland, NJ.

ON-LINE TEMPERATURE MEASUREMENT OF OPTICAL FIBER AND TELEPHONE WIRE

Don Willett

Luxtron Corporation
Santa Clara, CA

Manufacturers of optical fiber and telephone wire are increasingly under pressure to improve quality, while at the same time increase production speed. A reliable and repeatable system for on-line, non-contact temperature measurement and control can help ameliorate this situation.

The quality of optical fiber is highly dependent upon the temperature of the fiber as it enters the inner-primary coating cup. Particularly as line speeds increase to 1500 meters per minute and higher, the demand for tighter specifications calls for measuring and controlling the fiber temperature prior to coating.

With telephone wire a similar situation exists. The temperature of the bare wire prior to extrusion coating strongly affects the final insulation quality. Measuring the wire temperature after the preheater and sending a control signal to the preheater temperature controller virtually assures consistent wire quality, even at speeds of 2500 meters per minute and higher.

The non-contact temperature measuring systems described in this paper determine the temperature of both optical fiber and wire by measuring heat flow between the sensing head and the moving filament. By using two sets of sensors operating at different known temperatures, the system is fully auto-calibrating*. In operation, once the user sets the "setpoint temperature" with easy front panel switches, there are no future adjustments or calibration required.

Measuring Optical Fiber Temperatures During High-Speed Drawing and Coating

During high-speed drawing and coating of optical fiber, it is important that the temperature of the fiber at the entry to the inner-primary coating cup be within a few degrees of the target temperature to assure producing high quality, constant thickness fiber. Excessively high fiber temperatures will cause deterioration of the coating polymer, while fiber temperatures below the acceptable range will result in adherence problems and variations in coating thickness. In modern high-speed draw towers, forced convective cooling is used to cool the fiber. Particularly with forced cooling, it is important that the fiber temperature be measured at the entry to the inner-primary coating cup to assure proper fiber temperature.

*U.S. and Foreign Patents Pending

A schematic of a simplified draw tower and coating system is shown in Figure 1. Note that additional temperature measurement points of interest are prior to the outer-primary coating cup and after ultra-violet curing of the coatings.

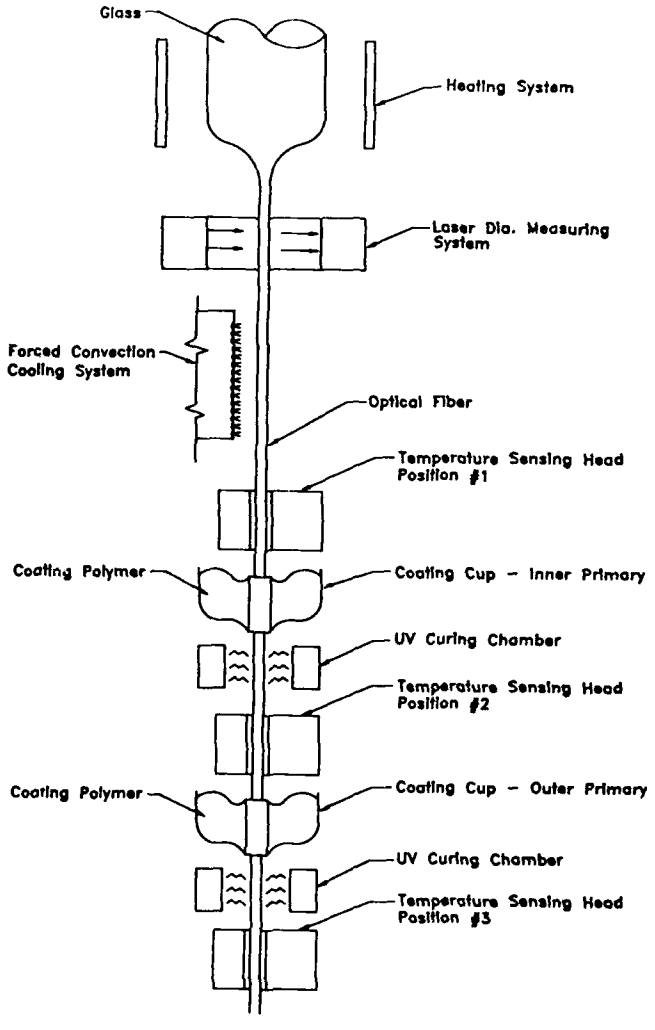


Figure 1 - Optical Fiber Draw Tower and Coating System

Optical fiber temperature measurement is difficult because (1) the diameter could be as small as 125 microns, (2) lateral movement could be as great as three diameters and (3) no contact is allowed because it would damage the optical characteristics of the fiber. Infrared temperature measurement devices are not usable because of the small target size and lateral movement of the fiber. Typical temperature of optical fibers prior to coating are in the range of 50-130°C depending on the point of measurement and the fiber making process being used.

Measuring Small-Gauge Telephone Wire Temperature Prior to Extrusion

The specifications for insulation characteristics of cellular and solid polyethylene and polypropylene insulated telecommunications wire are becoming increasingly tighter. Meeting these requirements in production requires reliable and consistent bonding of the plastic to the wire as well as proper foaming of the insulation. Particularly with today's higher line speeds, close preheat temperature control is an essential element in achieving these objectives.

Elevating the surface temperature of the metallic conductor above room temperature is critical to proper extrusion coating for both types of insulation. This becomes apparent when the product from automated extrusion lines is checked for uniformity of the principal parameters needed for paired telephone cable conductors.

Wire preheaters are used to heat the conductor to the desired temperature prior to extruding the coating. However, preheaters have no inherent mechanism for maintaining constant wire temperature. Basically, their function is to increase the wire temperature by a certain number of degrees as selected by an operator. So as the temperature of the wire entering the preheater changes, the temperature of the wire exiting the preheater changes by the same amount.

To control the actual wire temperature, it must be measured as it leaves the preheater and a feedback control signal sent to the preheater temperature controller. This not only assures constant wire temperature as other conditions change, it also makes frequent operator attention unnecessary.

Traditionally, the problem with wire temperature control has been that no easy-to-use, accurate and reliable method has been available to measure wire temperature, particularly small gauge wire running at high speed. Rotating contact thermocouples suffer from accuracy and reliability problems, while infrared devices have problems with small target size and variations in surface emissivity.

A Non-Contact, Auto-Calibrate Temperature Measurement System

The subject systems employ a convective heat flow sensing principle to determine the temperature of small, rapidly moving "products" (i.e., optical fiber or wire) without making contact. Earlier implementations of this technology suffered from the need for frequent and cumbersome on-line calibration. The current systems feature microprocessor-based electronics and sensing heads with two sections operating at different known temperatures to accomplish true auto-calibrate operation. See reference (1) for more details.

Figure 2 shows diagrammatically the relationship of the moving product to the two sections "A" and "B" of the sensing heads. The auto-calibrating system uses pairs of heat flow sensors that are matched to have the same sensitivity operating at two different measured temperatures. The "A" section of the head is heated under PID control to an operator determined "Setpoint Temperature" that is typically slightly higher than the product temperature. The "B" section is thermally coupled to the "A" section through a specially designed conductive path, causing it to come to equilibrium at a lower temperature than "A" and always tracking "A".

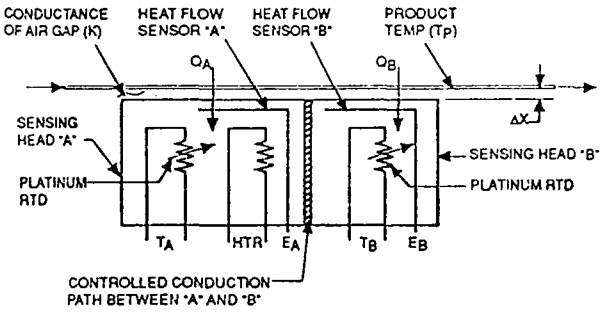


Figure 2 - The Auto-Calibrating Temperature Measurement Sensing Head

The signals from the heat flow sensors result from the conductive/convective heat flow rates between the sensors and the product. These signals are directly proportional to the difference in temperature between each sensor and the product. The heat transfer equations which govern the energy exchange and the resulting signals from the heat flow sensors in the two sections of the sensing head are:

$$(1)\ Q_A = C_A \cdot E_A = \left(\frac{K_A}{\Delta X_A} + h_A\right)(T_P - T_A)$$

RATE OF HEAT EXCHANGE BETWEEN PRODUCT AND SENSING HEAD "A"

$$(2)\ Q_B = C_B \cdot E_B = \left(\frac{K_B}{\Delta X_B} + h_B\right)(T_P - T_B)$$

RATE OF HEAT EXCHANGE BETWEEN PRODUCT AND SENSING HEAD "B"

Required Conditions:

T_A not equal to T_B.
ΔX (Thickness of air gap) the same for heat flow sensor "A" and "B".

K (thermal conductivity of air in gap) the same for heat flow sensor "A" and "B".
h (combined convection/radiation coefficient) the same for heat flow sensor "A" and "B".
Sensitivity of heat flow sensor "A" and "B" the same (i.e., $C_A = C_B$).

Subtracting (1) from (2):

$$C_A E_A - C_B E_B = \left(\frac{K_A}{\Delta X_A} + h_A\right)(T_P - T_A) - \left(\frac{K_B}{\Delta X_B} + h_B\right)(T_P - T_B)$$

Assumption: $T_A > T_B$

$C_A = C_B$; $K_A = K_B$; $\Delta X_A = \Delta X_B$; $h_A = h_B$

These assumptions are justified because T_A and T_B are relatively close in value by the design of the conducting path between A and B.

$$E_A - E_B = \frac{\left(\frac{K}{\Delta X} + h\right)}{C}(T_P - T_A - T_P + T_B) = \frac{\left(\frac{K}{\Delta X} + h\right)}{C}(T_B - T_A)$$

$$\frac{\left(\frac{K}{\Delta X} + h\right)}{C} = \left[\frac{E_A - E_B}{T_B - T_A}\right]$$

Substituting $\left[\frac{E_A - E_B}{T_B - T_A}\right]$ for $\frac{\left(\frac{K}{\Delta X} + h\right)}{C}$ in (1):

$$EA = \left[\frac{E_A - E_B}{T_B - T_A}\right](T_P - T_A)$$

Rearranging:

The following equation is solved by the microprocessor to continuously display product temperature (T_P)

$$(3)\ T_P = T_A + E_A \left[\frac{T_B - T_A}{E_A - E_B}\right]$$

Note that the terms for spacing (ΔX) and the conductance of the heat flow path ($K/\Delta X + h$), both drop out of the final equation because they are the same for both sensors.

The system design provides quick and easy start-up, as well as long-term trouble-free operation. All that is required to operate the system is to set the "setpoint temperature" using the front panel rocker switches; after that there are no adjustments or calibration required. The setpoint temperature need not be reset within a product temperature range of ±60°F (±33°C).

The system provides a choice of analog output signals for control applications: 4-20mA, 0-10V and ±5V. An RS-232C interface is provided for connection to dataloggers and control computers.

The Sensing Head for Optical Fiber

The salient requirements for a sensing head for measuring optical fiber temperature are:

- Fiber diameter range of 125 to 500 microns.
- Lateral fiber movement as high as ± three diameters.
- Measurement slot wide enough to prevent contact between the fiber and the sensing head.
- Measurement slot located and shaped so that fiber can be easily introduced.

Shown in Figure 3 is the design selected for optical fiber applications. It features dual-opposed heat flow sensors in both sections of the head. Using this approach allows a direct-access measurement slot for easy introduction of the fiber and slot width of 0.060" (1.5mm) to assure no contact with the fiber. The dual-opposed heat flow sensors are wired in series to produce a constant signal level even if the fiber is not perfectly centered in the slot. The direction of travel of the fiber through the sensing head is important because the entry section ("B") has been made longer than the exit section ("A"). This is done so the boundary layer of air is stripped off the fiber prior to the heat flow measurement.

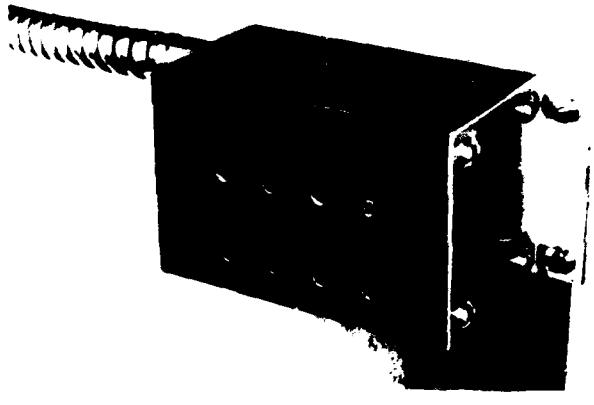


Figure 3 - Luxtron OPTICAL/FIBERTEMP Temperature Measuring System

The Sensing Head for Telephone Wire

Figure 4 shows the sensing head used for telephone wire applications. In this design there are four heat flow sensors surrounding the product in both sections of the sensing head. This is required because of the high speeds -- up to 8200 ft/min (2500 m/min) -- and wire diameters as small as 0.003" (0.075mm).

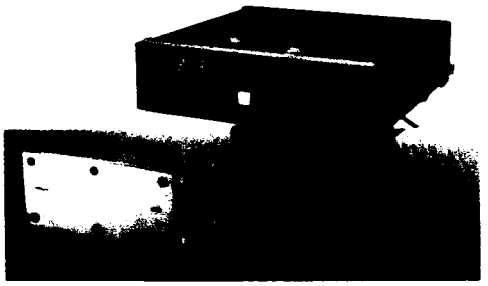


Figure 4 - Luxtron/WIRETEMP Temperature Measuring System

References

(1) Rall, D. L.; "Auto-Calibrating Non-Contact Temperature Sensing Based on a Convective Heat Flux Technique"; Proceedings of the Sensor Expo, September 11-13, 1990, Chicago, Page 301.

LONG TERM SERVICE EXPERIENCE OF XLPE AND EPR CABLES IN MV AND HV NETWORKS

F. Kraehenbuehl and J.J. Wavre

Câbles Cortaillod SA,
CH-2016 Cortaillod Switzerland

Abstract

Up to now, many comparative studies have been made between XLPE and EPR insulations, most often on short sample cables or on raw materials. This paper deals with the experience acquired these past 15 years with the two types of insulation.

The manufacturing experience on identical equipment shows that the characteristics of EPR cables are more sensitive prone to the components and production conditions than in the case of XLPE cables. This demonstrates the importance of quality control before and after manufacture, which contributes to excellent in-service results of XLPE and EPR cables.

Introduction

The swiss power grid is one of the most dense in the world, with approximately 45% of the MV lines running underground. The first cross-linked insulation cables were put on the market in the mid 1970's. The proportion of XLPE and EPR cables produced in Switzerland during the last ten years is shown in figure 1 below, in relation to the voltage level.

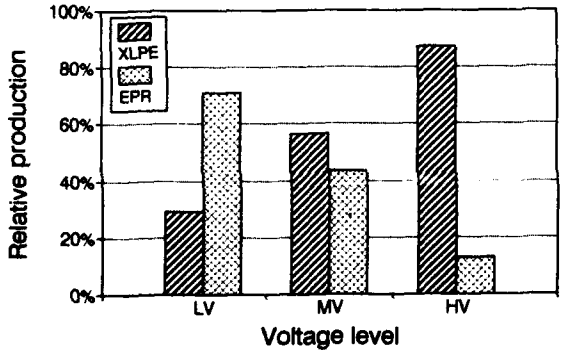


Figure 1: Relative quantities of cables produced from 1982 to 1991 as a function of the voltage and the type of insulation.

Manufacturing conditions

All the cables to which we refer have been produced on the same line which is a catenary continuous vulcanization line (dry-curing, length of the tube: 30m); the extrusion group is a "1+2" tandem system. The same conductor shield and easy strippable insulation shield were used, which means the same 240°C surface temperature in the curing tube was used. In order to be able to use the same tools (e.g. extruder, cross-head) for XLPE and EPR it was necessary to optimize the flow of materials, and to eliminate zones where scorching could occur. This meant that several precise in-factory developments had to be made. Obviously, for the two types of insulation, the screw and the extrusion conditions were different.

One of the most claimed advantages of EPR is the ease with which it is extruded and cross-linked, which allows production to be done at higher line speeds than for XLPE. Experience has shown that this is only partly true as summarized in table 1.

Table 1: Manufacturing conditions for different types of cables on the same catenary line.

Voltage	Insulation thickness [mm]	Relative line speeds	
		XLPE	EPR
10 kV	2.9	1	1.9
20 kV	5.0	1	1.6
60 kV	12.0	1	1.3
130 kV	17.0	1	1.0
150 kV	18.0	1	1.0

A comment should be made on this table: for insulation thicknesses of 12mm or greater, manufacturing speeds of XLPE and EPR cables become very similar due to other limiting parameters (screenpack).

Therefore the higher cost for raw materials in the case of EPR (140% higher for the same volume) cannot be compensated for by the higher manufacturing speeds. Even for 12 km of 20 kV cable with a 150mm2 conductor, the cost per meter, after the insulating operation, is still of approx. 20% higher despite different manufacturing speeds.

It is also important to know that the extrusion of EPR requires more sophisticated and precise equipment than that of XLPE, and it's abrasive nature (because of the presence of kaolin in the mixture) wears out the extrusion equipment in general and the screenpacks in particular.

Finally, from the point of view of extrusion characteristics, the quality of XLPE is more regular between suppliers than is that of EPR. In fact, the quality of EPR can vary greatly between different suppliers and even between different batches from the same supplier. It isn't a problem tied to the manufacturing procedure itself but rather to the quality of raw materials used in the compound.

Type and routine electrical tests

We have already mentioned the importance of electrical tests after production to guarantee the quality of the product. It is not surprising that in this case as well, to use different criteria and limit values for the two types of insulation. The routine electrical tests are summarized in tables 2 and 2a.

Table 2: Routine electrical tests for MV cables according to IEC standard 502 and internal requirements.

	IEC 502	Internal requirement
Dielectric losses		
XLPE EPR	$< 40.10^{-4}$ at U_o* $< 200.10^{-4}$ at U_o*	$< 10.10^{-4}$ at 2 U_o $< 50.10^{-4}$ at 2 U_o
Voltage test		
XLPE and EPR	2.5 U_o, 5 min	At least 4 U_o, 30 minutes
Partial discharges		
XLPE and EPR	1.5 U_o; PD < 20 pC	No PD increase between 0 and 4 U_o (max. noise: 2 pC)

* According to IEC 502 type test, at room Temp.

Table 2a: Routine electrical tests for HV cables according to IEC standard 840 and internal requirements.

	IEC 840	Internal requirements
Dielectric losses		
XLPE EPR	$< 10.10^{-4}$ at 2 U_o* $< 50.10^{-4}$ at 2 U_o*	$< 10.10^{-4}$ at 2 U_o $< 30.10^{-4}$ at 2 U_o
Voltage test		
XLPE and EPR	2.5 U_o, 30'	45 kV: ≥15 kV/mm 30' 60 kV: ≥15 kV/mm 30' ≥110 kV: ≥20 kV/mm 30'
Partial discharges		
XLPE and EPR	1.5 U_o, PD < 10 pC	No PD increase between 0 and 1.75 U_o (max. noise: 2 pC)

* According to IEC 840 type test, at 90°C.

Tests as severe as the ones described here inevitably reduce potential problems in service. Nevertheless, the in-factory rejection rate is relatively high, as shown in figure 2.

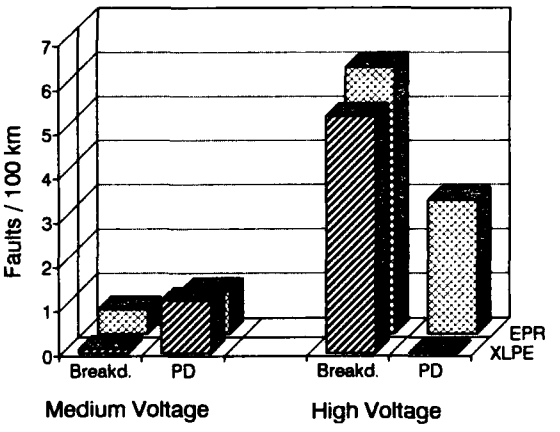


Figure 2: Comparison between in-factory refusal rates for XLPE and EPR.
PD = partial discharges
Breakd. = breakdowns.

The causes for refusal are, for MV cables, mostly mechanical in origin (rubbing, irregularities in the insulation shield, etc.) which push partial discharges above the specified limits. In the case of HV, breakdowns are due primarily to the presence of scorched particles in the insulation.

Accelerated aging

Accelerated aging tests are the most critical for the evaluation of a new product. In our case XLPE and EPR cables are submitted to the same testing conditions, which are for MV cables:

- a voltage of 3,5 Uo;
- water in the conductor and in the screen;
- conductor temperature cycles from 20°C to 90°C, 5hrs "on"/3hrs "off".

Measurements of breakdown strength at 50 Hz according to Weibull statistics are carried out at regular intervals (3000, 6000, and 12000 hours).

This aging procedure was applied to MV cables manufactured on the same line but at different production speeds. It has already been mentioned above that for cost reasons it is necessary to work at higher line speeds with EPR than with XLPE. Cables made with an EPR (that will be called EPR-1), identical in construction, were manufactured at two rates: the same speed as the XLPE and 1.4 times faster (this last value still is not the optimal production speed, see table 1).

All the cable samples produced at the higher speed broke down during aging within a very short 41 hour span, after only 54 days. However, none of the cable samples produced at the same speed as XLPE had defects after many thousands of hours of aging. The same test with a high voltage quality EPR (EPR-2) had no breakdowns during aging. It is equally important to mention that all the cables passed the routine electrical tests described in table 2 successfully.

From the aging tests we can gather the following conclusions (or confirmations):

1) the EPR-1 mixture is extremely homogenous, seeing the time span within which all the breakdowns occurred.
2) Unfortunately it is also extremely sensitive to processing conditions as other authors have already shown for this type of compound [1].
3) The EPR-2 material is remarkably less influenced by the processing conditions than EPR-1, which confirms the strong variation in quality for this type of insulation from one supplier to the next, already mentioned elsewhere [2].
4) It has often been assumed that for HV cables the main factor limiting the line speed was the extruder power, and for MV the speed of curing speed in the CV tube. The observations described here tend to show that it isn't an absolute rule.
5) To produce EPR cables in economically favourable conditions, the choice of the raw compound is essential. It is not possible, with EPR of any origin, to benefit from higher production speeds, relative to XLPE, without risks.

Recent developments

There are situations where EPR was claimed to have clear advantages over XLPE. This is the case, for example, concerning it's long-term behaviour contact with water (e.g. [3]). It is well known that EPR has less of a tendency to form water trees, and that those that do appear grow at a more moderate rate. However recent studies [4] show that though the length of water trees stabilizes rapidly in EPR, whereas it's electrical breakdown strength slowly deteriorates with time, but work remains to be done in this domain to better understand this phenomenon.

Whatever the results of this study, the introduction of TRXLPE about ten years ago noticeably improved XLPE's resistance to to water trees in particular, and to water and aging in general. Constant developments have made this product as reliable electrically as standard XLPE on new cables, while at the same time giving them a superior long-term behaviour. Figure 3 compares the conservation of electrical breakdown strength after ageing in MV cables produced with different materials.

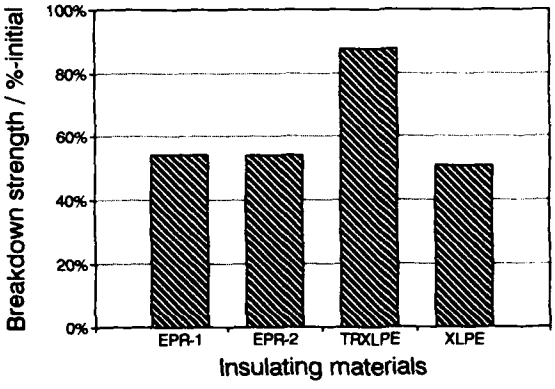


Figure 3: Comparison of the electrical breakdown strength of MV cables produced with different insulating materials, after 4000 hrs of accelerated ageing.
EPR-1 = EPR of MV quality
EPR-2 = EPR of HV quality
TRXLPE = tree retardant XLPE
XLPE = standard XLPE

The superior quality of TRXLPE is clear, as it has already been revealed in numerous publications (e.g. [5-8]).

Furthermore, it must be stated that the manufacturing conditions, the dimensions, and the design of cables insulated with TRXLPE are the same as that of standard XLPE, which facilitates the transition from one material to the other. Currently, its applications are limited to medium voltage, although there are a few quotations up to 110 kV (e.g. in Germany).

For high voltage cables the optimal production equipment (long die MDCV line, triple head extrusion), the cleanliness of the XLPE insulations, and the use of super-smooth semi-cons, are necessary for high quality and long lasting cables with a life span comparable to paper-oil insulated cables. On the other hand, as far as EPR is concerned, uncertainty linked to the quality of its numerous components remains, in spite of precautions taken by suppliers.

The grounds for choice

In view of what has been mentioned above, the reasons that go in favour of utilities using EPR cables can be different in nature.

- Historical reasons: a choice may have been made a few years ago and in order to conserve a certain homogeneity in the network, the customer continues to use the same materials.
- Excellent in-service results: the failure rate in cables insulated with EPR is very low, in comparison to the first thermoplastic HMWPE insulated cables, with a graphite insulation shield, which broke down excessively. The few faults, which did occur in Switzerland with EPR, were due to inadequate production processes of a cable manufacturer, as is the case in Germany with XLPE [9].
- Because of their better flexibility the installation of EPR cables is easier in sub-stations where little work space is available.

On the other hand, Bungay et McAllister [2] mention three main reasons for preferring XLPE to EPR:

- The quality of both the incoming compound and the finished cable.
- The fear of contaminating a dielectric: the fewer ingredients that have to be added to the polymer the better.
- The volume cost of XLPE is lower than that of EPR.

We wish to add, in the case of VHV cables, a fourth reason that goes in favour of XLPE: dielectric losses of EPR are too high for economical viability cables.

Note: For HV levels, the influence of water is less important because of a watertight metal protection applied on the cable.

Conclusion

The large number of additives in the composition of EPR improves its thermal and mechanical characteristics, and facilitates within certain limits its processing during extrusion.

The paper describes the direct correlation between the manufacturing equipment and line speed with short and long term cable performance. In order that EPR insulation has the right long-term resistance, production parameters must carefully be chosen with little consideration to cost or productivity. Moreover, it will be in direct competition in the near future with TRXLPE, especially in the MV field. But, because of its excellent flexibility, EPR will keep an edge in certain specific applications.

References

[1] C. Katz, M. Walker & J. Dyndul, "Comparative evaluation by laboratory aging of 15 and 35 kV extruded dielectric cables", IEEE Power Eng. Rev. 10, 69 (1990).

[2] E.W.G. Bungay & D. McAllister, "Electric Cables Handbook", BSP Professional Books, 2nd ed., Oxford, 1990.

[3] M. Cacciari et al., "Long-term experimental performance and life model fitting of XLPE and EPR insulated cables", *Proc. 1991 IEEE PES* Transmission & Distribution Conf., 135-42, Dallas, 1991.

[4] S.M. Rowland & S.V. Wolfe, "Comparison of the effect of watertree degradation on XLPE and EPR", 2nd Int. Conf. on Power Cables & Access. 10-180kV, 129-33, London, 1986.

[5] A.A. Farkas, "Investigation of water tree retardant XLPE-grades", 2nd Int. Conf. on Power Cables & Access. 10-180kV, 145-50, London, 1986.

[6] V.A.A. Banks, D.G. Roberts & A. Fitch, "Water tree retardant XLPE", 11th Int. Conf. on Electricity Distribution CIRED, Paper 3-12, Liège, 1991.

[7] L. Efraimsson & B. Rasmusson, "Modern XLPE-cable design with improved handling, installation and treeing properties", 11th Int. Conf. on Electricity Distribution CIRED, Paper 3-19, Liège, 1991.

[8] F. Krähenbühl & J.D. Umpleby, "Easy strippable tree retardant MV cable", ICC Meeting, Birmingham, England, 1992.

[9] H. Blechschmidt & L. Lithers, "Defects-developments on PE/XLPE insulated cables", Elektrizitätswirtschaft 88, 1831-45 (1989), in german.



Francis Kraehenbuehl was born on February 2, 1956. He received his B.Sc., and Ph.D. degrees in Chemical Engineering in 1980 and 1983 respectively. He was then Assistant Professor at the Physical Chemistry Dept., and joined Câbles Cortaillod in 1987, where he is head of Research and Development for Power Cables. Since 1988, he is the Swiss representative within CIGRE Study Committee 15 and is a Member of IEEE since 1992.

Mailing address :
Câbles Cortaillod SA
CH-2016 Cortaillod (Switzerland)



Jean-Jacques Wavre was born on December 5, 1939. He received his B.Sc. in Electrical Engineering in 1965 at the Swiss Federal Institute of Technology in Lausanne. In 1967, he became Research & Development engineer for the Ontario Hydro Research & Development Laboratory in Toronto, Canada. In 1971 he joined E. Haefely in Basel, and Câbles Cortaillod SA in 1981, where has been since 1986 head of the Power Cables department. He is the Swiss representative within CIGRE Study Committee 21 (High Voltage Cables) since 1986 and is a member of the board of the Swiss Electrotechnical Committee.

Mailing address :
Câbles Cortaillod SA
CH-2016 Cortaillod (Switzerland)

DEVELOPMENT OF A 220/230kV XLPE HIGH VOLTAGE CABLE AND ACCESSORIES

H. A. Mayer, E. Buczma, J. A. Adcock

Olex Cables a Division of Pacific Dunlop Ltd. Melbourne, Australia.

V. J. Boliver, M. Uzelac

G & W Electric Company
Blue Island, Illinois.

ABSTRACT

The development of a high voltage 127/220kV, 1200mm^2 copper Milliken conductor XLPE power cable and accessories is described. The cable and accessories were developed and manufactured for the State Electricity Commission of Victoria, Australia. The system comprising 27km of cable 39 joints and 6 terminations was installed over a complex 9km route on the outskirts of the Melbourne Central Business District.

To ensure the reliability of the system an optimum cable design has to be used which necessitates correct material selection. Also required are precise manufacturing techniques involving clean room conditions to prevent any contamination being introduced into the insulation materials. Together with the cable the system required compatible cable terminations and joints to be developed to ensure reliable performance. The type testing of cable and accessories to confirm the integrity of the system is outlined.

INTRODUCTION

Cross-linked polyethylene has been used as the insulation material for power cables for over 30 years. From initially being used in power cables in the low voltage range its use has now extended into high voltage power cables. This has occurred because of the material's excellent electrical and thermal properties, the ability for easy installation and ready monitoring of the cable's performance and also because of the overall favourable economics and performance of the installed systems.

In Australia the use of cross-linked polyethylene has developed initially from medium voltage cable up to 33kV[1] through to the high voltage cable range 66kV,110kV, 132kV, 150kV to 220kV which have all been manufactured in commercial quantities. These cables have all been installed into power grid systems with commercially available accessories. The integrity of these systems has been verified by extensive developmental testing, type testing to international standards and in service performance.

The need for a cable arose because of a rapid increase during the late 80's of high rise building developments in the Central Business District of Melbourne. Initially a new 220kV overhead power link was planned to supplement the reliability of Melbourne's power supply. However, because of public concern about its visual and environmental aspects the State Electricity Commission of Victoria chose to adopt an underground line.

The requirement for the cable manufacturer was for the complete project, including the manufacture, supply and installation of the cable system. The requirement for the manufacturer of the accessories was to provide suitable joints and terminations for the system.

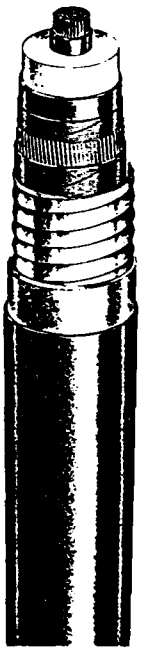


Figure 1. 220kV XLPE Cable

CABLE SPECIFICATION

At the time of preparation of the specification for the cable system no international standards were available for the voltage range required. The technical requirements for the cable were prepared by upgrading existing international high voltage cable specifications[2,3] to the required performance levels.

The insulated power cable specification[4] called for a conventional single core extruded polyethylene cross-linked solid dielectric type cable. The cable was to consist of a stranded copper conductor circular in cross-section, conductor semiconductive screen, XLPE insulation and insulation semiconductive screen all extruded and cross-linked, a screen consisting of screen wires and waterblocking tapes, means to prevent longitudinal water penetration, a welded or extruded metallic moisture impervious barrier or sheath and an extruded dual layer outer sheath of orange PVC and black HDPE.

The specification called for the conductor semiconductive screen, the insulation and the insulation semiconductive screen to be applied in the one manufacturing process using a single triple exrusion head and that the dielectric had to be dry cured.

Table 1. Requirements of the conductor screen

1. Conductor screen to consist of continuous layer of "Supersmooth" black thermosetting semiconductive material.
2. Material to be compatible with insulation and conductor.
3. Minimum thickness 0.8 mm.
4. Outer surface to be cylindrical and free from protrusions and irregularities, less than 125μm protrusion into the insulation.
5. Firmly bonded to insulation with no tendency to separate during installation or service.
6. Resistivity max. 1000 ohm-metre at max. operating temperature.

The conductor was also specified to be free from particles which could contaminate the semiconductive screens, causing high stress points at the surface of the semiconductive screen.

Some of the requirements of the specification for the conductor screen, insulation and insulation screen are set out in Tables 1, 2 and 3.

CABLE DESIGN

The 220kV XLPE cable is shown illustrated in Figure 1. Dimensions of the cable are shown in Table 4 with the performance criteria outlined in Table 5. The main features of the cable design are shown in Figure 2.

Table 2. Requirements of the insulation

1. Homogeneous extrusion of "Superclean" XLPE.
2. Insulation, conductor and insulation screens extruded using a single triple extrusion head.
3. Crosslinking by the dry cure process.
4. Design thickness of the insulation to be 27 mm.
5. The insulation of the cable and interfaces with semiconductive screens to have the following limits of voids and contaminants: voids : max. size 30 μm (1.2 mils) contaminants : black, metal, other foreign matter. max. size 100 μm (4 mils) amber : max. size 250 μm (10 mils)
6. Insulation material to be inspected for contaminants using a continuous sampling plan.

Table 3. Requirements of the insulation screen

1. Insulation screen to consist of extruded layer of black thermosetting semiconductive material applied directly over the insulation.
2. Inner surface to be smooth and free of protrusions and irregularities which extend more than 250 μm into the insulation.
3. Bonded to insulation with no tendency to separate during installation or service.
4. Resistivity max. 500 ohm-metre at maximum operating temperature.

The conductor is 1200mm^2 copper made up of four segments in a Milliken type configuration to reduce the skin effect. The segments are individually made up of stranded wires compacted together and taped to insulate the segments from each other. Design of the segments is such that no sharp corners or edges are produced and when laid up the segments form a tight close fitting construction. The segments are then taped together with semiconductive and metallic tapes to prevent any movement during subsequent processing.

The conductor screen, insulation and insulation screen are all applied in one manufacturing step in a triple head dry curing dry cooling continuous vulcanising plant. The semiconductive materials have to be of the "Supersmooth" category. The insulation has to be better than the typical "Superclean" classification in that no contaminants greater than 100μm are to be present in the insulation material. The three layers are applied simultaneously because this gives the best assurance that no contaminants will be introduced into any of the layers. This is also beneficial in maintaining a close size tolerance of all the individual layers and optimum concentricity of the cable.

The dry curing dry cooling concept eliminates any contact of the cable core

with water further improving XLPE cable characteristics and potential life of the cable.

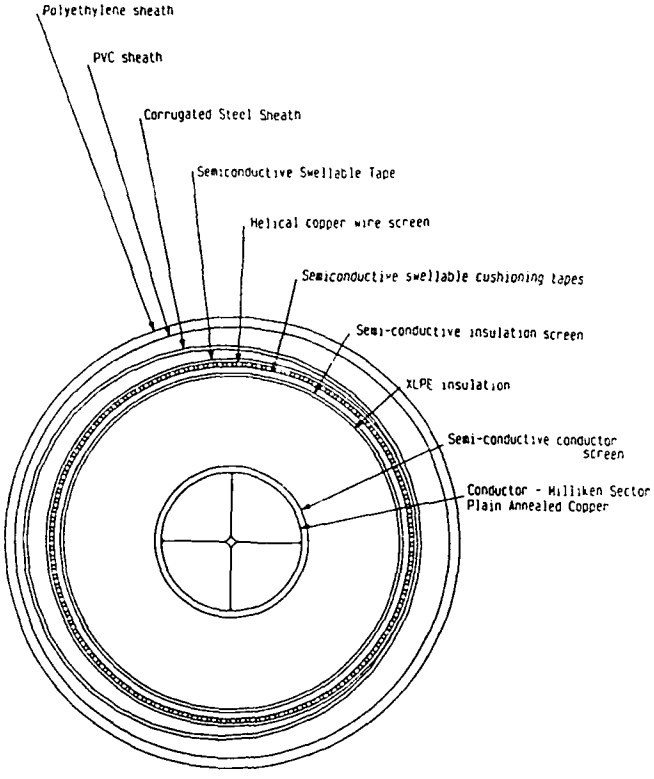


Figure 2. 220kV XLPE cable cross-section

As seen from Table 4, the thickness of the insulation used in the cable is 27mm. The general voltage levels on which stress calculations are based are the working voltage of $220/\sqrt{3}$ or 127kV line to ground and impulse levels of 1050kVp. The impulse level specified by the SECV was the maximum level given in standards for 220kV cable and switch yard accessories. With a conductor screen diameter of 46.5mm insulation diameter of 102.5mm and a minimum average thickness of 27.0mm stresses in the insulation are as follows:

at working voltage:
stress at conductor 6.9kV/mm
stress at insulation screen surface 3.1kV/mm
average stress 4.7kV/mm

at rated impulse level:
stress at conductor 57.1kVp/mm
Average stress 38.9kVp/mm

Over the cable core are applied cushioning tapes and water swellable semiconductive tapes beneath and over the screen wires. The cushioning tapes are used to cope with the expansion of the cable core under operating conditions.

The type testing of the cable involved cycling to a conductor temperature of 130 degrees C for part of the cycling regime. The cable as shown in Table 5 is required to cope with an emergency operating temperature of 105 degrees C. The applied tapes must be able to cope with these conductor temperatures and the expansion and contraction effects of the cable core induced by these elevated temperatures. No rupturing or tearing of the tapes should occur. The tapes should have adequate tensile and elongation properties at the cable service temperature to be encountered.

Table 4. Construction of the 220kV XLPE cable

Conductor		
cross-sectional area	mm^2	1200
material		copper
shape		4 sector Milliken
diameter	mm	42.1
Extruded conductor screen thickness	mm	2.0
Insulation thickness	mm	27
Extruded insulation screen thickness	mm	1.0
Stainless steel sheath thickness	mm	0.8
corrugation depth	mm	6
PVC sheath thickness	mm	2.5
HDPE sheath thickness		3.0
Outer diameter	mm	140
Weight	kg/m	28

The copper shielding wires are designed to carry the fault current with defined temperature limits and are applied with a lay which will not constrict the cable core on expansion during load cycling. This is in order to avoid embedding of the screen wires into the insulation screen and to maintain a smooth circular interface of the screen with the insulation.

The water swellable tapes prevent water travelling down the screen wires if accidental sheath damage occurs. The 220kV cable has a spirally corrugated stainless steel welded sheath. Stainless steel has a higher tensile strength compared with lead or aluminium resulting in a cable with an 0.8mm wall thickness of stainless steel having equivalent mechanical protection to an aluminium sheath of 3.4mm thickness. Stainless steel is also more corrosion resistant than the other alternative metal sheath materials.

A gap between the taped cable core and the welded corrugated metal sheath permits expansion and contraction during operating conditions. This prevents the corrugations causing excessive pressure onto the cable core when expansion of the core occurs at the normal conductor temperature and avoids any deformation of the insulation.

Table 5. Electrical and mechanical cable specifications

Max. d.c. resistance of conductor, 20 °C	ohm/km	0.0150
Max. a.c. resistance of conductor, 90 °C	ohm/km	0.0200
Max. capacitance per phase, 20 °C	μF/km	0.177
Max. dielectric stress at conductor screen	kV/mm	6.9
Nom. current carrying cross-sectional area copper wire/stainless steel	mm^2	173.5/323.5
Min. bending radius during installation	mm	2800
for cable setting	mm	2100
Max. pulling tension	kN	48
Max. side wall pressure	kN/m	22
Max. charging current, nom. voltage, 50 Hz /phase	A/km	7.06
Conductor continuous op. temp.	°C	90
emergency op. temp.	°C	105
short circuit temp.	°C	250
Max. permissible operating voltage	kV	245
Insulation impulse voltage withstand level	kVp	1050
Continuous power rating of cable	MVA	465

The gap cannot be too large otherwise damage to the cable sheath could allow water to travel between the cable core and the metallic sheath. The gap has to be a compromise between these two aspects.

The corrugations are continuous with the depth of corrugation being 6mm and the pitch of the corrugations 22mm nominal. Usually to waterblock this gap in a corrugated stainless steel sheath the use of waterblocking tapes is not sufficient and a new procedure was developed to prevent water travelling a significant distance down the cable.

A composite sheath made up of an inner layer of orange PVC and an outer layer of HDPE was applied. The PVC was extruded to fill-in the corrugations of the metallic sheath and provide a smooth surface to the HDPE. The density of the HDPE was in the upper end of the range to provide a high hardness value and high abrasion resistance. This composite sheath provides added mechanical and moisture protection during installation and service.

MATERIALS

Insulation

The insulation material used for the production of the cable was obtained from a raw material supplier. Requirements for the cable insulation are set out in Table 2 and the incoming raw material had to meet the contaminant requirements of the specification. To meet these requirements a special grade of "Extra Superclean" resin was used. The material was a natural cross-linkable low density polyethylene compound produced for the insulation of high voltage power cables containing a good balance of a non-staining antioxidant and a peroxide to ensure thermal stability and ease of processing. The "Super clean" material was produced on a production line specially designed for the manufacture of the superclean product. The line is separate from all other production from the base resin intake to the final packaging. All material passes through highly sensitive metal separators and through exhaustive continuous sampling and testing procedures for contaminant detection and other quality control testing.

The material had a density of 0.922 g/cm^3, typical melt flow index of 2g/10mins a dielectric constant of 2.3 and a dissipation factor at 50 Hz of 0.0005. Other electrical and mechanical properties were typical of these materials.

For extra high voltage cables very clean insulation materials are required and the manufacturers of these resins have improved their manufacturing technology to make these types of materials available.

Semiconductive Screens

It has long been recognised that the smoothness of the interfaces between insulation and semiconductive layers in power cables is of great importance for the cable life. Protrusions from the semiconductive layers into the insulation can give locally enhanced electrical field stress and enhanced risk for electrical tree growth. Therefore a very smooth extrudable semiconductive material has to be used for both the conductor and insulation screen layers.

The material used for the semiconductive screens was a "Supersmooth" type with a well dispersed high quality and high purity special conductive carbon black grade. Volume resistivity results obtained from cable measurements are shown in Table 8.

PROCESS DEVELOPMENT

For the extra high voltage cable range, in addition to using the best materials, the processes have been developed to a higher level of cleanliness, smoothness of layers and concentricity to ensure a uniform, dry cable insulation.

The vertical triple extrusion vulcanisation process (VCV) in a tower was used, which gives the best results. The tower is shown in Figure 3. The extrusion was made into a heat radiant tube filled with pressurised nitrogen the lower part of which has a section for cooling using nitrogen at the same pressure, i.e. a "dry during/dry cooling" process.

Material Handling

The XLPE insulation and semiconductive XLPE copolymers are handled in separate floor levels and conveyed in closed circuits. The upper floors of the tower are under positive pressure and filtered air is introduced with maximum 20µm particle size. All operators wear overalls.

The "extra clean" XLPE is brought into the tower in 1 tonne boxes with 2 outside shrink-wrap films and an inside film lining. It is then brought to a small cleaning room, where the wrapping is vacuum cleaned, then removed and the box is moved into another room. The box is opened and a tube at the bottom is connected to the material conveying system which conveys the XLPE to a bin, dryer, through magnets and a wind sifter.

From there the XLPE comes into a dryer - holding bin and is fed gravitationally into the extruder.

The super smooth semiconductive materials are conveyed in a separate area to dryers, using desiccated hot air and then to a bin and then by gravitation to the extruders.

The conductor passes through an accumulator, then vertically upwards, through a pre-heating system and then around a turn around wheel system where it changes direction and goes vertically downwards straight into the extrusion head.

Triple Extrusion

The 3 extruders are situated on the same floor and are arranged so that the material streams can flow into the same triple head and join in a smooth flow to form the extra smooth interfaces.

The temperature ranges of extruders and screw speeds are carefully controlled to avoid any scorching and to minimise amber formation during long continuous production runs using insulation material which contains the peroxide cross-linking agent but also must be sufficient to avoid formation of cold spots and to ensure good melt quality.

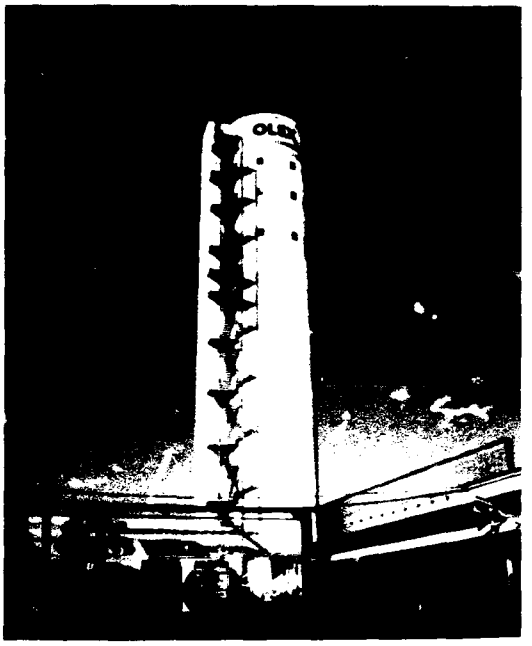


Figure 3. The VCV tower

Special tempered extruder screws allow a uniform material flow with high degree of concentricity and minimum variations of cable diameter. This is important for various reasons, including the jointing and terminating operation.

In addition to the use of extra super clean materials, high mesh screen packs are used for additional safety and their use must be optimised since they may cause an increase in melt pressure and temperature.

Dry Crosslinking and Dry Cooling

During the extrusion, barrel temperatures, extruder screw rotation speed, diameter variations, melt pressure and nitrogen gas pressure, are continuously monitored and recorded.

The 3 material layers then pass through the true triple head, which has carefully controlled and tempered zones and exit into the radiant heat cross-linking tube, filled with high purity nitrogen (residual oxygen content is monitored) under a pressure of the order of magnitude of 8-10 MPa.

The heat is produced by radiant heating elements and the tube walls can be heated to 350°C whereby the outer surface of the cable can reach temperatures of up to maximum 300°C. These temperature zones have been optimised using specially developed computer temperature prediction programs.[5] The cable then passes through

a vertical neutral (neither heated nor cooled) zone and then into the cooling zone which has forced circulation of cooled nitrogen. The first part of the cooling zone is vertical and the temperature of the crosslinked XLPE layers must be lower than the crystalline melting temperature of the XLPE when the cable passes the turn around wheel. The cable enters the second horizontal cooling zone still under pressurised nitrogen where the cooling is continued until the cable material is sufficiently cool and exits from the pressurised zone through a special seal into the open atmosphere.

Taping, Screening and Sheathing

After going through other special tempering treatments the cable is then passed into an integrated line where the various tapes are applied, the copper screen wires, followed by water swellable tapes and from there into the metal sheathing line, all in the one operation.

The stainless steel strip is first cleaned/degreased in a solvent bath, fresh edges are cut and the strip is formed to a round shape. Then the cable is introduced continuously into the formed strip, the strip closed around the cable and the edges are aligned perfectly for the following welding process.

The welding process is carried out in line by TIG welding under Argon gas and a hermetic welding seam has been achieved. A high quality welding is necessary to pass through the in-line corrugator which corrugates the cable with the 6mm deep corrugations, to confer to the cable a degree of flexibility and mechanical strength.

The polymer sheaths, flexible PVC and HDPE jacket over the corrugations are applied in a separate large extrusion line with cooling trough.

It should be mentioned that 220/230kV cables have been made consecutively on 2 different vertical VCV lines in the same tower.

Initially for development and type tests on the first line with triple extrusion and dry curing in pressurised nitrogen followed by a neutral zone and water cooling. These developmental 220kV cables have passed type tests as specified with similar results to those mentioned in this paper

Further development cables were made on the second "new" triple extrusion VCV line with dry curing and dry cooling as described in this paper and the type tests all passed, the results of which are mentioned in this paper. The manufacture of the 27km of the 220/230kV cable was carried out on the new second line with dry curing/dry cooling.

ACCESSORIES

Termination Development

The design concept for the termination is the modification of a field proven polybutene filled 161kV termination for solid dielectric cable to include internal capacitor grading as used on terminations for high pressure fluid filled cables at voltages of 230kV and above. A cutaway view of the 220/230kV termination is shown in Figure 4.

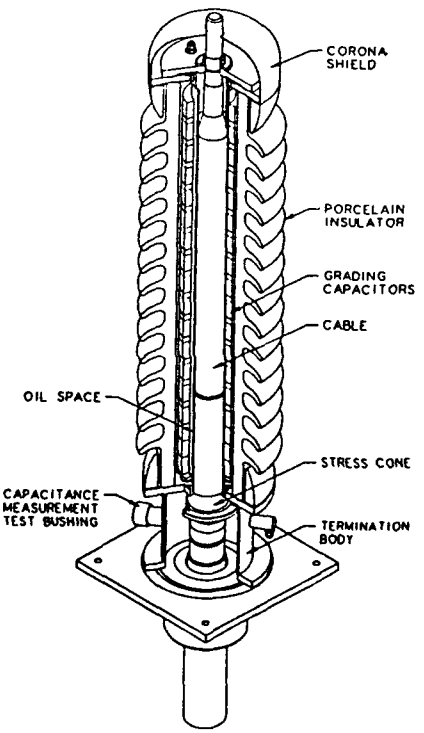


Figure 4. Cutaway view of 220/230kV XLPE cable termination

The capacitors grade the voltage along the porcelain insulator and thereby increase the flashover values in contaminated environments.[6] Likewise, the gradient is reduced along the unshielded length of the cable.

Figure 5 shows the voltage distribution at the end of the cable insulation screen. The stress is kept to acceptable levels by the use of a stress cone using an optimised computer developed contour.

The stress is reduced further by using tape with a high dielectric constant in the vicinity of the end of the cable screen. Maximum stress level in the oil is approximately 2.5kV/mm at operating voltage depending upon the cable size.

A unique feature of the stress cone design is that it does not compress on the cable insulation and thus cannot deform the cable insulation at high temperatures. The configuration permits an axial variation of 20mm in the location of the end of the cable screen. The cable is held rigidly in place within the termination by a threaded fitting on the crimp connector.

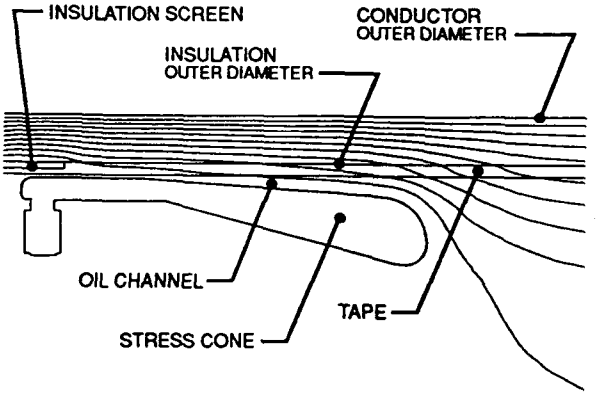


Figure 5. Dielectric stress distribution at stress cone

Special seals were developed for both vacuum and pressure sealing of the termination. The termination is put under vacuum prior to and during the oil filling process. An accumulator maintains the internal pressure at the desired value during oil volume changes that occur due to variations in operating temperature. The pressure is monitored by a gauge.

The termination is mounted on a base plate which in turn is mounted on the station structure. Insulators between the base plate and station structure provide a screen break capability to permit various bonding methods.

Joints

The joint is a prefabricated design filled with polybutene and illustrated in Figure 6. The cable is held in place within the stainless steel housing by epoxy nose cones. Each cable has a crimp connector that is joined together electrically and mechanically by a centre clamp. The clamping system can withstand a tensile force of 200kN without separation or damage.

Stress control is similar to that for the termination except for the addition of corona shields. Figure 7 shows the electrical field plot for the centre section. The stress level is 2kV/mm at operating voltage for this region.

The joint can be disassembled and reassembled should the need arise. The epoxy nose cone provides a screen break between the diaphragm seal assembly and the stainless steel housing for cross bonding. The screen break can be shorted with a metallic connection for solid bonding.

Pressure is monitored remotely by a fibre optic transducer.

Dielectric Fluid

The dielectric fluid is a synthetic high molecular weight, ultra pure polybutene oil. It is inert, has excellent dielectric and thermal properties and is environmentally safe. Extensive testing and in service use since 1970 demonstrate the compatibility with XLPE insulation.

The dielectric constant of the oil is virtually the same as that of XLPE which eliminates any stress enhancement. Thermal transfer greatly exceeds that of XLPE and solid insulating materials.

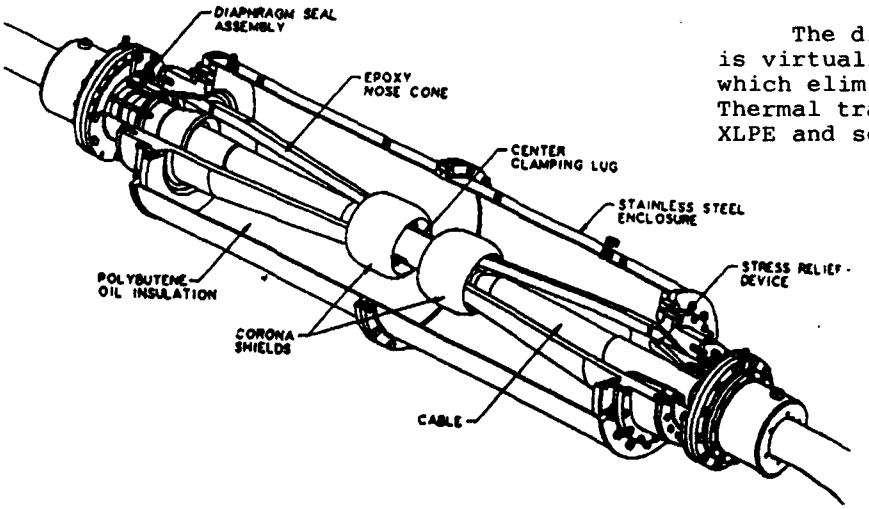


Figure 6.
Cutaway view of 220/230kV prefabricated XLPE cable joint

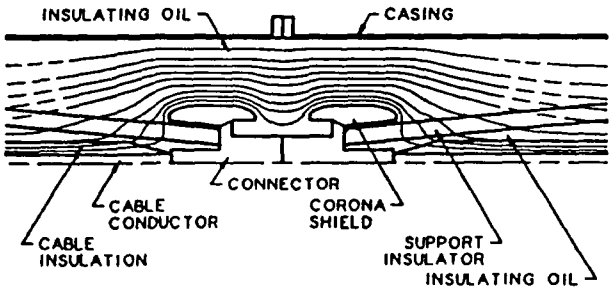


Figure 7. Dielectric stress distribution at the joint centre section

TESTING

Type Testing

The testing requirements are set out in the State Electricity Commission of Victoria specification.[4] For the type testing requirements of the cable the IEC 840 standard was followed with the heating cycle voltage test being replaced by the cyclic ageing test of AEIC CS 7-87. This latter standard for the cyclic ageing test requires that part of the cycling be carried out at a conductor temperature of 130°C. Because the cable standards are applicable to a lower voltage range of cable than the 127/220kV XLPE cable being developed the test voltages and conditions were extrapolated to the levels required for the 127/220kV cable system.

The terminations were evaluated to test requirements taking into account IEEE 48 while the joints to test requirements taking into account IEEE 404. Other special requirements of the State Electricity Commission of Victoria were also included into the testing schedule.

For the type testing of the cable and accessories the test assembly consisted of two terminations approximately 40 metres of cable and a joint. The type test involved simultaneous type qualification of the cable and accessories. The test sequence and results of the electrical type tests are shown in Table 6.

After the initial partial discharge test and high voltage test on the cable the cable sample was bend tested by bending the cable around a drum of diameter 2800mm three times in both directions. A partial discharge test was then carried out on the sample that was bend tested after which a piece of the cable was removed and examined for any damage to the cable core, metallic and plastic sheaths. The bend tested cable was then assembled with the cable accessories terminations and joint and the assembly subjected to cyclic ageing. The voltage and conductor temperature conditions for the cyclic ageing test are set out in Table 6. Each cycle consisted of 8 hours of load current followed by 16 hours of natural cooling. On the first and last cycle of the cyclic ageing test the tan δ determinations were made.

Table 6. Electrical Type Tests

Test	Requirement	Result
1.Partial Discharge of cable	< 5pC, 190 kV	1pC
2.High Voltage	318 kV,30 mins	no breakdown
3.Bending test then partial discharge	3 reverse bends on drum 2800mm diam. no cracks to any sheath, < 5pC,190kV	no cracks 1pC
Assembly of cable, terminations and joint.		
4.Tan δ of cable	< 0.001 ambient U_o to $1.5U_o$ 40°C U_o to $1.5U_o$ 90°C U_o to $1.5U_o$	pass
5.Variation tan δ 40°C to 90°C at U_o	< 0.0005	0.0002
6.Cyclic ageing test	7 cycles,40°C,$1.5U_o$ 14 cycles,90°C,$2.0U_o$ 14 cycles,130°C,$1.5U_o$	
7.Tan δ after cycling	< 0.001 ambient U_o to $1.5U_o$ 40°C U_o to $1.5U_o$ 90°C U_o to $1.5U_o$	pass
8.Variation tan δ 40°C to 90°C at U_o after cycling	< 0.0005	0.0001
9.Impulse withstand	conductor 100°C 10+, 10-, 1050kVp no breakdown	no breakdown
10.High Voltage test	318kV for 6 hrs. no breakdown	no breakdown
11.Partial Discharge on cable,joint and termination	< 5pC at 190 kV	< 2pC
12.High Voltage time test on cable,joint and termination	343 kV for 24 hrs. 381 kV for 30 min. 413 kV for 1 min. 460 kV for 1 min. no breakdown	no breakdown

The test assembly arrangement is shown in Figure 8. Because of the large physical size of the final test assembly after the final voltage test the cable was cut between each termination and joint and a final partial discharge determination was made on each section of the test assembly. The cable and accessories were then subjected to the AC voltage-time test.

The termination and joint used in the type test assembly are shown in Figure 9 and 10.

The electrical type test results in Table 6 show that excellent test performance was achieved with less than 2pC partial discharge on the cable and accessories after completion of the type testing schedule.

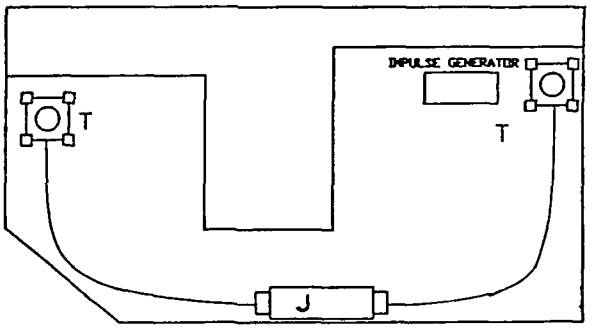


Figure 8. The type test assembly

As well as the electrical type tests physical and mechanical type testing was carried out on the cable to IEC 840 and AEIC CS7-87. The tests carried out are set out briefly in Table 7. Voids, contaminants and protrusions of the cable insulation and conductor and insulation screens were determined according to the methods set out in AEIC CS7-87 and the limits were as set out in Tables 1, 2, 3.



Figure 9. The 220kV termination in the type test assembly

Table 8 shows the results of the volume resistivity measurements obtained while Table 9 shows some results of the contaminant, void and screen protrusion testing carried out on the XLPE insulation and the semiconductive screens.

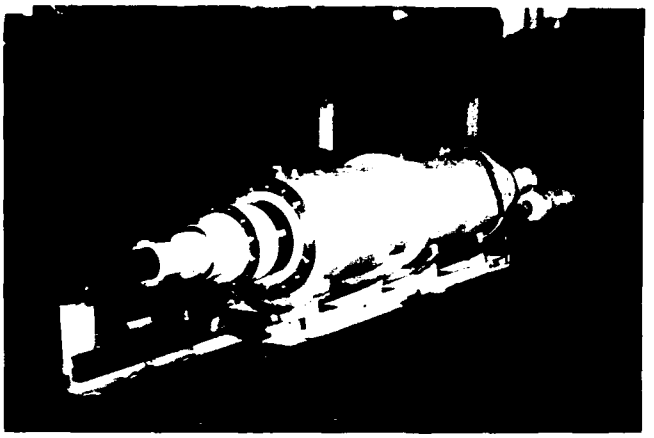


Figure 10. The 220kV joint

Other Type Tests

Sidewall bearing pressure test: The test was carried out on a 10 metre sample of 220kV cable in the test arrangement shown in Figure 11. The cable was tensioned to the required force using a chain block. The diameter of the fixed wheel used in the test was 2.4m. The load cell units were used on either side of the cable to enable the tension to be determined during the test. A lubricant was applied to the cable at the fixed wheel contact surface then maintaining the required tension the cable was pulled around the bend. The determined side wall pressure was 24.3kN/m. Table 5 shows that the requirement for the cable design was 22kN/m. A metre sample was cut from the 10 metre length and examined. No deformation was found to the plastic sheaths, corrugations of the stainless steel sheath, the screen wires, tapes or core insulation screen.

Table 7. Physical and Mechanical Type Tests

Cable examination after bend test.
Cable examination after cyclic ageing test.
Conductor screen: dimensions,voids and protrusions vol. resistivity 90°C, 130°C unaged/aged/cycled
Insulation: dimensions,tensile and elongation unaged/aged/cycled, hot set test, dimensional stability, shrinkage, voids and contaminants.
Insulation screen: dimensions,voids and protrusions, vol. resistivity 90°C, 130°C unaged/aged/cycled
sheaths: dimensions, tensile and elongation unaged and aged, loss of mass test, pressure test at high temp, behaviour at low temp, heat shock test, carbon black content.

Waterblocking test: This test was to determine the extent of water propagation beneath the metal sheath in case of sheath damage. The sample used for the test was from an initial development run of the cable. The cable sample was first bend

Table 8. Volume Resistivity Results

sample	units ohm-metres conductor screen 90°C	130°C	insulation screen 90°C	130°C
spec.limit	1000	1000	500	500
unaged cable	18	53	2.3	3.3
after cyclic ageing	26	34	5.9	11
complete cable aged 7days 100°C	96	88	4.9	11

tested as shown in Table 6 then a sample length of 3 metres with sheath with a length of exposed conductor for end connections was prepared for the test. A ring of the sheath 50mm wide was removed from the centre of the sample down to the core and a water column 1 metre high attached at the opening. The sample was subjected to 10 thermal cycles to 90°C. During the test and at the end of the test no water emerged from the ends of the cable.

Table 9. Contaminants, Voids, Protrusions on Type test cable

	max limits	test result
Conductor screen		
protrusions into screen	0.250mm	0
protrusions into insulation	0.125mm	0
voids		0
Insulation screen		
protrusions into screen	0.250mm	0
protrusions into insulation	0.125mm	0
voids		0
XLPE insulation		
size of voids	0.030mm	0
size of contaminants*	0.100mm	0
size of translucents*	0.250mm	0.100mm
no of voids per 16 cm^3	30	nil
no of contaminants per 16 cm^3	15	nil

* only greater than or equal to 0.050 mm (2 mils) recorded.

Mechanical test on joint protection box: A large pit was dug and the fibreglass joint protection box containing the joint complete with power cable and bonding leads and filled with compound was placed in the pit. This is shown in Figure 12. The pit was filled with consolidated dry sand and a load of 15,800kg placed on concrete cable protection covers. After 30 minutes the load was lifted off, the protective box completely exposed and examined for any deformation. During the test there was no movement of the assembly or displacement of any sand and on examination of the protection box no evidence of any deformation, fracture or disturbance to any part of the box.

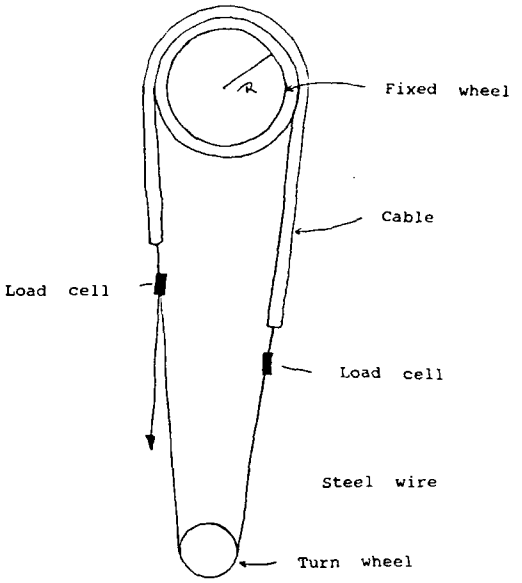


Figure 11. Test arrangement for side wall bearing pressure test

Short time current tests: These were carried out on the joint and joint housing. The joint was mounted on a frame with a length of bonding cable in place. A second cable was fitted in parallel with the main conductor and connected to carry the return current. This cable was placed 520mm from the main cable so as to create a force on the main conductor to simulate a fault condition. The test results are shown in Table 10. Two applications of short time current at 32kA for 0.32 secs.

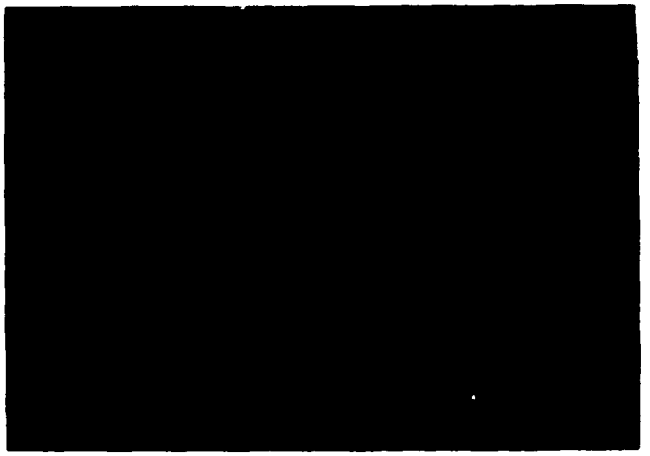


Figure 12. Mechanical test on joint protection box

were carried out. The short time current circuit was connected so that the return current for each application was alternatively connected via the inside and the outside conductors of the bonding cable. The connections were made in such a way that the effect of deflection was observed on the main conductor and every joint in every possible current path under fault conditions was tested. After the completion of the test examination revealed that there was no sign of damage to the corona shields or stress cones and no damage to the epoxy coating of the joint nose cones.

Table 10. Short time current test results

test	result
Partial discharge after assembly	< 2pC at 190 kV
High Voltage 318 kV, 30 min	no breakdown
DC resistance between cable ends	0.2065 milli-ohm
Short time current 32 kA 0.32 secs	
Inspection	no defects
DC resistance between cable ends	0.2042 milli-ohm
Partial discharge	< 2pC at 190 kV
Final inspection	no oil leaks no damage

Tests on the screen break bonding lead in the joint: Impulse tests were carried out to prove the integrity of the bonding lead and insulated gap in the joint screen circuit with the joint in the joint housing. Ten positive and ten negative impulses at 75kVp were applied between the inner and the outer conductors of the bonding lead also effectively testing the joint screen gap. No breakdowns occurred.

INSTALLATION

The 9km long route from the suburbs of Brunswick to Richmond involved freeway crossings, bridges, water, tramway tracks, railway lines and embankments. The cable route is shown in Figure 13.

In most cases the 3 cables were laid in 1.2m deep and 1m wide trenches on a mixture of sand and cement, using pulling techniques and then the cables were back filled with a layer of bedding material, covered with protective concrete slabs and soil.

In case of water crossings, the cable was installed in PVC piping set in concrete. At road and rail crossings, tunnelling and boring was used and ducts were installed in the tunnels. 3 joints were installed in each joint bay.

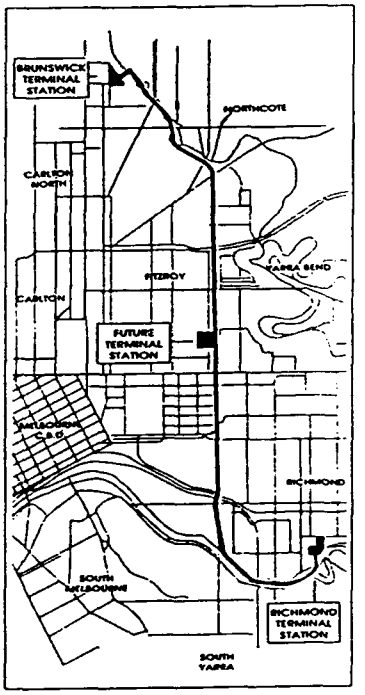


Figure 13. The cable route

Cables and accessories for the whole system were commissioned and are operational since early this year.

REFERENCES

1. Barber K. W., Mayer H. A., "Reliability of Medium and High Voltage XLPE Cables" Tech. Papers Vol. 2, Int. Conf. Distribution 2000, May 1991, Sydney, Australia.

2. IEC 840, 1988 "Tests for Power Cables with Extruded Insulation for Rated Voltages above 30kV up to 150kV".

3. AEIC CS7-87 "Specifications for Cross-Linked Polyethylene Insulated Shielded Power Cables Rated 46kV through 138kV"

4. SECV No. 200316 - 891348 Section F.

5. Kemp R. C., Stringer A., Zlatsin Y., "Estimation of Temperatures During Dry Crosslinking of High Voltage XLPE Insulated Cables", Proc. 41st IWCS 1992.

6. Boliver V. J., Uzelac M., Barber K. W. "Compatibility of Newly Developed 220/230kV Cable Accessories with XLPE Cable", Int. Meeting IEEE/ICC, Birmingham, July 1992.

Acknowledgements

The authors wish to acknowledge the valuable and significant contributions by the engineers of the Power Grid Development Department of the State Electricity Commission of Victoria in the project, in particular in the successful development of the accessories.
The authors also wish to thank their colleagues, engineers and scientists from Olex Cables and G&W for their valuable contributions and co-operation in the project.



Hans A. Mayer, after receiving his Dipl.-Ing. degree in Engineering (Technical University), he was 8 years in the Chemical, Plastics and Rubber Industry, mainly as Manager Technical, Quality & Laboratories. 1965-1983 he was at AEG-Telefunken Kabelwerke, AG, West Germany in various factories, mainly as Manager Central R&D, Materials and Processing and Chief Engineer. 1983 Hans joined Olex Cables, a Division of Pacific Dunlop Ltd. as a Technical Operations Manager with Group R&D responsibilities for new cable technologies. Hans is author/co-author of numerous patents to his Companies. He is Member of various Institutions of Engineers and Scientists in Australia and Germany and also Member of several CIGRE Working Groups.



Eugene Buczma graduated from the Department of Industrial Science, Melbourne University in 1971. He then joined Austral Standard Cables carrying out projects in the Materials Development section and in 1979 Hoechst Australia in the Plastics Technical Service section. In 1980 he received a Masters degree from Melbourne University for a thesis on extrusion of cellular polyethylene. In 1985 he joined Olex Cables where he now has the position of Manager Development Engineering and is responsible for process and product development.

Address:
Olex Cables, Melbourne
A Division of Pacific Dunlop Limited,
207 Sunshine Road, Tottenham, 3012,
Victoria, Australia.



John A. Adcock has a diploma in Electrical Engineering and is a Member of the Institute of Engineers Aust. After graduating he joined the SECV in 1954 and was involved in metering standards and calibration. In 1964 he joined AEE Capacitors Rifa where he designed capacitors and test equipment. From 1976 at Stanger and Co. he was involved in high voltage current transformer design and testing. In 1985 John joined Olex Cables where he is now the Senior Development Engineer-Electrical and has been involved in carrying out development and type testing on medium, high and extra high voltage power cables.



Vincent J. Boliver received a B.S. degree in Electrical Engineering from Worcester Polytechnic Institute and a M.S. degree in Electrical Engineering from the University of Massachusetts. He joined G&W Electric Company in 1990 as Manager of Cable Accessories. He is a registered Professional Engineer in New York State and holds 12 U.S. patents. He is a Member of IEEE.



Milan Uzelac received his B.S. degree in Power Electrical Engineering from the University of Belgrade, Yugoslavia in 1968. He has over 20 years of experience in development and manufacturing of high voltage equipment. He was a Member of the Yugoslav CIGRE Committee and published several papers in his field. He joined G&W Electric Company in 1989 as an Engineer for High Voltage Cable Accessories He is a member of IEEE.

Address:
G&W Electric Co.,
3500 West 127th Street,
Blue Island, Illinois 60406
USA

THE APPLICATION OF 154kV TRANSITION JOINT IN KOREA

* * * **
S. C. HWANG, C. S. LEE, W. K. PARK, J. Y. KOO

* Gold Star Cable Co.,Ltd. ** Dept. of Electrical Eng., Hanyang Univ.
Seoul, Korea

ABSTRACT

Since the successful development of 154kV XLPE cable in 1983, its commercial use has been drastically expanded due to technical advantages and high performance of insulation. Furthermore, the large conductor size of 1200 SQMM and 2000 SQMM has been mainly employed in Korea for the purpose of satisfying the bulk power demand in urban areas.

However, it is highly required to solve the problems at the level of the joint between the cables of different type such as existing OF and XLPE cables. In this respect, the OF/XLPE transition joint has been applied for the first time in Korea in 1989.

In this paper, considering the increasing demands of bulk power in Korea, the recent trend of underground power system is also reported for developing the 345kV XLPE cable and forced cooling system in enabling to ensure the stable power supply in urban area.

INTRODUCTION

In the case where it is not allowed to link the OF cables together for making the loop transmission network due to the topological and environmental constraintes, it is unavoidable to apply transition joints with XLPE cables. For the first time in Korea, the 154kV OF/XLPE transition joint was set up in the transmission lines between Shin-InCheon S/S and InCheon S/S in 1989.

In view of practical application, this report deals with the application backgrounds, requirements and test results of transition joint box (herewith referred as TJB). And technical countermeasures are described against the thermal expansion of installed power cables around TJB.

On the other hand, considering the increasing demands of bulk power in Korea, the recent trend of underground power system is also reported for developing the 345kV XLPE cable and forced cooling system in enabling to ensure the stable power supply in urban area.

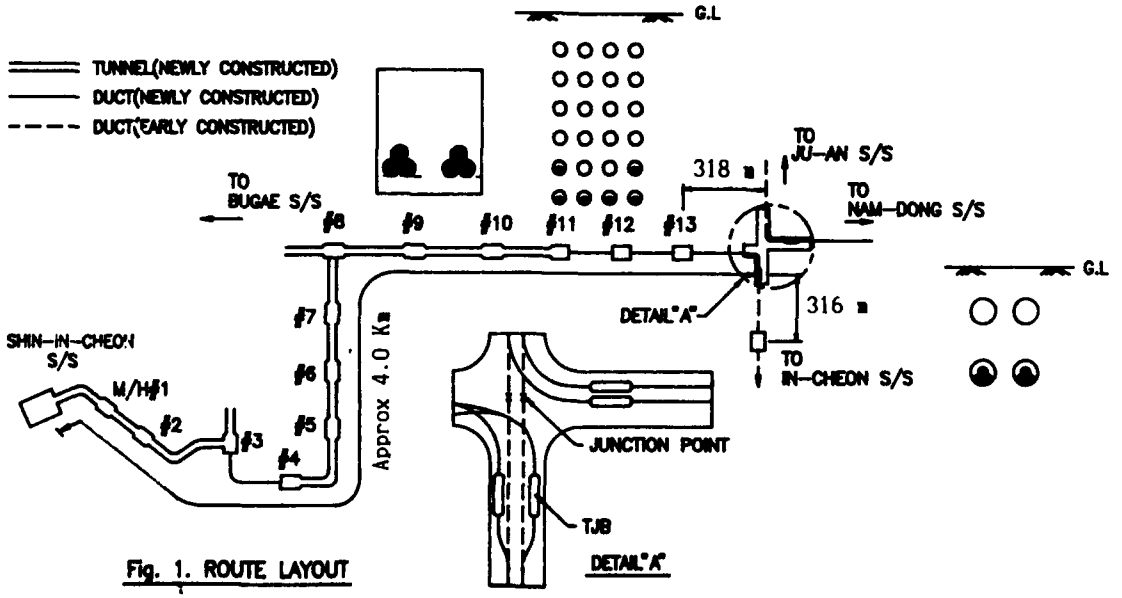


Fig. 1. ROUTE LAYOUT

BACKGROUNDS

The power transmission line between InCheon S/S and Ju-An S/S has been already under operation using three single core cable of 154kV OF 1200 SQMM which were installed as a trefoil formation in duct. But in 1989, the new lines using 154kV XLPE cable between Shin-InCheon S/S and Nam-Dong S/S were established in order to ensure the stability of power supply around these areas, for which TJB was constructed.

Route profile of underground transmission line is described in Fig 1.

OF cable was firstly considered for this new lines for the safety and easy jointing works, which might raise some technical inconveniences as follows :

- Considering the rapid temperature rise in tunnel due to the multi-circuit installation, it is indispensable to provide the forced cooling system in order to ensure the required transmission capacity for each circuit.

- Space for the stop joint and oil feeding equipment are required at the intermediate point of this long cable route with high difference in its elevation.

- More expenses should be reserved for the prevention devices against the fire incident of OF cables.

Therefore XLPE cable was considered as the better alternative to solve the above technical inconveniences and TJB was employed for the existing OF cables and newly established XLPE cables.

Electrical requirements of TJB

Table 1 describes the minimum electrical requirements determined for TJB. These values should be approximately equal to those of two different type of cables such as 154kV OF cable and 154kV XLPE cable.

Table 1. Electrical requirements for TJB

Item	Requirement
AC voltage withstand	400kV , 3 hours
Impulse withstand	-1135kV , 3 times
Partial discharge	Less than 5pc at 120kV

TJB, shown in Fig 2, was constructed by use of the symmetrical epoxy unit, for which a certain number of constraints are established as follows :

- adaptablity to the maximum conductor size up to 2000 SQMM of 154kV power cables

- compatibility of materials for any type of cables

- compactness

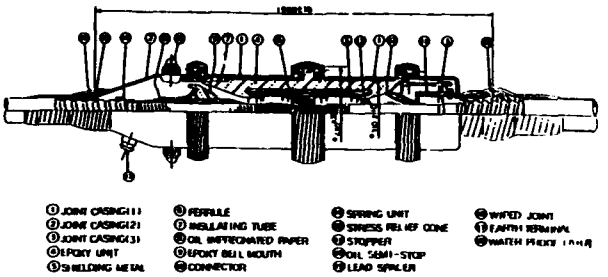


Fig. 2 Construction of TJB

Testing on TJB

(i) Behaviour of Epoxy Unit

Heat cycle test and partial discharge test have been performed to confirm the behaviour of the epoxy unit. Requirements and test results are shown in Table 2.

Table 2. Requirements and results of tests on the epoxy unit

Item	Requirement	Result
Heat cycle test	Sample should be put under the high temperature side during at least 1h, which is followed by the test under low temperature side during at least 1h. Temperature differences of both side should be greater than 80℃ and the low temperature side should be set 0℃ ~ 20℃. This process should be repeated 10 times, after which no evidence of abnomality should be noticed.	satisfied
Partial-discharge test	Less than 5pc at 120kV	satisfied

(ii) Initial performance

Table 3 illustrates the results and requirements of the tests carried out to verify the initial performance of TJB.

Table 3. Requirements and results of initial performance test

Item	Requirement	Result
Air-tightness test	Hydraulic test at ambient temperature during 30 min at 14 kg/㎠.G, through which no leakage should be detected at the OF cable side.	satisfied
Partial-discharge test	Less than 5pc at 120kV	satisfied
Impulse withstand	-1135kV, 3 times	satisfied
AC voltage withstand	400kV, 3 hours	satisfied

(iii) Long term thermal ageing test

Table 4 illustrates the testing condition of the long term thermal ageing for verifying the electrical, mechanical and thermal behaviour of TJB, for which a service life of 50 years based on the n=9 is assumed.

Table 4. Condition of long term thermal ageing test

Duration / Item	0	360	365 days
Applied voltage	144kV		
Conductor temperature	90℃	95℃	

Followed by the above test, residual test was also carried out in the same way as the initial performance test. No noticeable differences were observed.

Countermeasure of cable thermal expansion

In order to avoid the inconveniences occurred due to the thermal expansion of cables, two different countermeasures are taken : OFF-SET in manhole for the cables in duct and Snake installation for the cables in tunnel.

These two methods were designed to limit the strain of the metal sheath of cables within 0.3% .

For the junction at manhole where TJB was installed, L-type OFF-SET was used to absorb the thermal expansion of cables in each duct line as shown in Fig 3.

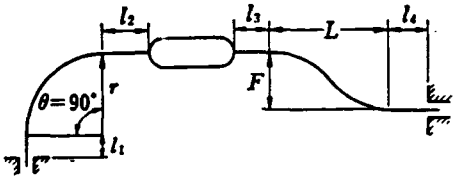


Fig.3 L-type OFF-SET

And for the curved part, the curve radius was set to be 3m considering the minimum permissible curve radius(20 times the average outer diameter of metallic sheath of cable). However, for the straight part, normal OFF-SET was designed according to the equations described below :

(1) $L \geq 4F$

(2) $L \geq \sqrt{(4RF-F^2)}$

(3) $.003 \geq \varepsilon = \dfrac{200\ Ds\ \Delta}{L^2+F^2} \left| \sqrt{\{5.2(1+L^2/F^2)+1\}-1} \right|$

where,

L : length of OFF-SET (mm)
F : Real width of OFF-SET (mm)
R : Permissible curve radius of OF cable (mm)
Ds: Average outer diameter of metallic sheath of cable (mm)
Δ : longitudinal displacement of cable due to thermal expansion (mm)

Table 5 shows the dimension of each part described in Fig 3.

Table 5. Dimension of L-type OFF-SET

L	F	l_1	l_2	l_3	l_4
1,200	3,600	100	200	200	100

The strain was calculated to be 0.23%, which satifies the requirement.

Recent trends of underground transmission system in Korea

Nowadays it is absolutely difficult to provide the new underground power cable route in Korean metropolitan area due to many a

different kind of underground utilities such as : subways , gas and water supply pipes, communication & power cable lines and etc. And thus underground tunnels for the new cable routes are now being constructed at the 30m ~ 50m lower than the ground level.

Electricity demand in Korea (21000MW in 1991) is expected to increase annually 6% ~ 10% to reach a high of 35000MW in 1996 and 47000MW in 2001. In order to supplement the forecasted load carrying capacity, a new underground transmission voltage level of 345kV and the forced cooling system will be introduced in near future.

345kV XLPE cable

345kV OF cable has been developed in 1989 and is about to be utilized commercially in 1993. However, it is highly required to develop the 345kV XLPE cables due to the progressed manufacturing facilities with improved dry-curing process. On the other hand, the users also pursue the excellent electric performance of power cables and the simplified installation with easy maintenance. Particularly, it is indispensably recommended to use the solid insulation power cables for the cable routes with great difference in height such as those of hydro power station or with insufficient space for oil feeding equipment.

The main technical problems to solved for the development of 345kV XLPE are as follows :

- Uniformity of insulation without any defects
- Cable manufacturing process ensuring to meet large thermal expansion of the insulation.

Considering 30 years of expected cable life, insulation thickness of 345kV cable is recommended to be approximately 34mm enabling to withstand both the maximum system voltage of 362kV and BIL of 1300kV.

Forced cooling method

Forced cooling methods will be introduced in Korea in order to increase the transmission capacity more efficiently for the safe power supply in urban area and to achieve the higher utilization efficiency of underground transmission facilities. Therefore, many a different type of forced cooling methods have been under consideration for introducing in our underground power system as follows :

- Tunnel direct and indirect water cooling
- Duct line direct cooling
- Internal cooling
- Pipe type freon cooling
- Cryogenic cooling

Among these, tunnel indirect water cooling technique will be adopted in view of the fact that this system is reliable with technical and economical advantages in connection with the construction and maintenance. Moreover this method is considered to be the most preferable for the long transmission line requiring large capacity. Fig 4 and Fig 5 describe the fire protection in tunnel and the arrangement of installations respectively which will be constructed in our underground power system.

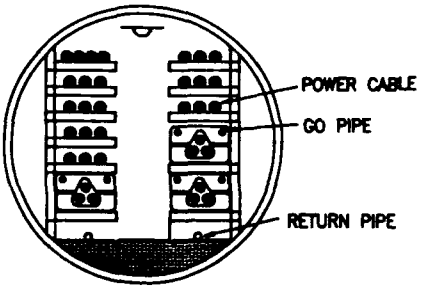


Fig. 4. CONFIGURATION OF FIRE-PROTECTION TROUGH IN TUNNEL

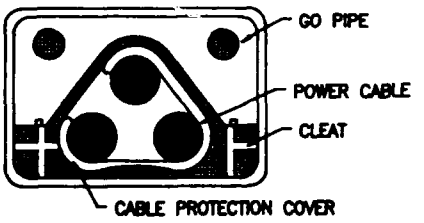


Fig. 5. SECTIONAL VIEW OF FIRE-PROTECTION TROUGH

It is also expected that this forced cooling system permits us to increase the transmission capacity by approximately 30% compared with that of natural air cooling system.

Conclusion

In this work, we have given the details of the 154kV OF/XLPE transition joint which was already installed into the main transmission line in Korea. And recent trends of underground transmission system in Korean urban area is also well reported.

Our TJB was proved, through the service records up to now, to be so reliable that it could be expected to envisage more advanced application to the other voltage grade in power transmission.

On the other hand, the electrical power company and cable makers in Korea make their investigations in developing power cables with large conductor size, for the higher rated voltage grade and in realizing appropriate forced cooling technique.

References

(1) H.Gokia et al., " Cable thermal expansion and its countermeasures " Power cable technical handbook, Jan.1989, pp.673-703.
(2) Yamaguchi et al.: Hitachi Cable Ltd., " Development of transition joint box for 275kV POF/CV cable " ,1992 national convention record I.E.E. Japan , Vol.12, Mar.1992,pp.105-106.
(3) M.Kanaoka et al. : Hitachi Cable Ltd., " Development of 500kV XLPE insulated power cable ", Hitachi Cable Review No.2, Aug.1983, pp.3-6.
(4) J.Y.SEO et al. : Korea Power Electric Co. Research Inc., " A study on the introduction of forced cooling system for under ground power cable ", Jan.1991, pp.36-79.



Soon Chul HWANG

Gold Star Co., Ltd.
Lucky-Goldstar Twin Tower E.6F
20, Yoido-Dong,Youngdungpo-Ku,
Seoul, 150-605, Korea

Soon- Chul HWANG was born in 1952 in Korea. He received the B.S degree from Seoul National University, Seoul, Korea in 1979. He then joined Gold Star Cable Co.,Ltd., and has been engaged in the area on the high voltage cables and its application. Mr.HWANG is now General Manager of Extra High Voltage System Dept. and a member of the Korean Institute of Electrical Engineers.



Chang Soo LEE

Gold Star Co., Ltd.
SUWON OFFICE
251-1 Woncheon-Dong,Kwonsun-Ku
Suwon city Kyonggi-Do,Korea

Chang- Soo LEE was born in 1948 in Korea. He received the B.S degree from Sung Kyun Kwan University, Seoul, Korea in 1969. During 1969 ~ 1982, he had worked for Korea Electric Power Company . Then 1983, he joined Gold Star Cable Co.,Ltd. and has been engaged in the area on installation of high voltage cables. Mr. Lee is now a General Manager of Electric Power Cable Installation Team.



Won Keun PARK

Gold Star Co., Ltd.
Lucky-Goldstar Twin Tower E.7F
20, Yoido-Dong,Youngdungpo-Ku,
Seoul, 150-605, Korea

Won-Keun Park was born in 1934 in Korea. He received the B.S degree from Seoul National University, Seoul, Korea in 1958. He then joined Gold Star Cable Co.,Ltd.in 1962 and has been engaged in the area on high voltage cables, communication cables and many other fields of wires and cables. Mr.PARK is now President of Goldstar Cable Co., Ltd. and a member of the Korean Institute of Electrical Engineers.



Ja Yoon KOO

Dept. of Electrical Eng.,
Hanyang University.
396 Ansanshi, Daehakdong
Kyeongki-Do, 425-791, Korea

Ja-Yoon KOO was born in 1951 in Korea. He received the B.S degree from Seoul National University, Seoul, Korea in 1975, M.S degree from ENSEEISH,Toulouse,France in 1980 and Docteur d'Ingenieur in High Voltage Insulating Dielectrics, from ENSIEG,Grenoble,France in 1984. He has joined Research Center of the Electricity of France, at th High Voltage and High Power Laboratory after his dissertation in France and then worked for Korea Advanced Institute of Science and Technology, Seoul, Korea. He has been with the Department of Electrical Engineering, Han Yang University, Seoul, Korea since 1988 as an associate professor.

He has been nominated by some international academic organizations representing Korea as follows: since 1990 a member of high voltage power cable study committee for CIGRE, since 1991 a member of technical committee for the JICABLE and a member of advisory committee member for the ICPADM.

His main research activities are in the area on the New Dielectrics used for High Power Engineering, Diagnosis of Electric Power Apparatus and the Protection of High Voltage Network System.

ESTIMATION OF TEMPERATURES DURING DRY CROSSLINKING OF HIGH VOLTAGE XLPE INSULATED CABLE

R. C. Kemp

CSIRO Division of Applied Physics, Sydney, Australia

A. Stringer and Y. Zlatsin

Olex Cables Division of Pacific Dunlop Ltd., Melbourne, Australia

ABSTRACT

A means of estimating temperature distributions within XLPE insulated extra high voltage cables undergoing manufacture in a harsh environment is described. The problem of estimating temperatures during dry curing in nitrogen in a VCV line was successfully accomplished in a collaborative project between a Research Organisation and a Cable Maker. The problem was addressed by constructing a computer model and a physical laboratory model of the vertical CV-line. In addition, the VCV-line was used as an experimental platform by embedding thermocouples and other temperature sensors in a variety of experimental cables so as to test and fine tune the computer model.

The project established that the cable temperatures exceed considerably those calculated by some popular programs which puts under review the existing correlation between the time of decomposition of peroxide and the degree of crosslinking of XLPE insulation as assessed by the hot set method.

The availability of the program has led to a better understanding and control of the manufacturing process.

INTRODUCTION

Ever increasing power demands in industrial centres, cities and urban areas means the use of high voltage (HV) and extra high voltage (EHV) underground cables is rapidly growing. In recent years polymers, especially crosslinked polyethylene (XLPE), are becoming a successful replacement for conventional oil filled paper cables.

A wide range of measures have been implemented in order to further the reliability of XLPE insulated cables, and in particular EHV cables, such as: cable design, materials and manufacturing technology. Replacement of traditional steam crosslinking processes by 'dry crosslinking' is one of the outstanding examples of progress in the field. The dry crosslinking is necessary to avoid water treeing and to obtain microvoid free insulation.

The processes which take place during the manufacture of an XLPE insulated cable have been described by a number of authors[1]. In essence, the layers of insulation and semiconductive materials are extruded simultaneously on to a metallic conductor by a multiple (triple) extruder system and the cable so formed passes down through a tubular heating environment, pressurised to 800-1000 kPa (120-150 p.s.i) with dry nitrogen, where the crosslinking process is initiated. The cable then passes through a cooling zone where it is cooled with forced dry nitrogen and/or water, again under pressure. In the case of a vertical plant, which can be 60-80m (180-240 feet) high, the cable direction is changed from vertical to horizontal by a large turnaround wheel at the base of the plant, before undergoing further cooling and then exiting into ambient conditions.

The crosslinking process itself, in this application, is activated by free radicals resulting from the decomposition of a peroxide caused by heating and is thus extremely temperature dependent. In addition, the surface of the cable must not be exposed to high temperatures for excessive periods, otherwise decomposition of the insulation material may occur. On exiting from the heating zones the cable must be cooled gently to avoid incorporating excessive strain in the insulation and to ensure the crosslinking process is effectively complete before the cable passes round the wheel so as to avoid deformation of the cable. Also, if water cooling is used, the cable surface must be below a particular temperature at entry to the water. Finally, at the point where the cable exits from the plant into atmospheric pressure the cable must be sufficiently cool to withstand the reduction in pressure, to avoid the formation of voids or bubbles in the insulation due to the by-products of the crosslinking process. The economics of the process also play a role, as the speed at which the cable passes through the plant must also be maximised so as to minimise the cost of manufacture.

The temperature distribution in the cable must therefore be known during the entire manufacturing process.

The determination of the temperature distribution in a cable undergoing manufacture in such a vertical continuous vulcanising (VCV) line is no easy task. The cable is moving and may also be oscillating perpendicular to its direction of travel. The pressurised tube in which the cable travels can be heated to $350 - 400°C$ up to a maximum of $450°C (840°F)$ and at the higher temperatures, some pyrolysis products can be emitted by the cable which tend to condense on the surface of the tube. Temperature sensors such as thermocouples cannot be embedded in production cable and temperature measurements on one or even a number of experimental cables do not provide information for the very large number of cable types of different size and configuration that can be manufactured in a VCV line.

Simulation of the dry curing process for XLPE insulated cable has been carried out by various firms and organisations with various degrees of accuracy. This project was undertaken because in the case of EHV cable there was a need for a considerably improved correlation between predicted and actual processes taking place in the cable.

The problem of estimating temperatures in a VCV line was successfully accomplished in a collaborative project between Research Organisation and a Cable Maker stretching over some 3 years. The problem was addressed by constructing a computer model of the VCV line to provide the temperature distribution within the cable in terms of temperatures and other parameters which could be measured on the line. Use of the computer model then enabled estimates to be made, at the accuracy required, of various measured line parameters and the extent of any necessary control. In addition, the VCV line was used as an experimental platform by embedding thermocouples and other temperature sensors in a variety of experimental cables so as to test and fine tune the computer model. The interactive development of the computer model aided in broadening the product range produced by the plant and in commissioning a second, larger plant for the production of larger-diameter cable.

This paper describes the course of the project, the development of the procedures used for the estimation of cable temperatures and the agreement achieved between calculation and experiment.

COMPUTER MODEL

Analyses of the processing of insulated cable have been carried out by Boysen[2] and Kodres and Phillip[3]. These analyses did not refer to the type of plant described here, were quite general and not applied to a real situation.

To obtain the transient temperature distribution within the cable as it passes through the plant it is necessary to solve the heat transfer equation within the layered cable structure. Experience showed that a number of simplifying assumptions could be made.

The solution procedure was confined to the interior of the cable with radiative and convective boundary conditions being set at the cable surface.

The stranded conductor was assumed to be of a uniform material with an appropriate effective density to take account of the voids and with a radial thermal conductivity very much less than the axial thermal conductivity [4]. Axial symmetry could then be assumed.

Axial thermal conduction in the cable was neglected as the heat conduction equation was solved at sufficiently small time intervals, Δt, for this to be a reasonable assumption.

These assumptions simplified the heat transfer equation to:

$$\frac{1}{r}\frac{\partial}{\partial r}\left(r\kappa\frac{\partial T}{\partial r}\right)+q=\rho C_p\frac{\partial T}{\partial t} \qquad (1)$$

where T is the temperature, r the radial distance from the cable axis, κ the thermal conductivity, ρ the density, C_p the specific heat and t the time. Heat is generated within the PE due to reactions associated with the crosslinking process and is represented by q.

Equation (1) was solved within the cable using the method of finite differences. A section of cable was considered as it moved through the manufacturing plant. The section was divided into a number of radial control volumes, Δr in width, appropriate to the cable dimensions. The temperature, thermal conductivity, density and specific heat were assumed to vary linearly within the control volumes.

The boundary conditions at the cable surface involve the convective heat transfer coefficients with dry nitrogen and/or water, the emissivities of the cable and surrounding tube and the temperatures of the media and tube. The boundary condition at the cable surface was established from the heat balance at the surface:

$$\kappa\frac{\partial T}{\partial R}=h(T_m-T)+FS_n((T_t+273.15)^4-(T+273.15)^4) \qquad (2)$$

where R is the cable radius, T_m is the temperature of the surrounding medium, T is the surface temperature of the cable, T_t is the temperature of the tube inner surface, h is the convective heat transfer coefficient at the cable surface and F is a configuration factor given by:

$$F=\frac{1}{1/E_c+(R/R_t)(1/E_t-1)} \qquad (3)$$

where R_t is the radius of the tube, E_c is the emissivity of the cable surface and E_t the emissivity of the tube.

The heat transfer coefficient in the water-cooling zones was taken from various values in the literature and was sufficiently large that variations in its value had little effect on the computer model. The heat transfer coefficient in the nitrogen-cooling zones was calculated as a separate exercise for a range of gas velocities, cable diameters and tube diameters. An empirical function was derived to describe the dependence of the heat transfer coefficient on gas velocities and cable diameter and included in the computer model. Values for the convective heat transfer coefficient were also calculated in the heating zones.

Values of the emissivity of the cable and tube surfaces were assumed and later empirically adjusted.

The transient solution of Eq. (1) was obtained by using the Crank-Nicolson(5) implicit method to move forward in time. The Crank-Nicolson method was chosen as being more robust than either pure implicit or explicit methods. The temperature at nodal position n and at timestep number i for a timestep size of Δt is given by:

$$T(n,i)=T(n,i-1)+\frac{1}{2}\Delta t\left(\frac{\partial T(n,i)}{\partial t}+\frac{\partial T(n,i-1)}{\partial t}\right) \qquad (4)$$

The time derivatives of temperature in Equ (2) were obtained by writing Equ (1) in finite difference form resulting in a set of linear equations which could be solved for the nodal temperatures.

Values for the thermal conductivity and specific heat for the XLPE materials obtained from various suppliers differed by almost a factor of 2. In addition, values obtained from the literature seemed quite variable. Accordingly, the various types of PE were examined using a differential scanning calorimeter to provide specific heat values and also to characterise the heat generated during the decomposition of the peroxide which initiates the crosslinking process.

The thermal conductivity of each PE material was measured by forming a cylinder of the PE, placing thermocouples on the axis and surface of the cylinder and then

heating and cooling the cylinder. The temperature profiles recorded by the thermocouples were stored in an IBM compatible personal computer. A computer model of the PE cylinder was developed in the same way as for the cable so that the temperature profile recorded on the axis of the cylinder could be calculated in terms of the surface temperature profile for trial values of the thermal conductivity which were adjusted until the measured and calculated values agreed. This enabled the thermal conductvity of the PE to be determined in terms of the specific heat over the appropriate temperature range in one experiment. This method had the advantage that the values of thermal conductvity being relative to the specific heat values were those most appropriate for use in the cable computer model. The apparatus constructed for this experiment is shown in Fig. 1

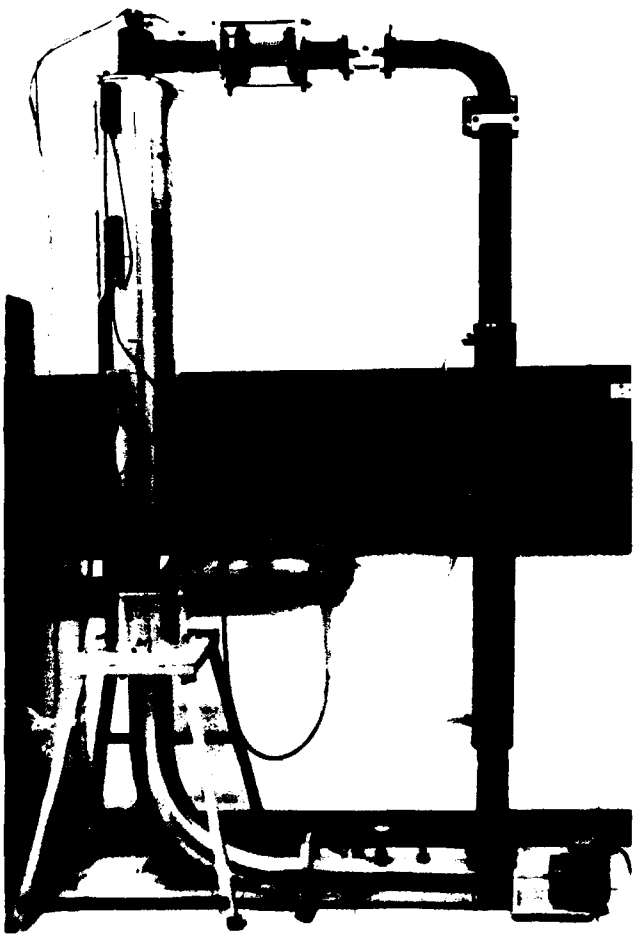


Figure 1. An experimental apparatus to simulate a heating and cooling zone of a pressurised dry cure CV line. The larger diameter vertical section contains the zones and the smaller diameter loop tube allows cooling gas to be recirculated by means of a fan and cooled by a water jacket.

The apparatus was actually a laboratory scale experimental simulation of a heating and cooling zone of a dry crosslinking CV-line. The apparatus could also be pressurised with dry nitrogen so as to simulate manufacturing conditions. A cylindrical sample could be lowered vertically between heating and cooling zones so that temperature profiles experienced by the sample were similar to those experienced by a cable in a pressurised VCV line. The apparatus thus provided a means of crosslinking polyethylene samples in the laboratory so as to verify numerical cure predictions.

These various data were included in the computer program, which existed in various versions, typically occupying less than 130 kbytes of computer memory and running in less than 8 seconds on an IBM compatible 386PC using a co-processor.

An expression relating the degree of crosslinking accumulated in the PE to temperature was included in the program as also was the ability to achieve a set degree of crosslinking by adjusting the speed of the cable.

EXPERIMENTAL RESULTS

Temperature measurements were made on a variety of cables as they passed through the VCV line.

On four experimental cables, a thermocouple was taped to the conductor and fed through the extruder system so as to provide a temperature profile as the cable passed through the plant. This procedure is not without its difficulties, as the presence of the thermocouple can cause the conductor to be asymmetrically located in the extruder resulting in a cable less symmetric than it would otherwise be as there is some manufacturing tolerance on symmetry.

On some of these cables, a thermocouple was also taped to the outer surface of the XLPE, enclosing the cable, and then passed through the VCV line. Measuring the surface temperature of the cable in this way is an extraordinarily difficult procedure as the XLPE at the output of the extruder is hot, perhaps 130°C, and quite soft. Consequently the thermocouple can sink into the polymer and the tape holding the thermocouple in place can restrict the expansion of the XLPE, causing the cable to have a neck at that point. The measurement procedure itself is also difficult because the thermocouples used were of the industrial variety and are relatively robust, and therefore large. Despite these difficulties a number of sensible-looking records of cable surface temperatures were obtained.

In Fig. 2, the best thermocouple measurements of the surface and conductor temperature profiles of a 110 kV cable are displayed together with computer simulations of the profiles followed by the conductor and cable surface during their passage through the plant.

The agreement between calculation and experiment is excellent, particularly when it is remembered that the simulation is of a large industrial plant and not that of a laboratory experiment. The most critical part of the temperature profile is that experienced by the conductor around its maximum value, as it is in this region where the XLPE close to the conductor is crosslinked. It will be seen that the computer program was very successful in simulating the conductor temperature profile around its maximum.

The agreement between measured maximum and predicted maximum conductor temperatures was within a few °C or °F for the four cables measured.

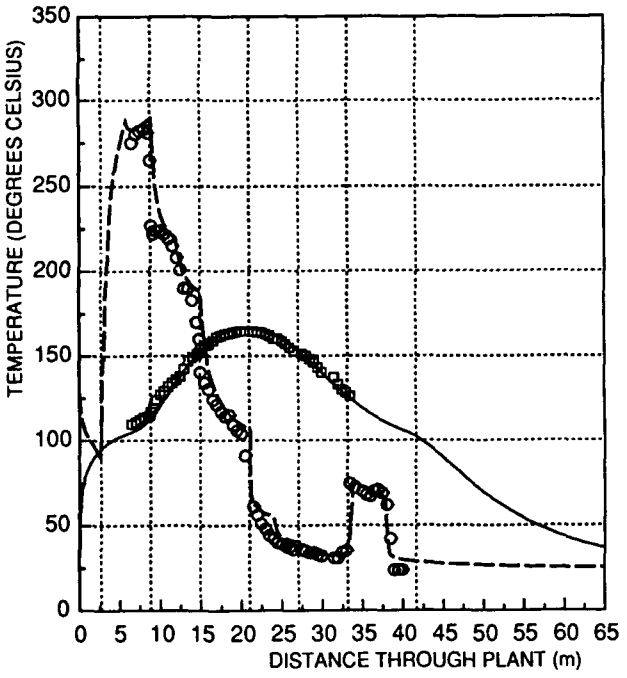


Figure 2. Simulation of the surface(dashed) and conductor(solid line) temperatures for a 110 kV cable on an Olex VCV line. Experimental measurements are represented by circles and squares for the surface and conductor temperature respectively

Additionally a different and less-informative means was also used to measure the maximum temperatures achieved by conductors for a variety of cables as they passed through the plant. A variety of temperature sensitive tapes which change colour permanently on exposure to temperature were placed on the conductors for a wide variety of experimental and production cable. The tape provided a range of values within which the temperature achieved by the tape was expected to be found. This tape performed reasonably well, and a test of a sample of 50 tapes resulted in most lying inside their specification of ±1% of their rating. These tapes were regarded as providing an indication of temperatures to within a few degrees Celsius. The agreement between the maximum temperature achieved by the conductor inferred from the temperature sensitive tape and computer simulations was determined for more than 30 cables. The mean deviation between the two estimates was 3°C over the range, which covered cable of insulation thickness ranging from 3 to 35 mm, *i.e.* covering the voltage range from 6.6 to 330 kV. This is considered to be an excellent result.

It has been established that in most cases actual temperatures measured exceeded, by 10°C or more, the temperatures predicted by existing well known programs. This in turn raises questions concerning the correlation between the time of decomposition of peroxide and the degree of crosslinking of the XLPE insulation as assessed by the hot set method.

Use of the program allows the speed of the cable through the plant to be maximised, while ensuring that the constraints on temperatures achieved by the cable are satisfied and a properly cross-linked cable is produced. The economics of the manufacturing process can thus be optimised.

CONCLUSION

The transient temperature distribution within XLPE insulated high voltage cable during the manufacturing process has been successfully simulated by means of a computer program. The agreement between temperatures predicted by the computer and those measured is excellent. The availability of the program has lead to a better-understood and better-controlled manufacturing process with economic benefits flowing from the elimination of waste and the use of optimal manufacturing conditions.

ACKNOWLEDGEMENTS

We would like to thank the engineers from Olex Cables, for their co-operation in and support of this project.

REFERENCES

1. T. Tanaka and A Greenwood: Advanced Power Cable Technology, CRC Press Inc. Vol II, 1-20 (1983)

2. R. L. Boysen: An Analysis of the continuous vulcanizing Process for Polyethylenes, IEEE Trans., PAS-90, 926-933 (1971)

3. C. A. Kodres and P. J. Phillips: A Numerical Model to Simulate the Processing of Electrical Distribution Cables - Part 1 (Heat and Mass Transfer), IEEE Trans. Elect. Ins. EI-16, No. 6 483-489 (1981)

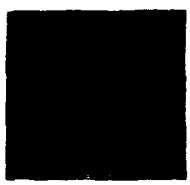
4. V. T. Morgan: The Radial Temperature Distribution and Effective Radial Thermal Conductivity in Bare Solid and Stranded Conductors,IEEE/PES Winter Meeting, Atlanta, Georgia 1990

5. J. Crank, and P. Nicholson: A Practical Method for Numerical Evaluation of Solutions of Partial Differential Equations of the Heat Conduction Type, Proc. Camb. Phil. Soc. 43, 50-67 (1947)



Ronald C Kemp
CSIRO Division of Applied Physics
National Measurement Laboratory
Bradfield Road
Lindfield NSW 2070
Australia

Ronald Kemp was born in Dursley, England. He graduated from the University of Bristol with a BSc Honours Degree in Physics in 1961 and received a PhD from the University of Birmingham in 1964. He then joined the CSIRO Division of Physics, Australia as a Research Fellow. Since then he has worked on electron spin resonance, temperature measurement and standards, heat transfer and more recently on various heat transfer related problems associated with the cable industry. He is now a Senior Principal Research Scientist with the CSIRO Division of Applied Physics.



Alan Stringer
Olex Cables
207 Sunshine Road
Tottenham Vic 3012
Australia

Alan Stringer was born in London, England. He graduated from the City University in London with a BSc Honours Degree in Electronics Engineering in 1979 and a PhD in Electronics and Electrical Engineering in 1984. He joined the Central Research Laboratories of BICC where he worked in the Measurement and Instrumentation Division of the Engineering Research Department. He emigrated to Australia in 1986 where he joined Olex Cables, a Division of Pacific Dunlop, as a Senior Development Engineer and is now the Technical Manager of the Optical Fibre Cables Division in the Communications Group.



Yefim Zlatsin
Olex Cables
207 Sunshine Road
Tottenham Vic 3012
Australia

Yefim Zlatsin received his Engineering Degree - Electrical Engineer Cable Design and Manufacture in 1956 and thereafter worked in the cable industry in the former USSR. He is the author of several inventions and publications. In 1980 he joined Olex Cables Australia, a Division of Pacific Dunlop where he is now a Senior Development Engineer. He is a Member of the Australian Institute of Engineers.

New Developments in Medium and High Voltage Cable with Laminate Sheaths as Moisture Barriers

Kenneth E. Bow

The Dow Chemical Company

Abstract There has been extensive development of moisture barrier medium and high voltage cables as a countermeasure to water treeing. The moisture barrier can take traditional forms including extruded or welded metallic tubes. The latest developments in moisture barrier cable design use laminate sheaths. This paper will discuss the traditional approaches and then present an evolution of the laminate sheath. An overview of the various designs, under-jacket with foil or sheet, or on-core, will be given. Design considerations will also be discussed. Information on deployment in the field and standardization activities will complete the report.

Introduction Where does one begin? As the reader will discover, an immense amount of data and information on moisture barrier cable has emerged. In spite of this body of knowledge on the effectiveness of moisture barriers against treeing and the commercialization of moisture barrier cable, the treeing phenomena is still being researched and studied. Well over a thousand papers have been presented on treeing related research. Great energy is still being expended to understand the mechanism and the material constraints. Yet the three things that cause or accelerate treeing are well known. They are electrical stress, the presence of water and the presence of ionic species. The evidence is indisputable that if moisture and ions are kept out of the insulation, then cable service life is assured. To this end, radial and longitudinal moisture barriers have been developed to the degree that practical, cost efficient cable designs are available. In point of fact, there has been a proliferation of moisture barrier or impervious cable designs in recent years. Field data on performance is starting to emerge and it is excellent.

This paper will overview the evolution of moisture barrier cables and the data that support their use. To set the stage, some background data on the use of jackets to increase moisture resistance will be presented, followed by general construction details with data on performance of moisture barrier sheaths. Details on the types of sheaths in use for both medium voltage and high voltage cable applications comprise the body of the report.

Background A lot of hope is being placed in the use of a cable jacket to provide moisture resistance to a cable. For a long time many medium voltage cables used by utilities in the U.S. were buried directly in the soil without a jacket (i.e., an "open neutral" design was used). This allowed water to contact the semi-conducting insulation screen directly. Neutral corrosion and water treeing led to field problems. Some utilities have been using jacketed cable for over 20 years to successfully control concentric neutral corrosion.[1,2] Recent survey data on the incidence of neutral corrosion indicates that jackets are indeed controlling neutral corrosion.[3]

What about treeing? Do the jackets help? The most comprehensive field data on the effect of polyvinyl chloride (PVC) jackets on treeing has been gathered by Mintz.[4] These data, shown in Table I, indicate that the trees in jacketed cable are not as long as those in unjacketed cables. The relative differences in performance between the jacketed and unjacketed cable on a statistical basis indicate that the use of a jacket resulted in 8% less failures versus the unjacketed cable.

Table I

Percentage of Samples with a Specified Cable Construction Trait and Water Trees Longer than a Specified Length

Jacket	Cables with Treeing Data	Percentage of Cables with Water Trees Longer Than X% of the Insulation Thickness			
		>0%	>25%	>50%	>75%
None	36	92	64	50	33
PVC	17	76	53	29	12

A polyvinyl chloride (PVC) jacket has a significantly higher water vapor transmission (WVT) rate than a polyethylene jacket, as shown in Table II.[5] These data show the effect of density on the rate of permeation as well. Typically, permeation is expressed as a transmission rate per unit thickness at a given vapor pressure and temperature. The data gathered by Hamilton[6] and shown in Figure 1 show the effect of polyethylene density and temperature on permeability of pure polyethylene. The data show that low density polyethylene has about three times the permeability of HDPE. The data of Ferrani[7] for a low density black cable jacketing compound indicate that it has about two

times the permeability of natural polyethylene. Temperature is also a factor. The data indicate that an increase in temperature from 20°C to 40°C doubles the permeability.

Table II

Moisture Vapor Transmission of Black Compounds

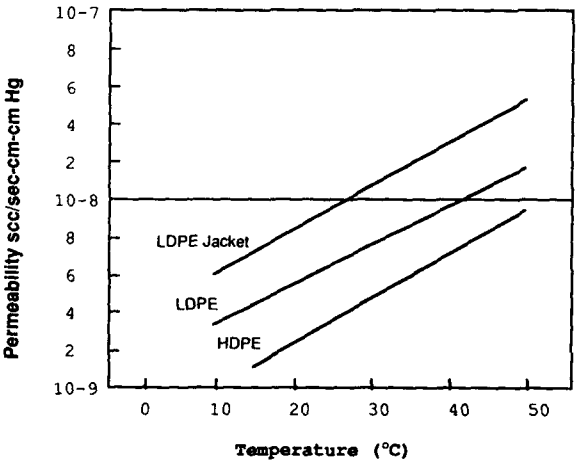
Compound	Base Resin Density (g/cc)	Moisture Vapor[2] Transmission (g/day/m²)
LDPE	.920	1.16
LLDPE	.920	0.74
MDPE	.930	0.51
HDPE	.941	0.58
HDPE	.948	0.32
PVC[1]	1.350	10.0

(1) PVC (90°C rating - 90 durometer pathalate plasticized)

(2) Moisture vapor transmission was run according to ASTM E 96-80 spec at 100°F and 90% R.H.

Figure 1

Permeability of Polyethylene Cable Jacket and Natural Polyethylene as a Function of Temperature



Source: Hamilton[6]

What about the use of polyethylene jackets? Several accelerated aging tests have been done to assess the effects of polyethylene jackets. The data shown in Table III were gathered by Katz, et al.[8] In this case, the cables were aged for 12 months in 31 m (101.7 ft) long coils in ambient temperature water at 2 1/2 times the rated voltage to ground (21.7 kV). The data show that cable with the polyethylene jacket and cross-linked polyethylene (XLPE) insulation has a somewhat reduced deterioration in impulse breakdown (-45% versus -37%), but a slightly greater amount of deterioration in ac breakdown (-38% versus -34%). For the jacketed cable with ethylene propylene rubber insulation, the degradation was greater with the jacketed cable versus the unjacketed (-43% versus -22%). The EPR had the lowest levels of ac and impulse breakdown after aging.

Table III

Results of 12 Month Test Program on 15 kV Cable

		AC Breakdown (V/mil)			Impulse (V/mil)		
Type	No.	Initial	End	Δ (%)	Initial	End	Δ (%)
EPR*	2	575	450	-22	1800	800	-56
EPR	5	840	480	-43	1770	1000	-44
XLPE	3	1375	850	-38	3350	2100	-37
XLPE*	1	910	600	-34	2900	1600	-45

Source: Katz[8]

* No jacket

Data on the effects of jackets and voltage stress have been reported by Landinger.[9] The samples were wet aged in water-filled insulated 3" (76.2 mm) PVC conduit with a 90°C maximum cycled conductor temperature. The vol-tage applied was 52 kV conductor to neutral. The results are shown in Table IV. They indicate that the use of a polyethylene jacket increases the time to failure. The data also indicate that reduced electrical stress increases the time to failure.

In summary, the data of Landinger generally indicate that a jacket is helping to retard electrical degradation, but, in comparison with the data of Katz, the effect may be test dependent. In both tests deterioration is taking place with a jacketed cable indicating that a jacket is not a permanent barrier to moisture ingress.

Table IV

Effect of Jacket and Voltage Stress on 35 kV Cable

Insulation Thickness (Inch)	Jacket	V/Mil	Time to Failure Day*	Failed at Test End** (%)
0.260	NO	200	101	100
0.260	YES	200	350	83
0.345	NO	150	448	79
0.345	YES	150	1090	33

Source: Landinger[9]

* Time at which 50% of the samples failed

** Test terminated at 1,031 days

None of these studies has taken into consideration the effect of ions in the soil water. Groeger[10] in a 1991 symposium paper demonstrated that ions were present in field aged cable as shown in Table V. These data indicate that ions contained in the soil can eventually find their way into the insulation. The rate at which they penetrate is dependent on the type of cable construction. Cables aged without a jacket have significant ionic contamination when compared to the unaged specimen. Cables with jackets have less ionic penetration. The cables with intact metallic moisture barrier, in this case a lead sheath, appear to be immune to the problem of ionic contamination. Groeger has also shown that the rate of vented water tree growth correlates with the presence of ionic impurities in the shielding materials.[11] He concludes "while ions present in cable materials play a significant role in the aging of cables, the ingress of ions associated with ground water dominates the system. Polymeric jackets afford limited long-term protection of the underlying cable components. Metallic moisture barriers

effectively exclude all extraneous ions, as long as they remain intact. Due to the influence of external ions, clean cable materials alone, in the absence of adequate moisture protection, will not assure long cable life."

Table V

Ion Concentration in Cable Insulation
Showing Effectiveness of Various Jacketing Materials

Jacket	Aging Condition:	Water-Soluble Ion Concentration (ppm) None	Intact	Punctured
PVC		125	850	1300
HDPE		220	1100	1000
None		300	1800	N/A
Lead		240	260	2100

Source: Groeger[10]

Moisture Barrier Cable Designs

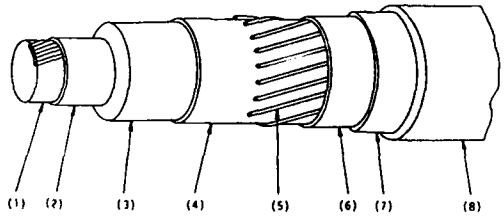
This background now brings us to the topic of moisture barrier sheaths and the theme of this paper.

There are four principal designs for moisture barrier power cable. The first is an under-jacket type that uses a laminate metallic moisture barrier over the neutrals of the cable. In the second under-jacket type, the laminate moisture barrier serves both as an electrical shield and moisture barrier. The third type is an on-core laminate moisture barrier in which the moisture barrier is a thin foil applied directly to the surface of the insulated conductor. The fourth type is an extruded or seam-welded metallic sheath. Each of these designs will be described in more detail.

Under-Jacket Laminate Moisture Barrier With Wire Neutral There are two variations of the under-jacket moisture barrier cable with wire neutral. The first variation uses a relatively thick (0.10 - 0.20 mm, 0.004 - 0.008 inch) metallic sheet over the neutrals. The second variation uses a relatively thin (0.5 mm or 0.02 inch) foil over the neutrals. The general construction is illustrated in Figure 2. The neutrals are retained for shielding and grounding purposes and are chosen according to the user's perceived short circuit considerations.

Figure 2

Cable Construction



(1) Conductor
(2) Conductor shield
(3) Insulation
(4) Insulation shield
(5) Copper wire shield
(6) Binder or water swellable tape
(7) Moisture Barrier
(8) Jacket

In both variations, a plastic coated metallic tape (metal plastic laminate) is longitudinally formed in a smooth configuration over the neutrals. The tape is chosen such that its coatings are adhesively compatible with jacket. Laminates are available which are compatible with various types of jackets such as chlorinate polyethylene, polyethylene, zero-halogens, and polyvinyl chloride.[12] The coatings are bonded to the cable jacket during the jacket extrusion process. The choice of wrap over the neutrals varies. Semi-conducting water swellable tapes are typically used with the thicker laminates while various types of non-conducting binder tapes are used with the foils.

The main benefits of using a laminate with the thicker metallic sheet are greater mechanical strength and assurance of a pinhole-free moisture barrier. Bonding the thicker laminate to the cable jacket gives the cable improved mechanical properties such as bend performance, impact or crush resistance, and improved side wall pressure capabilities. The use of sheet over 0.1 mm (0.004 mil) insures that pinholes and defects from the metal rolling process are relatively improbable and provides a metallic plastic laminate of sufficient thickness to achieve improved mechanical performance. The use of water swellable tapes over and/or under the neutrals allows for a longitudinal water block at the moisture barrier–neutral–core interface.[13] The water swellable tape can also serve as a cushion layer to handle thermal expansion. Typically a hot melt adhesive is placed in the overlap to insure a sufficient seal. This blocks both radial and longitudinal moisture flow through the overlap. (Interestingly, the concept of a sealed overlap as a moisture barrier was introduced over 25 years ago at this very symposium.[14] It's gratifying to see that the principles of performance for the sealed overlap as described in that paper are still valid today.) Finally, if a strand-filled conductor is used, the cable can be described as moisture impervious. A strand-filled or solid conductor forms a longitudinal water block in the conductor to go with the radial and longitudinal waterblocks of the sheath.

Most often a lead foil laminate is used with the second type of under-jacket moisture barrier. Typically, the lead foil is 50 microns (0.002 inch) thick. It is reinforced with a plastic layer 50 microns (0.002 inch) thick and an outer adhesive layer 50 microns (0.002 inch) thick. This adhesive layer bonds the foil to the jacket. A semi-conductive binder tape is wrapped over the neutrals to protect the moisture barrier from damage. This binder tape can be 100 to 300 microns (0.004 to 0.012 inch) thick. The lead foil laminate has some ability to expand and contract with the core allowing the cable to endure thermal loading. Lead is also preferred over aluminum or copper foil because of corrosion resistance and greater ability to withstand thermal expansion.

Under-Jacket Laminate Moisture Barrier Having Combination Moisture Barrier and Shield There are two variations of the under-jacket design. In one design, a metal plastic laminate is used as the combination shield or moisture barrier. Typically, the laminate is a plastic coated copper sheet.[15,16] The

thickness of the copper component of the laminate can range from 0.125 to 0.25 mm (0.005 to 0.010 inch). The metal plastic laminate may be one or two side coated. The one side coated provides a bond to the jacket and the bare side allows electric charge transfer from the core. Two side coated laminates may require semi-conducting coating to contact the core for charge transfer. Two side coated products with semi-conducting coatings enhance seam sealing and provide additional corrosion protection to the metallic component of the laminate.[17]

The laminate can be applied smooth or corrugated. The use of corrugated laminates is on the increase due to a number of factors. First the mechanical properties of the cable, bend performance in particular, are significantly improved by bonding the corrugated shield to the jacket. Second, the longitudinally applied corrugated shield provides electrical and mechanical improvements over helically-applied copper-tape shields. Third, the field experience in power cable with the corrugated shield has exceeded 20 years. This experience has been excellent. Fourth, hot melt adhesives have been developed which allow the overlap to effectively be sealed. At the same time, these hot melts are flexible enough to allow the overlap to give during thermal loading to accommodate some of the thermal expansion of the core.

On-Core Laminate Moisture Barrier In this third type of construction, a plastic metal laminate is used that consists of semi-conducting adhesive coatings on both sides of a lead foil.[18] The coating and foil are 0.05 mm (0.002 inch) thick. The moisture barrier laminate is placed directly over and sealed to the semi-conducting insulation screen of the cable core. The laminate is designed to expand and contract with the cable core. A semi-conducting bedding tape is then wrapped over the moisture barrier in order to protect the moisture barrier from the potential indenting effect of the neutral wires. These wires form the next layer in the cable construction and are placed over the bedding tape. Finally, the cable is jacketed with the desired type of jacketing material.

The principal feature of the on-core design is that by having the moisture barrier on the core, direct water contact with the cable core is prevented. Water may enter the neutral wire jacket interface, but it is radially blocked from the core over the entire length of the cable. It's noted that the laminate requires special properties in order to expand and contract with the cable core. The material considerations and testing of on-core moisture barriers has been extensively covered.[19,20]

Metallic Sheaths The fourth type of moisture barrier consists of a longitudinally formed and seam welded corrugated copper or aluminum sheet. Extruded lead or aluminum sheaths are also used. These sheath technologies have been in use for over 30 years and are quite familiar to the industry.[21] The metallic thickness can be chosen to give an adequate cross section so that it can be used as a combination shield/moisture barrier. Alternatively, a layer of concentric wires can be used as a screen beneath the metallic sheath. The sheaths may be protected on their outer side by a jacket or oversheath of extruded polymer. The welded sheath is finding use in high voltage applications in commercial power systems and for submarine applications such as lake crossings.[22]

Testing and Applications of Moisture Barrier Cable

In this section, the various applications of moisture barrier cable will be discussed. Appropriate test data as developed for this particular design will be presented. Finally, any available field data that has been developed for the design will be presented.

Lead Sheathed Cables Lead sheaths are one of the oldest forms of protection for cables, both power and telephone. General reader familiarity means there is little need to discuss lead sheath construction. Recently, however, Groeger has been able to document the degree of protection which lead sheaths have provided to synthetic insulation on medium voltage cable.[23] The data is quite informative, both from a historical point of view (i.e., the length of service history covered being 20 to 40 years) and from the technical point of view where the effectiveness of a metallic sheath as a barrier to moisture and ions can be documented. The data shown in Table VI were gathered by comparing the portion of a field aged cable with the sheath intact to the area where the sheath had been punctured, thereby exposing the core to water from the environment. As shown in Table VI, those locations containing a puncture were found to contain many vented water trees, a high concentration of water-extractable ions, and significantly reduced ac breakdown strength. The locations where the lead was intact were found to contain no detectable water trees, low levels of water extractable ions, and high ac breakdown strength. These cable were recovered from a urban environment where the cables had been installed in concrete ducts. Since this was a coastal location, the cables were frequently submerged in water containing salt. Concurrent work has shown that the ions such as those permeating into the insulation from the ground water are a key factor in tree initiation and growth.[24,25]

Table VI

Insulation Characteristics of Lead-Sheathed HMWPE Insulated Cables, Field-Aged Twenty Five Years, Comparing Protected and Non-Protected Areas of the Same Cable

Years of Service	Condition	Insulation	Ion Concentration (ppm)	Avg. Vented Tree (mm)	AC Breakdown Strength (kV/mm)
25	Intact	HMWPE	136	0.0	17.30
25	Punctured	HMWPE	1520	1.12	5.00
25	Intact	Butyl Rubber	354	0.0	13.25
25	Punctured	Butyl Rubber	2000	1.50	4.25

Source: Groeger[10]

Plastic Coated Aluminum or Copper as Combination Shield and Moisture Barrier One of the first installations of a moisture barrier medium voltage power cable design started in 1974 in Sweden.[26] A longitudinally formed copolymer coated aluminum was applied smooth over a triple extruded cross-linked polyethylene core. The single side coated aluminum was 0.30 mm (0.012 inch) thick and bonded to a cross-linked polyethylene jacket. A semi-conducting crepe paper tape was used to provide a thermal expansion layer between the aluminum shield and the cable core. More than 3000 km of the cable has been in use since 1974 with no failures attributed to water treeing. The development of this construction was driven by the need for a compact and low cost single conductor medium voltage cable for underground distribution.

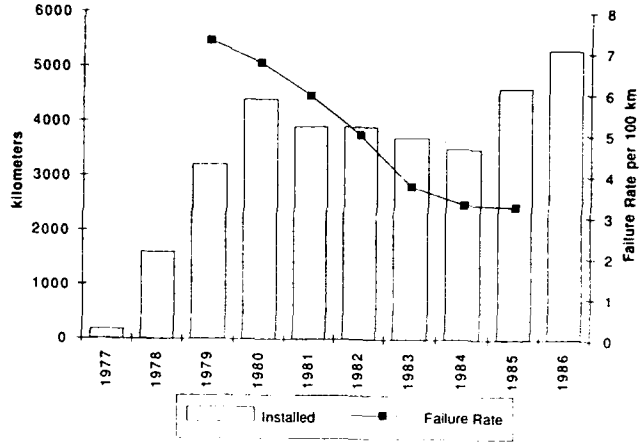
One of the largest applications of medium voltage cable with a plastic coated aluminum moisture barrier began in France in 1978.[27] The description of the cable, beginning from the outside, is as follows. The cable has an outer jacket or oversheath of a relatively thick (2 mm or 0.120 inch) polyvinyl chloride jacket to facilitate direct burial. Radial water tightness is achieved by way of an aluminum shield 0.10 mm (0.004 inch) thick which is longitudinally folded and bonded to the PVC oversheath. The sealing of the overlap is facilitated with a hot melt adhesive. Thermal expansion is handled by longitudinal grooves in the extruded semi-conducting insulation screen. The grooves compress during thermal loading to absorb the thermal expansion of the core. The grooves are filled with a swellable powder which expands upon contact with water to block the longitudinal flow of water in the shield–core interface. The cable meets the EDF Standard HN 37-S-23. The cable technology is fully developed and includes connectors for the moisture barrier, accessories, joints, and installation practices. The connectors do not require the jacket to be stripped. The connector slips between the core and sheath into the aluminum shield. The connector is clamped into place.

The field experience with this design has been excellent. At the end of 1986 a total of over 33,000 km of this cable, as a three phase network, has been installed. Figure 3 shows the lengths of the cable installed per year versus the failure rate per 100 km of circuit/yr. The mean national fault rate for all causes and all cable types combined has steadily decreased as more and more moisture barrier cable has been installed.

A laminate sheath with 0.5 mm aluminum to replace lead sheaths in high voltage (90 kV) applications has been developed by EDF.[28] The cable sheath met 10 kA fault current requirements for 0.5 - 2.5 seconds. The reliability of the sheath was proven by a series of tests for resistance to mechanical impact, abrasion and tearing, short circuit, corrosion, and moisture. A 6000 hour test was used to analyze thermo-mechanical behavior. The use of the laminate sheath reduced the weight of the cable versus lead by factors of 1.7 to 2.7, depending on cable diameter.

Figure 3

Use of Watertight Cable by Electricite De France



[1] Lengths of cable installed annually (km of three phase network)

[2] Failure rate per 100 km of circuit/year (all causes and cable types combined)

Prototype cables using plastic coated aluminum (0.19 mm or 0.008 inch) or plastic coated copper (0.15 mm or 0.006 inch) as moisture barrier were tested for moisture permeability.[29] The tests were conducted by filling 18 inch (0.4 m) samples of cable with water, covering both ends with aluminum caps, and sealing the caps with epoxy. The water filled cables were placed in an oven at 40°C and weight loss was measured monthly for five months. As a control, a hollow polyethylene tube of the same dimensions was sealed in the same fashion and subjected to the same conditions. The cable with metallic barriers exhibited no weight loss while the control showed substantial weight loss indicating high moisture permeability. The results are shown in Table VII. The study concluded that "the moisture barrier metal foil/polyolefin laminates protect the cable against moisture permeation without an adverse effect on the mechanical properties of the cable."

Table VII

Moisture Permeability of Extruded Cables

Moisture Barrier	Coating Type	Jacket Type	Moisture Permeability (g/5 months)
Coated Copper	Insulating	Conductive	0.0
Coated Aluminum	Insulating	Conductive	0.0
Coated Copper	Semi-Conducting	Conductive	0.0
Coated Aluminum	Semi-Conducting	Conductive	0.0
None	N/A	Polyethylene	14.5

Source: EPRI[29]

The Canadian Electrical Association sponsored a study to measure the effectiveness of moisture barriers.[30] The cable that was studied had a plastic coated aluminum moisture barrier (aluminum thickness of 0.2 mm or 0.008 inch). Samples of the cable with the moisture barrier were sealed with a port. Then 0.105 g/m of a water solution (0.2N NaCl) was injected into

the port. The control cables were immersed in the same solution with the moisture barrier removed. The cables were energized to 26.3 kV at room temperature for one year. After aging, an ac breakdown test using 5 minute voltage steps was conducted and water tree counts were taken of the insulation. The results are given in Table VIII. The difference in the ac breakdown voltage of the control cables, the dry cables, and the cables that were injected with water were well within the 90% confidence limits of the data. The cable saturated with water showed a significant reduction in ac breakdown. The water tree data indicated that the cable saturated with water had both streamer trees and bow-tie trees. The study concluded that "metal/polyethylene laminate moisture barriers can be very effective in reducing the ingress of moisture into the cable to the extent that water treeing is not a problem".

Table VIII

AC Breakdown Data Summary of 30 Dry-Cured XLPE Cables After the One Year Aging Test

Moisture Barrier	Water Content	Aging Voltage (kV)	Breakdown Strength (kV) Upper	Average	Lower
Coated Al	0.105 g/m	0	225.9	195.3	170.2
Coated Al	0.105 g/m	26.3	238.4	214.4	194.1
Coated Al	As Is	26.3	257.7	225.7	199.8
None	Saturated	26.3	102.6	89.7	79.3

From: CEA[30]

Plastic Coated Aluminum or Copper as Moisture Barrier Over Cable with Wire Screen Metal plastic laminates have been introduced to protect cables with metallic screens from the radial ingress of moisture.[31] The screen is retained to allow the cable users to meet their perceived needs for circuit protection. Typically the application of the laminated tape is in combination with swellable non-woven water blocking tapes over and/or under the metallic screen to protect the cable completely from radial and longitudinal entry of moisture.

One of the first installations of 220 kV cable with a moisture barrier in normal power network service took place in the Federal Republic of Germany in its Bergheinfeld transformer station in Bavaria.[32] The cable was insulated with cross-linked polyethylene. It had a core diameter of 95 mm (3.8 inches) and was fabricated on a horizontal machine using the MDCV method. A conductive paper wrapping was placed over the extruded semiconductive screen. This in turn was covered by the copper wire screen. The screen zone incorporated water swellable tapes to limit the longitudinal penetration of water to a limited area in the event of sheath damage. The sheath consisted of a polyethylene jacket laminated with coated aluminum (0.2 mm or 0.008 inch) to protect the insulation from the radial ingress of moisture through the intact sheath. The aluminum was applied longitudinally and bonded to the jacket and sealed at the overlap to provide the radial water-tightness. Improved mechanical properties also resulted from the laminate sheath which afforded additional protection against external mechanical impacts. Similar cable designs were developed for the voltage range 60 – 150 kV.

Another variation of the design for 64 and 76 kV service uses plastic coated copper.[33] This design consists of a layer of flat copper straps covered by swelling tapes and a laminated longitudinally overlapped copper tape. A semi-conductive bedding tape provides the mechanical and thermal contact between cable core and sheath while allowing for different rates of thermal expansion for the materials. A high density polyethylene oversheath is used for the outer protection. A 64 kV version of this cable has been tested for 2504 hours with a 10-hour-on/14-hour-off load cycle with no breakdown. An alternate version uses a 0.20 mm coated aluminum as the moisture barrier and aluminum strap as the neutral.

Medium voltage versions of the underjacket moisture barrier with wire neutral have been developed and are undergoing trial installations. One version of a 35 kV cable was subjected to extensive testing. It used a reduced concentric neutral wire screen and a plastic coated copper (copper thickness 0.125 mm or 0.005 inch) as the moisture barrier.[34] Semi-conducting water swellable tapes were placed over and under the wire screen. The copper was longitudinally applied. The overlap was sealed with a hot melt adhesive. The outer protection was a linear low density polyethylene jacket. This cable was tested for thermal loading, water blocking, and mechanical properties. A discussion of these results follows.

Table IX

Thermal Loading Test Results for Moisture Barrier Cable With 0.125 mm Copper Laminate

Test	Max. Cond. Temp. (°C)	No. of Cycles	Dissipation Factor (%)	Adhesion in N/mm Oversheath*	Overlap*
AEIC (in conduit)	130	20	<0.1	<2.01 / 2.22	9.96 / 4.54
IEC (in air)	90	20	<0.1	<2.01 / 2.45	9.96 / 4.47

* Initial / After Test

As shown in Table IX, the cable withstood 20 thermal load cycles to 130 and 93°C conductor temperatures. No mechanical damage was found at either temperature. Jacket bond and overlap seam seal strengths remained intact after both the 130 and 93°C load cycling. Dissipation factor measurements were below 0.1% indicating good electrical contact between the copper moisture barrier and the insulation shield. The water blocking tapes effectively stopped longitudinal water flow at 16 inches (406.4 mm) from the point of entry while being cycled to 93°C. The test indicated that water-swellable tapes can act both as a cushion for thermal expansion and as a water block in the longitudinal direction.

The mechanical properties of this cable were examined using a sidewall bearing pressure test, the results being shown in Table X. Cable samples pulled at sidewall bearing pressures of 1600 (23.4 kN/m) and 2000 lb/ft (29.2 kN/m) radius did not suffer damage.

Some minor wrinkling was observed in the overlap of the shield due to the stretching of the jacket during the pull, but the jacket bond and overlap seam seal values remained intact. There was no physical damage to the cable core. The data indicate that a bonded sheath should enhance the cable installation process.

Table X

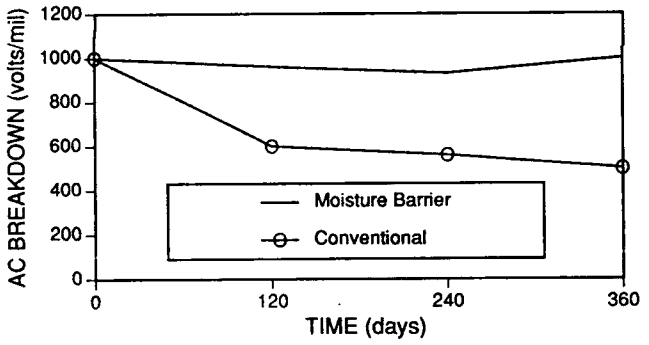
Side Wall Bearing Pressure (SWBP) Test Results for Cable with 0.125 mm Copper Laminate Moisture Barrier

SWBP (kN/m)	Core	Adhesion in N/mm Oversheath*	Overlap*
23.4	No Damage	2.01 / 2.89	9.86 / 10.47
29.2	No Damage	2.01 / 2.77	9.86 / 8.93

* Initial / After Test

An aluminum alternate version of this cable used a aluminum neutral and a coated aluminum (0.19 mm or 0.0075 inch) moisture barrier.[35] Samples of this cable were tested for thermo-mechanical properties in water filled insulated conduit at 90°C (194°F). The ac breakdown strength of this cable and a control cable, which was a conventional unjacketed open neutral design, was determined periodically. The results are shown in Figure 4. Note that the breakdown strength of the conventional design fell rapidly in the first 120 days of aging to about 600 V/mil, and then more gradually thereafter. The cable with the moisture barrier remained constant at about 1000 V/mil.

Figure 4



Welded and Corrugated Sheaths The use of longitudinally welded and corrugated sheaths for protection of cable from moisture is a technology with a long history.[36] The key to using this sheath design for higher voltage cables has awaited developments in the materials as well as the extrusion and vulcanization processes.[37] With the introduction of the horizontal MDCV process, triple extrusion, and insulating materials with fewer contaminates and smoother surfaces, it is now possible to use welded sheaths for high voltage applications. The principal advantages of the welded sheath are inherent water tightness and ability to be sized for use as the cable screen. Extensive type and long term tests of the copper sheath at various voltages have been conducted. The test sequence for the type tests consisted of 3 reverse bends around a 25X diameter mandrel, partial discharge, dissipation factor, 20 heating cycles with a 100°C - 105°C conductor temperature, repeat of partial discharge, impulse voltage, and power frequency voltage test. The long term test consisted of thermal cycling with a 10-hour-on/14-hour-off cycle to the 90°C rated temperature. The results of the long term test is shown in Table XI. The test results as of December 1990 indicate service life in excess of 40 years. Alternate versions using welded and corrugated aluminum are also commercial.

Table XI

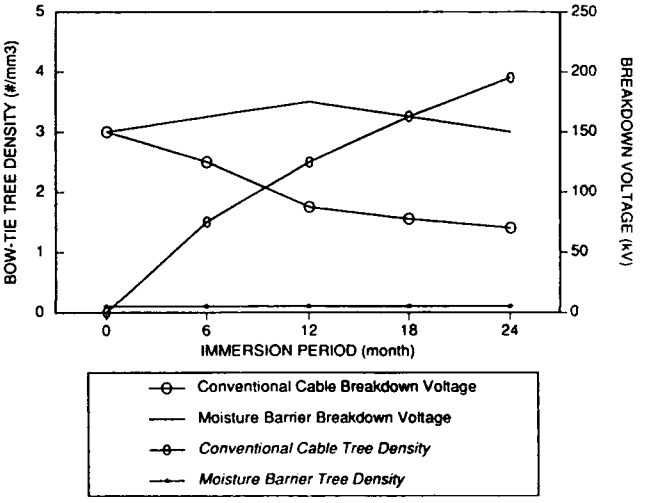
Summary of Long Term Test Results on Polymer Insulated Cables With Combination Shield/Moisture Barrier of Welded, Corrugated Copper

Type of Cable	Test Voltage (kV)	Dielectric Stress (kV/mm)	Service Hours	Comment
60 kV/500 mm^2	80	9.7	60686	no breakdown
110 kV/500 mm^2	140	13.1	44576	no breakdown
150 kV/500 mm^2	195	15.2	19368	no breakdown
230 kV/800 mm^2	195	11.8	5319	no breakdown
230 kV/800 mm^2	250	15.1	4050	no breakdown

Note: Status December 1990

Lead Laminate Moisture Barrier Cable Use of lead laminate moisture barriers is primarily a Japanese development. The prototype for the currently produced cables was first made in 1975.[38] A lead foil 0.05 mm (0.002 inch) is used as the moisture barrier. The lead foil is used because laminating polymer layers to the foil makes it possible for the foil laminate to expand and contract with the cable. The lead forms a single unit when in laminate form and acquires the plastic properties of the polymer layers. Both underjacket and on-core versions are commercial. The underjacket design was specified as standard by Tokyo Electric Power Company in 1984 for 66 kV and 154 kV cables.[39,40] Resistance to treeing was used to justify the change. The data shown in Figure 5 illustrates the effectiveness of an "on-core" metallic water barrier in reducing tree density as compared to a jacketed cable.

Figure 5



As a consequence of reduced tree density, the breakdown voltage of the insulation is maintained at a level consistent with its original value. These data were gathered by immersing cables jacketed with a PVC jacket with and without a metallic moisture barrier in water at 70°C (158°F) with 15 kV applied. The data aptly illustrate a cause and effect relationship between tree growth and a major reduction in cable breakdown strength.

The on-core type has been used in the United States for 15 kV and 35 kV for underground residential distribution service. Over 4000 km (2500 miles) has been installed by a large east coast utility. Much of this cable is 1000 mcm (507.0 mm^2) aluminum, 35 kV with XLPE insulation. Recently, a test program was initiated to check the condition and performance of this cable after seven years of service.[41] Cable manufactured near the start of the program was obtained and its ac breakdown and lighting impulse breakdown strength was compared to field aged samples and newly manufactured cable samples. The data shown in Table XII indicate that there was no significant deterioration of the cable electrical properties after seven years of service. A thorough, microscopic wafer examination of the field samples showed no electrochemical treeing.

Table XII

Lightning Impulse Breakdown Values

Sample Type	Average kV/mm	(V/mil)
New	115	(2921)
Unaged	145	(3683)
Field-Aged	135	(3429)

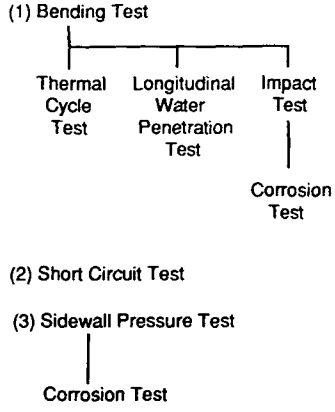
Standardization Activities for Moisture Impervious Cable

IEC Activities IEC 840 – "Tests for Power Cables with Extruded Insulation for Rated Voltages Above 30 kV Up to 50 kV" was published in 1988. At that time, the "water penetration test" (paragraph 5.6.16) was under consideration. An IEC working group was busy defining this test. A draft document, 20A(CO)99, under the six months rule, was later published as a secretariat document under 20A(Secretariat)164. This document describes a water penetration test for those cables where barriers to longitudinal penetration have been included. The test is applicable to barriers applied over the core and within the conductor. The water penetration test is applied after a length of cable has been subjected to the bending test. A 50 mm wide ring is removed from the center of the length including layers external to the insulation screen or, alternatively, the conductor. A tube at least 10 mm in diameter is placed vertically over the exposed ring and sealed to the surface of the oversheath. Normally tap water is used to fill the tube. A period of five minutes is allowed for filling. The height of the water in the tube is 1000 mm above the center of the cable. The water is allowed to stand for 24 hours. The sample is then subjected to 10 heating cycles. The conductor is heated until it reaches a temperature not less than 5°C or more than 15°C above the maximum rated temperature of the insulation in normal operation. The heating cycle is 8 hours on and 16 hours off.

A working group of CIGRE Study Committee 21 has prepared recommendations on tests for high voltage cables with synthetic insulation and laminated protective coverings as moisture barriers.[42] These tests will supplement those of IEC 840, First Edition, 1988. The recommendations were published in the Electra journal in 1992. The test sequence is shown in Table XIII.

Table XIII

CIGRE Recommended Test Procedure for High Voltage Cable



IEEE /ICC Task Group 6–23 Activities ICC Task Group 6–23 has undertaken, and is nearing completion, the preparation of an IEEE standard entitled "Guide on the Design, Testing, and Application of Moisture Impervious, Solid Dielectric, 5 – 35 kV Power Cable Using Metal/Plastic Laminates".[43] The task group is composed of representatives from utilities, industries, cable manufacturers, distributors, and materia! suppliers. As presently constituted, the guide includes sections on moisture barrier cable designs, metal/plastic laminates used for moisture barriers, cable performance and testing criteria, and installation guidelines. Also included is a complete bibliography of technical papers, patents, and specifications applicable to cables designed to preclude the effects of moisture.

Conclusions

There is overwhelming evidence that the use of moisture barriers on medium and high voltage power cables will solve the problem of water treeing. Alternately, however, the data is mixed on the effectiveness of a cable jacket or oversheath as a barrier to moisture. Penetration of ionic species from the soil through the jacket and into the insulation has been documented. Ionic contamination of the insulation has been shown to be a factor in water tree initiation and accelerated tree growth. Moisture barriers have been shown to be effective in keeping ions from the soil water from penetrating into the insulation.

There are many choices for a moisture barrier. Traditional lead sheaths or welded or extruded metallic sheaths have been shown to be effective moisture barriers. The evolving technologies are taking advantage of metal plastic laminates. Several different designs have been commercialized using laminates. A laminated metallic foil may be bonded to the oversheath. The foil is relatively thin (0.05 mm or 0.002 inch) and serves strictly as a moisture barrier. A relatively thicker plastic coated metallic sheet (0.125 to 0.25 mm) can also be bonded to the oversheath. In this case, the sheet can be used as the electric screen, can supplement the screen, or act simply as a moisture barrier. In any case, the cable receives mechanical reinforcement by bonding. Finally a laminated metallic foil can be applied over the insulation screen. In this case, the foil expands and contracts with the cable core. It serves strictly as a moisture barrier.

Material technologies for the metal plastic laminates have advanced as well as technologies for sealing the overlapped laminates with hot melt adhesives. Semiconducting coatings, coatings compatible with PVC jackets, and copper laminates have been developed. Non-woven water swellable tapes have been commercialized which allow the sheath interfaces to be blocked to the longitudinal flow of water. They may also act as cushion layers to accommodate thermal loading. As a consequence, moisture impervious cable designs with both radial and longitudinal water blocks have emerged.

Standardization activities for moisture blocked cable are proceeding in IEC, CIGRE, and the Insulated Conductors Committee (ICC) of the IEEE. These activities are fostering growing use of moisture barrier cables.

REFERENCES

1. R.H. Stevens, "Residential Underground Systems at Florida Power and Light Company", *Conference Record, IEEE Special Technical Conference on Underground Distribution, May 1969.*
2. A.S. Jones, "Utility Experience with Concentric Neutral Power Cables – With and Without Jacket", *Paper No. 234, Corrosion/1978.*
3. J.G. Valdes, *Appendix VI-C, Minutes of the Insulated Conductors Committee of the IEEE Power Engineering Society, 82nd Meeting, Spring 1988.*
4. J.D. Mintz, "Failure Analysis of Polymeric-Insulated Power Cable", *Paper No. 84 T&D 345-5, 1984 Transmission and Distribution Conference, Kansas City, MO.*
5. E.J. Fischer, "Polyethylene Jacketing Compounds", *Appendix VI-A, Minutes of the Insulated Conductors Committee of the IEEE Power Engineering Society, 75th Meeting, Fall 1984.*
6. R.L. Hamilton, "Water Vapor Permeability of Polyethylene and Other Plastic Materials", *The Bell System Technical Journal, February 1967.*
7. A.G. Ferrari, "Determining Permeability Constants of Wire Insulation and Cable Jacket", *Modern Plastics, June 1964.*
8. C. Katz, N. Walker, J. Dyndul, "Comparative Evaluation by Laboratory Aging of 15 kV and 34 kV Extruded Dielectric Cables", *Paper No. 89 TD 366-6 PWD, IEEE/PES, 1989 T&D Conference, New Orleans, LA.*
9. C. Landinger, *Appendix V-D, Minutes of the Insulated Conductors Committee of the IEEE Power Engineering Society, 85th Meeting, Fall 1989.*
10. J.H. Groeger, M.S. Mashikian, "Long-Term Service Degradation of Polyethylene and Rubber Insulated Power Cables", *International Wire and Cable Symposium Proceedings, pp. 388-396, 1991.*
11. M.S. Mashikian, J.H. Groeger, "Ageing Phenomena at Cable-Shield Interfaces Affecting the Propensity of the Insulation to Develop Water Trees", *Paper A.8.3, Jicable '91, Third International Conference on Polymer Insulated Power Cables, pp. 206-213.*
12. K.E. Bow, D.G. Pikula, B.K. Grosser, P.B. Leng, "Coated Metals Compatible with PVC Jackets for Bonded Sheath Cable Applications", *Antec '88, pp. 439-442.*
13. B.J. Nieuwhof, "Conductive and Non-Conductive Waterswellable Nonwovens for Longitudinal Waterblocking", *Jicable '84, International Conference on Polymer Insulated Power Cables., pp. 510-503.*
14. R.C. Mildner, W.E. Ropp, J.H. Snow, "The Evolution of Sheath Constructions for Communications Cable", *15th Annual Wire and Cable Symposium, Atlantic City, NJ , December 1966.*
15. K.E. Bow, B.K. Grosser, D. G. Pikula, "Coated Copper Shielding Tapes for the Wire and Cable Industry", *International Wire and Cable Symposium Proceedings, 1985, pp. 51-60.*
16. K.E. Bow, "Moisture Barrier Power Cable with a Plastic-Metal Laminate Sheath", *Jicable '84, International Conference on Polymer Insulated Power Cables, pp. 217-224.*
17. K.E. Bow, B. Bieringa, J.W. Smith, K. Zuercher, "Semiconductive Plastic Coated Metallic Shielding and Armoring Materials for Power Cables", *Paper A.1.3, Jicable '91, Third International Conference on Polymer Insulated Cables, pp. 12-18.*
18. T. Uchiyama, K. Ohata, T. Uematsu, T. Tanabe, Y. Takayama, "Development of Waterproof XLPE Cable", *Proceeding of the 52nd Annual Convention of the Wire Association International, Inc., Pittsburgh, PA, October 17-21, 1982, pp. 44-51.*
19. H. Furusawa, et al., "Water Impervious URD Cable Having Lead Foil on Conductor and on Core", *IEEE Transactions on Power Delivery, Vol. PWRD-1, No. 1, 1986, pp. 51-57.*
20. T. Uematsu, et al., "Thermal Fatigue Properties of Water Impervious Cable", *IEEE Transactions on Power Delivery, Vol. 5, No. 3, July 1990, pp. 1231-1238.*

21. K. Andresen, C.R. Stein, "Communication Cables with Welded and Corrugated Metallic Sheaths", *Paper No. 253, Eleventh Wire and Cable Symposium, 1962 (AD-6560701).*
22. H. Zimmerman, M. Schwarz, W.E. Mathis, "Results for Long Term Performance Tests on Polymer Insulated Cables up to 230 kV", *Proceedings of the 1991 Transmission and Distribution Conference, 91 CH3070-0, pp. 176-179.*
23. Ibid, Groeger, *Jicable '91.*
24. M.S. Mashikian, J.H. Groeger, "Ionic Impurities in Extruded Cable Insulation: Analytical Detection Techniques, Sources, Nature and Effects", *Jicable '87, Paper A.6.1, Second International Conference on Polymer Insulated Power Cables, pp. 199-205.*
25. A. Garton, J.H. Groeger, J.L. Henry, "Ionic Impurities in Crosslinked Polyethylene Cable Insulation", *IEEE Transactions on Electrical Insulation, Vol. 25, No. 2, April 1990, pp. 427.*
26. B. Dellby, G. Hjalmarsson, S.O. Olsson, "Water Tight XLPE Cables", *Paper No. 21-11, CIGRE, International Conference on Large High Voltage Electric Systems, 1982 Session.*
27. P. Bourjot, P. Gauthier, A. Pinet, "Thermomechanical Behavior and Water Tightness of MV Polymer Insulated Cables", *Jicable '84, International Conference on Polymer Insulated Power Cables, pp. 63-67.*
28. J.H. Fondeur, P.M. Dejean, "HV Cables with Corrugated Laminate Aluminum Sheath: Construction, Characteristics, Laying Advantages", *Jicable '87, Paper A.8.3, Second International Conference on Polymer Insulated Power Cables, pp. 405-412.*
29. B. Bernstein, "Development of Moisture Barriers for Extruded Dielectric Cables", *Appendix III-E-1, Minutes of the 81st Meeting of the Insulated Conductors Committee, November 1987.*
30. "Water Treeing as a Function of Moisture Present in XLPE Insulation", *Canadian Electrical Association Project 117D311, One Westmount Square, Suite 500, Montreal, Quebec, Canada H3Z 2P9.*
31. S.N. Parwal, "Reliability of XLPE-Insulated EHV Cables", *Wire Technology, November 1990.*
32. V. Fister, S.A. Hansen, W. Krieger, K. Oswald, T. Weinmann, "Germany's First 220 kV XLPE Cable System in Bayernwerk AG's Network", *Elektrizitaetswirtschaft Zeitschrift der Vereinigung Deutscher Eledrizitaetswerke Vol. 87 No. 26/88, 1988.*
33. Ibid., Zimmerman, et al.
34. K.E. Bow, "The Development of Under-Jacket Moisture Barrier Cable as a Counter Measure Against Treeing", *Paper No. 89 SM 635-4 PWRD, IEEE/PES 1989 Summer Power Meeting, Long Beach, CA, July 9-14, 1989.*
35. B. Robbins, "Evaluation of Power Cables with Moisture Barriers", *Appendix III-C-1, Minutes of the 77th Insulated Conductors Committee Meeting, November 1985.*
36. Ibid., Andresen, et al.
37. Ibid., Zimmerman, et al.
38. F. Teruo, "Technological Progress in High-Voltage XLPE Power Cables in Japan–Part II", *IEEE Electrical Insulation Magazine, Vol. 4, No. 6, November/December 1988, pp. 15.*
39. K. Takenouchi, H. Nakagawa, T. Nakabasami, A. Katsumata, "The Experience in Service for 66 kV XLPE Insulated Power Cables", *Jicable '84, International Conference on Polymer Insulated Power Cables, pp. 351-358.*
40. H. Nakagawa, T. Nakabasami, T. Tanabe, M. Aihara, A. Konda, "Development and Installation of 154 kV XLPE Cables", *Jicable '84, International Conference on Polymer Insulated Power Cables, pp. 359-366.*
41. P. Arnold, D.R. Jeter, C.D. Mercier, D.K. McDonald, "Evaluation and Comparison of Unaged and Field Aged Moisture Impervious Medium Voltage Cables", *Proceedings of the Transmission and Distribution Conference, 91CH3070-0, pp. 151-154.*
42. "Guidelines for Tests on High Voltage Cables with Extruded Insulation and Laminated Protective Coverings", *Working Group 21.14, Electra, No. 141, April 1992, pp. 53-61.*
43. "Guide on the Design, Testing and Application of Moisture Impervious, Solid Dielectric, 5-35 kV Power Cable Using Metal/Plastic Laminates", *P1142/D7, Prepared by Group 6-23 of the Sheaths and Coverings Subcommittee (No. 6) Insulated Conductors Committee, PES/IEEE, April 15, 1992.*



Kenneth E. Bow graduated with a B.S. degree in Electrical Engineering from Michigan State University in 1962.

He joined the Dow Chemical Company in 1962 as a special assignment engineer. He has been involved in the research and development of materials for the wire and cable industry for over 25 years. He is currently the Chief Scientist for wire and cable applications. He is responsible for the global development of coated metal shielding and armoring tapes for applications in cables. Mr. Bow is also the Technical Manager for the Engineered Laminates Technology Center.

Mr. Bow is a member of the IEEE Power Engineering Society, a voting member of the Insulated Conductors Committee, and chairman of Subcommittee No. 6 – Sheaths and Coverings. He is a member of the Wire Association International, the National Association of Corrosion Engineers, the Society of Plastics Engineers, the American Society of Materials, and Dow's primary representative to the Telecommunications Industry Association.

Mr. Bow can be reached at Dow U.S.A., P.O. Box 515, Building B, Granville, Ohio 43203.

An Experimental Investigations on the Degradation Characteristics of 22.9kV XLPE Insulated Power Cables Installed in Korea

Yun-Ok Cho, Hee-Suk Ryoo, Chong-Ho Sun
Korea Electrotechnology Research Institute, Changwon, Korea

Ja-Yoon Koo
Hangyang University, Seoul, Korea

Dong-Won Chung, Sang-Joon Kim
Korea Electric Power Cooperation, Daejeon, Korea

ABSTRACT

This paper presents the analysis on the main cause of insulation failures in 22.9kV XLPE insulated cables in Korea based on the laboratory experiments and statistic survey on the field failed cables from 1985 to 1989. It has been analysed that the Weibull distribution of failed cables in the field is very close to that of laboratory aged cables in the presence of water, and the expected life with 63.2% probability is 6.16 years for field failed cables and 5.6 years for laboratory aged cables in the presence of water. Also, bow-tie trees and vented trees have been observed in both the laboratory aged cables and the field aged cables. From these facts, it has been concluded that field failures are caused mainly by the water.

1. INTRODUCTION

In Korea, 22kV XLPE insulated semi-conductive tape shielded cables (CV) and 22.9kV XLPE insulated concentric neutral wire shielded cables (CNCV) have been installed from 1973 in the ungrounded systems, and from 1978 in the multi-grounded systems, respectively.

With this short time of service of XLPE insulated cables in the distribution systems, the insulation failure rates began to increase very sharply from 1985. Also, it was suspected that the failures might be caused mainly by the water penetration into the cables.

In this connection, laboratory aging experiments on the new cables and the field aged cables have been carried out to figure out the main cause of field failures by comparing the aging characteristics of laboratory aged cables with that of field failed cables. The sliced samples removed from the failed cables were observed through a microscope to figure out the failure mechanism. Also, tanδ and DC leakage current have been measured for the laboratory test samples to investigate the correlationship of those measurements to the cable deterioration.

Based on the above tests performed with the laboratory aged cables and failed cables in the field, it is pointed out that the failure of cables takes place most likely under the presence of water. Therefore, as a means to reduce the cable failures in Korea, it could be suggested to develop the watertight XLPE insulated cables for which it is predominantly necessary to introduce a long term accelerated test to examine the water penetration along the power cable conductor and to provide related appropriated specifications.

2. LABORATORY AGING TEST AND THE RESULTS

22.9kV, 325mm² CNCV cables were used for the laboratory accelerated aging test in this study. The length of samples was 20 meters. The tests have been carried out for the samples with and without introducing the water in the conductor and on the outer semiconductor layer. Cables in the presence of water have been preconditioned with water for 10 days without loading. The prepared test samples are shown in Table 1.

Table 1. Test samples

Sample No.	States	
No.1 - No.2	Dried	New Cables
No.3 - No.6	Wetted	New Cables
No.7	Wetted	Field aged for 7.5 years
No.8	Wetted	Field aged for 6 years

The test facility shown in Fig.1 for this work was composed of a voltage supplier, current supplier, a data acquisition system, and a control system.The basic flow of the aging test is shown in Fig.2. The controller was programmed to keep the voltage constant 45kV, and to adgust the current to maintain the cable temperature as 90℃. The controller turned on the loading current transformers for 8 hours and turned off those for 16 hours during a day of test period. Loading current corresponding to the values to keep the conductor temperature constant 90℃ has been calculated and applied to the cables every five minutes by the IEC 237 method based on the ambient and surface temperature measurements[1]. Tanδ and DC leakage current were measured to investigate the applicability of these measurements to

the diagnosis of cable failures during aging test period.

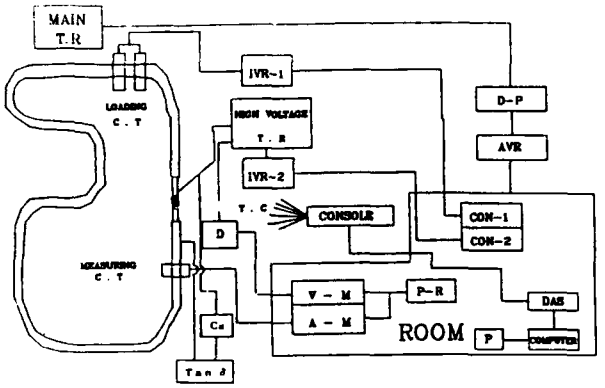


Fig 1. Test circuit diagram

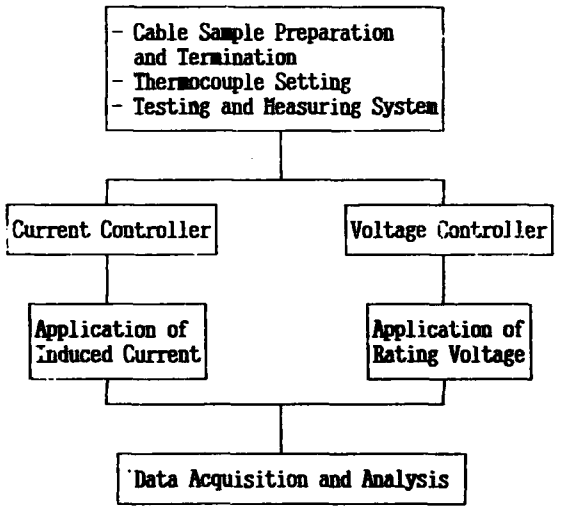


Fig 2. Basic flow of testing process

Table 2 shows the test results. Dried cables NO.1 and NO.2 were not failed despite of very long period of test corresponding over 40 years equivalent life. However, all the cables in the presence of water were failed in a short period of time. From this, it was concluded that water penetration to the cables degraded the cables very quickly.

From the equivalent life in Table 2, a Weibull distribution as shown in Fig.3 is obtained for the laboratory aged cables. In this figure, shape coefficient m and the expected life with 63.2% breakdown probability are known to be 1.2 and 5.6 years, respectively. Considering the minimum expected life of cables as 30 years, water in the cables decreases the cable life considerably.

Fig.4 and Fig.5 show the results of tanδ and DC leakage current measurements, respectively for the test samples NO.1, NO.6, and NO.8. From these figures, it is shown that any significant changes in the measurements can not be found in the dried samples. Also, DC leakage

Table 2. Test results

samples	Loading Time (days)	Final state	Equivalent life * (years)
1	60	Not Failed	Over 40
2	145	Not Failed	Over 40
3	14	Failed	1.5
4	15	Failed	1.6
5	18	Failed	2.0
6	42	Failed	4.6
7	0.5 hours	Failed	7.5 **
8	43	Failed	10.7 **

* Calculated by assuming that $V^n \cdot t$=const, n=3 [5]
** Service years are added in the calculation

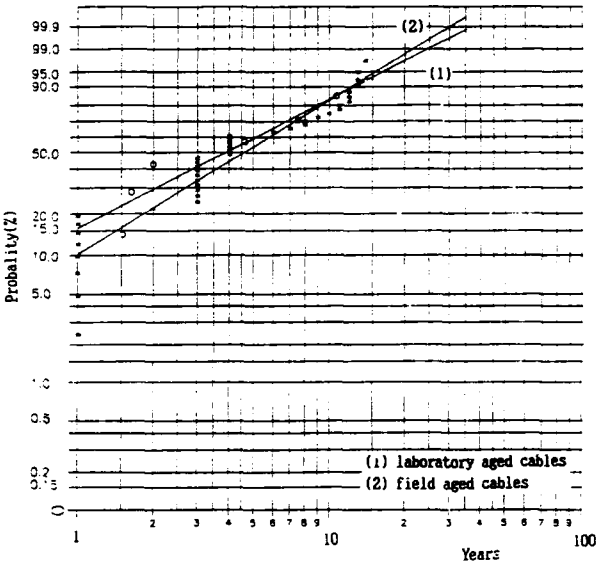
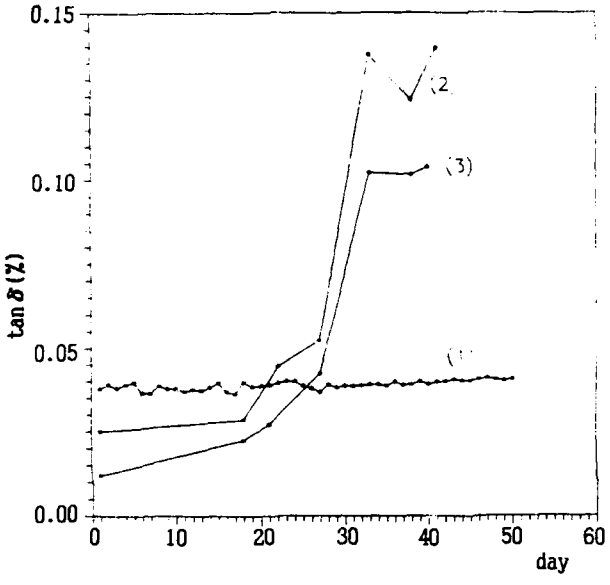


Fig 3. Weibull distribution for laboratory cables(1) and field failed cables(2)

current did not show any significant variations even for the cable samples with introduced water. Therefore, it is very doubtful that DC leakage current measurements could be applied in the failure monitoring. However, the tanδ measurements showed significant changes for the wetted cables. Table 3 shows the initial and final values of tanδ for the cable samples NO.6 and NO.8. From Table 3, it may be very cautiously concluded that tanδ value of 0.1% is a critical value for the normal cable operation.

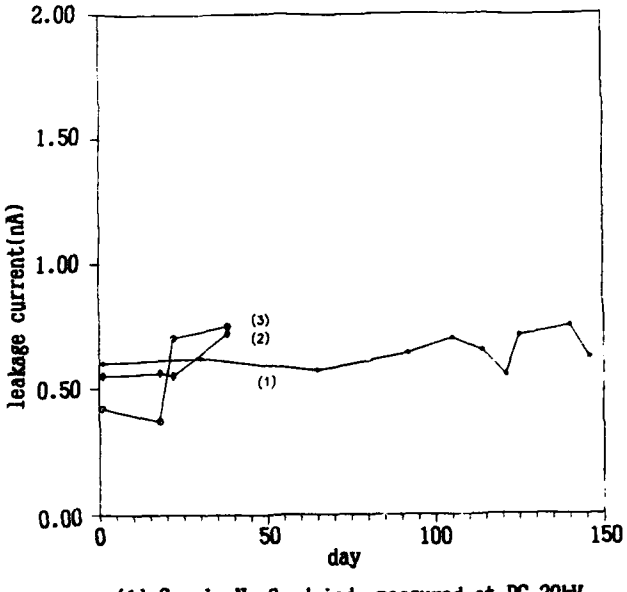
Table 3. The initial and final values of tanδ measured at 13.2kV

	Sample No.6 (%)	Sample No.8 (%)
Initial value	0.025	0.012
Final value	0.12377	0.10751



(1) Sample No.1, dried, measured at AC 45kV
(2) Sample No.6, wetted, measured at AC 13.2kV
(3) Sample No.8, wetted, measured at AC 13.2kV

Fig 4. Tan δ measuring results



(1) Sample No.2, dried, measured at DC 20kV
(2) Sample No.6, wetted, measured at DC 20kV
(3) Sample No.8, wetted, measured at DC 20kV

Fig 5. DC leakage current measuring results

3. MICROSCOPIC OBSERVATION

To understnd the failure mechanism, a microscopic observation has been carried out using the laboratory aged cable samples No.4 - No.8. Ten pieces of sliced samples of 0.4mm thickness for each failed cable were made by microtoming the XLPE insulation in the left-hand and right-hand sides of position separated from the breakdown spot by 5 cm. Table 4 shows the observation results of trees produced in the laboratory failed cables. Representative water trees observed through a microscope are shown in Fig.6.

Table 4. Trees produced in the failed cables

Cable Sample No.	Bow-tie Tree (Ea)						Vented tree	Equivalent Life (
	200 μm	300 μm	400 μm	500 μm	1000 μm	1300 μm	Maximum length(μm)	
4	1	1					100	1.6
5	1				1		75	2.0
6	3	3	1				80	4.6
7	3	1	1				70	7.5
8	4	1			1	1	160	10.7



(b)

Fig.6 Observed water trees in the laboratory aged cable. No 8
a) Bow-tie tree, b) Vented tree

Considering that the cable sample No.7 was failed right after the voltage application, water trees in No.7 sample are thought to be produced during the field service. Also, water trees in No.8 sample are considered to be produced during the field service considering that the tree length of No.8 is much longer than that of No.6 despite of similar loading time.

Maximum tree length in the failed cables is shown in Fig.7, where any distinct correlationship between the tree length and the equivalent service years can not be deduced.

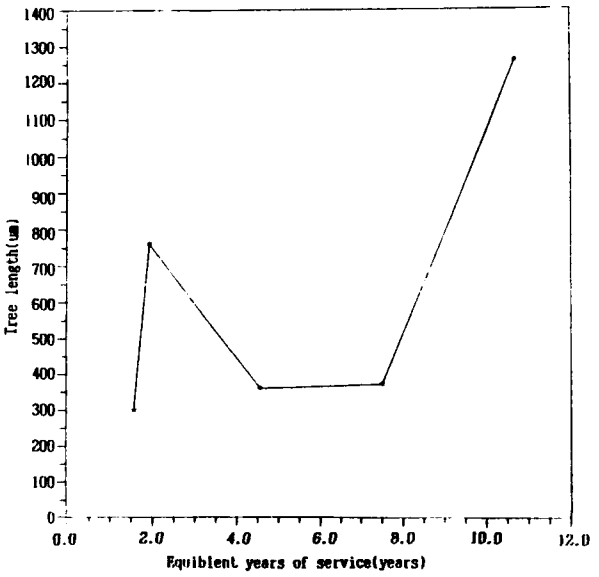


Fig. 7 Maximum tree length in the failed cables

Through the microscopic observation, it was known that 87% of bow-tie trees were caused by the contaminants in the insulation. From this, it could be assumed that the bow-tie trees were formed near contaminants in the insulation under the penetration of water into the cable. And they grow as the service time, and eventually breakdown the cable. The maximum size of the observed contaminants was 30㎛, which is smaller than the specified. Therefore, it is considered that any countermeasures to protect the cable fom the water penetration is the better solution to prevent cable failures than the control of contaminants.

4. STATISTIC SURVEY

Failure reports of cables installed in the distribution system in Korea from 1985 to 1989 were investigated to examine the failure statistics. The cables have been under operation in our underground distribution system during up to 14 years before being failed. Total number of failures from the reports was 43 as shown in Table 5.

From the table, it was shown that the longest life of failed cables was 14 years. Considering 30 years of cable life, it was thought that there might be a factor to reduce the cable life in the field. Fig.1 shows the Weibull distribution for the field failed cables. From this distribution, the shape coefficient m and the expected life with 63.2% breakdown probability were shown to be 1.22 and 6.16 years, respectively. This result and that for the laboratory aged cables are tabulated in Table 6.

Table 6. Weibull distribution of field and laboratory failed cables

	Field failed cable	Laboratory failed cable
Shape coefficient	1.22	1.02
Expected life	6.16 years	5.6 years

Table 6 shows that the shape coefficient and the expected life of field cables are very close to those of laboratory aged cables. Also, a microscopic observation have shown that water trees play the main role to breakdown the cables. Therefore, it may be concluded that the main cause of cable failures is the water penetration to the cables.

5. CONCLUSIONS AND CONTRIBUTIONS

The conclusions and contributions of the study are summarised as follows :

1) For the dried samples, there were not any insulation breakdowns and any changes in the tanδ

Table 5. Service years of field failed cables

Service years	0	1	2	3	4	5	6	7	8	9	10	11	12	13	14	not known	total
No. of failures	5	3	1	10	6	0	1	1	2	1	1	2	3	3	1	3	43

2) All the cables with water were failed in a short period of test time, and tanδ measurements changed significantly. 0.1% value of tanδ was shown to be critical in the cable operation. However, the DC leakage current did not show any significant changes.
3) A microscopic observation have shown that water trees play the main role to breakdown the cables.
4) Based on the laboratory aging test results and the failure rate of field-serviced cables, it has been concluded that the main cause of cable failures in Korea is the water penetration to the cables.

REFERENCES

[1] Koo, J.Y et al., "A syudy on the continuous permissible current rating in 22.9kV CN-CV underground distribution cables", JICABLE 91, pp 515-519
[2] L.Deschamps, "The aging of extruded dielectric cables", JICABLE/EPRI/CEA WORKSHOP,89
[3] AEIC CS55-87, "Spec. for thermoplastic and cross - linked polyethylene insulated shielded power cables rated 5 throuth 35kV"
[4] E.Occhini, "High voltage cables with extruded statistical controls and reliability evaluation", IEEE, Vol PAS-94, pp967-965(1975)
[5] Technical Reports of JIEE., Part II, V267 (1991.4)
[6] H.Fukagava et al., "Insulation Degradation by Water Treeing in XLPE Cables and Its Diagnostic Method" CRIEPI REPORT 113, (1983.5)



Yun-Ok Cho (P.O.BOX 20 Changwon City Korea) was born in 1952 in Korea. He received the B.S.degree from Seoul National University, Seoul, Korea in 1976, M.S.degree from Illinoi Institute of Techanology, U.S.A. in 1982 and Ph.d. from Iowa State University, U.S.A. in 1985. His main research activities are in the area on the High Voltage and High Power apparatus and its application.



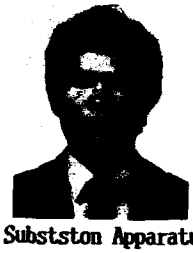
Hee-Suk Ryoo (P.O.BOX 20 Changwon City, South Korea) was born in 1958 in Korea. He received the B.s. degree and M.S.degree from Han Yang University, Seoul, Korea in 1979 and in 1985 respectively. His main research activities are in the area on the Power Cables and Power Apparatus.



Chong-Ho Sun (P.O.BOX 20 Changwon City, South Korea) was born in Korea. He received the B.S.degree and M.S.degree from Busan National University, Busan, Korea in 1986 and in 1988 respectively. His main research activities are in the area on the Power Apparatus and Power Cables



Ja-Yoon Koo (Dept. of Electrical Eng., Hangyang University, 396 Ansanshi, Daehadong, Kyeongki-Do, 425-791, Korea) was born in 1951 in Korea. He received the B.S. degree from Seoul National University, Seoul, Korea in 1975, M.S. degree from ENSEEISH, Toulouse, France in 1980 and Docteur d'Ingenieur in High Voltage Insulating Dielectrics, from ENSIEG, Grenoble, France in 1984. His main research activities are in the area on the New Dielectrics used for High Power Engineering, Diagnosis of electric Power Apparatus and the Protection of High Voltage Network System



Dong-Won Chung (KEPCO Research Center, Youngjundong, Dong-Gu,Daejun City, Korea) was born in 1946 in Korea. He received the B.S.degree from Busan Nation University, Busan, Korea in 1973 and M.S.degree from Yonse University, Seoul, Korea in 1981. His main Research activities are in the area on the Power Substston Apparatus and Power Cables.



Sang-Joon Kim (KEPCO Research Center, Youngjungdong, Dong-Gu, Daejun City, Korea) was born in 1951 in Korea. He received the B.S.degree from Seoul Industry University, and M.S.degree from Seoul National University, Korea in 1986 and in 1991 respectively. His main research activities are in the area on the Power Cables and Power Apparatus.

CURRENT ISSUES IN MECHANICAL RELIABILITY OF OPTICAL FIBERS

C. R. Kurkjian,[†] *H. Chandan*[*] *and D. Inniss*[†]

[†]AT&T Bell Laboratories, Murray Hill, NJ 07974
[*]Norcross, Georgia 30071

ABSTRACT

This paper illustrates the fundamental properties of silica fibers which control their general mechanical behavior, and then addresses some specific issues of immediate concern.

INTRODUCTION

An enormous amount of work has been done on the fracture of silica and silicate glasses in the past, and a great deal of understanding exists. However the emergence of silica lightguides in the last decade has led to the development of fibers of much higher quality than had been available previously as a result of concentrated research and development. Although new understanding has been achieved, some new problems have arisen because of very stringent mechanical requirements.

BRITTLE FRACTURE

Silicate glasses, and in particular silica, are perfectly elastic and perfectly brittle in tension at room temperature. A strength *distribution*[(1)] for the long lengths of fiber necessary for lightwave use is shown in Fig. 1 to illustrate the quality of fiber which is now produced, and the practical problems which are encountered in their application. This Fig. shows the cumulative failure probability when fibers are tested in 20 m lengths. The vast majority (~ 95%) of these fibers will fail at a tensile load of ~ 17 pounds, or for 125 μm diameter lightguide fibers, at a stress of ~ 750 ksi (~ 5.25 GPa) when tested to failure in 10-20 seconds. It has been shown that the steep slope of the high strength region of this plot (slope m ~ 100) results from the fact that no flaws are present in these fibers (or more correctly *on the surface* of these fibers) and thus there is *a strength*; i.e., the strength is single-valued and the fibers are most likely flaw-free.[(2)] Five percent of the fibers however, have both lower strengths and a much broader distribution of strengths (the slope $m \sim 5$, where $m \sim \frac{12}{v}$ and v is the coefficient of variation ~ 0.25). These fibers fail because of the presence of a wide variety of types and sizes of extrinsic manufacturing flaws. The flaws can be characterized by their length, c, and since at propagation they are likely to be "half-penny"-like, by $Y \sim \sqrt{\pi}$:

$$\sigma = \frac{K_{IC}}{Yc^{1/2}} \qquad (1)$$

where σ is the strength, and K_{IC} is a material constant, the fracture toughness (~ 0.8 MPa $m^{1/2}$ for silica). A given length of fiber will fail according to equation 1 at the largest flaw along its length. Since more flaws and larger flaws are likely to be found in longer lengths, longer fibers will be weaker according to an equation of the type:[(3)]

$$\ln \frac{\sigma_1}{\sigma_2} = \frac{1}{m} \ln \frac{L_2}{L_1} \qquad (2)$$

where σ_1 is the strength of length L_1, σ_2 is the strength of L_2, at some probability F, and m is the slope as described above. Equation 1 holds for "sharp" flaws. In some cases a flaw may *be* blunt, or *become* blunt and its strength is then characterized by:

$$\sigma = \frac{\sigma_i}{1 + 2(c/\rho)^{1/2}} \qquad (3)$$

where σ_i is the stress at the tip of the crack of radius ρ. Thus for a given crack length, greater bluntness leads to higher strength.

As seen in Fig. 1 the distribution of strength for reasonably long gage lengths is bimodal. At strengths below about 150 ksi (1 GPa), examination of the fracture surface can give valuable information about the fracture process itself. In particular, it is often possible to get detailed information about the origin of the fracture. Mecholsky et al[(4)] made early investigations of such fractography, and it is quite clear that at such low strength levels, cracks i.e., sharp flaws are responsible for failure and therefore eqn 1 will be obeyed. Figure 2 shows a typical fracture surface for a low strength failure.[(5)] The crack seen in the photo was produced by the stress generated as a result of the reaction of the foreign particle (ZrO_2) and the silica surface. When the crack is clearly seen and measurable it can be used to calculate the failure stress according to eqn. 1. If the crack is not measurable, the size of the smooth mirror-like region (for silica the mirror radius $r_m \sim 10\,c$) can be used to estimate the failure stress (eqn. 1). On the other hand fibers in the high strength mode are flaw-free and the failure mode in this case is less clear. The response of these two types of fibers to stress and time may thus be somewhat different.

INFLUENCE OF TIME ON STRENGTH

In vacuum,[6] or has recently been shown, in ambient if protected by a metal coating,[7] failure of a silica fiber will occur by breakage of Si-O-Si bonds. Under ordinary conditions however, fibers are covered by polymers which are permeable to water. Normally then, it should be assumed that the surface of the glass fiber is in equilibrium with the water in the ambient. Because of this, lightguide fibers undergo delayed failure or fatigue as shown in Fig. 3.[8] Although the details of fatigue are not understood, it is generally assumed that it is the result of stress assisted corrosion by water eg.

$$Si-O-Si + H_2O = SiOHHOSi \ .$$

For low strength fibers if the applied stress is less than that required by eqn 1, immediate failure will not occur. With the help of the above stress-assisted corrosion however, a crack may grow so that the eqn *is* satisfied at a later time and failure ie *delayed* failure, or fatigue will occur. In the absence of "real" flaws, however, the mechanism is less clear.

Although it is generally agreed that an exponential dependence of strength on time is expected from basic principles, most prediction are made on the basis of a power function extrapolation because of mathematical convenience. This simplification not only leads to quantitative errors, but possibly also qualitative errors. Figure 4 shows the differences which occur in both short and long time extrapolations. Although a choice cannot be made between power function and exponential models on the basis of measurements made over normal experimental times, Bubel and Matthewson[9] have shown the consequences of the assumption of four different lifetime expressions.

Because very long lifetimes (~ 25 yrs) are required of lightguide fibers, it has been normal practice to study such fibers under accelerated conditions - eg at T ~ 60–90°C in liquid water or high relative humidity. Under these circumstances a deviation from linearity on both log-log (power function) and semi-log plots (exponential) of stress and time is often seen.[10] France et al[11] and Krause[12] first showed that this "knee" in the fatigue curve could also been seen in aging (Fig. 5).[10,13] In aging experiments the fiber is held under the desired conditions with no applied stress. After the desired aging time has elapsed, ideally the inert strength is measured, but more normally, the fast fracture strength of the aged sample is measured. As with fatigue, a knee is often seen whether a log-log or semi-log plot is made. Yuce et al[14] and others[15,16] have recently shown that the strength reductions which occur under such accelerated conditions, correlate well with the growth of surface roughening as seen with the atomic force microscopy (AFM). A model which predicted this roughening was suggested by Kurkjian et al[17] and by Matthewson and Kurkjian.[13] It was suggested that random density and composition fluctuations intrinsic to the glassy state lead to non-uniform corrosion of the glass surface and give rise to the observed roughening. Support for this model has recently been given by Kurkjian et al.[18]

OUTSTANDING PROBLEMS

In the above discussion we have outlined the situation with respect to the general problems of strength, fatigue and aging. In this final section, a number of specific issues will be addressed which are either new, or if old have resisted resolution in the past.

1) Do large and small flaws (or *no* flaws) respond in the same way to stress and stress-assisted corrosion ie, fast and slow fracture?

Whatever the details of the processes responsible for failure in the two failure modes of Fig. 1, it is important to be able to predict their long time behavior. While many studies have been made of the variation of fatigue with variation in initial fast fracture strength, no clear understanding has emerged. Kurkjian et al[19] have shown that for the available data, there is no correlation between σ and n presumably because of the great variability in the character of the flaws present. The extremely high quality of fiber now produced makes it difficult to study the behavior of the infrequent, proof-test flaws. By using indentation flaws, Lin et al[20] have made a start at characterizing low strength behavior in fast and slow fracture but much more work is needed. It is also very important to study the aging behavior of low strength fibers. It has been suggested that the roughening which occurs on aging a flaw-free surface is due to local differences in total free energy inherent in glasses which gives rise to local differential solubility rates. When a crack exists on such a surface, the situation is completely changed. In the absence of stress or at low stresses, the solubility will be less at the tip of the crack and crack-tip blunting may be expected to occur, and instead of weakening, strengthening may occur.

2) Is there a fatigue (or aging) limit?

One of the major problems in defining the mechanical reliability of fibers is the prediction of fiber lifetimes on the basis of an incomplete understanding of aging and fatigue and thus an incomplete knowledge of appropriate analytical expressions governing the time dependence of strength. This problem would obviously be avoided if it could be shown (as has often been suggested) that there is a limit below which the strength would not drop ie, a *fatigue* or *aging* limit. Three lightguide related experiments have given indications that such may be the case. (1) Bogatyrjov et al[21] have shown an aging limit in silicone clad silica fiber in 80°C water of pH7. (2) Various experiments by Helfinstine and Quan[22] and Gulati et al[23] show increasing n-values with increasing time (decreasing stress) and (3) recent very impressive work by Helfinstine et al[24] and Gulati[25] have shown an apparent approach to a fatigue limit in a DCDC crack growth specimen of fused silica at very low crack velocities (K_i – 0.3 MPa $m^{½}$ and $v_c = 10^{-11}$ m/s). By using a scanning tunneling microscope to measure the position of timing markers they have made subcritical crack growth measurements in a regime which effectively extends the time of a *fatigue* measurement to *several years* in a real time of months.

3) Do liquid water and water vapor affect strength in the same way? If surface roughening and weakening is due to differential solubility, such behavior would not be expected in the absence of liquid water. On the other hand, both Yuce et al[14] and Kennedy et al[15] have observed such behavior. In fact Kennedy et al have shown that in some cases, substantially greater weakening occurs in vapor than in a liquid. Is the model wrong, or is there a mechanism for liquid formation in vapor – eg interaction of the polymer with water vapor?

4) How do different polymers affect mechanical behavior?

Some recent studies[26,27] have shown the importance of ambient chemistry on strength and fatigue. Other studies have shown that different polymers have a major impact on these properties.[14,15] It has been suggested that the detailed chemistry, as well as adhesion and water permeability affect this behavior. There is, however, very little understanding of the specific causes of these differences in polymer behavior. This is one of the most critical areas for additional work.

5) Can the behavior of lightguide fibers be predicted under combined loading eg combined tension and torsion. This reflects a practical condition which is frequently encountered, both in long cables and short coupled sections, but which has received essentially no attention. We have recently obtained some experimental data on the effect of combined uniaxial tension and twist on the strength of optical fibers; the effect on fatigue is still unexplored. The dynamic tensile strength of fibers with and without twist was measured at 23°C, 50% RH in an Instron tester. The twist was introduced in the gauge length by turning the top mandrel grip while the bottom mandrel grip was fixed. Fifty cm gauge length samples were tested at 2.5% per minute strain rate. For high strength coated fibers the tensile strength was essentially unaffected for up to 16 complete turns. However, with the extreme case of 128 turns, the strength was reduced from ~ 700 ksi to 352 ksi. When mechanically stripped (and thus damaged) the tensile strength was reduced and broadened (mean strength $\bar{\sigma} = 265 \pm 65$ ksi) with no twist. With 16 turns, the mean strength was 214 ± 90 ksi (95% confidence interval). This *suggests* the possibility of strength reduction, but more data are needed in this case. The principal stress in such a situation can be expressed as:

$$\sigma = (\sigma_T/2) + \sqrt{(\frac{\sigma_T}{2})^2 + \tau^2} \qquad (3)$$

where σ_T = tensile stress
τ = shear stress = $G(rd\phi/L)$

and G is the shear modulus, r is the fiber radius, ϕ the angular twist in radians and L the fiber length. Using G = 31.3 GPa, the shear stress for 16 turns in a 50 cm gauge length is 0.39 GPa or 57 ksi. For 128 turns, the shear stress is 456 ksi and thus the effective stress is 665 ksi which is within 5% of the value of 700 ksi measured in pure uniaxial tension with zero twist. The fracture in torsion has a unique appearance in that there is a zone of multiple fractures contained within the polymer coating which is apparently undamaged except for a corkscrew effect at the end (Fig. 7).

6) Effect of a filling compounds. Fibers in a cable are usually protected by a water-blocking or filling compound. These filling compounds are nonporous gels consisting of an oil, a rubber, an antioxidant and surface modified silica. Figure 6 illustrates the mean strength before and after aging the fibers at 85C/95% RH for 30 days. These fibers have an experimental dual polymer coating where corrosive components were intentionally introduced both in the primary and secondary coatings. The filling compound was applied as a thin coating on the fiber surface. The fibers with and without the filling compound were aged separately. Note that in the presence of a filling compound, the strength reduction after 30 days at 85C/95% RH was only 22% as compared with 53% reduction when there was no filling compound. Thus while the exact mechanism of the protective effect of the filling compound is not understood at present, the results shown here are encouraging.

The above discussion has concentrated on scientific and technological issues having to do with understanding and predicting the mechanical behavior of fibers. As the lightguide industry has grown and fiber has become a commodity, the issue of standards has become a more pressing one. Mechanical reliability of optical fibers is an active topic of discussion in the various standards bodies in U.S. and abroad. These standards groups have two main objectives. First, to develop standardized test procedures to allow direct comparison of fiber strength and fatigue parameters from different vendors. The second objective is to evaluate existing fiber lifetime models. The latter is a challenging task since there are many models which give widely different long-term predictions.

Fiber reliability is being discussed in many standards bodies; IEC (International Electrotechnical Commission), CCITT (Consultative Committee for International Telephony and Telegraph) EIA/TIA (Electronic Industries Association/Telecommunications Association), ETSI (European Telecommunications Standards Institute) and the Japanese National Standards Body. There is increasing communication among these bodies so that uniform world-wide standards may emerge. In the U.S., the Electronic Industries Association has a fiber reliability working group which meets quarterly to generate Fiber Optic Test Procedures (FOTP's). Representatives from various fiber vendors and users have developed FOTP's on measuring dynamic tensile strength (FOTP-28B), a fiber tensile proof test method (FOTP-31B), a method for measuring dynamic fatigue of optical fibers by tension (FOTP-76), a procedure for measuring the static fatigue of optical fibers in two-point bending (FOTP-97) and a fluid immersion aging procedure for optical fiber mechanical properties (FOTP-75). Procedures for static fatigue in tension, dynamic fatigue in two point bending and static fatigue in uniform bending (mandrel wrap method) are being currently discussed. Some other issues under discussion include the relationship between fatigue parameters measured by various test techniques, the effect of stripping the polymer coating on strength and fatigue, the effect of a mechanical twist on strength and fatigue of fibers, and the effect of

unloading time on prooftesting.

In addition to FOTP's, EIA has a document on fiber lifetime calculations based on a minimum time to failure model. Due to a large range of B values reported in the literature and its dependence on the fatigue parameter n, it is recommended that B value be determined for each fiber. Work is in progress to include predictions based on Mitsunaga's prooftest model.

SUMMARY

Although much progress has been made both practically and scientifically in the area of lightguide fiber strength, several outstanding problems require additional work. The application of new experimental techniques as well as new theoretical insights promise to provide the needed insights in the near future. Continuing work on standards for the mechanical characterization and testing is also of importance.

REFERENCES

(1) G. S. Glaesemann and S. Gulati, "Design Methodology for the Mechanical Reliability of Optical Fiber", Op. Eng., *30*, 709 (1991).

(2) C. R. Kurkjian and U. C. Paek, "Single-Valued Strength of Perfect Silica Fibers", Appl. Phys. Lett. *42*, 251 (1983).

(3) W. Weibull, "Statistical Distribution Function of Wide Applicability", J. Appl. Mech., *18*, 293 (1951).

(4) J. J. Mecholsky, S. W. Freiman and S. W. Morey, "Fracture Surface Analysis of Optical Fibers", in *Fiber Optics, Advances in Research and Development*, ed. B. Bendow and S. S. Mitra, Plenum (1979),

(5) H. C. Chandan, unpub. work (1988).

(6) C. R. Kurkjian and D. Inniss, "Strength and Fatigue of Silica", Proc. VII Intl Conf. Phys. Non-Cryst. Solids, Cambridge, Eng. (1991).

(7) V. A. Bogatyrjov, M. M. Bubnov, E. M. Dianov, A. M. Prokhorov, S. D. Rumyantsev and S. L. Semenov, "High Strength Hermetically Sealed Optical Fibers", Sov. Tech. Phys. Lett. *14*, 343 (1988).

(8) B. A. Proctor, I. Whitney and J. W. Johnson, "Tensile Strength of Fused Silica", Proc. Roy. Soc., *297A*, 534 (1967).

(9) G. M. Bubel and M. J. Matthewson, "Optical Fiber Reliability Implications of Uncertainty in the Fatigue Crack Growth Model", Opt. Eng. *30*, 737 (1991).

(10) C. R. Kurkjian and D. Inniss, "Understanding Mechanical Properties of Lightguides", Op. Eng. *30*, 681 (1991).

(11) P. W. France, W. J. Duncan, D. J. Smith and K. J. Beales, "Strength and Fatigue of Multicomponent Glass Fibers", J. Mater. Sci. *18*, 758 (1983).

(12) J. T. Krause, "Transitions in the Static Fatigue of Fused Silica Fiber Lightguides", in Proc. 5th Eur. Conf. Optical Commun. (Amsterdam, The Netherlands) pg 19.11 (1979).

(13) M. J. Matthewson and C. R. Kurkjian, "Environmental Effects on the Static Fatigue of Silica Optical Fiber", J. Am. Ceram. Soc. *71*, 177 (1988).

(14) H. H. Yuce, J. P. Varachi, J. P. Kilmer, C. R. Kurkjian and M. J. Matthewson, "Optical Fiber Corrosion: Coating Contribution to Zero-Stress Aging", OFC, 1992, post deadline paper.

(15) M. T. Kennedy, E. Cuellar and D. R. Roberts, "Stress-Free Aging in Liquid Water and Humid Environments", SPIE vol. 1580, Fiber Optic Components and Reliability, pg 152 (1991).

(16) W. Griffioen, W. Ahn, A. T. De Boer and G. Segers, "Stress-Induced and Stress-Free Aging of Optical Fibres in Water", IWCS, *40*, 673 (1991).

(17) C. R. Kurkjian, J. T. Krause and U. C. Paek, "Tensile Strength Characteristics of 'Perfect' Silica Fibers", J. de Phys. Coll., *43* suppl 12, 585 (1982).

(18) C. R. Kurkjian, M. J. Matthewson, V. V. Rondinella and W. M. Russ, "Effect of Activity of Glass Fiber Constituents in the Environment on Strength Degradation", Bull. Am. Ceram. Soc. *71*, 491 (1992).

(19) C. R. Kurkjian, J. T. Krause and M. J. Matthewson, "Strength and Fatigue of Silica Optical Fibers", J. Lightwave Tech. *9*, 1360 (1989).

(20) B. L. Lin, M. J. Matthewson and G. J. Nelson, "Indentation Experiments on Silica Optical Fibers", in *Fiber Optic Reliability: Benign and Adverse Environments*, Proc. SPIE *1366*, 157 (1990).

(21) V. A. Bogatyrjov, M. M. Bubnov, S. D. Rumyantsev and S. L. Semjonov, "Mechanical Reliability of Optical Fibers", in *Fiber Optics*, E. M. Dianov ed., Proc. Gen. Phys. Inst., Ac. Sci. USSR *23*, 66 (1990).

(22) J. D. Helfinstine and F. Quan, "Optical Fiber Strength/Fatigue Experiments", Opt. Laser Tech. *14*, 133 (1982).

(23) S. T. Gulati, J. D. Helfinstine, B. Justice, J. S. McCartney and M. Runyan, "Measurement of Stress Corrosion Constant n for Optical Fibers", Bull. Am. Ceram. Soc. *58*, 1115 (1979).

(24) J. D. Helfinstine, S. T. Gulati and D. G. Pickles, "Slow Crack Growth in High-Silica Glasses", Proc. VII Intl. Conf. Phys. Non-Cryst. Solids (1991).

(25) S. T. Gulati, "Mechanical Properties of SiO_2 vs SiO_2-TiO_2 Bulk Glasses and Fibers", Proc. Mat. Res. Soc. Symp. *224*, 67 (1991).

(26) V. V. Rondinella, B. Lin and M. J. Matthewson, "Cation Effects on the Strength and Fatigue of Silica Optical Fiber", Paper 3-JxII-90, 92nd Ann. Meeting, Am. Ceram. Soc., Dallas, TX 1991.

(27) D. Inniss, D. L. Brownlow and C. R. Kurkjian, "Effect of Sodium Chloride Solutions on the Strength and

Fatigue of Bare Silica Fibers'', J. Am. Ceram. Soc. *75*, 364 (1992).

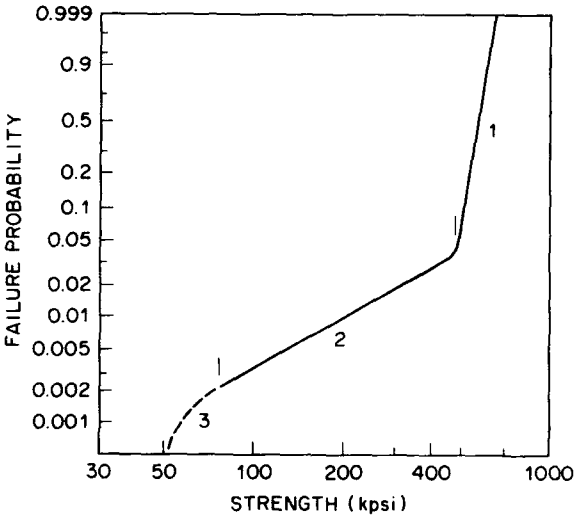


Fig. 1 Strength distribution of a standard polymer coated, silica clad fiber. Gauge length = 20 m.[1]

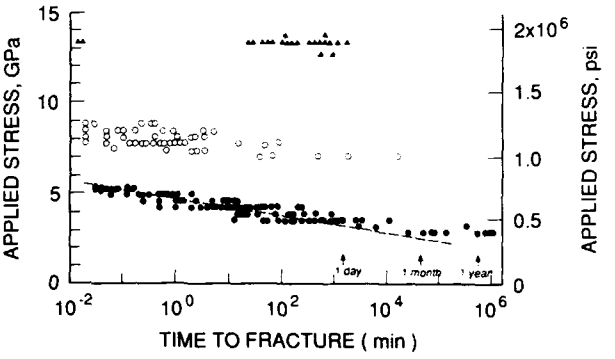


Fig. 3 Failure time of bare silica fibers under tensile stress in various ambients. Filled circles - room temperature, open circles - moderate vacuum (~ 10^{-4} Torr), triangles - ℓN_2.[8]



Fig. 2 Fracture surface of silica fiber. Both the mirror and flaw ($r_m \sim 10\ r_c$) can be seen.[5]

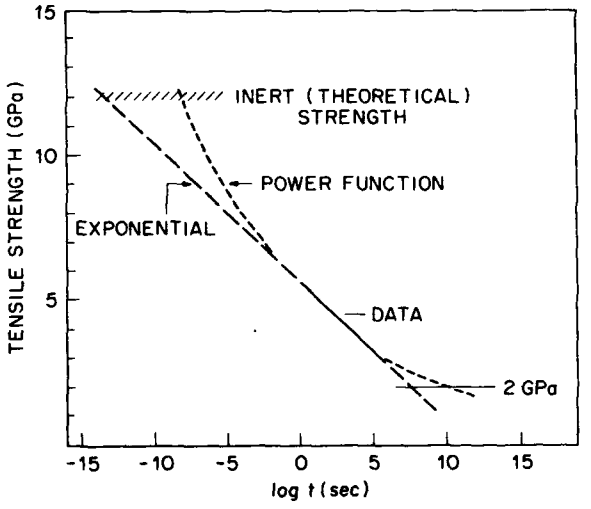


Fig. 4 Extrapolation of experimental static fatigue data as an exponential or a power function.[10]

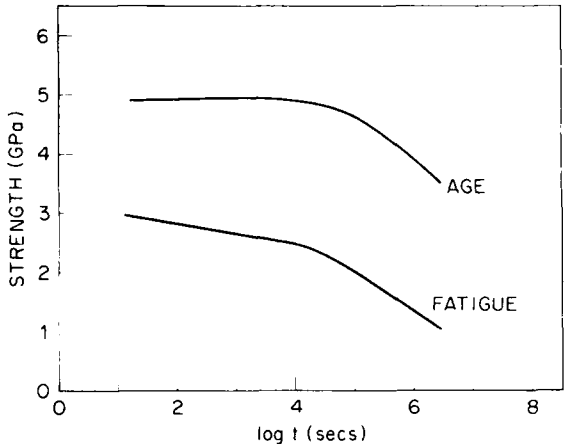


Fig. 5 Comparison of aging and fatigue of uncoated silica fibers in 90°C liquid water.[10]

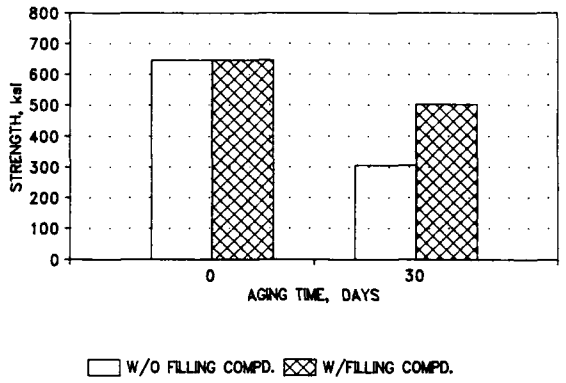


Fig. 6 Effect of filling compound on aging behavior in 85°C/95% RH.



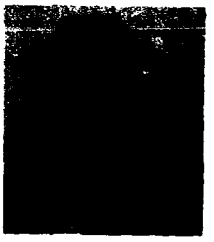
Fig. 7 Torsion-tension break.



Charles R. Kurkjian received the B.Sc. degree in ceramics from Rutgers University in 1952 and the Sc.D. degree in ceramics from MIT in 1955. After postdoctoral appointments at MIT and The University of Sheffield, England, he joined Bell Laboratories in 1959. He has worked in various areas of glass science, most recently with fracture and fatigue of silica fibers.



Daryl Inniss is a member of the technical staff of the Optical Fiber Research Department. He joined Bell Laboratories in 1988 and began his career working on the chemical mechanism that leads to fracture of silica optical fibers. Dr. Inniss was educated at Princeton University, where he received an A.B. in chemistry in 1983; he subsequently attended the University of California at Los Angeles and received a Ph.D. in chemistry in 1988.



Harish C. Chandan is a Member of Technical Staff at AT&T Bell Laboratories, Norcross, Georgia which he joined in 1977. His current activities include mechanical reliability and processing of optical fibers. Dr. Chandan holds a Ph.D. from Penn State University in Ceramics Science. He is active in the Fiber Reliability Working Group in the Electronic Industries Association. He is a member of American Ceramic Society.

AGING BEHAVIOR OF OPTICAL FIBERS

Hakan H. Yuce

Bellcore
Morristown, NJ 07962

ABSTRACT

This paper addresses some of the factors that may effect the aging behavior of silica fibers.

INTRODUCTION

Optical fibers in cables, splice closures, pedestals and optical network units (ONUs) often experience corrosive environments (e.g., water) which can degrade their strength. When these aged fibers are stressed later during routine maintenance or other field craft activity, they can fail at stress levels significantly below their typical strengths in short lengths.[1] The effect of aging on the mechanical reliability of optical fiber is therefore an important consideration in any system design.

Critical mechanical properties of optical fibers are high strength, small variability of strength, high fatigue resistance, and high aging resistance. With improvements in preform quality and drawing environment, long-length, high-strength optical fibers are being produced routinely.[2] Such fibers, with strengths in the range of ~10^6 psi in short gage lengths, are usually characterized by narrow, unimodal strength distributions with large Weibull slope parameters (~50-100). The commonly used UV-cured polymer coatings provide adequate fatigue resistance (as described by a fatigue parameter of ~20) in a benign environment.

However, since aging in adverse environments can severely degrade fiber strength and modify the fatigue resistance of optical fibers,[3-9] the long-term reliability of optical fibers in these environments is no longer assured. Some chemical species, especially water, are known to have detrimental effects on the mechanical properties of optical fibers. This is manifested in different ways depending on the stress state of the optical fiber: (1) time delayed failure mechanisms such as static or dynamic fatigue, and (2) zero-stress aging.

Static fatigue is the time-dependent failure of glass under a constant stress that is less than the instantaneous fracture strength. This delayed failure is a function of the coating, applied stress, temperature, and chemical species, particularly the presence of water. The stress-assisted hydrolysis of the silicon-oxygen network of the glass[10] results in the growth over time of microscopic surface flaws into larger critical cracks. The development of flaws is influenced by the surrounding environment, so the surface reactivity in a given environment determines the fiber's ultimate strength because of its effect on crack tip growth. Dynamic fatigue is the time-dependent failure of glass under a constant stressing rate, resulting in a fracture strength that is less than the strength measured in an inert environment.

The loss of strength in high-strength glass fibers in the absence of stress in some corrosive environments such as water is called zero-stress aging. The underlying mechanism of glass failure under static fatigue conditions has been well documented[11], but the reasons for loss of strength of glass fibers under zero stress are still under study. The topic is a controversial issue; proposed mechanisms involve adsorption of water molecules on the surface, promoting crack growth during subsequent strength testing[12], or corrosive reactions leading to surface flaws which can act as nuclei for cracks[5]. The surface reactivity of silica-based glasses in different environments determines the ultimate strength of these materials because of the effect on crack tip growth.

FACTORS EFFECTING AGING

In a first systematic study, Mould[13] showed that zero-stress aging of freshly abraded glass resulted in an increase in strength. Significant increases in strength were obtained after only 10 seconds, attributed to rounding of flaw tips by the action of water. An increase in strength after aging of scratched glass specimens was also reported by others[14,15]. These studies were conducted with bulk glasses with fresh abrasions so that the critical flaw sizes were large and the strengths were low (less than 20 kpsi).

Kurkjian et al,[16] observed that the strength of pristine fiber that has been aged for prolonged periods under zero stress falls to a level comparable to the strength of weak silica that has been etched or aged. Their explanation for this is that ellipsoidal pits for the two-types of silica are of different size but have the same shape and, hence, the same stress intensification factor. Under applied stress, differences in the local stress cause the

shape of the pits to evolve until a sharp crack is produced that subsequently leads to failure.

Direct evidence for surface roughening of pristine fiber during prolonged exposure to water was observed by scanning tunneling microscopy (STM)[17,18] (see Figure 1). Yuce et al showed that the roughness of the fibers increased with increasing exposure to the aqueous environment. They measured the inert strength of fibers aged under zero-stress conditions and showed that strength loss in the fibers is related to changes in surface roughness on the nanometer scale, and that the loss can be predicted by established models based on the surface roughness. In the original STM studies, fiber samples had to be DC sputter coated with gold grains having corrugations of 4 to 5 nm. Hence, precise measurement of flaw depth for features smaller than the grain size was not possible, as seen in Figure 2. Later, an atomic force microscope (AFM) was used[19] to compare the strength and morphological properties of fibers aged in the aqueous environments. The AFM offers the advantage over the STM that the sample need not be a conductor. With the help of AFM, Yuce and coworkers verified the pit formation (Figure 2) proposed by Kurkjian et al[16].

A recent study[20] showed that even subtle changes in coating chemistry can have an enormous effect on aging behavior of optical fibers. Fibers in this study, designated as Fibers X and Y, were made of *identical* fused silica, coated in-line with two *different* UV-curable epoxy polyurethane acrylate coatings. They were subjected to aging in both 85 °C deionized water (pH 7 ± 0.5) and 85 °C, 85% RH for up to sixty (60) days at zero-stress. Strength and surface morphology of the aged and unaged fibers were examined. The median strength values of unaged and aged fibers are shown in Figure 3 as a function of aging time and in Figure 4 as a function of surface roughness (obtained from the AFM measurements). These figures show that the median strength of fibers decreases and that the surface roughness of glass increases with increasing aqueous aging, particularly with Fiber Y. Figures 5 and 6 show the AFM images of Fiber X and Fiber Y, respectively, where (a) is the glass surface of the unaged fiber and (b) is the surface of the fiber aged for 1 month in deionized water. The roughening that occurred during the aging process is again evident in these figures. The surface roughness of the fibers increased with increasing aging time and was more dramatic in liquid water than in high humidity. Fiber Y experienced more severe aging, as shown in Figure 6. The roughened surface showed an increase in amplitude and wavelength of surface contour with increasing aging time, consistent with earlier findings.19

This study showed that coating composition can be designed to optimize zero-stress aging performance of optical fibers. In addition, it confirmed that the strength is inversely proportional to the measured surface roughness, regardless of the details of the aging experiment.

The formation of surface roughness requires removal of silica from the glass surface. This dissolution process is quite different from the mechanism of stress-assisted hydrolysis of the silicon-oxygen network of the glass[10]. Strength degradation due to aging can be improved if this chemical dissolution can be slowed. Matthewson et al[21] achieved this effect by introducing a small quantity of colloidal silica into the polymer coating of the fiber. Their results indicated that a modified polymer coating formulation increased the lifetime of the fiber almost thirty-fold. They proposed that the small particles are more soluble than the glass fiber due to their curvature and so preferentially dissolve as the environmental water penetrates the coating. The partially saturated water then has a reduced activity at the glass surface. Figure 7 shows the aging behavior of fibers with and without colloidal silica in the coating, measured at room temperature in a pH-7 buffer solution, as a function of aging time in 90 °C pH-7 buffer. As seen, the "with" fiber aged less than the "without" fiber.

CONCLUSIONS

Recent findings in the understanding of reliability of silica optical fiber indicate that the chemical durability of the fiber can control its long-term reliability. In particular, dissolution of surface material produces strength degradation. Recent studies have also demonstrated that coating chemistry can have an enormous effect on the degradation behavior of optical fibers. In order to improve reliability, coating composition must be designed to optimize aging performance.

REFERENCES

1. H. H. Yuce et al, *Proc of 40 th IWCS*, 700 (1991).
2. F.V. DiMarcello et al., *Opt. Fib. Comm.*, **1**, T. Li, Ed., Academic Press, Orlando, FL 179 (1985).
3. T.T. Wang, H.M. Zupko, *J. Mater. Sci.* **13**, 2241 (1978).
4. J.T. Krause, C.J. Shute, *Adv. Ceram. Mater.* **3**, 118(1988).
5. M.J. Matthewson, C.J. Kurkjian, *J. Amer. Ceram. Soc.* **71**, 171 (1988).
6. C.J. Kurkjian et al., *J. Lightwave Tech.* **7**, 1360 (1989).
7. H.C. Chandan, S.C. Perry, *J. Amer. Ceram. Soc.* **68**, C90 (1985).
8. H.H. Yuce et al., *Proc. SPIE 992* 211 (1989).
9. H. H. Yuce et al., Proc OFC' 90 171 (1990).
10. S. M. Wiederhorn, *J. Non-Cryst. Solids* **19** 169 (1975).
11. T. A. Michalske, S. W. Freimen, *J. Am. Ceram. Soc.*, **66** 284 (1983).
12. B.K. Tariyal, D. Kalish, Glass Div., Fall Mtg. Am. Ceram. Soc., Paper 8-CG-77F (1977).
13. R. E. Mould, *J. Am. Ceram. Soc.*, **43** 160 (1960).
14. W. C. Levengood, *J. Appl. Phys.* **29** 820 (1983)
15. A. J. Holland and W. E. S. Turner, *J. Soc. Glass Technol.* **21**, 383 (1937)
16. C.J. Kurkjian et al, *J. de Phys.*, **43** [12] C9-585 (1982).
17. H. H. Yuce et al, OFC '90 Postdeadline Paper, PD14 (1990).
18. R. S. Robinson and H. H. Yuce, *J. Amer. Ceram. Soc.* **74**, 814 (1991).
19. H. H. Yuce et al,*Trans* Electronic Div., Fall Mtg. Am. Ceram. Soc (1991).
20. H. H. Yuce et al, OFC '92 Postdeadline Paper, PD21, (1992)
21. M. J. Matthewson et al, to be published in *Proc. SPIE 1791*, (1992).

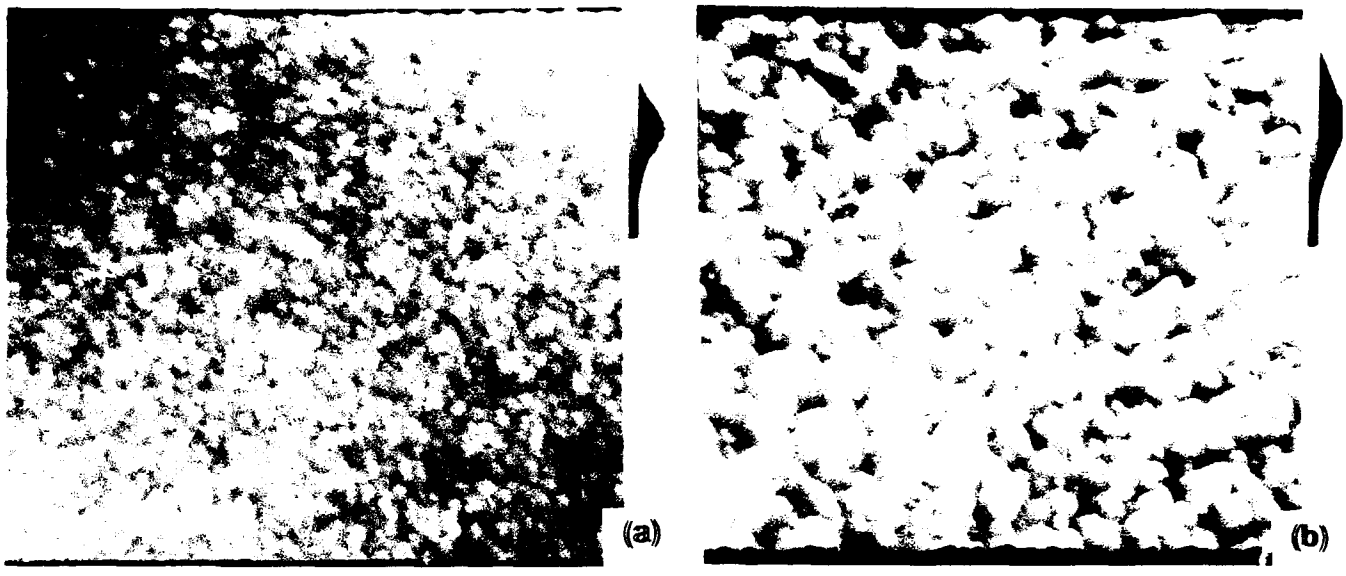


Figure 1 - STM images of surfaces of (a) unaged fiber, and (b) 3 months aged fiber (same magnification for both images; the scan area 900x900 nm) [after reference 17].

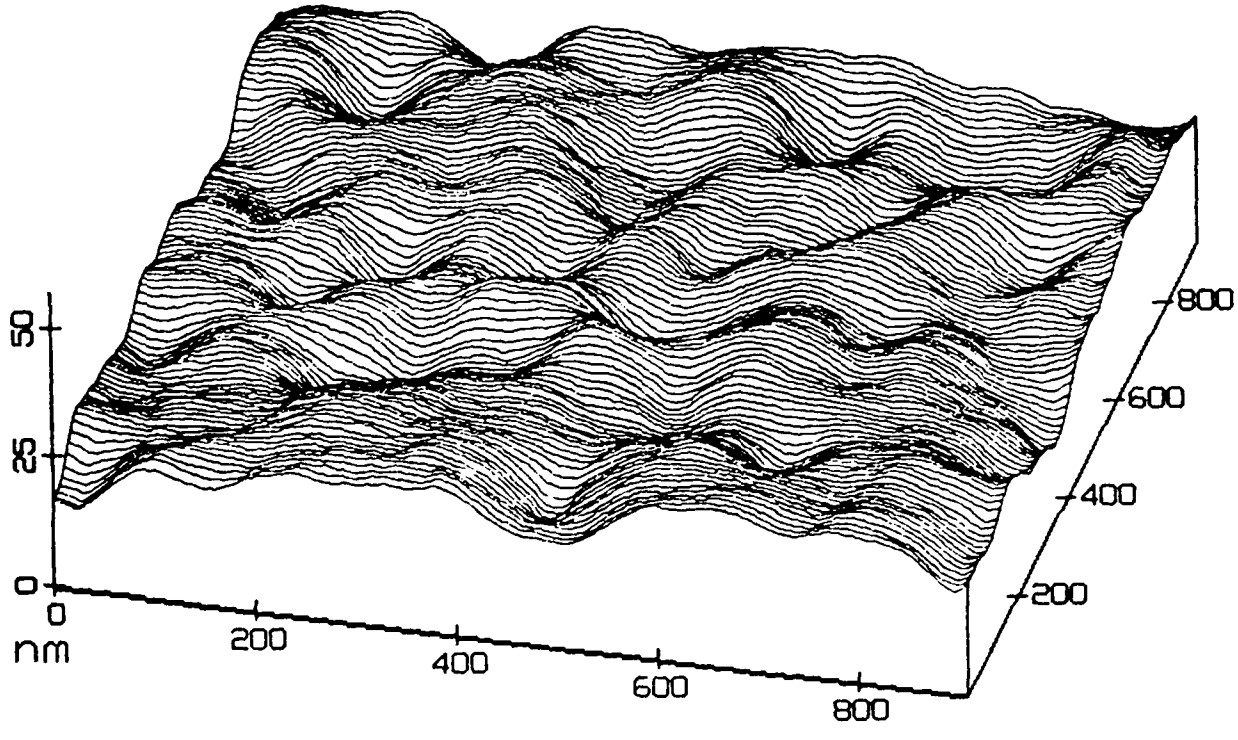


Figure 2 - AFM images of the surface of glass fiber after aging in 80° C deionized water for 3 months [after reference 19].

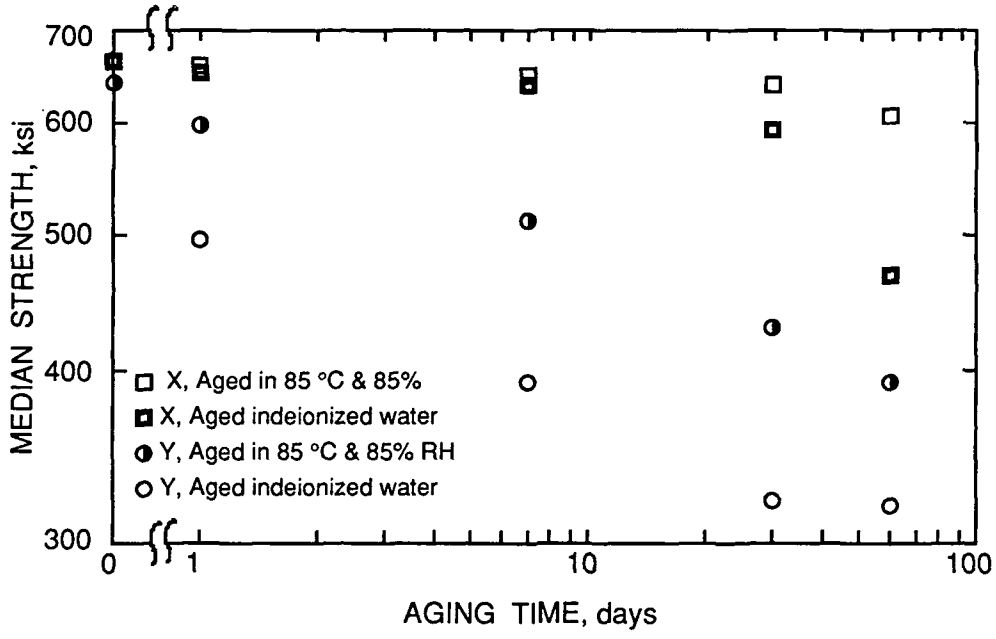


Figure 3 - Strength degradation after aging [after reference 20].

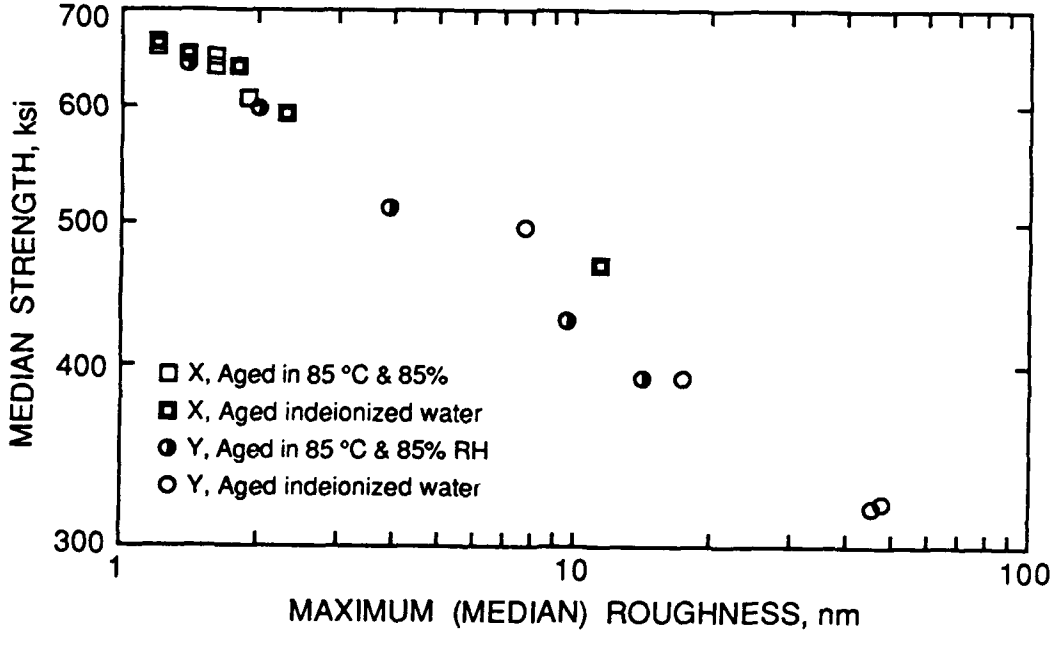


Figure 4 - Strength versus surface roughness [after reference 20].

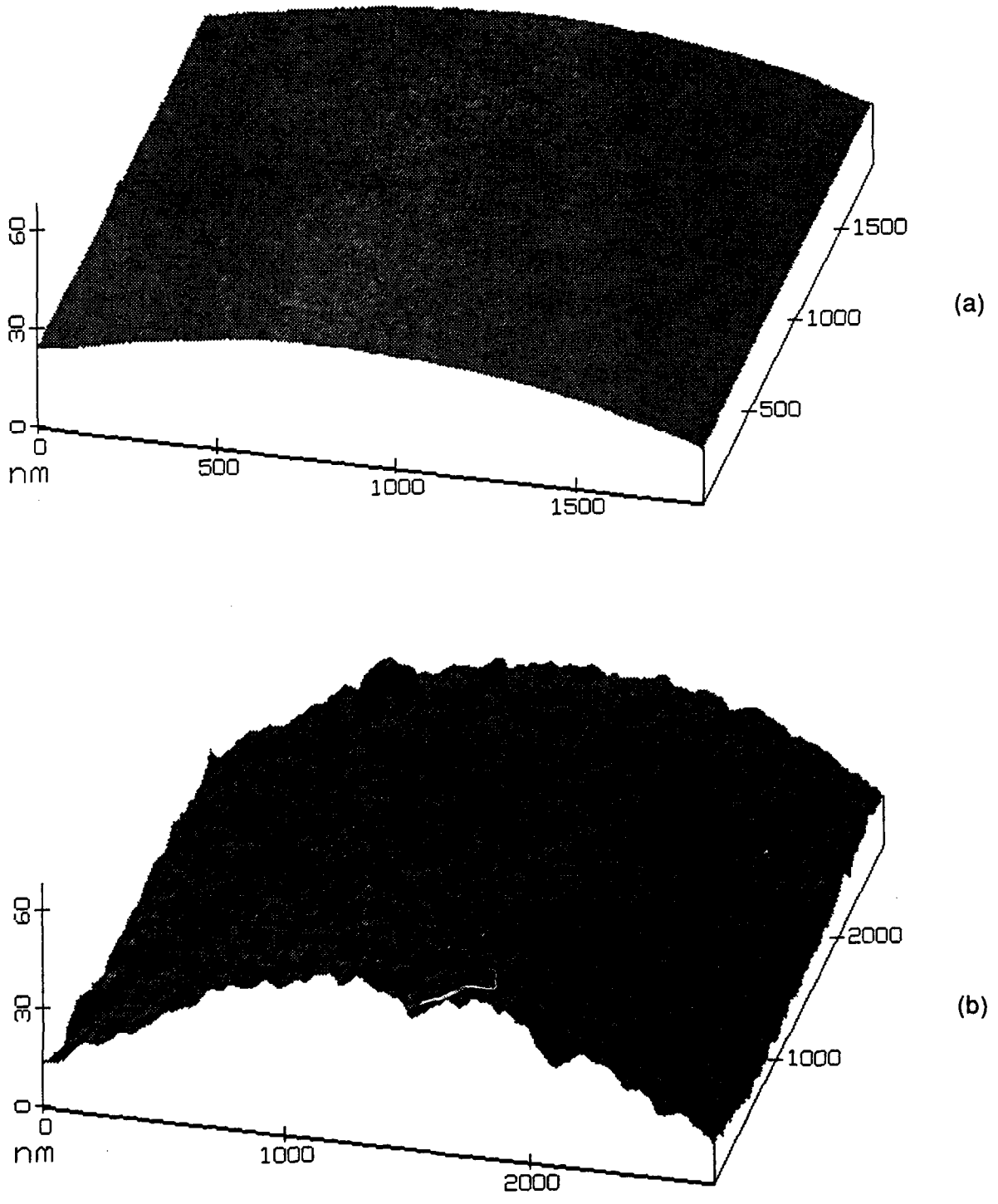


Figure 5 - Unfiltered AFM images of the glass surface of Fiber **X**: (a) unaged and (b) aged for 1 month in deionized water [after reference 20].

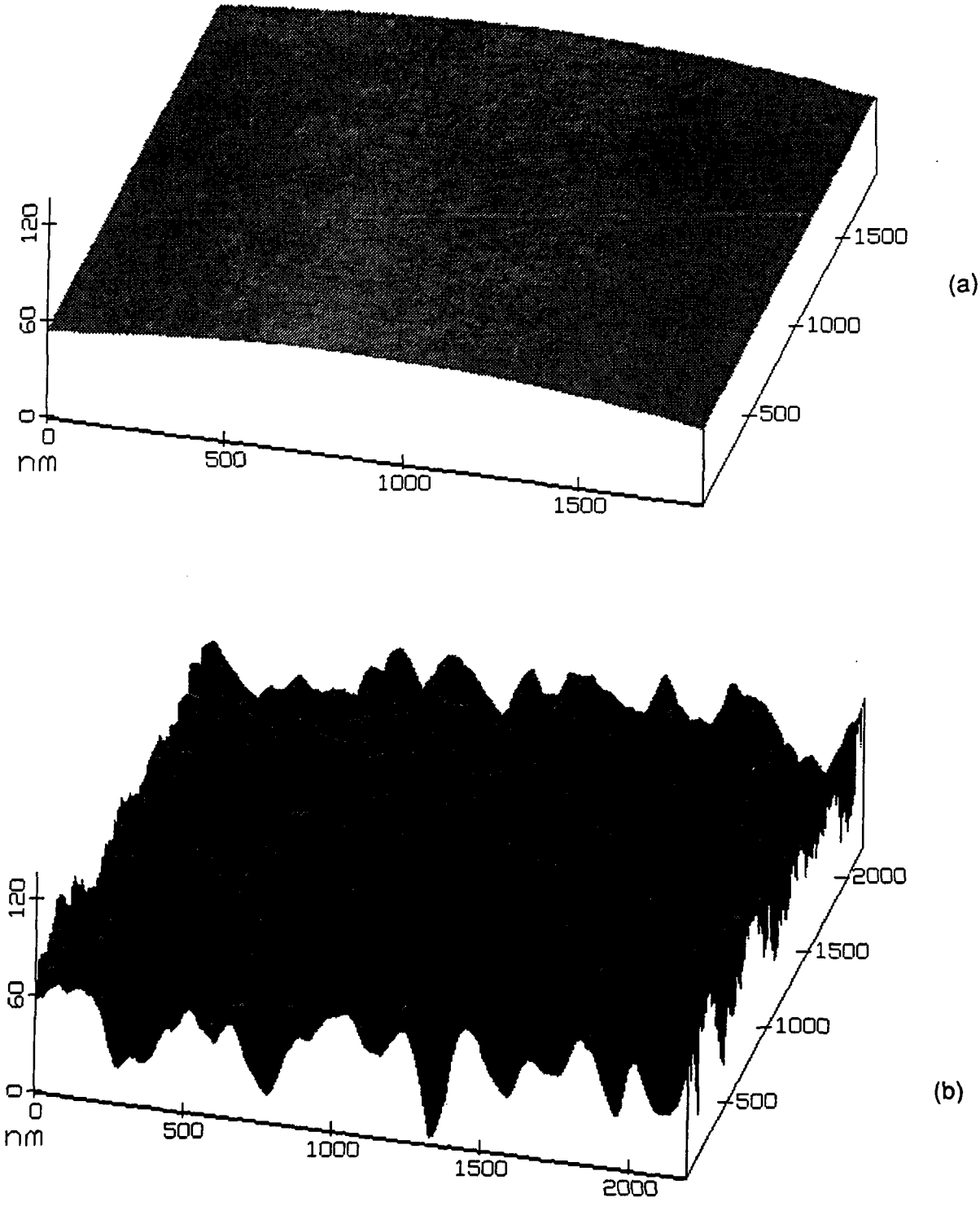


Figure 6 - Unfiltered AFM images of the glass surface of Fiber **Y**: (a) unaged and (b) aged for 1 month in deionized water [after reference 20].

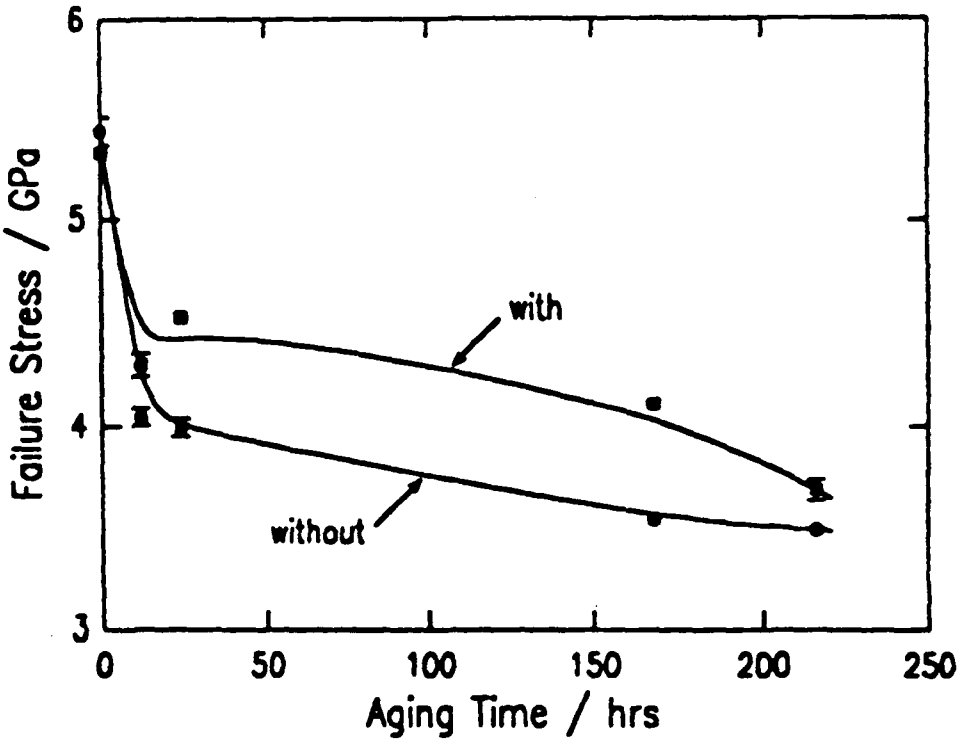


Figure 7 - Strength degradation after aging in 90° C pH-7 buffer [after reference 21].



Hakan H. Yuce is a member of technical staff in the "Fiber Distribution and Reliability Research" group at Bellcore. He leads a research program dealing with long-term mechanical reliability of optical fibers and interconnections. Hakan provides technical input and support to organizations responsible for generic requirements and responds to clients' immediate needs related to consultation on reliability and field failures. He also plays a active role in the establishment of U.S. and international standards within TIA and IEC regarding optical fiber test procedures to assure reliability. Hakan has a B.S. degree in Mechanical Engineering from Technical University of Istanbul, an M.S. in Mechanical Engineering from M.I.T.and a Ph.D degree in Mechanical Engineering and Material Science from Stanford University.

Reliability Considerations for Long Optical Fibers

Suresh T. Gulati

Corning Incorporated
Corning, NY 14831

Abstract

The three critical properties that impact the mechanical reliability of long-length optical fibers are flaw distribution, flaw growth behavior, and zero stress aging. Much progress has been made in the former areas by measuring the strength distribution to a 10^{-5} failure probability level using a continuous fiber strength measurement apparatus. Similarly, recent flaw growth studies for high silica and titania-doped silica glasses have provided further insight into fatigue resistance parameter n as a function of both the flaw size and test environment. In addition, zero stress aging experiments in various aging environments have revealed contrasting strength behavior for small vs. large flaws. The sum total of these data demonstrates that large flaws and their behavior in service are critical considerations for mechanical reliability of long-length optical fibers.

Introduction

Time-dependent fracture of brittle materials requires the knowledge of flaw statistics (flaw density vs. flaw size distribution) and stable crack growth kinetics, the latter being influenced by chemical reactive species and temperature field at the crack tip.[1] Most of the time dependence studies of optical fiber strength have neglected flaw statistics and focused on growth of a generic flaw from subcritical to critical size.[2-7] Furthermore, the majority of these studies deal with the high strength flaw—intrinsic flaw—which is relevant to short fiber lengths. Indeed, the distribution of such flaws is rather narrow, with large Weibull slope, which facilitates both the analysis and measurement of their growth. However, the results of such experiments are inapplicable to long fiber lengths containing large flaws, which means the reliability of structures such as fiber cables cannot be assessed appropriately. Although fewer in number, these larger flaws are the critical "weak links" in any cable structure. For the utmost reliability over long periods of time, the statistics and growth kinetics of large flaws are prerequisites for predicting either a safe allowable stress for a fixed life or for predicting the fiber life under specified operating conditions.[8] In most fiber structures the applied stress field is predominantly uniaxial, weather bending or tension, so that both the fast fracture and time-dependent fracture of such structures are governed primarily by the large flaws, making their study much more critical.[9]

The challenges posed by large flaws, however, are not trivial! In view of their low frequency in a given fiber population, a large sample size of long fibers is needed to measure their strength distribution and crack growth kinetics. This is indeed a formidable task both in terms of fiber utilization and the testing effort involved. Fortunately, the recent invention of a special continuous tensile tester[10] has facilitated the development of large flaw distribution with efficient utilization of fiber to failure probabilities approaching 10^{-5}. Similarly, the dynamic fatigue measurements for long fibers, over five decades of strain rate, have shed further insight into crack growth kinetics of large flaws.[3,11] Such data have demonstrated the nonconstancy of fatigue resistance parameter n, thereby, modifying lifetime predictions for long optical fibers. The measurement of crack velocity as function of stress intensity, using DCDC (double cleavage drilled compression) specimen and the scanning tunneling microscope,[12] has also shed further light on the form of such dependence—whether exponential or Power law—to crack velocities as low as 10^{-12} m/s. These data also help improve both the life prediction and safe stress estimates.

Despite above advances in measuring crack growth kinetics, there is a significant scatter in fatigue resistance constant or crack velocity data that figures heavily in lifetime predictions. Consequently, the predicted lifetimes can be in error by several orders of magnitude due to exponential or Power law dependence of lifetime on n or crack velocity. Furthermore, the commonly used fatigue models are based on a number of simplifying assumptions to keep the mathematics tractable.[13-16] The final impact of such assumptions, however, is to increase the error in predicted vs. measured lifetimes thus casting further doubt on the validity of computed lifetimes for real-life fiber structures.

Several fatigue models are available for predicting fiber lifetimes.[13-16] They involve a number of fatigue parameters whose evaluation requires either careful experimentation or certain simplifying assumptions to keep the mathematics tractable. However, certain other features of these models permit relaxation of

some of these assumptions thereby compensating for much of the uncertainty in designing fiber structures reliably. In particular, we take advantage of the experimentally determined large flaw distribution and use the Power law to determine a "safe" allowable stress which would minimize crack growth and ensure fiber integrity,[8] i.e. preserve fiber strength, over its functional lifetime. Such an approach neither requires the inert strength distribution nor calls for absolute crack growth computations, thereby alleviating two of the key assumptions used in fatigue models. Furthermore, the reaction kinetics of the Si-O bond with corrosive species like water vapor are so slow at the "safe" allowable stress that the "effective" crack velocity is negligibly small and remains relatively constant throughout the fiber's useful life.[2,17] The value of this characteristic crack velocity is estimated from the large flaw distribution and its impact on initial fiber strength examined via crack extension, if any. Hence, the above approach helps safeguard fiber's mechanical reliability and functionality over its useful life.

Fiber Reliability Issues

While a complete discussion of fiber reliability is beyond the scope of this paper, certain key issues from fiber manufacturers' and fiber users' points of view are worth summarizing.

Fiber manufacturers have long recognized that the mechanical integrity of optical fiber depends on its strength distribution following manufacturing, and strength retention during storage, cabling, installation and long-term service. The former is optimized by implementing appropriate controls in manufacturing processes including screening of raw materials, fabrication, consolidation and preparation of preform; drawing, coating, and proof testing of fiber; and winding and storage of proof-tested fiber in a controlled environment. The strength distribution of such fiber is obtained in pure tension using long lengths and special test apparatus capable of handling many kilometers of fibers.

The strength retention behavior during storage of optical fiber also is monitored experimentally by some of the fiber manufacturers and users as a function of coating composition, coating geometry, storage environment, and storage time. Any shift in the strength distribution automatically is recorded using the same procedure as for the initial strength distribution. Indeed, different flaws respond differently to zero stress aging.[18-23] From a reliability point of view, however, the aging data of those flaws that control fiber's long-term integrity (the largest flaws) are most meaningful. It is possible that such flaws may even exhibit a beneficial zero stress aging effect.

The strength retention behavior during cabling, installation and long-term service depends on both the stress-time history and environmental conditions to which the fiber is exposed. This includes processes like fiber handling, cable manufacturing, cable installation, cable splicing, cable repairs and the like. Each of these processes needs to be defined as a stress-time history together with the operating environment. Fiber users are in the best position to provide such information. This would allow the time-dependent strength behavior of fiber to be measured under realistic test conditions. The resulting data then could be used to determine the relevant fatigue resistance parameters for estimating the safe stress-time history necessary to ensure any specified level of reliability.[24] In the absence of user specific inputs, fiber suppliers may generate strength data that are not readily applicable to certain real-life conditions.

Another key issue pertinent to fiber reliability is the fatigue model one chooses to estimate the safe stress-time history for a given application. Several fatigue models have been proposed and evaluated in the literature with varied success.[13,17,25,26] Their complexities reside not only in the mathematical treatment of the models, but also in possible flaw-tip morphology changes (over long exposure times), which could alter the very fatigue parameters required for estimating the safe stress-time history.[14,15,27] It is suspected that the latter effect is facilitated by diffusion kinetics of aqueous species into certain coatings that modify the fiber/coating interfacial integrity and promote water transport to surface flaws.[28] In light of the above complexities the more amenable fatigue model, namely Power law, is often used to estimate the safe stress-time history, but here too the use of relevant fatigue resistance parameters is critical for arriving at reliable estimates.

We will elaborate on the foregoing reliability issues in the sections that follow and provide relevant data, wherever possible, to facilitate computation of safe stress-time histories or lifetime predictions for long fibers.

Strength Distribution

Figure 1 is a schematic of continuous fiber strength test apparatus,[10] developed recently, to obtain the

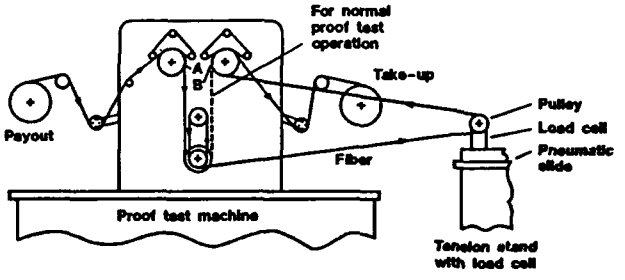


Figure 1. Schematic of Continuous Fiber Strength Test Apparatus

long-length strength distribution corresponding to failure probabilities approaching 10^{-5}; (Figure 2). When the long-length strength distribution is combined with the high strength region of 20 m fiber strength distribution (obtained by testing discrete 20 m gage lengths), the total strength distribution[8] is obtained as shown in Figure 3. The fiber population shown in Figures 2 and 3 had been proof-tested at 50 kpsi. Let us denote the high strength region by symbol I, intermediate strength region by symbol II, and the low strength region by symbol III. While region II data can be accumulated by testing a large sample of 20 m gage lengths, that for region III would require two orders of magnitude additional fiber and test effort—which would strain the resources of most fiber manufacturers. Indeed, the apparatus in Figure 1 facilitates such a task while minimizing time and material expense through continuous testing. In addition to the economic advantage afforded by this apparatus, it provides the most valuable flaw distribution, namely the large flaws, for predicting the reliability of long fibers under sustained loading.

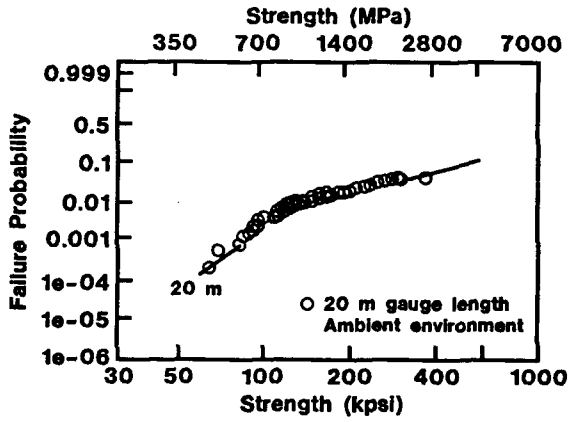


Figure 2. Strength Distribution of 386 km of Titania-Doped Silica-Clad Fiber in Low Strength Region

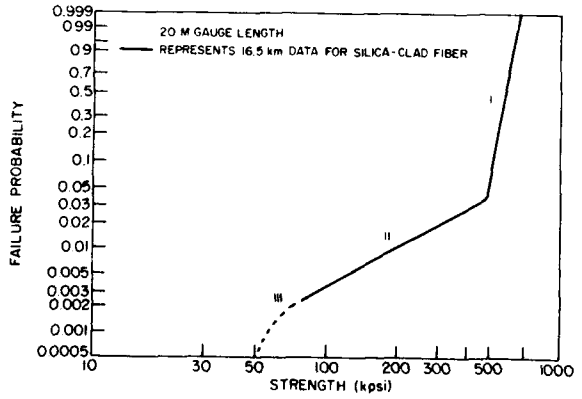


Figure 3. Total Strength Distribution of Silica Fiber in Tension (20 m gage length)

Referring to Figure 3, fiber manufacturers and users often measure only the high strength region of the distribution (region I), using a limited quantity of short gage length fiber. Measuring the strength distribution in this region requires the least amount of fiber and the data are relatively easy to obtain. The result is an invariable unimodal distribution, with a relatively high Weibull slope, indicative of uniform flaw population (known as intrinsic flaws) on the surface of optical fiber. These are also the smallest flaws whose aging and fatigue behaviors can differ significantly from those of large flaws. The study of intrinsic flaws, however, is useful mainly for theoretical modeling and adds little value for field functionality.[29]

As the cumulative length of tested fiber increases, the probability of encountering intermediate flaws also increases. This is illustrated by region II whose Weibull slope is lower and the strength range is also lower, typically by an order of magnitude. These intermediate flaws occur less frequently and, typically, result from handling damage inflicted during fiber and cable manufacturing, shipping, and subsequent cable processing. Their fatigue and aging behaviors also can vary from those of both the small and large flaws. As the total length of fiber tested increases further and the sample population grows by another order or two in magnitude, the probability of encountering a large flaw increases, thus giving rise to region III of Figure 3. The Weibull slope of region III is somewhere between that of regions I and II, indicating a tighter distribution than region II and representing large flaws that survived the proof test. Such large flaws, representing the minimum strength region, are most sensitive to fatigue damage under sustained loading. Flaws larger than region III would cause fiber failure during proof-testing while those smaller than region III would have survived the proof test.

The silica fiber in Figure 3 has survived a proof stress of 50 kpsi prior to strength measurement. In this example, the fiber manufacturers must exercise care to prevent crack growth during proof testing. This can be accomplished by limiting the unloading time to a fraction of a second and testing the fiber at a strain rate in excess of 2000% per min. The key parameters which the fiber manufacturers should control are unloading time and proof stress value to preserve fiber strength during proof testing since the allowable stress-time histories for long-term service are expressed in terms of proof stress which is assumed to represent the minimum strength.

Since the allowable service stress is a finite fraction of proof stress, the large flaws of region III would experience that fractional stress to a greater degree and be more prone to crack growth than either the intermediate flaws of regions II or small flaws of region I. Thus, the fatigue and aging behavior of flaws in region III is much more pertinent to predicting fiber reliability than that of small and intermediate flaws. Of

course, the random occurrence of large flaws as demonstrated by low failure probability in Figure 3 would require either a large fiber population or the use of abraded fiber to measure their aging and fatigue behaviors.[30] Such data for abraded silica fiber will be discussed in the next two sections.

Zero Stress Aging

Zero stress aging of silica fibers, with UV-acrylate coating, has been studied by several investigators.[18-23] The time dependence of strength of aged fibers depends on initial flaw size, aging environment, and coating formulation. The strength of unabraded fibers decreases with time due to diffusion of aqueous media and breakdown of glass/coating interfacial bond, which reduce the abrasion resistance of pristine glass surface during handling and post-processing of optical fibers. Strength losses of up to 50% have been reported for UV-acrylate coated fiber following 45 days of aging in 85°C water.[9,20,22] However, such data only pertain to the high strength region with submicron flaws whose post-aging strength is well above the proof stress and whose growth under service conditions is orders of magnitude smaller than that of large flaws.

From a reliability point of view, it is the large flaw (of "Region III") whose aging behavior is more critical. And as noted earlier, the behavior of these flaws is quite different from that of "Region I" flaws. Consequently, aging studies were carried out for abraded silica fibers in 80°C water.[9] Two types of abrasion were introduced, namely

i) draw abraded in which a 150 μm bare silica fiber was rubbed against the 125 μm bare silica fiber at right angle during drawing but prior to coating;

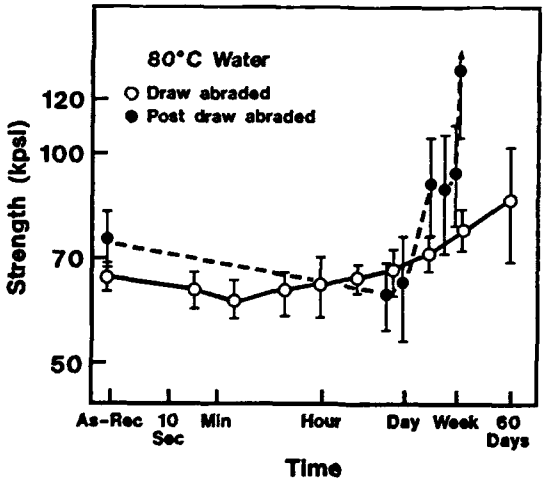


Figure 4. Effect of Zero Stress Aging on Tensile Strength of Abraded Silica Fiber (0.5 m gage length)

and

ii) post-draw abraded in which the coating was chemically removed over a small section of the fiber which was abraded by silica particles via free fall from a fixed height and subsequently recoated with UV-acrylate coating.

The mean flaw depth for draw abraded fiber was approximately 1.5 μm and that for post-draw abraded fiber was approximately 2 μm. The tensile strength of these two fiber populations following aging in 80°C water is shown in Figure 4 as function of aging time. Following initial weakening of 10-20% over the first day of aging, the strength of abraded silica fibers actually increases by 30 to 100%. The mechanism for initial weakening, which is small, is not well understood. However, the final strength increase, which is probably due to modifications in flaw tip morphology during aging, is very encouraging.

Thus, the large flaws in long optical fibers should either be unaffected by zero stress aging or should exhibit higher strength due, possibly, to residual stress release and/or crack tip blunting. Notwithstanding the well-known zero stress aging effect in high strength fibers of short gage length, the above data again point to the importance of flaw size in arriving at conclusions regarding the reliability of long-length optical fibers. What at first appears to be significant in a study of small flaw behavior, becomes less important for studying the behavior of large flaws.

Fatigue Behavior

As with strength and aging behavior, the fatigue behavior of silica fiber is also dependent on flaw depth, flaw tip morphology and the state of residual stress at crack tip. Much data exist in the literature for dynamic fatigue parameter n_d of high strength region of silica fiber (Figure 5).[11] Similarly, the static fatigue behavior of unabraded silica fiber over two years of test duration is shown in Figure 6. These data show that dynamic

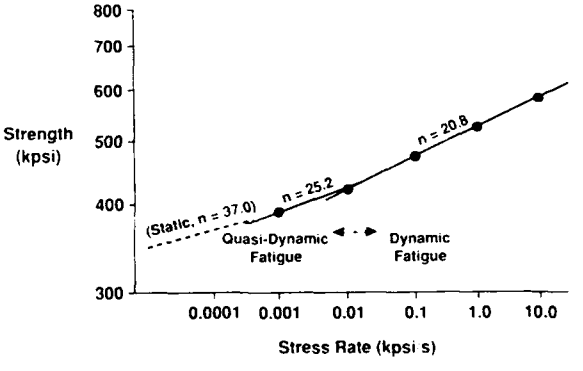


Figure 5. Strength vs. Stress Rate Dependence of Unabraded Silica Fiber in Tension (20 m gage length)

fatigue parameter n_d at moderate stress rates and the static fatigue parameter n_s have significantly different values, the former being about half of the latter.[31] However, if the dynamic fatigue measurements are carried out at lower stress rates, the ln (strength) vs. ln (stress rate) plot begins to show a distinct curvature with n_d value approaching n_s. These observations could imply flaw tip modifications, notably blunting during early stages of dynamic loading at low stress rates, which approach the geometry of flaws in long-term static fatigue experiments. Thus, the n value used for estimating fiber life from Power law fatigue model can vary significantly, resulting in a large spread in lifetime estimates. Although some spread is also observed in static fatigue data, its range is an order of magnitude smaller than that based on dynamic fatigue data. The use of dynamic fatigue parameter, n_d, provides a more conservative estimate of fiber life and/or safe allowable stress.

From a reliability point of view the fatigue behavior

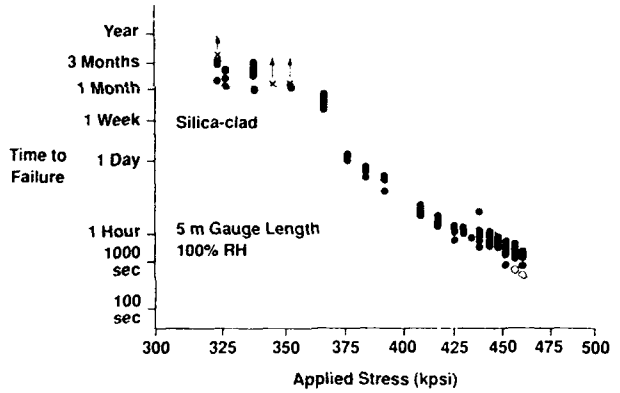


Figure 6. Static Fatigue Curve for Unabraded Silica Fiber in Tension (5 m gage length)

Table 1

Dynamic Fatigue Parameter n vs. Flaw Size for Silica

Flaw Size (μm)	n	Specimen Type and Loading Condition	Reference
0.01–1	20–23	Optical Fiber in Tension	Glaesemann and Gulati[11]
3–12	20–27	Optical Fiber in Tension	Glaesemann et al.[9]
8–15	28–38	Conc. Ring Flexure of Small Discs	Wiederhorn[32]
150–160	45	4-Point Flexure of Prismatic Bars	Gulati and Helfinstine[33]

of large flaws is of greater interest. Indeed, dynamic fatigue data for bulk silica with 10-200 μm deep flaws have been published with n values ranging from 28 to 45 indicative of higher fatigue resistance relative to silica fiber;[32,33] see Table 1. The dynamic fatigue experiments have also been carried out on abraded silica fibers with 3-12 μm deep flaws[9] (Figure 7). The type of abrasion chosen for these experiments was the post-draw abrasion described earlier for zero stress aging tests and is representative of the proof stress region (Region III) of the total strength distribution. The fatigue parameter n for post-abraded fibers has a value of approximately 20, as shown in Figure 7, although values as high as 27 have been recorded following aging of abraded fibers. Again, from a reliability point of view, the smaller n value of 20 would be more conservative and representative of large flaws, associated with proof stress region, which may or may not enjoy the benefit of aging in their final configuration in service. Accordingly, both the safe stress estimate and fiber life estimate for long optical fibers should be based on the smaller n value.

Safe Stress and Lifetime Estimates

From users' points of view, it is desirable to provide an estimate of safe allowable stress which the proof-tested fiber can support reliably throughout its functional lifetime. Such a stress can be estimated by invoking an appropriate fatigue model and specifying an acceptable level of flaw growth or strength loss. In view of its simplicity, versatility, familiarity and general acceptability, we will use the Power law model* in a conservative manner to minimize the impact of errors (resulting from assumptions implicit in the model) on safe stress estimate. Instead of designing the fiber to failure condi-

* *Furthermore, Power law is a first approximation of exponential law as may be verified by Taylor's series expansion[17].*

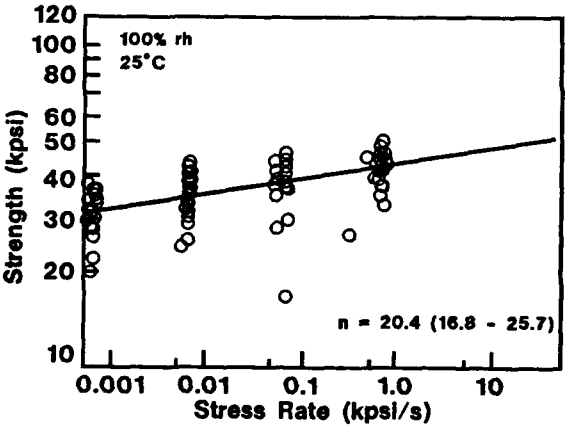


Figure 7. Strength vs. Stress Rate Dependence of Abraded Silica Fiber in Tension (0.5 m gage length)

tions, we will design for a surviving condition over a long period of time.

We can recast the Power law as[1,2]

$$\frac{da}{dt} = V_o \left(\sigma_a/\sigma_o\right)^n (a/a_o)^{n/2} \quad . \qquad (1)$$

Integrating equation 1 with respect to time for the case of constant applied stress σ_a, the time dependent flaw depth a(t) is given by

$$\frac{a(t)}{a_o} = \left[1 - \frac{V_o}{a_o}\left(\frac{n-2}{2}\right)\left(\frac{\sigma_a}{\sigma_o}\right)^n t\right]^{\left(\frac{2}{n-2}\right)} \qquad (2)$$

in which a_o denotes initial flaw depth, V_o the crack velocity at $a = a_o$ and $\sigma_a = \sigma_o$, and n is the fatigue parameter. Expanding the right side of eqn. 2 into Taylor's series and retaining the first term (since $\frac{2}{n-2} << 1$), we obtain

$$\frac{a(t)}{a_o} = 1 + \frac{V_o}{a_o}\left(\frac{\sigma_a}{\sigma_o}\right)^n t \qquad (3)$$

At this point we specify an acceptable flaw growth of 1% (or strength loss of 0.5%) after 40 years of applied stress $\sigma_a = \sigma_o$, whence $\frac{V_o}{a_o} = 7.9 \times 10^{-12} \text{sec}^{-1}$. The choice of 1% flaw growth after 40 yrs. is arbitrary, but necessary, to evaluate V_o/a_o which, interestingly, is independent of n. By specifying a negligible but nonzero flaw growth at $\sigma_a = \sigma_o$, we have essentially given a physical meaning to σ_o, namely the threshold stress. Furthermore, at $t = \frac{a_o}{V_o}$ and $\sigma = \sigma_o$ we note from eqn. 3 that $a = 2a_o$. Thus, the inverse of the system constant $\frac{V_o}{a_o}$ is the time required for the initial flaw a_o to grow to $2a_o$ at $\sigma_a = \sigma_o$, which for the arbitrary boundary condition specified above has a value of 4000 years.

It is also clear from the form of eqn. 1 that the crack velocity V depends primarily on the stress ratio $\frac{\sigma_a}{\sigma_o}$ and fatigue parameter n, i.e.

$$V = V_o \left(\sigma_a/\sigma_o\right)^n (a/a_o)^{n/2} \qquad (4)$$

Note that for $\sigma_a = \sigma_o$, a/a_o increases from 1 to 1.01 over a period of 40 years resulting in an increase of only 10% in the initial crack velocity V_o for an n value of 20. Furthermore, the value of V_o at $\sigma = \sigma_o$ is given by $7.9 \times 10^{-12}\ a_o$ and is insensitive to n for $\sigma_a \simeq \sigma_o$. For example, for $\sigma_o \le \sigma \le 1.05\,\sigma_o$, the crack velocity V ranges between V_o and $4\ V_o$ for a wide range of n values representing silica fiber ($20 < n < 28$). However, since $V_o = 7.9 \times 10^{-12}\ a_o$, the crack velocity V is a linear function of initial flaw size a_o which is physically consistent with the dependence of stress corrosion kinetics on activation volume.[34] It should also be noted from eqn. 4 that the crack velocity remains relatively constant for a good portion of fiber's functional life as long as σ_a and n remain constant.[17]

The magnitude of initial velocity for fibers with large flaws, which have survived a proof stress of 50 kpsi, is estimated from eqn. 4 to be 2×10^{-17} m/s at $\sigma_a = \sigma_o$, which agrees with previous estimates.[34] For the high strength flaw corresponding to 500 kpsi strength, the initial velocity is two orders of magnitude smaller with considerably reduced level of slow crack growth and associated strength loss. Thus, the large flaw is once again critical for assessing the impact of slow crack growth on the remaining strength and reliability of long fibers.

The threshold stress σ_o will be defined as the safe stress since it limits the flaw growth to 1% or strength loss to 0.5% over 40 years of service life. It can be estimated from the minimum fiber strength σ_f measured under fatigue conditions at a stress rate $\dot{\sigma}$. During such a test, the large flaw experiences significant crack growth with the result that the flaw ratio $a(t)/a_o$ approaches a large number and the quantity in square brackets on the right side of eqn. 2 becomes nonvanishingly small. Recalling that the equivalent static time for dynamic loading of fiber to a stress of σ_f at the stressing rate of $\dot{\sigma}$ is given by

$$t_d = \frac{\sigma_f}{(n+1)\,\dot{\sigma}} \quad , \qquad (5)$$

substituting $\sigma_a = \sigma_f$ and $t = t_d$ into eqn. 2, and setting the quantity in square brackets to zero, we obtain the following expression for safe allowable stress σ_o.

$$\sigma_o = \sigma_f \left[\frac{V_o}{2a_o}\left(\frac{n-2}{n+1}\right)\left(\frac{\sigma_f}{\dot{\sigma}}\right)\right]^{1/n} \qquad (6)$$

Equation 6 may be used to estimate the safe stress by substituting the minimum fiber strength σ_f corresponding to the desired failure probability level (such as shown in Figure 2). As an example, assuming the following representative values for long-length silica fibers,

$n = 20$

$\dot{\sigma} = 6667$ psi/sec (4% per min. strain rate)

$\sigma_f = 50$ kpsi

and recalling $\frac{V_o}{a_o} = 7.9 \times 10^{-12} sec^{-1}$, we obtain from eqn. 6 the following safe stress value:

$$\sigma_o = 0.30\ \sigma_f$$

i.e. a safe stress of 30% of minimum fiber strength under fatigue conditions is predicted by the Power law model for silica fiber.

This prediction has been evaluated at Corning by loading 100 silica fibers, of 2 m gage length, in deionized water to 30% of their proof stress value.[35] The test began in 1977 and is still in progress. None of the fibers has failed over the past 15 years. Granted, these were shorter lengths of fibers. However, as shown in Figure 8, their strength distribution included flaws approaching 100 kpsi (the proof stress level). The corresponding flaw depth was 0.75 μm, or two orders of magnitude larger than the crack tip radius. Such a flaw qualifies as a Griffith flaw[36] (i.e. large flaw) and may be modeled by Power law fatigue model.[34]

From users' points of view it is more desirable to express the safe stress σ_o in terms of proof stress σ_p. This is not as straightforward a task as expressing σ_o in terms of fatigue strength σ_f because the assumption leading to eqn. 6, namely $a(t)/a_o$ approaching a large number during strength testing, is no longer justified during proof testing of silica fibers. Traditionally, however, $\sigma_o = 0.3\ \sigma_p$ has been adopted for ensuring a reliable performance of glass and ceramic products in general.[35,37-42] Furthermore σ_o/σ_p values of 0.2 to 0.4 have also been reported in the literature[8,33] depending on the n value and proof test conditions.

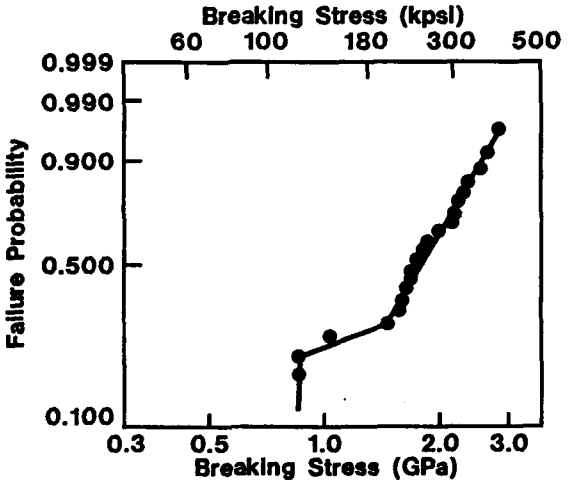


Figure 8. Strength Distribution of 2 m Long Silica Fiber, Proof-Tested at 100 kpsi, and Subjected to 30 kpsi Static Stress in Deionized Water for 15 Years

For the specific case of long-length silica fibers with large flaws, the growth of such flaws is negligible during proof testing due to two orders of magnitude higher strain rate, particularly during unloading,[43] than that used during strength testing in fatigue environment (room temperature and humidity). However, the same large flaws will experience stable crack growth during strength testing due to both the lower strain rate and corrosive test environment. The resulting minimum strength σ_f is reduced to below the σ_p value depending on the strain rate. An estimate of strength reduction, relative to σ_p, can be obtained from

$$\sigma_f/\sigma_p = \sqrt{a_o/a_f} \qquad (7)$$

in which the crack growth term (a_f/ a_o) is given by eqn. 2. Substituting

$$V_o/ a_o = 7.9 \times 10^{-12}\ sec^{-1}$$

$$n = 20$$

$$\sigma_a/ \sigma_o = \sigma_f/ \sigma_o = \frac{10}{3}$$

$$t = \frac{\sigma_f}{(n+1)\,\dot{\sigma}}$$

and

$\dot{\sigma} = 6667$ psi/sec (4% per min. strain rate)

in eqn. 2, it may be verified that a_f/ a_o ratio ranges from 1.08 to 1.96 and σ_f/ σ_p ratio ranges from 0.96 to 0.71 for σ_f values ranging from 35 to 68.5 kpsi. Thus, the minimum strength can range from 71% to 96% of proof stress value depending on initial flaw size and test conditions. Having estimated the minimum strength in terms of proof stress, the safe stress σ_o can now be expressed as

$$\sigma_o = 0.3\ \sigma_f = 0.21 \text{ to } 0.29\ \sigma_p$$

It should be pointed out that in addition to strength reduction due to fatigue as discussed above, the fiber may also encounter accidental damage during handling, shipping and cabling processes, following proof testing, which could reduce the strength further. Thus, for an ultraconservative design, the safe stress can be as low as $0.2\ \sigma_p$.

The above discussion relates to limiting the fiber stress to a safe level σ_o thereby promoting its reliability. If the applied stress exceeds the safe value, i.e.

$\frac{\sigma_a}{\sigma_o} > 1$, the crack growth will be larger, as shown by eqn. 2, and the fiber life will be shorter. An estimate of fiber life $t = t_s$ corresponding to an applied stress σ_s is obtained by substituting $\sigma_a = \sigma_s$ in eqn. 2 and letting the quantity in square brackets approach zero. We obtain

$$t_s = \left[\frac{V_o}{2a_o}(n-2)\left(\frac{\sigma_s}{\sigma_o}\right)^n\right]^{-1} \qquad (8)$$

It may be verified from eqn. 8 that for n = 20, the fiber life is reduced by an order of magnitude if $\sigma_s \simeq 1.12\ \sigma_o$ and by two orders of magnitude if $\sigma_s \simeq 1.26\ \sigma_o$ relative to its value at $\sigma_s = \sigma_o$. Thus, a small increase in applied stress can lead to significant reductions in fiber life pointing out the importance of not only defining the applied stress accurately but controlling it to promote fiber reliability. Again, the large flaw becomes the driving factor.

An alternate approach to assessing the effect of applied stress on fiber reliability is to estimate crack growth from eqn. 2 or 3 and examine its impact on fiber strength relative to proof stress. To this end, we suppose that the minimum value of initial fiber strength was σ_p, the proof stress value, and corresponded to an initial flaw of depth a_o. Following the application of a stress $\sigma_s > \sigma_o$ for time t, the initial flaw would have grown to a(t) given by eqn. 2 or 3. With the new flaw $a(t) > a_o$, the fiber would survive a proof stress σ_p' given by

$$\sigma_p' \sqrt{a(t)} = \sigma_p \sqrt{a_o} \qquad (9)$$

Since $a(t) > a_o$, $\sigma_p' < \sigma_p$, i.e. the fiber strength is reduced. Table 2 computes the strength reduction in silica fiber after 40 years of slow crack growth at σ_s values larger than safe stress σ_o. It is clear from this table that the fiber would experience a significant strength reduction if σ_s exceeded the safe stress by a small amount thereby jeopardizing its long-term reliability.

Table 2

Effect of Crack Growth on Strength Loss with Time

$\frac{\sigma_s}{\sigma_o}$	$\frac{a(40\ yrs)}{a_o}$	σ_p'/σ_p	Strength Reduction
1.0	1.01	0.995	0.5%
1.1	1.0673	0.968	3.2%
1.2	1.3834	0.850	15%
1.3	2.900	0.587	41.3%
1.33	4.0	0.5	50%

The above discussion points out the need for limiting the long-term stress in silica fiber to 20 to 30% of its proof test value to enhance its reliability. This means that both the proof stress and the applied stress should be measured accurately. In addition, since the fatigue parameter n can have a range of values, depending on test conditions, the smallest of these values should be used in eqn. 6 to estimate the safe stress for reliable performance of optical fiber. Finally, the importance of proper technical training of personnel involved in manufacturing, handling and utilization of fiber in cables and other structures cannot be over emphasized in terms of reducing the severity and frequency of large flaws.

Summary

The key points of this paper may be summarized as follows:

1. Large flaws affect both the fast fracture and time dependent fracture of long-length optical fibers, hence their frequency, morphology and stable growth under specified stress and environment are more critical to assessing fiber reliability than those of smaller flaws commonly studied and reported in the literature.

2. The recently developed continuous fiber strength tester is invaluable in obtaining the strength distribution of long fibers for stress regimes approaching proof stress level. Despite the large volume of fiber consumed, the resultant distribution extending to very low failure probabilities is indispensable for assessing fiber reliability.

3. Care must be exercised in minimizing the source, the frequency and the severity of large flaws during fiber manufacturing via quality architecture of highest standards. Once manufactured under these conditions, further growth of such flaws must be minimized and fiber strength preserved during storage, handling, shipping and utilization of fiber as it is cabled and deployed in service.

4. Large flaws behave differently than small flaws during zero stress aging. The former demonstrate crack tip blunting with a beneficial effect on initial strength distribution, while the latter exhibit crack tip sharpening resulting in a shift in high strength distribution. Despite such shift, fiber reliability is affected much more by the large flaws than small flaws.

5. Fiber users must define the stress-time history, both during installation and long term service, and the use environment so that fiber reliability under these conditions can be assessed by fiber manufacturers with the aid of relevant data and models. Such a close coordination between fiber manufacturers and users is imperative for optimizing fiber reliability.

In addition to these, the paper points out the importance of controlling proof test and aging procedures, and using an appropriate fatigue model and fatigue constant to arrive at a safe allowable stress:

i. Flaw growth during proof testing and the associated strength loss can be minimized by using a high strain rate during unloading.

ii. The time dependent strength behavior of large flaws under stressed or unstressed conditions provides the most relevant aging and fatigue data for estimating both the safe allowable stress and the lifetime of long optical fibers with high degree of reliability.

iii. The use of Power law fatigue model is better justified for large flaws than small flaws because

- they fit the Griffith flaw definition,[36]
- Inglis' stress concentration solution is applicable,[44]

and

- Irwin's stress intensity expression used in fatigue models is valid.[45]

iv. The safe allowable stress based on Power law and the large flaw fatigue behavior is estimated to be 20 to 30% of proof stress value. Under such a stress the maximum flaw growth and associated strength loss in a long fiber will be limited to 1% and 0.5%, respectively, over a period of 40 years—values that are acceptable to fiber users.

v. The expression for lifetime estimate, based on Power law and the large flaw fatigue behavior, shows that small increases in safe allowable stress can result in significant crack growth and loss of initial strength thereby jeopardizing fiber reliability. Thus, an accurate estimate and proper control of safe allowable stress are critical to fiber reliability.

Acknowledgements

The author is grateful to Scott Glaesemann, John Helfinstine, Tom Hanson, Jim Carr, Donna Taylor, Scott Robbins and Roy Love of Corning Incorporated for valuable discussions; and to Virginia Doud and Nancy Foster of Corning R,D & E for their assistance in the completion of this paper.

References

1. *X.Z. Hu, et al.; Phil. Mag. A, Vol. 58, No. 2; 1988.*
2. *S.T. Gulati; J. Non-Cryst. Solids, Vols. 38-39, pp. 475-480 (1980).*
3. *S.T. Gulati, et al.; SPIE Proceedings, Vol. 842, pp. 22-31 (1987).*
4. *D. Kalish and B.K. Tariyal; J. Am. Ceram. Soc. (USA) 61 p. 518 (1981).*
5. *D.R. Roberts et al.; Optical Engineering, Vol. 30, no. 6, pp. 716-27, (1991).*
6. *C.R. Kurkjian et al.; J. Lightwave Technol., Vol. 7, No. 16, p. 567 (1989).*
7. *F.P. Kapron; Proc. SPIE, Vol. 1366 , p. 136 (1990).*
8. *G.S. Glaesemann and S.T. Gulati; Opt. Eng., 30 (6) (1991).*
9. *G.S. Glaesemann et al.; Annual Mtg. Ceram. Soc., Minneapolis; April 1992.*
10. *G.S. Glaesemann and D.J. Walter; Opt. Eng., 30,(6) (1991).*
11. *G.S. Glaesemann and S.T. Gulati; Proc. Optical Fiber Communications Conference, 1989 Technical Digest Series, Vol. 5; Optical Society of America (OFC), Washington, DC;*
12. *J.D. Helfinstine et al.; Phys. Non-Cryst. Solids, Soc. Glass Tech., Cambridge, England, 1991.*
13. *K. Abé; Technical Digest of Conference on Optical Fiber Communication, p. 20; San Diego (1985).*
14. *W. Griffioen et al; "COST 218 Evaluation of Optical Fiber Lifetime Models," PTT Research, Leidschendam, The Netherlands; 1991.*
15. *W. Griffioen; "An Evaluation of Optical Fibre Lifetime Models II," Technical document of COST 218, WP 1, Turin, 1991.*
16. *Y. Mitsunaga; J. Appl. Phys. 53 (7), p. 136 (1990).*
17. *K. Abé et al.; Optical Engineering; special issue on "Optical Fiber Reliability;" SPIE, June 1991.*
18. *D.R. Roberts et al.; Opt. Eng., Vol. 30, No. 6; 1991.*
19. *D.R. Roberts et al.; SPIE Proc., 842; 1987.*
20. *M.T. Kennedy et al.; SPIE '91 Conf., Boston; 1991.*
21. *T.T. Wang et al.; J. Mat. Sci., Vol. 13, 1978.*
22. *M.J. Matthewson et al.; J. Am. Ceram. Soc., Vol. 71, No. 3; 1988.*
23. *J.E. Ritter et al., Glass and Optical Mat'ls Mtg of Am. Ceram. Soc., Arlington, VA; 1991.*
24. *G.S. Glaesemann and G. Kar; "Consideration of Mechanical Reliability of Optical Fiber in System Design," OEC '92, Tokyo; 1992.*
25. *P.K. Gupta; J. Am. Cer. Soc., Vol. 65, pp. C163-164 (1982).*
26. *K. Jakus et al., J. Am. Cer. Soc., Vol. 64, p. 372, 1981.*
27. *S. Ito and M. Tomozawa, J. Am. Ceram. Soc., Vol. 65, No. 8, pp. 368-377 (1982).*
28. *M.J. Matthewson and C.R. Kurkjian, J. Am. Cer. Soc., Vol. 71, p. 177, 1988*
29. *C.R. Kurkjian and U.C. Paek; App. Phys. Lett., Vol. 42; 1983.*
30. *K. Abé and R. Ernst; Elec. Lett., Vol. 21, pp. 926-928 (1985).*
31. *J.D. Helfinstine and F. Quan; Optics & Laser Tech., Vol. 14, No. 3, pp. 133-166 (1982).*
32. *S.M. Wiederhorn et al.; J. Am. Ceram. Soc., Vol. 57, No. 7; 1974.*

33. S.T. Gulati and J.D. Helfinstine; Annual Mtg. Am. Ceram. Soc., Dallas; April 1989.

34. P.C.P. Bouten and G. deWith, J. App. Phys., Vol. 64, No. 8; 1988.

35. J.D. Helfinstine; Unpublished Data.

36. A.A. Griffith; Phil. Trans. Royal Soc., Vol. 221A; London, England; 1920.

37. S.T. Gulati and J.S. McCartney; Proc. 1976 IASS World Congress on Space Enclosures; Montreal, Canada.

38. S.T. Gulati and J.D. Helfinstine; Ceram. Bull., Vol. 59, No. 4; 1980.

39. S.T. Gulati et al.; Metal Progress, Am. Soc. Metals; February, 1984.

40. S.T. Gulati and D.J.S. Wardale; Soc. Auto. Engr. Paper No. 741048; Toronto, Canada; 1974.

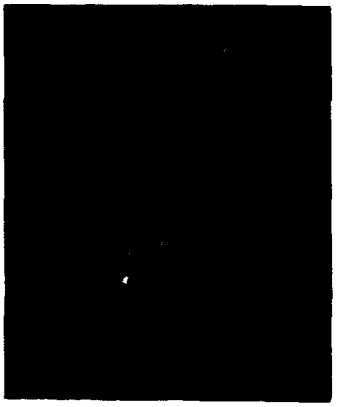
41. S.T. Gulati et al; Proc. 5th Int'l Conf. Phys. Noncryst. Solids; Montpellier, France; 1982.

42. S.T. Gulati et al.; Proc. XIV Int'l Cong. on Glass, New Delhi, India; 1986.

43. E.R. Fuller et al.; J. Mater. Sc., Vol. 15; 1980.

44. C.E. Inglis; Trans. Inst. Naval Arch., Vol. 55, p. 219; 1913.

45. G.R. Irwin; Encyclopedia of Physics, Springer-Verlag, Heidelberg; 1958.



Suresh T. Gulati is a research fellow responsible for the long-term reliability of Corning's products, including optical fiber, ceramic substrates, and fused-silica windows. Gulati joined Corning in 1967 as a senior research scientist in mathematics and mechanics. In 1974, he became a research associate in physical properties, advancing to senior research associate in 1979. Gulati was named a Corning research fellow in 1983. His research interests include the behavior of brittle materials subjected to mechanical and thermal loads, design of glass and ceramic products, strengthening methods for glasses, and fatigue and fracture of brittle materials. Before joining Corning, Gulati held positions with Cornell University, the University of Colorado, and Continental Can Company. Gulati holds a Ph.D. in mechanics from the University of Colorado, Boulder; an MS in mechanical engineering from Illinois Institute of Technology in Chicago; and a BS in mechanical engineering from University of Bombay, India. He is a member of the American Ceramic Society, American Society of Mechanical Engineers, and the Society of Glass Technology.

AGEING OF OPTICAL FIBRES IN WATER

W. Griffioen

PTT Research
Paulusstraat 4, 2260 AK Leidschendam, The Netherlands

Abstract

Measurements on fibres from different manufacturers in water are presented. The fibres were also tested in ribbons, in tight coatings and in cables. Fatigue knees and stress-free ageing were observed. A clear correlation between mechanical behaviour of the fibres and parameters from these fibres and their environments was not found. Three models to explain the anomalous mechanical behaviour of the fibres in water are discussed, one of these explaining fatigue knees, stress-free ageing and the formation of pits qualitatively. With such a model it should be possible to estimate lifetimes of the fibres in service, based on properly specified measurements.

Introduction

Recently the rate at which metal free fibre-optic cables are being installed has increased dramatically. This has been done to save costs and also to fully exploit the benefits of the dielectric optical fibre, such as the insensitivity to lightning and the absence of hydrogen formation caused by metal corrosion. The use of metal free cables brings with it the risk of the fibres being surrounded by water. In that case the description of fibre failure with stress-induced corrosion [1], the basis for most optical fibre lifetime models, is no longer valid. Fatigue knees, found in the static-fatigue behaviour of optical fibres immersed in water, are a reason to question whether existing lifetime estimations of the fibres are realistic [2,3,4]. Another anomalous effect which is found is stress-free ageing [3,4,5,6]. Long running (double-mandrel [7]) static-fatigue experiments in water and dynamic-fatigue (pulling and 2-point bending [8]) experiments after stress-free ageing in water are carried out in this work. These measurements were performed on standard fibres (different manufacturers), tight-coated fibres and fibre ribbons in water, also in a cable environment. Three models to explain the anomalous behaviour of the fibres in water are discussed.

Measurements

Fatigue knees were observed with static-fatigue double-mandrel experiments on standard fibre A [4] (see Figure 1). The fibres were placed in water of 30, 40 and 50 °C and a pH-value of about 7. The n-values (corrosion susceptibilities), obtained from the slopes in Figure 1, decrease from 21-25 to 6-8

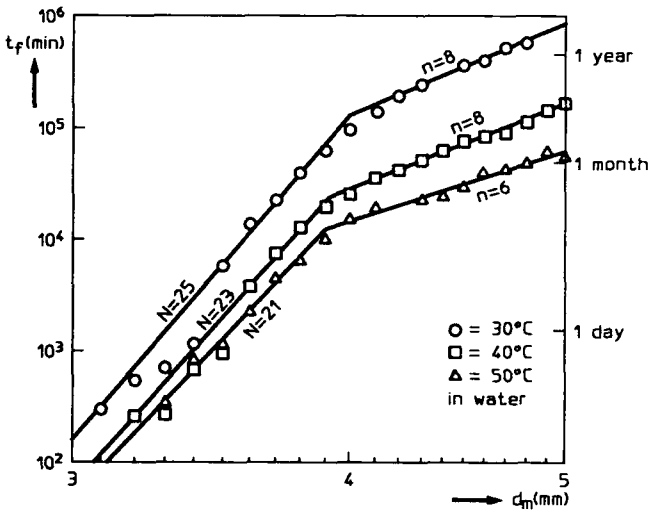


Figure 1 Median time to fracture t_f as a function of mandrel diameter d_m for standard fibre A in water of 30, 40 and 50 °C.

after the knees. With n-values of 6-8 no sufficient lifetime of an optical fibre is possible. Bending of the fibre with a bend radius of 1 m would already cause fracture [9] in service.

In order to investigate whether the fatigue knee is indeed a change in corrosion susceptibility, also experiments were performed where the (same) fibre was aged under stress free conditions. In this way effects of stress and time can be separated. With 2-point bending a decrease in fibre strength is observed when the fibre is stored (almost) stress free in water [4] (see Figure 2). This decrease was also present under inert conditions (vacuum) and with Scanning Tunneling Microscopy (STM) the formation of pits was shown [4]. These effects should, just as the fatigue knee, not occur according to the theory of stress-induced corrosion, which is commonly used to estimate lifetimes of fibres in service [9]. Probably the fatigue knees are caused by stress-free corrosion, superposed on the (normal) stress-induced behaviour. It is still unclear how these two effects work together. It should be noted that after ageing under stress-free conditions, no measurable change in n-value was found [4].

Later more fibres were investigated in water as a part of a COST-218 round robin, now under better defined conditions. In the preceding experiments the fibres were directly placed in the (large) water reservoirs of the temperature baths. Now the fibres

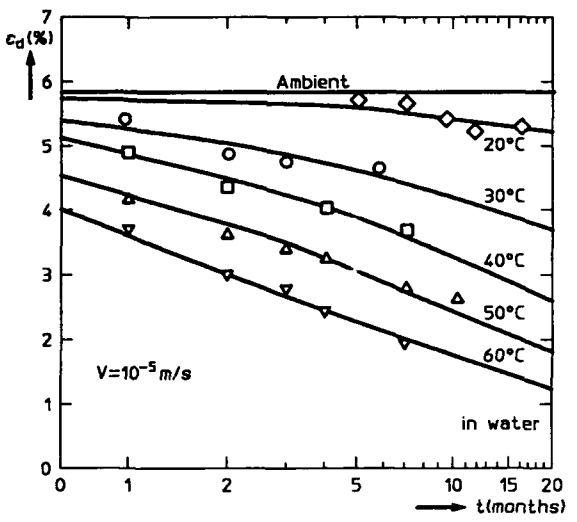


Figure 2 Median strain at fracture ϵ_d (2-point bending with 10^{-5} m/s) as a function of immersion time in water from 20 to 60 °C for standard fibre A.

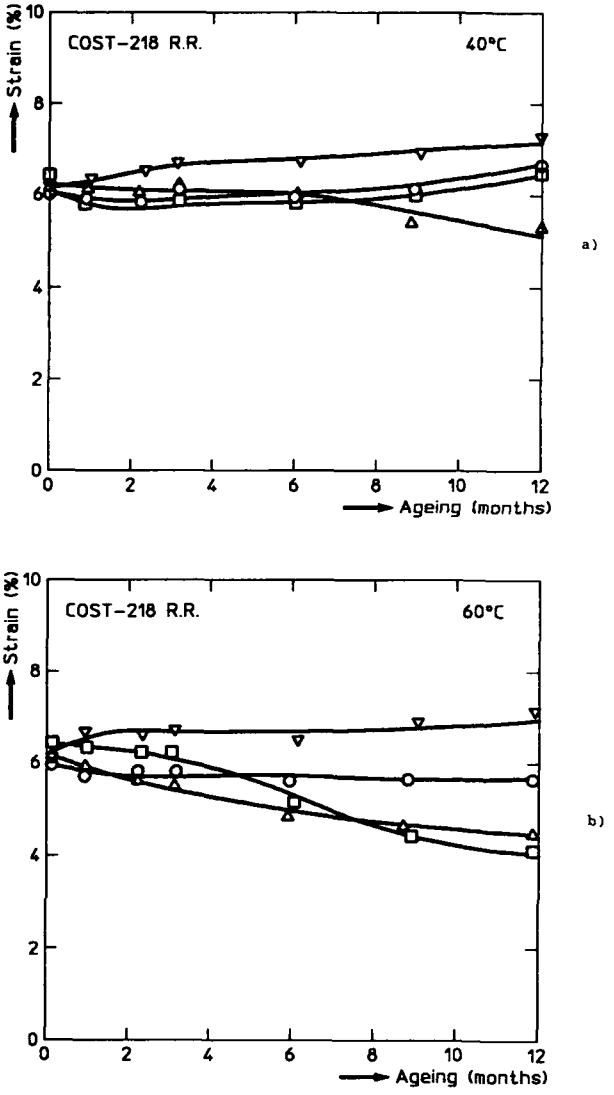


Figure 3 Median strain at fracture ϵ_d (2-point bending with 10^{-5} m/s) as a function of immersion time in water at a) 40 and b) 60 °C. The standard fibres B (circles), C (squares), D (triangles, top up) and E (triangles, top down) were measured for a COST-218 round robin.

were placed in well defined, water filled, poly-ethylene (PE) containers. For each 100 m of optical fibre one liter of water was used. In the "let go" experiments the pH-value now dropped to a value between 5 and 7. The speeds of the 2-point bender were also changed, unfortunately resulting in a lower accuracy of the measured *n*-value. Standard fibres B, C, D and E were aged stress free in water of 40 and 60 °C. The results are shown in Figure 3. At 40 °C only one fibre (D) dropped continuously in strength. Two fibres (B,C) increased in strength after an initial dip, and one fibre (E) increased continuously in strength. At 60 °C the fibre E also increased continuously in strength. The strength of fibre D, but now also fibre C, dropped continuously. The strength of fibre B remained remarkably constant. Visually nothing happened to fibre E, while the other fibres changed in colour, showed shiners or even loo ening of their coating.

In the same environmental conditions as for the COST-218 round robin, also some special fibres were tested (see Figure 4). The first fibre (F) was experimental. This fibre showed a good mechanical behaviour, but its coating looked rather poor. The second fibre (G) was an experimental multimode fibre with zero residual surface stress. This test was done to check if the small residual stress was responsible for the ageing under supposed stress free conditions [4]. It turned out that this fibre also showed a large stress free ageing. The third fibre (H) was a carbon coated fibre. This fibre is supposed to behave inert, and indeed no weakening was observed. The last experimental fibre (I) was titanium doped. This fibre possesses even a compressive residual surface stress. Stress free ageing occurs still but stabilizes after a while, just as with fibre G but a little earlier. With the special fibres no clear differences in behaviour were found for different temperatures. The effects were, of course, larger at 60 °C.

For comparison also fibre A is tested in the COST-218 conditions. The ageing is now a factor of 2 less than in the old test conditions, probably caused by the lower pH-values in the COST-218 conditions. In the COST-218 tests again no changes in *n*-values, within measuring accuracy, are found. Sometimes a weaker flaw is found, but with a strength considerably higher than for real weak flaws (the extrinsic distribution [9]. They should, however not occur, according to extrapolation of the Weibull plots (with values of the Weibull parameter *m* down to 10). Testing on longer samples is therefore recommended to investigate this effect. In the following tests longer samples are measured, and indeed the stress free ageing (of uncabled samples) looks more severe there.

The environment, not only water but also e.g. the filling gel, is important for the ageing of the fibres. Because the fibres themselves also influence

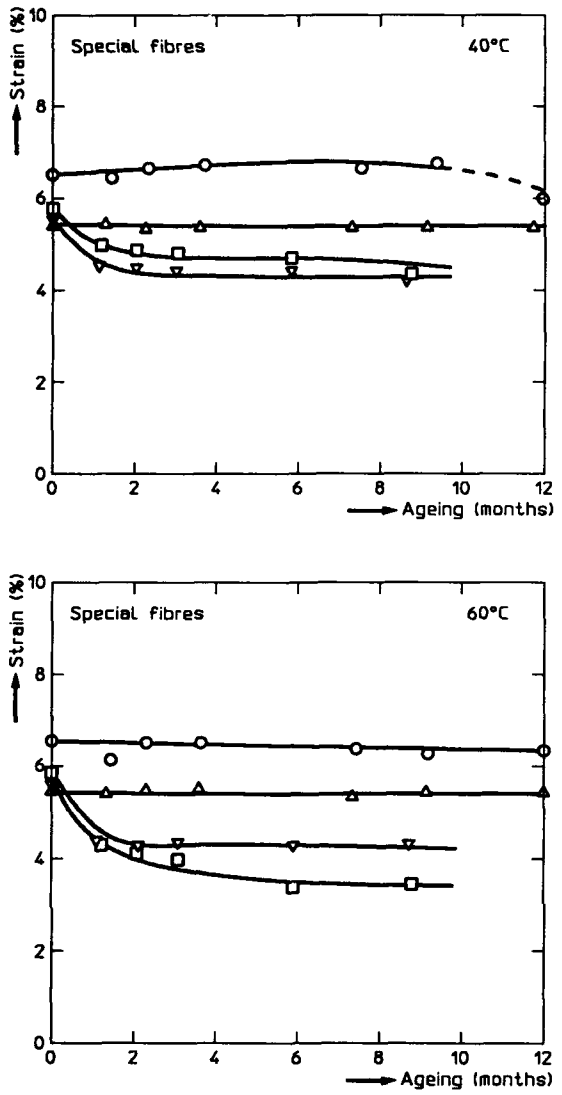


Figure 4 Median strain at fracture ϵ_d (2-point bending with 10^{-5} m/s) as a function of immersion time in water at a) 40 and b) 60 °C. The fibres F (circles), G (squares), H (triangles, top up) and I (triangles, top down) were special types: F is experimental, G experimental (zero surface stress), H carbon coated and I titanium doped.

their environment, the geometrical confinement around the fibres is also important. Therefore it was decided to perform tests in (metalfree) cables, placed in water [10]. These cables were, together with their reference fibres, immersed in large, water filled, milk containers with temperatures of 60 and 80 °C. In these "let go" experiments, now again with a large volume of water, the pH-value remained around 7. Two cable types were tested. Both are "slotted core" types. One cable is filled with fibre ribbons and with gel. The other (indoor) cable is filled with tight-coated fibres, but not with gel. The latter cable was difficult to saturate with water [10]. Therefore the 60 °C cable was artificially filled with water after 3 months. For the ribbon cable it was estimated that water saturation occurs after one day [10]. A third cable type, a gelly filled loose tube cable with coloured fibres, was not available with its reference fibres at the moment of starting the tests. Therefore the loose tubes were immersed in water instead of the cables. All fibres in the "cable tests" are of the same type as the previous tested standard fibre C.

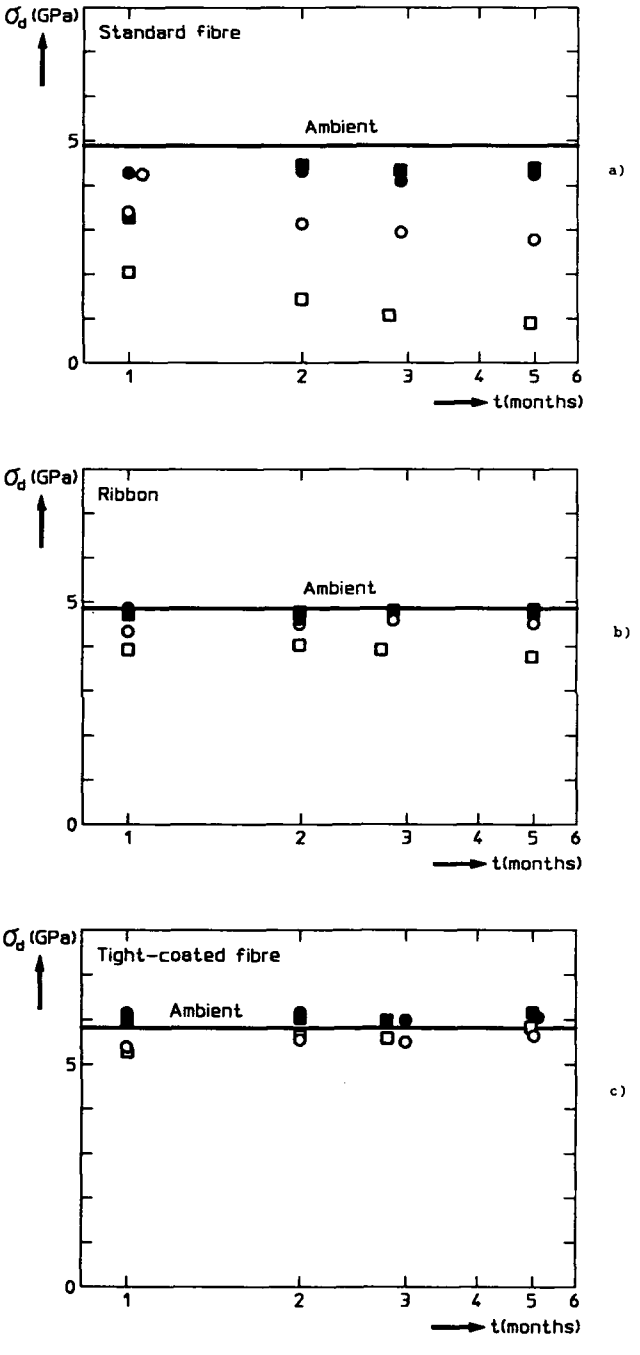


Figure 5 Median strength σ_d of 0.5 m samples (dynamic pulling with 50 mm/min) as a function of the immersion time in water, of a) standard fibres (C), b) ribbons and c) tight-coated fibres. Circles and squares represent temperatures of 60 and 80 °C respectively. The open and solid symbols represent direct immersion in water and protection by cable (loose tubes) respectively.

The measurements were done on 0.5 m samples with an Instron tensile tester. This tester was situated in a climate chamber (20°C, 50%RH) in which the fibres were stored for on week advancing the tests. First the ribbon was fractured as a whole, giving information about the weakest fibre in the ribbon. Later the ribbons were peeled, and the fibres measured separately. It turned out that a whole ribbon indeed fractures when the weakest fibre fractures. The data can be found in Figure 5. The standard fibres showed a large stress free ageing in water. At 80°C the strength even dropped down to 0.8 GPa showing a large spread (*m*-value of 5; this means that values down to 0.4 GPa are observed), while the process is still going on. With longer test lengths even lower strengths are expected. This is in contrast with reported observations that artificially abraded fibres, with strengths around the proof test level, increase in strength after immersion in water [11,12]. In the cable the ageing of the fibres was much less. Remarkable is the recovery in strength after two months of the 80°C sample. It looks as if the strength at both temperatures remains constant at a value of 4.2 GPa after 2 months.

The ribbons, and especially the tight-coated fibres (the latter fibres seem about 1 GPa stronger because of the contribution of the tight coating to the measured force) clearly weakened less than the bare (primary coated) standard fibres. For the samples that were not protected by the cable, also a constant strength level was reached. For the tight-coated fibre this level is the same for both temperatures. Especially the behaviour of the ribbons is remarkable. The protection of the ribbon, the matrix material, consists of just another layer of uv-acrylate, with physical properties close to those of the outer layer of the primary coating of its fibres. Further in this paper it is shown that changes from spool to spool in the properties of the, as received, standard fibre can be a reason for the apparent protection: the bare samples were from another spool than the fibres in the ribbon. The ribbons, aged in the cable, showed hardly any effect. The tight-coated fibres even increased in strength after ageing in the water immersed cable. Filling of the latter cable, from the 60°C container, with water did not result in any measurable change in the ageing behaviour.

In order to check the protective working of the ribbon material, ribbons with their reference fibres from the same spool were aged in water. In ribbon 1 the standard fibre C is used and in ribbon 2 an experimental fibre J. The ageing in ribbon 1 (see Table 1) was now more serious than in the same type of ribbons (it should be mentioned that both ribbons were still experimental) from the previous tests in water. Now the individual fibres in the ribbons showed also a different behaviour in ageing. This is not solely caused by the ribbon manufacturing process: The untreated standard fibres also showed different behaviour in ageing. Sometimes the fibres in the ribbon were even weaker than their reference fibres. This can however be caused by hard ribbon residues that influenced the results from the peeled ribbon. The results from ribbon 2 looked a little different, e.g. the spread in strengths is less. But still a predictable behaviour is not present.

Finally results from double-mandrel static-fatigue measurements, on ribbons in water of 50°C, are shown in Figure 6 [10]. The ribbon is another experimental ribbon with fibres C. Again "fatigue knees" are clearly visible. The different fibres in the ribbon show a slightly different behaviour.

Table 1

Dynamic strength (pulling speed 50mm/s) of fibres from ribbons and their separate fibres before the colouring and ribbon production. Results are given in GPa, before and after ageing in water for 1 month

Ribbon 1

Environment / Colour	bare samples ref	bare samples 60°C	bare samples 80°C	from ribbon ref	from ribbon 60°C	from ribbon 80°C
Red	5.00	2.32	2.14	4.79	2.93	2.55
Blue	4.74	3.00[2]	2.31[2]	4.88	2.30[1]	2.38[1]
White	4.83	——	——	4.85	2.78	2.41
Green	5.00	3.29	2.99	5.02	3.75	3.64

Ribbon 2

Environment / Colour	bare samples ref	bare samples 60°C	bare samples 80°C	from ribbon ref	from ribbon 60°C	from ribbon 80°C
Red	4.84	3.75	3.40	4.68	4.04	3.00
Blue	4.91	3.40	2.72	4.81	4.27[3]	3.94[3]
White	4.95	3.46	3.30	4.76	4.04	3.18
Green	4.94	3.67	3.44	4.76	4.10	3.25

1 Difficult to peel (hard ribbon residues)
2 One fibre was 1 GPa stronger than the rest
3 Colour removed by peeling

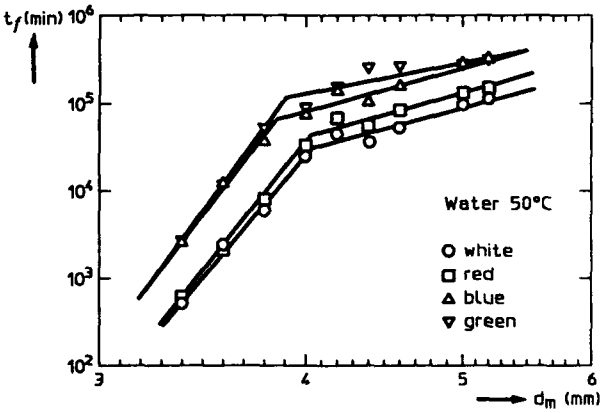


Figure 6 Median time to fracture t_f as a function of mandrel diameter d_m for fibres C in a ribbon in water of 50°C.

Search for Models

The behaviour of optical fibres in water is often not predictable. It depends on environment (e.g. temperature, water, pH-value and cabling) and on the fibre itself, probably especially on its primary coating. It would be extremely difficult to predict ageing in water, based upon the mentioned parameters. In this paper it is suggested not to bother about mentioned dependence, but rather to try to find a specification for measuring methods that can be used as a basis for lifetime estimations for fibres in water. For this a physically sound model is necessary that explains the anomalous behaviour, such as stress-free ageing and fatigue knees. In [4] an attempt was made by still using the power law with constant n-value (observed with measurements), but with a time dependent B-value. The latter assumption was based upon a change in corrosion speed due to a change in direct chemical environment of the fibre surface during ageing. After fitting the B-value to the measured stress-free ageing, fatigue knees were obtained that matched the measured knees quite reasonable. The observed pits (using STM) and decreases in inert strengths after stress-free ageing were however not explained [4].

For another attempt to explain stress-free ageing, let us return to the basics. Instead of the power law a, physically sounder, exponential law [13] is used, in which the speed of crack growth da/dt is given by:

$$\frac{da}{dt} = v_0 \exp\left[\frac{-E_0+bK_I}{RT}\right] \qquad (1)$$

Here v_0 is a scale constant, R the gas constant (8.31 J/K), T the temperature, E_0 the zero-stress activation energy and b a value which usually is assumed constant [14] (this is the same as assuming the n-value constant when using the power law). The exponential law has, in principle, a part which describes stress-free ageing (the term with E_0). This stress-free ageing will be relatively maximal when the initial crack is very small. Inert measurements, in which the strengths approach the theoretical limit [8], even suggest that optical fibres are pristine. A description with very small flaws (order of inter-atomic spacing), all of them about of the same size, which is necessary to fit experimental data, is unrealistic [15,16]. Therefore further analysis is made with the assumption that the initial flaw size is zero (the statistical nature of the first bond breaks and possible diameter variations of the fibre explain why a spread in measured strengths occurs). In this case the "sharp crack" assumption (Griffith [17]) of the calculated stress concentration around a crack (Inglis [18]) is no longer valid. Notation with a stress-intensity factor K_I [19] now results in:

$$K_I = (y\sqrt{a}+C_p)\sigma_a \qquad (2)$$

In this equation y is a geometrical constant (1.24 for a semi-circular crack [20]) and C_p is a constant, which becomes important for pristine fibres. The inert strength S_I for an initial crack size a_i follows with (2) for K_I equal to K_{Ic}:

$$S_I = \frac{K_{Ic}}{y\sqrt{a_i}+C_p} \qquad (3)$$

With K_{IC} = 0.8 MPam$^{1/2}$ [20] a pristine inert strength (a_i=0) of 12 GPa [4] results in C_p = 6.7x10^{-5}m$^{1/2}$. For constant stress σ_a, equations (1) and (2) can be solved analytically. Two solutions are of importance. First the ageing under stress free conditions results in:

$$a = v_0 \exp\left[\frac{-E_0}{RT}\right]\cdot t \qquad (4)$$

The second important solution is the fracture condition under static stress. In [13] it is pointed out that, just as in the derivation for the static condition for fracture using the power law [8], it is a good approximation if the crack size at fracture is taken infinity. Hence follows:

$$\log t + 2\log\sigma_a = C_1 - C_2\sigma_a \qquad (5)$$

with the (temperature dependent) constants C_1 and C_2:

$$C_1 = \log\left[\frac{2}{v_0}\right] + 2\log\left[\frac{RT}{by}\right] + \frac{E_0}{RT}\log(e) \qquad (6)$$

$$C_2 = \frac{bC_p}{RT}\log(e) \qquad (7)$$

This equation differs from the one in [13], where $by\sigma_a\sqrt{a_i}/RT$ is assumed much larger than 1, while a_i is assumed zero in this paper. In [14] a same kind of relation as (5) was reported. There this relation was used to find an explanation for the fact that optical (pristine) fibres show lower n-values (about 20) than bulk silica (about 40), with (larger) flaws. In this paper the relation is used to find an explanation for the "fatigue knees". When the data from the plot with "fatigue knees" from Figure 1 are plotted according to (5), as $\log t+2\log\sigma_a$ against $\log\sigma_a$, these knees indeed become less clear but do not completely disappear (see Figure 7). The fits do also not match with the inert-strength data of aged fibres from [4], when using (3) and (4). Even when a time dependent E_0-value is taken to fit the curves (same operation as time dependent B-value in [4]), flaw depths (pits) much smaller than one bond rupture are found for stress-free ageing during 7 months in water. This does not fit with the measured stress-free ageing in Figure 2 and with the decreases in inert strengths and observed (STM) pit

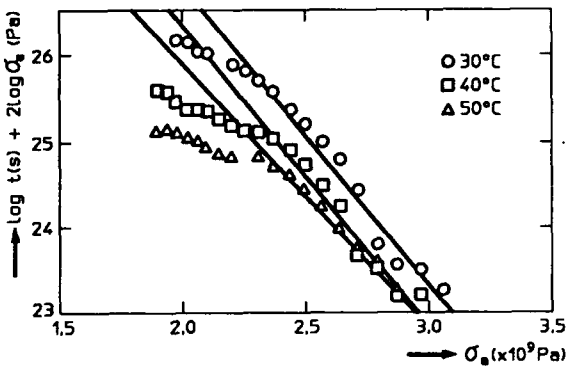


Figure 7 Static fatigue (double mandrel) tests in water of 30, 40 and 50 degrees Celsius from Figure 1, plotted according to (5).

sizes in [4]. Clearly a solution of flaw sizes less than one bond rupture has no physical meaning. This means that in that case a treatment with discrete bond ruptures is necessary instead of the presented continuous theory. Work on this subject is currently in progress, but it is not expected that the mentioned large differences can be explained.

The third attempt to relate stress-free ageing with fatigue knees makes use of the only thinkable assumption left: the reaction agent for stress-free ageing is not the same as for the stress-induced crack growth. Stress-free ageing is an etching process to which all possible aggressors can participate. Stress-induced crack growth is, however, only possible with aggressors that fit into the narrow crack and reach the tip, where the bond ruptures occur. Chemical analysis of the reaction products during stress-free ageing, e.g. with infrared spectroscopy [21], would be useful to prove above mentioned assumption. In this model it is assumed that the etching and stress-corrosion processes work independent of each other. The etching causes roughening of the surface, without the occurrence of sharp cracks (this is also how an aged fibre surface looks like under a STM [4]). In the bottom of the pits, sharp cracks may nucleate and propagate, caused by stress-induced corrosion (see Figure 8). It is assumed that the sharp crack is much smaller than the pit (for stress-induced corrosion especially the first bond ruptures are important for the time at which the crack causes fracture) and "sees" a uniform stress σ_{pit}, which is the concentrated stress at the bottom of the pit. Assume that the (non uniform) etching of the fibre surface results in the formation of pits and that the inert-strength decrease due to this can also be described with equations as (3) and (4). In that case follows:

$$S_I = \frac{K_{Ic}}{y\sqrt{v_0}\exp(-E_0/2RT)\cdot\sqrt{t} + C_p} \qquad (8)$$

Define f_{pit} as the quotient between inert strengths at t=0 and at t=t:

$$f_{pit} = \frac{y\sqrt{v_0}}{C_p}\exp\left(\frac{-E_0}{2RT}\right)\cdot\sqrt{t} + 1 \qquad (9)$$

The pits are not sharp and as a consequence the parameters in (8) and (9) have a different meaning. In the following the dependency of f_{pit} as a function of time is of importance. The only assumption is that the "shape" of f_{pit} in time is the same as in (9). The remaining parameters are fitted to the measurements. With measuring inert strengths after stress-free ageing in water of different temperatures the unknown parameters in (9) can be found. The data from [4], in which the inert strength S_I (the dynamic-fatigue strength of this fibre is shown in Figure 2) drops from 12 to 6.5, 4.5 and 2.5 GPa after 7 months of stress-free ageing in water of respectively 40, 50 and 60°C, result in E_0 = 132 kJ and v_0 = 11.2x10^5 m/s. If fracture occurred when the stress at the bottom of the pit σ_{pit} reached the pristine inert value (at t=0), then σ_{pit} can be written as $f_{pit}\cdot\sigma$. This time dependent value of the stress in the pit will form the starting point of the combined etching and stress corrosion, used to explain the knees in static-fatigue experiments. Analytic solution of stress-induced corrosion using the exponential law is not possible when the stress σ_{pit} depends on time [13]. Therefore an attempt to explain the knees is done first, using the power law for the stress corrosion. This law results, for a stress σ_{pit}, in [4]:

$$S_I^{n-2} = \int_0^t \frac{f_{pit}^{\,n}\cdot\sigma^n}{B}\,dt \qquad (10)$$

Here n is the corrosion susceptibility and B is a scale constant for the speed of crack growth. With (9) this equation can be solved analytically:

$$\log\sigma = \frac{1}{n}\left[\log\left(\frac{BS_I^{\,n-2}(f_{pit}-1)^2}{2t}\right) - \log\left(\frac{f_{pit}^{\,n+2}-1}{n+2} - \frac{f_{pit}^{\,n+1}-1}{n+1}\right)\right] \qquad (11)$$

Fits of (11) with a value of n of 30 and with values of $\log(BS_I^{n-2})$ of 288.9, 288.45 and 288.5 for respectively 30, 40 and 50°C are drawn in Figure 9, together with the measured data from Figure 1. In this case the theory explains both the fatigue knees and the stress-free formation of pits. The calculated curves are shifted downwards a little bit, when compared with the measured data. This can however be explained by the fact that the tested fibres (A) were from different spools (measurements in the preceding section showed that the ageing behaviour can differ significantly from spool to

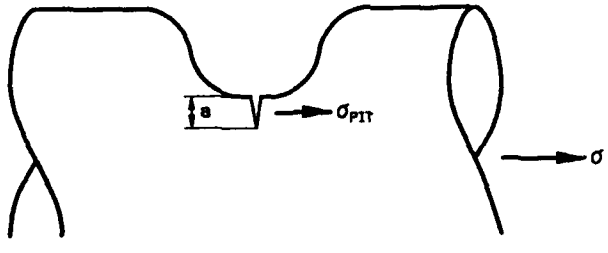


Figure 8 Model for a sharp crack, which grows under stress-induced corrosion, in the bottom of a much larger blunt pit, caused by stress-free etching.

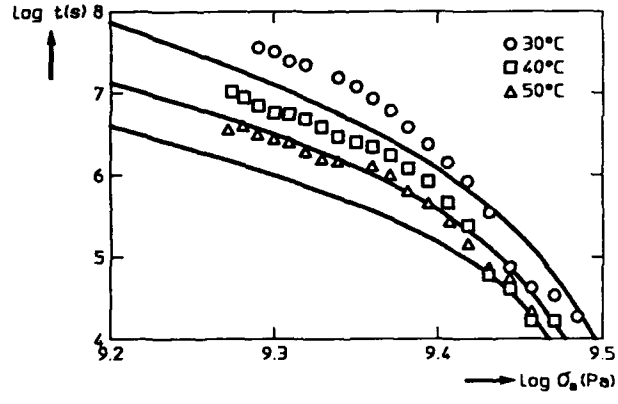


Figure 9 Calculated fits of the knees from figure 1, using the measured [4] decrease in inert strength after stress-free ageing in water.

spool). It is suggested to repeat static-stress and stress-free measurements on fibres from the same spool. Calculation (numerically) to check the curves in Figure 2 is currently in progress. It will also be checked if the change in measured B-values after stress-free ageing, observed in [4], can be explained with the presented model.

Conclusions

Measurements on fibres from different manufacturers in water are presented. The fibres were immersed as bare (primary coated) samples, in ribbons, in tight coatings and in (metalfree) cables. Fatigue knees and stress-free ageing were observed. The influence of the environment of the fibre on its mechanical behaviour in water turned out to be very important. In general it can be concluded that extra protection (material) around the fibre and low pH-values have a positive effect on the mechanical behaviour of the fibre. A prediction of this mechanical behaviour based on mentioned parameters is, however, very difficult. The type of primary coating of the fibre is also an important factor for this behaviour. It was not possible to find a correlation between primary coating behaviour, e.g. its visual performance (colouring, loosening), and the mechanical behaviour of the fibre. Moreover it was observed that the behaviour in water can be different from spool to spool with the same fibre from the same manufacturer. In this paper it is tried to find a, physically sound, model that explains the anomalous mechanical behaviour of the fibres in water. With such a model it should be possible to estimate lifetimes of the fibres in service, based on properly specified measurements. Three attempts are discussed. One of these models explains fatigue knees, stress-free ageing and the formation of pits qualitatively. The models are currently under further study.

Acknowledgements

The author wishes to thank A.T. De Boer from PTT Research, The Netherlands, and K. Jonsson and T. Volotinen, both from Ericsson Cables AB, Sweden, where a part of the presented work has been performed, for their valuable cooperation.

References

1 A.G. Evans, S.M. Wiederhorn, "Proof testing of ceramic materials- an analytical basis for failure prediction", Int. Journ. of Fracture, 10 (1974) 379-392.

2 P Hasloev, "Optical cables without metal elements", COST 218 temporary document 218TD(89)029 (Birmingham 1989).

3 C.R. Kurkjian, J.T. Krause, M.J. Matthewson, "Strength and fatigue of silica optical fibers", J. Lightwave Technol., 7 (1989) 1360.

4 W. Griffioen, W. Ahn, A.T. De Boer, G. Segers, "Stress-induced and stress-free ageing of optical fibres in water", Proc. 40th Int. Wire and Cable Symp. (1991) 673.

5 P Hasloev, "Lifetime of wet optical fibres- combined effects of stressed and unstressed ageing mechanism", COST 218 temporary document (Copenhagen 1992).

6 H.H. Yuce, J.P. Varachi, "Effect of zero stress aging on mechanical characteristics of optical fibers", Proc. SPIE, vol.1174 (1989) 279.

7 P.C.P. Bouten, H.H.M. Wagemans, "Double mandrel: a modified technique for studying static fatigue on optical fibres", Electron. Lett., 20 (1984) 280.

8 W. Griffioen, G. Segers, E. Van Loenen, "Two-point bending apparatus, fracturing optical fibres at different speeds in one run; measurements in standard and vacuum environment", Proc. Int. Wire and Cable Symp. (1990) pp.368-372.

9 W. Griffioen, T. Breuls, G. Cocito, S. Dodd, G. Ferri, P. Hasloev, L. Oksanen, D. Stockton, T. Svensson, "COST 218 evaluation of optical fibre lifetime models", to be presented at OE/FIBERS (Fiber Optics Reliability, Benign and Adverse Environment VI) (SPIE), Boston (1992).

10 W. Griffioen, K. Jonsson, "Ageing of optical fibres in water and in cable", proceedings 9th EFOC/LAN (1992) 245.

11 G.S. Glaesemann, "Safe stress model for mechanical reliability of optical fiber", presented at COST-218, WG1, Chester (UK), january 1992.

12 H.H. Yuce, P.L. Key, H.C. Chandan, "Aging behavior of low strength fused silica fibers", SPIE, Vol.1366 Fiber Optics Reliability, Benign and Adverse Environment IV (1990) 120-28.

13 K. Abe, G.S. Glaesemann, S.T. Gulati, T.A. Hanson, "Application of a phenomenological fatigue model to optical fibers", Optical Engineering, vol.30, no.6 (1991) pp.728-736.

14 P.C.P. Bouten, "Lifetime of pristine optical fibres", thesis, Eindhoven (The Netherlands), october 1987.

15 D.R. Roberts, E. Cuellar, M.T. Kennedy, J.E. Ritter, "Calculation of static fatigue lifetime of optical fiber", Optical Engineering, vol.30, no.6 (1991) pp.716-727.

16 C.R. Kurkjian, D. Inniss, "Understanding mechanical properties of lightguides: a commentary", Optical Engineering, vol.30, no.6 (1991) pp.681-689.

17 A.A. Griffith, "The phenomena of rupture and flow in solids", Proc. Roy. Soc. London, vol. 221A (1920) 163-198.

18 C.E. Inglis, "Stresses in a plate due to the presence of cracks and sharp corners", Proc. Inst. Naval Architects, march (1913) 219.

19 G.R. Irwin, "Encyclopedia of physics", Vol. VI, S Flugge, ed., Springer Berlin (1958) 551-590.

20 D. Kalish, B.K. Tariyal, "Static and dynamic fatigue of a polymer-coated fused silica optical fiber", J. Am. Ceram. Soc. (USA) 61 (1981) 518.

21 T.A. Michalske, B.C. Bunker, "The fracturing of glass", Scientific American, december (1987) 78-85.



Biography

Willem Griffioen received his M.S. degree in physics and mathematics in 1980 from Leiden University, The Netherlands. He worked at Leiden University from 1980 to 1984, where he investigated macroscopic quantum properties of liquid and solid ^{3}He/^{4}He-mixtures at ultra-low temperatures and in high magnetic fields. In 1984 he joined PTT Research, Box 421, 2260 AK Leidschendam, The Netherlands. His work includes research and development of optical cables, installation techniques and reliability of optical fibres. In the winter of 1991/92 he worked for half a year at Ericsson Cables AB, Hudiksvall, Sweden in the scope of an exchange project.

MAXIMUM VALUES OF STRENGTH AND FATIGUE PARAMETER n FOR HERMETICALLY COATED OPTICAL FIBERS

M.M.Bubnov, E.M.Dianov, S.L.Semjonov

General Physics Institute, Academy of Sciences of Russia
38 Vavilov Street, Moscow 117942, Russia

Abstract

The use of hermetic coatings on silica fibers can greatly improve fiber reliability by preventing static fatigue and hydrogen-induced loss increase. Yet, the initial strength of hermetically coated fibers usually turns out to be lower than that of polymer coated fibers. In this paper the factors limiting the maximum strength of metal- and carbon-coated fibers as well as those determining their static fatigue are considered.

Introduction

Up to now polymer coated fibers have been used in optical communication systems. The mechanical strength and reliability of such fibers are determined by stress corrosion of glass. In order to provide long-term (25-40 years) lifetime, such fibers are usually prooftested under the load 3-4 times exceeding the service stress affecting the fibers in the cable during use. Yet, recent investigations have shown catastrophic strength decrease of acrylate coated fibers under some special conditions.[1,2] Besides that, at the examination of the surface of fibers aged under zero-stress condition by means of scanning tunneling microscopy the growth of surface flaws has been observed, i.e. the loss of the fiber strength under zero stress has occured. [3] All these facts taken together make rather questionable the evaluations of the fiber lifetime based on the static fatigue model, and the idea of the coatings isolating the fiber surface from the environment becomes more and more attractive. Metal and carbon coatings allow to reduce significantly fiber static fatigue and to increase their reliability. Yet, up to now it is not quite clear what mechanism determines static fatigue of hermetically coated fibers and why the strengths of these fibers are somewhat less than those of polymer coated fibers. In this paper the factors limiting the strength of metal and carbon coated fibers as well as those determining their static fatigue are considered.

Theoretical strength snd static fatigue of silica glass under inert conditions

According to different theoretical estimates the maximum strength of silica glass reaches $\sigma_{th} \sim 25$ GPa.[4-7] These values were obtained without taking into consideration the microstructure of the glass surface. Yet, the calculations have shown that the surface crack (2 nm-deep and 0.3 nm-wide) leads to the reduction of tensile strength to $\sigma = \sigma_{th}/2 = 12.5$ GPa.[7] The roughness of just this size was observed on the surface of an "undamaged" silica fiber with the help of atomic force microscopy.[8] That is why the achieved by now for silica fibers strength level of about 14 GPa is, to our mind, the realistic strength limit.[9] Just this strength level could be expected in the case of hermetically coated fibers if these coatings could be applied without the damage of the fiber surface, and if the water presence under the coating could be avoided. The factors leading to the strength reduction of metal- and carbon-coated fibers will be considered lower.

The term silica glass "static fatigue" usually means moisture-enhanced stress corrosion cracking resulting in its fracture strength decrease. Static fatigue of hermetically coated fibers is much lower than that of polymer coated fibers, yet it does not equal zero (static fatigue parameter $n < \infty$). If we assume that there are no water molecules on the fiber surface under the hermetic coating, static fatigue of such fibers can be explained in terms of thermofluctuation theory. According to this theory the glass failure is considered as a sequential rupture of the atomic bonds at the microcrack tip due to thermal fluctuations. Stresses in this case reduce the activation barrier and apply direction to the failure process. The thermofluctuation mechanism of silica glass failure was

considered in a number of papers,[5,10-11] and it was experimentally observed at the investigation of silica fiber static fatigue in vacuum and at the liquid nitrogen temperature.[9]

According to the thermofluctuation model the dependence of time to failure on static load is given by[10]:

$$t_s = t_o \exp\left[\frac{U_o - \beta\sigma_s}{RT}\right] \qquad (1)$$

where t_o is the value approaching the period of the atom thermal oscillations ($\sim 10^{-13}$/s), U_o is the stress-free activation Si-O bond energy ($\sim$110 Kcal/mol), β is the parameter determined by the value of activation volume and size of the initial defect, R is the gas constant, and T is the absolute temperature. This relation can be transformed in the following way:

$$t_s = t_o \exp\left[\frac{U_o}{RT}\left(1 - \frac{\sigma_s}{S_{io}}\right)\right] \qquad (2)$$

where $S_{io} = U_o / \beta$ is the fiber strength in the absence of thermofluctuations (when $T = 0°K$). The dependence of the time to failure t_s on the static stress σ_s at the temperature of liquid nitrogen ($T = 77$ K) and room temperature ($T = 300°K$) is shown in Figure 1.

Usually the dependence of t_s on σ_s is described by the power function

$$t_s = B S_i^{n-2} \sigma^{-n} \qquad (3)$$

where n and B - parameters characterizing static fatigue, and S_i is the initial inert strength of the fiber.

In the logarithmic scale Equation (3) is a straight line with the slope (-n). When we use an exponential function (Eq.2), the slope is not a constant. Local value of parameter n in this case can be found from:

$$n = -\frac{\partial(\ln t_s)}{\partial(\ln \sigma_s)} = \frac{U_o}{RT}\frac{\sigma_s}{S_{io}} \qquad (4)$$

Calculations of parameter n by Eqs.(2) and (4) show that in the most important for applications range of the fiber lifetime from 1 s to 30 yr ($\sim 10^9$ s) parameter n changes in a narrow enough range from 155 to 135.

Much higher values of parameter n (400-1200) obtained in a number of papers for carbon coated fibers can be explained by the large experimental error, when parameter n exceeds 100.[12-14] For example, if the dynamic fatigue method is used, the difference between the maximum and minimum loading rates usually does not exceed 3 orders. At n = 150 the difference in the mean tensile strengths at the greatest and slowest rates would be $\sim$5%, and if the accuracy of these measurements is only 2%, the measured parameter n can change from 80 to 970. Static fatigue methods can improve the precision of n-value measurements, but there are some difficulties due to large variations in time to failure. For example, if the strength of the samples in series has a variance of 5% due to diameter variations, their time to failure at the same static load can change 1700 times (at n = 150).

Thus, our estimates of parameter n for the hermetically coated fibers in terms of thermofluctuation theory show that its maximum value should not exceed 150. Yet, this value can be even lower if the diffusion of the hydroxil groups from the fiber volume to the microcrack tip takes place.[15]

Metal coated optical fibers

A real hermetic seal is probably formed for the first time in the case of metal-coated fibers, at least aluminum coated ones, by the "freezing" method.[16,17] The essence of this method is the following. During drawing the fiber passes through an open hole filled with molten metal. If the fiber temperature is lower than melting point, fast freezing of the metal melt contacting with the fiber surface takes place. As a result, a smooth and thin (10-20 μm) metal coating is formed on the fiber. The fiber produced by this method has the strength of 5-7 GPa and comparatively low static fatigue (n~77).[18] Other methods used for fiber metallization (magnetron sputtering,[19] ion plasma deposition[20]) did not provide fiber hermetization.

The maximum strength of aluminum coated fibers is somewhat higher than that of polymer coated fibers but substantially less than the theoretical limit of glass strength. This lowering of the measured strength could be explained by chemical reaction of silica glass with molten aluminum, silica glass crystallization or fiber damaging by the film of aluminum oxide, formed on the melt surface in the metallizer. Taking into consideration all the factors mentioned above and using tin as a coating material (soft metal with low melting temperature) we managed to increase significantly the strength of sealed fibers to 10.9 GPa.[21] Investigations on different regimes of application showed that the structure of coating had

a great influence on the fiber strength. The maximum strength value of 14.6 GPa and sharp Weibull distribution were achieved if the tin coating had "monocrystalline"structure.[22] Later on this method was used to obtain lead, zink and aluminum coated fibers. These fibers had two-point-bending strength of 15.0 GPa, 11.7 GPa, 13.6 GPa and tensile strength of 7.5 GPa, 9.2 GPa, 8.1 GPa, respectively.[23,24]

During fiber sealing by the "freezing" method water molecules can be adsorbed on the surface of silica glass. So we have investigated the influence of atmospheric humidity between the draw furnace and the metallizer on strength and static fatigue of metal coated fibers. The fibers under consideration were drawn in ordinary laboratory atmosphere (60% RH) (environment 1) as well as in an atmosphere containing 300-400 ppm of water (environment 2), and in a dry inert gas containing 20-40 ppm of water (environment 3). The maximum strength of tin coated fibers measured by the two-point-bending technique did not depend on the concentration of water vapor in the atmosphere and turned out to be equal to 12.5 GPa, yet as the water content increased the spread in the strength values also increased (Figure 2). The static fatigue parameter $n = 135$ for the high strength mode of all Weibull distributions. Tensile test of these fibers showed that the tensile strength of tin-coated fibers decreased from 9.5 to 5.5 GPa with the increase of humidity (Figure 3).

During fiber drawing at 2000°C dehydration of the silica glass surface takes place. According to the generally adopted views concerning water adsorption on the glass surface during fiber cooling water molecules are mostly adsorbed on residual silanol (Si-OH) groups and not on the siloxane part of the surface.[25,26] The appearing hydroxilated parts on the fiber surface grow as separate spots while the hydration occurs along the boundary between hydroxilated and siloxane parts of the surface. In the two-point-bending test only 0.1 mm of a fiber experiences tensile stress. During metal deposition in very dry environment the probability of moisture presence on the fiber part under stress is very small. The strength in this case reaches a value of 12.5 GPa, which approaches that of the inert strength. As the humidity increases the probability of water presence becomes greater, and we observe the "tail" (low-strength part) of Weibull distribution, which however disappears at the temperature of liquid nitrogen. In the tensile test method 0.25 m of the fiber is under stress. Due to this, the probability of water presence on the stressed part of the fiber is rather high, and the Weibull distribution even for the fiber drawn in very dry environment is shifted to 9.5 GPa. Thus the observed difference in the results obtained by the two methods can be explained by the effect of residual moisture under the metal coating, which did not form a continuous layer.

The fiber lifetime is determined by the growth rate of the largest flaw after proof-test, so we carried out the investigation of strength and static fatigue of specially damaged tin coated fibers. The surface was damaged every 0.5 m by periodical touching of bare pristine fiber before metallization during the drawing process. 1 m-long samples under investigation had strength of about 1 GPa (Figure 4) with very small spread in values (the Weibull parameter $m \sim 20$). Figure 4 shows that the strength of damaged fibers increases monotonically with the reduction of the atmospheric humidity. Note that the strength of a fiber drawn in very dry atmosphere approaches the level of the liquid nitrogen strength. Sizes of the initial defects in fibers drawn at different humidities are the same due to the fact that tensile strength for all the fibers is the same in liquid nitrogen, as well as in the case when the metal coating was removed.

The results of static fatigue measurement are shown in Figure 5. The probability of water presence in the area of the largest defect is very small, so at small values of time-to-failure (at high load) the break of the fiber drawn in dry atmosphere occurs due to a thermofluctuation mechanism ($n \sim 100$). At great values of time-to-failure (at low load) the fiber break occurs due to the water-activated defect growth, so $n \sim 30$. Static fatigue of fibers drawn in the atmosphere containing more water is wholly determined by the mechanism of stress corrosion ($n \sim 30$-45). It should be noted that at the damaged regions dangling Si-O bonds are formed. Water adsorption on them occurs much quicker than on the surface of the undamaged fibers. So we suppose that for the undamaged fibers the phenomenon associated with the water adsorbed on the surface is not so prominent.

Our experiments have shown that metal coatings allow to increase the fiber strength to 10-14 GPa. High values of strength and low static fatigue of such fibers can be achieved if the water content in the atmosphere during the freezing process is less than 40 ppm.

Carbon coated optical fibers

Carbon is believed to be an excellent candidate for hermetic coating material.

Carbon coating improves the resistance of optical fiber to both static fatigue and hydrogen-induced attenuation, can be applied at sufficiently high drawing speed and does not cause additional microbending losses. At the same time the strength of 3.5-4.5 GPa is typical for carbon coated fiber, which is even less than the strength of polymer coated fibers.[12,27] While a correlation has recently been found between the fiber strength and roughness of a carbon coating,[13,14] fracture mechanism for carbon coated fibers is still unclear. Fiber damaging during the coating process[28] or tensile residual stress on the fiber surface due to carbon coating[27] were discussed as possible causes of the fiber failure.

Our investigations of dual hermetically coated optical (DHC) fibers help us to understand some problems connected with strength of carbon coated fibers.[29,30] DHC fiber has a primary coating of 500-600 Å carbon and a secondary coating of a metal. A tin or an aluminum coating (10-15 μm-thick) was applied over the carbon coated fiber from a melt by "freezing" method.

Our carbon coated fibers have two-point-bend strength of 4.6 GPa (Figure 6) corresponding to the strain of 5.3%, which is usual for this type of fibers. The two-point-bend strength of DHC fibers is 9 GPa. This is twice the strength of the carbon coated fiber, but substantially less than that of metal coated fiber. When the metal coating is removed from the DHC fiber, the resultant carbon coated fiber has the normal carbon coated strength.

To understand the mechanism of fiber failure better, a DHC fiber was loaded to the level greater than 4.6 GPa, i.e. greater than the ultimate strain of the carbon coated fiber. Upon unloading, it was tested by removing the metal coating and examining the carbon coating by immersion in hydrofluoric acid. The strength of fiber dramatically decreased. As hydrofluoric acid interacts with carbon weakly, but has a great influence on silica glass strength, this experiment demonstrates fracture of carbon coating at 5.5% -strain. Failure of the carbon coating could be clearly seen with the help of a microscope after the loading of carbon coated fibers in dry nitrogen atmosphere at strain exceeding 5.3%.[30] All these experiments demonstrate that the failure of carbon coated fiber in moisture environment takes place under the load corresponding to the ultimate elongation of the carbon coating. At the cracking of the carbon coating moisture activates the growth of surface microcracks, and as a result fiber failure occurs.

At the liquid nitrogen temperature the strength of carbon coated fibers equalling 9.5 GPa appeared to be less than that of polymer coated fibers (~ 14 GPa). Approximately the same strength had DHC fibers at the liquid nitrogen temperature (Figure 6). First we thought that this strength reduction was associated either with damage caused by the cracking of the carbon coating, or due to the stress concentration at the silica surface caused by the presence of the cracked carbon layer. However, our investigations on DHC fiber strength at the temperature exceeding 400°C showed that surface defects could appear under the carbon coating just in the process of coating application.

Figure 7 summarizes strength measurement data for DHC fibers after exposure at various temperatures. It is easily observed that change of temperature results in parallel shift of curves, but the curves shapes remain approximately the same. It is our opinion that various processes correspond to different regions in these curves. Interaction of carbon with silica glass and aluminum appears to take place in the first stage of strength degradation (region 1). When the carbon has reacted completely, it takes aluminum some time to get to silica glass surface through the layer of carbides. During this time the strength of fiber almost does not change and, consequently, plateau on the graph is observed (region 2). After that aluminum begins to react with silica, and the strength drops again (region 3). The activation energy E of strength reduction process can be obtained from such a relation:

$$\ln t_1 - \ln t_2 = E(1/T_1 - 1/T_2)/R \qquad (5)$$

where t_1 and t_2 are times of strength reducing to the same level at temperatures T_1 and T_2, R is the gas constant. Activation energy for the process of carbon interaction with silica glass turned out to be approximately 290 KJ/mol. Using strength reduction data for the DHC fiber at high temperature and relation (5), it is easy to get that inert strength of carbon coated fiber is reduced to 9.5 GPa after 0.003 s-exposure at 900°C or 0.05 s-one at 800°C. Similar time and temperature are typical for carbon coating process.

Static fatigue of carbon coated fibers is determined by the static fatigue of the coating, since our investigations have shown that fiber failure occurs just after the failure of the carbon coating. For the prepared fibers the static fatigue parameter n=200± 50, which approaches the value of parameter n = 178 for carbon.[31] Approximately the same values of parameter n

for the carbon coated fibers were cited in a number of papers.[12,27] The variations of the measurement results for parameter n in such fibers can be explained not only by the great value of experimental error when n> 100, but also by the strong static fatigue dependence of carbon on the deposition temperature.[32] The decrease in static fatigue of carbon coated fibers in water can be also explained by the change of parameter n for carbon.

Conclusion

Static fatigue of hermetically coated fibers can be explained in frames of thermofluctuation theory. Our estimates of parameter n for hermetically coated fibers showed that its maximum value should not exceed 150.

Metal coatings allow to increase fiber strength up to the level approaching the theoretical strength level of silica glass. High strength values (10-14 GPa) and low static fatigue (n $\sim$ 100) of metal coated fibers can be achieved if the water content in the atmosphere during the "freezing" process is less than 40 ppm.

The strength of carbon coated fibers is determined by the ultimate elongation of the carbon coating. The maximum strength of such fibers is limited by the strength decrease in the reactor during the coating deposition. The maximum values of static fatigue parameter n for such fibers is determined by the static fatigue of carbon coating.

References

1. M.J.Matthewson, C.R.Kurkjian, J.Am.Ceram Soc., 71, 177 (1988).
2. D.Roberts, E.Cuellar, L.Middleman, Proc. SPIE, 842, 31(1987).
3. R.S.Robinson, H.H.Yuce, J.Am.Ceram. Soc., 74, 814(1991).
4. I.Naray-Szabo, J.Ladik, Nature, 188, 226 (1960).
5. W.B.Hillig "Modern Aspects of the Vitreous State", ed.J.D.Mackenzie, 2, 152(1962).
6. D.M.Marsh, Proc.Roy.Soc.A., 279, 420 (1964).
7. T.F.Soules, R.F.Busbey, J.Chem.Phys., 78, 6307(1983).
8. H.H.Yuce, J.P.Varachi, P.L.Key, Proc. 40th Int.Wire and Cable Symp. (1991), 686.
9. B.A.Proctor, I.Whitney, J.W.Johnson, Proc.Roy.Soc.A., 297 534(1967).
10. S.N.Zhurkov Int.J.Fract.Mech., 1, 311 (1965).
11. S.M.Wiederhorn, H.Johnson, A.M.Diness, A.H.Heuer, J.Amer.Ceram.Soc., 57, 336 (1974).
12. J.T.Krause, C.R.Kurkjian, F.V.DiMarcello, R.G.Huff, Proc.EFOC/LAN (1988), 121.
13. N.Yoshizawa, Y.Katsuyama, Electron. Lett., 25,1429(1989).
14. N.Yoshizawa, Y.Katsuyama, J.Lightwave Technol., 9,417(1991).
15. W.T.Han, M.Tomozawa, J.Non-Cryst. Solids, 127, 97 (1991).
16. D.A.Pinnow, G.D.Robertson, J.A.Wysocki, Appl.Phys.Lett., 34, 17(1979).
17. J.A.Wysocki, A.Lee , Techn.Dig., 3rd Integr.Optics Opt.Fiber Commun. (1981), 24.
18. J.A.Wysocki, J.Am.Ceram.Soc., 66, C-38, (1983).
19. P.G.Hale, J.B.Almedia, C.J.R.Sheppard, Phys.Fiber Optics, ed.Bendow B. and Mitra S.S., 115(1981).
20. M.L.Stein, S.Aisenberg, J.M.Stevens, Phys.Fiber Optics, ed. Bendow B. and Mitra S.S., 124(1981).
21. V.A.Bogatyrev, M.M.Bubnov, E.M.Dianov et al., Sov.Tech.Phys.Lett., 14, 343 (1988).
22. V.A.Bogatyrjov, E.M.Dianov, S.D.Rumyantsev, Proc.Opt.Fiber Commun.Conf.(1992) 219.
23. V.A.Bogatyrjov, M.M.Bubnov, E.M.Dianov et al., Proc.Opt.Fiber Commun.Conf. (1991) 115.
24. V.A.Bogatyrjov, E.M.Dianov, S.D.Rumyantsev et al. Sov.Lightwave Commun., 1, 227(1991).
25. R.K.Iler "The Chemistry of Physica" (1979) ch.6.
26. C. Pantano "The Strength of Glass" ed. C.R.Kurkjian 37 (1985).
27. K.E.Lu, G.S.Glaesemann, M.T.Lee et al. Opt.Quant.Electron., 22, 227(1990).
28. R.G.Huff, F.V.DiMarcello, Proc.SPIE, 867, 40(1987).
29. M.M.Bubnov, E.M.Dianov, A.M.Prokhorov et al.,Proc.Opt.Fiber Commun.Conf. 400 (1992).
30. M.M.Bubnov, E.M.Dianov, A.M.Prokhorov et al., Sov.Lightwave Commun., 2(1992) in press.
31. J.S.Nadeau, J.Amer.Ceram.Soc., 57, 303 (1974).
32. W.P.Minnear, T.M.Hollenbeck, R.C.Bradt, P.L.Walker, J.Non-Cryst.Sol., 21, 107 (1976).

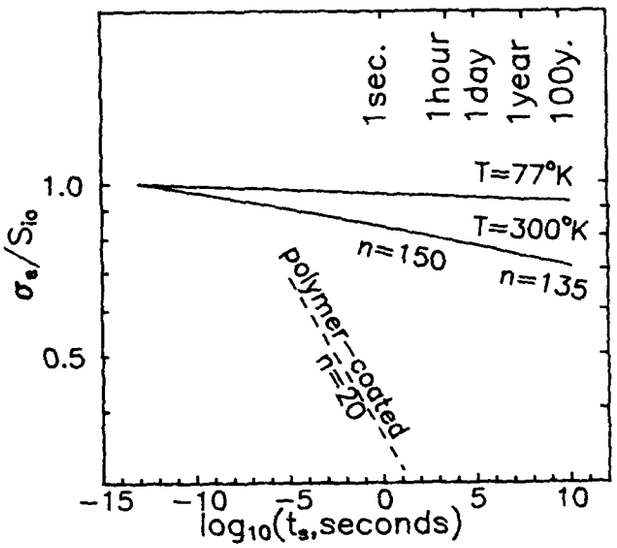


Figure 1. Static fatigue of hermetically coated silica fibers according to thermofluctuation theory.

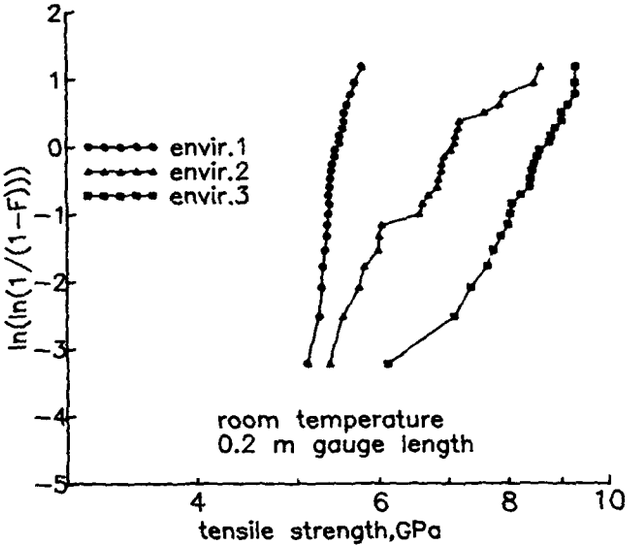


Figure 3. Tensile strength of undamaged tin-coated fibers tested at room temperature.

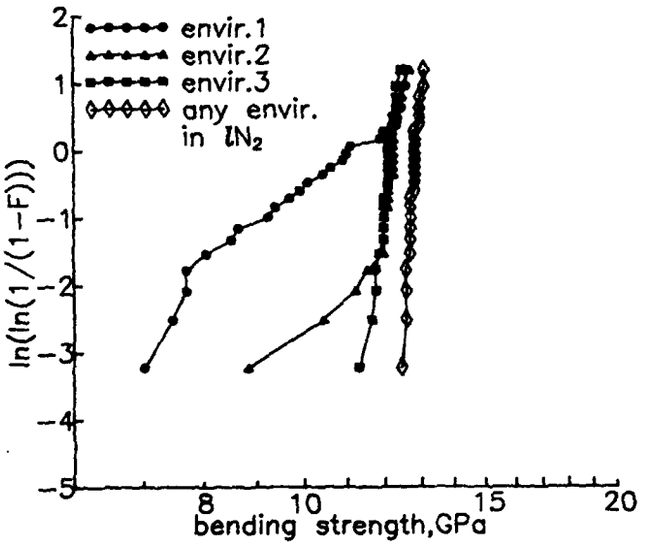


Figure 2. Bending strength of undamaged tin-coated fibers tested at room temperature and in liquid nitrogen (lN_2). F-failure probability.

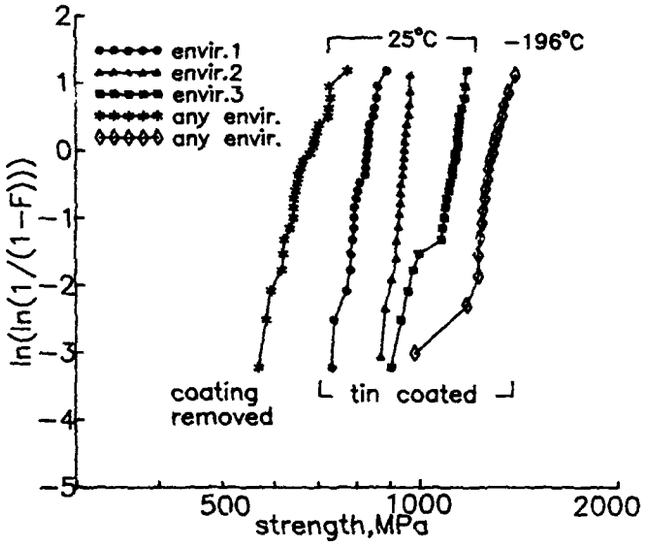


Figure 4. Tensile strength of damaged tin-coated fibers drawn in three types of atmosphere and tested at room temperature (20°C) and in liquid nitrogen (-196°C).

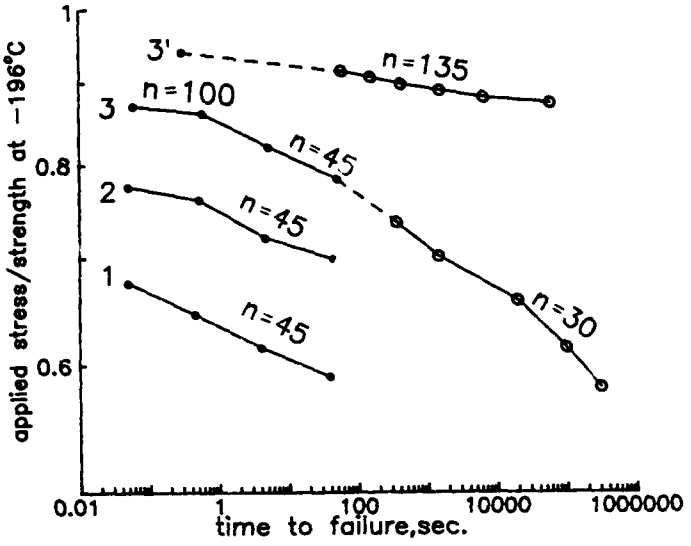


Figure 5. Static fatigue of damaged (1,2,3) and undamaged (3') tin-coated fibers drawn in environments 1,2 and 3, respectively. Damaged fibers were tensile tested and undamaged -in bending. Closed circles -reculculated results of dynamic fatigue measurements.

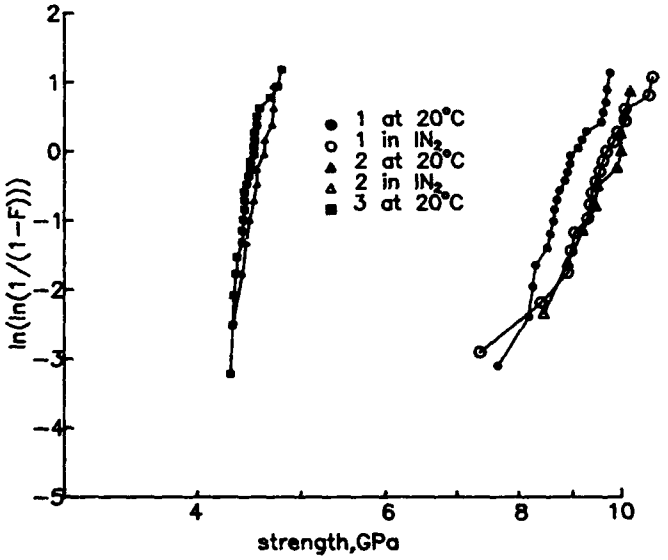


Figure 6. Strength of dual hermetic coated (DHC) fibers (1); DHC fibers after removal of metal coating (2); carbon coated fibers (3).

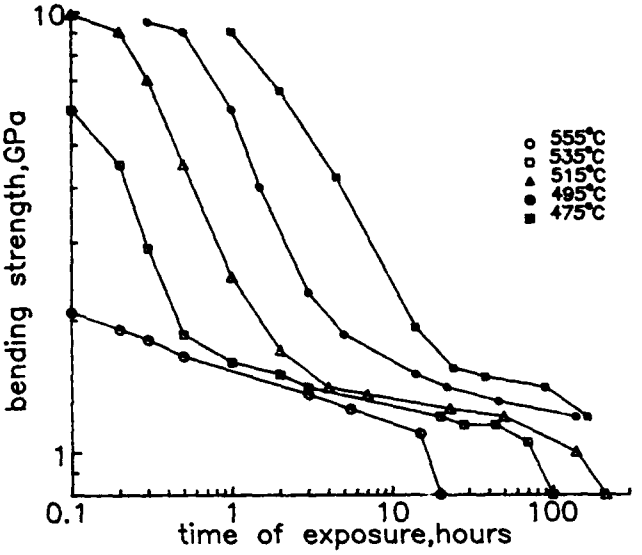


Figure 7. Strength measurement for DHC fibers after exposure at various temperatures.



Mikhail M.Bubnov was born in Moscow in 1946. He graduated from Moscow State University in 1970 and received in 1978 the Candidate of Science degree in physics from P.N.Lebedev Physical Institute of the USSR Academy of Sciences, where he worked on neodymium laser glass. Since 1978 he has been engaged in research on drawing technique, polymer coating and mechanical properties of optical fibers. He joined General Physics Institute of the USSR Academy of Sciences in 1982. He is currently involved in investigations on optical and mechanical properties of hermetically coated fibers.

E.M.Dianov was born in 1936 in Tula, Russia. He graduated from Moscow State University in 1960 and received the Ph.D.degree in physics from P.H.Lebedev Physical Institute of the USSR Academy of Sciences in 1966. From 1960 to 1982 he was with the P.N.Lebedev Institute. Since 1982 he has been with the General Physics Institute of the USSR Academy of Sciences. His early work was connected with the investigation of neodymium laser glasses. Since 1973 his research interests have been mainly in the field of fiber optics. He has contributed to the development of high strength optical fibers and to the investigations of defect centers and radia-

tion effects in silica glass and fibers. His present research efforts are in the areas of non-linear guided wave phenomena, integrated optics, and fiber lasers and amplifiers. He is the Head of Fiber Optics Department and Deputy Director of the General Physics Institute. Prof.Dianov is a fellow member of the Optical Society of America.



Sergey L.Semjonov was born in Zagorsk, USSR, in 1958. In 1982 he graduated from the Moscow Physical Technical Institute. Since 1982 he has been employed by the Fiber Optics Department of the General Physics Institute of the Russian Academy of Sciences. He works in the area of technology of optical fibers. His current activities are focused on fabrication of hermetically coated optical fibers and investigation of mechanical properties (strength and fatigue) of silica glass and fibers.

Reliability of waterproof optical fiber cables

Masaaki KAWASE

NTT Telecommunication Field Systems R&D Center
Tokai, Ibaraki, 319-11 Japan

Abstract

In order to construct reliable and economical optical fiber cable network, NTT have been used water-blocking optical fiber cable systems. This system consists of water-blocking cables, water sensors and supervision system. In this paper, strain design, water proofing and the other features of the water-blocking cable are described. The design of water sensor is also described.

In addition, design and performance of a new cable system which contains water-blocking cables, water sensors and the OTDR, is presented.

1. INTRODUCTION

Reliable and economical optical fiber cable technologies are required for use by future BISDN services. Optical fiber lifetime is determined by its history of stresses. Therefore, reduction of such stresses is a key factor in optical fiber cable design. In addition, the stress corrosion parameter n of an optical fiber is less in water than in air. Therefore, the environment of installed fibers should be considered.

In Japan, jelly-filled cables are not often used because jelly remaining on the fibers affects splicing work, and it is difficult to completely remove the jelly. Therefore, we developed water-blocking cables containing a water absorbent tape. The expansion of the absorbent material stops the flow of water which seeps into the cable through a broken sheath.

For reasons of economy, fiber ribbons are usually used in a high count optical fiber cable, in order to increase fiber density and to reduce splicing time.

This paper discusses fiber strain evaluation and the basic performance of water-blocking cables. Also, we study the reliability of an optical fiber cable network which consists of water-blocking cables and water sensors. Finally, we present experimental results from optical fiber cables and water sensors installed into a research facility over a period of three years.

2. WATER-BLOCKING OPTICAL FIBER CABLES

2.1 Structure and fiber strain

Optical fiber lifetime is determined by its history of stresses and by the atmosphere. The causes of stresses are back tensions during manufacturing, bending, torsion, installation force, temperature variation, etc. The stress diagram is most important when discussing fiber reliability. Such a diagram is shown in figure 1. Stresses can be divided into three categories: before installation, during installation, and after installation. We now calculate and evaluate theses stresses.

(1) Cable structure

Figure 2 shows a cross section of a 1000-fiber water-blocking cable. For high density packaging, we decided to use an 8-fiber ribbon which can be divided into two 4-fiber ribbons. Therefore, 8-fiber ribbon cables can be easily joined conventional 4-fiber ribbon cables.

(2) Fiber strains due to manufacturing

First, we consider structure induced strains which fall into three categories: elongation strain e_e, bending strain e_b, and twisting strain g.[1] e_e is caused by on the fiber ribbon during the manufacturing process. This value is less than 0.025%.[1] Figure 3 shows the calculation model for fiber strain caused by bending and twisting. This is based on one of the slotted rods shown in figure 2. The total fiber strain e caused by the structure and manufacturing process is calculated from by three kinds of strain by

$$e=(e_e+e_b)/2+(((e_e+e_b)/2)^2+g^2G_f^2/E_f^2)^{1/2} \quad (1)$$

where G_f is the modulus of elasticity in shear and E_f is Young's modulus of the fiber. For 1000-fiber water-blocking cable, the distance between cable center and slotted rod center a_1 is 13 mm, a_2 is 5.2 mm, E_f is 7200 kg/mm^2, and G_f is 3200 kg/mm^2. The calculated results are shown in figure 4. The fiber strain is required to be less than 0.05%. The area on the right of the line in figure 4 is a suitable combination of slotted rod stranding pitch p_1 and slot stranding pitch p_2. We selected the combination p_1=900mm and p_2=600mm. The measured stress was less than 0.03%.

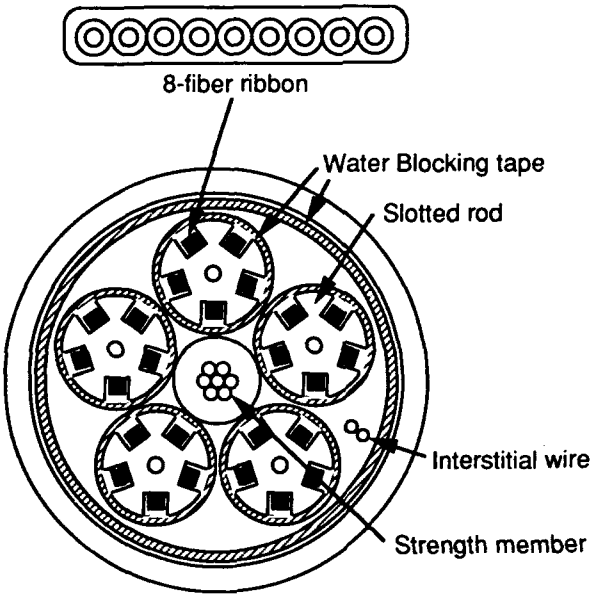


Figure 2 1000-fiber water-blocking cable

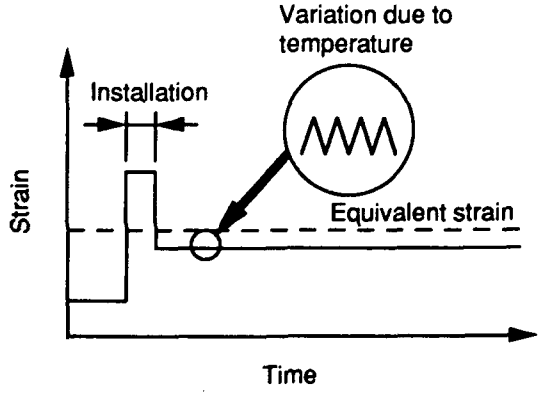


Figure 1 Strain diagram for reliability design

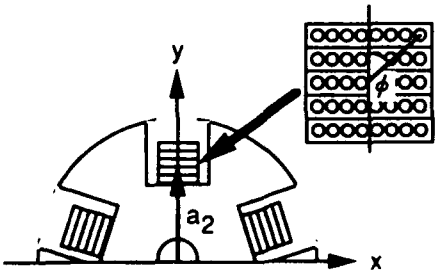


Figure 3 Calculation model for fiber strain

(3) Fiber strain due to installation

Fiber strain e_i during installation is expressed by

$$e_i=T/\Sigma E_iA_i \quad (2)$$

where T is the installation force, E_i is Young's modulus of each cable element, and A_i is the cross-sectional area of each element.

The strength member located at the center of the cable, was designed to keep fiber elongation below 0.15%, under maximum installation force.

(4) Fiber strain due to temperature variation

This cable will be installed in an underground conduit or an underground tunnel. Under these conditions the temperature range is from 0 to 40°C. Cable elongation due to temperature change is calculated by

$$e_C=\Delta t(\Sigma\alpha_iE_iA_i/\Sigma E_iA_i) \quad (3)$$

where Δt is temperature change, α_i is the coefficient of linear expansion of each cable element. The measured fiber elongation is less than 0.03% in over above temperature range.

2.2 WATERPROOFING

(1) Water-blocking mechanism

To satisfy the requirement of eliminating the use of jelly to trap water which seeps into the cable, we decided to use water-blocking tape.[2] This tape consists of absorbent powder, water-soluble adhesive, and base-tape as shown in figure 5. The water-soluble adhesive holds the absorbent powder on the base-tape. When water seeps into the cable, the water-soluble adhesive dissolves. thus releasing the absorbent powder to fill the empty spaces in the cable.

However, problems could be caused by the absorbed water remaining in the cable.

(2) Hydrogen generation

Hydrogen is generated by the reaction of some metals with water. We therefore changed the cable materials. Table 1 shows the conventional

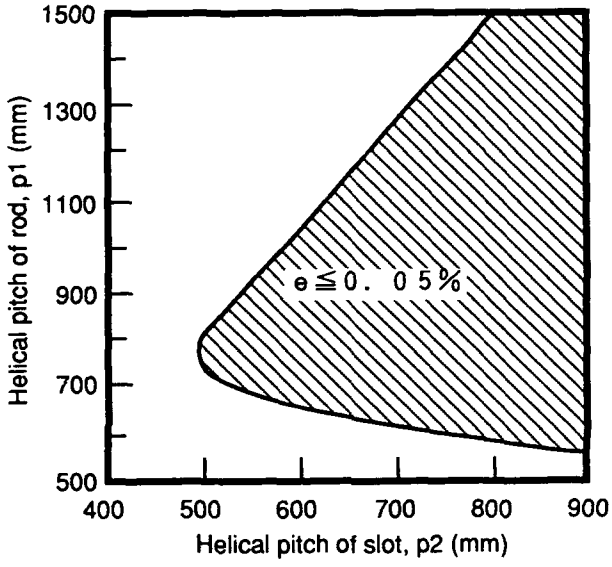


Figure 4 Appropriate combination between rod pitch p1 and slot pitch p2

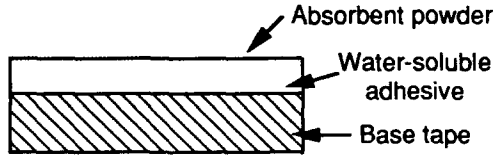


Figure 5 Structure of water-blocking tape

Table 1 Old and new components in the cable

Component	Conventional	Improved
Strength member	Steel wire plated with Zn	Cu cladding steel wire
Sheath	PE with laminated Al	Plain PE

and improved components. We measured the hydrogen generated by both the conventional and improved strength member in water at 80°C. Steel wire with a Cu cladding generated no detectable hydrogen. In addition, the sheath was replaced by PE. Therefore, it was unnecessary to consider increase in loss caused by the improved materials.

(3) Increase in loss caused by water below 0°C

Artificial seawater was pumped into a 10-m cable. We measured increases in loss of conventional and water-blocking cables. In the conventional cable, loss increase is 0.05 dB/10m at 1310 nm. However, in the water-blocking cable, we did not find any loss increase. Loss increase caused by the large lateral pressure of frozen water. However, in the water-blocking cable, the absorbed water did not freeze like ice but formed into a gel. Therefore, the lateral pressure was not so great as that of ice.

2.3 OTHER PERFORMANCE

The standard Single-Mode fiber was used in the manufactured cable. The cable diameter was 40 mm with a weight of 1.4 kg/m. There was no loss increase over the temperature range of -30 to +60°C. There was no loss increase during a squeezing test, with a tension of 800 kgf and a mandrel of 600-mm radius. The water penetration length was less than 3 m, using the conventional test set-up. Up to this distance, the loss increase caused by sub-zero water was negligible.

3. MAINTENANCE OF THE WATER-BLOCKING OPTICAL CABLE SYSTEM

3.1 Optical Fiber Characteristics Due to Water Penetration

Using this system, cables and closures are continue to be used after water penetration. Therefore, a consideration should be given to the adverse of this residual water. If the cable sheath is damaged by construction work, but the damage has not reached the core, the cable can still be used. The problem is not serious, because water penetration length is less than 3 m from the damaged sheath.

However, in a closure, fibers are bent to 30 mm radius to deal with the excess length of spliced fibers in high-density packaging.[3] This reduces the fiber lifetime because of greater bending stress compared with the cable. In addition, the probability of penetration is much higher than that of the cable, because a closure is often opened for operation or transfer of fibers.

(1) Reliability of optical fibers

Methods based on a screening test and strains are commonly employed for the design of optical fiber reliability .[4] The fiber failure ratio F is expressed by

$$F=1-\exp\left(NpL(1-(1+(\sigma_a/\sigma_p)^n(t_a/t_p))^{m/(n-2)})\right) \quad (4)$$

where L is the fiber length(m), σ_a is the fiber strain(%), σ_p is the screening strain 0.5%, t_a is the time during which the strain is applied (sec.), t_p and N_p are screening time (1 sec.) and fiber failure probability during screening (times/m),

and m is the Weibull distribution constant.[4]

In addition, n is the stress corrosion parameter and for presently used fiber with UV coating, it equals 23 in air and 20 in water.

(2) Failure probability of optical fibers

The calculated results of the fiber failure probability are shown in figure 6. The fiber equivalent strain σ_a is taken to be σ_a=0.17%. When using water-blocking cables, the water penetration length is less than 3 m. Assuming one water penetration per kilometer, increase in cable failure probability is very small.

The calculated results for the relationship between fiber failure probability and the water penetration period of the closure are shown in figure 7. The fiber strain σ_a is determined from the bending strain. The bending radius is 30 mm. The failure probability, after a fixed period of water penetration, is transformed from the dashed to the solid curves.

Based on the above discussion, we found that when using water-blocking cable, there is no adverse effect on the fiber reliability. However, the bent fibers in the closure are affected. Therefore, it is necessary to remove water when it penetrates a closure. Consequently, we study water sensing techniques for the splicing closure.

In addition, connectors and fusion splices in water were shown to be reliable for one year.[5]

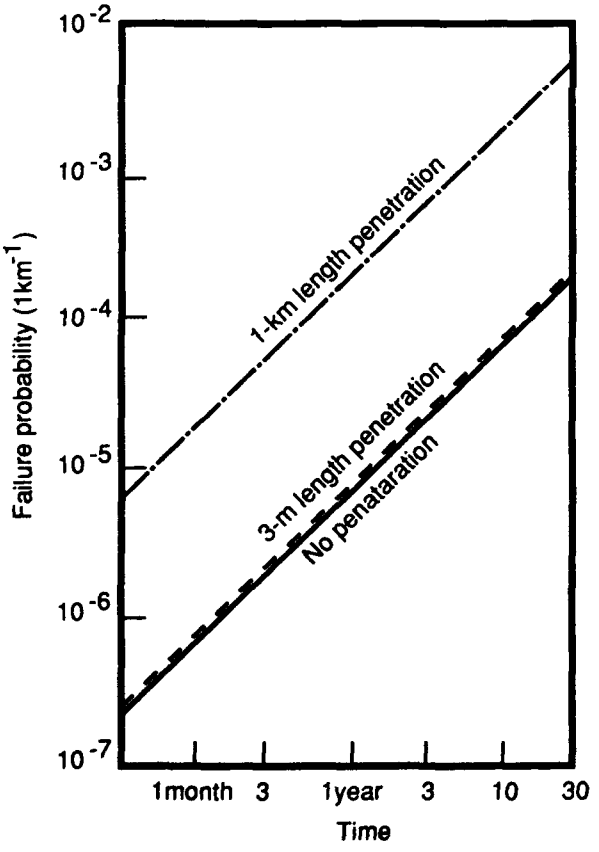


Figure 6 Failure probability of fiber in a cable

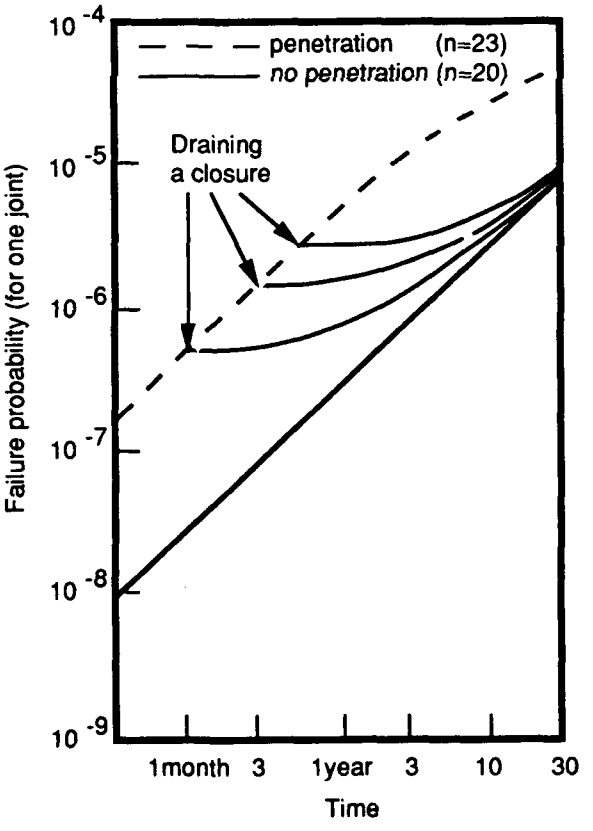


Figure 7 Failure probability of fiber in a closure

3.2 Design of water-blocking cable system

(1) Water penetration sensor

Two methods were considered for detection of water penetration: an electrical method that uses a metallic conductor [6], and a method which uses optical fiber bending loss[7]. It is desirable that sensors and monitor lines are dielectric to eliminate problems of induced current. Using the latter method, very small sensors are needed.

Figure 8 shows the basic structure of the water-penetration sensor. When water surrounds the sensor, it is absorbed by the absorbent material whose volume increase. This pushes a movable plate against the fiber thus bending it and increasing the optical loss. This additional bending loss is then detected by an OTDR (Optical Time Domain Reflectometer).

The fiber bending loss can be calculated with Marcuse's equation[8]. When using 1550 nm wavelength and bending radius is 5 mm, the bending loss is larger than 1 dB. Under these conditions, the failure probability calculated by equation [1], is less than 0.1% over 10 years, which is sufficiently very small.

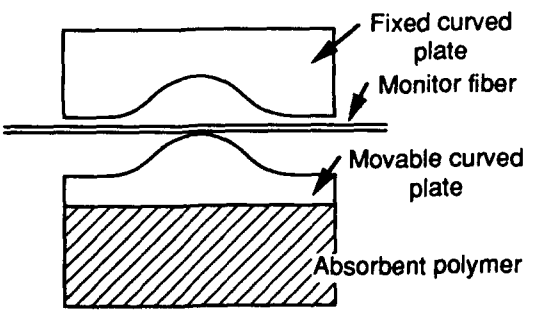


Figure 8 Structure of water sensor

(2) Reliability of the water-blocking cable system

The reliability can be maintained by providing a sensor to detect the penetrating water. As shown in figure 7, the fiber failure probability depends on the duration of water penetration of the joint. According to figure 7, the changes in reliability over less than 1 year is sufficiently small. Therefore, if the duration is assumed to be less than one year, the reliability of the water-blocking cable system is satisfactory. In practice, we monitor water penetration of closures, at three month intervals with automatic systems which consists of an OTDR, optical switch and fiber distribution frame[9].

4. EXPERIMENTAL RESULTS

We constructed the test systems in the laboratory using water-blocking cables and sensors. Total cable length is 930 m, and there are two splicing points in which water sensors are located.

To study water penetration effects, we filled one closure with water. Figure 9 shows the loss spectra of an optical fiber, under three conditions: before water penetration, 3 months after penetration, and 30 months after penetration. We found no increase in attenuation due to water penetration. Figure 10 shows the OTDR measurement results for the water sensor and monitor line. The closure is located the 708 m from the OTDR. Loss increases by 2.5 dB due to the water penetration. This shows that the water sensor was very effective.

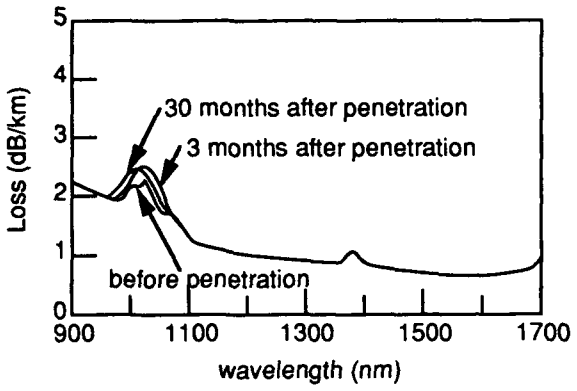


Figure 9 Loss spectra of fiber in the experimental cable

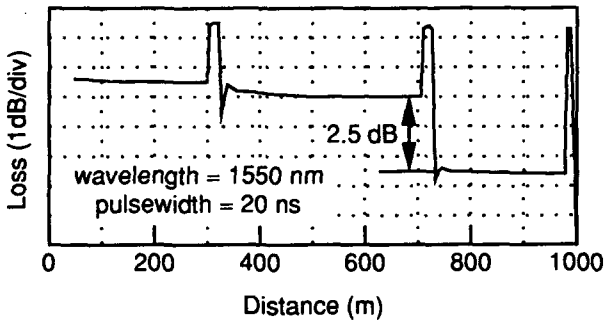


Figure 10 OTDR measurement when experimental closure is penetrated

5. CONCLUSION

We confirmed the long-term reliability and waterproofing performance of a 1000-fiber water-blocking cable.

(1) In order to ensure fiber reliability, we designed a slotted rod optical fiber cable. According to this design, the fiber strain due to manufacturing process is less than 0.05%, fiber elongation is less than 0.15% during installation and fiber elongation due to temperature variation is less than 0.03%.

(2) We prevented increase in loss caused by hydrogen by changing the components in the cable. We also prevented increase in loss caused by sub-zero water by using absorbent material.

(3) We calculated fiber failure probabilities in the cable and in the closure. With these results, cables are maintenance free, and closures should be checked at regular intervals.

(4) We developed water sensors for monitoring closures. In addition, we tested a water-blocking cable system, and found no problems.

NTT introduced this type of cable system in April 1990, and it is proving very useful for constructing optical fiber subscriber networks.

REFERENCES

[1] S. Hatano, Y. Katsuyama, T. Kokubun, and K. Hogari; "Multi-Hundred-fiber Cable composed of optical fiber ribbons inserted tightly into slots," Proc. of 35th IWCS, pp.17-23, 1986.

[2] S. Kukita, T. Nakai, A. Hayashi, and H. Koga; "New-Nonmetallic and waterproof optical fiber cable with absorbent polymer ribbon," Proc. of 36th IWCS, pp.357-371, 1987.

[3] N. Tomita, H. Kobayashi, M. Shimizu and J. Takagi; "A new high-density fiber organizer for optical fiber cable," J. of Lightwave Tech., LT-4, 8, 1988.

[4] Y. Mitsunaga, Y. Katsuyama, H. Kobayashi and Y. Ishida; "Failure prediction for long-length optical fiber based on proof testing," J. of Appl. Phys., No.53, 7, pp.4847-4853, 1982.

[5] M. Kawase, S. Tomita, N. Kasahara and T. Uenoya; "Non-pressurized optical subscriber cable systems"(in Japanese), Trans. of IEICE, J-73-B1, 10, pp.785-792, 1990.

[6] K. Sontag and A. Ross; "A fiber optic cable monitoring system," Proc. of 35th IWCS, pp.449-454, 1986.

[7] S. Tomita, H. Tachino and N. Kasahara; "Water sensor with optical fiber," J. of Lightwave Tech., No.8, vol.12 pp.1829-1832, 1990.

[8] D. Marcuse; "Curvature loss formula for optical fibers," Bell Syst. Tech. J., No.56, 5 pp.703-718, 1977.

[9] Y. Koyamada, N. Ohta and N. Tomita; "Basic concepts of fiber optic subscriber loop operation systems," Proc. of ICC'90, pp.1540-1544, 1990.



Masaaki KAWASE

NTT
Telecommunication Field
Systems R & D Center
Tokai, Naka, Ibaraki
319-11 JAPAN

Dr. Kawase received B.S., M.S. and Ph. D. degrees in electrical engineering from Hokkaido University in 1970, 1972 and 1991, respectively.

He joined NTT in 1972. He is engaged in the research and development of optical transmission lines.

He is a manager of Optical transmission cable systems laboratory, NTT Telecommunication Field Systems R & D Center.

Dr. Kawase is a member of IEEE and IEICE Japan.

OVERVIEW OF THE TRI-SERVICE FIBER OPTIC TECHNOLOGY PROGRAM

BRIAN M. HENDRICKSON

AIR FORCE ROME LABORATORY

ABSTRACT

This paper discusses Tri-Service activity in fiber optic technology developments. Programs discussed are divided into five major thrusts: Active and Passive Electro-Optic Components, Sensors, Radiation Effects, Point-to-Point Systems, and Network Systems. This paper is organized around the structure of the Tri-Service Fiber Optic Coordinating Committee and represents an annual investment of $50M.

Introduction

The Tri-Service Fiber Optic Technology is coordinated by the three services (Army - Navy - Air Force), DOF laboratories and NASA. It consists of six standing subcommittees with membership and expertise from each service and associate membership from other agencies based on their interests. The overall structure is shown in Figure 1. The committee reports to the Advisory Group on Electron Devices, Group C, and ultimately to OUSDDRE. The Fiber Optic Transition subcommittee also reports to the Fiber Optic Management Panel which reports to the Joint Commanders Group on Communications - Electronics (JCGCE) (see Figure 2).

Technology Thrusts

There are five technology thrusts embodied in the TSFOCS:

.Active & Passive EO Components
.Sensors
.Radiation Effects/Adverse Environments on Components
.Point-to-Point Systems
.Network Systems

Overall funding in the Tri-Service activity is approximately $50M.

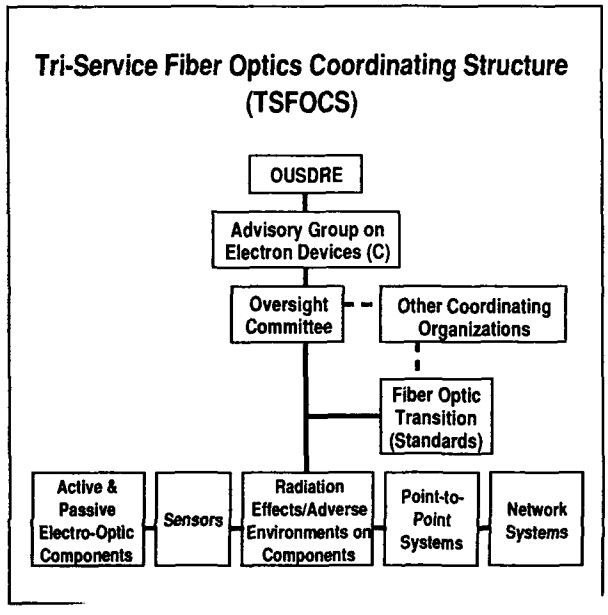


Figure 1 Tri-Service Fiber Optic Coordinating Structure

Active & Passive EO Components

The major long-term thrust in electrooptic component development is toward optoelectronic integrated circuits (OEIC) for the broad goal of optical signal processing. The earlier concept of "integrated optics" has been largely discarded in favor of the new approach which recognizes the desirability of combining both optical and electronic devices on the same substrate so as to capitalize on the best features of both. Thus optics excels at interconnection whereas signal processing is best done electronically. A number of approaches to OEIC are being pursued including III-V heteroepitaxy on silicon, Si and Si/Ge guided wave opticsw, pressure fusion of III-V semiconductor materials, organic on

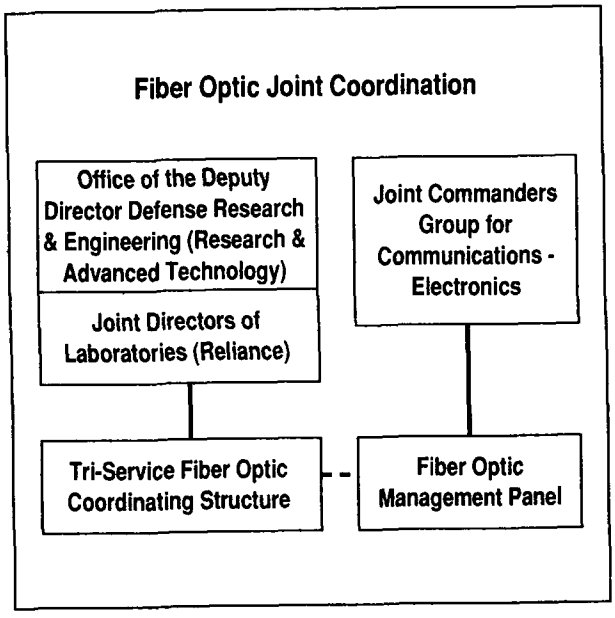


Figure 2 Fiber Optic Joint Coordination

inorganic semiconductor devices, the bipolar inversion channel FET (BICFET) and optically powered optoelectronics on III-Vs. Several programs are addressing the problem of the optoelectronically integrated source/driver and photodetector/preamplifier. Others are concerned with building blocks based on bandgap engineering in the III-Vs.

Discrete components are still being developed, notably laser diodes optimized and packaged for high-speed broadband analog direct modulation and also waveguide modulators for similar applications where wide dynamic range and extreme frequency range are needed. Modulators based on LiNbO3 and GaAs are being developed for ultra high-speed performance presently limited by velocity walk-off. Velocity equalization by burying the microstrip should raise the frequency limit to the vicinity of 100 GHz. Future performance to 500 GHz is conceivable when microwave dispersion and skin effect resistance are eliminated. Directly modulated lasers are close to the 20 GHz mark with the fundamental limit probably around 40 GHz in the VCSEL devices. Low power, high efficiency laser arrays for 2-dimensional optical processors based on the VCSEL technology are on the horizon.

Discrete modulation and switching devices based on multi quantum well structures are in the research phase but will be an important factor in future OEIC. Organic nonlinear optical materials are also potentially for compact modulators and switches in OEIC. A new class of organic semiconductors based on the polycyclic aromatic tatracarboxylic acid anhydrides have extremely interesting and potentially important electronic and optical properties.

A crucially important emerging technology in which there is presently relatively little Triservice activity is optical amplification in fibers and in semiconductor devices. This technology will open up a whole new range of applications including long-haul fiber communications without repeaters, fiber to the home and multiple access local area networks. The Air Force is currently involved in semiconductor amplifiers for a programmable infinite impulse response filter based on fiber delay lines. The Navy is reporting some work on a tilted-facet ridge waveguide amplifier and a diode-pumped fiber laser which is closely related to the fiber amplifier. This technology seems destined to be important in long-line undersea communications and in optical signal processing application such as the recirculating delay line problem alluded to above.

Point-to-point monomode fiber optic communications is maturing so that future trends of the technology will be toward optical processing. In addition to the challenging problem of fabricating 2-dimensional laser and detector arrays advances are also needed in spatial light modulators and rebroadcasters, pixellated arrays which can accept an optical input and provide an optical output with some intermediate processing performed electronically. The BICFET and the optically powered OEIC are current approaches to this formidable problem.

Sensors

Air Force fiber optic sensor programs encompass the following broad technology areas: explosive pressure, detonation velocity and temperature; fiber optic gyro technology; aircraft health monitoring; smart structures; environmental and chemical sensors. This work is being accomplished at Wright Laboratory's Armament, Avionics and Flight Dynamics Directorates; Phillips Laboratory Astronautics Directorate; and the Air Force Engineering and Services Laboratory.

Fiber Optic Technology Program Office development work is continuing on fiber optic sensors and sensor systems over a wide technology base. The objective of the program is to develop new classes of fiber optic sensors for the measurement of acoustic and magnetic fields, engine performance and environmental parameters. These devices would provide improved performance at a lower cost with a savings in weight and size. In addition, optical multiplexing of these type sensors has the capability for greater flexibility and reliability in providing the detailed sensing information at the location where it is most needed.

The All Optical Towed Array Acoustic Sensor (AOTA) which includes heading, pressure and temperature sensors has successfully completed an Advanced Technology Demonstration Program. This program was a collaborative effort with the Naval Underwater Systems Center, Naval Ocean Systems Center and contractors. Related to the AOTA program has been the fiber optic planar sensor array development effort for ship hull mounting.

Point-to-Point Systems

The Army successfully fielded tactical fiber optic subsystems including the CECOM-developed Tactical Fiber Optic Cable Assembly (TFOCA) in key systems such as Patriot in the recent conflict in the Middle East. In addition, the Optical Communication Set AN/GAC-4 replacing the 26 pair cable was fielded to meet the local area communications needs.

At this time, the fiber optic technology has been introduced and accepted to meet the needs of the five Battlefield Functional Areas. Prototype systems carrying the local area networks communications, command and control have been developed using the same TFOCA which is used to replace the twin coax and the twenty-six pair cables. The replacement of two metallic communications cables by only one has resulted in significant cost savings and reduction of the logistics burden.

The TFOCA is currently considered by NATO to become a NATO standard. The Army successfully demonstrated its capability to provide key fiber optic subsystems to meet field requirements. This success has been recognized by the other services and requests for cooperation have been increasing. This will result in significant cost savings for the taxpayer and will help field a standard product supportable by all parties involved.

Future Air Force thrust areas to be pursued:

- Additional work in improvement of linearity of fiber optic links using alternate modulation techniques

- Improved wider band performance of high linearity fiber optic links

- Increasing the upper frequency limit of fiber optic links including both conventional and high linearity links

- Improved/reduced size opto-electronic integrated circuits for phased array antenna applications

Thrust areas that need to be addressed:

- Low loss integrated photonic waveguide

- Higher efficiency, hirher frequency, lower noise, higher dynamic range, active photonic components - such as sources, modulators, and detectors - for point-to-point systems

- Higher efficiency, lower loss, passive components - such as couplers, isolators, and switches - for point-to-point systems

Navy Thrusts Are:

- Development of fiber optic tether cables

- Development of fiber optic tactical data link

- Providing fully operational digital fiber optic communication links at several military sites worldwide

Network Systems

The Fiber Optic Tactical Local Area Network (FOTLAN) is a continuing program. Its objective is to demonstrate real-time voice, video and data traffic transmission on a 100 Mb/s fiber optic packet LAN. To date, it has completed Network Interface Unit (NIU) board simulation, achieved real time full resolution NTSC compressed video transmission (10 Mb/s), and implemented fiber optic module interchangeability and bypass capability. Current efforts are directed toward developing FDDI NIUs that process real time voice, video and data, then integrating them into Army testbeds. This is the only network program which has made a transition, from 6.2 to 6.3A.

Survivable Adaptive Systems Technology Demonstration is a new program. Its objective is the development of a communication and information processing infrastructure which supports connectivity demands of evolving C3 systems. The approach is to build upon the Army Tactical Command and Control System (ATCCS), transfer any hardware or software developments to the Common Hardware Software Program and demonstrate evolutionary growth to the ATCCS objective system.

The Very High speed Optical Networks program seeks to develop a very high speed optical (500-2000 Mb/s) network capable of supporting the requirements for advanced avionics architectures such as PAVE PILLAR and PAVE PACE. To achieve the objective, requirements will be investigated and potential technologies examined such as optical switching and wavelength division multiplexing (WDM).

The Fiber Optic Active Star Coupler program focusses on developing and demonstrating an active optical star coupler as a drop-in replacement for the 64-port passive transmissive star coupler in the High Speed Data Bus system, a 50 Mb/s token passing bus. Although not a network within the entire sense of the definition, the fiber optic star coupler is a major component and its capabilities bear directly on the performance of a network into which it is inserted. The program is conducting tradeoff studies and lab experiments to determine the best approach for implementing the star coupler with a single transmitter and receiver, then extending the result to the remainder of the ports.

Another program which examines components integral to network performance is the Advanced Aircraft Avionics Packaging Technology - Photonic Connector and Backplane Technology. Its objective is to investigate alternate approaches to reduce the demands on electrical backplanes for common modules by using optical interconnects. The Standard Hardware Acquisition and Reliability Program (AATD-SHARP) will demonstrate a MIL-STD-1553 to MIL-STD-1773 SEM-E converter module production prototype. The plan is to rework the laboratory demonstration model developed earlier in the program and flight test with fiber optic control systems aboard a NASA F-18. To support AATD and SHARP, the Optical Backplane program is working on an optical backplane. It is developing technology and fabrication processes, performing environmental testing and developing embedded fiber approaches. Ultimately, it will produce and flight test a prototype.

Supporting high speed data communications, the AATD Sensor Data Distribution Network is developing a prototype fiber optic switched network. Results from evaluation of the prototype will go into a Tri-Service specification.

Implementation of networks based on the Survivable Adaptable Fiber Optic Embedded Network (SAFENET) standard is slated for the near future. The standard is being developed under the auspices of the Next Generation Computer Resources program. The program seeks the development of LAN standards which are applicable to mission critical computer resources on air, surface and subsurface platforms. It involves a joint Navy/industry effort along with participation with applicable national and international standards efforts. Two programs furthering the development via implementation of the standards are the SAFENET Development Facility and the AEGIS LAN prototype project. The SAFENET Development Facility, located at the Naval Ocean Systems Center, San Diego, provides the Navy with an experimental testbed for developing SAFENET II in conformance with the standard. Currently, a SAFENET II LAN has been implemented up through the ISO logical link layer and performance evaluations are planned. The AEGIS LAN prototype project is evaluating fiber optic LAN interconnection techniques which will provide benefit to the AEGIS program. It will develop a SAFENET testbed at the Naval Surface Warfare Center, Dahlgren, VA, using MULTIBUS II backplanes and commercially developed components.

Two programs are looking at specific NAVY applications requiring LANs. The Rapid Anti-Ship Missile Integrated Defense System (RAIDS) requires distribution of common data and recommendations for display to key tactical watch standers. Data from approximately 8 existing tactical systems is interconnected with 3 watch stations via a fiber optic Ethernet LAN. Another application is a Fiber Optic Network for the MK-7 Arresting Gear Control Readiness System. Work is focussed on developing a physical layer that is 100% independent of control layer protocols to ensure portability into the network choice for the MK-7 Arresting Gear Communications System.

For future applications, there are the Fiber Optic LANs for Shipboard Voice Systems and the High Speed Optical Network (HSON). The Fiber Optic LANs for Shipboard Voice Systems is looking at innovative concepts for fiber optic LAN based shipboard voice communication systems by developing a working prototype.

The prototype will be based on OSI standards and military and commercial components. To serve an entire ship's communications needs, including linking LANs like SAFENET, HSON is developing networking and fiber optic technology concepts which will lead to a standardized approach. This is realized in a first step high speed fiber optic network operating at 1.7 Gb/s. Current efforts center on acquiring the high speed switches and three SONET nodes and demonstrating data transmission between them.

Acknowledgement

The author would like to acknowledge the TSFOCS Subcommittee Chairmen who provided the information for this paper: Mr. Robert Baumback (Sensors), Dr. Richard Payne (EO Components), Mr. Edward Taylor (Radiation Effects), Mr. Vasilios Kalomiris (Point-to-Point Systems) and Mr. Clifford Carlson (Network Systems).

GaAs INTEGRATED OPTOELECTRONIC TRANSCEIVER FOR FIBER-OPTIC LINK APPLICATIONS

R.W. Ade, D.E. Bossi, J.M. Berak, R.N. Sacks, and L.A. Newman

United Technologies Research Center
East Hartford, CT 06108

Abstract

This paper describes a GaAs transmit/receive optoelectronic integrated circuit (OEIC) for optical communication and sensing applications. Significant progress toward the monolithic realization of this OEIC has been achieved. In particular, high-performance GaAs electro-optic waveguide modulators with monolithic MESFET drive electronics and low-loss channel waveguides with integrated multi-GHz metal-semiconductor-metal (MSM) photodetectors have been demonstrated. The monolithic integration of these passive and active waveguide components with photodetectors and electronic circuitry represents the enabling device and process technologies for realizing transmit/receive OEICs that utilize external modulation of a cw optical source.

Introduction

Optoelectronic transceivers are critical for the development of several fiber-optic communication systems, including optically controlled phased-array radars, and a hybrid microwave-to-photonic transceiver module has recently been demonstrated.[1] This paper describes progress toward the development of a *monolithic* transmit/receive (T/R) OEIC, which utilizes semiconductor integrated optics to externally modulate a cw optical source and to provide photonic signal routing. Monolithic realization of the transceiver provides increased interconnection reliability, reduced external drive power through on-chip amplifier gain, and decreased size, weight, and parasitic reactance. The external modulation format is chosen to facilitate high-linearity, wide-dynamic-range operation at high optical power levels.

The GaAs/AlGaAs material system is attractive for guided-wave optoelectronic integration because of the maturity of GaAs electronic device and processing technology, the radiation hardness of GaAs electronics, and the transparency of these semiconductors at 0.8-, 1.3-, and 1.55-μm fiber-communication wavelengths. Figure 1 illustrates the proposed transceiver OEIC, which can be realized by combining the indicated optical waveguide components with photodetectors and electronic control circuitry on a common GaAs substrate. The waveguide directional coupler is used to actively switch the circuit between the transmit and receive modes, enabling a single optical fiber to carry both the input and output signals. Key components of the proposed T/R OEIC are: passive waveguides; active electro-optic devices, such as the directional coupler switch and the optical intensity modulator; a waveguide-coupled photodetector; and MESFET driver and receiver electronics.

The transceiver OEIC of Fig. 1 is currently under development and the enabling device and process technologies for realizing this structure have been demonstrated, as described below. In particular, several advancements in the area of opto-electronic integration are reported. First, a high-performance GaAs electro-optic waveguide modulator with monolithic MESFET drive electronics is described. High-contrast (>15 dB) optical intensity modulation is achieved in this device for an input voltage swing of only 0.26 V. Second, a low-loss channel waveguide with an integrated multi-GHz GaAs metal-semiconductor-metal (MSM) photodetector operating at $\lambda = 0.8$ μm is reported in a structure compatible with both high-performance modulator and electronics integration. Finally, high-speed operation of a back-illuminated 1.3-μm InGaAs MSM photodetector fabricated on a GaAs substrate is described.

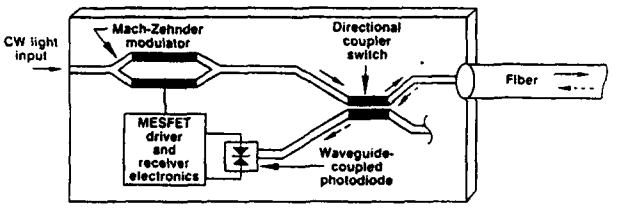


Fig. 1. Proposed single-fiber transmit/receive GaAs OEIC realized by integrating optical waveguide components with photodetectors and MESFET electronics.

Transceiver Integration

Waveguide modulator with monolithic drive electronics

A novel epitaxial structure and optoelectronic processing sequence have been developed, permitting monolithic integration of high-performance electro-optic waveguide components and GaAs MESFET circuitry.[2] Using this technology, the external-drive-voltage requirement of a GaAs/AlGaAs Mach-Zehnder modulator has been substantially reduced through the integration of a MESFET drive amplifier. A circuit schematic and a cross-sectional profile of the integrated modulator/MESFET structure are shown in Fig. 2. The waveguide in Fig. 2(b) is designed for single-mode operation at $\lambda = 1.3$ μm; a similar structure for $\lambda = 0.8$ μm operation is readily achieved by increasing the Al content of the waveguide core and cladding layers. The approach outlined in Fig. 2 enables the modulator drive voltage to be reduced through the integration of the MESFET amplifier with no adverse impact on the modulator propagation loss, optical contrast and bandwidth.

The inherent electro-optic efficiency of the Mach-Zehnder modulator is characterized by directly modulating the voltage applied to the bias-control arm. In agreement with calculations based on the linear electro-optic effect, the half-wave voltage is 6 V for 8-mm electrodes, as shown in Fig. 3(a). For comparison, Fig. 3(b) shows the optical transfer characteristic of the same device with the drive voltage applied to the amplifier input. This latter characteristic represents a combination of the amplifier and Mach-Zehnder transfer functions; both the amplifier and modulator are operating in their linear regimes in the central switching portion of the curve. As a result of on-chip amplifier gain, the integrated device exhibits >15 dB optical extinction for an input voltage swing of only 0.26 V.

Measured propagation losses in the passive and active waveguide sections of the amplifier/modulator circuit are 0.3 and 1.5 dB/cm, respectively, resulting in a total on-chip loss <4 dB for 2.2-cm-long Mach-Zehnders with 8-mm electrodes. The measured ~1 GHz bandwidth of the modulator/amplifier OEIC is determined by the capacitive charging time of the 8-mm lumped-element modulator electrode. By utilizing a traveling-wave electrode configuration, the present device could operate at frequencies to ~5 GHz. For higher-frequency operation, a MESFET-compatible modulator structure fabricated on a semi-insulating GaAs substrate is currently under investigation.

Waveguide-integrated photodiode with total-internal-reflection coupling

In addition to requiring the integration of electro-optic waveguide devices with electronics, the transceiver of Fig. 1 calls for monolithic waveguide-to-photodetector coupling in a structure compatible with active waveguide devices. Efficient optical coupling between a low-loss AlGaAs channel waveguide and a monolithic high-speed GaAs MSM photodetector has been demonstrated using a vertically deflecting total-internal-reflection (TIR) mirror formed by wet chemical etching.[3] A cross-sectional profile of the integrated waveguide/photodetector is shown in Fig. 4(a). Optical radiation at $\lambda = 0.84$ μm is incident from an AlGaAs

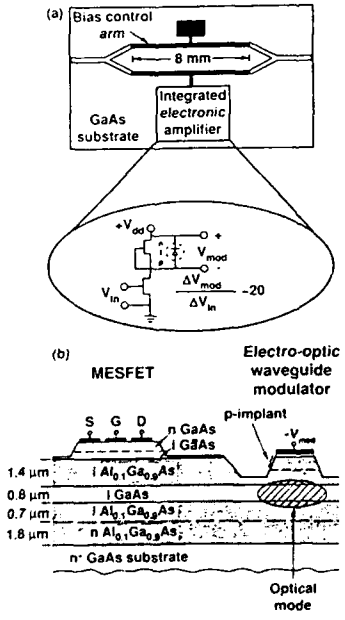


Fig. 2. (a) GaAs Mach-Zehnder optical intensity modulator with monolithically integrated MESFET amplifier.
(b) Cross-sectional profile of GaAs electro-optic modulator and integrated MESFET.

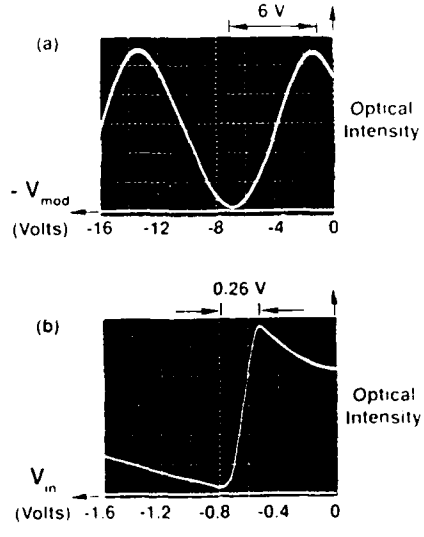


Fig. 3. Intensity vs. voltage response of GaAs modulator/amplifier OEIC. On/off optical switching occurs for a voltage swing of either (a) 6 V applied to the modulator's bias-control arm or (b) 0.26 V applied to the amplifier input. The supply voltage, V_{dd}, is 9.5 V.

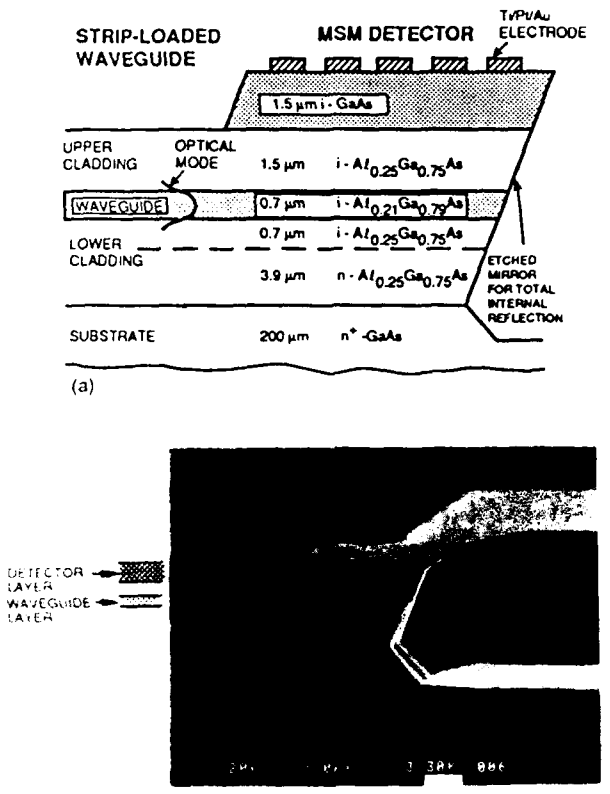


Fig. 4. (a) Cross-sectional profile of a waveguide-integrated photodetector utilizing a total-internal-reflection coupling mirror. (b) SEM photograph of a fabricated device with wet-etched mirror.

single-mode strip-loaded waveguide onto an etched TIR mirror. The mirror redirects the optical beam upward through the transparent cladding, onto the backside of an overlying GaAs MSM photodetector. The AlGaAs waveguide and cladding are sufficiently thick to confine >99.9% of the guided mode within these transparent layers, ensuring low propagation loss, yet the optical path from the mirror to detector through the upper cladding is sufficiently short to prevent appreciable spreading of the unguided beam. Hence, the TIR mirror provides efficient coupling between a low-loss waveguide and small-area photodetector. A key feature of the structure in Fig. 4(a) is its compatibility with the previously described integration of MESFET electronics and active waveguide devices.

Figure 4(b) shows a SEM photograph of an integrated waveguide/detector with a wet-chemical-etched TIR mirror. The key step in the device fabrication sequence involves etching the retrograde mirror, whose surface must be angled greater than 17° from the wafer normal in order to satisfy the TIR condition. Both Cl_2-assisted ion beam etching and wet chemical etching in 1 H_2SO_4:8 H_2O_2:1 H_2O have been used to produce suitably angled (18° - 22°) reflectors.

An internal responsivity of 0.56 A/W (photocurrent divided by power in waveguide) is measured at $\lambda = 0.84$ μm for the waveguide-coupled photodetector, corresponding to an internal quantum efficiency, $\eta_{int} = 0.83$. The calculated value of $\eta_{int} = 0.82$, which assumes unity carrier collection efficiency, is in close agreement with the measured value, indicating a low recombination velocity at the etched surface. Low dark current (<1 nA at 10 V) and high breakdown voltage (>25 V) provide additional evidence that mirror etching does not degrade photodetector performance. The waveguide-illuminated photodetector, with 2-μm finger spacing, exhibits a 5-GHz 3-dB bandwidth. Currently, the photodetector bandwidth is limited by the (150 x 100 μm^2) bond pad-to-backplane capacitance. Reducing the bond pad area and finger spacing will extend the detector bandwidth to >10 GHz while maintaining high quantum efficiency.

Long-wavelength InGaAs-on-GaAs photodiodes

The two preceding technology demonstrations are sufficient for realizing a $\lambda = 0.8$ μm GaAs transceiver OEIC. The transceiver could also operate at the 1.3-μm minimum-fiber-dispersion wavelength if a suitable long-wavelength photodetector could be fabricated on a GaAs substrate. Through the incorporation of a 1.3-μm-sensitive $In_{0.4}Ga_{0.6}As$ absorbing layer, a high-speed long-wavelength MSM photodiode on GaAs has recently been demonstrated.

The 1.3-μm photodetector employs thick deliberately lattice-mismatched InGaAs layers to force dislocations to loop and terminate within a thin region at the heterointerface, far from the carrier collection electrodes.[4] A cap layer graded from $In_{0.4}Ga_{0.6}As$ to $In_{0.4}Al_{0.6}As$, which is grown at the surface of the device, serves to enhance the Schottky barrier height of the MSM contacts. Because this cap layer is lattice-matched to the underlying absorbing layer, it provides a dislocation-free path for collection of photogenerated carriers, while reducing photodiode dark current.

The fabricated MSM photodiodes consist of 6 pairs of 2 x 50 μm^2 Ti/Pt/Au fingers with 2-μm spacing, for a 50 x 50 μm^2 active area. The total device area including bond pads is 3×10^{-4} cm^2. Typical dark currents for these detectors are <200 nA at 10 V and breakdown occurs at ~35 V. The dc photoresponse is characterized at $\lambda = 1.3$ μm under both frontside and backside illumination and a 90% internal quantum efficiency is measured for both cases. For a back-illuminated 0.5-μm-thick detector with no anti-reflection (AR) coating, the measured external responsivity is 0.4 A/W. From this measurement a 0.9-A/W responsivity is predicted for a 1-μm-thick back-illuminated device with backside AR-coating. This value approximates the internal responsivity expected for a waveguide-integrated photodetector using the TIR-coupling technique described above. The measured 3-dB bandwidth for these detectors is 4.5 GHz.

Summary

A single-fiber transmit/receive OEIC incorporating optical waveguide devices, photodetectors, and electronic circuitry on a common GaAs substrate has been discussed, and the enabling technologies for fabricating this OEIC for operation at both 0.8– and 1.3–μm wavelengths have been demonstrated. Monolithic realization of optical transceiver modules offers significant benefits in terms of performance, reliability, size, and cost, making these devices particularly attractive for a variety of fiber-optic communications applications.

References

1. E. Ackerman, S. Wanuga, K. Candela, R. Scotti, W. MacDonald, J. Gates, "A 3 to 6 GHz microwave/photonic transceiver for phased-array interconnects," *Microwave Journal*, vol. 35, pp. 60-71, 1992..

2. R. W. Ade, D. E. Bossi, R. P. Basilica, and J. M. Berak, "Monolithic integration of a GaAs-waveguide optical intensity modulator with MESFET drive electronics," *Electron. Lett.*, vol. 28, pp. 702-704, 1992.

3. R. W. Ade, D. E. Bossi, R. P. Basilica, and J. M. Berak, "Vertically integrated AlGaAs waveguide and GaAs photodetector with efficient total-internal-reflection coupling," in *Integrated Photonics Research*, Vol. 10, OSA Technical Digest Series, (Optical Society of America, Washington, DC 1992), pp. 46-47.

4. D.L. Rogers, J.M. Woodall, G.D. Pettit, and D. McInturff, "High-speed 1.3-μm GaInAs detectors fabricated on GaAs substrates," *IEEE Electron Device Lett.*, vol. 9, pp. 515-517, 1988.

TEST PATTERNS OF OPTICALLY CONTROLLED TWO-BAND PHASED ARRAY ANTENNA

Serey Thai
Norman Bernstein and James Hunter

Rome Laboratory
RL/C3DB
Griffiss AFB, New York 13441

ABSTRACT

The advantages of true time delay RF beam forming and beam steering are well known. True time delay with wideband radiating elements permits large transmit and receive frequency excursions without beam wander (beam squint) as the frequency is changed, and also permits the use of wideband waveforms . A number of different approaches are being investigated to implement true time delay beam steering for RF phased array antennas. This paper discusses beam pattern generation and analysis using an early model transmit phased array implemented with fiber optic delay lines. Two arrays, one at X-band and one at L-band, each have the same physical length and split into four subarrays, use a common time delay generator for each corresponding subarray on both bands. This paper reveals how far-field patterns confirm earlier near-field pattern generation and that true time delay beam pointing does not significantly change with frequency.

INTRODUCTION

The main principle of this microwave multiband phased array antenna is the use of optically controlled photonic delay lines for beam forming and steering. The use of fiber optic delay lines in the phased array antenna instead of phase shifters or RF waveguide or coaxial cable has the following advantages: weight, compact, flexibility, wide band operation, nondispersive over multiple bands of microwave frequencies, and immunity to electromagnetic interference. This system is suitable for spaceborne and airborne phased array applications.

The far-field pattern development is under sponsorship of Rome Laboratory (formerly Rome Air Development Center). Hughes Aircraft Company developed the two-band Optically Controlled Phased Array Transmitter under contract to Rome Laboratory. The content of this paper is devoted to understand the functionings of the transmitter and results of beam pattern development.

THEORY OF LINEAR PHASED ARRAYS

The radiating elements of the transmitter are one-dimensional (linear) arrays which are mostly used in microwave applications. It consists of N isotropic radiators with equispacing at a distance d ($d = \lambda/2$) apart. The radiation pattern of this array is called the array factor. For uniform amplitude excitation in the absence of errors, it can be written :

$$E(\theta) = \frac{1}{N}\sum_{n=1}^{N} e^{jnKd\sin\theta} \qquad (1)$$

and

$$K = \frac{2\pi f}{c} = \frac{2\pi}{\lambda} \qquad (2)$$

Where K is the wave number
f is an operating frequency
θ is the beam angle
(ndsinθ) is n^{th} phased delay distance
1/N is normalized factor of array pattern
$n_r = 1 \equiv$ index of refraction

The expanding series in equation (1) can be summed to give

$$E(\theta) = \frac{\sin(\frac{NKd\sin\theta}{2})}{N\sin(\frac{Kd\sin\theta}{2})} \qquad (3)$$

The far-field intensity pattern of this linear array can be written as follows:

$$I(\theta) = |E(\theta)|^2 = \left[\frac{\sin(\frac{NKd\sin\theta}{2})}{N\sin(\frac{Kd\sin\theta}{2})}\right]^2 \qquad (4)$$

The far-field range R of the antenna can be determined by the following equation:

$$R \geq \frac{2L^2}{\lambda} \qquad (5)$$

Where L is the largest dimension of the antenna array and λ is the operating wavelength.

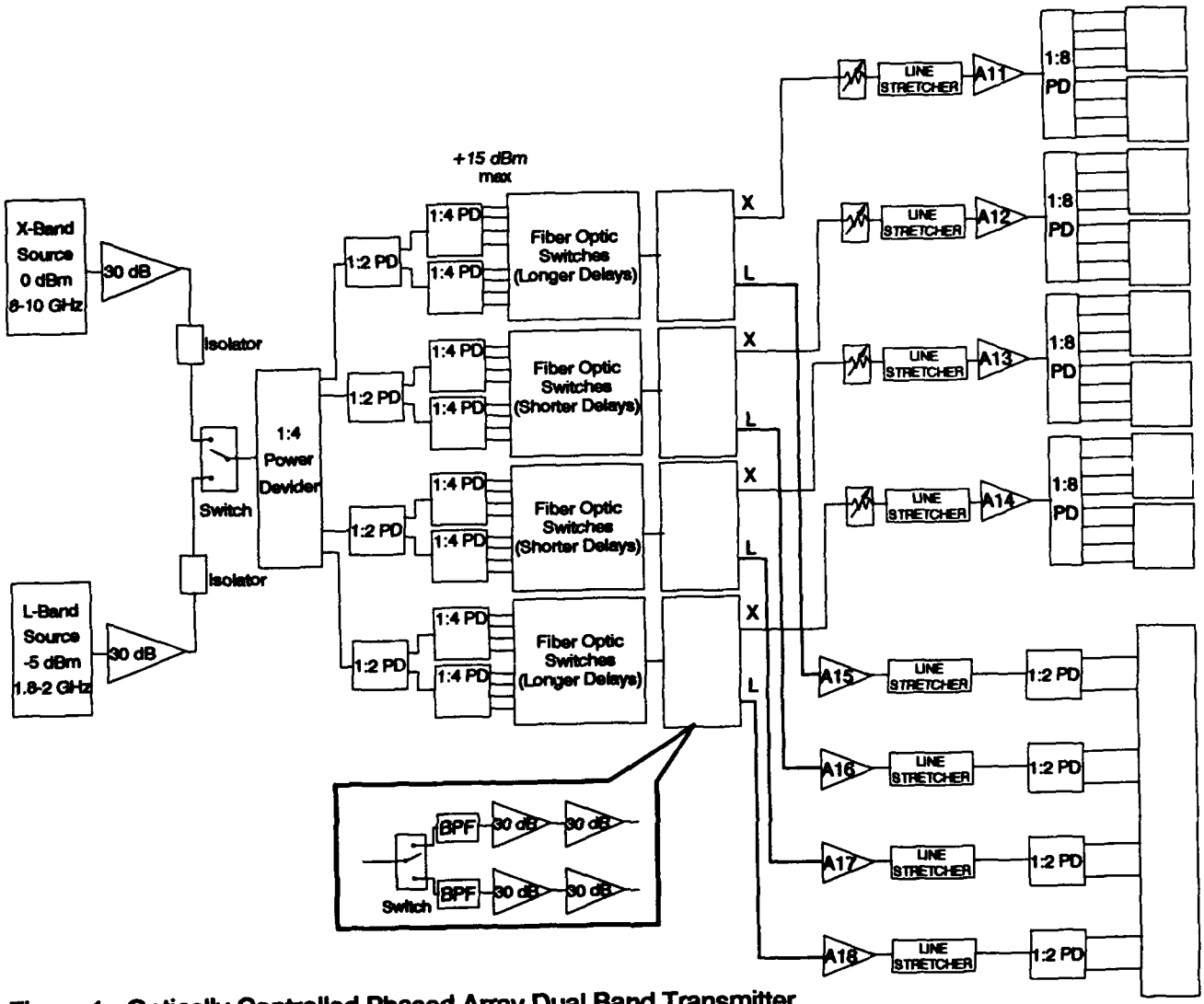


Figure 1. Optically Controlled Phased Array Dual Band Transmitter

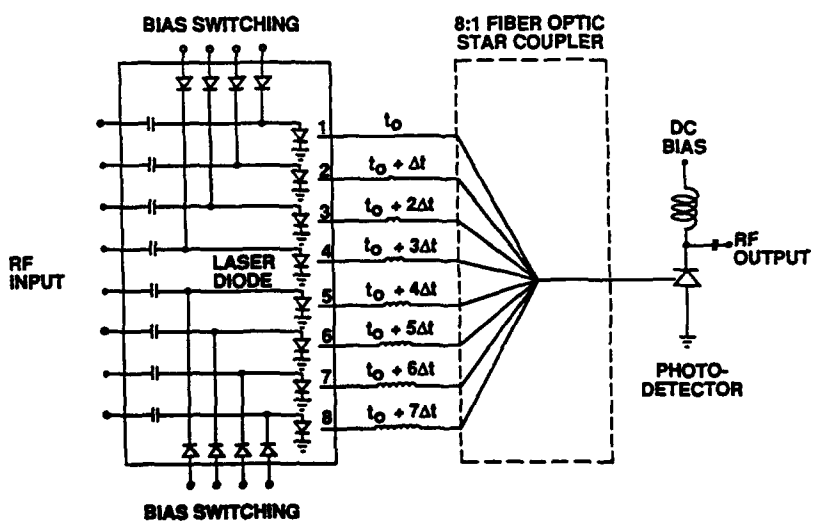


Figure 2. Schematic of 3-bit fiber optic switching network.

OPTICALLY CONTROLLED PHASED ARRAY

The optically controlled phased array dual band transmitter with true time delay beamsteering is depicted in Figure 1. The operating frequencies in far-field testing at the Newport Short Range Test Site were 1.8 GHz to 2.0 GHz for L-band, and 8.5 GHz to 9.5 GHz for X-band. The RF analog input signal of both bands of the optically controlled phased array transmitter will split four ways to feed four linear subarrays (the radiating elements of either band were divided into four subarrays). The divided signal in each channel will again split into eight analog fiber optic links. At this point the insertion loss is approximately 15 dB. The eight fibers were spliced into an eight-to-one star coupler as shown in Figure 2. This module is called true time delay, and will be discussed in detail later on.

The RF insertion loss at the output of the GaInAs/InP detector is approximately 90 dB. A nonuniform distribution of insertion losses between all channels and RF paths is a valid concern. Therefore steps must be taken to ensure the minimum relative insertion loss differences. The matched performance of all four channels is crucial for the proper functioning of the beamforming.

Each output signal of the photodiodes will feed two radiating elements in each L-band subarray, or feed eight radiating elements in each X-band subarray.

There are four subarrays in the system. The X-band has eight elements in each subarray which are used to construct a baseline of 32 dipole radiating elements. There are two modules in each subarray, and four dipole elements in each phase shifter module. L-band has two elements in each subarray which are used to construct a baseline of eight vertical monopole elements arranging side by side and lined up in a parallel structure. The polarization is horizontal along the linear dimension for X-band, and vertical for L-band. The array size of both band is 20.8" (~ 53 cm) in length. The element spacing is 0.65" (~ 1.65 cm) for an X-band antenna, and 2.6" (~ 6.60 cm) for an L-band antenna.

The band pass filters (BPF) were used to prevent cross band interferences. The purpose of a line stretcher is to compensate the relative phased differences between the fiber optic beam steerer and the array system. The line stretcher calibration adjustment was set to minimize errors in the system.

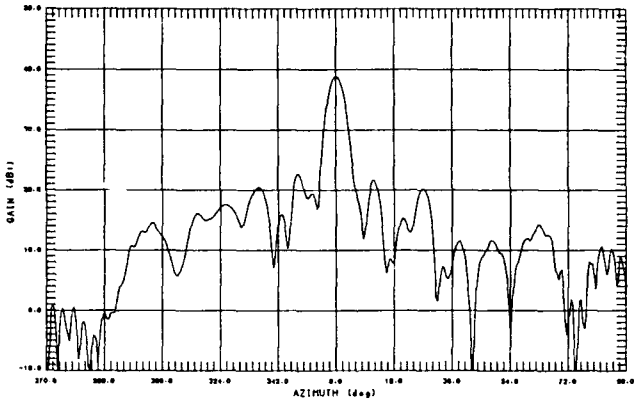
The gain trimmer was used only in X-band for amplitude equalization between the channels in X-band because the angular width of each subarray (channel) falls within the angular scan limit, whereas the angular width of each subarray in L-band is much larger than the maximum angular scan limit. If the amplitudes of each channel in X-band are nonuniformly distributed, it may cause a lower and wider main lobe, and in turn raise the amplitudes of the side lobes. This process is called destructive beamforming.

This transmitter was designed for maximum angular scan limit of ± 28°. The L-band 2-element pattern has an angular width of 60°. Therefore it causes minimal concern for constructive beam interferences because its angular width is much larger than the maximum angular scan limit. On the other hand, the X-band 8-element subarray pattern has an angular width of approximately 16.4°, this would cause destructive beamforming. These errors can be corrected by using additional optical delay lines or a microwave phase shifter for each element in the array. The decision was made to use phase shifters based on the resources available at the time. Also the high insertion losses in the optical true time delay module helped influence the decision.

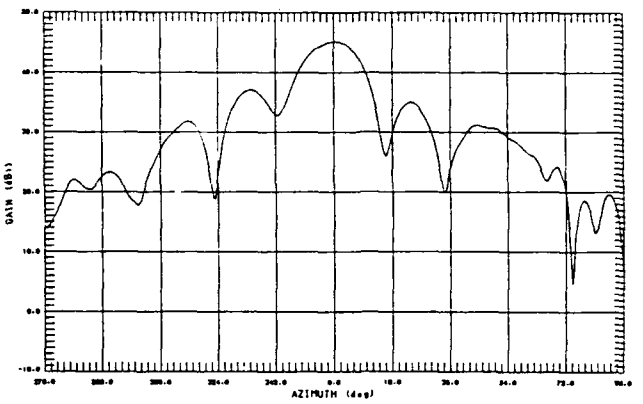
Again, due to the resources available, the decision was made to have four sets of fiber optic switches with channel #1 and #4 having longer delays, and channel #2 and #3 having shorter delays. Channels 1 and 4 feed the outer ends subarrays of the horizontally arranged one-dimensional radiating elements, whereas channels 2 and 3 feed the middle subarrays as shown in Figure 1. This arrangement will provide the proper delay values for forming a radiated phase front.

This transmitter was built not only for manual operation but also for computer control, therefore the switches must have a 3-bit variable switch. 2^3 provides 8 combinations of delay increments which can be used to achieve all possible settings for microwave beam direction. In turn, an eight-to-one (8:1) star coupler is required in optical true time delay. The true time delay is an independent frequency delay. The beamforming or beamsteering to the desired angle can be accomplished independent of frequency. This process minimizes the beam squint as compared to the frequency operation alone, and no decorrelation between channels occurs. It is important to recognize that both band signals share a common feed fiber optic delay network and are controlled by one set of delay lines which help to simplify the beamforming architecture of the transmitter.

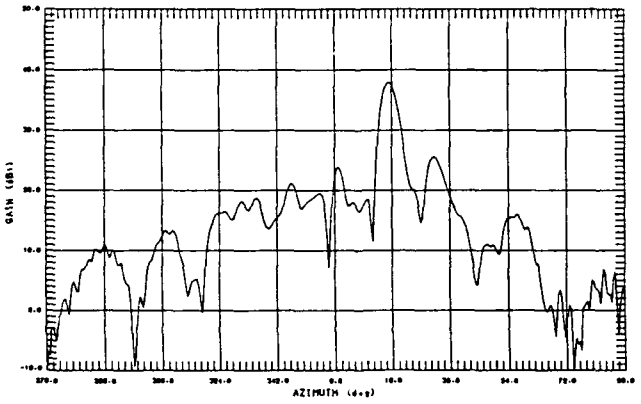
The 8:1 star coupler is coupled to 8 GaInasp/InP buried crescent lasers operating at 1.3 μm wavelength. The optical output is coupled to a GaInAs/InP detector with a bandwidth of about 11 GHz. Multimode fiber is used with an index of refraction of 1.47 (n_r = 1.47) and fiber dispersion of 0.2 ps/(km-nm). The antenna aperture and maximum steering angle determine fiber optic lengths, and the lengths were cut to 0.5 mm precision. The incremental time delay is 89 ps for channels 1 and 4 (ΔT = 89 ps), and 59 ps for channels 2 and 3 (ΔT = 59 ps). The total time delay setting for each path in one of the four optical delay channel can be expressed as follows :



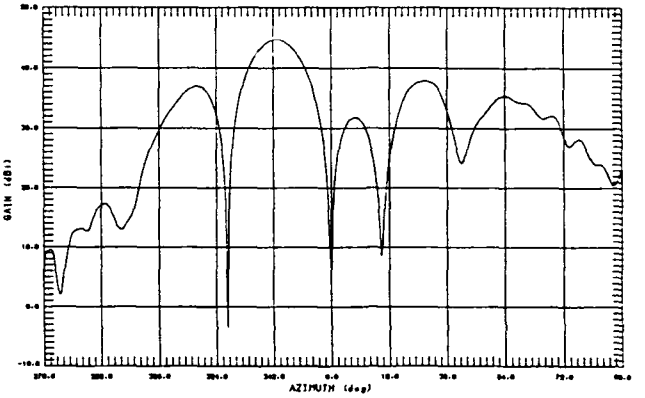
(A) FREQUENCY: 9.0 GHz SCAN ANG: 0°



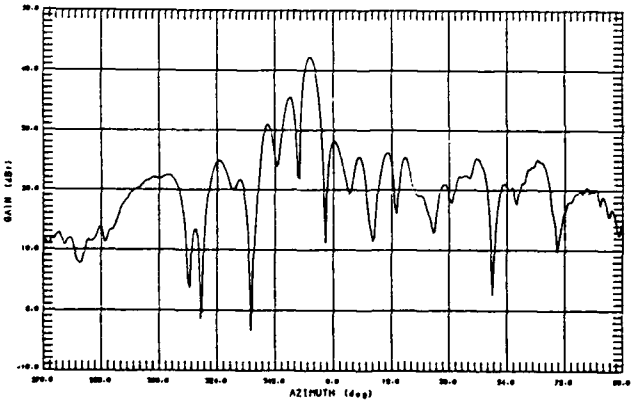
(D) FREQUENCY: 1.9 GHz SCAN ANG: 0°



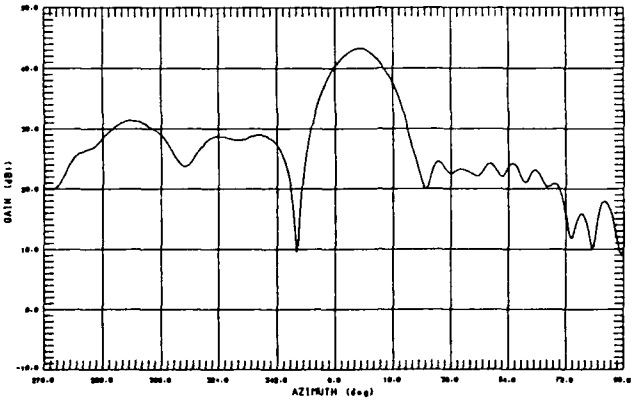
(B) FREQUENCY: 9.0 GHz SCAN ANG: +16°



(E) FREQUENCY: 1.9 GHz SCAN ANG: -16°



(C) FREQUENCY: 9.0 GHz SCAN ANG: -8°



(F) FREQUENCY: 1.9 GHz SCAN ANG: +8°

Figure 3. Radiation patterns of phased array antenna.

$$T_{d,i} = T_o + \sum_{i=0}^{7} i\Delta T \qquad (6)$$

Where T_o is the reference time delay
$T_{d,i}$ is the i^{th} path total time delay

The differential fiber optic length (ΔL) can be determined by using equation (7) below. For channels 1 and 4, ΔL = 1.81 cm (ΔL = 0.71"), and ΔL = 1.20 cm (ΔL = 0.47") for channels 2 and 3.

$$V = \frac{c}{n_r} = \frac{\Delta L}{\Delta T} \qquad (7)$$

Figure 2 is the laser switched module for a 3-bit time delay line. The true time delay also can be accomplished by switching the photodetectors instead of lasers. There is no real distinctive advantages between two methods, therefore, cost and availability are the decision factors. Other methods of true time delay beam forming and steering are also being investigated but they are more futuristic than this fiber optic delay line switching technique.

ANTENNA RADIATION PATTERN

The pattern characterization tests were conducted at the Rome Laboratory Tanner Hill Newport Short Range Test Site. The X-band and L-band receive gain horns were mounted 674 ft (~205 m) from the transmitter. According to equation (5), the calculations will yield the far-field results as follows:
$R_x \geq 55$ ft for X-band and $R_L \geq 12$ ft for L-band. Therefore, the radiation patterns of the antenna were far-field cuts. A boresight beam squint of 3.5° was observed between L and X-band and main lobes of the different frequencies in a band at broadside (0° scanning) stayed within 0.5° of each other. However within 3°, beam squints have been observed within each single frequency testing in each band of both bands if the scanned angles were steered between ± 28°. This 3° error is believed to be due to a slight misalignment between the parallel antennas and errors in RF coaxial line lengths. The test was conducted at frequencies (1.8, 1.9, 2.0 GHz) for L-band, and (8.5, 9.0,9.5 GHz) for X-band. The 1.9 and 9.0 GHz radiation patterns are the most appropriate representations of each band. A few radiating patterns were chosen to represent the patterns of both bands as shown in Figure 3. The 3-dB beamwidths of the 1.9 and 9.0 GHz pattern were approximately 17° and 5°, respectively, and these 3-db beamwidths remain somewhat constant as the beam steered off to the different scanned angle. The pattern characterization tests have shown that the beam squints would be much larger if the true time delays were not implemented.

CONCLUDING REMARKS

This technical work confirms that the implementation of photonic beam forming and steering into an RF phased array antenna will permit frequency hopping over wide frequency ranges without the resultant beam squint present in a conventional RF phased array antenna. The advantage also extends to both communications and surveillance applications where the beam wander off target could occur without the use of the true time delay beam forming and steering.

REFERENCES

1. Dr. G. L. Tangonan, Dr. W. W. Ng, J. J. Lee, M. Wechsburg, "EHF Optical Fiber Based Subarrays," Hughes Research Laboratories, RL-TR-91-355, Final Technical Report, December 1991.

2. R. Tang, R. W. Burns, "Phased Arrays," Chapter 20, Antenna Engineering Handbook, 2nd Edition pp. 20-1 - 20-5, New York: McGraw Hill,1984.

SINGLE MODE FIBER OPTIC CABLE FOR SPACE APPLICATIONS

P.A. Michaels
AT&T Bell Laboratories, Whippany, NJ 07981

A.E. Miller, M.F. Yan
AT&T Bell Laboratories, Murray Hill, NJ 07974

V.E. Kalomiris
U.S. Army CECOM, Fort Monmouth, NJ 07703-5203

ABSTRACT

A fiber optic cable has been developed for use in space applications. The unique requirements for the cable were derived from the operating conditions encountered in a space environment. Radiation hardened hermetic optical fibers were developed in the first phase of a concurrent development program. Using these fibers, five experimental cable designs were built and subjected to a comprehensive test and evaluation program. One cable design has met optical and mechanical operating requirements at temperature extremes ranging from -150°C to +150°C, resulting in a fiber optic cable suitable for space applications.

INTRODUCTION

The development program of a single mode fiber optic cable for space applications included two phases. The first phase resulted in the development of an optical fiber, successfully tested to operate in a long term, low dose rate radiation space environment. Parallel to the fiber development phase, cable designs were developed around the optical fiber to withstand the environmental conditions of space. The experimental radiation hardened optical fibers were manufactured into five different single fiber cable designs that were then evaluated through a comprehensive test program. Through the test and evaluation period, one cable has exhibited good performance characteristics over the required operating conditions. The development process and the results of the test and evaluation program are presented in this paper.

CABLE REQUIREMENTS

The requirements for a fiber optic cable to be used in space applications are severe. The design specifications (given in Table 1) for this cable were intended to simulate operation of a cable directly in the open space environment. These specifications were aggressive design goals that would result in a highly reliable fiber optic cable.

The temperature requirement of -150°C to +150°C provide an exceptional design challenge. This is further compounded when these extreme temperatures are the operating temperatures for subsequent mechanical requirements such as cyclic flexing, impact, and cold bend. The low temperature requirement of -150°C presents a most challenging requirement in two respects. As shown in Figure 1, the optical fiber developed for this application

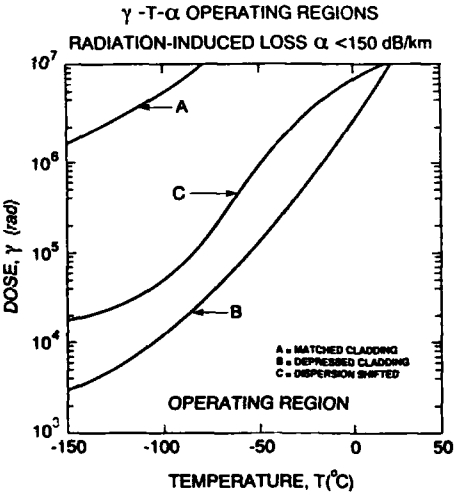


Figure 1. Operating Range of Optical Fibers

exhibits increasing radiation sensitivity, indicated by optical losses greater than 150 dB/km, with decreasing temperature. Additionally, most standard cable materials and constructions will not exhibit working properties at temperatures as low as -150°C.

Table 1. Cable Design Specifications

TEST DESCRIPTION	REQUIREMENT
OPTICAL ATTENUATION per FOTP-78	< .24 dB/km at 1310 nm < .30 dB/km at 1550 nm
THERMAL CYCLING 5 cycles -150 °C to +150 °C	< 5 dB/km rel. optical attenuation
THERMAL SHOCK -150°C to +150 °C	< 5 dB/km rel. optical attenuation
CYCLIC FLEXING per DOD-1678, Method 2010 Temp + 25°C, 500 cycles Temp +150°C, 500 cycles Temp -150°C, 500 cycles	< 0.5 dB rel. optical attenuation
COLD BEND per DOD-1678, Method 2030 5 wraps around mandrel at -150°C	< 0.5 dB rel. optical attenuation.
IMPACT per DOD-1678, Method 2030 Temp -150°C, 50 impacts Temp +25°C, 50 impacts Temp +150°C, 50 impacts	<0.5 dB rel. optical attenuation
FLAMMABILITY per DOD-1678, Method 5010	Flame travel < 4 time cable OD
TENSILE STRENGTH	> 1000 N (225 lbs) breaking strength
RADIATION 1×10^7 rad gamma radiation	> 70 % of tensile strength after exposure
ULTRAVIOLET RESISTANCE exposure equivalent to 12 years in space	> 70% of tensile strength after exposure
TENSION-ELONGATION 10 cycles to 490 N	< .25% strain at 76 N < .45% strain at 135 N <1.6% strain at 490 N
TENSION-OPTICS	<0.5 dB/km rel. optical attenuation at 490 N

CABLE DESIGN

Based on a survey of available cable materials and designs, the qualification of an existing cable was not considered feasible. Driven by the need to satisfy the operating temperature range, several cables were designed on an experimental basis to determine the most suitable construction.

The key elements of the cable design are the fiber, fiber buffer, strength member and outer jacket. The optical fiber, developed during the concurrent fiber phase, provided the core element. The remaining cable elements were varied to create the five

resulting cable designs.

The fiber buffer design began with a review of polymeric materials capable of spanning the operating temperature range. The original buffer material considered was a PCTFE fluorocarbon thermoplastic. The special processing techniques needed to extrude this material were impractical to develop on an experimental basis, thus the material was changed to an FEP fluorocarbon thermoplastic. The buffer construction, designed to be extruded directly over the fiber, was the result of a tradeoff between a large outer diameter to provide greater impact resistance, and a smaller diameter which would provide better temperature performance by minimizing the effects of the thermal expansion mismatch between the fiber coating and the buffer. Three of the manufactured cables included the same fiber buffer, while the other two cables omitted the buffer altogether.

The strength member for all five cables was selected to be parallel lay aramid fibers, directly surrounding the buffered or unbuffered fiber. Aramid fiber, used in space applications and throughout the fiber optic cable industry, exhibits the required operating temperature range along with high tensile strength.

The outer jacket was designed to be of a braided textile fiber construction. This approach was chosen to allow better low-temperature flexibility, ease of inspection and repair, and to eliminate jacket creep and shrink-back. A braided fiber jacket avoids the dimensional instability of an extruded plastic jacket that can cause excessive optical attenuation over a wide temperature range. Four cables were manufactured with a polyester braided jacket, with one cable having a thin tape separating the strength member fibers from the jacket. The fifth cable was made with a glass fiber braided jacket. The five completed cables are shown in cross section in Figure 2.

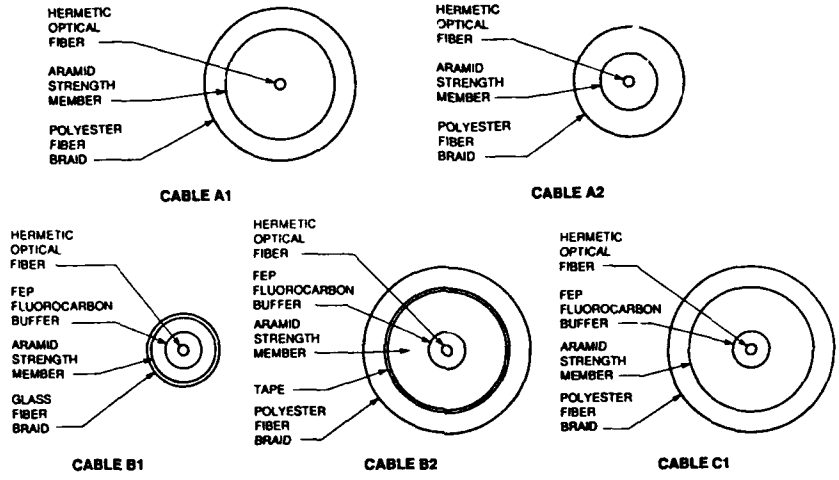


Figure 2. Cable Designs

CABLE EVALUATION

The cables were manufactured and delivered to the test lab for evaluation. Immediately, the two cables that did not include fiber buffers were found to be unacceptable designs. During handling, the unbuffered optical fiber was easily broken as it moved unprotected between the aramid fibers.

All tests requiring an operating temperature ranging from -150°C to +150°C were performed in a temperature chamber specifically modified for this test program. Mechanical test fixtures for cyclic flexing, cold bend and impact testing were built into the test chamber, and designed to be operable and controllable throughout the temperature range.

Optical Attenuation

The optical attenuation in the remaining three buffered fiber cables was measured by the cutback method per EIA-455-78A. Measurements were made at 1300 nm and 1550 nm with the results indicated in Table 2. All three cables exhibited higher attenuation than specified as a result of the cabling and spooling process.

Table 2. Optical Attenuation of Manufactured Cables

#	Optical Attenuation		Fiber Type
	1300 nm	1550 nm	(see Fig 1)
B1	4.8 dB/km	1.1 dB/km	depressed cladding
B2	3.2	18.3	depressed cladding
C1	7.1	57.0	matched cladding

Temperature Cycling

The three cables were placed in the temperature chamber with one laser source split between the three cables and a reference optical power meter. During temperature cycling, the relative optical attenuation of the three cables, specified to be lower than 5 dB/km, was measured per EIA-455-20. Five cycles to the temperatures indicated in Table 3 were repeated.

Table 3. Temperature Cycle Profile

Temperature	Dwell Time
-150°C	8 hours
+25°C	16 hours
+150°C	30 hours

Data acquisition for the optical measurements and temperature control for the chamber was automatic with optical attenuation sampled every 5 minutes over the duration of the test. Both the B2 and C1 cables failed on the first cycle as the temperature was rising from +25°C to +150°C. Cable B1 was subjected to 5 complete cycles while remaining within specification. Cycle 1 is shown in Figure 3.

The failure mode analysis of cables B2 and C1 revealed a high frequency of buckling in the aramid fiber, caused by unmatched thermal expansion between the aramid fiber and the polyester braided jacket. The buckling resulted in a periodic wave in the fiber buffer and fiber. In at least one section of cable C1, the buckling was enough to cause a break in the fiber. Some localized buckling of cable B1 was observed periodically throughout the cable, but

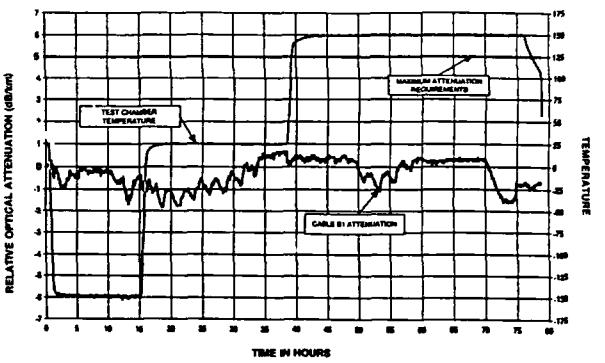


Figure 3. Temperature Cycling Cable B1

the effect on the buffer and fiber was not as severe. The success of cable B1 is attributed to the material property of the glass fiber braid, which forms a more compliant jacket allowing the aramid fiber strength member to expand and contract without as much buckling. Additionally since there was less aramid fiber in cable B1, the buckling that did occur did not exert as much force on the buffer. The net effect on cable B1 resulted in an end of test, room temperature optical attenuation of 6.25 dB/km and 5.75 dB/km at 1300 and 1550 nm respectively. Tests were continued on the B1 cable only.

Thermal Shock

The B1 cable was exposed to thermal shock per DOD-STD-1678, Method 4020. The cable was placed for 4 hours in a -150°C chamber and then immediately transported to a chamber at +150°C. After 4 hours, the cable was transported back to the -150°C chamber, followed by a final shock back to the +150°C chamber. Optical attenuation was automatically and continually measured, with an increased data sampling rate during the shock periods. The results indicated that the relative optical attenuation did not increase by more than the specified 5 dB/km over the duration of the test. Post test measurements on the cable optical attenuation measured 3.75 dB/km and 4.58 dB/km at 1300 nm and 1550 nm respectively.

Cyclic Flexing

The B1 cable was tested in cyclic flexing per DOD-

STD-1678, Method 2010, with relative optical attenuation measured continuously. The test consisted of a 180 degree arc bend over a mandrel 2.5 times the diameter of the cable with the cable under 5 kg tension. Consecutive trials on three sections of cable, for 500 cycles at +25°C and 500 cycles at +150°C, resulted in relative optical attenuation 'ower than the 0.5 dB limit. The attenuation during a +150°C cycle is shown in Figure 4. Mechanically, the cable was not damaged, so long as the vertical motion of the cable was eliminated during flexing. In cases where there was vertical motion, the braided jacket was worn away by

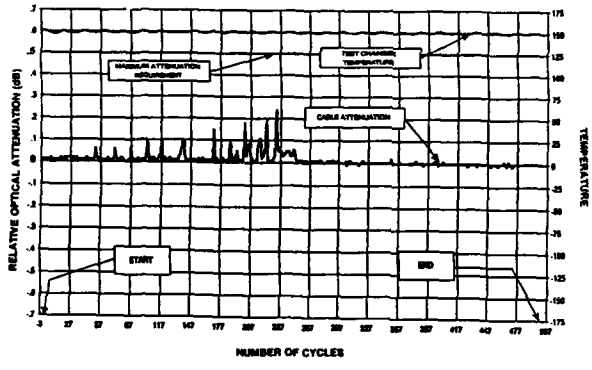


Figure 4. Cyclic Flexing +150°C

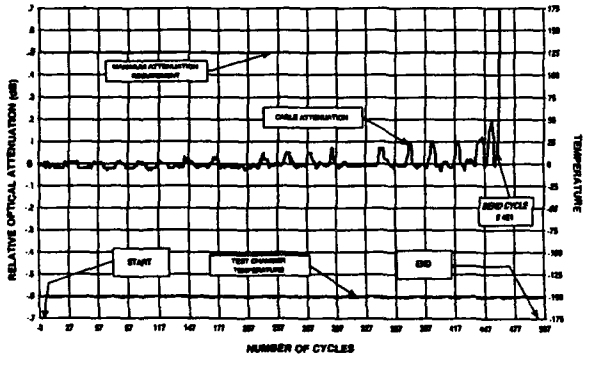


Figure 5. Cyclic Flexing -150°C

the rubbing on the mandrel. Even though the jacket was completely broken at times, the optical performance remained within specification.

Cyclic flexing at -150°C resulted in the buffer and fiber breaking at 461 cycles as shown in Figure 5. Repeated tests at -150°C on inactive cables revealed the same failure mode. The mechanism of failure was determined to be the brittle fracture of the thermoplastic buffer, resulting in the optical fiber break.

Cold Bend

The B1 cable was subjected to low temperature flexibility (cold bend) tests per DOD-STD-1678 Method 2020. The test was configured to have two ends of the cable, each supporting a 5 kg mass, simultaneously wrapped around a mandrel of 7 times the diameter of the cable, while at -150°C. Through automatic control and data acquisition, the cable was wrapped around the mandrel 5 times and then unwrapped. The first cable tested was successful, resulting in relative optical attenuation much less than the required maximum .5 dB as shown in Figure 6. The next two samples tested failed, resulting in localized breaks in the optical fibers and buffers, but no damage elsewhere in the cable or in the other cable elements. Inspection of the failed

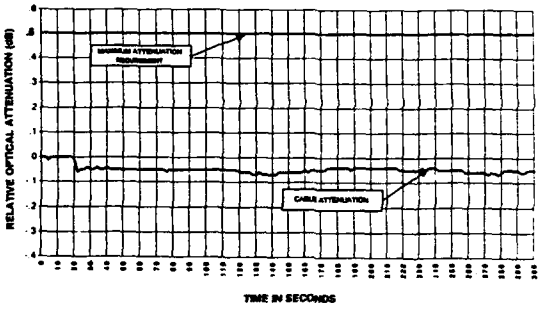


Figure 6. Cold Bend

cables revealed that when areas of the cable that had buckled from temperature cycling were wrapped onto the mandrel, the buffer had split, consequently breaking the fiber. With this knowledge, we were able to successfully predict the location where a fourth cable ultimately failed, as the fiber broke at the point when the buckled section was bent over the mandrel. A cable that has not been temperature cycled will not have buckled areas, and should be expected to consistently pass the cold bend test.

Impact Test

The B1 cable was subjected to impact testing per DOD-STD-1678 Method 2030.. A mass of 0.5 kg

was set up to repeatedly free drop a distance of 150 mm, impacting the cable with a striking surface of radius 12.5 mm. Data acquisition and control of the impact mass were automatic. Results of the test consistently showed no relative optical attenuation until failure. The survival duration for each test sample is shown in Table 4. In all cases, the

Table 4. Impact Test Results

Temp	Impacts to Failure			
	Trial 1	Trial 2	Trial 3	Trial 4
-150°C	30	28	50*	28
+25°C	50*	2	2	-
+150°C	2	2	-	-

braided jacket was completely damaged after five impacts. The Aramid strength member, on the other hand, had only minimal damage after 50 impacts. In the two cases where the B1 cable lasted for the full duration of 50 impacts, the relative optical attenuation was negligible..

Flammability

The cable was subjected to a flammability test per DOD-STD-1678. A sample of cable was fixed at a 60 degree angle and exposed to a propane torch flame of temperature 1100°C at the hottest location. A tissue paper was located under the section of cable exposed to the flame. There was no flame travel up the cable during exposure or continued burning of the cable after removal of the flame. No burning particles or drippings were found. Repeated tests showed the same results, indicating the cable to be nonflammable.

Tensile Strength

The tensile strength of the cable was measured on three samples with the ends terminated by capstans. The optical continuity of the cable was monitored to determine the load where the fiber breaks. Results of the tests are shown in Table 5.

The optical fiber showed little or no relative optical attenuation until within 22 N (5 pounds) of the fiber break load. These results demonstrate the cables ability to meet the minimum break strength and operating load.

Table 5. Tensile Strength Results

Minimum Break Strength	% elongation at break	Minimum load at optical fiber break
1090 N (245 lbs)	6.0	467 N (105 lbs)

Radiation

Three lengths of the B1 cables were subjected to Cobalt 60 radiation at -150°C. Each cable received a total radiation dosage of 8×10^6 rad over a 24 hour period. After receiving the dosage of radiation, the three cables were tested to determine the tensile strength as before. The minimum break strength was 1129 N (254 pounds), indicating that there was no mechanical degradation of the cable.

UV Radiation

Ultraviolet radiation exposure tests were not performed on the cable. The glass fiber material comprising the braided jacket is unaffected by ultraviolet radiation and should thus provide ultraviolet protection to the underlying cable elements. It is expected that the cable will retain greater than 70% of its tensile strength after an ultraviolet radiation exposure equivalent to 12 years in space.

CONCLUSION

The test results on the fiber optic cable are encouraging. The performance characteristics of the cable as determined through testing are summarized in Table 6. Of great significance is the ability of the cable to repeatedly operate at the temperature extremes.

Through material selection and design experimentation, this program has developed a cable that has met many requirements other cables were not able to meet. Further research of materials and improvements in the manufacturing process should lead to a cable that will consistently meet all of the requirements. The results of this program indicate that the tested cable, along with the radiation hardened optical fiber developed in the fiber phase of this program, will provide a single mode fiber optic cable usable in space applications.

ACKNOWLEDGEMENTS

The authors would like to acknowledge the initial cable design and development efforts provided by J.P. Kurt, M.L. Dowell, M.M Mekawi and F.J. Laritz of AT&T Bell Laboratories, and the test apparatus design, operation and data acquisition provided by I. Pelech and Z. Onufryk of AT&T Bell Laboratories.

Table 6. Cable Performance

TEST DESCRIPTION	REQUIREMENT
OPTICAL ATTENUATION per FOTP-78	< 4.8 dB/km at 1310 nm < 1.2 dB/km at 1550 nm
THERMAL CYCLING 5 cycles -150°C to +150°C	< 5 dB/km rel. optical attenuation
THERMAL SHOCK -150 °C TO +150°C	< 5 dB/km rel. optical attenuation
CYCLIC FLEXING per DOD-1678, Method 2010 Temp + 25°C, 500 cycles Temp +150°C, 500 cycles Temp -150°C, 500 cycles	< 0.5 dB rel. optical attenuation 500 cycles (no failure) 500 cycles (no failure) 461 cycles (no failure)
COLD BEND per DOD-1678, Method 2030 5 wraps around mandrel at -150°C	< 0.5 dB rel. optical attenuation. 1 of 4 samples passed
IMPACT per DOD-1678, Method 2030 Temp -150°C, 50 impacts Temp +25°C, 50 impacts Temp +150°C, 50 impacts	<0.5 dB rel. optical attenuation 28 impacts to failure 2 impacts to failure 2 impacts to failure
FLAMMABILITY per DOD-1678, Method 5010	Not flammable
TENSILE STRENGTH	> 1090 N (225 lbs) breaking strength
RADIATION 1 X 10^7 rad gamma radiation	No change in tensile strength after exposure
ULTRAVIOLET RESISTANCE exposure equivalent to 12 years in space	estimated > 70% of tensile strength after exposure
CABLE DIAMETER	1.8 mm (0.070 in)
CABLE WEIGHT	3.8 kg/km



Peter A. Michaels is a Member of Technical Staff at AT&T Bell Laboratories, Whippany, New Jersey. He received a B.S. degree in Mechanical Engineering from The Pennsylvania State University and an M.S. degree in Mechanical Engineering from Lehigh University. He joined AT&T Bell Laboratories in 1988 and has been working on the design and development of undersea fiber optic cable and cable systems for military applications. He is a member of the American Society of Mechanical Engineers.



Man F. Yan is a supervisor in the Optical Fiber Research Department at AT&T Bell Laboratories, Murray Hill, NJ. He joined AT&T Bell Laboratories in 1976. His current research activities focus on preform process technology and optimization. He received B.S. and Sc.D. degrees from Massachusetts Institute of Technology, Cambridge, MA in 1970 and 1976 respectively. He also received a M. Eng. degree from University of California at Berkeley, CA in 1971. Dr. Yan is a member of the Optical Society of America, Materials Research Society, the American Society for Metals and he is a fellow of the American Ceramic Society. He authored or coauthored more than 80 publications in processing and characterizations of ceramics, optical fibers and semiconductors. He has also received 9 patents and edited 5 books.



Anne E. Miller graduated from Princeton University in 1983 with a B.S.E. in Chemical Engineering and started working for AT&T Bell Laboratories, Murray Hill, NJ in the optical materials research department on glasses for fiber optic application superconductors, and crystal growth. She received an M.S. in Materials Science in 1987 from Stevens Institute of Technology and a PhD in Ceramic Science in 1991 from Rutgers University. She is currently working in the Optical Fiber Research department on radiation effects in optical fiber and optical preform processing.



Vasilios E. Kalomiris is Chief Scientific Advisor for Local Area Communications Division at CECOM's Command, Control and Communications Directorate. Previously he was the Branch Chief for Local Area Networks and Fiber Optics. He joined U.S. Army CECOM twelve years ago. Prior to joining CECOM, he was employed by ITT-EOPD as a project engineer responsible for the design and development of various fiber optic cable systems. One of his projects was the design and development of the first air-layable fiber cable system. He also worked for General Cable Corporation R&D, as a research engineer involved with the design, development and manufacture of a prototype super conductive power cable with flexible core. Vasilios holds three patents in fiber optic connector design.

Education and Professional Activities: B.A. in Mathematics, B.S. in Electrical Engineering, and M.S. in Electrical Engineering, all from New York University, and an M.B.A. from Fairleigh Dickinson University. He is a member of AFCEA, the Technical Chamber of Greece (Society of Professional Engineers) and Senior member of IEEE. He received the 3rd Annual Engineering Excellence Award for 1986 from CECOM; served for three years as Chairman of the Tri-Service Group on Fibers, Cables and Connectors; and is currently chairing the Point-to-Point Systems group.

FIBER OPTIC CABLE SYSTEMS FOR NAVY SHIPS

Dennis R. Knudsen, Joseph P. Ingold, Gair D. Brown

Dahlgren Division
Naval Surface Warfare Center
Dahlgren, Virginia

Abstract

As fiber optic systems are implemented on Navy ships, emphasis is being given to fiber optic cable systems for the ships. Different systems share fibers within the same cable to achieve efficiency. Redundant trunk cables are provided to increase survivability. The components are standardized to reduce logistic burdens. Design standards are being developed and prototype cable systems are being installed.

Introduction

Fiber optic technology is beginning to be incorporated into Navy ships. The technology has been proven and is being engineered into shipboard systems. A system engineered cable system is critical to successful implementation of these systems.

Systems on Navy ships have requirements for widely varying signal types including voice, video, and data. Each of these can be either analog or digital. These signals can all be handled by the same type of optical fiber. This characteristic significantly reduces the numbers and types of different components needed for logistics support of installed systems.

Fiber optics offers many benefits for naval surface combatants. The use of fiber optics allows higher data transmission rates, reduces electromagnetic interference (EMI), reduces cable weight and space requirements and allows systems designers greater flexibility in the design of systems.

The benefits in using fiber optics in Navy ships were discussed in detail in reference 1. In that paper, three essential items were identified as being critical to a beneficial implementation of fiber optics in surface combatants. These are a system engineered cable system that meets the needs of the shipboard systems, components that meet system requirements, and design guidelines to assure that system requirements are met. The concepts for an effective fiber optic cable plant are discussed below.

Cable Plant Description

The fiber optic cable system or cable plant consists of all of the trunk fiber optic cables and fiber optic interconnection equipment within the ship including connectors, splices and interconnection boxes. The fiber optic cable plant is a totally passive system only serving to transport optical signals between equipments (e.g. computers, displays, network nodes, etc.). To obtain the greatest ship-wide benefits from fiber optic upgrades, a ship-wide design approach must be used. Maximum benefits can be obtained by designing the fiber optic cable plant using a critical compartment interconnection box approach.

The cable plant primarily consists of trunk cable runs and interconnection boxes. Trunk cables optically interconnect critical compartment interconnection boxes and are typically run through the main cableways. Local equipment cables are used to optically connect the equipment to the cable plant at the compartment interconnection box and typically are not run through the main cableways. Trunk cables generally have higher fiber counts per cable than that found in local cables.

In past installations, eight-fiber cables have been used for trunk cables and two or four-fiber cables have been used for local cables. Higher fiber count cables are desirable and may be used in the future for the trunk cable application. The data path is established between equipments by connecting fibers in the local cables to common fibers in a trunk cable via single-fiber connectors or splices within a interconnection box. A typical link is shown in Figure 1.

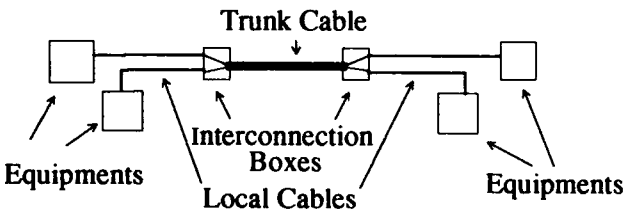


Figure 1. Typical Fiber Optic Link

Cable Plant Concepts

The interconnection box approach to fiber optic connections takes advantage of the fact that many types of signals can be carried on one type of fiber. This characteristic means that only a few types of components are required for all shipboard applications, which reduces logistic requirements. Since fibers are naturally immune to electromagnetic interference (EMI), electromagnetic pulse (EMP), and other electromagnetic perturbations, multiple fibers may be run in the same cable, any of which will meet the requirements of an equipment interconnection. Thus multiple signals from one system or multiple systems can be run in the same cable, which further reduces cable space and weight requirements. These characteristic, together with the fact that long runs are possible, also reduce routing restrictions.

Since the transfer from electrical cables to fiber optic cables will save space and weight within the ship's cableways, spare fibers and extra trunk cables can be pulled at the time of ship construction to serve as survivable spares for all critical fiber optic cables. In the event of fire or battle damage, fiber optic systems can be manually reconfigured by the ship's crew from the damaged cables to functional redundant cables at each interconnection box location (see Figure 2).

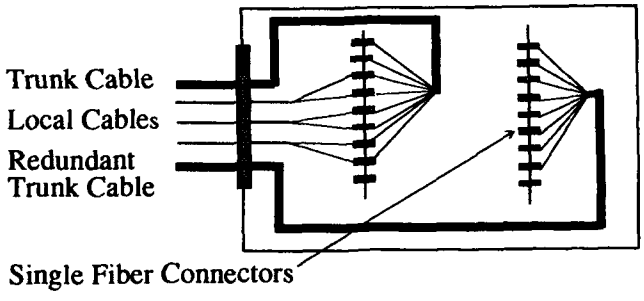


Figure 2. Typical Fiber Optic Interconnection Box Configuration

Similarly, extra cables can also be pulled with the specific purpose of supporting future upgrades, since the installed fibers will meet the requirements of most future systems. This pre-installation of cable for future upgrades will allow quicker and much less costly additions to the ship's capabilities at later dates. Also, systems can be change or are replaced and still use the same fiber optic cables for their intended lifetime.

Cable Plant Design Issues

There are presently three issues in designing a cable plant such that it will have an overall beneficial effect on the total ship as a system and not have a negative effect on a given system served by the cable plant. These are (1) the impact of additional connections on the power budget of a given system, (2) the impact upon the survivability of a given system by maximizing the collective survivability of all the systems, and (3) the impact of additional connections on the reliability of a given system.

Power Budgets

Special provisions must be made for systems with critical power budgets to minimize the adverse effect that additional connections would have. For example, local area network implementations that use ring architectures and bypass switches have critical power budgets and have difficulties allowing for additional connections. By designing the cable plant around these systems and putting the bypass switches in the interconnection box, the cable plant can be implemented without adding additional connectors to these systems.

Survivability

Since one of the reasons for implementing the cable plant is to increase survivability by providing reconfiguration, one must be careful not to configure the cable plant so it adversely affects the survivability of a given system. For example, the location of the bypass switches in a local area network is critical to the survivability of the network. While striving to achieve efficiency in the cable plant by putting bypass switches in interconnection boxes along with connections for other systems, one must be careful not to locate the bypass switches in improper locations.

Reliability

At first, one might be concerned about the impact of additional connections on the reliability of a given system. This issue is not really significant, however since the connectors are very reliable and the availability is increased by providing the redundant cable path.

Cable Plant Design Standards

The Naval Sea Systems Command is undertaking a project called Fiber Optic Topology, the objective of which is to produce documentation and qualify

components to *design, install, maintain and manage* a fiber optic topology (or cable plant). Much of this information is equally applicable to fiber optic cable dedicated completely to one system. The products of this project are:

Topology Design Standard
System Design Standard
Installation Standard
General Ship Specification Update
Navy Training Plan & Curriculum
Naval Ship Technical Manual
Reliability and Lifetime Predictions
Qualified Products

Topology Design Standard

A Topology design standard has been written to define the implementation of the cable plant. The standard defines the design requirements, the design process and methodology.

Design Process

The design process is divide into a three phase approach which corresponds to a typical ship design process. The process starts with a review of the ship specification, configuration, and fiber optic systems planned for that ship. This information together with the design requirements is used to produce the cable plant design.

Design Methodology and Requirements

The three phase of the topology design process are the conceptual, preliminary and detailed design.

Conceptual Design: The inputs to the conceptual design are the:

Ship Specification
Ship Configuration
System Specifications
Conceptual Design Requirements

The vital spaces from the ship specification and the location of equipments are used to determine service areas. Each service area is served by one interconnection box. These services areas are then documented on block diagrams showing general interconnection box locations and trunks between service areas.

A trunk cable is provided between each interconnection box and an interconnection box in damage control to provide dedicated fibers for damage control assessment. Fibers for a maintenance phone system may also be provided.

Preliminary Design: The inputs to the preliminary design are the:

Conceptual Design Block Diagrams
Detailed System Requirements
Preliminary Design Requirements
Ship Configuration

The number and type of fibers, termination type and link performance are used to determine the size, type and location of interconnection boxes. Trunk cable capacities are also identified at this point. The preliminary design is then documented on block diagrams. A cable plant specification which identifies all the general performance and environmental specifications is imposed on the cable plant and its components.

A link loss budget and a link rise time budget are developed for each link in the cable plant to ensure that system performance requirements are met for each user. If performance requirements are not met, the configuration is changed.

Requirements for redundant trunk and local cables are also determined at this time. Also, fibers are identified as to function including those allocated for systems, spares and growth.

The preliminary design block diagrams and the specification define the cable plant and serve as input to the detailed design of the ship and the cable plant.

Detailed Design: The output of the preliminary design is used to lay out the detailed design on the detailed ship construction drawings. Items produced are

Block Diagram
Fiber Run Lists
Cable Pull Charts
Interconnection Box Configuration Drawings
Detailed Parts List

Requirements for local and trunk cable routing are included to maximize survivability. Requirements for interconnection box configuration exist to ensure standard arrangement for ease of access and reconfiguration. Requirements for components are given to ensure standardization.

This standard is presently in the Navy review process; current shipboard cable plant design efforts are using this standard as a model.

Key Cable Plant Components

The paragraphs below describe the components and point out the first set of components that are being qualified.

Optical Fiber

There currently are two standard fibers recommended for use in Navy systems (per MIL-F-49291). The first of these is the 62.5 micron core/ 125 micron cladding graded index multimode fiber. For shipboard interconnection lengths this fiber is capable of handling data rates up to approximately 1 GHz depending upon the optical source characteristics and the exact link length. For those applications where the data capacity of the multimode fiber is inadequate the other recommended fiber is the singlemode fiber.

It should be noted that each of the recommended fibers have the same outside diameter so the same connector can be used for each application.

Fiber Optic Cable

The general requirements that a Navy fiber optic cable must meet are given in MIL-C-85045. Cable specified to this point is of the Optical Fiber Cable Component design. This is a type of cable consisting of individual single-fiber cables called Optical Fiber Cable Components (OFCCs) laid with strength members around a central member and overjacketed for environmental and mechanical protection. The OFCC consists of a buffered fiber (900 microns total diameter) surrounded by strength members and a protective jacket with an outer diameter of approximately 2 millimeters.

For future use in high density applications, stranded cable may be used. This is a type of cable in which the buffered fibers (900 microns total diameter) are stranded down the center of the cable surrounded by strength members and a protective jacket.

These cable designs must meet minimum levels of performance in safety (low smoke generation, low toxicity, low halogen content, flame resistant, etc.), durability (able to withstand shock, vibration, mechanical abuse, fluids, etc.), ease of installation and repair, and optical performance.

Interconnection Equipment

Interconnection equipment consists of single- fiber light duty connectors or splices, multifiber heavy duty connectors, and interconnection boxes. Each of these components are described in more detail in MIL-C-83522, MIL-S-24623, MIL-C-28876, and MIL-I-24728. The design of each of these components was chosen in order to optimize their performance for the application in which they are used as well as to minimize problems due to human factors.

Single Fiber Light Duty Connectors: The single fiber connectors (per MIL-C-83522/16) are intended only for use inside of interconnection boxes or equipments. Ceramic ferrules are preferred because of their tighter tolerances and improved environmental performance.

Single Fiber Light Duty Splices: The single fiber splices (per MIL-S-24623) are also intended only for use inside of interconnection boxes or equipments. Their primary purpose is to provide a higher grade optical performance in those cases when the single fiber connectors are not adequate. In general, they are used when connectors would introduce too much loss into the system, but may also be used when low reflection interfaces are needed such as for high speed single mode communications systems. The splice is intended to be a permanent connection, but may be demated and remated to another splice with only a slight degradation in performance if emergency reconfiguration is necessary.

Multifiber Heavy Duty Connectors: The multifiber heavy duty connectors (per MIL-C-28876) are required to withstand the severe naval environment while showing only a limited performance degradation. They are intended to be used to connect equipment in any application where the fiber optic connector is exposed and not housed within the interconnection box. These connectors are expected to withstand the full rigors of the Navy shipboard environment including shock, vibration, temperature extremes, fluids including salt water, and humidity.

Interconnection Boxes: The interconnection boxes used (per MIL-I-24728) are also intended to withstand the full rigors of the Navy shipboard environment and, to the maximum extent possible, to protect and isolate the connectors and splices from that environment. The boxes are modular in nature with current versions

containing one, two, or three modules. Each module may contain up to 48 connectors or 72 splices. Connector and splice modules may be mixed in the same box. The connectors are mounted on a flat plate which slides out of the box when it is open to allow for easy access and to minimize the chance of secondary damage when performing repairs within the box. The splices are mounted in removable drawers which organize the splices as well as provide limited mechanical protection. The front cover of the box is hinged in a fashion so that it may either be completely removed from the box or be held out from the box to function as a work table. Both the connector panel and the splice drawers are securely locked into place when the cover is closed and secured. The design of the box structure itself is based on the design of existing lightweight electrical interconnection boxes.

Cable Plant Installations

Some prototype installations have been accomplished and larger scale installations are planned.

AEGIS Cruiser Installations

Cable plants were installed on two AEGIS Ticonderoga class guided missile cruisers, USS Valley Forge (CG 50) and USS Mobile Bay (CG 53). The installation of 5800 feet of fiber optic cable and 16 interconnection boxes on the USS Valley Forge in 1985 showed the feasibility of the concept. The installation also showed that fiber optic cable and connectors could be installed in a shipyard environment.

The installation of 3000 feet of cable and 8 interconnection boxes on the USS Mobile Bay in 1987 has supported evaluations during shock trials (reference 2) and long term evaluation (reference 3). The evaluation during shock trials showed that fiber optic systems could operate in a combat environment. The long term evaluation has shown that there are no long term effects on fiber optic cable and connectors in a shipboard environment.

Land-Based Evaluation Facilities

One land-based cable and interconnection box installation has been accomplished at the Naval Surface Warfare Center's Interim Combat System Engineering Facility at Wallops Island, Virginia. This installation in 1991 supported the Integrated Interior Communications and Control proof of concept demonstration (reference 4). (The Integrated Interior Communications and Control program is an initiative to coordinate the development of architectures based on fiber optic networks for shipboard interior communications.)

A larger scale installation has been designed per the Topology Design Standard and is currently being installed. This installation will support the evaluation of shipboard cable plant designs, installation and repair procedures as well as the 1993 Integrated Interior Communications and Control system evaluation. This installation will include 7400 feet of multimode cable, 1500 of single mode cable and nine interconnection boxes.

USS George Washington (CVN 73)

A fiber optic cable plant was installed on this aircraft carrier in 1991-1992 to support a fiber optic network comprised of an FDDI backbone with ethernet subnets. The installation included 45,000 feet of multimode cable and 202 interconnection boxes, of which 187 were special small-size boxes with a capacity of eight connectors. Similar systems may be installed on carriers in the future.

Future AEGIS Destroyers

A fiber optic cable plant is being designed for future AEGIS Arleigh Burke class guided missile destroyers. The cable plant will support ten fiber optic systems. The systems range from single point to point links to FDDI Local Area Networks. The information on the different links is either video, voice or data. These systems are candidates for destroyers beginning construction in 1994.

Acknowledgments

The authors wish to acknowledge the support of the Fiber Optics Program Office (SEA 06KR22) of the Naval Sea Systems Command and the AEGIS Program. The authors also acknowledge David Owen and Jack Paxton of NTL Inc. for developing the Topology Design Standard and the design of the cable plant for the land-based evaluation facility at Wallops Island.

References

1. Knudsen. D. R. et al., A Ship-Wide System Engineering Approach for Fiber Optics For Surface

Combatants, Naval Engineers Journal, May 1990. pp. 127-137.

2. Ingold, J. P. et al., Fiber Optic Integrity Testing During U.S. Navy Shock Trials, DOD Fiber Optics Conference '88, March 1988. pp. 173-174.

3. Paxton, J.G.,Jr., et al. Long Term Performance Measurements of Shipboard Fiber Optic Cable Plants, DOD Fiber Optics '92, March 1992. pp.135-138.

4. Carle, G. and J.P. Ingold, Integrated Interior Communications and Control, DOD Fiber Optics '92, March 1992. pp. 348-350.



JOSEPH INGOLD received a B.S. degree in physics (1985) and an M.S. degree in electrical engineering with concentration in fiber optics (1990) from Virginia Polytechnic Institute and State University. Since joining the Naval Surface Warfare Center in 1985 he has worked in the Photonics Group in the Combat Systems Technologies Branch, performing environmental tests on fiber optic components, shipboard experiments on fiber optic sensors, and development, design test and evaluation of shipboard cable plants.



DENNIS KNUDSEN received a Ph.D. in physical chemistry from North Dakota State University in 1970. At the center from 1970 to 1986 he developed shipboard equipment for vapor and radioactive particulate detection, methods for testing protective clothing for torpedo workers, and methods for the thermal destruction of hazardous waste. As head of the Photonics Group in the Combat Systems Department for the past five years Dr. Knudsen has directed projects for the AEGIS Program and the NAVSEA Fiber Optic Program Office. The projects have involved fiber optic component development, cable plant development and system implementation issues. Dr. Knudsen is a member of the American Chemical Society.



GAIR BROWN graduated summa cum laude in May 1985 from West Virginia Institute of Technology with a B.S. in physics and mathematics. He has worked in the Photonics Group in the Combat Systems Technologies Branch at the Center since 1985, concentrating on environmental testing of fiber optic components, component specifications, and system design standards, shipboard cable plant design, and light launch conditions for shipboard applications.

Hydrogen - Caused Signal Attenuation in Buried Optical Fiber Cables

George Schick, Karen A. Tellefsen, Casey J. Wieczorek
Robert M. Kanen and Aaron J. Johnson

Bell Communications Research
Morristown, NJ

Abstract

Submarine optical fiber cables experience significant hydrogen-caused darkening, but there is no report of this problem in buried plant. The purpose of this work was to determine whether buried optical cables can darken excessively under adverse conditions because of hydrogen.

Experiments were conducted in wet sand environments, simulating that of direct buried plant. The hydrogen was generated by: (1) hydrogen-producing bacteria, and (2) the corrosion of the corrugated steel shield at outer jacket defect sites. The results show that the bacterial hydrogen production was limited both in magnitude and in time of duration. The corrosion-generated hydrogen was still negligible after 307 days. Furthermore, optical fiber cables in the buried plant are unlikely to develop hydrogen-caused signal attenuation problems because: (1) oxidizing and well-aerated soils do not support the growth of hydrogen-producing bacteria, (2) the cables are buried at a 0.76 - 1.1 meter (2.5 - 3.5 feet) depth, and the worse case hydrogen partial pressure is limited to 1 atm as opposed to >8 atm at deep water crossings.

INTRODUCTION

It has been established by both laboratory and field investigations that hydrogen diffusion into optical fiber cables can cause signal attenuation.[1-12] The source of hydrogen may be inside the cable: (1) break-down of organic materials in the cable,[13] (2) corrosion of metallic cable components,[6,7,15] and (3) microbiological break-down of a water absorbent polymer.[14] The source of hydrogen may also be the corrosion of the submarine cable's, metallic armor wires, [5,8,11,12,15] or it may be microbiological activity in the environment near the cable, independent of any cable material.[11,12] The field studies referenced above pertain only to submarine optical fiber cables.

Prior to the studies described in this paper, we have established that armor wire corrosion, stray dc current pick-up by the armor wires, and fermentation of hydrocarbon by hydrogen-producing bacteria can generate large quantities of hydrogen.[11,12] Our experiments also showed that cables manufactured with an overlapped corrugated metal shield cannot keep the hydrogen out of the core where it can darken fibers.[12] Furthermore, corrosion tests on submarine cables with known levels of signal attenuation, and analysis of mud samples, collected near the same cables, indicate that our laboratory tests are based on realistic field conditions.[16] Consequently, a generic requirement and a pass/fail test was developed to prevent signal attenuation in newly installed submarine optical fiber cables. The requirements and the test are in Bellcore Document TA-NWT-000020, Issue 8, December 1991.

Since direct buried optical fiber cables are widely used, our attention is now focused in this direction. This paper is a report on laboratory experiments concerning the effects of hydrogen-producing bacteria and the corrosion of corrugated steel shield at outer jacket defect sites on buried optical cable. As before,[12] our goal is to establish whether or not additional generic requirements for buried optical fiber cables are needed in the appropriate Bellcore Technical Reference(s).

Experimental Method

The experiments were conducted in the same test chambers used in our previous studies[12] (Fig. 1). A slight modification was made to the PVC cover; the heating unit was removed, and the large central opening was used to introduce sand into the system (Fig. 2). The reason for removing the heater was twofold. First, the wet sand would have created an unrealistically large temperature gradient, and the high temperature near the heater might have killed the hydrogen producing bacteria. Secondly, our previous work showed that bacteria (the reason for using elevated temperature) can survive at room temperature without any appreciable effect on hydrogen production. This was learned when the heater in one of the test chambers containing hydrogen-producing bacteria culture only, was replaced, exposing it to room temperature for four days.

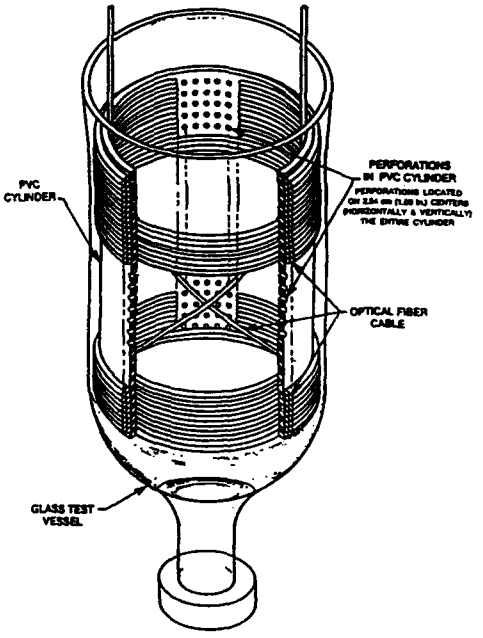


Figure 1. Illustration of the cable sample on PVC cylinder inside the glass test chamber.

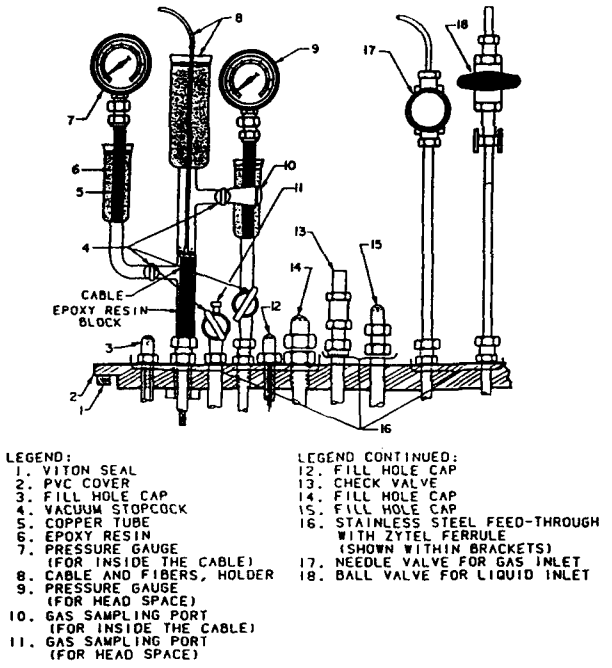


Figure 2. A segment of the PVC cover of the glass test chamber with the cable end holder, pressure gauge, gas sampling port, gas inlet and liquid inlet valves.

The test environments are fine sand saturated with either a 3.5 percent (by weight) NaCl solution or with hydrogen-producing bacteria culturing solution. In the former environment, cables with defective outer polyethylene jackets were exposed, and in the latter, the cable was undamaged. As of 6/11/92, the cables had been exposed to these environments for 307 days (NaCl solution saturated sand) to 373 days (hydrogen-producing bacteria containing sand). During this time, we monitored the signal attenuation in the 1.1 to 1.6 μm range, and measured the partial pressures of hydrogen both inside and outside the cables (Fig. 3).

A. Materials and Sample Preparation

The optical fiber cables used in these experiments had a 1.02 cm (0.4 in.) OD, and a corrugated, overlapped steel shield, coated with a thin green polymer, that improves adhesion between the steel and the polyethylene outer jacket. It also functions as a corrosion barrier. The 12 fibers were enclosed in a plastic center tube.

Four 50-meter sections were cut from this cable and coiled in 2 layers on the outer surface of a rigid PVC cylinder of 30.5 cm (12 in.) length, 23.9 cm (9.4 in.) OD, and 0.64 cm (0.25 in.) wall thickness (Fig. 1). The cylinder had 1.27 cm (0.5 in.) OD holes 2.54 cm (1 in.) apart on its entire surface. On the outer jacket of three of the cables, 2, 4, or 8 evenly spaced, 1.27 cm x 1.27 cm (0.5 in. x 0.5 in.) defects were introduced. These polyethylene squares were removed with a sharp blade and a small screwdriver. Consequently, the underlying thin green polymer film was also scratched in small areas. The cable was placed carefully so that half the jacket defects were located on the outer surface of the outer layer of cable, and the other ones were facing holes in the PVC cylinder. Thus, all the jacket defects were directly exposed to the corrosive environment. The fourth cable which had no sheath defects, was coiled on the PVC cylinder. The last 2 meters of both ends of each cable were brought inside the cylinder through long, smooth channels cut in the bottom of the PVC cylinder. These channels allowed a gradual transition between the inside and the outside of the cylinder without causing a sharp bend in the cable. The cable samples were placed in 30 liter capacity glass test chambers (Fig. 1). These test chambers had rigid PVC covers secured to their tops (Fig. 2). Gas tightness of the test chambers was ensured with VITON seals. The outer jacket, metal shield, and inner plastic tube were removed from the cable ends approximately 16.5 cm (6.5 in.) above the PVC cover, leaving 152.4 cm (5 ft.) sections of exposed fibers. The fibers were cleaned with turpentine and ethyl alcohol. The two cable ends and exposed fibers were pulled through glass structures (Fig. 2) and 15.2 cm (6 in.) of the jacketed cable ends were sealed with epoxy resin inside the glass tube to position the cable and form a gas tight seal. The upper 8.8 cm (3.5 in.) sections of the glass structures were filled with epoxy resin to form a gas tight seal around the exposed fibers. The spaces between the two epoxy resin seals were equipped with vacuum stopcocks and gas sampling ports, allowing the gases inside the cables to be sampled. The fibers above the upper seals were concatenated with fusion splices to form a continuous ~600m light path and placed into splice organizer trays.

Other associated equipment: pressure gages, valves for N_2 gas blanketing, liquid inlets, pressure check valves, gas sampling ports (for gases generated outside of the cable), were installed as shown in Fig. 2.[11,12] Glass tubes were passed through the PVC cover via stainless steel feed-throughs, threaded into the PVC with ZYTEL ferrules around the glass tubes (Fig. 2) to ensure gas tightness. The test chamber design, especially the cable end and fiber holders, enabled gas sampling and measurement of the overall pressure in both the head space and in the spaces at the two cable ends, (Fig. 2).

B. Test Environments

The experiments were conducted in two different environments: (a) fine clean sand saturated with 3.5 percent (by weight) NaCl solution, and (b) fine clean sand saturated with a culturing solution (Table I) inoculated with a hydrogen-producing bacteria (Clostridium acetobutylicum, ATCC* 824). The NaCl solution saturated sand was used to establish whether corrosion of the exposed steel at outer jacket defect sites, can generate sufficient hydrogen to cause signal attenuation. The sand saturated with hydrogen-producing bacteria inoculated culturing solution was used to determine the upper limit of bacterial hydrogen production in wet soil and its effect on the direct buried optical fiber cable.

TABLE I

Culturing Solution for Clostridium Acetobutylicum

5 gram	Bacto-peptone
5 gram	Bacto-tryptone
5 gram	Yeast extract
10 gram	Glucose
0.005 gram	Hemin
0.2 ml	0.5% solution of vitamin K, in 95% ethanol
20 ml	Salts solution
1000 ml	Deionized water

The solution pH was adjusted to 7.3 ± 0.2 and degassed with N_2.

After transferring the culturing solution into the test chambers and further purging with N_2, 1 millimole of Na_2S was added as reducing agent.

Salts Solution contains per 1000 g. of deionized water

0.23 gram	$CaCl_2 \cdot 2H_2O$
0.48 gram	$MgSO_4 \cdot 7H_2O$
1.0 gram	K_2HPO_4
10.0 gram	$NaHCO_3$
2.0 gram	NaCl

* ATCC = American Type Culture Collection
1203 Parklawn Drive, Rockville, MD 20852

After placing the cables in their respective test chambers and concatenating the fibers, about one third of the sand was poured in to the test chamber through the center fill hole. Then, enough solution was poured through the liquid fill tube to thoroughly wet the sand. This procedure was repeated twice. The sand totally covered the cable samples, and an additional two inch of liquid was added on the top of the sand to ensure constant wetness. The hydrogen-producing bacteria were inoculated into the second liquid fill, and the last part of the sand was poured in under a N_2 gas blanket to ensure anaerobic conditions during the filling process.

C. Measuring Equipment

The signal attenuation in the fiber was monitored between 1.1μm and 1.6μm with equipment similar to that described in the Electronic Industries Association Standard EIA-455-78. The gas samples were analyzed for hydrogen content with a Gow-Mac isothermal 580 type gas chromatograph with a 2.5m long 3mm diameter molecular sieve 5A column and thermal conductivity detector. Argon carrier gas (99.998%) was introduced at a flow rate of 30 cc/min. The column detector and injector temperatures were set to 50, 135, and 135°C respectively, and the detector current was 40mA. The detector signal was recorded and processed on a Spectra Physics integrator.

D. Testing Procedure

The signal attenuation, against two unexposed reference fibers, was measured for the cables in all the test chambers at 54 different wavelengths between 1.1 and 1.6μm. A typical spectral attenuation plot is illustrated in Figure 3 for a fiber with and without hydrogen. From these data, the Hydrogen indicator, H_{ind}, defined by Anderson et. al.[9] as signal attenuation at 1.24μm less that at 1.31μm, was calculated and plotted as a function of time.

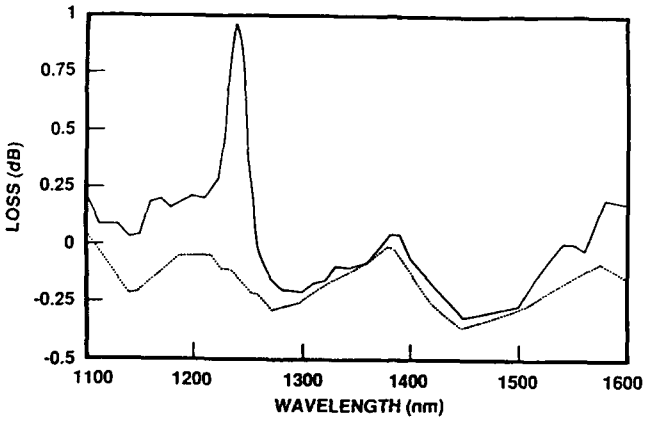


Figure 3. Typical spectral attenuation of optical fiber with (solid line) and without (dotted line) hydrogen.

Gases were sampled in each test chamber from the test chamber head space (outside the cable) and at the two cable ends (inside the cable) using a 0.5 ml gas-tight syringe with a valve. The chromatograph was calibrated, each day that gas analyses were made, with duplicate samples of 0.250 ml of 99.9% hydrogen and 0.500 ml of room air (about 21% oxygen and 78% nitrogen). The partial pressure of hydrogen [$p(H_2)$] data were also plotted as a function of time.

The overall pressure of the gas in the head spaces and at the two cable ends was also measured so as to be taken into account at the calculation of the $p(H_2)$ values.

Results

The results prior to 6/11/92, representing exposure times of 307 days in the NaCl containing sand and 373 days in the hydrogen-producing bacteria containing sand, are considerably different from those obtained in fully liquid environments.[12]

A. The effect of hydrogen-producing bacteria

The data plotted in Figure 4 indicate that the level of hydrogen production in the liquid saturated sand can approach that in liquid alone. However, the available fermentable hydrocarbon is more limited, and consequently the hydrogen production abates more rapidly. The H_{ind} values obviously follow the same trend. After an initial period of hydrogen production (~800 hours), the $p(H_2)$ and H_{ind} inside the cable are reduced to negligible levels. After 1800 hours of exposure, an additional 160 grams of dextrose, dissolved in deionized water, was added to the liquid phase. The ensuing bacterial fermentation quickly produced hydrogen (up to $p(H_2) = 0.4$ atm.). Consequently, the hydrogen rapidly permeated the cable causing a fast rise of the H_{ind} (up to 2.2 dB/km). However, the high partial pressure of the hydrogen in the cable was not maintained for long, as indicated by the diminishing H_{ind} less than 500 hours after the additional dextrose was introduced, and, about 1700 hours after introducing the sugar, the H_{ind} was negligible.

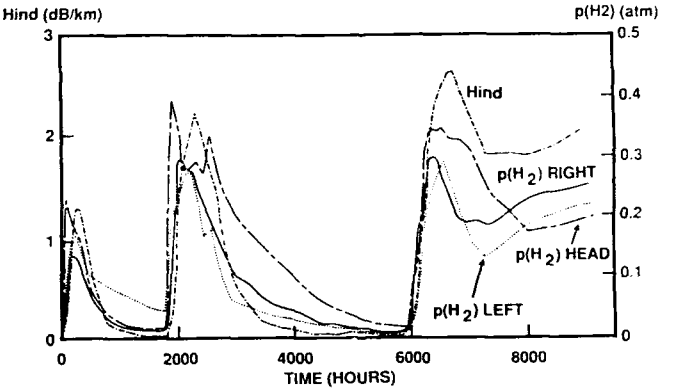


Figure 4. Hydrogen indicator (H_{ind}) and hydrogen partial pressure [$p(H_2)$] curves vs. time for an optical fiber cable (without cable sheath damage) exposed to fine sand saturated with hydrogen-producing bacteria inoculated culturing solution.

At approximately 6000 hours of exposure an additional 160 grams dextrose was introduced into the test chamber. This time a 91.4 cm (36 inch) long, 2.54 cm (1 inch) diameter glass tube was sealed on one end and was pushed into the wet sand to approximately 2.5 cm (1 inch) from the bottom. The dextrose and deionized water mixture was poured into this glass tube, then using a clean stainless steel rod the sealed bottom of the glass tube was broken and the dextrose solution was emptied in the wet sand phase. As a result, the $p(H_2)$ in the head space increased to 0.35 atm. and the H_{ind} reached 2.6 dB/km. Both the $p(H_2)$ and the H_{ind} started to decrease after 780 hours. However, they did not go down to a negligible level continuously but leveled off after about 660 hours at $p(H_2) = 0.2$ atm. and $H_{ind} = 2.0$ dB/km (Fig. 4).

B. The effect of cable shield corrosion

Among the three cables exposed to NaCl solution saturated sand, the only difference was the number of defects in the outer jacket. As of 6/11/92, the analysis of gas samples for the cables with 2 and 4 defects showed only traces of hydrogen. Consequently, these cables showed no measurable H_{ind}.

The third cable sample with 8 defects, showed extremely low H_{ind} (Fig. 5). This is in spite of the fact that the cable shield is thoroughly flooded (water accumulation and rust at the cable ends are visible). The $p(H_2)$ inside the cable at the two cable ends, was detectable only after 1000 hours and 1500 hours of exposure. The average of these two values is plotted in Figure 5.

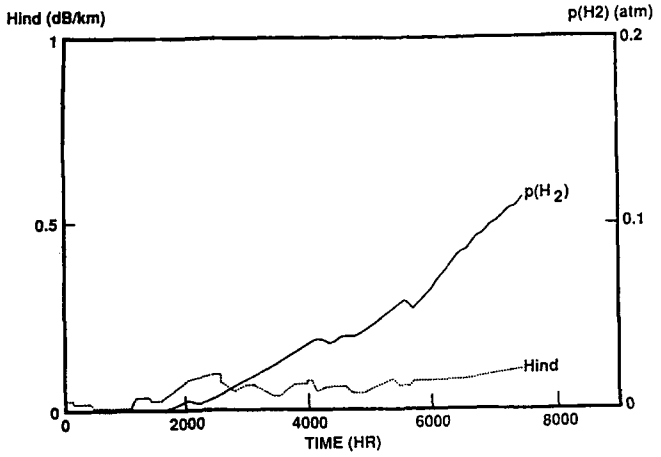


Figure 5. Hydrogen indicator ($H_{ind.}$) and hydrogen partial pressure [$p(H_2)$] curves vs. time for an optical fiber cable with eight 1.27 cm x 1.27 cm. (0.5 in x 0.5 in) cable sheath defects exposed to fine sand saturated with 3.5 percent (by weight) NaCl solution.

The $H_{ind.}$ is negligible up to 6/11/92. Because we have only ~600 meter test length of fiber and the hydrogen level is very low, the $H_{ind.}$ data are not reproducible. A trend of $H_{ind.}$ increase starts only after about 1500 hours of exposure time.

Discussion of the Results

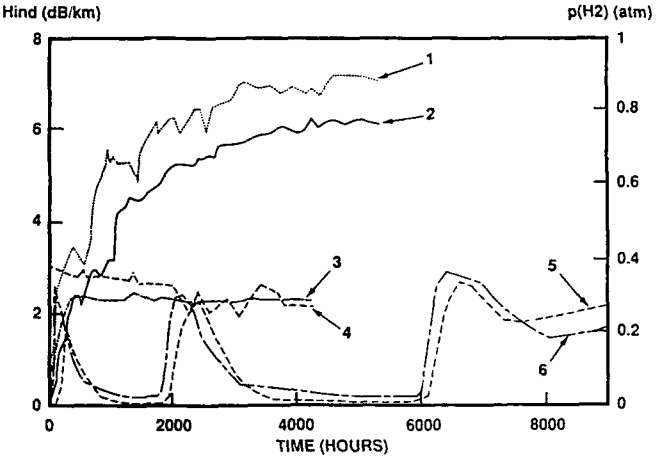
The experiment conducted in fine sand, saturated with inoculated hydrogen-producing bacteria culturing solution, indicates that hydrogen production and the ensuing increase of $H_{ind.}$ is smaller and shorter in duration than the same occurring in a totally liquid environment. This is partially due to the fact that the liquid saturated sand contains approximately half as much fermentable hydrocarbon (dextrose) as that in the previous experiments conducted in the inoculated culturing solutions.[12] This is supported further by the introduction of dextrose into the environment after 1800 hours of exposure which presumably largely remained in the liquid phase. The partial pressure of hydrogen and $H_{ind.}$ developed after adding extra sugar are similar to that measured earlier in a similar test in a totally liquid medium.[12] The short duration of high $p(H_2)$ and $H_{ind.}$ also points to the possibility that replenishment of fermentable hydrocarbons in wet sand, around the cable, is slower than in liquids.

The addition of the second extra 160 gram dextrose to the wet sand phase produced approximately the same $p(H_2)$ max. value as the first extra addition. However, the $p(H_2)$ at a lower level (0.2 atm.) persists for an appreciably longer time. This may be explained by the fact that the total dextrose content of the wet sand environment, after the extra additions is 440g, while the dextrose content of the experiments in totally liquid culturing solutions was only 240g.

In order to compare the hydrogen production and the ensuing $H_{ind.}$ in environments where the active component was inoculated hydrogen-producing bacteria culturing solution, the $p(H_2)$ and $H_{ind.}$ data were plotted from three separate experiments (Fig. 6). These curves indicate that corrosion of the submarine cable armor wire is the primary contributor to the hydrogen-caused signal attenuation. In order to obtain semi-quantitative information about the hydrogen generation under various conditions we graphically integrated the areas under the $p(H_2)$ vs. time curves in Figure 6 and divided the obtained values with their individual exposure times. This calculation gave us average $p(H_2)$ values over the time of the experiments as follows.

Cable and exposure	Avg. $p(H_2)$ (atm.)
Submarine cable with galvanized steel armor wire	0.69
Submarine cable without armor wire	0.31
Buried cable	0.12*

* The test environment contained 83 percent more fermentable hydrocarbon than the submarine cable test environments.



Legend

1. $H_{ind.}$ of submarine cable, with galvanized steel armor wire, in hydrogen-producing bacteria culturing solution
2. $p(H_2)$ over the submarine cable, with galvanized steel armor wire, in hydrogen-producing bacteria culturing solution
3. $H_{ind.}$ of submarine cable, without armor wire, in hydrogen-producing bacteria culturing solution
4. $p(H_2)$ over the submarine cable, without armor wire, in hydrogen producing bacteria culturing solution
5. $H_{ind.}$ buried cable (no armor wire) in a mixture of fine sand and hydrogen-producing bacteria culturing solution
6. $p(H_2)$ over the buried cable, (no armor wire) in a mixture of fine sand and hydrogen-producing bacteria culturing solution

Figure 6. Hydrogen indicator ($H_{ind.}$) and partial pressure of hydrogen [$p(H_2)$] in the head space for submarine and direct buried optical fiber cables.

The experiments conducted in 3.5 percent (by weight) NaCl solution indicate that only very small areas, that is, the cut edge of the corrugated steel shield and the scratched areas of the green polymer film, are exposed to corrosion (Fig. 5). These results also suggest that the thin, green polymer film is not only an adhesive between the steel shield and the outer jacket, but is also a good corrosion barrier.

The following findings indicate very limited likelihood of hydrogen caused signal attenuation in direct buried optical fiber cables:

- The data from this study shows appreciably less bacterial hydrogen production in wet soil than in the environments simulating water crossings.
- Although, the hydrogen-producing bacteria were present at every water crossings where we collected bottom sediments in the vicinity

of the cables, the specimens without fermentable hydrocarbon additive produced only trace to 0.6 percent hydrogen.[16] Because such low level of hydrogen causes negligible $H_{ind.}$, and the soil around buried cables are even less likely to contain a continuous source of fermentable hydrocarbons, we can safely disregard microbiologically generated hydrogen as a threat to buried optical fiber cables.

- Hydrogen-producing bacteria do not thrive in oxidizing and well aerated soils.
- The corrosion of the steel shield at defects produces negligible hydrogen when compared to that of galvanized steel armor wires.
- The depth of the cables in buried plant cannot increase the overall pressure at the cable, unlike cables at deep water crossings, thus, the $p(H_2)$ cannot be more than 1 atm. as opposed to >8 atm. in deep waters.

Summary

Hydrogen-caused signal attenuation experiments were conducted in simulated buried plant environments. The experiments showed that bacterially fermented hydrogen formation, and the ensuing development of $H_{ind.}$ is limited both in magnitude and time of duration. Also, corrosion of the steel shield at outer jacket defect sites produced negligible hydrogen and H_{ind} after 307 days.

The results indicate that the buried optical fiber cable plant is unlikely to have significant hydrogen-caused signal attenuation problems. Consequently, we conclude that no additional generic requirements for buried optical fiber cables are needed in Bellcore Technical Reference(s).

References

1. S. R. Nagel, "Reliability Issues in Optical Fibers", in Reliability *Considerations in Fiber Optic Applications, D. K. Paul ed., Proc.* SPIE 717, 8 (1987)
2. B. Wiltshire and M. H. Reeve, J. Lightwave Technology, 6 (2), 179 (1988)
3. J. Stone, Lightwave Technology, LT-5 (5), 712 (1987)
4. K. W. Plessner and S. J. Standard-Powell, "Attenuation/Time Relation for OH^- Formation in Optical Fibers Exposed to H_2" Electr. Lett. 20 (6) p. 250-254 (1984)
5. S. R. Barnes, N. Pitt, and J. N. Russell, "The Effect of Hydrogen on Submarine Optical Cables", Electrical Communications *59 (4) 429* (1983)
6. D. L. Philen and C. H. Gartside III, "Prevention of Hydrogen Gas Induced Loss in Optical Fibers by Proper Lightguide Cable Design", Proceedings of the 33rd International Wire and Cable Symposium, p. 415 (1984)
7. K. Amano and Y. Iwamoto, "Optical Fiber Submarine Cable Systems", J. Lightwave Technology 8 (4) p. 595 (1990)
8. N. E. Hardwick, III, L. C. Hotchkiss, J. J. Blee, and D. L. Philen, "*Corrosion-Resistant Armor to Prevent* H_2-Induced Loss in Underwater (Wire-Armored) Fiber Optic Cable", Proceedings of the 38th International Wire and Cable Symposium, p. 689 (1989)
9. W. T. Anderson, A. J. Johnson, J. P. Kilmer, and R. M. Kanen, "Hydrogen Gas Effects on Installed Submarine Single-Mode Fiber Cables", Proceedings of the 37th International Wire and Cable Symposium, p. 188 (1988)
10. W. T. Anderson, A. J. Johnson, and A. DeVito, "Field Measurements of the Effect of Hydrogen Gas on Installed Submarine Single-Mode Fiber Cables", Proceedings of the 38th International Wire and Cable Symposium, p. *611 (1989)*
11. G. Schick, K. A. Tellefsen, A. J. Johnson, and C. J. Wieczorek, "Hydrogen Sources for Signal Attenuation in Optical Fibers", Optical Engineering 30 (6), 790-801 (1991)
12. G. Schick, K. A. Tellefsen, A. J. Johnson, C. J. Wieczorek, and R. M. Kanen, "Hydrogen Sources for Signal Attenuation in Submarine Optical Fiber Cables and the Effect of Cable Design", Proceedings of the 40th International Wire and Cable Symposium, p. 643-652 (1991)
13. I. Plitz and P. Warren, "Evaluation of Hydrogen Generation from Optical Fiber Cable", Proceedings of the 36th International Wire and Cable Symposium, p. 616 (1987)
14. S. Kukita, T. Nakai, A. Hayashi, and H. Koga, "Design and Performance of Nonmetallic Waterproof Optical Fiber Cable Using Water-Absorbent Polymer, "J. Lightwave Technology, 7 (4), 740 (1989)
15. G. Haynes and R. Baboian, "Conditions and Mechanisms for the Formation of Damaging Hydrogen in Fiber Optic Cable", Proceedings of the 39th International Wire and Cable Symposium, p. 255-260 (1990)
16. G. Schick and K. A. Tellefsen, "The Effect of Corrosion on Submarine Optical Fiber Cables" Paper #460, Corrosion/92, Nashville, TN, 4/27-5/1/92

AUTHORS



George Schick received a Dipl. Eng. degree in Electrochemistry and Electrometallurgy from the Ecole Nationale Superieure d'Electrochimie et d'Electrometallurgic de Grenoble, France in 1958, the MS degree in Metallurgy from Massachusetts Institute of Technology in 1961, and the Ph.D. in Metallurgy and Materials Science from New York University in 1972. He worked at Bell Telephone Laboratories from 1961 to 1983 in the area of corrosion. In 1984 he joined Bell Communications Research where he is working on corrosion control and on the effects of the environment on optical fibers. Dr. Schick is a member of the National Association of Corrosion Engineers and the American Society for Testing and Materials.



Karen A. Tellefsen received the B.S. degree in Chemistry from Stevens Institute of Technology in 1977 and the Ph.D. degree in Physical Chemistry from the University of Ottawa, Ontario in 1988. She worked for Energetics Science, Inc. between completing her B.S. degree and beginning her Ph.D. program, where she worked on the development of an electrochemical hydrazine vapor detector. She joined Bell Communications Research in 1988, where she is working on corrosion control and on the effects of the environment on optical fibers. Dr. Tellefsen is a member of the National Association of Corrosion Engineers, the American Society for Testing and Materials, the Electrochemical Society and the American Chemical Society.



Casey J. Wieczorek is a member of the Optical Cable Group in Bellcore, Morristown, NJ. He joined Western Electric in 1967 and worked on various cable designs and manufacturing processes. He is currently responsible for the development of generic requirements and test procedures for optical cables. He holds a B.S. degree in Mechanical Engineering from Fairleigh Dickinson University and did graduate work at Stevens Institute of Technology.



Robert M. Kanen Came to work for Bell Communications Research in 1986. He attended Champlain College and Worcester Polytechnic Institute. During the twenty years before working at Bellcore, he was employed by ITT-Federal Electric, HRB-Singer, Singer Co., R.H. Wagner Co., as well as four years of Naval Electronics.



Aaron J. Johnson received the B.S. degree in Electrical Engineering and Economics from Carnegie-Mellon University in 1980 and the M.S. degree in Electrical Engineering from Georgia Institute of Technology in 1981. He worked for IIT Research Institute from 1982 to 1984, where he was engaged in electromagnetic compatibility analysis. Since 1984, he has been with Bell Communications Research where he has been developing novel optical fiber measurements and writing generic requirements for optical fibers and optical fiber cables. Mr. Johnson is a member of the Optical Society of America.

ANALYSIS OF FIBER OPTIC CABLE DESIGN CONDITIONS IN VICINITY OF STEAM LINES - RUPTURED AND PRISTINE

Nathan E. Hardwick, III and Kris Kathiresan

AT&T Bell Laboratories, Norcross, Georgia 30071

J. G. Hartley

School of Mechanical Engineering, Georgia Institute of Technology, Atlanta, Georgia 30332

ABSTRACT

Fiber optic cables installed in close proximity to steam lines are vulnerable to serious damage. If the high pressure, high temperature steam emanating from a steam pipe rupture impinges directly on a standard fiber optic cable, the jacket will either degrade or melt. Also, standard cables that are in the vicinity of pristine steam lines can be damaged by (1) secondary steam generated when water covers the hot steam pipes as well as (2) normal heat transfer modes. Understanding the thermodynamic conditions of the harsh steam environments is important in optimizing the design of a steam-resistant cable. Thermodynamic and fluid flow analyses provide temperature and velocity profiles for steam pipe rupture of different diameters. The rates of decrease for steam jet centerline and fanout temperatures are shown to be much more pronounced for smaller rupture diameters while the jet velocities remain substantial for significant distances from the rupture. Implications for bracketing design limits are that cables designed to withstand a temperature of 140°C (284°F) should survive even a direct steam jet from ruptures as large as 2.5 cm (1 in.) in the highest pressure steam lines.

In cases where steam-resistant cables are not used, the steam effects mechanisms are identified and methods for alleviating their impact discussed.

INTRODUCTION

As the evolution of optical fiber transmission systems continues to saturate the communications networks, an increasing number of hostile environment applications are being encountered. Understanding such environments and characterization of the corresponding physical conditions are extremely important in optical fiber cable design. One of the most demanding environments frequently encountered in large cities is the high temperature, high humidity conditions that may exist when optical fiber cables are installed in close proximity to steam pipes. Telecommunication cables are now being designed to withstand steam-related conditions because of the extensive repair expense that has been incurred in large cities for a number of years. Also, with today's high capacity fiber optic media, even a single transmission failure is considered too many in the telecommunications industries. Despite these considerations, no published work exists that analyzes the steam jet exiting a pipe rupture or brackets the worst case design conditions. This work was undertaken to provide these inputs which are necessary for an appropriate design and development of a steam-resistant fiber optic cable. Another goal was to provide insights for avoiding or alleviating telecommunication cable steam problems.

This paper is divided into four sections. In the first two sections, the steam line damage potential is summarized and the most common steam problem mechanisms are identified. The third section presents a quantitative analysis that reveals the conditions that cables can encounter when they are close to a steam pipe rupture or leak. This third section is extremely important because; (1) it provides the first reported analysis that addresses this problem and (2) the resulting temperature and velocity profiles define the design limits that a steam-resistant fiber optic cable must be capable of withstanding. The fourth section provides basic strategies for alleviating the steam problem areas along with discussions of some potential pitfalls.

1.0 ENVIRONMENT IN PROXIMITY OF STEAM LINE

As indicated above, the most prevalent hostile environment occurs when optical fiber cables are installed below street level near steam lines where they are vulnerable to damage or even failure when the steam lines rupture or crack. High pressure, high temperature steam released from the steam pipe could impinge directly on the cable and either melt the outer jacket or degrade the cable because of long-term exposure. Because typical steam line operating pressures and temperatures are set at 2.8 MPa (400 psig) and 245°C (473°F) for high pressure lines as well as 1.4 MPa (200 psig) and 212°C (413°F) for low pressure lines, the maximum temperature to be expected outside a rupture can be as high as 171°C (340°F). This extreme environment is too harsh for general purpose cables that have economical designs. Thus, the temperature and velocity profiles outside the steam pipe rupture must also be known to accurately bracket the worst case design limits.

Even when steam lines are in pristine condition (i.e., being in a state of not leaking steam), the extremely hot lines can significantly elevate the temperatures of nearby fiber optic cables by traditional heat transfer modes. Of course, the temperature levels that the cables can attain depend upon the spatial separation and characteristics of the surrounding media as will be discussed in the next section.

2.0 TELECOMMUNICATION CABLES STEAM DAMAGE REGIMES

In designing a special telecommunication cable for potential steam damage environments as well as installing a standard cable in such a manner as to alleviate detrimental steam-induced conditions, three distinct steam effects regimes must be understood and addressed. These steam effects regimes for telecommunication cables are identified by the mechanisms of thermal interactions causing the damage and will be referred to as the Thermal Vicinity Damage Regime, the Steam Condensation Damage Regime, and the Steam Jet Impingement Damage Regime. The steam damage regimes will be explained in the following three subsections.

2.1 Thermal Vicinity Damage Regime

The first and probably most prevalent steam line damage mechanism occurs when telecommunication cables reside in the close vicinity of pristine steam lines. In this case, the cables are affected by the large thermal energy transfer from the steam line to the telecommunication cables. This thermal energy transfer can be either by conduction through the soil (or other intervening media), radiation, or natural convection as well as any combination of these heat transfer modes. In this regime, the most widespread problem occurrences are caused by "clean" heat transfer from the steam line resulting in a large temperature rise in nearby telecommunication cables. The temperature increase is generally caused by either (1) conduction through moist soil between the cable and steam line or (2) radiation and convection heat transfer via air at severe conflict areas in shared manholes.

2.2 Steam Condensation Damage Regime

The Steam Condensation Damage Regime is the second most prevalent steam effects regime. It accounts for the majority of the severe cable damage when the telecommunication cables and the steam lines are not extremely close to each other. The Steam Condensation Damage Regime can be initiated by two steam line occurrences that are similar in effect but wholly different in cause as will be discussed below.

The most dominant Steam Condensation Damage Regime occurrence results from secondary steam generated when the water table rises and covers the hot steam pipes. The high temperature pipes, in turn, boil the water creating the secondary steam which then condenses on the telecommunication cables. The change of phase process causes large amounts of thermal energy (the latent heat of condensation of the vapor) to be transferred to the cable at 100°C (212°F). (Usually the water table rises in urban steam areas because of low lying locations and/or tidal conditions in coastal cities.)

A smaller percentage of steam condensation problems results from direct escape from the steam lines because of leaks and ruptures in the pipe walls. Steam generated by either of these means can affect cables significantly far away from the steam lines because of the ability of steam to travel through devices or underground openings leading to the cables.

2.3 Steam Jet Impingement Damage Regime

The third steam line damage mechanism is the most severe but is less prevalent than the first two regimes discussed. This damage mechanism occurs when steam jets emanating from leaks and ruptures of steam lines impinge directly upon the telecommunication cables. Although this source of damage does not occur as often, when it does occur standard fiber optic cables are usually damaged to an extent that service is or will be interrupted. Understanding the steam jet impingement conditions is very important because they determine the design limits for steam-resistant cable.

3.0 FIBER OPTIC CABLE DESIGN CONDITIONS NEAR STEAM LINE RUPTURES

To bracket the design limits, analyses of the steam temperature and velocity distributions in the vicinity of a steam pipe rupture were completed. This study led to an understanding of the gas flow dynamics in the vicinity of a steam pipe break as well as the exposure risks for cables installed near steam ducts.

3.1 Theoretical Characterization of Steam Pipe Leak

The flow of steam through a hole or crack in a steam pipe is likely to be similar to that of the flow through a converging nozzle. Because the steam pressure is much higher than the surrounding atmospheric pressure, the steam cannot expand completely to the atmospheric pressure before it exits the crack or hole. Instead, the flow is choked and the steam pressure is still very high immediately outside the opening. These conditions create a highly underexpanded jet[1,2] such as the one depicted in Figure 1. The initial velocity of this steam jet is extremely high, and shock waves develop and persist downstream of the opening until the pressure of the flow finally approaches atmospheric pressure. At that point, the flow of the steam should be similar to that of a free turbulent jet,[2] illustrated in Figure 2, whose diameter increases as the stagnant air is entrained in the flow until the jet dissipates. In these figures, the absolute pressure in the steam line is P_o, the atmospheric pressure is P_∞, and the pressure at the exit of the nozzle is P_e.

To further explain the decay of subsonic jets issuing into a quiescent medium (represented by Figure 2), the subsonic jet is characterized by a potential core surrounded by a region in which mixing between jet and ambient fluid takes place. At a length downstream equal to z_c (c refers to core), the mixing region has spread inward enough to reach the centerline, and the core no longer exists. Further downstream from this point, the mixing region continues to spread as the velocity decays at a rate required to conserve axial momentum.

For sonic exit pressure ratios, $P_e/P_\infty > 2$, the form of the shock structure in the initial shock cells are extremely severe. For a high degree of under-expansion, such as our expected P_e/P_∞ = 14.9, the subsonic core region is quickly accelerated and becomes supersonic once again near the beginning of the second cell. For these very high pressure ratios, the structure downstream of the first cell is dominated for a great distance

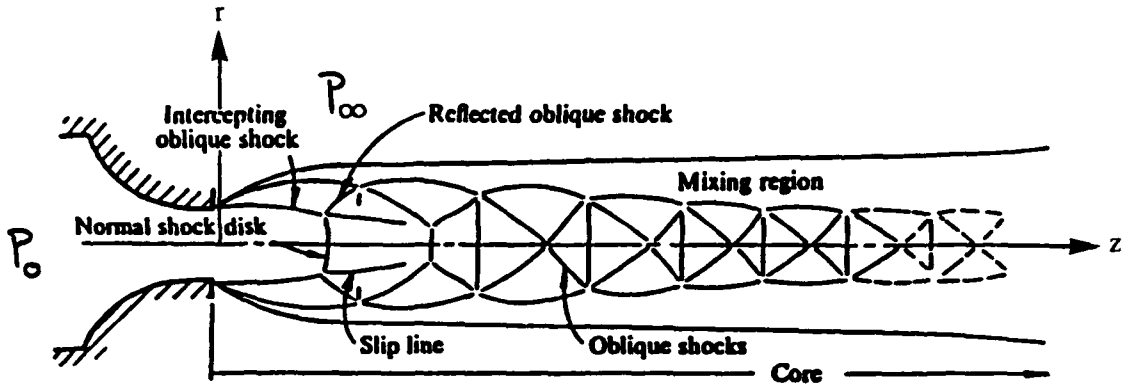


Figure 1. Highly Underexpanded Jet. (From Reference [1].)

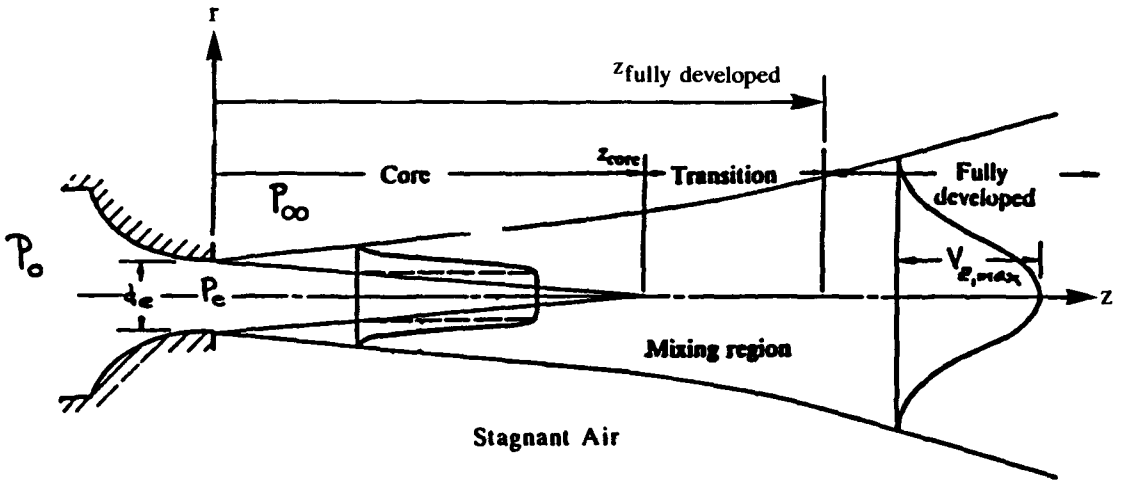


Figure 2. Development of a Fully Developed, Free Turbulent Jet. (From Reference [1].)

by the very strong normal shock in the first cell, and no other normal shocks are present. The flow then decays through a structure of oblique shocks as shown in Figure 1. The mixing region surrounds the core as discussed earlier, but its radial diffusion is small, with the result that the core of the highly underexpanded jet can be extremely long.[1]

3.2 Thermodynamic Analysis of Steam Jet

Based on nozzle flow measurements, Donaldson and Snedeker[1] suggest that the distance required for the pressure of a highly underexpanded jet to approach atmospheric pressure is more than 40 times the exit diameter. Thereafter, the jet should behave as a free turbulent jet.[1,2] The equations that describe the behavior of the free turbulent jet have the same form as the boundary layer equations for incompressible flow.[3] Although the flow of the steam is not incompressible, the results presented by Donaldson and Snedeker[1] confirm that even the highly underexpanded jet exhibits the characteristics of an incompressible, free turbulent jet after the jet reaches a pressure that is nearly atmospheric. Thus the appropriate equations consist of the continuity equation (see Appendix for Nomenclature),

$$\frac{\partial V_z}{\partial z} + \frac{1}{r}\frac{\partial (rV_r)}{\partial r} = 0 \ , \qquad (1)$$

the z-momentum equation,

$$V_z \frac{\partial V_z}{\partial z} + V_r \frac{\partial V_z}{\partial r} = \nu \left[\frac{1}{r}\frac{\partial}{\partial r}\left[r\frac{\partial V_z}{\partial r}\right]\right] \ , \qquad (2)$$

and the energy equation,

$$V_z \frac{\partial h}{\partial z} + V_r \frac{\partial h}{\partial r} = \frac{k}{\rho}\left[\frac{1}{r}\frac{\partial}{\partial r}\left[r\frac{\partial T}{\partial r}\right]\right] \ . \qquad (3)$$

If we integrate the z-momentum equation over the area normal to the z axis, from r = 0 to r = ∞, then

$$\frac{\partial}{\partial z}\int_0^\infty V_z^2\, 2\pi r dr = 0 \ . \qquad (4)$$

Thus, the axial momentum of the free jet is independent of z or

$$\int_0^\infty V_z^2\, 2\pi r dr = \text{Constant} = \frac{\pi d_e^2 V_c^2}{4} \qquad (5)$$

where the constant has been determined by noting that the axial momentum of the free turbulent jet would originate from steam flowing from the nozzle exit at velocity, V_c, if the flow were incompressible. A similar integration of the energy equation reveals that the "energy flow rate" in the axial direction is also independent of z, i.e.,

$$\int_0^\infty V_z h_z\, 2\pi r dr = \text{Constant} = \frac{\pi d_e^2 V_c h_c}{4} \quad . \qquad (6)$$

The free turbulent jet has a velocity profile that is "similar" and is described with a Gaussian curve,[4]

$$\frac{V_z}{V_{z,max}} = \exp\left[-\frac{r^2}{C^2 z^2}\right] \qquad (7)$$

and an envelope of the radius, r_5, at which the velocity decreases to one-half of the maximum centerline velocity, described by $r_5/z = \tan\alpha$. Because a characteristic of axisymmetric free turbulent jets is that the angle α is 5°, the constant C can be determined and an expression for $V_{z,max}$ found by substituting V_z from Equation (7) into Equation (5) and integrating. After noting from Reference [1] that $V_{z,max}$ is equal to the actual exit velocity of the steam at $z/d_e = 23$, the resulting expression reduces to

$$\frac{V_{z,max}}{V_e} = \frac{23}{(z/d_e)} \quad . \qquad (8)$$

3.3 Steam Jet Temperature Profiles

Although no previous work exists for the temperature profiles of a free turbulent jet, Schlichting[5] states that the profile is also "similar" and can be expressed with a Gaussian curve. Assuming that the steam and the air of the free turbulent jet are in local thermodynamic equilibrium and are perfectly mixed where the enthalpy, h_z, is an approximate average value for the mixture of steam and air,

$$\frac{h_z}{h_{max}} = \exp\left[-\frac{r^2}{b^2 z^2}\right] \quad . \qquad (9)$$

An expression for $h_{z,max}$ can be determined by substituting h_z from Equation (9) into Equation (6), performing the integration, and determining the constants using the same arguments as above. Thus,

$$\frac{h_{z,max}}{h_e} = \frac{23}{(z/d_e)} \quad . \qquad (10)$$

Even though the axial momentum remains constant as the jet radius increases because only initially stagnant fluid is entrained in the jet, the mass flow rate, $\dot{m}_z$, in the jet increases as z increases and the jet expands. The mass flow rate in the z direction, $\dot{m}_z$, is evaluated as

$$\dot{m}_z = \int_0^\infty \rho\, V_z 2\pi r dr = \rho\, V_{z,max} \pi C^2 z^2 \quad . \qquad (11)$$

The average enthalpy of the mixture is defined as

$$h_z = \frac{\dot{m}_s h_s + \dot{m}_a h_a}{\dot{m}_z} \qquad (12)$$

where $\dot{m}_z = \dot{m}_s + \dot{m}_a$ and the subscripts s and a denote steam and air, respectively. Assuming that each component of the mixture behaves as an ideal gas, the jet centerline temperature is obtained from

$$\frac{T_{z,max} - T_\infty}{T_e - T_\infty} = \left[\frac{c_{ps}}{c_{pa} + \dfrac{11.5(c_{ps} - c_{pa})}{(z/d_e)}}\right] \frac{23}{(z/d_e)} \qquad (13)$$

where c_p denotes the specific heat at constant pressure. Finally, the temperature $T_z = T_z(r)$ at any radial or axial position can be determined from

$$\frac{T_z - T_\infty}{T_e - T_\infty} = \exp\left[-\frac{r^2}{C^2 z^2}\right]\left[\frac{T_{z,max} - T_\infty}{T_e - T_\infty}\right] \qquad (14)$$

where the term in the second bracket is given by Equation (13).

3.4 Quantitative Implications of Steam Leak Profiles

Using the above expressions and assuming a typical steam pipe with a pressure of 2.8 MPa (400 psig) the temperature drop in the vicinity of the steam pipe is approximately as shown in Figure 3 for various sizes of pipe ruptures. The dashed portions of each curve represent an extrapolation because the theoretical model only provides analytical results for the nozzle exit and for distances greater than 40 diameters away from the nozzle where the flow becomes a fully developed free turbulent jet. As expected, the rate of temperature decrease with distance is much greater for smaller size ruptures. For example, with a 0.3 cm (1/8 in.) rupture diameter, the temperature decreases from 171°C (341°F) at the exit to 102°C (215°F) in only 22.2 cm (8-3/4 in.) while the temperature for a rupture with a diameter of 5 cm (2 in.) does not drop to this level until 356 cm (140 in.) away from the steam pipe. One mechanism causing the differences is that the larger jet has to entrain a larger amount of the cooler ambient air before the centerline velocity becomes equally diminished because of the larger cross-sectional area of the jet. Also, the larger rupture hole inherently creates a longer length of shock waves to unravel the underexpanded jet conditions prior to the development of the free turbulent jet regime.

The temperature profiles fanning away from the steam jet centerlines are presented because the likelihood of a direct alignment of a rupture with a cable is remote. The

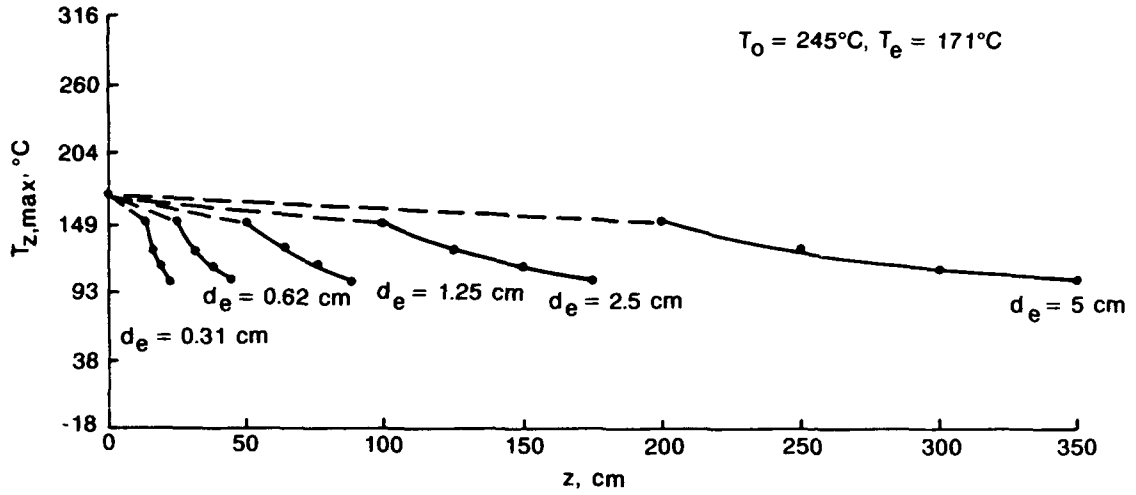


Figure 3. Maximum (Centerline) Temperature of Steam Jet, $T_{z,max}$, versus Distance, z, from Steam Pipe Ruptures of Various Sizes.

temperature profiles for the steam jet cross-section emanating from a 0.6 cm (1/4 in.) and a 5 cm (2 in.) diameter steam pipe hole are shown in Figures 4 and 5 for typical high pressure steam line conditions.

Temperatures are provided for two flow envelopes in addition to the maximum centerline temperatures. The outside envelope represents temperatures where the entraining air has reduced the velocity to 0.1 that of the centerline velocity and the intermediate envelope represents temperatures where the entraining air has reduced the velocity to 0.5 of the centerline velocity. The curves reveal that the temperatures drop off significantly at radii away from the centerline while the centerline temperatures do not decrease much until the fully developed flow regime begins. These temperature profiles also indicate that the fanout angle is relatively small, so extremely severe temperatures would not be experienced unless a cable sustains almost a direct hit.

The maximum centerline velocities of jets from steam pipe ruptures that match the centerline temperatures are shown in Figure 6. Note that the primary velocity plots do not appear to begin at the exit velocity. This graphical license is taken for visual clarity because the flow velocity in the initial portion of each curve fluctuates wildly as shock waves form in the highly underexpanded region immediately following the exit. The insert to Figure 6 gives an example of these fluctuations that represent the initial portion of the top plot for a 5 cm (2 in.) pipe rupture. Velocity fluctuations for the smaller diameter ruptures are similar but would occur over a correspondingly shorter distance. The profiles indicate that the centerline velocities remain substantial for relatively large distances away from a steam pipe rupture.

4.0 METHODS OF ALLEVIATING DETRIMENTAL EFFECTS OF STEAM ON FIBER OPTIC CABLE

Methods for alleviating or preventing the detrimental effects caused by steam lines in the vicinity of fiber optic cables are discussed in the following three subsections. Guidelines are provided for initial installation procedures, retrofitting protection methods, and replacement options.

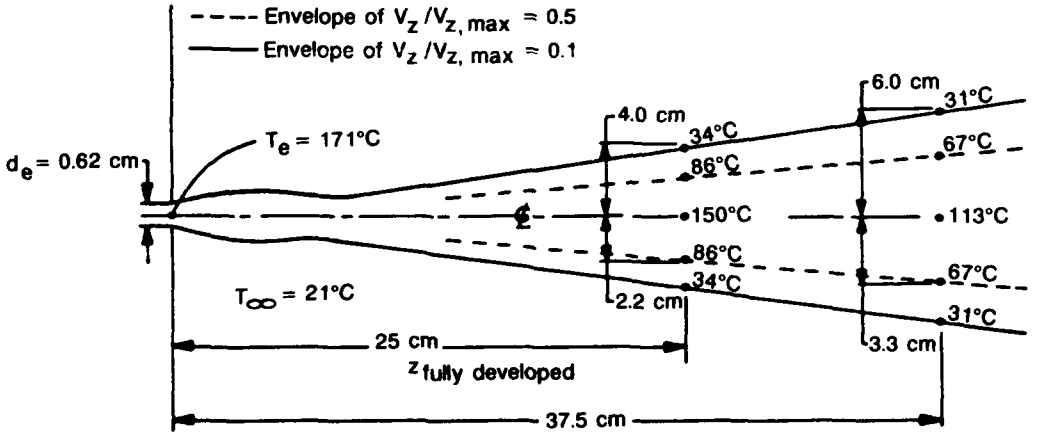


Figure 4. Temperature Profile of Fluid Jet Cross Section Emanating from 0.62 cm Diameter Steam Pipe Rupture [245°C (473°F) and 2.8 MPa (400 psig)Inside Temperature and Pressure].

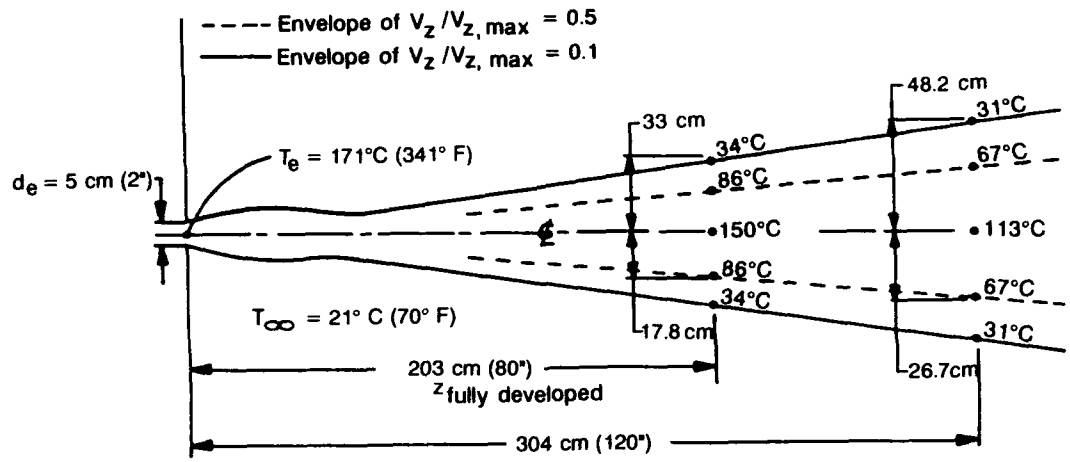


Figure 5. Temperature Profile of Fluid Jet Cross Section Emanating from 5 cm (2") Diameter Steam Pipe Rupture [245°C (473°F) and 2.8 MPa (400 psig) Inside Temperature and Pressure].

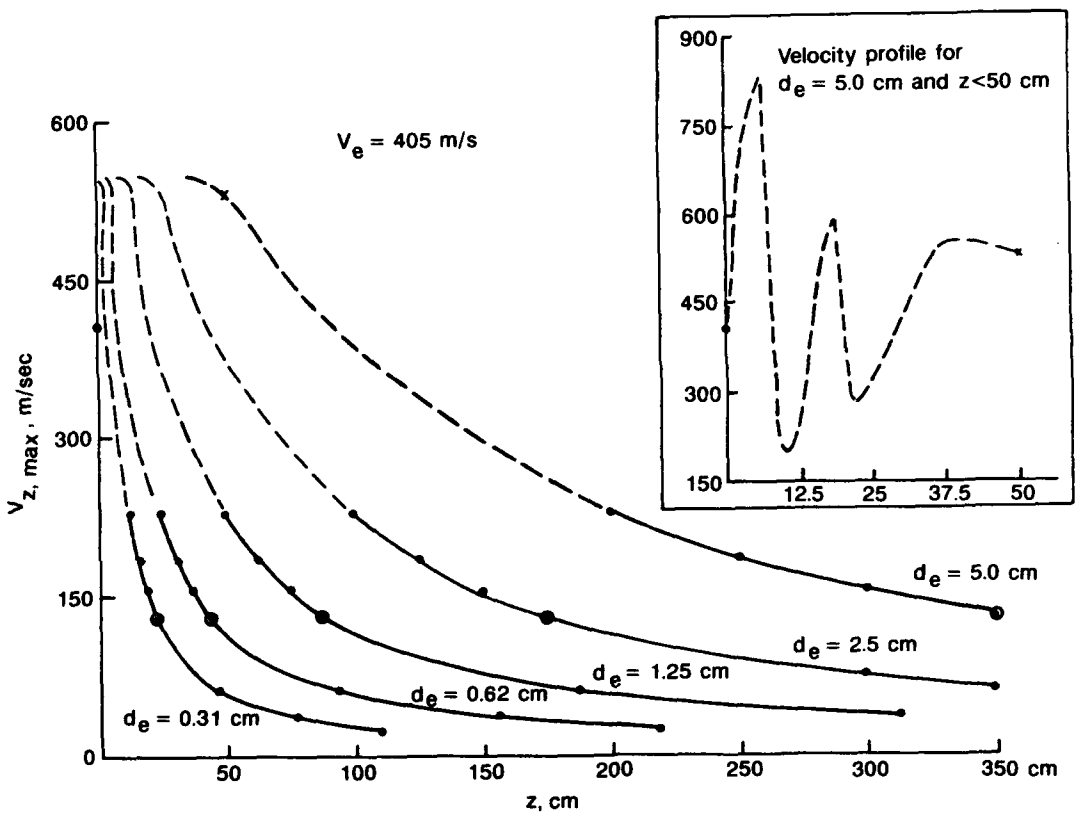


Figure 6. Maximum (Centerline) Velocity of Steam Jet, $V_{z,max}$, versus Distance, z, from Steam Pipe Ruptures of Various Sizes. (Insert Shows Typical Velocity Fluctuations Caused by Shock Waves in Underexpanded Jet from Reference [1].)

4.1 Use of Steam-Resistant Cable

The easiest and probably surest method of protecting a fiber optic cable in the vicinity of a steam pipe is to use a steam-resistant cable that will withstand the harsh steam conditions (see, for example, Reference [6]). Using a sheath that is sufficiently robust to withstand the absolute worst conditions imaginable would not be economically feasible, however. Even designing a fiber optic cable that is capable of withstanding the worst conditions encountered in a high percentage of the conflict areas could result in a significant sheath cost premium. For this reason, an analysis of the expected thermodynamic conditions as presented in Section 3.0 is essential to any steam-resistant cable design to ensure that the costly high temperature materials are optimized for cost/value performance.

4.2 Initial Installation Suggestions

The thermal energy potential in a foot of steam duct is alarming. The basic rule for protecting standard fiber optic cables from these potent steam lines for generating thermal energy is straightforward although difficult to achieve in some real world situations.

The basic design objectives should be as follows: (1) Increase the thermal resistance to heat transfer between the high-energy steam line and the fiber optic cable to a maximum. (2) Concurrently, the thermal resistance between the cable and a heat sink (e.g., cool environment) should be made as small as possible so the cable temperature does not rise significantly higher than the environment temperature. (See electrothermal analog in Figure 7.)

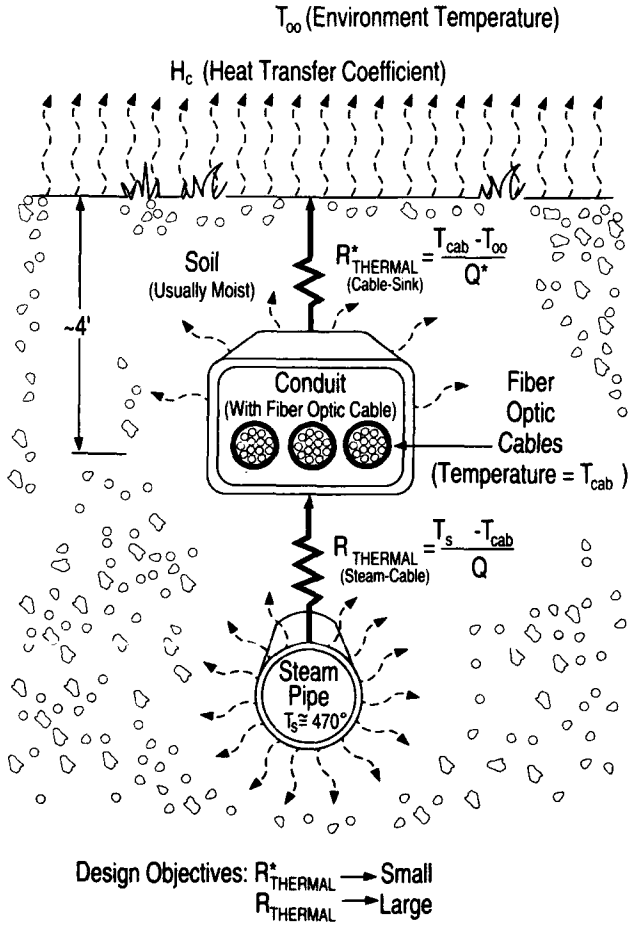


Figure 7. Electro-Thermal Analog Representing Thermal Paths for Heat Flow, Q, from Steam Line to Telecommunication Cable and Q* from Cable to the Environment.

For initial designs, the obvious best way of achieving these objectives is to put as much distance between the steam line and the fiber optic cable as possible while locating the cable as close to a cooler environment as practical. (This generally means putting the cables closer to the ground surface and above the steam lines.) An important caveat to this approach is to avoid a condition that commonly occurs in which primary or secondary steam becomes trapped underneath city streets. This steam can travel horizontally and vertically through crevices in the soil, surround the cable, condense on the cable, and impart thermal energy to the cable. A sketch illustrating this scenario is shown in Figure 8. Note that the trapped steam violates the second design objective of providing a low thermal resistance path from the fiber optic cable to a cooler environment.

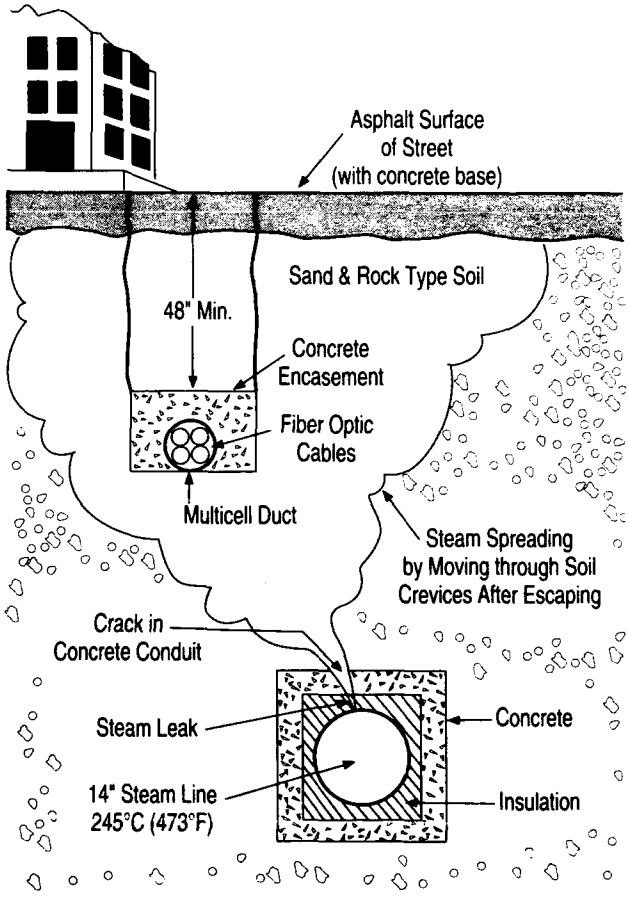


Figure 8. Typical Steam Leak Entrapment Conditions Underneath City Streets.

In situations where the likelihood of steam being trapped around the fiber optic cable is recognized initially, the lower thermal resistance path for the cable may not be toward the street. On the other hand, installing grates above the cable to vent the trapped steam may be possible in these cases.

Constructing a special housing to protect cables from steam damage in extreme conflict areas that incorporate the design objectives of Figure 7 is possible. These protective housing designs have been documented but are usually more expensive than using a steam-resistant sheath as discussed in the previous section.

4.3 Restoration Guidelines for Existing Plant Problems

Existing fiber optic cable in steam conflict areas can only be protected after repair by either (1) using costly special insulated duct construction or ground vents that achieve the thermal resistance objectives of Figure 7, (2) retrofitting a steam-resistant cable, (3) installing special barriers to block the steam access and/or reduce heat transfer to the cable, or (4) convincing the utility company to repair and monitor the problem steam line.

One of the most frequent steam damage problems that occurs in existing plant leads to the conditions shown in Figure 8 and discussed in the last subsection. The problem source is a leaking steam line near the fiber optic cables that is not costing the utility company enough to justify the repair expenses. In a number of these cases, local engineering firms have advised the telecommunication companies to replace the damaged cables and insulate them for protection. Typically this "so-called" fix results in the city streets having to be reexcavated immediately afterwards. The reason for the problem recurrence is that having the cables heavily insulated is useless because the entire cable interior will eventually reach the surrounding steam temperature. The simplest actual solution (other than a steam cable retrofit) is to insert a barrier that blocks the flow of leaking steam from reaching the cable.

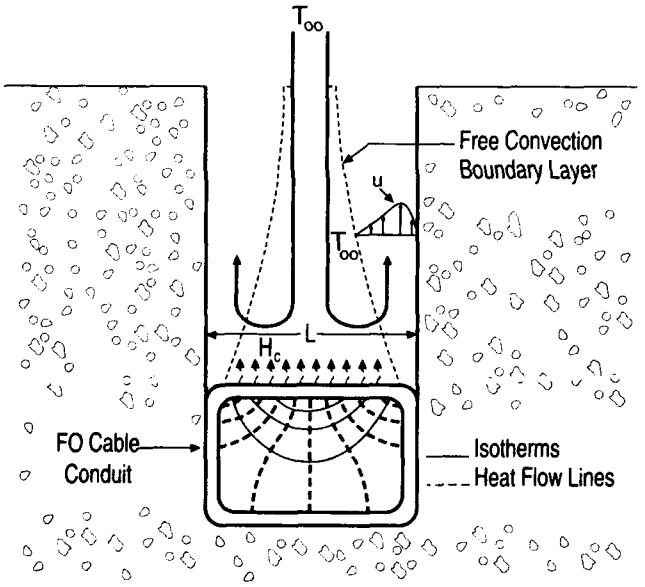


Figure 9. Approximate Temperature Gradient for Natural Convection Cooling of a Heated Conduit Surface with an Open Cavity Above it.

Another temporary solution to many steam problems in existing plant is to use ground vents with a chimney to permit enhanced natural convection cooling. Figure 9 shows a vertical cavity opening immediately above the surface of a heated cable. Note the heat dissipation capability is reduced because the rising boundary layers in the cavity will interfere with each other. Also, with the simple excavation shown, the sides and bottom of the cable or conduit would still be exposed to the moist soil at elevated temperatures. A fourfold increase in the thermal energy removal capacity can be achieved by providing an air space completely around the cable or conduit. This configuration, shown in Figure 10, isolates the conduit from the hotter earth that is in close thermal communication with the heat source and also sweeps away portions of the convective and conductive thermal paths before the conduit becomes overheated. The chimney addition shown further enhances the gravity flow capacity by an amount proportional to the square root of chimney height.

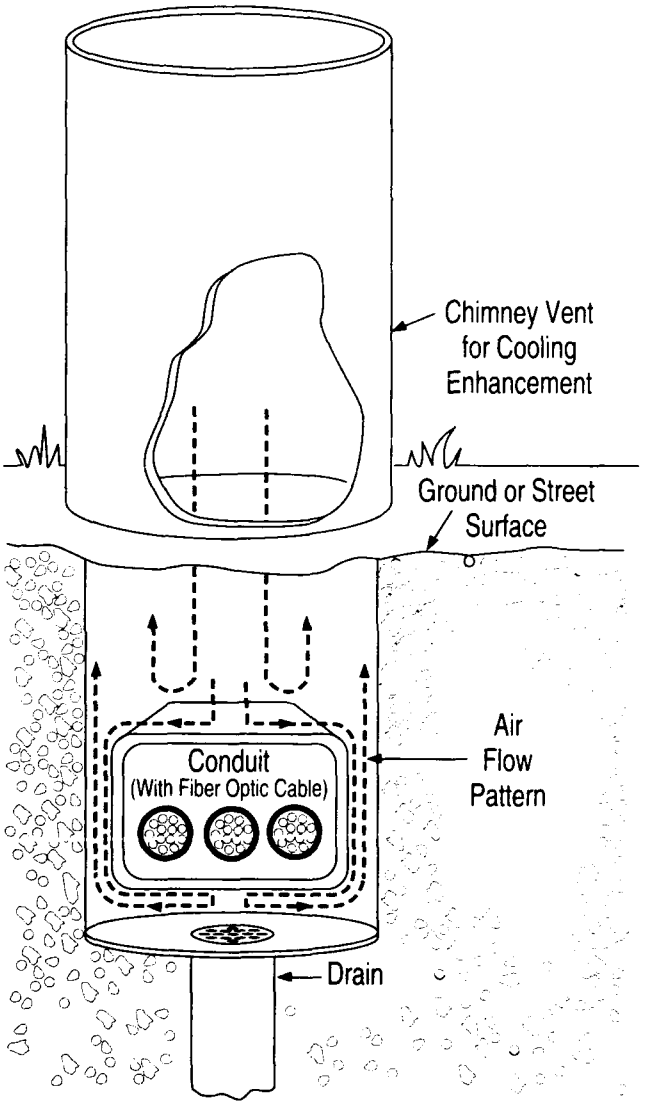


Figure 10. Vertical Cavity Vent with Air Spacing Around Periphery of the Conduit and Chimney Vent for Further Cooling Enhancement.

Both types of ground vent discussed above are efficient if positioned directly over a discrete high temperature hot spot. However, only the cavity constructed with air spacings around the periphery of the conduit possesses sufficient heat dissipation potential to permit intermittent skipping of high temperature conduit lengths which is usually imperative for economical venting.

CONCLUSIONS

As optical fiber telecommunications continues to spread, the need for defining and having solutions for hostile environment conditions grows in importance. Quantitative results are provided that bracket the conditions for one of the most frequently encountered and most severe hostile environments (i.e., high pressure steam).

The temperature and velocity profiles that would emanate from a high pressure steam pipe rupture were generated and presented graphically. The temperature profiles reveal that temperatures up to 71°C (133°F) greater than the atmospheric pressure vaporization temperature, 100°C (212°F), could theoretically be encountered when cables are intersected by steam jets exiting from a steam line rupture. As expected, the rate of temperature decrease with distance was found to be much greater and the fanout of high temperature much less for smaller size ruptures. Although the steep dropoff in temperatures as the steam jets fan out from the centerline indicates that the damage to optical fiber cables offset by approximately a meter is minimized if the cable can withstand moist 100°C (212°F) temperatures for long lengths of time, this is only part of the story. The advantage of this steep transverse offset temperature drop is countered by the slow centerline temperature decrease. For example, for a 5 cm (2 in.) diameter rupture the centerline temperature drops to only 113°C (236°F) at a distance of 3.04 meters (10 feet). Also, temperatures significantly above 100°C (212°F) can be incurred in cables located within several meters of even pristine steam lines due to pure radiation and conduction heat transfer. Based on this study, cables with sheaths designed for temperatures of 140°C (284°F) should survive almost all conceivable pure heat transfer interactions and even a direct steam jet from up to a 2.5 cm (1 in.) hole in the highest pressure steam line if not extremely close to the rupture.

The most common steam damage regimes for telecommunication cables were also identified and methods for alleviating the steam effects discussed. If a steam-resistant cable is not used, the design objectives for steam environments are to maximize the thermal resistance to heat transfer between the steam line and the cable and minimize the thermal resistance between the cable and a heat sink.

ACKNOWLEDGEMENTS

The authors would like to acknowledge M. R. Santana and K. W. Jackson of AT&T Bell Laboratories for their helpful discussions and suggestions throughout this project.

REFERENCES

1. Donaldson, C. duP. and Snedecker, R. S., "A Study of Free Jet Impingement, Part 1. Mean Properties of Free and Impinging Jets," *J. Fluid Mechanics*, Vol. 45, 1971, pp. 281-319.
2. Ardon, K. H., Baum, M. R. and Lee, M. H., "On the Evaluation of Dynamic Energies Arising in a Water Reactor Loss-of-Coolant Accident," *J. Br. Nucl. Energy Soc.*, Vol. 16, No. 1, 1977, pp. 81-96.
3. Bejan, A., *Convection Heat Transfer*, John Wiley & Sons, York, 1984.
4. Daily, J. W. and Harleman, D. R. F., *Fluid Dynamics*, Addison-Wesley, Reading, MA, 1966.
5. Schlichting, H., *Boundary Layer Theory*, McGraw-Hill, New York, 1978.
6. Kathiresan, K., et al, "A Fiber Optic Cable for Hostile Environments Such as Steam, Petroleum, and High Temperature," *Proceedings of the 41th International Wire and Cable Symposium*, Reno, Nevada, November 16-19, 1992.

APPENDIX

Nomenclature

c_p	Specific Heat at Constant Pressure
d_e	Diameter at Nozzle Exit
H_C	Surface Heat Transfer Coefficient
h_e	Enthalpy per Unit Mass (at nozzle exit)
h_z	Enthalpy at Location z
k	Thermal Conductivity
$\dot{m}$	Mass Flow Rate
$\dot{m}_s$	Mass Flow Rate of Steam in the Jet
P	Pressure
Q	Heat Flow
R	Thermal Resistance to Heat Flow Between Steam Line and Telecommunication Cable
R*	Thermal Resistance to Heat Flow Between Telecommunication Cable and a Cooler Environment
r	Magnitude of Radius
T	Temperature
T_{cab}	Telecommunication Cable Temperature
T_s	Steam Pipe Temperature
u	Velocity Due to Bouyancy Forces
V	Velocity
$V_{z,max}$	Velocity at Jet Centerline at Location z
Z_c	Apparent Core Length

Greek Symbols

γ	Ratio of Specific Heats
ρ	Mass Density
ν	Kinematic Viscosity

Subscripts

a	Air
c	Core Location
e	Nozzle Exit
o	Stagnation State
r	Radial Direction
s	Steam
∞	Ambient Conditions
z	z-Direction
z,max	Maximum Condition at Jet Centerline for Location z



NATHAN E. HARDWICK, III
AT&T Bell Laboratories
Norcross, Georgia 30071

Nathan E. Hardwick, III is a Distinguished Member of Technical Staff in the Fiber Optic Cable and Materials Development and Engineering Department at AT&T Bell Laboratories, Norcross, Georgia. He has received B.S. and M.S. Degrees in Mechanical Engineering from the University of South Carolina and a Ph.D. in Mechanical Engineering from Lehigh University. After joining Bell Laboratories in 1965, Dr. Hardwick initially designed and thermally characterized integrated circuit packages. Later work included responsibility for the design and the initial installation of the outside plant hardware system for FT3 lightguide cable, SM multifiber splice design, and splice mechanisms analyses. In his current assignment, he is responsible for the design and development of outside plant and underwater fiber optic cables. Dr. Hardwick spent one year as a Bell Laboratories Visiting Professor at N.C. A&T State University.



JAMES G. HARTLEY
Georgia Institute of Technology
Atlanta, Georgia

James G. Hartley is Professor of Mechanical Engineering in the George W. Woodruff School of Mechanical Engineering at the Georgia Institute of Technology in Atlanta, Georgia. He earned B.S. and M.S. Degrees in Mechanical Engineering from Louisiana Tech University and a Ph.D. in Mechanical Engineering from Georgia Tech. Dr. Hartley developed methods for analyzing and characterizing the thermal stability of underground power cables and worked extensively in combined heat and moisture transfer in unsaturated porous media. His current research interests include high heat flux heat transfer, heat transfer in composite media, and thermal systems. He is a member of the the American Society of Mechanical Engineers and has received the 1986 ASEE Meriam/Wiley Distinguished Author Award, the 1990 AT&T Foundation Award for Excellence in Instruction of Engineering Students, and the 1992 Georgia Tech Outstanding Teacher Award.



KRIS KATHIRESAN
AT&T Bell Laboratories
Norcross, Georgia 30071

Kris Kathiresan is a Distinguished Member of Technical Staff in the Fiber Optic Cable and Materials Development and Engineering Department at AT&T Bell Laboratories in Norcross, Georgia. He is responsible for the design and development of outside plant fiber-optic cables. Prior to his current assignment, he was responsible for the design and development of military and specialty fiber-optic cables. Dr. Kathiresan joined AT&T Bell Laboratories in 1985. He has a B.E. Hons in Mechanical Engineering from University of Madras, India, and M.E. in Aerospace Engineering from Indian Institute of Science, India, and a Ph.D. in Engineering Science and Mechanics from Georgia Institute of Technology, Atlanta, Georgia. Dr. Kathiresan is a Senior Member of AIAA and a Member of ASME. He is a registered Professional Engineer (Mechanical) in the States of Georgia and Florida.

STATIC FATIGUE TESTING OF OPTICAL FIBERS IN WATER IMMERSION

Enrique Cuellar, Michael T. Kennedy, Daniel R. Roberts#

Raynet Corporation
155 Constitution Drive
Menlo Park, CA 94025

Abstract

Polymer coated optical glass fibers can exhibit, under severe environmental conditions, an accelerated static fatigue behavior at long times and under moderate stresses. This behavior is manifested as a transition towards shorter times to failure in the static fatigue plot of *ln* (time to failure) versus *ln* (applied stress). To better understand this effect, a wide variety of polymeric coatings on optical glass fibers were tested for their effectiveness in inhibiting this transition. Two-point bending static fatigue data were obtained in either 80°C or 85°C water immersion. The coatings included in the testing were ultraviolet (u.v.) curable acrylates, fluorinated acrylates, polyimides, and silicones. Also tested were several generations of fiber containing titania doping in the glass cladding surface. It was found that the most effective coatings in increasing the resistance of the fiber to accelerated fatigue were phenyl-methyl silicone and polyimide.

Introduction

It is now well established that polymer coated optical glass fibers can exhibit a transition in slope of their static fatigue behavior that can severely limit their long term reliability in certain harsh environments. This transition was first observed by Wang and Zupko[1] after about 20 days for fibers coated with a u.v.-curable epoxy-acrylate at 32.6°C and 90% r.h. Subsequently, others have shown that this transition depends upon the environmental conditions as well as the polymer coating. For example, Krause and Paek[2] reported the change in slope occurring in shorter time scales for static fatigue tests in 90°C water. In this environment, the transition occurred after about 1 hour for fibers coated with a u.v.-curable epoxy acrylate and a silicone-nylon composite, and about 6 hours for a u.v.-curable polyester. Chandan and Kalish[3] tested the static fatigue of a u.v.-curable polyurethane acrylate coated fiber, in water, in 10°C intervals from 40°C to 90°C. The transition was experimentally verified at all temperatures in the range tested, increasing from about 10 hours at 90°C to about 5 days at 40°C. Cuellar *et al.*[4] observed the transition in water at 80°C for a laboratory drawn acrylate coated fiber in about 1 day, while the same glass coated with a silicone showed no transition in tests extending to 1.5 years. Roberts *et al.*[5] reported no transition in tests at various levels of relative humidity, ranging from 0% r.h. to 90% r.h., and 80°C. Krause[6,7] also reported fatigue results of stripped fiber, demonstrating that the transition in slope is an intrinsic characteristic of the bare glass which can be modified by the presence of the coating material. In addition, Matthewson and Kurkjian[8] and Krause and Shute[9] showed that the fatigue transition is sensitive to pH, occurring more rapidly at higher pH for both bare fiber, stripped of its polymeric coating, and fiber with a u.v.-curable urethane acrylate coating.

The fatigue transition appears to be strongly influenced by the chemistry of the coating. Attempts at modeling it[3,9] have resulted in empirical expressions not founded on physical models. While reasonable fits to the data were obtained, these authors cautioned against extrapolation outside of the bounds of the data. Regardless, the existence of the transition should be considered for conservative service life predictions. Due to its practical importance, we undertook an extensive research program to test the effectiveness of a wide variety of different polymer coated optical fibers in inhibiting the transition.

Raychem GmbH, Ottobrunn, Germany.

Experimental

Fourteen different optical glass fibers were included in this study. Both commercial telecommunications fibers purchased over a five year period as well as samples specially prepared in this laboratory were tested. The fibers are described below:

Polyurethane Acrylate Coated Fibers:

- Corning Corguide™ 1508 (100/140μm multimode fiber, 250 μm CPC2 coating)
- Corning Corguide 1528 (singlemode fiber, 125μm cladding, 250μm CPC3 coating)
- Corning Corguide 1528 (custom singlemode fiber, 125μm cladding, 250μm CPC5 coating)
- Corning HFRC (developmental singlemode fiber with titania-doped cladding, CPC3 coating)
- Corning Titan™ (singlemode fiber with titania-doped cladding, 125μm cladding, 250μm CPC5 coating)
- AT&T (singlemode fiber, 125μm cladding, 250μm pre-D-Lux 100™ coating)
- AT&T D-Lux 100 (singlemode fiber, 125μm cladding, 250μm D-Lux 100 coating)
- Raychem lab drawn (480μm silica fiber, no cladding, 600μm DeSolite™ 950-131 coating)
- Sumitomo (100/140μm multimode fiber, 250μm coating)

Fluorinated Acrylates:

- Ensign-Bickford HCS™ (Hard Clad Silica, 200/220μm multimode fiber, with fluorinated acrylate cladding)

Polyimides:

- Raychem lab drawn (480μm silica fiber, no cladding, with DuPont Pyrolin™ P12525 polyimide coating, 520μm coating)
- Raychem VSI™ (100/120μm multimode fiber, with permanent polyimide primary coating and silicone overcoat)

Silicones:

- Raychem lab drawn (480μm silica fiber, no cladding, with a 625μm coating consisting of a 75% phenyl-, 25% methyl-silicone primary coating and a dimethyl silicone overcoating)
- Sumitomo (100/140μm multimode fiber, 250μm methyl-phenyl silicone coating)

The static fatigue behavior of the fibers was measured using a two-point bending geometry. Two types of bending fixtures were used, both made of anodized aluminum. One consisted of two parallel plates with 20 or 30 precision-machined V-grooves to hold the fibers in place. Accurate stainless steel spacers were used to separate the plates to the desired values. The second fixture type consisted of a block 2.5 cm high with 20 precisely reamed identical holes. The ends of the fiber were pulled through each hole until the fiber bends were inside the holes. Applied stresses were systematically varied from 1100 to 4100 MPa. Each fixture was submerged in a Pyrex tank of deionized water at 80°C or 85°C and whose temperature was carefully regulated to ± 0.2°C. Each tank was equipped with an overflow drain, and deionized water (16-18 Mohm-cm) was continuously dripped into the tank. The rate of addition of water was sufficient to replace the loss due to evaporation and to turn over the water in the tank every 12 hours. The pH and conductivity of the water in each tank were monitored regularly. The pH remained constant at about 4 to 6, and the conductivity at 1 to 2 micromho/cm. The tanks were insulated and outfitted with polycarbonate lids to reduce contamination by dust.

Fiber breaks were monitored acoustically with a hydrophone and confirmed visually. The voltage generated by the hydrophone was amplified, filtered, and either recorded on strip chart recorders or by a data acquisition system and computer. All fiber breaks were entered into a data base for analysis. The results of each experiment were analyzed using Weibull statistics. Typically, 20 specimens were tested at each condition of applied stress and temperature, and the Weibull probability function $ln\ln (1/(1-F))$, where F is the cumulative failure probability, was plotted against the experimentally determined time to

failure. This data were regressed linearly to calculate the median time to failure at a cumulative failure probability F=0.5. Static fatigue data were then plotted as *ln* (median time to failure) versus *ln* (applied stress). The strain, ε on the fibers was calculated from[10]

$$\varepsilon = 1.1978\left(\frac{2r}{D-d}\right) \quad (1)$$

for the test fixtures using precision reamed holes, and

$$\varepsilon = 1.1978\left(\frac{2r}{D+2\Delta-d\sqrt{2}}\right) \quad (2)$$

for the test fixtures using parallel plates. In these equations, r is the glass fiber radius, D is the plate separation or hole diameter, Δ is the average groove depth, and d is the coated fiber diameter.

The applied stress σ is given by

$$\sigma = \varepsilon E \quad (3)$$

where E is the secant modulus and is related to the strain by[11]

$$E = E_0(1+3\varepsilon) \quad (4)$$

E_0 is the modulus of the fiber, 70.3 GPa for pure silica cladding fibers, and 65.5 for fibers with titania doped claddings.

Results and Discussion

Figures 1 and 2 illustrate the significant effect that different u.v.-curable polyurethane acrylate coatings can have on the static fatigue transition. The time of the transition can increase from 0.5 days for the Raychem lab drawn fiber with DeSolite 950-131 acrylate coating (at 80°C) to 230 days for the AT&T D-Lux 100 coated fiber (at 85°C). Table 1 summarizes the static fatigue transition times for these various optical fibers. The transition time was determined graphically and defined as the time at which the fatigue data deviated from the straight line. Also included in Table 1 is the stress corrosion constant *n*, equal to the negative of the slope of the static fatigue plot before the occurrence of the transition. For pure silica cladding fibers, it can be seen that different u.v.-curable polyurethane coatings can also significantly affect the stress corrosion constant, which varied from 22 for Corguide 1508, CPC2 (at 80°C) to 48 for Corguide 1528, CPC3 (at 85°C).

It is interesting to examine in greater detail the data presented for Corning and AT&T fibers. All of these fibers have dual layer polyurethane acrylate coatings, with a lower modulus inner primary coating applied directly to the fiber cladding surface and a higher modulus outer primary coating which is adhered to the inner coating. The CPC2, CPC3

TABLE 1. Summary of the Static Fatigue Behavior of UV-Curable Polyurethane Acrylate Coated Fibers.

Fiber	Test Environment	Transition Time ln (time, seconds)	Stress Corrosion Constant, n
Corguide 1508 CPC2	80°C Water	12.0 (+0.5/-1.0)[a]	22 (± 1.0)[b]
Corguide 1528 CPC3	80°C Water	15.5 (+0.2/-0.2)	30 (±1.0)
Corguide 1528 CPC3	85°C Water	14.5 (+0.2/-0.5)	48 (±8.0)
Corguide 1528 CPC5	85°C Water	14.4 (+0.2/-0.5)	38 (±4.0)
AT&T (Pre-D-Lux 100)	85°C Water	12.5 (+0.1/-0.3)	30 (±1.0)
AT&T D-Lux 100	85°C Water	16.8 (+0.2/-0.3)	24 (±2.0)
Raychem	80°C Water	10.7 (+0.2/-0.2)	31 (±6.0)
Sumitomo	80°C Water	12.1 (+0.2/-0.2)	24 (±1.0)
Corning HFRC CPC3	80°C Water	17.8 (+0.1/-0.3)	98 (±20.0)
Corning Titan CPC5	80°C Water	15.5 (+0.2/-0.2)	126 (±22)
Corning Titan CPC5	85°C Water	15.4 (+0.1/-0.3)	>70

[a] Estimate of the uncertainty in the transition time.
[b] Standard error of the estimate in n from linear regression.

and CPC5 coatings represent successive generations of Corning coatings. In the change from CPC2 to CPC3, the inner primary was modified for improved adhesion and its hardness was increased. There was no change to the outer primary coating. On the other hand, the change from CPC3 to CPC5 involved increasing the hardness of the outer coating to provide better abrasion resistance and toughness, while the inner primary coating was left unchanged[12]. As can be seen in Table 1 and Figures 1 and 2, changes in the time of the transition are well correlated with these changes in the coatings. The change from CPC2 to CPC3, corresponding to a change in inner coating, increased the time of the fatigue transition from 2 days to 62 days, while the change to CPC5, which was a change in the outer coating only, resulted in no change in the time of the transition, 23 days for CPC3 vs. 21 days for CPC5 in 85°C water. Similarly, AT&T D-Lux 100 coatings were formulated to minimize moisture absorption into the coating, improve and maintain adhesion to the cladding, and enhance hydrolytic stability with aging over the standard, previous coating[13]. These changes increased the time of the fatigue transition from 2 days to 230 days in 85°C water.

Significantly more dramatic effects on the static fatigue behavior are observed for fibers with other polymeric coatings, as shown in Figure 3 and Table 2. The short term fatigue resistance of these non-polyurethane coated fibers are similar to each other and not significantly different from those of the acrylate-coated fibers, but the fatigue transition can be very effectively inhibited. For example, the Raychem laboratory drawn fiber with phenylated polysiloxane primary coating showed no transition in 80°C water in tests extending out to 4.2 years. These tests were terminated at a time when the data point indicated by the arrow had two fiber breaks out of 20 fibers under test. Similarly, both polyimide coated fibers under test show no indication of a transition in tests extending out to >200 and >910 days respectively. Biswas[14] has also reported tensile static fatigue tests with no transition of polyimide coated fibers in 80°C distilled water, but the test durations were not as extensive as those reported here.

Small changes in the chemistry of the coatings can apparently have dramatic effects in inhibiting the fatigue transition. For example, Hiskes *et al.*[15] reported test data on a fiber with a polydimethyl siloxane coating. Fiber samples 1 m in length wound on mandrels and immersed in 98°C water showed a transition in the static fatigue in about 10 hours. In Table 2 and Figure 3, data are shown for two other silicone coated fibers. Both the Raychem and the Sumitomo fiber coatings were methyl-phenyl silicones, and in both cases the transition was greatly inhibited compared to the dimethyl silicone coated fiber. This slight change in functionality results in an impressive difference in the time of the transition, 230 days for the Sumitomo fiber and >1500 days for the Raychem fiber. Note that Sumitomo fiber did not show a transition until almost 1 year of testing. A second example is provided by the Ensign-Bickford HCS fiber. The fluoroacrylate functionality of this fiber

TABLE 2. Summary of the Static Fatigue Behavior of Various Non-Acrylate Polymer Coated Fibers.

Fiber	Test Environment	Transition Time ln (time, seconds)	Stress Corrosion Constant, n
Ensign Bickford HCS	80°C Water	16.9 (+0.9/-0.9)[a]	30 (± 4.0)[b]
Raychem Polyimide	80°C Water	>18.0	27 (±2.0)
Raychem Polyimide/Silicone	80°C Water	>18.2	28 (±2.0)
Raychem Silicone	80°C Water	>18.7	25 (±1.0)
Sumitomo Silicone	80°C Water	16.8 (+0.2/-0.5)	36 (±3.0)

[a] Estimate of the uncertainty in the transition time.
[b] Standard error of the estimate in n from linear regression.

inhibits the transition compared to conventional polyurethane acrylate. Lastly, Yuce *et al.*[16] have also concluded that subtle changes in the coating chemistry can have an enormous effect on fiber aging behavior. However, they did not identify the nature of the coating changes.

An alternative approach to inhibiting or eliminating the fatigue transition is to modify the surface of the fiber cladding. Figure 4 shows two-point bending static fatigue data for two generations of Corguide fibers with TiO_2 dopant in the cladding surface. The earlier developmental High Fatigue Resistant Composition (HFRC) fiber with CPC3 coating was followed by the commercialized TITAN fiber with CPC5 coating. Table 1 shows that this dopant is very effective in increasing the short term fatigue resistance. The static stress corrosion constant n of Corguide 1528 with CPC3 coating is 30, that of the HFRC fiber, also with CPC3 coating, is about 100. Changes in the glass composition are also effective in changing the time of the fatigue transition. The HFRC fiber with CPC3 coating showed the possible start of a fatigue transition after 620 days in 80°C water. On the other hand, the TITAN fiber with CPC5 coating showed a transition after about 62 days in the same environment. As discussed above, there was no difference in the time of the transition for pure silica cladding fibers (Corguide 1528) with CPC3 or CPC5 coatings. Thus, we deduce that a possible cause of the difference in fatigue behavior between the HFRC and TITAN fibers is a change in the level of titania doping in the cladding. Glaesemann *et al.*[17] have reported dynamic fatigue n values as a function of TiO_2 weight %. The dynamic n value was found to increase linearly with TiO_2 concentration up to about 10 wt. %. Above this level, the dynamic n increased at a far faster rate.

Summary

Two-point bending static fatigue data have been obtained on commercially available and laboratory drawn optical fibers with a variety of polymeric coatings: u.v.-cured acrylates, polyimides and silicones. Also tested were acrylate coated fibers whose cladding surface composition was modified by doping with TiO_2. The static fatigue transition, representing an accelerated fatigue behavior at long times and moderate stress levels, can be dramatically inhibited by the choice of polymeric coating. Changes to the coating chemistry such as the addition of fluorine functional groups to u.v.-cured acrylates or phenyl functional groups to thermally cured silicones can inhibit and possibly eliminate the transition. The short term static fatigue resistance of fibers can also be significantly increased by titania doping of the cladding surface. The static fatigue transition time appears to be a function of the doping level.

Acknowledgements

The authors wish to thank Maria Stipek, Michael Feldman and Rick Ayers for their technical assistance.

References

1. T.T. Wang and H.M. Zupko, "Long-Term Mechanical Behaviour of Optical Fibres Coated with a U.V.-Curable Epoxy Acrylate", J. Mater. Sci. 13, 2241-2248 (1978).

2. J.T. Krause and U.C. Paek, "Aging and Static Fatigue of Plastic-Coated Fused-Silica Fibers", in Proc. Topical Meeting on Optical Fiber Communication, Washington, D.C., 18-19 (1979).

3. H.C. Chandan and D. Kalish, "Temperature Dependence of Static Fatigue of Optical Fibers Coated with a Uv-Curable Polyurethane Acrylate", J. Am. Ceram. Soc. 65(3), 171-173 (1982).

4. E. Cuellar, D. Roberts and L. Middleman, "Static Fatigue Lifetime of Optical Fibers in Bending", Fiber and Integrated Optics 6(3), 203-213 (1987).

5. D.R. Roberts, E. Cuellar and L.M. Middleman, "Static Fatigue of Optical Fibers in Bending II: Effect of Humidity and Proof Stress on Fatigue Lifetimes", in Proc. SPIE, 842, 32-40 (1987).

6. J.T. Krause, "Transitions in the Static Fatigue of Fused Silica Fiber Lightguides", in Proc. 5th European Conference on Optical Communications, Postdeadline Papers, Amsterdam, 19.1.1-19.1.4 (1979).

7. J.T. Krause, "Zero-Stress Strength Reduction and Transitions in Static Fatigue of Fused Silica Fiber Lightguides", J. Non-Cryst. Solids 38&39, 497-502 (1980).

8. M.J. Matthewson and C.R. Kurkjian, "Environmental Effects on the Static Fatigue of Silica Optical Fiber", J. Am. Ceram. Soc. 71(3), 177-183 (1988).

9. J.T. Krause and C.J. Shute, "Temperature Dependence of the Transition in Static Fatigue of Fused Silica Optical Fiber", Adv. Ceram. Mater. 3(2), 118-121 (1988).

10. M. J. Matthewson, C.R. Kurkjian and S. T. Gulati, "Strength Measurement of Optical Fibers by Bending", Am. Ceram. Soc. 69(11), 815-821 (1986).

11. S.T. Gulati, J.D. Helfinstine, G.S. Glaesemann, D.R. Roberts, E. Cuellar and L.M. Middleman, "Improvements in Optical Fiber Reliability via High Fatigue Resistant Composition", in Proc. SPIE 842, 22-31 (1987).

12. Michael Reunert, personal communication.

13. Tom Chapin, personal communication.

14. D. R. Biswas, "Characterization of Polyimide-Coated Optical Fibers", Opt. Eng. 30 (6), 772-775 (1991).

15. R. Hiskes, C.A. Shantz, E.G. Hanson, L.S. Mittelstadt, C.J. Scott, C.S. Joiner, G.F. Knutsen and J.G. Pound, "High Performance Hermetic Optical Fibers", in Proc. OFC'84, Postdeadline Papers, WI6.1-WI6-4 (1984).

16. H.H. Yuce, J.P. Varachi, Jr., J.P. Kilmer, C.R. Kurkjian and M.J. Matthewson, "Optical Fiber Corrosion: Coating Contribution to Zero-Stress Aging", in Proc. OFC'92, 395-399 (1992).

17. G.S. Glaesemann, M.L. Elder and J.W. Adams, "Dependence of Fatigue Resistance on Titania Doping of Silica-Clad Optical Fiber", in Proc. OFC'90, Postdeadline Papers, PD13.1-PD13.4 (1990).

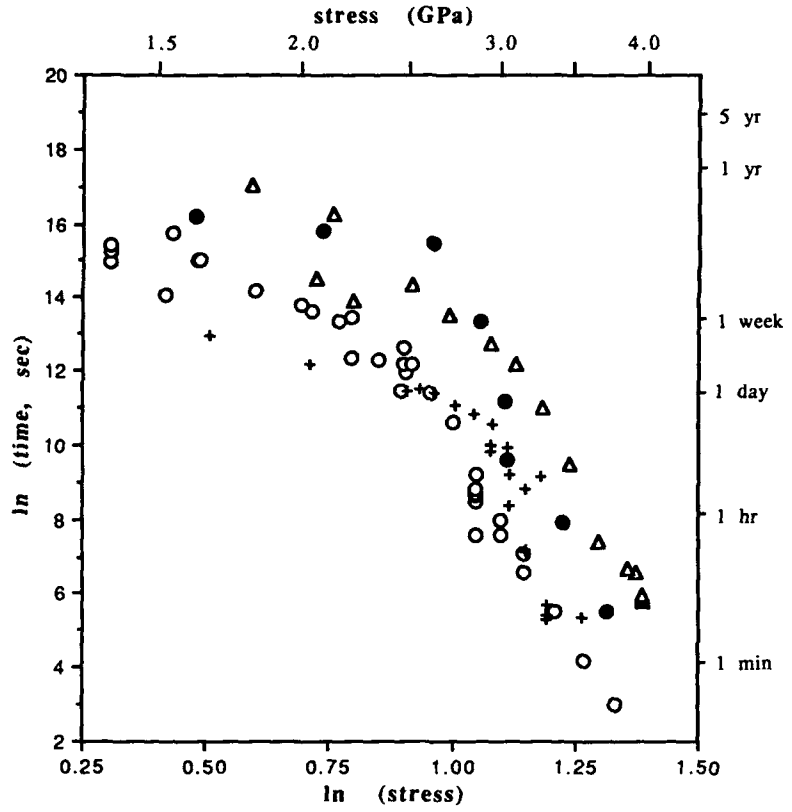


Figure 1. Static fatigue data in two-point bending of polyurethane acrylate coated fibers, in 80°C water.

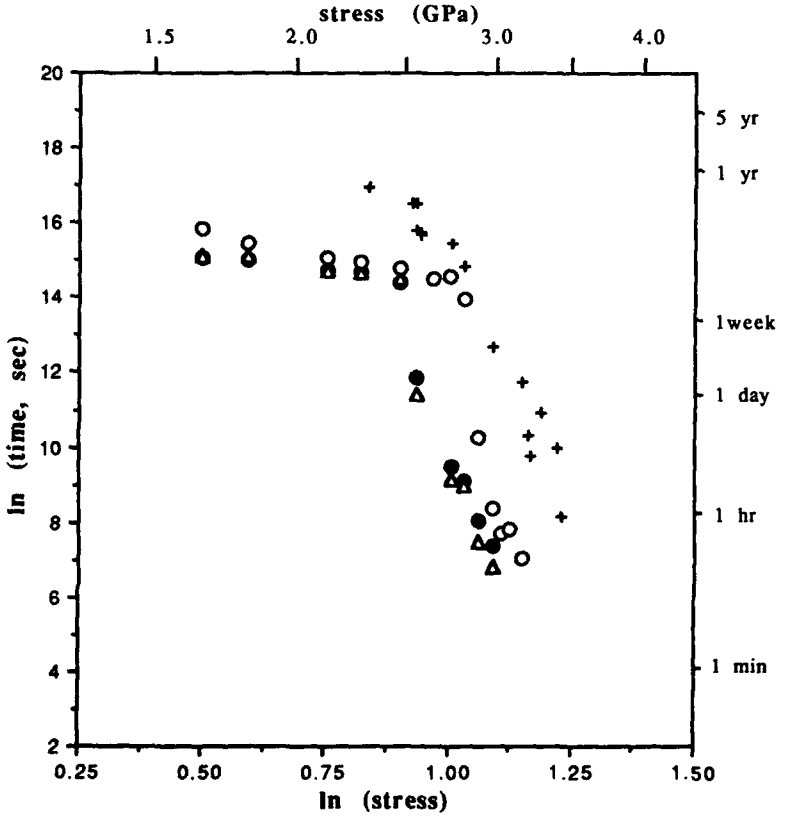


Figure 2. Static fatigue data in two-point bending of polyurethane acrylate coated fibers, in 85°C water.

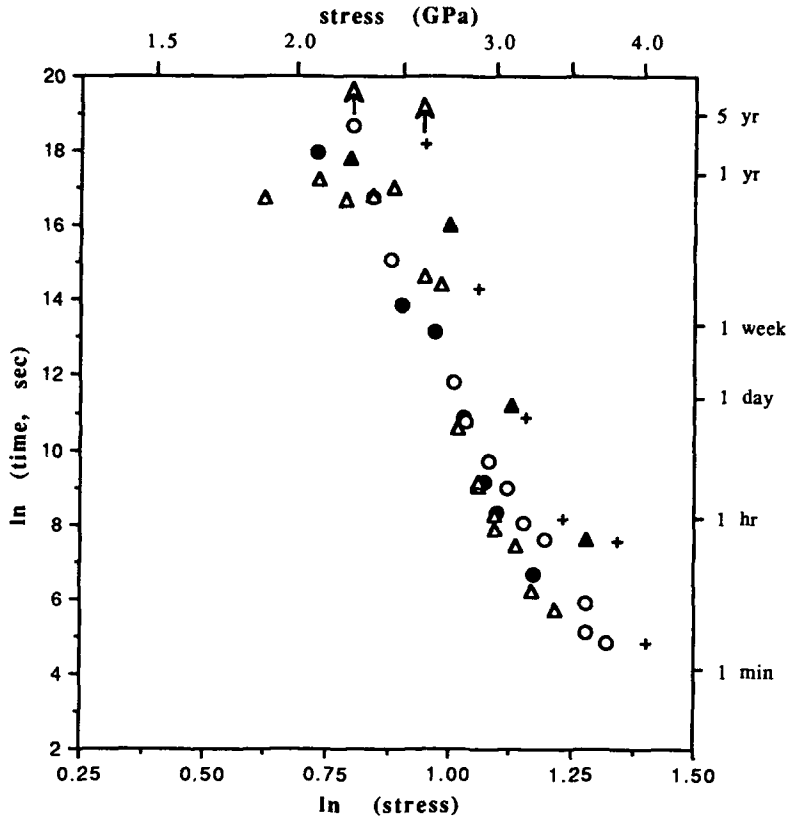


Figure 3. Static fatigue data in two-point bending of fibers with other polymeric coatings, in 80°C water. Data points with arrows represents tests which were terminated with no fiber failures.

- ● Raychem Polyimide
- \+ Raychem VSI
- ○ Raychem Silicone
- △ Sumitomo Silicone
- ▲ Ensign Bickford HCS

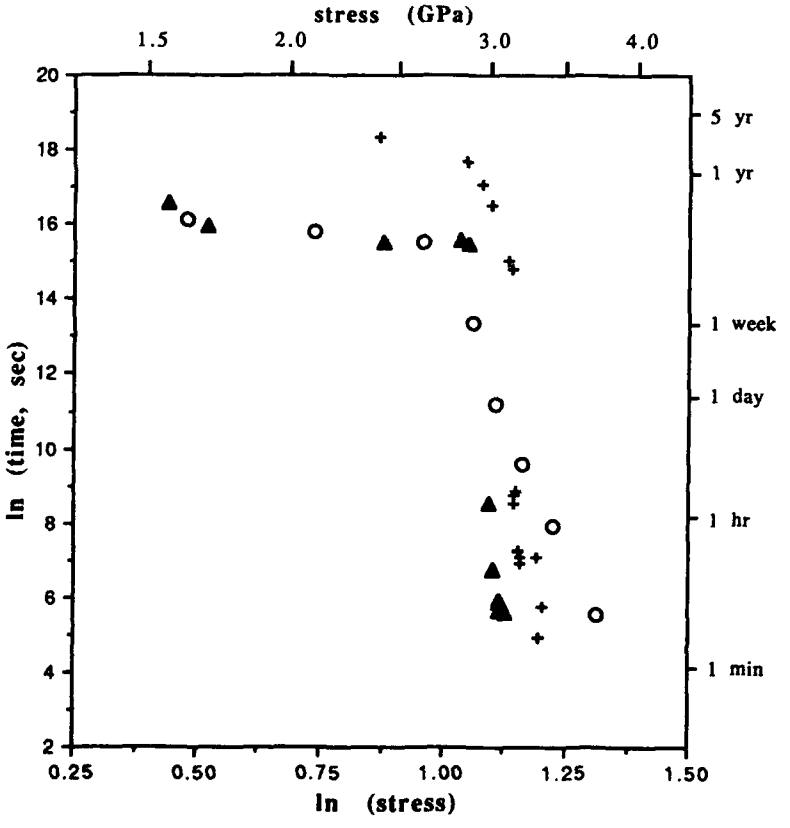


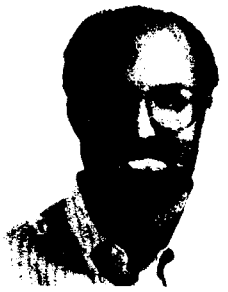
Figure 4. Comparison of static fatigue data in two-point bending of pure silica clad and titania doped clad fibers, in 80°C water.

- \+ Corning HFRC CPC3
- ○ Corning 1528 CPC3
- ▲ Corning TITAN CPC5



Enrique Cuellar
Raynet Corporation
155 Consitution Drive
Menlo Park, CA 94025

Enrique Cuellar received his B.A. in Chemistry in 1970 from Oberlin College and his Ph.D. in physical chemistry from the University of California at Berkeley in 1975. He joined Raychem Corporation in 1982 and Raynet Corporation in 1987, where he has managed the non-invasive coupler product development and the research on fiber and passive component reliability. He is presently Director of International FITL Standards and Fiber Optic Product Line.



Michael T. Kennedy
Raynet Corporation
155 Consitution Drive
Menlo Park, CA 94025

Michael T. Kennedy received his B.S. in Engineering Physics from the University of California at Berkeley in 1980, and his M.S. in Mechanical Engineering at Berkeley in 1983. He spent four years at Hewlett Packard designing fiber optic components for data communications. During the past four years he has been conducting research on long term fiber and passive component reliability at Raynet Corporation in Menlo Park, CA.



Daniel R. Roberts
Raychem GmbH
Am Haidgraben 6
8012 Ottobrunn, Germany

Daniel R. Roberts received his B.S. in Chemistry in 1974 from the University of Wisconsin at Madison, and his Ph.D. in Polymer Science in 1981 from the Massachusetts Insitute of Technolgy. Following four years at Dow Chemical Company he joined Raychem Corporation in 1981. While at Raynet Corporation, Raychem's fiber optic subsidiary, he conducted research in fracture mechanics of optical fibers. He is currently with the Raychem Energy Products Division in Germany.

THE MECHANICAL BEHAVIOR OF LARGE FLAWS IN OPTICAL FIBER AND THEIR ROLE IN RELIABILITY PREDICTIONS

G.S. Glaesemann

Corning Incorporated
Corning, New York

Abstract

The flaws in optical fiber of greatest reliability risk are those below the high strength region. The fatigue behavior of proof stress size flaws is similar to that of flaws in the high strength region. The strength of such flaws after aging in 80°C water is markedly different than that of pristine fiber surfaces. Whereas pristine fiber surfaces degrade in strength with aging, large flaws in fiber actually increase in strength with aging. The risk of mechanical failure for fiber in most applications is governed primarily by the fatigue and aging behavior of relatively large flaws.

Introduction

In a previous study, a nearly 400 km fiber strength distribution was statistically scaled for failure probability predictions for a range of fiber lengths in tension and bending.[1] The predicted distributions for the case of bending are replicated in Figure 1. Not surprisingly, for long lengths in tension or bending, such as those found in typical stranded cable designs, the probability of encountering a flaw near the proof stress level is high. Of particular interest are typical short length applications where it is usually assumed only pristine fiber is stressed. By way of example, consider a typical splice enclosure where approximately one meter of fiber is stored in bending. The strength distribution appropriate for this situation is shown in Figure 1. For a common failure probability requirement of 10^{-4} to 10^{-6}, the flaws of greatest risk can be as low as 70 kpsi in strength and are significantly weaker than the strength of pristine fiber (> 500 kpsi). Therefore, regardless of the application, the fatigue and aging behavior of these flaws must be understood in order for engineers to make accurate reliability predictions. The purpose of this paper is to present data on the aging and fatigue behavior of flaws near the proof stress level.

Background

Aging of optical fiber

The aging of fiber in harsh environments has received much attention in the last few years. Strength degradation of pristine optical fibers after exposure to hot water has been well documented. For example, Figure 2 shows the results of Matthewson and Kurkjian[2] where pristine silica-clad fiber was strength tested in 2-point bending after aging in 100°C water. The strength degradation with aging time was attributed to the dissolution of the silica surface. For a pristine fiber surface, as found on short test lengths, aging results in surface roughening and strength degradation.[3] This phenomenon is one of flaw introduction for pristine fiber surfaces.

What about the aging of extrinsic flaws in optical fiber, since they are the ones of greatest reliability risk? Little data exists on the aging of the lower strength region of optical fiber strength distributions due to difficulty in finding such flaws with typical strength testing equipment. However, strength increases with aging time have been reported for bulk silica glass.[4,5] Strength of both abraded and indented silica glass is plotted in Figure 3 versus aging time in silicic acid and water at 90°C. With the exception of indentation cone cracks strength increases of 25 to 35% were measured. Ito and Tomozawa[4] attributed the strength increase of abraded silica glass to a change in the crack tip morphology best described by "rounding". Rounding of the crack tip leads to a strength increase because it lowers the stress intensity factor over sharp cracks. Marshall and Lawn[5] argued that a strength increase during aging is caused by relieving of localized residual stresses generated by the indentation or abrasion event. They illustrated their point by showing that the strength increase for indentation cone cracks, produced by sphere on flat glass, is negligibly small. Cone cracks are produced by purely elastic deformation and do not have an associated residual stress field. In this study we will attempt to provide some understanding of the aging behavior of flaws near typical proof stress levels on silica-clad optical fiber.

Fatigue of optical fiber

Figure 4 is a plot of the fatigue parameter n versus fracture strength for silica-clad fibers and bulk silica glass. The data and references for Figure 4 are summarized in Table 1. This plot is similar to that found in reference 6 with the exception that the data here is confined just to silica fiber and bulk silica glass. The fatigue parameter n for as-received silica-clad fiber is approximately 20 down to strength levels as low as 100 kpsi. The exceptions are n values greater than 25 where extremely slow dynamic fatigue stressing rates were used. Bulk silica glass clearly has n values greater than high strength fiber. Of particular interest are two studies[10,14] where abraded fibers with strengths less than 100 kpsi demonstrated n values approaching bulk silica glass as shown in Figure 4. It appears then that there is a transition to higher n values for fiber strengths below 100 kpsi.

Several researchers have argued that the transition to higher n values with lower strengths is a fundamental transition in flaw geometry from a mere surface impression to a more well defined "Griffith" type flaw.[16,21,22] The technique used to create model flaws in bulk silica glass and optical fiber is that of indentation, where flaws are introduced onto the glass surface using a diamond microhardness indenter.[21] Results from this technique are shown in Figure 5 where the strength of indentation flaws on fiber and bulk silica glass is plotted versus indentation size. The transition to a more well-defined crack system at an indentation size between 10 and 30

microns is described as moving from a surface impression (subthreshold) to a flaw with well defined radial cracks emanating from the impression (postthreshold) and is characterized by a significant drop in strength. The localized residual stress that accompanies indentation flaws is believed to play a crucial role in the subcritical growth or fatigue of such flaws by assisting in the growth with the end result that subthreshold flaws have a lower measured n (20) than postthreshold flaws (30).[15] This is shown in Figure 6 where measured n values are plotted versus indentation load from reference 15. Postthreshold flaws without the influence of residual stress have measured n values near 40. Comparing the fatigue values in Figure 4 with the strength values in Figure 5 suggests that the indentation flaws near 100 kpsi are subthreshold in form and that the abrasion flaws on fiber near 50 kpsi behave as postthreshold flaws without residual stress.

It has been stated that the residual stress effect on subthreshold flaws does not account for the n of 20 for flaws in the high strength region since the near perfect as-drawn fiber surface is not believed to contain regions of concentrated residual stress.[2] Also, it has been postulated that the localized residual stress on proof stress level flaws stimulates radial cracks to unexpectedly transition from subthreshold to postthreshold, i.e.,"pop-in", during in-service use; and therefore, the ultimate reliability of fiber is ultimately controlled by crack "pop-in" and not subcritical growth of pre-existing flaws.[23] This report will attempt to provide additional fatigue data and understanding of flaws in this strength region.

Experimental Details

Aging.

To examine aging behavior of extrinsic flaws in optical fibers, 125 μm fibers were first mechanically abraded during the drawing process by intentionally touching the fiber with an uncoated 150 μm fiber just before applying a 250 μm dual acrylate coating. The resulting flaws from this abrasion procedure are believed to be more similar to that of blunt indentation, as with the cone indenter for bulk silica in Figure 3. The draw-abraded fibers were aged in 80°C water buffered to pH 7 for up to 60 days. Strength testing of the aged fiber was performed under uniaxial tension in 45% relative humidity and 23°C using a gauge length of 0.5 meters. A strain rate of 70 %/min. was used to minimize crack growth during strength testing. Prior to strength testing all specimens were preconditioned in the test environment for a minimum of 8 hours.

Also included in this study are the aging results from the Honors Thesis by Estep.[24] Estep abraded fibers after drawing by chemically removing a one inch section of polymer coating, dropping 30 grams of silica particles onto the fiber surface from a height of 9 cm, and recoating the fiber using a standard fusion-splice recoating apparatus. This abrasion technique is believed to more closely replicate the abrasion or sharp indentation surface conditions in Figure 3 than that of blunt indentation cone cracks. The aging condition for these fibers was 85°C water. The strength testing procedure consisted of baking the fibers at 60°C and a soft vacuum for 24 hours and subsequent loading to failure in less than 15 seconds. This preconditioning procedure was intended to minimize strength degradation during the tensile test.

Fatigue.

For this part of the study draw-abraded fibers were prepared as discussed above. Also, post-draw abraded specimens were prepared using an abrasion process similar to Estep's[24]. Fibers from both abraded surface conditions were dynamic fatigue tested at 23°C and 100% RH using rates of 0.4, 0.04, 0.004, and 0.0004%/min. A fiber gauge length of 4 meters was used for the dynamic fatigue tests. Also, specimens for fatigue testing were preconditioned a minimum of 2 hours in 100% RH. Fibers from both surface conditions were also aged in 80°C water and fatigue tested in the same manner. A minimum of 10 specimens per strain rate was used for all fibers. For some of the aged draw-abraded fibers a fifth rate of 0.00004%/min was also used to investigate any curvature in the data, but the resulting strengths did not depart from the best fit line of the 4 faster rates.

Results and discussion

Aging.

Strength distributions from the draw-abraded fibers in this study and the post-draw abraded fibers from reference 24 are shown in Figure 7. It is of particular interest that the strengths produced by these abrasion techniques are greater than that needed to produce post-threshold flaws according to the indentation results in Figure 5. It is postulated that indentation flaws model the large flaws in optical fibers. It follows that the flaws with strengths shown in Figure 7 are believed to be subthreshold in morphology.

The tensile strength of the aged abraded fibers is plotted versus aging time in Figure 8. The strength of both abraded fiber types is shown to initially decrease slightly followed by a significant increase in strength to values significantly greater than their initial value. For example, the draw-abraded fiber has an initial strength of 66 kpsi and after 150 days of aging the strength increases to 106 kpsi. The post-draw abraded fiber of Estep starts at 75 kpsi and increases to 133 kpsi after 10 days, a value nearly twice its original strength.

It is interesting that the post-draw abraded fiber increased in strength more rapidly than the draw-abraded. The post-draw abraded reaches 100 kpsi in 10 days, whereas, the draw-abraded attains 100 kpsi after 150 days. One explanation for this difference is that the higher aging temperature for the post-draw abraded fiber, 85°C versus 80°C, simply causes the aging process to proceed at a faster rate. This is unlikely since the published activation energies of 45 to 75 kJ/mol, postulated for the aging process at these temperatures,[2] greatly underestimate the observed difference in rate. Another possible explanation is that the aging behavior is dependent on the type of flaw produced by the abrasion method. For example, recall the results in Figure 3 where cone flaw produced by blunt indentation responded more slowly to the aging environment than abrasion and Vickers indentation. It was speculated earlier that draw-abrasion is more reflective of blunt indentation like that produced by a sphere on a flat plate, whereas, post-draw particle abrasion is more similar to sharp indentation. Clearly more research is needed to better understand the aging differences in Figure 8, nevertheless, the strength of abraded fiber increased with aging time irrespective of the flaw introduction method and aging temperature.

Fracture mechanics developed for modelling localized residual stresses around indentations predicts that the

maximum strength increase by residual stress relief is twice its original value.[25] Measured strength increases for abraded soda-lime glass, known for its ability to retain localized residual stresses, are on the order of only 40% when annealed at 400°C for 3 hours.[26] Now in the case of silica, it is well known that the level of residual stress retained in this anomalous glass as a result of surface damage is much less than that of soda-lime glass due to densification of the silica structure during abrasion.[25,27,28] Silica falls far short of retaining the residual stress needed to produce a doubling in strength after aging. Assuming that fracture mechanics applies to the damage created in this study, the two-fold increase in strength of the post-draw abraded fiber is best explained by a modification of the crack tip geometry by a process like rounding. It is speculated that the smaller strength increase of the draw-abraded fiber is an indication that the flaws are more of a surface impression, a geometry less affected by aging.

The fact that abraded fiber strength increases with aging time suggests that if the abrasion flaws are in fact subthreshold in form, they do not transition from subthreshold into postthreshold form. The transition from subthreshold flaw to postthreshold is characterized by the emanation of radial cracks from the impression region created during abrasion or indentation. Figure 5 shows a strength decrease of nearly one order of magnitude over this transition. The abraded fibers do not experience this transition to lower strengths, rather the strength increases with aging time. Also, considering the fact that the aging environment in this study is more severe than that experienced by fiber in most applications, it is believed that proof stress level flaws in optical fiber are not at risk of catastrophic failure from radial crack "pop-in". Furthermore, the above results also suggest that fracture mechanics modeling of the "pop-in" event may not be necessary for normal fiber proof stress levels.

The increase in abraded fiber strength with aging time is in sharp contrast to that of pristine fiber in Figure 2 which degrades in strength over the same aging period. Evidence of surface roughening has been recently obtained for aged pristine fiber surfaces[3] and dissolution of silica has been the most common explanation for the formation of pits on the pristine fiber surface.[2] This phenomenon of silica dissolution at high temperatures is the same argument proposed by Ito and Tomozawa[4] for the strengthening of large flaws. Whereas, silica dissolution degrades the strength of pristine fiber through flaw formation, it rounds the tip of preexisting flaws leading to a strength increase. Clearly, the concern over the aging behavior of high strength fiber cannot be extended to flaws near the proof stress.

It also is worth noting that the variability in strength appears to increase with aging time and higher strengths for both abraded fibers. Estep[24] suggests that this increase in variability with increasing strength is a further indication crack tip rounding. He argues that one would expect the overall magnitude of the flaw depth distribution to decrease with rounding, but a relative difference between flaws in specimens to remain.

Fatigue.

The strength distributions of draw and post-draw abraded fibers used for fatigue testing are shown in Figure 9. Abrading on the draw provides a relatively uniform strength distribution just above a typical proof stress level of 50 kpsi with a Weibull modulus, m, of 13. Post-draw particle abrasion yields a distribution of strength values just below 50 kpsi and modulus of 9. Figure 10 is a dynamic fatigue plot for the post-draw abraded fibers. The best fit line through all the data is shown and the calculated n value of 20.4 was obtained. A similar analysis of the draw-abraded fiber yielded an n value of 23.4. The results from dynamic fatigue testing draw-abraded and post-draw abraded fibers are plotted in Figure 11 along with large flaw fatigue data from Table I. Also included in Figure 11 is fatigue data for fiber abraded to 20 kpsi. The error bars on n were determined from the 95% confidence interval of the slope of the best fit line through the dynamic fatigue data. The results from this study do not agree with data from other studies on fiber abraded to 50 kpsi where n values equal to that of bulk silica glass were measured. Rather, results from this study match the fatigue of subthreshold flaws and abraded fibers with strengths of 100 kpsi.

The reason for the difference between the results for flaws near 50 kpsi from this study and the previously published results at 50 kpsi is not clear. However, if one were to hold to the fracture mechanics framework developed for indentation type flaws, the 50 kpsi flaws with high n values would be postthreshold in form and, as previously discussed, the flaws in this study are subthreshold, even though the strengths are the same. If postthreshold flaws in fiber are possible, then one would expect that a further abrasion of the fiber in this study would eventually provide such a flaw. The achievement would be marked by a decrease in strength and a dramatic increase in n over the present results near 20. To test this argument, fibers were abraded to 20 kpsi using the post-draw particle abrasion method and the fatigue testing yielded an n of 32. This data point is shown as a triangle in Figure 11. This increase in n from 23 to 32 is the same as shown in Figure 6 for the transition from subthreshold to postthreshold flaws.

The dynamic fatigue behavior of the 50 kpsi draw-abraded fiber is plotted in Figure 12 versus aging time in 90°C water. The n value increases from an initial 23 to 40 after 20 days of aging, but with further aging decreases to approximately 27. Due to the significant uncertainty in n it is difficult to determine if an actual increase in n has been realized. Interestingly, an increase in n from 23 to 27 is approximately what one would predict from residual stress relief that comes with aging of subthreshold flaws.[29,30]

The data presented on n of aged abraded fiber is important because it enables those making reliability predictions to have a certainty about n over 30 year life on the flaws that matter most; namely, those near the proof stress level. There are two reasons for this statement. First, in the previous section on strength after aging of abraded fiber it was concluded that one need not be concerned about strength degradation due to phenomena other than fatigue. Secondly, the fatigue data presented here shows that an n value in the low 20s is conservative even after exposure to a severe aging environment.

Summary

- Flaws produced by particle abrasion or draw abrasion are a convenient means for examining the mechanical behavior of proof stress level flaws.

- Large flaws in silica-clad optical fiber do not exhibit the zero-stress-aging strength degradation found on pristine fiber surfaces. Results confirm a process of strengthening with

aging attributed to a modification of the flaw tip geometry.

• The fatigue behavior of large flaws is at least maintained with aging.

• The mechanical reliability of optical fiber is best served by continued study of the large flaw region. This is consistent with failure probability requirements, the experimental findings in this and other studies, and the most likely application of fiber (cabling, installation, termination, and long-term life of long fiber lengths)

Acknowledgments

The author would like to thank M.G. Estep for his helpful discussions, D.J. Walter and D.A. Clark for their experimental work and patience, R.L. Bennett and T.L. Jacoby for developing the draw-abrasion technique, and to D.R. Powers and R.V. VanDewoestine for their support and guidance.

References

1. G.S. Glaesemann, "Optical Fiber Failure Probability Predictions from Long-Length Strength Distributions," pp.819-825 in proceedings of the 40th International Wire and Cable Symposium, St. Louis, Mo., 1991.

2. M.J. Matthewson and C.R. Kurkjian, "Environmental Effects on the Static Fatigue of Silica Optical Fiber," J. Am. Ceram. Soc., **71** [3] 177-83 (1988).

3. R.S. Robinson and H.H. Yuce, "Scanning Tunneling Microscopy of Optical Fiber Corrosion: Surface Roughness Contribution to Zero-Stress Aging," J. Am. Ceram. Soc., **74** [4] 814 (1991).

4. S. Ito and M. Tomozawa, "Crack Blunting of High-Silica Glass," J. Am. Ceram. Soc., **65** [8] 368-371 (1982).

5. D.B Marshall and B.R. Lawn, "Surface Flaws in Glass," in: Strength of Inorganic Glass, ed. C.R. Kurkjian (Plenum, New York, 1985).

6. C.R. Kurkjian, J.T. Krause, and M.J. Matthewson, "Strength and Fatigue of Silica Optical Fibers," J. Lightwave Tech., **7** [9] 1360-1370 (1989).

7. D. Kalish and B.K. Tariyal, "Static and Dynamic Fatigue of a Polymer-Coated Fused Silica Optical Fiber," J. Am. Ceram. Soc., **61** [11-12] 518-23 (1978).

8. S.P. Craig, W.J. Duncan, P.W. France, and J.E. Sodgrass, "The Strength and Fatigue of Large Flaws in Silica Optical Fibres," in Proc. 8th ECOC (Cannes, France), 1982.

9. G.S. Glaesemann, Masters Thesis, University of Massachusetts, 1983.

10. H.H. Yuce, P.L. Key, and D.R. Biswas, "Investigation of the Mechanical Behavior of Low Strength Fibers," in Fiber Optics Reliability: Benign and Adverse Environments III, Proc. SPIE 1174, 272-278 (1989).

11. G.S. Glaesemann and S.T. Gulati, "Dynamic Fatigue Data for Fatigue Resistant Fiber in Tension vs. Bending," in 1989 Technical Digest Series, Vol. 5, Proc Optical Fiber Communication Conference, 48 (1989).

12. J.E. Ritter, Jr, J.M. Sullivan, and K. Jakus, "Application of Fracture Mechanics Theory to Fatigue Failure of Optical Glass Fibers," J. Appl. Phys., **49** [9] 4779-82 (1978).

13. F.A. Donaghy and D.R. Nicol, "Evaluation of the Fatigue Constant n in Optical Fibers with Surface Particle Damage," J. Am. Ceram. Soc., **66** [8] 601-4 (1983).

14. S. Sakaguchi and Y. Hibino, "Fatigue in Low-Strength Silica Optical Fibers," J. Mater. Sci., **19**, 3416-20 (1984).

15. T.P. Dabbs and B.R. Lawn, "Strength and Fatigue Properties of Optical Glass Fibers Containing Microindentation Flaws," J. Am. Ceram. Soc., **68** [11] 563-69 (1985).

16. M.J. Matthewson, "Strength and Reliability of Fused Silica Optical Fiber," BROADBAND (FOC/LAN) '90 (Baltimore, MD.), 1990.

17. J.E. Ritter, Jr., and C.L. Sherburne, "Dynamic and Static Fatigue of Silicate Glasses," J. Am. Ceram. Soc., **54** [12] 601-605 (1971).

18. S.T. Gulati, "Mechanical Properties of SiO2 versus SiO2-TiO2 Bulk Glasses and Fibers," in proceedings of 1991 MRS Fall Meeting, Boston.

19. S.M. Wiederhorn, A.G. Evans, and D.E. Roberts, pp. 829-41 in Fracture Mechanics of Ceramics, Vol. 2. Edited by R.C. Bradt, D.P.H. Hasselman, and F.F. Lange. Plenum Press, New York, 1974.

20. S. Sakaguchi, Y. Sawaki, Y. Abe, and T. Kawasaki, "Delayed Failure in Silica Glass," J. Mat. Sci., **17**, 2878-86 (1982).

21. T.P. Dabbs, D.B. Marshall, and B.R. Lawn, "Flaw Generation by Indentation in Glass Fibers," J. Am. Ceram. Soc., **63** [3-4] 224-25 (1980).

22. K. Jakus, J.E. Ritter, Jr, S.R. Choi, T.J. Lardner, and B.R. Lawn, "Failure of Fused Silica Fibers with Subthreshold Flaws," J. Non-Cryst. Sol., **102** 82-87 (1988).

23. F.A. Donaghy and T.P. Dabbs, "Subthreshold Flaws and Their Failure Prediction in Long-Distance Optical Fiber Cables," J. Lightwave Tech., **6** [2] 226-32 (1988).

24. M.G. Estep, "The Effects of Zero Stress Aging on the Strength of Large Flaws Introduced to the Surface of Optical Waveguides," Honors Thesis, New York State College of Ceramics at Alfred University, Alfred, New York, 1990.

25. M.A. Israel, J.E. Ritter, Jr., and K. Jakus, "Strength and Dynamic Fatigue Behavior and Indented Borosilicate and Soda-Lime Glasses," Phy. and Chem. Glass., **28** [4] 133-38 (1987).

26. D.H. Roach and A.R. Cooper, "Effect of Contact Residual Stress Relaxation on Fracture Strength of Indented Soda-Lime Glass," J. Am. Ceram. Soc., **68**

[11] 632-36 (1985).

27. C.R. Kurkjian, "Mechanical Stability of Oxide Glasses," J. Non-Cryst. Sol., **102,** 71-81 (1988).

28. J.T. Hagan, "Cone Cracks around Vickers Indentations in Fused Silica Glass," J. Mat. Sci. **14**, 462-66 (1979).

29. S.R. Choi, J.E. Ritter, Jr., and K. Jakus, "Failure of Glass with Subthreshold flaws," J. Am. Ceram. Soc., **73** [2] 268-74 (1990).

30. D.B. Marshall and B.R. Lawn, "Flaw Characteristics in Dynamic Fatigue: The Influence of Residual Contact Stresses," J. Am. Ceram. Soc., **63** [9-10] 532-536 (1980).

Table I. Summary of Fatigue Data for Silica-Clad fiber and Bulk Silica Glass.

Silica form	Surface Condition	Strength (kpsi)	n			RH (%) *	comments	ref.
			crack velocity	dynamic fatigue	static fatigue			
fiber	as-drawn	700		15.9	14.3	97	tension	7
fiber	as-drawn	800		25.5		amb.	tension	8
fiber	as-drawn	800		22.5		water	tension	8
fiber	as-drawn	700		22		water	tension	9
fiber	as-drawn	700		21.1	19.7	45	tension	10
fiber	as-drawn	700		22.1		water	bending	11
fiber	as-drawn	530		29.9		water	bending	11
fiber	as-drawn	600		20.8		100	tension	11
fiber	as-drawn	420		25.5		100	tension	11
fiber	as-drawn	700		21.7		amb.	tension	12
fiber	abraded	180		22.1	19.8	50	tension	13
fiber	abraded	150		22.3	20.2	45	tension	10
fiber	abraded	80		26	22.2	45	tension	10
fiber	abraded	50		33.7		45	tension	10
fiber	abraded	50			35.6	water	tension	14
fiber	abraded	50		42.6		60	tension	14
fiber	abraded	100		20.5		water	tension	8
fiber	abraded	100		25.5		amb.	tension	8
fiber	indented	70		19		water	tension	15
fiber	indented	100		20		amb.	sub-threshold	16
bulk	indented	10		30.7		water	sub-threshold	15
bulk	abraded	14		37.8		water		17
bulk	abraded	10		45		water		18
bulk	compact tension		42			water		14
bulk	DCB		36			100		19
bulk	compact tension		36-44			20 to water	24 to 70 °C	20

* test temperatures 20 - 25 °C except where otherwise noted.

Figure 1. Failure Probability Predictions for Optical Fiber in Bending.

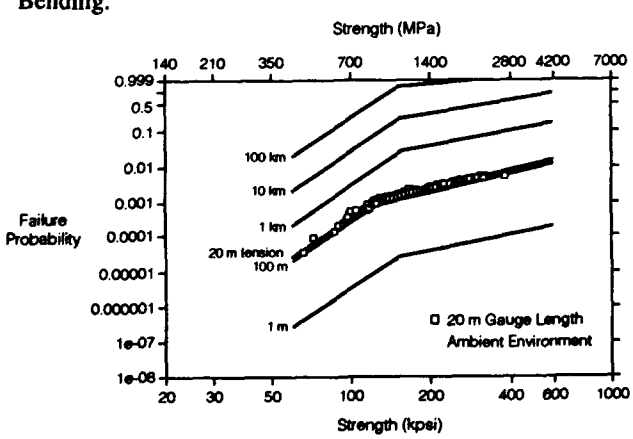


Figure 2. Effect of Aging on the Strength of Optical Fiber. From Ref. 2.

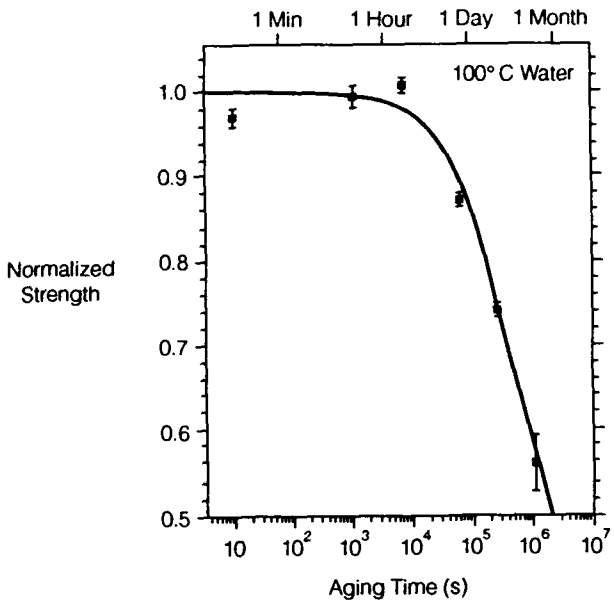


Figure 3. Fracture Strength of High Silica Glass as a Function of Aging Time in 90°C Silicic Acid. From Ref. 5.

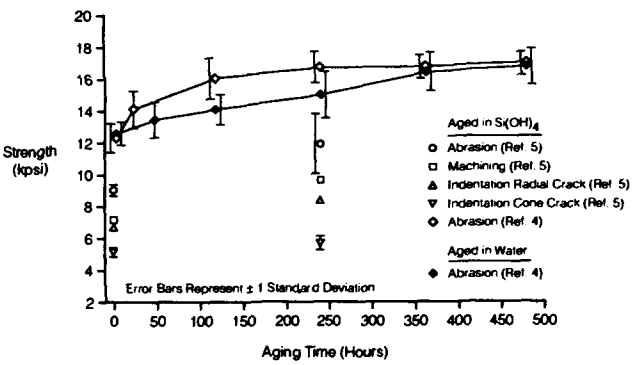


Figure 4. Fatigue Susceptibility n of Silica. References and Data in Table I.

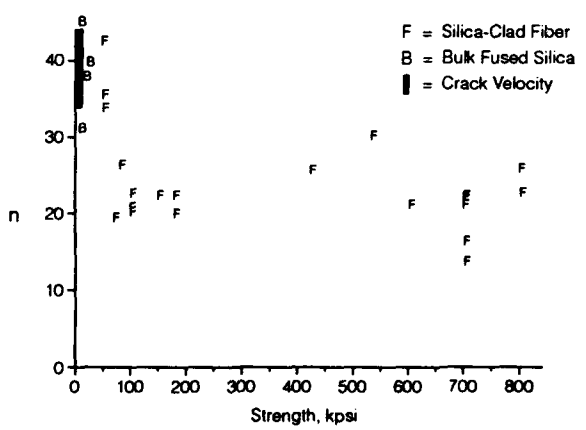


Figure 5. Strength of Indented Silica-Clad fibers and Bulk Silica Glass.

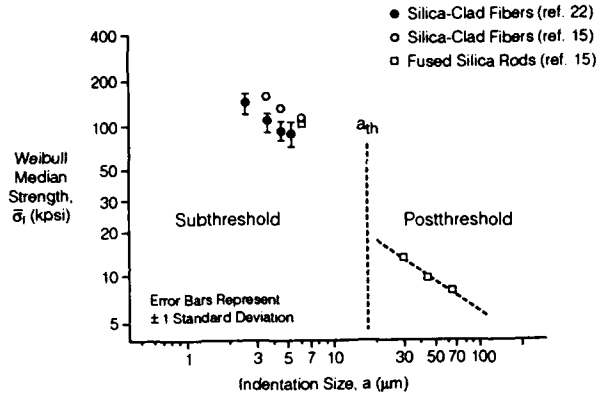


Figure 6. Plot of n for Indentation Flaws in Silica.

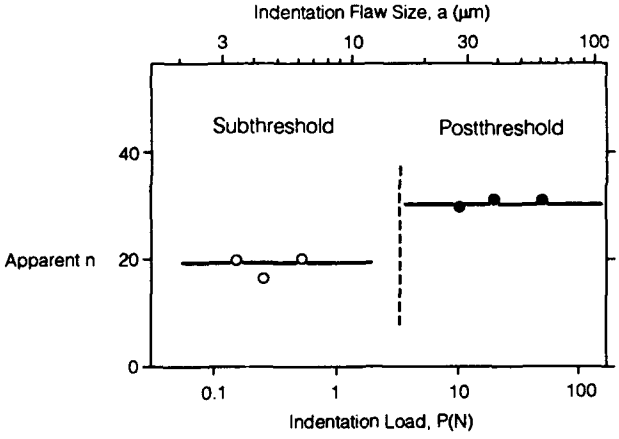


Figure 7. Strength of Abraded Silica-Clad Fibers.

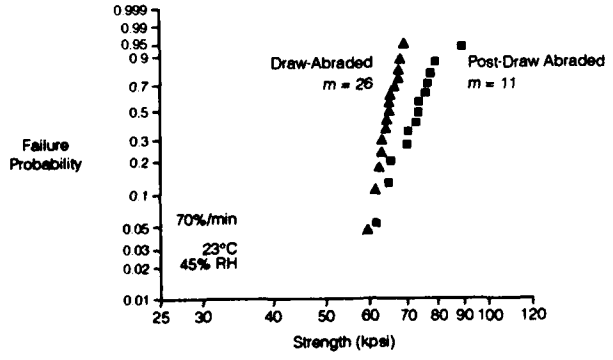


Figure 8. Strength of Abraded Silica-Clad Fiber as a Function of Aging Time in 80°C Water.

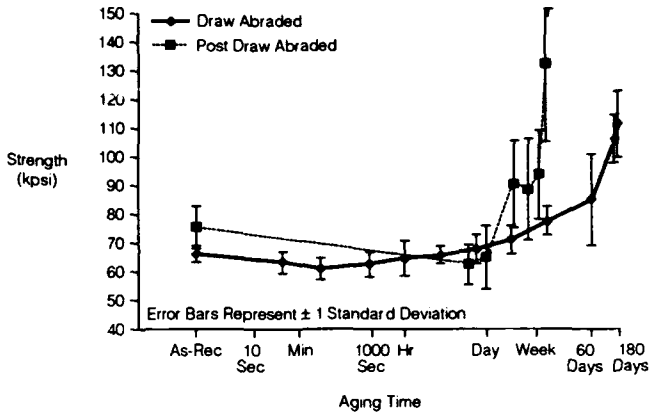


Figure 9. Strength of Abraded Silica-Clad Fibers for Fatigue Testing.

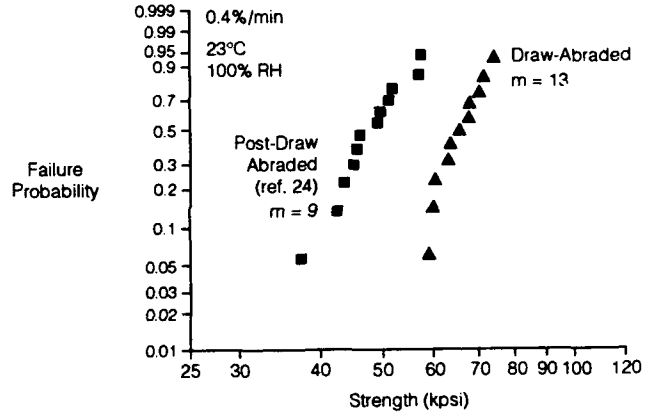


Figure 10. Dynamic Fatigue of Post-Draw Abraded Silica-Clad Fiber.

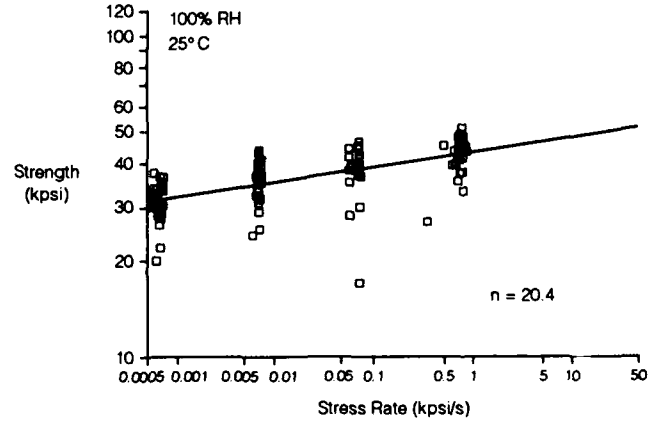


Figure 11. Fatigue Susceptibility n of Abraded Silica-Clad Fibers.

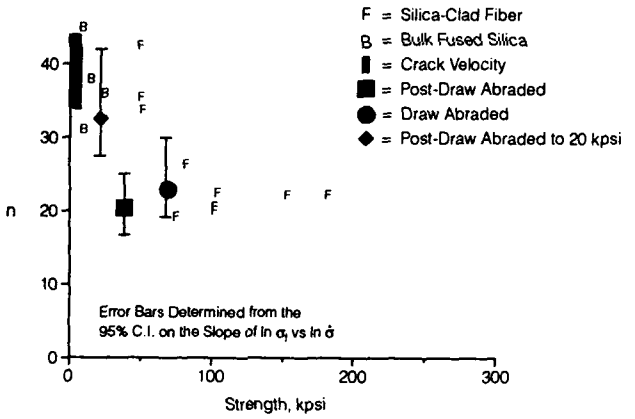


Figure 12. Effect of Aging in 80°C Water on n of Draw-Abraded Silica-Clad Fibers.





G. Scott Glaesemann, SP-DV-01-8 Corning Inc., Corning, N.Y., 14831. Glaesemann is a senior development engineer responsible for the optical fiber strength laboratory at Corning. His research focuses on the mechanical properties and reliability of optical fiber. He has been employed by Corning for six years at the Sullivan Park technology facility. Glaesemann received his master's degree and Ph.D. in mechanical engineering from the University of Massachusetts and a B.S. in mechanical engineering from North Dakota State University.

Fiber Reliability Study of Field Aged Optical Cables

H. H. Yuce, T. Wei**, R. Estes*, C. J. Wieczorek*,*
*B. T. Devlin**, J. P. Kilmer*, and J. P. Varachi, Jr.**

** Bellcore, Morristown, NJ*
*** GTE Laboratories Inc., Waltham, MA*

ABSTRACT

The effects of aging on the mechanical properties of optical fiber have been widely reported [1-8]. Both strength degradation and changes in coating properties have been observed after optical fiber has been aged in water or a humid environment at elevated temperatures [2-8]. Although fiber aging has not been implicated in many field failures, one particular case of fiber failure was reported [9] that was attributed to exposing an unprotected cable reel to extreme environmental conditions for almost five years. This failure prompted a broader investigation of field aged optical cable (e.g., aerial, closures, pedestals, etc.). In this paper, we report the results of an investigation of the mechanical properties of field-aged optical cable. More than twenty cable samples, of ages 2 to 9 years, were investigated. These included samples from unprotected cable reels, aerial cables, pedestals, and aerial splice closures. Mechanical and physical measurements on the fiber specimens showed no significant mechanical degradation. In the worst case, the fiber strength in an aerial splice closure (seven years old) was measured to be about 18% lower than that of unaged cable samples. Some correlation between coating strip force and fiber strength was observed. Atomic force microscopy examination of the fiber samples showed that fiber cables exposed to typical field environments are not subjected to extreme reliability risk except in isolated cases where severe environmental conditions (e.g., steam damage) or highly undesirable coating properties are encountered.

1. INTRODUCTION

There are four possible failure mechanisms that may affect the performance of a cabled fiber over time. First, the attenuation of fibers may increase due to the presence of molecular hydrogen [10-11] or exposure to high doses of ionizing radiation. Second, fatigue (time delayed failure under constant or varying load) may cause fiber breaks to occur years after the cable is installed [12]. To minimize such breaks, fibers must be screened at sufficiently high proof test levels to eliminate low strength flaws. The cable structure is generally designed to maintain the fibers tension free in the installed cable and to maintain a sufficient radius of curvature to minimize bending stresses. Consequently, this failure mechanism is unlikely to occur with properly designed cable structures. The third failure mechanism is thermal aging of the cable structure and fiber coating, which can lead to microbending-induced attenuation increases [13]. Cable materials, therefore, have to be selected and the structure optimized such that dimensional cable changes expected over time do not increase fiber loss. In the final failure mechanism, exposure of a fiber in the cable to a high temperature/high humidity conditions in the absence of stress can reduce its strength [9]. This is known as *zero-stress aging*.

The underlying mechanism of glass failure under static fatigue conditions has been well documented [14]. But the reasons for loss of strength of glass fibers under zero-stress aging are still under study. Proposed degradation mechanisms include absorption of water molecules on the surface, which promote crack growth during subsequent stressing [15] and corrosive reactions leading to surface flaws [1-8], which can act as nuclei for cracks. The surface reactivity of silica-based glasses in different environments determines the ultimate strength of these materials because of its effect on crack tip growth.

The effect of low or zero-stress aging of optical fibers is of considerable importance in cables or in splice cases because fibers can encounter high humidity and high temperatures (e.g., in pedestals and aerial cables) or other chemical species such as water (e.g., in manholes) which can degrade fiber strength. These aged fibers may then be subsequently stressed during routine maintenance or other craft activity. The effect of zero-stress aging on the mechanical reliability of optical fibers is therefore an important consideration in any cable installation.

In this study, we investigate the mechanical properties of fiber specimens taken from aged optical cable samples to assess the risk of exposing optical cables to typical field environments. More than twenty cable samples of ages 2-9 years were collected for this study. These included unprotected spare cables from cable yards, cable sections removed from aerial cables and pedestal installations, and fiber samples from seven aerial splice closures. The study included the full mix of cable structures (buffer tube, slotted core, and core tube) and fiber designs. The fiber samples collected from the field-exposed splice closures/cables and pedesdals were studied to determine the effect of the environment on long-term mechanical/physical reliability of fibers (fiber strength, fatigue, and fiber coating properties). The mechanical properties of the aged fibers were compared with those of unaged fibers from the same vendor and vintage whenever possible.

2. MECHANICAL CHARACTERISTICS OF FIELD AGED FIBERS

2.1 Experimental

A computer controlled, two-point bending apparatus [16,17] was used to determine the strength and dynamic fatigue behavior of unaged and aged fibers. The test apparatus consists of two parallel platens, one fixed and one moving, between which a fiber loop is bent until it breaks, as shown in Figure 1. The moving platen is driven by a computer controlled stepper motor; the rate of closure can be varied so that the maximum stress in the fiber loop changes at a constant rate. Fiber failure is sensed by an acoustic transducer which signals the computer to stop the moving platen and record the platen separation at failure. The stress at failure is calculated from the platen separation, the elastic modulus of the glass, and the dimensions of the fiber.

Because the effective gage length is small [18], the probability of stressing a fiber section containing a large flaw is also small, so the test results tend to be uniform and unimodal. Bending tests were conducted at a range of stress rates (60, 6, 0.6, and 0.06 MPa/second) so that the dynamic fatigue behavior could be characterized. The experiments were conducted in a laboratory environment of 23 °C and 50% relative humidity (RH). For each case and stress rate, 21 samples were tested.

To determine the coating integrity after field aging, the coating strip force was measured. The force required to strip the coating was measured using a commercial stripping tool mounted on a screw-driven universal tensile testing machine. The gage length of the stripped section was 1.2 inches and the test was conducted at the rate of 20 in/min. The experiments were conducted in a laboratory environment of 23 °C and 50% RH. We tested 11 fibers for each set of samples.

A commercial atomic force microscope (AFM) was used to examine the surfaces of the aged and unaged fibers at magnifications up to several million times. The AFM allowed us to make direct observations of any surface imperfection caused by aging. The AFM has a very sharp tip, a few atoms wide at the end, attached to a micro-cantilever arm (Figure 2) that is on the order of 100-200 microns long. The tip is brought into contact with a sample and is scanned across the surface, usually in a raster pattern. The deflection of the cantilever is monitored as the tip is scanned. The deflection signal is used in a feedback loop to control the tip heights. In our unit, the scanning is accomplished with a piezoelectric tube scanner. The data can be acquired by measuring the cantilever deflection signal as the tip is scanned, or by adjusting the height of the tip using feedback to maintain a constant cantilever deflection signal. In our AFM, the deflection signal is produced by focusing the output of a laser diode on a spot on the back side of the cantilever and measuring the reflected light from this spot with a photodetector. The polymer coating on the fiber was removed before AFM examination by dipping the fiber briefly in hot (200° C) sulfuric acid and rinsing in distilled water. In order to insure representative results, a number of samples from each cable or splice closure were used. Each sample was also examined with at least two different AFM tips, minimizing the possibility of misinterpreting tip-induced artifacts in the images.

2.2 Results and Discussions

2.2.1 Dynamic [Two-Point Bending] Strength

The strength data for two-point bending plotted in Figure 3 show a good fit to a Weibull distribution of the form:

$$F = 1 - e^{-\left[\frac{\sigma}{\sigma_0}\right]^{m_d}} \qquad (1)$$

In this equation, F is the cumulative probability of failure at a stress less than or equal to σ; σ_0 and m_d are empirical distribution parameters. The values of the Weibull exponent m_d and the median strength (F=0.5) for two-point bending tests are summarized in Table 1. No extreme degradation was observed among the field aged samples. The worst degradation occurred in splice closure # 7 and cable # 7, in which the fiber strengths were about 18% and 14%, respectively, lower than those of unaged samples. We also observed lower fiber strength in splice closures than in cables. This is attributed to the higher temperatures and humidities that closures may experience. For comparative purposes, the results from earlier studies [9] (i.e., the unprotected cable reel and steam exposed cable) are also included in Table 1. Clearly, the decrease in fiber strength appears to be correlated to the severity of environmental exposure and cables that are exposed to higher temperatures and humidities obviously influence the trends of strength reduction.

2.2.2 Dynamic (Two-Point Bending) Fatigue

In Table 2, dynamic fatigue (two-point bending) results for fiber samples taken from different cable samples are summarized. Assuming that the rate of growth of flaws in the presence of stress depends upon the stress intensity factor at the tip of the flaws raised to a power n, then it can be shown that the failure stress is related to the rate of stressing $\dot{\sigma}$ by:

$$\sigma = B\dot{\sigma}^{\frac{1}{n_d+1}} \qquad (2)$$

where n_d is a "fatigue parameter", i.e., the crack growth exponent associated with the power law dependence of the crack growth rate, and B is an experimental parameter. The effects of aging conditions on the values of n_d are well documented [3,7]. In this study, no significant change in the fatigue parameter was observed in the field aged samples.

2.2.3 Coating Behavior

The coating stripping test was performed on fiber samples from each layer of the cable. The strip force results are summarized in Table 3 which shows a general decrease in strip force in field-aged samples. We observed some correlation between coating adhesion and fiber strength (see Tables 1 and 3). The worst degradation again occurred in splice case # 7 and cable # 7. In this sample there was almost no coating adhesion to the glass making it difficult for the fiber to be handled by a craft person. We also observed lower strip force in splice closures than in cables. This degradation is attributed to higher temperatures and moisture that closures may experience.

2.2.4 Glass Behavior

A series of AFM images of some of the aged and unaged fibers are shown in Figures 4-7. Figure 4 shows a typical roughness observed on the surface of unaged fibers. The surface of unaged fibers can be characterized as having pits ~0.1-1.5 nm[1] across with a depth of ~0.1-2 nm. In contrast, the surface of the steam aged fibers (Figure 7) showed a corrugation amplitude of ~100-130 nm with features 100-200 nm across. The relative surface roughness can be put on a more quantitative basis, as given in Table 4, by measuring the maximum value of flaw depth obtained from the AFM.

Figures 5 and 6 show surface profiles of the fibers aged in splice closure-1 and splice closure-7. The median strength values for fibers from both cables and aerial closures are shown in Figure 8 as a function of the depth of surface roughness obtained from the AFM. This figure shows that the degree of surface roughness of the aged fibers is consistent with the strength results of Table 1, as expected [4-8]. The roughness of the fibers increased with increasing exposure to the hostile environment, with the most dramatic roughening occurring in the fiber samples that were aged in high temperatures and moisture (i.e, steam).

[1] 1 nm = 10^{-7} cm = 3.94×10^{-8} in.

Table 1 - Summary of Strength [Two-Point Bending] Test

SAMPLES FROM	AGING TIME (yrs)	UNAGED σ (ksi)	UNAGED m_d	AGED σ (ksi)	AGED m_d	D^2 %
Aerial Cable-1	7	673	69	645	57	4
Aerial Splice Closure-1	7	673	69	616	48	8
Aerial Cable-2	7	685	66	651	47	5
Splice Closure-2	7	685	66	635	44	7
Aerial Cable-3	7	N/A[3]	-	672	57	-
Aerial Splice Closure-3	7	-	-	655	46	-
Aerial Cable-4	7	669	62	641	54	4
Aerial Splice Closure-4	7	669	62	627	48	6
Aerial Cable-5	7	611	58	589	46	4
Aerial Splice Closure-5	7	611	58	576	40	6
Aerial Cable-6	7	635	54	587	51	8
Aerial Splice Closure-6	7	635	54	584	40	8
Aerial Cable-7	7	570	78	502	34	14
Aerial Splice Closure-7	7	570	78	484	25	18
Aerial Cable-8	5	621	69	606	61	2
Buried Cable-1	9	678	61	657	55	3
Buried Cable-2	3	710	78	702	74	1
Pedestal-1	2	724	82	709	75	2
Pedestal-2	3	710	78	699	71	2
Submarine Cable	3	725	79	719	70	1
Splice Closure from manhole[4]	7	645	56	550	39	14
Unprotected Cable Reel[5]	5	685	66	326	14	52
Steam Exposed Cable[5]	2	685	66	102	3	85

[2] Strength degradation of the field aged fibers [relative compared to unaged fiber]
[3] Fiber samples from the same vintage vendor were not available.
[4] Splice case was filled with water. Exact date of water entrance is not known.
[5] From reference 9.

Table 2 - Summary of Dynamic Fatigue [Two-Point Bending] Tests

Samples From	n_d [Unaged]	n_d [Aged]
Aerial Cable-1	21	21
Aerial Cable-2	19	20
Aerial Cable-3	N/A	22
Aerial Cable-4	20	20
Aerial Cable-5	18	18
Aerial Cable-6	20	22
Aerial Cable-7	21	21
Aerial Cable-8	19	19
Buried Cable-1	19	19
Buried Cable-2	19	19
Pedestal-1	21	21
Pedestal-2	20	19
Submarine Cable	22	21
Splice Closure from manhole	19	19
Unprotected Cable Reel	19	23
Steam Exposed Cable	19	25

Table 3 - Summary of Median Coating Strip Force

Samples From	Strip Force [Unaged], lb_f	Strip Force [Aged], lb_f
Aerial Cable-1	1.06	0.95
Aerial Splice Closure-1	1.06	0.81
Aerial Cable-2	1.16	0.88
Splice Closure-2	1.16	0.91
Aerial Cable-3	N/A	1.23
Aerial Splice Closure-3	N/A	1.06
Aerial Cable-4	1.35	0.65
Aerial Splice Closure-4	1.35	0.66
Aerial Cable-5	1.23	0.78
Aerial Splice Closure-5	1.23	0.72
Aerial Cable-6	1.08	0.73
Aerial Splice Closure-6	1.08	0.60
Aerial Cable-7	0.90	0.12[6]
Aerial Splice Closure-7	0.90	0.08
Aerial Cable-8	0.95	0.91
Buried Cable-1	0.70	0.45
Buried Cable-2	0.83	0.66
Pedestal-1	1.10	0.91
Pedestal-2	0.85	0.69
Submarine Cable	0.77	0.70
Splice Closure from manhole	0.89	0.38
Unprotected Cable Reel	1.08	0.62
Steam Exposed Cable	1.08	-

Table 4 - Summary of Maximum Value of Surface Roughness Height Obtained from the AFM Measurements

Samples From	Median Roughness Height [Unaged], nm	Median Roughness Height [Aged], nm
Aerial Cable-1	1.1	1.8
Aerial Splice Closure-1	1.1	2.2
Aerial Cable-2	1.4	2.9
Splice Closure-2	1.4	3.3
Aerial Cable-3	N/A	3.1
Aerial Splice Closure-3	N/A	3.4
Aerial Cable-4	1.2	3.9
Aerial Splice Closure-4	1.2	4.1
Aerial Cable-5	1.7	5.7
Aerial Splice Closure-5	1.7	5.8
Aerial Cable-6	1.5	5.2
Aerial Splice Closure-6	1.5	5.9
Aerial Cable-7	1.9	10.1
Aerial Splice Closure-7	1.9	11.8
Aerial Cable-8	1.7	2.5
Buried Cable-1	1.3	2.7
Buried Cable-2	1.0	1.2
Pedestal-1	1.0	1.2
Pedestal-2	0.9	1.1
Submarine Cable	0.9	1.1
Splice Closure from manhole	1.8	6.7
Unprotected Cable Reel	1.4	59.
Steam Exposed Cable	1.4	139.0

[6] This does not meet Bellcore TR-20 requirements.

3. FIBER-TEMPERATURE ENVIRONMENT

Because fiber aging is accelerated by severe environments, some knowledge of the expected field environment is necessary to estimate the long-term reliability of fiber. To gauge the expected temperature environment, we developed a simple thermal model of an aerial cable in the field. This model considered the effects of solar heat load on the cable, wind-induced heat convection to the ambient air, and long-wavelength radiation to the low atmosphere. Weather data used in the model were the ASHRAE (American Society of Heating, Refrigeration, and Air-Conditioning Engineers) WYEC (Weather Year for Energy Calculations) data [19,20], which consists of 8,760 hours (one year) of real weather data for each of 51 locations in North America. A WYEC "year" for a given location is a composite of twelve separate months chosen from thirty years (1951 to 1980) of data from the US Weather Service. The individual months were selected because of their closeness to the long-term means of both ambient air temperature and insolation (solar radiation per unit horizontal surface). Thus, the WYEC data are a good representation of both the average and the coincidence of weather conditions.

Normal maximum annual cable temperatures estimated from the model are shown in Fig. 9. In the contiguous United States, these range from 44 °C (Seattle, WA) to 68 °C (Las Vegas, NV). The maximum temperature depends on the size of the cable, and Fig. 9 was generated assuming a cable diameter of 1-3/8 inches. To estimate temperatures in aerial splice closures, an "equivalent" diameter of 8 inches was input to the model. Maximum temperatures generated for this diameter were about 4-1/2 °C higher than those shown in Fig. 9. Since aging is accelerated by temperature, these higher temperatures may be a factor in the lower fiber strength observed in splice closures.

Note that, because they were generated from the WYEC data, the modeled "maximum" cable temperatures represent *average* rather than extreme values. Extreme (maximum recorded) ambient temperatures in the United States range from 3 °C to 16 °C higher than normal maximum values [21]; however, the largest deviations from the normal maximums appear to occur where the normals are low. If, as a first approximation, it is assumed that maximum cable temperature tracks maximum ambient temperature, then the extreme maximum temperature for a 1-3/8 inch aerial cable could range 58 °C (Tallahassee, FL) to 76 °C (Phoenix, AZ). These temperatures should not represent an extreme reliability risk to the aerial cable.

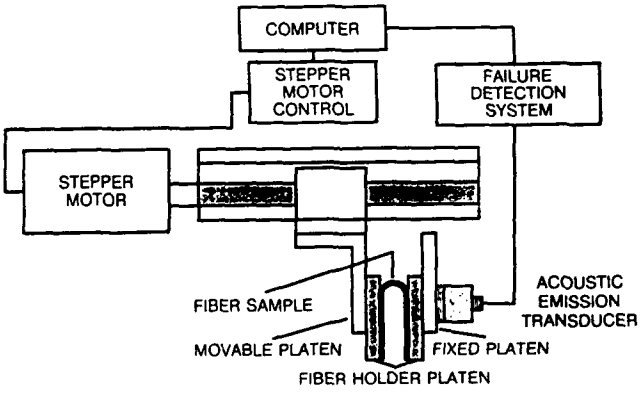


Figure 1 - Two-point fiber strength testing apparatus.

4. CONCLUSIONS

In summary, we have compared the mechanical and morphological properties of field-aged fibers and unaged fibers of the same vintage. Fibers in this study did not experience the extreme aging that was observed in an earlier study of fibers from the outside layer of the unprotected cable reel [9]. The difference in aging can be attributed to differences in fiber coating chemistry [8], cable core materials (e.g., filling compound) and construction, and local environment. Based on this study, it is concluded that fiber cables exposed to typical field environments are not subjected to extreme reliability risk except in isolated cases where severe environmental conditions (e.g. steam damage) or highly undesirable coating properties are encountered.

REFERENCES

1. J. T. Krause, *J Non-Cryst. Solids* **38-39**, 497 (1980).
2. M. J. Matthewson, C.J. Kurkjian, *J Amer Ceram Soc* **71**, 171 (1988).
3. H.H. Yuce et. al., *Proc. SPIE 1174*, 279 (1989).
4. H. H. Yuce et al, OFC '90 Postdeadline Paper, Paper PD14 (1990).
5. H. H. Yuce et al, *Trans of Am. Ceram. Soc.*, Glass Fall Meeting, Orlando, FL., (November, 1990).
6. R. S. Robinson and H.H. Yuce, *J. Am. Ceram. Soc.*, **74** [4] 814(1991).
7. M. T. Kennedy et al, *Proc. SPIE 1580* , 152 (1991).
8. H. H. Yuce et al, OFC '92 Postdeadline Paper, Paper PD21 (1992).
9. H. H. Yuce et al, *Proc. 40th IWCS,* 700 (1991).
10. W. T. Anderson et al, *Proc. 37th IWCS,* 188 (1988).
11. W. T. Anderson et al, *Proc. 38th IWCS,* 675 (1989).
12. H. H. Yuce et al, *Proc. 38th IWCS,* 611(1989).
13. W. T. Anderson, Bellcore, Personal Communications.
14. T. A. Michalske, S. W. Freimen, *J. Am. Ceram. Soc.*, **66** *[4] 284(1983).*
15. B.K. Tariyal, D. Kalish, Glass Div., Fall Mtg. Am. Ceram. Soc., Paper 8-CG-77F (1977).
16. P. W. France et. al., *J Mater Sci,* **15**, 825 (1980).
17. H. H. Yuce, et.al., *Proc. Seventh Int. Conf. on Integrated Optics* **2** 44(1989).
18. M. J. Matthewson and C. R. Kurkjian, *J. Am. Ceram. Soc.*, **69** [11] 815(1986).
19. L. W. Crow, *ASHRAE Journal* 23, 37 (October 1981).
20. L. W. Crow, *ASHRAE Journal* 26, 42 (June 1984).
21. *Weather Atlas of the United States*, Detroit, MI: Gale Research Co. (1975).

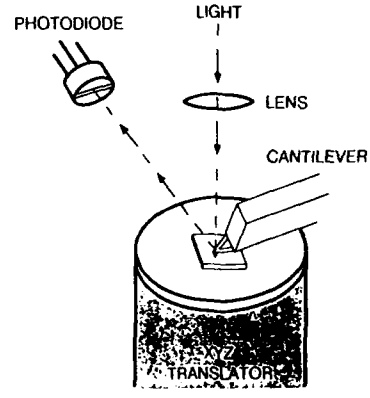


Figure 2 - Schematic of atomic force microscope.

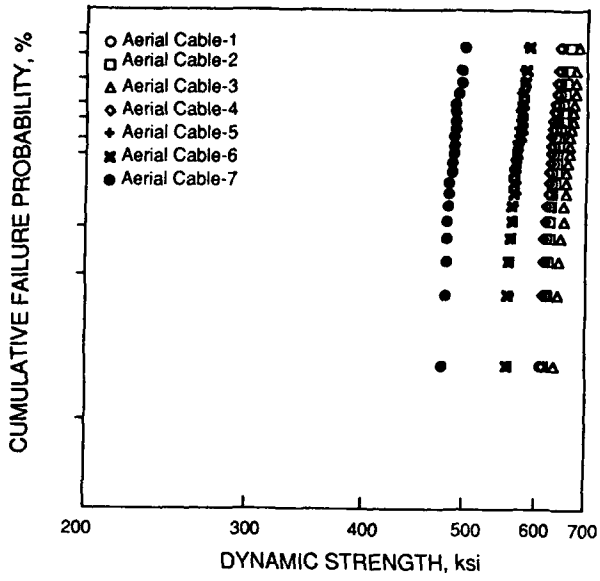


Figure 3 - Two-point bending Weibull strength distribution.

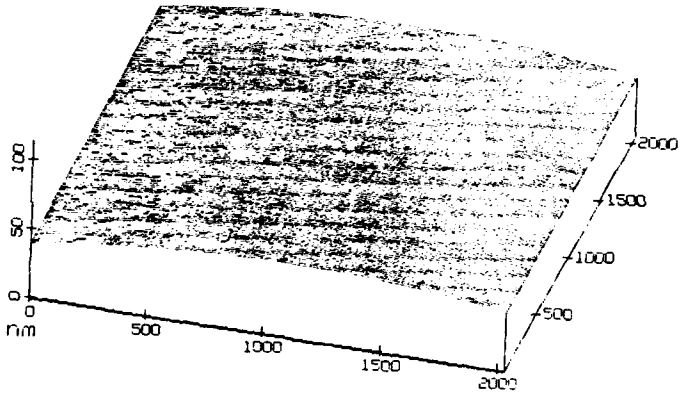


Figure 4 - Unfiltered AFM image of a typical glass surface of a typical unaged fiber [the same vintage of fibers from aerial cable/closure # 1]

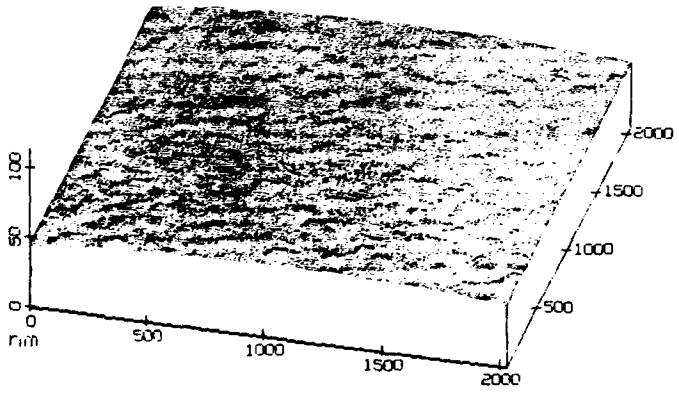


Figure 5 - Unfiltered AFM image of a typical glass surface of fibers inside aerial splice closure # 1. Surface roughness is about 3-5 nm, showing slight aging degradation after seven years.

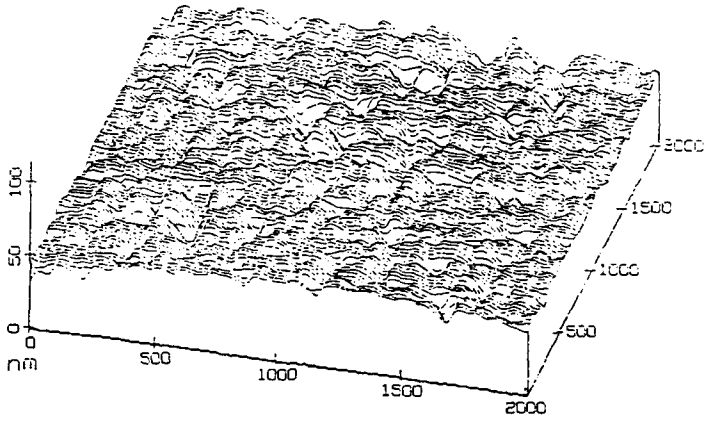


Figure 6 - Unfiltered AFM image of a typical glass surface of fibers inside aerial splice closure # 7. Surface roughness is about 10-12 nm, showing aging degradation after seven years.

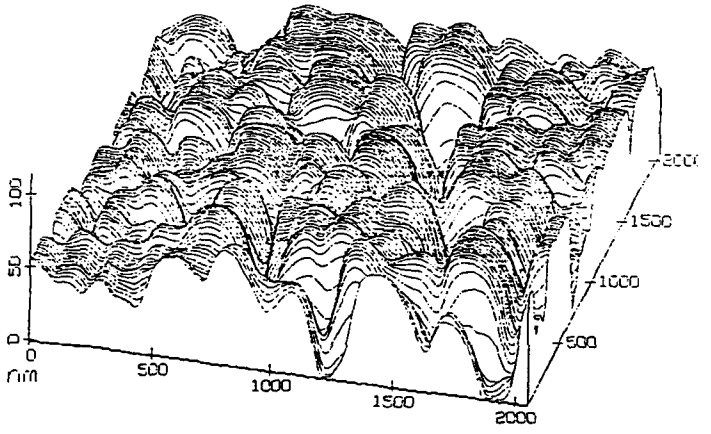


Figure 7 - Unfiltered AFM image of the glass surface of fibers aged in a cable after two years of hot steam exposure. Surface roughness is about 100-140 nm, showing severe aging degradation.

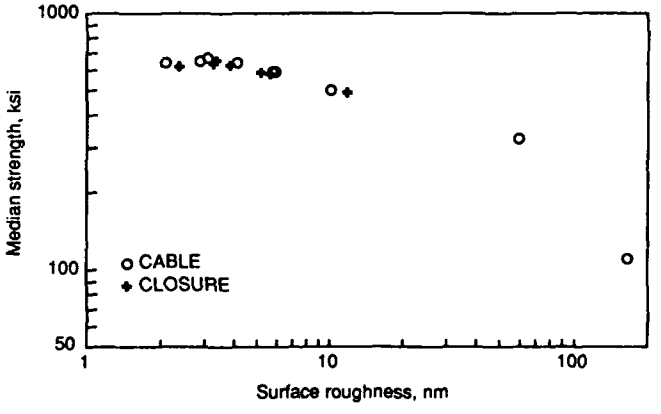


Figure 8 - Strength versus surface roughness.

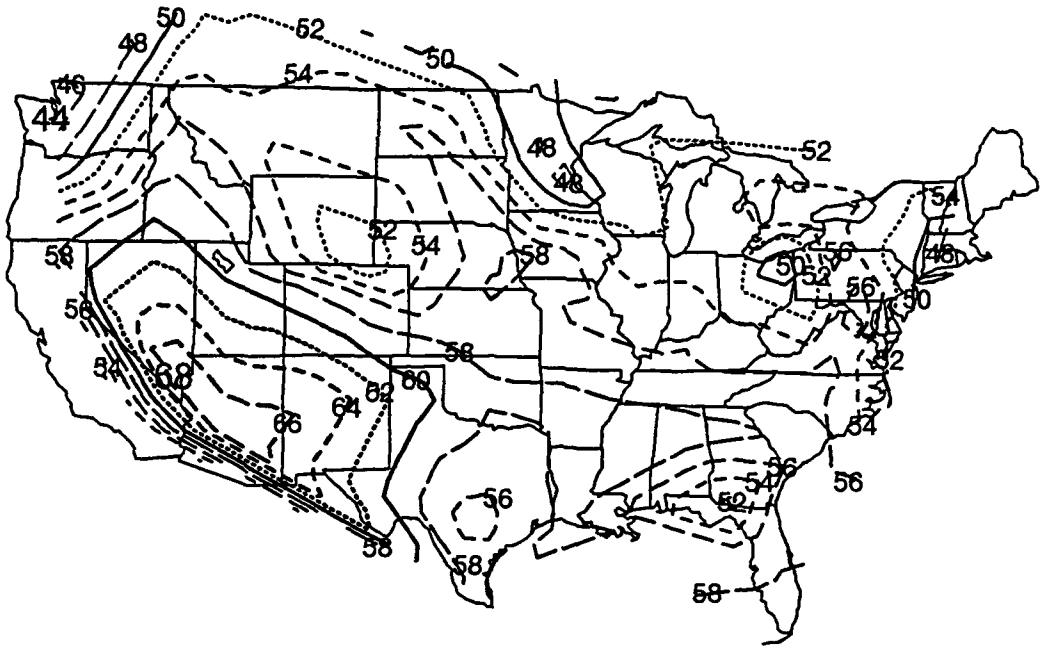


Figure 9 - Expected annual-maximum cable temperature. (Temperatures in degree C)





Hakan H. Yuce is a member of technical staff in the "Fiber Distribution and Reliability Research" group at Bellcore. He leads a research program dealing with long-term mechanical reliability of optical fibers and interconnections. Hakan provides technical input and support to organizations responsible for generic requirements and responds to clients' immediate needs related to consultation on reliability and field failures. He also plays a active role in the establishment of U.S. and international standards within TIA and IEC regarding optical fiber test procedures to assure reliability. Hakan has a B.S. degree in *Mechanical Engineering from Technical University* of Istanbul, an M.S. in Mechanical Engineering from M.I.T.and a Ph.D degree in Mechanical Engineering and Material Science from Stanford University.

T. (Mike) Wei is a Research Supervisor - Network Quality and Reliability at GTE Laboratories Incorporated, Waltham, MA, responsible for operations support and component reliability activities. He received the B.S. degree in physics from National Tsing Hua University, Hsinchu, Taiwan; and the Ph.D. degree in physics from University of Pennsylvania, USA. He is a member of the APS, IEEE, OSA, and SPIE. He has over 50 technical publications and holds two U.S. patents.



Renee Estes received a B.S.M.E and M.S.M.E degree from New Mexico State University and a Ph.D. degree in mechanical engineering from Columbia University. She has worked in the areas of thermal control and energy systems at Bell Laboratories, Singer Corporate Research & Development Labs, and Lockheed Electronics Company. Since 1984, she has been with Bellcore, where she is currently a Member of Technical Staff in the Energy Systems Technology Research Group.



Casey J. Wieczorek is a member of the Optical Cable group in Bellcore, Morristown, NJ. He joined western Electric in 1967 and worked on various cable designs and manufacturing processes. he is currently responsible for the development of generic requirements and test procedures for optical cables. He holds a B.S degree in Mechanical Engineering from Fairleigh Dickinson university and did graduate work at Stevens Institute of Technology.



Dr. Joyce P. Kilmer received his Ph.D. in Electrical Engineering from the University of Florida and joined Bellcore as a Member Technical Staff of the Optical Cables District in the Fiber Optic Technology Division in 1984. In 1988, he was temporarily reassigned to Fiber Optic Systems District to study the effects of reflections on fiber optic system performance. In 1989, he was promoted to District Manager of the Optical Connector, Splicing and Closures District. In 1990, he was reassigned to District Manager of the Optical Cables & Distribution Terminals/Closures District. In this capacity he is responsible for writing generic requirements, performing product and post-mortem analyses, and developing long term reliability testing of optical fiber, optical fiber cable, and distribution terminals for Fiber-in-the-Loop (FITL).



John Varachi is Director of Fiber Distribution and Reliability Research, at Bellcore. He is responsible for research in the areas of optical fiber and fiber-optic component reliability and new low-cost installation methods for fiber-in-the-loop deployment. He is an active participant in industry standards related to fiber-optic component reliability at the national and international level within TIA and IEC. Previously, John was a Member of Technical Staff in the Loop Transmission Division at Bell Laboratories where he was involved in systems engineering and physical design. John received Bachelor of Science and Master of Science degrees in Mechanical Engineering from Fairleigh Dickinson University and The Polytechnic Institute of New York and is a registered Professional Engineer in the State of New Jersey.

PREDICTING THE LIFETIME OF OPTICAL FIBRE CABLES USING APPLIED STRESS HISTORIES AND RELIABILITY MODELS

Mr K G Hodge & Mr C S Pegge, BICC Cables Ltd.

Dr G S Glaesemann & Mr M Hopiavuori, Corning Incorporated.

Summary

The mechanical reliability of optical fibres is better understood and intrinsically improved as a result of the advancements in fibre production techniques. The industry is taking advantage of the opportunities this presents. In particular, the traditional approach adopted in the form of 'fibre strain free' optical cables has been complemented by the development of higher fibre packing density designs. In these 'tight' designs applied stresses on the cable are transmitted directly to the fibre and it is necessary for manufacturers and operators alike to be assured of the installed system reliability. This paper discusses the relationship between realised fibre strains in cable, required lifetime, and reliability models in association with cabling the dedicated fibre solution to the distribution network.

Introduction

The use of optical fibre technology in the distribution network is driving the development of new generations of cable products. Dedicated fibre network topologies especially in urban localities will require a high channel density. One solution is the tight cable design which offers a high fibre count in a minimum diameter. The traditional 'zero fibre strain' loose tube designs, such as those described by Farmer et al.[1], impart only bending stresses to the fibre. Conversely, the newer 'tight' designs transfer stresses directly to the fibre in the cable structure. As fibre under strain represents a potential reliability hazard it is necessary to build robust models of the lifetime under such circumstances. We present here a methodology for approaching this crucial issue based on a fibre reliability model[2&3]. Alternative reliability models are being considered and it may well be necessary before settling on a definitive model to test the robustness and conservatism of these other models.

In this paper the strain history of a fibre, in a 'tight' design product, linking exchange to subscriber, is modelled using a typical cable system as an example. Developed calculus enables comparative tensile modelling for a variety of applied stresses, affording the use of tensile strength test data for lifetime prediction. A method for selecting a suitable level of screened fibre for specific applications is described. Finally, the theoretical mechanical reliability of the fibre in the total system and each dedicated link is calculated[4] and the implications to cable design discussed.

Reliability Models

Minimum Strength Design

The minimum strength of a fibre under fatigue conditions after proof screening can be expressed as a function of its screen level, as for example has been reported by Glaesemann & Gulati[3]. In this model fibre failure is interpreted as a 1% growth in flaw size. A time dependent crack growth parameter is derived from normalising the power law fit to the standard crack growth kinetics equation. Finally, a 'safe' boundary condition is realised by accounting for post proof test strength degradation in the fatigue condition.

$$\sigma_o = 0.7\,\sigma_p \left[0.35 \left(\frac{n-2}{n+1}\right) \frac{V_o}{a_o} \frac{\sigma_p}{\dot{\sigma}} \right]^{\frac{1}{n}} \quad (1)$$

Where, for the case where $\frac{a}{a_o} = 1.01$ when $\sigma_a = \sigma_o$:

$$\frac{V_o}{a_o} = \frac{\left[1 - 1.01^{-\left(\frac{n-2}{2}\right)} \right]}{\left(\frac{n}{2} - 1\right) t}$$

: σ_o = safe stress

σ_p = proof stress

σ_a = applied stress

$\dot{\sigma}$ = stress rate

$\frac{V_o}{a_o}$ = crack growth parameter

t = time

n	=	stress corrosion parameter
a	=	crack size
a_o	=	Initial crack size

Hence for a given 'n' value the model allows graphical representation of 'safe' strain vs strain duration. Figure 1 shows the tensile strains which silica fibre (n=20) screened to various levels can sustain safely over time. Calculations used a nominal stress rate of 300 kpsi/s consistent with that used in long length dynamic strength testing, the equation shows relative independence from stress rate.

Interestingly, from these curves, a 'safe' in service strain, for 1% screened all silica fibre (n=20), for 30 years life (~ 10^9 secs), would be approximately 0.2%.

Failure Probability Design

'The strength of fibre can be represented as a statistical parameter reflecting the distribution of flaw sizes on the glass surface'[3]. Employing the results of long length dynamic strength testing to predict failure probabilities of long lengths of fibre suffering applied stress reduces the risks associated with extrapolating lesser data across several orders of magnitude. For instance, acknowledging Weibullian statistical theory and assigning failure probabilities by the median rank method, a 1400km distribution is required to yield data down to 1 x 10^{-5} / 20m. This scale of testing (70000 20m lengths) can only practicably be achieved using continuous strength testing apparatus, such as that described by Glaesemann[2]. Probabilistic theory supports the scaling of such collated data to longer lengths. Clearly very long length testing is required to gain real data at the levels of failure probability which are becoming industry requirements.

Conversely, for short fibre lengths the probability of encountering a flaw in the low strength end of the distribution is negligible and the high strength region dominates. Therefore Weibull parameters pertaining to both the low and high strength regions on the bi-modal cumulative failure distribution plot are required to recommend a 'safe' stress for a given length and failure probability requirement. Following the model developed for the minimum strength design the following expression can be used to calculate a safe stress for a required failure probability :

$$\sigma_o = \exp\left[\frac{1}{m}\ln\ln\frac{1}{1-F}+\ln\sigma'\right] x \left[0.5\left(\frac{n-2}{n+1}\right)\frac{V_o}{a_o}\frac{\sigma_f}{\sigma}\right]^{\frac{1}{n}} \qquad (2)$$

:	σ_o	=	safe stress
	σ'	=	Weibull scaling parameter
	F	=	failure probability
	m	=	Weibull modulus
	σ_f	=	strength appropriate to the F region of interest

The Weibull parameters are available from cumulative failure distributions built up from dynamic testing of 20m gauge lengths. See figure 2.

Application Models

This section is devoted to developing expressions, for use within Weibull calculus, to model complex stress situations on a fibre as an equivalent tensile stress. Real tensile data can then be applied to more complex situations.

Tensile Load

The failure probability at an applied tensile stress, σ_f is given by :

$$F = 1 - \exp\left[-\int\left(\frac{\sigma_f}{\sigma_o}\right)^m \frac{dA}{A_o}\right] \qquad (3)$$

:	σ_o	=	characteristic strength
	A_o	=	surface area of gauge length

For the case of simple uniform tension the result of the integral is :

$$F = 1 - \exp\left[-\frac{L}{L_o}\left(\frac{\sigma_f}{\sigma_o}\right)^m\right] \qquad (3a)$$

Bend

In bending only a fraction of the fibre surface is under tension. The length in bending, L_b which would have the same failure probability as an equivalent length in tension, L_{eq} when the maximum bending strain equals the tensile strain has been shown by Glaesemann[2] to be given by :

$$L_{eq} = \frac{G(m)}{\pi} L_b \qquad (4)$$

where : $$G(m) = \frac{\sqrt{\pi}}{2}\frac{\Gamma\left(\frac{m+1}{2}\right)}{\Gamma\left(\frac{m+2}{2}\right)}$$

Note : For the case where m=2, $L_{eq} = \frac{L_b}{4}$

Hence for long lengths of all silica fibre (m=2) in bending the failure probability can be determined by equating the maximum bending stress to tensile stress and using 1/4 of the length in bending to scale to the Weibull distribution.

Tensile Load as a Function of Length

When the tensile strain on a fibre gradually increases along its length, as depicted in figure 3. A relationship can be derived describing the fibre stress, σ_f, at any point along the it's length, L, as follows :

$$\sigma_f = \sigma_a\left(1-\frac{L}{L_t}\right)+\sigma_t\left(\frac{L}{L_t}\right) \qquad (5)$$

Substituting for the above σ_f in equation (3) results in :

$$F = 1 - \exp\left[-\int_0^{Lt}\left(\frac{\sigma_a\left(1-\frac{L}{L_t}\right)+\sigma_t\left(\frac{L}{L_t}\right)}{\sigma_o}\right)^m \frac{dL}{L_o}\right]$$

$$F = 1 - \exp\left[-\frac{1}{m+1}\,\frac{L_t}{L_o}\left(\frac{\sigma_a{}^{m+1}\,\sigma_t{}^{m+1}}{\sigma_o{}^m\left(\sigma_a-\sigma_t\right)}\right)\right] \qquad (6)$$

For the case where $\sigma_a = 0$, where the fibre stress increases directly proportionately with its length, the developed expression given in equation (6) reduces to :

$$F = 1 - \exp\left[-\frac{1}{m+1}\,\frac{L_t}{L_o}\left(\frac{\sigma_t}{\sigma_o}\right)^m\right] \qquad (7)$$

: σ_a = stress at L=0
σ_t = stress at L = Lt
σ_o = characteristic strength
L_t = total length
L_o = gauge length

Hence, by comparing equations 7 and 3a, the case of tension increasing gradually along a fibre length can be compared directly with the case for constant tension . For instance, a fibre with an m=2, experiencing a constantly increasing stress along its length would have the same failure probability as 1/3 the length in uniform tension when the maximum applied stress equalled the uniform stress.

Combined Bend and Tensile Load

When, as in most practical applications with tight cable constructions, a fibre suffers tensile and bending stresses the fraction of the fibre surface under tension changes with the magnitude of each force. See figure 4. The stress on the surface of the fibre can be described by :

$$\sigma_f \approx \sigma_a + \sigma_b \sin\theta \qquad (8)$$

$$\sigma_b \approx E\frac{r}{R} \quad \text{(for strain levels < 1\%)} \qquad (9)$$

Substituting for σ_f in equation 3, the developed expression becomes :

$$F = 1 - \exp\left[-\iint\left(\frac{(\sigma_a+\sigma_b\sin\theta)}{\sigma_o}\right)^m \frac{r\,dL\,d\theta}{A_o}\right] \qquad (10)$$

Two distinct solutions exist :
When $\sigma_a < \sigma_b$

$$F = 1 - \exp\left[-\frac{rL_t}{A_o\sigma_o{}^m}\int_{-\theta}^{\pi+\theta}\left(\sigma_a+\sigma_b\sin\theta\right)^m d\theta\right] \qquad (11)$$

and, when $\sigma_a \geq \sigma_b$

$$F = 1 - \exp\left[-\frac{rL_t}{A_o\sigma_o{}^m}\int_{0}^{2\pi}\left(\sigma_a+\sigma_b\sin\theta\right)^m d\theta\right] \qquad (12)$$

: σ_f = stress on surface of fibre
σ_a = tensile stress
σ_b = maximum bending stress
σ_o = characteristic strength

For the applications examined in this study the case described by equation 12 is appropriate. Further, when the Weibull modulus, m, is an integer value reflecting the low strength region of the cumulative distribution, precise solutions exist for the integral in equation 12, see table 1 below.

m	$\int_0^{2\pi}\left(\sigma_a+\sigma_b\sin\theta\right)^m d\theta$
2	$\pi\left(2\sigma_a{}^2+\sigma_b{}^2\right)$
3	$2\pi\sigma_a{}^3+3\pi\sigma_a\sigma_b{}^2$
4	$2\pi\sigma_a{}^4+6\pi\sigma_a{}^2\sigma_b{}^2+\frac{3\pi\sigma_b{}^4}{4}$

Table 1 : Solutions of integral

eg. For m=2 and $\sigma_a \geq \sigma_b$:

$$F = 1 - \exp\left[-\frac{rL_t}{2\pi rL_o\sigma_o{}^2}\left(\pi\left(2\sigma_a{}^2+\sigma_b{}^2\right)\right)\right]$$

$$= 1 - \exp\left[-\frac{L_t}{L_o}\left(\frac{2\sigma_a{}^2+\sigma_b{}^2}{2\sigma_o{}^2}\right)\right] \qquad (13)$$

Historically engineers have simply summed the maximum bending and uniform tensile stresses to estimate the failure probability of this combined stress situation as a uniform applied tensile stress. For example, substituting for $\sigma_t=\sigma_a+\sigma_b$ in the original Weibull equation (3a), for a fibre with an m=2 yields :

$$F = 1 - \exp\left[-\frac{L_t}{L_o}\left(\frac{(\sigma_a+\sigma_b)^2}{\sigma_o^2}\right)\right] \qquad (14)$$

Graphical comparisons of the developed applied stress components of equations 13 and 14 are given in figure 5. In this figure the components of the equations have each been normalised to tensile stress alone and the results plotted against the tensile stress to bending stress ratio. The curves 'F(A)' and 'F(B)' refer to the expressions contained within equations 14 and 13 respectively.

Figure 5 clearly illustrates the conservative nature of treating the maximum bending stress as a uniform tension. It also shows that it is more appropriate to account for combined tensile and bending stresses.

However, the most important finding must be that for situations where $\sigma_a > 4\sigma_b$ the bending stress contribution becomes insignificant and may be ignored in subsequent analysis.

Distribution Network Architecture

The network architecture which is the subject of this study is a hypothetical dedicated fibre network supplying 300 subscribers. The cable designs are based on the likely requirements of the distribution network in the UK. The chosen design methodology is ribbon in slotted core cable employing 8 fibre ribbons. Figure 6 details the network topology and indicates the route lengths and fibre count of the primary and secondary links. All cables except for subscriber drop cable are underground duct installed. A two fibre overhead drop cable connects the subscriber. Details of these cables are included in the following sections. Excess cable is accommodated in coils in the pedestal or footway boxes.

Ribbon in Slotted Core Cable for Duct Installation

A number of stacks of fibres in ribbon construction are implanted in an appropriately designed slotted core profile. The residual strains experienced by the fibres in the manufactured cable are a mix of tensile, bending and torsional elements. In a typical design (represented in figure 7) the magnitude of the extreme values of these strains may be:

Tensile strain due to array position :	0.01%
Tensile strain due to insertion tension :	0.02%
Torsional strain (ribbon twist per lay) :	negligible
Bending strain due to lay :	0.006%

The overall strains realised by the fibres during their operational lifetime can then be projected by analysing the relationship between cable and fibre strain. The mechanical response of a 'tight' design cable is shown in figure 8.

In addition, coated fibres experience thermally induced strains caused by their different expansion with respect to the cable on temperature change. These strains can be modelled by calculating the effective thermal expansion of each element across the operational temperature range.

Effective thermal expansion coeff.

$$\alpha(T) = \frac{\sum_{i=1}^{n} E_i(T).A_i.\alpha_i(T)}{\sum_{i=1}^{n} E_i(T).A_i} \qquad (15)$$

$E(T)$ = Modulus of elasticity functional with temperature
A_i = Cross sectional area
$\alpha_i(T)$ = Thermal expansion coeff. as a function of temp.

$$\text{Thermal strain} = \frac{L.\left(1+\int_{T_1}^{T_2}(\alpha(T)_{cable}-\alpha(T)_{fibre})dT\right)}{L} \qquad (16)$$

: L = Original length
T = Temperature

At 20°C above ambient the predicted thermally induced fibre strain in the cable construction shown in figure 7 ≈ 0.06%.

Understanding and quantifying the strains induced by these separate mechanisms is important because, in this type of cable design, they are directly additive to the fibre strains realised in cable installation.

Cables hauled into ductwork experience tensile strains which are both length and time dependant. Figure 10 describes expected load variance with load duration and length during installation for the general case of a cable hauled through a straight duct.

The cable will experience the maximum load (T_{max}) at the pulling end of the route for short durations only. The following expression relates tensile strain to time and length :

$$\text{Strain, } \varepsilon(L, t) = \frac{\mu W L\left(1-\frac{t}{t_{max}}\right)}{AE} \qquad (17)$$

: ε = Strain
L = Distance along duct route
μ = Friction coefficient : cable to duct
W = Cable weight
t = Time
A = Area of strength member
E = Modulus of strength member

$$\text{Strain energy (t)} = \int\int AE\varepsilon\,(L, t)\,dl\,dt$$

$$= \frac{\mu W L^2 t\left(1-\frac{t}{2t_{max}}\right)}{2} \qquad (18)$$

Once installed the cables retain a stress profile along their length, caused by frictional forces opposing stress relaxation. This effect has been reported by Caviglia et al.[5] and Hsieh et al.[6]. Although tensile elements in the cable products may creep with time, reducing the magnitude of the residual installation stress, the perfectly elastic glass fibres do not stress relax. Therefore, it would seem reasonable to show the cables' original residual stress profile unchanging over the fibres' installed lifetime. See figure 11.

The following expressions apply :

$$\varepsilon\,(L, t) = \frac{\mu W L}{AE} \qquad \left(0 \le L \le \frac{L_{max}}{2}\right) \qquad (19a)$$

$$\varepsilon\,(L, t) = \frac{\mu W (L_{max}-L)}{AE} \qquad \left(\frac{L_{max}}{2} \le L \le L_{max}\right) \qquad (19b)$$

$$\text{Strain energy (t)} = \int\int AE\varepsilon\,(L, t)\,dl\,dt$$

$$= \frac{\mu W L^2 t}{2} \qquad \left(0 \le L \le \frac{L_{max}}{2}\right) \qquad (20a)$$

$$= \mu W L t\left(L_{max} - \frac{L}{2}\right) \qquad \left(\frac{L_{max}}{2} \le L \le L_{max}\right) \qquad (20b)$$

Traditionally the cable design engineer would have based his selection of fibre proof screen level on the maximum load, over the entire length of cable in the duct for the duration of its lifetime. The corresponding equations for this case are :

$$\text{Total strain, } \varepsilon = \frac{\mu W L_{max} t_{max}}{AE} \qquad (21)$$

$$\text{Total strain energy} = AE\varepsilon$$

$$= \mu W L_{max} t_{max} \qquad (22)$$

Clearly, comparing equations 18,20 and 22 (which describe the volumes enclosed within the curves in figures 10 and 11), designing to the maximum load, length and duration for installation and installed lifetime is a conservative approach for cost effective design of 'tight' fibre cable products. Hence, for the purposes of analysing the fibre strains in duct installed 'tight' design product the stress will be modelled as function of time and length.

Overhead Drop Cable

The residual strains in the fibre, from manufacture, in the type of cable depicted in figure 9 are negligible. Fibre strain is driven by the thermo-mechanical response of the cable to its environment. In tensile testing the cable has shown the same characteristic response to load as the 'tight' design product.

A length of this product installed on an access network simulation test facility with environmental, mechanical, optical and fibre strain monitoring has shown that the fibre strain response is directly proportional to the realised cable strain.
The design of these products is a complex task involving a compromise between the products' elastic modulus, breaking load and environmental response governed by its size and weight. A larger, heavier, stronger design creates higher loading at suspension points. A lighter design may be too elastic, sag too much or even break. The tensile response of the cables to the environment is governed by well documented change of state equations[8]. Generally, for short span applications, an approximation to the catenary is used in the form of parabolic expressions. The general formula is :

$$C_o = L + \frac{f_o^2 L^3}{24 T_o^2} + \frac{H^2}{2L} \qquad (23)$$

: C_o = Catenary length at state 0, installation
L = Span length
H = Suspension point height difference
T_o = Tension at state 0
f_o = Resultant load at state 0

The new cable tension, caused by a change in environmental conditions, state 1, is derived by substituting for C_1 and C_o in the following relationship :

$$\Delta C = C_1 - C_o = \Delta C_{elastic} + \Delta C_{thermal}$$

$$= \frac{C_o}{EA}(T_1 - T_o) + (\alpha C_o (t_1 - t_o)) \qquad (24)$$

Given the new tension, the new catenary length C_1 can be calculated, this value yields the resultant strain in the fibre.

For the cable shown in figure 9, with an installation tension of 200N and for a 68m span case, the following range of tensile strains are expected to be experienced by the fibre during its lifetime :

Condition (temp., ice, wind)	Duration	Cable strain (%)	Including creep (%)
Installation @ 20°C	30 years	0.12	0.17
-7°C, 0mm, 19.2m/s	30 days	0.19	0.24
-7°C, 3mm, 19.2m/s	30 days	0.35	0.40
0°C, 3mm, 0m/s	30 days	0.21	0.26
0°C, 3mm, 19.2m/s	30 days	0.37	0.42
0°C, 0mm, 22.8m/s	30 days	0.28	0.33
20°C, 0mm, 22.8m/s	30 days	0.34	0.39
60°C, 0mm, 0m/s	30 days	0.27	0.32

Table 2 : Overhead drop cable strains

Higher strains are seen for short durations only. The every day strain is governed by the installation condition. For overhead cables, the installed span length, the creep under load[8] and any initial constructional elongation must be built into the resultant total strain.

System Reliability

This section uses the application models developed for various stress situations, applies the stress history of the installed fibre and uses established probabilistic theory to calculate a system reliability.

Primary and Secondary Links

Working from the exchange to the home (see figure 6), a 1km length of the high fibre count, tight design, ribbon in slotted core cable is hauled through ductwork to the primary flexibility point. 500m lengths of 120f and 20f cables of similar design extend through the secondary flexibility points to the footway boxes. For the purposes of this investigation we have chosen to examine the 120f cable design described earlier and assumed that the ductwork in question is level and straight.

Installation

Postulating that the tensile load developed at the hauling end is realised as a strain level of up to, for instance, 0.5% in the cable, and that the installation takes a nominal eight hours. Then, for the cable previously described the total applied tensile strains can be determined :

Extreme value of tensile strain due to fibre's array position and ribbon insertion tension : 0.03%
Thermally induced tensile strain realised by installing the cable at, say, 10°C above ambient : 0.03%
Steadily increasing strain experienced by the fibre along its length due to hauling into the duct : 0 to 0.5%

The resultant magnitude of the tensile strain range experienced by the fibre during installation may be 0.03 to 0.56%.

The bending strain due to lay is 0.006%. Clearly $\sigma_b < \sigma_a/4$ therefore, following the argument previously presented, bending strains can be ignored. Hence for reliability analysis, the magnitude of the tensile strains realised by fibres in the construction remain unchanged by the strain due to bending, and range from 0.03% at the 'pulling in' end to 0.56% at the hauling end.

The level of stress seen by the fibre increases with distance along the duct, whereas the stress duration is inversely proportional (see figure 10). Consequently, the calculation to determine a reliability for the installation must involve an integration over stress, length and time. Solving this using numerical integration methods, by repeatedly applying eqn 17 with small step sizes of length and strain duration would enable a safe equivalent tensile strain to be recommended for a given failure probability requirement. However, this approach should account for the changing strength distribution after each iteration and the solution becomes over complex. For the purposes of this paper we have assumed that the strength distribution remains practically unchanged after each stress event provided we adhere to the recommended 'safe' stress levels.

Figure 12 represents an assumed strength distribution for approx. 400km of all silica fibre[2]. This figure may be considered to be a design diagram for all silica fibre.

The accumulated 20m gauge length data is first scaled to the application length (500m) and then further scaled by 1/3 (for m=2) to represent the constantly increasing strain case experienced by the duct cable, ie. the equivalent length under uniform tension is 167m. Referring to the 'duct cable' curve superimposed on fig. 12 the expected failure probability at an 'in service' strain of up to 0.56% for 8 hours is too high ($\approx 4\times10^{-3}$) therefore a minimum strength design is preferred.

Overlaying a graphical representation of the installation strains realised by the fibre on the curves shown in figure 1, provides a recommendation for a minimum proof screen level. See figure 13. The minimum proof screen level, for an all silica fibre (n=20), required to support the aforementioned installation case would be approximately 1.5%.

Installed case

Assuming that the fibre has not been damaged by installation a similar approach can be adopted to estimate the reliability of the installed cable where the residual stress profile is described by figure 11. In this situation the fibre sees a residual strain level after installation which changes with length and is virtually time independent. Differential thermal expansion of cable components may cause an additional fibre strain up to 0.06% at 20°C above ambient. The magnitude of the realised strains may vary, in this case, from 0 to 0.34% for the installed lifetime. Referring to the 'duct cable' curve superimposed on figure 12 the expected failure probability at an 'in service' strain of up to 0.34% for 30 years is again too high ($\approx 6\times10^{-3}$) therefore a minimum strength design is again preferred. Referring to figure 13, the minimum proof screen level, for an all silica fibre (n=20), required to support the installed case would be approximately 1.8%.

Analysis of the results shows the reliability of the product to be installed life dependant. To support allowing a tensile strain of up to 0.5% in the tight design cable shown in figure 7 during duct installation, and ensure that there is a negligible probability of breaking a fibre through the products installed lifetime, a proof screen level of up to 1.8% would be recommended for all silica fibre (n = 20).

Fatigue resistant fibre (n=30) however, shows screen level choice balanced between installation and installed lifetime of the product, see figure 14. In this case a 1.25% screened fibre would be required.

Splice Cassette

The splice cassettes typically contain up to 0.8m of fibre in pure bending with a bend radius of 30mm (maximum bending strain = 0.21%). The predicted strength distribution is shown in the design diagram in figure 12. Referencing figure 12, the safe strain recommended at $F=1x10^{-5}$ can be read down from the 'splice cassette' curve to the 30 year time scaled axis, and is 0.38%. Comparatively, the minimum design strength theory would suggest that a 1.2% proof screened would be required. Clearly, designing to a failure probability requirement is justified in this case and a only nominal 0.5% proof screen level is required for fibre in the cassette.

Since the fibre in the cassette will be drawn from the duct cables or overhead drop cable this analysis shows that the fibre handling in the joint is not a dominant factor in proof screen level selection. Knowledge of the low strength portion of the strength distribution of the all silica fibre has afforded the possibility of utilising a greater proportion of its strength allowing failure probability design.

Footway Box

Several metres of excess cable length may be contained in the footway box in large diameter coils, the case of pure bending applies at ambient temperatures. Referring to figure 12, and the 'footway box' curve for 8m in bending, the calculated 'safe' strain for a 30 year life with $F=1x10^{-5}$, is 0.14%. This is greater than the maximum bending strain realised in the 1m dia. coil ≈0.0125%. Conversely, the expected failure probability at this strain level is of the order $5x10^{-8}$, this figure is so small as to be considered to be zero.

During temperature changes the fibre would experience a cyclic change in tensile stress due to differential thermal expansion of components and see a range of strains from 0 to 0.06%. In the worst case the thermally induced tensile strain is greater than four times the maximum bend strain and therefore the bending contribution may be ignored (as previously shown). Referring to the 'footway box' curve on figure 12 for 8m in tension and assuming a 30yr life and $F=1x10^{-5}$, the 'safe' strain is 0.075%. Therefore, again 0.5% screen fibre suffices.

The Drop Cable

Fibre in the drop cable, packaged as shown in figure 9, sees only bending stresses coiled in the footway box and no thermally induced tensile stresses because it is de coupled from the cable packaging. Cable fixed to the pole transmits no tensile strains to the fibre and the weight of the fibre is supported along its vertical length by the 'viscous' gel. The span of the drop cable to the customer suffers a range of levels and durations of strains whose extreme values are shown in table 2. In this case the choice between the failure probability or minimum strength design is not distinct. When designing to higher failure probability levels (e.g. $1x10^{-3}$) real data can apply (see the 'overhead cable' curve on figure 12) and safe strain recommendations for all silica fibre of 0.29% for 30 days and 0.22% for 30 years result. However, at the high levels of strain seen by the fibre in the span failure probabilities are high and a minimum strength design is preferred to advise a higher proof screen level.

Superimposing the strains experienced by the cable during its lifetime on figure 1 a choice of screen level can be made (figure 15).

From analysis of the curves produced the minimum recommended screen level required would be ~1.6% (~1.2% for fatigue resistant fibre). Further, it is clear that the choice of screen level is governed by the short term high strain level.

The remainder of the drop cable exists in a relatively benign environment and the screen level of fibre required for the span length is more than sufficient to assure its lifetime.

Overall Reliability

The overall mechanical reliability of the fibre in the system depicted in fig. 6 can be calculated by taking the sum of the product of the calculated survivability's of the component parts of each link[4]. The failure probability of each component part can be estimated by taking the product of the calculated survivability's for each stress event seen by that part. Assuming that the reliability's of all the fibres in the duct installed cables are equal, and that fibre in the cable coiled in the footway boxes, and fibre in the splice cassettes, and fibre in the overhead cables can be treated similarly. Then the system failure probability can be found from the following expression :

$$F_{system} = \sum_{k=1}^{q} \left(1 - \prod_{j=1}^{s} \prod_{i=1}^{r} R_{iJ} \right)_k \qquad (25)$$

$R = 1 - F$
F = failure probability
R_i = reliability of a fibre in a component part of a link subject to a particular strain event
r = no. of different strain events
R_j = reliability of the fibre in a component part of a link
s = no. of separate components in the link
q = no. of links in the system

For example, in the notional system we have discussed, breaking the link route down to 3 lengths of duct cable, 6 loops of cable in footway boxes, 3 splice cassettes and an overhead span, the expected failure probability in a two fibre link from the exchange to a subscriber can be estimated as follows (note that minimum strength design was preferred for the longer lengths of fibre hence these regions essentially show a reliability of 1) :

$$F_{\text{subscriber link}} = 2.\{1 - (R_{\text{duct cable}})^3.(R_{\text{footway box}})^6 .(R_{\text{splice cassette}})^3.(R_{\text{overhead cable}})\}$$

:

$F_{\text{duct cable}}$	≈ 0
$F_{\text{footway box}}$	$<1\times10^{-5}$
$F_{\text{splice cassette}}$	$<1\times10^{-5}$
$F_{\text{overhead cable}}$	≈ 0

$$F_{\text{subscriber link}} < 1.8\times10^{-4}$$

ie. The probability of a duplex fibre link from exchange to subscriber failing within 30 years $< 1.8\times10^{-4}$.

In similar fashion the probability of any one link in the entire system failing within 30 years can be calculated :

$$F_{600\text{ fibre system}} < 5.4\times10^{-2}$$

Clearly designing component parts to the low levels of failure probability advised, and using a knowledge of the fibre strength distribution, results in a reasonably high system reliability. The chances of accidental damage occurring to the network's outside plant within it's 30 year lifetime would far outweigh the probability of a stressed fibre breaking by crack growth.

Duct installed cable can be constrained by design to some pre-determined strain level to suit the fibre type and screen level employed. The overhead cable, however, lies at the mercy of the elements, compromises in its design to meet local requirements must be made and therefore rather than being able to design around the fibre, the converse is true. If the same screen level of fibre is employed throughout the system, then for the cabling and environments discussed, the link reliability will depend on the length of fibre contained within the span of the drop cable.

Re-routing of the final drop via local ductwork would therefore offer a more reliable solution. Where this proves impractical, allowing a higher failure probability for the final drop may prove an attractive alternative. The re-installation costs of the final short link being relatively low.

Conclusions

In this paper the strains realised by fibre, in a link in the outside plant in a generic representation of the local dedicated fibre network employing 'tight' design cable products, have been estimated.

Existing reliability models have been developed to apply to the various stress situations seen by the installed fibre. Specifically, where combined bending and tensile stresses are seen, and $\sigma_a > 4\sigma_b$, the bending stress contribution has been shown to be insignificant when calculating a failure probability. Also, we have developed a means to simply scale to the tensile strength distribution to accommodate the example of a fibre experiencing a constantly increasing strain along its length.

Distinctions have been made between designing to a minimum strength for prescribing a proof screen level to suit the application and using the failure probability distribution data to recommend a 'safe' strain.

We have shown that a knowledge of the strength distributions affords the possibility of allowing greater stresses on shorter lengths of fibre whilst still achieving a high system reliability.

Design diagrams, on which installation and installed cabled fibre tensions can be readily superimposed, were developed to ease the selection of a suitable fibre screen level and fibre type for an application. The developed analysis is relatively straight forward and provides a means towards estimating the overall reliability of a system.

The analysis showed that employing fatigue resistant fibre, or hermetic coated fibre, in the network would afford cable manufacturers the luxury of designing to greater levels of cable strain whilst still assuring product lifetime.

We suggested that the chances of accidental damage occurring to a network far outweigh the probability of a fibre, under controlled stress, failing.

Finally, we recommended some possible alternatives to cabling the local loop network using the reliability of the fibre as the driving force in product design.

References

1. A.R.Farmer, J.E.Taylor, "Fibre optics in a power transmission environment" SPIE Volume 374 p16-24, April 1983

2. G. S. Glaesemann, "Optical fiber failure probability predictions from long-length strength distributions" IWCS '91 p819-825

3. G. S. Glaesemann, S.T.Gulati, "Design methodology for the mechanical reliability of optical fiber" Optical engineering /June 91/Vol. 30 No.6 p709-715

4. BS 5760 : "Reliability of systems, equipments and components"

5. F.Caviglia, F.Esposto, F.Nanni, P.Ricaldone, D.Suino, "Optical fibre strain measurement during cable laying" E-FOC 90 p92-97

6. R-C. Hsieh, P.Boes, A.Kruijshoop "Lifetime of optical fibres installed in underground plant" - ACOST 16, Adelaide (1991) p238ff

7. R.W.Bond, "O.C.S. Design manual", Balfour Beatty PLC.

8. J.Bradbury, P.Dey, G.Orawski, K.H.Pickup "Long term creep assessment for overhead-line conductors" Proc IEE Vol 122 No.10, October 1975

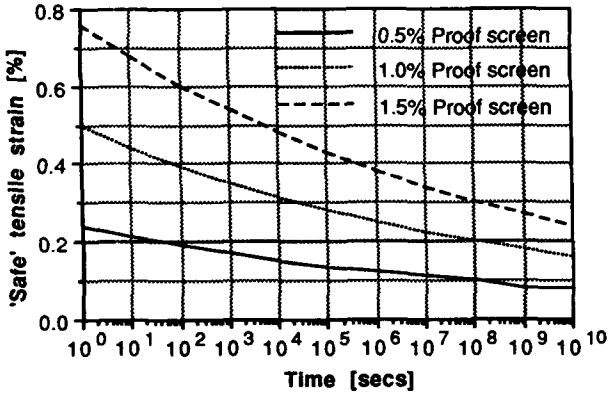


Figure 1 : Minimum strength design for all silica fibre (n=20)

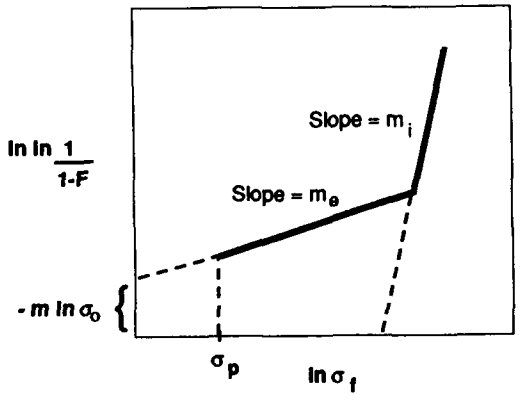


Fig 2 : Representation of post proof test strength distribution (dynamic)

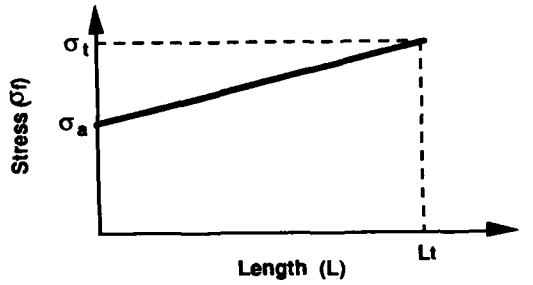


Fig 3 : Stress vs length

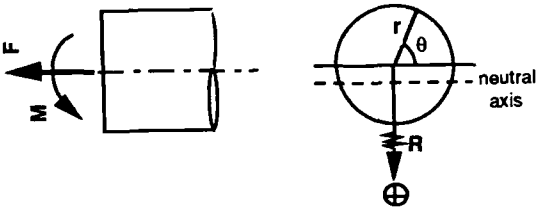


Fig 4 : Fibre under bending and tension

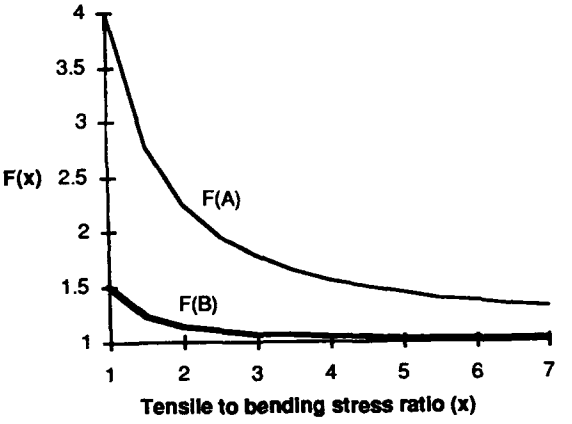


Fig 5 : Realised stresses in tension and bending

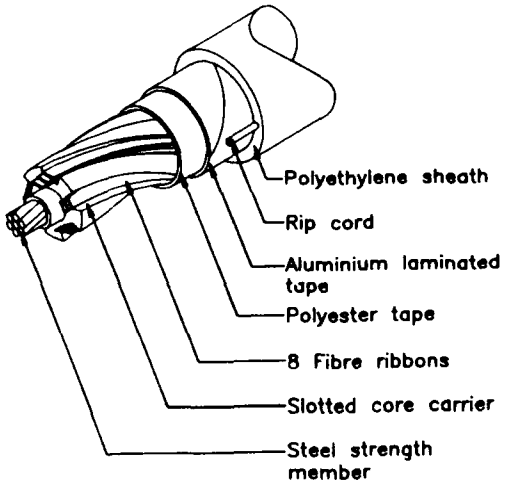


Fig 7 : Schematic of a ribbon in slotted core cable

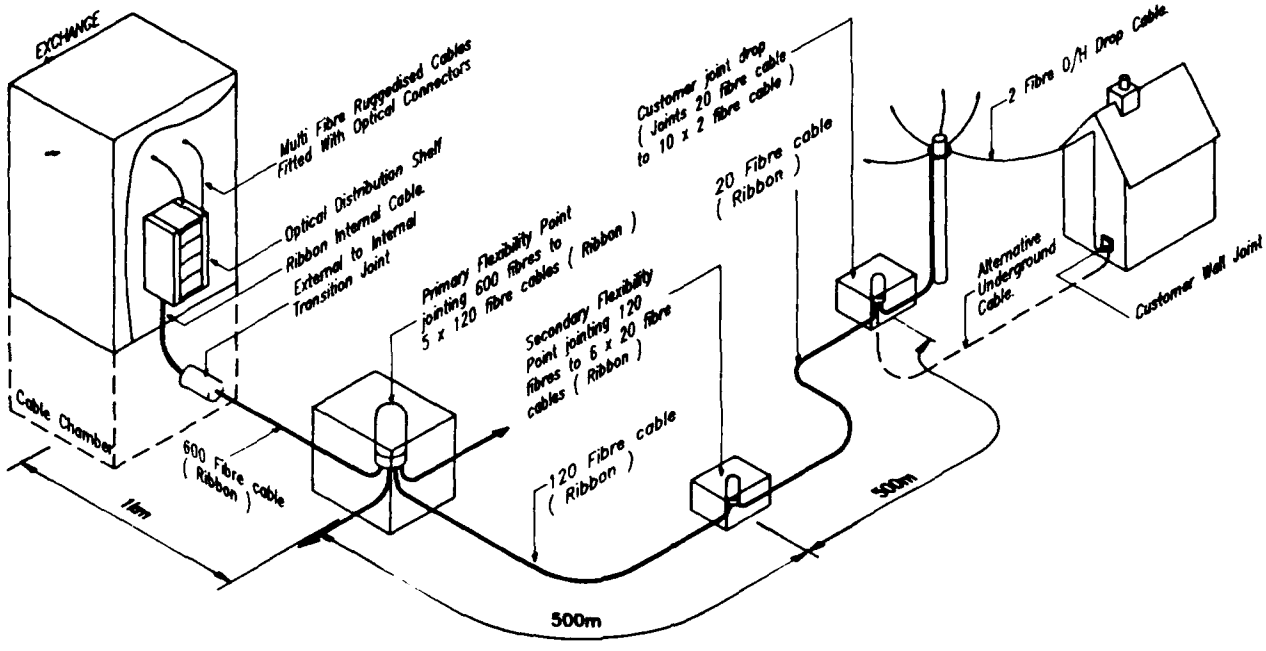


Fig 6 : Topological representation of a dedicated fibre network

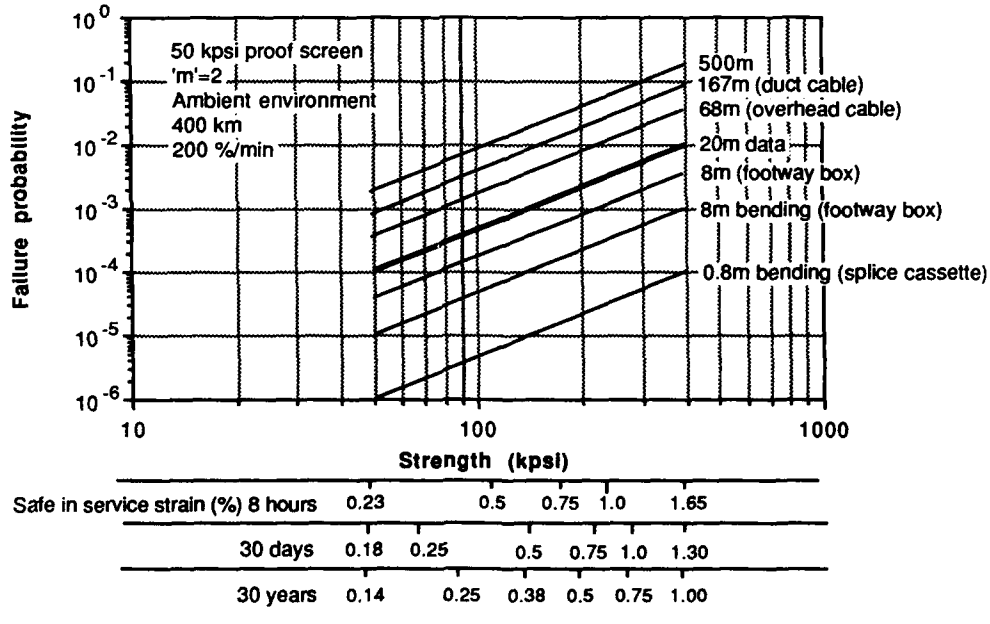


Fig 12 : 'Safe' strain design diagram for all silica fibre (n=20)

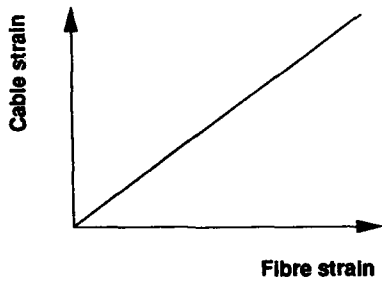


Fig 8 : Fibre strain vs cable strain for 'tight' design cables

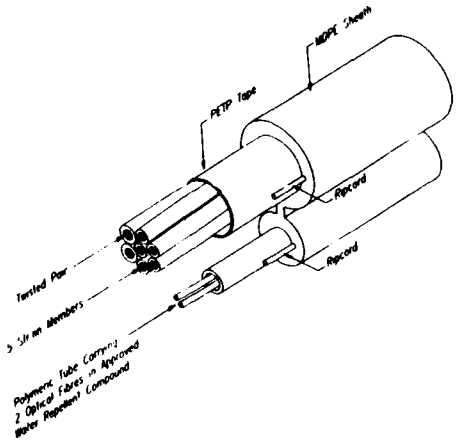


Fig 9 : Schematic of an overhead subscriber drop cable

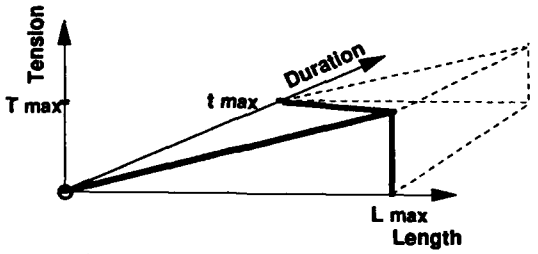


Fig 10 : Cable tension vs length vs time during installation in ductwork

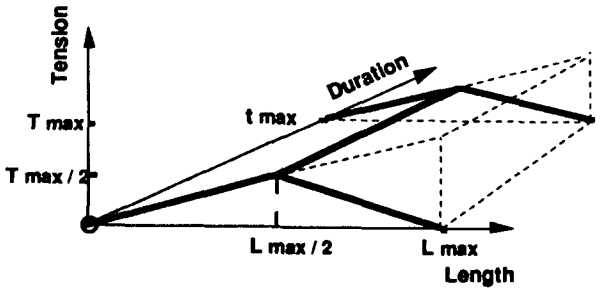


Fig 11 : Cable tension vs length vs time installed in ductwork

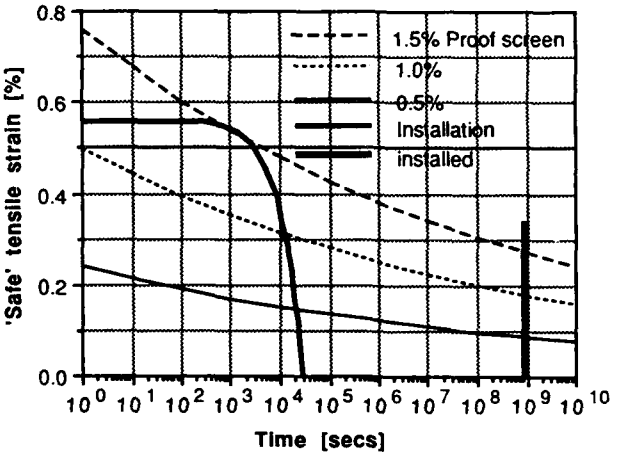


Figure 13 : Minimum strength design for all silica fibre (n=20)

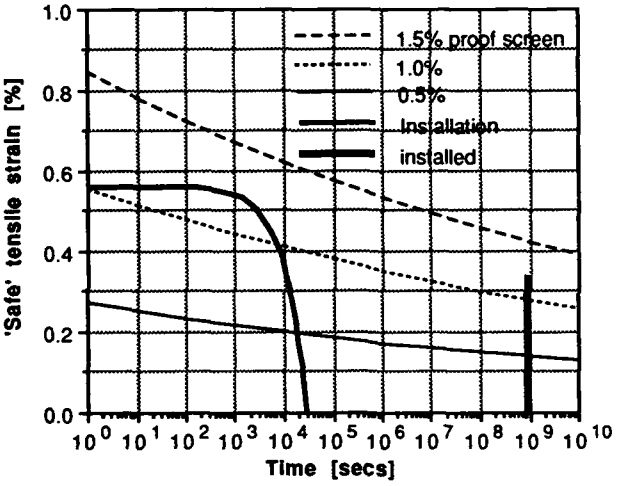


Figure 14 : Minimum strength design for Ti clad silica fibre (n=30)

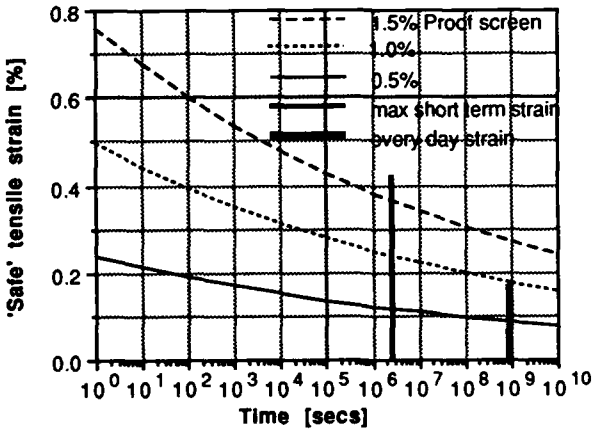


Figure 15 : Minimum strength design for all silica fibre (n=20)



Ken Hodge
Senior Optical Cable Design Engineer
Helsby Technology Centre
BICC Cables Ltd.

Ken Hodge is a Senior Optical Cable Design Engineer in the Helsby Technology Centre.

He joined BICC as a graduate trainee in 1982 and has been engaged in the development and design of optical fibre cables since 1983.

Mr. Hodge graduated from Liverpool University with an honours degree in Mechanical Engineering.



Chris Pegge
Group Leader, Optical Cable Design
Helsby Technology Centre
BICC Cables Ltd.

Chris Pegge has worked in the field of optical cable and connector technology since graduating from Bristol University with an honours degree in Mechanical Engineering in 1985. He joined BICC in 1988 and currently holds the title of Group Leader, Optical Cable Design within the Helsby Technology Centre. This centre provides a central research and development facility in optical and advanced material technology for the BICC Group worldwide.



Matti E.Hopiavuori
Senior Engineer
International Operations
Corning Incorporated

E. Matti Hopiavuori is a senior engineer responsible for technical product, process, and application support to cable manufacturers, end customers, and Corning's joint ventures involved in optical fiber technology.

Mr. Hopiavuori joined Corning in 1984 as a senior application engineer. He held a number of technical positions supporting different markets and applications before assuming his current responsibilities in May 1990.

Mr. Hopiavuori holds the Master of Science in Electrical Engineering degree from Tampere University of Technology, Finland.



G. Scott Glaesemann
Senior Development Engineer
Optical Waveguide Development
Corning Incorporated

G. Scott Glaesemann is a senior development engineer responsible for modelling and measuring the mechanical behaviour and reliability of optical fibre.

Glaesemann received his Master's degree and Ph.D. from the University of Massachusetts. He is a member of the American Ceramics Society and Sigma Xi.

DISTRIBUTED STRAIN- A RATIONAL TEST OF FIBER FATIGUE

Torbjörn Svensson
Erland Sundberg

Telia Research AB, Systems Research,
Fibre Technology, Sff
S-136 80 HANINGE

Abstract

The evaluation of the fatigue parameter "n" of optical fibers always has required testing of several samples, on which a series of loads, or stress rates, have been applied during the test.

Great advantage would be, if testing series of samples were eliminated by a single operation. Such a test, the distributed strain test, now has been analyzed theoretically. Formulas are derived, which enables the evaluation of n from a series of measurements of failures in one fiber specimen. The mounting operation of a single specimen, loading, and the completion of the measurement compose the total test. In this respect, it will be a radically new test of fiber fatigue.

A brief guidance is given on the design of an instrument, and limitations of the test.

Introduction

The prediction of lifetime of optical fibers under stress is limited by the model employed, and by the reliability of long-term fatigue data. Reliable, and extensive data are accessible, e.g. by the expander test, in which static and dynamic tests are made on medium length fibers under uniaxial stress. When using an expander, the failure statistics are quickly obtained by testing a single specimen.[1,2] This relatively new method, based on uniform fiber strain, is now being used as a routine test for quality approval of optical fibers, at Swedish Telecom. The instrument also has proven useful for the study of low strength fibers, in experiments aiming at modeling the fatigue behaviour of weak flaws.[3] See Figure 1.

When using the established expander test, the stress corrosion susceptibility parameter "n" has to be evaluated following the regular procedure used in other tests. The n-parameter must be determined from a series of measurements at varied conditions as the strain rate, in dynamic tests, or at different values of constant load when static testing is applied. A common requirement for most tests is the preparation of a large number of specimens, in order to obtain accurate average values of failure stress or time. However, the number of specimens is quite limited in expander tests. All data in Figure 1 were obtained from two specimens only. A series of loads, or stress rates, must still be applied, though.

Great advantage would be, if testing series of samples were eliminated by a single operation. A potential successor to the original expander test has therefore been studied, the distributed strain test, or DS test. With a load distribution based on a linearly increasing strain along the fiber, this modified expander test enables even more effective tests of fiber fatigue.

The mounting operation of a single specimen, loading, and the completion of the measurement compose the total test. In this respect, it will be a radically new test of fiber fatigue.

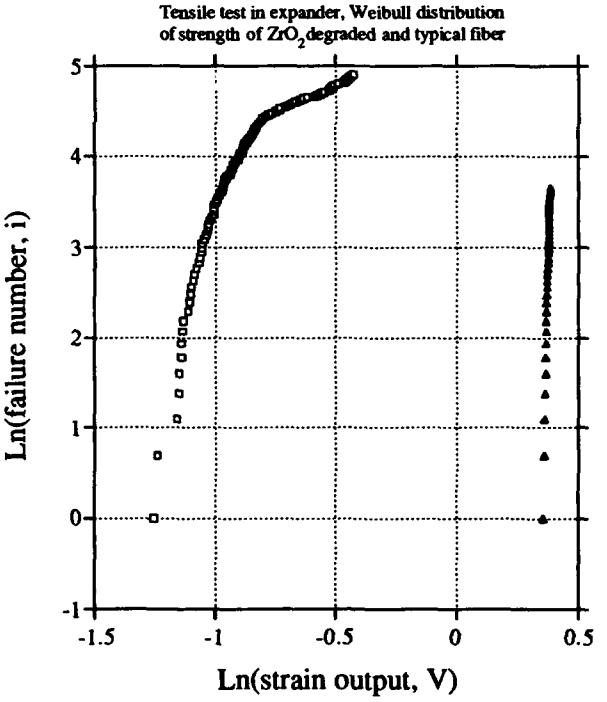


Figure 1. Expander tests of low- and high-strength optical fibers.

Design

The DS test is based on the expander test, in which a uniform tensile strain is applied on the fiber, by winding it onto an expandable drum. The diameter of the drum is large, so

stresses caused by bending are negligible.

The significant idea of DS test is to apply the strain in a way that gradually increases the load from one end of the fiber to the other. Owing to the the same principles as the original expander test, there will be no interference between fractures occuring at different loads.

Two ways of accomplishing this can be distinguished: either the load is applied by increasing it during winding the fiber onto a stiff drum (this may be complicated due to premature fiber failures, however), or by winding at zero strain, and asymmetrically expanding the drum at the beginning of test, according to Figure 2.

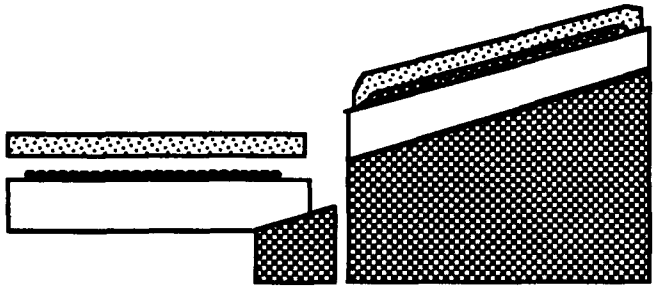


Figure 2. Principle of the DS test

A design based on an expanding drum is preferable, because it can be used both for dynamic and static testing. Also, the time to mount the fiber will not be critical.

An ideal instrument should enable a synchronized capture of both strain and time. But also if the simplest possible design and instrumentation is chosen, it will be useful for the evaluation of the stress corrosion susceptibility parameter, n. This will be shown theoretically, for optical fibers having a constant value of n.

Such a low cost design will only capture the time-to-failure, any information on the value of strain will be lost. In the test, weak parts may fail at a small stress, and strong parts at higher stress, at the same time. Obviously, there is a need for a statistical method to evaluate the value of "n" from such a mess. A method will be suggested below.

DS test simulation

The function of a low cost DS test can be simulated numerically by studying the times-to-failure of a fiber exposed to a static load, which increases linearly between its ends, independently of occuring failures.

A large number of data may represent the lowest values of strength, in different parts of similar length, along the fiber. Data are assigned a known Weibull distribution of strength. These data are randomly distributed along the fiber.

Finally, a static load is applied, linearly increasing along the fiber, and the time-to-failure is calculated for all strength data. The ordinal number of times-to-failure is studied.

Strength and fatigue of fiber

A Weibull distribution of initial strength is created by assigning values of initial strength σ_{Ii}, in ascending order from i=1 to N using the expression[4]

$$Ln(i) = Ln\left[\frac{L_{tot}}{L_o}\left(\frac{\sigma_{Ii}}{\sigma_{Io}}\right)^m\right]$$

where

σ_{Ii} = initial strength of order i
σ_{Io} = site parameter of initial strength
m = Weibull modulus
L_o = reference length
L_{tot} = total length under stress

i.e.:

$$\sigma_{Ii} = \sigma_{Io}\left(i\,\frac{L_o}{L_{tot}}\right)^{1/m}$$

In order to simplify the study the assumptions σ_{Io} =1 GPa, and L_o =1 m, will be made. The total length, L_{tot}, is not significant for the study, but so is the maximal number of (measurable) data, N. In practice, this number is limited by pressure, friction and stress relaxation close to the fractures. Because of the proportionality $N \propto L_{tot}$, it is possible to do the substitution $L_{tot} = N$, which yields an expression of reduced complexity:

$$\text{Assumption: } \sigma_{Ii} = \left(\frac{i}{N}\right)^{1/m}$$

This expression simplifies both the analysis and the computer code. For this reason the assumption N = 1024 has been made here. The resulting Weibull distribution is shown for m = 80 according to Figure 3.

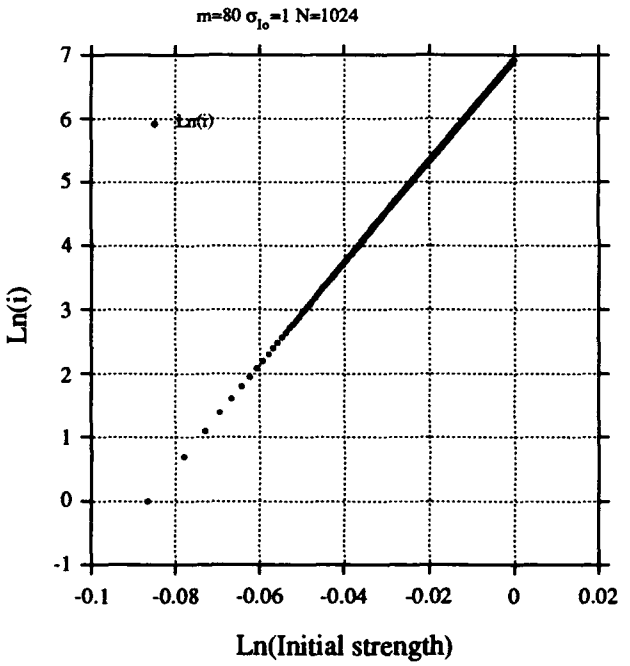


Figure 3. Ideal Weibull distribution of strength

The failure sites are then randomly distributed along the fiber. Finally is applied a constant stress, σ_s, which increases linearly from one end of the fiber to the other. According to crack propagation theory, the time-to-failure, t_s , for each failure site "i" of initial strength σ_{Ii} is given by[5]

$$t_s = \frac{B}{\sigma_{Ii}^2}\left(\frac{\sigma_{Ii}}{\sigma_s}\right)^n$$

where

n = stress corrosion parameter, assumedly being constant

B = fatigue initiation parameter

Frequent values for optical fibers[2] are B = 0.05 $(GPa)^2$s, and n = 20. The stress is varied along the fiber within the limits $[0.4 \le \sigma_s/\sigma_{IO} \le 0.8]$.

Because of the varying strength of failure sites, and their exposure to different stresses, the static fatigue of failure sites will proceed with widely varying rapidness.

If all failure sites could be identified, and thus the original order reestablished according to their increasing values of strength, i =1, 2, .., N, one would find a new order of failures with time, severely distorted from the original order of strength. The somewhat caotic result is shown in Figure 4.

Ideally, there is un unlimited number of failure sites to be activated in a uniform strain test. In practise, the relaxation of tensile stress close to failed parts of the fiber will cause a limited number of failures, N, which are easily discerned from failures "out-of-order". More important: it is also feasible to pin-point a certain number by means of instrumental design. In this study the maximal number of failures is assumed to be N = 1024.

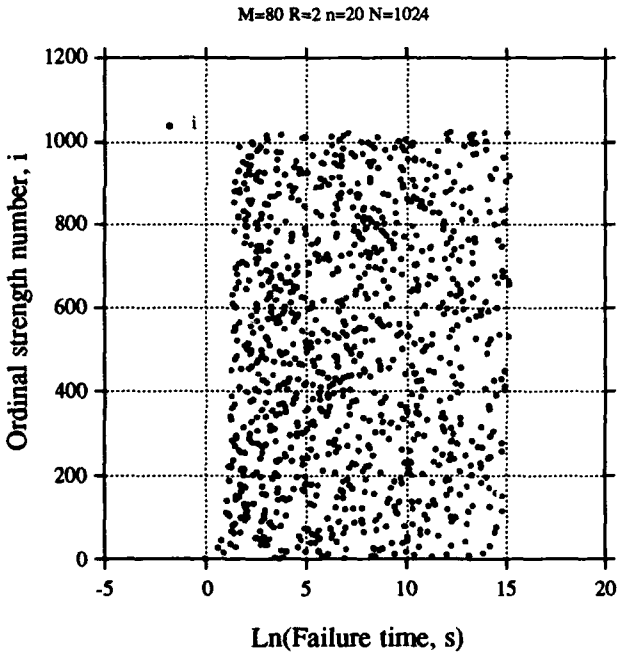


Figure 4. Ordered failures lost in time

Capture of stress and time

An elaborate equipment would enable identification of both the time-to-failure *and* the applied stress, corresponding to a certain failure. Such measurements would allow data to be plotted according to Figure 5.

From linear regression, the slope factor $d\ln\sigma/d\ln t_s = -1/n$ is obtained. Such a simple evaluation of the stress corrosion susceptibility parameter, n, would be very attractive.

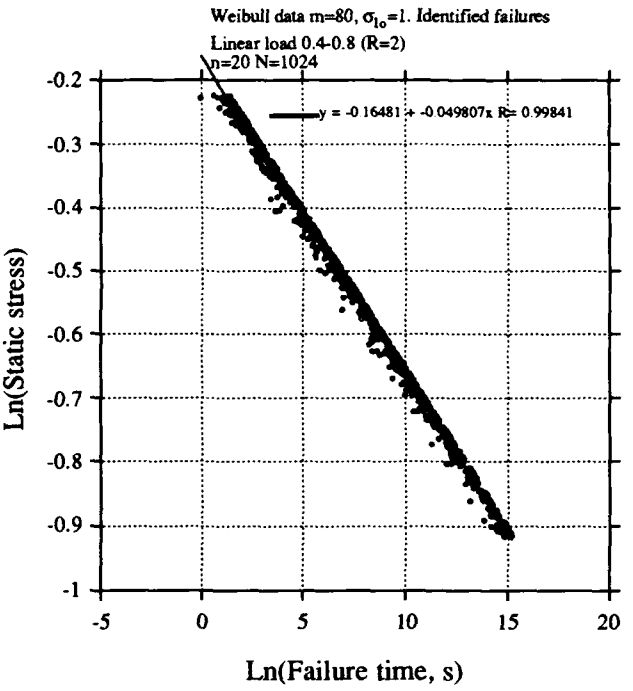


Figure 5. Pin-pointing stress-time data in the DS test

Capture of time alone

A low cost DS test can not identify the stress which causes a certain failure. *Only* the time-to-failure can be measured. A reasonable assumption though, is that there is usable information in just the measured series of time-to-failure. The problem is how to extract the essential part of information, i.e the value of n.

In Figure 6a, failures are presented in an ascending order of failure times: k = 1, 2,.., N, for N = 1024. Generally, k≠i.

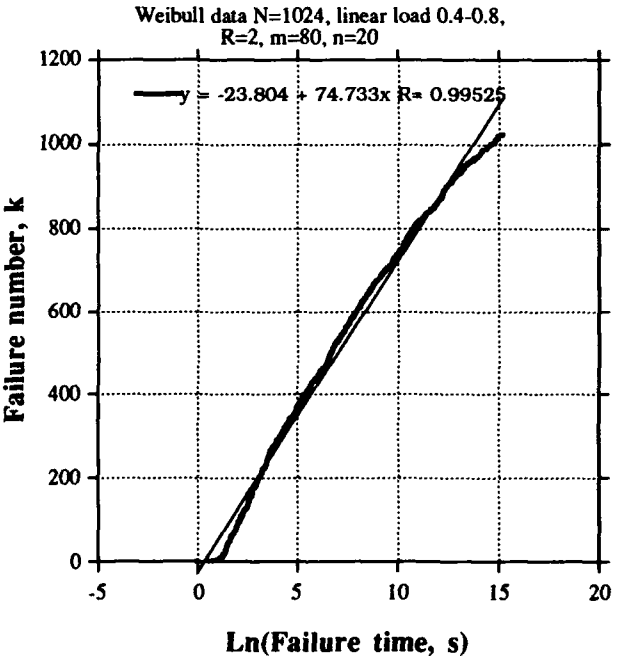


Figure 6a. Assorted failure times in DS test

Evidently, there is a reasonably linear relation between k and the logarithm of the failure time. Following the same procedure, an approximately linear relation is obtained also for N = 50, Figure 6b. Now the slope has a new value.

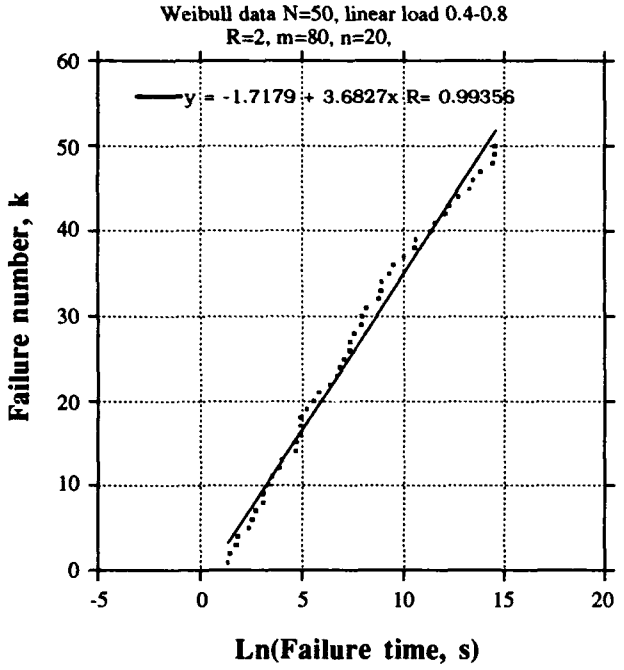


Figure 6b. Assorted failure times in DS test

For the sake of amusement, a series of similar studies can be made, applying different values of the ratio R between the previously assumed value of maximal static stress, 0.8, and the minimal stress, $R=\sigma_{max}/\sigma_{min}$

By doing this for a series of different values on the initial Weibull modulus m, a table of data will give a hint of what relations might be hidden in the DS test data, Table I.

m	R	$\Delta k/\Delta Ln(t_s)$	$N/[n \cdot Ln(R)]$
10^4	11/79	4065	4070
240	11/3	173.7	178.0
240	2	74.04	73.8
240	4	38.48	36.9
80	11/15	682	793
80	11/3	175.1	178.0
80	2	74.7	73.8
80	4	38.2	36.9
20	11/3	151.6	178.0
20	2	72.6	73.8
20	4	37.5	36.9

N=1024 and n=20

Table I. Slopes from linear curve fit

The third column, $\Delta k/\Delta Ln(t_s)$, is the slope of linear estimates of calculated data. The fourth column is a sound choice by guess. Obviously there seems to be a relation; $\Delta k/\Delta Ln(t_s) \approx N/[n \cdot Ln(R)]$, within a wide range of values of m, R, and N.

Higher values of m usually give better linear estimates. The influence of R on linearity varies, however. Using a typical value for high strengh optical fibers, m = 80, shows an improved estimation when R is reduced from 8 to 2. See Figure 7.

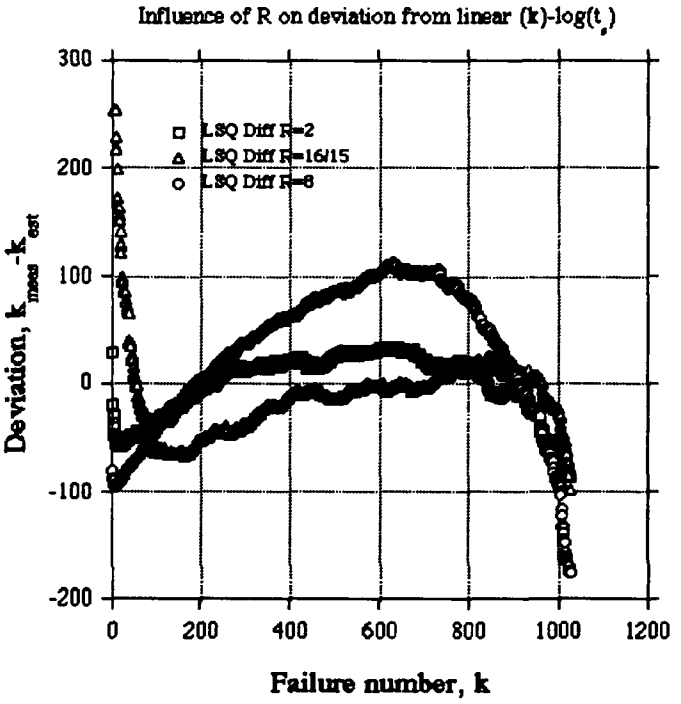


Figure 7. Deviation from linear k-Ln(t) relation

Apparently an optimum is being passed after having applied even smaller values, $R \approx 1$. This is evident in Figure 7 for the curve R = 16/15 which deviates significantly from linearity. The initial part of data now better follows another relation: $Ln(k) \propto Ln(ts)$

Generally, the function $k(\ln(t_s))$ is crescent-shaped. This is more pronounced for higher values of R. A significant improvement of the linearity may be obtained by plotting k versus $[1+k/N(1-k/N)\ln(R)]\ln(t_s)]$. The slope of the line also is quite well in accordance with the previous observations in Table I. However, the slope is consequently about 5% smaller than the factor $N/[nLn(R)]$. Further, the replacement of $\ln(t_s)$ is not well justified, physically. Finally, the choice of $\Delta k/\Delta \ln(t_s)$ turns out to be surprisingly good, according to Table II. This table shows simulations using typical values of m and n for optical fibers, and very reasonable values of test parameters: N=1024, and R=2.

$\Delta k/\Delta Ln(t_s)$	75.42, 73.11, 74.82, 74.296, 74.899, 74.831, 71.909, 72.548, 73.827, 74.251
average	73.99
std dev.	1.14
N/[n·Ln(R)]	73.86

N=1024, R=2, m=80, and n=20

Table II. Repeatability of DS test simulations

The conclusion is, that the value of $\Delta k/\Delta \ln(t_s)$, from a linear curve fit to all data should agree well with a value calculated from the expression N/[n·Ln(R)]. The proven relation enables the determination of the stress corrosion parameter, n, from the formula

$n \approx N/[\Delta k/\Delta \ln(t_s) \cdot Ln(R)]$

In cases with a ratio R very close to unity, the logarithm of "k" versus $\ln(t_s)$ will give the best fit to a straight line, see Figure 8.

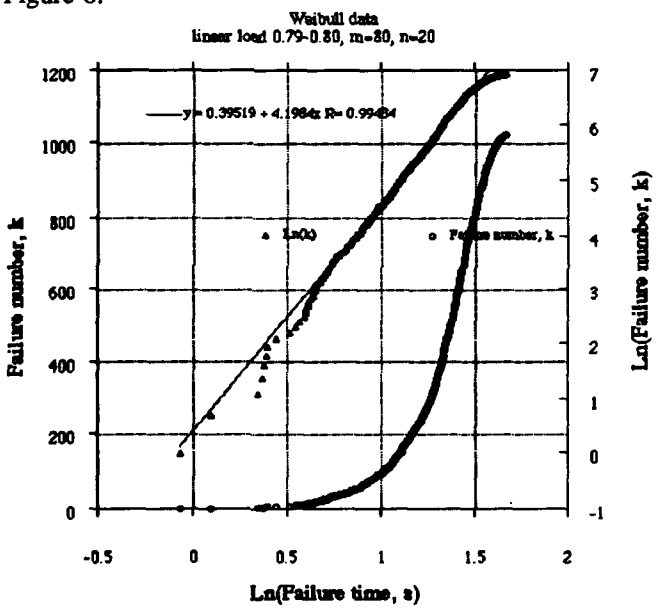


Figure 8. Logarithmic plot (left curve), and linerar plot of k (right curve).

Figure 8 is showing the same data plotted alternatively as k, and ln(k), respectively, versus $\ln(t_s)$. The data were calculated using R=80/79, and m=80. The slope of $\Delta \ln(k)/\Delta \ln(t_s)$ is very close to the theoretical value, $d\ln(k)/d\ln(t_s) = m/(n-2)$.[6]

The ideal case of R≡1 is studied in Figure 9. This corresponds to one and the same load all along the fiber. As expected, the calculated data plotted in a log(k) versus $\log(t_s)$ diagram will join a line with the theoretical slope, m/(n-2).

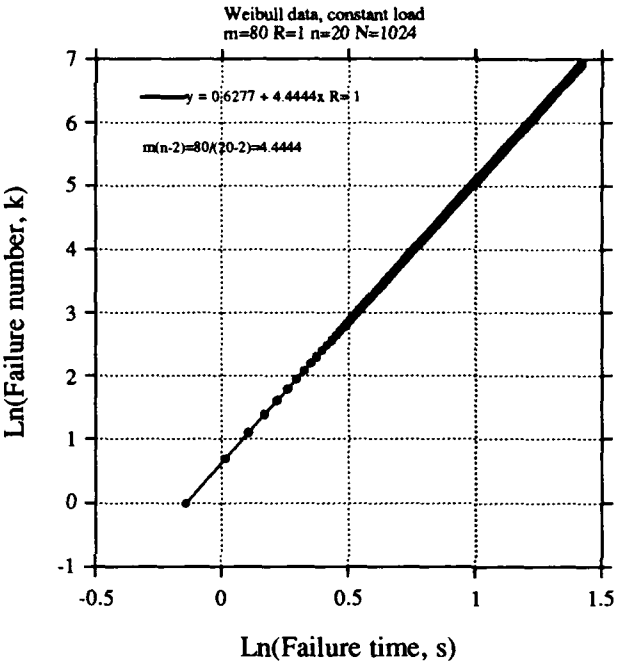


Figure 9. Logarithmic plot applied on R=1.

Supported by the results from simulations, an attempt was made to analytically derive expressions for the relations between time-to-failure, t_s, and failure sequence, k. See equation (1), (2), and (3) in the Appendix.

Although an exact expression could not be derived for the general case, there is a number of special cases for which exact formulas can be derived. They describe the relations between k and t_s, and the parameters n, R, and m, respectively. In order to complete this subject, their derivation will be shown in the appendix.

Summary

Without knowing the value of N, the exact expression

$$\frac{d\ln(k)}{d\ln(t_s)} = \frac{m}{n-2} \qquad (3)$$

can be used to theoretically determine the value of n from a single test at constant load (R=1). In practice, the Weibull modulus, m, varies, making this method unreliable.

Also under a linearly varying load along the fiber (R>1), a single test is sufficient to determine the value of n. For a *fiber of uniform strength* ($m \to \infty$) *the exact expression is*

$$\frac{dk}{d\ln(t_s)} = \frac{N-1}{n\ln(R)} \qquad (2)$$

According to the simulations made, this expression can also be applied on real fiber. For a fiber with a constant value of n, within the ratio of R used, the parameter n can be evaluated from the formula

$n \approx N/[\Delta k/\Delta \ln(t_s) \cdot Ln(R)]$

Though being approximate, the results from the formula are quite good for optical fibers with a typical distribution of strength (m=80).

An ideal, evenly distributed strain along the fiber implies that all failures occur without interference. Theoretically, there is an infinite number of failure sites, hence there will be no upper limit of N. The analysis made, and the DS test suggested, only works for a limited value of N, however.

This is an apparently intricate problem, but it is believed to be solved, either by the fact that an ideal load can not be sustained in a real instrument, or by means of design. The friction can be controlled periodically along the fiber, thus allowing up to a fixed number of failures during test. Such a design is equivalent to a division of the specimen into a number of N independent specimens, which is also assumed in the analysis.

The value of N has a very small influence on the evaluation of the parameter n. In practise, the value of N will be in the range 100-1000, which is sufficient to allow an accurate evaluation of n for typical optical fibers, using a design with a ratio R≈2.

Before testing, a proper combination of σ_{smin} and R should be chosen, to allow capture of all failures within reasonable time. A suitable design of the instrument will facilitate the control of N during the DS test.

Acknowledgements

This work was financially supported by Swedish Telecom Network Services. Appreciation is directed to Mr. Nils Artlöve, and to Mr. Anders Ekblad, at the ST Network Services.

References

1. J. Björkman and T. Svensson, "Quick-Access to Fracture Statistics at Ultra-Wide-Range Tensile Test of Optical Fibers", *Proc of the 39th IWCS*, pp 373-378, Nov. 1990
2. T. Svensson, "Long-duration tensile test of titania-doped, carbon coated, and all-silica base optical fibres", *COST 218TD(91)088* (1991)
3. T. Svensson, "COST 218 round robin test of strength degraded optical fibre", *Telia Research report Sf 6008/92*, 1992.
4. T. Svensson, "Mekanisk provning av optofiber med expander", *Tvt Rapport Plm 87 018* (1987)
5. J. E. Ritter et al. "Application of fracture-mechanics theory to fatigue failure of optical glass fibers", *J. Appl. Phys. 49(9)*, pp 4779-4782 (1978)
6. T. Svensson, "Static fatigue of optical fiber using expander technique. A comparison between static and dynamic failure data", paper presented at the *10th Management Committee Meeting of COST 218*, Berne, Schweiz, Oct. 1991

Biographies

Torbjörn Svensson received his MS and Ph.D. from the Royal Institute of Technology, Stockholm. In 1976 he joined the Dept of Physical Metallurgy at RIT where he worked on mechanisms of plastic deformation. In 1979 he joined the Dept of Materials at the National Defence Research Institute of Sweden, essentially working on high-strain-rate effects in solids. During 1985-91 he was engaged in quality assurance and techniques for testing fibers and cables, at Swedish Telecom. He is now at Telia Research AB.

Erland Sundberg received his MS from the Royal Institute of Technology, Stockholm, 1983, in the field of Optics and Solid State Physics. He joined Swedish Telecom in 1984 where he was engaged in development and standardization of techniques for optical fiber measurements. His present employment is at Telia Research AB.

Appendix

Derivation of failure sequence versus time-to-failure

A number of expressions can be derived, which describe the relation between the sequence of failures in time, k, and the time-to-failure, t_s, for each failure, under static stress.

In two cases, R=1, and $m \rightarrow \infty$, the relation can be expressed exactly.

A derived general-case expression is only approximate, due to the randomness involved.

In order to keep the derivation clear, the assumptons made are: $\sigma_{I0} = 1$ GPa, $L_0 = 1$ m. These assumptions will not influence the results.

Definitions The variation of strength and applied stress are given by two expressions. The first expression is

$$\sigma_{Ii} = \left(\frac{i}{N}\right)^{1/m}$$

where

σ_{Ii} = initial strength of order i
m = initial value of Weibull modulus
i = ordinal number of strength
N = maximal number of failures, asummedly being fixed.

According to the previous chapters, this simplified expression models the initial strength of a failure site with ordinal number i, in an ascending order of strength.

The other expression is

$$R = \left(\frac{\sigma_{smax}}{\sigma_{smin}}\right)$$

R is a design parameter which defines the limits of applied static stress along the fiber. $R \geq 1$.

Failure sequence at general variation The sequence of failures in time is k = 1, 2,..., N. N is the last failure. In general, $k \neq i$, but doing the approximation i = k enables analysis.

The first failure, at k = 1, having an initial strength of σ_{I1}, will assumedly occur at the highest stress, $\sigma_s = R \cdot \sigma_{smin}$. The corresponding time-to-failure is

$$t_{s1} = \frac{const}{\sigma_{I1}^2}\left(\frac{\sigma_{I1}}{R \cdot \sigma_{smin}}\right)^n$$

The last failure, at k = N, is assumed to occur at the lowest stress, $\sigma_s = \sigma_{smin}$. The initial strength is σ_{IN}, and the corresponding time-to-failure is

$$t_{sN} = \frac{const}{\sigma_{IN}^2}\left(\frac{\sigma_{IN}}{\sigma_{smin}}\right)^n$$

The assumption $R \geq 1$ implies that $t_{s1} \leq t_{sN}$. Combination of the time-to-failure at k=1 and k=N yields

$$\frac{\Delta k}{\Delta \ln(t_s)} = \frac{N-1}{\ln(t_{sN}) - \ln(t_{s1})} = \frac{N-1}{\ln\left[\left(\frac{\sigma_{I1}}{\sigma_{IN}}\right)^2 \left(\frac{R \cdot \sigma_{IN}}{\sigma_{I1}}\right)^n\right]}$$

or

$$\frac{dk}{d\ln(t_s)} = \frac{N-1}{n\ln(R) + (n-2)\ln\left(\frac{\sigma_{IN}}{\sigma_{I1}}\right)}$$

The expression can be simplified, by applying the definition of the initial strength at i = 1 and i = N,

$$\frac{dk}{d\ln(t_s)} = \frac{N-1}{n\ln(R) + \frac{n-2}{m}\ln(N)} \qquad (1)$$

The above expression is not exact since, in general, $i \neq k$.

Failure sequnce at uniform strength. The case $m \rightarrow \infty$ implies that $\sigma_{IN} = \sigma_{I1}$. Insertion in equation (1) gives

$$\frac{dk}{d\ln(t_s)} = \frac{N-1}{n\ln(R)} \qquad (2)$$

The data will thus lie along a straight line in a (k) versus $\log(t_s)$ diagram.

Failure sequence at uniform stress. Another case of interest is when $R \rightarrow 1$. The equality $R \equiv 1$ implies that the sequence of time-to-failure exactly follows the sequence for initial strength, $i \equiv k$. Apply this equality on the definition of initial strength,

$$\sigma_{Ik} = \left(\frac{k}{N}\right)^{1/m}$$

The strength ratio between two following failures, k resp k+1, is

$$\left(\frac{\sigma_{Ik+1}}{\sigma_{Ik}}\right) = \left(\frac{k+1}{k}\right)^{1/m} = \left(1 + \frac{1}{k}\right)^{1/m}$$

Insertion in equation (1) yields

$$\frac{dk}{d\ln(t_s)} = \frac{k+1-k}{n\ln(R) + (n-2)\ln\left(1 + \frac{1}{k}\right)^{1/m}}$$

By applying $R \equiv 1$ and $k >> 1$ one gets

$$\frac{dk}{d\ln(t_s)} = \frac{m}{(n-2)\ln\left(1 + \frac{1}{k}\right)} = \frac{k \cdot m}{n-2}$$

or

$$\frac{d\ln(k)}{d\ln(t_s)} = \frac{m}{n-2} \qquad (3)$$

Evidently, the data will now lie along a straight line in a log(k) versus $\log(t_s)$ diagram. ■

ULTRA-HIGH-BANDWIDTH HEAT RESISTANT LEAKY COAXIAL CABLE

K.Aihara, Y.Sakata, N.Tago

Sumitomo Electric Industries, Ltd.
1 Taya-cho, Sakae-ku, Yokohama 244, Japan

Abstract

The available frequency band for mobile communication is generally divided into tree zones(150MHz, 400MHz, 800MHz) for service , and the LCX cable has been widely used in the field of mobile communication system.
Recently the frequency band tends to expand wider according to diversification of various services, but no conventional LCX cable could cover whole frequency band by one cable.
We present radiating design concept and evaluated charactoristics of new LCX cables which has advantageous radiating and low transmission loss in whole frequency band with high performance of heat resistant.

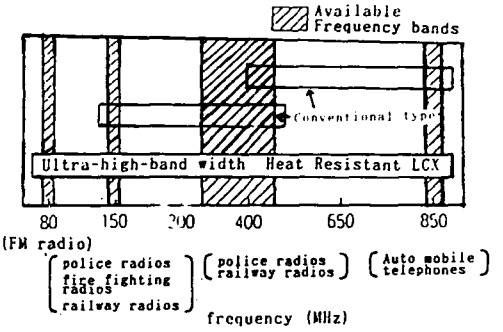


Fig.1 Zone of available frequency

1. Introduction

Leaky coaxial (hereinafter called LCX) cables provide an antenna function as well as a function for supplying electric power to distributed repeaters. LCX cables are widely used in Japan mainly for railway radios, police and fire fighting radios, automobile telephones and portable telephones.
In addition, they are also used extensively as a countermeasure of communication tool in tunnel sections and underground shopping areas, which impede radio wave propagation. Moreover, LCX cables are widely used for mobile radio communication. Their available frequency bands are generally divided into three zones: 150 MHz zone, 400 MHz zone, and 800 MHz zone .
In recent years, mobile radio communication is one of the market fields that has grown rapidly, and the diversion of the services causes the users to have a strong need for the broadband frequencies. And it has been strongly demanded to develop a new type LCX Cable which is capable of covering the wide range of frequency zone from 80MHZ to 800MHZ (we call it as "ultra-high-bandwidth").
This paper describes a ultra-high-bandwith, heat resistant LCX cable which meets the growing demands of bandwidth as shown in Figure 1, so as to satisfy the requirements of the 80 MHz zone in addition to the 150 MHz to 800 MHz zone.
This paper also introduces two types of newly developped ultra-high-bandwidth, heat resistant LCX cables of different feed loss levels, taking into account grating in a real system.

2. Cable Structure

Figure 2 shows the structural drawing of ultra-high-bandwidth, heat resistant LCX cable and the structural specifications.
The center conductor is an annealed copper pipe of approx.17.3 mm in outside diameter and approx.1.0 mm in thickness. Insulating material of polyethylene string is extruded around the center conductor in a spiral fashion. In addition, the spiraly string is covered with extruded polyethylene tube of approx.43 mm in outside diameter to form insulation structure. Glass tape is wound in layers around the insulation to form a heat resistant layer. An outer conductor adopts an annealed copper tape of approx.0.15 mm in thickness. Holes called "slots" are arranged on the outer conductor to generate radiation of radio waves, determining the characteristics of radio wave radiation. For the sheath, flame retardant, polyvinyl chloride is extruded in the shape of a figure-eight crosssection together with a support wire (galvanized stranded steel wire).
Structural key points include a slot arrangement design for the outer conductor for bandwidth, and the use of copper pipe and copper tape in place of conventional aluminium pipe and aluminium tape for both conductor for reducing transmission loss in the high frequency range.

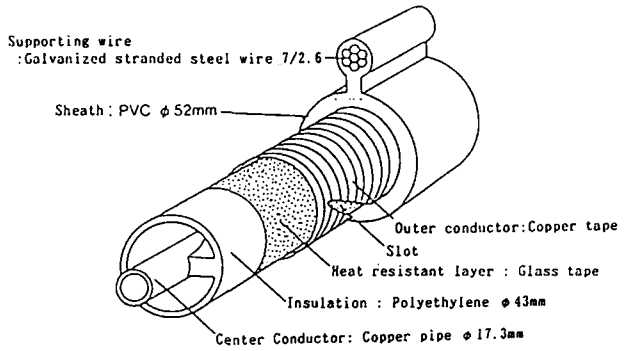


Fig. 2 Cable structure

3. Broadband Radiation Characteristics and Grating

This section outlines the broadband of LCX cable radiation characteristics as well as grating characteristics which is part of the structure of a general LCX cable communication system.

3-1 Radiation principle

Electric current flows in the cable axis direction through an outer conductor of normal coaxial cable which is not adopting the slot structure (Figure 3 (a)). Arrangement of slots on the outer conductor causes the electric current to be disturbed, resulting in the generation of an electric field in the slot in vertical direction to slot lengthwise (Figure 3 (b)). This field is the source of radio wave leakage to the outside of the cable (Figure 3(c)). This paper considers such an electric field with slots periodically arranged. Under this case it is assumed that a long array antenna is used; the paper analyzes the situation as a case of an array antenna of infinite length.

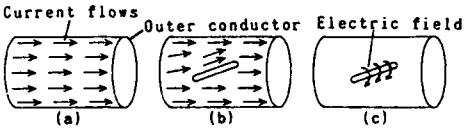


Fig. 3 Leakage from slots

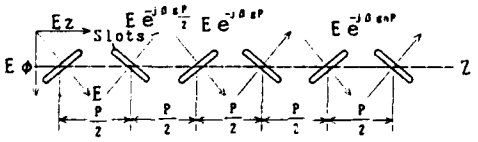


Fig. 4 Zigzag slots array



Fig. 5 Transmission of electromagnetic waves

As shown in Figure 5, transmission of electromagnetic waves radiated from arrays S_1, S_2, etc., of waves sources having equal wave source strength in a direction of ξ viewed totally requires establishing the following relationship:

(Phase of wave source S_{i+1} - $K \cdot \overline{S_{i+1} W_{i+1}}$)
- (Phase of wave source S_i - $K \cdot \overline{S_i W_i}$) $= 2n\pi$ (1)

However, the following must be satisfied:
$n = 0, \pm 1, \pm 2 \ldots$
$K = 2\pi / \lambda$ (λ: wave length in free space)

If this relationship is applied to Figure 4:
(1) Component of the electromagnetic wave by the array of Ez component

$$-Bg \frac{P}{2} + K \frac{P}{2} \sin \xi_{z,m} = 2n\pi$$

$$\therefore \xi_{z,m} = \sin^{-1} \left(\frac{m\lambda}{P} + \frac{1}{V} \right) \quad (2)$$

However, the following must be satisfied:
$m = 2n$, $Bg = 2\pi / \lambda g$ (λg: wave length in the cable)
V: wave length reduction factor ($\lambda g = V\lambda$)

(2) Component of the electromagnetic wave by the array of $E\phi$ component

$$\left(-Bg \cdot \frac{P}{2} - \pi\right) + K \frac{P}{2} \sin \xi_{\phi,m} = 2n\pi$$

$$\therefore \xi_{\phi,m} = \sin^{-1} \left(\frac{m\lambda}{P} + \frac{1}{V} \right) \quad (3)$$

However, the following must be satisfied:
$m = 2n + 1$
The following is obtained with formulae (2) and (3) thrown into one:

$$\xi_m = \sin^{-1} \left(\frac{m\lambda}{P} + \frac{1}{V} \right) \quad (4)$$

$m = 0, \pm 1, \pm 2, \ldots$

Existence of a real number solution in formula (4) generates radiation waves, and the transmission of radio waves is put into effect in the direction away from the cable axis. The condition of having a real number solution is as follows:

$$\left| \frac{m\lambda}{P} + \frac{1}{V} \right| \leq 1 \quad (5)$$

3-2 Broadband radiation characteristics

Since radio waves are radiated in the range given in the formula (5), this formula indicates that radio waves are radiated in various modes by m. Applications of the cables to mobile radio communication requires that components be radiated for only one of m and to add a condition for surface waves for the other m. Without this condition,

leakage of waves having multiple modes with different space transmission constants can be existent, resulting in being accompanied by many standing waves which are interfering with each other. Thereby, a favorable communication line is difficult to construct.

In order to satisfy above condition, "zigzag slots" as shown in Figure 4 has been widely used as one of the most typical slot arrangement and has been satisfying the requ-irement of ordinary frequency zone. In the case of "zigzag slot" pattern, the following inequalityis obtained owing to the formula (5).

$$\frac{1}{2}\left(1+\frac{1}{\forall}\right) < \lambda_p < \left(1+\frac{1}{\forall}\right) \qquad (6)$$

This inequality means that the ratio of the upper limit to the lower limit in the available frequency zone is 2:1 because of m-th higher modes radiation which is determined by "zigzag slots" pattern. So this concluded that radio waves can be radiated from 70MHz(that is the lower limitof 80MHZ frequency zone) upto maximum frequency of only 140 MHz.

In order to obtain much wider frequency zone of radiated waves, it is nessesaly to control m-th modes radiation. The electromagnetic waves in the m-th mode are radiated by the m-th higher harmonic wave resulting from Fourier series expansion of the δ function in which the strength distibution of the wave source expressed. If distribution of wave source strength is in sine wave, none of the m-th higher harmonic wave is radiated except only one mode.

So we studied the slot structure where the strength of the wave source is distributed in the sine wave as shown in Figure 6. In the case of this sophisticated "sine wave slots" pattern, the following inequality shall be obtained owing to the formula (5).

$$\frac{1}{14}\left(1+\frac{1}{\forall}\right) \leq \lambda_p \leq \left(1+\frac{1}{\forall}\right) \qquad (7)$$

This inequality means that the arrangement shown in Figure 6 allows the ratio of the upper limit to the lower limit in the available frequency zone to be broadened up to 14:1 which is determined by " sine wave slots" pattern. This conclude that radio waves at the lower limit frequency of 70 MHz can be radiated upto a maximum of 980 MHz.

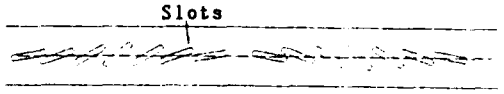


Fig. 6 Ultra-High-Band Width Slots Construction

3-3 Grating

Figure 7 shows a configuration of a communication system that uses grating. When radio waves are received by an antenna to which the power is supplied from the end of an LCX cable, and which allow a certain distance from the cable, the radio wave reception level in the direction of the cable axis becomes lower because of cable transmission loss when the length of the cable is longer. However, if the antenna is connected to another LCX cable, whose radio wave leakage is more than that of the above LCX cable, the reception level is recovered. This recovery should be determined by a transmission system configuration called "grating". Characteristic of LCX cables that compensates the reduction of reception level due to the cable transmission loss with the increase of wave leakage. Generally, the difference in radio wave leakage be tween these LCX cables is approximately 10 dB.

Two types of ultra-high-bandwidth, heat resistant LCX cables have been manufactured, taking into account the frequency dependency in the radio wave leakage and the difference of 10 dB in leakage level.

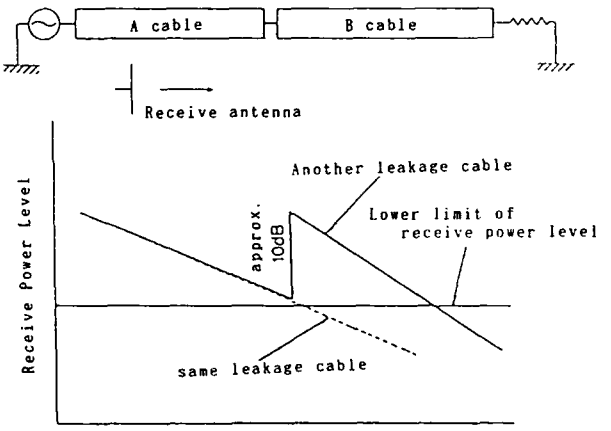


Fig. 7 Outline of grating system

4. High Frequency Characteristics

The two types of cables manufactured were measured with respect to three items: coupling loss, transmission loss, and voltage standing-wave ratio(hereinafter called VSWR). These three items are general high frequency characteristics that up to now have been a requirement for LCX cables.

4-1 Coupling loss

Figure 8 outlines the measurement of coupling loss. The coupling loss indicates value for the amount of radio wave leakage. The coupling loss is a ratio between the power of the transmission signal (Pt) through an LCX cable of approx. 50 m extended on concrete surface and the power of reception (Pt)

for continuously receiving circumference directional components of radiation waves in a lengthwise direction from the cable, when a half-wave length dipole antenna is installed at a point which is above and 1.5 m away from the cable. The coupling loss is defined as shown in the following formula:

$$(\text{Coupling loss}) = -10 \log \frac{Pr}{Pt} \text{ (dB)} \quad (8)$$

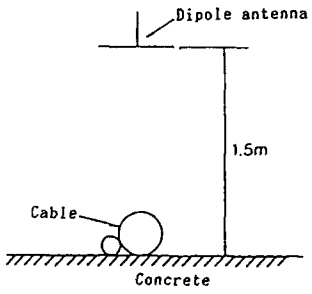


Fig. 8 Measurement method of coupling loss

Figure 9 shows the measurement results for each representative frequency used. Figure 10 shows the frequency dependence in the coupling loss.
In Figure 10, the area marked by slanted lines indicates an area of coupling loss(range of normal coupling loss) applicable to existing LCX cables. In an area of the working frequency zone which 80 to 800 MHz, both newly developed cables A and B are found to provide sufficient radiation characteristics. In addition, a difference in the coupling loss between the two prototype of cable was approximately 10 dB, an optimum value for grating.

4-2 Transmission loss

Figures 11 and 12 show the results of having measured the transmission loss in a condition where an LCX cable is extended on concrete, in the same way as described in Paragraph 4-1. For the reference, a standard transmission loss is indicated when aluminium are adopted for both center and outer

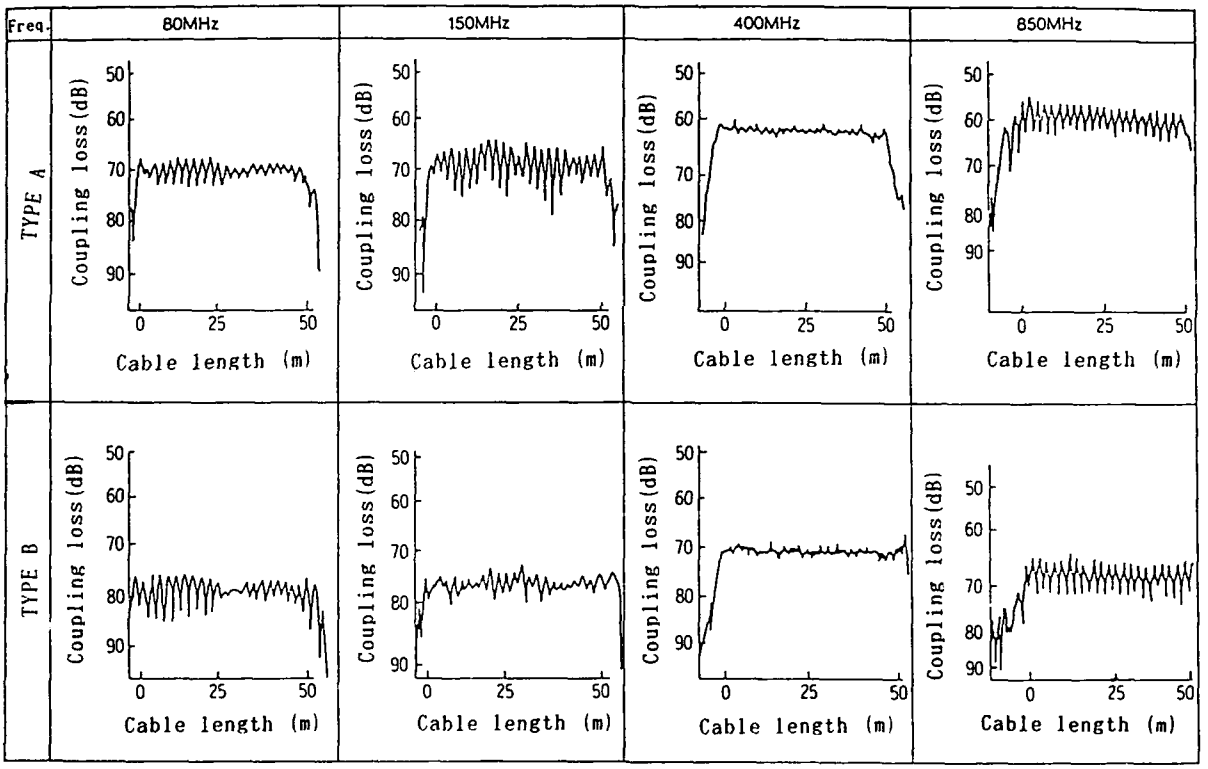


Fig. 9 Coupling Loss ①

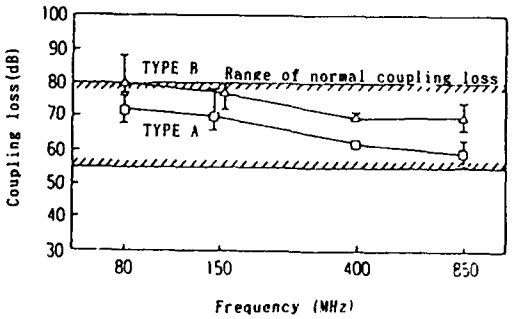


Fig. 10 Coupling loss ②

conductors. From the results, transmission loss is found to be reduced in the high frequency area.

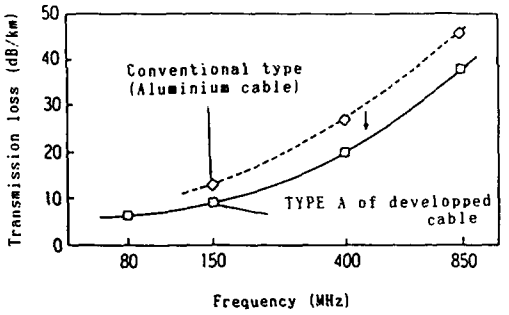


Fig. 11 Transmission loss for TYPE A

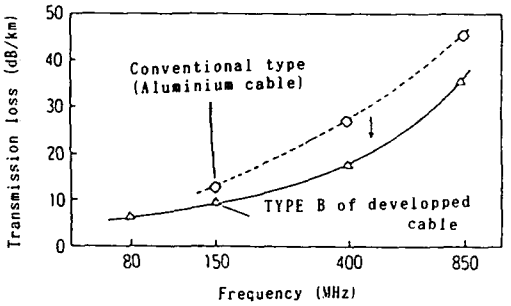


Fig. 12 Transmission loss for TIPE B

4-3 VSWR

Figure 13 shows the maximum value of VSWR in each frequency zone. Moreover, for reference purposes, the standards of existaing LCX cables are shown in Figure 13. The VSWR of existing LCX cables is defined as being 1.5 or less in the working frequency range. The ultra-high-bandwidth LCX cable described at this time was confirmed to have a maximu m VSWR of 1.5 in each frequency range.

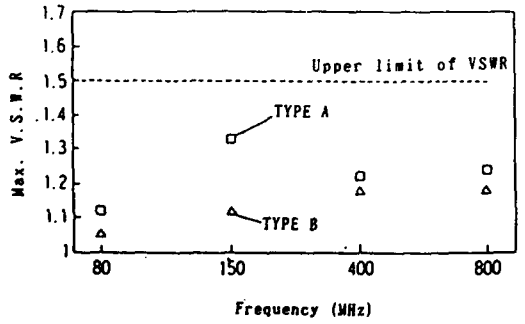


Fig. 13 Maximum value of VSWR

5. Mechanical Characteristics

Table 1 shows the evaluation of mechanical characteristics provided by the cables.

5-1 Bending test

Though a general bending test requires that the LCX cable be bent twice in different directions by 180 degrees, using a mandrel whose diameter is 30 times of the LCX outer diameter.

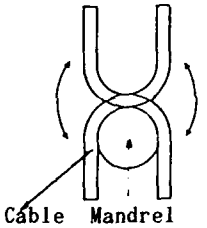
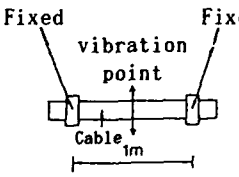
The bending test was carried out under more severe conditions; i.e., the diameter of the mandrel used for the test was 23 times that of the cable outer-diameter. This test confirmed that there was no cracks at neither the center conductor nor the outer conductor.

5-2 Vibration test

This test assumes vibrations due to wind force,etc., created primarily by a fast moving trains. This test confirmed that none of the center conductors, outer conductors, insulating materials and sheath of these cables were cracked after having received vibrations 200,000 times.

It was confirmed from the above results that these newly developed cables provide characteristics higher than or equal to those of existing cables with respect to estimated bend at the time of installation and vibrations after installation.

Table 1 Outline of mechanical tests

Item	Test method	Condition
Bending test		·Cable length 5m ·Mandrel dia. 1200mm ·Bending times twice ·Bending angle 180°
Vibration test		·Cable length 1.3m ·Amplitude ±2.5mm ·frequency 30Hz

6. Heat Resistant Characteristics

Since LCX cables are to be frequently used facilities in tunnel sections and underground areas etc where disaster should be prevented. LCX cable shall also be required to have heat resistance performance characteristics to meet such applications. To confirm the heat resistanceperformance characteristics of these cables, a heat resistant test was carried out as described below.

6-1 Test method

Figure 14 outlines the test method. A test piece of about 1.3m in length, given a weight twice that of cable under testing, is fixed at the position shown in figure 14 in a furnace specified by JIS

(Japanese Industrial Standard) A 1305 "Vertical and Compact Heating Furnace and its Adjustment." According to the heating curve specified by JIS A 1304 "Fire Resistance Test for Building Construction," the test piece is then heated to a maximum of 420 ℃ using a 1/2 standard heating curve for 30 minutes to measure the items listed in Table 2.

6-2 Test results

Table 2 provides the results of the test and general standards. The test confirmed that these cables have sufficient heat resistant characteristics with respect to each test items.

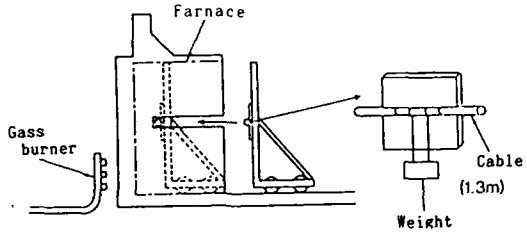


Fig. 14 Heat resistant test

7. Conclusion

We have developed the ultra-high-bandwidth, heat resistant leaky coaxial cables that are applicable in the whole working range of existing leakage coaxial cables and are capable of expanding their band areas to 80 MHz - 800 MHz frequency zone. As the results of evaluation tests, developped cables were prove to have sufficient radio wave radiation characteristics and low loss transmission characteristics and are excellent in mechanical strength.

8. References

1. N. Kurauchi et al.: Wideband Leaky Coaxial Cable, Electronics and Communications in Japan, Vol. 54-B, No. 11, 1971.

2. T. Kishimoto et al.:LCX communication system, Electronics and Communications in Japan, pp15-26, 1982.

Table 2 Test items and result for heat resistant test

	Item	Short circuit	Insulation Resistance	Burned cable length	V.S.W.R.
	Measuring Method Condition etc.	A.C.Voltage of 600V shall be applied between center and outer conductor.	D.C. Voltage of 500V shall be applied between center and outer conductor	Burned cable length of outside of furnace shall be measured.	80MHz zone 150MHz zone 400MHz zone 800MHz zone
Results	sample 1	Good	100 MΩ ≦	0 mm	Max.1.5
	sample 2	Good	100 MΩ ≦	0 mm	Max.1.2
	sample 3	Good	100 MΩ ≦	0 mm	Max.1.4
General Standard		Good	0.4 MΩ ≦	150 mm ≧	5.0 ≧



Katsuyuki Aihara
Sumitomo Electric
Industries,Ltd.
1,Taya-cho
Sakae-ku
Yokohama 244
Japan

Katsuyuki Aihara received the B.E. degree in physics from Tsukuba University in 1987 and joined Sumitomo Electric Industries,Ltd.He has been engaged in the development and design of communication cables. He is now an engineer of Communications Division.



Yasuo Sakata
Sumitomo Electric
Industries,Ltd.
1,Taya-cho
Sakae-ku
Yokohama 244
Japan

Yasuo Sakata received the B.E. degree in engineering from Osaka University in 1974. He then joined Sumitomo Electric Industries,Ltd. and worked on the development of low loss unbalanced type cables and multipair jelly filled communication cables. Thereafter, he concentrated on the development of coaxial cables and optical fiber cables. He is now Manager of Communications Division at Sumitomo Electric Industries,Ltd.



Noriyuki Tago
Sumitomo Electric
Industries,Ltd.
1-1-3,Symaya,
Konohana-ku
Osaka
Japan

Noriyuki Tago received the B.E. degree in electronics and communication engineering from Waseda University in 1980 and joined Sumitomo Electric Industries,Ltd. and worked on the development and design of communication cables. He is now an senior engineer of Radio & Optical Wave Systems Division. He is a member of the Institute of electronics & Communication Engineers of Japan.

LEAKY OR RADIATING ? RADIATION MECHANISMS OF RADIATING CABLES AND LEAKY FEEDERS - CHANNEL TUNNEL APPLICATIONS

André LEVISSE

RFS FRANCE - Département Haute Fréquence

Abstract: Radiating mode cables show major advantages: low coupling loss, field stability, insensitivity towards surroundings, etc. They are propagative solutions of Maxwell's equations and correspond at finite distances to radiation pattern lobes at infinity; they rely on in-phase addition of the fields radiated by all slots. This property is frequency-independent: there is no resonance effect.

The new generation of radiating mode cables is based on a periodic pattern of slots that generates one single radiating mode over a very broad frequency range. Such cables have already been widely used in major projects: more than 260 kilometers of 7/8" radiating cable make up the radiating cable system of the Channel tunnel between France and Great Britain.

I - THEORETICAL APPROACH
 I-1 Coupled modes-Radiating modes
 I-2 Lobes and modes
 I-3 Wide band tuning
II - ADVANCED DESIGN
 II-1 Higher modes
 II-2 Design
 II-3 Performances
III - CHANNEL TUNNEL APPLICATIONS
 III-1 Tunnel system
 III-2 Shuttle system
CONCLUSION
Acknowledgements
References

Mobile radio communications today show the following trends:
-towards higher frequencies: applications shift from 50-150 MHz to 450-1800 MHz ranges.
-towards higher quality links: digital transmissions, high baud rates...
-towards a denser integration in urban zones and confined areas: tunnels, half-buried motor ways, underground parking lots, etc.

Due to multipath and absorption in these areas, transmission by means of antennas is often difficult; this is why a major interest in devices such as radiating cables has developed in the recent years. Radiating cables permit reliable communication whatever the intrinsic quality of the propagating environment may be. Several years ago, the RFS group launched an extensive research program to overcome limitations of leaky feeders:

-high coupling loss, increasing with frequency.
-strong environmental influences, leading to high "safety factors" in power budgets.
-high scattering of fields, this being inappropriate for high quality links

Research directions were:

-to manufacture long slots instead of small apertures in the outer conductor of the coaxial cable. Long slots would behave as much better antennas .
-to determine if RADIATING MODES, which are theoretically calculated, could be found experimentally and produced by a periodic array of slots.

Results:

A large amount of data has been collected by computerized test equipment and shows the influences of the various parameters: distance, polarisation, environment, phenomena of the end effect and frequency...

Experimental evidence of radiating modes has been found and theory has been fully confirmed. Radiating modes have shown major advantages:

-Slots act "in-phase", thus leading to very good radiation efficiency (low coupling loss)

-Only one definite mode propagates, thus avoiding nulls and scattering of fields.

-Environment sensitivity is strongly reduced.

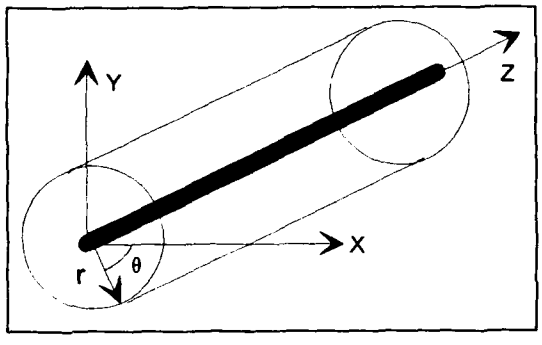
-Broad band use (100-1800 MHz for ex.) and operation of receiving-transmitting devices are maintained.

This article is an introduction to radiating mode cables; its main objective is to educate the reader. It quickly leaves Maxwell's equations and adopts a more intuitive approach based on long-wire antenna radiation pattern lobes. The design of the new generation of radiating cables is then introduced, and aspects of real-scale applications in the Channel Tunnel between Great Britain and France will be given as a conclusion.

I-THEORETICAL APPROACH

I-1 Coupled modes - Radiating modes

Cylindrical co-ordinates are of course fitted to the application of Maxwell's equations governing the fields around the radiating cable:



We start from Helmholz's equation in free space:

$$\Delta^2 H - \frac{1}{c^2}\frac{\partial^2 H}{\partial t^2} = 0 \qquad (1)$$

where H is the magnetic field vector, t, the time, and c is the velocity of light , = 3.10^8 m/s.

we look for solutions of the form:

$H(r, \theta, z, t) = M(r)\ e^{-j\beta z}\ e^{j\omega t}$,

where:

r is the distance to the cable's axis,

z is the distance along this axis

ω is the angular frequency of the wave

t is the time

β is the phase velocity along the z-axis

M(r) describes the decrease of the field versus distance.

Helmoltz's equation is transformed into an expression which only depends on M(r): ($k^2 = \frac{\omega^2}{c^2}$):

$$\frac{\partial^2 M}{\partial r^2} + \frac{1}{r}\frac{\partial M}{\partial r} + (k^2 - \beta^2)\, M = 0 \qquad (2)$$

The solution M(r) which satisfies equation (2), can be expressed in terms of Bessel-type functions, as usual when using cylindrical co-ordinates. The behaviour of these functions is fundamentally dependant on the sign of expression (3):

$$(k^2 - \beta^2) \qquad (3)$$

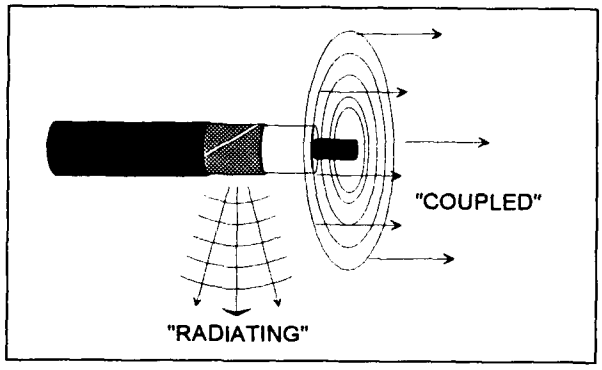
If negative, M(r) is similar to an exponential decrease of r (Vanishing field); if positive, M(r) is similar to an imaginary exponential of r (Propagating field)

Coupled modes:

If quantity (3) is negative (k_r pure imaginary), we speak of Coupled modes. These solutions show a power flow which is parallel to the cable axis. Electromagnetic energy is concentrated in the close vicinity of the cable and decreases quickly with distance: this is why these modes are sometimes referred to as "surface waves". The modes, confined around the cable axis, are partially diffracted by surrounding obstacles and discontinuities (clamps, walls) : a fraction of the power is randomly radiated radially[1].

Radiating modes:

If quantity (3) is positive (k_r real), we speak of radiating modes. These modes correspond to in-phase addition of all apertures. They appear for only very well defined slot arrangements, and over a well defined "Radiated mode frequency" F_r, BUT ARE NOT NARROW BAND: there is no tuning effect comparable to those encountered with antennas.

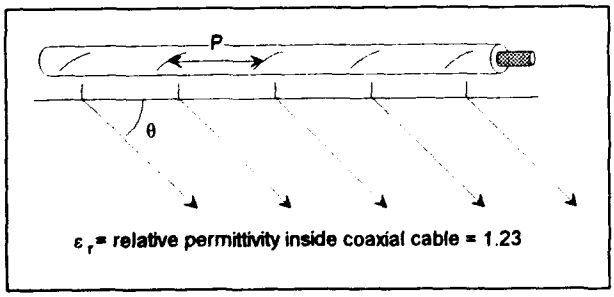


I-2 Lobes and modes

Most radiating cables rely on an periodic array of slots manufactured in the outer conductor of a coaxial cable. We have so far given the basic definitions of the modes of a radiating cable. For such periodic structures, we can now leave Maxwell's equations to adopt a more intuitive approach based one the following principle:

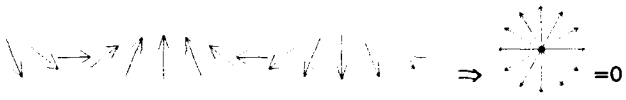
A MODE is the finite distance corresponding to a LOBE on a far-field radiation pattern.

For this, let us consider radiation in one direction characterized by the angle θ, of an infinite array of apertures, fed by a travelling wave. The radiation of all apertures will add up with respect to their phase delay $k(\sqrt{\varepsilon_r} - \cos\theta)P$,



We can represent each radiation contribution by a small arrow whose length represents the amplitude of the radiation, and whose direction represents the phase. As we move far from the array, all lengths are equal.

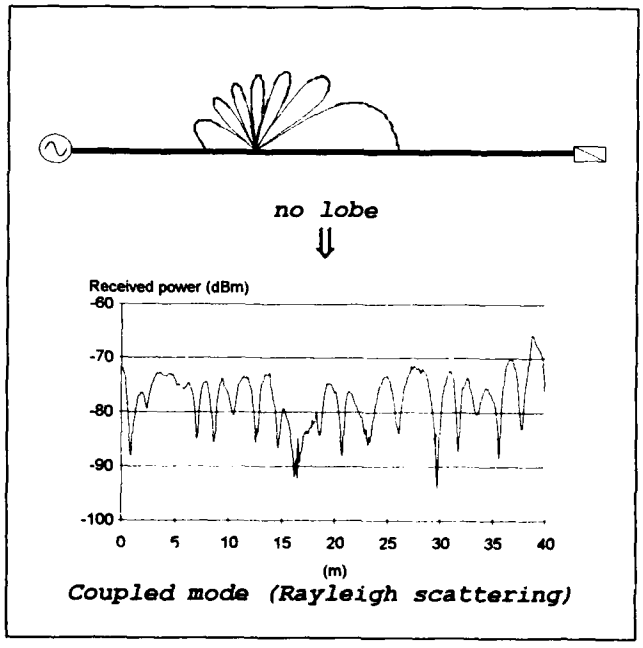
If the phase difference between two adjacent apertures is different from 360 degrees, the arrows will constantly turn, and the overall radiation will be null: there is no radiation in this direction.



If the phase delay between two adjacent apertures is 360 degrees, all radiation's will add up to give a tremendous radiation in the corresponding direction: a LOBE.



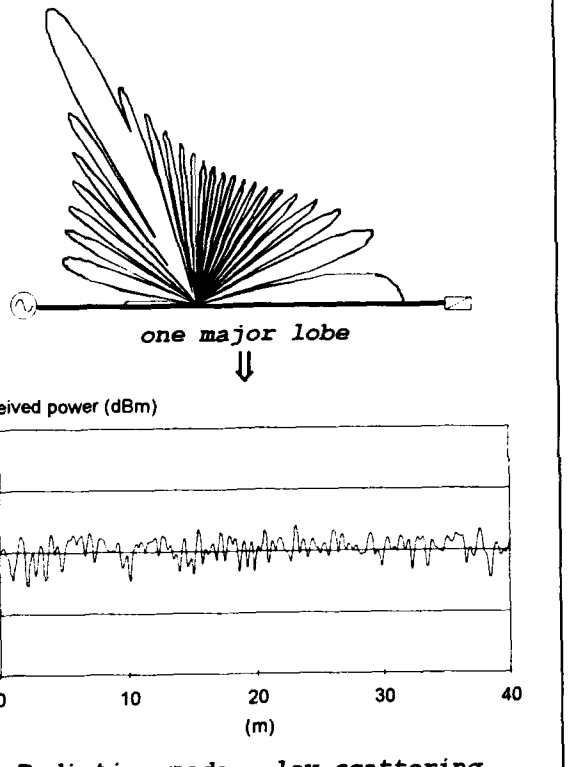
If the distance between slots is small compared to the wavelength, the phase delay between two adjacent apertures will always remain much smaller than 360 degrees, and fields will not add up: we are in the COUPLED MODE configuration:
-low radiation
-high scattering
This is typical at low frequencies.



If a major lobe exists, then the behaviour drastically changes:
-low scattering
-definite waves
-high radiation.

This behaviour appears as soon as the wavelength becomes comparable to the distance between two apertures, over the frequency F_r defined by:

$$F_r = \frac{c}{(1+\sqrt{\varepsilon_r})} \qquad (4)$$



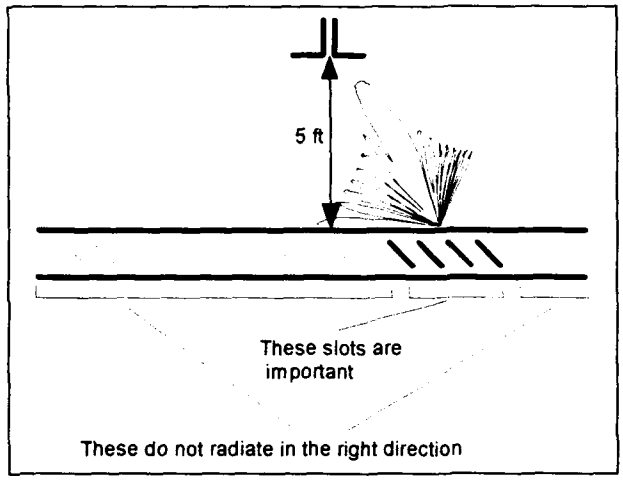
Radiating mode - low scattering

RADIATING MODES correspond to in-phase addition of the radiation of the apertures, this explains their efficiency.

I-3 Wide band tuning

If we try to push this approach forward, we encounter some difficulty: The radiation lobe of an array of antennas changes direction as frequency changes: such an array is narrow-band. How can this be compatible with wide band radiating cables?

Let us consider the same array as above, at a definite frequency. We suppose it shows a lobe at infinity in the 45 degree direction. This means that in this direction, slot radiation add up, and that in other directions, they somehow cancel. Let us come back to a finite distance, i.e 5 feet from the cable, and try to answer to the question *"Which part of the cable makes the major contribution to the power that the antenna receives ?"*



Of course, it is produced by the group of slots which radiate at a 45 degree angle towards the receiving antenna. Radiation of all other slots can almost be forgotten. This group of slots is about 5 / cosine(45) = 7 feet away from the antenna. For another frequency, the lobe of the array turns to for example 60 degrees, because the phase relation between apertures has changed. The group of slots that radiate in the right direction has changed as well, but we find one other at a 6 feet distance.

As soon as the angle becomes large enough, we can find a group of slots acting "in-phase" CLOSE TO THE RECEIVING ANTENNA; the resulting power is not significantly affected by the frequency. This is what we call "Wide band tuning": tuning because slots act in phase, wide band because this co-operative action is frequency independent.

RADIATING MODES: the receiving antenna can always find a group of slots that radiate in phase close to its vicinity.

[The mathematics behind this entire paragraph is of course stationary phase calculations[2]. To compute precisely *how many* slots are in this important group requires deep analysis; this approach is aimed to give a better understanding of phenomenons involved in radiating cables, not to get accurate prediction of coupling loss figures]

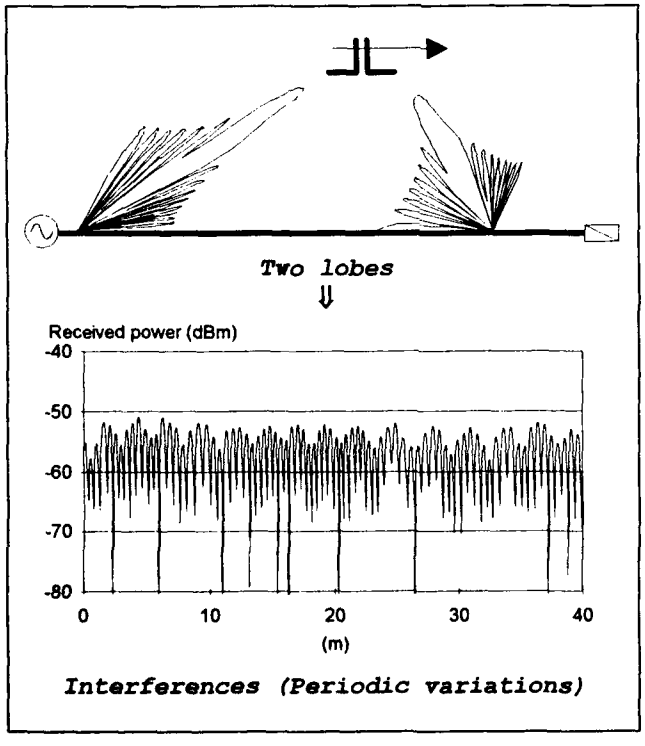
We have seen how the basic properties of radiating mode cables could be easily found:
-high efficiency (low coupling loss) due to in-phase radiation of slots
-low scattering because one definite wave propagates
-environment insensitivity because radiation relies on the array by itself that radiates, not on an excitation of the environment.

We will now see how this property can be practically obtained with a slotted coaxial cable.

II - ADVANCED DESIGN

II-1 Higher modes

We have until now carefully avoided one difficulty: we know what happens when zero or one lobe/mode exists, but what happens if several lobes appear ?



Interferences (Periodic variations)

With the concepts developed above, this is now easy:
-we have two different lobes, characterized by two different radiation angles.
-we thus get two different groups of slots radiating in phase
-as the receiving antenna moves, it reveals the interference pattern between the two sources.

This happens as frequency increases, and could have cancelled one major advantage of radiating modes: their field stability. After this analysis, the target for the RFS radiating cable designers was:
-to obtain a radiating mode
-to avoid obtaining too many of them.

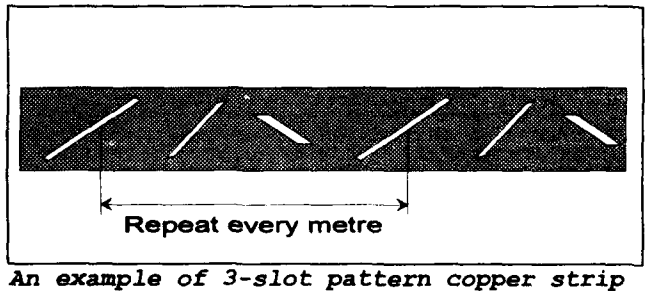
For this, we decided to use a pattern of slots instead of just repeating a single slot.

II-2 Design

The new radiating cable is made out of a copper inner conductor, a low-loss foam polyethylene insulator, and a copper outer conductor in which slots are manufactured. Sizes range from 5/8" up to 1 5/8".

The long thin slots are typically 150 x 3 mm, with a carefully chosen pitch angle.

The new pattern used here is exclusive, patented and optimized. By optimized, we mean that radiating modes are obtained on a given frequency range (e.g. 100-1600 MHz, or 400-2000 MHz) by using a minimum number of slots in one pattern. All other possible arrangements will be more complicated, thus leading to less cost effective designs and extra electrical losses. Odd numbers of slots are used, such as 3,5 and 7.



An example of 3-slot pattern copper strip

These patterns are repeated every meter or less. This ensures the existence of a radiating mode from 90 MHz up to 2000 MHz depending on the cable technology. Some cables are more specifically designed for use from 400 to 1800 MHz, they show better performances in this band, BUT CAN BE USED AT OTHER FREQUENCIES: they then just behave as leaky cables.

As an example, the 7/8" radiating cable presented in the next paragraph is built around a 3-slot pattern repeated every P = 50 centimeters. Expression (4) gives F_r = 281 MHz. It must be emphasized that below this radiating mode frequency, such cables can still be used: they just operate as standard (leaky) cables. When several radiating modes are present, operation is possible with most of the interesting properties of radiating cables but low scattering.

II-3 Performances

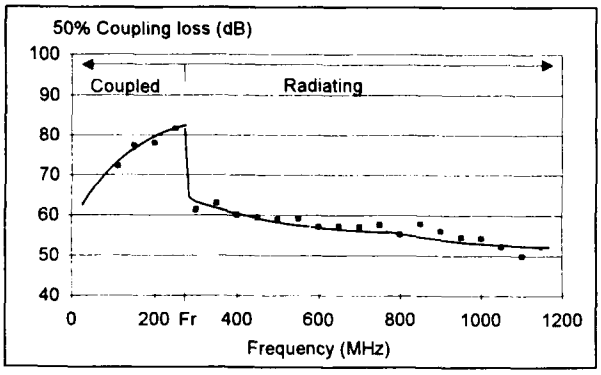
Measurements are performed according to IEC 96 method. We give below values obtained on a 7/8" cable for both coupling loss and longitudinal loss. 95% coupling loss characterizes a level which only 5% of the receiving points fall under.

		450MHz	900 MHz
Longitudinal loss		10.4 dB/1000ft	18.6 dB/1000ft
Coupling loss	50%	60 dB	55 dB
	95%	63 dB	59 dB

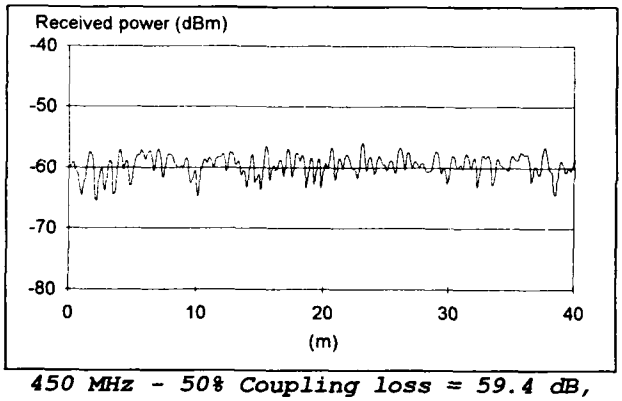
The plot of 50% coupling loss vs. frequency is given on the next page. It clearly points out the influence of the coupled mode/radiating mode transition: coupling loss figures are drastically reduced (from 15 to 20 dB); we can also notice that in the first zone (low frequencies), the coupling loss grows with frequency, while for radiating modes it decreases as frequency grows: this is especially interesting since it compensates for the increase of longitudinal loss.



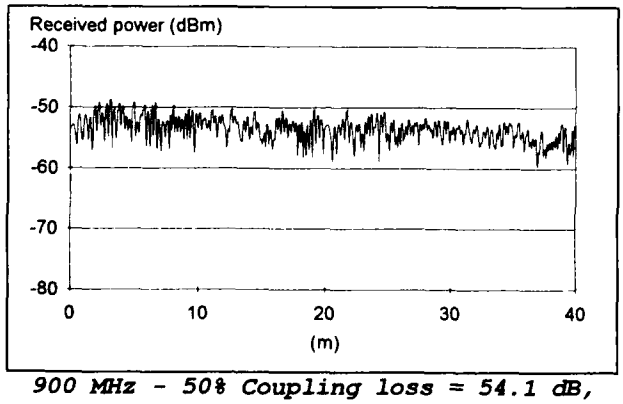
Pict. 1: New generation radiating cables: different sizes and sheathings. On the right, versions with mica tape fire barrier.



Notice in the table the small gap between 50% and 95% coupling loss; to give qualitative aspects of the fields received, records at 450 MHz and 900 MHz are given below. It must be emphasized that at 900 MHz, 3 modes are present and should interfere. The smoothness of the plot confirms that upper modes are almost perfectly cancelled by the new generation pattern.



450 MHz - 50% Coupling loss = 59.4 dB, 95% Coupling loss = 62.8 dB



900 MHz - 50% Coupling loss = 54.1 dB, 95% Coupling loss = 57.3 dB

III - CHANNEL TUNNEL APPLICATIONS

The Channel Tunnel between France and Great Britain is one of the most important tunnels built recently. Three pipes, each more than 50 kilometers-long, will ensure very high speed link between England and the European continent by mid-1993. In such a structure, communication is a major issue and several points were carefully studied:

- Communications reliability
- Durability over time
- Fire safety.

III-1 Tunnel system

Temporary communication systems were used during the construction months, before the installation of the definitive radiating cable system. More than 250 kilometers of 7/8" radiating cable has been used to cover all Channel Tunnel facilities, from main tunnels to small service galleries, from terminals to pumping stations. Planned frequencies range from FM (100 MHz) to 450 MHz, with possible extensions to 900 MHz. Any personnel, in any area within the site, can be communicated with by means of a 450 MHz-band portable radio. Of course, traffic control, video and conversations can transit through the same installation.

In order to ensure a minimum 20 year life in a harsh environment, drastic levels of safety and quality have been met:

-mechanical resistance: radiating cables must be separated from walls by some distance; they are more submitted than other cables to vibrations and air vortex. The cable and the connectors are designed to withstand the passage of high speed trains for 20 years.

-harsh environment: salt water, 100% humidity, dust, must not affect performances nor reliability over time.

-catenary fall: surge protection and grounding is provided to avoid personal injuries in case of induced surges or short-circuit.

-fire and smoke: two jackets made of an exclusive halogen-free compound and separated by a mica film ensure that in case of fire:

- no opaque fumes and no toxic gases are emitted.
- fire is not propagated by the cable.

-quality assurance: all drums have been fully measured during factory acceptances, including sample measurements of parameters such as coupling loss and longitudinal loss. Complementary tests are performed on site.

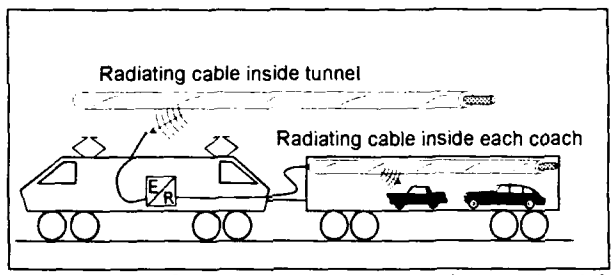
By Summer 1992, more than 220 kilometres of radiating cables were laid and tested. Electromagnetic measurements on site fully comply with what stated. The tunnel should be opened to the public by mid-1993.

III-2 Shuttle system

If one does not care for its size, difficulty and symbolic importance, the subsystem described above is rather classical: radio communication inside a tunnel. We will now present a very original application of radiating cables.

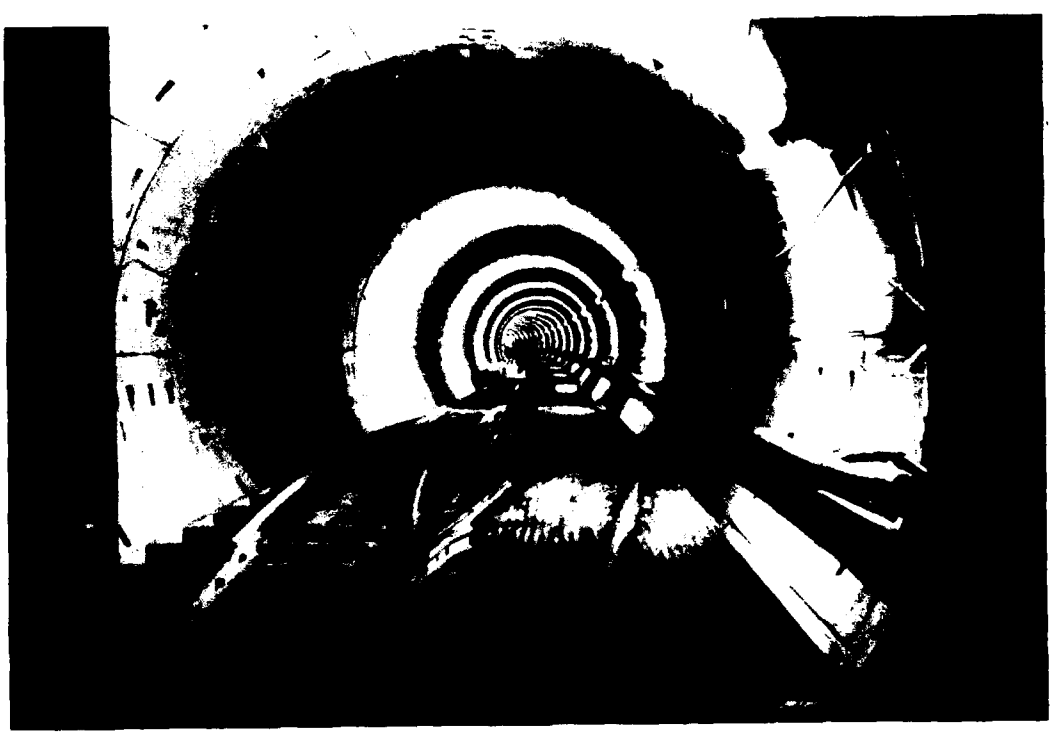
The Channel Tunnel is exclusively a rail tunnel: cars and trucks must embark inside big coaches to be transferred by train for a 30 minute trip. During this time, passengers remain seated in their vehicles and the tunnel management need to pass them information, entertainment, or warning messages.

To allow RF transmission towards car radios in confined environments such as aluminium coaches without reflections, masking effects and disturbances, radiating cables have been chosen. The overall system has the following aspect.



Principle of transmission inside shuttles by radiating cables

For this sole use, about 8 kilometres of radiating cable have been used. Such subsystems are until now very innovative but will widely spread in the near future.



Pict. 2: Channel Tunnel: one of the three pipes, today totally equipped with 7/8" radiating mode cable. (Photo Eurotunnel - Q.A.)

CONCLUSION

Radiating modes are a major breakthrough because of their electromagnetic properties:
-low coupling loss, because of in-phase addition of the fields radiated by all slots
-one only definite wave propagating around the cable
-slow radial decrease of fields.
-low scattering.
-low sensitivity towards environment: the surroundings of the cable are not involved in its radiating properties.

Radiating modes are also interesting because they allow a good prediction accuracy for coupling loss values predictions: computer simulations give for one slot configuration a typical ±3 dB difference with what measured on our test range.

We tried to show through this paper different aspects of radiating cables: from theory to real-scale applications through technological design. The example of applications such as transmission inside trains show that transmission by mobile radio in any area, whatever the propagation conditions, is made possible by the use of radiating cables.

ACKNOWLEDGEMENTS

This project has been initiated and supported by the *Direction Technique* of RFS, with the help of all RFS members in different countries. Mr M. Devicque developped this range of cables and Mr J. Boby dealt with system aspects.

REFERENCES

[1]P. Delogne "Leaky feeders and subsurface radio communications", IEE Electromagnetic waves series 14, Peter Peregrinus Ltd.

[2]L.B. Felsen and N. Marcuwitz, "Radiation and scattering of waves", Prentice Hall 1973, chapter 4.

[3]RFS FRANCE, "Radiating cable handbook", a summary of RFS work on radiating cables, 1991. Available on request.

[4] D.A. Hill and J.R Wait "Electromagnetic characteristics of a coaxial cable with periodic slots" IEEE Trans. Electrom. Compat., Nov 1980, pp 303-307

[5] D.J.R Martin " A general study of the leaky feeder principle" Radio ands Electron. Engr. May 1975, vol 45 pp 205-214

[6] M. Abramowitz and I.A. Stegun, "Handbook of Mathematical Functions", Nat. Bur. of Standards, 1980, pp 355-379



André LEVISSE has graduated in mathematics and telecommunications from the French *Ecole Polytechnique* and from the *Ecole Nationale Supérieure de Télécommunications* (Paris). He worked on FM antennas at RFS Cablewave Systems (CT, USA) and is currently in charge of Radiating Cable Systems development at RFS France.

RFS FRANCE - CGTI
Département Haute Fréquence
35, rue Jean Jaurès BP 20
95871 BEZONS CEDEX
FRANCE
Tel: 33-1 34 23 62 00
Fax: 33-1 39 47 81 51

In the USA:
RFS Inc.
Cablewave Systems Div.
60, Dodge Ave
North Haven CT 06473
USA
Tel: 1 203 239 33 11
Fax: 1 203 234 77 18

Leaky Coaxial Cable with Length Independent Antenna Receiving Level

* Alessandro Coraiola, SIRTI S.p.A. Milano, Italy
o Helmut G. Haag, Karl Schulze-Buxloh, Günter Thönneßen

* SIRTI S.p.A. Via E. Fermi, 2 - I-20060 Cassina de`Pecchi (Milano), Italy
o KABEL RHEYDT AG (former AEG KABEL AG) Bonnenbroicher Str. 2-14,
4050 Mönchengladbach 2, Germany

Abstract

Starting from the characteristics of classic leaky coaxial cables the system performances are deduced. The fact of decreasing receiving level with increasing longtudinal attenuation of the leaky cable with increasing distance from the amplifier limits the length of the unamplified section. This limitation can be overcome by a leaky cable with almost constant receiving level. For the concept of VARIO leaky cable this is achieved by increasing the radiation power over the cable length by increasing the number of radiation slots. The by this enforced increase in longitudinal attenuation is compensated by shortening the subsequent lengths of equal radiation power.
This contribution describes such a VARIO leaky cable and compares the results with conventional leaky cables.

1. Introduction

The transmission between stationary and mobile units in confined areas with leaky cables is well known since more than 20 years.

The ongoing development of new transmission systems leads to higher frequencies such as 960 MHz for GSM together with digital transmission. This limits the repeater section lengths of those leaky cable systems by frequency-dependent higher longitudinal attenuation of the cable. Moreover the confined areas especially the tunnels become longer by the better techniques for tunnel construction. As examples are nominated the Channel-tunnel and the planned Alpes-Basis tunnel.

These two each other enforcing effects cannot only been overcome by thicker this means lower attenuating cables, but new solutions must be found. One step in this direction is the VARIO leaky cable which will be described here.

2. Design and operation characteristics of a conventional leaky cable

The leaky cable has a coaxial design. It consists of a central conductor, a concentric insulating dielectric, an outer conductor which covers the dielectric and a thermoplastic sheath. The conductors are made of copper. The dielectric is composed of polyethylen disks which are extruded around the inner conductor with a regular mutual distance. Over these disks a thin polyethylen tube is extruded. By this a system of closed air chambers is formed which shows good electrical and mechanical properties as for example:

- low dielectric constant,
- low longitudinal attenuation,
- good bending characteristics,
- high lateral stability,
- watertightness (longitudinal and transverse).

Because of its similarity with a bamboo-tree this type of insulation is called "bamboo dielectric" which is well known in CATV-cabling /1/. The outer conductor tape has a pre-punched configuration of apertures, normally rectangular slots.

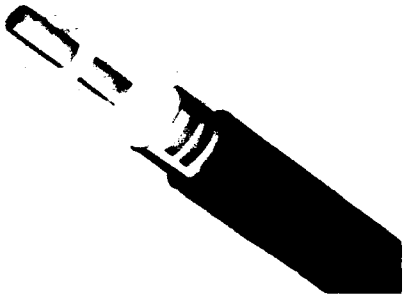


Fig. 1 Leaky Cable

The configuration of apertures determines the radiation characteristics and is described later. Over the outer conductor a thermoplastic sheath is extruded. The standard material is a black fire-retardent non-halogenuous material (Fig.1).

The main attributes of a leaky cable are its longitudinal attenuation and its coupling loss. A coaxial cable attenuates the signal running inside depending on the used frequency. This longitudinal attenuation is mainly influenced by the type of dielectric and the size of the cable. By applying apertures to the outer conductor of a coaxial cable a part of the energy running inside the cable is transferred to the outside surroundings. Also energy can intrude into the cable from the environment.
The mechanism of coupling the interior of the coaxial cable to its surroundings is distinguished depending on the design of the apertures in the outer conductor into

- coupled mode cables,
- radiated mode cables.

Coupled mode cables have a continuous slot along the total cable length or a row of small apertures with mutual distances short or very long compared to the operational wavelength.

Radiated mode cables show a periodic configuration of apertures with a periodicity length in the range of the operational wavelength. The most simple configuration is a row of small apertures in mutually constant distance which equals approximately half of the desired operational wavelength. For a regular configuration of apertures the leaky cable shows at each frequency a constant longitudinal attenuation per unit length and a constant radiation. So the signal level is decreasing from the maximum value at the feeding point monotonuously to the cable end (Fig. 2).

If system structures consisting of leaky feeders and amplifiers are considered, it is necessary to distinguish between one-way and two-way systems /2/ (Fig. 3).

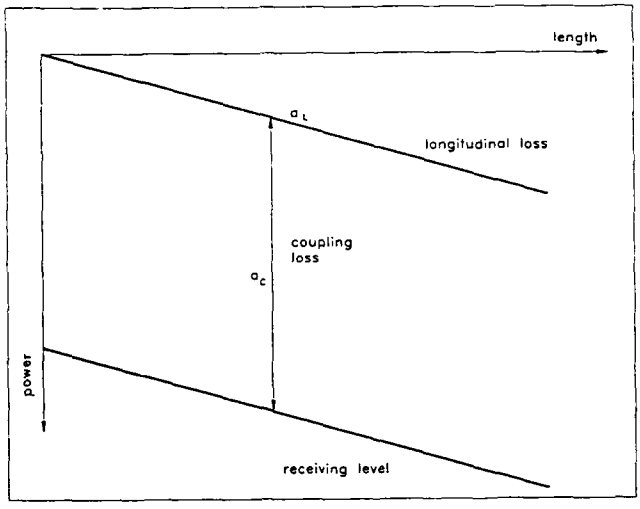


Fig. 2 Longitudinal loss and receiving level versus cable length for normal leaky cable

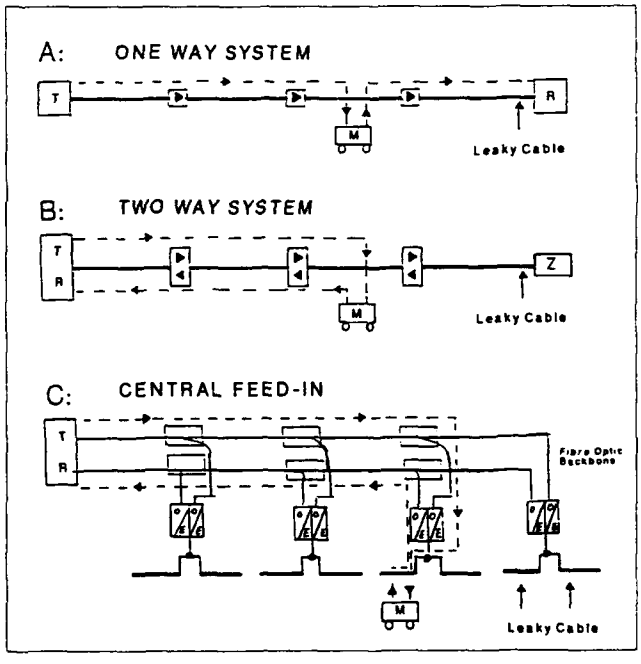


Fig. 3 System configurations for leaky cables

Ref. /3/ shows how, for two-way systems, the use of several cascade leaky cables with different characteristics instead of a single type of cable provides considerably longer amplified sections. It is a fact that the uniform leaky cable is not an optimized radiating means for two-way systems.

This can be presumed if we consider that a uniform leaky cable, due to its longitudinal attenuation, gives a receiving unit moving parallelly to the cable variable electromagnetic field values depending on the position of the receiving unit.
The received field, which is very high at the beginning of the section, progressively decreases as the mobile unit moves away from the amplifier parallelly to the cable.
This field variation, due to the longitudinal attenuation, entails a waste of radiated power in the cable segment near the amplifier and consequently makes it necessary to limit the section length considerably.
In the opposite link direction, the signal transmitted by the mobile unit to the base station arrives at line amplifiers with remarkably variable levels. The amplifiers will therefore work with a high signal dynamics and, for multicarrier operation, this involves a considerable increase in their power requirement to avoid intermodulation problems.
In the following the relations required to obtain a theoretical and practical solution for an uniform field distribution along the whole cable extension (except for the short range Rayleigh-distributed variations) are given.

3. Main relations of a system using leaky feeders

Fig 3B shows a repeater system to connect a base station to a mobile unit located inside a tunnel. The repeater is supposed to be a two-way system which means that the two information signals - to and from the mobile unit - run in opposite directions using different frequency bands.
The line amplifier gain is supposed to compensate exactly the loss of the cable section. If we presume that equal sections are used, the following relations can be considered for both directions:

$$P_{RM} - P_{Rm} = H + D \quad \text{(to basestation)} \qquad (1a)$$

$$P_0 - P_S = A_M + D \quad \text{(to mobile unit)} \qquad (1b)$$

where:

P_{RM}: maximum power per carrier at the amplifier output (dBm)

P_{Rm}: minimum power per carrier at the amplifier output, to ensure that the link will have a correct signal to noise ratio (dBm)

H: signal dynamics due to the length extension of a leaky cable section (dB). H corresponds to the maximum loss variation between the mobile antenna connector and the line amplifier input, evaluated for a complete route of the mobile unit along the section (dB)

D: margin including Rayleigh fading (dB)

P_0: power per carrier towards mobile (dBm)

P_S: minimum power to be granted at mobile input (dBm)

A_M: maximum loss between amplifier output towards a leaky cable section and mobile antenna connector, evaluated for a complete route of the mobile unit along the section (dB)

Relations (1a) and (1b) make it possible to evaluate the carrier levels P_{RM} and P_0 which usually are the highest of the system.
A good system design must aim at reducing such levels in order to limit the cost of the amplifiers and of the power supply.
The noise introduced by the repeater system depends on the number of line amplifiers and the longitudinal loss of the leaky cable sections.
The effects of this noise in both directions can be considered through a receiver threshold degradation included in the terms P_{RM} and P_S of Rel.s (1a) and (1b).

Considering a constant amount of the system noise, Rel.s (1a) and (1b) show how P_{RM} and P_0 (and hence the final amplifier powers) can be reduced by reducing the terms A_M and H.

This is an important result since such terms depend almost entirely on the leaky cable sections used.

H and A_M can be expressed as the fluctuation and the maximum value of the overall attenuation (system loss) between section origin and mobile unit antenna connector.

The system loss A(l,f) is generally a function of the mobile position l within a section and of the frequency f, and can be expressed as:

$$A(l,f) = L(l,f) + T(l,f) \qquad (2)$$

where:

L(l,f): longitudinal loss of the leaky cable from section origin to the mobile position (dB)

T(l,f): coupling loss of the leaky cable (dB).

Then H and A_M are given by

$$H = \max_{(l)} A(l,f) - \min_{(l)} A(l,f) \qquad (3)$$

$$A_M = \max_{(l)} A(l,f). \qquad (4)$$

4. The compensated leaky cable

The signal dynamics may be virtually reduced to zero for a given frequency f_i, assuming the system loss as defined by Rel.(2) is equal to a constant. Hence for $A(l,f_i)=A(l)$ the condition of zero dynamics is:

$$A(l) = \text{constant}$$

or in differential form:

$$dA = \alpha\, dl + dT = 0 \qquad (5)$$

where α is the specific attenuation of the cable (in dB/m) at the frequency f_i.

(5) can be put in the following form:

$$dT/dl = -\alpha \qquad (dB/m) \qquad (6)$$

Rel.(6) shows how a situation of zero cable dynamics can be reached by a cable with the coupling loss decreasing along the length. In order to completely define the compensated cable the following functions are considered at the frequency f_i:

$$T = T(g) \qquad (dB) \qquad (7a)$$

$$\alpha = \alpha(g) \qquad (dB/m) \qquad (7b)$$

$$\alpha = \alpha(T) \qquad (dB/m) \qquad (7c)$$

g is a "geometric variable" which specifies the linear density or the dimensions of the slots which enable the cable to radiate (slot configuration) and is a function of the distance l of the cable portion considered from the section origin. The first two functions can be determined experimentally. An analysis of T(g) and $\alpha(g)$ is under study.

The third function can be deduced from the previous two.

From Rel.(6), and functions (7a) and (7b) the following differential equation can be written:

$$\frac{dT}{dg} + \alpha(g)\ \frac{dl}{dg} = 0 \qquad (8)$$

with:

$$l(g_0) = 0 .$$

The solution of (8) provides the distance l, at which slot configuration g must be located in order to obtain a wholly compensated cable.

g_0 is the geometric variable evaluated at the beginning of the cable (l = 0).

The section length l_1 can be calculated through (8) or directly from integration of (5) using (7c):

$$l_1 = \int_{T_1}^{T_0} dT / \alpha(T) \qquad (9)$$

where T_1 and T_0 are the coupling losses at the end and beginning of the cable section respectively.

The overall longitudinal loss of the cable section at the frequency f_i can also be deduced from (5) and is given by:

$$L = \int_0^{l_1} \alpha \, dl = T_0 - T_1 \qquad (10)$$

The maximum attenuation as defined by (4) for frequency f_i is given by T_0. This is because the function A(l,f) for $f=f_i$ is always equal to T_0.

Figure 4 shows as an example the comparison of a normal leaky cable with constant longitudinal loss (α_1) and constant coupling loss (T_1) to a leaky cable with same geometrical dimensions but varying longitudinal loss and coupling loss (VARIO-concept).

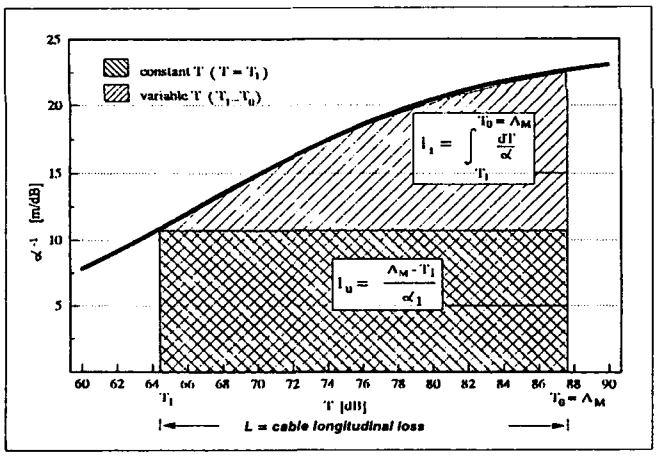


Fig. 4 Cable length calculation for standard and VARIO leaky cable

The reciprocal of the actual longitudinal loss is plotted versus the actual coupling loss. For a normal leaky cable the constant longitudinal loss leads to a straight horizontal line, for the VARIO-concept it results in a curve. This curve was obtained through measurements, some of which are reported in /4/, performed on leaky cables with the same diameter and in which only the slot density has been changed. With respect to a tolerable maximum loss $A_M = T_0$ and equal total longitudinal loss $L = T_0 - T_1$ for the two different cable sections, the length of the VARIO-cable is obtained as the area below the curve:

$$l_1 = \int_{T_1}^{T_0 = A_M} \frac{dT}{\alpha} \qquad (11)$$

whereas for the normal leaky cable the length is represented by the area of the rectangle

$$l_u = \frac{A_M - T_1}{\alpha_1} \qquad (12)$$

It is evident, that the area below the curve is considerably larger than the area of the rectangle, i.e. the VARIO-concept enables considerable advantages in reach for equal cable dimensions /5/.

5. Implementation of the VARIO-concept

To compensate the level drop at the antenna, either longitudinal loss or coupling loss must change with cable length.

The cable attenuation mainly is predetermined by the dimensions of the cable and the dielectric material. In practice it is impossible during cable manufacturing, either to change cable dimensions or to vary the dielectric constant of the insulating material in an adequate extent.

Consequently the coupling loss must be changed to reach the aim. This can be done by enlarging the size of the apertures in the outer conductor.

Another way is to increase the number of apertures per periodicity length.

As the apertures are pre-punched in the copper tape, it is, with regard to the punching process, complicated to vary the size of the punching tools.

For practical reasons it is substantially easier to change the distance between the apertures, i.e. to change the number of apertures per periodicity length.

This leads to the concept of the VARIO leaky cable.

6. Slot configurations and segment lengths of a VARIO leaky cable

As an approximation to a continuous change the variation of coupling loss is done in discrete steps.

Starting from the transmitter point the first segment of the VARIO leaky cable has one small slot per periodicity length perpendicular to the cable axis. By this a certain radiation level is adjusted in the desired frequency band, for example 890 - 960 MHz (GSM). As soon as the signal level has decreased the same amount that is gained by for example doubling the number of slots per periodicity length, the slot configuration is changed accordingly. The signal level at the mobile antenna increases to the value which was measured at the feeder point (Fig. 5). This results in a certain length for the first segment with "one slot configuration". The slot configuration of the second segment shows a slightly higher longitudinal attenuation because of its higher radiation. So the length must be reduced compared to the first segment.

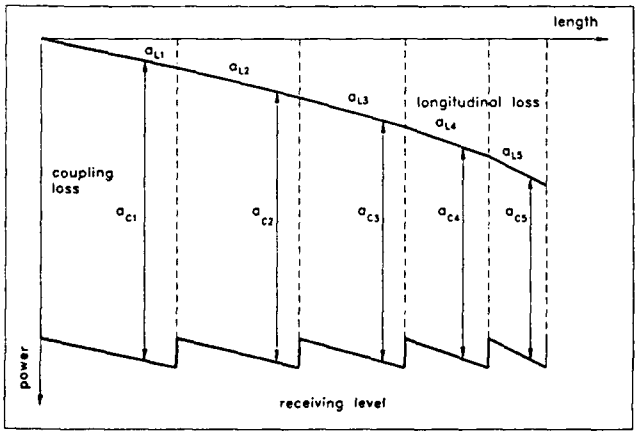


Fig. 5 Longitudinal loss and receiving level versus cable length for VARIO leaky cable

This procedure can be repeated several times as long as there is enough space for placing more slots on the cable. The lengths of the following segments are reduced according to the growing of the specific longitudinal attenuation of the respective segment.

Fig. 6 shows as an example the "one slot configuration" of the first VARIO-segment and the "multi slot configuration" of the last segment.

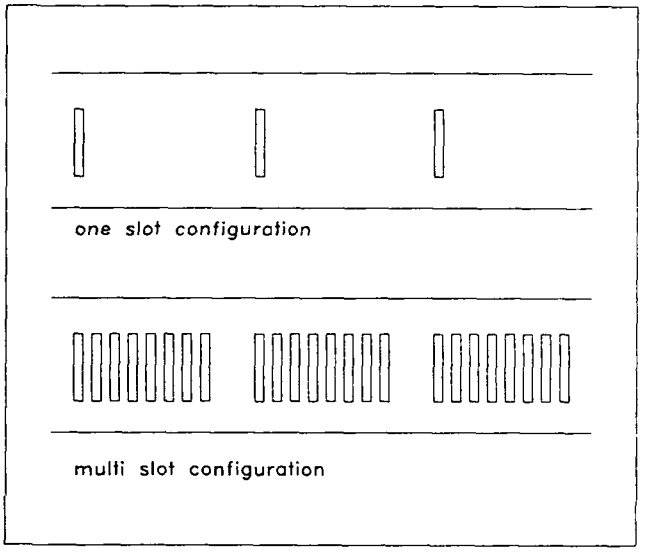


Fig. 6 Slot configuration at beginning and end of the VARIO leaky cable

7. Measurements and results

In contrary to normal leaky cables, where it is sufficient to test a short portion (approximately 100 m) of a cable to describe the total cable length, with VARIO cables the complete cable length must be measured in order to verify the efficiency of the compensation. For this the cable was installed in a tunnel at the ceiling about 5 m above ground. A distance of 12 cm between cable and ceiling is provided by non metallic stand-off clamps with a mutual spacing of 1 m. The distance of 12 cm has resulted as an optimum for a variety of effects on leaky cable properties especially proximity to the wall and humidity.

The VARIO leaky cable was 750 m long and the transmitter output into the leaky cable was 16 dBm. The test vehicle was a small van which carried the mobile antenna and the receiver. It passed parallelly along the VARIO cable in constantly 2,5 m distance. Measurements at different frequencies were taken. Details of the measuring technique are described in /6/.

In the following figures for selected frequencies the signal level at the mobile antenna connector is recorded for a VARIO cable and a corresponding normal leaky cable. Both cables have diameters of 11,9 mm for the inner conductor and 28,9 mm over dielectric.

The distance of the mobile antenna from the transmitter is recorded as the X-axis and the received level at the antenna is plotted in Y-direction.

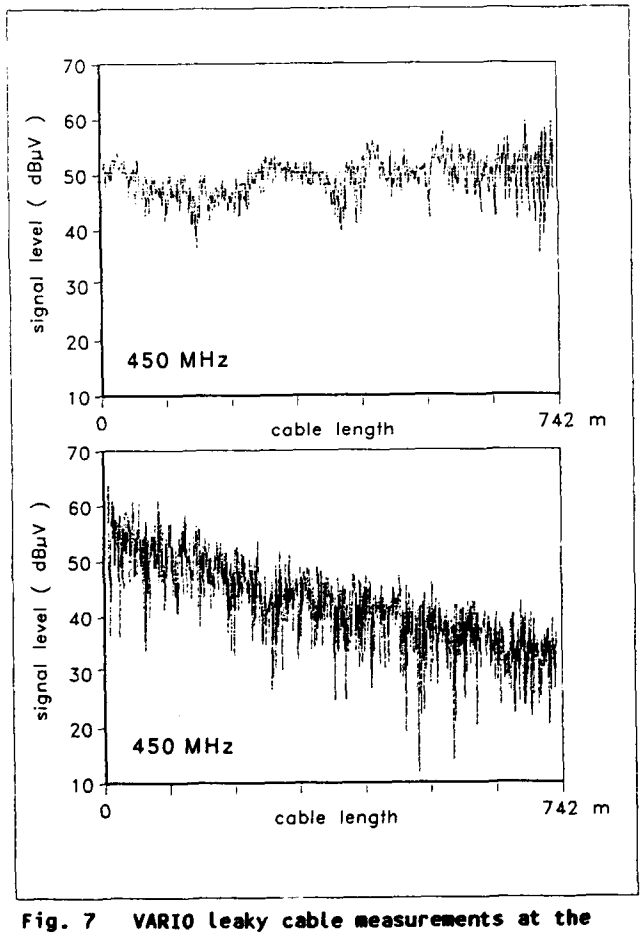


Fig. 7 VARIO leaky cable measurements at the compensated frequency (upper) compared to normal leaky cable (lower)

The most important difference is the decrease of the signal strength for the normal leaky cable. This cannot be noticed in the VARIO cable recording in the "compensated" frequency band (Fig. 7, 450 MHz). The difference in coverage between the best and the worst part of the length of the cable is minimized by the VARIO-concept, i.e. for equal lengths the VARIO cable needs less transmitter power for equal quality of transmission. For equal transmitter power section length can be improved considerably by using VARIO cables, e.g. at 900 MHz:

500 m for normal leaky cable

750 m for VARIO leaky cable.

The measured curves show in good approximation that the VARIO-concept is the right way to the desired compensation of the influence of the longitudinal attenuation of a leaky cable in a certain frequency band.

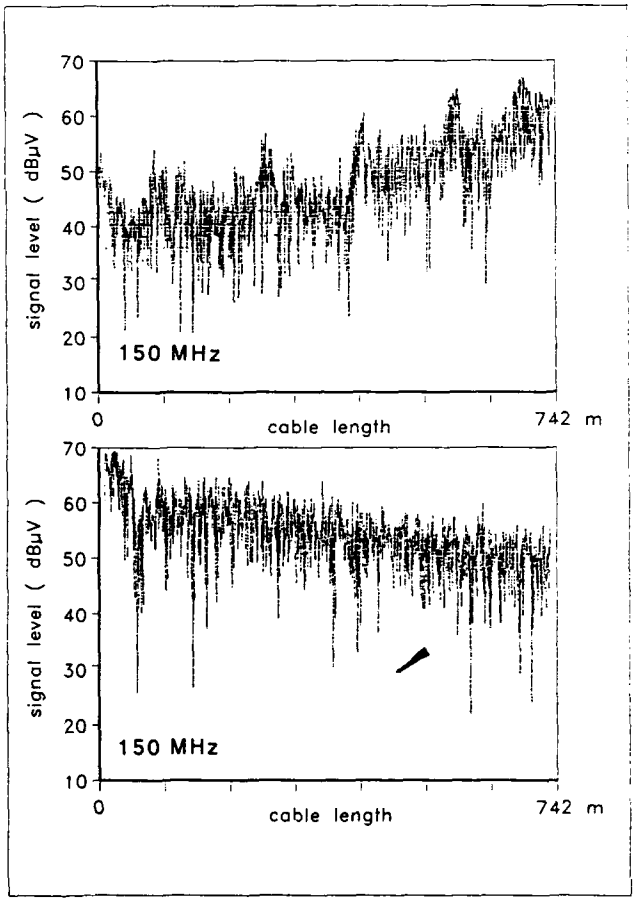


Fig. 8 VARIO leaky cable measurements at lower than the compensated frequency (upper) compared to normal leaky cable (lower)

Even outside the "compensated" frequency band the VARIO cable shows reduced attenuation along its total length.
For lower frequencies than the "compensated" ones (Fig. 8, 150 MHz) the signal level is different but the structure of the "compensated" curve remains with a tendency of "over-compensation".

So the signal level slowly grows with increasing distance between feeding point of the VARIO cable and mobile antenna.

For higher frequencies than the "compensated" ones (Fig. 9, 900 MHz) the signal level slowly decreases because the segment lengths are relatively too long.

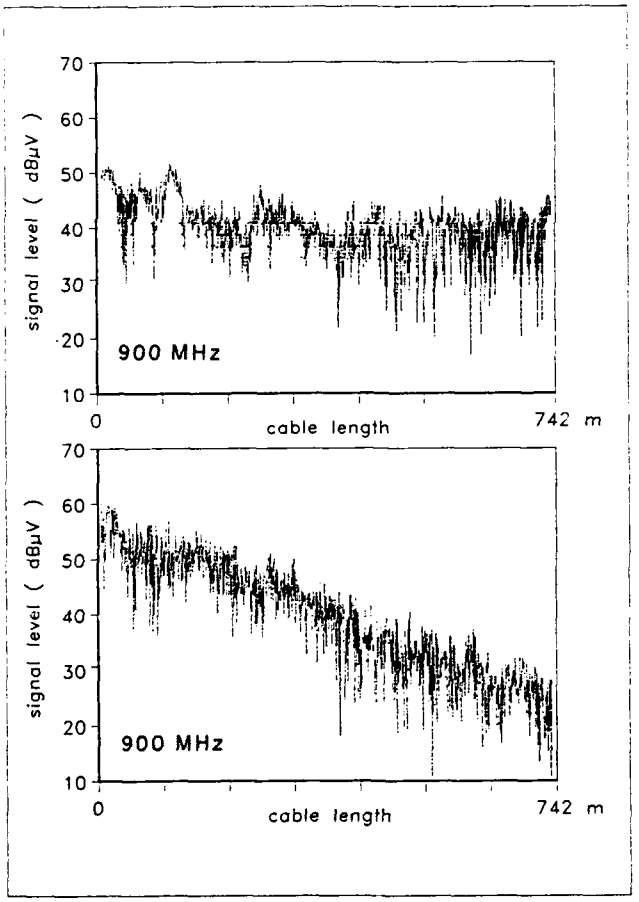


Fig. 9 VARIO leaky cable measurements at higher than the compensated frequency (upper) compared to normal leaky cable (lower)

So, the VARIO-concept has impressively demonstrated its advantages not only theoretically but also in a realistic tunnel environment in direct comparison to a normal leaky cable.

Finally it can be stated that the described general design method can be used to produce VARIO leaky cables optimized for other specific frequencies with clearly better properties than normal leaky cables. This is important especially for higher frequencies like 960 MHz (GSM).

8. Conclusions

Out of the present situation with leaky cables the limitations were appointed which result mainly from the increasing longitudinal loss along the cable section. By theoretical investigations and calculations a compensated leaky cable was proposed. Engineering and development were undertaken to design such a leaky cable of VARIO type. Even if the continuous radiation increase was not performed, the discrete radiation variation leads to excellent results.

This newly developed cable opens the possibility to further activities with acceptable effort for radio communication in confined areas.

Literature

/1/ G. Thönneßen, Kabeltechnik für Breitband-Verteilnetze, TELEMATICA 1986 (Proceedings Part 3), pp 359

/2/ CCIR, Leaky-feeder Systems in the Land Mobile Service, Rep. 902-1, Annex 1 to Volume VIII,- Geneva 1990.

/3/ Toshio Suzuky, Tetsuro Hanazawa, Shiegeru Kozono, Design of a Tunnel Relay System with a Leaky Coaxial Cable in an 800 MHz Band Land Mobile Telephone System, IEEE Transaction on Vehicular Technology, Vol. VT-29, No. 3, August 1980.

/4/ H. Haag, G. Thönneßen, K. Schulze-Buxloh, Leaky Coaxial Cables for Mobile Communication, International Wire & Cable Symposium Proceedings, pp 266, Atlanta 1989.

/5/ A. Coraiola, K. Schulze-Buxloh, Variable leaky Feeders for Cellular Radio Systems, International Conference on Wireless Communication Proceedings, pp 111, Vancouver 1992.

/6/ H. Haag, K. Lehan, K. Schulze-Buxloh, W. Stremme, Leaky Coaxial Cable Systems for High Speed Trains in Tunnels and other Environmental Conditions - Theory and Experience, International Wire & Cable Symposium Proceedings, pp 71, Reno 1990.



Helmut G. Haag (Speaker)
KABEL RHEYDT AG
Director Sales Division
Mönchengladbach, Germany

Helmut G. Haag (44) is Director of the Technical Sales Division for Telecommunications. After reaching his Dipl.-Physiker-degree from the University of Stuttgart he joined AEG KABEL in 1975 for the development of coaxial cables. Later he has been also responsible for the development of optical fibre cables. From 1980 to 1983 he built up the production plant for these cables. In 1991 he took his present position.



Karl Schulze-Buxloh
KABEL RHEYDT AG
Telecommunications Development
Mönchengladbach, Germany

Karl Schulze-Buxloh (36) is Engineer in the Development Department for Telecommunication Cables. He finished his studies at Ruhr-Universität Bochum in 1986 as Dipl.-Ing. In 1986 he joined AEG KABEL. Since this time he is engaged in the development of leaky coaxial cables.



Alessandro Coraiola
SIRTI S.p.A.
Transmission System Division
Milano, Italy

Alessandro Coraiola (42) graduated with full marks in telecommunication engineering in 1976 at the University of Pisa and has been working with SIRTI since 1978. Since 1976 he worked abroad in the installation and commissioning of Earth Station for satellite communications. Since 1988 he is responsible for the mobile sector and has contributed to the definition and development of RF plants including new'y designed systems for cellular coverage.



Günter Thönneßen
KABEL RHEYDT AG
Telecommunications Development
Mönchengladbach, Germany

Günter Thönneßen (54) is head of the Development Department for Telecommunication Cables. He finished his studies at Technische Hochschule Aachen in 1964. After a 3 years employment as a development engineer for CF measuring instruments he returned to Technische Hochschule Aachen, where he graduated as a Dr.-Ing. In 1971 he joined AEG KABEL.

Return Loss of Metallic Telecommunications Cables Due to Periodic and Random Structural Variation and Temperature

L. M. Hore

Bellcore

Morristown, New Jersey 07962-1910

Abstract:

The various industry standards organizations currently propose structural return loss (SRL) as a new transmission requirement for category 3, 4 and 5 premises wires that are intended to transmit signals for STARLAN 1, Token Ring 4 and 5, IEEE 802.9, TPDDI (twisted pair distributed data interface), etc., systems up to 100 megabits/sec. Studies are conducted by researchers to improve the technique of SRL measurements, its relationship with other transmission parameters, any environmental effect on SRL level, etc. This paper deals mostly with the SRL measurement technique and the effect of temperature on the SRL level of premises wires intended for use in the carrier side of the network interface or demarcation point, as well as in building premises.

The effect of temperature on the losses from both conductors and dielectric of a coaxial cable and also on the coaxial cable's SRL level has been discussed. Both theoretical and experimental proof indicates that a cable operating at a lower temperature has a worse SRL level than the same cable at a higher temperature and vice versa.

Similar study has been conducted on unshielded twisted pair wires by exposing them at room temperature and higher than room temperature. Measurements on the wires at these temperatures also show that the wires exposed at higher temperature improve the SRL level over the same wires exposed to room temperature.

The relationship of SRL versus temperature shows independence of the type of structural variations; e.g., random variation of twisted pair wires versus periodic variation of coaxial wire and cable. The magnitude of SRL variations due to impedance discontinuity or impedance mismatch of both twisted pair wires and coaxial cable, although, is different, but follows the same principle which shows that any twisted pair wire or coaxial cable increases its loss at elevated temperature allowing the signal to travel through a shorter distance. This results in reduced number of reflections at the impedance mismatch and produces an improvement in SRL level.

1. Introduction

EIA/TIA-568 for Commercial Building Telecommunications Wiring Standard and NEMA Premise Wiring Standard have been active to develop structural return loss (SRL) limits of higher grade of inside wire products which include unshielded twisted pair (UTP), shielded twisted pair (STP) and coaxial wires. Friesen[1], among others, provided information on SRL measurement techniques of UTP wires. This was followed by a proposal from him[2] at the EIA/TIA TR-41.8.1 Committee meeting held in December 1991 on the development of SRL limits for category 3, 4 and 5 (also designated Level 3, 4 and 5) horizontal wiring. Both EIA and NEMA premises wiring standards groups have been working to include the SRL limits in the premises wiring standards. At the present time, SRL limits are already established for coaxial cable television systems. Since the coaxial cables are also being used for DSX-3 (44.736 Mbit/s) signal transmission[3] in the central office and for other data transmission systems in commercial buildings[4], it is felt necessary to develop similar SRL limits for coaxial wire and cable used for high grade data transmission and other systems.

The transmission parameters of the twisted and coaxial wires depend on the design criteria, materials used in the wire, and the environmental conditions of the wire during its service life. Normally plenum wire operates at room temperature (RT) because it is located in air return plenums. In some buildings, however, wire and cable could run parallel to steam pipes or may be exposed to other heat sources and thereby become heated above ambient temperature, especially in cold weather. In some other buildings, cable could be placed in wiring closets and other non-plenum areas where there is no air conditioning provided and where temperature can rise during summer. With this scenario in mind, the twisted and coaxial wires exposed to elevated temperatures were measured and analyzed to determine if the structural irregularity of the wire poses any additional loss at the elevated temperatures.

2. Periodic Structural Variation and Transmission Parameters

2.1 Periodic Structural Variation versus SRL and Attenuation

The characteristic impedance of a coaxial cable depends on three basic components of the cable: (1) the center conductor; (2) the insulation; and (3) the outer conductor. In practice, the successful manufacture of any given cable design reduces to accurate control of cable components dimensions. In any cable, minute impedance changes along its length cannot be eliminated due to finite instabilities of the production processes. The dimensional variations, which are often periodic, can be caused either by the rolling process of the metal strip forming the outer conductor, from the drawing operations of the center conductor, from minute irregularities of the equipment used for application of the insulation, or from the machine sheaves.

Various papers have been published outlining the theories of structural return loss in coaxial cables expressed in terms of attenuation, length of cable, reflection coefficients, etc.[5,6,7] which treated theoretically random and periodic changes of cable impedances.

Using a model similar to Olszewski and Lubars[5], expressions have been developed in the Appendix for the SRL degradation of a coaxial cable due to the reduction of attenuation by the introduction of lower dissipation factor dielectric material. In computing the SRL, assumptions made are (1) the irregularity periods are symmetrical or periodic, and (2) the reflection coefficients (ρ) are unaffected due to change of dielectric.

Under these conditions, the SRL degradation of the cable due to lower loss can be expressed by the following:

For a finite length,

$$|\Delta SRL| = 20\left[\log_{10}\left(1-R\right) - \frac{0.02461\,V_p RA}{f} + \log_{10}\left\{\frac{1-e^{-0.23AL}}{1-e^{-0.23\left(1-R\right)AL}}\right\}\right] dB \qquad (1)$$

For an infinite length,

$$|\Delta SRL| = 20\left[\log_{10}\left(1-R\right) - \frac{0.02461\,V_p RA}{f}\right] dB \qquad (2)$$

where variables are as listed in the Appendix.

For the measurement of SRL level, due to periodic and random structural variation, an SRL test set developed by Automation Dynamics was used. By adjusting the variable termination bridge, the characteristic impedance of the coaxial cable under test was matched for minimum reflection and the cable was swept between 5 MHz to 300 MHz. Any random minute impedance discontinuities occurring on the coaxial cable are found to produce an SRL trace having small spikes. Only a periodic impedance discontinuity in the cable produces a prominent spike on the SRL trace between the frequency band of interest. It has been observed that if the distance between the periodic discontinuities corresponds to the half wave length or its multiple of the signal transmitted through the cable, a prominent SRL spike will appear at the resonance frequency. A typical sweep frequency SRL trace is shown in Figure 1.

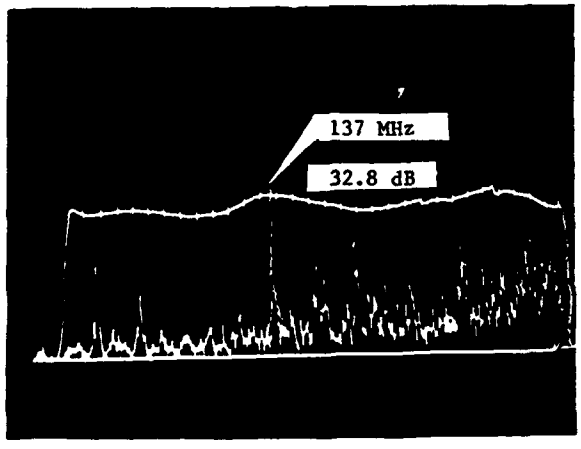


Fig. 1: Sweep Frequency SRL Trace

By utilizing the above equation (1) for finite length, the SRL degradation for any type or any size of coaxial cable with reference to a same type and size of cable of higher loss can be computed. A series of curves were generated for 10.4 mm (0.412") coaxial cable showing their SRL degradation versus percent reduction of attenuation. These are presented in Figure 2 for a cable of finite length of 2000 ft. at frequencies 50, 100, 150, 220 and 300 MHz.

The SRL degradation has also been computed for infinite length at various frequencies using the above infinite length equation (2).

Although the expression in equation (2) is dependent on frequency, the second factor within the parenthesis is practically negligible. For all practical purpose the SRL degradation for any size cable of infinite length with respect to the reference cable is independent of frequency and attenuation of the reference cable, but dependent on the attenuation reduction factor (R). This factor is defined in the Appendix. The computed values for the infinite length are also plotted in the same graph (Fig. 2) for ease of comparison.

As the cable sizes become smaller, the SRL degradation values of both finite and infinite lengths become comparable due to higher attenuation of such cables.

Series of similar curves for any other length of cable can also be generated.

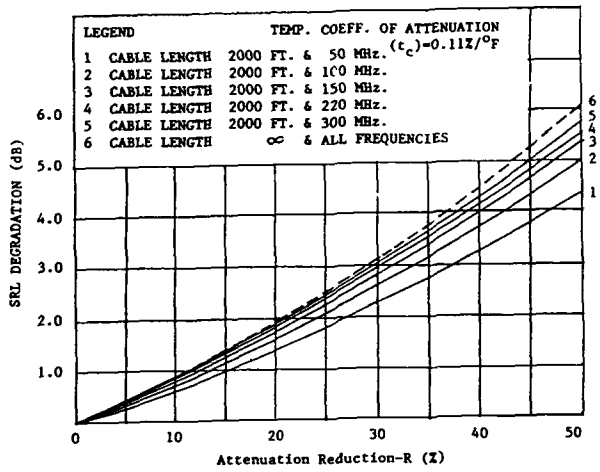


Fig. 2: SRL Degradation as a function of % reduction in attenuation, 10.4 mm (0.412") coaxial cable.

To prove the theory derived in the Appendix, a 10.4 mm (0.412") coaxial cable having equally spaced polyolefin discs was stabilized at an elevated temperature of 140°F (60°C), and both the attenuation and the SRL level of the cables were measured at this temperature. The attenuation and the SRL level of the cables were then measured at different temperatures in the range of 140 to -40°F (60°C to -40°C). Using 140°F measurement data as reference, the percent reduction of attenuation at lower temperature and the SRL degradation of the cable at that temperature were determined.

Fig. 3 is a plot of the measured SRL degradation versus percent reduction of attenuation of 10.4 mm coaxial cable under study. The solid lines represent the theoretical results based on equation (A-10) in the Appendix. The measured results, in some cases, deviate slightly from the estimated values. These discrepancies can be attributed to small changes in average cable input impedance with temperature and imperfect equipment balancing. In general, the measured data are in excellent agreement with the theory.

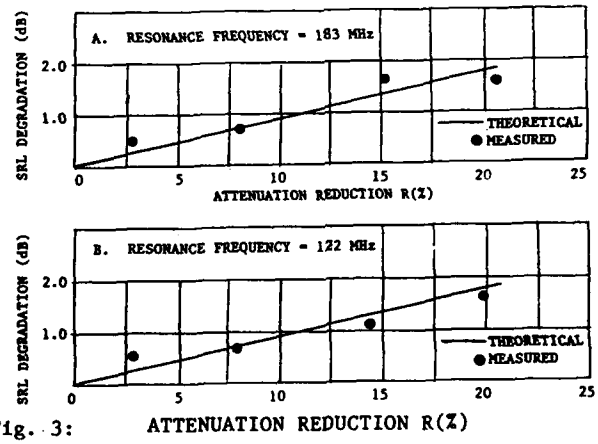


Fig. 3: ATTENUATION REDUCTION R(%)
Theoretical and measured values of SRL degradation -a function of % reduction in attenuation, 10.4 mm (0412") coaxial cable; length of cable, 1692 ft.

2.2 Periodic Structural Variation versus SRL and Temperature

It follows from the same theory that if any cable measured or operating at room temperature of 68°F (20°C) is exposed to an elevated temperature, its SRL level will improve due to the increase in attenuation. Similarly, if the cable is exposed to a lower temperature its SRL level will degrade due to reduction of attenuation assuming, of course, a positive temperature coefficient of attenuation for the cable.

Fig. 4 represents SRL deviation for 10.4 mm coaxial cable of both finite and infinite lengths respectively at any temperature from that of 68°F computed by using equations (A-13) and (A-14) in the Appendix. In these computations, the temperature coefficient of attenuation of cable was measured and found to be 0.11%/°F at all frequencies. The dielectric material used in the coaxial cable samples consisted of a small portion of acrylic acid copolymer and polyethylene whose dissipation factor (tan δ) is relatively constant at the temperature and frequency ranges mentioned above.

It may be of interest to note that the temperature coefficients of attenuation (t_c) of some of the plenum wires using different dielectric materials were measured by the author in the frequency range of 64 KHz to 40 MHz and found to be in the range of 0.08%/°F to 0.30%/°F[8]. The temperature coefficients of PVC were even higher and found to be in the range of 0.25%/°F to 1%/°F within the same frequency band of 64 KHz to 40 MHz. These insulating materials, if used in coaxial cable, are expected to result in the SRL deviation of higher magnitude than those shown in Fig. 4.

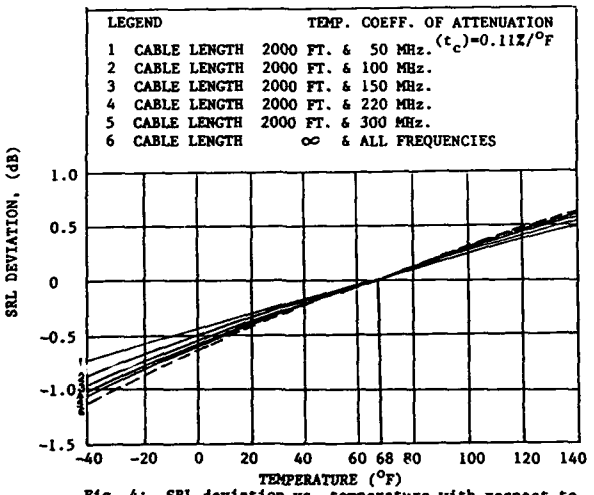


Fig. 4: SRL deviation vs. temperature with respect to 20°C (68°F), 10.4 mm (0.412") coaxial cable.

3. Random Structural Variation and Transmission Parameters

Unshielded twisted pair wires in general exhibit random structural variations due to variations in conductor dimension, DOD (diameter over dielectric), variation of spacing between the wires of a pair, variation in the effective dielectric constant, especially of foam dielectric, etc, unless the manufacturing processes are very well controlled.

The recently proposed method of determining the SRL level of twisted pair wire by Friesen[2] involves measurement of input impedances and by using a least square fitting algorithm the characteristic impedance of the wires. From the characteristic impedance and the input impedances data, the SRL level can be estimated by using the following well known equation:

$$SRL = -20\log_{10}\left|\frac{Z_{in}-Z_o}{Z_{in}+Z_o}\right| \qquad (3)$$

In this paper, the author is interested to show the relative difference in SRL levels between operating temperature viz. room temperature of 73°F (23°C) and high temperature of 150°F (65°C). Instead of proceeding with the least square fitting technique with the aid of an algorithm to determine the characteristic impedance value, which requires extensive computation work, the author is taking a different approach as suggested by Poulsen in his proposal to EIA/TIA 41.8.1 Committee meeting held in June 1992 at St. Johns. This technique proposes that the characteristic impedance (Z_o) can reasonably be estimated by averaging the input impedance (Z_{in}) values within the frequency range of 1 MHz to 16 MHz for level 3, 1 MHz to 20 MHz for level 4, and 1 MHz to 100 MHz for level 5 wires.

Figure 5 and Figure 6 are the input impedance traces of white-orange (W-O) pair of a 4 pair/24 AWG plenum wire designated Level 5. The wire was placed inside a box like a bird's nest to minimize interference between adjacent turns and stabilized at each of the test temperatures of 73°F and 150 °F for 24 hours before any measurements were made. An HP 4194A Impedance Analyzer was used to measure the input impedance obtained from open and short circuit measurements according to the following equation:

$$Z_{in} = \sqrt{Z_{open} * Z_{short}} \qquad (4)$$

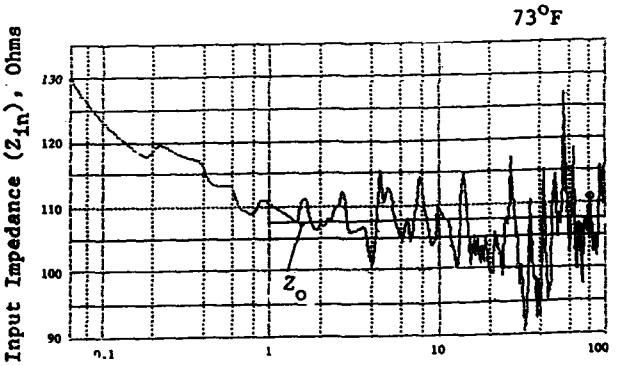


Fig. 5: Measured Input Impedance of Level 5 Wire @ 73°F.

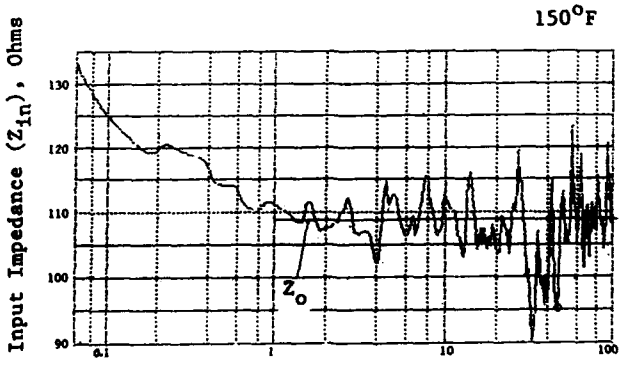


Fig. 6: Measured Input Impedance of Level 5 Wire @ 150°F

The average of the input impedance values is computed and designated as characteristic impedance (see Figures 5 and 6). Fig. 7 represents the input impedance traces of both temperatures, 73°F and 150°F, superimposed.

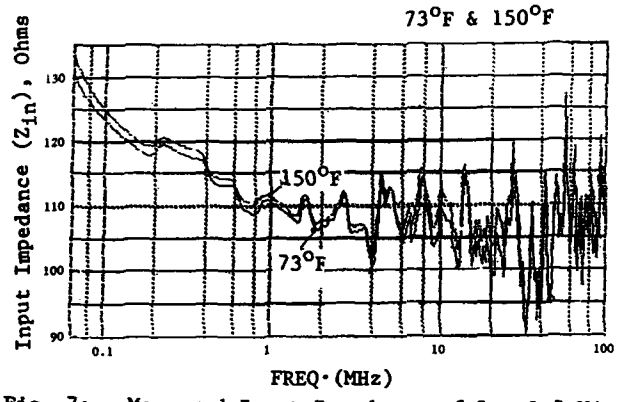


Fig. 7: Measured Input Impedance of Level 5 Wire at 73°F and 150°F Superimposed

To compute the SRL, at first all the frequencies and the corresponding input impedance values where impedance spikes occurred are noted. In between 1 MHz and 100 MHz, there are 250 data points. All the pertinent frequency points within the range have been included for the computation of SRL by using equation (3). The impedance is a complex quantity. Since we are interested in the high frequency range where the phase angle of the impedance is close to 0°, therefore, it is assumed that the

$Z_o = \left(\sqrt{\frac{L}{c}}\right)$ is not a complex quantity.

The computed SRL values at 73°F and 150°F are plotted in Fig. 8 and Fig. 9. A regression line is drawn through the data points by using a programmable calculator. The equations for the best fit lines for 73°F and 150°F are as follows:

73°F:

$$y = -4.02 \log x + 39.08 \quad (5)$$

150°F:

$$y = -3.89 \log x + 40.08 \quad (6)$$

where y: SRL in dB
x: frequency, MHz

The SRL traces of both temperatures are superimposed and shown in Fig. 10.

It is important to note that the SRL values are computed for single reflection only at the location of impedance discontinuity for simplicity's sake. In reality, multiple reflections may take place which could change the SRL values. Since the objective of the study is to make a relative assessment of the effect of temperature on the SRL values, it is appropriate to deal with single reflection only at the point of impedance discontinuity or impedance mismatch.

From equations 5 and 6, we find that the slope of the regression line is -4.02 dB for 73°F and -3.89 dB for 150°F per decade of frequency increase. In Fig. 11, the difference in SRL values between 73°F and 150°F expressed in percent are plotted. Most of the ΔSRL values are positive, indicating that the SRL values are higher (without considering -ve sign) at higher temperatures. The separation of about 1.7 dB between the two regression lines indicates that at elevated temperature, the attenuation of the wire increases allowing the signal to travel through a shorter distance. Some total effect of the increase in attenuation is the improvement of SRL.

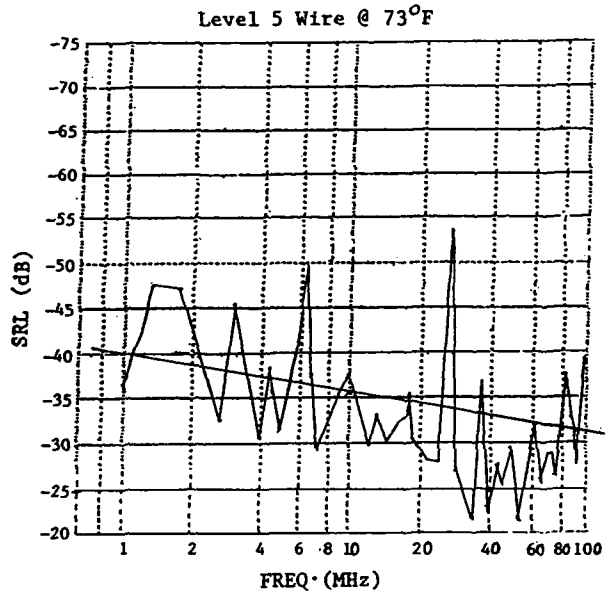


Fig. 8: SRL Values Computed From Input Impedance Data

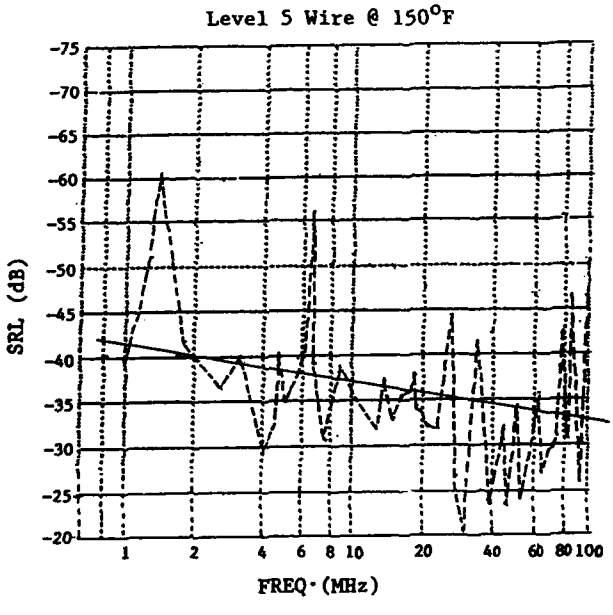


Fig. 9: SRL Values Computed From Input Impedance Data

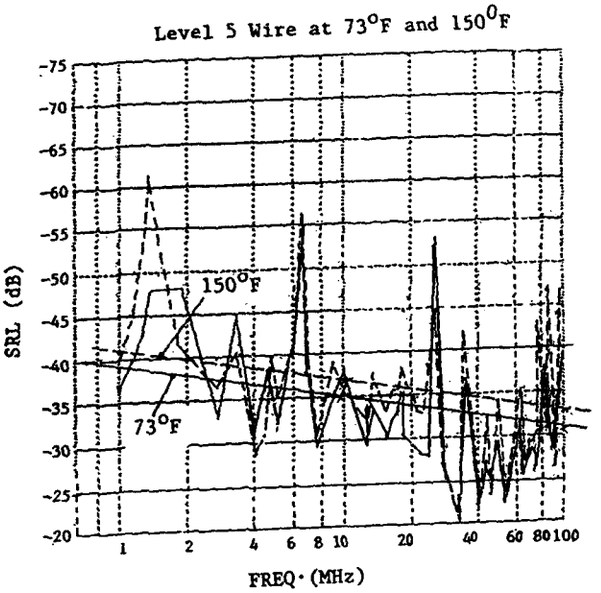


Fig. 10: SRL Values Computed From Input Impedance Data at 73°F and 150°F and Superimposed

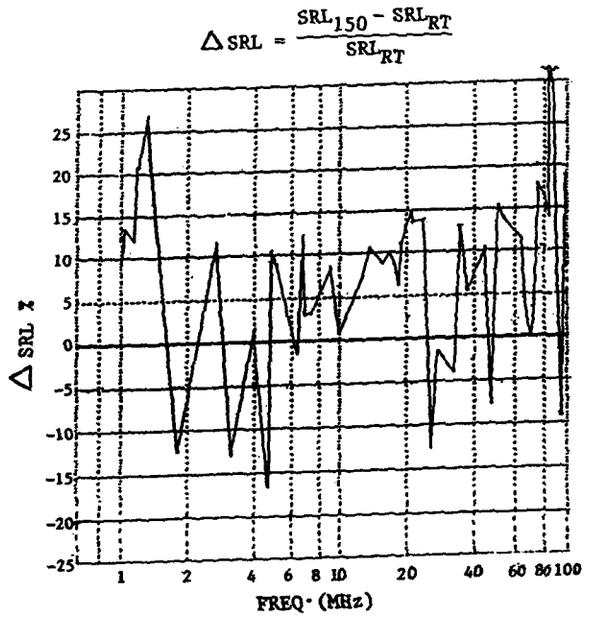


Fig. 11: SRL Versus Frequency of Level 5 Wire

4. Summary and Conclusions

4.1 Periodic Structural Variation

I. The structural variation of a coaxial cable is assumed to follow a periodic pattern.

II. The SRL level of a coaxial cable is degraded if the attenuation of the cable is reduced by utilizing a dielectric of lower loss and vice versa.

III. The SRL degradation of any coaxial cable with respect to a reference cable of the same size and design reduces as the frequency is lowered and the length of the cable is shortened - all because of lower attenuation value.

IV. The SRL degradation of infinite length of a coaxial cable does not depend on cable size or frequency but is a function of the attenuation reduction factor (R) only, as shown in the following expression:

Δ SRL = SRL degradation factor X attenuation reduction ratio (%)

$$= D_{F(R)X} R \qquad (7)$$

where $D_{F(R)} = 0.093$

Note: By drawing a regression line through the different values of $D_{F(R)}$, plotted against R (Table 1) in Appendix, an empirical relationship can be found. From this relationship, $D_{F(R)}$ is estimated to be 0.093.

4.2 Random Structural Variation

i. Unshielded twisted pair wires in general exhibit random structural variations

ii. Within the frequency range of 1 MHz to 100 MHz, the average input impedance values can be considered the same as the characteristic impedance of the wire.

iii. SRL values computed from characteristic impedance and input impedances at different temperatures and frequencies can give a relative picture of the SRL levels versus temperature.

iv. At higher temperature, SRL values improve with respect to room temperature. This is due to the fact that the increased attenuation of the wire at elevated temperature allows the signal to travel through a shorter distance resulting in reduced number of reflections at the impedance mismatches. This means an improvement of SRL level.

5. Acknowledgement

The author acknowledges with thanks the help received from Mark Carangi, Kathie Smith, Tony Stephenson and Chuck Avant of Bellcore, Ketan Pastakia, Bellcore summer student, and Jeff Poulsen of General Cable during the experiment setup, measurements and preparation of the paper. Al Gambardella's help in setting up the HP Impedance Analyzer and generating input impedance data in a short time is commendable. The author expresses his deep appreciation to Al.

6. References

1. H. W. Friesen, "An Evaluation of Measurement Techniques For Determining Copper Cable Structural Effects," 40th International Wire & Cable Symposium Proceedings, 1991, pp. 93-104.

2. H. W. Friesen, presentation on "Development of SRL Limits for Category 3, 4 and 5 Horizontal Wiring" at the EIA/TIA TR-41.8.1 Committee Meeting, December 1991

3. American National Standard for Telecommunications - Digital Hierarchy Electrical Interface, ANSI T1.102-1987.

4. EIA/TIA Standard for "Commercial Building Telecommunications Wiring Standards" ANSI/EIA/TIA 568, July 1991.

5. J. A. Olszewski and H. Lubars, "Structural Return Loss Phenomenon in Coaxial Cables," Proceedings of the IEEE (July 1970), 58, no. 7, 1036-1050.

6. G. Fuchs, "Reflections in a Coaxial Cable due to Impedance Irregularities," Proceedings of the IEEE (London: April 1952), 99, part 4, 121-137.

7. A. E. Karbowiak, "Investigation of Signal Distortion in Cables Caused by Imperfections in Cable Manufacture," Proceedings of the IEEE (June 1974), 1, no. 6, 419-431.

8. L. M. Hore, "Temperature Effect of High Frequency Data Transmission Through Plenum Wires," 40th International Wire & Cable Symposium Proceedings, 1991, pp. 251-259.

9. J. Poulsen, presentation on "A Simplified Alternative Method for Calculation of Structural Return Loss or Input Impedance Limits on Inside Product Wire" at the EIA/TIA TR-41.8.1 Committee Meeting, June 1, 1992.

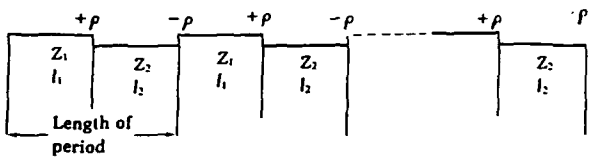


Lal M. Hore
Bellcore
445 South St.,
Morristown,
NJ 07962

Lal Hore is responsible for the preparation of Bellcore's Technical Requirements for Outside Plant Cables and the development of high speed transmission requirements for wire products. After receiving a M.Sc. Tech. degree in Applied Physics from the University of Calcutta and a Dr. Tech. degree from the Technical University of Budapest in Electrical Engineering, he joined Bell Northern Research in 1970 to design and develop communications cables. In 1972, Lal moved to General Cable Company where he worked as a Senior Research Engineer and next as a manager in Communications Cable Research and later as a Staff Project Manager in Applications Engineering until 1987 when he joined Bellcore.

Dr. Hore has authored numerous technical papers on dielectric materials and telecommunications wire and cable and holds a number of patents on telecommunications cables.

Appendix



Transmission line model

Symbols:

$(l_1 + l_2)$	= Length of period
Z_1 (ohms)	= Characteristic impedance of 1st section
Z_2 (ohms)	= Characteristic impedance of 2nd section (let $Z_1 > Z_2$)
n	= Number of periods
α (neper)	= Average attenuation of the line per in.
α_1, α_2 (neper)	= Average attenuation of cables No. 1 and 2 per in.
A (dB)	= Average attenuation of reference cable per 1000 ft.
$\beta = \frac{2\pi}{\lambda}$ (radian)	= Phase constant per in.
V_i (volt)	= Input voltage
V_r (volt)	= Reflected voltage at $(l_1 - l_2)$ junction
$+ \rho = \frac{V_r}{V_i}$	= Reflection coefficient of section $(l_1 - l_2)$
$-\rho$	= Reflection coefficient of section $(l_2 - l_1)$
$V_t = V_i(1 + \rho)$	= Transmitted voltage at $(l_1 - l_2)$ junction.
L (kilofoot)	= Length of cable.
V_p	= Velocity of propagation as a function of velocity of light in vacuum.
f (MHz)	= Frequency of signal.
$(SRL_1 - SRL_2)$ dB	= SRL degradation between cable No. 1 & 2 = Δ SRL.
$R = \Delta\frac{\alpha}{\alpha}$ or $\Delta\frac{A}{A}$	= Attenuation reduction ratio between two cables.
ΔT (°F) = (T − 68) °F	= Temperature difference.
t_c/°F	= Temperature coefficient of attenuation of cable.
$D_{f(R)}$	= SRL degradation factor.

SRL degradation due to attenuation reduction:

It has been shown (ref 5) that if the period corresponds to signal the length of sections l_1 and l_2 are equal the SRL level of coaxial half wave length or its multiple, and cable can be written as

$$SRL = 20\log_{10} R' \left[\frac{1-K^{2n}}{1-K^2}\right] \qquad \text{(A-1)}$$

where

$$R' = \rho_{12} e^{-2\alpha l_1} \sqrt{\left[\cos 2\omega t_2 - \left(1-\rho_{12}^2\right)e^{-2\alpha l_2}\right]^2 + \left[\sin 2\omega t_2\right]^2} \qquad \text{(A-2)}$$

and

$$K = \left[1-\rho_{12}^2\right] e^{-\alpha\left(l_1+l_2\right)} \qquad \text{(A-3)}$$

Further simplifying

$$R' = \rho_{12} e^{-2\alpha l_1} \sqrt{1 - 2\cos 2\omega t_2 \left[1-\rho_{12}^2\right] e^{-2\alpha l_2} + \left[1-\rho_{12}^2\right]^2 e^{-4\alpha l_2}}$$

For maximum SRL, $\omega t_1=\omega t_2=\pi/2$, and $l_1=l_2=l$ therefore, $\cos 2\omega t_2=-1$, therefore

$$R'=\rho e^{-2\alpha l}\sqrt{1+2\left(1-\rho^2\right)e^{-2\alpha l}+\left(1-\rho^2\right)^2 e^{-4\alpha l}}$$

$$=\rho e^{-2\alpha l}\sqrt{\left[1+\left(1-\rho^2\right)e^{-2\alpha l}\right]^2}$$

$$=\rho e^{-2\alpha l}\left[1+\left(1-\rho^2\right)e^{-2\alpha l}\right]$$

$$=\rho e^{-2\alpha l}\left[1+K\right] \qquad \text{(A-4)}$$

Equation (A-1) can be written as

$$SRL=20\log_{10}\rho e^{-2\alpha l}\frac{\left[1+K\right]\left[1-K^{2n}\right]}{\left[1-K^2\right]}$$

$$=20\log_{10}\rho e^{-2\alpha l}\frac{\left[1-K^{2n}\right]}{\left[1-K\right]}$$

Substituting for K

$$SRL=20\log_{10}\rho e^{-2\alpha l}\frac{\left[1-\left(1-\rho^2\right)^{2n}e^{-4n\alpha l}\right]}{\left[1-\left(1-\rho^2\right)e^{-2\alpha l}\right]} \qquad \text{(A-5)}$$

For infinite length, $n\rightarrow\infty$, therefore $K^{2n}\rightarrow 0$, therefore

$$SRL=20\log_{10}\rho e^{-2\alpha l}\frac{1}{\left[1-\left(1-\rho^2\right)e^{-2\alpha l}\right]} \qquad \text{(A-6)}$$

From equation (A-6)

$$\frac{\rho e^{-2\alpha l}}{1-\left(1-\rho^2\right)e^{-2\alpha l}}=\log_{10}^{-1}\left[\frac{SRL}{20}\right]$$

or

$$\rho e^{-2\alpha l}=\log_{10}^{-1}\left[\frac{SRL}{20}\right]-e^{-2\alpha l}\log_{10}^{-1}\left[\frac{SRL}{20}\right]+\rho^2 e^{-2\alpha l}\log_{10}^{-1}\left[\frac{SRL}{20}\right]$$

or

$$\rho^2 e^{-2\alpha l}\log_{10}^{-1}\left[\frac{SRL}{20}\right]-\rho e^{-2\alpha l}+\log_{10}^{-1}\left[\frac{SRL}{20}\right]\left[1-e^{-2\alpha l}\right]=0 \qquad \text{(A-7)}$$

Solving the above quadratic equation for ρ,

$$\rho=\frac{e^{-2\alpha l}\pm\sqrt{\left(e^{-2\alpha l}\right)^2-4e^{-2\alpha l}\left[\log_{10}^{-1}\left(\frac{SRL}{20}\right)\right]^2\left(1-e^{-2\alpha l}\right)}}{2e^{-2\alpha l}\log_{10}^{-1}\left(\frac{SRL}{20}\right)} \qquad \text{(A-8)}$$

If in Eq (A-5), ρ^2 is neglected since $\rho\ll 1$, the ΔSRL between two cables of same size and design but of different attenuation can be expressed as,

$$|\Delta SRL|=\left(|SRL_1|-|SRL_2|\right)$$

$$=20\left[\log_{10}\rho_1 e^{-2\alpha_1 l}\frac{1-e^{-4n\alpha_1 l}}{1-e^{-2\alpha_1 l}}-\log_{10}\rho_2 e^{-2\alpha_2 l}\frac{1-e^{-4n\alpha_2 l}}{1-e^{-2\alpha_2 l}}\right]dB$$

If the reflection coefficients, ρ_1, ρ_2 are considered equal on the assum ption that the same manufacturing line is employed to make the cables, ΔSRL can be simplified to:

$$|\Delta SRL|=20\left[\log_{10}\left(\frac{\alpha_2}{\alpha_1}\right)+2l\left(\alpha_2-\alpha_1\right)\log_{10}\rho+\log_{10}\left\{\frac{1-e^{-4n\alpha_1 l}}{1-e^{-4n\alpha_2 l}}\right\}\right]dB \text{ (A-9)}$$

Employing the conversion factors for the actual,length of the cable L, in EQ (A-9), for finite length:

$$|\Delta SRL|=20\left[\log_{10}\left(1-R\right)-\frac{0.02461\,V_p RA}{f}+\log_{10}\left\{\frac{1-e^{-0.23AL}}{1-e^{-0.23\left(1-R\right)AL}}\right\}\right]dB \qquad \text{(A-10)}$$

For infinite length:

$$|\Delta SRL|=20\left[\log_{10}\left(1-R\right)-\frac{0.02461\,V_p RA}{f}\right]dB \qquad \text{(A-11)}$$

SRL vs. temperature:

Attenuation of a cable A_T per 1000 feet at any temperature $T\,^{\circ}F$ can be expressed with reference to its 68 $^{\circ}F$ value by the following expression using the temperature coeifficient of attenuation of the cable $t_c/\,^{\circ}F$

$$A_T=A_{68}\left[1+t_c\left(T-68\right)\right]$$
$$=A_{68}+A_{68}t_c\Delta T$$

or

$$\frac{\left(A_T-A_{68}\right)}{A_{68}}=t_c\Delta T$$

or

$$R\approx t_c\Delta T \qquad \text{(A-12)}$$

Substituting R from Eq (A-12) in Eq (A-10) and Eq (A-11), ΔSRL can be expressed as:

for finite length

$$|\Delta SRL|\approx 20\left[\log_{10}\left(1-t_c\Delta T\right)-\frac{0.02461\,V_p t_c\Delta TA}{f}+\log_{10}\left\{\frac{1-e^{-0.23AL}}{1-\rho-0.23\left(1-t_c\Delta T\right)AL}\right\}\right]dB \qquad \text{(A-13)}$$

and for infinite length

$$|\Delta SRL|\approx 20\left[\log_{10}\left(1-t_c\Delta T\right)-\frac{0.02461\,V_p t_c\Delta TA}{f}\right]dB \qquad \text{(A-14)}$$

Empirical relationship for SRL degradation of infinite cable lengths:

Let ΔSRL be expressed by the following relationship for infinite length of cable of all sizes and all frequencies.

$$\Delta SRL \approx SRL degradation Factor\left(D_{F(R)}\right) * R, dB \qquad \text{(A-15)}$$

Using Eq (A-11), ΔSRL values are computed as noted in Table 1.

Table 1

R (%)	ΔSRL	$D_{f(R)}$
2	.176	0.0880
5	.446	0.0893
7	.632	0.0903
10	.918	0.0918
12	1.113	0.0928
15	1.415	0.0943
20	1.943	0.0971
25	2.505	0.1002
30	3.105	0.1035

By drawing a regression line through the different values of $D_{F(R)}$, plotted against R, an emperical relationship can be found for limited range of attenuation reduction for ΔSRL. From this relationship $D_{F(R)}$ is estimated to be 0.093.

RADIO-FREQUENCY CABLES IN RUSSIA

A. A. Pavlov, I. B. Peshkov and M. F. Popov

All-Russian Scientific Research Institute of the Russian Cable Industry
111112 Shosse Entusiastov 5 Moscow, Russia

Summary

Radio-frequency cables are used in radio communication and radar systems, in electronic equipment and computers, in control and television systems, in above-ground, underground and submarine applications and in aircraft and spacecraft applications. The extensive use of radio-frequency cables which serve as links for the reception and transmission of radio signals, pulses and digital data both of low and high energy rendered necessary the development of cables with a wide range of dimensions and constructions (range of diameters over dielectric: 0.15 to 80 mm - .006 in. to 3.15 in.), for operating temperatures between -269° and 500°C. Practically all types of cable construction with characteristic impedances of 50, 75, 100, 150 and 200 ohms have been developed and are being produced in Russia. The national standard (GOST 11326.0-78) which includes more than 300 cable types is based on IEC (Subcommittee 46A) recommendations which also takes into account a number of requirements of the U.S. MIL-C-17F as well as national standards of other countries.

Facilities

The Special Design Bureau of the Cable Industry (known as "OKB KP") in Mytishchi, near Moscow which is a unit of the All-Russian Scientific Research Institute for the Cable Industry and the "Sevkabel" factory group (St. Petersburg) deal with the design and the production technology and provide engineering services for the cable manufacturing plants. A number of scientific-technical investigations of radio-frequency cable designs for new and developing technical applications have been completed. Calculations of design parameters and construction data have been developed for different cable types, including radiating cables, cables with corrugated metallic conductors, multi-conductor cables operating in frequency ranges up to 18 - 20 GHz as well as phase-stable cables for radar systems and super-flexible cables for spacecraft communication applications.

General Purpose Coaxial and Twin Conductor Radio-Frequency Cables (-60° to +85°C)

This series of PE-insulated cables (solid, air dielectric and foam PE) includes about one hundred types with diameters over the insulation ranging from 0.6 to 33.0 mm (0.024 in. to 1.3 in.). The inner conductors (solid or stranded) consist of bare, tinned or silver-plated copper wire. The outer conductors are braids. The jackets are made from PE or PVC. The larger cable types carry protective jackets and armor. A number of cables include under the PVC jacket a barrier layer of polyamide tape which prevents component migration from the jacket to the insulation. This feature protects the service life of the cables at maximum operating temperatures.

General Purpose Heat-Resistant Coaxial Cables (-60° to +200°C)

These cables are used in electronics and radio transmission (including rf power transmission) and for aviation or cosmic applications in elevated temperature environments. The insulation consists of multi-layered PTFE tape. In miniature cables PTFE or FEP insulation materials (applied by ram presses or extruders, respectively) are used. The inner and outer conductors are made of silver-plated wires. The jacket materials are FEP, silicon rubber or wrapped PTFE tapes over which a braid of glass filaments is applied. Diameters over the insulation, which is impregnated with PTFE particles and subsequently baked, range between 0.6 and 17.3 mm (.023 in. to .68 in.).

Coaxial Semi-Flexible Cables with Welded and Corrugated Conductors

These cables are used in television and broadcasting systems, radio communication and radar systems and in radio measuring equipment. The cables of this series have air dielectric (PE or PTFE) insulations, with different percentages of air volume. They are standardized by their reflection coefficients (average and maximum values) for the operating frequency bands.

This series includes cables designed for specific requirements (for example: phase-stable cables for phased arrays of radar installations). It is known that conventional cables significantly change their electrical length $\beta\ell$ with a change in temperature (β = phase coefficient, ℓ = length). The above-mentioned changes are due to variations of conductor length and the dielectric constant (ε) of the insulation as a function of temperature.

The normal value of the temperature phase coefficient of a solid PE-insulated cable is between 90 and 200 x 10^{-6}/°C. The temperature phase coefficient of phase-stable cables will not exceed 10 to 15 x 10^{-6}/°C. The low values of the temperature phase coefficient are obtained by using air dielectric with a strictly defined dielectric volume (about 10%), whereby the variation of the dielectric constant ε compensates for the change in conductor lengths. Fig. 1 illustrates the phase variations as a function of temperature

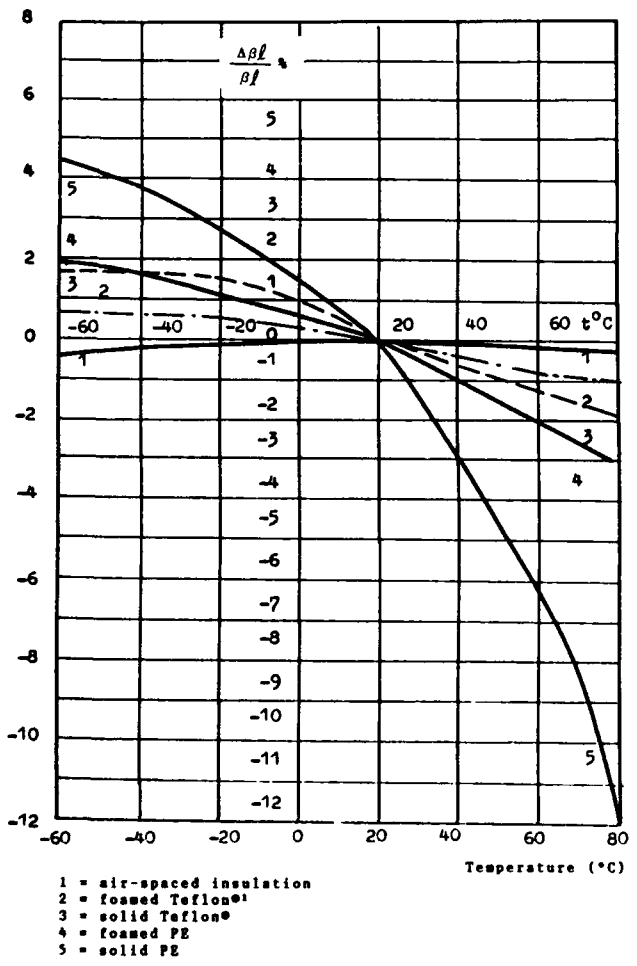


Fig. 1 Phase-temperature characteristics of cables with different insulations

for semi-flexible cables with various types of insulation. It can be seen that the electrical length of phase-stable cables (curve 1) changes between one and two orders less than in conventional cable designs.

The standardization of phase-stable cables according to the reflection coefficient within distinctly defined limits (0.1 to 0.2) ensures the uniformity of their amplitude and phase-shift-frequency characteristics, for it is known that these parameters are interrelated.[2]

Fig. 2 shows test results of the dependence of the phase-shift frequency relationship on the value of the cable input reflection coefficient.

The construction parameters of some types of the semi-flexible cables are listed in Table 1.

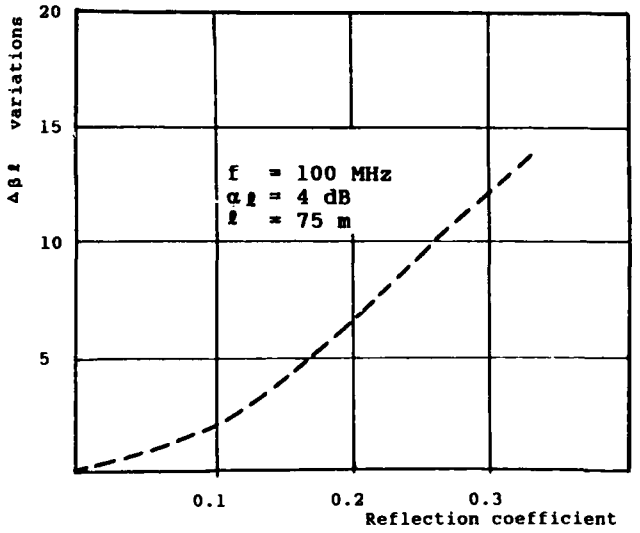


Fig. 2 Increase in phase coefficient $\Delta\beta\ell$ due to periodical non-uniformities depending on reflection coefficient at the resonant frequency.

Semi-flexible cables for connecting test equipment are made with outer conductors of welded thin metal tapes with deep corrugations, with 50 ohms impedance. The longitudinal section is shown in Fig. 3. In order to ensure phase-temperature and phase-mechanical stability a combination PTFE insulation of perforated and foamed tapes is used.

Owing to the deep corrugation (height/corrugation pitch ratio: >1) the cables can withstand about 5,000 double flexures about a 200 mm (7.87 in.) radius. Fig. 4 shows the frequency dependence of

the attenuation constant of the mentioned cable.

Measurements of the phase-mechanical parameters confirm that the phase change of the signal in a cable of 1.5 m (4.92 ft.) length during a flexure cycle with a 200 mm (7.87 in.)radius represents between 0.6 and 1.0 electrical degrees in the frequency range up to 15 GHz and 1.0 to 1.5 electrical degrees in the range up to 18 GHz.

Coaxial Semi-Rigid Cables with Outer Conductors of Solid Copper Tubes

These cable types are used in microwave electronics, instruments and computers. Their insulation is PTFE or FEP. This series includes cables with diameters over the insulation of 0.15, 0.3, 0.6, 1.0, 1.5, 2.2, 2.95 and 4.6 mm (.006, .012, .024, .039, .059, .087, .116 and .181 in.). Constructional details and parameters of cables of this series are given in Table 2.

Radiating Cables for Communication with Moving Objects, Surveillance and CATV Systems

Radiating cables are widely known for their dual function as transmission lines and linear antennas in the metric frequency band resulting from the slots in the outer conductor.

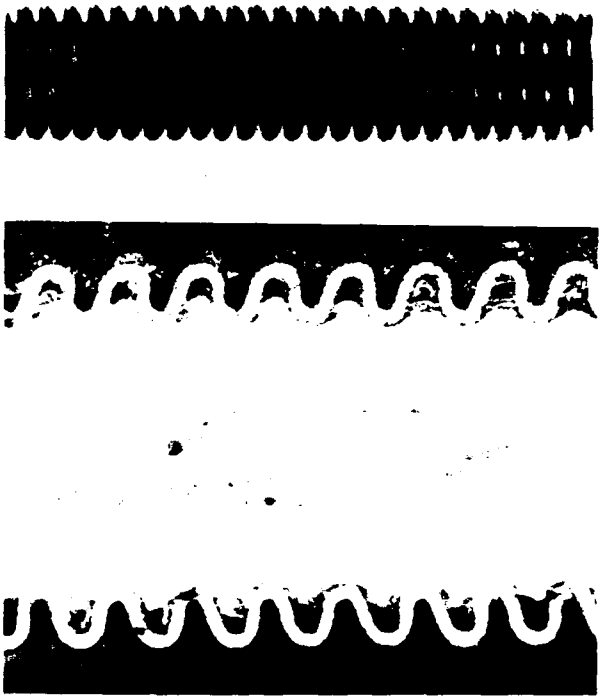


Fig. 3 External view and longitudinal section of a cable with deep corrugations

	RK 50-3,7-31	RK 50-4-32	RK 50-7-58	RK 50-17-51	RK 75-75-52
Characteristic Impedance (ohms)	50±1.5	50±2	50±1.5	50±1.5	75±2
Inner conductor dia. (mm)	Cu wire 1 x 1.2	Cu wire 1 x 1.75	Cu wire 1 x 3.2	Cu tube 7.5	Cu tube 23.0
Insulation dia. (mm)	PE 3.7	Foamed PE 4.6	PE helix 7.25	PE helix 17.3	Teflon® helix 75.0
Outer conductor dia. (mm)	5.1	Corrugated copper tube 6.2	17.3	21.3	86.0
Jacket outer dia. (mm)	6.5	7.6	Light stabilized PE 11.2	24.3	92.0
Weight (kg/km)	62	81	189	439	3,120
Attenuation (● 3 GHz) dB/m, nominal/max.	0.72/0.9	0.42/0.5	0.21/0.28	0.11/0.13	0.0040/0.0045
Phase-temperature coeff. 10^{-6}/°C	200	80	10	10	not specified
VSWR (aver./max.)	1.3/1.5	1.3/1.5	1.2/1.4	1.2/1.4	not specified

Table 1. Semi-Flexible Radio-Frequency Cables (Typical examples)

	RK 50-0,3-21S	RK 50-0,6-25S	RK 50-1-23S	RK 50-1,5-22S	RK 50-2-25S	RK 50-3-29S	RK50-4-27S
Characteristic Impedance (ohms)	50±5	50±3	50±2	50±2	50±2	50±1	50±2
Inner conductor dia. (mm)	0.1	0.18	0.32	0.47	0.68	0.895	1.42
Insulation dia. (mm)	0.3+0.02 -0.05	0.6+0.00 -0.05	1.0±0.05	1.5±0.05	2.2±0.05	2.95	4.6±0.1
Outer dia. (mm)	0.45±0.05	0.8±0.05	1.5±0.05	2.0±0.05	2.8±0.05	3.43±0.05	5.2±0.1
Weight (kg/km)	1.08	3.13	14.6	21	36.3	41.5	90.3
Attenuation (dB/m)							
● 1 GHz	4	2					
● 3 GHz			2.2	1.7	1.1	0.8	0.55
● 10 GHz	15	10	4.4	3.4	2.2	1.7	
Capacitance (pF/m)	95	95	95	95	95	94	94
Operating Temp. range (°C)	-60 to +85	-60 to +85	-60 to +155	-60 to +155	-60 to + 125	-60 to +125	-60 to +85
Min. bending radius (mm)	2	3	3	4	5	8	20

Table 2. Radio-Frequency Cables with Solid Teflon● Insulation and Smooth Copper Tube Outer Conductor

These cables are used in communication systems with mobile stations (railways, subways, tunnels, surveillance systems (including private properties). The application to local radio-telephony systems (indoor applications and in large warehouses) and to CATV (for example, in the open country and in mountainous areas) is being investigated.

The optimum combination of transmission and radiating properties is obtained by selection of the shape of the slots and their size and location along the longitudinal axis of the cable. Radiating cables are excellent means for the establishment of local broadcast networks in areas, such as subways, tunnels, offices, airports, etc.

In selecting a radiating cable for specific radio-communication or surveillance applications, the users must consider the following four main factors:

- Attenuation;
- Coupling efficiency through the slots in the outer conductor;
- The structure of the external electro-magnetic field;
- Cost.

To provide the necessary radiated power level for communication rather large slots are necessary. These lead to changes in the main electrical characteristics of the cable when compared to a similar cable with a solid outer conductor. As the capacitance decreases, inductance, characteristic impedance and attenuation increase and the transfer impedance and transfer capacitance exceed by 10 to 1,000 times those of conventional braided radio-frequency cables.

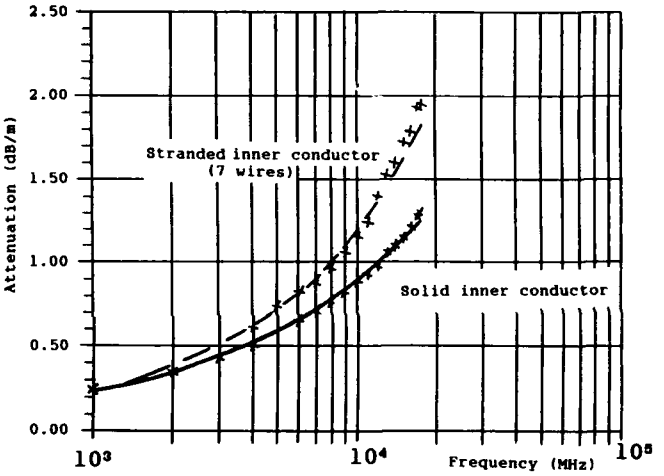


Fig. 4 Frequency dependence of attenuation of cables with deep corrugations
D = 4.6 mm, Z = 50 ohms

In the design of radiating cables it is necessary to consider not only the cable parameters but also those of the external electro-magnetic field.

The theoretical calculation of the external electro-magnetic field parameters and the characteristics of radiating cables are given in [3,4].

In particular, the impedance of a radiating cable, unlike that of a conventional cable, is described in Eq.1:

$$Z_B = \frac{60 \ln (D/d)}{\sqrt{\varepsilon}} \sqrt{1 + \frac{2 (M + P)}{\pi D^2 h \ln (D/d)}} \quad (1)$$

wherein:

M and P = magnetic and electrical polarization characteristics of the slots
d and D = diameters of the inner and outer conductors
h = distance between slots
ε = relative dielectric constant of the insulation

The quantities M and P are quantitative representations of the electrical and magnetic field energies which pass through the slots, respectively.

The attenuation constant of a radiating cable, unlike that of a conventional cable, has not only two components (metal losses α_m and dielectric losses α_d) but three additional ones: losses in the protective jacket (α_j), radiation losses (α_r) and losses resulting from installation conditions (α_i)[4]. Thus,

$$\alpha = \alpha_m + \alpha_d + \alpha_j + \alpha_r + \alpha_i \qquad (2)$$

For cables in which the surface waves predominate, the radiation loss component is negligibly small for sufficiently long cable lengths. Depending on the type of outer conductor, the α_i component determined by the installation conditions may increase the total attenuation constant from 20% to 100% when the cable is laid on concrete or buried. For example, Fig. 5 shows the percentage attenuation ratio contributed by all components for the type RI 50-7-11 cable in free air installation.

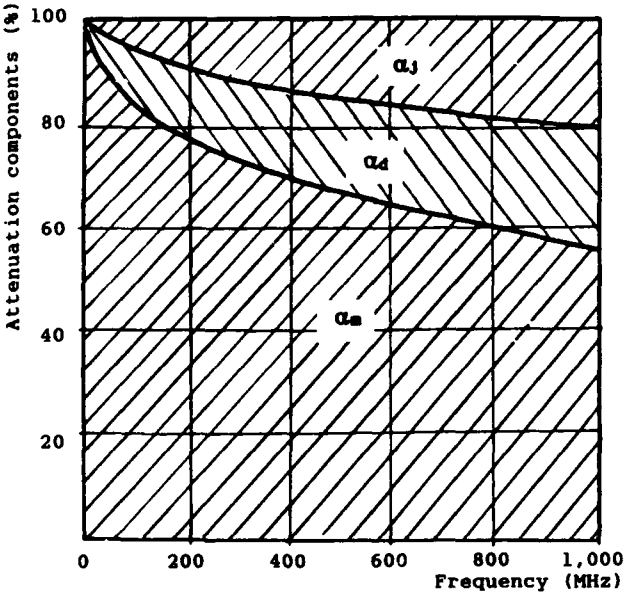


Fig. 5 Attenuation components of type RI-50-7-11 radiating cable upon installation in free space

Complete electro-dynamic analysis disclosed, as a general solution, that all six components lie in the cylindrical coordinate system for a cable of infinite length. In this case, the surface wave components E_z, E_ρ and H_φ are always present. Furthermore, in the case where the distance between slots is comparable to the wavelength, one has to deal with the radiated wave components. If the slots are at an angle to the cable axis both surface and radiated waves with components E_φ, H_ρ and H_z may be generated.

In the case of a finite cable length, additional radiated wave components E_z, E_ρ and H_φ appear even when the distance between the slots is significantly shorter than the wavelength. In general, the cable is surrounded by a combination of various wave types. In the case of radiating cables, the electro-magnetic field level is usually estimated by the coupling losses, as measured with a dipole. Fig. 6 shows a typical example of coupling loss dependence for a 120 m (393.7 ft.) length of type RI 50-7-11 cable with the dipole placed parallel to the cable and at a certain distance from its center in the radial direction.

Developments completed in our research center in the 1980s led to the creation of a series of radio-frequency cables with constant slot parameters in which the external electro-magnetic field is a surface wave. The parameters of this cable series are shown in Table 3.

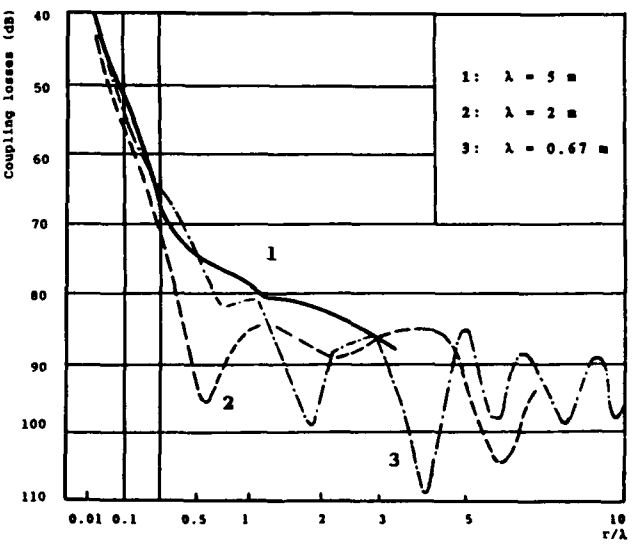


Fig. 6 Coupling losses as a function of r/λ, wherein r = distance from the cable axis, λ = wavelength in free space.

	RI 75-4-11	RI 75-7-11	RI 50-7-11	RI 50-17-31	RI 75-17-33
Characteristic Impedance (ohms)	75±3	75±3	50±2	50±2	50±2
Inner conductor dia. (mm)	Cu wire 0.83	Cu wire 1.3	Cu wire 2.5	Cu tube 7.2	Cu tube 7.2
Insulation dia. (mm)	PE 4.6±0.2	PE 7.75±0.2	PE 7.75±0.2	PE helix+tube 17.3±0.6	Foamed PE 17.3±0.6
Outer conductor, thickness (mm)	0.05	Longitudinally applied corrugated copper tape 0.10	0.10	0.10	0.10
Jacket outer dia. (mm)	7.0	7.0	Light stabilized PE 11.2	22.3	22.3
Weight (kg/km)	45	120	151	365	365
Max. attenuation (dB/100 m)					
● 60 MHz	9	6	6		
150 MHz				3.2	3.0
450 MHz				6.5	6.0
600 MHz	27	22	20		
1,000 MHz				12.0	11.0
Min. transfer impedance (Ohms/m)	2.7	3.0	2.7	1.0	1.0
Aver. coupling loss (dB)					
● 2.5 m, 60 MHz	70	70	70		
2.0 m, 150 MHz				75	75
Min. bending radius (mm)	75	110	110	250	250
Permissible number of bends over 300 mm dia.	30	30	30	not specified	not specified

Table 3. Radiating Radio-Frequency Cables

At present we are engaged in the development of a radiating cable series with variable slot parameters, in particular, for CATV applications and high-speed railway radio-communication systems. The initial design requirement is based on the frequency range of the application. For example, in CATV systems in the 110 to 790 MHz range radiating cables have a sinusoidal distribution of oval slot sizes with 2.2 to 2.5 m (7.22 to 8.2 ft.) distance between slots. In particular, a radiating cable with air-spaced insulation of 17.3 mm (.68 in.) diameter designed for the above frequency range, has coupling losses at 25 m distance of 75 to 80 dB, while the maximum attenuation at 230 MHz is 20 dB/km.

Special test equipment for the measurement of the external electromagnetic field of radiating cables has been designed. Fig. 7 represents the schematic diagram of this unit.

Miniature and Sub-Miniature Cables for Computer Wiring (Wrapping and Soldering)

A series of new sub-miniature and miniature radio-frequency cables has been developed for the internal wiring (by wrapping or soldering) of electronic equipment, computers and diagnostic equipment. To enhance the operational reliability and for ease of wiring the cable construction contains a drain wire. The cross-section of the cable is shown in Fig. 8.

The main characteristics of cables with drain wires for wrapping or soldering terminations are shown in Table 4.

Our Center is manufacturing sub-miniature twin-conductor radio-frequency cables (Table 5).

Coaxial and twin-conductor cables can be incorporated in ribbon cables or cable bundles with practically any number of pairs.

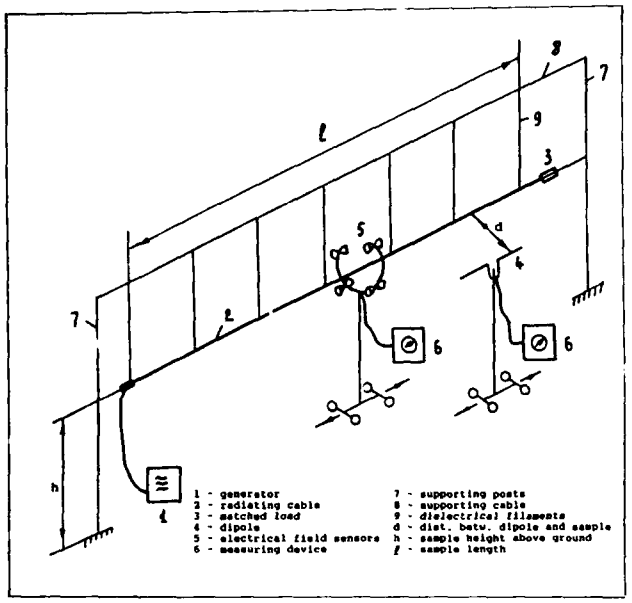


Fig. 7 Set-up for the measurement of the external electro-magnetic fields of radiating cables

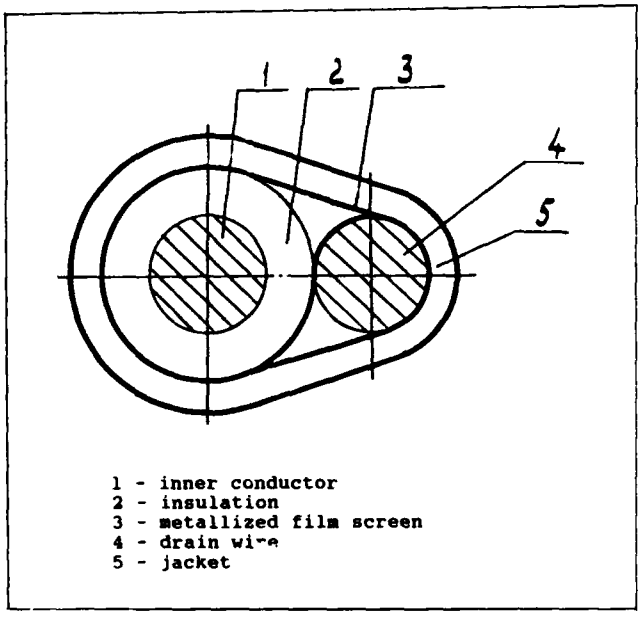


Fig. 8 Cross-section of Miniature and/or Sub-Miniature Cable

Super-Flexible Coaxial Cables for the -150 to +200°C Temperature Range

For communication, navigation and radar systems for aircraft and spacecraft, super-flexible heat- and cold-resistant radio-frequency cables, with a high degree of flexibility and resistance to multiple flexures in the 150 to +200°C temperature range have been developed and are being produced.

These cables feature reinforced, stranded inner conductors of silver-plated wires and braided outer conductors of silver-plated wires. The insulation consists of a closely-spaced PTFE helix. Protective jackets are made from PTFE tapes and braids of durable heat-resistant fibers. The cables retain their flexibility down to liquid nitrogen temperatures (-196°C). The bending moment values are standardized. The main applications consist of flexible cable links in antenna feeder systems operating at low temperatures (for example, in space environment).

The main electrical characteristics and mechanical properties of some of these cables are given in Table 6.

Methods for calculating conductor resistance at high frequencies and attenuation constant over a broad range of frequencies and temperatures have been developed. These methods take into account the stranded construction of the conductors and the contact resistance between the wires[5,6]. It has been shown that the angle of the stranding or braiding of the conductors has a major influence on the attenuation constant in the frequency range between 1 to 20 GHz within the given temperature range (Figs. 9 and 10).

This phenomenon has been studied both experimentally and theoretically as a function of contact resistance between the wires. It shows up most clearly in the frequency range above 3 GHz. Note, that in the IEC recommendations (Committee 46A, Publication 96-0) this phenomenon is not considered.

For the measurement and standardization of bending moments special methods and equipment have been developed. In the test the cable specimen is bent over a circular arc during the entire test cycle. The bending radius is cyclically changed within predetermined limits. In this procedure the cable specimen is subjected to bending forces only whereby the bending strain is distributed uniformly over the entire cable specimen (except for the parts near the clamps). This pure bending test allows measurement of the bending moment as a function of the cable bending radius as well as phase changes of the microwave signal at cable flexure for a specified radius.[7]

Figs. 11 and 12 illustrate the measurement methods and the physical significance of the measured values.

	RK 50-1,5-31	RK 75-1,5-32	RK 50-0,87-11	RK 50-0,6-27
Characteristic Impedance (ohms)	50±3.5	75±3.5	50±3.5	50±3.5
Inner conductor dia. (mm)	CuSn 7x0.20	CuSn 7x0.12	CuSn 0.25	CuAg 7x0.07
Insulation dia. (mm)	Foamed PE 1.5	Foamed PE 1.5	PE 0.87	Teflon● 0.6
Outer conductor, thickness (mm)	Laminated plastic foil (PE/Al) 0.05	0.05	Copper foil 0.015	0.015
Drain wire dia. (mm)	CuSr. 7x0.15	CuSn 7x0.15	CuSn 0.25	CuSn 7x0.10
Jacket material	PE	PE	PE	Teflon●
Outer dia. (mm)	2.5	2.5	1.8	1.6
Weight (kg/km)	7.3	6.1	3.85	4.0
Attenuation (dB/m) ● 10 MHz			0.14	0.16
100 MHz	0.2	0.2	0.45	0.5
200 MHz	0.3	0.3	0.7	0.8
1,000 MHz	0.9	0.9		
Capacitance (pF/m)	75	55	96	94
Min. bending radius (mm)	10	10	10	10

Table 4. Miniature and Sub-Miniature Radio-Frequency Cables

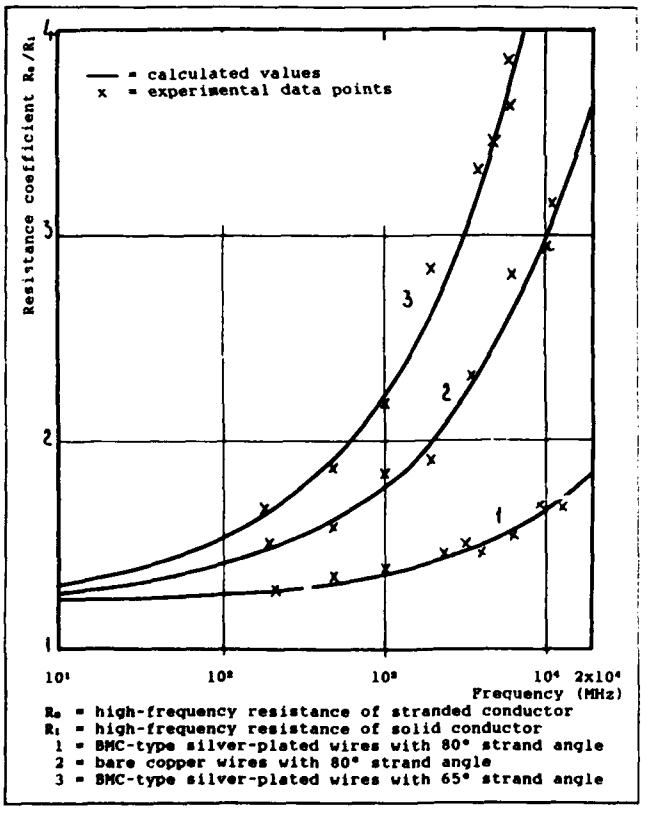


Fig. 9 Frequency dependence of resistance coefficient of a stranded conductor (19 wires) of silver-plated and bare copper wires of 0.32 mm diameter.

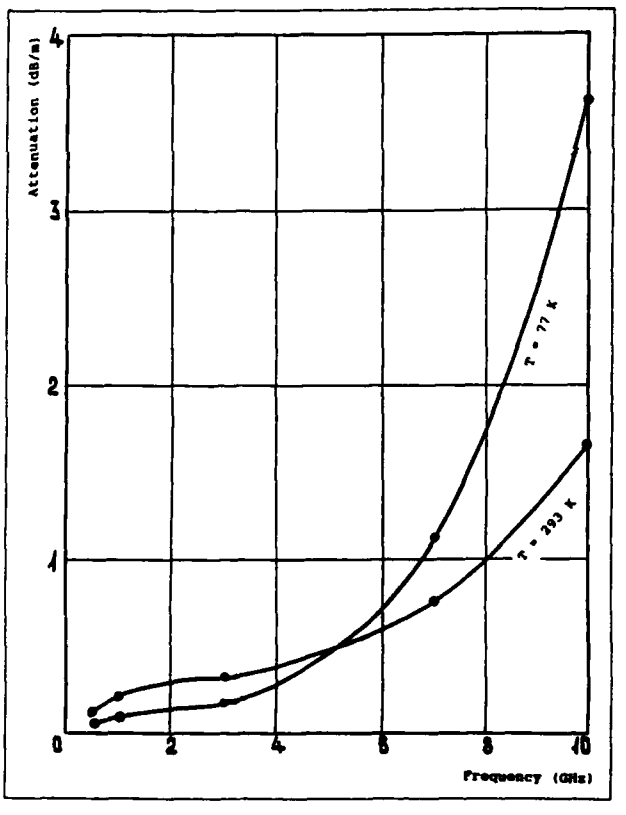


Fig. 10 Frequency dependence of the attenuation of cable type PK-50-7-22 at 77 K and 293 K

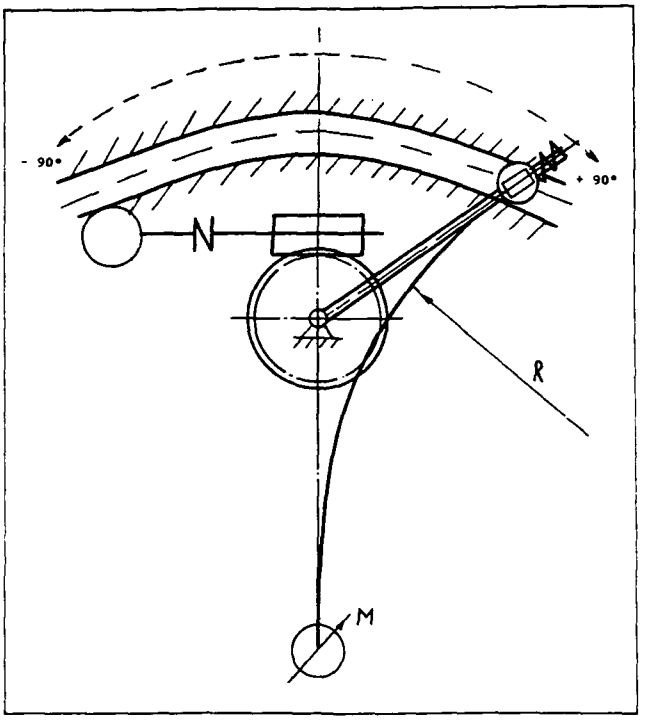


Fig. 11 Functional diagram of the device for the measurement of pure bending stress

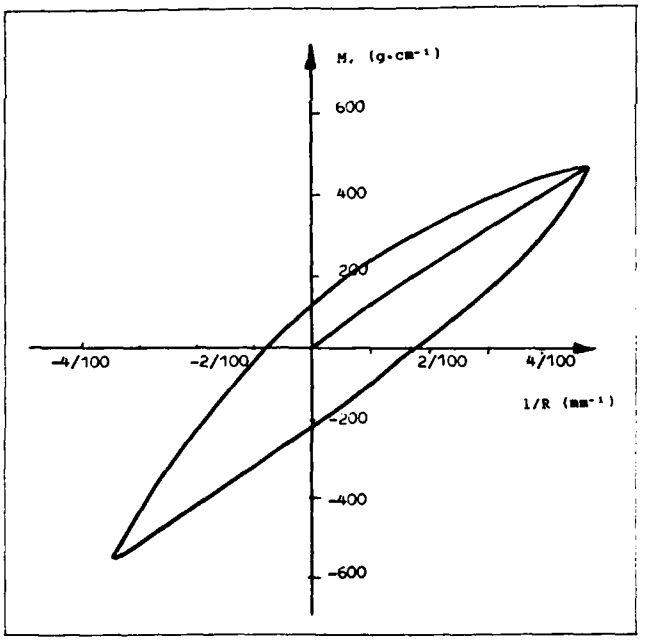


Fig. 12 Bending moment as a function of cable bending radius

Miniature and Sub-Miniature Radio-Frequency Cable Series with Non-Braided Outer Conductors

It is well known that the production process of the outer braided conductor for radio-frequency cables involves large amounts of noise and low production rates, especially when it concerns miniature and sub-miniature cables (0.1 - 0.5 m/min. - .33 to 1.64 ft./min.).

Our Center has developed cable designs, technologies and equipment for the longitudinal application of wires (instead of braid) for miniature and sub-miniature cables. This innovation increases the production rates by a factor of about 5 to 8.

The mechanical properties and electrical parameters of cables with longitudinally-applied wires differ little from braided cables. However, they offer smaller dimensions and weight. By means of the above-mentioned technology a miniature flexible cable with stranded conductors, with FEP insulation and a 0.6 mm (.024 in.) outer diameter over the jacket has been produced (Table 7). This cable has applications, for example, in medicine for the insertion of intravenous sensors and for the introduction of radiation sources in humans (even into the veins of an infant).

Anti-Vibrational (Anti-Noise) Cable

All wires and cables subjected to vibration generate electrical noise which relates to piezo-electricity and charge separation at the conductor-insulation interface. Thus, for signal transmission, for example, from the output of a piezo-electric sensor for vibration measurement to the input of a high-impedance amplifier or instrument, low-noise cables are used. A particular feature of these cables is a conductive layer on the surface of the insulation (both on the outer and inner surface) which is formed by fluoro-suspension or conductive PE.

The inner conductor is a strand and the outer conductor (screen) consists of a braid of tinned, silver-plated or nickel-plated copper wires.

Depending on the materials used, these cables are divided into two groups:

- group of normal heat-resistance (from -60 to +85°C): PE-insulated cables with PE or PVC jackets, ABK-1, ABK-2 and ABK-3 types;

- high-temperature cable group (-60 to +250°C): cables with Teflon● or silicon rubber insulation, ABKT-4, ABKT-5 and ABKT-6 types.

They are, again, subdivided into two groups according to the design:

- coaxial cable types: ABK-1, ABK2(3), ABKT-6 and ABKTMP-1;

- twin conductor cables: ABKT (II), ABKTM-2 and ABKTMP-2 types.

These cables feature long-term stability of low-noise properties under environmental and mechanical exposure. The noise reduction obtained through the use of these cables is at least 40 dB.

More than ten cable plants are producing radio-frequency cables in Russia. They are equipped with all necessary instruments and test equipment for standard tests. Our Center has a set of test equipment for all types of radio-frequency cable parameter measurements in the frequency range between 0.1 and 40 GHz as well as for environmental and mechanical tests.

Acknowledgments

The authors wish to express their appreciation to Mr. Dimitri R. Stein for suggesting, organizing and editing this paper. Thanks are also due to Mr. Henry Hofheimer for preparing the manuscript for printing. Mr. Stein is President and Mr. Hofheimer is Vice President of Cable Consultants Corp., Larchmont NY 10538.

	RD 50-0,6-21	RD 50-1-11	RD 75-1-11	RD 100-1,5-11
Characteristic Impedance (ohms)	50+10,-0	50+7.5,-5	75±7	100±10
Conductor dia. (mm)	CuAg 0.15 & 0.18	CuSn 0.3	CuSn 0.3	CuSn 0.3
Insulation material	Teflon●	Polyimide	Polyimide	Teflon●
Dia. over insul. (mm)	0.2	0.35	0.41	0.5
Jacket material	Teflon●	PE	PE	PE
Max. outer dia. (mm)	0.75	1.4	1.5	1.7
Weight (kg/km)	1.21	2.2	2.42	2.76
Attenuation ● 200 MHz (dB/m)	3.0	1.6	1.4	1.2
Capacitance (pF/m)	98	100	70	45
Min. bending radius (mm)	2	3	3	3

Table 5. Sub-Miniature Twin-Conductor Radio-Frequency Cables

	RK 50-7-415	RK 50-7-416	RK 50-4-49	RK 50-1,5-213	RK 50-2-212	RK 50-2-213
Characteristic Impedance (ohms)	50±3	50±3	50±2	50±3	50±3	50±3
Inner conductor dia. (mm)	stranded wire 2.45	stranded wire 2.37	(19x0.32) 1.6	(19x0.10)	(19x0.15)	(19x0.15)
Insulation dia. (mm)	Teflon®/air 7.25±0.20	Teflon®/air 7.25±0.20	Teflon®/air 4.6±0.20	Teflon®/solid 1.5+0.00,-0.15	Teflon®/solid 2.2+0.00,-0.15	Teflon®/solid 2.2+0.00,-0.15
Braided outer cond. wire dia. (mm)	single braid 0.15	single braid 0.15	single braid 0.15	single braid 0.1	single braid 0.1	two braids 0.1
Outer dia. (mm)	8.49±0.30	8.45±0.30	5.8±0.5	2.8±0.3	3.3±0.3	4.0±0.3
Weight (kg/km)	186	126	83.6	12	25	33
Attenuation (dB/m)						
● 0.2 GHz			0.16			
1 GHz	0.4	0.55	0.4			
3 GHz	0.8	1.4	0.75			
10 GHz				4	3	3
Min. bending radius (mm)						
● +20°C			30	4	5	5
● -200°C	100	100	100			
Permissible number of bends						
● +20°C	50,000	50,000	10,000	30,000	30,000	30,000
● -200°C	15,000	15,000	3,000			

Table 6. Super-Flexible Radio-Frequency Cables

	RK 50-0,6-23N	RK 50-1-24N	RK 50-1,5-23N	RK 50-1-13N	RK 75-1-13N
Characteristic Impedance (ohms)	50±5	50±2	50±3.5	50±3.5	75±5
Inner conductor (mm)	CuAg 7x0.08	CuAg 7x0.12	CuAg 7x0.18	CuAg 7x0.11	CuAg 7x0.06
Insulation thickness (mm)	FEP 0.6	FEP 1.0	FEP 1.5	PE 1.0	PE 1.0
Jacket material	FEP	FEP	FEP	PE	PE
Outer dia. (mm)	1.2	1.7	2.4	1.9	1.9
Weight (kg/km)	3.27	6.85	15	5.4	5.1
Attenuation (dB/m)					
● 0.2 GHz	0.9	0.62		0.65	0.65
3 GHz	4	2.8			
10 GHz			4.2		
Capacitance (pF/m)	95	95	95	100	67
Operating temp. range (°C)	-60 to +200	-60 to +200	-60 to +200	-60 to +85	-60 to +85
Min. bending radius (mm)	5	9	15	10	10

Table 7. RF Cables with Outer Conductors Consisting of Longitudinally-Applied Wires held together by a Wire Wrap and Jacket

References

1. Teflon® is a registered trademark of E. I. Du Pont de Nemours & Co.

2. N. I. Dorezuk, M. F. Popov, "Radio-Frequency Cables of High Uniformity", Svyaz Publisher, Moscow, 1979, 104 pp.

3. V. N. Korotkov, "The Parameters of the External Electromagnetic Field of Radiating Coaxial Cables. - Investigation and Manufacture of Cables and Wires", Sbornik Nauchnykh Trudov VNIIKP (Collection of Scientific Papers of the Research Institute of the Cable Industry), 1988, pp. 67-80.

4. P. R. Bazanskaya, V. N. Korotkov, "The Parameters of RF Coaxial Cables with Openings in Outer Conductors - Theory, Investigation, Cable Design, Manufacturing Technology, Materials". Published in Sbornik Nauchnykh Trudov VNIIKP, December 1987, pp. 59-62.

5. B. V. Malkov, A. A. Pavlov, "The Numerical Analysis of the High-Frequency Resistance of Multiwire Conductors", Elektrotechnika, No. 1, 1989, pp. 52-55, publ. by Elektroatomizdat.

6. D. Ya. Galperovich, A. A. Pavlov, N. N. Khrenkov, "Radio-Frequency Cables". Energoatomizdat, 1990, 256 pp.

7. M. L. Strupinsky, "Numerical Method for Calculation of Flexible Rods as Applied to the Analysis of the Mechanical Characteristics of RF Cables". Author's abstract of a dissertation submitted for a PhD. degree.



Anatolij Pavlov
Special Design Bureau of the Cable Industry, 141002 Jadreevskaya, 4 Mytishchi, Moskovskaya Oblast, Russia

Anatolij Pavlov graduated in 1971 from the Moscow Power Engineering Institute with a degree in Electrical Engineering. He then joined the Special Design Bureau of the Cable Industry (OKB KP) as a development engineer and, in 1986, became the chief of its radio-frequency cable department. He received a Doctor of Science degree for research in cable engineering. Dr. Pavlov is the author and co-author of books and articles dealing with radio-frequency cable theory, design and technology.



Izyaslav Peshkov
All-Russian Scientific Research Institute of the Russian Cable Industry, 111112 Shosse Entusiastov 5, Moscow, Russia

Izyaslav Peshkov graduated in 1960 from the Moscow Power Engineering Institute with a degree in Electrical Engineering. He then joined the All-Russian Scientific Research Institute of the Russian Cable Industry as a development engineer and, in 1970, became its director. He received a Doctor of Science degree for research in cable engineering and was appointed a Professor at the Moscow Power Engineering Institute. Dr. Peshkov is the author and co-author of numerous books and articles dealing with cable design and technology. He is presently director-general of the All-Russian Scientific Research Institute of the Russian Cable Industry, Chairman of the Board of the Russian Cablemakers Association and Member of the Council of the International Cablemakers Federation.



Michail Popov
Special Design Bureau of the Cable Industry 141002 Jadreevskaya, 4 Mytishchi, Moskovskaya Oblast, Russia

Michail Popov graduated in 1962 from the Moscow Power Engineering Institute with a degree in Electrical Engineering. He then joined the Special Design Bureau of the Cable Industry (OKB KP) as a development engineer and, in 1981, became the chief of its fiber optic cable department. In 1986 he became its director. He received a Doctor of Science degree for research in cable engineering. Dr. Popov is the author and co-author of books and articles dealing with radio-frequency and fiber optic cable theory, design and technology.

Automated Equipment to Assemble Connectors for Telecommunication Cables

Tadahisa HARAKAWA , Naoki NAKAO and Satoshi MATSUHASHI

Nippon Telegraph and Telephone Corporation, Telecommunication Field System R&D Center

Abstract - **Automated equipment to assemble connectors for telecommunication cables is proposed. The equipment can pick up a conductor from a set of twisted conductors, identify the conductor number by the color of its insulation, and arrange it on a connector. Using experiments on test versions, the basic requirements are determined and evaluated, and the process control method for lines is confirmed. Based on the experimental results, estimations, and human interface, the equipment is designed and a prototype is manufactured. The use of this equipment is expected to reduce assembly time and eliminate human error.**

1. INTRODUCTION

Robotics and automation technology have recently become important in outside plant construction, due to soaring labor costs. In addition, it is expected that it will be difficult to obtain a highly skilled labor force in the near future [1]. In assembling outside telecommunication cables, splicing the cable conductors requires a great amount of work and a high level of skill. This is because cable conductors are spliced by manually twisting them or by using the manual twist-and-solder method. It is therefore advantageous to automate and simplify cable conductor splicing.

Furthermore, the required reliability and flexibility of cable splicing have increased with the advances in telecommunication technology. For example, Integrated Services Digital Networks (ISDN), which provide simultaneous voice, data, and image services incorporating a digital switching and transmission system, were recently introduced under the guidance of the International Telegraph and Telephone Consultative Committee (CCITT) [2][3][4][5]. Nippon Telegraph and Telephone Corporation (NTT) began providing ISDN service, INS-Net 64, in April 1988 [6]. INS-Net 64 has been growing steadily and requires high reliability and flexibility. The development of the pair transferable connector (PAT connector) and the cable transfer splicing system (CATS system) satisfy some of these requirements, but connector assembly is still not automated [7]. Therefore, additional work is needed to eliminate human errors and reduce assembly time.

Automated equipments to assemble electronic connectors are already on the market. However these equipments are not applicable to telecommunications for two reasons. The first reason is the fundamental problem that to assemble connectors at one end of the cable, an electrical signal must be sent from the other end of the cable in order to identify the conductor number. For telecommunications, it is necessary to operate at only one end of the cable, because the ends of the cable are too distant from each other. Moreover, a method to pick up a conductor from the twisted conductors is not provided. Automating only the conductor arrangement process is not enough to eliminate human error and decrease assembly time. The second reason is that the outdoor environment is much worse than in a factory. It is usually narrow, wet, dusty, and unstable. The above equipments were developed for a factory environment. A few researchers have developed automatic equipments to assemble connectors for telecommunication. One of the most interesting results has been reported by Ebrey, Sckerl and Seaman [8]. They proposed automatic connectorizing machines to manipulate wires at high speeds. However, because they identify the conductor number using electrical signals and were developed for a factory environment, it does not satisfy the requirements for assembling connectors in manholes.

In this paper, we will first explain the background of copper cable splicing. Next, through experiments using test

versions, we will determine and evaluate the basic requirements and confirm the process control method. Then, using the experimental results, estimations, and human interface, the equipment is designed and a prototype is manufactured.

2. Background

A. Cables

The cable used is PEC cable, which has polyethylene foam (PEF) insulation and is color-coded. The conductor gauges and PEF thicknesses are shown in Table 1. As shown in Fig. 1, four conductors twisted together make a quad, five quads are assembled to form a subunit, and ten subunits constitute a unit. The conductors are identified by their insulation colors. Blue, yellow, green, red, and violet identify the quad number. The other conductors in each quad are white, brown, and black. The largest cable consists of 3,600 pairs (7,200 conductors).

B. Connectors and Assembly Method

Fig. 2 shows a PAT connector which is designed to connect ten conductor pairs at a time and to easily separate or mate them. It has a plastic body with metallic U-connecting elements, which makes it possible to splice the conductor and connect two PAT connectors. It is superior to regular connectors for the following reasons:

a) Conductors are spliced using highly reliable U-connecting elements, so the splicing points have long-term stability.

b) It can be used for both regular splicing of newly installed cable and transfer splicing.

c) It has holes for electrical contact, so it is useful for transfer splicing with transfer equipment, making it possible to maintain the splice points easily and effectively.

PAT connectors are assembled using the equipment shown in Fig. 3. And the cable splicing process is shown in Fig. 4.

TABLE 1
Conductor Gauges and PEF Insulation Thicknesses.

Conductor Gauge	PEF Insulation Thickness
0.32 mm	0.08 mm
0.40 mm	0.09 mm
0.50 mm	0.11 mm
0.65 mm	0.13 mm
0.90 mm	0.18 mm

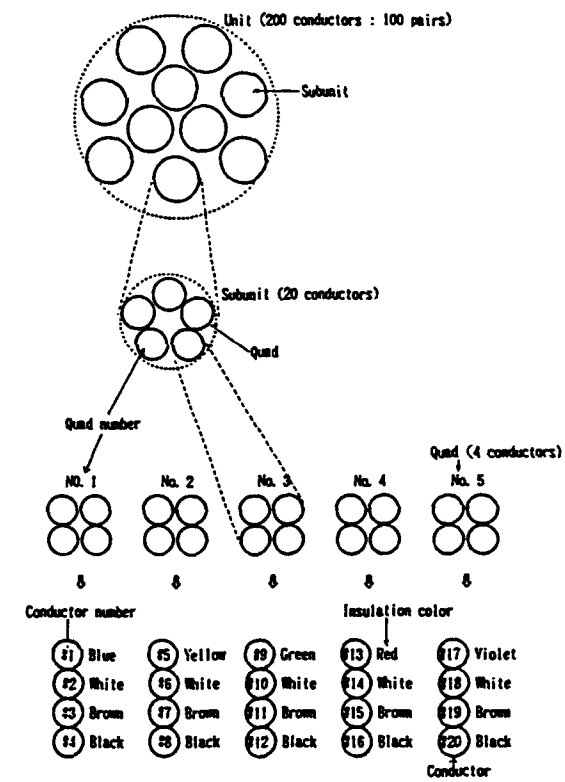


Fig. 1: Cable Structure.

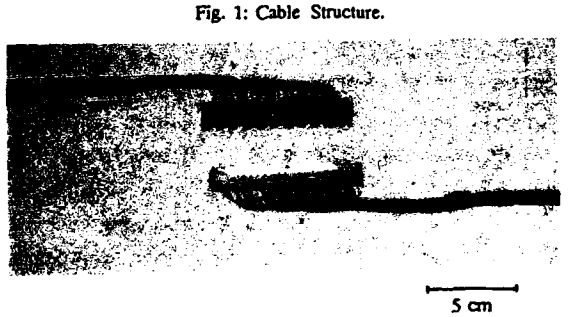


Fig. 2: PAT Connector.

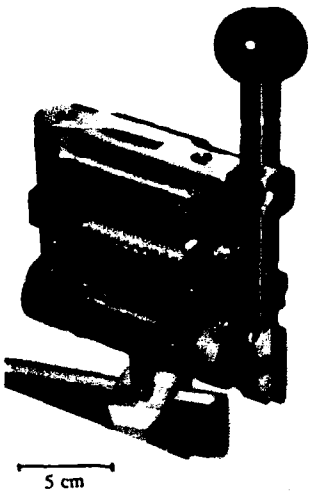


Fig. 3: PAT Connector Assembly Equipment.

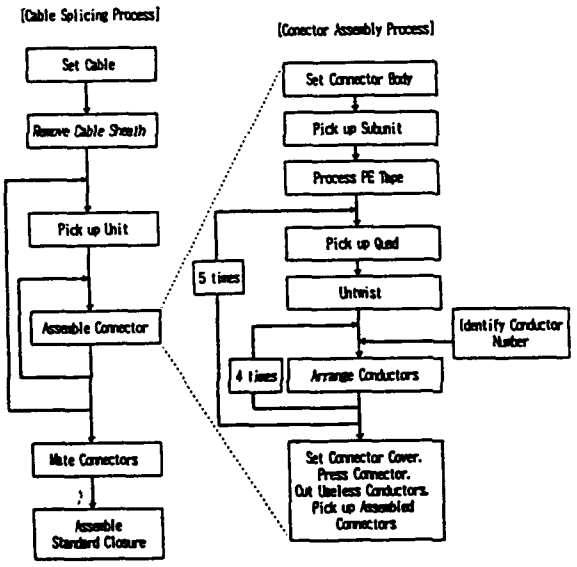


Fig. 4: Cable Splicing Process.

3. ASSEMBLY PROCESS

This section discusses the processes used by the automated equipment to assemble connectors. Each process is explained, and the fundamental characteristics are determined by experiment and estimation.

A. Quad Pick-Up

1) Process: Fig. 5 shows the process for the picking up a quad. Without automation, the worker places a subunit in a slit slightly larger than the diameter of one quad. With automation, the equipment picks up a quad as shown in the figure. In this process, the approach to the quad is most important. The pickup head must not force the quad, otherwise the quad will remain untwisted and the process will fail. So the pickup head must approach the quad gently. We thus use a spring-loaded R-shaped pickup head.

2) Experiment: Fig. 6 shows the experimental setup used for picking up a quad. The pickup head is driven by position-controlled robotic arms. Eliminating the force controller simplifies the process. This experiment showed that the results are affected by human actions. A subunit is considered to be in good condition if every quad is twisted. It is in bad condition if some quads are left untwisted. In the experiments, the ratio of successes (good conditions) to failures (bad conditions) was 987:13. In the final equipment, the person must be able to place the quads easily.

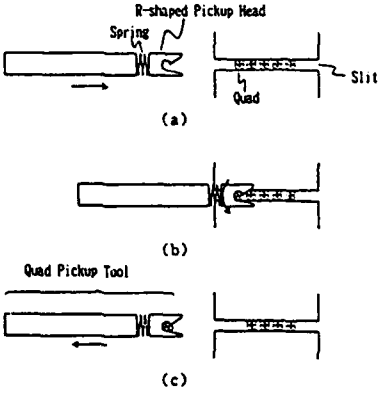


Fig. 5: Quad Pick-Up Process.

B. Untwisting

1) Process: After the quad is picked up, it is untwisted by stroking it, as shown in Fig. 7. Each stroke must untwist about one twist pitch (3-7 cm) of the quad. To untwisted a length of 10 cm, at least three strokes are necessary,

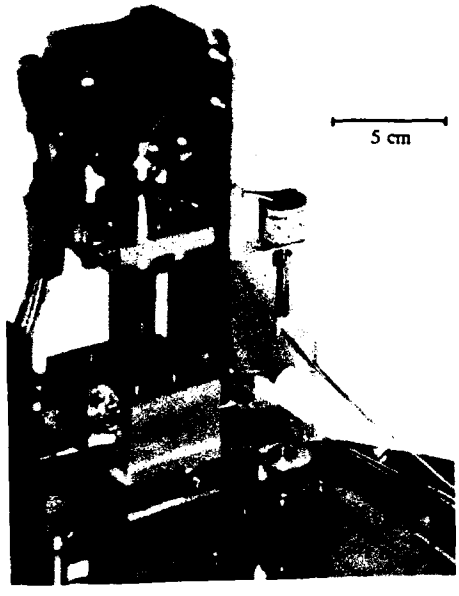


Fig. 6: Experimental Setup for Picking up Quad.

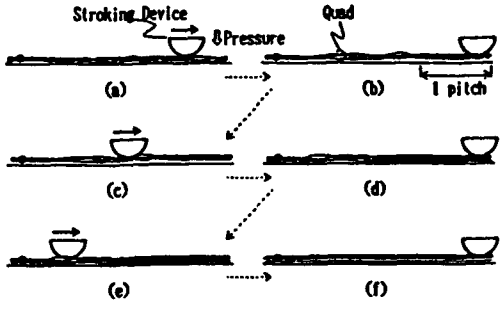


Fig. 7: Untwisting Process.

because if the equipment tries to untwist a quad-long length (more than two twist-pitches) in one stroke, the conductor insulation is usually damaged. Also, the stroking device must not press down too hard or the insulation may be damaged. When the equipment fails to untwist the quad, the stroking device should pass over it without damaging the insulation.

Fig. 8 shows the untwisting tool structure. It has several stroking devices moving on a track, and a plate with a step. The stroking device can only untwist a quad on the upper portion of the plate. It cannot untwist a quad on the lower portion, because of insufficient pressure. The quads are gradually untwisted with increasing upper portion.

With this technique, the friction of the stroking device is an important factor in controlling the conductors. The proper friction makes the conductors straight, and thus easy to pick up. This helps in arranging the conductors on the connector.

2) Experiment: The experiment was executed to confirm the untwisting principles shown in Fig. 8. Fig. 9 shows the experimental setup. The experiment confirmed that the equipment can untwist quads without damaging the insulation.

C. Conveying and Picking up a Conductor

1) Picking up a Conductor: We will first explain how to pick up a conductor using an easy example. The untwisted conductors are first conveyed to the pick-up position. Then a comb separates the conductors, as shown in Fig. 10. The comb has several slits, slightly wider than the conductor diameter.

Preliminary experiments were conducted to determine the requirements for picking up a conductor. The requirements are as follows:

a) In order to avoid picking up two conductors, the openings in the upper and lower plates must be as small as possible, but still large enough to ensure one conductor is picked up.

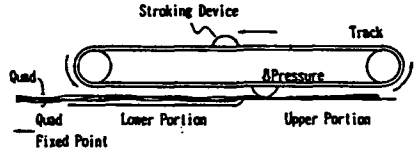


Fig. 8: Untwisting Tool Structure.

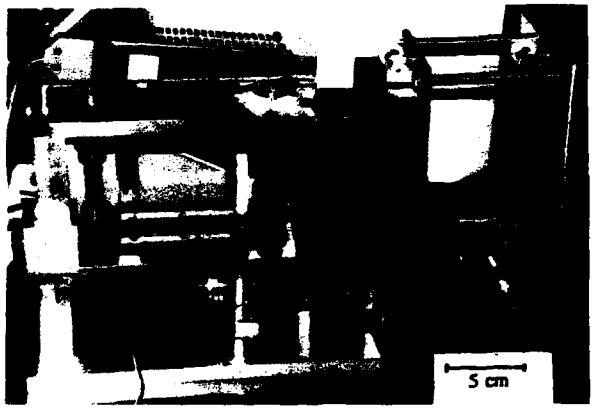


Fig. 9: Setup for Untwisting Experiment.

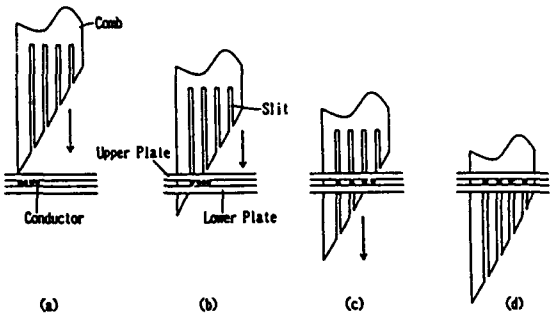


Fig. 10: Conductor Pick-Up Process.

b) To avoid damaging the insulation, the comb must be 1 to 2 mm thick and the conductors must be perpendicular to the comb.

2) Process: Our process for conveying and picking up a conductor meets the above requirements. It is shown in Fig. 11. There is a different conductor screw for each of the five conductor gauges. Each conductor screw has a slightly larger groove than the corresponding conductor diameter. The quad screw has a somewhat larger groove than the quad diameter for a conductor gauge of 0.9 mm. It can be used for all sizes of conductors. After the quad is picked up, it is conveyed to the quad screw. While the quad is being conveyed, the conductors are untwisted. By the time the quad reaches the conductor screw, they are untwisted. The conductor screw then picks up the untwisted conductors and conveys them, as shown in Fig. 11.

3) Experiment: Fig. 12 shows the experimental setup used to evaluate the conductor pick-up process. The experiments were carried out using many different conductor screws. Some of the requirements for picking up conductors without damaging the insulation are:

1) The conductor screw groove must be slightly larger than the corresponding conductor diameter.
2) The conductors must be straight.
3) The conductors must be pushed gently to the conductor screw.

D. Conductor Number Identification

There is a color sensor in the conductor support to identify the conductor number. Fig. 13 shows the structure of the color sensor. Its output is an RGB signal. This color sensor is already on the market, but has not been

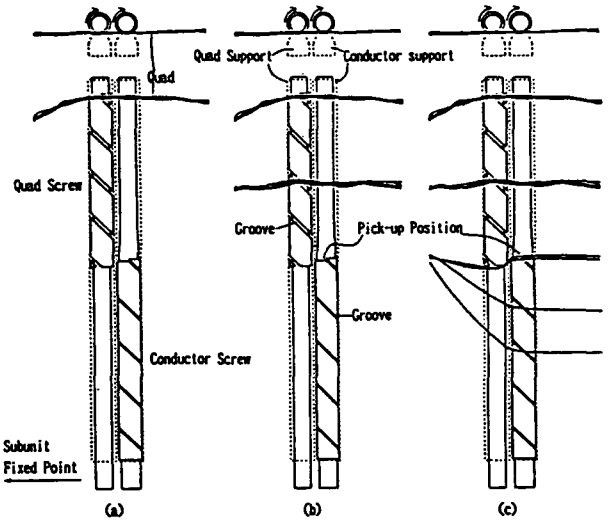


Fig. 11: Conveying and Picking up a Conductor.

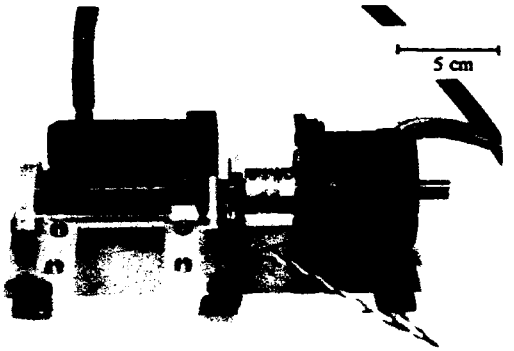


Fig. 12: Experimental Setup for Conductor Pick-Up.

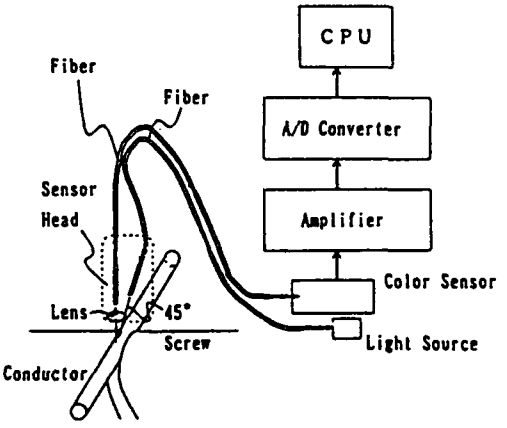


Fig. 13: Color Sensor Structure.

used for assembling connectors. So new software was developed to process the RGB signals.

As explained earlier, eight colors are used to identify the conductor numbers. These eight colors are measured and used to set the color standards. A color is represented as a 3-dimensional vector, $\mathbf{I} = (I_1, I_2, I_3)$. The values I_i are

$$I_1 = M_R - W_R, \quad I_2 = M_G - W_G, \quad \text{and} \quad I_3 = M_B - W_B \qquad (1)$$

where M_X is the measured RGB signal intensity and W_X is the standard RGB signal intensity of white. Each conductor color is determined by the following equation:

$$D(C_1,C_2) = \{M - (C_1 + C_2) / 2\} \cdot (C_2 - C_1), \qquad (2)$$

where C_1, and C_2 are the standard color vectors, and M is the measured color vector. $D(C_1,C_2)$ shows which standard color vector the measured color vector is nearer to in 3-dimensional space. If $D(C_1,C_2) < 0$, the measured color vector is nearer to C_1, and if not, it is nearer to C_2. $D(C_1,C_2)$ is checked for all combinations of standard color vectors (C_1,C_2). Then the measured color is judged to be the nearest standard color.

This technique was confirmed using the experimental setup for conveying and picking up a conductor, as shown in Fig. 12. There were no errors during 2000 trials.

E: Conductor Arrangement

Equipments to arrange conductors are already on the market. Based on our work on various techniques for automated connector assembly for telecommunication cables, the technique shown in Fig. 14 was chosen for the following reasons:

1) It reduces the size of the equipment that assembles connectors.
2) The conductors can be arranged without damaging the insulation.
3) It fits well with the related processes.

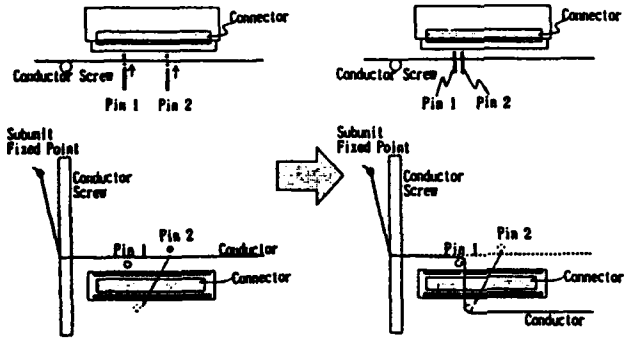


Fig. 14: Conductor Arrangement Process.

After this process, the following processes are carried out manually: place the connector cover, press the connector, cut useless conductors, and pick up the fully assembled connector. How to combine the machine operation with human operation is evaluated in the following discussion.

4. Equipment Design

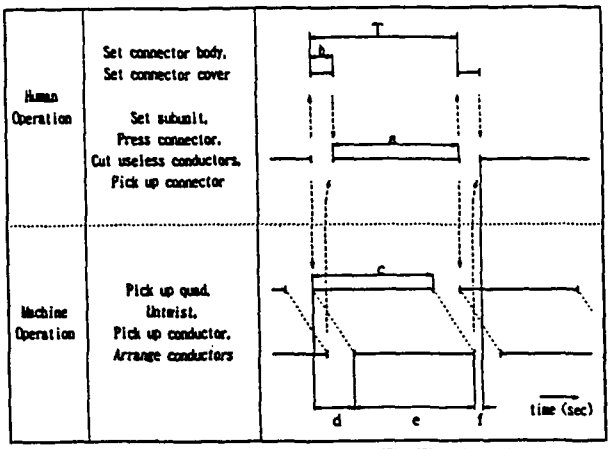
A. Requirements

The previous sections have described the processes used by the automated equipment to assemble connectors. This section discuss, as the overall equipment design. Table 2 shows the process used to assemble a connector.

Processes (5), (6), (7), and (8) have been automated to eliminate human error, decrease repetition, and match the machine operation with human operation. With automation, assembly time is only one third of what it was. To evaluate the basic equipment requirements, a diagram of the timing of the connector assembly processes is shown in Fig. 15. It shows that when the process times for "a" and "b" are the same as in the present process, the connector assembly time can be decreased to 27.9% of that of the present process. Table 4 shows the requirements to minimize the connector assembly time. To synchronize the machine with the human, and to decrease the connector assembly time, the best conditions are c=a+b and d+e=a+2b.

Table 2
Present Connector Assembling Process.

Process	Ratio [%]	Repetition
(1) Set Connector Body	3.8	1
(2) Pick up Subunit	5.1	1
(3) Set Subunit	3.8	1
(4) Process PE Tape	5.1	1
(5) *Pick up Quad*	5.1	1
(6) *Untwist*	17.7	5
(7) *Arrange Conductors*	49.3	20
(8) *Determine Color*	Included in (7)	20
(9) Set Connector Cover	3.8	1
(10) Press Connector	1.3	1
(11) Cut Useless Conductors	2.5	1
(12) Pick up Assembled Connector	2.5	1



a Human operation time for processes (2), (3), (4), (10), (11), and (12).
b Human operation time for processes (1) and (9).
c Machine operation time for picking up five quads.
d Time between when the equipment starts picking up a quad and when it starts arranging conductors.
e Machine operation time for arranging twenty conductors.
f Time between when the equipment finishes arranging conductors and when the human starts pressing a connector.

Fig.15: Connector Assembly Processes.

Table 3
TIMING REQUIREMENTS.

Process	Requirements
"c": machine operation time for picking up five quads	$c \le a + b \ (= T)$
"d": time between when the equipment starts picking up a quad and when it starts arranging conductors & "e": machine operation time for arranging 20 conductors	$d + e \le a + 2b$

B. Design and Composition of the Equipment

This section discusses in detail the optimal design of the equipment. The conductor arrangement process is repeated the most, so it requires the most time and determines the connector assembly time. In addition, the motion of the equipment has to be synchronized with the conductor arrangement motion, because the quad screw and the conductor screw are key parts of the whole process. For example, while a conductor is being arranged, the conductor screw must be stopped. And when the arrangement is completed, the conductor screw must start revolving again. With these requirements in mind, the connector assembly diagram was designed as shown in Fig. 16. The process

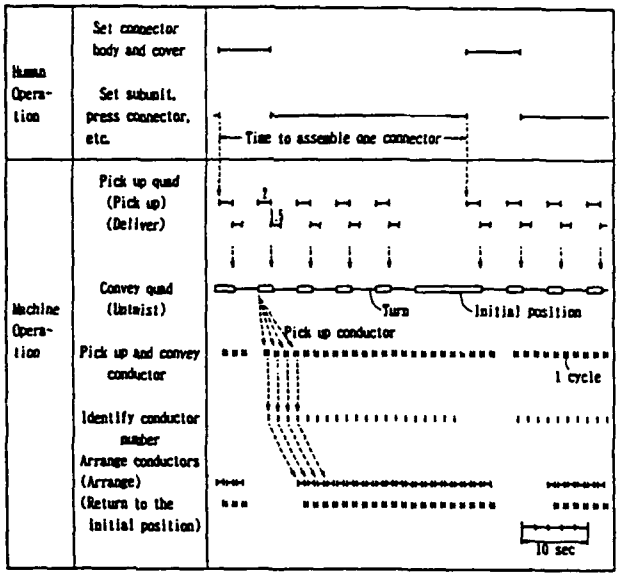


Fig. 16: Connector Assembly Diagram.

specifications are as follows:

1) The quad pick-up process takes about two seconds.
2) The quad is untwisted in revolutions of the quad screw.
3) The conductor screw picks up a conductor in one revolution.
4) The distance between the color sensor position and the conductor pick-up position equals one pitch of the conductor screw.
5) The distance between the conductor arrangement and removal position is less than one pitch of the conductor screw.
6) The arrangement process takes 1.5 seconds per conductor.

Using the results of these experiments and considerations, we manufactured a prototype as shown in Fig. 17. In future, we will present the characteristics of this equipment.

5. CONCLUSIONS

In this paper, the following conclusions concerning the design of automated equipment to assemble connectors were reported.

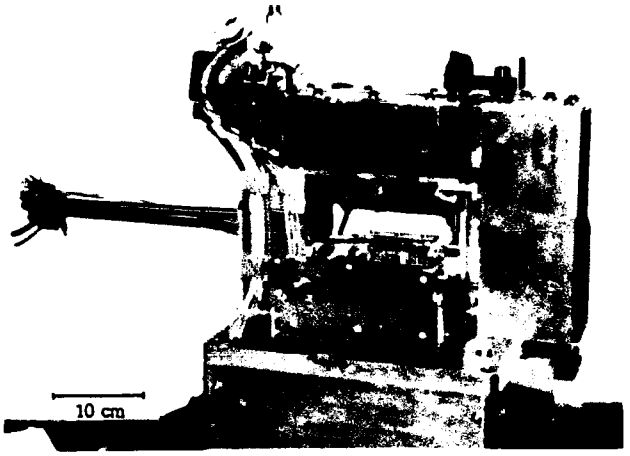


Fig. 17: Prototype of Automated Equipment to Assemble Connectors.

1) Automated equipment to assemble connectors for telecommunication cables was proposed.
2) Through experiments using test versions, the basic requirements were determined and evaluated, and the control method for lines was confirmed.
3) Based on the experimental results, estimations, and human interface, automated equipment to assemble connectors was designed and a prototype was manufactured.
4) The use of this equipment is expected to reduce assembly time and eliminate human error.

It is easy to automate the "set connector body," "set connector cover," and "press connector" processes. However our equipment does not automate these processes, because they are simple and not prone to human error. If the time of arrange conductor can be further reduced, the processes can be automated to synchronize the machine operation with human operation and thus reduce assembly time. After evaluating the characteristics of the prototype, a version for practical use will be designed, manufactured, and field-tested.



Tadahisa Harakawa

NTT Telecommunication Field Systems R&D Center

1-7-1 Hanabatake, Tsukuba, Ibaraki, 305 Japan

Tadahisa Harakawa received his B. E. degree in electronics engineering from Tokyo Denki University in 1982. He joined NTT in 1982. He is engaged in the development of cable splicing technique at NTT Telecommunication Field Systems R&D Center, Japan.



Naoki Nakao

NTT Telecommunication Field Systems R&D Center

1-7-1 Hanabatake, Tsukuba, Ibaraki, 305 Japan

Naoki Nakao received his M. E. degree in electronics engineering from Okayama University in 1987. He joined NTT in 1987. He is engaged in the development of cable splicing technique at NTT Telecommunication Field Systems R&D Center, Japan.



Satoshi Matsuhasi

NTT Telecommunication Field Systems R&D Center

1-7-1 Hanabatake, Tsukuba, Ibaraki, 305 Japan

Satoshi Matsuhasi is a Senior Engineer at NTT Telecommunication Field Systems R&D Center, Japan. He received his B. E. degree in electronics engineering from Hokkaido University in 1981. He joined NTT in 1981 He is engaged in the development of aerial cable installation technique and cable splicing technique. Mr. Matsuhashi is a member of the Institute of Electronics, Information and Communication Engineers of Japan.

Evaluation Method and Performance of Advanced Low-Reflection Optical Connectors

Kazunori Kanayama, Yasuhiro Ando, Ryo Nagase* and Shin'ichi Iwano

NTT Opto-electronics Laboratories, Ibaraki, Japan
* NTT Communication Switching Laboratories, Tokyo, Japan

Abstract

The performance of a newly developed advanced low-reflection Physical Contact (PC) optical connector and a method for evaluating it are presented. The advanced PC (APC) optical connector with an average return loss of 46 dB has been realized using an SC connector while maintaining a reliability as high as that of conventional PC optical connectors. The high return loss and reliability of the APC has been achieved by removing the most of damaged layer caused by the polishing process and by maintaining a slight fiber withdrawal from the ferrule endface. A new method of return loss evaluation that ensures the realization of the minimum return loss of randomly concatenated connectors is proposed for low-reflection connectors. Experimental results for the new method indicate that over 99% of connections achieve the expected minimum return loss.

1. Introduction

Low-reflection optical connectors will be indispensable for future analog video and high-speed digital transmission systems. The return loss of conventional Physical Contact (PC) connectors is, however, limited to about 30 dB. A finite reflection remains at the point of physical contact because a thin damaged layer is produced by the fiber endface polishing process. The difference between the refractive index of this layer and that of the fiber core produces a slight optical reflection. To eliminate this reflection, the damaged layer must be removed. In addition, the amount of fiber withdrawal from the ferrule endface must be limited[1] in order to maintain high reliability under a variety of environmental conditions.

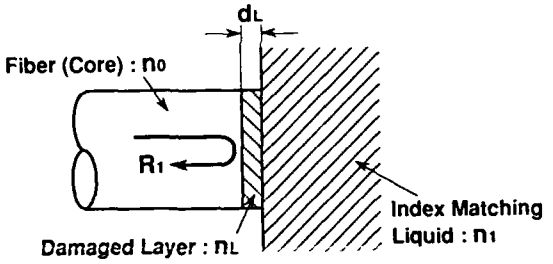
Recently, we have developed an Advanced Physical Contact (APC) optical connector that considerably improves the reflection characteristics while maintaining the same reliability as that of the existing PC optical connectors[2].

This paper clarifies the relationship between the damaged layer and the return loss with the APC and compares it with a conventional PC. The dependence of the optical characteristics under various conditions with respect to fiber withdrawal is elucidated. We also propose a new method of return loss evaluation that ensures the realization of the minimum return loss for randomly concatenated low-reflection connectors.

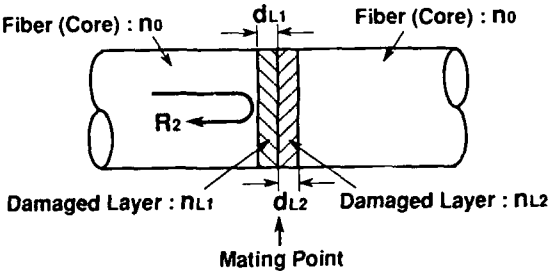
2. Advanced Physical Contact

2.1 Features of APC Optical Connectors

The domed ferrule endfaces of conventional PC connectors are produced by polishing the fiber with a diamond polishing agent. This polishing process results in a damaged layer at the fiber endface. In silica fiber, the refractive index of the damaged layer is slightly higher than that of the original fiber core. Therefore this high refractive index layer generates optical reflection at the connection interface. It is necessary to remove this damaged layer to eliminate optical reflection at the connection interface.



(a) Reflection from single damaged layer



(b) Reflection from mating point

Fig.1 Model of reflection from damaged layer

On the other hand, the combination of domed ferrule endfaces and axial compressive force can allow physical contact without generating Fresnel

reflection, because the ferrule endfaces are deformed elastically by the force, even if there is slight fiber withdrawal at the ferrule endface. To maintain stable PC connections under various environmental conditions, it is necessary to limit initial fiber withdrawal to less than 0.05 μm[2].

APC technology has satisfied the above two requirements through the use of additional fine grain SiO_2 polishing[3] after the conventional PC polishing process. APC polishing can remove the damaged layer without excessive fiber withdrawal. We estimated the refractive index and thickness of the damaged layer , on the assumption that it is a homogeneous single layer at the APC fiber endface. When we take the plane-wave multiple reflection at the damaged layer into consideration, the optical reflection from the fiber endface, which is coated with refractive index matching liquid, is given by

$$R_1 = \left| \frac{n_0 A + n_0 n_1 B - C - n_1 D}{n_0 A + n_0 n_1 B + C + n_1 D} \right|^2 \quad (1)$$

with

$$A = D = \cos\delta,\ B = (i/n_L)\sin\delta,$$

$$C = (in_L)\sin\delta,\ \delta = 2\pi n_L d_L/\lambda, \quad (2)$$

where n_0, n_1, n_L and d_L are the refractive indexes of the fiber core, index matching liquid and damaged layer and the thickness of the damaged layer, respectively. A model of the reflection from the interface between the damaged layer and the index matching liquid is shown in Fig. 1(a). The refractive index and the thickness of the damaged layer, which are calculated from the measured optical reflection for various n_1 values, are shown in Table 1. The refractive index of the APC surface is 1.460 as compared to a value of 1.540 for the PC surface. Because the refractive index of the APC is very close to that of the silica fiber core(=1.452), the reflection of the APC is essentially lower than that of a conventional PC.

Table 1 Refractive index and thickness of damaged layer

Connector	Refractive Index (λ =1.3μm)	Thickness (μm)
APC	1.46	0.07
Conventional PC	1.54	0.05

As the polishing rate for a zirconia ferrule and a silica fiber are almost identical, the amount of fiber withdrawal from the ferrule endface can be adjusted to less than ±0.05 μm, which is the same as that for the PC optical connector. Figure 2 shows the return loss dependence on temperature for the APC connector and other low-reflection PC connectors with relatively large fiber withdrawals. With the exception of the APC ferrule, the ferrules were polished with cerium oxide to increase the amount of fiber withdrawal. This experimental result indicates that if the fiber withdrawal is not sufficiently small, physical contact is not achieved at high temperatures due to the difference between the thermal expansion coefficients of the fiber and the ferrule. Only APC technology can provide stable optical characteristics and long term reliability.

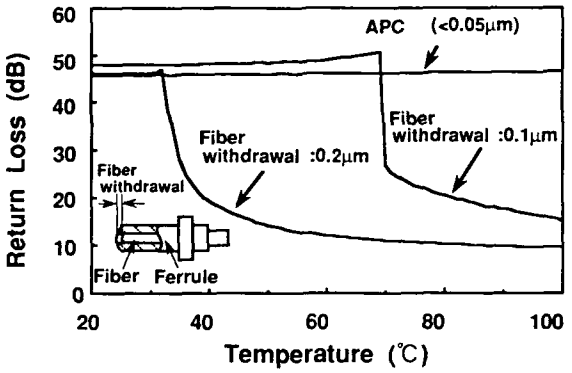


Fig.2 Temperature dependence of return loss for APC and other low-reflection PC connectors with relatively large fiber withdrawals

2.2 Characteristics of APC Optical Connectors

An SC connector was used in our experiments to evaluate the APC technology. Figure 3 shows the setup for the return loss measurement of an APC or conventional PC connector with the Optical Continuous Wave Reflectometry (OCWR) method. This setup consists of a 2x2 fusion fiber coupler, an optical power meter and an 1.3 μm optical light source. Ports 1 and 2 of the fiber coupler, whose internal reflection is less than -60 dB, are terminated with oblique ferrule end connectors. One end of the sample optical cable is terminated with an objective connector (APC or conventional PC) and the other end is terminated with an oblique ferrule end connector. The angle of these oblique ferrule ends is about 8°. These connectors were used to reduce the optical reflection at all mating points except at the objective connector. The return loss of the objective connectors (mating point) L_r [dB] is given by the following equation.

$$L_r = -10\log\frac{P_1}{P_0} + 14.7 \quad (3)$$

The value of 14.7 in Eq.(3) is the Fresnel reflection between the air (refractive index of 1.0) and the silica fiber core (refractive index of 1.452). Return loss histograms for APC and PC connectors are shown for comparison in Fig. 4. The histogram

represents the random concatenation of each objective connector measured by the above mentioned method. The average APC connector return loss is 46 dB, an improvement of more than 15 dB over that of conventional PC connectors.

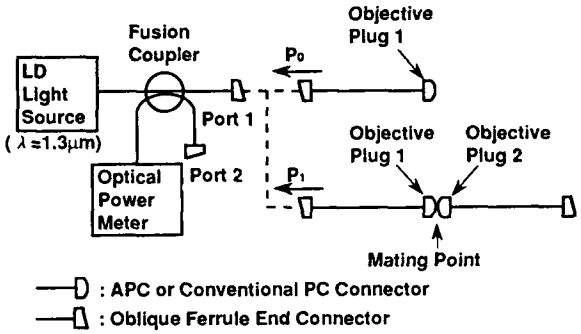


Fig.3 Return loss measurement setup for APC and conventional PC connectors

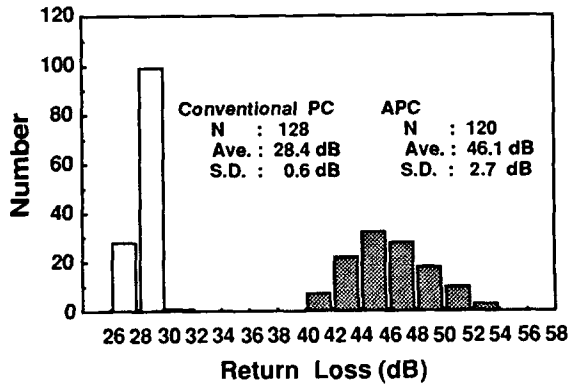


Fig.4 Histogram of return loss for APC and conventional PC connectors

The return loss distribution with APC is somewhat broad. This is because the refractive index of the damaged layer is close to that of the silica fiber. The relationship between the return loss and the damaged layer with PC and APC, are shown in Fig. 5. The plots represent the measurement data in Table 1, and the solid lines are calculated by using the above mentioned multiple reflection theory. A slight deviation in the refractive index of the APC damaged layer affects the return loss distribution much more than with conventional PC.

Test results on the mechanical and environmental characteristics of APC optical connectors are presented in Table 2. The evaluation was made by return loss measurement which can detect changes in characteristics with high sensitivity. The mechanical characteristics were satisfactory in terms of durability (mating/demating), vibration, and impact. No degradation in characteristics was observed in a variety of environmental tests including temperature cycling, high/low temperature endurance, and temperature/humidity cycling. It was concluded that the APC optical connectors had sufficient reliability in practical use.

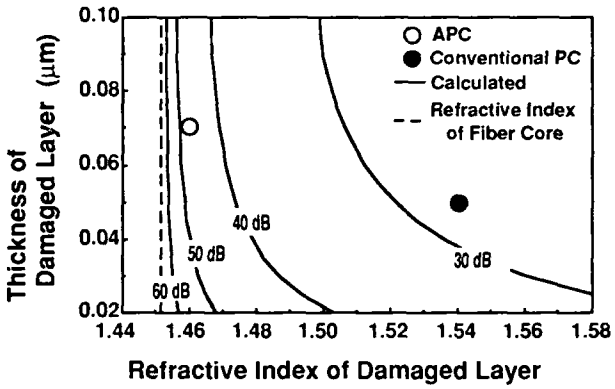


Fig.5 Relationship between return loss and damaged layer for PC and APC

Table 2 APC connector test results

Items		Conditions	Results
Optical Characteristics	Return loss	λ=1.3μm LD	Ave. 46.1dB S.D. 2.7dB
	Insertion loss	λ=1.3μm LD	Ave. 0.06dB S.D. 0.07dB
Mechanical Tests	Durability	500 times, measured every 10 times	No degradation
	Vibration	10 to 55Hz, Amp. 1.5mm, 2 hours	
	Impact	100G, 6ms duration, 10times, 3 directions	
Environmental Tests	Temperature cycling	-25 to 70℃, 4h/cycle, 100 cycles	
	High temp. endurance	85±2℃, 960 hours	
	Low temp. endurance	-25±2℃, 960 hours	
	Temp. and humidity cycling	-10 to 65℃, 93%R.H., 20 cycles	

3. Evaluation Method for Low-Reflection Optical Fiber Connectors

When optical connectors are in practical use, it is necessary to ensure that the minimum return loss of connector mating point has been realized. For this purpose, a new evaluation method for low-reflection connectors is investigated and proposed.

3.1 Theoretical Background

The return loss distribution is estimated with a Monte Carlo simulation. A theoretical model of the reflection from the connector mating point is shown in Fig.1(b). Optical reflection occurs from damaged layers. The return loss of a connector mating point is estimated by using the refractive index and the thickness of the damaged layers and these values vary for each connector due to the polishing process. It is assumed that the refractive index and the thickness of a damaged layer is represented by a Gaussian distribution. Probability densities of the refractive index $f(n_L)$ and the thickness $f(d_L)$ are given by the following equations,

$$f(n_L) = \frac{1}{\sqrt{2\pi}\sigma_n} \exp\left[-\frac{1}{2\sigma_n^2}(n_L - n_\mu)^2\right], \quad (4)$$

$$f(d_L) = \frac{1}{\sqrt{2\pi}\sigma_d} \exp\left[-\frac{1}{2\sigma_d^2}(d_L - d_\mu)^2\right], \quad (5)$$

where, n_μ and d_μ are average values of the damaged layer refractive index and thickness, σ_n and σ_d are the standard deviations of the damaged layer refractive index and thickness, respectively. $f(n_L)$ and $f(d_L)$ are not correlated. Measured values of n_μ, d_μ, σ_n and σ_d are shown in Table 3. The reflection from a connector mating point is calculated with the following equation.

$$R_2 = \frac{\left[\left(\frac{n_{L1}}{n_{L2}} - \frac{n_{L2}}{n_{L1}}\right)n_0 E\right]^2 + \left[\left(\frac{n_0^2}{n_{L2}} - n_{L2}\right)G + \left(\frac{n_0^2}{n_{L1}} - n_{L1}\right)H\right]^2}{\left[2n_0 F - \left(\frac{n_{L1}}{n_{L2}} + \frac{n_{L2}}{n_{L1}}\right)n_0 E\right]^2 + \left[\left(\frac{n_0^2}{n_{L2}} + n_{L2}\right)G + \left(\frac{n_0^2}{n_{L1}} + n_{L1}\right)H\right]^2}, \quad (6)$$

with

$$E=\sin\delta_1\sin\delta_2, F=\cos\delta_1\cos\delta_2,$$

$$G=\cos\delta_1\sin\delta_2, H=\sin\delta_1\cos\delta_2,$$

$$\delta_1=2\pi n_{L1}d_{L1}/\lambda, \delta_2=2\pi n_{L2}d_{L2}/\lambda, \quad (7)$$

where n_{L1} and d_{L1} are the refractive index of the damaged layer and the thickness of one connector, n_{L2} and d_{L2} are corresponding values for the other connector, respectively. A set of n_{Li} and d_{Li} corresponds to a combination of randomly selected connectors. As it is assumed that these values have Gaussian distributions as expressed by Eq.(4) and (5), each set of n_{Li} and d_{Li} is determined from normal random numbers. The normal random numbers can be generated by the Box-Muller method. Therefore, the return loss distribution is obtained for generated values of n_{L1}, n_{L2}, d_{L1} and d_{L2} calculated with Eq.(6).

The measured and calculated return loss distributions are compared in Fig.6. The calculation was carried out using the values in Table 3. The measured and calculated distributions agree well. From this result, it is concluded that the return loss distribution of low-reflection connectors can be estimated and predicted by means of the Monte Carlo simulation for random connection.

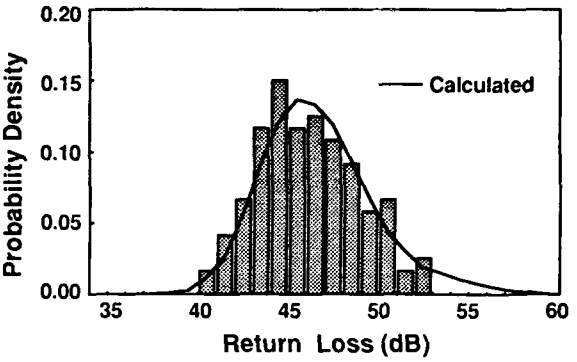


Fig.6 Distribution of return loss for randomly concatenated connectors

Table 3 Statistical characteristics of APC damaged layer

Items	Average	S. D.
Refractive Index (λ =1.3μm)	1.460	0.0038
Thickness (μm)	0.069	0.0125

3.2 New Evaluation Method for Low-Reflection Optical Connectors

As the return loss characteristics of the master connector are unknown in the conventional evaluation method, it is difficult to measure a specific return loss. Measured return loss values vary because of the differences in the damaged layers of the master connectors[4]. Therefore, it is necessary to determine the return loss characteristics of the master connector. We propose a new evaluation method for return loss measurement which uses a defined master connector to ensure that the designed minimum return loss is realized for random connection. This new method also ensures the realization of the designed minimum return loss of one mating point of the objective patch cord with connectors on either side. Furthermore, new method is applicable to a measurement setup in which be spatial reflection can not be resolved. The setup for return loss evaluation is shown in Fig.7. This method employs OCWR with a 2x2 fusion fiber coupler and reflection-standard connectors that is to say the above mentioned master connectors. The procedure is as follows when the designed minimum return loss is L_{r_s} [dB], namely specification

(a) The objective patch cord is connected between the preselected reflection-standard connectors A and B.

(b) The return loss L_r [dB] from the two mating points of the objective cord and the reflection-standard connectors is measured.

(c) When L_r is greater than L_{r_s}, the objective patch cord is passed as a screened cord.

As shown in Fig. 7, standard connectors are selected on condition that their return loss from the mating point is $L_{r_s} + \alpha$ [dB]. In brief, objective cord (con

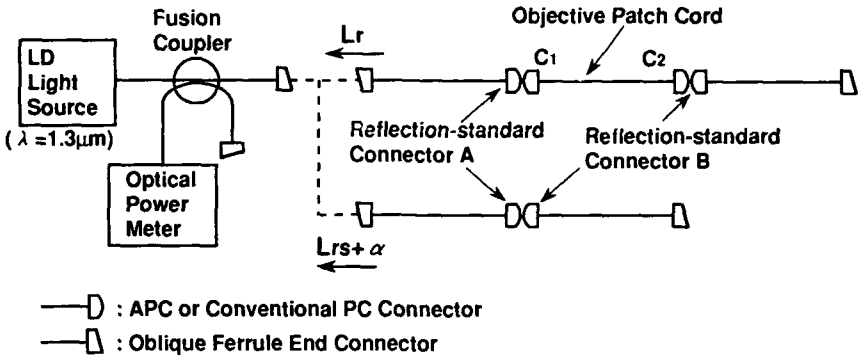


Fig.7 Setup for return loss evaluation

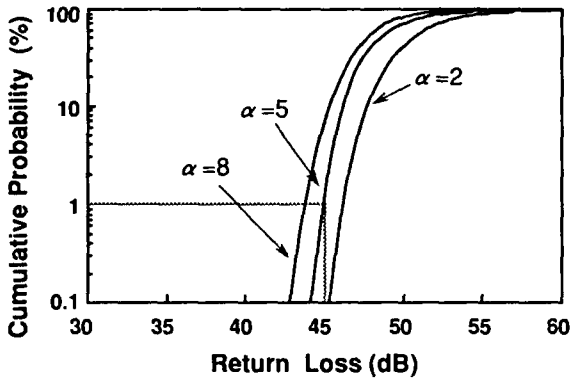


Fig.8 Simulated cumulative probability for return loss with respect to parameter α

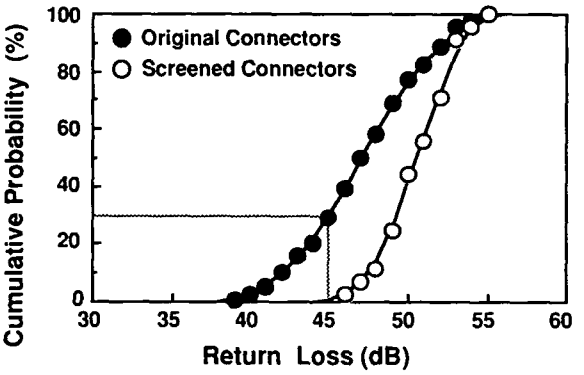


Fig.9 Experimental cumulative probability for return loss

nectors) are screened out by using of reflection standard connectors. Parameter α is determined based on a statistical simulation, which takes into consideration the above mentioned damaged layer distribution. Simulated return loss results for different α values are shown in Fig. 8. The solid lines represent the cumulative probability of return loss, when the screened cords which are selected from objective cords, are randomly concatenated using the parameters α=2, 5 and 8. Calculations are also carried out using the values in Table 3. The designed minimum return loss L_{rs} is 45 dB in this case. From the result in Fig.8, it is demonstrated that over 99% of connectors achieve the designed minimum return loss, provided that parameter α is less than 5 dB.

3.3 Experimental Result

The simulated result of the evaluation method was verified experimentally. In the experiment, the designed minimum return loss L_{rs} was 45 dB and parameter α was 2 dB. After evaluation the objective patch cords were cut at their center. The experimental return loss of randomly concatenated connectors was obtained from these cut cords (i.e. C_1 and C_2 combination in Fig. 7). The experimental results are shown in Fig.9. 30% of the original objective cord combinations were unsuitable. On the other hand, all the cords screened by the new method satisfied the designed minimum return loss of 45 dB. Therefore, the proposed evaluation method is very effective for ensuring that the minimum return loss of randomly concatenated connectors is realized.

4. Conclusion

An advanced PC optical connector with an average return loss of 46 dB has been realized which maintains a reliability as high as that of conventional PC optical connectors. The high return loss and reliability of the APC connector have been achieved by removing most of the damaged layer and by maintaining a slight fiber withdrawal from the ferrule endface with a fine grain SiO_2 polishing process. It has also been confirmed that the return loss value and distribution of the APC connector is significantly affected by the remaining damaged layer, because the refractive index of the layer is very close to that of the silica fiber core.

A new method of return loss evaluation that ensures the realization of the minimum return loss of randomly concatenated connectors is proposed for low-reflection connectors. This method employs a fusion fiber coupler and reflection-standard connectors. These standard connectors are selected based on a statistical simulation, which takes into consideration variations in the thin damaged layer on the fiber endface. Experimental results for the new method

designed to ensure the minimum return loss of over 99% of connections, indicate that all the connections achieve the expected minimum return loss. Therefore, the proposed evaluation method is very effective for ensuring that the minimum return loss of randomly concatenated connectors is realized.

Acknowledgments

The authors wish to thank E.Sugita, M.Horiguchi and M.Kobayashi for their helpful guidance and encouragement, and F. Ohira, K.Matsunaga and T.Saito for their collaboration in the development of the polishing machine.

References

[1] T.Shintaku, R. Nagase and E.Sugita, "Connection mechanism of physical-contact optical fiber connectors with spherical convex polished ends," Appl. Opt., vol. 30, no. 36, pp. 5260-5265, Dec. 1991.

[2] Y.Ando, S.Iwano, R.Nagase, K.Kanayama and E.Sugita, "Advanced optical connectors for single-mode fibers," NTT Review, vol. 3, no. 3, pp. 110-121, MAY 1991.

[3] T.Saitoh, K.Matsunaga and K.Kanayama, "Polishing technology for very high return loss optical fiber connector," in Paper of the Technical Group on Electromechanical Components, IEICE Japan, 1990, EMC90-23.

[4] R.Nagase, K.Kanayama and Y.Ando, "Method for return loss measurement of PC optical fiber connectors," in Nat. Conf. Rec., IEICE Japan, Autumn 1990, no. C-284 (in Japanese).



Kazunori Kanayama

NTT Opto-electronics Laboratories
Tokai, Naka-Gun, Ibaraki
319-11 Japan

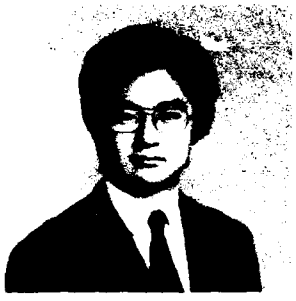
Kazunori Kanayama received his B.E. and M.E. degrees in mechanical engineering from Waseda University in 1984 and 1986, respectively. Since joining NTT Electrical Communications Laboratories in 1986 he has been engaged in research on optical fiber connectors. He is presently a Research Engineer in the NTT Opto-electronics Laboratories.



Yasuhiro Ando

NTT Opto-electronics Laboratories
Tokai, Naka-Gun, Ibaraki
319-11 Japan

Yasuhiro Ando received his B.E. and M.E. degrees in electronic engineering from Osaka University in 1974 and 1976. Since joining NTT Electrical Communications Laboratories in 1976, he has been engaged in research on electric contact and optical connection technology, and in the development of electrical/optical connectors for advanced digital communication systems. He is presently a Senior Research Engineer, Supervisor, in the NTT Opto-Electronics Laboratories.



Ryo Nagase

NTT Communication
Switching Laboratories
Midorityo, Musashino-Shi,
Tokyo 180 Japan

Ryo Nagase received his B.E. and M.E. degrees in precision engineering from Tohoku University, Miyagi, Japan, in 1983 and 1985, respectively. Since joining NTT Electrical Communications Laboratories in 1985, he has been engaged in the research and development of optical fiber connectors. He is presently a Senior Research Engineer in the NTT Communication Switching Laboratories. He is now working in the field of photonic switching systems.



Shin'ichi Iwano

NTT Opto-electronics
Laboratories
Tokai, Naka-Gun, Ibaraki
319-11 Japan

Shin'ichi Iwano received his B.E. and M.E. degrees in electronic engineering from Kyushu University, Fukuoka, Japan, in 1981 and 1983, respectively. Since joining NTT Electrical Communications Laboratories in 1983, he has been engaged in research on optical fiber connections and the development of optical fiber connectors. He is presently a Senior Research Engineer in the NTT Opto-electronics Laboratories.

PERFORMANCE OF CERAMIC-FERRULE OPTICAL CONNECTORS

L.A. Reith, R.M. Fagerstrom, G.D. Kiss, E.M. Vogel*, W.W. Wood and H.H. Yuce*

Morris Research and Engineering Center, Bellcore, Morristown, New Jersey 07962
**Red Bank Research and Engineering Center, Bellcore, Red Bank, New Jersey 07701*

ABSTRACT

The ultimate goal of this work is to correlate the performance of ceramic ferrule optical fiber connectors to measurable physical characteristics of the fiber endfaces. These characteristics include the geometry of the fiber/ferrule endface and the quality of the polished fiber surface. Connector performance is not solely a function of an individual plug, however, but is determined by the interaction of two mated plugs, i.e., mateability. We therefore began our investigation by performing statistical analyses of loss and reflectance performance on different groups of connectors. We present details of our results showing that significant differences can exist between both homogeneous and heterogeneous groups. Once significantly different groups were identified, we used a variety of techniques to characterize the fiber/ferrule endfaces, including atomic force microscopy, scanning electron microscopy, and interferometry.

1. INTRODUCTION

As fiber deployment escalates into the loop portion of the telephone network, so too will the deployment of optical fiber connectors. Reliable performance of these connectors will become increasingly critical. A basic understanding of the relationship between quantifiable surface properties and connector performance is thus desirable. Knowledge of critical properties and the subsequent ability to control them will result not only in more reliable performance, but will also help to ensure intermateability of connectors from different vendors.

We began our study by using a modified concatenation test method[1] to measure the performance (loss and reflectance) of eight different groups of ceramic ferrule-type connectors. Our goal was to first characterize the performance of homogeneous vendor groups and then to intermate plugs from different groups, in order to find significant performance differences between homogeneous and heterogeneous groups. This work will be described in Section 2.

Once groups with significantly different performance were identified, we proceeded to characterize the properties of the ferrule endfaces in an attempt to correlate performance to some measurable physical quantities. The characterization techniques we used and the results of these measurements are described in Section 3. Conclusions are given in Section 4.

2. MATEABILITY MEASUREMENTS

2.1 Experimental Setup

Figure 1 shows a detailed block diagram of the experimental setup. A dual-wavelength source provides both 1300 and 1550 nm outputs for the loss and reflectance measurements. The wavelength is selected by means of an optical switch. For transmission-loss measurements, the source output travels through the coupler and SW 4, and through the connection on test to detector head B of an optical power meter. For reflectance measurements, the reflected light from the test connection travels back through the coupler through SW 2, which is connected to detector head A of the power meter.

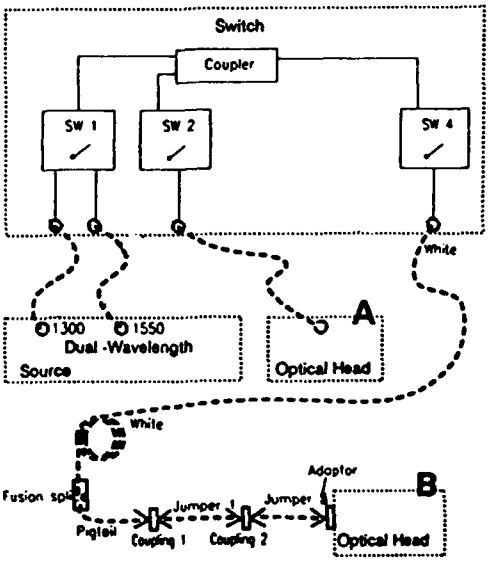


Figure 1 - Block diagram of experimental setup.

Figure 2 shows generalized block diagrams describing the modified concatenation test. The testing system uses a source, S, coupler, and two detectors, D_1 and D_2. As detailed in Fig. 1, the source S is connected to one arm of the coupler, which is in turn connected to the connector cable assemblies on test. One detector, D_1, acts as a photon bucket, capturing essentially all the light output through the connector cable assemblies. Detector D_2 is connected to the second input arm of the coupler, and is used to detect the reflected light from the connector under test. All of the instruments in the testing system are controlled by an HP computer via a GPIB interface.

At the START-OF-TEST condition, one connector jumper assembly is cut in half and fusion spliced to the output of the coupler. A complete jumper assembly, 1, is connected between the spliced connector and D_1. The transmitted power is measured at D_1. This is used as a reference value.

A second jumper assembly, 2, is then connected between jumper 1 and D_1. The connector under test is the mating of jumpers 1 and 2. The loss at this connection is simply given by the difference
between the measured loss and the reference value. Thus, system losses are subtracted out. Similarly, the system reflectance is found by putting a 40 dB mandrel wrap in jumper 2 and measuring power at D_2. This reflected power includes system reflectances plus that of the connector under test. Then the mandrel wrap is relaxed and moved to jumper 1 so that the reflected power measured by D_2 includes the system reflectances only. The net reflectance at the connector under test is simply given by the difference between the two measured values.

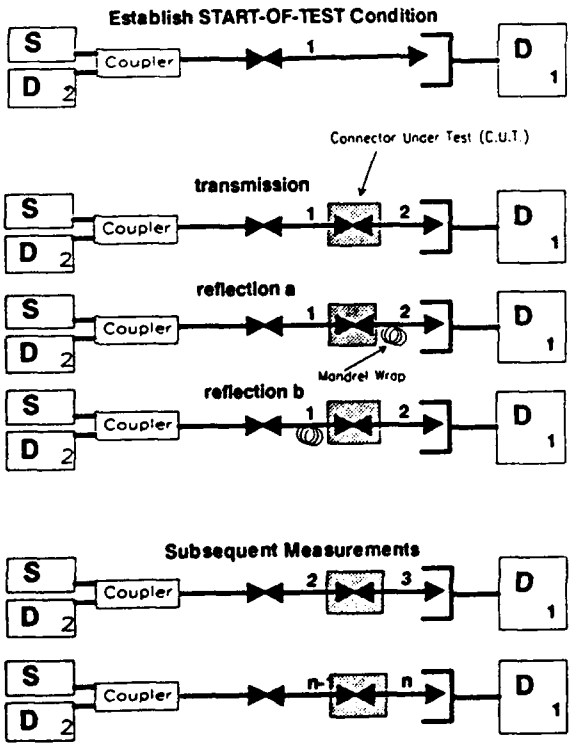


Figure 2 - Generalized block diagrams of modified concatenation test.

For these experiments, we used three complete jumper assemblies (marked as jumpers 1, 2, 3, sides W(hite) and R(ed)) to make a total of 12 possible connections for each homogeneous group. For heterogeneous groups, we used jumper 1 (W and R) from one vendor and jumper assemblies 1, 2, and 3 (W and R), from a second vendor to again make up 12 possible connections. Each connector was cleaned carefully with a lint-free wipe, first soaked in alcohol, then dried, followed by blowing with an air gun. This was done before every reconnection. If loss or reflectance was unusually high, the connectors were cleaned carefully and the measurement was retaken.

2.2 Results

Boxplots for eight different homogeneous groups are shown in Fig. 3 (a) and (b) for the loss and reflectance at 1300 nm, respectively. The horizontal lines around each box denote the 25th and 75th percentiles. The filled circles denote the median values, and the dashed whiskers from each box extend upward (downward) as far as 1.5 times the interquartile range or to the maximum (minimum) value, whichever is less (more). Any values beyond the whiskers are denoted by open circles.

The eight groups correspond to eight different lots from four different vendors. Group F includes only eight, rather than twelve data points, because several connections did not make

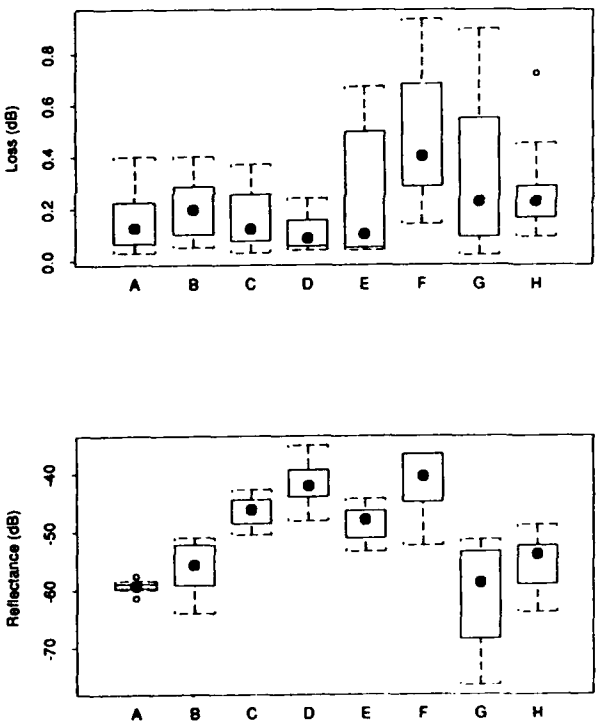


Figure 3 - Boxplots of Loss and Reflectance for groups A through H at 1300 nm.

physical contact due to large eccentricities of the polished endface surface. This resulted in extremely high reflectances and these data points were therefore neglected as anomalous.

Intermated, heterogeneous groups AB, AC, and BC, as well as DE, DF, EF, and DG were also characterized. Figure 4 shows sample boxplots comparing groups (A, AB, B), (A, AC, C), and (B, BC, C) at 1300 nm for both loss and reflectance. Note that there is much overlap of all the groups in loss performance, but little overlap in reflectance between (A, AC, C) and (B, BC, C).

To determine if the differences in performance between different groups were statistically significant, we calculated group means and standard deviations, and did an analysis of variance for each set of three groups. This analysis yields the probability that populations with no differences in mean performance will have group means with differences as large as those which we observed. If this probability, or p-value, is less than 5%, we conclude that the difference between the group means is statistically significant. For group means that were significantly different, a subsequent test, Fisher's least-significant-difference test, was performed to determine which pairs of group means were significantly different.

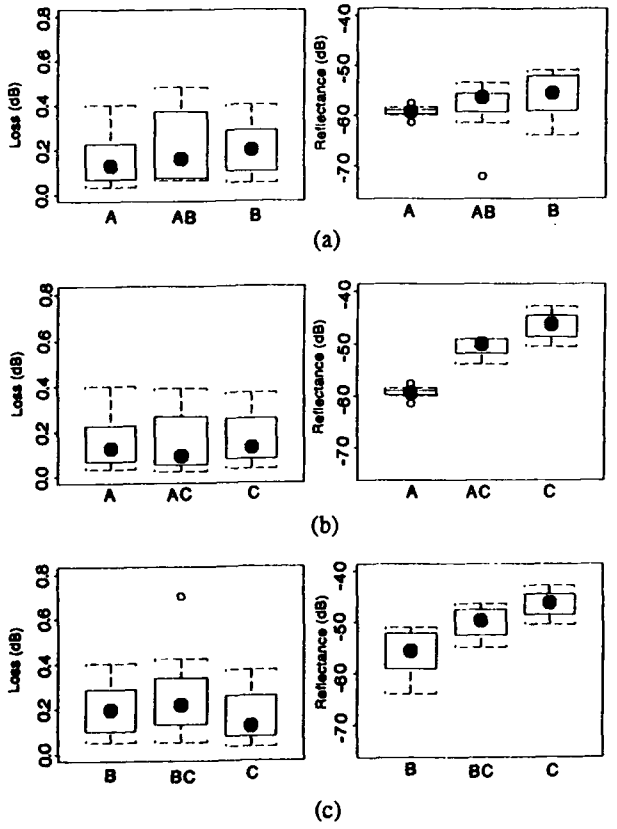


Figure 4 - Boxplot comparisons of loss and reflectance for homogeneous and heterogeneous groups at 1300 nm. (a) Boxplot comparing the two homogeneous groups, A and B, with the heterogeneous group, AB. (b) compares groups (A, AC, C) and (c) compares (B, BC, C).

Table 1 presents group means and standard deviations for loss and reflectance at 1300 nm for all the groups. Solid lines drawn between groups indicate that the performance differences between those groups are significant. For example, groups (A, AC, C), had no significant differences between any of the groups for loss performance. However, there were significant reflectance differences between both of the homogeneous groups and the intermated group, and the performance of the intermated group fell between that of its parents.

Table 1 - Group means and standard deviations for loss and reflectance at 1300 nm for cell groups. solid lines connecting groups indicate that the performance differences between those groups are significant.

	LOSS (dB)		REFLECTANCE (dB)	
	Mean	Std. Dev.	Mean	Std. Dev.
A	.16	.12	-59.3	.9
AB	.22	.15	-58.3	4.9
B	.20	.11	-56.1	4.2
A	.16	.12	-59.3	.9
AC	.15	.13	-50.6	1.6
C	.16	.12	-46.5	2.4
B	.20	.11	-56.1	4.2
BC	.25	.18	-50.2	3.1
C	.16	.12	-46.5	2.4
D	.11	.06	-42.0	3.9
DE	.36	.25	-47.1	1.5
E	.24	.24	-48.5	3.0
D	.11	.06	-42.0	3.9
DF	.25	.16	-46.8	2.6
F	.48	.27	-41.7	5.9
E	.24	.24	-48.5	3.0
EF	.29	.26	-46.8	5.6
F	.48	.27	-41.7	5.9
D	.11	.06	-42.0	3.9
DG	.23	.14	-52.3	3.5
G	.34	.31	-61.4	9.3

2.3 Summary

Homogeneous groups A, B, and C and their intermated heterogeneous groups AB, AC, and CB, showed no significant differences in loss performance. The reflectance of group C, however, was significantly higher than that of A and B. The intermated groups, AC and BC, had significantly different reflectances from any of the parent groups, and their reflectances fell between the extremes of the parent groups.

Homogeneous groups D, E, and F and their intermated heterogeneous groups DE, DF, and EF, had significantly different loss performance between groups D and F, and DF and F, as well as between D and DE. Group F had a significantly higher loss than D, and the intermated group, DF, had a loss significantly better than F, but not significantly worse than its other parent, D. Similarly, group DE, although significantly higher in loss than D, was not significantly different from its other parent, E. In the case of reflectance performance, group D was significantly higher than E and DE, but DE was not significantly different from E. Similar results were obtained for groups F, E, and EF. Group DF had unusual behavior not seen with any other group. This group was significantly better than either of its parents. The cause is not yet understood.

Finally, there were significant differences in loss performance between homogeneous groups D and G, but the heterogeneous group DG was not significantly different from either of its parents. In the case of reflectance performance, there were significant differences between D, G, and DG. The mean reflectance of group DG fell between that of its parents.

Therefore, in all cases, whether or not there were any significant differences between homogeneous groups, the intermated groups were never worse than the worst performing parents. In one case, the heterogeneous group was actually better than its parents. This result is not yet understood. Although data was taken for both 1300 and 1550 nm, the results were essentially the same at the two wavelengths. Thus, only results at 1300 nm were shown here.

3. ENDFACE CHARACTERIZATION

3.1 Experimental Techniques

3.1.1 Environmental Scanning Electron Microscopy

The use of a conventional scanning electron microscope is limited when the samples are wet, oily, or electrically insulating, such as glass or ceramic surfaces. Conductive surfaces at high vacuum are required for good imaging. With an environmental electron microscope (ESEM), however, the electron gun still requires high vacuum (10^{-6} torr), but the specimen chamber can be observed at 25 torr or higher. High chamber pressure is a key element in the charge-neutralization of insulating surfaces and electron-detection processes, so that conductive coatings are no longer necessary. A gas such as water vapor, oxygen, argon, or methane is introduced to the chamber to maintain a selected pressure. Secondary electrons and ions are detected by a gaseous detector device using ionization of the ambient gas molecules.

In order to gain sufficient signal, we found it necessary to use higher water-vapor pressure to image the core of a fiber, which has different chemical composition than the surrounding fiber cladding or the ceramic ferrule. In addition to imaging with secondary and backscattered electrons, ESEM is also equipped with an energy dispersive x-ray analyzer for elemental analysis. We operated the ESEM at 20 kV and pressures of about 5 torr.

3.1.2 Atomic Force Microscopy

A commercial atomic force microscope (AFM) was also used to study the surface morphology of the connectors. The AFM, like the ESEM, does not require the sample to be a conductor. It measures the topography of a sample with sub-nanometer resolution regardless of the size of the sample. The AFM can be used directly on large samples. The AFM can be thought of as an ultra sensitive profilometer which operates with an extremely low applied force. A cylindrical piezoelectric tube scans a very sharp probe, which is mounted on a flexible cantilever over the sample surface. A compact interferometric detection system mounted on the end of the piezo tube senses the deflection of the cantilever as features in the sample are encountered. In the most common operating mode, the control system varies the voltage applied to the piezo to keep the cantilever deflection nearly constant as the probe is scanned over the sample surface in a raster pattern. The variation in the voltage applied to the piezo translates directly into the variation in height across the sample[2].

The constant-force mode was used for this study, and the samples were imaged in air. No special sample preparations were required. We used xyz translators with two different scan widths: 150 and 20 μm. Using different translators allowed us to image with tremendous resolution (0.3 nm laterally and 0.1 nm vertically), depending upon the sample. Scanning frequencies were in the range of 5 to 100 Hz with the higher frequencies for smaller scan widths. To ensure representative results, several samples from each group were used. Each sample was also examined with at least two different AFM tips, minimizing the possibility of misinterpreting tip-induced artifacts in the images.

3.1.3 Interferometric Measurements

Interferometric measurements were made using a unit specifically adapted to measure ferrule-endface parameters, including radius of curvature of the ferrule as well as eccentricity of the polished endface, and fiber protrusion/undercut with respect to the ferrule. In this implementation, the ferrule endface contacts a thin glass flat illuminated with an LED. Interference fringes are formed with a half-wavelength spacing, corresponding to a height variation across the ferrule endface of 0.315 μm.

Eccentricity and radius of curvature of the polished ferrule endfaces were measured from pictures of the ferrule endfaces as shown in Fig. 5(a). The polishing eccentricity was defined as the distance between the center of the fringe "bullseye" pattern, where the connector contacted the optical flat, and the center of the fiber in the ferrule. Connectors were always inserted in the same orientation and the relative direction of the eccentricity was noted.

Radius of curvature was calculated from the fringe spacing of the first five rings emanating from the center of the "bullseye" (an area of approximately 400-μm diameter). The fringe spacing was measured at 90 degree intervals, and the curvatures calculated using a least-squares fit.

Fiber extension with respect to the ferrule can also be measured by tilting the optical flat so that at least two fringes fall across the fiber and ferrule as shown in Fig. 5(b). If the fiber endface is perfectly spherical, and matches that of the ferrule, the fringe pattern will still be perfectly circular. Thus, fiber protrusion or undercut from a spherical surface is obtained by measuring variations in the fringe radius between the edge of the ferrule and the center of the fiber. This technique gives results reproducible to 0.05 μm.

3.1.4 Index-Matching Fluids

A potential cause of reflectance between two physically contacting connector plugs is the modification of the glass surface layer[3,4,5]. This is a polishing-induced effect, resulting in a higher refractive index of the glass over a distance a few tens of nanometers deep across the polished surface. In order to determine if such an effect was present in the connectors we tested, we immersed the end of a connector plug in a number of different index-matching gels, ranging from n = 1.418 to 1.500 and measured the reflectance. If there was an increase in

refractive index at the fiber endface due to compaction, there should always be some residual reflectance regardless of the value of the refractive index of the matching fluid[6].

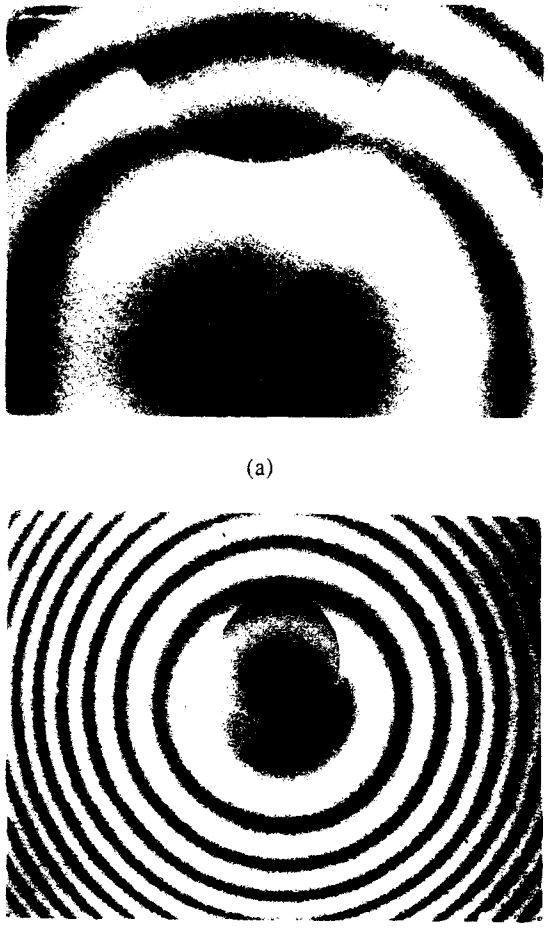


Figure 5 (a) - Fringe pattern formed when a connector endface contacts an optical flat in the interferometer. Center of the fringe "bullseye" is the endface contact point to the flat. **(b)** shows fringes falling across the fiber surface to measure protrusion/undercut.

3.2 Results

3.2.1 ESEM

ESEM images in Fig. 6(a), (b), and (c) show the physical topography of connectors from groups A, B, and C, respectively. Group C showed consistently more and deeper polishing scratches than A or B. Note that group C also had higher reflectance than either A or B. Elemental analysis of the surfaces showed no particulate matter indicative of polishing residue.

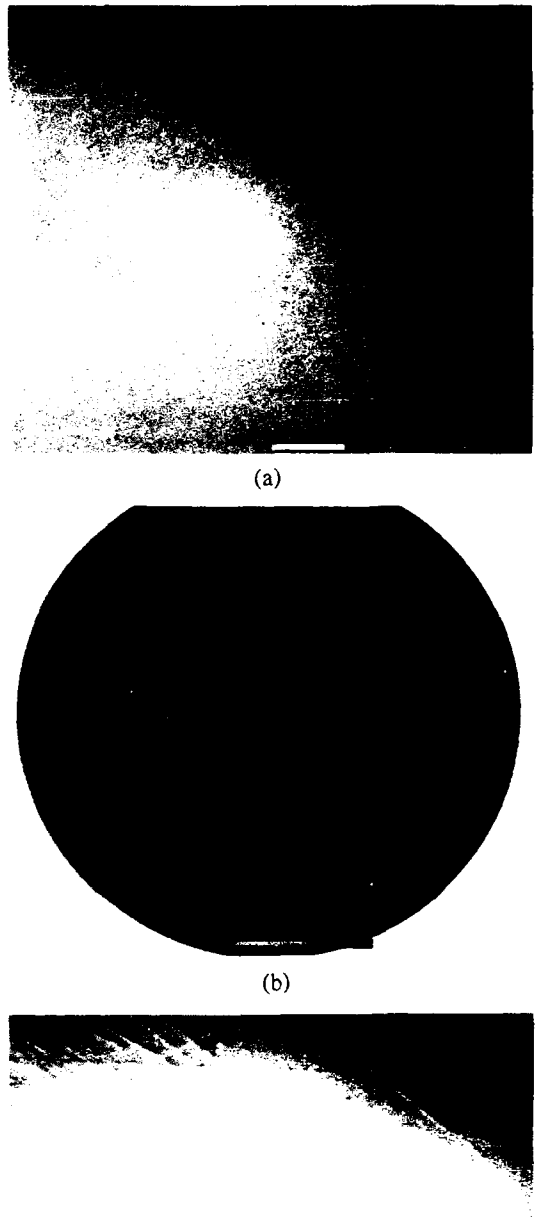


Figure 6 - ESEM images of connectors from groups (a) A, (b) B, and (c) C.

3.2.2 AFM

A series of AFM images of connector ends are shown in Fig. 7 which shows a 150 μm square area across the endface of three different connectors. Units are in nanometers. Note that the vertical scale is one-hundred times as sensitive as the horizontal scale. The surface of the fiber in the center of the image in Fig. 7(a) (group A) can be characterized as almost scratch free and flush with the ferrule. In contrast, the surface of a connector from group E (Fig. 7(b)) shows a number of scratches 0.01 - 0.1 μm deep and 0.05 - 0.3 μm across. Most of this roughness can be attributed to the polishing technique. Figure 7(c) shows an image of a connector from group B. Note the crevice on the left side of the fiber, where the soft epoxy has been eroded away. The epoxy is below the surface of the fiber and the surface of the ferrule. A number of pits, as well as some dirt, can be observed on the fiber surface.

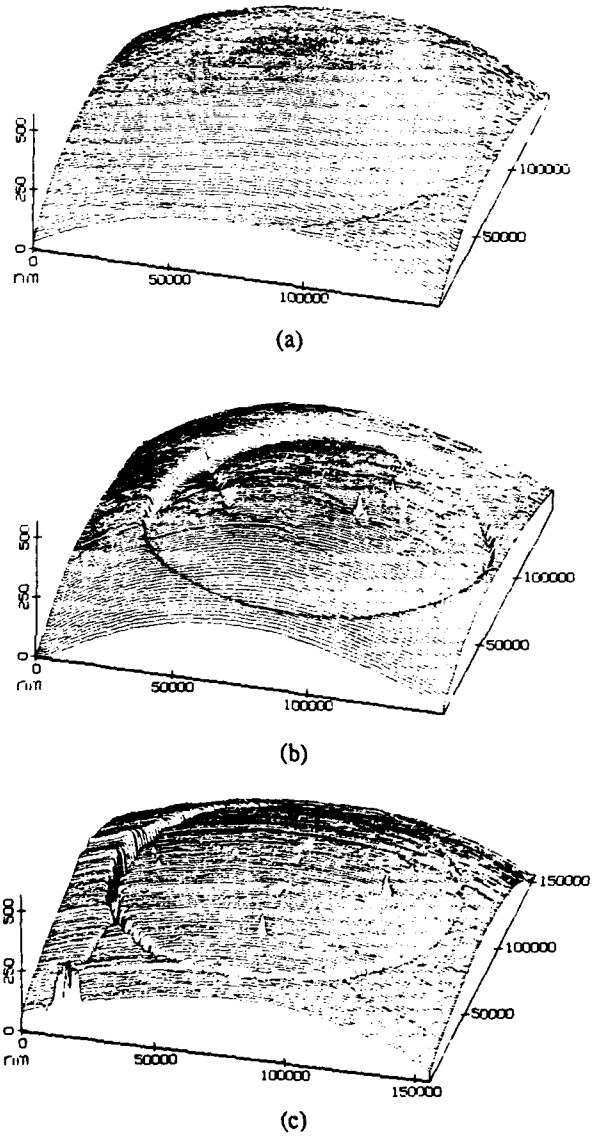


Figure 7 - AFM images of connector endfaces from groups (a) A, (b) B, and (c) E.

3.2.3 Interferometer

The gap between the fiber cores of any pair of connector plugs without spring loading (zero insertion force) could be estimated from values of radius of curvature and location and size of the eccentricity of each of the connector plugs. Results of such calculations for groups F (filled circles) and EF (open circles) are shown in Fig. 8, where reflectance for mated connector pairs is plotted as a function of the total estimated gap between the fiber cores assuming zero insertion force. This figure clearly indicates that for gaps greater than approximately 0.5 μm, the fibers will not achieve physical contact, resulting in high reflectances. This implies that ferrule deformation in mated, spring loaded connectors must be approximately 0.5 μm. Such behavior is highly dependent on the particular plug combination, since two plugs with large eccentricities can compensate each other if their eccentricities are in opposite directions.

This plot does not take into account the relative fiber protrusion/undercut with respect to the spherical surface of the ferrule. On the basis of our interferometric measurements, the connectors from all groups were typically slightly undercut, usually less than 0.1 μm. Only groups G and H showed protrusions, by as much as 0.1 μm.

Figure 8 includes data from the total groups. Performance data presented in Section 2 does not include interconnects with reflectances greater than -25 dB, which were clearly the result of non-physical contact.

Radii of curvature of different groups of connector ferrules ranged from approximately 10 to 30 mm, with deviations from a perfect sphere ranging from 0 to 3 mm.

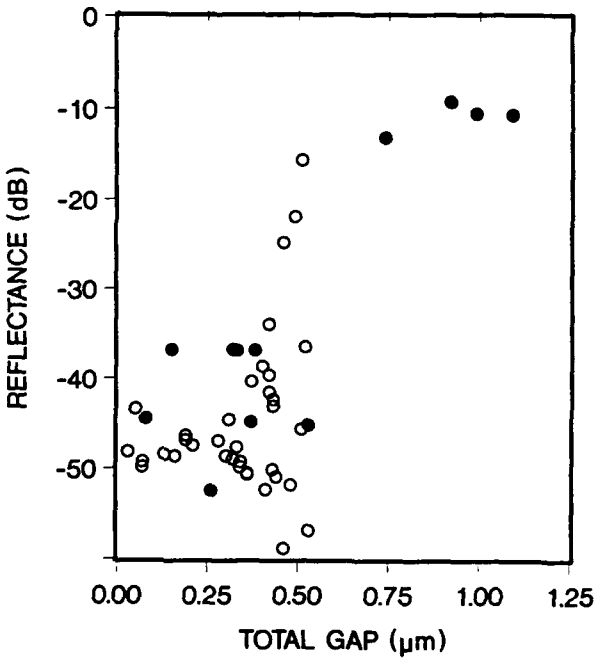


Figure 8 - Measured reflectance for all combinations of mated connector pairs, plotted as a function of the estimated gap between the two fiber cores (assuming zero insertion force). Filled circles are group F values, and open circles are group EF values.

3.2.4 Index-Matching Fluid

An example of results from these measurements are shown in Fig. 9. Reflectances from two different connector plugs are plotted as a function of the refractive index of the matching fluid applied to the end of the connector plug. Results are plotted for 1300 nm wavelength. The open symbols denote results from a connector plug from group A, which had a very small reflectance, and the filled symbols from a connector plug from group D, which had much higher reflectance. The solid line shows ideal reflectance for a perfectly perpendicular fiber endface, assuming a refractive index of 1.464 in the bulk glass. Although there are small differences in the reflectances between the two groups as plotted in Fig. 9, these differences are not large enough to explain the large difference in performance between the two groups of mated pairs. We also measured connector plugs from groups B and C, and saw no evidence of a higher-index surface layer.

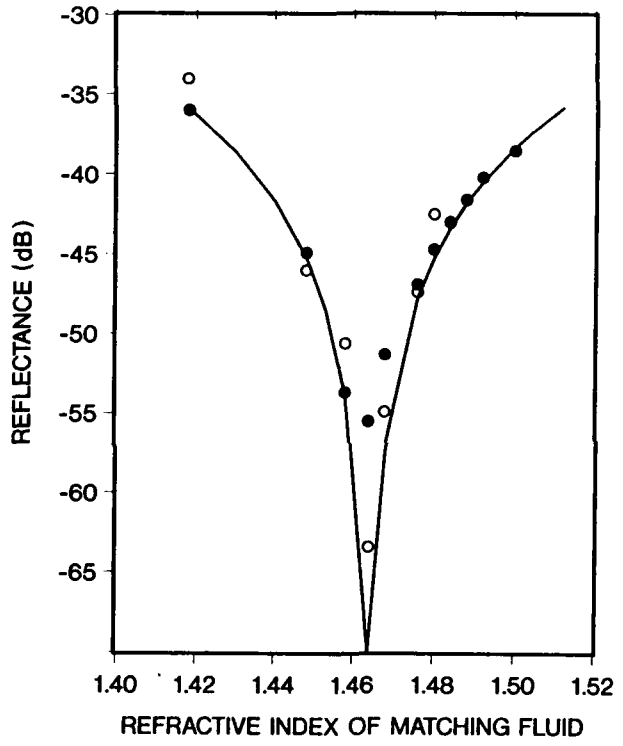


Figure 9 - Reflectances for two different, open-ended connector plugs, immersed in fluids of varying refractive index. The open circles are for a plug from group A, and the filled circles are for a plug from group D. The solid line is an ideal plot of reflectance.

3.3 Summary

Connectors from various groups have been characterized using a variety of techniques. Evidence of non-physically contacting connections were found, which could be correlated to eccentricity of the polished ferrule. This was based on an interferometric measurement. Interferometry was also used to measure radii of curvature of the connector endfaces, as well as protrusion/undercut of the fiber with respect to the ferrule.

AFM and ESEM measurements of the fiber surfaces showed clear differences between connectors from different groups. Sources of poor surface quality, such as scratches, pitting, dirt, etc. could be identified by these techniques.

No conclusive evidence of a high-index due to polishing was found on any connector we measured. This was to be expected, since all physically contacting connectors had quite low reflectances[5].

4. CONCLUSIONS

The loss and reflectance performance of eight different vendor groups was characterized on a statistical basis. Significant differences in performance were found. Intermated groups were also characterized. The performance of the intermated groups typically fell between that of its parents and in no case was significantly worse than the worst parent.

Connectors from these same groups were then characterized using various techniques, including AFM, ESEM, and interferometry. Eccentricity of the polished ferrule endface, measured with an interferometer, was found to correlate to connector performance in those cases where the eccentricity was so large as to result in non-physical contact. Other techniques show promise of yielding information on very small scale surface features which may lead to a more detailed understanding of connector reflectance performance.

5. ACKNOWLEDGEMENTS

We would like to acknowledge the hard work of J.C. Parisis, in completing the concatenation tests and interferometric measurements, and K.W. Moyers for his assistance with the microscopy.

6. REFERENCES

1. W.W. Wood and G.D. Kiss, "Procedures for Measuring Optical Performance of Fiber Optic Connectors", Proc. NFOEC, Vol. I, April, pp. 383-394, 1992.
2. H.H. Yuce, J.P. Kilmer, and J.P. Varachi, "Atomic Force Microscopy Measurements to Study Optical Fiber Aging", To appear in Proc. Symp. Opt. Fiber Meas., Boulder, CO, Sept. 15-17, 1992.
3. Lord Rayleigh, "The Surface Layer of Polished Silica and Glass with Further Studies on Optical Contact", Proc. R. Soc. London, Ser. A, Vol. 160, pp. 507-526, 1937.
4. V. Shah, W.C. Young and L. Curtis, "Large Fluctuations in Transmitted Power at Fiber Joints with Polished Endfaces", OFC Technical Digest, paper TUF4, 1987.
5. V. Shah, L. Curtis, and W.C. Young, "Reflectance Considerations in Optical Interconnection Devices", Proc. NFOEC, Vol. I, April, pp. 341-360, 1992.
6. J.B. Clayton, G.M. Alameel and G.F. DeVeau, "Low-Reflection Polish for Ferrule-Based Mechanical Splices and Straight-Tip Connectors", OFC Technical Digest, Paper THJ4, 1989.



Leslie A. Reith received a B.A. degree from New York University in 1975, the M.Phil. degree from the City University of New York in 1979, and the Ph.D. degree from The University of Texas at Austin in 1981, all in physics. In 1981 she joined AT&T Bell Laboratories as a Member of Technical Staff. In 1984 she subsequently joined Bellcore, where she is presently a member of the Fiber Distribution and Reliability Research group in Morristown, N.J. Her research at Bellcore currently includes reliability issues related to optical splices and connectors. She is an APS and IEEE member.

Richard Fagerstrom is a Member of Technical Staff at Bellcore in Red Bank, New Jersey. He works in the Reliability & Maintainability Methods group, where most of his time is devoted to developing mathematical reliability models at the device, system, and network levels. He holds a Ph.D. in statistics from Florida State University. Prior to his present position, he was Assistant Professor of Biomathematical Sciences at the Mount Sinai School of Medicine in New York.

Gabor Kiss was born in Budapest, Hungary. His parents emigrated during the Revolution of 1956, first to Canada, then to the USA in 1961. He earned an undergraduate degree in Polymer Science, Case Institute of Technology, Cleveland, Ohio (1974), and a PhD in Polymer Science, University of Massachusetts, Amherst MA (1978). His thesis work studied the flow properties of liquid crystals. He then completed a post-doctoral year in Strasbourg, France (1979). He later earned a Master's degree in Computer Science from NJIT, in night school, obtained in 1987. Prior to Bellcore, he was a Research Chemist at Celanese Corp. He is presently a Member of Technical Staff at Bellcore, specializing in optical splice and connector reliability.



Eva M. Vogel is a Member of Technical Staff in Metals and Glass Research Group at Bellcore, Red Bank, NJ. She is a graduate of the Slovak Technical University, Faculty of Chemical Engineering, Department of Physical Chemistry, Bratislava, Czechoslovakia. During her career at Bell Telephone Laboratories from 1970-1984, she was involved in many facets of materials research, including glass compositions for optical fibers, solid-state electrolytes, perovskite catalysts and new dispersants for ferrite processing. Her research at Bellcore since 1984 has focused on novel properties of electronic and optical materials. Vogel is internationally recognized for her research in the area of nonlinear optical properties of glasses. Currently she also is involved in reliability issues of optical components. Her work has resulted in 80 publications and four patents. Vogel is a Fellow of The American Ceramic Society and is Chair-elect of the Electronics Division of the ACerS.



William Wood is a Member of Technical Staff at Bellcore, Morristown, NJ. His current responsibilities include the analysis of fiber optic splices and connectors. Mr. Wood received a Bachelor of Science degree in Mechanical Engineering from Newark College of Engineering in 1955, and a Master of Science Degree in Engineering Mechanics from Columbia University in 1960. He joined Bell Telephone Laboratories in 1957 where he worked on the development of tools and equipment for use in the telephone system. He joined Bellcore in 1984.



Hakan H. Yuce is a member of technical staff in the "Fiber Distribution and Reliability Research" group at Bellcore. He leads a research program dealing with long-term mechanical reliability of optical fibers. Hakan provides technical input and support to organizations responsible for generic requirements and responds to clients' immediate needs related to consultation on reliability and field failures. He also plays a active role in the establishment of U.S. and international standards within TIA and IEC regarding optical fiber test procedures to assure reliability. Hakan has a B.S. degree in Mechanical Engineering from Technical University of Istanbul, an M.S. in Mechanical Engineering from M.I.T.and a Ph.D degree in Mechanical Engineering and Material Science from Stanford University.

Push-on Pull-off Multi-Fiber Connector

Y. Nomura Y. Kikuchi H. Hirao
Fujikura Ltd. Opto-Electronics Lab
Chiba, Japan

Abstract

We have successfully developed a push-on pull-off type connector for multi-fiber ribbons which can connect optical fiber cables quickly and reliably with a low insertion loss. This connector can easily and quickly connect one to eight fiber ribbon in a single motion.This connector is capable of easy and stable connection due to its housing structure which features an unique locking mechanism.

The physical contact between connectors is secured by projecting fibers from the end face of a ferrule by 1 μm thereby attaining low insertion losses and high reliability. The average insertion loss was 0.5 dB for single mode fibers which is low for multi fiber connectors. The connector also achieved return losses of as low as -50 dB through a custom diagonal polishing process.

We also developed a novel polishing method exclusively for this connector and succeeded in achieving a flatness of 1 μm or less and a polishing angle accuracy of ±0.1° or less.

We have conducted various performance tests and reliability tests on this connector and verified its consistency. The tests confirmed that the connector can be successfully used in the field.

1. Introduction

Optical fiber networks are expanding globally due to their superior performance and large information carrying capacity. The number of fibers in a single cable has been continuously increasing in response to the demand of subscribers for various services. This has led to the use of multi fiber ribbons which offer greater efficiency in connection.

Consequently, the time and skill required for connection jobs has increased tremendously[1]. In order to simplify this task, various connectors have been developed and have been reported[2] on previously. As part of these efforts, we have developed this novel push-on/ pull-off connector which can connect multi-fiber ribbons quickly and reliably and does not require any special operator skills or experience.

This connector has the following features which contribute to its superior performance :

1. Applicable to multi fiber ribbons
 It can easily connect multi fiber ribbons consisting of from one to eight fibers.
2. Low return loss
 Reflection is significantly reduced by polishing the end face of the ferrule diagonally. A return loss of -50 dB was obtained.
3. High stability
 By projecting fibers from the ferrule end face by 1 μm through the improved polishing method, the connector is able to achieve stable connection characteristics. The fluctuation in the insertion loss is ±0.3 dB or less.
4. High precision end face
 The polishing method for the ferrule end face was improved to achieve a flatness of 1 μm or less and a polishing angle precision of ±0.1°.
5. Reliable locking mechanism
 The locking mechanism are pawls which can be locked under a predetermined pressure. During connection, a constant pressure is maintained on the ferrule end faces to reduce effects of variations in environmental conditions such as temperature and vibration .
6. Improved performance
 The connector can connect multi fiber ribbons in a dry condition without the necessity of using index matching material for reducing reflection. The connector assembly operation is also made easier as compared to conventional connectors.

2. Structure

2.1 Connection Principle

As shown in Fig. 1, the connection principle lies in the structure obtained by polishing a multi-fiber ferrule end face diagonally so as to make the fiber tips protrude out. The fibers can therefore be connected directly resulting in a low return loss.

The effects of Fresnel reflection can be eliminated by polishing the end face at an angle of 8°. Since the fiber tips protrude from the ferrule end face, any fluctuation inthe return loss which may be caused by receding of the fibers can be minimized.

The connector can be connected in a dry state without the use of index matching material. This contributes to easy installation and subsequent reconnection.

Fibers are positioned by means of alignment holes and pins provided on the ferrules. At present, this method is being widely used for positioning multi-fiber connectors precisely and accurately.

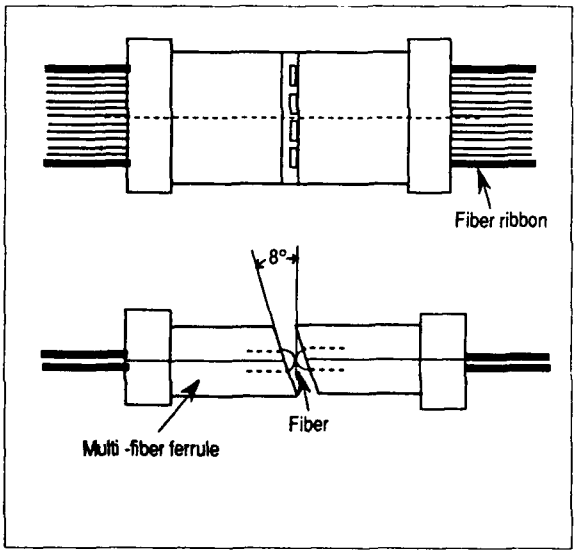


Fig. 1 Principle of Connection

2.2 Housing Structure

The housing is designed to to apply pressure on the ferrule from behind by means of a coil spring. It however allows the ferrule a certain degree of movement during insertion and extraction. This structure enables the ferrule end faces to be connected securely with a low insertion loss. As the end faces are constantly kept under a certain pressure by the spring, the connector is stable against environmental changes (especially changes in the temperature).

Ferrules are positioned by means of alignment holes and pins on the ferrules. An alignment pin is fixed on one of the housings via a pin clamp. The pin clamp is of a ring spring type with a slit which allows the pins to be easily fitted or pulled out upon application of a predetermined pressure.

The housing is structured such that the locking pawls are force fitted with the pawls of an adaptor when the housing is inserted into an outer case. Connectors can be efficiently engaged with one another without errors because their pawls are fit together with a predetermined outer pressure unlike the conventional method where pawls are locked merely with their elasticity. When disconnecting, connectors can easily and automatically be detached by the pressure of the spring by simply pulling the outer case.

Fig. 2 shows an assembled connector with its adaptor.

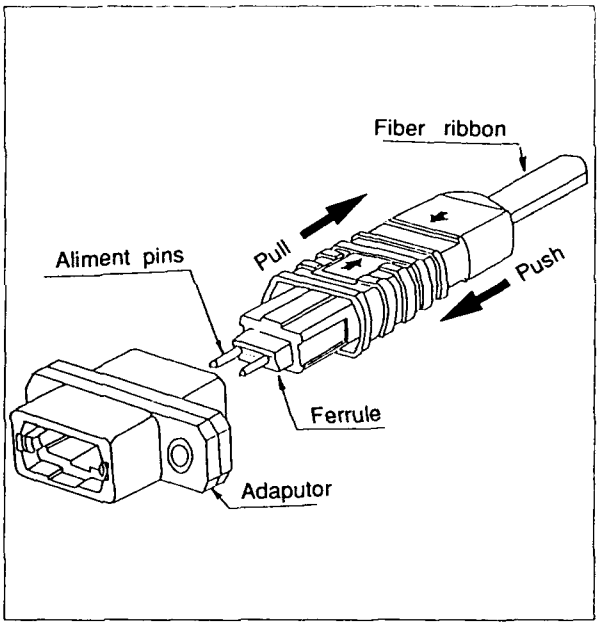


Fig. 2 Structure of Connector

2.3 Ferrule end face

As ferrule end faces are abutted against each other, they must have a high degree of flatness and angular precision. In order to minimize fluctuation in insertion loss caused by attachment/detachment as well as environmental factors, the fibers should be abutted too. It is known that the insertion loss increases due to Fresnel reflection as the adhesive applied between ferrules contracts at high temperatures leading to fibers being pulled back to widen the interstice between the

end faces of a ferrule.

To eliminate this, we developed a novel polishing technique to make the fibers project from the ferrule end face by 1 μm. A new high precision polishing machine was developed and is capable of achieving an end face flatness of 1 μm with an angular precision of 0.1°. A typical value of the end face angle accuracy is given in Table 1.

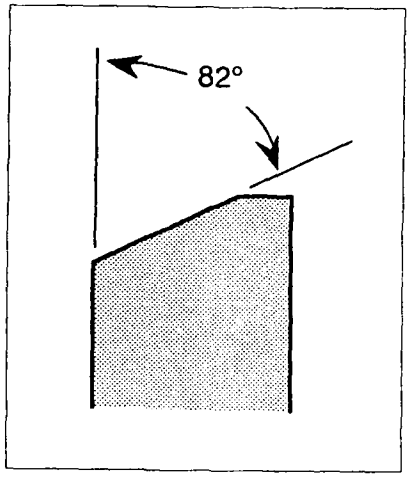


Fig. 3 End Face Angle

Item	Precision
Diagonal polishing	0.07°

Table 1 Angular Precision

3. Optical Characteristics

The optical characteristics of the connector were verified. The results are shown below.

3.1 Insertion Loss

The insertion loss was measured when the connector was connected to a master connector. As is illustrated in the histogram shown in Fig. 4, the insertion loss averaged 0.5 dB for an eight fiber ribbon connector.

Fig. 5 shows the results of the repeatability measurement test. The insertion loss was measured after repeatedly attaching and detaching a connector five times.

Based on these tests, we have verified that the connector has stable connection characteristics and has a low insertion loss for a multi-fiber connector.

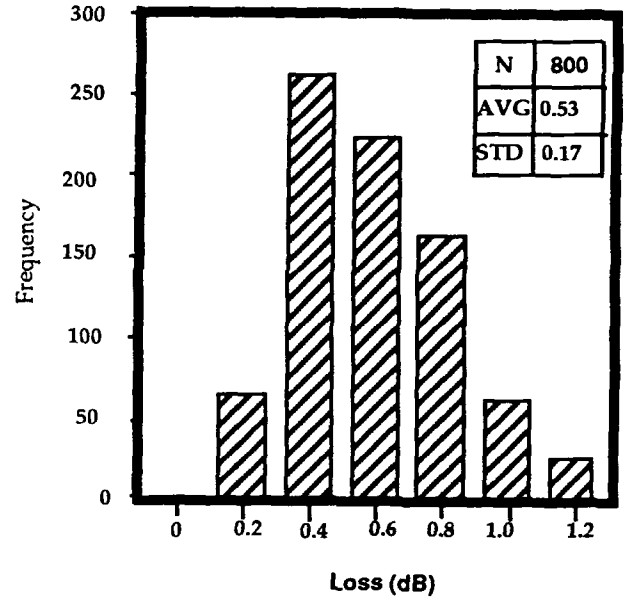


Fig. 4 Insertion Loss

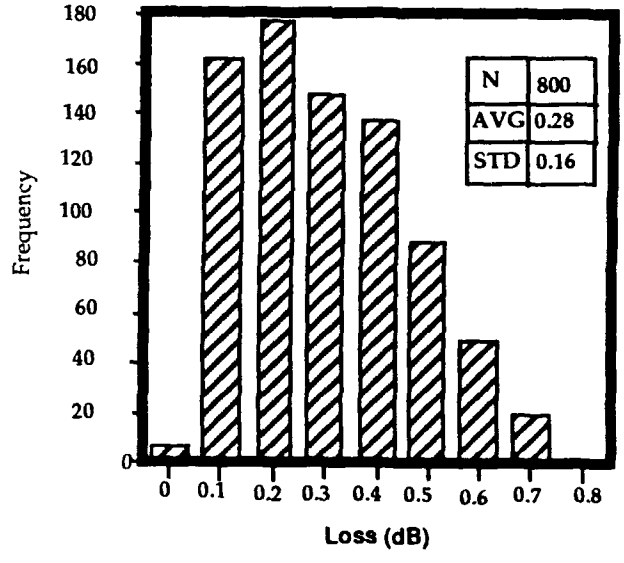


Fig. 5 Insertion Loss Repeatability

3.2 Return Loss

The return loss was measured with the connector mated with a master connector. The histogram of the results of the test is given in Fig. 6. The return loss was as low as -50 dB or less for the case of a 8-fiber ribbon connector.

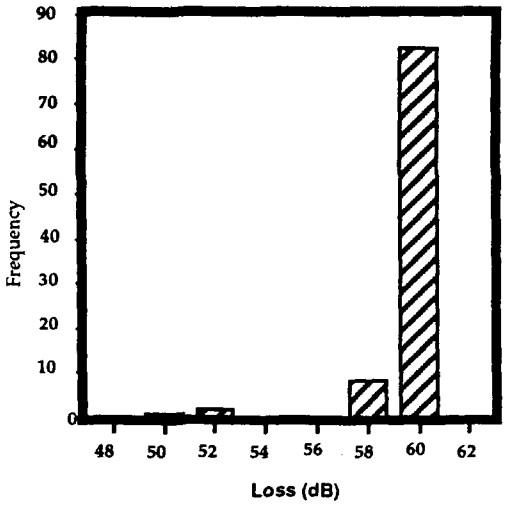


Fig. 6 Return Loss

4. Reliability

In order to ascertain the field worthiness of the connector, various reliability tests including those for mechanical characteristics and resistance to environmental factors were conducted. The results of these tests are elaborated below.

4.1 Heat Cycle characteristics

The insertion loss fluctuation of the connector was measured by repeating a 4 hour cycle of -20°C to 70°C ten times. This cycle is shown in Fig. 7. The results of the measurement is shown in Fig. 8. The loss fluctuation was within ±0.1 dB.

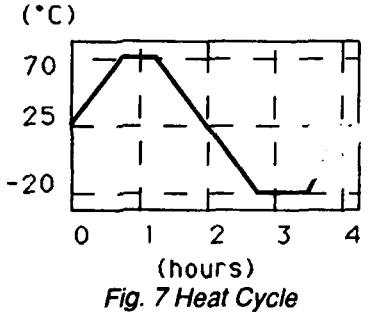


Fig. 7 Heat Cycle

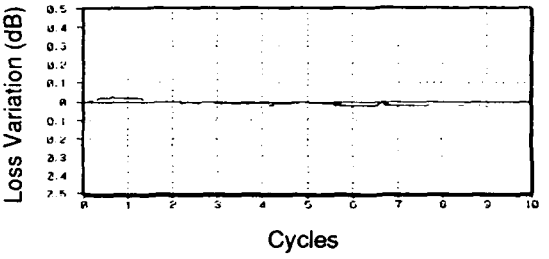


Fig. 8 Heat Cycle Test Results

4.2 High Temperature Characteristics

The insertion loss fluctuation was measured at a high temperature in a constant temperature test apparatus in the laboratory where the connector was connected via an adaptor. The test was conducted continuously for 100 hours at 70°C. The results of are shown in Fig. 9. The loss fluctuation was within ±0.1 dB.

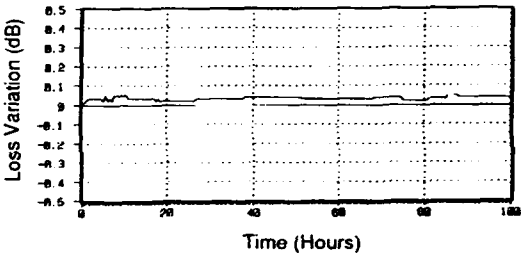


Fig. 9 High Temperature Fluctuation

4.3 Low Temperature characteristics

The above test was repeated for a temperature of -20 °C. The results of the test can be found in Fig. 10. Once again the loss fluctuation was within ±0.1 dB.

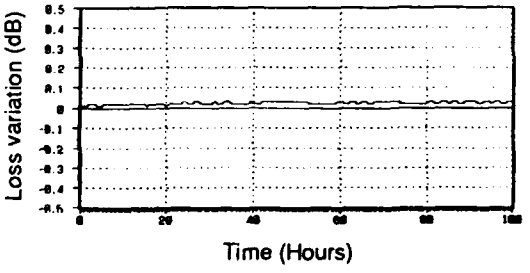


Fig. 10 Low Temperature Fluctuation

4.4 Vibration Test

To evaluate the mechanical stability of the connector, a vibration test was conducted under the conditions listed below. The insertion loss of the connector which was connected via an adaptor was measured continuously.

Frequency	: 10 - 55 Hz
Amplitude	: 1.5 mm
Direction	: All axes
Duration	: 2 hours per axis

Fig. 12 shows that the fluctuation was within a small range of 0.05 dB.

5. Conclusions

This push-on/pull-off connector has demonstrated through various tests a high reliability and characteristics which suitable for use in challenging field environments. This connector is expected to be implemented widely in optical fiber networks in the future.

References

[1] L. Resnick, *Connector suppliers set sights on rapid installation,* Laser Focus World, p149-156, Aug 1990.

[2] S. Nagasawa et al., *A Single Mode Multi-Fiber Push-OnType Connector with Low Insertion and High Return Loss* , IOOC-ECOC'91 Paper MoB1-7, Paris, France Sep 1991.



Yoshikazu Nomura
FUJIKURA LTD.
Opto-Electronics Lab.
1440 Mutsuzaki
Sakura City, Chiba
Japan

Yoshikazu Nomura was born in 1951. He graduated in mechanical engineering from Shinshu University. He has been engaged in the research and development of telecommunication cables and accessories.
He is presently a manager in the Fiber and Cable Accessory Department.



Yoshio Kikuchi
FUJIKURA LTD.
Opto-Electronics Lab.
1440 Mutsuzaki
Sakura City, Chiba
Japan

Yoshio Kikuchi was born in 1955. He joined Fujikura after his graduation from Tohoku University with a M.E. degree in 1980.
Since then, he has been involved in the research and development of optical fibers, cables and accessories.
He is now an assistant manager in the Fiber and Cable Accessory Section. Mr. Kikuchi is a member of the IEICE of Japan.



Hideo Hirao
FUJIKURA LTD.
Opto-Electronics Lab.
1440 Mutsuzaki
Sakura City, Chiba
Japan

Hideo Hirao was born in 1951. He received the B.E.M. degree in agricultural mechanical engineering from Mie University in 1974.
He subsequently joined Fujikura and has been engaged in the research and development of telecommunication cables and accessories.
He is presently a manager in the Fiber and Cable Accessory Department.

Development of High-density Extensible Mechanical Switching System

TAKEO KOMIYA, SHUNICHI MIZUNO, TOMOMI SANO,
KAZUMASA OZAWA, KEIJI OSAKA, YASUO ASANO

Sumitomo Electric Industries Ltd.
1,Taya-cho,Sakae-ku,Yokohama,Japan

ABSTRACT

A 8X2000 mechanical matrix switch composed of 250 8-Singlemode fiber connectors was developed. A master head with one 8-fiber connector moves along three orthogonal axes by DC servo motors and optical encoders under 16-bit CPU control and joins 250 access connectors which are arranged 10 x 25 matrix. By employing compliant master head mechanism, an extensible optical matrix switch with high performance was realized. The average connection loss of 0.35dB and the repeatability less than 0.1dB were obtained through 10000 time repeated connections.

1. INTRODUCTION

In subscriber networks, it is very important to economically and effectively perform optical measurement, where a high-count cable is used. Such a high-count cable will be a ribbon-fiber based one and a multiple connector will be used. To reduce the size of the switch and the number of connecting point, directly switching multiple connector is a promising choice. It will be one of the major requirement that after the initial installation, a newly laid cable connectors can be added to the matrix switch on the site in response to the demand. Therefore the demands for the flexible and extensible optical matrix switching system with high performance will increase very much.

2.SYSTEM CONFIGURATION

For the purpose of choosing one optical fiber among high-count cable, combining 1xN type switch and NxM type switch is a practical solution.(Fig.1)

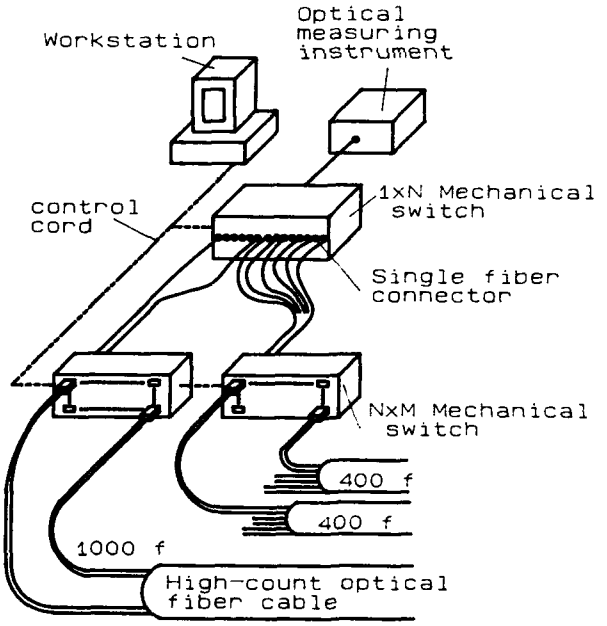


Fig.1 Typical configuration of Flexible switching system

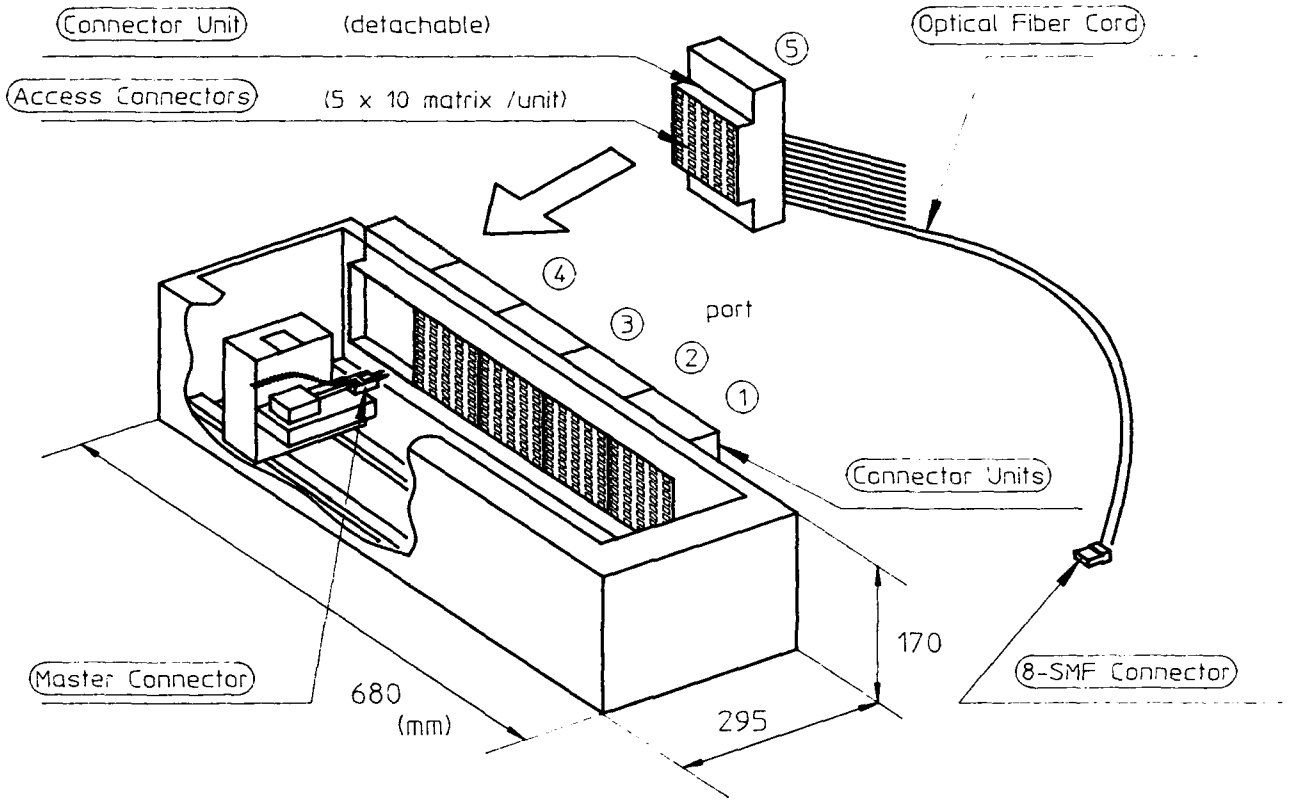


Fig.2 The structure of the matrix switch

3.DESIGN OF THE MATRIX SWITCH

3.1 Structure of matrix switch

Fig.2 shows the structure of the matrix switch. The dimension of this switch is 680(W) x 295(L) x 170(H) mm^3. It is composed of 251 8-SM fiber connectors. One master connector is placed on the master head and the other 250 access connectors are fixed on 5 separate connector units opposite to the master connector.

The master connector moves along three orthogonal axes by DC servo motors and ball screws and joins against one of the access connectors by the command from the workstation. It takes about 10 seconds to change from the left end access connector to the right end access connector. The positioning accuracy is within 5 μ m along each axes.

The master connector fibers and access connector fibers are protected by PVC jacketing.

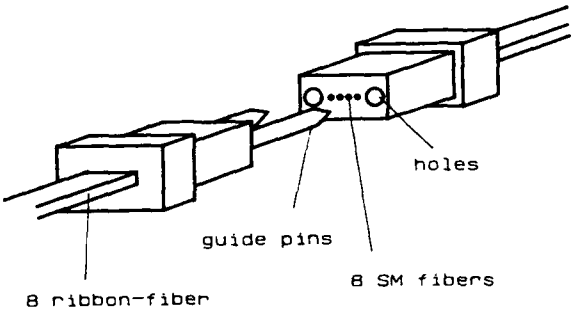


Fig.3 The structure of 8 SM-fiber connector

3.2 Floating arm

This switch uses a transfer molded square shaped connector into which the eight single-mode fibers with 10 μ m core and 125 μ m cladding diameter are positioned. This connector has two holes beside the fiber holes and connects together by the aid of guide pins, as shown Fig.3 .The size of the hole is 0.7mm and the diameter of the guide pin is 0.7mm.The end of the pin is sharp.It is physically possible to insert the guide pin into the hole when their axes offset is as large as 0.3mm, however the connector loss is very high. Therefore two mating connectors should be aligned within 10um accuracy.

In order to realize an optical matrix switch with high performance, there were two problems. One is to prevent the connectors from the external force.The force may raise the connecting loss or shorten the lifetime of the connectors. The other is the precise initial positioning of the master connector for jointing the master to one of the access connectors situated on some 100mm square plane.

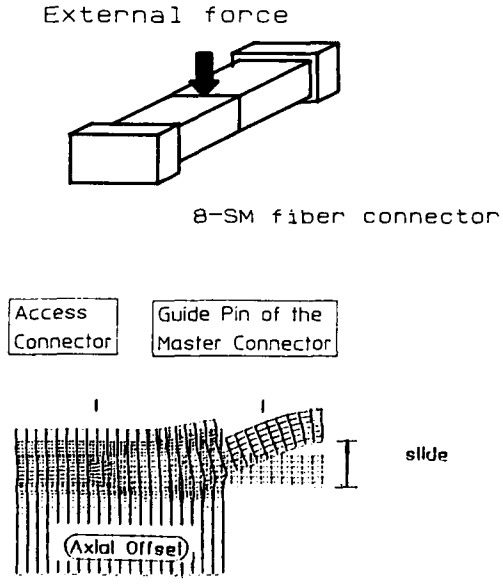


Fig. 4 The example of the finite element method

To solve both problems, the highly compliant floating arm has been developed after FEM analysis .(Fig.4)

Fig.5 shows the relations of the external force and change of the connecting loss and the comparison between calculation and the experiment is made.Both results are slightly different ,however it was expected that external force less than 25gram would not cause a significant loss increase.

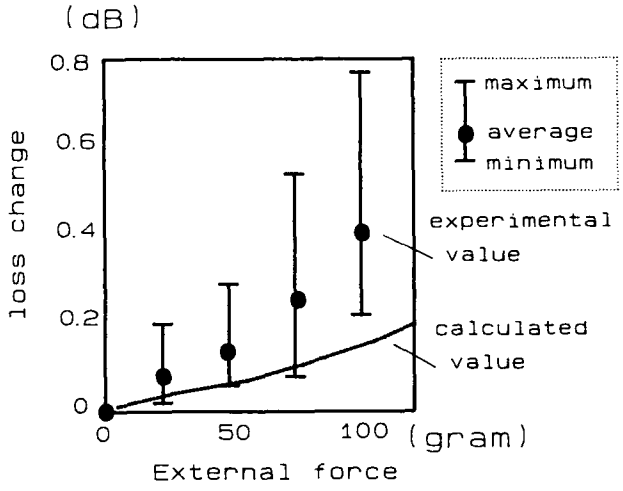


Fig. 5 Results of the external force and loss change

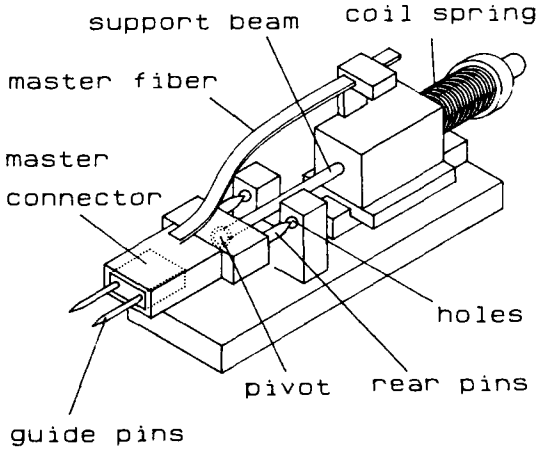
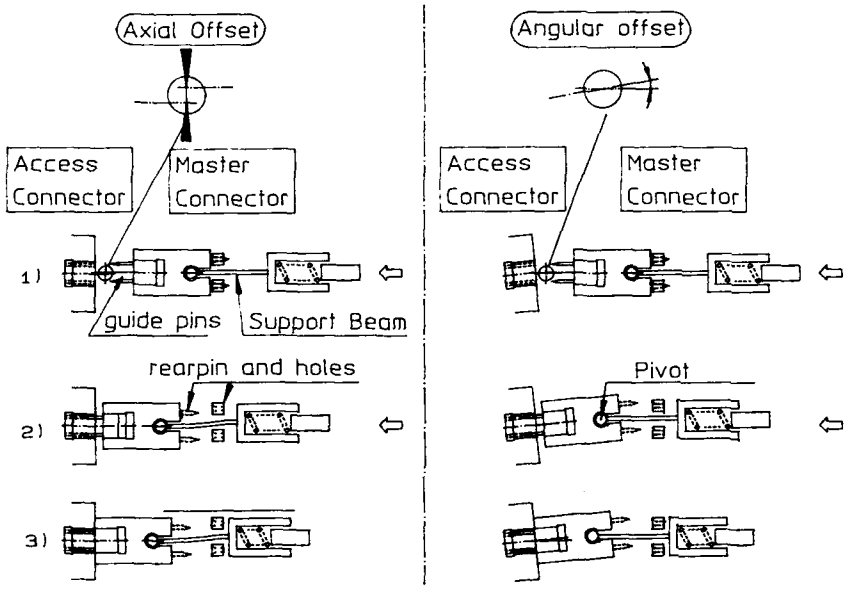


Fig. 6 The structure of the floating arm

Fig.6 and Fig.7 show the structure ,and the mechanism of the floating arm. The axial and angular offset of position are allowed by the bend of the supporting beam or the small rotation of the head.
The initial position of the master connector is kept precisely at the center by the stiffness of the beam and the combination between the rear pin and the hole.

Fig.8 indicates connecting loss dependence on the offset in case of 8-fiber connector. The result shows that the arm has wide-ranged compliance against axial and angular offset.



1) Initial position

2) The guide pins of the master connector are inserted in the holes of the access connectors

The axial offset is mainly allowed by the bend of the support beam. The angular offset is mainly allowed by the small rotation of the beam.

3)The master connector and the access connecter are joined. The coil spring give the suitable force to the master connectors to attain stable connection.

Fig.7 The mechanism of the floating arm

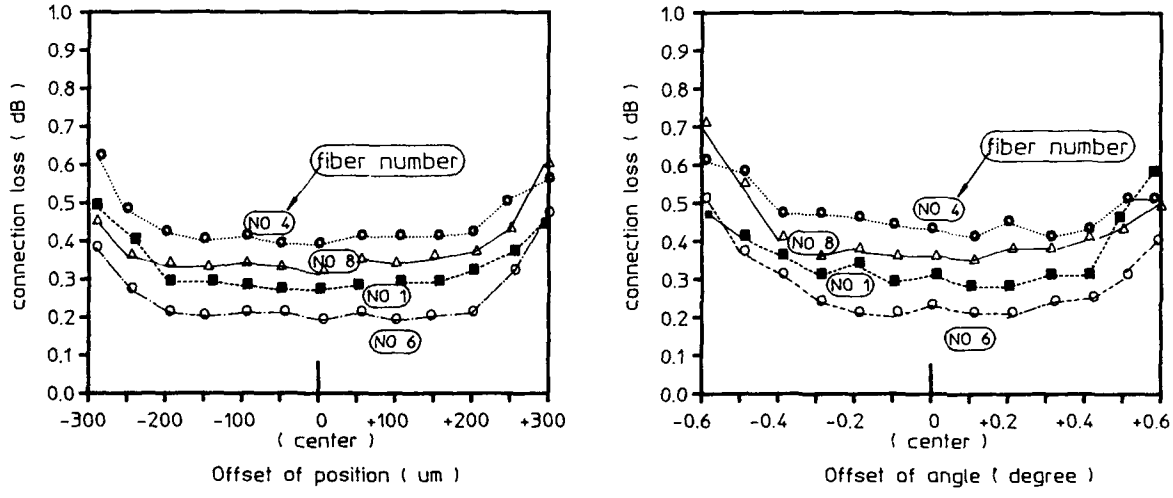


Fig.8 Loss dependence on axial and angular offset

3.3 Connector unit

This switch has 5 ports on one side. At the maximum 5 access connector units each of which is composed of a plate and 50 multi-fiber connectors can be attachecd to the ports. These connectors are arrayed as 5x10 matrix. This unit is roughly positioned in the switch in accordance with the combination between the pin and the groove as shown Fig.9. The number of connector unit is chosen on the customer's request.

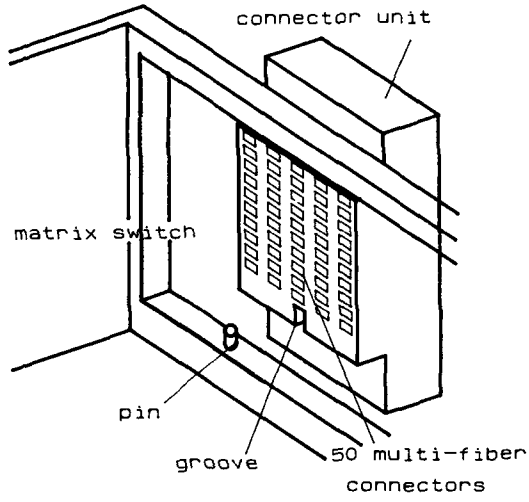


Fig.9 The structure of the connector unit

4. PERFORMANCE

2000 connecting losses of one optical matrix switch were measured using 1.31 μ m LED as a light source. Histogram of connecting losses of 250 MT-8 SM connectors(total 2000 fibers) are shown in Fig 10. The average loss was 0.35dB in case of 8-SMfiber connectors.Fig.11 shows the connecting loss change of one fiber during 10000 times repeated connections. The variaton was less than 0.1dB.

The return losses of the matrix switch were measured at 1.3 μ m and were found greater than 35dB.

Table 1 shows the results of the movement of the same connector unit to each port. No sigimificiant dependence on the port was found. Thereby the connector unit was proved to be added easily.

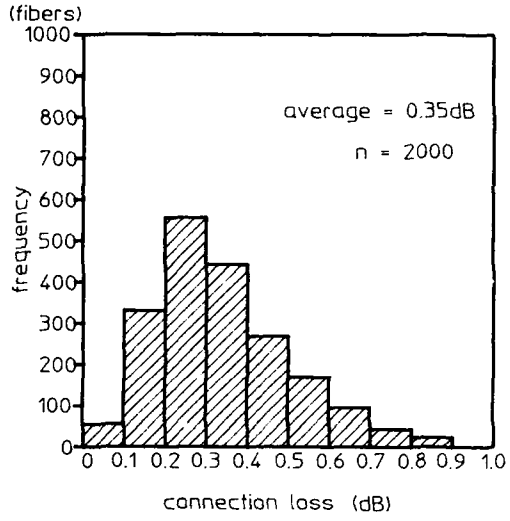


Fig. 10 Histogram of connecting loss

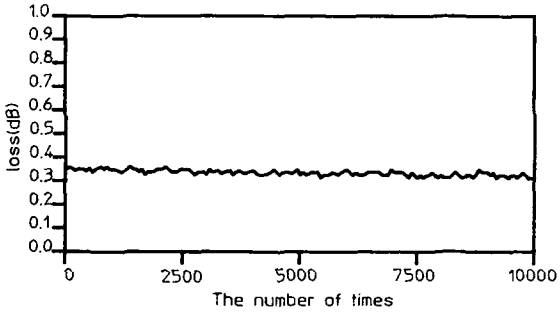


Fig. 11 Repeatability test

Table 1 The connectingloss dependence on the port No of the matrix switch

Port No.	Average loss
1	0.34 dB
2	0.32 dB
3	0.33 dB
4	0.34 dB
5	0.33 dB

Various kinds of mechanical and enviromental tests were carried out and the variations in connecting loss were measured. The vibrations test was carried out at the frequency of 10Hz ~ 40Hz sweep and the amplitude of 0.5mm for 1 hour, and the fluctuation in connecting loss before and after the test was within 0.1dB.
Fig.12 shows the results of heat cycling test, from which connecting loss change was within 0.1dB over temperature range of 0°C to 40°C. The results concerning other test items are summerized in Table 2. Results of these testing demonstrate that newly developed matrix switch exibits stable connection performance.

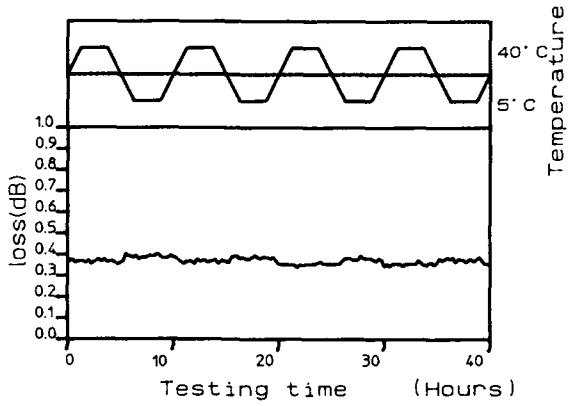


Fig. 12 Temperature cycling test

Table 2 Performance of the matrix switch

Testing item	Condition	Result
Average loss	1.31umLED	0.35dB
Return loss	1.31umLD	More than 35dB
Repeatability	10000 times	Within 0.1dB
Heat cycling	From 5° C to 40° C 100hrs	Within 0.2dB
Humidity	40° C ,80%RH 100hrs	Within 0.1dB
Vibration	10Hz-40Hz sweep 0.5mm 1hr	Within 0.1dB
Tensile strength	5Kg,10 min for fiber cord	Within 0.1dB

5. CONCLUSION

8X2000 mechanical matrix switch for the use in optical communication networks have been developped. They are composed of one 8-fiber multiple connector and 250 access connectors. By the aid of compliant master head mechanism and the precise positioning controller,the matrix switch was proved to connect one of 250 connectors quite easily.

The average connection loss of matrix switch is 0.35dB. A series of mechanical and environmental tests were conducted to prove the long-term stability and reliability of the matrix switch.
The matrix switch is expected to be practically used in optical subscriber networks and to play a role in reducing the testing time of the optical fiber cables or networks.



Takeo Komiya

Sumitomo Electric
Industries.Ltd

1,Taya-cho,Sakae-ku
Yokohama,Japan

akeo komiya recieved his B.S. degree in precision mechanical engineering from Tokyo university in 1986. He jointed Sumitomo Electric Industries the same year and has been engaged in research and development of optical fiber jointing and switching technologies. He is a member of Optomechatronics System R&D Dept Yokohama Reserch Labo.,and a member of Electronics, Information and Communication Engineering of Japan.



Shunichi Mizuno

Sumitomo Electric
Industries.Ltd

1,Taya-cho,Sakae-ku
Yokohama,Japan

Shunichi Mizuno recieved his M.S. degree in mechanical engineering from Tokyo Institute of Technology in 1985. He jointed Sumitomo Electric Industries the same year and has been engaged in research and development of optomechanical matrix switch.He is a member of Electronics, Information and Communication Engineering of Japan.



Tomomi Sano

Sumitomo Electric
Industries.Ltd

1,Taya-cho,Sakae-ku
Yokohama,Japan

Tomomi Sanoa recieved his M.S. degree in electric engineering from Tokai University in 1990. He jointed Sumitomo Electric Industries the same year and has been engaged in research and development of optical fiber jointing and switching technologies.He is a member of Optomechatronics System R&D Dept. Yokohama Reserch Labo.,and a member of Applied Physics.



Kazumasa Ozawa

Sumitomo Electric
Industries.Ltd

1,Taya-cho,Sakae-ku
Yokohama,Japan

Kazumasa Ozawa recieved his M.S. degree in chemical engineering from Tokyo university in 1989. He jointed Sumitomo Electric Industries the same year and has been engaged in research and development of optical fiber mesuring technologies. He is a member of Optomechatronics System R&D Dept.Yokohama Reserch Labo.,and a member of Electronics, Information and Communication Engineering of Japan.



Keiji Osaka

Sumitomo Electric
Industries.Ltd

1,Taya-cho,Sakae-ku
Yokohama,Japan

Keiji Osaka recieved his M.S. degree in precision mechanical engineering from Kyoto university in 1981. He jointed Sumitomo Electric Industries the same year and has been engaged in research and development of fusion splicing technologies and optical switching system. He is a member of Optomechatronics System R&D Dept.Yokohama Reserch Labo.,and a member of Electronics and Information and Communication Engineering of Japan.



Yasuo Asano

Sumitomo Electric
Industries.Ltd

1,Taya-cho,Sakae-ku
Yokohama,Japan

Yasuo Asano recieved his B.S. degree in mechanical engineering from Waseda university in 1968. He jointed Sumitomo Electric Industries in 1971 and has been engaged in research and development of fjointing technologies for coaxial cables and optical fiber cables. He is now a manager of Optomechatronics System R&D Dept. Yokohama Reserch Labo.,and a member of Japan Society of Mechanical Engineers and The Institute of Electronics, Information and Communication Engineering of Japan.

Mechanical-Type Optical Switch For DSF

Koji Yoshida Toshihiko Ohta Hiroyoshi Sueki
Hiroyuki Yamada Takashi Shigematsu Takahide Kimura

The Furukawa Electric CO., LTD.

Abstract

According to the optical fiber telecommunication networks, many new optical components are required. Particularly the optical switch is one of the key components in the optical fiber networks. We have already developed, under the guidance of NTT, mechanically transferable connector (MT connector) that is a high-performance plastic connector for single mode multi-fiber. The optical switch development has been progressed utilizing this high precision plastic molding technology. As the result, we have been developing a new connector transfer type optical switch that is a new pin-referenced indirect slide type optical switch.

This paper presents a structure of a newly developed 2x2 mechanical switch and its initial characteristics and the results of reliability evaluation tests with 1.55um dispersion-shifted fibers (DSF).

1. Introduction

With the ISDN era approaching, the function of optical fiber communication systems has become more diversified. And the application has extended to locally specialized networks such as local area networks and intelligent buildings, centering on subscriber networks. In such a wide application, the importance of operation systems that efficiently conduct operations and maintenance of huge networks, with an aim of better service, has been pointed out by many fields. The systems aiming at supervising and switching of optical fiber networks have already been in practical use and their running has already started. Optical switches would be required to change active lines into spare (inactive) lines at the time of malfunction of devices or relocation works of lines. They are vital parts for the systems and are required the following properties.

(1) Low insertion loss
(2) High-speed switching
(3) Good switching repeatability
(4) Long-term stability
(5) Compact size and low cost

Currently, although various kinds of optical switches are being proposed, mechanical ones have been generally using in the practical use. Among them, connector transfer type switches have become a mainstream of optical switches, because they do not require expensive optical devices and they can possess low loss characteristics.

2. Connector Transfer Type Optical Switch

Generally, the pin-referenced direct slide type is proposed as a switching mechanism of connector transfer type optical switch, by taking advantage of reference pins. Reference pins are fixed in the connector (switching ferrule) as switching operation and these pins are pressed against the side of positioning holes that are formed in the connector. Fig.1 shows the operating principle of pin-referenced direct slide type optical switch. This optical switch consists of reference pins for positioning reference,

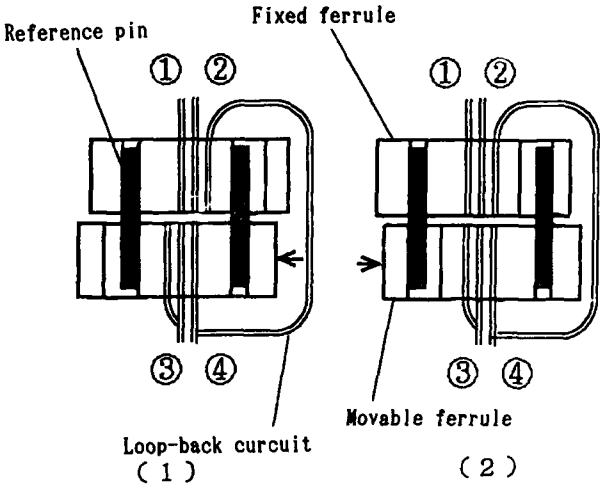


Fig.1 Mechanism of 2×2 pin-referenced direct slide optical switch

movable ferrule and fixed ferrule. These ferrules are same shaped connectors with reference pins for positioning reference. In each ferrule, long slide holes are formed that are as long as a moving stroke. Such a device as solenoid is used for switching operation. By applying force directly to the side of the movable ferrule by solenoid, the ferrule moves along fiber array to conduct switching operation. During that process, an optical route 2-4 switches to 2-3 and another route 1-3 switches to 1-4 by making light pass through a loop-back route. Still, the force should be constantly added to maintain the state in case of pin-referenced direct slide type optical connector even after the switching operation is completed. Fig. 2 shows structure of switching ferrule for this switch. Many such V-grooved type ferrules are made of a hard and brittle material as ceramic. However, its processing is costly because V-grooves must be processed with high accuracy. And the fiber assembly process has a weak point as requiring high skill of trained personal.

In case that a switching ferrule is made of plastic, with an aim to improve productivity, this switch has a problem in its long-term reliability. Because, positioning holes in plastic ferrule are apt to creep deformation. Consequently, We developed a pin-referenced indirect slide type optical switch, a new switching type, to solve such a problem.

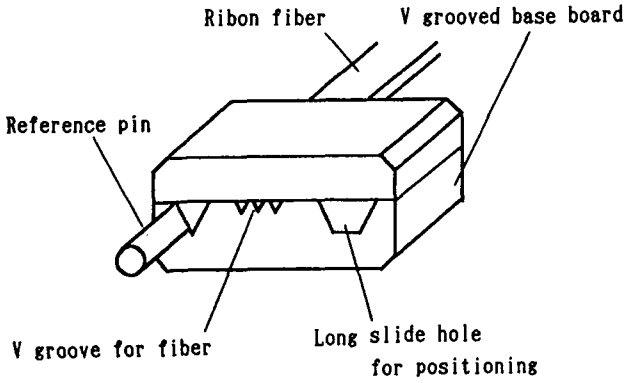


Fig.2 Structure of ferrule for pin-refernced direct slide optical switch

3. Structure of Pin-Referenced Indirect Slide Type Optical Switch and Its Mechanism

3-1 Principle of Mechanism

Fig. 3 shows a principle of mechanism of pin-referenced indirect slide type optical switch. This optical switch is

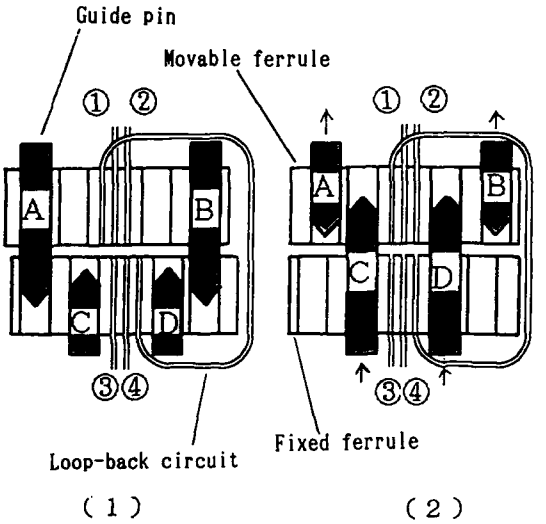


Fig.3 Mechanism of 2×2 pin-refernced indirect slide optical switch

predominantly featured by transfer systems for switching ferrules. Above pin-referenced direct slide type optical switch can be given switching operation by adding direct driving force to the side of switching ferrule. But pin-referenced indirect slide type switch can be done the operation by simultaneously four guide pins moving in and out in unilateral direction that is vertical to the fiber array. Exactly, it is designed to convert the insertion force of guide pins into the sliding force of switching ferrules horizontally by taking advantage of the angle of the edges of the guide pins. Under the condition shown in Fig. 3(1), two guide pins at the outside (A and B) insert into the ferrule's holes and ferrule's positioning is completed. Then optical route is the connecting condition of 1-3 and 2-4. During the process inner guide pins (C and D) are moved out from the other ferrule.

Switching operation is performed by a bistable solenoid. Guide pins, A, B, C and D, move simultaneously to the same direction that is vertical to fiber array. As shown in Fig. 3(2), ferrule positioning is set by guide pins, C and D, enabling the optical routes to change to 1-4 and 2-3. As it also shown in Fig. 3, this type optical ferrule does not need an external force for positioning. Constantly external force is not add to the switching ferrule, so it can reduce the occurrence of creep phenomenon on it.

3-2 Structure of Switching Ferrules

Fig. 4 shows structure of a switching ferrule for a pin-referenced indirect slide type optical switch. The switching ferrule is entirely made of plastics and is similar to MT connector structure. The difference is another couple of guide pin holes formed at the outside of positioning holes.

The structure of a switching ferrule is designed as follows. Reference pin holes at the outside are equal distant (L1) from fiber 1 as the standard point. And the other holes at the inside are deviated the half fiber pitch horizontally (L3). This structure allows a stroke of one pitch to be secured, when two same shaped ferrules fit each other.

Above ferrule's design makes it possible to reduce to effect on the insertion loss characteristics caused by misalignment of the holes. Because using ferrules that are made by the same die, the deviations of the position misalignment of holes are equal when those ferrules fit each other.

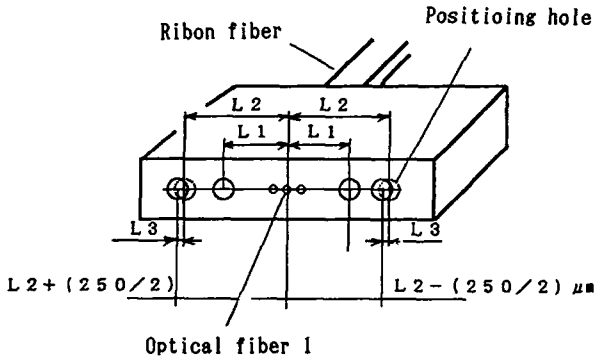


Fig.4 Structure of ferrule for pin-referenced indirect slide optical switch

3-3 Entire Configuration

Fig. 5 shows the structure of a pin-referenced indirect slide type optical switch. One of the switching ferrules is installed to the switch body. And it is pressed against an opposite ferrule (movable side) by means of spring. Four guide pins for both outside and inside holes are jointed through a bracket to an axle of a bistable solenoid. This structure enables four guide pins to be transfer simultaneously. And these switching ferrules are dipped in reflective index matching oil to prevent the reflection of their edge.

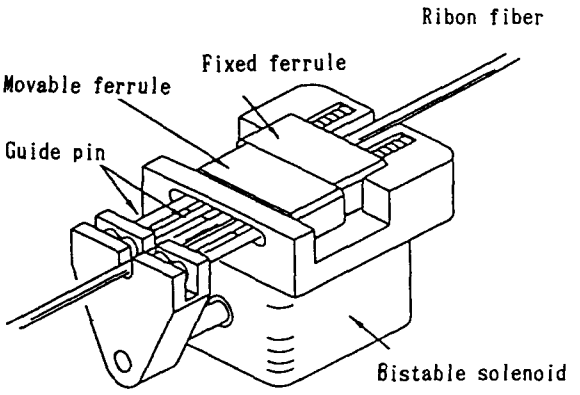


Fig.5 Structure of 2×2 pin-refernced indirect slide optical switch

4. Initial Characteristics

4-1 Insertion Loss Characteristic

Fig. 6 shows the result of insertion loss measurement assembled with DSF. Data are maximum values of insertion loss when the switch was operated repeatedly 20 times. We obtained good insertion loss, with 0.27dB in average and standard deviation of 0.26dB.

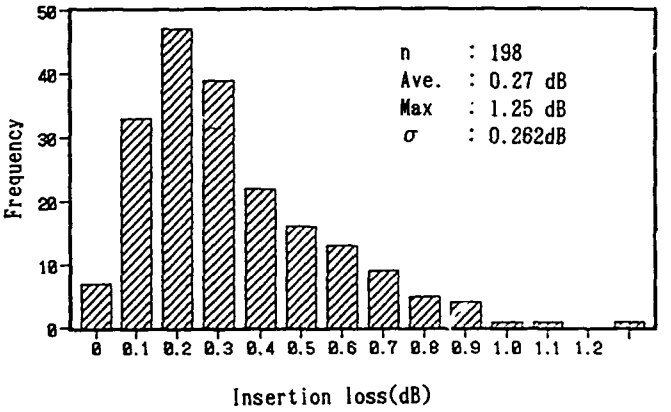


Fig.6 Initial Insertion Loss of 2×2 pin-referenced indirect slide optical switch

4-2. Switching Time

Fig. 7 shows wave-form data when the switch operated. As it is shown in the graph, one of features of this switch is very short optical transfer time (t1) that is below 1ms. Fig. 8 shows the histogram of switching time (t2) from the input of a trigger signal to the completion of switching. This switch has a very high

speed switching characteristic. The switching time averaged 7.0ms with its maximum value of 8.3ms, and its standard deviation was 0.40ms.

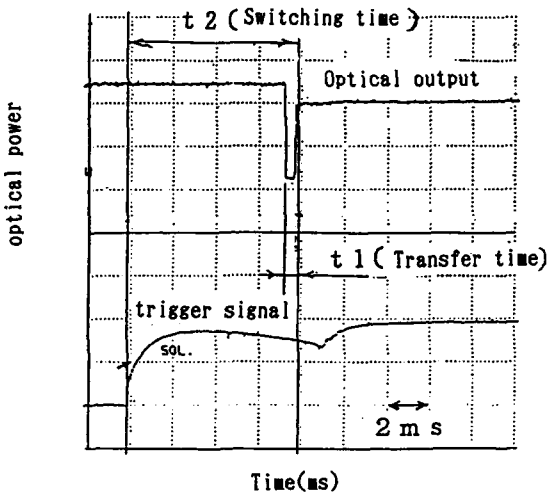


Fig.7 Switching wave form of pin-referenced indirect slide optical switch

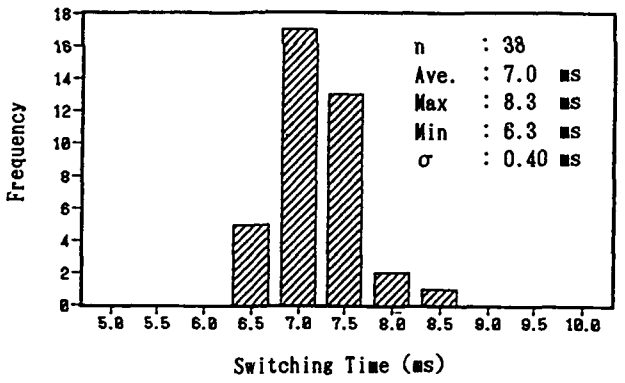


Fig.8 Histogram of Switching Time

4-3 Value of Back Reflection

Fig. 9 shows the results of back refection measurement. Good back reflection characteristic was obtained, with the average of reflective attenuation of 51.1dB and minimum value of 42dB.

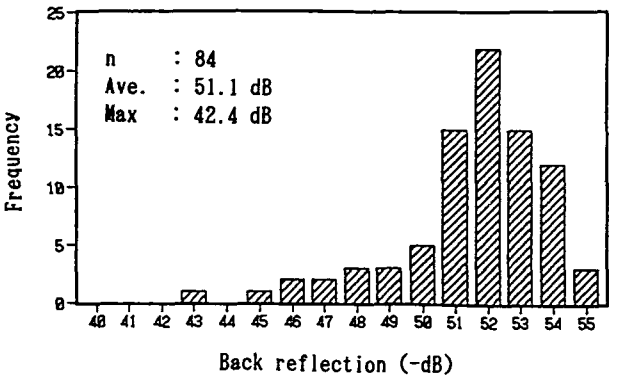


Fig.9 Histogram of value of back reflection

5. Result of Reliability Evaluation

The reliability evaluation of the switch was made in series. It is a very critical condition. The number of test samples is 8. Table 1 shows the evaluated items, test condition and evaluated results.

Tablel Result of reliability evaluation test

Evaluated Items	Test Condition	Result
Heat cycle	-10～+60℃ 10cycle	loss variation ≦0.1dB
Low temparature	-10℃×2hr	loss variation ≦0.1dB
	-10℃ 100 times switching	switching time ≦10ms
High temparature	60℃×2hr	loss variation ≦0.1dB
	60℃ 100 times switching	switching time ≦10ms
Humidity test	60℃,90%RH 100hr	loss variation ≦0.1dB
Vibration test	10～55～10Hz/2min p.p 1.5mm 6dir×2hr	loss variation ≦0.1dB
Impact test	100G 6dir×2hr	loss variation ≦0.1dB
Repeated switching (500times)	continuous switching of 500 times repetition at R.Temp	loss variation ≦0.1dB
		switching time ≦10ms

5-1 Switching Repeatability

Fig. 10 shows a variation in switching time under various surrounding conditions. No significant change was observed in switching time, regardless of the change of the surrounding condition. The switching time was less than 10ms under every condition. No malfunction was also observed after switching operation of more than 1000 times in total. Among the results of switching repeatability test, Fig. 11 shows the result of switching repeatability at 500 times repeated switching test. The fluctuation in the switching time was in the range of maximum 0.33ms, which shown good result.

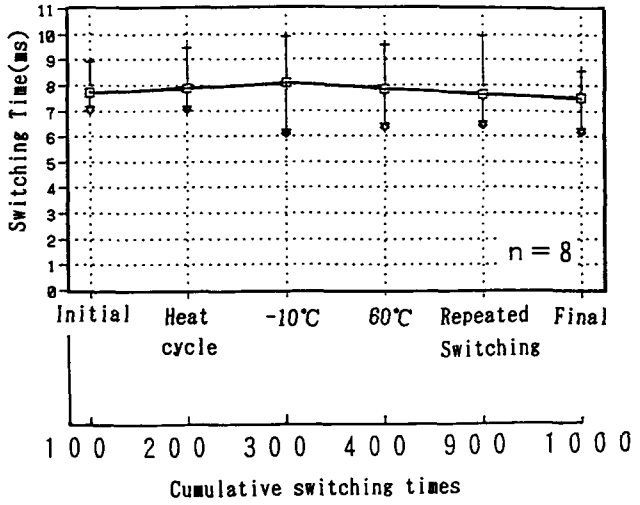


Fig.10 Change in switching time under various surrounding condition

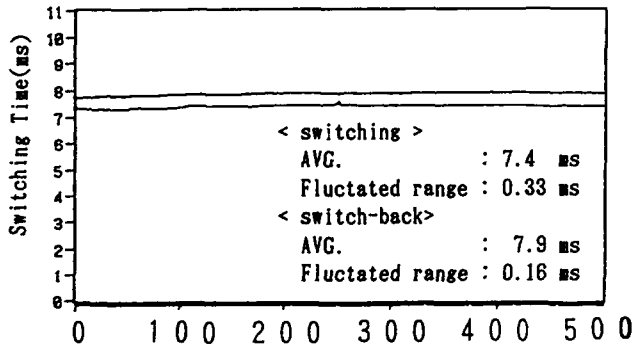


Fig.11 Repeatability of switching time at 500 times repeated switching test

5-2 Repeatability of Insertion Loss

Fig. 12 shows repeatability of the insertion loss at 500 times repeated switching test. The variation in the insertion loss was in the range of maximum 0.4dB, showing good repeatability. Fig. 13 shows the variation in the insertion loss during heat cycle test. Slight dependency can be observed with temperature changes, but the variation was in the range of maximum 0.09dB, a good result.

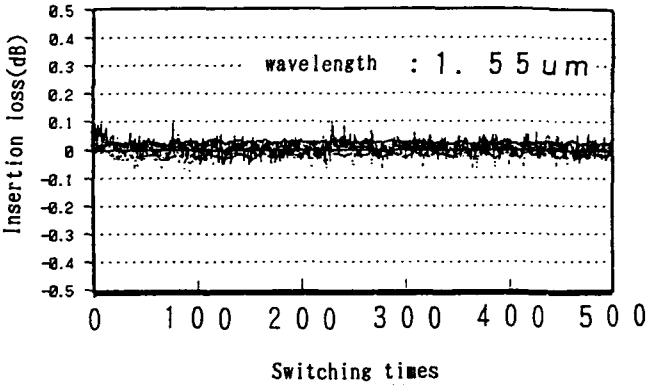


Fig.12 Repeatability of insertion loss at 500 times repeated switching test

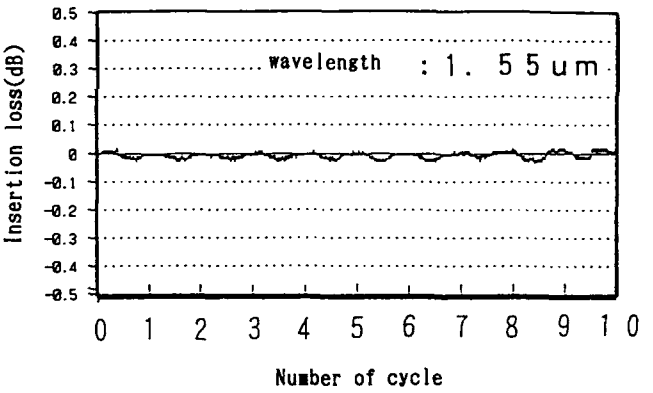


Fig.13 Repeatability of insertion loss during heat cycle

6. Conclusion

Application of both the high-precision plastics molding technology and a new concept as a pin-referenced indirect slide type made it possible to develop a highly productive optical switch. As the evaluation results, we can prove that this switch has a good insertion loss characteristic and high speed and stable switching characteristics. It was also confirmed that it has superior characteristic in terms of long-term reliability.

With network systems growing, optical

switches must meet demands for further higher reliability, more compactness, weight reduction and lower costs that are expected to arise from now.

We are going to make progress in the development of optical switches to meet those demands.

7. Reference

1) S.Nagasawa,H.Furukawa,T.Satake and N.Kashima; "New Type of Optical Switch with a Molded Ferrule ",Trans.IEICE,Vol E70,8,PP696-698,1987
2) S.Nagasawa, H.Kobayashi and F.Ashiya; "A Low-Loss Multifiber Mechanical Switch for 1.55um Zero-Dispersion Fibers", Trans.IEICE,Vol.E73,7,pp.1147-1149,1990
3) T.Satake,S.Nagasawa and N.Kasima ; "Design and Characteristics of Plastic-Molded Multi-fiber Connector ", Trans. IEICE Japan,J68-B,3,PP.427-434,1987
4) H.Kobayasi,M.Simizu,I.Watanabe, S.Nagasawa; "High Reliability Service utilizing high-speed switching of Optical Fiber ", NTT Technology Journal pp.15-17, August,1990



Koji Yoshida

The Furukawa Electric Co.,Ltd.
6,Yawatakaigandori, Ichihara,Chiba,290, Japan

Koji Yosida was born in Fukuoka, Japan, in 1964. He received the B.E. degree in metal engineering from Kyushu Institute of Technology, Fukuoka, Japan, in 1986.
He jointed The Furukawa Electric Company, in 1986. Since 1991 he has been engaged in R&D on optical component. Mr.Yosida is a member of the Institute of Electronics, Information and Communicaton Engineers of Japan.



Toshihiko Ohta

The Furukawa Electric Co.,Ltd.
6,Yawatakaigandori, Ichihara,Chiba,290, Japan

Toshihiko Ohta was born in Gifu, Japan, in 1962. He received the B.S. degree in physics from Shinshu University, Nagano, Japan, in 1985.
He jointed The Furukawa Electric Company, in 1985. He has been engaged in R&D on optical component. Mr.Ohta is a member of the Institute of Electronics, Information and Communicaton Engineers of Japan.



Hiroyoshi Sueki

The Furukawa Electric Co.,Ltd.
6,Yawatakaigandori, Ichihara,Chiba,290, Japan

Hiroyoshi Sueki was born in Hokkaido, Japan, in 1965. He received the B.S. degree in physics from University of Electro Communications, Tokyo, Japan, in 1990.
He jointed The Furukawa Electric Company, in 1990. He has been engaged in R&D on optical component. Mr.Sueki is a member of the Institute of Electronics,Information and Communicaton Engineers of Japan.



Hiroyuki Yamada

The Furukawa Electric Co.,Ltd.
6,Yawatakaigandori, Ichihara,Chiba,290, Japan

Hiroyuki Yamada was born in Kanagawa, Japan,in 1960. He received the B.E. degree in mechanical engineering from Tokyo Metropolitan University , Tokyo, Japan, in 1983.
He jointed The Furukawa Electric Company, in 1983. He has been engaged in plant and facilities Div.



Takashi Shigematu

The Furukawa Electric Co.,Ltd.
6,Yawatakaigandori,
Ichihara,Chiba,290,
Japan

Takasi Sigematu was born in Sizuoka, Japan, in 1963. He received the B.E. degree in precision engineering from Yamagata University , Yamagata, Japan, in 1986.
He jointed The Furukawa Electric Company, in 1986. He has been engaged in R&D on plant and facilities Div.



Takahide Kimura

The Furukawa Electric Co.,Ltd.
2-6-1,Marunouti,
Chiyoda,Tokyo,
110,Japan

Takahide Kimura was born in Tokyo, Japan, in 1958. He received the M.E. degree in mechanical engineering from Tokyo University , Tokyo, Japan, in 1983.
He jointed The Furukawa Electric Company, in 1981. He has been engaged in plant and facilities Div.

MT-type Fiber Selector for Optical Fiber Monitoring System

Y.TAMAKI Y.ISONO S.GOTO

Fujikura Ltd.
1440, Mutsuzaki Sakura-shi, Chiba, 285, Japan

Abstract

As optical fiber cable networks expand maintenance technologies for optical lines assume increasing importance in the operation of the network.

A system that quickly and automatically forecasts and locates defects on the optical line has been designed and implemented. Defects can be forecast and automatically located because the optical line is continuously monitored. The monitoring system consists of measuring instruments like the light source, optical power meter, OTDR, and an optical switch to select the monitor line.

The optical switch, which determines the reliability of the entire system, is one of the most important system elements. In order to reliably select a monitor line from the multicore optical line, the optical switch must have loading consistency and durability.

1.Introduction

Since optical fiber cables were introduced to subscriber lines, the number of cores used has been increasing each year. In Japan particularly , high-density optical fiber cables of 4-and 8-core ribbon fibers are being used, and a large subscriber network is being constructed.

As the density of optical fiber cables increases, there is a need for efficient construction and maintenance technologies. An optical line monitoring system has been developed and implemented to perform optical line tests and automatic remote control of cables.

The optical line monitoring system consists of an optical fiber coupler, an optical fiber switch, and a test unit. The optical fiber switch consists of a switch to select the measuring unit and another switch to select the optical fiber line that is to be tested.

The two optical fiber switches are an important system component for system design. In particular, the switch that selects the optical line determines the performance of the overall system.

Therefore, this switch must have low losses and consistency.

Based on our research, we developed a multicore optical switch which can meet the above requirements and also perform switching of multiple cores.

In this paper, we describe the design and characteristics of this multicore optical switch.

2.System Configuration

Fig.1 shows the configurations of an optical line monitoring system and an optical fiber selector used in this system.(1)

This system is principally used to measure and monitor the optical line by automatic remote control without adversely affecting the on-going transmission signal.

Monitoring and measurement is carried out using an OTDR, light source, and optical power meter. The measurement light is emitted through an optical fiber coupler installed in the optical line to measure optical line loss and return loss.

Monitoring of an optical line which is being used is through OTDR generally. A measurement light wavelength of 1.55um is used for a transmission signal light of 1.3um.

A light source and an optical power meter are used for measuring line losses caused during installation work of optical lines, as well as during shifting of an optical line due to interference, or when connectors need to be replaced.

The optical fiber selector, one of the main components of the optical line control system, comprises of MT-and SC-type fiber selectors.(2)

The MT-type fiber selector chooses on a tape basis the line to be monitored from among the optical lines consisting of tape fibers; the SC-type fiber selector further chooses the line to be monitored, on a core basis. Simultaneously, the fiber selector also selects a test unit to be used for monitoring (measurement).

The end of the optical fiber core of the

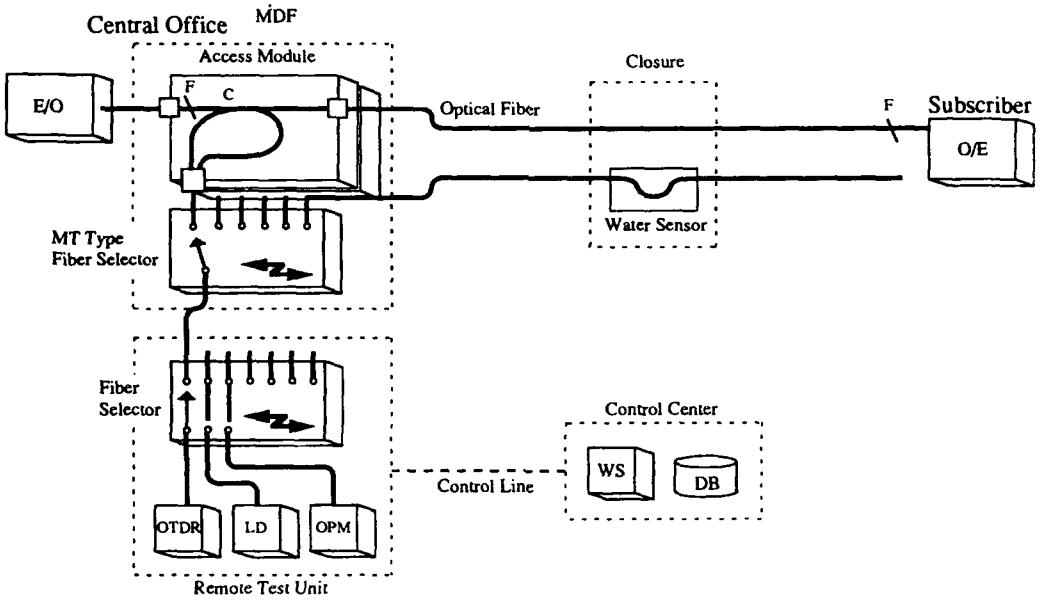


Fig .1 System Configuration

MT-type fiber selector moving head is connected to the SC-type fiber selector. The SC-type fiber selector allows a maximum of six MT-type fiber selectors to be connected.

Monitoring and test operation of the optical line are controlled using a workstation and is continuously carried out. The workstation acquires test data to identify whether the line is functioning normally.

3.MT-type Fiber Selector

3.1 Basic function

As noted in the system configuration, the MT-type fiber selector is used to select the optical line that is to be monitored. Since this unit selects an optical line on a tape fiber basis, its basic connection element is an MT connector.

A single MT-type fiber selector can handle a maximum of 1000 cores. When return lines at the optical fiber coupler are included, the maximum number of cores that can be installed is 2000 (250 eight-core tape fibers).

The MT-type fiber selector has to be installed in an optical end frame and its size is a compact 685mmWx295mmDx170mmH.

3.2 Mechanism

3.2.1 Equipment configuration

Fig.2 shows the internal structure of the MT-type fiber selector.

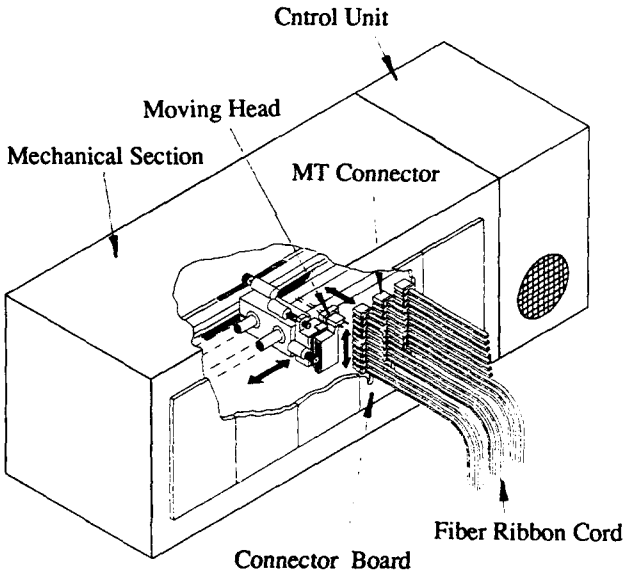


Fig .2 MT-type Fiber Selector Configuration

The MT-type fiber selector is basically composed of a mechanical section (including optical fiber) and a control unit. For easy maintenance as well as future expansion, these sections can be easily separated.

The mechanical section consist of a moving head and connector boards with MT connectors which are the ends of the tape fibers connected to an optical line. The moving head is capable of moving in all three axes when selecting a MT connector on the connector board. One connector board has 50 MT-connector plugs, and the fiber selector allows up to five connector

boards (250 MT-connector plugs) to be installed on the mechanical section. A connector board can be installed on the mechanical section by inserting a location pin provided on the edge of the connector board into a location hole provided on the edge of the fiber selector. This allows connector boards to be installed precisely enabling the MT-type fiber selector to acquire optimum optical characteristics without having to make fine adjustments during installation.

Individual connector boards are fastened to the fiber selector using four screws.

The driving system of the moving head consists of a compact DC motor and a rack & pinion gear.

3.2.2 Positioning Control System

The MT-type fiber selector employs a closed loop control system using a linear scale for position control in the X and Y axes.

This control system feeds back the position of the moving head to a position controller. This allows real-time identification of the present location, so that the moving head can be moved to the desired position accurately. Furthermore, since the origin can always be identified, this positioning control system allows the moving head to be moved to a different position directly without having to return to the origin first.

3.2.3 Structure of connector

Connections of connectors on the moving head and connector boards use an MT connector as shown in Fig.3.
A pin similar to the alignment pin shown in the figure is installed on the MT connector plug on the moving head. The tip of this pin is chamfered to a larger degree than the pins of ordinary MT connectors. This is to ensure that the pin does not damage the pin hole in the mating connector when the pin is inserted into the hole for connection.

MT connectors are mounted in a floating construction both in the moving head and the connector boards to absorb any variations in the connecting position. This ensures constant optical characteristics even when there are variations in the moving head stopping position.
Furthermore, the MT connectors are constructed so that the end of an MT connector always moves in a fixed direction when disconnected. This is to prevent problems such as the alignment pin not fitting into the hole in the mating connector upon connection and so on.

Connecting force is applied by a coil spring provided at the rear of the MT connector plug. The intensity of this force is 1kg, which is the same as that of an MT connector.

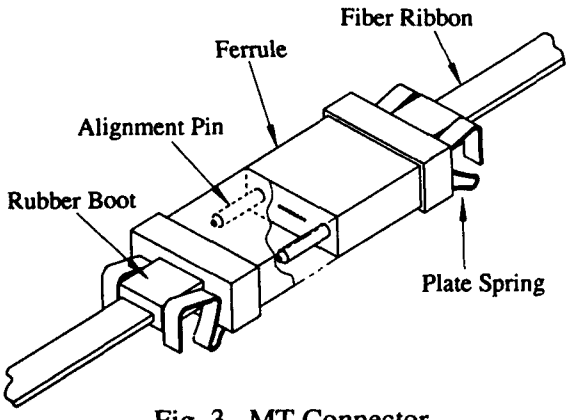


Fig .3 MT Connector

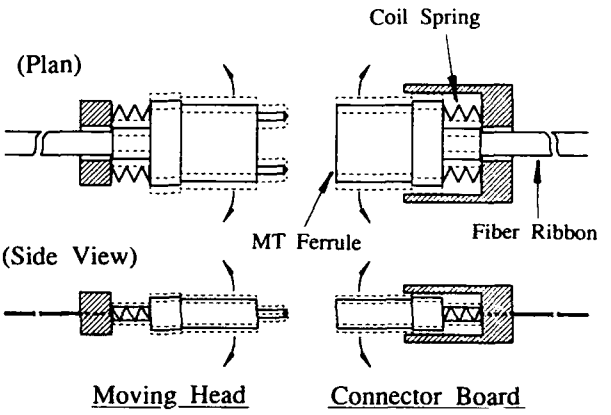


Fig .4 Structure of Connector Holder

3.3 Characteristics
3.3.1 Connecting characteristics

We investigated the relationship between the moving head positional deviation and the connection loss. The moving head positional deviation was measured in both X and Y axes. The maximum moving head positional deviation was predicted to be about 25um in both the X and Y axes as viewed from the mechanism. Based on the results of the test, a positional deviation of 100um caused a loss change of less than 0.1dB as shown in Fig.5.
This reveals that the connection of the MT connectors is very stable with respect to positional deviation.

3.3.2 Position repeatability

We checked the positional repeatability of the moving head in the X direction using a proximity sensor.

In this test, starting from the origin, we repeated a positioning operation 1000 times in succession and measured the stop position at a measurement point every 100 times to check for variations. The measurement results show that the deviation was less than 10um, verifying the positional accuracy.

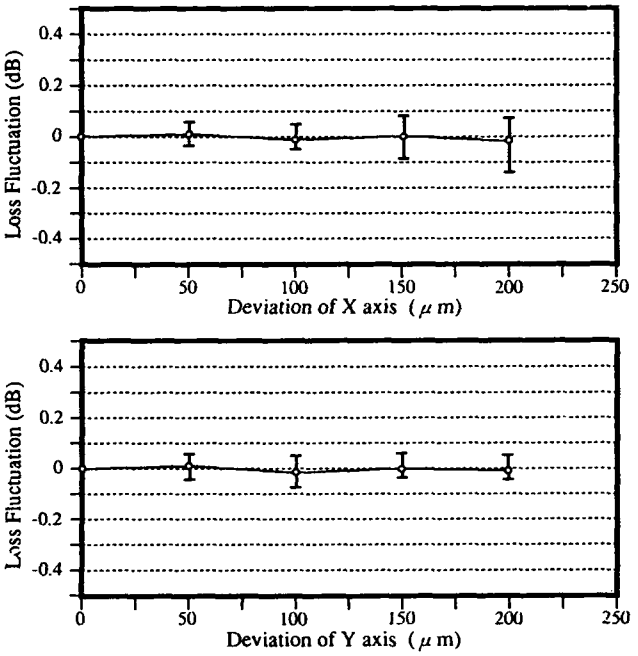


Fig .5 Relationship Between the Moving Head Deviation and Connection Loss

3.3.3 Temperature characteristics

We measured the connection loss and its repeatability at set temperatures of 0, 25 and 40 C. This was repeated 1000 times at each set temperature. The connection loss was measured at the end of every 10 repetitions. The measurement results show stable temperature characteristics at all the set temperatures. Fig.6 shows the measurement results.

3.3.4 Vibration characteristics

The MT-type fiber selector was vibrated under the following conditions to evaluate changes in connection loss before and after the vibration test.

* Frequency : 10 to 55Hz
* Amplitude : 5mm p-p
* Vibrating time : 20min

The test results show that change in connection loss before and after the vibration test was 0.05dB on average and 0.10dB maximum. This indicates stable vibration characteristics.

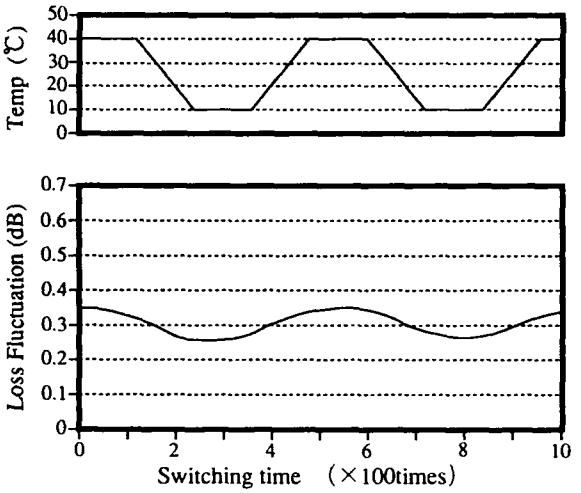


Fig .6 Temperature Cycle Test Result

3.3.5 Other Characteristics

Table 1 shows the target values of other characteristics and the obtained results. For connection loss characteristics, an MT connector was connected using an MT clip and also connected in the fiber selector to compare the connection losses. As shown in Fig.7, the connection losses did not show a significant variation. As for the return loss, we obtained an average value of 49dB and a minimum value of 42dB as compared to a target value of 35dB or more. The measurement results are shown in Fig.8.

We also conducted a repetitive loading test of 22000 connections/disconnections. As shown in Fig.9, connection loss variations are less than 0.2dB throughout the test. This verifies that the MT -type fiber selector has very stable characteristics.

As for switching speed, switching time from port 1 on one end of the fiber selector to a port at the center(average switching time) was 6sec and the switching time from port 1 of the fiber selector to

Table 1 Characteristics of MT-type Fiber Selector

Item	Target	Result
Insertion Loss	≦ 0.90dB	AVE : 0.32dB MAX : 0.75dB
Return Loss	≧ 35dB	AVE : 49.3dB MIN : 42.0dB
Loss Fluctuation	≦± 0.17dB/10 times	≦± 0.1dB/10 times ≦± 0.2dB/10000 times

the furthest end port(maximum switching time) was 8sec as compared to a target value of 15sec or less.

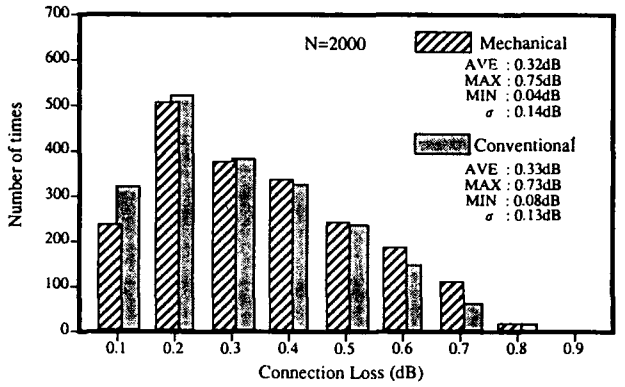


Fig .7 Connection Loss Histogram

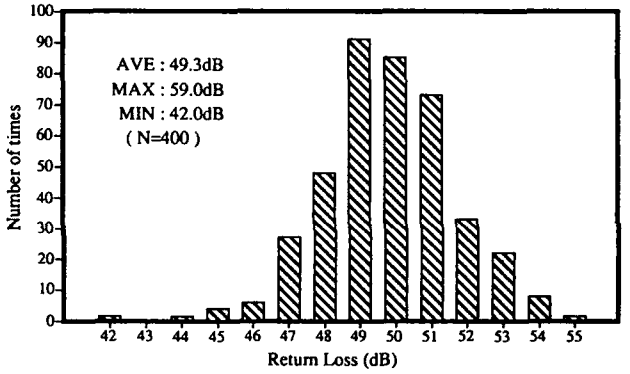


Fig .8 Return Loss Histogram

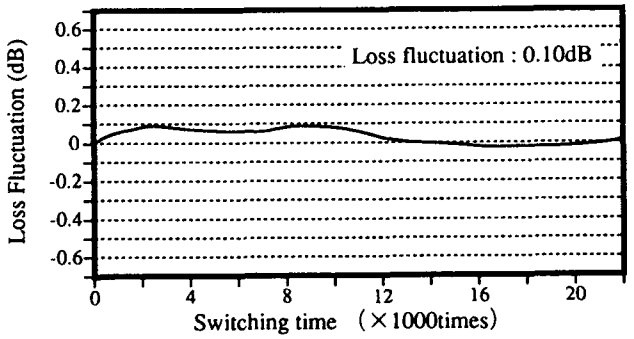


Fig .9 Loss Fluctuation for Repeat Switching

4.Conclusions

As described above, we have developed a fiber selector with stable characteristics and high reliability. This fiber selector has already been implemented as part of an optical line monitoring system. This system is presently in use in Japan. Since it displays stable optical characteristics, this MT-type fiber selector can also be used in other automatic loss measurement systems. We believe that it has the potential to be widely used for applications other than optical line monitoring systems in the future.

In addition, we are presently studying optical fiber selectors that are more compact, accommodate optical fibers at higher densities, and are capable of faster switching.

References

(1) N.Tomita, et al.,"Automatic Remote Optical Fiber Line Test and Administration System Design", in 1990 Spl.Nat.Conf. Rec.Common. IEICE, Japan, NO.B-888.

(2) H.Takasugi, et al.,"Design and Evaluation of Automatic Optical Fiber Operation Support System", 39th IWCS, pp.623-628, 1990.



Yasuhiro Tamaki

FUJIKURA LTD.
Opto-Electronics
Laboratory

1440,Mutsuzaki,
Sakura-shi,Chiba,285
Japan

Yasuhiro Tamaki was born in 1955. He received the B.E. degree in mechanical engineering in 1977 from Saitama University.

He joined Fujikura Ltd. in 1982 and has been engaged in the research and development of telecommunication cables and accessories.

Mr. Tamaki is a member of the Institute of Electronics, Information and Communication Engineers of Japan.



Yoshiya Isono

FUJIKURA LTD.
Opto-Electronics
Laboratory

1440,Mutsuzaki,
Sakura-shi,Chiba,285
Japan

Yoshiya Isono was born in 1956. He received the B.E. degree in mechanical engineering in 1977 from Waseda University.

He joined Fujikura Ltd. in 1982 and has been engaged in the research and development of telecommunication cables and accessories.

Mr. Isono is a member of the Institute of Electronics, Infomation and Communication Engineers of Japan.



Shigenori Goto

FUJIKURA LTD.
Opto-Electronics
Laboratory

1440,Mutsuzaki,
Sakura-shi,Chiba,285
Japan

Shigenori Goto received the B.E. degree from Iwate University.

He joined Fujikura Ltd. in 1974 and has been engaged in the research and development of telecommunication cables and accessories.

Mr.Goto is the manager of the Cable Maintenance System Section.

He is a member of the Institute of Electronics, Infomation and Communication Engineers of Japan.

A LARGE-SCALED 1xN OPTOMECHANICAL MATRIX SWITCH

Shun'ichi Mizuno Hisao Maki Naoshi Hakamata Yasuo Asano

Optomechatronics systems R&D Dept., Yokohama Research Labs..
Sumitomo Electric Industries, LTD.

1. Abstract

A large-scaled 1xN optomechanical matrix switch for use in the "optical line switching test system", designed to effectively implement construction, maintenance and operation of the optical communication trunk lines has been developed. This switch employs DC servo motors and LED arrays for driving and positioning, and has achieved stable optical characteristics and high reliability by a newly developed master head with a compliance mechanism.

2. Introduction

Recently trunk optical fiber cable networks, have been deployed rapidly. A new operation system that provides a major advance in construction and maintenance efficiency is necessary to construct the extensive optical fiber cable networks.

Some results for the operation systems were reported.[1] The equipment which can select freely one of the optical fibers in some cables and can interconnect it to a master connector plays a very important role in these operation systems.

This paper describes a large-scaled 1xN optomechanical matrix switch which has been developed and its optical performance.

3. Function of a 1xN optomechanical matrix switch

The configuration of the new operation system is shown in Fig.1. In that system the 1xN optomechanical matrix switch has the function of selecting an optical fiber to be measured from the trunk optical cables. This switch is composed of connectors arranged in a matrix and a master head opposing to the matrix and movable in 3 directions.

The monitor light of which wavelength is defferent from that of the in-service light is injected from the matrix switch into an in-service fiber line through a coupler. The other end of an optical fiber from the master head is connected to the measuring instruments such as an OTDR (Optical Time Domein Reflectometer). The same system is installed in telephone offices or tandem offices, and it enables supervision of transmission characteristics.

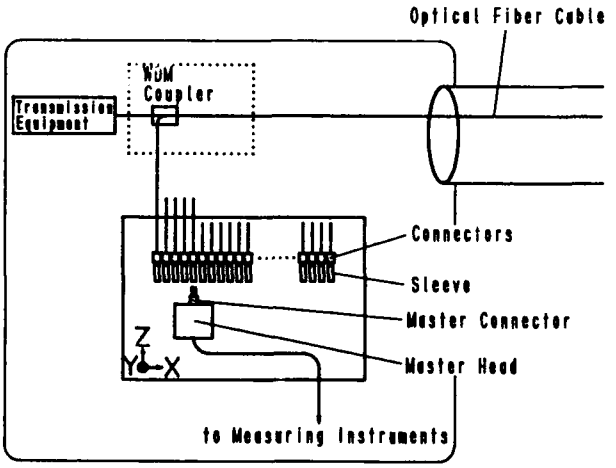


Fig.1 System Configuration

4. Structure

As shown in Fig.2, a large number of holes are dug in the baseplate. An optical connector is set in each hole.

Figure 3 shows the schematic view of a 1xN optomechanical matrix switch. This matrix switch employs DC servo motors for driving in each

direction. A means to drive the sliders is rack & pinion in X direction and ballscrews in both Y and Z directions. The sliders in X and Y directions are positioned by LED arrays corresponding to each connectors, and the slider in Z direction is positioned by the rotary encoder coupled to the motor-rotating-axis.

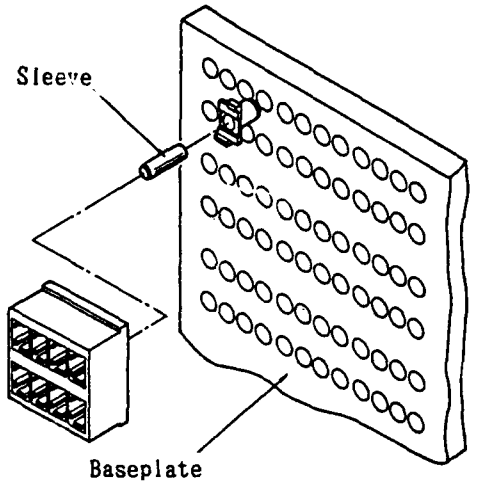


Fig.2 Structure of Baseplate

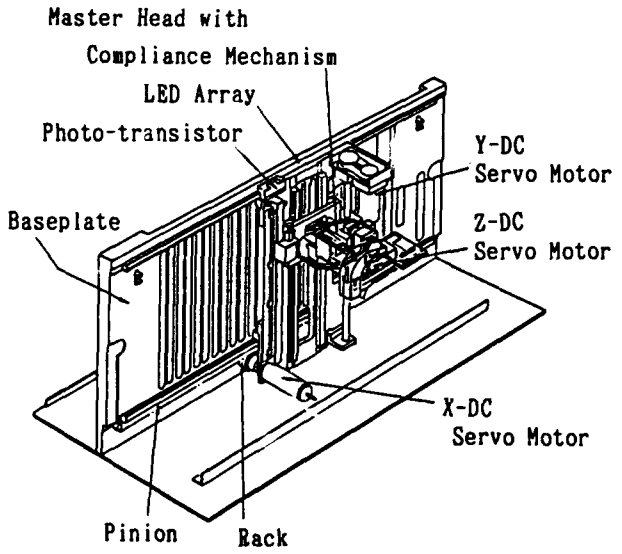


Fig.3 Schematic View of ..N Optomechanical Matrix Switch

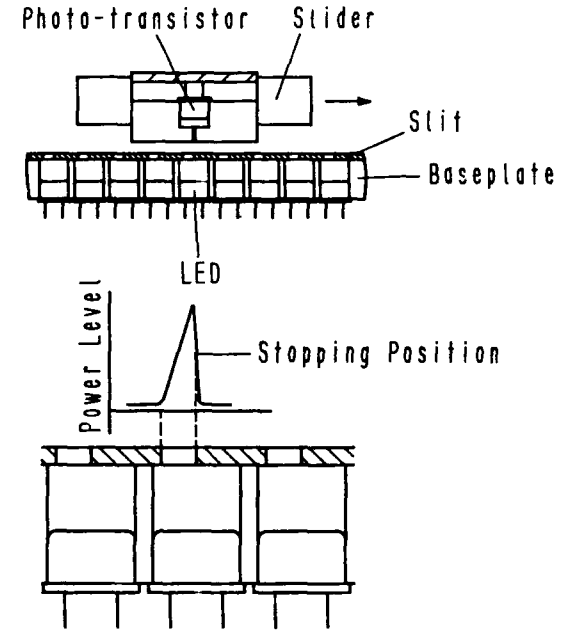
5.Positioning method & Compliance master head

5-1.Positioning by LED array

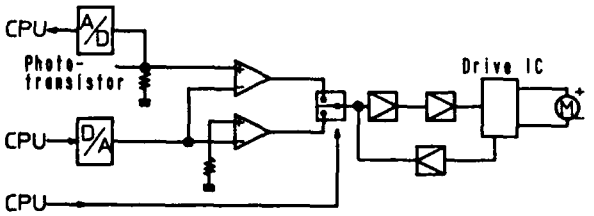
Generally a machine which employs a DC servo motor is positioned by a rotary or linear encorder and a counter circuit which counts the number of pulses from the encorders. In such positioning methods, we need to adjust and memorize the each X, Y and Z address where the master connector should be stopped and interconnected to the connector arranged in a matrix.

In the developed 1xN optomechanical matrix switch, LEDs are arranged in arrays in both X and Y directions corresponding to connectors arranged in a matrix. A photo-transistor is set on the master head.

Figure 4 shows the positioning method by LED array. Holes corresponding to connectors are dug in the baseplate of the matrix switch, and LEDs are set in each hole. A slit plate is stacked



(a) Structure



(b) Block Diagram

Fig.4 Positioning Method by LED Array

over the LED array to sharpen the propagation of the LED's beam flow. It improves the accuracy of positioning.

The photo-transistor set on a master head receives the LED's beam flow. In case of positioning, the process is as follows;

(1)A LED just before point to be stopped is lighted.

(2)The master head can detect the light by the photo-transistor.

(3)The master head is decelerated.

(4)The master head detects the first light from the deceleration point and stopped there.

For deciding the stopping position, we set the threshold at the mid point between the maximum and the minimum power level on the side of beam propagation distribution cut by the edge of the slit plate.

The above positioning method by LED array makes it unnecessary that we preadjust the each X and Y address where the master connector should be interconnected.

5-2.Master head with compliance mechanism

The positioning method by LED array has the above merit, however the fine adjustment of the positioning point isn't easy in comparison with the positioning method by a rotary encorder. So we developed the master head with compliance mechanism which can invalidate a bad effect on an optical performance with the misalignment during the interconnection. Figure 5 shows the experimental results of connection loss without any compliance mechanism. As shown in Fig.5, the connection loss increases by 0.2dB while the master connector is shifted 0.2mm from the connection center. In case the misalignment is more than 0.25mm, the master connector is not able to connect.

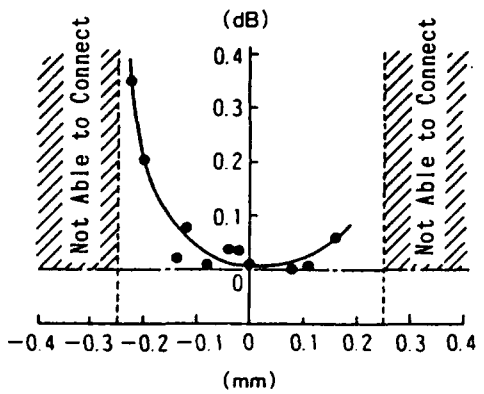


Fig.5 Relationship between Connection Loss and Offset without Compliance Mechanism

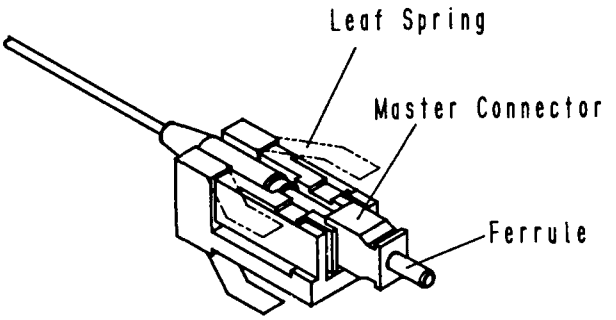
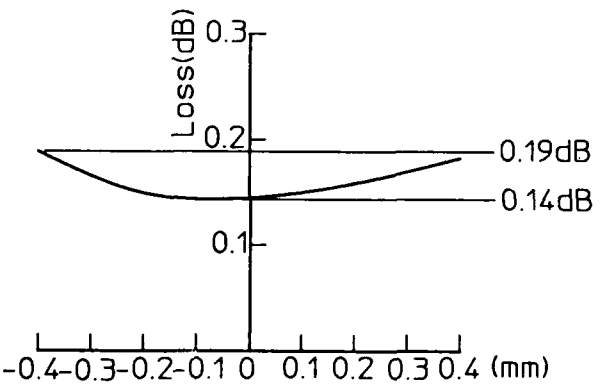
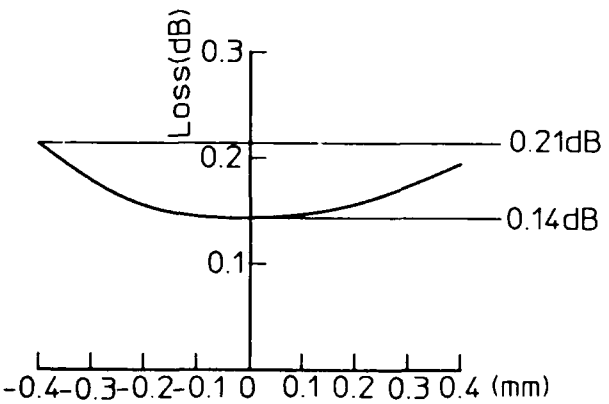


Fig.6 Structure of Compliance Mechanism



(a)Offset in X Direction



(b)Offset in Y Direction

Fig.7 Relationship between Connection Loss and Offset with Compliance Mechanism

Figure 6 shows the newly developed structure of compliance mechanism. It has two pairs of parallel leaf springs. The mechanism can cancel the misalgnment due to not only the scattered positioning, but also the scattered arranging of the connectors in a matrix.

Figure 7 shows the experimental results of a connection loss with the compliance mechanism. By this compliance mechanism, we can controll the connection loss increase less than 0.05dB and 0.07dB in X and Y direction respectively, while we limit the lateral offset within ±0.4mm.

6.Performance

Overall performance for the mechanical and optical characteristics of the 1xN matrix switch have been tested including repeated switching, heat cycle, and vibration. Results are summarized in Table 1. Figure 8 shows the connection loss histogram. The mean connection loss was 0.10dB, and the maximum loss was 0.32dB. Figure 9 shows the reflection loss histogram. The mean reflection loss was 30.4dB. Figure 10 shows the loss fluctuation during repeated switching test of 12000 times. It can be seen that the loss fluctuation is less than 0.03dB. A heat cycle test was conducted to measure the changes of the connection loss with changes in temperature. As shown in Fig.11, the loss fluctuation was less than 0.03dB when the temperature was changed from 0℃ to +45℃. And we obtained a good results on vibration tests.

Table 1 Evaluation Test Results

Items	Results
Connection Loss	Ave. = 0.1dB
Reflection Loss	Ave. = 30.4dB
Repeated Switching	12000 times Loss Variation < 0.03dB
Heat Cycle	0～+45℃ Loss Variation < 0.03dB
Vibration	10～45Hz, 0.5mm p-p →No problem

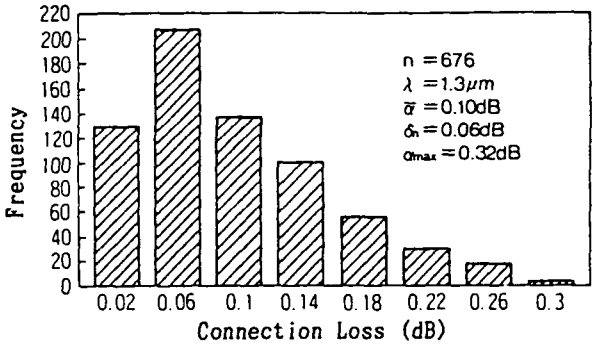


Fig.8 Loss Histogram

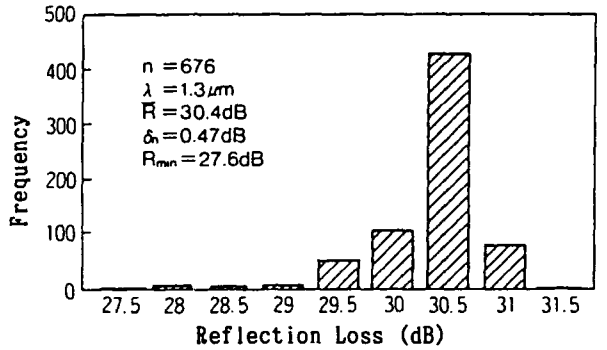


Fig.9 Reflection Loss Histogram

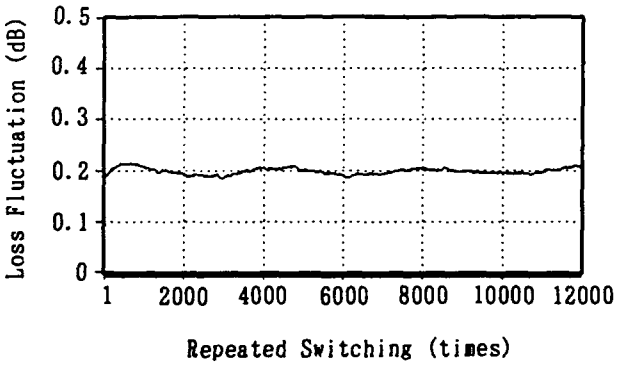


Fig.10 Loss Fluctuation of Repeated Switching

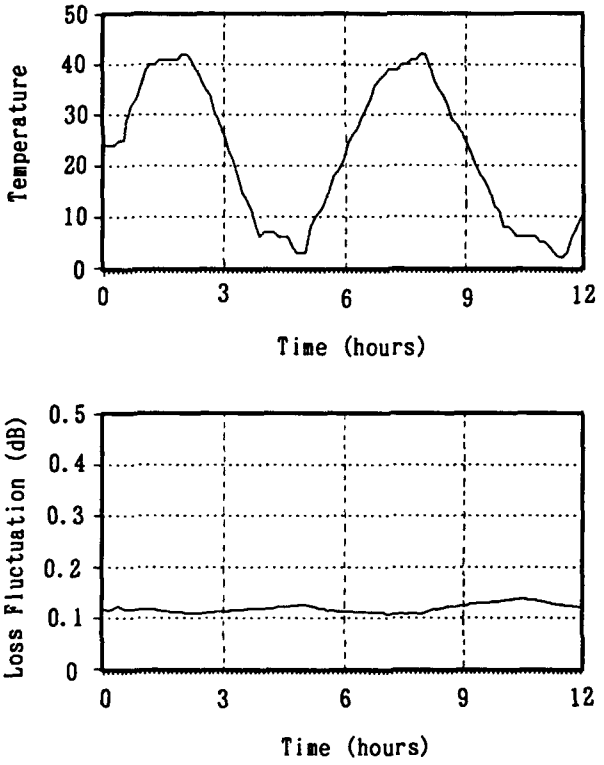


Fig.11 Heat Cycle Tests

7.Conclusions

A large-scaled 1xN optomechanical matrix switch using single fiber connector has been developed. The matrix switch has achieved stable optical characteristics and high reliability.

References

(1) H. Matsumoto, et al., "Cable transfer and supervisory system for trunk optical fiber cables" 40th IWCS(1991), 787.

Shun'ichi Mizuno



Sumitomo Electric Industries, Ltd.

1, Taya-cho, Sakae-ku
Yokohama, Japan

Shun'ichi Mizuno was born in 1959 and received his M.S. degree in mechanical engineering from Tokyo Institute of Technology in 1985. He joined Sumitomo Electric Industries the same year and has been engaged in research and development of optomechanical matrix switches. He is a member of the Institute of Electronics, Information and Communication Engineering of Japan.

Hisao Maki



Sumitomo Electric Industries, Ltd.

1, Taya-cho, Sakae-ku
Yokohama, Japan

Hisao Maki was born in 1958 and received his M.S. degree in system engineering from Kobe University in 1983. He joined Sumitomo Electric Industries the same year and has been engaged in research and development of automatic optical measuring instruments. He is now a senior engineer of Optomechatronics Systems R&D Dept. Yokohama Research Labs. He is a member of the Institute of Electronics, Information and Communication Engineering of Japan.

Naoshi Hakamata



Sumitomo Electric
Industries, Ltd.

1, Taya-cho, Sakae-ku
Yokohama, Japan

Naoshi Hakamata was born in 1960 and received his B.S. degree in electronic engineering from Nagoya University in 1983. He joined Sumitomo Electric Industries the same year and has been engaged in research and development of fusion splicing technologies for optical fibers. He is a member of the Institute of Electronics, Information and Communication Engineering of Japan.

Yasuo Asano



Sumitomo Electric
Industries, Ltd.

1, Taya-cho, Sakae-ku
Yokohama, Japan

Yasuo Asano received his B.S. degree in mechanical engineering from Waseda University in 1968. He joined Sumitomo Electric Industries in 1971 and has been engaged in development of jointing technologies for coaxial cables and optical fiber cables. He is now a manager of Optomechatronics Systems R&D Dept. Yokohama Research Labs, and a member of Japan Society of Mechanical Engineers and the Institute of Electronics, Information and Communication Engineering of Japan.

AUTHORS INDEX

Name	Page
ADCOCK, J. A.	561
ADE, R. W.	650
AIHARA, K.	732
AIKAWA, H.	119
AKASAKA, N.	13, 428
AMANO, T.	46
ANDO, Y.	785
AOYAMA, A.	261
ARAKI, S.	111
ASANO, Y.	119, 806, 826
AZUMA, Y.	97
BEECH, S. C.	349
BERAK, J. M.	650
BERNSTEIN, N.	654
BERTHELSEN, G.	25
BISHOP, J.	356
BISHOP, T.	442
BLYLER, L. L.	239
BOES, P.	64, 285
BOLIVER, V. J.	561
BOSCHER, G.	126, 447
BOSSI, D. E.	650
BOW, K. E.	583
BOWMER, T. N.	310
BRIGGS, JR., P. R.	533
BROWN, G. D.	667
BRÜCKNER, H. W.	406
BUBNOV, M. M.	629
BUCZMA, E.	561
CARLTON, G.	59
CARLTON, L. T.	158
CARTER, C. N.	59
CHANDAN, H.	599
CHANDAN, H. C.	239
CHANG, T. C.	435
CHAWLA, C.	442
CHEN, K. Y.	435
CHEN, T. H.	183
CHENG, L. P.	539
CHO, Y.-O.	594
CHU, F. L.	545
CHUNG, D.-W.	594
CONNAUGHTON, M.	332
CORAIOLA, A.	748
CORTINES, C.G.	25
CUELLAR, E.	689
D'AMICO, J. N.	310, 526
DANESHVAR, O.	417
DAVIES, A. E.	356
DAWSON, T.	338
DE VEAU, G. F.	104
DE VECCHIS, M.	145
DEBSKA, A.	548
DELAGE, P.	373
DEVLIN, B. T.	705
DI MINICO, C.	228
DIANOV, E. M.	629
DOBLE, I. R.	349
DYE, K. D.	298
ECKARD, A.	548
EMMERICH, M.	197
ENDO, S.	249
ESTES, R.	705
FAGERSTROM, R. M.	792
FANN, D. M.	435
FERNANDO, P. L.	497
FICKE, W. H.	158
FIJITA, I.	119
FINZEL, L.	447
FORD, J. R.	349
FOY, P. R.	253
FRANKEN, G.	406
FRANTZ, R. A.	279, 467
FROST, P.	53
FUJISAKI, A.	208
FUJITA, I.	395
FUKUOKA, K.	46
FURUKAWA, H.	234
FURUKAWA, S.-I.	81
GAU, Y.	298
GEBIZLIOGLU, O. S.	279, 526
GIRBIG, R.	373
GLAESEMANN, G. S.	698, 713
GOTO, S.	820
GOULD, C. A.	451
GRABANDT, O.	293
GREEN, G. D.	253
GRIFFIOEN, W.	622
GRIMADO, P. B.	457
GRÜNER-NIELSEN, L.	321
GULATI, S. T.	612
HAAG, H. G.	748
HAKAMATA, N.	826
HAKOZAKI, J.	506
HALL, C. E.	521
HAMADA, M.	119
HAMADE, T.	481
HARA, M.	20
HARAKAWA, T.	777
HARDWICK, III, N. E.	679
HARTLEY, J. G.	679
HASEMI, A.	476

Name	Page
HASHIMOTO, S.	506
HASLØV, P.	321, 423
HATTORI, T.	428
HAYAKAWA, H.	476
HENDRICKSON, B. M.	645
HERSHKOWITZ, E. E.	533
HILL, J.	417
HILL, J. A.	521
HIRAO, H.	801
HODGE, K. G.	713
HOFFART, M.	267, 373
HÖG, G.	373
HOPIAVUORI, M.	713
HOPLAND, S.	492
HORE, L. M.	757
HORIGUCHI, T.	81
HORII, K.	481
HORIMA, H.	46
HORNUNG, S.	53
HSIAO, J. M.	435
HSIEH, R.-C.	64
HUNTER, J.	654
HWANG, S. C.	573
IGARASHI, K.	261
INGOLD, J. P.	667
INNISS, D.	239, 599
ISHIKAWA, H.	395
ISONO, Y.	820
IWANO, S.	785
JENSEN, K. B.	423
JOHNSON, A. J.	673
JOSEPH, E. J.	332
JOSTAN, J. L.	267
KAIDE, T.	273
KAKUTA, T.	13
KALOMIRIS, V. E.	659
KAMIKATANO, M.	176
KANAYAMA, K.	785
KANEN, R. M.	673
KATHIRESAN, K.	158, 679
KATSURASHIMA, W.	13, 428
KAUFMAN, S.	345
KAWASE, M.	637
KELLER, D.	25
KEMP, R. C.	578
KENNEDY, M. T.	689
KERRY, J.	53
KEY, P. L.	462
KHAN, M. J.	511
KHAN, S. A.	533
KIKUCHI, Y.	801
KILMER, J. P.	705
KIM, S.-J.	594
KIMURA, T.	813
KINOSHITA, K.	208
KISS, G. D.	792
KITAYAMA, Y.	13, 395
KLYKKEN, A.	492
KNUDSEN, D. R.	667
KÖLSCHBACH, V.	75
KOMIYA, T.	806
KONIK, W. S.	104
KOO, J. Y.	573
KOO, J.-Y.	594
KOSSAT, R.	126
KOVAC, R. J.	253
KOYAMADA, Y.	81
KRAEHENBUEHL, F.	556
KRUIJSHOOP, A.	64
KUBO, Y.	171
KUME, N.	384
KUN, Z. Y.	183
KURKJIAN, C. R.	599
KUROSAWA, Y.	151
KUWAKI, N.	88, 97
KYLEN, G.	25
LASNE, C.	25
LATOSZYNSKI, P.	285
LEE, C. S.	573
LEEUWEN, J. H. V.	293
LEVISSE, A.	739
LEVY, A. C.	253
LIN, Y.-C.	435
LOCH, M.	126
MACHIDA, T.	401
MAKI, H.	826
MATSUDA, Y.	428
MATSUHASHI, S.	777
MATSUMAE, Y.	481
MATSUMOTO, M.	5
MATSUOKA, R.	384
MAYER, H. A.	561
MENDAT, L.	447
MIAYAZAKI, Y.	417
MICHAELS, P. A.	659
MILLER, A. E.	659
MILLS, G. A.	472
MISHIMA, S.	132
MIYAMOTO, M.	151, 176, 389
MIZUNO, S.	806, 826
MIZUTANI, A.	249
MOCK, J. L.	104
MOERS, H.	373
MORITANI, Y.	506
NAGASAWA, S.	5
NAGASE, R.	785
NAGAYAMA, K.	119
NAITO, Y.	261
NAKAHARA, S.	273
NAKAO, N.	777
NELSON, E. D.	298
NEWMAN, L. A.	650

Name	Page
NIMURA, H.	208
NOMURA, Y.	234, 801
NONAKA, T.	428
NYAAS, K.	369
OHNO, N.	32
OHSUMI, K.	481
OHTA, I.	476
OHTA, T.	813
OHTSUKI, F.	220
OHZAWA, K.	140
OISHI, K.	13
OKADA, N.	384
OKAGAWA, S.	20
OOHASHI, K.	111
OSAKA, K.	395, 806
OTAKE, A.	20, 213
OZAWA, K.	806
PANUSKA, A. J.	158
PARK, W. K.	573
PARMAR, D. S.	406
PATTERNOSTRO, G.	25
PAVLOV, A. A.	765
PEACOCK, A. J.	59
PEGGE, C. S.	713
PELLEGRINO, A.	457, 462
PESHKOV, I. B.	765
PETISCE, J. R.	239
PLITZ, I. M.	279, 467
POKLACKI, E.	442
POPOV, M. F.	765
PRESNELL, M. J.	104
PRESTON, J.	539
RACHCOFF, J.	285
REITH, L. A.	457, 467, 792
RITCHIE, J.	486
ROBERTS, D. R.	689
ROCHESTER, C. J.	349
ROGERS, L.	332
RUEGENBERG, G.	126
RUSSELL III, H. J.	332
RYOO, H.-S.	594
SACKS, R. N.	650
SAEGUSA, M.	401
SAITHO, D.	249
SAITO, S.	389
SAKAMOTO, T.	506
SAKATA, Y.	732
SAKURAI, K.	88
SANKAWA, I.	81
SANO, T.	806
SANSHIGE, Y.	132
SANTANA, M. R.	158
SATO, K.	32
SATO, N.	111, 151, 176
SAWANO, H.	151, 176, 389
SAWYER, D.	539
SCHICK, G.	673
SCHULTE, J.	25
SCHULZE-BUXLOH, K.	748
SEMJONOV, S. L.	629
SHEA, J. W.	158, 239
SHEPHERD, L.	239
SHIBATA, Y.	97
SHIELDS, K. B.	521
SHIGEMATSU, T.	813
SHIMIZU, M.	476
SHIMIZU, S.	213
SHIMO, Y.	481
SHIMOMICHI, T.	111
SHINDO, Y.	384
SKOVGAARD, N. H.	321, 423
SLAVIN, L. M.	533
SNYDER, J. R.	253
SOMMER, R. G.	267
SONTAG, K.	486
STRINGER, A.	578
STYZINSKI, M.	285
SUEKI, H.	813
SUETSUGU, Y.	171
SUGIYAMA, N.	401
SUGIYAMA, Y.	132
SUN, C.-H.	594
SUNDBERG, E.	725
SUTEHALL, R.	59
SUZUKI, I.	140
SUZUKI, K.	213
SVENSSON, T.	725
SZUM, D.	442
TAGO, N.	732
TAKASE, A.	213
TAKEDA, T.	273
TAMAKI, Y.	820
TAMURA, S.	97
TANAKA, H.	273
TANAKA, S.	171, 395
TANIFUJI, T.	5
TAYA, H.	140
TAYLOR, C. R.	158, 239
TAYLOR, J.	539
TELLEFSEN, K. A.	673
TERASAWA, Y.	171
THÖNNEßEN, G.	748
THAI, S.	654
THALMAN, W. J.	548
TIBBETTS, D. J.	451
TITCHMARSH, J. G.	411
TOMITA, S.	5
TOMITA, Y.	481
TONYALI, K.	304, 497
TOYOSHIGE, S.	140
TRÖNDLE, H.	75
UENOYA, T.	5

Name	Page
UKACHI, T.	261
UNAMI, Y.	88
UZELAC, M.	561
VARACHI, JR., J. P.	462, 533, 705
VOGEL, E. M.	792
VOKEY, D.	486
WANG, S. I.	435
WARDEBERG, J.	369
WARGOTZ, W. B.	362
WARREN, J.	53
WAVRE, J. J.	556
WEI, T.	462, 705
WESTFALL, W. B.	104
WIECZOREK, C. J.	673, 705
WILLEMSEN, S.	293
WILLETT, D.	552
WOOD, W. W.	792
YAMADA, H.	813
YAMADA, T.	88
YAMAMOTO, Y.	220
YAMASHITA, K.	220
YAMAUCHI, O.	32
YAMAZAKI, T.	46
YAN, M. F.	659
YING, X. N.	183
YODO, S.	476
YOKOSUKA, H.	234
YONECHI, S.-I.	38
YOSHIDA, K.	813
YOSHINUMA, M.	140
YOSHIOKA, K.	32
YOSHIOKA, N.	249
YOW, S. C.	234
YUCE, H. H.	279, 462, 605, 705, 792
YUMOTO, M.	88
ZAMZOW, P. E.	373
ZLATSIN, Y.	578
ZUSHI, T.	273

IWCS

International Wire & Cable Symposium, Inc.

SPONSORED BY:
INTERNATIONAL WIRE & CABLE SYMPOSIUM, INC. (IWCS)
174 Main Street, Eatontown, NJ 07724
Tel: 908-389-0990

With Participation By:
U.S. Army Communications-Electronics Command (CECOM)
Fort Monmouth, New Jersey

AUTHOR'S ABSTRACTS

Please provide a 300–500 word abstract (25 copies) of proposed technical or poster papers on such subjects as applications and field evaluation; process & manufacturing; copper and fiber optic cables; systems; design & testing; military applications; disposal, recycling and reutilization of copper cables; power and industrial cables; cost reduction and quality improvement programs of interest to the commercial and military electronics industries. Send 25 copies of this abstract before 12 March 1993 to: IWCS, Inc., 174 Main Street, Eatontown, NJ 07724.

To submit a technical or poster session paper, prepare a comprehensive abstract using the format below:

- Author's name(s) and association
- Contact for Correspondence (Name, address, telephone and fax number)
- Indicate if paper is submitted for technical or poster session
 - I Title of paper
 - II Primary conclusion or result (one paragraph)
 - III Background - Why was work undertaken? (one paragraph)
 - IV Abstract

NOTE: Items II, III and IV should not be less than 300 words nor more than 500 words total in order to be considered by the Committee.
The substance of submitted papers shall not have been previously published or presented and must satisfy the Committee's criteria for content, originality and minimal commercial content.

Acceptance by the Committee will be based on the abstract; notification of acceptance will be mailed by May 21, 1993. The full manuscript will be required by August 13, 1993. The committee reserves the right to reject any final paper manuscript, if in its judgment, it does not comply with the guidelines on content, originality and minimal commercial content.

Fold Here

Stamp

IWCS, Inc.
Crystal Brook Professional Bldg.
174 Main Street
Eatontown, NJ 07724

Fold Here